Introduction to Aircraft Aeroelasticity and Loads

Jan R. Wright
University of Manchester and
J2W Consulting Ltd, UK

Jonathan E. Cooper
University of Liverpool, UK

John Wiley & Sons, Ltd

Introduction to Aircraft Aeroelasticity and Loads

Introduction to Aircraft Aeroelasticity and Loads

Jan R. Wright
University of Manchester and
J2W Consulting Ltd, UK

Jonathan E. Cooper
University of Liverpool, UK

BICENTENNIAL
1807
WILEY
2007

John Wiley & Sons, Ltd

Copyright © 2007

John Wiley & Sons Ltd, The Atrium, Southern Gate, Chichester,
West Sussex PO19 8SQ, England

Telephone (+44) 1243 779777

Email (for orders and customer service enquiries): cs-books@wiley.co.uk
Visit our Home Page on www.wileyeurope.com or www.wiley.com

All Rights Reserved. No part of this publication may be reproduced, stored in a retrieval system or transmitted in any form or by any means, electronic, mechanical, photocopying, recording, scanning or otherwise, except under the terms of the Copyright, Designs and Patents Act 1988 or under the terms of a licence issued by the Copyright Licensing Agency Ltd, 90 Tottenham Court Road, London W1T 4LP, UK, without the permission in writing of the Publisher. Requests to the Publisher should be addressed to the Permissions Department, John Wiley & Sons Ltd, The Atrium, Southern Gate, Chichester, West Sussex PO19 8SQ, England, or emailed to permreq@wiley.co.uk, or faxed to (+44) 1243 770620.

This publication is designed to provide accurate and authoritative information in regard to the subject matter covered. It is sold on the understanding that the Publisher is not engaged in rendering professional services. If professional advice or other expert assistance is required, the services of a competent professional should be sought.

Other Wiley Editorial Offices

John Wiley & Sons Inc., 111 River Street, Hoboken, NJ 07030, USA

Jossey-Bass, 989 Market Street, San Francisco, CA 94103-1741, USA

Wiley-VCH Verlag GmbH, Boschstr. 12, D-69469 Weinheim, Germany

John Wiley & Sons Australia Ltd, 42 McDougall Street, Milton, Queensland 4064, Australia

John Wiley & Sons (Asia) Pte Ltd, 2 Clementi Loop #02-01, Jin Xing Distripark, Singapore 129809

John Wiley & Sons Canada Ltd, 6045 Freemont Blvd, Mississauga, Ontario, Canada L5R 4J3

Wiley also publishes its books in a variety of electronic formats. Some content that appears in print may not be available in electronic books.

Anniversary Logo Design: Richard J. Pacifico

British Library Cataloguing in Publication Data

A catalogue record for this book is available from the British Library

ISBN 978-0470-85840-0

Typeset in 9/11pt Times by Aptara, New Delhi, India.
Printed and bound in Great Britain by Antony Rowe Ltd, Chippenham, Wiltshire
This book is printed on acid-free paper responsibly manufactured from sustainable forestry in which at least two trees are planted for each one used for paper production.

To our wives, Joy and Sarah

Contents

Preface **xv**

Introduction **xix**

Abbreviations **xxv**

Part I Background Material 1

1 Vibration of Single Degree of Freedom Systems **3**
- 1.1 Setting up equations of motion for single DoF systems 3
- 1.2 Free vibration of single DoF systems 5
- 1.3 Forced vibration of single DoF systems 7
- 1.4 Harmonic forced vibration – frequency response functions 7
- 1.5 Transient/random forced vibration – time domain solution 10
- 1.6 Transient forced vibration – frequency domain solution 14
- 1.7 Random forced vibration – frequency domain solution 16
- 1.8 Examples 17

2 Vibration of Multiple Degree of Freedom Systems **19**
- 2.1 Setting up equations of motion 19
- 2.2 Undamped free vibration 21
- 2.3 Damped free vibration 24
- 2.4 Transformation to modal coordinates 27
- 2.5 ‘Free–free’ systems 31
- 2.6 Harmonic forced vibration 31
- 2.7 Transient/random forced vibration – time domain solution 33
- 2.8 Transient forced vibration – frequency domain solution 34
- 2.9 Random forced vibration – frequency domain solution 34
- 2.10 Examples 35

3 Vibration of Continuous Systems – Assumed Shapes Approach **37**
- 3.1 Rayleigh–Ritz ‘assumed shapes’ method 38
- 3.2 Generalized equations of motion – basic approach 39
- 3.3 Generalized equations of motion – matrix approach 44
- 3.4 Generating aircraft ‘free–free’ modes from ‘branch’ modes 46
- 3.5 Whole aircraft ‘free–free’ modes 49
- 3.6 Examples 50

4 Vibration of Continuous Systems – Discretization Approach **53**
4.1 Introduction to the finite element (FE) approach 53
4.2 Formulation of the beam bending element 54
4.3 Assembly and solution for a structure with beam elements 58
4.4 Torsion element 63
4.5 Combined bending/torsion element 64
4.6 Comments on modelling 65
4.7 Examples 66

5 Introduction to Steady Aerodynamics **69**
5.1 The standard atmosphere 69
5.2 Effect of air speed on aerodynamic characteristics 71
5.3 Flows and pressures around a symmetric aerofoil 72
5.4 Forces on an aerofoil 74
5.5 Variation of lift for an aerofoil at an angle of incidence 75
5.6 Pitching moment variation and the aerodynamic centre 76
5.7 Lift on a three-dimensional wing 77
5.8 Drag on a three-dimensional wing 81
5.9 Control surfaces 82
5.10 Supersonic aerodynamics – piston theory 83
5.11 Transonic flows 84
5.12 Examples 84

6 Introduction to Loads **87**
6.1 Laws of motion 87
6.2 D'Alembert's principle – inertia forces and couples 90
6.3 Externally applied/reactive loads 93
6.4 Free body diagrams 94
6.5 Internal loads 95
6.6 Internal loads for continuous representation of a structure 96
6.7 Internal loads for discretized representation of a structure 100
6.8 Intercomponent loads 102
6.9 Obtaining stresses from internal loads – structural members with simple load paths 103
6.10 Examples 103

7 Introduction to Control **107**
7.1 Open and closed loop systems 107
7.2 Laplace transforms 108
7.3 Modelling of open and closed loop systems using Laplace and frequency domains 110
7.4 Stability of systems 111
7.5 PID control 118
7.6 Examples 119

Part II Introduction to Aeroelasticity and Loads 121

8 Static Aeroelasticity – Effect of Wing Flexibility on Lift Distribution and Divergence **123**
8.1 Static aeroelastic behaviour of a two-dimensional rigid aerofoil with spring attachment 124
8.2 Static aeroelastic behaviour of a fixed root flexible wing 127

8.3 Effect of trim on static aeroelastic behaviour 129
8.4 Effect of wing sweep on static aeroelastic behaviour 134
8.5 Examples 139

9 Static Aeroelasticity – Effect of Wing Flexibility on Control Effectiveness 141
9.1 Rolling effectiveness of a flexible wing – the steady roll case 141
9.2 Rolling effectiveness of a flexible wing – the fixed wing root case 146
9.3 Effect of spanwise position of the control surface 149
9.4 Full aircraft model – control effectiveness 149
9.5 Effect of trim on reversal speed 151
9.6 Examples 151

10 Introduction to Unsteady Aerodynamics 153
10.1 Quasi-steady aerodynamics 153
10.2 Unsteady aerodynamics 154
10.3 Aerodynamic lift and moment for a harmonically oscillating aerofoil 157
10.4 Oscillatory aerodynamic derivatives 159
10.5 Aerodynamic damping and stiffness 160
10.6 Unsteady aerodynamics related to gusts 161
10.7 Examples 165

11 Dynamic Aeroelasticity – Flutter 167
11.1 Simplified unsteady aerodynamic model 167
11.2 Binary aeroelastic model 168
11.3 General form of the aeroelastic equations 171
11.4 Eigenvalue solution of flutter equations 171
11.5 Aeroelastic behaviour of the binary model 172
11.6 Aeroelastic behaviour of a flexible wing 180
11.7 Aeroelastic behaviour of a multiple mode system 182
11.8 Flutter speed prediction for binary systems 182
11.9 Flutter conic 184
11.10 Divergence of aeroelastic systems 186
11.11 Inclusion of unsteady reduced frequency effects 187
11.12 Control surface flutter 191
11.13 Whole aircraft model – inclusion of rigid body modes 193
11.14 Flutter in the transonic regime 194
11.15 Flutter in the supersonic regime – wing and panel flutter 194
11.16 Effect of nonlinearities – limit cycle oscillations 197
11.17 Examples 198

12 Aeroservoelasticity 201
12.1 Mathematical modelling of a simple aeroelastic system with a control surface 202
12.2 Inclusion of gust terms 203
12.3 Implementation of a control system 204
12.4 Determination of closed loop system stability 204
12.5 Gust response of the closed loop system 205
12.6 Inclusion of control law frequency dependency in stability calculations 206
12.7 Response determination via the frequency domain 208
12.8 State space modelling 208
12.9 Examples 209

13 Equilibrium Manoeuvres **211**
13.1 Equilibrium manoeuvre – rigid aircraft under normal acceleration 213
13.2 Manoeuvre envelope 217
13.3 Equilibrium manoeuvre – rigid aircraft pitching 218
13.4 Equilibrium manoeuvre – flexible aircraft pitching 225
13.5 Flexible corrections to rigid aircraft pitching derivatives 238
13.6 Equilibrium manoeuvres – aircraft rolling and yawing 239
13.7 Representation of the flight control system (FCS) 243
13.8 Examples 243

14 Flight Mechanics Model for Dynamic Manoeuvres **245**
14.1 Aircraft axes 246
14.2 Motion variables 247
14.3 Axes transformations 248
14.4 Velocity and acceleration components for moving axes 250
14.5 Flight mechanics equations of motion for a rigid aircraft 252
14.6 Representation of disturbing forces and moments 255
14.7 Equations for flexible aircraft in longitudinal motion 257
14.8 Solution of flight mechanics equations 262
14.9 Flight control system (FCS) 263

15 Dynamic Manoeuvres **265**
15.1 Dynamic manoeuvre – rigid aircraft heave/pitch due to elevator input 266
15.2 Dynamic manoeuvre – flexible aircraft heave/pitch due to elevator input 271
15.3 General form of longitudinal equations 278
15.4 Dynamic manoeuvre – rigid aircraft roll due to aileron input 279
15.5 Dynamic manoeuvre – flexible aircraft roll due to aileron input 283
15.6 Flexible corrections to flight mechanics equations 290
15.7 Representation of the flight control system (FCS) 290
15.8 Examples 290

16 Gust and Turbulence Encounters **293**
16.1 Gusts and turbulence 294
16.2 Gust response in the time domain 295
16.3 Time domain gust response – rigid aircraft in heave 297
16.4 Time domain gust response – rigid aircraft in heave/pitch 303
16.5 Time domain gust response – flexible aircraft 306
16.6 General form of equations in the time domain 312
16.7 Turbulence response in the frequency domain 314
16.8 Frequency domain turbulence response – rigid aircraft in heave 317
16.9 Frequency domain turbulence response – rigid aircraft in heave/pitch 320
16.10 Frequency domain turbulence response – flexible aircraft 323
16.11 General form of equations in the frequency domain 325
16.12 Representation of the flight control system (FCS) 326
16.13 Examples 326

17 Ground Manoeuvres **329**
17.1 Landing gear 329
17.2 Taxi, take-off and landing roll 333

17.3 Landing 340
17.4 Braking 345
17.5 ‘Spin-up’ and ‘spring-back’ condition 348
17.6 Turning 350
17.7 Shimmy 350
17.8 Representation of the flight control system (FCS) 353
17.9 Examples 353

18 Aircraft Internal Loads 355
18.1 Limit and ultimate loads 356
18.2 Internal loads for an aircraft 356
18.3 General internal loads expressions – continuous wing 358
18.4 Effect of wing-mounted engines/landing gear 360
18.5 Internal loads – continuous flexible wing 361
18.6 General internal loads expressions – discretized wing 366
18.7 Internal loads – discretized fuselage 370
18.8 Internal loads – continuous turbulence encounter 373
18.9 Loads generation and sorting to yield critical cases 374
18.10 Aircraft dimensioning cases 376
18.11 Stresses from internal loads – complex load paths 377
18.12 Examples 377

19 Potential Flow Aerodynamics 381
19.1 Elements of inviscid, incompressible flow analysis 381
19.2 Inclusion of vorticity 386
19.3 Numerical steady aerodynamic modelling of thin two-dimensional aerofoils 388
19.4 Steady aerodynamic modelling of three-dimensional wings using a panel method 391
19.5 Unsteady aerodynamic modelling of wings undergoing harmonic motion 394
19.6 AICs in modal space 397
19.7 Examples 400

20 Coupling of Structural and Aerodynamic Computational Models 401
20.1 Mathematical modelling – static aeroelastic case 401
20.2 Two-dimensional coupled static aeroelastic model – pitch 403
20.3 Two-dimensional coupled static aeroelastic model – heave/pitch 404
20.4 Three-dimensional coupled static aeroelastic model 405
20.5 Mathematical modelling – dynamic aeroelastic response 409
20.6 Two-dimensional coupled dynamic aeroelastic model – bending and torsion 410
20.7 Three-dimensional flutter analysis 411
20.8 Inclusion of frequency-dependent aerodynamics for state space modelling – rational fraction approximation 412

Part III Introduction to Industrial Practice 417

21 Aircraft Design and Certification 419
21.1 Aeroelastics and loads in the aircraft design process 419
21.2 Aircraft certification process 421

22 Aeroelasticity and Loads Models **427**
22.1 Structural model 427
22.2 Aerodynamic model 432
22.3 Flight control system 435
22.4 Other model issues 435
22.5 Loads transformations 436

23 Static Aeroelasticity and Flutter **437**
23.1 Static aeroelasticity 437
23.2 Flutter 439

24 Flight Manoeuvre and Gust/Turbulence Loads **443**
24.1 Evaluation of internal loads 443
24.2 Equilibrium/balanced flight manoeuvres 443
24.3 Dynamic flight manoeuvres 446
24.4 Gusts and turbulence 449

25 Ground Manoeuvre Loads **455**
25.1 Aircraft/landing gear models for ground manoeuvres 455
25.2 Landing gear/airframe interface 456
25.3 Ground manoeuvres – landing 456
25.4 Ground manoeuvres – ground handling 457
25.5 Loads processing 458

26 Testing Relevant to Aeroelasticity and Loads **461**
26.1 Introduction 461
26.2 Wind tunnel tests 461
26.3 Ground vibration test 462
26.4 Structural coupling test 463
26.5 Flight simulator test 464
26.6 Structural tests 464
26.7 Flight flutter test 465
26.8 Flight loads validation 466

Appendices 467

A Aircraft Rigid Body Modes **469**
A.1 Rigid body translation modes 469
A.2 Rigid body rotation modes 469

B Table of Longitudinal Aerodynamic Derivatives **471**

C Aircraft Symmetric Flexible Modes **473**
C.1 Aircraft model 473
C.2 Symmetric free–free flexible mode 474

D Model Condensation **481**
D.1 Introduction 481
D.2 Static condensation 481
D.3 Dynamic condensation – Guyan reduction 482

D.4 Static condensation for aeroelastic models 483
D.5 Modal condensation 483
D.6 Modal reduction 484

E Aerodynamic Derivatives in Body Fixed Axes 485
E.1 Longitudinal derivative Z_{w} 485
E.2 Lateral derivatives L_p, L_ξ 486

F Aircraft Antisymmetric Flexible Modes 489
F.1 Aircraft model 489
F.2 Antisymmetric free–free flexible modes 489

References 491

Index 495

Programs Accessible (on the Companion Website) via the Internet

G MATLAB/SIMULINK Programs for Vibration
G.1 Forced response of an SDoF system
G.2 Modal solution for an MDoF system
G.3 Finite element solution

H MATLAB/SIMULINK Programs for Flutter
H.1 Dynamic aeroelastic calculations
H.2 Aeroservoelastic system

I MATLAB/SIMULINK Programs for Flight/Ground Manoeuvres and Gust/Turbulence Encounters
I.1 Rigid aircraft data
I.2 Flexible aircraft data
I.3 Flight case data
I.4 Aerodynamic derivative calculation
I.5 Equilibrium manoeuvres
I.6 Dynamic manoeuvres
I.7 Gust response in the time domain
I.8 Gust response in the frequency domain
I.9 Ground manoeuvres

Preface

Aeroelasticity is the study of the interaction of aerodynamic, elastic and inertia forces. For fixed wing aircraft there are two key areas: (a) static aeroelasticity, where the deformation of the aircraft influences the lift distribution, can lead to the statically unstable condition of divergence and will normally reduce the control surface effectiveness, and (b) dynamic aeroelasticity, which includes the critical area of flutter, where the aircraft can become dynamically unstable in a condition where the structure extracts energy from the air stream.

Aircraft are also subject to a range of static and dynamic loads resulting from flight manoeuvres (equilibrium/steady and dynamic), ground manoeuvres and gust/turbulence encounters. These load cases are responsible for the critical design loads over the aircraft structure and hence influence the structural design. Determination of such loads involves consideration of aerodynamic, elastic and inertia effects and requires the solution of the dynamic responses; consequently there is a strong link between aeroelasticity and loads.

The aircraft vibration characteristics and response are a result of the flexible modes combining with the rigid body dynamics, with the inclusion of the flight control system (FCS) if it is present. In this latter case, the aircraft will be a closed loop system and the FCS affects both the aeroelasticity and loads behaviour. The interaction between the FCS and the aeroelastic system is often called aeroservoelasticity.

This book aims to embrace the range of basic aeroelastic and loads topics that might be encountered in an aircraft design office and to provide an understanding of the main principles involved. Colleagues in industry have often remarked that it is not appropriate to give some of the classical books on aeroelasticity to new graduate engineers as many of the books are too theoretical for a novice aeroelastician. Indeed, the authors have found much of the material in them to be too advanced to be used in the Undergraduate level courses that they have taught. Also, the topics of aeroelasticity and loads have tended to be treated separately in textbooks, whereas in industry the fields have become much more integrated. This book is seen as providing some grounding in the basic analysis techniques required which, having been mastered, can then be supplemented via more advanced texts, technical papers and industry reports.

Some of the material covered in this book developed from Undergraduate courses given at Queen Mary College, University of London and at the University of Manchester. In the UK, many entrants into the aerospace industry do not have an aerospace background, and almost certainly will have little knowledge of aeroelasticity or loads. To begin to meet this need, during the early 1990s the authors presented several short courses on Aeroelasticity and Structural Dynamics to young engineers in the British aerospace industry, and this has influenced the content and approach of this book. A further major influence was the work by Hancock, Simpson and Wright (1985) on the teaching of flutter, making use of a simplified flapping and pitching wing model with strip theory aerodynamics (including a simplified unsteady aerodynamics model) to illustrate the fundamental principles of flutter. This philosophy has been employed here for the treatment of static aeroelasticity and flutter, and has been extended into the area of loads by focusing on a simplified flexible whole aircraft model in order to highlight key features of modelling and analysis.

The intention of the book is to provide the reader with the technical background to understand the underlying concepts and application of aircraft aeroelasticity and loads. As far as possible, simplified mathematical models for the flexible aircraft are used to illustrate the phenomena and also to demonstrate the link between these models, industrial practice and the certification process. Thus, fairly simple continuum models based upon a small number of assumed modes (so avoiding partial differential equations) have been used. Consequently, much of the book is based upon strip theory aerodynamics and the Rayleigh–Ritz assumed modes method. By using this approach, it has been possible to illustrate most concepts using a maximum of 3 degrees of freedom. Following on from these continuum models, basic discretized structural and aerodynamic models are introduced in order to demonstrate some underlying approaches in current industrial practice. The book aims to be suitable for final year Undergraduate or Masters level students, or engineers in industry who are new to the subject. For example, it could provide the basis of two taught modules in aeroelasticity and loads. It is hoped that the book will fill a gap in providing a broad and relatively basic introductory treatment of aeroelastics and loads.

A significant number of different topics are covered in order to achieve the goals of this book, namely structural dynamics, steady and unsteady aerodynamics, loads, control, static aeroelastic effects, flutter, flight manoeuvres (both steady/equilibrium and dynamic), ground manoeuvres (e.g. landing, taxiing), gust and turbulence encounters, calculation of loads and, finally, finite element and three-dimensional panel methods. In addition, a relatively brief explanation is given as to how these topics might typically be approached in industry when seeking to meet the certification requirements. Most of the focus is on commercial and not military aircraft, though of course all of the underlying principles, and much of the implementation, are common between the two.

The notation employed has not been straightforward to define, as many of these disciplines have tended to use the same symbols for different variables and so inevitably this exercise has been a compromise. A further complication is the tendency for aeroelasticity textbooks from the US to use the reduced frequency k for unsteady aerodynamics, as opposed to the frequency parameter ν that is often used elsewhere. The reduced frequency has been used throughout this textbook to correspond with the classical textbooks of aeroelasticity.

The book is split into three parts. After a brief introduction to aeroelasticity and loads, Part A provides some essential background material on the fundamentals of single and multiple degree of freedom (DoF) vibrations for discrete parameter systems and continuous systems (Rayleigh–Ritz and finite element), steady aerodynamics, loads and control. The presentation is not very detailed, assuming that a reader having a degree in engineering will have some background in most of these topics and can reference more comprehensive material if desired.

Part B is the main part of the book, covering the basic principles and concepts required to provide a bridge to begin to understand current industry practice. The chapters on aeroelasticity include static aeroelasticity (lift distribution, divergence and control effectiveness), unsteady aerodynamics, dynamic aeroelasticity (i.e. flutter) and aeroservoelasticity; the treatment is based mostly on a simple two DoF flapping/pitching wing model, sometimes attached to a rigid fuselage free to heave and pitch. The chapters on loads include equilibrium and dynamic flight manoeuvres, gusts and turbulence encounters, ground manoeuvres and internal loads. The loads analyses are largely based on a three DoF whole aircraft model with heave and pitch rigid body motions and a free–free flexible mode whose characteristics may be varied, so allowing fuselage bending, wing bending or wing torsional deformation to be dominant. Part B concludes with an introduction to three-dimensional aerodynamic panel methods and simple coupled discrete aerodynamic and structural models in order to move on from the Rayleigh–Ritz assumed modes and strip theory approaches to more advanced methods, which provide the basis for much of the current industrial practice.

The basic theory introduced in Parts I and II provides a suitable background to begin to understand Part III, which provides an outline of industrial practice that might typically be involved in aircraft design and certification, including aeroelastic modelling, static aeroelasticity and flutter, flight manoeuvre and gust/turbulence loads, ground manoeuvre loads and finally testing relevant to aeroelastics and loads. A number of MATLAB/SIMULINK programs are available on a companion website for this book at http://www.wiley/go/wright&cooper.

The authors are grateful to the input from a number of colleagues in the UK University sector (John Ackroyd, Philip Bonello, Grigorios Dimitriadis, Zhengtao Ding, Dominic Diston, Barry Lennox and Gareth Vio). The authors greatly valued the input on industrial practice from Mark Hockenhull, Tom Siddall, Peter Denner, Paul Bruss, Duncan Pattrick, Mark Holden and Norman Wood. The authors also appreciated useful discussions with visiting industrial lecturers to the University of Manchester (namely Rob Chapman, Brian Caldwell, Saman Samarasekera, Chris Fielding and Brian Oldfield). Some of the figures and calculations were provided by Colin Leung, Graham Kell and Gareth Vio. Illustrations were provided with kind agreement of Airbus, Messier-Dowty, DLR, DGA/CEAT, ONERA, Royal Aeronautical Society and ESDU. Use of software was provided by MATLAB.

The authors would also like to acknowledge the encouragement they have received over the years in relation to research and teaching activities in the areas of structural dynamics, aircraft structures, loads and aeroelasticity, namely Alan Simpson (University of Bristol), Mike Turner (deceased) (British Aircraft Corporation), Geoff Hancock and David Sharpe (Queen Mary College), Colin Skingle, Ian Kaynes and Malcolm Nash (RAE Farnborough, now QinetiQ), Jer-Nan Juang (NASA Langley), Peter Laws (University of Manchester), Geof Tomlinson (University of Sheffield, formerly at Manchester), Otto Sensburg (MBB) and Hans Schwieger (EADS).

Jan Wright and Jonathan Cooper
Manchester, UK

Series Preface

This book addresses the science of aeroelastics as it applies to aircraft and air vehicle design and as such is just one of a wide ranging variety of topics that contribute to the over-arching subject of aerospace systems and their integrated solutions.

Over the past fifty years or so, a wealth of knowledge associated with aerospace systems has been gleaned by many aerospace engineering specialists who have witnessed a unique transition of available technologies including the invention of the transistor and its extension to the remarkable levels of solid state electronics and software integration that we now take for granted. Many of these specialists who have lived through these technology revolutions from mechanical, structural, electronic and aerodynamic backgrounds are retiring from full time positions. It is important that the expertise established by this community of gurus be captured and documented to support the up-coming generation of aerospace engineers that consider a career in aerospace engineering to be both exciting and fulfilling.

The *Aerospace Series* by John Wiley & Sons provides a practical and topical series of books authored by established experts in industry and academia that provide a unique insight into the issues facing the engineering communities associated with the design development and certification of modern air vehicles. The range of topics available from this *Series* is intended to provide a valuable background of knowledge to industry professionals, operators, and professional institutions. The *Series* is also intended to be an important source of aircraft systems knowledge and know-how to aspiring aerospace engineers at both under-graduate and graduate levels.

Ian Moir, Allan Seabridge, and Roy Langton

Introduction

Aeroelasticity is the subject that describes the interaction of aerodynamic, inertia and elastic forces for a flexible structure and the phenomena that can result. This field of study is summarized most clearly by the classical Collar aeroelastic triangle (Collar, 1978), seen in Figure 1, which shows how the major disciplines of stability and control, structural dynamics and static aeroelasticity each result from the interaction of two of the three types of force. However, all three forces are required to interact in order for dynamic aeroelastic effects to occur.

Aeroelastic effects have had a major influence upon the design and flight performance of aircraft, even before the first controlled powered flight of the Wright Brothers. Since some aeroelastic phenomena (e.g. flutter and divergence) can lead potentially to structural failure, aircraft structural designs have had to be made heavier (the so-called aeroelastic penalty) in order to ensure that structural integrity has been maintained through suitable changes in the structural stiffness and mass distributions. The first recorded flutter problem to be modelled and solved (Bairstow and Fage, 1916; Lanchester, 1916) was the Handley–Page 0/400 bomber in 1916, shown on the front cover of this book. Excellent histories about the development of aeroelasticity and its influence on aircraft design can be found in Collar (1978), Garrick and Reid (1981) and Flomenhoft (1997), with surveys of more recent applications given in Friedmann (1999) and Livne (2003).

Of course, aeroelasticity is not solely concerned with aircraft, and the topic is extremely relevant for the design of structures such as bridges, Formula 1 racing cars, wind turbines, turbomachinery blades,

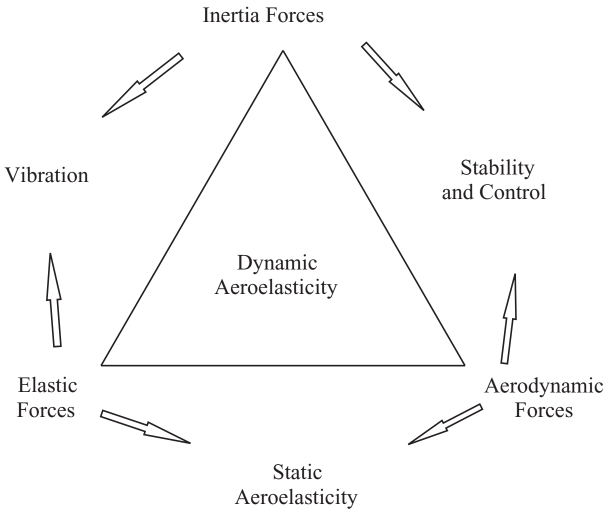

Figure 1 Collar's aeroelastic triangle.

helicopters, etc. However, in this book only fixed wing aircraft will be considered, with the emphasis being on large commercial aircraft, but the underlying principles have relevance to other applications.

It is usual to classify aeroelastic phenomena as being either static or dynamic. *Static aeroelasticity* considers the nonoscillatory effects of aerodynamic forces acting on the flexible aircraft structure. The flexible nature of the wing will influence the in-flight wing shape and hence the lift distribution in a steady (or so-called equilibrium) manoeuvre (see below) or in the special case of cruise. Thus, however accurate and sophisticated any aerodynamic calculations that are carried out, the final in-flight shape could be in error if the structure is modelled inaccurately; drag penalties could result and the aircraft range could reduce. Usually static aeroelastic effects can also lead to a reduction in the effectiveness of the control surfaces and eventually to the phenomenon of control reversal; here, for example, the aileron has the opposite effect to that intended because the rolling moment it generates is negated by the wing twist that accompanies the control rotation. There is also the potentially disastrous phenomenon of divergence to consider, where the wing twist can increase without limit when the aerodynamic pitching moment on the wing due to twist exceeds the structural restoring moment. It is important to recognize that the lift distribution and divergence are influenced by the trim of the aircraft, so strictly speaking the wing cannot be treated on its own.

Dynamic aeroelasticity is concerned with the oscillatory effects of the aeroelastic interactions, and the main area of interest is the potentially catastrophic phenomenon of flutter. This instability involves two or more modes of vibration and arises from the unfavourable coupling of aerodynamic, inertial and elastic forces; it means that the structure can effectively extract energy from the air stream. The most difficult issue when seeking to predict the flutter phenomenon is that of the unsteady nature of the aerodynamic forces and moments generated when the aircraft oscillates, and the effect the motion has on the resulting forces, particularly in the transonic regime. The presence of flexible modes influences the dynamic stability modes of the rigid aircraft and so affects the flight dynamics. Also of serious concern is the potential unfavourable interaction of the flight control system (Pratt, 2000) with the flexible aircraft, considered in the topic of *aeroservoelasticity* (also known as structural coupling).

There are a number of textbooks on aeroelasticity, e.g. Broadbent (1954) Scanlan and Rosenbaum (1960), Fung (1969), Bisplinghoff *et al*. (1996), Hodges and Pierce (2002) and Dowell *et al*. (2004). These offer a comprehensive and insightful mathematical treatment of more fundamental aspects of the subject. However, the approach in most of these books is on the whole somewhat theoretical and often tends to restrict coverage to static aeroelasticity and flutter, considering cantilever wings with fairly sophisticated analytical treatments of unsteady aerodynamics. All, except Hodges and Pierce (2002) and Dowell *et al*. (2004), were written in the 1950s and 1960s. The textbook by Forsching (1974) must also be mentioned as a valuable reference but there is no English translation from the German original. There is some material relevant to static aeroelasticity in the ESDU Data Sheets. A further useful source of reference is the AGARD *Manual on Aeroelasticity* 1950–1970, but again this was written nearly 50 years ago. Further back in history are the key references on aeroelasticity by Frazer and Duncan (1928) and Theodorsen (1935).

Aeroelastic considerations influence the aircraft design process in a number of ways. Within the design flight envelope, it must be ensured that flutter and divergence cannot occur and that the aircraft is sufficiently controllable. The in-flight wing shape influences drag and performance and so must be accurately determined requiring careful consideration of the jig shape used in manufacture. The aircraft handling is affected by the aeroelastic deformations, especially where the flexible modes are close in frequency to the rigid body modes.

Collar's aeroelastic triangle may be modified to cater for loads (mainly dynamic) to generate a loads triangle, as shown in Figure 2. Equilibrium (or steady/trimmed/balanced) manoeuvres involve the interaction of elastic and aerodynamic effects (cf. static aeroelasticity), dynamic manoeuvres involve the interaction of aerodynamic and inertia effects (cf. stability and control, but for a flexible aircraft, elastic effects may also be important), ground manoeuvres primarily involve the interaction of inertia and elastic effects (cf. structural dynamics) and gust/turbulence encounters involve the interaction of inertia, aerodynamic and elastic effects (cf. flutter).

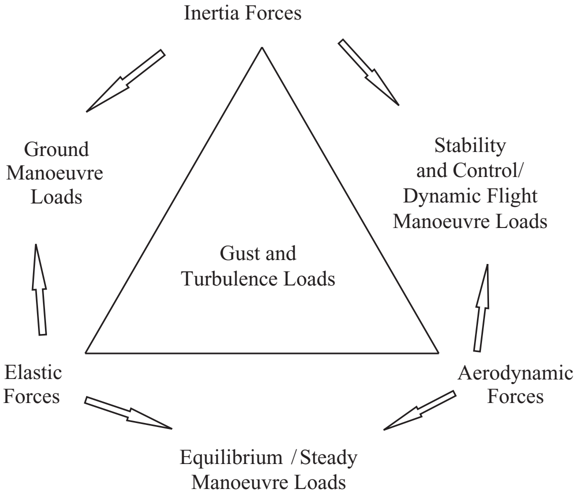
Inertia Forces
Ground Manoeuvre Loads
Stability and Control/ Dynamic Flight Manoeuvre Loads
Gust and Turbulence Loads
Elastic Forces
Aerodynamic Forces
Equilibrium / Steady Manoeuvre Loads

Figure 2 Loads triangle.

Equilibrium manoeuvres concern the aircraft undergoing steady longitudinal or lateral manoeuvres, e.g. a steady pull-out from a dive involving acceleration normal to the flight path and a steady pitch rate. *Dynamic manoeuvres* involve the aircraft responding dynamically to transient control inputs from the pilot or else to failure conditions. *Ground manoeuvres* cover a number of different steady and dynamic load conditions (landing, taxiing, braking, turning) where the aircraft is in contact with the ground via the landing gear. Finally, *gust/turbulence encounters* involve the aircraft responding to discrete gusts (represented in the time domain) or continuous turbulence (represented in the frequency domain).

The different load cases required for certification under these four main headings may be considered in one of two categories: *bookcase* refers to a load case where in essence a relatively artificial state of the aircraft, in which applied and inertia loads are in equilibrium, is considered whereas *rational* refers to a condition in which the aircraft dynamic behaviour is modelled and simulated as realistically as possible. Bookcase load cases apply primarily to equilibrium manoeuvres and to some ground manoeuvres, whereas rational load cases apply to most dynamic and ground manoeuvres as well as to gust/turbulence encounters. These load cases in the certification process provide *limit loads*, which are the maximum loads to be expected in service and which the structure needs to support without 'detrimental permanent deformation'; the structure must also be able to support *ultimate* loads (limit loads × factor of safety of 1.5) without failure/rupture.

The resulting distributions of bending moment, axial force, shear force and torque along each component (referred to in this book as 'internal loads'), due to the distribution of aerodynamic and inertial forces acting on the aircraft, need to be determined as a function of time for each type of loading across the entire design envelope. The critical internal loads for design of different parts of the aircraft structure are then found via a careful process of sorting the multitude of results obtained; the load paths and stresses within the structure may then be obtained by a subsequent analysis process for the critical load cases in order to allow an assessment of the strength and fatigue life/damage tolerance of the aircraft. The aircraft response in taxiing and particularly in gust and turbulence encounters will influence crew and passenger comfort. The flight control system (FCS) is a critical component for aircraft control that has to be designed so as to provide the required stability and carefree handling qualities, and to avoid unfavourable couplings with the structure; it will in turn influence the loads generated and must be represented in the loads calculations. Manoeuvre load alleviation and gust load alleviation systems are often fitted to the aircraft to reduce loads and improve ride comfort.

There are a number of textbooks on classical aircraft structural analysis, but in the area of loads there are far fewer relevant textbooks. The AIAA Education Series book on structural loads analysis (Lomax, 1996) is extremely useful and deals with aircraft loads in an applied manner, using relatively simplified aircraft models that may be used to check results from more sophisticated approaches used when seeking to meet certification requirements; it also aims to present somewhat of a historical perspective. The book on aircraft loading and structural layout (Howe, 2004) covers approximate loading action analysis for the rigid aircraft, together with use of results provided in initial load estimates and hence layout and sizing of major structural members in aircraft conceptual design. The AIAA Education Series book on gusts and turbulence (Hoblit, 1988) provides a comprehensive introductory treatment of loads due to gusts and particularly due to continuous turbulence. Some of the classical books on aeroelasticity also include an introductory treatment of gust response (Scanlan and Rosenbaum, 1960; Fung, 1969; Bisplinghoff *et al*., 1996) and so partially bridge the aeroelasticity/loads fields. The ESDU Data Sheets provide some coverage of loads in steady manoeuvres, linked to static aeroelastic effects, and also an introductory item on gusts and turbulence. The AIAA Education Series book on landing gear design (Currey, 1988) provides a very practical treatment of design issues but is not aimed at addressing the associated mathematical modelling required for estimation of loads in ground manoeuvres. Niu (1988) provides a useful chapter on aircraft loads but the main focus is on practicalities of airframe structural design. Donaldson (1993) and Megson (1999) are primarily aimed at covering a wide range of aircraft structural analysis methods, but also provide introductory chapters on loads and aeroelasticity.

Historically, loads and aeroelasticity have often been treated separately in industry, whereas in recent years they have been considered in a much more integrated manner; indeed now they are often covered by a single department. This is because the model for a flexible aircraft has traditionally been developed for flutter calculations and the aircraft static and dynamic aeroelastic effects have gradually become more important to include in the flight/ground manoeuvre and gust/turbulence load calculations. Also, as the rigid body and flexible mode frequencies have grown closer together, the rigid body and FCS effects have had to be included in the flutter solution. The flight mechanics model used for dynamic manoeuvres would be developed in conjunction with the departments that consider stability and control/handling/FCS issues since the presence of flexible modes would affect the aircraft dynamic stability and handling. There also needs to be close liaison with the aerodynamics and structures departments when formulating mathematical models. The models used in loads and aeroelastic calculations are becoming ever more advanced. The model of the structure has progressed from a ‘beam-like’ model based on the finite element (FE) method to a much more representative ‘box-like’ FE model. The aerodynamic model has progressed from one based on two-dimensional strip theory to three-dimensional panel methods and, in an increasing number of cases, computational fluid dynamics (CFD).

The airworthiness certification process requires that all possible aeroelastic phenomena and carefully defined range of load cases should be considered in order to ensure that any potentially disastrous scenario cannot occur or that no critical load value is exceeded. The analysis process must be supported by a ground and flight test programme to validate the aerodynamic, structural, aeroelastic and aeroservoelastic models. The certification requirements for large aircraft in Europe and the United States are CS-25 and FAR-25 respectively. The requirements from Europe and the United States are very similar and use essentially the same numbering system; here, for convenience, reference is made mostly to the European version of the requirements.

In recent years there has also been an increasing interest in the effect of aerodynamic and structural nonlinearities and the effect they have on the aeroelastic behaviour. Of particular interest are phenomena such as limit cycle oscillations (LCO) and also the transonic aeroelastic stability boundaries. In addition the FCS has nonlinear components. More advanced mathematical models are required to predict and characterize the nonlinear phenomena, which cannot be predicted using linear representations. However, in this book nonlinear effects will only be mentioned briefly.

This book is organized into three parts. Part I provides some essential background material on the fundamentals of single and multiple degree of freedom vibrations for discrete parameter systems and continuous systems (namely the Rayleigh-Ritz and finite element methods), steady aerodynamics, loads and control. The presentation is relatively brief, on the assumption that a reader can reference more comprehensive material if desired.

Chapter 1 introduces the vibration of single degree of freedom discrete parameter systems, including setting up equations of motion using Lagrange's equations, and in particular the response to various types of forced vibrations. Chapter 2 presents the equivalent theory for multiple degree of freedom systems with reference to modes of vibration and modelling in modal space, as well as free and forced vibration. Chapter 3 employs the Rayleigh–Ritz assumed shapes approach for continuous systems, primarily slender structures in bending and torsion, but also considering use of branch modes and whole aircraft 'free–free' modes. Chapter 4 describes the most common discretization approach for vibration of continuous structures, namely the finite element method.

Chapter 5 introduces a number of basic steady aerodynamics concepts that will be used to determine the flows, lift forces and moments acting on simple two-dimensional aerofoils and three-dimensional wings, including two-dimensional strip theory. Chapter 6 describes simple dynamic solutions for a particle or body using Newton's laws of motion or D'Alembert's principle and introduces the use of inertia loads to generate an equivalent static problem, leading to internal loads for slender members experiencing nonuniform acceleration. Chapter 7 introduces some basic concepts of control for open and closed loop feedback systems.

Part II is the main part of the book, covering the basic principles and concepts required to provide a link to begin to understand current industry practice. A Rayleigh–Ritz approach for flexible modes is used to simplify the analysis and to allow the equations to be almost entirely limited to three degrees of freedom to aid understanding. A strip theory representation of the aerodynamics is employed to simplify the mathematics, but it is recognized that three-dimensional panel methods are more commonly used in practice. The static and dynamic aeroelastic content makes use of wing models, sometimes attached to a rigid fuselage. The loads chapters combine a rigid body heave/pitch model with a whole aircraft free–free flexible mode (designed to permit fuselage bending, wing bending or wing torsional motions as dominant), and consider a range of flight/ground manoeuvre and gust/turbulence cases.

Chapter 8 considers the effect of static aeroelasticity on the aerodynamic load distribution, resulting deflections and potential divergence for a flexible wing, together with the influence of wing sweep and aircraft trim. Chapter 9 examines the impact of wing flexibility on aileron effectiveness. Chapter 10 introduces the concept of quasi-steady and unsteady aerodynamics and the effect that the relative motion between an aerofoil and the flow has on the lift and moment produced. Chapter 11 explores the critical area of flutter and also how aeroelastic calculations are performed where frequency-dependent aerodynamics is involved. Chapter 12 introduces aeroservoelasticity and illustrates the implementation of a simple feedback control on an aeroelastic system.

Chapter 13 considers the behaviour of rigid and flexible aircraft undergoing symmetric equilibrium manoeuvres and a rigid aircraft experiencing simple lateral manoeuvres. Chapter 14 introduces the two-dimensional flight mechanics model with body fixed axes and extends it to include a flexible mode. Chapter 15 shows how the flight mechanics model may be used to examine dynamic manoeuvres in heave/pitch and pure roll, and how the flexibility of the aircraft can affect the response, dynamic stability modes and control effectiveness. Chapter 16 considers discrete gust and continuous turbulence analysis approaches in the time and frequency domains respectively. Chapter 17 presents a simple model for the nonlinear landing gear and considers taxiing, landing, braking, wheel 'spin-up'/'spring-back', turning and shimmy. Chapter 18 introduces the evaluation of internal loads from the aircraft dynamic response and any control/gust input, applied to continuous and discretized components, and also loads sorting. Chapter 19 describes potential flow aerodynamic approaches and how they lead to determination of aerodynamic influence coefficients (AICs) for three-dimensional panel methods in both steady and unsteady flows. Chapter 20 considers the development of simple coupled two- and three-dimensional structural/aerodynamic models in steady and unsteady flows.

Finally, Part III provides an outline of industrial practice that might typically be involved in aircraft design and certification. It references the earlier two parts of the book and indicates how the processes illustrated on simple mathematical models might be applied in practice to 'real' aircraft.

Chapter 21 introduces the design and certification process as far as aeroelasticity/loads are concerned. Chapter 22 explains how the mathematical models used for aeroelasticity and loads analyses can typically be constructed. Chapter 23 considers the calculations undertaken to meet the requirements for static aeroelasticity and flutter. Chapter 24 presents the calculation process involved for determination of loads in meeting the requirements for equilibrium and dynamic flight manoeuvres and gust/continuous turbulence encounters. Chapter 25 introduces the analyses required for determining the ground manoeuvre loads and loads post-processing, and finally Chapter 26 describes briefly the range of ground and flight tests performed to validate mathematical models and demonstrate aeroelastic stability.

Abbreviations

AC	aerodynamic centre
AC	Advisory Circular
AIC	aerodynamic influence coefficient
AMC	Additional Means of Compliance
AR	aspect ratio
CFD	computational fluid dynamics
CoM	centre of mass
COTS	commercial-off-the-shelf
CRI	certification review item
CS	Certification Specifications
DL	doublet lattice
DoF	degree of freedom
EAS	equivalent air speed
EASA	European Aviation Safety Agency
FAA	Federal Aviation Administration
FAR	Federal Aviation Regulation
FBD	free body diagram
FCS	flight control system
FD	frequency domain
FE	finite element
FFT	flight flutter test
FRF	frequency response function
FT	Fourier transform
GVT	ground vibration test
IRF	impulse response function
ISA	International Standard Atmosphere
JAA	Joint Airworthiness Authorities
LCO	limit cycle oscillation
LDHWG	Loads and Dynamics Harmonization Working Group
LE	leading edge
MDoF	multiple degree of freedom
NPA	Notice of Proposed Amendment
PSD	power spectral density
RMS	root-mean-square
SDoF	single degree of freedom
SRF	step response function
TAS	true air speed
TD	time domain
TE	trailing edge
TF	transfer function
WA	wing aerodynamic (axis)
WF	wing flexural (axis)
WM	wing mass (axis)

Part I

Background Material

1

Vibration of Single Degree of Freedom Systems

In this chapter, some of the basic concepts of vibration analysis for single degree of freedom (SDoF) discrete parameter systems will be introduced. The term 'discrete (or sometimes lumped) parameter' implies that the system is a combination of discrete rigid masses (or components) interconnected by flexible/elastic stiffness elements. Later it will be seen that a single DoF representation may be employed to describe the behaviour of a particular characteristic (or mode) shape of the system via what are known as modal coordinates. Multiple degree of freedom (MDoF) discrete parameter systems will be considered in Chapter 2. The alternative approach to modelling multiple DoF systems, as so-called 'continuous' systems, where components of the system are flexible and deform in some manner, is considered later in Chapters 3 and 4.

Much of the material in this introductory part of the book on vibrations is covered in detail in many other texts, such as Tse *et al.* (1978), Newland (1987), Rao (1995), Thomson (1997) and Inman (2006) and it is assumed that the reader has some engineering background so should have met many of the ideas before. Therefore, the treatment here will be as brief as is consistent with the reader being reminded, if necessary, of various concepts used later in the book. Such introductory texts on mechanical vibration should be referenced if more detail is required or if the reader's background understanding is limited.

There are a number of ways of setting up the equations of motion for an SDoF system, e.g. Newton's laws and D'Alembert's principle. However, consistently throughout the book, Lagrange's energy equations will be employed, although in one or two cases other methods are adopted as they offer certain advantages. In this chapter, the determination of the free and forced vibration response of an SDoF system to various forms of excitation relevant to aircraft loads will be considered. The idea is to introduce some of the core dynamic analysis methods (or tools) to be used later in aircraft aeroelasticity and loads calculations.

1.1 SETTING UP EQUATIONS OF MOTION FOR SINGLE DoF SYSTEMS

A single DoF system is one whose motion may be described by a single coordinate, i.e. a displacement or rotation. All systems that may be described by a single degree of freedom may be shown to have an identical form of governing equation, albeit with different symbols employed in each case. Two examples will be considered, a classical mass/spring/damper system and an aircraft control surface able to rotate about its hinge line but restrained by an actuator. These examples will illustrate translational and rotational motions.

Introduction to Aircraft Aeroelasticity and Loads J. R. Wright and J. E. Cooper
© 2007 John Wiley & Sons, Ltd

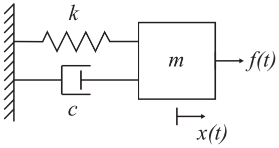

Figure 1.1 SDoF mass/spring/damper system.

1.1.1 Example: Classical Single DoF System

The classical form of an SDoF system is shown in Figure 1.1, and comprises a mass m, a spring of stiffness k and a viscous damper whose coefficient is c; a viscous damper is an idealized energy dissipation device where the force developed is linearly proportional to the relative velocity between its ends (note that the alternative approach of using hysteretic/structural damping will be considered later). The motion of the system is a function of time t and is defined by the displacement $x(t)$. A time-varying force $f(t)$ is applied to the mass.

Lagrange's energy equations are differential equations of the system expressed in what are sometimes termed 'generalized coordinates' but written in terms of energy and work quantities (Wells, 1967; Tse *et al.*, 1978). These equations will be suitable for a specific physical coordinate or a coordinate associated with a shape (see Chapter 3). Now, Lagrange's equation for an SDoF system with a displacement coordinate x may be written as

$$\frac{\mathrm{d}}{\mathrm{d}t}\left(\frac{\partial T}{\partial \dot{x}}\right) - \frac{\partial T}{\partial x} + \frac{\partial \Im}{\partial \dot{x}} + \frac{\partial U}{\partial x} = Q_x = \frac{\partial(\delta W)}{\partial(\delta x)}, \tag{1.1}$$

where T is the kinetic energy, U is the potential (or strain) energy, $\Im$ is the dissipative function, Q_x is the so-called generalized force and W is a work quantity.

For the SDoF example, the kinetic energy is given by

$$T = \frac{1}{2}m\dot{x}^2, \tag{1.2}$$

where the overdot indicates the derivative with respect to time, namely d/dt. The strain energy in the spring is

$$U = \frac{1}{2}kx^2. \tag{1.3}$$

The damper contribution may be treated as an external force, or else may be defined by the dissipative function

$$\Im = \frac{1}{2}c\dot{x}^2. \tag{1.4}$$

Finally, the effect of the force is included in Lagrange's equation by considering the incremental work done δW obtained when the force moves through an incremental displacement δx, namely

$$\delta W = f\,\delta x. \tag{1.5}$$

Substituting Equations (1.2) to (1.5) into Equation (1.1) yields the ordinary second-order differential equation

$$m\ddot{x} + c\dot{x} + kx = f(t). \tag{1.6}$$

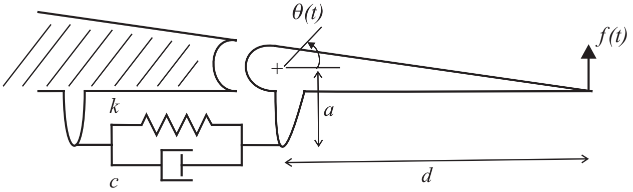

Figure 1.2 Single degree of freedom control surface/actuator system.

1.1.2 Example: Aircraft Control Surface

As an example of a completely different SDoF system that involves a rotational coordinate system, consider the control surface/actuator model shown in Figure 1.2. The control surface has a moment of inertia J about the hinge, the effective actuator stiffness and damping values are k and c respectively and the rotation of the control surface is θ rad. The actuator lever arm has length a. A force $f(t)$ is applied to the control surface at a distance d from the hinge. The main surface of the wing is assumed to be fixed rigidly as shown.

The energy, dissipation and work done functions corresponding to Equations (1.2) to (1.5) may be shown to be

$$T = \frac{1}{2}J\dot{\theta}^2, \qquad U = \frac{1}{2}k(a\theta)^2, \qquad \Im = \frac{1}{2}c(a\dot{\theta})^2, \qquad \delta W = (f\,d)\,\delta\theta, \tag{1.7}$$

where the angle of rotation is assumed to be small, so that, for example, $\sin\theta = \theta$. The work done term is a torque multiplied by a rotation. Then, applying the Lagrange equation with coordinate θ, it may be shown that

$$J\ddot{\theta} + ca^2\dot{\theta} + ka^2\theta = d\,f(t). \tag{1.8}$$

Clearly, this equation is of the same form as that in Equation (1.6). All SDoF systems have equations of a similar form, albeit with different symbols and units.

1.2 FREE VIBRATION OF SINGLE DoF SYSTEMS

In free vibration, an initial condition is imposed and motion then occurs in the absence of any external force. The motion takes the form of a nonoscillatory or oscillatory decay; the latter corresponds to the low values of damping normally encountered in aircraft, so only this case will be considered. The solution method is to assume a form of motion given by

$$x(t) = X\mathrm{e}^{\lambda t}, \tag{1.9}$$

where X is the amplitude and λ is the characteristic exponent defining the decay. Substituting Equation (1.9) into Equation (1.6), setting the applied force to zero and simplifying, yields the quadratic equation

$$\lambda^2 m + \lambda c + k = 0 \tag{1.10}$$

The solution of this ‘characteristic equation’ for the oscillatory motion case produces two complex roots, namely

$$\lambda_{1,2} = -\frac{c}{2m} \pm \mathrm{i}\sqrt{\left(\frac{k}{m}\right) - \left(\frac{c}{2m}\right)^2}, \tag{1.11}$$

where the complex value $\mathrm{i} = \sqrt{-1}$. Equation (1.11) may be rewritten in the nondimensional form

$$\lambda_{1,2} = -\zeta\omega_n \pm \mathrm{i}\omega_\mathrm{n}\sqrt{1-\zeta^2} = -\zeta\omega_\mathrm{n} \pm \mathrm{i}\omega_\mathrm{d}, \tag{1.12}$$

where

$$\omega_\mathrm{n} = \sqrt{\frac{k}{m}}, \qquad \omega_\mathrm{d} = \omega_\mathrm{n}\sqrt{1-\zeta^2}, \qquad \zeta = \frac{c}{2m\omega_\mathrm{n}}. \tag{1.13}$$

Here ω_n is the (undamped) natural frequency (frequency in rad/s of free vibration in the absence of damping), ω_d is the damped natural frequency (frequency of free vibration in the presence of damping) and ζ is the *damping ratio* (i.e. c expressed as a proportion of the critical damping c_crit, the value at which motion becomes nonoscillatory); these parameters are basic and unique properties of the system.

Because there are two roots to Equation (1.10), the solution for the free vibration motion is given by the sum

$$x(t) = X_1\mathrm{e}^{\lambda_1 t} + X_2\mathrm{e}^{\lambda_2 t}. \tag{1.14}$$

After substitution of Equation (1.12) into Equation (1.14), the motion may be expressed in the form

$$x(t) = \mathrm{e}^{-\zeta\omega_\mathrm{n}t}\left[(X_1+X_2)\cos\omega_\mathrm{d}t + \mathrm{i}(X_1-X_2)\sin\omega_\mathrm{d}t\right]. \tag{1.15}$$

Since the displacement must be a real quantity, then X_1, X_2 must be complex conjugate pairs and Equation (1.15) simplifies to one of the classical forms

$$x(t) = \mathrm{e}^{-\zeta\omega_\mathrm{n}t}\left[A_1\sin\omega_\mathrm{d}t + A_2\cos\omega_\mathrm{d}t\right] \qquad \text{or} \qquad x(t) = A\mathrm{e}^{-\zeta\omega_\mathrm{n}t}\sin(\omega_\mathrm{d}t+\psi), \tag{1.16}$$

where the amplitude A and phase ψ (or amplitudes A_1, A_2) are unknown values, to be determined from the initial conditions for displacement and velocity. Thus this 'underdamped' motion is sinusoidal with an exponentially decaying envelope, as shown in Figure 1.3 for a case with general initial conditions.

1.2.1 Example: Aircraft Control Surface

Using Equation (1.8) for the control surface actuator system and comparing the expressions with those for the simple system, the undamped natural frequency and damping ratio may be shown by inspection to be

$$\omega_\mathrm{n} = \sqrt{\frac{ka^2}{J}} \qquad \text{and} \qquad \zeta = \frac{\mathrm{ca}}{2\sqrt{\mathrm{kJ}}}. \tag{1.17}$$

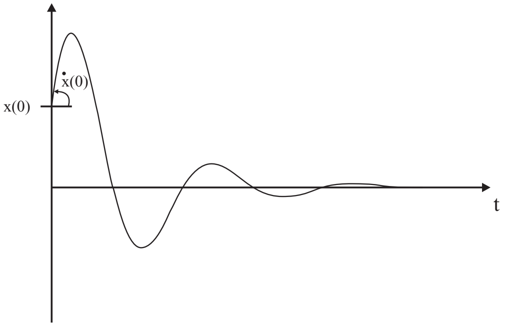

Figure 1.3 Free vibration response for an underdamped single degree of freedom system.

1.3 FORCED VIBRATION OF SINGLE DoF SYSTEMS

In determining aircraft loads for gusts and manoeuvres (see Chapters 13 to 17), the aircraft response to a number of different types of forcing functions needs to be considered. These tend to divide into three categories:

1. *Harmonic excitation* is primarily concerned with excitation at a single frequency (for engine or rotor out-of-balance and as a constituent part of continuous turbulence analysis).
2. *Nonharmonic deterministic excitation* includes the '1-cosine' input (for discrete gusts or runway bumps) and various shaped inputs (for flight manoeuvres); such forcing functions often have clearly defined analytical forms and tend to be of short duration, often called transient.
3. *Random excitation* includes continuous turbulence and runway profiles, the latter required for taxiing. Random excitation can be specified using a time or frequency domain description (see later).

The aircraft dynamics are sometimes nonlinear (e.g. doubling the input does not double the response), which complicates the solution process, but in this chapter only the linear case will be considered. The treatment of nonlinearity will be covered in later chapters, albeit only fairly briefly. In the following sections, the determination of the response to harmonic, transient and random excitation will be considered, using both time and frequency domain approaches. The extension to MDoF systems will be covered later in Chapter 2.

1.4 HARMONIC FORCED VIBRATION – FREQUENCY RESPONSE FUNCTIONS

The most important building block for forced vibration requires determination of the response to a harmonic (i.e. sinusoidal) force with frequency ω rad/s (or $\omega/(2\pi)$ Hz). The relevance to aircraft loads is primarily in helping to lay important foundations for behaviour of dynamic systems, e.g. continuous turbulence analysis. However, the real-life cases of engines or rotors and propellers can introduce harmonic excitation to the aircraft.

1.4.1 Response to Harmonic Excitation

When a harmonic force is applied, there is an initial transient response, followed by a steady-state phase where the response will also be sinusoidal at the same frequency as the excitation but lagging it in phase; only the steady-state response will be considered here, though the transient response may often be important.

The excitation input is defined by

$$f(t) = F \sin \omega t \tag{1.18}$$

and the steady-state response is given by

$$x(t) = X \sin(\omega t - \phi), \tag{1.19}$$

where F, X are the amplitudes and ϕ is the amount by which the response 'lags' the excitation in phase (so-called 'phase lag'). In one approach, the steady-state response may be determined by substituting these expressions into the equation of motion and then equating sine and cosine terms using trigonometric expansion.

However, an alternative approach uses complex algebra and will be adopted since it is more powerful and commonly used. In this approach, the force and response are rewritten in a complex notation as follows:

$$\begin{aligned} f(t) &= F\mathrm{e}^{\mathrm{i}\omega t} = F\cos\omega t + \mathrm{i}F\sin\omega t, \\ x(t) &= X\mathrm{e}^{\mathrm{i}(\omega t-\phi)} = (X\mathrm{e}^{-\mathrm{i}\phi})\mathrm{e}^{\mathrm{i}\omega t} = \tilde{X}\mathrm{e}^{\mathrm{i}\omega t} = \tilde{X}\cos\omega t + \mathrm{i}\tilde{X}\sin\omega t. \end{aligned} \tag{1.20}$$

Here the phase lag is embedded in a new complex amplitude quantity $\tilde{X}$. Only the imaginary part of the excitation and response will be used for sine excitation; an alternative way of viewing this is that the solutions for both the sine and cosine excitation will be found simultaneously. The solution process is straightforward once the concepts have been grasped. The complex expressions in Equations (1.20) are now substituted into Equation (1.6). Noting that $\dot{x} = \mathrm{i}\omega\tilde{X}\mathrm{e}^{\mathrm{i}\omega t}$ and $\ddot{x} = -\omega^2\tilde{X}\mathrm{e}^{\mathrm{i}\omega t}$ and cancelling the exponential term, then

$$(-\omega^2 m + \mathrm{i}\omega c + k)\tilde{X} = F. \tag{1.21}$$

Thus the complex response amplitude may be solved algebraically so that

$$\tilde{X} = X\mathrm{e}^{-\mathrm{i}\phi} = \frac{F}{k-\omega^2 m + \mathrm{i}\omega c} \tag{1.22}$$

and equating real and imaginary parts from the two sides of the equation yields the amplitude and phase as

$$X = \frac{F}{\sqrt{\left(k-\omega^2 m\right)^2 + (\omega c)^2}} \qquad \text{and} \qquad \phi = \tan^{-1}\left(\frac{\omega c}{k-\omega^2 m}\right). \tag{1.23}$$

Hence, the time response may be calculated using X, ϕ from this equation.

1.4.2 Frequency Response Functions (FRFs)

An alternative way of writing Equation (1.22) is

$$H_{\mathrm{D}}(\omega) = \frac{\tilde{X}}{F} = \frac{1}{k-\omega^2 m + \mathrm{i}\omega c} \tag{1.24}$$

or in nondimensional form

$$H_{\mathrm{D}}(\omega) = \frac{1/k}{1-(\omega/\omega_{\mathrm{n}})^2 + \mathrm{i}2\zeta\,(\omega/\omega_{\mathrm{n}})} = \frac{1/k}{1-r^2+\mathrm{i}2\zeta r} \quad \text{where} \quad r = \frac{\omega}{\omega_{\mathrm{n}}}. \tag{1.25}$$

Here $H_{\mathrm{D}}(\omega)$ is known as the displacement (or receptance, (Ewins, 1995)) frequency response function (FRF) of the system and is a system property. It dictates how the system behaves under harmonic excitation at any frequency. The equivalent velocity and acceleration FRFs are given by

$$H_{\mathrm{V}} = \mathrm{i}\omega H_{\mathrm{D}}, \qquad H_{\mathrm{A}} = -\omega^2 H_{\mathrm{D}} \tag{1.26}$$

since multiplication by $\mathrm{i}\omega$ in the frequency domain is equivalent to differentiation in the time domain ($\mathrm{i}^2 = -1$).

The quantity $kH_{\mathrm{D}}(\omega)$ is a nondimensional expression, or dynamic magnification, relating the dynamic amplitude to the static deformation for several damping values. The well-known 'resonance'

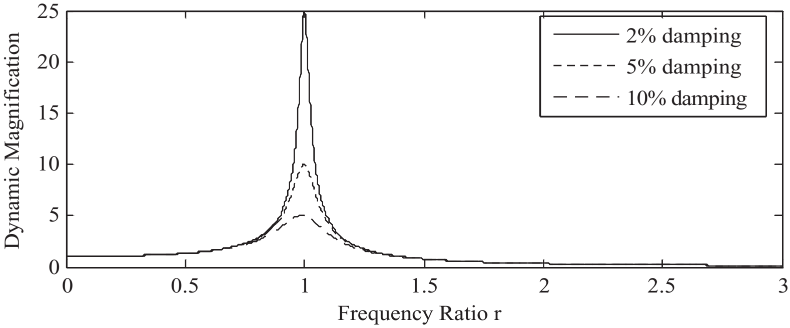

Figure 1.4 Displacement frequency response function for a single degree of freedom system.

phenomenon is shown in Figure 1.4 by the amplitude peak that occurs when the excitation frequency ω is at the 'resonance' frequency, close in value to the undamped natural frequency ω_{n}; the phase changes rapidly in this region, passing through 90° at resonance. Note that the resonant peak increases in amplitude as the damping ratio reduces and that the dynamic magnification (approximately $1/2\zeta$) can be extremely large.

1.4.3 Hysteretic (or Structural) Damping

So far, a viscous damping representation has been employed, based on the assumption that the damping force is proportional to velocity (and therefore to frequency). However, in practice, damping measurements in structures and materials have sometimes shown that damping is independent of frequency but acts in quadrature (i.e. is at 90° phase) to the displacement of the system. Such an internal damping mechanism is known as hysteretic (or sometimes structural) damping (Rao, 1995). It is common practice to combine the damping and stiffness properties of a system having hysteretic damping into a so-called complex stiffness, namely

$$k^* = k(1 + \mathrm{i}g), \tag{1.27}$$

where g is the structural damping coefficient or loss factor (not to be confused with the same symbol used for acceleration due to gravity) and the complex number indicates that the damping force is in quadrature with the stiffness force. The SDoF equation of motion amended to employ hysteretic damping may then be written as

$$m\ddot{x} + k(1 + \mathrm{i}g)x = f(t). \tag{1.28}$$

This is a rather peculiar equation, being expressed in the time domain but including the complex number; it is not possible to solve this equation in this form. However, it is feasible to write the equation in the time domain as

$$m\ddot{x} + c_{\mathrm{eq}}\dot{x} + kx = f(t), \tag{1.29}$$

where $c_{\mathrm{eq}} = gk/\omega$ is the equivalent viscous damping. This equation of motion may be used if the motion is dominantly at a single frequency. The equivalent damping ratio expression may be shown to be

$$\zeta_{\mathrm{eq}} = \frac{g}{2}\left(\frac{\omega_{\mathrm{n}}}{\omega}\right) \tag{1.30}$$

or, if the system is actually vibrating at the natural frequency, then

$$\zeta_{\mathrm{eq}} = \frac{g}{2} \tag{1.31}$$

Thus the equivalent viscous damping ratio is half of the loss factor, and this factor of 2 is often seen when comparing flutter damping plots from the US and Europe (see Chapter 11).

An alternative way of considering hysteretic damping is to convert Equation (1.28) into the frequency domain, using the methodology employed earlier in Section 1.4.1, so yielding the FRF in the form

$$H_{\mathrm{D}}(\omega) = \frac{\tilde{X}}{F} = \frac{1}{k(1 + \mathrm{i}g) - \omega^2 m} \tag{1.32}$$

and now the complex stiffness takes a more suitable form. Thus, a frequency domain solution of a system with hysteretic damping is acceptable, but a time domain solution assumes motion at essentially a single frequency. The viscous damping model, despite its drawbacks, does lend itself to more simple analysis, though both viscous and hysteretic damping models are widely used.

1.5 TRANSIENT/RANDOM FORCED VIBRATION – TIME DOMAIN SOLUTION

When a transient/random excitation is present, the time response may be calculated in one of three ways.

1.5.1 Analytical Approach

If the excitation is deterministic, having a relatively simple mathematical form (e.g. step, ramp), then an analytical method suitable for ordinary differential equations may be used (i.e. combination of complementary function and particular integral). Such an approach is impractical for more general forms of excitation. For example, a *unit step* force applied to the system initially at rest may be shown to give rise to the response (or so-called 'step response function') $s(t)$.

$$s(t) = x_{\mathrm{SRF}}(t) = \frac{1}{k}\left[1 - \frac{\mathrm{e}^{-\zeta\omega_{\mathrm{n}}t}}{\sqrt{1-\zeta^2}}\sin(\omega_{\mathrm{d}}t + \psi)\right] \qquad \text{with} \tan\psi = \frac{\sqrt{1-\zeta^2}}{\zeta}. \tag{1.33}$$

Note that the term in square brackets is the ratio of the dynamic-to-static response and this ratio is shown in Figure 1.5 for different dampings. Note that there is a tendency of the transient response to 'overshoot' the steady-state value, but this initial peak response is hardly affected by damping; this behaviour will be referred to later as 'dynamic overswing' when considering manoeuvres in Chapters 13 and 24.

Another important excitation is the *unit impulse* of force. This may be idealized crudely as a very narrow rectangular force–time pulse of unit area (i.e. strength) of 1 N s (the ideal impulse is the so-called Dirac-δ function, having zero width and infinite height). Because this impulse imparts an instantaneous change in momentum, the velocity changes by an amount equal to the impulse strength/mass), so the case is equivalent to free vibration with a finite initial velocity and zero initial displacement. Thus it may be shown that the response to a unit impulse (or the so-called 'impulse response function') $h(t)$ is

$$h(t) = x_{\mathrm{IRF}}(t) = \frac{1}{m\omega_{\mathrm{d}}}\mathrm{e}^{-\zeta\omega_{\mathrm{n}}t}\sin\omega_{\mathrm{d}}t. \tag{1.34}$$

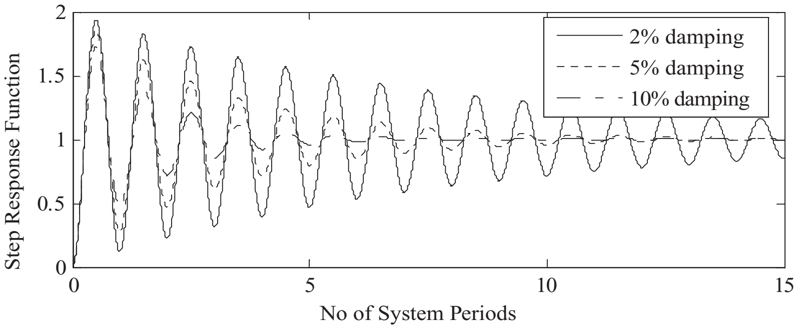

Figure 1.5 Dynamic-to-static ratio of step response for a single degree of freedom system.

The impulse response function (IRF) is shown plotted against nondimensional time for several dampings in Figure 1.6; the response starts and ends at zero. The y axis values depend upon the mass and natural frequency. The IRF may be used in the convolution approach described in Section 1.5.3.

1.5.2 Principle of Superposition

The principle of superposition, only valid for linear systems, states that if the responses to separate forces $f_1(t)$ and $f_2(t)$ are $x_1(t)$ and $x_2(t)$ respectively, then the response $x(t)$ to the sum of the forces $f(t) = f_1(t) + f_2(t)$ will be the sum of their individual responses, namely $x(t) = x_1(t) + x_2(t)$.

1.5.3 Example: Single Cycle of Square Wave Excitation – Response Determined by Superposition

Consider an SDoF system with an effective mass of 1000 kg, natural frequency 2 Hz and damping 5 % excited by a transient excitation consisting of a single cycle of a square wave with amplitude A and period τ_{square}. The response may be found by superposition of a step input of amplitude 1000 N at $t = 0$, a negative step input of amplitude 2000 N at $t = \tau_{\text{square}}/2$ and a single positive step input of amplitude 1000 N at $t = \tau_{\text{square}}$, as illustrated in Figure 1.7. The response may be calculated using the MATLAB program in appendix G in the companion website.

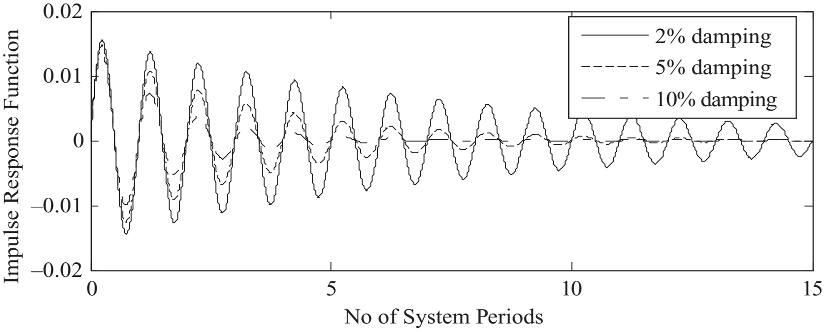

Figure 1.6 Impulse response function for a single degree of freedom system.

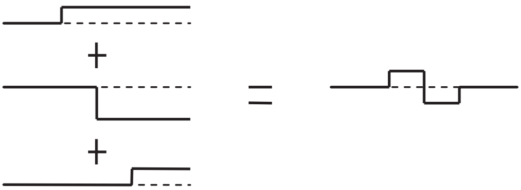

Figure 1.7 Single cycle of a square wave described by the principle of superposition.

Figure 1.8 shows the response when $\tau_{\text{square}} = 0.5$ s, the period of the system; the dashed line shows the time scale of the input. In this case, the square wave pulse is nearly 'tuned' to the system (i.e. near to the resonance frequency) and so the response is significantly larger (by almost a factor of 2) than for a single on/off pulse. This is the reason why the number of allowable pilot control input reversals in a manoeuvre is strictly limited.

1.5.4 Convolution Approach

The principle of superposition illustrated above may be employed in the solution of the response to general transient/random excitation. The idea here is that a general excitation input may be represented by a sequence of very narrow (ideal) impulses of different heights (and therefore strengths), as shown in Figure 1.9. A typical impulse occurring at time $t = \tau$ is of height $f(\tau)$ and width $\mathrm{d}\tau$. Thus the corresponding impulse strength is $f(\tau)\,d\tau$ and the response to this impulse, using the unit impulse response function in Equation (1.34), is

$$\begin{aligned} x_\tau(t) &= \{f(\tau)\,\mathrm{d}\tau\}\; h(t-\tau) = \frac{\{f(\tau)\,\mathrm{d}\tau\}}{m\omega_{\mathrm{n}}} \mathrm{e}^{-\zeta\omega_{\mathrm{n}}(t-\tau)} \sin\omega_{\mathrm{d}}(t-\tau) \quad \text{for} \quad t \geq \tau, \\ x_\tau(t) &= 0 \quad \text{for} \quad t < \tau. \end{aligned} \tag{1.35}$$

Note that the response is only nonzero *after* the impulse at $t = \tau$. The response to the entire excitation time history is equal to the summation of the responses to all the constituent impulses. Given that each impulse is $\mathrm{d}\tau$ wide, and allowing $\mathrm{d}\tau \to 0$, then the summation effectively becomes an integral, given by

$$x(t) = \int_{\tau=0}^{t} f(\tau)\,h(t-\tau)\,\mathrm{d}\tau. \tag{1.36}$$

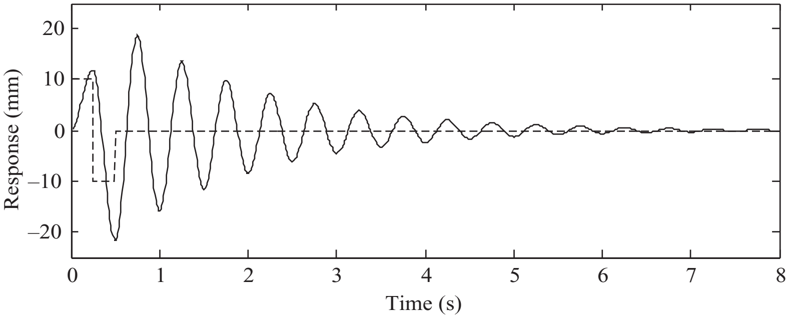

Figure 1.8 Response to a single cycle of square wave, using superposition.

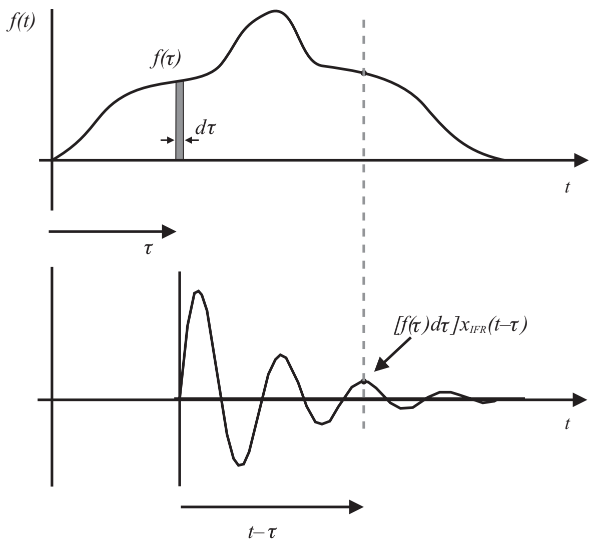

Figure 1.9 Convolution process.

This is known as the convolution integral (Newland, 1989; Rao, 1995) or, alternatively, the Duhamel integral (Fung, 1969). A shorthand way of writing this integral, where $*$ denotes convolution, is

$$x(t) = h(t) * f(t). \tag{1.37}$$

An alternative form of the convolution process may be written by treating the excitation as a combination of on/off steps and using the step response function $s(t)$, thus yielding a similar convolution expression (Fung, 1969)

$$x(t) = f(t)s(0) + \int_{\tau=0}^{t} f(\tau)\,\frac{\mathrm{d}s}{\mathrm{d}t}(t-\tau)\,\mathrm{d}\tau. \tag{1.38}$$

This form of convolution will be encountered in Chapters 10 and 16 for unsteady aerodynamics and gusts.

In practice, the convolution integrations would be performed numerically and not analytically. Thus the force input and impulse (or step) response function would need to be obtained in discrete, and not continuous, time form. The impulse response function may in fact be obtained numerically via the inverse Fourier transform of the frequency response function (see later).

1.5.5 Direct Solution of ODEs

An alternative approach for solving the ordinary differential equation, not requiring a closed form solution or performing a convolution, is to employ a numerical integration approach such as the Runge–Kutta or Newmark-β algorithms (Rao, 1995). To present one or both of these algorithms in detail is beyond the scope of this book. Suffice it to say that, knowing the response at the jth time value, the differential equation expressed at the $(j+1)$th time value is used, together with some assumption for the variation of the response within the step length, to predict the response at the $(j+1)$th time value.

In this book, time responses are sometimes calculated using numerical integration in the SIMULINK package called from a MATLAB program. The idea is illustrated using the earlier superposition example.

1.5.6 Example: Single Cycle of Square Wave Excitation – Response Determined by Numerical Integration

Consider again the SDoF system excited by the single square wave cycle as used in Section 1.5.3. The response may be found using numerical integration and may be seen to overlay the exact result in Figure 1.8 provided an adequately small step size is used (typically at least 30 points per cycle). The response is calculated using a Runge–Kutta algorithm in a MATLAB/SIMULINK program (see companion website).

1.6 TRANSIENT FORCED VIBRATION – FREQUENCY DOMAIN SOLUTION

The analysis leading up to the definition of the frequency response function in Section 1.4 considered only the response to an excitation input comprising a single sine wave at frequency ω rad/s. However, if the excitation was made up of several sine waves with different amplitudes and frequencies, the total steady-state response could be found by superposition of the responses to each individual sine wave, using the appropriate value of the FRF at each frequency. Again, because superposition is used, the approach only applies for linear systems.

1.6.1 Analytical Fourier Transform

In practice the definition of the FRF may be extended to cover a more general excitation by employing the Fourier transform (FT), so that

$$H(\omega) = \frac{X(\omega)}{F(\omega)} = \frac{\text{Fourier transform of } x(t)}{\text{Fourier transform of } f(t)}, \tag{1.39}$$

where, for example, $X(\omega)$, the Fourier transform of $x(t)$, is given for a continuous signal by

$$X(\omega) = \int_{-\infty}^{+\infty} x(t)\mathrm{e}^{\mathrm{i}\omega t}\,\mathrm{d}t. \tag{1.40}$$

The Fourier transform $X(\omega)$ is a complex function of frequency (i.e. spectrum) whose real and imaginary parts define the magnitude of the components of $\cos\omega t$ and $-\sin\omega t$ in the signal $x(t)$. The units of $X(\omega)$, $F(\omega)$ in this definition are typically m s and N s and the units of $H(\omega)$ are m/N. The inverse Fourier transform (IFT), not defined here, allows the frequency function to be transformed back into the time domain.

Although the Fourier transform is initially defined for an infinite continuous signal, and this would appear to challenge its usefulness, in practice inputs of finite length T may be used with the definition

$$X(\omega) = \frac{1}{T}\int_{0}^{T} x(t)\mathrm{e}^{\mathrm{i}\omega t}\,\mathrm{d}t. \tag{1.41}$$

In this case, the units of $X(\omega)$, $F(\omega)$ become m and N respectively, while units of $H(\omega)$ remain m/N. What is being assumed by using this expression is that $x(t)$ is in effect periodic with period T; i.e. the signal keeps repeating itself in a cyclic manner. Provided there is no discontinuity between the start and end of $x(t)$, then the analysis may be applied for a finite length excitation such as a pulse. If a discontinuity does exist, then a phenomenon known as 'leakage' occurs and additional incorrect Fourier amplitude components are introduced to represent the discontinuity; in practice, window functions (e.g.

Hanning, Hamming, etc.) are often applied to minimize this effect (Newland, 1987). The choice of the parameters in the analysis must be made carefully to minimize this error.

1.6.2 Discrete Fourier Transform

When using the Fourier transform in solving real problems, the discrete version (as opposed to the analytical version above) must be used. A detailed discussion of this is beyond the scope of the book, and other references should be studied, but some of the ideas will be seen in the example to follow Section 1.6.3 and in the MATLAB program (see companion website). In summary, the data record of length T $(= N\Delta t)$ is represented by a sequence $\{x(j\Delta t),\ j = 0, 1, 2, \ldots, (N-1)\Delta t\}$, with N (usually a power of 2) values at equal time intervals Δt s.

The resulting discrete Fourier transform (or DFT) is a sequence of discrete frequency domain values $X((j-1)\Delta f),\ j = 1, 2, \ldots, N/2+1$, i.e. from DC (zero frequency) to the so-called Nyquist frequency $(f_{\mathrm{Nyq}} = 1/(2\Delta t))$ at frequency intervals of$\Delta f = 1/T$. The values at the DC and Nyquist frequency are real but all the remaining values are complex, catering for the cosine and sine components.

It should be emphasized that it is important to understand the way in which the data are handled when performing forward and inverse transforms and this is well worth checking, e.g. using a simple case with a limited number of sine or cosine components and data points. Typically, the Fourier transform in the frequency domain is stored in a vector of N numbers (mostly complex), namely

$$\{X(0)X(\Delta f)X(2\Delta f) \cdots X(f_{\mathrm{Nyq}} - \Delta f)X(f_{\mathrm{Nyq}})X^{*}(f_{\mathrm{Nyq}} - \Delta f) \cdots X^{*}(2\Delta f)X^{*}(\Delta f)\}. \tag{1.42}$$

It can be seen that the so-called ‘negative’ frequency values are conjugates of the positive frequency values (i.e. have the opposite sign for the imaginary parts, shown by $*$, which is not to be confused with convolution). They are stored further along the transform vector in the reverse direction. Thus the additional complex numbers provide no extra information, but when using numerical functions or subroutines to carry out the inverse transform to return to the time domain, it is essential to retain the data in this form. Again, a simple check may prevent considerable difficulty and possibly error later on.

1.6.3 Frequency Domain Response – Excitation Relationship

It may be seen that rearranging Equation (1.39) leads to

$$X(\omega) = H(\omega)\ F(\omega) \tag{1.43}$$

and it is interesting to relate this to the time domain convolution Equation (1.37). The FRF and IRF are in fact Fourier transform pairs, e.g. the FRF is the Fourier transform of the IRF. Further, it may also be shown that by taking the Fourier transform of both sides of Equation (1.37), then Equation (1.43) results, i.e. convolution in the ‘time domain’ is equivalent to multiplication in the ‘frequency domain’. The extension of this approach for an MDoF system will be considered in Chapter 2.

A useful feature of Equation (1.43) is that it may be used to determine the response of a system, given the excitation time history, by going via a frequency domain route. Thus the response $x(t)$ of a linear system to a finite length transient excitation input $f(t)$ may be found by the following procedure (taking care over data storage):

1. Fourier transform $f(t)$ to find $F(\omega)$.
2. Determine the FRF $H(\omega)$ for the system.
3. Multiply the FRF and $F(\omega)$ using Equation (1.43) to determine $X(\omega)$.
4. Inverse Fourier transform $X(\omega)$ to find $x(t)$.

1.6.4 Example: Single Cycle of Square Wave Excitation – Response Determined via Fourier Transform

Consider again the SDoF system excited by a single square wave cycle as used in Section 1.5.3. The response is calculated using a MATLAB program (see companion website). Note that only a limited number of data points are used in order to allow the discrete values in the frequency and time domains to be seen; only discrete data points are plotted in the frequency domain functions. The results agree well with those in Figure 1.8 but the accuracy would improve as more data points were used to represent the signals.

1.7 RANDOM FORCED VIBRATION – FREQUENCY DOMAIN SOLUTION

There are two cases in aircraft loads where response to a random-type excitation is required: flying through continuous turbulence and taxiing on a runway with a nonsmooth profile. For continuous turbulence, it is normal practice to use a spectral approach based on a linearized model of the aircraft (see Chapter 16). When the effect of significant nonlinearity is to be explored, a time domain computation would need to be used. However, for taxiing (see Chapter 17), the solution would be carried out in the time domain using numerical integration of the equations of motion, as they are highly nonlinear due to the presence of the landing gear.

When a random excitation is considered, then a statistical approach is normally employed by defining the so-called power spectral density (PSD) of the excitation and response (Newland, 1987; Rao, 1995). For example, the PSD of $x(t)$ is defined by

$$S_{xx}(\omega) = \frac{T}{2\pi} X(\omega)^* X(\omega) = \frac{T}{2\pi} \left| X(\omega)^2 \right|, \tag{1.44}$$

where * denotes the complex conjugate (not to be confused with convolution). Thus the PSD is essentially proportional to the modulus squared of the Fourier amplitude at each frequency and would have units of density (m^2/rad s if $x(t)$ were a displacement). It is a measure of how the ‘power’ in $x(t)$ is distributed over the frequency range of interest. In practice, the PSD of a time signal could be computed from a long data record by employing some form of averaging of finite length segments of the data.

If Equation (1.43) is multiplied on both sides by its complex conjugate then

$$X(\omega)\, X^*(\omega) = H(\omega)F(\omega)\;\; H^*(\omega)F^*(\omega) = |H(\omega)|^2\;\; F(\omega)\, F^*(\omega) \tag{1.45}$$

and if the relevant scalar factors present in Equation (1.44) are accounted for, then Equation (1.45) becomes

$$S_{xx}(\omega) = |H(\omega)|^2\;\; S_{FF}(\omega). \tag{1.46}$$

Thus, knowing the definition of the excitation PSD $S_{FF}(\omega)$ (units N^2/rad s for force), the response PSD may be determined given the FRF for the system (m/N for displacement per force). It may be seen from Equation (1.46) that the spectral shape of the excitation is carried through to the response, but is filtered by the system dynamic characteristics. The extension of this approach for an MDoF system will be considered in Chapter 2. This relationship between the response and excitation PSDs is useful but phase information is lost.

In the analysis shown so far, the PSD $S_{xx}(\omega)$, for example, has been ‘two-sided’ in that values exist at both positive and negative frequencies; the latter are somewhat artificial but derive from the mathematics in that a positive frequency corresponds to a vector rotating anticlockwise at ω, whereas a negative frequency corresponds to rotation in the opposite direction. However, in practice the ‘two-sided’ (or double-sided) PSD is often converted into a 'one-sided' (or single-sided) function $\Phi_{xx}(\omega)$, existing only at nonnegative frequencies and calculated using

$$\Phi_{xx}(\omega) = 2S_{xx}(\omega), \qquad 0 \leq \omega < \infty. \tag{1.47}$$

Single-sided spectra are in fact used in determining the response to continuous turbulence considered in Chapter 16, since the continuous turbulence PSD is defined in this way.

The mean square value is the corresponding area under the one-sided or two-sided PSD, so

$$\overline{x^2} = \int_0^{+\infty} \Phi_{xx}(\omega)\,\mathrm{d}\omega \qquad \text{or} \qquad \overline{x^2} = \int_{-\infty}^{+\infty} S_{xx}(\omega)\,\mathrm{d}\omega, \tag{1.48}$$

where clearly only a finite, not infinite, frequency range is used in practice. The root-mean-square value is the square root of the mean-square value.

1.8 EXAMPLES

Note that these examples may be useful preparation when carrying out the examples in later chapters.

1. An avionics box may be idealized as an SDoF system comprising a mass m supported on a mounting base via a spring k and damper c. The system displacement is $y(t)$ and the base displacement is $x(t)$. The base is subject to acceleration $\ddot{x}(t)$ from motion of the aircraft. Show that the equation of motion for the system may be written in the form $m\ddot{z} + c\dot{z} + kz = -m\ddot{x}(t)$ where $z = y - x$ is the relative displacement between the mass and the base (i.e. spring extension).

2. In a flutter test, the acceleration of an aircraft control surface following an explosive impact decays to a quarter of its amplitude after 5 cycles, which corresponds to an elapsed time of 0.5 s. Estimate the undamped natural frequency and the percentage of critical damping. [10 Hz, 4.4 %]

3. Determine an expression for the response of a single degree of freedom undamped system undergoing free vibration following an initial condition of zero velocity and displacement x_0.

4. Determine an expression for the time t_p at which the response of a damped SDoF system to excitation by a step force F_0 reaches a maximum $[\omega_\mathrm{n} t_\mathrm{p} = \pi/\sqrt{1-\zeta^2}]$. Show that the maximum response is given by the expression $xk/F_0 = 1 + \exp(-\zeta\pi/\sqrt{1-\zeta^2})$, noting the insensitivity to damping at low values.

5. Using the complex algebra approach for harmonic excitation and response, determine an expression for the transmissibility (i.e. system acceleration per base acceleration) for the base excited system in Example 1.

6. A motor mounted in an aircraft on four antivibration mounts may be idealized as an SDoF system of effective mass 20 kg. Each mount has a stiffness of 5000 N/m and a damping coefficient of 200 N s/m. Determine the natural frequency and damping ratio of the system. Also, estimate the displacement and acceleration response of the motor when it runs with a degree of imbalance equivalent to a sinusoidal force of ±40 N at 1200 rpm (20 Hz). Compare this displacement value to the static deflection of the motor on its mounts. [5.03 Hz, 63.2%, 0.128 mm, 2.02 m/s^2, 9.8 mm]

7. A machine of mass 1000 kg is supported on a spring/damper arrangement. In operation, the machine is subjected to a force of 750 cos ωt, where ω (rad/s) is the operating frequency. In an experiment, the operating frequency is varied and it is noted that resonance occurs at 75 Hz and that the magnitude of the FRF is 2.5. However, at its normal operating frequency this value is found to be 0.7. Find the normal

operating frequency and the support stiffness and damping coefficient. [118.3 Hz, 2.43×10^8 N/m, 1.97×10^5 N s/m]

8. An aircraft fin may be idealized in bending as an SDoF system with an effective mass of 200 kg, undamped natural frequency of 5 Hz and damping 3 % critical. The fin is excited via the control surface by an 'on/off' force pulse of magnitude 500 N. Using MATLAB and one or more of the (a) superposition, (b) simulation and (c) Fourier transform approaches, determine the pulse duration that will maximize the resulting response and the value of the response itself.
9. Using MATLAB, generate a time history of 16 data points with a time interval Δt of 0.05 s and composed of a DC value of 1, a sine wave of amplitude 3 at 4 Hz and cosine waves of amplitude -2 at 2 Hz and 1 at 6 Hz. Perform the Fourier transform and examine the form of the complex output sequence as a function of frequency to understand how the data are stored and how the frequency components are represented. Then perform the inverse FT and examine the resulting sequence, comparing it to the original signal.
10. Generate other time histories with a larger number of data values, such as (a) single (1-cosine) pulse, (b) multiple cycles of a sawtooth waveform and (c) multiple cycles of a square wave. Calculate the FT of each and examine the amplitude of the frequency components to see how the power is distributed.

2

Vibration of Multiple Degree of Freedom Systems

In this chapter, some of the basic concepts of vibration analysis for multiple degree of freedom (MDoF) discrete parameter systems will be introduced, as there are some significant differences to a single degree of freedom (SDoF) system. The term 'discrete (or sometimes lumped) parameter' implies that the system in question is a combination of discrete rigid masses (or components) interconnected by flexible stiffness and damping elements. Note that the same approaches may be employed when a modal coordinate system is used (see later). On the other hand, 'continuous' systems, considered later in Chapters 3 and 4, are those where all components of the system are flexible/elastic and deform in some manner.

The focus of this chapter will be in setting up the equations of motion, finding natural frequencies and mode shapes for free vibration and determining the forced vibration response with various forms of excitation relevant to aircraft loads. Some of the core solution methods introduced in Chapter 1 will be considered for MDoF systems. For simplicity, the ideas will be illustrated for only two degrees of freedom. The general form of equations will be shown in matrix form to cover any number of degrees of freedom, since matrix algebra unifies all MDoF systems. Further treatment may be found in Tse *et al.* (1978), Newland (1989), Rao (1995), Thomson (1997) and Inman (2006).

2.1 SETTING UP EQUATIONS OF MOTION

There are a number of ways of setting up the equations of motion for an MDoF system. As before in Chapter 1, Lagrange's energy equations will be employed. Two examples will be considered: a classical 'chain-like' discrete parameter system and a rigid aircraft capable of heave and pitch motion while supported on its landing gears. The latter example will be used later when considering the taxiing case in Chapter 17.

2.1.1 Example: Classical 'Chain-like' Two DoF System

A classical form of a two DoF system is shown in Figure 2.1. All other systems that may be described by multiple degrees of freedom may be shown to have an identical form of governing equation, albeit with different parameters. This basic system comprises masses m_1, m_2, springs of stiffness k_1, k_2 and viscous dampers of coefficient c_1, c_2. The motion of the system is a function of time t and is defined by the displacements $x_1(t), x_2(t)$. Time varying forces $f_1(t), f_2(t)$ are also applied to the masses as shown.

Although there are now two DoF, and therefore two equations of motion, the energy and work terms required are obviously still scalar and therefore additive quantities. Firstly, the kinetic energy is given by

$$T = \frac{1}{2}m_1\dot{x}_1^2 + \frac{1}{2}m_2\dot{x}_2^2. \tag{2.1}$$

Introduction to Aircraft Aeroelasticity and Loads J. R. Wright and J. E. Cooper

© 2007 John Wiley & Sons, Ltd

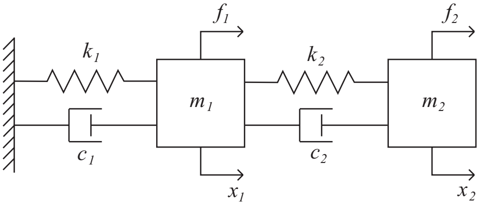

Figure 2.1 Two degree of freedom chain-like mass/spring/damper system.

The strain energy in the springs depends upon the relative extension/compression of each and is given by

$$U = \tfrac{1}{2}k_1x_1^2 + \tfrac{1}{2}k_2\,(x_2 - x_1)^2 \tag{2.2}$$

and the dissipative term for the dampers depends upon the relative velocities and is written as

$$\Im = \tfrac{1}{2}c_1\dot{x}_1^2 + \tfrac{1}{2}c_2(\dot{x}_2 - \dot{x}_1)^2. \tag{2.3}$$

Finally, the effect of the forces is included in Lagrange's equation by considering the incremental work done δW obtained when the two forces move through incremental displacements δx_1, δx_2, namely

$$\delta W = f_1\,\delta x_1 + f_2\,\delta x_2. \tag{2.4}$$

Now, Lagrange's equation for a system with multiple degrees of freedom N may be written as

$$\frac{\mathrm{d}}{\mathrm{d}t}\left(\frac{\partial T}{\partial \dot{x}_j}\right) - \frac{\partial T}{\partial x_j} + \frac{\partial \Im}{\partial \dot{x}_j} + \frac{\partial U}{\partial x_j} = Q_j = \frac{\partial(\delta W)}{\partial(\delta x_j)} \quad \text{for } j = 1, 2, \ldots, N. \tag{2.5}$$

Then substituting Equations (2.1) to (2.4) into Equation (2.5) and performing the differentiations for $N = 2$ yields the ordinary second-order differential equations

$$\begin{aligned} m_1\ddot{x}_1 + (c_1 + c_2)\,\dot{x}_1 - c_2\dot{x}_2 + (k_1 + k_2)\,x_1 - k_2x_2 &= f_1(t), \\ m_2\ddot{x}_2 - c_2\dot{x}_1 + c_2\dot{x}_2 - k_2x_1 + k_2x_2 &= f_2(t). \end{aligned} \tag{2.6}$$

These equations of motion are most easily expressed in matrix form as

$$\begin{bmatrix} m_1 & 0 \\ 0 & m_2 \end{bmatrix}\begin{Bmatrix} \ddot{x}_1 \\ \ddot{x}_2 \end{Bmatrix} + \begin{bmatrix} c_1 + c_2 & -c_2 \\ -c_2 & c_2 \end{bmatrix}\begin{Bmatrix} \dot{x}_1 \\ \dot{x}_2 \end{Bmatrix} + \begin{bmatrix} k_1 + k_2 & -k_2 \\ -k_2 & k_2 \end{bmatrix}\begin{Bmatrix} x_1 \\ x_2 \end{Bmatrix} = \begin{Bmatrix} f_1 \\ f_2 \end{Bmatrix} \tag{2.7}$$

where the mass matrix is diagonal (so the system in uncoupled inertially) whereas the damping and stiffness matrices are coupled. In general matrix notation this becomes

$$\mathbf{M}\ddot{\boldsymbol{x}} + \mathbf{C}\dot{\boldsymbol{x}} + \mathbf{K}\boldsymbol{x} = \boldsymbol{f}(t) \tag{2.8}$$

where $\mathbf{M}$, $\mathbf{C}$, $\mathbf{K}$ are the mass, damping and stiffness matrices respectively, and $\boldsymbol{x}$, $\boldsymbol{f}$ are the column vectors of displacements and forces. Note that the matrices are symmetric. In this book, the bold symbol will be used to indicate a matrix quantity and bold italics for a vector, as seen in the above equation. It is assumed that the reader is familiar with basic matrix concepts, and if not another reference should be consulted (Stroud and Booth, 2007).

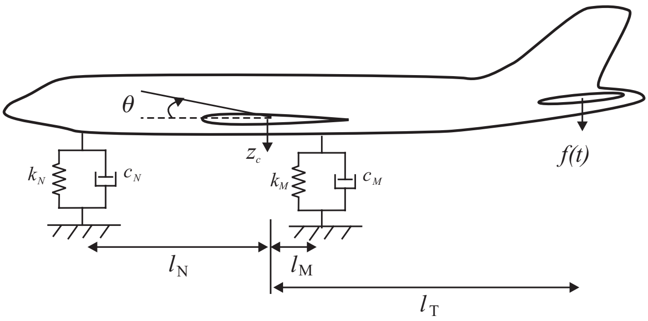

Figure 2.2 Two degree of freedom rigid aircraft in heave/pitch supported on landing gear.

2.1.2 Example: Two DoF Rigid Aircraft

As an example of a completely different two DoF system that involves both translational and rotational coordinates, consider the rigid aircraft supported on linear landing gears as shown in Figure 2.2. The aircraft has mass m, pitch moment of inertia about the centre of mass I_y, nose and main landing gear stiffness $K_{\mathrm{N}}, K_{\mathrm{M}}$ respectively, and viscous damping $C_{\mathrm{N}}, C_{\mathrm{M}}$. In order to demonstrate how excitation forces are treated, consider an arbitrary input excitation force $f(t)$ to be applied vertically downwards at the tail. The coordinates describing the motion are the centre of mass heave displacement z_{C} (downwards positive to be consistent with axes systems used often later on) and pitch angle θ (nose up positive). The geometry is shown in the figure.

The energy, dissipation and work functions corresponding to Equations (2.1) to (2.4) depend upon the expressions for the extension/compression of the springs and dampers, and for small angles are given by

$$\begin{aligned} T &= \tfrac{1}{2}m\dot{z}_{\mathrm{C}}^2 + \tfrac{1}{2}\mathrm{I}_y\dot{\theta}^2, \qquad U = \tfrac{1}{2}K_{\mathrm{N}}(z_{\mathrm{C}} - l_{\mathrm{N}}\theta)^2 + \tfrac{1}{2}K_{\mathrm{M}}(z_{\mathrm{C}} + l_{\mathrm{M}}\theta)^2 \\ \Im &= \tfrac{1}{2}C_{\mathrm{N}}(\dot{z}_{\mathrm{C}} - l_{\mathrm{N}}\dot{\theta})^2 + \tfrac{1}{2}C_{\mathrm{M}}(\dot{z}_{\mathrm{C}} + l_{\mathrm{M}}\dot{\theta})^2, \qquad \delta W = f\,(\delta z_{\mathrm{C}} + l_{\mathrm{T}}\delta\theta). \end{aligned} \tag{2.9}$$

Then, applying Lagrange's equations with physical coordinates z_{C} and θ, the aircraft equations of motion are

$$\begin{aligned} &\begin{bmatrix} m & 0 \\ 0 & I_y \end{bmatrix}\begin{Bmatrix} \ddot{z}_{\mathrm{C}} \\ \ddot{\theta} \end{Bmatrix} + \begin{bmatrix} C_{\mathrm{N}} + C_{\mathrm{M}} & -l_{\mathrm{N}}C_{\mathrm{N}} + l_{\mathrm{M}}C_{\mathrm{M}} \\ -l_{\mathrm{N}}C_{\mathrm{N}} + l_{\mathrm{M}}C_{\mathrm{M}} & l_{\mathrm{N}}^2C_{\mathrm{N}} + l_{\mathrm{M}}^2C_{\mathrm{M}} \end{bmatrix}\begin{Bmatrix} \dot{z}_{\mathrm{C}} \\ \dot{\theta} \end{Bmatrix} \\ &\qquad + \begin{bmatrix} K_{\mathrm{N}} + K_{\mathrm{M}} & -l_{\mathrm{N}}K_{\mathrm{N}} + l_{\mathrm{M}}K_{\mathrm{M}} \\ -l_{\mathrm{N}}K_{\mathrm{N}} + l_{\mathrm{M}}K_{\mathrm{M}} & l_{\mathrm{N}}^2K_{\mathrm{N}} + l_{\mathrm{M}}^2K_{\mathrm{M}} \end{bmatrix}\begin{Bmatrix} z_{\mathrm{C}} \\ \theta \end{Bmatrix} = \begin{Bmatrix} f(t) \\ l_{\mathrm{T}}f(t) \end{Bmatrix}. \end{aligned} \tag{2.10}$$

It can be seen clearly that this equation is of the same general form as that in Equation (2.8). Depending upon the parameter values, the damping and stiffness matrices will in general be coupled whereas there is no inertia coupling for this choice of coordinate system. Further analysis of this problem will be shown later in this chapter and also in Chapter 17, where the taxiing problem will be examined.

2.2 UNDAMPED FREE VIBRATION

Initially, the free vibration for the *undamped* MDoF system will be considered; the damped case will be introduced later. Because of the compact nature of matrix algebra in illustrating the theory, where possible any analysis will be carried out in matrix form for N degrees of freedom, and an example shown for $N = 2$.

Rather as for the SDoF system, the solution method is to seek a form of free vibration motion given by

$$\boldsymbol{x}(t) = \boldsymbol{X} \sin \omega t, \tag{2.11}$$

where $\boldsymbol{X}$ is the amplitude vector and ω is the frequency of free vibration. All coordinates are assumed to move in or out of phase at the same frequency. Substituting Equation (2.11) into Equation (2.8), setting the damping and forcing values to zero and simplifying yields the expression

$$\left[\mathbf{K} - \omega^2 \mathbf{M}\right] \boldsymbol{X} = 0. \tag{2.12}$$

The solution to this equation recognizes that $\boldsymbol{X}$ must be nontrivial and therefore that the matrix in brackets must be singular (i.e. have a zero determinant). By setting the determinant $\left|\mathbf{K} - \omega^2 \mathbf{M}\right|$ to zero, an Nth-order polynomial in ω^2 is obtained. The solution of this polynomial yields roots ω_j, $j = 1, 2, \ldots, N$. These are the so-called *(undamped) natural frequencies* of the system, one for each DoF, and are the frequencies at which motion of the type described by Equation (2.11) may be found. They are a property of the system.

For each natural frequency ω_j, the response may be characterized by the vector $\boldsymbol{X}_j$, given by the solution of

$$\left[\mathbf{K} - \omega_j^2 \mathbf{M}\right] \boldsymbol{X}_j = 0 \quad \text{for } j = 1, 2, \ldots, N. \tag{2.13}$$

These characteristic vectors may be found by solving Equation (2.13) directly, though only ratios of the vector elements and not absolute values are obtained. This process will be illustrated later by an example.

As an alternative approach, Equation (2.12) may be rewritten as

$$\mathbf{K}\boldsymbol{X} = \omega^2 \mathbf{M}\boldsymbol{X} \qquad \text{or} \qquad \mathbf{M}^{-1}\mathbf{K}\boldsymbol{X} = \omega^2 \boldsymbol{X}, \tag{2.14}$$

which is equivalent to the classical eigenvalue notation

$$\mathbf{A}\boldsymbol{X} = \lambda \mathbf{B}\boldsymbol{X} \qquad \text{or} \qquad \mathbf{A}\boldsymbol{X} = \lambda \boldsymbol{X}, \tag{2.15}$$

where $\mathbf{A}, \mathbf{B}$ are symmetric matrices and $\lambda \, (= \omega^2)$ is referred to as an eigenvalue. The eigenvalues are λ_j, $j = 1, 2, \ldots, N$ (leading to the corresponding natural frequency values ω_j, $j = 1, 2, \ldots, N$), and these are readily obtainable using matrix methods (Golub and van Loan, 1989). Also, it may be recognized that the corresponding vectors $\boldsymbol{X}_j$, $j = 1, 2, \ldots, N$, are in fact the eigenvectors, also known as the *(undamped) normal mode shapes* of the system, a further property of the system. Each mode shape yields the relative displacements of each of the physical coordinates when the system vibrates at the corresponding natural frequency.

The so-called *modal matrix* is defined as the matrix having the mode shapes (i.e. eigenvectors) as columns, so

$$\boldsymbol{\Phi} = [\boldsymbol{X}_1 \boldsymbol{X}_2, \ldots, \boldsymbol{X}_N]. \tag{2.16}$$

The undamped free vibration motion can be shown to be comprised of the sum of all the mode shapes, each vibrating at its corresponding natural frequency, with amplitudes and phases determined by the initial conditions. Because there is no damping, the motion will not decay.

2.2.1 Example: Classical 'Chain-like' Two DoF System

Consider the example of the classical two DoF system shown in Figure 2.1 and introduced earlier in Section 2.1.1. However, now assign numerical values as follows: $m_1 = 2\,\text{kg}$, $m_2 = 1\,\text{kg}$, $k_1 = 2000\,\text{N/m}$ and $k_2 = 1000\,\text{N/m}$. Damping and force values are set to zero. Substituting these values into Equation (2.7) to determine the equation of motion, and then using the mass and stiffness matrices in Equation (2.12) yields

$$\begin{bmatrix} 3000 - 2\omega^2 & -1000 \\ -1000 & 1000 - \omega^2 \end{bmatrix} \begin{Bmatrix} X_1 \\ X_2 \end{Bmatrix} = 0. \tag{2.17}$$

Setting the determinant of the matrix equal to zero,

$$(3000 - 2\omega^2)(1000 - \omega^2) - (-1000)^2 = 0, \tag{2.18}$$

leads to the quadratic equation in ω^2, namely

$$2(\omega^2)^2 - 5000(\omega^2) + 2\,000\,000 = 0. \tag{2.19}$$

The two equation roots are $\omega_1^2 = 500$, $\omega_2^2 = 2000$, so $\omega_1 = 22.36$, $\omega_2 = 44.72$ rad/s and so 3.56 and 7.12 Hz are the (undamped) natural frequencies at which the system will respond in free vibration when disturbed.

To determine the mode shapes, the characteristic vector must be solved for each natural frequency. For this two DoF system, Equation (2.17) may be used to find the ratio of X_1/X_2 from either of the two equations, so

$$\frac{X_1}{X_2} = \frac{1000}{3000 - 2\omega^2}. \tag{2.20}$$

Now, substituting the values for each natural frequency into this equation yields the ratios

$$\left(\frac{X_1}{X_2}\right)_{\text{Mode 1}} = 0.5 \qquad \text{and} \qquad \left(\frac{X_1}{X_2}\right)_{\text{Mode 2}} = -1. \tag{2.21}$$

These ratios imply that in mode 1 the second mass moves twice as much as the first mass but in phase with it; however, in the second mode both masses move an equal amount but out-of-phase. It is not possible to assign absolute values to X_1, X_2 for each mode. The ratios may be written as mode shape vectors by choosing some suitable form of normalization. Here the vector is written with a maximum element of unity, e.g.

$$\boldsymbol{X}_1 = \begin{Bmatrix} 0.5 \\ 1 \end{Bmatrix} \qquad \text{and} \qquad \boldsymbol{X}_2 = \begin{Bmatrix} -1 \\ 1 \end{Bmatrix} \tag{2.22}$$

and so the modal matrix is

$$\boldsymbol{\Phi} = \begin{bmatrix} 0.5 & -1 \\ 1 & 1 \end{bmatrix}. \tag{2.23}$$

The same result would be obtained using an eigenvalue solver (see the MATLAB program in Appendix G in the companion website).

2.2.2 Example: Two DoF Rigid Aircraft

Consider further the example of the aircraft considered earlier in Section 2.1 and shown in Figure 2.2. However, now assign numerical values as follows: $m = 4000\,\mathrm{kg}$, $I_y = 12\,000\,\mathrm{kg\,m^2}$, $l_\mathrm{N} = 4\,\mathrm{m}$, $l_\mathrm{M} = 1\,\mathrm{m}$, $K_\mathrm{N} = 40\,000\,\mathrm{N/m}$ and $K_\mathrm{M} = 120\,000\,\mathrm{N/m}$. Damping and force values are set to zero for the determination of natural frequencies and mode shapes. Substituting into Equation (2.10) yields the following mass and stiffness matrices:

$$\mathbf{M} = \begin{bmatrix} 4000 & 0 \\ 0 & 12\,000 \end{bmatrix} \quad \text{and} \quad \mathbf{K} = \begin{bmatrix} 160\,000 & -40\,000 \\ -40\,000 & 760\,000 \end{bmatrix}. \tag{2.24}$$

The determinant $\left|\mathbf{K} - \omega^2\mathbf{M}\right|$ must be set to zero, so

$$\begin{vmatrix} 160\,000 - 4000\omega^2 & -40\,000 \\ -40\,000 & 760\,000 - 12\,000\omega^2 \end{vmatrix} = 0. \tag{2.25}$$

Expanding the determinant and simplifying by dividing through by 10^6 yields a quartic polynomial which is actually a quadratic in ω^2:

$$48\omega^4 - 4960\omega^2 + 120\,000 = 0. \tag{2.26}$$

This equation has roots $\omega_1^2 = 38.65$ and $\omega_2^2 = 64.68\,\mathrm{rad/s}$, so the undamped natural frequencies are 0.989 and 1.280 Hz. Solving Equation (2.13) for the mode shape vector yields

$$\boldsymbol{X}_1 = \begin{Bmatrix} 1 \\ 0.135 \end{Bmatrix} \quad \text{and} \quad \boldsymbol{X}_2 = \begin{Bmatrix} -0.405 \\ 1 \end{Bmatrix} \tag{2.27}$$

and thus the modal matrix is

$$\boldsymbol{\Phi} = \begin{bmatrix} 1 & -0.405 \\ 0.135 & 1 \end{bmatrix}. \tag{2.28}$$

The mode shape vectors need to be interpreted physically since the two values in the vector refer to the motion of the centre of mass (downwards positive) and the pitch angle (nose up positive). The downwards motion at the nose and main landing gear positions, for example, may be found using $z_\mathrm{C} - l_\mathrm{N}\theta$ and $z_\mathrm{C} + l_\mathrm{M}\theta$ respectively; e.g. the values 1 and 0.135 imply that the corresponding nose and main gear displacements in the mode shape are 0.460 and 1.135 whereas the values −0.405 and 1 imply nose and main gear modal displacements of −4.405 and 0.595. These values may be shown graphically, as in Figure 2.3, though it should be noted that these shapes have unknown absolute values and only show the ratio between the deflections.

Each displaced shape is essentially a snapshot in time of the motion in the mode. Mode 1 is a motion of heave down/up and pitch nose up/down with a stationary point (or ‘node’) at a position 7.407 m in front of the centre of mass, whereas mode 2 is primarily a pitching motion with a node point 0.405 m behind the centre of mass. Altering the value of the nose gear stiffness to 30 000 N/m would eliminate coupling in the stiffness matrix and mean that the two modes would be pure heave and pure pitch respectively.

2.3 DAMPED FREE VIBRATION

Now consider the free vibration of a damped MDoF system. The mathematical form of the motion of the damped system following release from an initial condition is rather complicated so will not be covered in detail here.

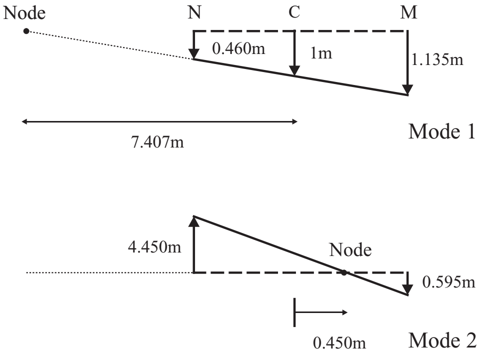

Figure 2.3 Mode shapes for the rigid aircraft example.

2.3.1 Form of the Damped Solution

Rather as for the SDoF system, if the response vector is assumed to be

$$\boldsymbol{x}(t) = \boldsymbol{X}\mathrm{e}^{\lambda t} \tag{2.29}$$

and this solution is substituted into Equation (2.8) with no excitation and the exponent term cancelled, then

$$[\lambda^2\mathbf{M} + \lambda\mathbf{C} + \mathbf{K}]\boldsymbol{X} = 0. \tag{2.30}$$

Since the matrix determinant is zero for a nontrivial solution, a $2N$th-order characteristic polynomial in λ may be obtained and the N complex roots determined. Alternatively, the problem can be solved using a matrix based approach by transforming to first-order (state space) form (illustrated later for flutter in Chapter 11).

For systems where damping is small enough for oscillatory motion to occur in each mode, there will be N complex conjugate pairs of roots of Equation (2.30) of the form $\lambda_j = -a_j + \mathrm{i}b_j$, $\lambda_j^* = -a_j - \mathrm{i}b_j$ for $j = 1, 2, \ldots, N$ and corresponding (nominally) complex conjugate pairs of eigenvectors $\tilde{\boldsymbol{X}}_j$, $\tilde{\boldsymbol{X}}_j^*$ for $j = 1, 2, \ldots, N$. Because the constituent solutions for the free vibration in Equation (2.29) will be governed by the term $\exp[(-a_j \pm \mathrm{i}b_j)t] = \exp(-\zeta_j\omega_j t \pm \mathrm{i}\omega_j\sqrt{1-\zeta_j^2 t})$ then, somewhat akin to the SDoF approach used in Chapter 1, the eigenvalues can be used to obtain the 'effective' natural frequency and damping ratio values of $\omega_j = \sqrt{a_j^2 + b_j^2}$, $\zeta_j = a_j/\omega_j$ for $j = 1, 2, \ldots, N$.

2.3.2 Proportional (or Rayleigh) and Nonproportional Damping

The behaviour of an MDoF viscously damped system is dependent upon the relationship between the damping matrix and the mass and stiffness matrices. If the physical damping matrix **C** can be written as a linear combination of the physical mass and stiffness matrices (**M**, **K**), e.g.

$$\mathbf{C} = \alpha\mathbf{M} + \beta\mathbf{K}, \tag{2.31}$$

where α, β are scalar coefficients, then such a damping model is known as *proportional* (or Rayleigh) damping (Rao, 1995; Thomson, 1997). If this relationship is not satisfied, then the damping is said to be *nonproportional*. The two DoF rigid aircraft example will be used to illustrate the effect of these two damping models on the free damped vibration behaviour.

2.3.3 Example: Two DoF Rigid Aircraft with Proportional Damping

Consider the same two DOF rigid aircraft example as earlier, but now define nose and main gear damping values of $C_\mathrm{N} = 400$ Ns/m and $C_\mathrm{M} = 1200$ Ns/m; these values are 1 % of the corresponding numerical stiffness values and so describe a *proportional damping* model with Rayleigh coefficients $\alpha = 0$ and $\beta = 0.01$. Thus the mass, proportional damping and stiffness matrices are

$$\mathbf{M} = \begin{bmatrix} 4000 & 0 \\ 0 & 12\,000 \end{bmatrix}, \qquad \mathbf{C} = \begin{bmatrix} 1600 & -400 \\ -400 & 7600 \end{bmatrix}, \qquad \mathbf{K} = \begin{bmatrix} 160\,000 & -40\,000 \\ -40\,000 & 760\,000 \end{bmatrix}. \tag{2.32}$$

Solution of the relevant eigenvalue problem (see Chapter 11) for the damped two DoF system gives $\lambda_1 = -0.193 \pm 6.214\mathrm{i}$ and $\lambda_2 = -0.323 \pm 8.036\mathrm{i}$, leading to 'effective' natural frequencies of 0.989 and 1.280 Hz, with damping ratio values of 0.031 (i.e. 3.1 % critical) and 0.040 for the two modes. Note that for this proportional damping case the 'effective' natural frequencies obtained are identical to the undamped natural frequencies found earlier. The corresponding eigenvectors are found to be

$$\tilde{\boldsymbol{X}}_1 = \begin{Bmatrix} 1 \\ 0.135 \end{Bmatrix} = \boldsymbol{X}_1 \qquad \text{and} \qquad \tilde{\boldsymbol{X}}_2 = \begin{Bmatrix} -0.405 \\ 1 \end{Bmatrix} = \boldsymbol{X}_2. \tag{2.33}$$

These vectors $\tilde{\boldsymbol{X}}_j$ are termed the (damped) mode shapes; for the proportional damping case they are real and are exactly the same as the undamped normal modes $\boldsymbol{X}_j$ found for the undamped case considered in Section 2.2.2. Thus motion in any such mode will involve each coordinate being in-phase or out-of-phase, with an invariant nodal point location and simultaneous maximum and minimum excursion of all the coordinates.

The implication of these results is that the free vibration of a proportionally damped MDoF system will consist of the summation of decaying responses in each of N normal modes with shape $\boldsymbol{X}_j$, 'effective' natural frequency ω_j (rad/s) and damping ratio ζ_j; thus in effect the general free vibration response is expressed as the combination of modes, each behaving like SDoF systems. Each component in the summation will have an amplitude and phase that depend upon the initial conditions.

2.3.4 Example: Two DoF Rigid Aircraft with Nonproportional Damping

Now consider the nose gear damping value C_N doubled to 800 N s/m, while the nose gear stiffness value remains unchanged; this means that the damping will be *nonproportional*, with the damping matrix

$$\mathbf{C} = \begin{bmatrix} 2000 & -2000 \\ -2000 & 14\,000 \end{bmatrix}. \tag{2.34}$$

The solution of the relevant eigenvalue problem for the damped MDoF system gives $\lambda_1 = -0.203 \pm 6.215\mathrm{i}$ and $\lambda_2 = -0.630 + 8.016\mathrm{i}$, leading to 'effective' natural frequencies of 0.990 and 1.280 Hz, with damping values of 0.033 and 0.078 for the two modes. Note that the 'effective' natural frequency is now slightly different to the undamped natural frequency of the system, but nevertheless governs its free vibration decay. The damping value has increased as expected. The corresponding eigenvectors are found to be

$$\tilde{\boldsymbol{X}}_1 = \begin{Bmatrix} 1 \\ 0.138 + 0.016\mathrm{i} \end{Bmatrix} \qquad \text{and} \qquad \tilde{\boldsymbol{X}}_2 = \begin{Bmatrix} -0.416 - 0.061\mathrm{i} \\ 1 \end{Bmatrix} \tag{2.35}$$

and these are clearly seen to be complex and different to the values in Equation (2.33). The vectors are termed complex (or damped) mode shapes and are only the same as the undamped normal modes for the proportionally damped case. A complex mode involves each coordinate having a fixed relative amplitude and phase with respect to the other coordinates (usually different to 0 or 180°), points reaching their maximum excursion at different instants of time and nodal point locations that vary with time during a cycle of vibration. Note that the presence of complex modes will be found in the flutter solution (see Chapter 11).

The free vibration response will now be a summation of the decaying complex mode responses as opposed to normal mode responses for the proportionally damped system.

2.4 TRANSFORMATION TO MODAL COORDINATES

A particularly powerful feature of mode shapes of vibration is that they may be used to transform the coupled equations of motion in physical coordinates into a different (principal/modal) coordinate form where coupling is absent. The analysis will be presented in matrix form for a general MDoF system and illustrated for the two DoF examples. Damping and excitation terms are now included since the approach is generally applicable.

Firstly, define a coordinate transformation based on the modal matrix and 'modal' (or 'principal') coordinates $\boldsymbol{q}$:

$$\boldsymbol{x} = \boldsymbol{\phi}\boldsymbol{q}. \tag{2.36}$$

Now substitute for $\boldsymbol{x}$ using Equation (2.36) in Equation (2.8) and pre-multiply by the transpose of the modal matrix; therefore

$$\begin{gathered} \boldsymbol{\phi}^{\mathrm{T}}\mathbf{M}\boldsymbol{\phi}\ddot{\boldsymbol{q}} + \boldsymbol{\phi}^{\mathrm{T}}\mathbf{C}\boldsymbol{\phi}\dot{\boldsymbol{q}} + \boldsymbol{\phi}^{\mathrm{T}}\mathbf{K}\boldsymbol{\phi}\boldsymbol{q} = \boldsymbol{\phi}^{\mathrm{T}}\boldsymbol{f} \\ \text{or} \\ \mathbf{M}_q\ddot{\boldsymbol{q}} + \mathbf{C}_{\mathbf{q}}\dot{\boldsymbol{q}} + \mathbf{K}_q\boldsymbol{q} = \boldsymbol{\phi}^{\mathrm{T}}\boldsymbol{f} = \boldsymbol{f}_q, \end{gathered} \tag{2.37}$$

where

$$\mathbf{M}_q = \boldsymbol{\phi}^{\mathrm{T}}\mathbf{M}\boldsymbol{\phi}, \qquad \mathbf{C}_q = \boldsymbol{\phi}^{\mathrm{T}}\mathbf{C}\boldsymbol{\phi}, \qquad \mathbf{K}_q = \boldsymbol{\phi}^{\mathrm{T}}\mathbf{K}\boldsymbol{\phi}, \qquad \boldsymbol{f}_q = \boldsymbol{\phi}^{\mathrm{T}}\boldsymbol{f}. \tag{2.38}$$

The matrices $\mathbf{M}_q$, $\mathbf{C}_q$, $\mathbf{K}_q$ are known as the modal mass, damping and stiffness matrices, and $\boldsymbol{f}_q$ is the modal force vector. It may be shown that the modal mass and stiffness matrices are in fact diagonal (i.e. uncoupled), with diagonal elements equal to the modal mass m_j and modal stiffness k_j for the jth mode. This diagonalization occurs because the modes of vibration are 'orthogonal' with respect to the mass and stiffness matrices (Rao, 1995); this is an extremely useful feature, as will be illustrated later. The statement of orthogonality with respect to the mass matrix, for example, may be expressed as

$$\boldsymbol{X}_i^T\mathbf{M}\boldsymbol{X}_j = \begin{cases} 0, & i \neq j, \\ m_j, & i = j. \end{cases} \tag{2.39}$$

The properties of the modal damping matrix are less clear-cut. Provided that the physical damping matrix $\mathbf{C}$ can be written as a linear combination of the physical mass and stiffness matrices ($\mathbf{M}$, $\mathbf{K}$), as described above in Section 2.3.2, then the damping is *proportional* and the modal damping matrix $\mathbf{C}_q$ will also be diagonal. However, if the damping is *nonproportional*, then the modal damping matrix will include cross-coupling terms. At the initial analysis stage, it is normal to assume proportional damping so that the equations of motion expressed in 'modal space' in Equation (2.37) are in fact fully uncoupled.

The power of the modal transformation defined by Equation (2.36) may now be seen by writing out the modal equation of motion for the jth mode in Equation (2.37), with the assumption of proportional damping, so that

$$m_j \ddot{q}_j + c_j \dot{q}_j + k_j q_j = f_{qj}(t) \quad \text{for} \quad j = 1, 2, \ldots, N, \tag{2.40}$$

where m_j, c_j, k_j and f_{qj} are the modal mass, damping, stiffness and force for the jth mode. Using the SDoF concepts introduced in Chapter 1, the damping ratio for each mode is given by $\zeta_j = c_j/(2m_j\omega_j)$, where $\omega_j = \sqrt{k_j/m_j}$ is the jth mode natural frequency. The modal equation in nondimensional form is

$$\ddot{q}_j + 2\zeta_j\omega_j\dot{q}_j + \omega_j^2 q_j = \frac{f_{qj}(t)}{m_j} \quad \text{for } j = 1, 2, \ldots, N. \tag{2.41}$$

The coupled MDoF equations of motion originally derived in physical coordinates have now been expressed as a set of uncoupled single degree of freedom equations in modal coordinates. An MDoF system may therefore now be treated as a summation of SDoF systems. All the SDoF concepts (e.g. forced response) introduced in Chapter 1 may then be applied to each modal equation. Such a transformation will later be seen to be a fundamental part of the analysis approach used for aircraft aeroelasticity and loads calculations.

2.4.1 Example: Classical ‘Chain-like’ Two DoF System

To illustrate the transformation to modal coordinates, the classical two DoF system introduced earlier in Section 2.1.1 will be used, together with proportional damping defined by $\alpha = 0$ and $\beta = 0.002$, so $c_1 = 4$ and $c_2 = 2$ N s/m. The general physical forces f_1, f_2 will be included, without numerical values defined as yet. Firstly, the modal mass matrix defined in Equation (2.38) may be calculated as

$$\mathbf{M}_q = \boldsymbol{\phi}^{\mathrm{T}}\mathbf{M}\boldsymbol{\phi} = \begin{bmatrix} 0.5 & 1 \\ -1 & 1 \end{bmatrix}\begin{bmatrix} 2 & 0 \\ 0 & 1 \end{bmatrix}\begin{bmatrix} 0.5 & -1 \\ 1 & 1 \end{bmatrix} = \begin{bmatrix} 1.5 & 0 \\ 0 & 3 \end{bmatrix} \tag{2.42}$$

and it is clearly diagonal. Repeating this procedure for the modal damping and stiffness matrices yields

$$\mathbf{C}_q = \begin{bmatrix} 1.5 & 0 \\ 0 & 12 \end{bmatrix} \quad \text{and} \quad \mathbf{K}_q = \begin{bmatrix} 750 & 0 \\ 0 & 6000 \end{bmatrix}. \tag{2.43}$$

Also, the modal force vector is given by

$$\boldsymbol{f}_q = \boldsymbol{\phi}^{\mathrm{T}}\boldsymbol{f} = \begin{bmatrix} 0.5 & 1 \\ -1 & 1 \end{bmatrix}\begin{Bmatrix} f_1 \\ f_2 \end{Bmatrix} = \begin{Bmatrix} 0.5f_1 + f_2 \\ -f_1 + f_2 \end{Bmatrix} \tag{2.44}$$

Thus, writing out the two modal equations separately as illustrated in Equation (2.40) yields

$$\begin{aligned} 1.5\ddot{q}_1 + 1.5\dot{q}_1 + 750q_1 &= 0.5f_1(t) + f_2(t), \\ 3\ddot{q}_2 + 12\dot{q}_2 + 6000q_2 &= -f_1(t) + f_2(t). \end{aligned} \tag{2.45}$$

The coupled two DoF equations in physical coordinates have been transformed into uncoupled SDoF equations in modal coordinates. Each SDoF equation has the natural frequency for the corresponding undamped normal mode, with each mode having an effective damping ratio of $\zeta_j = c_j/(2m_j\omega_j)$, so $\zeta_1 = 0.022$ (i.e. 2.2 % critical) and $\zeta_2 = 0.045$. These results may be seen when running the MATLAB program in the companion website.

It is clear that values of force may be chosen to excite one or both modes; e.g. if the forces f_1, f_2 are equal then mode 1 can be excited but mode 2 will not be excited. This is in fact the principle of multiple exciter testing sometimes used to isolate and measure modes in the aircraft Ground Vibration Test (see Chapter 26).

2.4.2 Example: Two DoF Rigid Aircraft with Proportional Damping

In this example, even though the physical coordinates are mixed translation and rotation, the transformation to modal coordinates is still possible. If damping is again proportional, defined by $\alpha = 0$ and $\beta = 0.01$, then $C_{\mathrm{N}} = 400$ and $C_{\mathrm{M}} = 1200$ Ns/m, as described earlier. The tail force is applied at $l_{\mathrm{T}} = 6$ m. After performing the modal transformation, the two modal equations may be shown to be

$$\begin{aligned} 4219\ddot{q}_1 + 1631\dot{q}_1 + 163\,060 q_1 &= 0.81 f(t), \\ 12\,657\ddot{q}_2 + 8187\dot{q}_2 + 818\,670 q_2 &= -5.595 f(t). \end{aligned} \tag{2.46}$$

The natural frequencies are 0.989 and 1.280 Hz, with modal dampings $\zeta_1 = 0.031$ and $\zeta_2 = 0.040$.

2.4.3 Example: Two DoF Rigid Aircraft with Nonproportional Damping

Pre- and post-multiplying the nonproportional damping matrix (equation 2.34) by the modal matrix gives

$$\mathbf{C}_q = \begin{bmatrix} 1715 & -810 \\ -810 & 15\,949 \end{bmatrix}, \tag{2.47}$$

so clearly, although the mass and stiffness matrices would be diagonalized as for the proportional case above, the resulting modal damping matrix is not diagonal. Thus the equations of motion in modal space become

$$\begin{aligned} 4219\ddot{q}_1 + 1715\dot{q}_1 - 810\dot{q}_2 + 163\,060 q_1 &= 0.81 f(t), \\ 12\,657\ddot{q}_2 - 810\dot{q}_1 + 15\,949\dot{q}_2 + 818\,670 q_2 &= -5.595 f(t). \end{aligned} \tag{2.48}$$

Modal damping cross-coupling terms are now present, thus implying that excitation of one mode causes a response in the other. Clearly, the equations have not been uncoupled using the classical normal mode transformation; it is only possible to generate uncoupled equations using the first order form (Tse *et al.*, 1978).

2.4.4 Mode Shape Normalization

Note that it is important to recognize that the values of modal mass, and therefore modal damping, stiffness and force, depend upon the normalization used in defining the modal matrix. Thus, for example, modal mass does not have a unique value and the statement ‘this mode has a high modal mass’ needs qualifying; it is quite meaningless unless the mode shape normalization employed when generating the modal mass is also defined. However, provided the definitions used are consistent throughout the analysis, it does not matter what normalization is used and the same final result will emerge for, say, the response to an excitation.

Common normalization approaches for mode shapes are:

- mode shape normalized so as to generate a unit modal mass (‘mass normalized’ mode shape),
- mode shape normalized to a maximum value of unity or
- mode shape normalized such that the vector norm is unity.

In the above two examples, the modal quantities correspond to the mode shapes normalized to a maximum value of unity. However, if, for example, the first mode for the aircraft system was to be defined by a unit modal mass, then the mode shape vector $\{1 \quad 0.135\}^{\mathrm{T}}$ would need to be multiplied by $1/\sqrt{4219}$, the square root appearing because the mode shape appears twice in the modal mass calculation.

2.4.5 Meaning of Modal Coordinates

At this point, it is helpful to consider the physical meaning of modal (or principal) coordinates. The coordinate q_j indicates the amount of the *j*th mode present in the motion. In the example of the aircraft, q_1 describes the dominantly heave mode while q_2 describes the pitch mode. Thus it is not possible to place a transducer on the system and measure a modal coordinate – it defines a characteristic 'shape' and the absolute value of the coordinate in any given response depends upon the mode shape normalization employed.

2.4.6 Dimensions of Modal Coordinates

2.4.6.1 Consistent coordinates

The units of mode shapes, modal coordinates and other modal quantities are interesting to consider as they can cause confusion. Consider first the chain-like two DoF system, where all the coordinates have the same dimensions. It is sensible to think of the mode shape vectors as being dimensionless since they have no absolute values; the consequence of this choice is that the modal mass has dimensions of mass (kg), the modal coordinates have dimensions of displacement (m) and the modal equation is then a force equation (N). If, instead, the mode shapes were taken as having displacement units, then the modal coordinates would be dimensionless, modal mass would be in kg m^2 and the equation would be in terms of moments; this is not consistent with a classical description of the terms, so the former approach is preferable.

2.4.6.2 Mixed coordinates

However, the position is less clear when considering the aircraft example where the mode shapes have mixed (i.e. both translational and rotational) coordinates. In order for the modal transformation and the modal equation to be dimensionally consistent and produce a modal mass in kg and modal force in N, the mode shapes will need to be treated rather differently to the earlier consistent coordinate case. In fact, the mode shape vector needs to be nondimensionalized in some way, and since it cannot be nondimensionalized independently in both displacement and rotation, it is normalized to, say, 1 m, and so the mode 2 vector is $\{-0.405 \quad 1\ \mathrm{rad/m}\}^{\mathrm{T}}$. Thus only the displacement term has been made dimensionless; when modal equations are considered, the dimensions are consistent with the simpler system.

2.4.7 Model Order Reduction

A further benefit in working in modal coordinates for systems with a large number of DoF (and therefore many modes of vibration) is that it allows the number of modes included in a solution to be considerably reduced. The frequency range of interest is limited and so it may be advantageous to reduce the scale of the analysis by only considering a subset of the modes in the modal transformation. By reducing the number of modes, the residual effect of higher frequency modes would be omitted, so it is normal to include modes with natural frequencies somewhat higher than the maximum frequency of interest to make some allowance for this effect. Consider only including $n\ (< N)$ of the modes; therefore $\boldsymbol{\Phi}_n = [\boldsymbol{X}_1 \boldsymbol{X}_2 \cdots \boldsymbol{X}_n]$ would be the reduced modal matrix and the transformation to the reduced set of principal coordinates would be

$$\boldsymbol{x} = \boldsymbol{\Phi}_n \boldsymbol{q}_n. \tag{2.49}$$

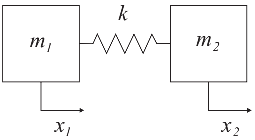

Figure 2.4 Two degree of freedom free–free system.

Thus the final set of transformed equations would simply be reduced to n instead of N SDoF equations. For example, a system with 200 000 (N) physical degrees of freedom from a finite element analysis (see Chapter 4) could be analysed using only 20 (n) modal equations.

2.5 'FREE–FREE' SYSTEMS

A 'free–free' system is one that is not connected to 'earth' via any support stiffness, i.e. it is effectively freely floating in space. An aircraft in flight is a typical example of a free–free system and it is therefore important to recognize the particular features of such systems. Consider the simple chain-like two DoF system in Figure 2.4.

The equations of motion may be shown to be given by

$$\begin{bmatrix} m_1 & 0 \\ 0 & m_2 \end{bmatrix} \begin{Bmatrix} \ddot{x}_1 \\ \ddot{x}_2 \end{Bmatrix} + \begin{bmatrix} k & -k \\ -k & k \end{bmatrix} \begin{Bmatrix} x_1 \\ x_2 \end{Bmatrix} = 0, \tag{2.50}$$

where the stiffness matrix is singular. Applying the usual method for calculating natural frequencies yields the quadratic equation

$$\omega^2[m_1 m_2 \omega^2 - k(m_1 + m_2)] = 0. \tag{2.51}$$

The natural frequencies of the two modes are $\omega_1 = 0$ and $\omega_2 = \sqrt{k(m_1 + m_2)/(m_1 m_2)}$. The first mode shape is $\{1 \quad 1\}^{\mathrm{T}}$, which is known as a 'rigid body' mode, with both masses moving together and having zero natural frequency. The second mode shape is $\{1 \quad -\mu\}^{\mathrm{T}}$, where $\mu = m_1/m_2$ is the mass ratio; this is a flexible mode with the two masses moving in opposite directions in such a way that there is no net inertia force acting on the system. For these mode shape normalizations, the two modal masses are $m_1 + m_2$, the total mass, and $m_1(1 + \mu)$ respectively. Similar features will be seen later in Chapter 3 when considering a free–free continuous system.

2.6 HARMONIC FORCED VIBRATION

The response to harmonic excitation may be determined via equations expressed in physical or modal coordinates using a similar approach to that in Chapter 1, except that matrix algebra is appropriate.

2.6.1 Equations in Physical Coordinates

In this section, the solution will be based upon the equations of motion expressed in physical coordinates. The similarity of the SDoF and MDoF expressions will be seen. The excitation and response are now column vectors and in complex algebra form are assumed to be

$$\boldsymbol{f}(t) = \boldsymbol{F}\mathrm{e}^{\mathrm{i}\omega t} \qquad \text{and} \qquad \boldsymbol{x}(t) = \tilde{\boldsymbol{X}}\mathrm{e}^{\mathrm{i}\omega t}, \tag{2.52}$$

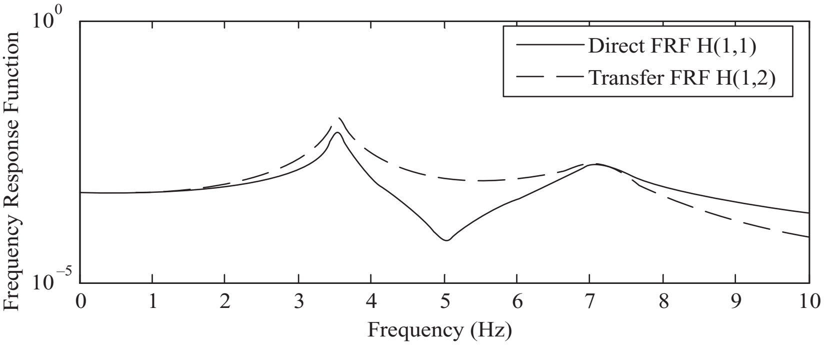

Figure 2.5 Sample driving point and transfer FRFs for the chain-like two DoF system.

where again $\sim$ indicates a complex quantity. The complex expressions in Equations (2.52) are now substituted into the equation of motion (2.8) and after cancelling the exponential term the result is

$$\left[-\omega^2\mathbf{M} + \mathrm{i}\omega\mathbf{C} + \mathbf{K}\right]\tilde{\boldsymbol{X}} = \boldsymbol{F}. \tag{2.53}$$

Thus the response may be solved using a matrix inverse operation so that

$$\tilde{\boldsymbol{X}} = [-\omega^2\mathbf{M} + \mathrm{i}\omega\mathbf{C} + \mathbf{K}]^{-1}\boldsymbol{F} \qquad \text{or} \qquad \tilde{\boldsymbol{X}} = \mathbf{H}(\omega)\boldsymbol{F}. \tag{2.54}$$

Here $\mathbf{H}(\omega)$ is the frequency response function (FRF) matrix, given by

$$\mathbf{H}(\omega) = \left[-\omega^2\mathbf{M} + \mathrm{i}\omega\mathbf{C} + \mathbf{K}\right]^{-1}, \tag{2.55}$$

where the matrix inversion must be carried out at every frequency of interest. A typical term in the FRF matrix $H_{kr}(\omega)$ is a complex quantity representing the modulus and phase of coordinate k when a unit harmonic force is applied at coordinate r at a frequency ω. The diagonal terms $H_{rr}(\omega)$ are known as direct or driving point FRFs whereas the off-diagonal terms $H_{kr}(\omega),\ k \neq r$, are transfer FRFs. Sample driving point and transfer FRFs are shown in Figure 2.5 for the two DoF chain-like system considered above. The direct FRF shows antiresonance behaviour (i.e. a trough) between each pair of modal peaks, which is characteristic for all systems; the transfer FRF behaviour depends upon the number of nodal points between the excitation and response positions. The phase behaviour could also be examined using the MATLAB program in the companion website.

2.6.2 Equations in Modal Coordinates

In Section 2.4, it was shown how a transformation to modal coordinates, based on the modal matrix, could yield uncoupled SDoF equations of motion provided the damping was proportional. With such uncoupled equations, a different approach to forced vibration is possible. Basically, the response of each mode may be determined from Equation (2.40) or (2.41) using the SDoF methods introduced in Chapter 1; the results can then be transformed back into physical coordinates using Equation (2.36). However, it is also possible to write the response vector and the FRF directly from the full set of modal equations defined in Equation (2.37) using a similar approach to that taken above in Section 2.6.1. Now, in addition to the physical force and response vectors defined in Equation (2.52) above, the modal response may be written as

$$\boldsymbol{q}(t) = \tilde{\boldsymbol{Q}}\mathrm{e}^{\mathrm{i}\omega t}. \tag{2.56}$$

Applying the methodology used in Section 2.6.1 to Equation (2.37) then an equation of similar form to Equation (2.54) will result and it may be seen that

$$\tilde{\boldsymbol{Q}} = [-\omega^2\mathbf{M}_q + \mathrm{i}\omega\mathbf{C}_q + \mathbf{K}_q]^{-1}\boldsymbol{\phi}^{\mathrm{T}}\boldsymbol{F}. \tag{2.57}$$

Transforming back to physical coordinates using Equation (2.36) then yields

$$\tilde{\boldsymbol{X}} = \boldsymbol{\phi}\tilde{\boldsymbol{Q}} = \boldsymbol{\phi}[-\omega^2\mathbf{M}_q + \mathrm{i}\omega\mathbf{C}_q + \mathbf{K}_q]^{-1}\boldsymbol{\phi}^{\mathrm{T}}\boldsymbol{F}, \tag{2.58}$$

so by inspection the FRF matrix in physical space is

$$\mathbf{H}(\omega) = \boldsymbol{\phi}[-\omega^2\mathbf{M}_p + \mathrm{i}\omega\mathbf{C}_p + \mathbf{K}_p]^{-1}\boldsymbol{\phi}^{\mathrm{T}}. \tag{2.59}$$

Note that if the damping is proportional, then the FRF matrix inverse in Equations (2.57) to (2.59) is straightforward to compute since the matrix is diagonal. The FRF matrix may then be calculated by a summation of the modal contributions and it may be shown that a typical [*k*,*r*] element of the matrix for an *N* DoF system is

$$H_{kr}(\omega) = \sum_{j=1}^{N} \frac{\Phi_{kj}\Phi_{rj}}{k_j - \omega^2 m_j + \mathrm{i}\omega c_j}, \tag{2.60}$$

where Φ_{kj} is the *j*th mode shape value at coordinate *k*. This expression is often used in curve fitting experimentally derived FRF data in ground vibration testing (see Chapter 13). The FRF numerator shows the importance of the mode shape at the excitation and response points in determining the contribution of a particular mode to the FRF; the denominator shows how each mode contributes to the resonant peaks.

2.7 TRANSIENT/RANDOM FORCED VIBRATION – TIME DOMAIN SOLUTION

In Chapter 1, the methods available for solution of the response to transient excitation for an SDoF system were discussed. In this section, the suitability of these methods for an MDoF system is considered briefly.

2.7.1 Analytical Approach

An analytical approach may still be used for the solution of the response of linear MDoF systems to transient excitation, provided the excitation has a relatively simple mathematical form such that a closed form solution is possible. In particular, when the damping is proportional, then the uncoupled SDoF modal equations may be used to solve for the response to transient excitation. For example, since the response to a step excitation is known for a linear SDoF system, then the modal response for each mode of an MDoF system to a step modal force may be determined and the results combined using the modal transformation in Equation (2.36).

2.7.2 Convolution Approach

Convolution for a linear SDoF system (see Chapter 1) may be extended to a linear MDoF system to relate the response vector $\boldsymbol{x}(t)$ to the excitation vector $\boldsymbol{f}(t)$ by using the matrix form of the convolution equation, namely

$$\boldsymbol{x}(t) = \int_{\tau=0}^{t} \mathbf{h}(t-\tau)\boldsymbol{f}(\tau)\,\mathrm{d}\tau, \tag{2.61}$$

where $\mathbf{h}(t)$ is the IRF (impulse response function) matrix, the inverse Fourier transform of the FRF matrix. A typical term in the IRF matrix is $h_{kr}(t)$, the response of the kth coordinate due to a unit impulse at the rth coordinate. The FRF and IRF matrices can also be calculated where aerodynamic terms are present.

2.7.3 Solution of ODEs

It is possible to solve the equations of motion for an MDoF system directly using a numerical integration approach as explained briefly in Chapter 1. The algorithms are adapted to handle response and excitation vectors instead of scalars. The approach is powerful and suitable for highly nonlinear systems, such as would be encountered when landing gear dynamics or flight control systems are present.

2.8 TRANSIENT FORCED VIBRATION – FREQUENCY DOMAIN SOLUTION

In Chapter 1, it was shown for an SDoF system that the response to a finite length general excitation input could be determined by a process based upon the Fourier transform (FT) and multiplication in the frequency domain. A similar approach is possible for an MDoF system, and potentially for a multiple input–multiple output (MIMO) system, except that the analysis needs to be expressed in matrix form and the FT of the excitation and response vectors are involved.

2.9 RANDOM FORCED VIBRATION – FREQUENCY DOMAIN SOLUTION

In Chapter 1, it was shown that the power spectral density (PSD) of the response of an SDoF system to a random excitation input could be determined using a spectral approach, with the response and excitation PSDs being related via the modulus squared value of the FRF. In the case of an MDoF system, multiple independent random sources may be applied simultaneously and a matrix spectral relationship would then be developed; however, in this book, such a case is not required. Since turbulence acts as a single excitation source, each response can be treated separately using the relevant MDoF FRF. Thus the PSD relationship is

$$S_{x_k x_k}(\omega) = |H_{ka}(\omega)|^2 \; S_{aa}(\omega), \quad k = 1, 2, \ldots, N, \tag{2.62}$$

where the kth response term is being considered, $H_{ka}(\omega)$ is the FRF relating the kth response to the source and $S_{aa}(\omega)$ is the source PSD. It may be seen that all the modes will be included in the response via the FRF.

2.10 EXAMPLES

Note that these examples may be useful preparation when carrying out the examples in later chapters.

1. For the two DoF lumped parameter system shown in Figure 2.6, determine (a) the equations of motion in matrix form, (b) the undamped natural frequencies and mode shapes, (c) the modal masses, (d) the modal dampings and (e) the modal stiffnesses. Write the uncoupled equations in modal space. Repeat the calculations using MATLAB (see companion website).

   [(a) $\mathbf{M} = \text{diag}[m \;\; m], \mathbf{K} = [2k \;\; -k; -k \;\; 2k]$, (b) $\omega_1 = \sqrt{k/m},\; \omega_2 = \sqrt{3k/m}$ and $\{1 \;\; 1\}, \{1 \;\; -1\}$, (c) $2m, 2m$, (d) $2c, 6c$, (e) $2k, 6k$]

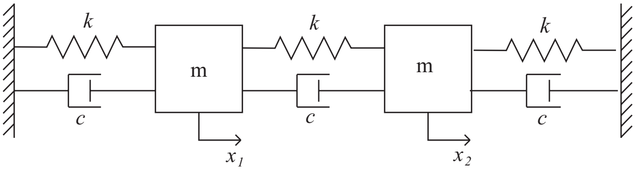

Figure 2.6

2. For the aircraft plus landing gear example investigated earlier in this chapter, obtain the equations of motion written in terms of the vertical displacements $z_{\mathrm{N}}, z_{\mathrm{M}}$ at the nose and main gears instead of z_{C}, θ. (Note that the pitch rotation will need to be written in terms of the displacements in order to obtain the kinetic energy of rotation.) For the parameter values used in the example, obtain the undamped natural frequencies and mode shapes and show that they are the same as those determined earlier. Determine the modal masses. Repeat the calculations using MATLAB.

   [$\mathbf{M} = [(I_y + ml_{\mathrm{M}}^2),\; (ml_{\mathrm{N}}l_{\mathrm{M}} - I_y);\; (ml_{\mathrm{N}}l_{\mathrm{M}} - I_y),\; (I_y + ml_{\mathrm{N}}^2)], \mathbf{K} = [K_{\mathrm{N}}(l_{\mathrm{N}} + l_{\mathrm{M}})^2,$ $0;\; 0,\; K_{\mathrm{M}}(l_{\mathrm{N}} + l_{\mathrm{M}})^2]$, 0.989 and 1.280 Hz, $\{0.4405 \;\; 1\}, \{1 \;\; -0.135\}$, 81 870, 16 310 kg]

3. An aerofoil section has a mass m and moment of inertia I_{O} about the point O, where it is supported in heave and pitch by a linear spring k and a rotational spring K respectively (see Figure 2.7). The centre of mass C is a distance e ahead of O. Determine the equations of motion for two coordinate sets (a) z_{C}, θ and (b) z_{O}, θ, where $z_{\mathrm{C,O}}$ are measured downwards from points C and O respectively and θ is the nose up pitch angle. Note the different types of coupling term in the equations of motion.

   [(a) stiffness coupled $\mathbf{M} = [m, 0;\; 0,\; (I_{\mathrm{O}} - me^2)], \mathbf{K} = [k,\; ke;\; ke,\; (K + ke^2)]$ and
   (b) inertia coupled $\mathbf{M} = [m,\; -me;\; -me,\; I_{\mathrm{O}}], \mathbf{K} = [k,\; 0;\; 0,\; K]$]

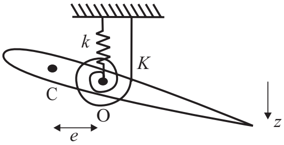

Figure 2.7

4. The system shown below in Figure 2.8 consists of two masses ($m = 1$ kg) mounted on a rigid member of length $3a$ ($a = 1$ m), supported by springs ($k = 1000$ N/m) and dampers ($c = 2$ N s/m). Determine (a) the equations of motion in matrix form, (b) the undamped natural frequencies and mode shapes,

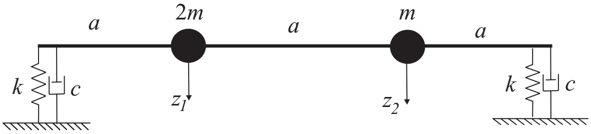

Figure 2.8

(c) the modal masses and (d) the modal damping ratios. Note that expressions need to be determined for the compressions of the springs in terms of $z_{1,2}$.

$[M = \text{diag}[2, 0; 0, 1]$ and $K = [5000, -4000; -4000, 5000]$, mode 1: 4.08 Hz, $\{1 \quad 0.921\}$, 2.848 kg, 0.0256, mode 2: 13.17 Hz, $\{1 \quad -2.171\}$, 6.713 kg, 0.0826]

5. For the system in Example 4, write down the modal equations. Then, ignoring damping, using a superposition of the modal responses, obtain an expression for the response of the system at point 1 due to (a) a 100 N step input at point 2 and (b) a sine input of 100 N at a frequency of 5 Hz (close to the resonance of mode 1). Results from Chapter 1 may be helpful.

$$[\text{(a) } z_1(t) = 0.0443 - 0.0492\cos 25.65t + 0.0047\cos 82.72t \text{ and}$$
$$\text{(b) } z_1(t) = 0.083\sin(31.4t + 32.1^\circ) - 0.0052\sin(31.4t - 20.1^\circ)]$$

6. For the system in Example 4 without damping, determine expressions for the FRFs H_{12}, H_{22} using both the (a) physical and (b) modal coordinate models. Sketch the amplitudes of these functions against frequency.
7. Describe how the analyses in Examples 5 and 6 would change for the case where modal damping is present in each mode. Sketch the changes in the responses and FRFs.
8. For the three DoF free–free system shown in Figure 2.9, with $m = 100$ kg and $k = 10\,000$ N/m, determine expressions for the undamped natural frequencies, mode shapes and modal masses.

[0, 1.591 and 2.757 Hz, $\{1 \quad 1 \quad 1\}$, $\{-1 \quad 0 \quad 1\}$, $\{-0.5 \quad 1 \quad -0.5\}$ and 300, 200 and 150 kg]

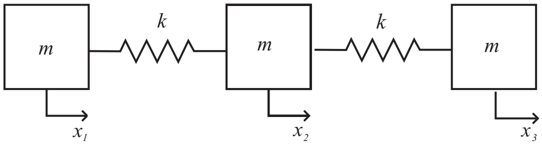

Figure 2.9

3

Vibration of Continuous Systems – Assumed Shapes Approach

In Chapters 1 and 2, some basic concepts were introduced for single and multiple DoF 'discrete parameter' systems, where motion was defined via displacement or rotation coordinates. However, for most problems encountered in aircraft aeroelasticity and loads, the systems are 'continuous', involving mass and stiffness properties distributed spatially over the system. An aircraft wing or fuselage may be considered as elastic continuum components able to bend and twist, but these require a different analysis approach.

There are several ways of modelling 'continuous' systems, namely:

(a) an exact approach using the partial differential equations of the system to achieve exact modes,

(b) an approximate approach using a series of assumed shapes to represent the deformation or

(c) an approximate approach using some form of spatial 'discretization'.

The exact approach is satisfactory for simple systems such as slender members under bending, torsional or axial deformation, but is impractical for 'real' systems with complex geometry. (The term 'slender member' is used here in place of the many terms often used to describe what are essentially similar members that experience different types of loading, namely beams, shafts, bars and rods. The term 'slender' implies that their length is significantly greater than their cross-section dimensions.)

In this chapter, the Rayleigh–Ritz approach for modelling a system using a series of assumed shapes will be introduced as a way of representing continuous systems with relatively simple geometries (e.g. uniform built-in wings). Also, special cases where the assumed shapes are in fact normal modes of the whole aircraft, or 'branch (normal) modes' of parts of the aircraft, will be considered. All these approaches will yield models of the system expressed in terms of so-called 'generalized', and not physical, coordinates; the generalized coordinates define the amount of each assumed shape present in the motion. Such models will be used to demonstrate the basic concepts of aeroelasticity and loads in Part II of the book, since by doing so the number and complexity of equations will be minimized to avoid obscuring the underlying principles. It will then be seen that the MDoF methods introduced in Chapter 2 may be employed to determine the vibration characteristics of the set of simultaneous ordinary differential equations in the unknown generalized coordinates.

Before progressing with the Rayleigh–Ritz analysis, the difficult issue of which appropriate symbols to use in expressing deformation will be discussed. It is normal in stress/structural analysis to consider the geometric position coordinate using the symbol z and the bending deformation using the symbol w. However, later in the book it will be seen that the symbol w is also used in the flight mechanics model to denote downwards velocity and the symbol w_g to denote the gust velocity. Also, in aeroelastic calculations, the symbol z is often used to describe the downwards deformation of the aircraft. It has therefore been

Introduction to Aircraft Aeroelasticity and Loads J. R. Wright and J. E. Cooper
© 2007 John Wiley & Sons, Ltd

decided to use a notation throughout that is more consistent with the aircraft usage. Therefore in this chapter and the next, the bending deformation will be denoted using the symbol z; the context of a particular analysis should clarify what is being considered in any given case. For convenience when comparing the Rayleigh–Ritz treatments given here with that in other books, the bending displacement will be considered as positive upwards. Later in Part II, when aeroelastic and loads models are considered, a downwards positive displacement will be used.

3.1 RAYLEIGH–RITZ 'ASSUMED SHAPES' METHOD

The Rayleigh–Ritz approach is used to represent the deformation of the system by a finite series of known assumed deformation shapes multiplied by unknown coefficients. The method (Tse *et al.*, 1978; Rao, 1995) was introduced when a practical approximate methodology was required in the absence of computers. It is an extension of Rayleigh's method (where only a single shape is employed).

3.1.1 One-Dimensional Systems

For a system where the deformation varies in only one dimension, the bending deformation $z(y, t)$ (see earlier remarks on notation) can be represented by the series

$$z(y,t) = \sum_{j=1}^{N} \psi_j(y)\, q_j(t), \tag{3.1}$$

where $\psi_j(y)$ is the jth assumed deformation shape (a function of y), $q_j(t)$ is the jth unknown coefficient (the 'generalized coordinate'), which is a function of time, and N is the number of terms in the series. The idea is that this combination of shapes represents the true deformation of the system as closely as possible, as shown in Figure 3.1 for $N = 2$. The more shapes used, the more accurate will be the approximation. Also, the degree to which the shapes satisfy the boundary conditions (see later) is important. If the assumed shapes are identical to the undamped normal mode shapes, then the generalized coordinate $q_j(t)$ is equivalent to the modal coordinate introduced in Chapter 2. The principle of assumed shapes is somewhat akin to using a Fourier series to represent a time signal by the summation of a series of sinusoids of different amplitude and phase.

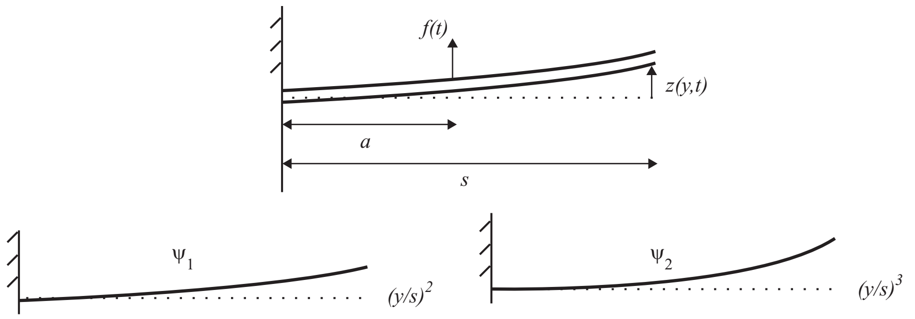

Figure 3.1 Deformation of a slender member in bending ($N = 2$): $z(y, t) = \psi_1(y)q_1(t) + \psi_2(y)q_2(t)$.

3.1.2 Two-Dimensional Systems

Where the deformation varies in two dimensions (e.g. a thin plate that can both bend and twist), the assumed shapes may be a product of functions that vary along each dimension, for example $\phi(x)\psi(y)$, or else a combined shape accounting for deformation in both coordinates simultaneously, for example $\chi(x, y)$.

3.1.3 Choice of Assumed Shapes

The assumed shapes are classically of polynomial, trigonometric or hyperbolic form. It is essential that each shape satisfies the geometric (or 'kinematic') boundary conditions of the system, e.g. no transverse deformation at a simple/built-in support and also no rotation at a built-in support. However, the accuracy of the representation will be improved if the shapes also satisfy the load (or natural) boundary conditions. For a slender member built in at one end and under bending, the load boundary conditions at the free end are zero curvature and zero rate of change of curvature (i.e. zero bending moment and shear force); for the torsion case, the load boundary condition is a zero rate of twist (i.e. zero torque) at the free end. A better choice of shapes implies that fewer terms are required for the same accuracy. However, whereas the kinematic boundary conditions are relatively simple to satisfy, it is much more difficult to satisfy the natural boundary condition.

The choice of shapes is better served by example than by attempting to generalize further. However, because the aim in this book is simply to generate systems with a small number of equations that may be used to demonstrate aircraft aeroelasticity and load concepts, only simple polynomial assumed shapes will be employed. It is recognized that the results will be less accurate than if more terms in the series, and better shapes, were to be used.

Having defined the assumed shapes, an energy principle is employed to minimize the error in the approximation and so generate equations in the unknown generalized coordinates; Lagrange's equations will be used again.

3.1.4 Normal Modes for a Continuous System

When a continuous system is considered, then theoretically there are a near-infinite number of normal modes, with each mode defined by a continuous mode shape and having its own natural frequency, damping ratio and modal mass. When using a finite number *N* of assumed shapes, then the analysis will yield estimates of *N* normal modes, with the accuracy being superior for the lower frequency modes.

3.2 GENERALIZED EQUATIONS OF MOTION – BASIC APPROACH

In this section, an analysis will be performed for a uniform built-in member (or 'wing') under bending or torsional vibration, with one or two simple polynomial terms used in the series. Results will be compared to those from an exact analysis. Later, the use of matrix algebra to set up the equations will be shown. It should be recognized that when only a single shape is used, the method is actually Rayleigh's method.

3.2.1 Built-in Member in Bending – Single Assumed Shape

The member shown in Figure 3.1 has length s, mass per length μ, material Young's modulus E and relevant section second moment of area for vertical bending I (sometimes incorrectly termed the second moment of inertia). The product *EI* is known as the flexural rigidity. A force *f*(*t*) is applied at position

$y = a$ as shown. No damping is included. Firstly, only one term in the series will be chosen and the polynomial will be a simple quadratic function, namely

$$z(y,t) = \psi(y)\, q(t) = \left(\frac{y}{s}\right)^2 q(t). \tag{3.2}$$

This function is shown in Figure 3.1 and satisfies the requirement for zero displacement and zero slope/rotation at the clamped end (i.e. the kinematic boundary condition) but not the load boundary condition at the free end (because the curvature there is finite, not zero). In this case, it may be seen that the assumed shape has been chosen to be dimensionless, so the generalized coordinate has dimensions of displacement.

The use of Lagrange's equations, as described in Chapters 1 and 2, requires various energy and work terms to be determined for discrete systems, but in this continuous case the quantities need to be found by integration over the member. The kinetic energy dT for an element of length dy and mass $\mu\,\mathrm{d}y$ is

$$\mathrm{d}T = \tfrac{1}{2}(\mu\,\mathrm{d}y)\dot{z}^2 \tag{3.3}$$

and the kinetic energy T is calculated by summing up (i.e. integrating) the elemental energies; thus

$$T = \tfrac{1}{2}\int_0^s \mu\,\dot{z}^2 \mathrm{d}y. \tag{3.4}$$

Substituting the expression for $z(y,t)$ from Equation (3.2) into Equation (3.4) and performing the integration yields

$$T = \frac{1}{2}\int_0^s \mu \left[\left(\frac{y}{s}\right)^2 \dot{q}\right]^2 \mathrm{d}y = \frac{\mu\, s}{10}\dot{q}^2. \tag{3.5}$$

The strain energy in bending depends upon the curvature and flexural rigidity (Benham *et al.*, 1996) and is

$$U = \frac{1}{2}\int_0^s EI \left(\frac{\partial^2 z}{\partial y^2}\right)^2 \mathrm{d}y. \tag{3.6}$$

Thus, substituting the expression for $z(y,t)$ from Equation (3.2) into Equation (3.6) and integrating yields the strain energy

$$U = \frac{1}{2}\int_0^s EI \left(\frac{2}{s^2}\, q\right)^2 \mathrm{d}y = \frac{2EI}{s^3} q^2. \tag{3.7}$$

Finally, the work done by the applied force moving through an incremental displacement δz at $y = a$ will be

$$\delta W = f(t)\ \delta z(a,t) = f(t)\ \left(\frac{a}{s}\right)^2 \delta q, \tag{3.8}$$

where it should be noted that the incremental physical displacement may be expressed in terms of an increment δq in the generalized coordinate. The effectiveness of the force depends upon the value of the assumed shape at the point of application; e.g. applying a force at a nodal point will have no effect.

Taking Lagrange's equation (see Chapters 1 and 2), rewritten in terms of generalized coordinates q_j,

$$\frac{\mathrm{d}}{\mathrm{d}t}\left(\frac{\partial T}{\partial \dot{q}_j}\right) - \frac{\partial T}{\partial q_j} + \frac{\partial \Im}{\partial \dot{q}_j} + \frac{\partial U}{\partial q_j} = Q_j = \frac{\partial(\delta W)}{\partial(\delta q_j)} \quad \text{for } j = 1, 2, \ldots, N, \tag{3.9}$$

and substituting the energy and work expressions for the single generalized coordinate $q(t)$ $(N = 1)$ yields

$$\frac{\mu s}{5}\ddot{q} + \frac{4EI}{s^3}q = \left(\frac{a}{s}\right)^2 f(t) \tag{3.10}$$

By inspection of this SDoF equation (see Chapter 1), the undamped natural frequency is given by

$$\omega = 4.47\sqrt{\frac{EI}{\mu s^4}} \tag{3.11}$$

This is an overestimate by 27 % on the exact value of $3.516\sqrt{EI/(\mu s^4)}$ (Rao, 1995), the difference occurring because the member is effectively constrained (or forced) into the assumed shape (i.e. by not satisfying the tip load boundary conditions) and so is over-stiff. Note that this assumed shape has led to an estimate of the lowest, or fundamental, natural frequency. One reason that this estimate is so much in error is that relatively small errors in the assumed shape can make a significant difference when differentiated twice within the strain energy expression. For a slender member problem, it can be shown (Thompson, 1997) that by evaluating the strain energy via the bending moment that corresponds to the distributed inertia loading the errors are much smaller. However, the standard approach adopted here is simpler to apply and using sufficient shapes will yield adequate results.

3.2.2 Built-in Member in Bending – Two Assumed Shapes

To show how the analysis changes and the accuracy improves, when more than a single shape is used, consider the expression for displacement of the member in bending with two assumed shapes, given by

$$z(y,t) = \psi_1(y)\, q_1(t) + \psi_2(y)\, q_2(t) = \left(\frac{y}{s}\right)^2 q_1(t) + \left(\frac{y}{s}\right)^3 q_2(t). \tag{3.12}$$

The second shape is now a cubic polynomial which also satisfies the kinematic boundary condition, as shown in Figure 3.1, but not the load condition. The energy and work done terms may be determined in a similar way to that in Section 3.2.1 above, but now there are two terms in the series. Thus the kinetic and strain energies are

$$\begin{aligned} T &= \frac{1}{2}\int_0^s \mu \left[\left(\frac{y}{s}\right)^2 \dot{q}_1 + \left(\frac{y}{s}\right)^3 \dot{q}_2\right]^2 \mathrm{d}y = \frac{\mu s}{10}\dot{q}_1^2 + \frac{\mu s}{14}\dot{q}_2^2 + \frac{\mu s}{6}\dot{q}_1\dot{q}_2 \\ &\text{and} \\ U &= \frac{1}{2}\int_0^s EI\left(\frac{2}{s^2}\, q_1 + \frac{6y}{s^3}q_2\right)^2 \mathrm{d}y = \frac{2EI}{s^3}q_1^2 + \frac{6EI}{s^3}q_2^2 + \frac{6EI}{s^3}q_1 q_2. \end{aligned} \tag{3.13}$$

The work done term is

$$\delta W = f(t)\ \delta z(a,t) = f(t)\ \left[\left(\frac{a}{s}\right)^2 \delta q_1 + \left(\frac{a}{s}\right)^3 \delta q_2\right], \tag{3.14}$$

where now increments in both generalized coordinates are required. Finally, applying Lagrange's equations for the generalized coordinates q_1 and q_2 ($N = 2$) yields the simultaneous equations of motion,

$$\begin{aligned}\frac{\mu s}{5}\ddot{q}_1 + \frac{\mu s}{6}\ddot{q}_2 + \frac{4EI}{s^3}q_1 + \frac{6EI}{s^3}q_2 &= \left(\frac{a}{s}\right)^2 f(t),\\ \frac{\mu s}{6}\ddot{q}_1 + \frac{\mu s}{7}\ddot{q}_2 + \frac{6EI}{s^3}q_1 + \frac{12EI}{s^3}q_2 &= \left(\frac{a}{s}\right)^3 f(t).\end{aligned} \tag{3.15}$$

Note that it is possible to perform the differentiations required by Lagrange's equations prior to carrying out the integrals for the kinetic and strain energies; this would reduce the amount of integration involved. This idea will be used later when the matrix approach is introduced. Equations (3.15) may be rewritten in matrix form as

$$\begin{bmatrix} \frac{\mu s}{5} & \frac{\mu s}{6} \\ \frac{\mu s}{6} & \frac{\mu s}{7} \end{bmatrix} \begin{Bmatrix} \ddot{q}_1 \\ \ddot{q}_2 \end{Bmatrix} + \begin{bmatrix} \frac{4EI}{s^3} & \frac{6EI}{s^3} \\ \frac{6EI}{s^3} & \frac{12EI}{s^3} \end{bmatrix} \begin{Bmatrix} q_1 \\ q_2 \end{Bmatrix} = \begin{Bmatrix} \left(\frac{a}{s}\right)^2 \\ \left(\frac{a}{s}\right)^3 \end{Bmatrix} f(t). \tag{3.16}$$

The equations are in the classical MDoF form shown in Chapter 2, with 'mass' and 'stiffness' matrices and a 'force' vector. However, in this case both the matrices are coupled; this would not be the case if the assumed shapes were identical to the normal mode shapes. Also, the 'mass' matrix, for example, is not a classical mass matrix since the generalized coordinates are multipliers of assumed shapes and not physical coordinates.

Using the approach introduced in Chapter 2 for determining the natural frequencies and undamped mode shapes, the natural frequencies predicted using this approximate method based on two simple shapes are

$$\omega_1 = 3.533\sqrt{\frac{EI}{\mu s^4}} \quad \text{and} \quad \omega_2 = 34.81\sqrt{\frac{EI}{\mu s^4}} \tag{3.17}$$

The frequency values in Equation (3.17) may be compared to the exact values of

$$\omega_{1_{\mathrm{Exact}}} = 3.516\sqrt{\frac{EI}{\mu s^4}} \quad \text{and} \quad \omega_{2_{\mathrm{Exact}}} = 22.03\sqrt{\frac{EI}{\mu s^4}} \tag{3.18}$$

The first natural frequency is now predicted much more accurately (only 0.5 % overestimated) because the combination of shapes approximate the true first mode shape more accurately; however, the second natural frequency is overestimated by 58 %. To improve this latter estimate would require further or better shapes; e.g. including a quartic shape would yield the second natural frequency to within 1 % error and a further quintic shape would give the third natural frequency to within 2.5 %. Note that the mode shapes for the first two bending modes of a built-in member are shown in Figure 3.2; these are

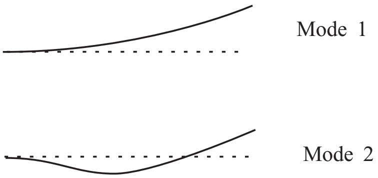

Figure 3.2 Mode shapes for the first two normal modes.

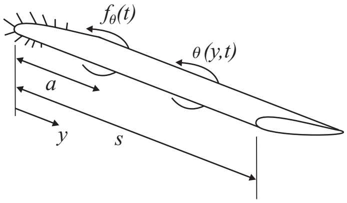

Figure 3.3 Slender member in torsion.

the modes estimated using the Rayleigh–Ritz approach. The number of nodal points (see Chapter 2) will increase with the mode number.

It can be seen that to obtain an estimate for the natural frequencies of a tapered built-in member would be fairly straightforward since all that would be required would be to include the mass per length μ and the flexural rigidity *EI* as functions of *y*/*s*, with the same assumed shapes being used. If the mass and/or stiffness properties varied along the member in a piecewise manner, this could be handled by piecewise integration. To obtain equivalent exact results using the partial differential equation approach for either of these nonuniform scenarios would be much more difficult.

3.2.3 Built-in Member in Torsion – One Assumed Shape

A related problem to bending is that of torsion, since commercial aircraft have high aspect ratio wings that have often been treated as slender members (or ‘sticks’) under combined bending and torsion. Later in the book, the importance of wing twist will become apparent, so an introduction to torsional vibration analysis is appropriate.

The uniform member in Figure 3.3, built in at one end, now has a moment of inertia in twist per unit length of χ and a torsional rigidity *GJ* (*G* is the material shear modulus and *J* is the section torsion constant, which is not equal to the polar second moment of area, as is sometimes incorrectly stated, except for the special case of a circular section). Here, the assumed shapes describe the twist $\theta(y,t)$, so for a single assumed shape then typically

$$\theta(y,t)=\gamma(y)q(t)=\left(\frac{y}{s}\right)\ q, \tag{3.19}$$

where a linear twist shape is assumed and q is effectively the tip twist. This shape satisfies the kinematic condition of zero twist at the root but not the load condition at the tip (zero torque and rate of twist $\mathrm{d}\theta/\mathrm{d}y$).

Given that the moment of inertia in torsion of an element d*y* is χ d*y*, the torsional kinetic energy is given by

$$T=\frac{1}{2}\int_0^s \chi\,\dot{\theta}^2\mathrm{d}y=\frac{1}{2}\int_0^s \chi\,\left(\frac{y}{s}\dot{q}\right)^2\mathrm{d}y=\frac{\chi s}{6}\dot{q}^2 \tag{3.20}$$

and the strain energy is (Benham *et al.*, 1996)

$$U=\frac{1}{2}\int_0^s GJ\left(\frac{\partial\theta}{\partial y}\right)^2\mathrm{d}y=\frac{1}{2}\int_0^s GJ\left(\frac{1}{s}q\right)^2\mathrm{d}y=\frac{GJ}{2s}q^2. \tag{3.21}$$

Finally, a torque of value $f_\theta(t)$ is to be applied at position $y = a$, so the incremental work done is

$$\delta W = f_\theta(t)\ \delta\theta(a) = f_\theta(t)\ \frac{a}{s}\delta q. \tag{3.22}$$

When Lagrange's equations are used, the equation of motion becomes

$$\frac{\chi s}{3}\ddot{q} + \frac{GJ}{s}q = \frac{a}{s}\ f_\theta(t). \tag{3.23}$$

The estimated natural frequency is therefore $1.73\sqrt{GJ/(\chi s^2)}$ and this value is a 10 % overestimate compared to the exact value of $1.57\sqrt{GJ/(\chi s^2)}$. Clearly, the application to more than one assumed shape is a straightforward extension and will improve the accuracy. Also, the analysis of a combined bending/torsion problem is possible, using both bending and torsion shapes, since the energy terms are scalar and therefore additive.

3.2.4 Flexural Axis and Shear Centre

In the above examples, bending and torsional vibrations were assumed to occur independently (i.e. be uncoupled). This means that the axis about which the bending displacement and twist were defined is the so-called flexural axis, the locus of the shear centres of each cross-section along the member. The shear centre is the point in the cross-section where a transverse (or shear) load causes no twist and a torque causes no bending (Megson, 1999). Also, for no coupling to occur, the mass and flexural axes must be coincident. If the member mass axis is offset from the flexural axis, then the bending and torsion motions will be coupled by inertia terms.

3.3 GENERALIZED EQUATIONS OF MOTION – MATRIX APPROACH

Having seen how the process works for more than one assumed shape, it is possible to approach the problem in a general form using matrix algebra. This approach is particularly useful when using large numbers of shapes or considering exact modal representations (see later). The idea will be illustrated for the one-dimensional slender member problem in bending with two assumed shapes, considered earlier in Section 3.2.2.

3.3.1 Representation of Deformation

Firstly, the assumed series expression must be written in matrix form, so

$$z(y,t) = \sum_{j=1}^{N} \psi_j(y)\ q_j(t) = \boldsymbol{\psi}^{\mathrm{T}}\boldsymbol{q} \quad \text{or} \quad \boldsymbol{q}^{\mathrm{T}}\boldsymbol{\psi},$$

where (3.24)

$$\boldsymbol{\psi}(y) = \{\psi_1(y)\ \psi_2(y)\ \cdots\ \psi_N(y)\}^{\mathrm{T}}, \qquad \boldsymbol{q}(t) = \{q_1(t)\ q_2(t)\ \cdots\ q_N(t)\}^{\mathrm{T}}.$$

Note that because $\boldsymbol{\psi}$ and $\boldsymbol{q}$ are column vectors and $z(y,t)$ is a scalar, the inner product of these vectors may be written in either order, as shown in Equation (3.24). In the above $N = 2$ example, these vectors will be given by

$$\boldsymbol{\psi} = \begin{Bmatrix} (y/s)^2 \\ (y/s)^3 \end{Bmatrix}, \qquad \boldsymbol{q} = \begin{Bmatrix} q_1 \\ q_2 \end{Bmatrix} \tag{3.25}$$

3.3.2 Kinetic Energy

The kinetic energy may now be written in matrix form as

$$T = \tfrac{1}{2}\int_0^s \mu\ \dot{z}^2 \mathrm{d}y = \tfrac{1}{2}\int_0^s \mu\,(\dot{\boldsymbol{q}}^{\mathrm{T}}\boldsymbol{\psi})(\boldsymbol{\psi}^{\mathrm{T}}\dot{\boldsymbol{q}})\,\mathrm{d}y,$$

so

$$T = \tfrac{1}{2}\dot{\boldsymbol{q}}^{\mathrm{T}}\left[\int_0^s \mu(\boldsymbol{\psi}\boldsymbol{\psi}^{\mathrm{T}})\ \mathrm{d}y\right]\ \dot{\boldsymbol{q}} = \tfrac{1}{2}\dot{\boldsymbol{q}}^{\mathrm{T}}\mathbf{M}_q\,\dot{\boldsymbol{q}}, \tag{3.26}$$

where the order of the vector products is chosen carefully so that the vectors of generalized coordinates may be taken outside the integral since they are not functions of *y*. Note that the expression for *T* is a quadratic form involving the generalized mass matrix $\mathbf{M}_q$. In the two shape notation, the kinetic energy would be given by

$$T = \frac{1}{2}\{\dot{q}_1 \quad \dot{q}_2\}\begin{bmatrix} \dfrac{\mu\,s}{5} & \dfrac{\mu\,s}{6} \\ \dfrac{\mu\,s}{6} & \dfrac{\mu\,s}{7} \end{bmatrix}\begin{Bmatrix} \dot{q}_1 \\ \dot{q}_2 \end{Bmatrix} \tag{3.27}$$

3.3.3 Strain Energy

The strain energy may be written in a similar way, involving the generalized stiffness matrix $\mathbf{K}_{q,}$ as

$$U = \frac{1}{2}\int_0^s EI\left(\frac{\partial^2 z}{\partial y^2}\right)^2 \mathrm{d}y = \frac{1}{2}\int_0^s EI(\boldsymbol{q}^{\mathrm{T}}\boldsymbol{\psi}'')(\boldsymbol{\psi}''^{\mathrm{T}}\boldsymbol{q})\,\mathrm{d}y,$$

so

$$\mathrm{U} = \frac{1}{2}\boldsymbol{q}^{\mathrm{T}}\left[\int_0^s EI(\boldsymbol{\psi}''\boldsymbol{\psi}''^{\mathrm{T}})\ \mathrm{d}y\right]\ \boldsymbol{q} = \frac{1}{2}\boldsymbol{q}^{\mathrm{T}}\mathbf{K}_{\mathbf{q}}\boldsymbol{q}, \tag{3.28}$$

where the dash notation – indicates partial differentiation with respect to *y*.

3.3.4 Incremental Work Done

The incremental work done for force *f*(*t*) applied at position $y = a$ is expressed as a vector inner product

$$\delta W = f(t)\ \delta z(a,t) = [\delta\boldsymbol{q}^{\mathrm{T}}\boldsymbol{\psi}(a)]\ \ f(t), \tag{3.29}$$

where $\boldsymbol{\psi}(a)$ is the shape vector at $y = a$. For the two assumed shape examples, $\boldsymbol{\psi}(a) = \{(a/s)^2\ (a/s)^3\}^{\mathrm{T}}$.

3.3.5 Differentiation of Lagrange's Equations in Matrix Form

Lagrange's equations may also be expressed in matrix form, namely

$$\frac{\mathrm{d}}{\mathrm{d}t}\left(\frac{\partial T}{\partial\dot{\boldsymbol{q}}}\right) - \frac{\partial T}{\partial\boldsymbol{q}} + \frac{\partial\Im}{\partial\dot{\boldsymbol{q}}} + \frac{\partial U}{\partial\boldsymbol{q}} = \boldsymbol{Q} = \frac{\partial(\delta W)}{\partial(\delta\boldsymbol{q})}, \tag{3.30}$$

and since energy and work terms are available in matrix form, an efficient approach is to use matrix differentiation rules (Graupe, 1972). Energy terms *E* (scalar) may be expressed in the quadratic form, namely $E = \boldsymbol{x}^{\mathrm{T}}\mathbf{A}\boldsymbol{x}$, and if $\mathbf{A}$ is symmetric then $\mathrm{d}E/\mathrm{d}\boldsymbol{x} = 2\mathbf{A}\boldsymbol{x}$. Work terms *W* (scalar) are in the inner product form $W = \boldsymbol{a}^{\mathrm{T}}\boldsymbol{x} = \boldsymbol{x}^{\mathrm{T}}\boldsymbol{a}$ and then $\mathrm{d}W/\mathrm{d}\boldsymbol{x} = \boldsymbol{a}$. These expressions may be proven by expanding into scalar form and carrying out the differentiations recognizing that, for example, $\mathrm{d}E/\mathrm{d}\boldsymbol{x} = \{\,\mathrm{d}E/\mathrm{d}x_1\ \ \mathrm{d}E/\mathrm{d}x_2\,\}^T$.

Following the rules of matrix differentiation for the kinetic and strain energies (quadratic form) and work terms (inner product), the *N* equations in matrix form for this slender member in bending are given by

$$\left[\int_0^s \mu\left(\boldsymbol{\psi}\boldsymbol{\psi}^{\mathrm{T}}\right)\mathrm{d}y\right]\ddot{\boldsymbol{q}} + \left[\int_0^s EI\left(\boldsymbol{\psi}''\boldsymbol{\psi}''^{\mathrm{T}}\right)\mathrm{d}y\right]\boldsymbol{q} = \boldsymbol{\psi}(a)\,f(t). \tag{3.31}$$

It should be noted that the integrals for a plate or other type of structure would differ but the principles would be the same. Equation (3.31) may then be written in the generalized matrix form

$$\mathbf{M}_q\,\ddot{\boldsymbol{q}} + \mathbf{K}_q\boldsymbol{q} = \boldsymbol{\psi}(a)\,f(t). \tag{3.32}$$

When the series with two assumed shapes is used, the result using this equation may be shown to be identical to that in Equation (3.16), the equations obtained by the longhand method. However, such a matrix approach is more compact and because the *N* by *N* matrices are symmetric, some integrals need not be calculated. If the chosen assumed shapes $\boldsymbol{\psi}$ corresponded to the *exact* normal mode shapes, which are orthogonal, then both the 'mass' and 'stiffness' matrices in Equation (3.32) would be diagonal since the generalized coordinates would in fact be the same as modal coordinates (see Chapter 2).

The remainder of this chapter addresses some of the issues encountered when analysing an aircraft structure made up of simple slender members.

3.4 GENERATING AIRCRAFT 'FREE–FREE' MODES FROM 'BRANCH' MODES

In some aircraft applications, the modes of vibration are determined from separate models of parts (or 'branches') of the structure, each constrained in some way as illustrated in Figure 3.4, e.g. wing with root built in. However, it is possible to 'free' such constraints in order to generate a model for a free–free (unconstrained) structure by effectively introducing additional rigid assumed shapes (i.e. effectively rigid body modes). The process is also known as component mode synthesis (Cook *et al.*, 1989), where the structure is divided into components or substructures.

Consider the simple example of an aircraft consisting of two uniform flexible wings of mass per length μ_{W} and flexural rigidity *EI*, plus a rigid fuselage of mass m_{F} as shown in Figure 3.5. The aircraft of mass *m* is assumed not to undergo any pitch motion so the wings only bend and the fuselage only heaves. Assume that the first two *exact* normal 'branch' mode shapes (subscript b), for a single wing constrained/built in at its root, are known and given by the functions $\psi_{\mathrm{b}1}$ and $\psi_{\mathrm{b}2}$.

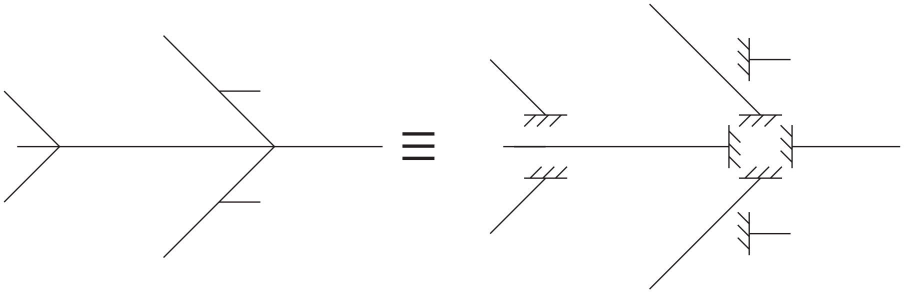

Figure 3.4 Aircraft 'branches'.

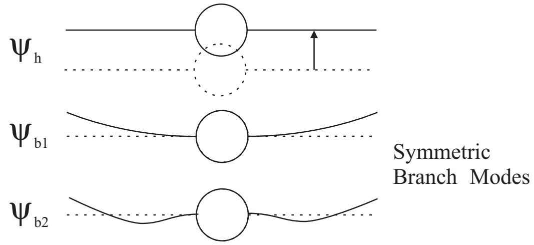

Figure 3.5 Aircraft with 'branch mode' representation for the wing.

In order to 'free' the aircraft so that it behaves as a free–free structure, and so be able to determine the equivalent free–free flexible modes, the constraints must be 'released'. This can be achieved by assuming that the displacement of the aircraft is a combination of the exact flexible branch modes $\psi_{\mathrm{b}1,2}$ and a rigid body heave assumed shape (or heave mode) ψ_{h}. Thus the assumed total displacement along the wing ($y \geq 0$) is given by

$$z(y,t) = \psi_{\mathrm{h}}(y) q_{\mathrm{h}}(t) + \psi_{\mathrm{b}1}(y) q_{\mathrm{b}1}(\mathrm{t}) + \psi_{\mathrm{b}2}(y) q_{\mathrm{b}2}(\mathrm{t}) \quad \text{where } \psi_{\mathrm{h}}(y) = 1 \tag{3.33}$$

and the constituent shapes are shown in Figure 3.5. Now, recognizing that the two wings move in-phase (if only symmetric modes are required) and that the fuselage width is ignored in the integrals, the total kinetic energy is

$$T_{\mathrm{Aircraft}} = T_{\mathrm{Wings}} + T_{\mathrm{Fuselage}}, \tag{3.34}$$

where

$$T_{\mathrm{Wings}} = 2\left(\frac{1}{2}\int_0^s \mu_{\mathrm{W}} \dot{z}^2 \,\mathrm{d}y\right) = 2\left[\frac{1}{2}\int_0^s \mu_{\mathrm{W}} (\psi_{\mathrm{h}}\dot{q}_{\mathrm{h}} + \psi_{\mathrm{b}1}\dot{q}_{\mathrm{b}1} + \psi_{\mathrm{b}2}\dot{q}_{\mathrm{b}2})^2 \,\mathrm{d}y\right], \tag{3.35}$$

$$T_{\mathrm{Fuselage}} = \frac{1}{2} m_{\mathrm{F}} \dot{z}(0)^2 = \frac{1}{2} m_{\mathrm{F}} \left(\psi_{\mathrm{h}}\dot{q}_{\mathrm{h}} + \psi_{\mathrm{b}1}(0)\dot{q}_{\mathrm{b}1} + \psi_{\mathrm{b}2}(0)\dot{q}_{\mathrm{b}2}\right)^2 = \frac{1}{2} m_{\mathrm{F}} \left(\psi_{\mathrm{h}}\dot{q}_{\mathrm{h}}\right)^2, \tag{3.36}$$

because the value of the branch mode shapes (built in at the root) is zero at $y = 0$. Also, since strain energy is only present in wing bending for this simple system then

$$U = 2\left(\frac{1}{2}\int_0^s EI z''^2 \,\mathrm{d}y\right) = 2\left[\frac{1}{2}\int_0^s EI(\psi_{\mathrm{h}}'' q_{\mathrm{h}} + \psi_{\mathrm{b}1}'' q_{\mathrm{b}1} + \psi_{\mathrm{b}2}'' q_{\mathrm{b}2})^2 \,\mathrm{d}y\right]. \tag{3.37}$$

Since the additional rigid shape has no elastic deformation, then $\psi_h'' = 0$, which will simplify the final expression. When Lagrange's equations are used, it may be shown that the generalised equations of motion are

$$\begin{bmatrix} m_{\mathrm{h}} & 2m_{\mathrm{hb}1} & 2m_{\mathrm{hb}2} \\ 2m_{\mathrm{hb}1} & 2m_{\mathrm{b}1} & 0 \\ 2m_{\mathrm{hb}2} & 0 & 2m_{\mathrm{b}2} \end{bmatrix} \begin{Bmatrix} \ddot{q}_{\mathrm{h}} \\ \ddot{q}_{\mathrm{b}1} \\ \ddot{q}_{\mathrm{b}2} \end{Bmatrix} + \begin{bmatrix} 0 & 0 & 0 \\ 0 & 2k_{\mathrm{b}1} & 0 \\ 0 & 0 & 2k_{\mathrm{b}2} \end{bmatrix} \begin{Bmatrix} q_{\mathrm{h}} \\ q_{\mathrm{b}1} \\ q_{\mathrm{b}2} \end{Bmatrix} = 0, \tag{3.38}$$

where

$$m_{\mathrm{h}} = m = m_{\mathrm{F}} + 2\mu_{\mathrm{W}} s, \qquad m_{\mathrm{hb}j} = \int_0^s \mu_{\mathrm{W}} \psi_{\mathrm{b}j} \mathrm{d}y, \qquad m_{\mathrm{b}j} = \int_0^s \mu_{\mathrm{W}} \psi_{\mathrm{b}j}^2 \mathrm{d}y \qquad \text{and}$$

$$k_{\mathrm{b}j} = \int_0^s EI \psi''^2_{\mathrm{b}j} \mathrm{d}y, \qquad j = 1, 2.$$

Firstly, it may be seen that there are no stiffness terms associated with the rigid shape as there is no corresponding strain energy (i.e. zero top left-hand corner term in the stiffness matrix). Then, because the branch mode shape $\psi_{\mathrm{b}j}$ is the exact *j*th normal mode shape for the built in wing, it should be noted that the terms $m_{\mathrm{b}j}$ and $k_{\mathrm{b}j}$ are in fact the modal mass and stiffness for the *j*th branch mode and so $k_{\mathrm{b}j} = \omega_{\mathrm{b}j}^2 m_{\mathrm{b}j}$, where $\omega_{\mathrm{b}j}$ is the natural frequency of the *j*th branch mode. The orthogonality of these modes means that there are no mass or stiffness cross-coupling terms between the branch modes as seen in Equation (3.38). However, there is an inertia coupling term $m_{\mathrm{hb}j}$ between the rigid body and the *j*th flexible branch mode; it is this coupling that enables the aircraft flexible motion to be 'released' and free–free modes produced.

If the eigenvalue solution of Equation (3.38) is carried out, then three generalized mode shapes will result, expressed as the proportion of each of the three constituent shapes. In this example, there will be one rigid body mode (with no contribution from the flexible branch modes) and two free–free flexible modes (involving flexible branch and rigid heave components). Note that the analysis approach may be extended to more modes, to include overall aircraft motions other than heave (e.g. pitch, roll), and also antisymmetric modes.

3.4.1 Example

Consider the above example with values of $m_{\mathrm{F}} = 1200$ kg, $\mu_{\mathrm{W}} = 50$ kg/m, $s = 6$ m and $EI = 500\,000$ Nm^2. However, in order to solve the eigenvalue problem in Equation (3.38), the exact mode shapes must be known for a continuous member built in at one end. From the exact partial differential equation analysis approach (Bishop and Johnson, 1979; Rao, 1995; Thomson, 1997), not covered in this book, it has been shown that for the built-in member of length s and mass per length μ_{W}, built in at one end, the *j*th mode natural frequency is given by

$$\omega_{\mathrm{b}j} = (\beta_j s)^2 \sqrt{\frac{EI}{\mu_{\mathrm{W}} s^4}}, \tag{3.39}$$

where for the first two modes $\beta_1 s = 1.875,\ \ \beta_2 s = 4.694$. The natural frequencies corresponding to the parameters chosen in this example are 1.55 and 9.74 Hz. The corresponding mode shapes (Bishop and Johnson, 1979) are given by

$$\psi_{\mathrm{b}j}(y) = (\cosh \beta_j y - \cos \beta_j y) - \sigma_j (\sinh \beta_j y - \sin \beta_j y), \tag{3.40}$$

where

$$\sigma_j = \cos \beta_j s + \cosh \beta_j s / \sin \beta_j s + \sinh \beta_j s.$$

The modal mass values for these mode shapes are given in Bishop and Johnson (1979) as $m_1 = m_2 = \mu_{\mathrm{W}} s$. Thus, knowing the branch mode natural frequencies, the modal stiffness values may be calculated. By integrating the mode shapes, the mass coupling terms may be shown to equal $m_{\mathrm{hb}1} = 0.734 \mu_{\mathrm{W}} s$, $m_{\mathrm{hb}2} = 1.018 \mu_{\mathrm{W}} s$.

Then, solving the eigenvalue problem based on Equation (3.38), the rigid body heave mode has a frequency of 0 Hz and generalized mode shape $\{1, 0, 0\}$. The natural frequencies of the two free–free elastic modes of the aircraft are 1.74 and 10.15 Hz and the generalized mode shapes are $\{-0.261, 1, -0.004\}$ and $\{-0.183, 0.147, 1\}$. These generalized mode shapes are the proportion of each of the three shapes in the series used; when the three shapes are weighted by these values, then the resulting free–free flexible mode shapes are sketched in Figure 3.6. When additional branch modes are added in, these frequencies barely alter.

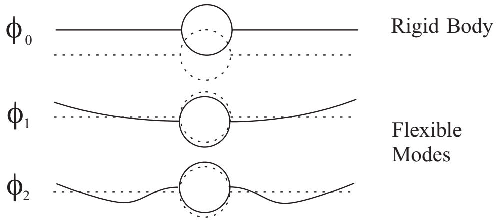

Figure 3.6 Aircraft 'free–free' mode shapes.

3.5 WHOLE AIRCRAFT 'FREE–FREE' MODES

In Section 3.4, it was shown that the branch modes for one or more built in components, such as a wing, could be combined with rigid body shapes for the whole aircraft to generate free–free rigid body and flexible modes for the combined system. In the approach used, the number of modes calculated for each branch was reduced, before combining with modes from the other branches and with the rigid body displacements, so as to generate the final solution, thus economizing on computing requirements. However, in practice nowadays, the aircraft is usually modelled as a whole using a discretization approach, such as the finite element method (see Chapter 4), and rigid body and free–free flexible modes are then produced for the whole aircraft in a single calculation.

In later parts of the book, simple whole aircraft flexible models composed of rigid body and free–free flexible modes will be used, particularly in manoeuvre and gust load calculations, to illustrate the effect of flexibility. In this section, the form of such models will be introduced.

Consider the 'stick' representation of a flexible aircraft shown in Figure 3.7, with only symmetric deformations shown for simplicity. However, this time the displacement will be expressed in matrix form as a summation of the whole free–free aircraft rigid body (subscript r) and flexible/elastic (subscript e) normal modes:

$$z(x, y, t) = \boldsymbol{\varphi}_{\mathrm{r}}^{\mathrm{T}} \boldsymbol{q}_{\mathrm{r}} + \boldsymbol{\varphi}_{\mathrm{e}}^{\mathrm{T}} \boldsymbol{q}_{\mathrm{e}} = \boldsymbol{\varphi}^{\mathrm{T}} \boldsymbol{q}, \tag{3.41}$$

where $\boldsymbol{\varphi}$ are normal mode shapes and $\boldsymbol{q}$ are generalized/modal coordinates; simple examples of the aircraft free–free modes were shown in Figure 3.6. Following the usual approach of writing the

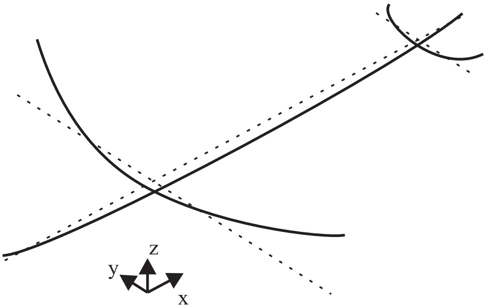

Figure 3.7 Flexible aircraft with free–free symmetric modes.

kinetic and strain energy terms and using Lagrange's equations, it may be shown that the equation of motion is

$$\begin{bmatrix} \mathbf{m}_\mathrm{r} & \mathbf{0} \\ \mathbf{0} & \mathbf{m}_\mathrm{e} \end{bmatrix} \begin{Bmatrix} \ddot{\boldsymbol{q}}_\mathrm{r} \\ \ddot{\boldsymbol{q}}_\mathrm{e} \end{Bmatrix} + \begin{bmatrix} \mathbf{0} & \mathbf{0} \\ \mathbf{0} & \mathbf{k}_\mathrm{e} \end{bmatrix} \begin{Bmatrix} \boldsymbol{q}_\mathrm{r} \\ \boldsymbol{q}_\mathrm{e} \end{Bmatrix} = \mathbf{0}, \tag{3.42}$$

where the modal mass matrices for the rigid body and flexible modes are given by

$$\mathbf{m}_\mathrm{r} = \int \boldsymbol{\varphi}_\mathrm{r}^\mathrm{T} \boldsymbol{\varphi}_\mathrm{r} \, \mathrm{d}m = \mathrm{diag}[m_{\mathrm{r}1}, m_{\mathrm{r}2} \ldots], \qquad \mathbf{m}_\mathrm{e} = \int \boldsymbol{\varphi}_\mathrm{e}^\mathrm{T} \boldsymbol{\varphi}_\mathrm{e} \, \mathrm{d}m = \mathrm{diag}[m_{\mathrm{e}1}, m_{\mathrm{e}2} \ldots] \tag{3.43}$$

and where integrations are taken over the entire aircraft. It should be noted that these modal mass matrices are diagonal and that the mass coupling terms seen for the branch mode analysis in Equation (3.38) are zero, because the rigid body and flexible modes are orthogonal. The modal stiffness matrix $\mathbf{k}_\mathrm{e}$ is also diagonal, being found from the modal mass and the modal frequencies; there is no rigid body modal stiffness.

As an example of such equations, consider an aircraft undergoing heave and pitch motion in two dimensions. If the rigid body free–free mode shapes are given by pure heave and pitch motion about the centre of mass, namely $\phi_{\mathrm{r}1} = 1$ and $\phi_{\mathrm{r}2} = -x$, it may be shown that the modal mass terms are equal to the aircraft mass m and pitch moment inertia I_y respectively (see Appendix A). Clearly, the corresponding generalized coordinates are equal to the vertical motion of the centre of mass and the nose up pitch angle, namely $q_{\mathrm{r}1} = z_\mathrm{C}$ and $q_{\mathrm{r}2} = \theta$. Adding a single flexible mode, governed by the generalized coordinate q_e (subscript e) with modal mass m_e and stiffness k_e, would then lead to the equations of motion (without aerodynamics present)

$$\begin{bmatrix} m & 0 & 0 \\ 0 & I_\mathrm{y} & 0 \\ 0 & 0 & m_\mathrm{e} \end{bmatrix} \begin{Bmatrix} \ddot{z}_\mathrm{C} \\ \ddot{\theta} \\ \ddot{q}_\mathrm{e} \end{Bmatrix} + \begin{bmatrix} 0 & 0 & 0 \\ 0 & 0 & 0 \\ 0 & 0 & k_\mathrm{e} \end{bmatrix} \begin{Bmatrix} z_\mathrm{C} \\ \theta \\ q_\mathrm{e} \end{Bmatrix} = 0. \tag{3.44}$$

This result, and others similar to it, will be used later in Part II of the book to show how the flexible aircraft may be treated when experiencing ground or flight manoeuvres, or when encountering gusts or turbulence.

3.6 EXAMPLES

Note that some of these examples may be useful preparation when carrying out the examples in later chapters.

1. A wing is idealized as a uniform slender member of semi-span s, mass per length μ and flexural rigidity EI, built in at one end. Find an expression for the natural frequency of the fundamental bending mode using each of the following assumed bending deformation shapes:

   (a) $z(y,t) = (1 - \cos \pi y/s)\, q(t)$ and (b) $z(y,t) = (y/s)^2 (3 - y/s) q(t)$.

   Compare the results with those for the basic quadratic shape and the exact result, both quoted earlier in this chapter. Consider how well these three assumed shapes satisfy the kinematic and load boundary conditions.

   [(a) $\omega = 5.70\sqrt{EI/(\mu s^4)}$ and (b) $\omega = 3.57\sqrt{EI/(\mu s^4)}$; cf. 4.47 for polynomial shape and 3.52 exact]

2. A wing is idealized as a uniform slender member of semi-span s, moment of inertia in twist per length χ and torsional rigidity GJ, built in at one end. Find an expression for the natural frequency of the

fundamental torsional mode using each of the following assumed torsional deformation shapes:

$$\text{(a)}\quad \theta(y,t)=\sin\left(\frac{\pi y}{2s}\right)q(t)\qquad \text{and}\qquad \text{(b)}\quad \theta(y,t)=(y/s)\left[3-(y/s)^2\right]q(t).$$

Compare the results with those for the basic linear shape and the exact result, both quoted earlier in this chapter. Consider how well these three assumed shapes satisfy the kinematic and load boundary conditions.

[(a) $1.571\sqrt{GJ/(\chi s^2)}$ and (b) $1.572\sqrt{GJ/(\chi s^2)}$; cf. 1.73 for linear shape and 1.571 exact]

3. For a uniform slender member of length s, moment of inertia in twist per length χ and torsional rigidity GJ, built in at one end, find an expression for the natural frequency of the fundamental torsional mode using a deformation with two assumed shapes, namely $\theta(y,t)=(y/s)\,q_1(t)+(y/s)^2\,q_2(t)$. Repeat the analysis using matrix algebra. Note that the eigenvalue calculation could be performed using the 'eig' MATLAB function once the symbols had been ignored (see Appendix A).

   [$1.576\sqrt{GJ/(\chi s^2)}$; cf. 1.571 exact]

4. An aircraft is idealized as a rigid fuselage of mass 1200 kg with two wings, each represented as a flexible member of mass per length 50 kg/m, length (or semi-span) 6 m and flexural rigidity 500 000 N m^2, built in at the fuselage. Assume that the series representation for the bending deformation of the wings is a combination of a rigid body heave and a flexible 'branch' shape, namely $z(y,t)=q_0(t)+(y/s)^2\,q_1(t)$. Obtain an estimate for the frequency of the free–free bending mode of the aircraft. If desired, the matrix form of analysis may be used. Note that the mass matrix is not diagonal because the assumed shape for the wing deformation is not a free–free mode shape and therefore is not orthogonal to the rigid body shape. Note also that the result may be compared to the example in Section 3.4 where exact mode shapes for the built-in member were used.

   [2.19 Hz; cf. 1.74 Hz when the exact built-in mode shape was used]

5. An unswept, rectangular wing has a semi-span s, chord c, bending rigidity EI and torsional rigidity GJ. The shear centre (centre of twist) and the mass centre lie at distances of $0.35c$ and $0.45c$ respectively aft of the leading edge. The mass per unit length of the wing is μ and the moment of inertia per unit length about a spanwise axis through the mass centre is $\chi=0.1\mu c^2$. Assuming that the wing is built in at one end and that the bending deflection z, measured from the flexural axis, and angle of twist ϑ (positive nose up) are given by $z(y,t)=(y/s)^2\,q_{\mathrm{b}}(t)$ and $\vartheta(y,t)=(y/s)\,q_{\mathrm{t}}(t)$, obtain the coupled equations of motion in generalized coordinates. For values of the parameters given by mass per length of 50 kg/m, semi-span 6 m, chord 1.2 m, torsional rigidity 240 000 N m^2 and flexural rigidity 500 000 N m^2, determine estimates for the first two natural frequencies. By noting the mode shape in generalized coordinates, indicate whether the modes are dominantly bending or torsion. Note that, as a check, the coupling term in the generalized mass matrix is $-0.1\,\mu cs/4$.

   [2.16 and 8.39 Hz with generalized mode shapes $\{1\ \ 0.045\}$ and $\{-0.16\ \ 1\}$]

6. Using Example 5, determine the expressions for the two generalized forces corresponding to a force F acting upwards on the leading edge at mid-span.

   [$Q_{\mathrm{b}}=F/4$ and $Q_{\mathrm{t}}=0.35Fc/2$]

7. A wing/tip store combination may be idealized as a uniform member, built in at one end, with an offset tip store (e.g. fuel tank). The wing has a mass per length of 75 kg/m, moment of inertia in twist per length 25 kg m^2/m, span 6 m, flexural rigidity 2×10^6 N m^2 and torsional rigidity 5×10^5 N m^2. The tip store has a mass of 100 kg and moment of inertia in pitch of 25 kg m^2 about its centre of mass, which itself is offset by 0.5 m forward of the wing centre line. Using simple quadratic bending and linear torsional assumed shapes, estimate the first two natural frequencies of the combination and sketch the expected mode shapes. Assume that the flexural and mass axes both lie along the mid-chord.

Note that the inertia coupling term will be given by tip mass × distance forward of the mid-chord = +50 kg m, with the sign depending upon the twist sign convention; a sign error will be shown by incorrect mode shapes.

[2.18 and 5.48 Hz]

8. An idealized wing structure built in at the root ($y = 0$) has a semi-span of $2L$ and the internal structure is such that the flexural stiffness is nonuniform, being $2EI_0$ for the inner half of the wing ($L > y \geq 0$) and EI_0 for the outer half ($2L \geq y > L$), whereas the mass per unit length μ is constant. Using two assumed shapes in the form of simple quadratic and cubic functions, determine the fundamental natural frequency and mode shape. Write down the additional terms that would need to be included in the analysis if a landing gear of stiffness K was positioned at mid-span?

   [$0.2\sqrt{EI_0/(\mu L^3)}$; mode shape in generalized coordinates $\{1, \quad -0.174\}$ and in physical coordinates $\{0.33$ at mid-span and 1 at the tip$\}$]

9. For a nonuniform tapering member, built in at one end, with mass per length and flexural stiffness distributions $\mu(y) = \mu_0\,(1 - y/s)$, $EI(y) = EI_0\,(1 - y/s)$, use a quadratic assumed shape to estimate the fundamental natural frequency in bending.

   [$3.87\sqrt{EI_0/(\mu_o s^3)}$]

4

Vibration of Continuous Systems – Discretization Approach

In Chapter 3 the vibration of continuous systems was considered using a summation of assumed shapes to describe the motion. The approximate analysis led to differential equations of motion expressed in terms of the unknown coefficients (or generalized coordinates) that multiply each assumed shape. Standard MDoF analysis approaches as described in Chapter 2 could then be employed to solve for natural frequencies, normal modes and the response to various forms of excitation.

In this chapter, the vibration of continuous systems will be approached using a physical discretization of the system, i.e. the structure is divided into finite width strips (or elements) and the motion of the structure is described via the displacements and rotations of the strips. An early approach to this discretization was using the flexibility influence coefficients (Rao, 1995), but this was superceded by the finite element (FE) approach (NAFEMS, 1987; Cook *et al.*, 1989; Rao, 1995). In this chapter, the FE method will be introduced, where the deformation within each strip (or so-called 'finite element') is approximated using a polynomial representation and the distributed stiffness and mass behaviour is represented by stiffness and mass matrices for each element. The FE approach will be illustrated upon simple slender 'beam-like' members (e.g. representing a wing or fuselage by a 'stick-like' model). Such approaches have been traditionally employed in the aerospace industry for high aspect ratio wings. However, it is now common practice to develop a more comprehensive finite element model of the structure (see later in this chapter and in Chapter 22 where the application of the finite element approach to more complex structural representations will be considered briefly); specialist texts and papers should be referenced for further detail. The move towards using the finite element method has been aided by the availability of many dedicated software packages.

4.1 INTRODUCTION TO THE FINITE ELEMENT (FE) APPROACH

The finite element (displacement) approach (NAFEMS, 1987; Cook *et al.*, 1989; Rao, 1995) is the most widely used method for static and dynamic theoretical modelling of aircraft structures, providing the basic equations involving mass and stiffness terms for both aeroelastic and loads calculations. The idea of the finite element (FE) method is to 'divide' the structure into so-called 'finite elements' (effectively strips when a wing is analysed as a beam), connected together at discrete points on the elements called 'nodes'. The displacements (and, where relevant, rotations) at the nodes become the unknowns for which the equations of motion are formulated, so the continuum structure is reduced to a discretized one with finite DoF. It is important to recognize that damping can be incorporated into an FE model but only as an approximation based on past experience or measured data.

Introduction to Aircraft Aeroelasticity and Loads J. R. Wright and J. E. Cooper
© 2007 John Wiley & Sons, Ltd

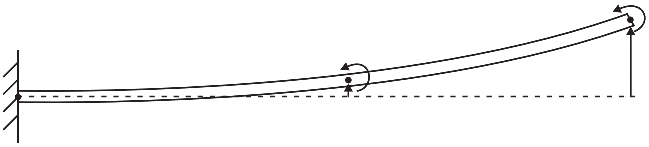

Figure 4.1 Built-in beam represented by two finite elements.

For typical commercial aircraft with high aspect ratio wings, there are two main approaches to FE modelling of the thin-walled box-like (or tube-like) nature of the major aircraft components (e.g. wing, fuselage):

- to represent each component by a 'beam-like' model using beam 'elements' of known bending, torsional and shear properties or
- to represent each component using a full structural model with membrane + bar or shell + beam elements, with the 'box-like' nature of the component (and relatively detailed load paths) retained.

However, in this chapter, for simplicity only the 'beam-like' representation will be discussed in any detail. An example of a beam represented by two beam finite elements joined at a node is shown in Figure 4.1; note that the term 'beam' is commonly used in FE theory, and in general refers to a member including bending, shear, axial and torsional effects. Later on in this chapter and in Chapter 22, the more comprehensive representation of the full structural model will be considered briefly, since this is current aircraft industry practice.

The FE solution approach is firstly to determine the dynamic properties of each element in the form of *element* stiffness and mass matrices and then to assemble all the elements to form *global* (or overall structure) mass and stiffness matrices from which modes and responses may be determined. The assembly process satisfies exact *compatibility* of displacements/rotations between elements (i.e. the nodes common to adjacent elements have the same displacements/rotations); however, *equilibrium* is normally only satisfied in an approximate manner over the entire structure except for very simple problems (such as the uniform beam under point loading) where there are no approximations.

The stiffness and mass matrices for each finite element are obtained by an energy approach, assuming a form for the displacement variation *within* the element. This is somewhat similar to the Rayleigh–Ritz approach, described in Chapter 3, except that in the latter the displacement variation over the *whole* structure is represented by a summation of assumed shapes. Thus the finite element methodology is rather like a 'piecewise' Rayleigh–Ritz approach, as illustrated in Figure 4.2, where three assumed shapes are compared with two finite elements, each having an assumed cubic displacement variation (see the next section). The advantages of the finite element method are that more elements may be used in regions where the displacement and/or stress is expected to vary more rapidly and that more complex geometries and problems may be handled.

4.2 FORMULATION OF THE BEAM BENDING ELEMENT

4.2.1 Stiffness and Mass Matrices for a Uniform Beam Element

For simplicity, bending in only one plane, with no shear deformation or torsion, is considered. A typical uniform beam element of length L, mass per unit length μ and flexural rigidity EI is shown in Figure 4.3. It should be noted that in this chapter, the bending deformation will again be denoted using the symbol z; the context of a particular analysis should clarify what is being considered in any given case.

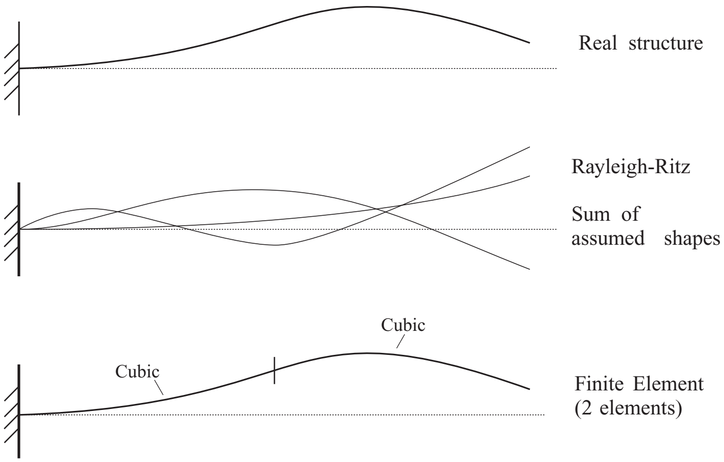

Figure 4.2 Complete versus piecewise displacement representation.

4.2.1.1 Element shape functions

The nodal 'displacements' (it is usually implied that some are rotations) are denoted by the vector $\boldsymbol{d} = \{d_1 \quad d_2 \quad d_3 \quad d_4\}^{\mathrm{T}}$. In order to write the strain energy and the kinetic energy terms for the element, the variation of displacement within the element will need to be expressed as a function of the nodal displacements. It is assumed that the variation of the transverse displacement $z(y)$ along the beam element is expressed as a cubic polynomial in y, namely

$$z = a_0 + a_1 y + a_2 y^2 + a_3 y^3, \tag{4.1}$$

where $a_0, \ldots, a_3$ are unknown coefficients that must be determined such that the assumed polynomial matches the nodal displacements at the ends $y = 0, L$. When the displacements and slopes at each end of the beam, determined from the polynomial, are equated to the nodal displacements $d_1, \ldots, d_4$, then the following equations are found:

$$\begin{aligned} &y = 0 \quad \textit{displacement} \quad d_1 = a_0, \\ &y = 0 \quad \textit{slope} \quad d_2 = a_1, \\ &y = L \quad \textit{displacement} \quad d_3 = a_0 + a_1 L + a_2 L^2 + a_3 L^3, \\ &y = L \quad \textit{slope} \quad d_4 = a_1 + 2a_2 L + 3a_3 L^2. \end{aligned} \tag{4.2}$$

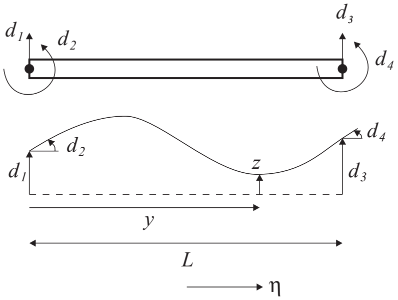

Figure 4.3 Two-node beam bending element.

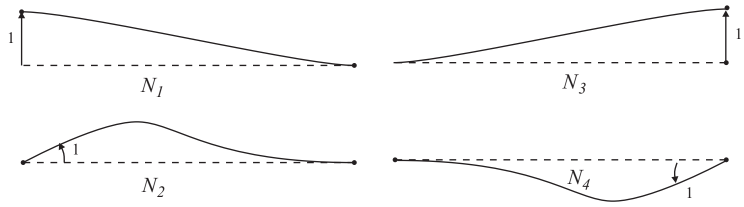

Figure 4.4 Shape functions for a two-node beam element.

Equations (4.2) may be solved to yield expressions for the polynomial coefficients $a_0, \ldots, a_3$ in terms of the nodal displacements $d_1, \ldots, d_4$. The final polynomial may then be written in the following form:

$$z = N_1 d_1 + N_2 d_2 + N_3 d_3 + N_4 d_4 = \boldsymbol{N}^{\mathrm{T}} \boldsymbol{d}, \tag{4.3}$$

where $\boldsymbol{N}$ is a column vector of the so-called 'shape functions' $N_1, \ldots, N_4$, each being a cubic polynomial in y. For example, it can be shown that the shape functions N_1, N_2 are given by the polynomials

$$N_1 = \frac{1}{4}(1-\eta)^2(2+\eta), \qquad N_2 = \frac{L}{8}(1-\eta)^2(1+\eta), \tag{4.4}$$

where $\eta = 2y/L \ (+1 \geq \eta \geq -1)$ is a nondimensional local coordinate commonly used in FE analysis (see Figure 4.3); the shape functions N_3, N_4 are very similar to N_1, N_2. The shape functions, shown in Figure 4.4, have distinctive shapes in that N_k is the polynomial corresponding to $d_k = 1$ and $d_j = 0$, $j \neq k$.

The fact that the displacement is assumed to vary as a cubic function of y along the element means that the bending moment (proportional to curvature), and therefore the bending stress, will vary linearly along the element. Thus in a complex problem, sufficient elements must be used to allow the exact stress variation along the beam to be represented reasonably well by a piecewise linear approximation. The accuracy of the FE method depends upon the number and type of elements used; e.g., the assumed polynomial is a quintic for the higher order three-node beam element.

4.2.1.2 Element equation of motion

In the FE representation, forces and moments may only be applied to the element at the nodes, as shown in Figure 4.5; these are termed nodal 'forces' (usually implied that some are moments) $\boldsymbol{P} = \{P_1 \quad P_2 \quad P_3 \quad P_4\}^{\mathrm{T}}$. The element equation relating nodal forces, displacements and accelerations will then be sought. The mass and stiffness matrices are known for each element and may be assembled for any structure of interest.

To determine the equation of motion for the beam element, Lagrange's equations may be used, with nodal displacements $\boldsymbol{d}$ acting as the coordinates, so ensuring that equilibrium applies on average over the element. The strain and kinetic energy terms are the same as those used in Chapter 3, but with the

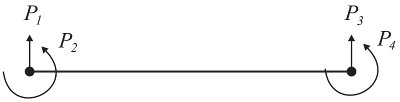

Figure 4.5 Nodal forces for a two-node beam element.

revised displacement description in Equation (4.3) being used. Thus the strain energy is

$$U = \frac{1}{2}\int_0^L EI\left(\frac{\partial^2 z}{\partial y^2}\right)^2 \mathrm{d}y = \frac{1}{2}\int_0^L EI(\boldsymbol{d}^{\mathrm{T}}\boldsymbol{N}'')(\boldsymbol{N}''^{\mathrm{T}}\boldsymbol{d})\,\mathrm{d}y, \quad \text{so} \quad U = \frac{1}{2}\boldsymbol{d}^{\mathrm{T}}\left[\int_0^L EI(\boldsymbol{N}''\boldsymbol{N}''^{\mathrm{T}})\,\mathrm{d}y\right]\boldsymbol{d}, \tag{4.5}$$

where the shorthand notation $'' = \partial/\partial y$ is used, and the kinetic energy is

$$T = \frac{1}{2}\int_0^L \mu\,\dot{z}^2\,\mathrm{d}y = \frac{1}{2}\int_0^L \mu(\dot{\boldsymbol{d}}^{\mathrm{T}}\boldsymbol{N})(\boldsymbol{N}^{\mathrm{T}}\dot{\boldsymbol{d}})\,\mathrm{d}y, \quad \text{so} \quad T = \frac{1}{2}\dot{\boldsymbol{d}}^{\mathrm{T}}\left[\int_0^L \mu(\boldsymbol{N}\boldsymbol{N}^{\mathrm{T}})\,\mathrm{d}y\right]\dot{\boldsymbol{d}} \tag{4.6}$$

Here the matrix approach introduced in Chapter 3 has been used. The incremental work done by the applied nodal forces acting through the nodal displacements will be given by

$$\delta W = P_1\delta d_1 + P_2\delta d_2 + P_3\delta d_3 + P_4\delta d_4 = \boldsymbol{P}^{\mathrm{T}}\boldsymbol{\delta d}. \tag{4.7}$$

When Lagrange's equations are employed, the differential equation of motion for the element may be written as

$$\mathbf{m}\ddot{\boldsymbol{d}} + \mathbf{k}\boldsymbol{d} = \boldsymbol{P}, \tag{4.8}$$

where **m**, **k** are the element mass and stiffness matrices respectively, given by

$$\mathbf{m} = \left[\int_0^L \mu(\boldsymbol{N}\boldsymbol{N}^{\mathrm{T}})\,\mathrm{d}y\right] \quad \text{and} \quad \mathbf{k} = \left[\int_0^L EI(\boldsymbol{N}''\boldsymbol{N}''^{\mathrm{T}})\,\mathrm{d}y\right]. \tag{4.9}$$

Note that the transformation from y to η would need to be carried out on these integrals. Introducing the relevant shape function polynomials $N_1, \ldots, N_4$ into Equations (4.9) and performing the matrix multiplications and integrations, it may be shown that, for a *uniform* beam element, these matrices are given by

$$\mathbf{m} = \frac{\mu L}{420}\begin{bmatrix} 156 & 22L & 54 & -13L \\ 22L & 4L^2 & 13L & -3L^2 \\ 54 & 13L & 156 & -22L \\ -13L & -3L^2 & -22L & 4L^2 \end{bmatrix}, \qquad \mathbf{k} = \frac{EI}{L^3}\begin{bmatrix} 12 & 6L & -12 & 6L \\ 6L & 4L^2 & -6L & 2L^2 \\ -12 & -6L & 12 & -6L \\ 6L & 2L^2 & -6L & 4L^2 \end{bmatrix}. \tag{4.10}$$

Here it may be seen that both the matrices are symmetric. The matrices quoted are only in this precise form provided that the ordering and sign convention of the element displacements and rotations are preserved. Clearly, a tapering beam element may be handled by using the nonuniform functions $\mu(y)$ and $EI(y)$; normally the integrations are performed numerically over η varying from -1 to $+1$.

This mass representation is known as a **'consistent'** mass matrix because it is the most accurate, matching the kinetic energy corresponding to the assumed deformation of the element. An alternative mass representation is the more simple **'lumped'** mass model, where for a two-node beam element, half the mass is 'lumped' at each node. The other rotational terms may be zero or else take on some intermediate value to allow for rotary inertia effects (Cook *et al.*, 1989). The lumped mass matrix is diagonal, namely

$$\mathbf{m}_{\text{Lumped\_No\_Rotary\_Inertia}} = \frac{\mu L}{24}\mathrm{diag}\begin{bmatrix} 12 & 0 & 12 & 0 \end{bmatrix}$$

or (4.11)

$$\mathbf{m}_{\text{Lumped\_Rotary\_Inertia}} = \frac{\mu L}{24}\mathrm{diag}\begin{bmatrix} 12 & L^2 & 12 & L^2 \end{bmatrix}.$$

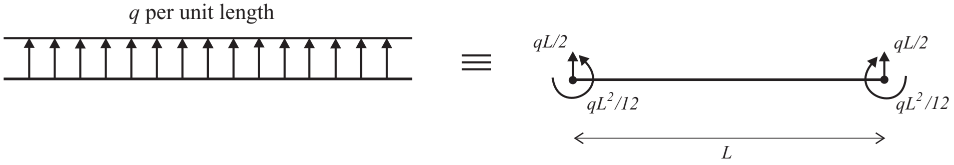

Figure 4.6 Kinematically equivalent nodal forces for a two-node beam element under distributed Loading.

However, although the consistent mass matrix is the rigorous approach to handling distributed inertia, it should be noted that when an aircraft component (such as a wing) is idealized using FE beam elements, then the masses will tend to be lumped at or offset from each node (see Chapter 22) and so are not consistent; by employing sufficient elements, the errors involved using this approximation will be considered small.

4.2.1.3 Kinematically equivalent nodal forces

When forces are distributed over the structure then, as part of the FE idealization, they need to be replaced by forces acting at the nodes themselves, usually called ‘kinematically equivalent nodal forces’. Such nodal forces are defined on the basis that they do equivalent work to the true distributed forces when the element experiences its assumed deformation. For the two-node beam element example, if a uniformly distributed force of q per length is applied over the element, as shown in Figure 4.6, then the distributed load needs to be represented by nodal loads acting at each node. The principle involved is that the distributed and nodal forces do the same work when acting through the assumed displacement variation for the element. The vector of so-called ‘kinematically equivalent nodal forces’ (Cook *et al.*, 1989) may be shown to be given by

$$\boldsymbol{P}_{\mathrm{KinEq}} = \frac{qL}{2}\left\{ 1 \quad \frac{L}{6} \quad 1 \quad -\frac{L}{6} \right\}^{\mathrm{T}}. \tag{4.12}$$

Similar equivalent nodal forces need to be determined to account for other effects distributed over the element, such as thermal loading, initial strains, etc. However, although the kinematically equivalent loading is the rigorous approach to handling distributed loading and will be considered further in Chapter 20, it should be noted that when an aircraft component (such as a wing) is idealized using FE beam elements, then the inertia and aerodynamic loads will tend to be added at each node (see Chapter 22) and so are not kinematically equivalent; by employing sufficient elements, the approximation will be considered as small.

4.3 ASSEMBLY AND SOLUTION FOR A STRUCTURE WITH BEAM ELEMENTS

Once the element mass and stiffness matrices have been determined for all the elements on the structure, the matrices may be assembled to generate the global mass and stiffness matrices for the entire structure. This process is automated when an FE package is employed, with the user providing the structure geometry, properties, boundary conditions, and the element type and topology (i.e. how the elements are interconnected).

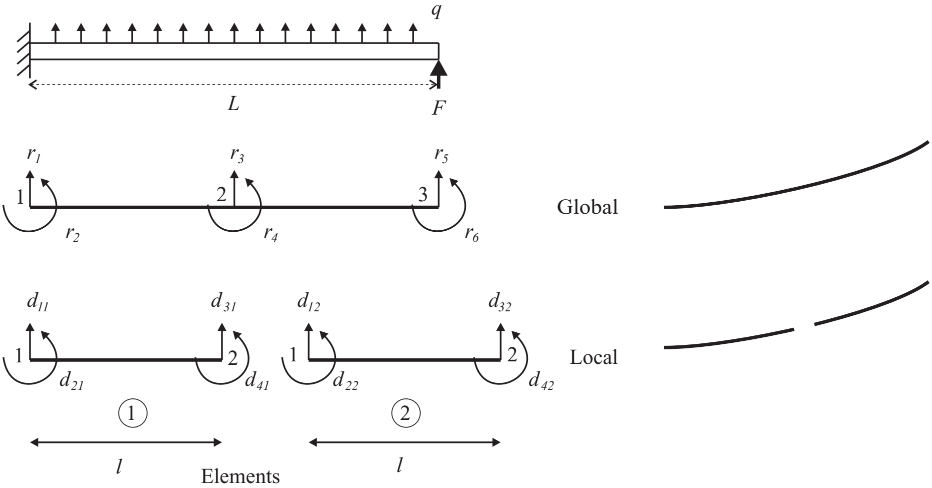

Figure 4.7 Built-in beam assembly with two elements.

4.3.1 Structure and Element Notation

At this introductory stage, the assembly process will be shown longhand using the two-element/three-node built-in beam example shown in Figure 4.7; the structure ('global') displacements at the three nodes are given by $\boldsymbol{r} = \{r_1, r_2, \ldots, r_6\}^{\mathrm{T}}$ and the structural forces by $\boldsymbol{R} = \{R_1, R_2, \ldots, R_6\}^{\mathrm{T}}$. The element ('local') nodal displacements are given by $\boldsymbol{d}_1, \boldsymbol{d}_2$, where the subscripts 1 and 2 refer to the two elements, and the element nodal force sets by $\boldsymbol{P}_1, \boldsymbol{P}_2$. The structure forces are either applied (e.g. applied point loads at nodes, distributed loads represented by kinematically equivalent nodal forces) or reactive (supplied via the supports). Note that nodal forces are a combination of external loads and the equal and opposite forces acting between the elements.

4.3.2 Imposing Compatibility

For *compatibility* of displacements between the assembled elements, the nodal displacements of all the elements meeting at a common node must be equal to each other, and for consistency must also equal the structure displacements at that node. Thus, referring to Figure 4.7, the displacements at nodes $\{1\ 2\}$ for elements 1 and 2 must map on to structure nodes $\{1\ 2\}$ and $\{2\ 3\}$ respectively, so

$$\begin{aligned} \{d_{11}\quad d_{21}\quad d_{31}\quad d_{41}\} &= \{r_1\quad r_2\quad r_3\quad r_4\} \quad \text{for element 1} \\ \{d_{12}\quad d_{22}\quad d_{32}\quad d_{42}\} &= \{r_3\quad r_4\quad r_5\quad r_6\} \quad \text{for element 2}, \end{aligned} \tag{4.13}$$

or, in matrix form,

$$\boldsymbol{d}_1 = \begin{Bmatrix} d_{11} \\ d_{21} \\ d_{31} \\ d_{41} \end{Bmatrix} = \begin{bmatrix} 1 & 0 & 0 & 0 & 0 & 0 \\ 0 & 1 & 0 & 0 & 0 & 0 \\ 0 & 0 & 1 & 0 & 0 & 0 \\ 0 & 0 & 0 & 1 & 0 & 0 \end{bmatrix} \begin{Bmatrix} r_1 \\ r_2 \\ r_3 \\ r_4 \\ r_5 \\ r_6 \end{Bmatrix} = \boldsymbol{\Gamma}_1 \boldsymbol{r}, \quad \boldsymbol{d}_2 = \begin{Bmatrix} d_{12} \\ d_{22} \\ d_{32} \\ d_{42} \end{Bmatrix} = \begin{bmatrix} 0 & 0 & 1 & 0 & 0 & 0 \\ 0 & 0 & 0 & 1 & 0 & 0 \\ 0 & 0 & 0 & 0 & 1 & 0 \\ 0 & 0 & 0 & 0 & 0 & 1 \end{bmatrix} \begin{Bmatrix} r_1 \\ r_2 \\ r_3 \\ r_4 \\ r_5 \\ r_6 \end{Bmatrix} = \boldsymbol{\Gamma}_2 \boldsymbol{r}. \tag{4.14}$$

The *j*th element 'maps' on to the structure via $\boldsymbol{d}_j = \boldsymbol{\Gamma}_j \boldsymbol{r}$, where $\boldsymbol{\Gamma}_j$, $j = 1, 2$, is the assembly matrix.

4.3.3 Assembly of the Global Stiffness Matrix – Imposing Equilibrium

The imposition of **equilibrium** at each structure node is essentially a statement that the structure force is 'shared' between the elements at that node and when combined with the element load/displacement relationships will yield the structure load/displacement relationship based on assembled element stiffness matrices. More formally, equilibrium is imposed because the incremental work done by the two equivalent sets of loads moving through the corresponding incremental displacements must be equal, so

$$\delta W = \boldsymbol{\delta r}^{\mathrm{T}} \boldsymbol{R} = \sum_{j=1}^{2} \boldsymbol{\delta d}_j^{\mathrm{T}} \boldsymbol{P}_j. \tag{4.15}$$

If the mass terms are ignored at this stage in order to simplify the equations, the relationship between the nodal forces and displacements for the two elements is

$$\boldsymbol{P}_j = \mathbf{k}_j \boldsymbol{d}_j \quad j = 1, 2, \tag{4.16}$$

where $\mathbf{k}_1, \mathbf{k}_2$ are the 4 × 4 element stiffness matrices derived earlier. What is being sought is the global force/displacement relationship for the structure, namely

$$\boldsymbol{R} = \mathbf{K}_r \boldsymbol{r}, \tag{4.17}$$

where $\mathbf{K}_r$ is the 6 × 6 structure stiffness matrix (prior to boundary conditions being imposed). Now, combining Equations (4.15) to (4.17) with the compatibility relationship in Equation (4.14), and simplifying, yields

$$\delta W = \boldsymbol{\delta r}^{\mathrm{T}} \mathbf{K}_r \boldsymbol{r} = \sum_{j=1}^{2} \delta(\boldsymbol{\Gamma}_j \boldsymbol{r})^{\mathrm{T}} (\mathbf{k}_j \boldsymbol{\Gamma}_j \boldsymbol{r}) = \boldsymbol{\delta r}^{\mathrm{T}} \left[\sum_{j=1}^{2} \boldsymbol{\Gamma}_j^{\mathrm{T}} \mathbf{k}_j \boldsymbol{\Gamma}_j \right] \boldsymbol{r}$$

and so

$$\mathbf{K}_r = \sum_{j=1}^{2} \boldsymbol{\Gamma}_j^{\mathrm{T}} \mathbf{k}_j \boldsymbol{\Gamma}_j. \tag{4.18}$$

In practice, the complete assembly matrices are not stored, and the matrix operation in Equation (4.18) is not actually carried out, because of the considerable number of zero values present in the assembly matrices. Instead, it may be seen that the effect of Equation (4.18) is that the element stiffness matrices are 'added into' the structure stiffness matrix in positions corresponding to the 'mapping' between the structure and element displacements, i.e. the so-called 'element topology' defined by the nonzero values in the assembly matrices.

4.3.4 Example of Stiffness Matrix Assembly for the Two-Element Beam

Consider the two-element example in Figure 4.7 with the length of *each* element being taken as l for convenience. Using the element stiffness matrix derived earlier in Equation (4.10) and substituting into the assembly Equation (4.18) yields the assembled 6 × 6 structure stiffness matrix

$$\mathbf{K}_r = \frac{EI}{l^3} \begin{bmatrix} 12 & 6l & -12 & 6l & 0 & 0 \\ 6l & 4l^2 & -6l & 2l^2 & 0 & 0 \\ -12 & -6l & 12+12 & -6l+6l & -12 & 6l \\ 6l & 2l^2 & -6l+6l & 4l^2 & -6l & 2l^2 \\ 0 & 0 & -12 & -6l & 12 & -6l \\ 0 & 0 & 6l & 2l^2 & -6l & 4l^2 \end{bmatrix}. \tag{4.19}$$

On careful examination, it may be seen that the first element stiffness matrix appears in rows/columns 1–4 and that the second element stiffness matrix is added into rows/columns 3–6; this matrix structure is defined by the assembly matrices. An equivalent result may be obtained for the assembled mass matrix.

4.3.5 Global Matrix Equation for the Assembled Structure

The mass matrix is included into the assembly process by adding the inertia terms from Equation (4.8) into Equation (4.16). The final equation of motion for the assembled elements in the structure is

$$\mathbf{M}_r\ddot{\boldsymbol{r}} + \mathbf{K}_r\boldsymbol{r} = \boldsymbol{R}, \tag{4.20}$$

where $\mathbf{M}_r$ is the structure mass matrix and $\boldsymbol{R}$ represents all the assembled external applied forces.

4.3.6 Solution Process

Once the structure mass and stiffness matrices have been assembled, the solution can proceed as follows:

(a) The 'boundary conditions' need to be defined (corresponding to zero or prescribed nodal displacements). Since the beam is built in at node 1, as shown in Figure 4.7, the boundary conditions are $r_1 = r_2 = 0$. The forces R_1, R_2 are the corresponding reaction forces required to prevent support movement.

(b) The applied loads need to be defined at unconstrained nodes 2 and 3. Loads may be applied directly at the nodes or be distributed over the structure, when the kinematically equivalent condition defines nodal forces.

(c) Once the boundary conditions and applied loads are defined, the solution of the structure equations of motion is best seen by partitioning the equation of motion in (4.20) so as to separate out the equations for reactions and those for unknown responses, namely

$$\begin{bmatrix} \mathbf{M}_{\mathrm{aa}} & \mathbf{M}_{\mathrm{ab}} \\ \mathbf{M}_{\mathrm{ba}} & \mathbf{M}_{\mathrm{bb}} \end{bmatrix} \begin{Bmatrix} \ddot{\boldsymbol{r}}_{\mathrm{a}} \\ \ddot{\boldsymbol{r}}_{\mathrm{b}} \end{Bmatrix} + \begin{bmatrix} \mathbf{K}_{\mathrm{aa}} & \mathbf{K}_{\mathrm{ab}} \\ \mathbf{K}_{\mathrm{ba}} & \mathbf{K}_{\mathrm{bb}} \end{bmatrix} \begin{Bmatrix} \boldsymbol{r}_{\mathrm{a}} \\ \boldsymbol{r}_{\mathrm{b}} \end{Bmatrix} = \begin{Bmatrix} \boldsymbol{R}_{\mathrm{a}} \\ \boldsymbol{R}_{\mathrm{b}} \end{Bmatrix}, \tag{4.21}$$

where a and b refer to the partitioned quantities. In this equation, $\boldsymbol{r}_{\mathrm{a}}$ are the known (or prescribed) support displacements (i.e. r_1, r_2 $(= 0)$ in the above example), $\boldsymbol{R}_{\mathrm{a}}$ are the corresponding unknown reactions at the supports (or the forces required to impose any prescribed displacements), $\boldsymbol{R}_{\mathrm{b}}$ are the known applied forces and $\boldsymbol{r}_{\mathrm{b}}$ are the corresponding unknown displacements. Once the partition has been defined, the solution can proceed. The second equation in Equation (4.21) may be written

$$\mathbf{M}_{\mathrm{ba}}\ddot{\boldsymbol{r}}_{\mathrm{a}} + \mathbf{M}_{\mathrm{bb}}\ddot{\boldsymbol{r}}_{\mathrm{b}} + \mathbf{K}_{\mathrm{ba}}\boldsymbol{r}_{\mathrm{a}} + \mathbf{K}_{\mathrm{bb}}\boldsymbol{r}_{\mathrm{b}} = \boldsymbol{R}_{\mathrm{b}} \tag{4.22}$$

and assuming that $\boldsymbol{r}_{\mathrm{a}} = \mathbf{0}$ (i.e. fixed support), then Equation (4.22) may be rewritten as

$$\mathbf{M}_{\mathrm{bb}}\ddot{\boldsymbol{r}}_{\mathrm{b}} + \mathbf{K}_{\mathrm{bb}}\boldsymbol{r}_{\mathrm{b}} = \boldsymbol{R}_{\mathrm{b}}, \tag{4.23}$$

where this is in essence a four DoF set of equations for this example. For a static problem where $\boldsymbol{R}_{\mathrm{b}}$ is known, then Equation (4.23) may be solved for the unknown displacements $\boldsymbol{r}_{\mathrm{b}}$. The result may then be substituted back into the first equation in Equation (4.21) in order to find the corresponding support reactions $\boldsymbol{R}_{\mathrm{a}}$ if required. If the applied load is time varying, then the dynamic response may be determined by solving the equations by numerical integration, for example. If there is no applied force, then the normal modes of the structure may be determined using classical matrix eigenvalue methods (see Chapter 2).

4.3.7 Examples of Solution for the Built-in Beam

Consider now the solution of the two-node built-in beam example used above in Figure 4.7 to illustrate the assembly process. Assume that the beam has length $s = 2l = 10$ m, flexural rigidity $EI = 4 \times 10^6$ N m^2 and mass per length $\mu = 100$ kg/m and that the elements have equal length $l = 5$ m. Two examples will be considered, namely a static load and a normal modes analysis. Increasing the number of elements will be considered. In both examples, the assembled stiffness matrix shown earlier in Equation (4.19) will be used.

4.3.7.1 Static loading analysis: two elements

Consider an applied force $F = 1000$ N acting upwards at the tip and a distributed load of $q = 100$ N/m acting over the entire length. Using the earlier result for kinematically equivalent loads, the applied force vector is

$$\boldsymbol{R}^{\mathrm{T}} = \left\{ R_1 \quad R_2 \quad 0 \quad 0 \quad F \quad 0 \right\} + \frac{ql}{2}\left\{ 1 \quad \frac{l}{6} \quad 1 \quad -\frac{l}{6} \quad 0 \quad 0 \right\} + \frac{ql}{2}\left\{ 0 \quad 0 \quad 1 \quad \frac{l}{6} \quad 1 \quad -\frac{l}{6} \right\}. \tag{4.24}$$

Here the first term in the expression is for the point loads, with R_1, R_2 being the unknown reactions, whereas the second and third terms are the kinematically equivalent forces for the two elements; the component of the distributed load at the support is ignored as it acts at a fixed point.

Once the equations are partitioned and boundary conditions imposed, the final load/displacement equation is

$$\mathbf{K}_{\mathrm{bb}}\boldsymbol{r}_{\mathrm{b}} = \boldsymbol{R}_{\mathrm{b}} \quad \text{or} \quad \frac{EI}{l^3}\begin{bmatrix} 12+12 & -6l+6l & -12 & 6l \\ -6l+6l & 4l^2 & -6l & 2l^2 \\ -12 & -6l & 12 & -6l \\ 6l & 2l^2 & -6l & 4l^2 \end{bmatrix}\begin{Bmatrix} r_3 \\ r_4 \\ r_5 \\ r_6 \end{Bmatrix} = \begin{Bmatrix} ql \\ 0 \\ F + ql/2 \\ -ql^2/12 \end{Bmatrix}. \tag{4.25}$$

Using the numerical parameter values leads to a value for tip displacement (r_5) of 32.7 mm, agreeing with the exact value. The theoretical displacement is a quartic function, matched well by the two cubic functions.

4.3.7.2 Normal modes analysis: two elements

The structure stiffness matrix may now be combined with the mass matrix to yield normal modes for the structure. Using Equation (4.10) and the assembly process to assemble the full structure mass matrix, and then partitioning it, yields the consistent mass matrix for the structure

$$\mathbf{M}_{\mathrm{bb}} = \frac{\mu l}{420}\begin{bmatrix} 312 & 0 & 54 & -13l \\ 0 & 8l^2 & 13l & -3l^2 \\ 54 & 13l & 156 & -22l \\ -13l & -3l^2 & -22l & 4l^2 \end{bmatrix}. \tag{4.26}$$

Performing an eigenvalue analysis based on this matrix and the stiffness matrix in Equation (4.19) yields the normal modes for the beam. Using the numerical parameter values gives the first two natural frequencies of 2.095 and 13.23 Hz; this compares to the exact values of 2.094 and 13.12 Hz. The equivalent result for the lumped mass representation is that the frequencies are (a) 1.808 and 8.61 Hz for the case where rotary inertia effects are included or (b) 1.879 and 9.68 Hz for the case where rotary inertia effects are ignored. The consistent mass approach yields more accurate results than the lumped mass representation, as expected.

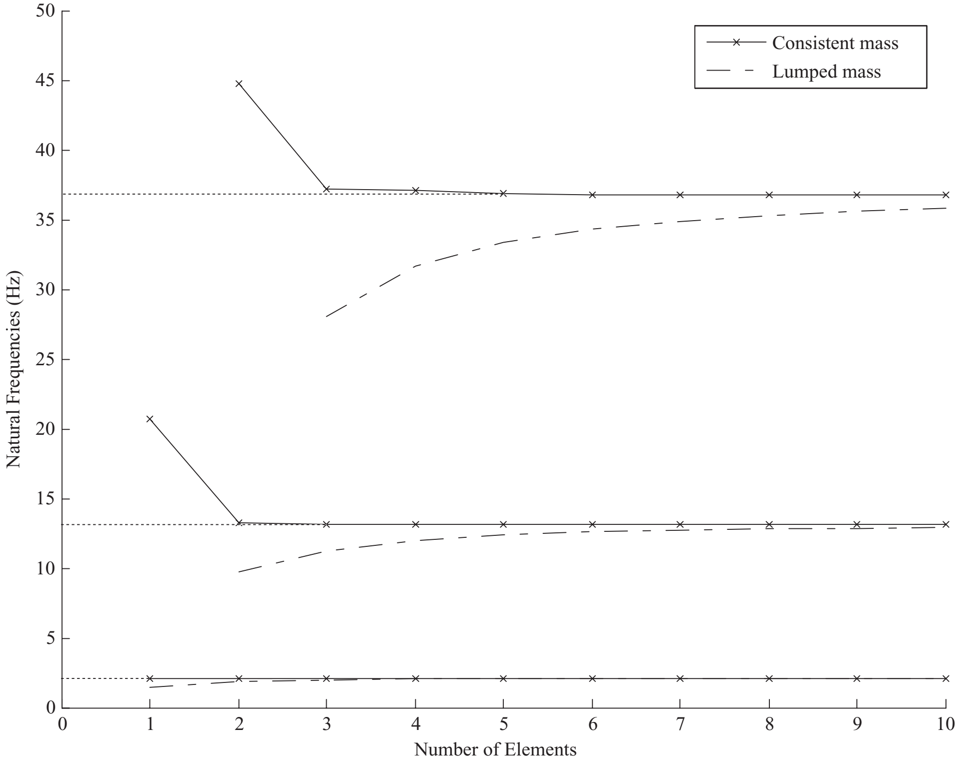

Figure 4.8 Variation of modes 1 to 3 natural frequencies with number of elements for consistent and lumped masses (no rotary inertia effects) (- - - - - exact values).

4.3.7.3 Normal modes analysis – effect of increasing the number of elements

The accuracy of the results for these, and higher, modes may be improved by introducing more elements. It is good practice to increase the number of elements until the results of interest stabilize, as seen in Figure 4.8 for the consistent and lumped mass matrix representations, where the natural frequencies for the first three modes are shown plotted against the number of elements used. The exact values are also shown and clearly the consistent mass results converge far more quickly than for the lumped mass. However, what is somewhat surprising is that the results shown for the lumped mass matrix are with the rotary inertia effects ignored, and these are better than the results for the rotary inertia included.

4.4 TORSION ELEMENT

So far, the focus has been on two-node beam bending elements. However, in aircraft applications, it is important to model torsional behaviour of slender members and so a brief introduction will be given here. A typical two-node torsion element is shown in Figure 4.9. In the same way that the displacement variation for a bending element may be represented by a cubic polynomial, the twist for a two-node torsion element varies linearly along its length. The two shape functions are therefore linear polynomials and the element stiffness and mass matrices may be evaluated as before; the strain and kinetic energy

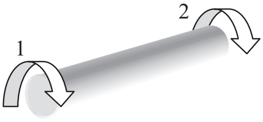

Figure 4.9 Two-node torsion element.

terms for a member under torsion are the same as used earlier in Chapter 3. It may be shown that the element stiffness and consistent mass matrices are as follows:

$$\mathbf{k} = \frac{GJ}{L}\begin{bmatrix} 1 & -1 \\ -1 & 1 \end{bmatrix}, \qquad \mathbf{m} = \frac{\chi L}{6}\begin{bmatrix} 2 & 1 \\ 1 & 2 \end{bmatrix}, \tag{4.27}$$

where *GJ* is the torsional rigidity, *L* is the length and χ is the torsional moment of inertia per unit length.

It may also be shown that the element stiffness and mass matrices for a two-node bar element under axial extension/compression are the same as those for the torsion element except that the axial rigidity *EA* replaces the torsional rigidity *GJ* and the mass per unit length μ replaces the torsional moment of inertia per unit length χ.

4.5 COMBINED BENDING/TORSION ELEMENT

Having obtained the element mass and stiffness matrices for the beam bending and torsion elements based on using independent notations for nodal displacements, the elements may be combined using an integrated set of nodal displacements to obtain a single element having 6 × 6 matrices and able to bend and twist. The nodal displacements are conveniently defined with reference to the flexural axis (i.e. the axis where a bending load causes no twist and a torque causes no bending). The form of the matrices depends upon the numbering system for the nodal displacements. For example, if $\left\{ d_1 \quad d_2 \quad d_4 \quad d_5 \right\}$ corresponds to the bending displacements/rotations and $\{d_3 \quad d_6\}$ to the twists, as shown in Figure 4.10, this would lead to matrices where the bending and torsion terms are interspersed, as shown later in Chapter 20. There would be no stiffness coupling in the stiffness matrix and no mass coupling if the mass and flexural axes are coincident.

However, if the mass axis does not coincide with the flexural axis then there will be inertia coupling present, so that inertia forces associated with bending acceleration will cause torsional motion and vice versa. Then, whether the mass is distributed or else lumped and attached to each node via a rigid connection (often the case for an aircraft, as discussed in Chapter 22), a mass matrix will be generated

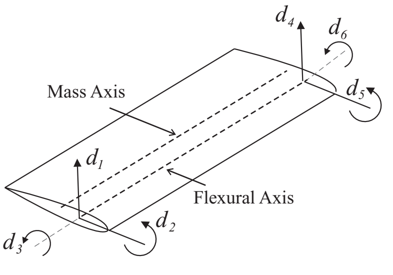

Figure 4.10 Combined bending/torsion element.

having bending/torsion coupling terms involving the mass offset (i.e. the product of the mass and the offset distance, with an appropriate sign, but negative if the mass axis is aft of the flexural axis).

4.6 COMMENTS ON MODELLING

4.6.1 ‘Beam-Like’ Representation of Slender Members in Aircraft

When an aircraft component such as a wing or fuselage is to be represented by a ‘beam-like’ model using the FE method, a three-dimensional beam element, more complete than the two-dimensional bending version considered in this chapter, needs to be developed. The element will have bending in two directions, axial extension and torsion defined by six DoFs per node, plus allowance for shear deformation. In effect, the final 12 × 12 element stiffness and mass matrices for the three-dimensional element may be built up using a combination of two 4 × 4 matrices for bending in the two orthogonal directions, a 2 × 2 matrix for torsion and a 2 × 2 matrix for axial extension/compression. The location of these submatrices within the full matrices will depend upon the numbering system for the nodal displacements/rotations. Note that a simple example of bending / torsion will be considered in Chapter 20.

Clearly, models may be set up for individual ‘branches’ (called substructures) or for the whole aircraft (see Chapter 3). If the free–free modes of the aircraft are required, then the boundary conditions are fully free for all nodes and six rigid body modes with zero frequency will be found. Note that since the stiffness matrix is singular for a free–free structure, the eigenvalue problem needs to be formulated using the inverse of the mass matrix instead of the stiffness matrix.

4.6.2 ‘Box-like’ Representation of Slender Members in Aircraft

So far, the emphasis has been upon the analysis of slender structures (such as wings) using a ‘beam-like’ representation. The distributions of flexural and torsional rigidities (*EI* and *GJ*) along the wing have traditionally been estimated from the structural stiffness behaviour of the wing box boom/skin model (Donaldson, 1993; Megson, 1999; Sun, 2006). However, to perform more accurate analyses, it is important to represent the stiffened structure and its complex load paths more comprehensively in the FE model. In order to do this, the structure may be represented by a ‘box-like’ FE model such as the simple untapered and unswept box shown in Figure 4.11.

Here booms are represented by axial (or rod/bar) elements that react the axial loads (i.e. tension/compression), and cover skins/spar webs/rib webs are modelled using membrane elements that carry

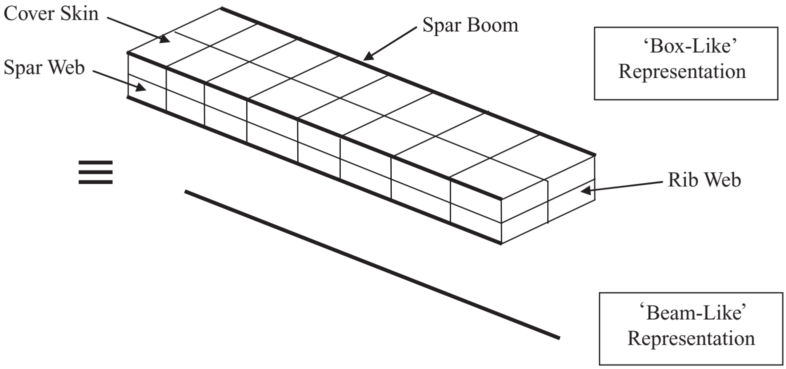

Figure 4.11 Simple ‘box-like’ representation of a wing box structure.

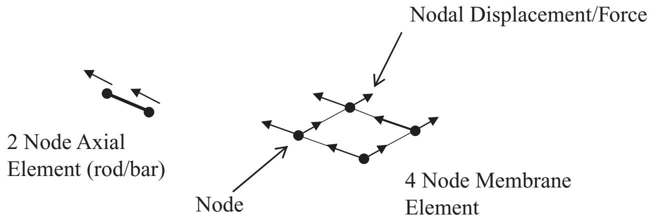

Figure 4.12 ‘Low order’ axial and membrane finite elements.

in-plane axial and shear loads. Typical two-node axial and four-node membrane elements are shown in Figure 4.12; these elements are known as ‘low order’ elements, because the assumed variation of displacement within the element is linear and so the variation of stress (NAFEMS, 1987) may be shown to be (approximately) constant. On the other hand, the ‘higher order’ three-node axial and eight-node membrane elements are more accurate, since the displacement variation within the element is represented as a quadratic function and the stress variation as (approximately) linear. It is also possible to represent the booms by beam elements and the skins by shell elements, where these elements allow for local bending of the booms and skin; shell elements allow for both membrane and plate bending/twisting effects. It should be remembered that the two-node beam element considered earlier had a cubic displacement and linear bending moment and bending stress variation along the element.

In practice, the aircraft wing is much more complex than the simple geometry shown here, so the model has to use significant approximations of local structural features. For example, a stiffened cover panel with holes may be represented by a uniform panel of equivalent thickness; once the load paths (i.e. how the loads are distributed through this panel) are known from a preliminary FE analysis using the relatively coarse type of model discussed above, a local FE or other type of analysis (e.g. a plate buckling analysis or an analysis based on data sheets) may be performed on a more detailed representation of the panel. It should be noted that for a complex aerospace type structure, many parts of the FE model are not suitable for direct extraction of stresses due to the approximations made in the idealization. Instead, nodal forces are obtained and employed to define the external loads acting on the relevant local structure.

Having obtained such a box-like model, it is possible to use an approach known as static ‘condensation’ (see Chapter 22 and Appendix D) to reduce the size of the FE model and to replace the box-like model by an equivalent beam, as illustrated in Figure 4.11 (see also Chapter 22); this beam can be used in the aeroelasticity and loads analyses (see Chapter 20), being coupled with inertia loads (see Chapter 6) and aerodynamic loads (obtained using strip theory or panel methods, see Chapters 5, 19 and 22). Thus a ‘beam-like’ model may now be extracted from a more realistic ‘box-like’ FE model, and will be much more accurate than if a traditional beam with crudely estimated stiffness properties were employed from scratch.

4.7 EXAMPLES

1. Using the same approach as taken above for developing the element stiffness matrix for a two-node bending element, determine the shape functions and hence the 2 × 2 stiffness and consistent mass matrices for a two-node torsion element of length L, torsional rigidity GJ and torsional moment of inertia χ per unit length. (An equivalent result may be obtained for a two- node bar element, i.e. one under axial loading.)

$$\left[k = \frac{GJ}{L}\begin{bmatrix} 1 & -1 \\ -1 & 1 \end{bmatrix}, \qquad m = \frac{\chi L}{6}\begin{bmatrix} 2 & 1 \\ 1 & 2 \end{bmatrix}\right]$$

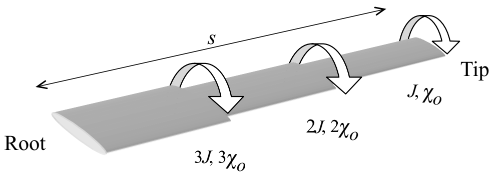

Figure 4.13

2. Consider a clamped–clamped component with length $4l$, flexural rigidity EI and mass per length μ. The fundamental natural frequency is to be obtained and since the corresponding mode shape will be symmetric, only half of the component needs to be modelled, in this case using 2 two-node bending finite elements. Determine the 3 × 3 overall stiffness and consistent mass matrices, recognizing the zero slope boundary condition at the line of symmetry. Then determine the fundamental natural frequency and mode shape using MATLAB (the symbols may be ignored in the calculations and added in later).

$$[1.400\sqrt{EI/\mu l^4};\ \text{cf. exact } 1.398]$$

3. The element stiffness and consistent mass matrices for the two-node torsion element shown in Example 1 above may be used in this question. In order to estimate the first torsional natural frequency of a tapered unswept wing, the wing is modelled by three equal length uniform torsion elements of different dimensions, as shown in Figure 4.13. The wing is clamped at the root. The relevant parameters for each section are shown on the diagram, i.e. the torsion constants for the three sections are $3J$, $2J$, J (root to tip) and the equivalent torsional moments of inertia per unit length are $3\chi_0,\ 2\chi_0,\ \chi_0$. Determine the 3 × 3 stiffness and consistent mass matrices for the overall system after boundary conditions have been applied. Use MATLAB to determine the natural frequency estimates (again ignoring symbols and adding in later) and the mode shape. If a tank with moment of inertia I_t in torsion were to be added to the wing tip, explain how the analysis would change.

$$[\mathbf{K} = GJ/s\,[15\quad -6\quad 0;\ -6\quad 9\quad -3;\ 0\quad -3\quad 3],$$
$$\mathbf{M} = \chi_0/6\,[10\quad 2\quad 0;\ 2\quad 6\quad 1;\ 0\quad 1\quad 2],\ 1.209\sqrt{GJ_0/I_0 s};$$

cf. 1.225 using Rayleigh–Ritz with linear assumed shape and piecewise integration]

4. A wing/tip store combination may be idealized as a uniform member, built in at one end, with an offset tip store (e.g. fuel tank). The wing has a mass per length of 75 kg/m, moment of inertia in twist per length of 25 kg m^2/m, span 6 m, flexural rigidity 2×10^6 N m^2 and torsional rigidity 5×10^5 N m^2. The tip store has a mass of 100 kg and moment of inertia in pitch of 25 kg m^2 about its centre of mass, which itself is offset by 0.5 m forward of the wing centre line. It may be assumed that the flexural and mass axes coincide at mid-chord so there are no couplings between the bending and torsional behaviour for the basic wing. Using a single finite element comprising both bending and torsional behaviour (this 6 × 6 matrix is a simple combination of the 4 × 4 bending and 2 × 2 torsional matrices), obtain the 3 × 3 stiffness and mass matrices for the built-in member. Then add suitable mass terms to the mass matrix in order to account for the store inertia. One approach for doing this is to consider the inertia forces and moments acting on the store, then apply them to the FE model as right-hand side forces and express the force vector as a matrix multiplied by an acceleration vector; rearranging the equations then yields a mass matrix augmented with the store effect. Use MATLAB to obtain the first two natural frequencies and sketch the mode shapes. Compare the results with those from the Rayleigh–Ritz assumed modes of Example 7 in Chapter 3.

[1.81 and 5.00 Hz; cf. 2.18 and 5.48 Hz]

5

Introduction to Steady Aerodynamics

Aircraft are able to fly because the lift generated by the airflow over the wings and horizontal tail surfaces supports their weight. For a flexible aircraft, these lift forces give rise to deflections in the aerodynamic shape, which in turn change the characteristics of the airflow, hence leading to aeroelastic phenomena and affecting the dynamic loads. An understanding of how aerodynamic flow around a two-dimensional aerofoil (a section of a typical wing profile) or a three-dimensional aerodynamic surface generates the forces and moments that are applied to aircraft during flight is very important in order to be able to develop mathematical models that describe the aeroelastic behaviour. In this book, the majority of the mathematical treatment concerns lifting surfaces that are described as continuous, but in some cases the surfaces are discretized, as discussed earlier in Chapter 4.

In this chapter, some of the fundamentals of fluid mechanics and aerodynamics are reviewed, with particular emphasis on the lift/drag forces and moments that occur when air flows around a two-dimensional aerofoil or three-dimensional aerodynamic surface (i.e. wing, tailplane or fin). Other parts of the chapter examine the atmosphere, as well as the effect of adding camber and control surfaces to the wing. The final sections briefly discuss supersonic and transonic flows. Both continuous and discretized wings are considered. More detail about the material in this chapter can be found in Anderson (2001) and Houghton and Carpenter (2001).

5.1 THE STANDARD ATMOSPHERE

Aircraft fly at a range of altitudes and air speeds. It will be shown that the aerodynamic forces and moments that act upon the lifting surfaces (e.g. wings, tail) depend in part upon the air density and pressure, and therefore these quantities must be determined at all altitudes. However, the characteristics of the atmosphere vary with altitude, position on the globe, time of day and time of year (Anderson, 2001). Consequently, the International Standard Atmosphere (ISA) has been defined, which enables aircraft performance to be related to a common reference. The ISA has been determined from experimental measurements and relates temperature, air density and pressure to the altitude above sea level ($h_0 = 0$ m). At extremely high altitudes, the varying values of the acceleration due to gravity also need to be considered, but they will be ignored here and gravity will be assumed to remain constant at all altitudes. Table 5.1 shows the values of a number of important atmospheric parameters for the International Standard Atmosphere (ISA) in both SI and Imperial units.

Here, only the range of altitudes from sea level to 11 000 m (33 528 ft), known as the *troposphere*, will be considered. In this range, the temperature T (in degrees Kelvin) of the standard atmosphere decreases with altitude h (in m) in a linear manner such that

$$T = 288.15 - 0.0065\,h = T_0 - \chi h, \tag{5.1}$$

Introduction to Aircraft Aeroelasticity and Loads J. R. Wright and J. E. Cooper
© 2007 John Wiley & Sons, Ltd

Table 5.1 International Standard Atmosphere properties

T_0 (sea level temperature)	288.16 K	518.69 R
P_0 (sea level air pressure)	101325 N/m^2	21162 lbf/ft^2
ρ_0 (sea level air density)	1.225 kg/m^3	0.0023769 slug/ft^3
a_0 (speed of sound at sea level)	340.29 m/s	1116.43 ft/s
R (gas constant)	287.05 m^2/s^2 K	1716 ft^2/s^2 R
$\gamma = \frac{c_p}{c_v} = \frac{\text{specific heat at constant pressure}}{\text{specific heat at constant volume}}$	1.4	1.4

where constant $\chi = 0.0065$ (i.e. the temperature decreases by 6.5 °C for each 1000 m climbed). Equation (5.1) can be rewritten to relate the change in temperature dT to the height above sea level, so that

$$\mathrm{d}T = T - T_0 = -\chi\, h. \tag{5.2}$$

Assuming that the atmosphere behaves as a perfect gas, then the state equation, and the hydrostatic equation that relates the change in pressure dP due to a change in height, can be written as

$$P = \rho RT \qquad \text{and} \qquad \mathrm{d}P = P - P_0 = -\rho g h, \tag{5.3}$$

where P is pressure, ρ is air density, R is the gas constant and g is the acceleration due to gravity. Then, combining Equations (5.2) and (5.3) to eliminate altitude and integrating gives an expression that relates the pressure to the temperature, such that

$$\int_{P_0}^{P} \frac{\mathrm{d}P}{P} = \frac{g}{\chi R}\int_{T_0}^{T} \frac{\mathrm{d}T}{T} \Rightarrow \frac{P}{P_0} = \left(\frac{T}{T_0}\right)^{g/\chi R}. \tag{5.4}$$

A similar approach can also be used to determine how the density changes with temperature. Applying the state Equation (5.3) at some given altitude and at sea level gives

$$\frac{P}{P_0} = \frac{\rho T}{\rho_0 T_0} = \left(\frac{T}{T_0}\right)^{g/\chi R} \quad \Rightarrow \quad \frac{\rho}{\rho_0} = \left(\frac{T}{T_0}\right)^{g/(\chi R)-1}. \tag{5.5}$$

Thus, using Equations (5.1), (5.4) and (5.5) it is possible to determine the temperature, pressure and air density for any altitude within the troposphere. At 11 000 m, the temperature, pressure and air density reduce to 75.19, 22.3 and 29.7 % respectively of the sea level values.

A further property of the atmosphere that has an important effect on the aerodynamic properties is the speed of sound, defined by the symbol a. The speed of sound is a function of the ratio of specific heats of air γ, the gas constant R and the ambient absolute temperature T, and is defined as

$$a = \sqrt{\gamma RT} = \sqrt{\frac{\gamma P}{\rho}} = a_0\sqrt{\frac{T}{T_0}}, \tag{5.6}$$

where a_0 is the speed of sound at sea level. Hence, the speed of sound reduces with increasing altitude, for instance at 11 000 m it is 86.7 % of the sea level value.

5.2 EFFECT OF AIR SPEED ON AERODYNAMIC CHARACTERISTICS

The airflow and the resulting pressure distribution around a two-dimensional aerofoil changes depending upon the air speed and altitude. These characteristics can be defined in terms of several dimensionless quantities.

5.2.1 Mach Number

One particularly important influence upon the characteristics of all fluid flows is the compressibility of the air at the air speed of interest, which alters depending upon the ratio between the local flow velocity V at some point in the flow and the speed of sound a. This ratio is known as the Mach number (M), defined as

$$M = \frac{V}{a}. \tag{5.7}$$

The value of M has a significant effect on the flow characteristics around aerofoils, and specific flow regimes can be defined approximately as shown in Table 5.2 (note that the symbol M will be used in different ways in the book, particularly for pitching or bending moment, but the context will indicate the usage).

Shock waves (or 'shocks') appear in transonic and supersonic flows and effectively act as boundaries across which there are significant abrupt changes in Mach number and pressure. A commercial jet aircraft will typically cruise in the transonic regime at around $M = 0.85$, while fighter aircraft often fly at around $M = 2$.

5.2.2 Reynolds Number

The Reynolds Number (Re) is a further nondimensional quantity that influences the flow around aerofoils and is defined as

$$Re = \frac{\rho V c}{\mu}, \tag{5.8}$$

where c and μ are the aerofoil chord and air viscosity respectively. The Reynolds number defines whether a viscous flow, particularly in the boundary layer (region close to the aerofoil surface where the flow velocity is slowed down due to the surface friction) is laminar (i.e. flow velocity varies smoothly close

Table 5.2 Flow regimes defined by Mach number

$M < 0.75$	Subsonic	No shocks present in the flow	Gliders/propeller aircraft/some jet transports
$0.75 < M < 1.2$	Transonic	Shocks are attached to the aerofoil	Civil transports (typically $M = 0.8$ to 0.9)
$M = 1$	Sonic	Flow at the speed of sound	Fighter aircraft
$1.2 < M < 5$	Supersonic	Shocks present but not attached to the aerofoil	Fighter aircraft
$M > 5$	Hypersonic	Viscous interaction, entropy layer, high temperature effects become important	Missiles

to the surface of the aerofoil) or turbulent (i.e. flow velocity varies randomly and irregularly close to the surface). It is in effect the ratio of inertia to viscous forces in the flow.

5.2.3 Inviscid/Viscous and Incompressible/Compressible Flows

The simplest form of aerodynamic modelling, the so-called *inviscid* flow, assumes that there are no effects from the viscosity of the air. This assumption implies that the flow past an aerofoil, even at the surface, incurs no friction. In practice, viscosity does have an effect on the flow (*viscous* flow) and this is most notably demonstrated by the presence of the boundary layer, where the flow slows down from the velocity in the free stream to zero velocity on the surface.

A common simplification is to assume that the density of the air is constant (i.e. *incompressible*) throughout the flow, and this is valid for flows where $M < 0.3$. Beyond this Mach number, *compressibility* effects need to be taken into account and the density will vary through the flow field.

5.2.4 Dynamic Pressure

The dynamic pressure q is defined as $\frac{1}{2}\rho V^2$, where the density ρ and velocity V need to be defined consistently. It is common practice to define it in terms of the *equivalent air speed* V_{EAS}, which is the speed at sea level that gives the same dynamic pressure as at some altitude, i.e.

$$\frac{1}{2}\rho V^2 = \frac{1}{2}\rho_0 V_{\mathrm{EAS}}^2 \quad \Rightarrow \quad V_{\mathrm{EAS}} = \sqrt{\frac{\rho}{\rho_0}}V = \sqrt{\sigma}V, \tag{5.9}$$

where σ is the ratio of the air density at some altitude to the sea level density ρ_0. Strictly, V should be referred to as V_{TAS}, the *true air speed*, when ρ is the density at altitude. These air speeds will be referred to later in the book when aeroelasticity and loads are considered.

5.3 FLOWS AND PRESSURES AROUND A SYMMETRIC AEROFOIL

An aerofoil is a two-dimensional shape that is the cross-section of some three-dimensional aerodynamic surface; two-dimensional flows are fundamental for gaining understanding whereas three-dimensional flows are more complex and are what occur in practice. The flow over an aerofoil moving in a fluid at rest is said to be *steady* when the velocity at any fixed point is constant with time. Figure 5.1 shows how 'streamlines' map the fluid motion around a symmetric aerofoil at zero angle of incidence. There is no flow across the streamlines; however, the velocity and pressure can change along them. Any element of fluid experiences a static pressure from adjacent elements as it is moving.

Figure 5.2 shows the same streamlines but this time with the aerofoil at some small positive angle of incidence α, defined as the angle between the chord line and the free-stream direction of the oncoming flow. It can be seen how the flow is altered by the change of incidence, and how the symmetry of Figure 5.1

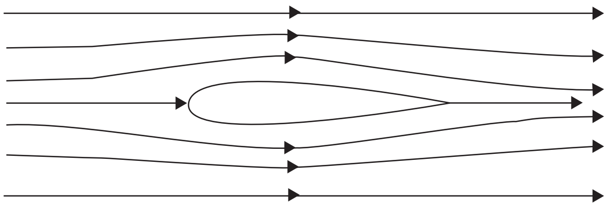

Figure 5.1 Flow around a symmetric aerofoil at zero incidence.

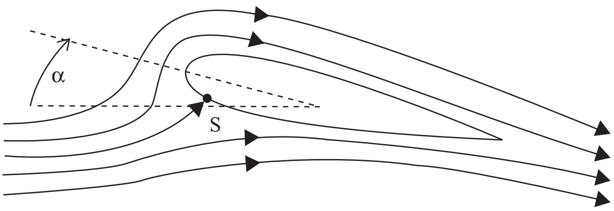

Figure 5.2 Flow around a symmetric aerofoil at a small angle of incidence to the flow.

is lost. Lift occurs because the flow is deflected downwards by the aerofoil; this leads to the flow over the upper surface being faster than that on the lower surface. Note that this difference in speeds is *not* because the upper surface flow has further to travel but rather due to the aerofoil shape. Point S is the stagnation point where the flow is brought to rest.

Making use of Newton's laws of motion (see Chapter 6) and neglecting gravitational effects, Bernoulli's equation (Anderson, 2001) for constant ρ (incompressible flow) can be derived to relate the pressure, density and velocity such that

$$P + \tfrac{1}{2}\rho V^2 = \text{constant}. \tag{5.10}$$

For compressible flow it can be shown that Bernoulli's equation, again neglecting gravitational effects, becomes

$$\left(\frac{\gamma}{\gamma - 1}\right)\frac{P}{\rho} + \frac{1}{2}V^2 = \text{constant}. \tag{5.11}$$

Consider the flow along a typical streamline starting in the free stream at pressure P_∞ and velocity V_∞ and then changing to pressure P and velocity V at some point close to the aerofoil. Applying Bernoulli's equation gives

$$P_\infty + \tfrac{1}{2}\rho V_\infty^2 = P + \tfrac{1}{2}\rho V^2 \quad \Rightarrow \quad P = P_\infty + \tfrac{1}{2}\rho\left(V_\infty^2 - V^2\right). \tag{5.12}$$

Hence for a velocity $V > V_\infty$, pressure $P < P_\infty$, so an increase in velocity leads to suction (pressure reduction); for velocity $V = V_\infty$, pressure $P = P_{\infty,}$; and for velocity $V < V_\infty$, pressure $P > P_\infty$, so a decrease in velocity leads to compression (pressure increase).

The maximum pressure occurs at the *stagnation point* S where the flow comes to rest on the aerofoil ($V = 0$), so

$$P_s = P_\infty + \tfrac{1}{2}\rho V_\infty^2. \tag{5.13}$$

It is usual to describe the pressure distribution in terms of the nondimensional *pressure coefficient* C_p, which is defined for a point in the flow (or on the aerofoil) as

$$C_p = \frac{P - P_\infty}{\frac{1}{2}\rho V_\infty^2} = 1 - \left(\frac{V}{V_\infty}\right)^2, \tag{5.14}$$

which is a measure of the ratio of the local static pressure on the aerofoil (relative to the free stream pressure P_∞) to the free stream dynamic pressure. In terms of C_p, the pressure distribution of a typical symmetric aerofoil at an angle of incidence below stall (see later) is plotted in Figure 5.3.

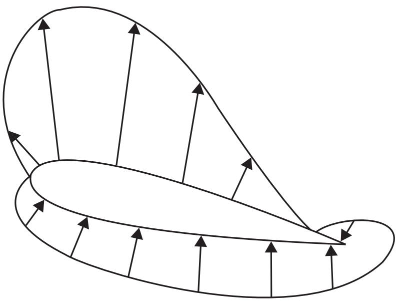

Figure 5.3 Typical pressure distribution for a symmetric aerofoil at a small angle of incidence.

Note that the pressure always acts normal to the surface. A common way of presenting the pressure distribution on both surfaces is shown in Figure 5.4, where it can be seen that the lift is dominated by suction on the upper surface. The ratio of chordwise distance from the leading edge normalized to the aerofoil chord is x/c. There is a greater rate of change in pressure close to the leading edge.

5.4 FORCES ON AN AEROFOIL

For an aerofoil moving at velocity V in a fluid at rest, the pressure distribution acting over the surface of the aerofoil gives rise to a total force. The position on the chord at which the resultant force acts is called the *centre of pressure,* as shown in Figure 5.5. If the angle of incidence α (angle between the mean airflow and the chord line of the aerofoil, measured in radians) alters, then the pressure distribution over the aerofoil changes, which leads to a repositioning of the centre of pressure. The changing centre of pressure position with respect to different angles of incidence leads to difficulties in any simple aeroelastic analysis, since the forces and moments need to be recalculated continually. For convenience, the net force is usually replaced by two resultant orthogonal forces, acting at a chosen reference point on the aerofoil, and a moment as seen in Figure 5.5.

The lift (L) is the force normal to the relative velocity of the aerofoil and fluid, the drag (D) is the force in the direction of relative velocity of the aerofoil and fluid, and the pitching moment (M) is the

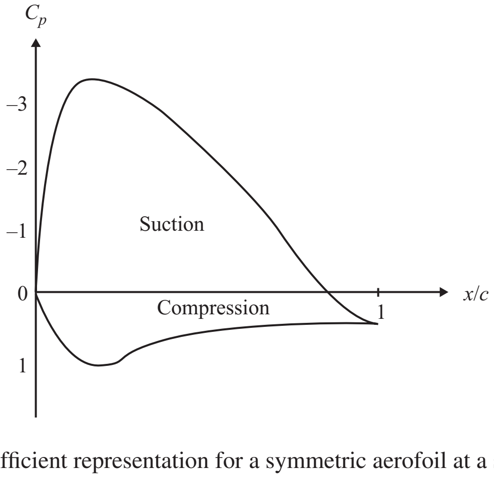

Figure 5.4 Pressure coefficient representation for a symmetric aerofoil at a small angle of incidence.

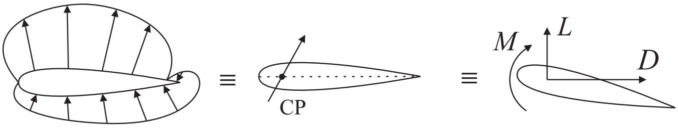

Figure 5.5 Resultant aerodynamic force acts at the centre of pressure.

moment due to offset between the centre of pressure and the reference point (+ve when pushing the nose upwards as shown in Figure 5.5).

It is usual to use coefficients which relate the above quantities to the dynamic pressure and chord for a unit span of aerofoil (since it is two-dimensional), so that the lift, drag and moment coefficients are defined as

$$C_{\mathrm{L}} = \frac{\text{Lift } L}{\frac{1}{2}\rho V^2 c}, \qquad C_{\mathrm{D}} = \frac{\text{Drag } D}{\frac{1}{2}\rho V^2 c}, \qquad C_{\mathrm{M}} = \frac{\text{Pitching moment } M}{\frac{1}{2}\rho V^2 c^2}$$

respectively, where c is the aerodynamic aerofoil chord and lift, and drag and pitching moment are defined per unit span of the aerofoil. It is often more useful to use the coefficients rather than the total lift, drag and pitching moment per unit length as they are normalized by dynamic pressure and the aerofoil chord. Note that the forces and pitching moment can be defined with reference to any point on the chord.

Aerofoil sections usually have unsymmetric cross-sections and incorporate camber, as shown in Figure 5.6, to improve the lift performance. Later on, equivalent coefficients will be defined for the entire three-dimensional lifting surface (e.g. wing) and these will be based upon the total force (or moment) and normalized by the wing area instead of the chord for a unit span of the two-dimensional aerofoil.

5.5 VARIATION OF LIFT FOR AN AEROFOIL AT AN ANGLE OF INCIDENCE

Figure 5.7 shows the variation of lift coefficient with incidence. The lift coefficient C_{L} is seen to increase linearly with an increase in the angle of incidence α from the zero lift angle until stall is reached, when the flow detaches and the lift drops off. The maximum lift coefficient obtained is $C_{\mathrm{L_{MAX}}}$. Also, at some angle of incidence known as the *zero lift angle* α_0, all aerofoils have zero lift, with $\alpha_0 = 0$ for a symmetric aerofoil. Note how the use of a cambered aerofoil enables C_{L} to be increased, but at the expense of stall occurring at lower angles of incidence.

Hence, in the linear range

$$C_{\mathrm{L}} = a_1 (\alpha - \alpha_0) \quad \Rightarrow \quad C_{\mathrm{L}} = a_0 + a_1 \alpha, \tag{5.15}$$

where $a_1 = dC_{\mathrm{L}}/d\alpha$ is the two-dimensional *lift curve slope*, which has a theoretical value of 2π/rad. However, measurements show that in practice this has a value between 5.5 and 6 per radian and a value of $a_1 = 5.73$ is often taken as this corresponds to 0.1 per degree (Houghton and Brock, 1960). Note that a_0 is the lift at zero angle of incidence, having a value of zero for a symmetric aerofoil.

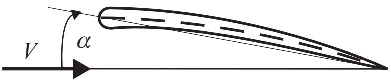

Figure 5.6 Cambered aerofoil.

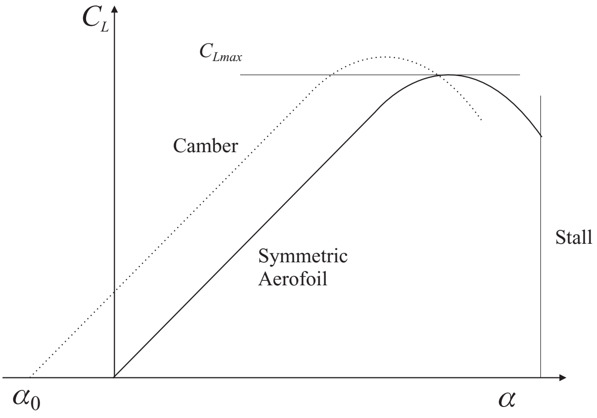

Figure 5.7 Variation of the lift coefficient with the angle of incidence.

As the Mach number M increases, compressibility of the air has a greater influence on the aerodynamic forces and changes the two-dimensional lift curve slope to become

$$a_1' = \frac{1}{\sqrt{1 - M^2}} a_1. \tag{5.16}$$

It is usual to ignore compressibility effects for $M < 0.3$, and in this book, for simplicity, Mach number effects will be ignored in any modelling.

5.6 PITCHING MOMENT VARIATION AND THE AERODYNAMIC CENTRE

If the pitching moment coefficient C_{M} is determined about the leading edge for a varying angle of incidence and hence lift coefficient, then the results shown in Figure 5.8 are found. Note that C_{M_0} is the moment coefficient at the zero lift condition.

The relationship between the moment and lift coefficients below stall can be represented by a straight line, so

$$C_{\mathrm{M_{LE}}} = C_{\mathrm{M}_0} + bC_{\mathrm{L}}, \tag{5.17}$$

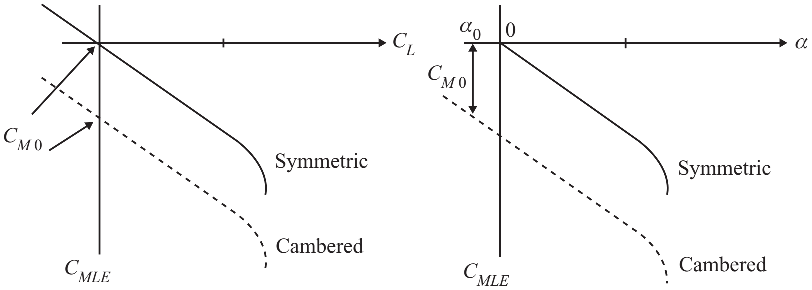

Figure 5.8 Variation of the moment coefficient about the leading edge with the lift coefficient and angle of incidence.

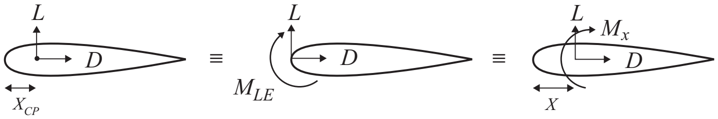

Figure 5.9 Forces and moments acting on an aerofoil for different reference points.

where it is found that $b = \mathrm{d}C_{\mathrm{M_{LE}}}/\mathrm{d}C_{\mathrm{L}} \approx -0.25$ for all aerofoils and therefore

$$C_{\mathrm{M_{LE}}} = C_{\mathrm{M_0}} - 0.25C_{\mathrm{L}}. \tag{5.18}$$

The pitching moment value and coefficient depend upon where the reference point for the lift and drag are chosen, with Figure 5.9 showing three possible arrangements that must be statically equivalent, i.e. at the centre of pressure, leading edge and a general point. Considering the forces and moments acting on the aerofoil shown in Figure 5.9 and taking moments about the leading edge, then

$$-Lx_{\mathrm{CP}} = M_{\mathrm{LE}} = M_x - Lx. \tag{5.19}$$

Dividing by $\frac{1}{2}\rho V^2 c$ gives the equivalent expression in coefficient form:

$$-C_{\mathrm{L}}\frac{x_{\mathrm{CP}}}{c} = C_{\mathrm{M_{LE}}} = C_{\mathrm{M}_x} - C_{\mathrm{L}}\frac{x}{c}, \tag{5.20}$$

and comparison of Equations (5.18) and (5.20) shows that for x $= 0.25c$ (quarter chord) then $C_{\mathrm{M}_x} = C_{\mathrm{M_0}}$ = constant.

This quarter chord point is called the *aerodynamic centre* and is where the pitching moment coefficient C_{M_x} equals $C_{\mathrm{M_0}}$ and does not vary with C_{L} or incidence unlike any other point on the chord. The aerodynamic centre position is independent of incidence and section shape, and is the point where any incremental lift due to any incremental change in incidence acts. Note that for a symmetric aerofoil section, $C_{\mathrm{M_0}}$ is zero and therefore the centre of pressure would be at the quarter chord. These characteristics make it convenient to use the aerodynamic centre for the aeroelastic and load modelling covered in later chapters.

5.7 LIFT ON A THREE-DIMENSIONAL WING

So far, most of the attention has been focused on the flow around two-dimensional aerofoil sections and on the forces and moment acting; however, now the aerodynamic behaviour of a wing will be considered. In practice, the lifting surfaces on an aircraft (e.g. wing) are three-dimensional and there will be changes in the behaviour. Most of the focus in this book will be on unswept and untapered wings to keep the mathematics as simple as possible.

5.7.1 Wing Dimensions

Dimensions of a tapered but unswept wing are shown in Figure 5.10; here the semi-span is s and the root and tip chords are c_{R}, c_{T}. The mean chord is c and the wing planform area is given by $S_{\mathrm{W}} = 2sc$, thus

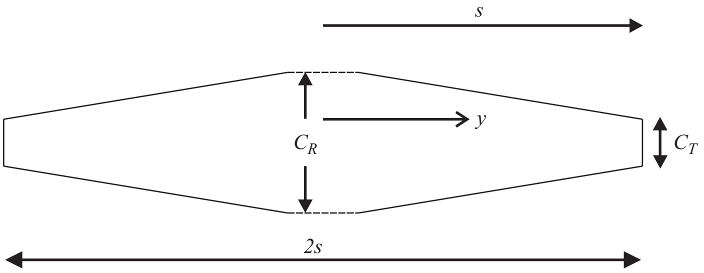

Figure 5.10 Dimensions of an unswept wing.

including the section of wing passing though the fuselage. The aspect ratio of the wing is a measure of the slenderness of the wing planform and is given by

$$\mathrm{AR} = \frac{2s}{c} = \frac{(2s)^2}{S_\mathrm{W}}. \tag{5.21}$$

Commercial aircraft tend to have relatively high aspect ratio wings (∼6 to 8) for reasons that will become apparent later when drag is considered.

5.7.2 Lift Curve Slope of a Three-Dimensional Wing

There are a number of simple adjustments that can be made to the value of the lift curve slope for a two-dimensional aerofoil in order to account approximately for finite span wings and also the effects of compressibility. For three-dimensional finite span wings, the value of the lift curve slope is given the symbol a_W.

Assuming that the lift distribution across a three-dimensional wing of aspect ratio AR is elliptically shaped, with lift falling off to zero at the wing tips (see later), then the effective wing lift curve slope can be shown to take the form (Fung, 1969)

$$a_\mathrm{W} = \frac{a_1}{1 + a_1/(\pi \mathrm{AR})}, \tag{5.22}$$

so the lift curve slope reduces for a finite span wing, with the largest reduction for low aspect ratio wings.

5.7.3 Force and Moment Coefficients for a Three-Dimensional Wing

Sectional lift, drag and pitching moment coefficients were defined earlier for the two-dimensional aerofoil in terms of force/moment per unit span. For a three-dimensional wing, the equivalent coefficients may be defined in terms of the total lift, moment, etc., over the wing. The wing lift and pitching moment coefficients are defined by

$$C_\mathrm{L} = \frac{L}{\frac{1}{2}\rho V^2 S_\mathrm{W}}, \qquad C_\mathrm{M} = \frac{M}{\frac{1}{2}\rho V^2 S_\mathrm{W} c}, \tag{5.23}$$

where L, M are the total lift and pitching moment for both wings. The drag coefficient C_D may be defined similarly.

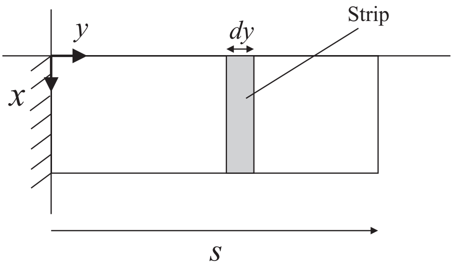

Figure 5.11 Aerodynamic ‘strip’ on a continuous rectangular wing.

5.7.4 Strip Theory for a Continuous Wing

There are a number of different ways of modelling the spanwise lift distribution of a wing. In this first part of the book the simplest, known as *strip theory*, will be considered, initially for a continuous untapered wing and then for a discretized wing.

In strip theory, the wing is considered to be composed of a number of elemental chordwise ‘strips’ and it is assumed that the lift coefficient on each chordwise strip of the wing is proportional to the local angle of incidence $\alpha(y)$ and that the lift on one strip has no influence upon another. In its basic form, root and tip effects are ignored along with the effects of compressibility. In practice these assumptions imply that the air speed is low ($M < 0.3$) and that the wing has a high aspect ratio ($\mathrm{AR} \geq 6$). Note that strip theory cannot be used for drag calculations.

Consider an elemental strip of the wing, having width $\mathrm{d}y$ and chord c as shown in Figure 5.11. Then the lift $\mathrm{d}L$ on the strip is taken to act at its aerodynamic centre (i.e. quarter chord) and is defined as

$$\mathrm{d}L = \tfrac{1}{2}\rho V^2 c \,\mathrm{d}y\, a_1 \alpha(y), \tag{5.24}$$

so in essence the two-dimensional lift curve slope value is employed. Thus, the total lift acting on a single wing of semi-span s is found by integrating the effect of all the strips, so

$$L_{\mathrm{TOTAL}} = \int_0^s \mathrm{d}L = \tfrac{1}{2}\rho V^2 c a_1 \int_0^s \alpha(y)\,\mathrm{d}y. \tag{5.25}$$

If the wing had been tapered, then the chord would be a function of the spanwise coordinate $c(y)$ and would be included under the integral. Note that an expression for the wing pitching moment about, for example, the leading edge or axis of aerodynamic centres (i.e. quarter chord) could be obtained using a similar approach. Also, the rolling moment about the root could be obtained.

Strip theory in its basic form assumes that the lift on each strip of the wing is the same as if the strip were part of an infinite span two-dimensional wing, i.e. that aerofoil sectional properties would be used. However, when applied to a finite wing, the presence of lift in the tip region implies a pressure discontinuity at the tip that cannot occur in practice. The suction on the upper surface and compression on the lower surface must be equal at the wing tip. In practice, as shown in Figure 5.12, the spanwise lift distribution falls off to zero at the tip. A consequence of the difference in pressures between the upper and lower surfaces in the tip region is the ‘trailing tip vortex’ that occurs on all wings due to the flow around the tip from lower to upper surfaces (see the later section on drag).

For elliptically shaped or tapered wings, where the lift predicted by strip theory drops off towards the wing tip due to the reduced chord, the finite wing effect can be accounted for through the use of Equation (5.22) to adjust the value of the lift curve slope and then using a_W in place of a_1 in Equations (5.24) and (5.25). However, for wings without a significant taper, then strip theory may be modified

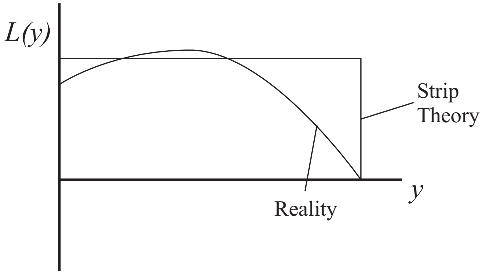

Figure 5.12 Spanwise lift distribution for a realistic wing and strip theory model.

(Yates, 1966) to account for the reduction towards the tip. In this case, the lift curve slope may be varied across the span, either by assuming functions of the form

$$a_W(y) = a_1\left[1-\left(\frac{y}{s}\right)^2\right] \quad \text{or} \quad a_W(y) = a_1\left[1-\left(\frac{y}{s}\right)\right]^2 \quad \text{or} \quad a_W(y) = a_1\cos\left(\frac{\pi y}{2s}\right) \tag{5.26}$$

to replace a_1, or by using a more sophisticated aerodynamic theory. Alternatively, experimental pressure measurements can be used to determine the variation of lift curve slope and aerodynamic centre position along the span.

5.7.5 Strip Theory for a Discretized Wing

In Chapter 4, the treatment of slender members was considered where a discretization was employed. If a method such as strip theory (or modified strip theory) is to be employed in conjunction with a finite element 'beam-like' model (see later in the book, Chapters 20 and 22), then the continuous expressions used above will need to revised. In effect, the wing will be treated as if it is divided into N sections (i.e. finite width 'strips') of width Δy.

Consider the kth 'strip' (or section) located at a distance of y_k from the root. Following the previous approach for the elemental strip on the continuous wing, the lift force acting upon the kth strip will be given by the expression

$$L_k = \tfrac{1}{2}\rho V^2 c\Delta y\ a_W\alpha(y_k), \tag{5.27}$$

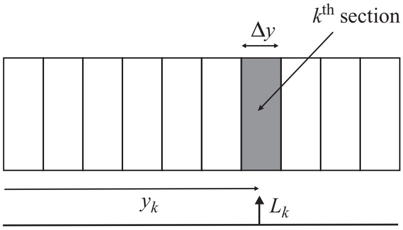

Figure 5.13 Aerodynamic 'strips' on a discretized rectangular wing.

where again the local chord could have been used for a tapered wing and the lift curve slope a_{W} is corrected in some way. Thus the total lift on the single starboard wing would be given by

$$L_{\mathrm{TOTAL}} = \sum_{k=1}^{N} L_k. \tag{5.28}$$

A pitching moment per section could also be calculated. Again, the lift curve slope could be adjusted over the sections and the section width need not be constant.

5.7.6 Panel Methods

Even with the use of modified strip theory, there are still inaccuracies primarily due to the lack of interaction effects between different parts of the lifting surfaces (for instance, T-tails cannot be modelled with a strip theory approach) and more sophisticated approaches must be used instead. Current industry practice is to make use of the so-called *panel methods* whereby the lifting surface is divided up into panels and the lift distribution is modelled using potential flow elements such as vortices or doublets acting over each panel. The key calculation in such an approach is to determine the aerodynamic influence coefficients (AICs) that determine the aerodynamic effect that each panel has on another. These methods are described in more detail for both steady and unsteady flows in Chapter 19 and applied to simple aeroelastic models in Chapter 20. Further comments are made on the practical implementation in Chapter 22.

5.8 DRAG ON A THREE-DIMENSIONAL WING

As well as generating lift, wings also produce drag. Commercial aircraft designers aim to achieve a maximum lift/drag ratio as this gives the maximum flight range. There are two main contributions to drag: profile drag and induced drag. Noting that the total drag D can be defined as

$$D = \tfrac{1}{2}\rho V^2 S C_{\mathrm{D}}, \tag{5.29}$$

the drag coefficient can be defined as

$$C_{\mathrm{D}} = C_{\mathrm{D}_0} + C_{\mathrm{D}_I} = C_{\mathrm{D}_0} + \frac{C_{\mathrm{L}}^2}{\pi e' \mathrm{AR}}. \tag{5.30}$$

Now C_{D_0} is the *profile drag* (the drag that is inherent from the aerofoil shape, i.e. when there is zero lift, $C_{\mathrm{L}} = 0$). However, $C_{\mathrm{D}_\mathrm{I}}$ is the *induced* or lift-dependent drag that is mainly due to the presence of the wing tip trailing vortex, but also includes the effects of the fuselage and engine nacelles and is proportional to the (lift)^2. The value e' is the span efficiency factor, which is unity if the wing planform is elliptical. For typical commercial aircraft, the value is within the range $0.85 < e' < 0.95$. Note that the induced drag can be decreased by increasing the aspect ratio and by using as close to an elliptical wing planform as possible (tapered wings can give a good approximation of an elliptical planform). The addition of winglets effectively increases the aspect ratio and so reduces the drag.

Figure 5.14 shows how both types of drag vary with dynamic pressure. At low dynamic pressures, the induced drag dominates, whereas at high dynamic pressures the profile drag dominates. Figure 5.15 shows how the *drag polars* of C_{D} versus C_{L} vary for increasing Mach number. Although the drag does not directly affect most aeroelastic calculations, the static aeroelastic wing bending deflection and twist in flight do have a significant effect on the drag and are one of the key components in efficient aerodynamic wing design (see Chapters 8 and 23). Drag will also have an impact upon aircraft handling via the flight mechanics equations (see Chapter 14) and therefore indirectly upon loads. Once the transonic

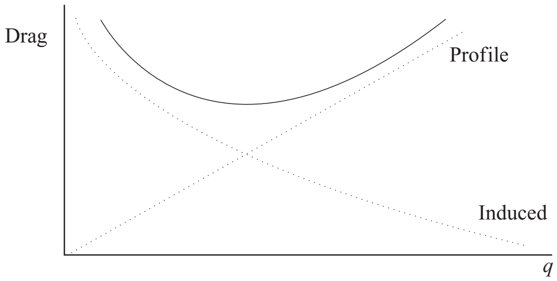

Figure 5.14 Variation of drag with dynamic pressure q.

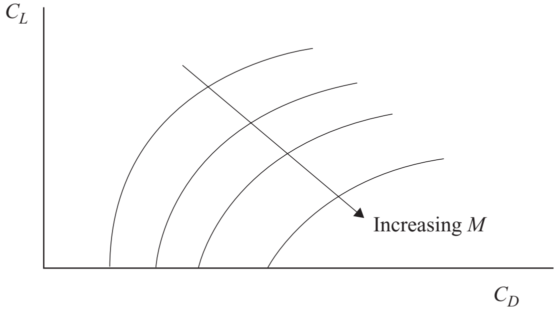

Figure 5.15 C_L versus C_D for different Mach numbers.

flight regime is reached, the presence of shock waves creates the onset of *wave drag*, which produces a significant increase in the overall drag.

5.9 CONTROL SURFACES

Control surfaces are used primarily to manoeuvre the aircraft by changing the pressure distribution over the aerofoil. Consider the two-dimensional aerofoil and control surface, shown in Figure 5.16, where the control angle β (not to be confused with later usage for a sideslip angle in Chapter 13) is taken as +ve downwards.

Figure 5.17 shows how the C_L versus α curves vary for changing β. It can be seen that the lift coefficient is increased by increasing β while the slope of each curve remains the same. Consequently, the application of the control surface *increases the effective camber* of the aerofoil. Note also that the stall speed decreases and $C_{M_{LE}}$ becomes more negative.

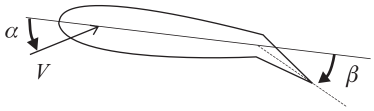

Figure 5.16 Two-dimensional aerofoil with a control surface.

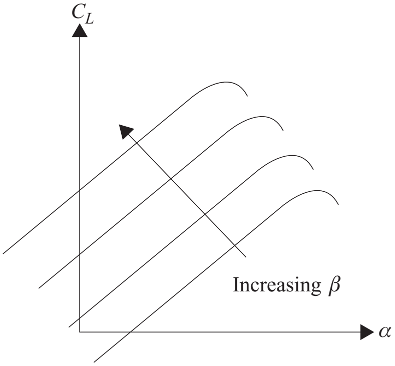

Figure 5.17 Variation of the lift coefficient for different incidence and control surface angles.

Figure 5.18 shows how the pressure distribution changes with the applied control surface, with the centre of pressure moving aft. Application of the control surface therefore increases the lift but imparts an additional nose down pitching moment. The influence of the control surface on the lift coefficient and pitching moment about any point in the section can be modelled as

$$C_{\mathrm{L}} = a_0 + a_1\alpha + a_2\beta \qquad \text{and} \qquad C_{\mathrm{M}} = b_0 + b_1\alpha + b_2\beta, \tag{5.31}$$

where a_2 is the control surface lift slope and b_2 is the control surface pitching moment slope. The coefficients a_2 and b_2 for a two-dimensional aerofoil are defined (Fung, 1969) as

$$a_2 = \frac{a_1}{\pi}\left[\cos^{-1}(1-2E) + 2\sqrt{E(1-E)}\right] \qquad \text{and} \qquad b_2 = -\frac{a_1}{\pi}(1-E)\sqrt{E(1-E)} \tag{5.32}$$

where E is the ratio of the control surface chord to the total chord. When strip theory is applied to the entire three-dimensional wing in Chapter 9, then subscripts 1 and 2 become W and C respectively.

5.10 SUPERSONIC AERODYNAMICS – PISTON THEORY

In many aspects, the analysis of supersonic flows is simpler than subsonic flows and the simplest approach for the analysis of supersonic flows using piston theory is analogous to modelling subsonic flows using strip theory. Consider a steady supersonic flow passing over the unit chord two-dimensional aerofoil

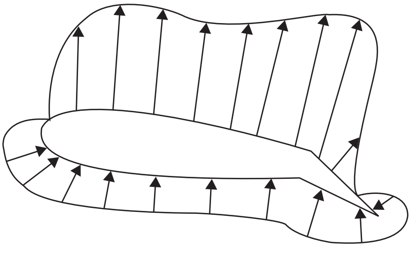

Figure 5.18 Pressure distribution for an aerofoil with an applied control surface.

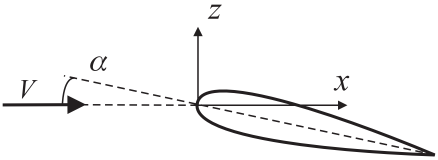

Figure 5.19 Supersonic flow over an aerofoil.

shown in Figure 5.19. The pressure acting upon the aerofoil section can be approximated using the so-called piston theory (Dowell *et al.*, 2004) at high speeds ($M \gg 1$) to be

$$P = \rho a V \alpha = \frac{\rho V^2}{M}\alpha, \tag{5.33}$$

where ρ, a and M are the air density, speed of sound and Mach number respectively. The lift acts uniformly over the chord and therefore the aerodynamic centre is positioned at the semi-chord.

Piston theory is a very simplified modelling approach and typically the so-called Mach box method is used in industry whereby the lifting surface is divided into panels and aerodynamic interaction effects between the panels calculated. The extension from piston theory to the Mach box method is analogous to moving from strip theory to panel methods for subsonic flows.

5.11 TRANSONIC FLOWS

The transonic flight regime is characterized by the presence of shock waves on the wing surface. The shocks represent a sudden change in the pressure and their position is dependent upon the flight condition and also the chordwise wing geometry. It is consequently not possible to model accurately the transonic pressure distributions using either strip theory or the potential flow panel methods that will be covered in Chapter 19 since neither approach enables shock waves to be modelled. No further mention will be made in this book about transonic flows, except to consider their effect on the flutter speed and possible nonlinear aeroelastic effects in Chapter 11 and to mention some relevant applications of computational fluid dynamics (CFD) in Part III.

5.12 EXAMPLES

1. Write a MATLAB program to determine:
   (a) the temperature, air density and pressure at any given altitude;
   (b) the Mach number for a given air speed and altitude;
   (c) the air speed for a given altitude and Mach number.
2. Calculate P/P_0, ρ/ρ_0 and T/T_0 for the standard atmosphere at $h = 3$, 7 and 11 km.
3. The aerodynamic centre for an aerofoil is at 27 % chord, and the pitching moment coefficient at zero lift C_{M_0} is -0.05. What is the pitching moment coefficient about the mid-chord point when $C_L = 1.5$, assuming that C_L and C_M vary linearly with incidence?

   [0.295]
4. Find the values of C_L for which the centre of pressure of an aerofoil is (a) at 30 % chord behind the leading edge and (b) at the trailing edge, if the aerodynamic centre is at 25 % chord and $C_{M_0} = -0.03$.

   [0.6, 0.04]

5. An aerofoil was suspended from a balance in a wind tunnel and its nominal lift and drag were measured normal to and along the wind tunnel axis. The balance readings indicated that at a value of C_{L} of 0.6 the lift/drag ratio for the aerofoil was 20. However, it was found subsequently that in the working section in the region where the model was suspended the air stream was inclined downwards by 0.5° relative to the tunnel axis. Find the correct value of the lift/drag ratio. (Note that since the model is suspended in the tunnel, positive lift is downwards.)

   [17]

6. An aerofoil of 2 m chord has $C_{\mathrm{M}_0} = -0.02$, $\alpha_0 = -1^\circ$, $a_1 = 5.7$/rad. The aerodynamic centre is at $0.25c$ behind the leading edge. It is at an incidence of 5° in a wind speed of 50 m/s ($\rho = 1.225$ kg/m^3). Find the lift and pitching moment about the leading edge per unit span when a trailing edge flap angle is set at 10°. Take $b_1 = 2.0$/rad and assume that the lift increment due to the flap acts through the mid-chord point.

   [2897N, 2107 Nm (nose down)]

7. The above aerofoil with the flap at 10° is found to stall at $\alpha = 12^\circ$ and C_{L} varies linearly with α up to the stall. The aerofoil is then fitted with a leading edge slat of chord $0.15c$ and the stall is consequently delayed to $\alpha = 17^\circ$ (a_1 and b_1 being unchanged by the presence of the slat). Find $C_{\mathrm{L}_{\max}}$ and $C_{\mathrm{M}_{\mathrm{LE}}}$ at the stall with the slat in operation. It may be assumed that the pitching moment coefficient increment due to the slat is given by $\Delta C_{\mathrm{M}_{\mathrm{LE}}} = 0.9$ slat chord/wing chord. (Note that all coefficients are still referred to the same chord c).

   [2.140, −0.508]

8. For a rigid wing of root chord 2 m and semi-span 6 m with incidence 2°, write a MATLAB program to compare the different lift distributions obtained using strip theory and modified strip theory described in Equation (5.26). Determine the taper ratio that gives the closest strip theory lift distribution compared to the modified strip theories.

6

Introduction to Loads

In this book, the topics covered divide naturally into those related to (a) stability (e.g. flutter), (b) static deformation (e.g. static aeroelastic effects, steady flight manoeuvres) and (c) dynamic response (e.g. manoeuvres, gusts, turbulence). The aircraft dynamic response needs to be calculated for ground manoeuvres (e.g. taxiing, take-off and landing), flight manoeuvres (e.g. response to control movements) and gust/turbulence encounters. However, once the response deformations and accelerations are obtained, the loads and stresses generated in the aircraft must also be determined so that the strength and fatigue/damage tolerance behaviour may be assessed.

'Loads' is a general term that incorporates both forces and moments, discrete and distributed, external and internal. In this chapter, various basic concepts relevant to loads in general will be introduced, including Newton's laws of motion for a particle and their generalization to a body, D'Alembert's principle (leading to discrete inertia forces/couples and distributed inertia forces), externally applied/reactive loads, free body diagrams (FBDs), loads generated internally within a structure (i.e. internal loads) and intercomponent loads. It will be shown how loads within a structure may be determined in an accelerating slender member by introducing distributed inertia loads so as to bring the structure into an effective static equilibrium condition.

In this chapter, the way in which internal loads (or so-called 'stress resultants', such as bending moments and shear forces) are determined for slender members subject to uniformly or nonuniformly distributed loading will be explained; both continuous and discretized members will be considered. Then the classical way in which stresses are obtained from these internal loads for simple structures will be outlined. However, for complex aircraft structures, this classical approach is not always suitable; the different methodology for such structures, and the potential confusion in terminology, will be explained later in Chapters 18 and 24.

The treatment in this chapter aims to serve as a reminder of key concepts and an introduction to analysing loads on structures experiencing uniform or nonuniform distributions of acceleration; other texts should be referred to for more information and further explanation of basic concepts if required (Donaldson, 1993; Benham *et al*., 1996, Megson, 1999). The examples given in this chapter will be for simple continuous slender members under uniformly or nonuniformly distributed loading, so as to allow a fundamental understanding to be gained of the kind of analyses relevant to slender wing and fuselage structures, represented in either a continuous or discretized manner. The application of these approaches to aircraft loads will be covered later in Chapter 18.

6.1 LAWS OF MOTION

In Chapters 1 and 2, and indeed later on in the book, Lagrange's equations are normally used to set up the differential equations of motion. However, Newton's second law of motion could have been used instead

Introduction to Aircraft Aeroelasticity and Loads J. R. Wright and J. E. Cooper
© 2007 John Wiley & Sons, Ltd

to achieve the same end. In this chapter, Newton's laws will be introduced for completeness (as well as being sometimes simpler to employ) and because they are important for loads purposes.

6.1.1 Newton's Laws of Motion for a 'Particle'

Newton's laws (Meriam, 1980) are originally stated for a 'particle', a body of negligible dimensions but finite mass, such that acceleration occurs in translation, but without any rotation. The laws may be stated as follows:

1. Every 'particle' continues in a state of rest or of uniform motion unless acted upon by a net force.
2. When a net force acts upon a 'particle', it produces a rate of change of momentum equal to the force and in the same direction.
3. To every action, there is an equal and opposite reaction.

The second law is the most commonly used, and states mathematically that

$$F = \frac{\mathrm{d}}{\mathrm{d}t}(mv) = m\frac{\mathrm{d}v}{\mathrm{d}t} + v\frac{\mathrm{d}m}{\mathrm{d}t}, \tag{6.1}$$

where F is the net force acting, m is mass and v is velocity. If the rate of change of mass is insignificant, as is the case in most practical situations (except, for example, in rockets), then Equation (6.1) reduces to the better known form

$$F = m\frac{\mathrm{d}v}{\mathrm{d}t} = ma, \tag{6.2}$$

where a is the acceleration. When a 'particle' is not accelerating, there must be no net force, so $F = 0$ and the forces acting on it must be in equilibrium, a most important concept for loads.

Strictly speaking, acceleration should be measured with respect to an inertial axes system (i.e. one fixed relative to the stars). However, for most engineering analyses, the motion of the earth may be ignored so that an axes system fixed to the earth may be used; this is obviously inappropriate for space flight. When expressed in two dimensions, Equation (6.2) is written for components aligned with two orthogonal axes. Also, the double dot notation seen in earlier chapters will be employed to represent acceleration in most of the book, but in this chapter the simple symbolic representation for acceleration often used when introducing basic dynamic principles will be retained.

6.1.2 Generalized Newton's Laws of Motion for a 'Body'

When the applied forces cause both translation and rotation of a body of finite size, then Newton's second law as expressed for a particle no longer strictly applies. However, if the body is considered as an assembly of particles with equal and opposite forces acting between them, then it may be shown (Meriam, 1980) that this law can be extended to cover a body that is both translating and rotating.

6.1.2.1 Translation

For a body accelerating in translation, the generalized Newton's second law may be stated (in two dimensions) as

$$F_x = ma_x, \qquad F_y = ma_y, \tag{6.3}$$

where the subscripts x and y refer to the components acting in the Oxy axes directions and the acceleration is that of the centre of mass of the body. Thus, Newton's second law for a particle may effectively be used for a finite sized body, but only provided that the accelerations are considered at its centre of mass; the net force may be considered along any axis direction although usually two orthogonal axes are used.

Note that the term 'centre of mass' is used in this book to describe the point where the mass of a body may be assumed to act; it is a property of the body and remains the same whatever gravitational field the body is under. However, in aerospace applications, the term 'centre of gravity' is also in common usage; strictly speaking, this has a different definition to centre of mass in that the centre of gravity will change if the gravitational field is nonuniform, but the two are synonymous if a uniform gravitational field acts over the system.

6.1.2.2 Rotation

For a body accelerating in rotation, the generalized Newton's second law may be stated (in two dimensions) as

$$M_c = I_c \alpha, \tag{6.4}$$

where M_c is the applied moment about the centre of mass, α is the angular acceleration (rad/s^2) and I_c is the moment of inertia about an axis through the centre of mass. It is very important to recognize that for dynamic problems, this equation only applies for moments about the centre of mass (Meriam, 1980); the only exception is that moments may be taken about any fixed pivot point in the body (if one exists), with subscript 'o' replacing 'c' in Equation (6.4). If the body is not accelerating, then these two equations reduce to the equations of *equilibrium* and moments may then be taken about *any* axis. Note that for a body in three dimensions, the net force is usually expressed in three orthogonal directions and moments, about the three orthogonal axes that are employed.

6.1.3 Units

In using the second law of motion as defined above, it is essential that consistent sets of units are used, given that both metric (SI) and Imperial units are still in use within the international aerospace industry. For Newton's equation in translation, the appropriate units of force, mass and acceleration are given in Table 6.1.

The term kilogram (or pound) force refers to the force produced by a kilogram (or pound) mass acting in the gravity field (the so-called 'weight' associated with the mass); however, 'lb' is often used to denote force instead of 'lbf', though the authors would prefer to use 'lb' for mass only and to retain the symbol 'lbf' for force. It may be seen that the definition of 'slug' for mass in Imperial units derives from the second law. Clearly the unit sets A, D and E defined by kg m s N, slug ft s lbf and lb ft s poundal are suitable for use in Newton's law for translation (and indeed rotation), though lbf is far more common than poundal in Imperial use; they also yield consistent results when used in natural frequency calculations involving mass and stiffness. However, the other two sets of units B and C are deemed unsuitable for dynamic calculations.

Table 6.1 Units for force, mass and acceleration

Unit set	A	B	C	D	E
A force of	1 N (Newton)	1 kgf (kilogram force)	1 lbf (pound force)	1 lbf	1 poundal
accelerates a mass of	1 kg (kilogram)	1 kg	1 lb (pound mass)	1 slug (= 32.2 lb)	1 lb
at	1 m/s^2	9.81 m/s^2 (1*g*)	32.2 ft/s^2	1 ft/s^2 (1*g*)	1 ft/s^2

If the reader is ever faced with needing to convert between SI and Imperial units, then conversion factors are readily available for most common units. Alternatively, a procedure based on introducing conversion ratios of basic units may be employed as shown in the example following for a moment (or work done) unit, namely

$$\begin{aligned}1\,\mathrm{lbf\,ft} &= 1\left(\mathrm{slug}\frac{\mathrm{ft}}{\mathrm{s}^2}\right)\mathrm{ft} = 32.174\,\mathrm{lb}\frac{\mathrm{ft}^2}{\mathrm{s}^2} = 32.174\,\mathrm{kg}\left(\frac{\mathrm{lb}}{\mathrm{kg}}\right)\mathrm{m}^2\left(\frac{\mathrm{ft}}{\mathrm{m}}\right)^2\frac{1}{\mathrm{s}^2}\\ &= 32.174\,\mathrm{kg}\left(\frac{\mathrm{lb}}{2.2046\,\mathrm{lb}}\right)\mathrm{m}^2\left(\frac{\mathrm{ft}}{3.2808\,\mathrm{ft}}\right)^2\frac{1}{\mathrm{s}^2} = \left(\frac{32.174}{2.2046\times 3.2808^2}\right)\frac{\mathrm{kg\,m}^2}{\mathrm{s}^2} = 1.3558\,\mathrm{N\,m}.\end{aligned} \tag{6.5}$$

6.2 D'ALEMBERT'S PRINCIPLE – INERTIA FORCES AND COUPLES

In this section, D'Alembert's principle will be introduced to show how a dynamic problem may be reduced to an equivalent static one via so-called 'inertia forces (and couples)', even for a flexible aircraft in accelerated flight (see Chapter 18). This approach will allow the internal loads for a dynamic problem to be determined.

6.2.1 D'Alembert's Principle for a Particle

D'Alembert's principle (Meriam, 1980) allows the dynamic problem solved by Newton's second law to be converted into an *equivalent static* problem by changing the reference axes system from an inertial set to one fixed in the particle (or 'body') and accelerating with it. The effect of the acceleration is handled by introducing a fictitious 'inertia force' equal to (mass × acceleration), acting in the *opposite* direction to the acceleration vector. The applied force and the inertia force are then simply in equilibrium ('dynamic equilibrium'), as the problem has been reduced to an equivalent static one. In essence, the observer accelerating with the particle/body considers it to be in equilibrium and concludes that an inertia force must be acting to balance the applied force.

The idea is illustrated for a particle, and compared with Newton's law, in Figure 6.1. Thus the equation of equilibrium associated with D'Alembert's principle becomes

$$F - F_{\mathrm{Inertia}} = 0, \tag{6.6}$$

where $F_{\mathrm{Inertia}} = ma$. Note of course that this gives exactly the same result as may be found using Newton's second law. Newton's law and D'Alembert's principle are equivalent in outcome, and care should be taken not to use them together in a problem – otherwise the effective mass may end up being doubled.

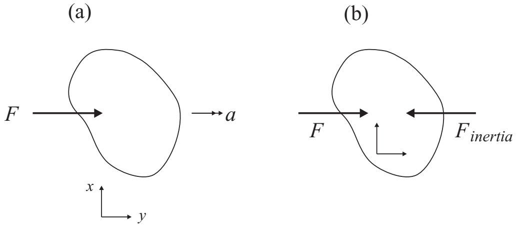

Figure 6.1 Comparison of (a) Newton's law and (b) D'Alembert's principle for a particle in translation.

The reader might wonder whether there is any point in using D'Alembert's principle; indeed Meriam (1980) recommends against using it. However, it is particularly powerful when determining the internal loads of a flexible accelerating body such as an aircraft. By employing D'Alembert's principle, a complex dynamic problem, with different parts of the aircraft accelerating by different amounts, is reduced to an equivalent static problem where simple static analysis methods may be employed. Indeed, so established is this approach in determining aircraft loads that the airworthiness requirements refer to the use of inertia forces and couples (CS-25 and FAR-25).

6.2.2 Application of D'Alembert's Principle to a Body

The approach described above for a particle may also be employed for a rigid body of finite size under the action of an applied force, except that the inertia forces must be introduced at the centre of mass. Also, a body subject to a net moment M_c about the centre of mass, and experiencing a rotational acceleration, is handled by introducing an *inertia couple* M_{Inertia} equal to moment of inertia about the centre of mass $I_c \times$ angular acceleration α, acting at the centre of mass and in the opposite direction to the angular acceleration, so

$$M_c - M_{\text{Inertia}} = 0, \tag{6.7}$$

where $M_{\text{Inertia}} = I_c\alpha$. The two approaches are illustrated in Figure 6.2.

Note that a 'couple' is a pure moment, such as would be provided by turning a screwdriver. It derives in essence from the effect of two parallel and equal forces acting in opposite directions and has the effect of rotating a body but providing no tendency to translate.

6.2.3 Extension to Distributed Inertia Forces

The concept of a *discrete* inertia force (or couple) was introduced above for a body accelerating under an applied force (or couple). However, the idea of inertia forces is extremely powerful when considering the internal loads (see later) present in a body under an accelerated condition because inertia forces can be *distributed* over the body and the problem can be reduced to one that is in equivalent static equilibrium. The use of distributed inertia forces will be illustrated for the problem of a rigid *continuous* member for two different load cases.

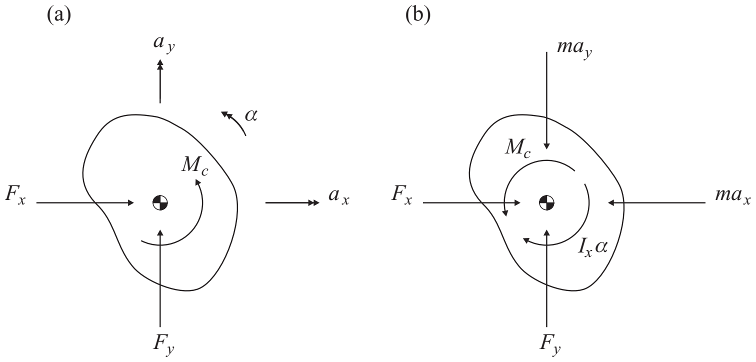

Figure 6.2 Comparison of (a) Newton's law and (b) D'Alembert's principle for a body.

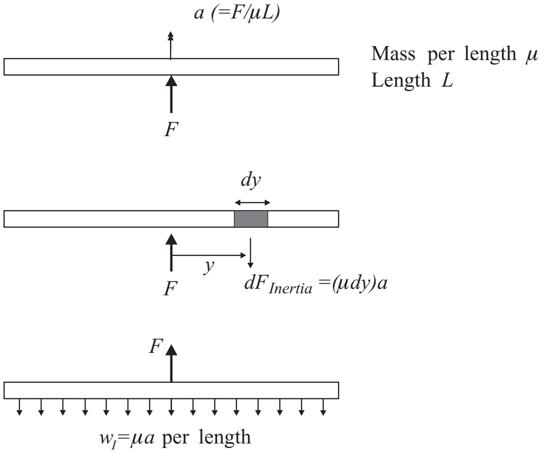

Figure 6.3 Distributed inertia forces on a body under uniform acceleration.

6.2.3.1 Translation

Consider firstly the example of a uniform continuous *rigid* body (or slender member) of length L and mass per length μ, accelerating in the horizontal plane (to avoid having to consider gravity) under the action of a force F applied at the centre of mass as shown in Figure 6.3. In the *steady* condition, the whole member, and thus every element $\mathrm{d}y$ of it, experiences a uniform acceleration of $a = F/(\mu L)$. Thus, using D'Alembert's principle for each element of mass $\mu\mathrm{d}y$ means that an elemental inertia force $\mathrm{d}F_{\mathrm{Inertia}}$ given by

$$\mathrm{d}F_{\mathrm{Inertia}} = (\mu \mathrm{d}y)a \tag{6.8}$$

may be considered as acting on each element of mass (in the opposite direction to the acceleration), as shown in Figure 6.3. The inertia force per unit length is given by $w_{\mathrm{I}} = \mu a$. The member is then effectively in static equilibrium because the applied force F and the total inertia force F_{Inertia} (obtained by integration of Equation (6.8)) are in balance. What is particularly useful, as a consequence of introducing distributed inertia forces, is that the internal loads for the member in the steady accelerating condition may be examined just as if it was subjected to a central static force, balanced by a uniformly distributed load.

6.2.3.2 Rotation

A further example allows the ability of the approach to cater for a *nonuniformly distributed acceleration* to be shown. Consider the same uniform rigid member, but it is now accelerated in rotation by a moment M_{c} applied at the centre of mass as shown in Figure 6.4. Since the moment of inertia of a uniform slender member about its centre of mass is given by $I_{\mathrm{c}} = \mu L^3/12$, the angular acceleration of the member is

$$\alpha = \frac{M_{\mathrm{c}}}{I_{\mathrm{c}}}. \tag{6.9}$$

Hence the acceleration of a typical element $\mathrm{d}y$, at distance y from the centre of mass, will be given by

$$a = \alpha y, \tag{6.10}$$

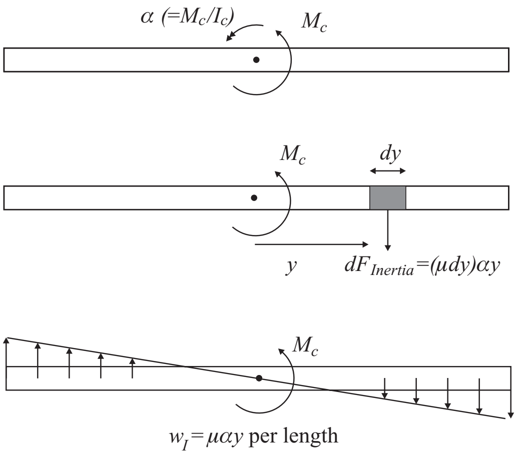
α (=M_c/I_c)
M_c
M_c
dy
y
$dF_{Inertia}$=(μdy)αy
M_c
$w_I = \mu\alpha y$ per length

Figure 6.4 Distributed inertia forces on a member under nonuniform acceleration.

and this may be seen to vary linearly with the distance from the centre of mass. Thus, when inertia forces are introduced for each element then, as shown in the figure, the inertia force per unit length varies linearly and is given by $w_{\mathrm{I}} = \mu\alpha y$. The applied couple is then in equilibrium with the net moment of the inertia forces acting on all the elements. Once again the internal loads could be determined by static methods, but this time an approach based on integrating elemental contributions will be required; this process is relevant to the real aircraft in dynamic response and will be illustrated in Chapter 18.

6.3 EXTERNALLY APPLIED/REACTIVE LOADS

6.3.1 Applied Loads

Externally applied loads are defined as loads that may be considered as acting *on* the whole body (and not a part of it), and may be constant or vary with time. They may be categorized as being:

(a) *Distributed over a surface* (e.g. aerodynamic pressure loads),
(b) *Discrete* (e.g. engine thrust) or
(c) *Distributed over the body volume* (e.g. weight and inertia forces, see later).

In practice, no force ever acts precisely at a ‘point’ but may often be represented as doing so for convenience of analysis (e.g. thrust will be considered as a discrete force for overall aircraft handling and load calculations but is actually distributed, and a discrete force representation is inappropriate for engine load considerations).

6.3.2 Reactive Loads (i.e. Reactions)

For an aircraft, many of the load cases involve the aircraft being airborne and so there would be no reactions to the ground. However, ground manoeuvres such as taxiing, landing, turning and braking involve the aircraft being in contact with the ground via the landing gear. Any such support arrangement has the effect of constraining one or more displacements and/or rotations, usually to zero, as shown in Figure 6.5 for a two-dimensional scenario with several different constraint arrangements. This concept readily extends to the three-dimensional case.

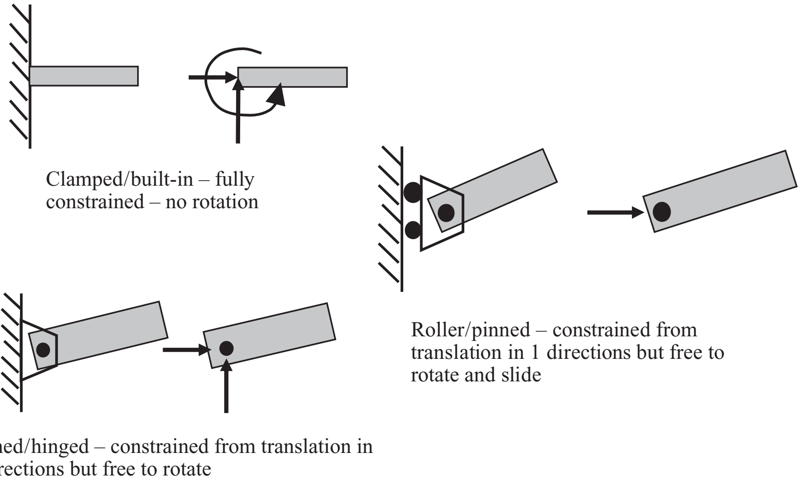
Clamped/built-in – fully constrained – no rotation
Roller/pinned – constrained from translation in 1 directions but free to rotate and slide
Pinned/hinged – constrained from translation in 2 directions but free to rotate

Figure 6.5 Constraints and reactions in two dimensions.

When analysing a body supported in some way, the body must be 'released' from the support (or ground) and equal and opposite reactions considered, corresponding to Newton's third law. The effect of the support on the body is replaced by the unknown equal and opposite reactions provided by the support to the body, shown in Figure 6.5; every constrained component of motion (translation or rotation) must be replaced by a reactive force or moment. A free body diagram (FBD) is then drawn (see the next section); the reactions are added to the FBD and the magnitudes determined using equilibrium considerations. An example is shown in the next section.

6.4 FREE BODY DIAGRAMS

A free body diagram (FBD) is a diagrammatic representation of the forces acting on a whole body, or part of it. The body is isolated from its supports and all the applied and reactive forces are drawn on a diagram of the body, positioned at their effective points of action (e.g. centre of mass for inertia forces, centre of pressure for aerodynamic forces). This is because only their total effect is required for *overall* considerations; however, when the internal loads are required (see later), then the *distributed* nature of the loads will need to be retained. Once an FBD is available, then generalized Newton's laws of motion may be applied so as to yield relationships between the forces and any resulting accelerations; alternatively, D'Alembert's principle may be applied.

As an example of an FBD, consider an aircraft supported against vertical motion at the nose and main landing gear positions but free to roll horizontally, as shown in Figure 6.6; it is accelerating forward under thrust loading with friction effects ignored. The mass is m, weight $W(= mg)$, thrust T and total support reactions R_N, R_M. The acceleration at the instant of interest is $a = T/m$. The dimensions are shown in the figure with the centre of mass being a distance d above the thrust line and h above the ground. The forces acting are shown on an FBD in the lower part of the figure. The arrows are the forces acting upon the aircraft if the generalized Newton's law were to be employed. On the other hand, were D'Alembert's principle to be applied, an additional horizontal inertia force ma would need to be present (not shown here). There is no pitch acceleration or inertia moment because both landing gears are assumed to remain in contact with the ground. Consider determining the nosegear reaction using

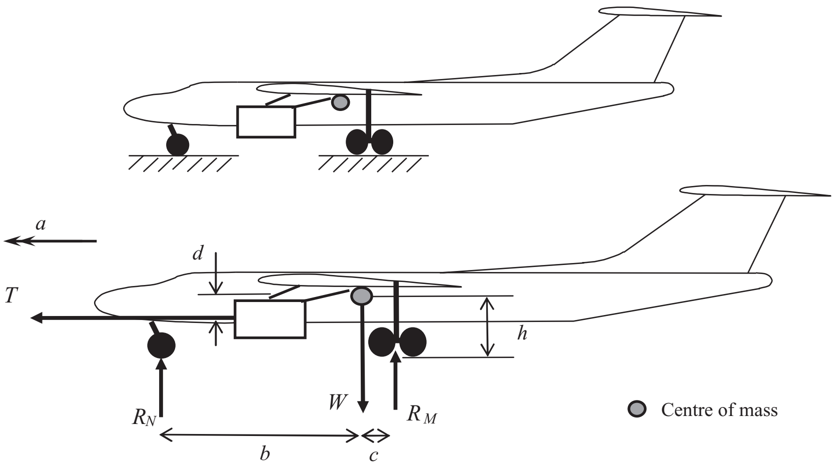

Figure 6.6 Free body diagram example when using Newton's law.

Newton's law; the equations for translation and rotation *about the centre of mass* are

$$T = ma, \qquad R_N + R_M - W = 0, \qquad R_N b - R_M c + Td = I_c \alpha = 0, \tag{6.11}$$

and solving for the nose gear reaction yields

$$R_\mathrm{N} = \frac{Wc - Td}{b + c}. \tag{6.12}$$

If, on the other hand, moments are taken about the point of contact of the main landing gear with the ground instead of about the centre of mass, then the resulting reaction would be incorrect because the basis of the generalized Newton's law is that moments must be taken about the centre of mass for a dynamic problem (this is a common error). However, if D'Alembert's principle were to be employed, the inertia force *ma* is included in the FBD and the problem is a static one, so it is immaterial where moments are taken.

6.5 INTERNAL LOADS

So far, the external loads present on a body have been considered. However, in order to see whether the body can sustain the external loads applied to it, the so-called 'internal loads' present *within* the body must be determined. These internal loads will depend upon the *distribution* of the external loads over each component, and not simply on their net values. Internal loads may be determined for steady or dynamic load cases, for the latter by employing D'Alembert inertia forces/couples in order to create an effective static equilibrium condition.

Typical internal loads for a relatively slender body (or member/beam/shaft/rod/bar, see Chapter 3) are shear force, bending moment (hogging/sagging), axial force (tension/compression) and torque (twisting moment) – a suitable acronym might be 'MAST' loads (moment/axial/shear/torque). The examples considered in this chapter will only cover shear force and bending moment, with the others introduced later in Chapter 18. More detailed coverage of internal loads may be found in many references, e.g. Benham *et al.* (1996), but here the focus will be on members with distributed loads such as those induced by inertia loading. Internal loads are sometimes referred to as ‘stress resultants’ since they are the aggregate of the stresses acting. The body will be treated initially as *continuous* and later a *discretized* representation will be considered.

6.6 INTERNAL LOADS FOR CONTINUOUS REPRESENTATION OF A STRUCTURE

The treatment of a slender member (such as a wing) represented as a continuous structure will be considered for uniformly and then nonuniformly distributed loadings. Later, discretized members will be considered.

6.6.1 Internal Loads for Uniformly Distributed Loading

The idea of internal loads and how they can be determined will be illustrated for the earlier dynamic example of the uniform member in effective static equilibrium under a uniform accelerating condition as shown in Figure 6.3.

6.6.1.1 ‘Exposing’ internal loads

To ‘expose’ and so determine the internal loads at a particular point on a member, then the analyst must ‘imagine’ the member as being ‘cut’ into two subsections at this point. However, when doing so, equal and opposite ‘internal loads’ must be introduced at the ‘cut’ to represent the effect of the missing structure (i.e. what has been ‘cut’ away); this is in effect a consequence of Newton’s third law. The internal loads are then determined by considering the equilibrium of one or other subsection.

The FBDs for the two subsections generated by the ‘cut’ AA at position y from the centre of mass are shown in Figure 6.7, with equal and opposite internal ‘shear force’ Q and ‘bending moment’ M (a pure couple) introduced; these internal loads quantities will be discussed below. In order to simplify the

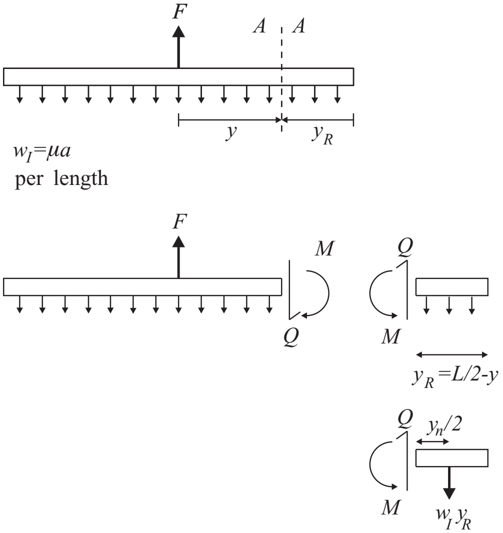

Figure 6.7 Free body diagrams showing internal loads on a member with uniformly distributed loading.

resulting equilibrium expressions, a different coordinate measured from the right hand end will be used in place of y, namely $y_{\mathrm{R}} = L/2 - y$. There are two versions of the FBD shown for the right-hand cut section, one with the distributed load per unit length w_{I} shown explicitly and the other showing the net force due to the distributed load acting on the relevant subsection; it is this latter version which is used for analysis and because the force is uniformly distributed, the net force $w_{\mathrm{I}} y_{\mathrm{R}}$ on the cut subsection may be placed at the centre of the subsection as shown.

6.6.1.2 Determining internal loads via equilibrium of 'cut' sections

Each 'cut' subsection must be in equilibrium under the relevant external and internal loads acting on it. In this example, it is simpler to apply the equilibrium condition for the right-hand subsection, namely that there will be no net force or moment (moments are usually taken about the 'cut' to avoid including the shear force Q), so

$$Q - w_{\mathrm{I}} y_{\mathrm{R}} = 0, \qquad M - w_{\mathrm{I}} y_{\mathrm{R}} \frac{y_{\mathrm{R}}}{2} = 0, \tag{6.13}$$

Note the function of the two types of internal load introduced; the shear force Q balances the distributed external load $w_{\mathrm{I}} y_{\mathrm{R}}$ and the bending moment M resists the tendency of the member to rotate due to the offset of the net force from the cut. Rewriting the equations leads to expressions in terms of y or y_{R}, namely

$$Q = w_{\mathrm{I}} y_{\mathrm{R}} \quad \text{or} \quad w_{\mathrm{I}} \left(\frac{L}{2} - y \right), \qquad M = \frac{1}{2} w_{\mathrm{I}} y_{\mathrm{R}}^2 \quad \text{or} \quad \frac{1}{2} w_{\mathrm{I}} \left(\frac{L}{2} - y \right)^2 \tag{6.14}$$

Exactly the same expressions would have been obtained were the equilibrium of the left-hand subsection in Figure 6.7 to have been considered instead, but the applied force $F(= \mu a L)$ would have been included. Note that the internal load expressions only apply for the subsection of the member covered by cut AA, namely $y > 0$ or $y_{\mathrm{R}} < L/2$; the internal loads in the left-hand half of the member ($y < 0$) could be obtained by repeating the process for a cut in the left hand half, or more simply by exploiting symmetry.

The variation of these internal loads along the entire member is shown graphically in Figure 6.8. It may be seen that the shear force varies linearly and the bending moment quadratically with an increase

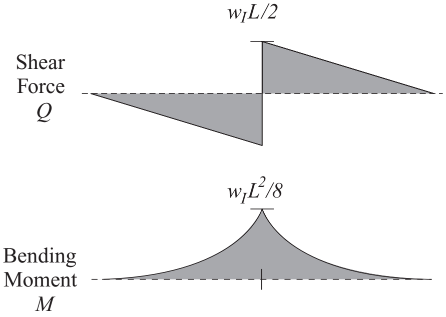

Figure 6.8 Internal load diagrams for a member accelerating under a central force.

in y_R, and that the maximum internal loads occur at the centre where the external load is applied and there is a step change in shear force. Note that the signs of these internal loads depend upon the sign convention chosen. What is important is to be consistent with the choice of sign convention within a particular problem.

So far, internal loads have been shown for the dynamic load case of steady acceleration using a simple continuous, rigid and uniform body. In practice, an aircraft will be subject to transient dynamic loading and will be flexible; also the loads (inertia and aerodynamic) will be nonuniformly distributed. Resulting deformations and internal loads would then be required as a function of time and maximum values found. Such a problem may be treated as in the above example but the effective static equilibrium condition needs to be considered at every instant of time. Also, calculation of internal loads for a structure with nonuniform loading will require an integral approach, as shown later in this chapter. The calculation of loads for a rigid or flexible aircraft under steady/dynamic manoeuvres or gusts will be considered in Parts II and III of the book.

6.6.2 Internal Loads for Nonuniformly Distributed Loading

In this section, the analysis shown above will be extended to a member with time-varying applied loads and nonuniformly distributed inertia loading. The focus will be on how to handle the nonuniformly distributed loading when determining internal loads. Consider a uniform continuous rigid member of length L, mass per length μ, mass m and moment of inertia I_c, subject to centrally applied dynamic loads $F(t)$ and $M_c(t)$, as shown in Figure 6.9. The acceleration over the member varies nonuniformly and is defined by $a(\eta, t) = a_0(t) + \alpha(t)\eta$, where $a_0(t) = F(t)/m$, $\alpha(t) = M_c(t)/I_c$ and η is the distance from the centre of mass.

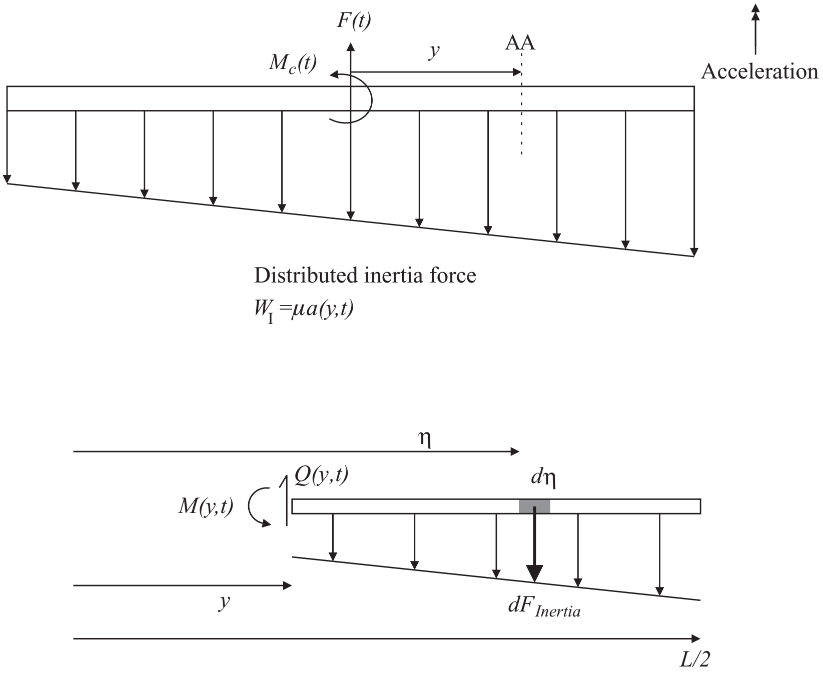

Figure 6.9 Internal loads for nonuniformly distributed loading – continuous member.

6.6.2.1 Distributed inertia forces for a continuous structure

Knowing that the acceleration at time t of an element $\mathrm{d}\eta$ of the member at position η from the centre is given by the function $a(\eta, t)$, introduce a distributed inertia force to bring the member into effective static equilibrium at a chosen instant of time t (based on D'Alembert's principle). The inertia force acting on the element is

$$\mathrm{d}F_{\text{Inertia}}(\eta, t) = \mathrm{d}m\, a(\eta, t) = \mu \mathrm{d}\eta\, a(\eta, t), \tag{6.15}$$

which acts in the opposite direction to the acceleration as shown in Figure 6.9. Thus the distributed inertia force per unit length is $w_{\mathrm{I}} = \mu\ a(\eta, t)$ and this will have a non-uniform spatial distribution.

6.6.2.2 Internal loads for a continuous structure under nonuniform loading

Consider a 'cut' AA in the member at position y (> 0) and introduce an instantaneous shear force $Q(y, t)$ and bending moment $M(y, t)$, as shown in Figure 6.9. For equilibrium of the right-hand subsection at time t, there will be no net force or moment about the cut. Previously, where the loading was uniformly distributed, the net load could be positioned at the centre of the cut section. However, the effect of the nonuniformly distributed inertia force needs to be included by integration (or summation) of the elemental contributions over the right-hand subsection, so that

$$Q(y, t) = \int_{\eta=y}^{L/2} \mathrm{d}F_{\text{Inertia}}(\eta, t) = \mu \int_{\eta=y}^{L/2} a(\eta, t)\mathrm{d}\eta$$

and (6.16)

$$M(y, t) = \int_{\eta=y}^{L/2} (\eta - y)\mathrm{d}F_{\text{Inertia}}(\eta, t) = \mu \int_{\eta=y}^{L/2} (\eta - y)a(\eta, t)\mathrm{d}\eta.$$

Knowing the time histories for the applied force, and hence the acceleration along the member, the shear force and bending moment at every position along the member and at every instant of time may be calculated. Results are typically plotted against time for each internal load of interest at critical positions in order to determine maximum values for design (see Chapters 18 and 25).

6.6.2.3 Example of nonuniformly distributed loading for a continuous structure

Consider the case where only the pure moment $M_{\mathrm{c}}(t)$ is applied, so $F(t) = 0$. The linearly varying acceleration of the member at position η is $a(\eta, t) = \eta\alpha(t)$, where $\alpha(t) = M_{\mathrm{c}}(t)/I_{\mathrm{c}}$ and $I_{\mathrm{c}} = \mu L^3/12$ for a uniform member. If these values are substituted into Equation (6.16), then the internal loads are given by

$$Q(y, t) = \frac{M_{\mathrm{c}}}{L}\left[\frac{3}{2} - 6\left(\frac{y}{L}\right)^2\right], \qquad M(y, t) = M_{\mathrm{c}}\left[\frac{1}{2} - \frac{3}{2}\left(\frac{y}{L}\right) + 2\left(\frac{y}{L}\right)^3\right]. \tag{6.17}$$

The shear force and bending moment at every position along the member may then be calculated as a function of time, and antisymmetry may be employed for the left-hand half of the member. The variation of internal loads along the member at a particular instant of time is shown in Figure 6.10; note in this case that there is a step change in moment at the centre due to the presence of the applied moment.

Clearly, for an aircraft in flight, some applied forces will be aerodynamic in origin, a function of the response, and will also be distributed over the component in question. Also, the mass will not be uniformly

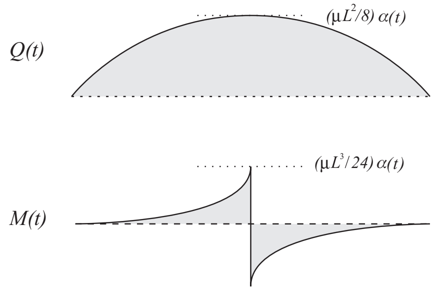

Figure 6.10 Internal loads for a member under rotational acceleration due to a central couple.

distributed. Thus the analysis for the aircraft case will be more complex than in these examples, but the principles will be the same.

6.7 INTERNAL LOADS FOR DISCRETIZED REPRESENTATION OF A STRUCTURE

The above analysis applies to continuous bodies, i.e. where both the structure and distributed loads are treated as continuous and the internal load expressions required integration over the member. However, for a real structure such as an aircraft, while the structure and loading are still nominally continuous, they are far too complex to treat as analytic functions. Since only a finite set of loads is required, the structure is idealized by dividing it into discrete sections/elements, with the loads being applied to each section. The analysis is approximate, with the analytic integral being replaced by a summation, but provided an adequate number of sections are used, the accuracy should be satisfactory. The idea will be illustrated for the earlier example of a member under the action of a central force and moment, but this time the treatment is discretized. It should be recognized that the treatment of a discretized member is essentially the same whether the loading is uniformly or nonuniformly distributed, since in either case a summation approach would be required. Note that discretized structures were considered in Chapters 4 and 5, and will be considered further in Chapters 18 and 20.

6.7.1 Distributed Inertia Forces for a Discretized Structure

Consider the uniform rigid member of length L and mass per length μ, subject to a centrally applied dynamic load $F(t)$ and moment $M_c(t)$, as shown in Figure 6.11. The member is approximated by discretizing it into N sections/elements, each of equal length $\Delta y(= L/N)$ and mass $m_k = \mu L/N$; the left-hand end of the kth element is at a distance y_k from the centre of the member. The mass is lumped at the centre of each section. D'Alembert's principle may then be applied to this discretized structure by introducing,

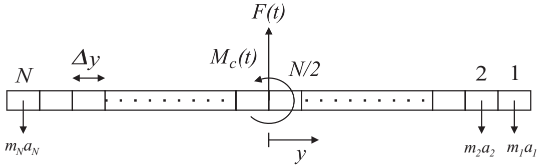

Figure 6.11 External loads for nonuniformly distributed loading – discretized member.

at the kth section/element, an inertia force equal to the product of the section mass m_k and the section acceleration $a_k(t)$ at a chosen instant of time t. The inertia force on the kth element at time t is then given by

$$F_{\text{Inertia\_k}}(t) = m_k a_k(t). \tag{6.18}$$

The inertia forces are shown in Figure 6.11 and the structure is in static equilibrium under the applied and inertia forces. The acceleration at each mass point can be found using the structure mass $m = \sum m_k$ and moment of inertia $I_c = \sum m_k r_k^2$, where r_k is the distance from the centre of mass to the kth mass point.

6.7.2 Internal Loads for a Discretized Structure

For a discretized member, the internal loads are only determined at the interfaces between the sections/elements. Consider a cut in the right-hand half of the member at the interface between the jth and $(j+1)$th elements, with internal loads $Q_j(t)$ and $M_j(t)$ introduced to the subsection, as shown in Figure 6.12. For equilibrium of the right-hand subsection, there is no net force or moment at the cut, so

$$Q_j(t) = \sum_{k=1}^{j} F_{\text{Inertia\_k}}(t) - F_{\text{Applied}}$$

and (6.19)

$$M_j(t) = \sum_{k=1}^{j} F_{\text{Inertia\_k}}(t)\left(y_k + \frac{\Delta y}{2} - y_j\right) - F_{\text{Applied}}\left(\frac{L}{2} - y_j\right).$$

Thus the approach is the same as for the continuous system, except that integration is replaced by summation.

6.7.3 Example of Distributed Loading – Discretized Structure

The above case will now be considered using numerical values. Consider the example of the member under uniform acceleration from an applied force alone (no couple acting), with $N = 10$ sections, $\mu = 100$ kg/m, $L = 1$ m (i.e. total mass of 100 kg) and $F = 1000$ N, so that $\Delta y = 0.1$ m, $m_{1-10} = \mu\,\Delta y = 10$ kg, $a_{1-10} = F/\mu L = 10$ m/s^2 and $F_{\text{Inertia}1-10} = 100$ N. Applying Equation (6.19) yields the internal

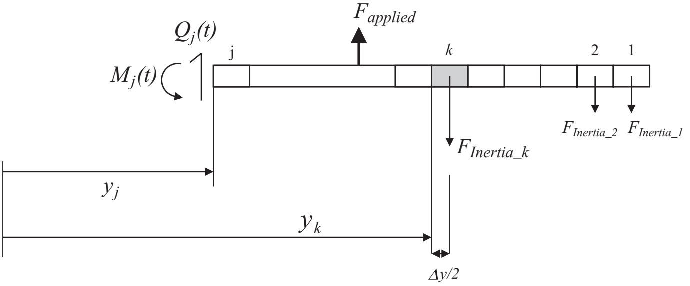

Figure 6.12 Internal loads for nonuniformly distributed loading – discretized member.

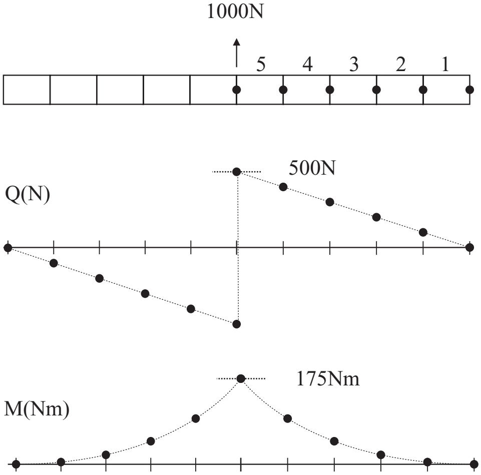

Figure 6.13 Internal load diagrams for a member accelerating under a central force.

load diagram shown in Figure 6.13. The results may be compared to those in Figure 6.8 for the continuous member and there is good agreement.

6.8 INTERCOMPONENT LOADS

A body is often composed of several interconnected major components (e.g. wing, fuselage, tailplane, fin, landing gear and engines for an aircraft). It can be helpful to consider a particular component in isolation from the rest of the body; this is achieved by 'cutting' it away and introducing equal and opposite 'intercomponent' loads at the interface – actually the internal loads there. Thus Figure 6.14 shows, in two dimensions only, an example where the FBDs for the two components are shown separately, with intercomponent forces and moments introduced. Once such diagrams are drawn and the external loads applied to each component are known, each component may then be analysed separately in order to determine the intercomponent loads. A further example of 'separating' a wing and fuselage is shown in Chapter 18.

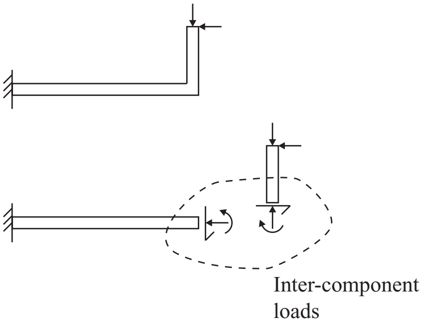

Figure 6.14 Intercomponent loads example.

6.9 OBTAINING STRESSES FROM INTERNAL LOADS – STRUCTURAL MEMBERS WITH SIMPLE LOAD PATHS

The process of obtaining internal loads, described so far in this chapter, is essentially the first stage of a calculation aimed eventually at obtaining stresses. For a slender member with well-defined load paths (e.g. a circular tube or T-section member), once any moment, axial, shear and torsion ('MAST') internal loads present have been determined at any cross-section, it is then possible to determine the stresses at that cross-section from basic stress analysis theory using the cross-sectional properties (Benham *et al.*, 1996).

As an example, the direct stress σ for bending about the neutral axis (i.e. the axis in the cross-section where this stress is zero) of a member is given by

$$\sigma = \frac{My}{I}, \tag{6.20}$$

where M is the bending moment, I is the cross-section second moment of area and y is the distance from the neutral axis (Benham *et al.*, 1996). Similar expressions apply for other loadings on simple structures (Young, 1989; Benham *et al.*, 1996) and for simple aerospace structures (Donaldson, 1993; Megson, 1999), but a treatment of stress analysis is beyond the scope of this book. Such methodologies may be employed for structures with well-defined load paths.

However, it should be noted that such classical formulaic approaches are not suitable for complex aerospace structures where the load paths are not well defined. Instead, additional analyses will need to be carried out to determine loads and stresses in structural elements using the 'MAST' internal loads described earlier; this will be explained briefly in Chapters 18 and 21.

6.10 EXAMPLES

Note that the signs of the internal loads depend upon the sign convention used.

1. Convert the following quantities into SI or Imperial units as appropriate: (a) 10 N m, (b) 5 lbf ft, (c) 10 N/m^2, (d) 5 lbf/ft^2, (e) 10 kg m^2 and (f) 5 slug ft^2.

   [7.376 lbf ft, 6.779 N m, 0.209 lbf/ft^2, 239.4 N/m^2, 7.376 slug ft^2, 6.779 kg m^2]

2. Draw the free body diagram and find the support reactions in magnitude and direction for the member shown in Figure 6.15.

   [left-hand support 1.73 kN upwards and 5.50 kN to the left and right-hand support 0.87 kN upwards; do not forget the moment produced by the horizontal 5 kN force]

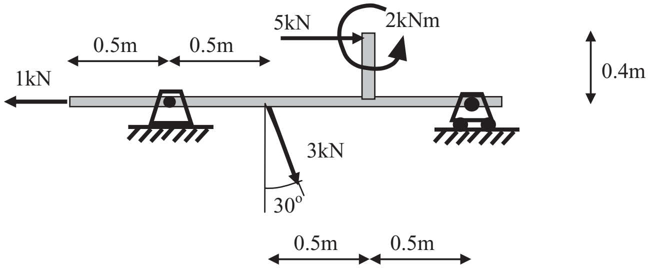

Figure 6.15

3. A nose landing gear is subject to a set of loads as shown in Figure 6.16. Find the force and moment reactions at the support.

[11 kN down, 4 kN to the right and 4.75 kN m anticlockwise]

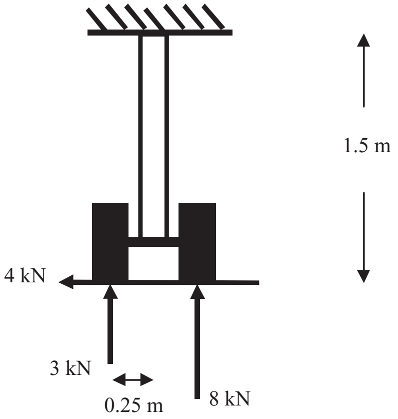

Figure 6.16

4. Replace the lift force L acting at the centre of pressure (CP) on the aerofoil shown in Figure 6.17 by an equivalent force and couple arrangement at the aerodynamic centre position (AC). Hint: place a pair of equal and opposite forces L at AC and replace one parallel force pair by a couple.

[force L and couple Lh nose down]

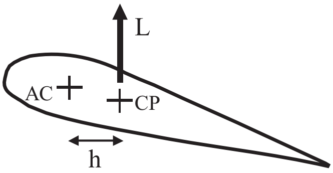

Figure 6.17

5. For the built-in slender member shown in Figure 6.18, draw each ‘cut’ part together with external and internal loads. Use equilibrium to determine expressions for the shear force and bending moment at each cut. Then draw the internal load diagrams and find the support reactions.

[maximum bending moment −10 kN m at 9 kN load position, reactions 4 kN and 2 kN m at root]

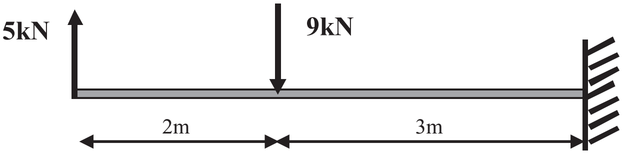

Figure 6.18

6. For the simply supported slender member shown in Figure 6.19, determine the reactions and draw each 'cut' part together with external reaction components and internal loads. Use equilibrium to determine expressions for the shear force and bending moment at each cut. Then draw the internal load diagrams and indicate the support reactions.

   [maximum bending moment 12 kN m at the left-hand support, reactions 10 kN up at the left-hand support and 4 kN down at the right-hand support]

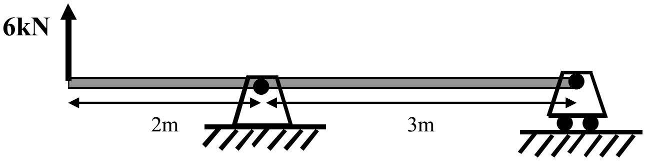

Figure 6.19

7. For the simply supported slender member shown in Figure 6.20, determine the reactions and draw each 'cut' part together with external and internal loads. Use equilibrium to determine expressions for the shear force and bending moment at each cut. Then draw the internal load diagrams and indicate the support reactions.

   [bending moment varying parabolically, with maximum 5.625 kN m at centre, reactions 7.5 kN at each end]

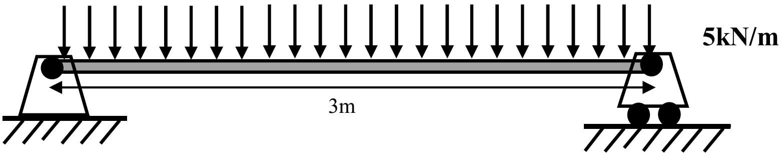

Figure 6.20

8. A uniform member of length L and mass per length μ is subject to applied forces $F/2$ acting normal to the member axis at a distance $b/2$ either side of its centre. Determine the inertia loading distribution and draw an FBD for the member in effective static equilibrium for an accelerated condition. Then determine the bending moments at the centre and at one load point. Sketch the bending moment variations for values of $b/L = 0, \frac{1}{3}, \frac{2}{3}, 1$ and note how the load position influences the behaviour.

   [load point $(-FL/8)(1 - b/L)^2$ and centre $(FL/4)(b/L - \frac{1}{2})$]

9. For the built-in slender member shown below in Figure 6.21, draw each 'cut' part together with external and internal loads. Use equilibrium to determine expressions for the shear force and

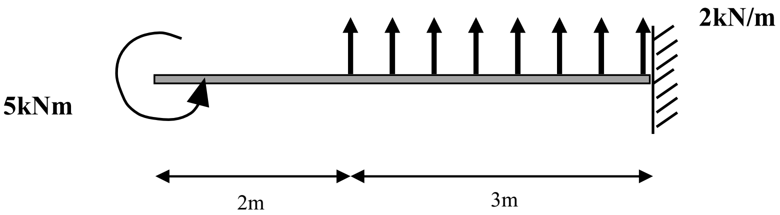

Figure 6.21

bending moment at each cut. Then draw the internal load diagrams and indicate the support reactions.

[bending moment is constant at 5 kN m in the left-hand section, changing parabolically to −4 kN m at the support, where the other reaction is 6 kN]

10. The slender member shown in Figure 6.22 is built in at point A and loaded by torques at points B and C. Draw each ‘cut’ part together with external and internal torsional loads. Use equilibrium to determine expressions for the torque at each cut. Then draw the internal load diagrams and indicate the support reaction.

    [torque is 4 kN m at root, essentially the same diagram as for the shear force in Example 5]

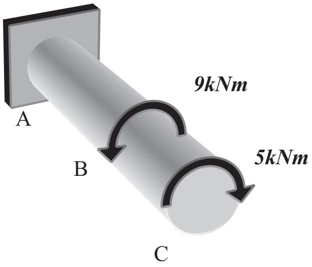

Figure 6.22

11. A uniform member of length 10 m and mass per length 200 kg/m is subject to an applied force of 10 kN acting normal to the member axis at its centre. Determine the inertia loading distribution and draw an FBD for the member in effective static equilibrium for this accelerated condition. Then determine the bending moment at the centre (a) assuming the member is continuous and (b) assuming the member is discretized into 10 sections.

    [both 12.5 kN m]

12. A uniform member of length L and mass per length μ is subject to an applied force F acting normal to the member axis at one end of the member. Determine the inertia loading distribution and draw an FBD for the member in effective static equilibrium for this accelerated condition. Then determine the bending moment at the centre.

    [centre $3FL/8$]

7

Introduction to Control

Control systems are used in a wide range of engineering applications and industries, to enable a system (e.g. an aircraft) to respond in some desired way when subjected to some form of external input. For example, a gust load alleviation system might use acceleration measurements on the aircraft to detect the motion due to turbulence and then employ the control surfaces in such a way as to reduce the loads acting on the aircraft structure. Other inputs could be provided by the pilot and the control system could limit the loads generated. The systems used on aircraft for control in flight may be electrical, mechanical, hydraulic or pneumatic and perform a widely differing range of tasks, e.g. provision of required stability and handling properties, carefree handling, manoeuvre load alleviation, etc. Modern aircraft have extremely sophisticated flight control systems (Pratt, 2000) that play an important role in the aeroelastic and loads behaviour of the aircraft, so it is important to understand key issues of control.

This chapter will examine some of the basic control tools and definitions that need to be understood before the application of control systems to aeroelastic systems, the science of aeroservoelasticity (or structural coupling), which will be tackled in Chapter 12. The aircraft flight control system will be considered further in Chapters 14 and 22. Many textbooks cover basic control theory, e.g. Raven (1994) and Dorf and Bishop (2004).

7.1 OPEN AND CLOSED LOOP SYSTEMS

Consider the system in Figure 7.1 that responds in some way, known as the output, to some given input. This representation of the resulting output due to an applied input could, for example, be used to describe the direction that an aircraft flies in, subject to the application of the control surfaces.

A controller can be added to the set-up, as shown in Figure 7.2, and is used to define the control inputs needed in order to manoeuvre the aircraft so that it flies on a particular heading. This is known as an *open loop* system. The controller may be designed using trial and error or past experience to dictate what control surface deflections are needed to change the direction of the aircraft. However, no account is made of any external influences, e.g. the wind direction and speed, and the consequent effect this has on the aircraft.

In order to steer the aircraft accurately, a continually updated comparison between the required direction and that actually being flown needs to be made. The aircraft's heading can be continually changed until the difference between the required and actual direction is zero. Figure 7.3 shows this set-up, known as a *closed loop* system, where it can be seen that the output is fed back into the system and compared with the desired input value. The difference (error) between the two is then passed through the controller element which is designed to produce the required output from the system. Such a closed loop system is the basis of all control systems, e.g. flight control systems, but there are many different ways of implementing the control.

Introduction to Aircraft Aeroelasticity and Loads J. R. Wright and J. E. Cooper
© 2007 John Wiley & Sons, Ltd

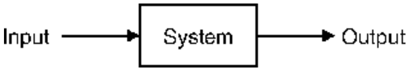

Figure 7.1 Basic open loop system.

The ratio between any two points in the system (often the output and input) in either the Laplace or frequency domains (Raven, 1994) is known as the *transfer function* (TF). Note however, that in vibration analysis the ratio between output and input signals is also commonly called the *frequency response function* (FRF; see Chapter 1).

7.2 LAPLACE TRANSFORMS

The Laplace transform is one of the key mathematical tools used to model control systems. Essentially, it is simply a mathematical transformation that enables functions of time t to be reformulated in terms of the so-called Laplace operator s. One particular benefit is that differential equations in t can be expressed as algebraic expressions in s, which can then be used to determine the system transfer function with or without a control system present. The transfer function then enables the stability and dynamic characteristics of the system to be investigated. A further advantage of employing the Laplace approach is that, by the use of a transformation between s and ω, the transfer function can be expressed in the frequency domain.

The Laplace transform $F(s)$ of a time function $f(t)$ is defined as

$$L\{f(t)\} = F(s) = \int_0^{\infty} f(t)\mathrm{e}^{-st}\mathrm{d}t, \tag{7.1}$$

where the usual convention of time functions being written in lower case and Laplace operator functions written in upper case is followed. It is also possible to invert the process so that the corresponding time function for a given Laplace function can be found.

In general, the integral does not have to be solved since tables are available giving the Laplace transforms of the most common functions, some of which are shown in Table 7.1. More complicated expressions can be tackled through the use of simple rules that apply to linear systems (Raven, 1994). Note in the table that $f(0)$, for example, is the initial condition of $f(t)$.

7.2.1 Solution of Differential Equations using Laplace Transforms

As an example of the use of Laplace transforms, the solution of differential equations will be illustrated with a single degree of freedom system, subjected to a unit step function at time $t = 0$ (with initial conditions $x(0) = 0$, $\dot{x}(0) = 0$). As was determined in Chapter 1, the equation of motion is

$$m\ddot{x} + c\dot{x} + kx = f(t) \qquad \text{or} \qquad \ddot{x} + 2\zeta\omega_{\mathrm{n}}\dot{x} + \omega_{\mathrm{n}}^2 x = \frac{f(t)}{m} \tag{7.2}$$

and for this example $f(t)$ is taken as the unit step function.

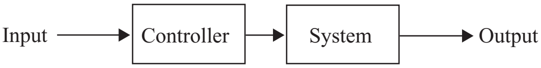

Figure 7.2 Open loop system with open loop controller.

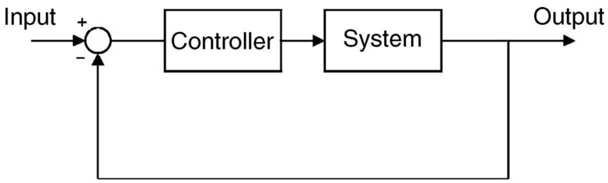

Figure 7.3 Closed loop system.

The idea of the analysis is to use the Laplace transform to transform a differential equation in time into an algebraic equation in the Laplace variable. The algebraic equation may be solved readily and transformed back to the time domain to yield the response solution.

Transforming each term in Equation (7.2) using the Laplace transforms given in the above table leads to

$$m[s^2X(s) - sx(0) - \dot{x}(0)] + c[sX(s) - x(0)] + kX(s) = \frac{1}{s} \tag{7.3}$$

or, with zero initial conditions,

$$(ms^2 + cs + k)X(s) = m\left(s^2 + 2\zeta\omega_{\mathrm{n}}s + \omega_{\mathrm{n}}^2\right)X(s) = \frac{1}{s}. \tag{7.4}$$

This algebraic equation shows that a differential equation in time has been transformed into an algebraic expression in s. Rearranging this equation yields

$$X(s) = \frac{1}{ms\left(s^2 + 2\zeta\omega_{\mathrm{n}}s + \omega_{\mathrm{n}}^2\right)}. \tag{7.5}$$

This expression now needs inverse transformation to get back to the time domain, but the form of the expression needs modifying so as to be able to use the table below. Rewriting Equation (7.5) in terms of a partial fraction expansion gives

$$X(s) = \frac{1}{m}\left(\frac{A}{s} + \frac{Bs + C}{s^2 + 2\zeta\omega_{\mathrm{n}}s + \omega_{\mathrm{n}}^2}\right) = \frac{1}{m}\left[\frac{A\left(s^2 + 2\zeta\omega_{\mathrm{n}}s + \omega_{\mathrm{n}}^2\right) + Bs^2 + Cs}{s\left(s^2 + 2\zeta\omega_{\mathrm{n}}s + \omega_{\mathrm{n}}^2\right)}\right], \tag{7.6}$$

Table 7.1 Example time functions and corresponding Laplace transforms

Time domain function *f*(*t*)	Laplace domain function *F*(*s*)	Time domain function *f*(*t*)	Laplace domain function *F*(*s*)
Unit impulse	1	Unit step function	$\frac{1}{s}$
Exponential decay e^{-at}	$\frac{1}{s+a}$	$\sin\omega t$ and $\cos\omega t$	$\frac{\omega}{s^2+\omega^2}$ and $\frac{s}{s^2+\omega^2}$
$\frac{d}{dt}f(t)$	$sF(s) - f(0)$	$\frac{d^2}{dt^2}f(t)$	$s^2F(s) - sf(0) - \frac{df(0)}{dt}$
$e^{at}\sin\omega t$	$\frac{\omega}{(s-a)^2+\omega^2}$	$e^{at}\cos\omega t$	$\frac{s-a}{(s-a)^2+\omega^2}$

where the unknown constants A, B and C are found by comparing coefficients of s in Equation (7.5). Thus the partial fraction expansion becomes

$$X(s) = \frac{1}{mw_{\mathrm{n}}^2}\left(\frac{1}{s} - \frac{s + 2\zeta\omega_{\mathrm{n}}}{s^2 + 2\zeta\omega_{\mathrm{n}}s + \omega_{\mathrm{n}}^2}\right). \tag{7.7}$$

The final step is to transform back into the time domain, using the relationships shown in Table 7.1, thus

$$x(t) = \frac{1}{k}\left[1 - \frac{\omega_{\mathrm{n}}}{\omega_{\mathrm{d}}}e^{-\zeta\omega_{\mathrm{n}}t}\sin(\omega_{\mathrm{d}}t + \psi)\right], \tag{7.8}$$

which is the same answer as found using the analytical approach described in Chapter 1. Responses to other inputs may be obtained using a similar approach. Note that it is usual nowadays to use software such as MATLAB and SIMULINK to solve such systems rather than relying upon the solution using Laplace transforms.

7.3 MODELLING OF OPEN AND CLOSED LOOP SYSTEMS USING LAPLACE AND FREQUENCY DOMAINS

The control of a system is achieved through either open or closed loop control systems. If the Laplace transform of the open loop system is $G(s)$ in Figure 7.1, then the transfer function (TF) between the input $X(s)$ and output $Y(s)$ is given as

$$\mathrm{TF}_{\mathrm{system}} = G(s) = \frac{Y(s)}{X(s)}. \tag{7.9}$$

The inclusion of a controller $H(s)$ as part of the open loop system as shown in Figure 7.2 results in the transfer function between the output and input

$$\mathrm{TF}_{\mathrm{open\ loop}} = \frac{Y(s)}{X(s)} = H(s)G(s). \tag{7.10}$$

However, if the system is made *closed loop* so that the output to the system $G(s)$ is fed back into the input via a controller in the feedback path represented by$H(s)$, as shown in Figure 7.4, then it becomes possible to influence directly the input to the system in order to control the output. This system makes use of *negative feedback* shown by the minus sign on the feedback loop, and the error is input to the system.

There are two separate transfer functions to consider for each part of the system shown in Figure 7.4:

- between the input $E(s)$ to the system and the output $Y(s)$, $G(s) = \frac{Y(s)}{E(s)}$;
- between the output $Y(s)$ and the feedback path output $F(s)$, $H(s) = \frac{F(s)}{Y(s)}$.

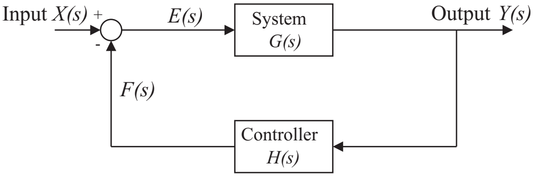

Figure 7.4 Closed loop system with controller in the feedback loop.

In addition the relationship between the actual input $X(s)$, the error signal $E(s)$ and the feedback path output $F(s)$ can be written as

$$E(s) = X(s) - F(s). \tag{7.11}$$

Rearranging these expressions gives the overall TF of the closed loop system as

$$\mathrm{TF}_{\text{closed loop}} = \frac{Y(s)}{X(s)} = \frac{G(s)}{1 + G(s)H(s)}. \tag{7.12}$$

The transfer functions of far more complicated systems can be determined simply by following the above approach. It will be seen later how it can be useful to convert transfer functions based in the Laplace domain into the frequency domain simply through the use of the transformation $s = \mathrm{i}\omega$, where $\mathrm{i} = \sqrt{-1}$ is the complex variable used in this book (though the symbol j is normally used by control engineers).

7.4 STABILITY OF SYSTEMS

Control systems are used to influence the behaviour of the system that is being controlled, in particular to manipulate the response to different inputs. Care must be taken that the characteristics of the closed loop system are favourable and that instabilities do not occur due to the interaction between the feedback control and the system. For example, the use of an incorrectly designed flight control system on an aircraft might result in flutter (refer to Chapter 12). Although time simulations of the system could be used to determine whether the application of a particular control loop results in a stable response, this is a very inefficient approach, particularly when the effect of changing many system and control parameters needs to be investigated.

In this section, a range of commonly used tools are described that can be used to determine whether a system is stable or not, and also to determine what the critical conditions are that define the boundary between stable and unstable behaviour.

7.4.1 Poles and Zeros

Consider the representation of the transfer function of a general closed loop system

$$G(s) = \frac{K(s^m + b_{m-1}s^{m-1} + \cdots + b_1 s + b_0)}{s^n + a_{\mathrm{n}-1}s^{n-1} + \cdots + a_1 s + a_0}, \tag{7.13}$$

where K is known as the gain of the system. This equation can be written in terms of the roots of the denominator p_i, known as *poles* (TF reaches a peak at these roots), and the roots of the numerator z_i, known as *zeros* (TF reaches a minimum at these roots), such that

$$G(s) = \frac{K(s - z_1)(s - z_2)\cdots(s - z_m)}{(s - p_1)(s - p_2)\cdots(s - p_{\mathrm{n}})}. \tag{7.14}$$

The poles are the roots of the *characteristic equation* of the system, which is found by setting the denominator of the TF to zero; they determine the stability of the closed loop system. For an oscillatory system (as usually encountered in aeroelastic or mechanical systems), the roots occur in complex conjugate pairs of the form

$$\sigma \pm i\theta = -\zeta\omega \pm i\omega\sqrt{1 - \zeta^2} \tag{7.15}$$

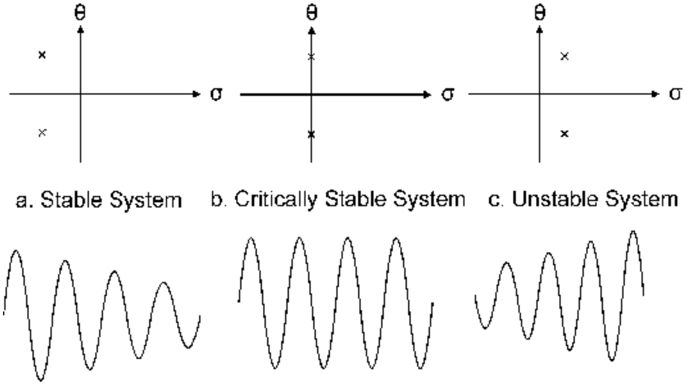

Figure 7.5 Relation of position of poles to system stability.

It can be shown that the system becomes unstable if the real part of any of the poles is positive ($\sigma > 0$). Figure 7.5 shows s plane plots (Argand diagrams) for three different cases of a single degree of freedom oscillatory system and the corresponding time response to an initial disturbance. Since this is a second order system, there are two poles that occur as a complex conjugate pair. When there are negative real parts of the poles ($\sigma < 0$), a stable time response occurs, as seen in Figure 7.5(a). Figure 7.5(b) shows the result for poles with a zero real part ($\sigma = 0$) and this leads to a critical response whereby the amplitude of the time history remains constant. Finally, in Figure 7.5(c), when the poles move to the right-hand side of the s plane the system response becomes unstable. If the imaginary part of a pole is zero ($\theta = 0$), then the motion relating to this pole cannot be oscillatory (but could still become unstable in a static sense if the real part is positive). For an MDoF system, the motion with all of the poles being damped is far more complicated than that shown in Figure 7.5(a). However, the motion of a single critically stable, or unstable, mode will dominate the response of an MDoF system and the resulting motion will be similar to that in Figures 7.5(a), (b) and (c) respectively.

7.4.2 Routh-Hurwitz Method

Although the roots of a polynomial can be determined using numerical software such as the ROOTS function in MATLAB, there can be occasions when the stability of a system needs to be determined without explicitly calculating the roots. The Routh–Hurwitz method (Bisplinghoff *et al*., 1996) can be used to check whether a system is stable just by considering the coefficients of the characteristic polynomial. The technique will be used later on in Chapter 11 as a means to determine when flutter occurs. Only the method, and not the proof, will be described here.

Any nth-order polynomial

$$a_n s^n + a_{n-1} s^{n-1} + \cdots + a_1 s + a_0 = 0 \tag{7.16}$$

will have stable roots if all the coefficients $a_i > 0$ and the n determinants $T_1 \cdots T_{\mathrm{n}} > 0$ where T_{n} is the $n \times n$ determinant that takes the form

$$\begin{vmatrix} a_{\mathrm{n}-1} & a_{\mathrm{n}-3} & \cdots & 0 & 0 & 0 \\ a_{\mathrm{n}} & a_{\mathrm{n}-2} & \cdots & a_0 & 0 & 0 \\ 0 & a_{\mathrm{n}-1} & \cdots & a_1 & 0 & 0 \\ \vdots & a_{\mathrm{n}} & \cdots & a_2 & a_0 & 0 \\ \vdots & \vdots & & a_3 & a_1 & 0 \\ 0 & 0 & \cdots & a_4 & a_2 & a_0 \end{vmatrix}. \tag{7.17}$$

The subdeterminants $T_1 \cdots T_{n-1}$ are found as

$$T_1 = |a_{n-1}|, \qquad T_2 = \begin{vmatrix} a_{n-1} & a_{n-3} \\ a_n & a_{n-2} \end{vmatrix}, \qquad T_3 = \begin{vmatrix} a_{n-1} & a_{n-3} & a_{n-5} \\ a_n & a_{n-2} & a_{n-4} \\ 0 & a_{n-1} & a_{n-3} \end{vmatrix}, \qquad \text{etc.} \tag{7.18}$$

A comparison of Equations (7.17) and (7.18) shows how these subdeterminants are formed. An increasing number of terms from the $n \times n$ determinant are taken, starting at its top left-hand corner. Note that if the subscript of any of the above terms is negative, then the term is taken as zero.

For example, consider the quartic equation $a_4s^4 + a_3s^3 + a_2s^2 + a_1s + a_0 = 0$ and set up the determinants up to 4×4 in size; therefore

$$T_4 = \begin{vmatrix} a_3 & a_1 & 0 & 0 \\ a_4 & a_2 & a_0 & 0 \\ 0 & a_3 & a_1 & 0 \\ 0 & a_4 & a_2 & a_0 \end{vmatrix}, \qquad T_3 = \begin{vmatrix} a_3 & a_1 & 0 \\ a_4 & a_2 & a_0 \\ 0 & a_3 & a_1 \end{vmatrix}, \qquad T_2 = \begin{vmatrix} a_3 & a_1 \\ a_4 & a_2 \end{vmatrix}, \qquad T_1 = a_3.$$

The polynomial has stable roots if $a_i > 0$ for $i = 0,1,2,3,4$ (includes $T_1 > 0$), $a_3a_2 - a_1a_4 > 0$ (T_2) and $a_1a_2a_3 - a_0a_3^2 - a_1^2a_4 > 0$ (T_3). There is no need to calculate the largest determinant T_4 as this is equal to a_0T_3.

7.4.3 Frequency Domain Representation

When designing a control system, it is often of interest to examine the effect of changing the gain and/or phase of the system in order to determine if and when stability is lost. Such investigations can be carried out in the Laplace domain using root locus plots or in the frequency domain using Nyquist or Bode plots. The figures can also be used to define how much the gain or phase can be increased before instability occurs.

7.4.3.1 Root locus

Root locus plots are used to show the effect of changing the control system gain on the position of the closed loop poles (the so-called root loci) (see Figure 7.6). Instability occurs when any denominator root crosses the imaginary axis and the real part becomes positive. The gain at which oscillatory roots become nonoscillatory (i.e. the imaginary part becomes zero) can also be determined. It is possible to use the root locus plot to adjust the open loop zeros and poles in order to affect the behaviour (damping, frequencies and occurrence of instabilities) of the closed loop poles.

There are a number of rules for drawing the root loci by hand (Raven, 1994). However, as it is usual nowadays to simply plot them out using numerical software, they will not be considered here.

As an example, consider the closed loop feedback system shown in Figure 7.4. The open loop transfer function is taken as $G(s) = K/[s(s^2 + 4s + 8)]$ with a feedback loop term $H(s) = 1$ and gain K. This gives a closed loop transfer function using the approach defined earlier as

$$\frac{Y(s)}{X(s)} = \frac{K}{s^3 + 4s^2 + 8s + K}. \tag{7.19}$$

Figure 7.6 shows how the root loci change with values of gain K varying from 1 to 40. It can be seen that there is an oscillatory pair of (complex conjugate) poles and a single nonoscillatory pole (zero imaginary part). The system is stable for all values of $K < 32$ (this can be verified using the Routh–Hurwitz criteria). However, beyond this critical value the system becomes unstable and the real parts of the complex poles become positive. Note that as the poles change, the values of the corresponding frequency and damping ratio of the closed loop system alter as well.

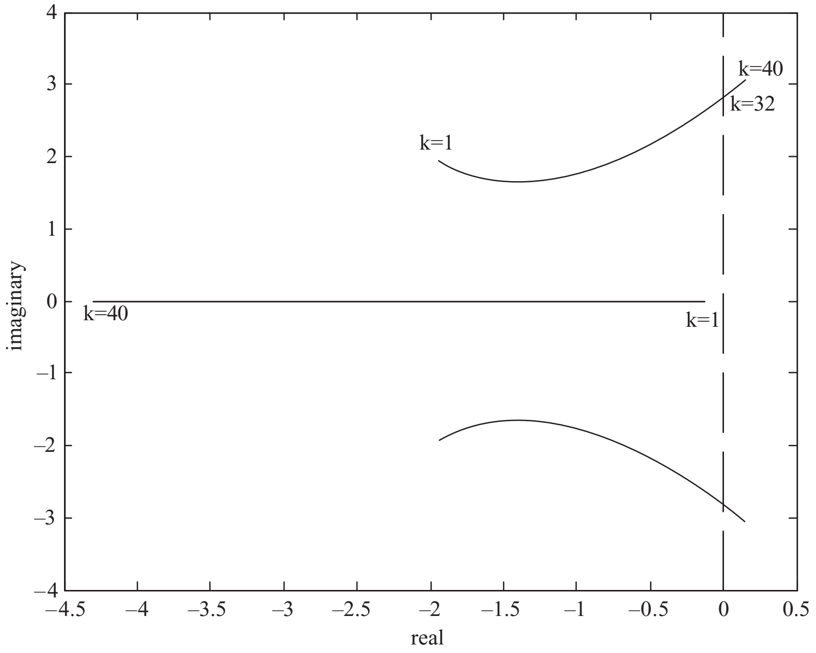

Figure 7.6 Root loci trends for different gain values.

It can be seen from the above example that the introduction of a feedback loop has allowed the system characteristics to be altered from those of the basic system. In control design, the form and gain of the feedback controller $H(s)$ are chosen to achieve the desired closed loop characteristics, such as overshoot, rise time and settling time. These requirements vary for different types of system.

7.4.3.2 Stability analysis using Nyquist and Bode plots

By application of the transformation ($s = \mathrm{i}\omega$) the transfer function in the Laplace domain is transformed into the frequency domain and thus Equation (7.12) becomes

$$\mathrm{TF}_{\text{closed loop}}(\omega) = \frac{G(\mathrm{i}\omega)}{1 + G(\mathrm{i}\omega)H(\mathrm{i}\omega)}. \tag{7.20}$$

It is usual to display this type of representation in terms of the Bode plot (gain (dB) and phase angle versus frequency) or the Nyquist plot (real part versus imaginary part for different frequencies).

Considering the denominator of the above expression for the transfer function, then a system can be shown to be stable if the term $G(\mathrm{i}\omega)H(\mathrm{i}\omega)$ has an amplitude ratio on the Bode plot less than 0 dB when the phase angle is -180°. On the Nyquist diagram this is equivalent to an amplitude ratio of less than -1 at a phase angle of -180°; thus the transfer function must not enclose the point (-1) on the real axis. Figure 7.7 shows typical Nyquist plots for a stable and an unstable system.

It is useful for control law design to determine how far from instability the system is, and this can be defined by the gain and phase margins. The gain margin defines at the -180° phase how much the magnitude is below 0 dB (Bode) or 1 (Nyquist), whereas the phase margin defines at 0 dB (Bode) or

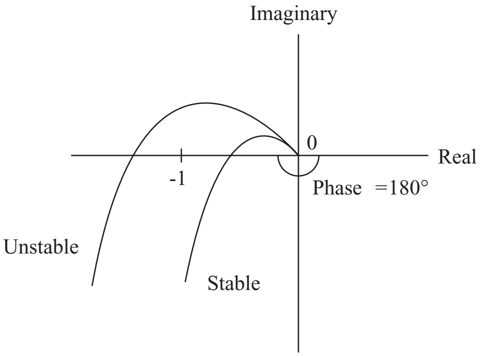

Figure 7.7 Nyquist representations of stable and unstable systems.

amplitude of 1 (Nyquist) how much the phase is greater than -180°. Schematic representations of the gain and phase margins for both Bode and Nyquist plots are shown in Figures 7.8 and 7.9.

Returning to the above example, defined by Equation (7.19), and making use of the substitution $s = \mathrm{i}\omega$, then Bode and Nyquist plots of $G(\mathrm{i}\omega)H(\mathrm{i}\omega)$ are shown for gain values of 20 and 32 in Figures 7.10 and 7.11. Note that they both have the same phase plot as the gain does not affect the phase in this case. It can be seen that when $K = 32$ the system is marginally stable, with the TF magnitude of 0 dB corresponding to the -180° phase.

Airworthiness certification regulations define the amount of gain and phase margins that must be present when flight control systems are used for civil and military aircraft.

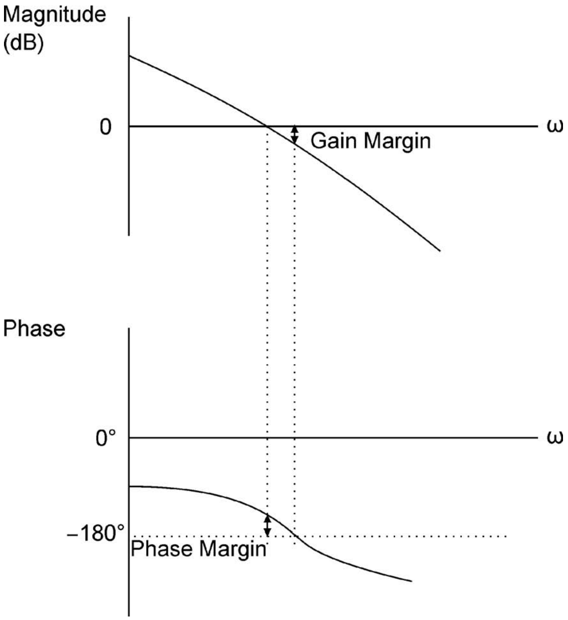

Figure 7.8 Bode plot showing gain and phase margins.

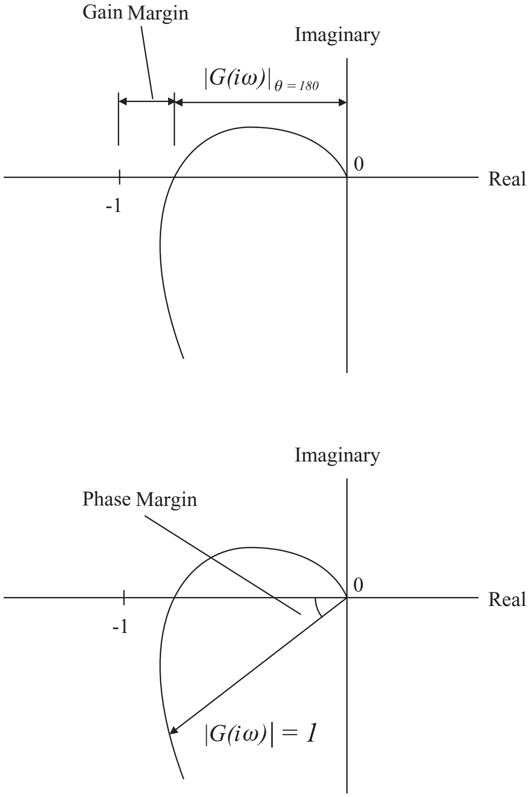

Figure 7.9 Nyquist plot showing gain and phase margins.

7.4.4 Time Domain Representation

The alternative to performing a control system analysis in the Laplace or frequency domains is to use the time domain, often deriving models in terms of acceleration, velocity or displacement.

7.4.4.1 State space representation

For a time domain analysis, it is convenient to make use of the so-called *state space models*, which are based upon the so-called system *states*. The states are any sets of variables that must be linearly independent and sufficient in number to define the dynamic behaviour of the system, but cannot be the system inputs (or linear combinations of the inputs). State space models can be used to model any set of differential equations.

For example, consider a second-order mechanical system with input u and output y in the form

$$\ddot{y} + 2\zeta\omega_{\rm n}\dot{y} + \omega_{\rm n}^2 y = u, \tag{7.21}$$

which can be rewritten in terms of two first-order differential equations with the states defined as $x_1 = y$ and $x_2 = \dot{y}$ such that

$$\begin{aligned} \dot{x}_1 &= x_2, \\ \dot{x}_2 &= u - \omega_{\rm n}^2 x_1 - 2\zeta\omega_{\rm n} x_2. \end{aligned} \tag{7.22}$$

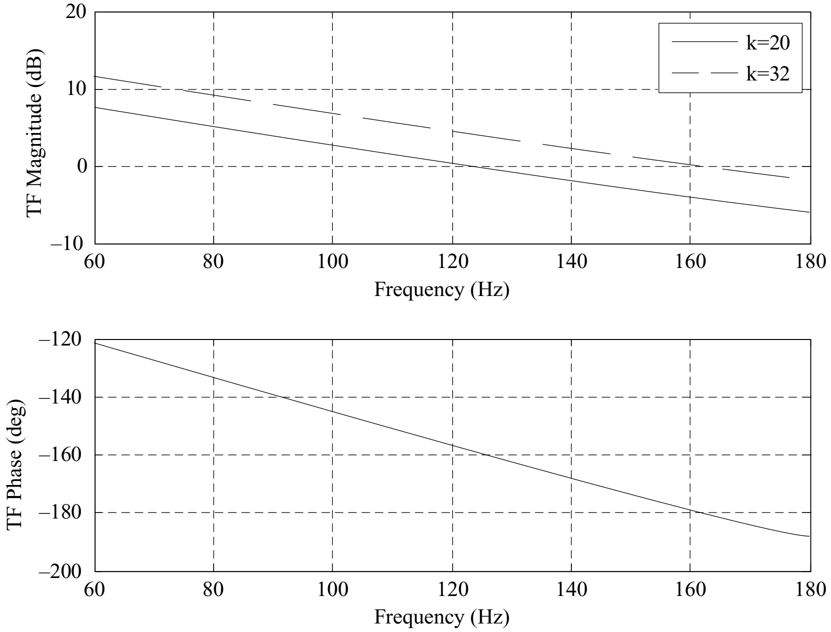

Figure 7.10 Bode plot for a system with two different gain values.

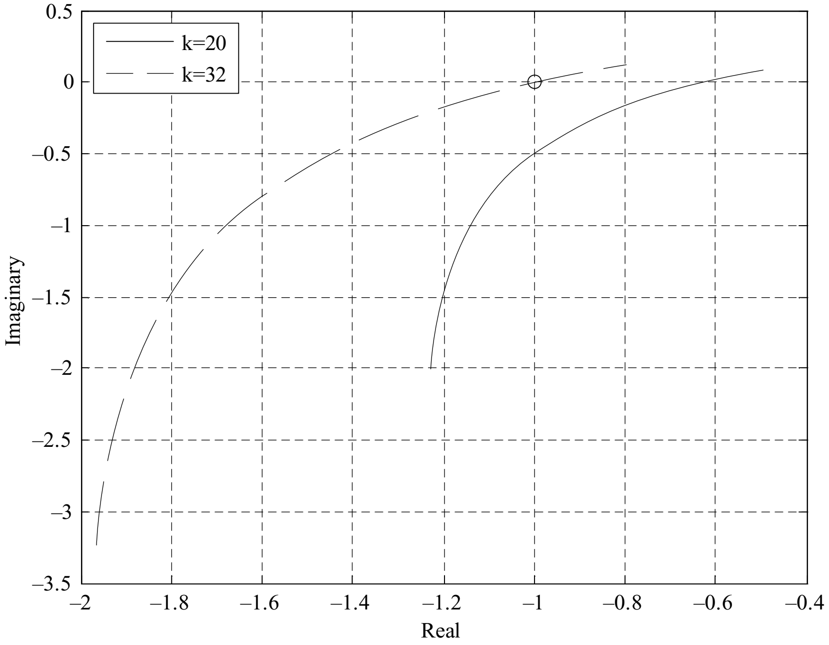

Figure 7.11 Nyquist plot for a system with two different gain values.

In matrix form, these equations may be expressed as

$$\left\{\begin{matrix}\dot{x}_1\\ \dot{x}_2\end{matrix}\right\}=\begin{bmatrix}0 & 1\\ -\omega_{\mathrm{n}}^2 & -2\zeta\omega_{\mathrm{n}}\end{bmatrix}\left\{\begin{matrix}x_1\\ x_2\end{matrix}\right\}+\begin{bmatrix}0\\ 1\end{bmatrix}\{u\}\quad\text{and}\quad\{y\}=\begin{bmatrix}1 & 0\end{bmatrix}\left\{\begin{matrix}x_1\\ x_2\end{matrix}\right\}+[0]\{u\}. \tag{7.23}$$

Equations (7.23) are in the form of the so-called *state space equations*:

$$\dot{\boldsymbol{x}}=\mathbf{A}_{\mathrm{s}}\boldsymbol{x}+\mathbf{B}_{\mathrm{s}}\boldsymbol{u}\qquad\text{and}\qquad\boldsymbol{y}=\mathbf{C}_{\mathrm{s}}\boldsymbol{x}+\mathbf{D}_{\mathrm{s}}\boldsymbol{u}, \tag{7.24}$$

where for an Nth-order system with NI inputs and NO outputs, $\boldsymbol{x}$ is the $N\times 1$ state vector, $\boldsymbol{u}$ the input vector $NI\times 1$, $\boldsymbol{y}$ the $NO\times 1$ output vector, $\mathbf{A}_{\mathrm{s}}$ the $N\times N$ system matrix, $\mathbf{B}_{\mathrm{s}}$ the $N\times NI$ input matrix, $\mathbf{C}_{\mathrm{s}}$ the $NO\times N$ output matrix and $\mathbf{D}_{\mathrm{s}}$ the $NI\times NO$ feedforward matrix.

The use of the subscript ‘s’ for these matrices is nonstandard for state space analysis, but the subscript is added to avoid confusion with different matrices in the general aeroelastic and loads equations presented later.

The state space Equations (7.24) can then be solved in the time domain using numerical integration to obtain the response of the system to any input. For multivariable problems they are a succinct method for describing the dynamics, and advanced matrix tools can be used to analyse the systems. Note that the eigenvalues of the system matrix $\mathbf{A}_{\mathrm{s}}$ are the same as the poles of the Laplace domain transfer function. Also, the number of first-order state space equations is twice that of the second-order representation.

It is a straightforward operation to transform from a state space model to a transfer function model. Taking Laplace transforms of Equation (7.24), with zero initial conditions, gives

$$s\boldsymbol{X}(s)=\mathbf{A}_{\mathrm{s}}\boldsymbol{X}(s)+\mathbf{B}_{\mathrm{s}}\boldsymbol{U}(s)\Rightarrow\boldsymbol{X}(s)=[s\mathbf{I}-\mathbf{A}_{\mathrm{s}}]^{-1}\mathbf{B}_{\mathrm{s}}\boldsymbol{U}(s). \tag{7.25}$$

Hence

$$\boldsymbol{Y}(s)=\left(\mathbf{C}_{\mathrm{s}}[s\mathbf{I}-\mathbf{A}_{\mathrm{s}}]^{-\mathbf{1}}\mathbf{B}_{\mathrm{s}}+\mathbf{D}_{\mathrm{s}}\right)\boldsymbol{U}(s)=\mathbf{G}(s)\boldsymbol{U}(s), \tag{7.26}$$

where, of course, $\mathbf{G}(s)$ is now, in general, a matrix of transfer functions corresponding to the multiple inputs and outputs.

There is a large body of work devoted to the use of digital control systems (Kuo, 1995) as opposed to the continuous time model considered above. However, these are beyond the scope of this book.

7.5 PID CONTROL

The simplest and most commonly used type of control strategy typically sets the controller of the system in Figure 7.3 as linear multiples of the error E (proportional) along with its integral (I) and derivative (D) multiplied by some gain values. Hence the proportional-integral-derivative (PID) controller can be written as

$$h_{\mathrm{PID}}(t)=K_{\mathrm{p}}E+K_{\mathrm{i}}\int E\,\mathrm{d}t+K_{\mathrm{d}}\frac{\mathrm{d}E}{\mathrm{d}t}, \tag{7.27}$$

where K_{p}, K_{i}, K_{d} are the proportional, integral and derivative gains. In the Laplace domain this becomes

$$H(s)=K_{\mathrm{p}}+\frac{K_{\mathrm{i}}}{s}+K_{\mathrm{d}}s. \tag{7.28}$$

There are various empirical schemes that can be used for setting the three gain values, but tuning of the gains often still has to be executed in order to get optimal performance. The proportional term determines the speed of the response, the integral term improves the accuracy of the final steady state, while the derivative term helps to stabilize the response.

State feedback control typically used the set-up in Figure 7.4 with the controller feedback equal to $-\mathbf{K}\boldsymbol{x}$. Such an approach leads to optimal control techniques (Whittle, 1996), which specify that the gain matrix **K** is such that some cost function is minimized.

7.6 EXAMPLES

1. For the feedback control system in Figure 7.3, determine the closed loop transfer function for the combinations of $G(s)$ and $H(s)$ given below.

$G(s)$	$H(s)$
$\frac{K}{s^2+3s+9}$	1
$\frac{K}{s(s^2+3s+9)}$	$(s+1)$
$\frac{K}{s(s+1)(s+3)}$	$(s+1)(s+2)$
$\frac{K(s+2)}{s(s^2+3s+9)}$	$K_\mathrm{p}+\frac{K_\mathrm{i}}{s}+K_\mathrm{d}s$

2. Repeat Example 1 but this time using the control system shown in Figure 7.4.
3. By plotting out the root locus, determine when the above systems in Example 1 become unstable.
4. By plotting Bode and Nyquist plots, determine the gain and phase margins of the above systems in Example 1.
5. Use the Routh–Hurwitz method to determine whether the roots of the following polynomials are stable:

$$x^2+x+4=0,\qquad x^3+x^2+2x+1=0,\qquad 3x^3+x^2+2x+1=0$$

and

$$x^4+3x^3+x^2+2x+1=0.$$

6. Use the Routh–Hurwitz method to determine the values of p for which the roots of the following polynomials are stable:

$$x^3+px^2+2x+1=0,\qquad x^3+x^2+px+1=0,\qquad x^3+2x^2+2x+p=0$$

and

$$x^4+2x^3+x^2+x+p=0.$$

7. Confirm the results of Example 3 using the Routh–Hurwitz method.

Part II

Introduction to Aeroelasticity and Loads

8

Static Aeroelasticity – Effect of Wing Flexibility on Lift Distribution and Divergence

Static aeroelasticity is the study of the deflection of flexible aircraft structures under aerodynamic loads, where the forces and motions are considered to be independent of time. Consider the aerodynamic lift and moment acting upon a wing to depend solely upon the incidence of each chordwise strip (i.e. strip theory; see Chapter 5). These loads cause the wing to bend and twist, so changing the incidence and consequently the aerodynamic flow, which in turn changes the loads acting on the wing and the deflections, and so on until an equilibrium condition is usually reached. The interaction between the wing structural deflections and the aerodynamic loads determines the wing bending and twist at each flight condition, and must be considered in order to model the static aeroelastic behaviour. The static aeroelastic deformations are important as they govern the loads in the steady flight condition, the lift distribution, the drag forces, the effectiveness of the control surfaces, the aircraft trim behaviour and also the static stability and control characteristics. The aeroelastic wing shape at the cruise condition is of particular importance as this has a crucial effect on the drag and therefore the range.

Through the elimination of time-dependent forces and motion, the inertial forces can be ignored in the equilibrium equations as these are dependent upon acceleration. Also, only steady aerodynamic forces need to be included in the analysis. Consequently, the modelling of static phenomena is much easier than dynamic aeroelastic phenomena where unsteady aerodynamic effects must be considered (see Chapter 10).

There are two critical static aeroelastic phenomena that can be encountered, namely *divergence* and *control reversal*. The latter will be considered in Chapter 9. Divergence is the name given to the phenomenon that occurs when the moments due to aerodynamic forces overcome the restoring moments due to structural stiffness, so resulting in structural failure. The most common type is that of wing torsional divergence. On a historical note, it is thought that Langley's attempt to fly some months before the Wright Brothers' successful flights in 1903 failed due to the onset of divergence (Collar, 1978; Garrick and Reid, 1981). When the Langley aircraft was rebuilt some years later by Curtis with a much stiffer wing structure, the aircraft flew successfully. In general, for aeroelastic considerations the stiffness is of much greater importance than the strength.

In modern aircraft, the flutter speed (the air speed at which flutter, a dynamic aeroelastic instability, occurs; see Chapter 11) is usually reached before the divergence speed (the air speed at which divergence occurs) so divergence is not normally a problem. However, the divergence speed is a useful measure of the general stiffness of the aircraft structure and must be considered as part of the certification process (CS-25 and FAR-25).

In this chapter, the aerodynamic lift distribution acting upon a flexible wing fixed at the root will be considered using a simple aeroelastic model involving wing twist, and the divergence condition will

Introduction to Aircraft Aeroelasticity and Loads J. R. Wright and J. E. Cooper
© 2007 John Wiley & Sons, Ltd

be shown. The influence of the aircraft trim on the divergence speed and lift distribution for a simple heave/pitch model combined with a flexible wing torsion branch mode will also be considered. Later, in Chapter 13, aircraft trim and the related issue of the equilibrium manoeuvre will be examined using a whole aircraft heave and pitch model with a free–free flexible mode, including other features such as the steady pitch rate, accelerated flight condition, wing camber, thrust and drag out-of-line, and downwash effects on the tailplane. Later in Chapter 18, the internal loads (see Chapter 6) in the manoeuvre will be obtained.

8.1 STATIC AEROELASTIC BEHAVIOUR OF A TWO-DIMENSIONAL RIGID AEROFOIL WITH SPRING ATTACHMENT

The static aeroelastic behaviour is considered initially using an iterative approach and then a direct approach.

8.1.1 Iterative Analysis

As a first example of static aeroelastic behaviour, consider the two-dimensional aerofoil in Figure 8.1 with unit span and chord c. The rigid aerofoil section is symmetric (so has no inherent camber) and is attached to a torsional spring of stiffness K_θ at a distance ec aft of the aerodynamic centre on the quarter chord. The lift-curve slope is a_1. The aerofoil has an initial incidence of θ_0 and twists through angle θ due to the aerodynamic loading.

The lift acting on the aerofoil at air speed V (true air speed, or TAS) and initial angle of incidence θ_0 causes a pitching moment of

$$M = \left[\tfrac{1}{2}\rho V^2 c a_1 \theta_0\right] ec = \tfrac{1}{2}\rho V^2 ec^2 a_1 \theta_0 = q\, ec^2 a_1 \theta_0 \tag{8.1}$$

to act about the flexural axis, where q is the dynamic pressure (not to be confused with the later usage of q for the pitch rate and q_e for the flexible mode generalized coordinate) and ρ is the true air density. The equation for the aerofoil will be obtained using Lagrange's equations, introduced in Chapter 1. Since only static aeroelastic effects are being considered, the kinetic energy term can be ignored. The potential (or strain) energy U is found from the twist of the torsional spring, namely

$$U = \tfrac{1}{2}K_\theta \theta^2. \tag{8.2}$$

The generalized moment may be obtained from the incremental work done by the pitching moment acting through the incremental angle $\delta\theta$ and is given by

$$Q_\theta = \frac{\partial(\delta W)}{\partial(\delta\theta)} = \frac{\partial\left(q\, ec^2 a_1 \theta_0 \delta\theta\right)}{\partial(\delta\theta)} = q\, ec^2 a_1 \theta_0. \tag{8.3}$$

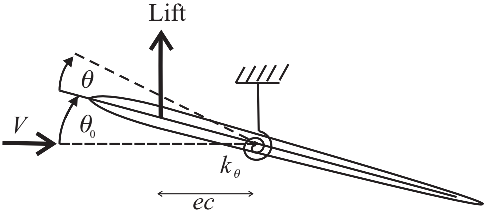

Figure 8.1 Two-dimensional aerofoil with a torsional spring.

Then application of Lagrange's equations for coordinate θ gives

$$K_\theta \theta = q\, ec^2 a_1 \theta_0 \qquad \Rightarrow \qquad \theta = \frac{q\, ec^2 a_1}{K_\theta}\theta_0 = qR\theta_0 \tag{8.4}$$

where $R = ec^2 a_1 / K_\theta$. Thus having applied the initial aerodynamic loading, the aerofoil has twisted by angle θ, as determined in Equation (8.4). In performing this calculation, it has been assumed that the pitching moment has not changed due to the twist. However, as a consequence of the twist, the aerodynamic moment now changes to allow for the new angle of incidence. This new loading, in turn, causes the aerofoil twist to change again, leading to a further modification in the aerodynamic loading, and so on.

The stepping between application of the aerodynamic load on the aerofoil, changing the aerofoil twist and then determining the new aerodynamic loading illustrates the fundamental interaction between a flexible structure and aerodynamic forces that gives rise to aeroelastic phenomena.

8.1.1.1 First iteration

The incidence of the aerofoil now includes the initial incidence and the estimate of twist, so the revised pitching moment becomes

$$M = q\, ec^2 a_1 (\theta_0 + qR\theta_0) \tag{8.5}$$

and, since the potential/strain energy term remains the same as in Equation (8.2), application of Lagrange's equations gives a revised elastic twist angle of

$$\theta = q\, ec^2 a_1 \frac{1 + qR}{K_\theta}\theta_0 = qR(1 + qR)\theta_0. \tag{8.6}$$

8.1.1.2 Further iterations

Repeating the above process continues by using the updated elastic twist value in the pitching moment and work expressions, leading to an infinite series expansion for the elastic twist in the form

$$\theta = qR\left[1 + qR + (qR)^2 + (qR)^3 + (qR)^4 + \cdots\right]\theta_0. \tag{8.7}$$

Now, remembering that the binomial series is written as

$$(1 - x)^{-1} = 1 + x + x^2 + x^3 + \cdots \quad \text{with} \quad |x| \le 1, \tag{8.8}$$

in the limit, the aerofoil twist becomes

$$\theta = \frac{qR}{1 - qR}\theta_0. \tag{8.9}$$

This example will be reconsidered in the next section, but using an approach that enables determination of the twist in a single calculation. It should be noted, however, that the single step (strongly coupled) approach is only feasible if there is a direct mathematical relationship between the aerodynamic forces and the deflections. If advanced static aeroelastic calculations for an entire aircraft, involving the coupling of computational fluid dynamics (CFD) methods with finite element methods, are applied, then such an approach requires use of a loosely coupled approach somewhat similar to the iterative process shown above. However, the more common and traditional methodology for static aeroelastic calculations is a single step approach.

8.1.2 Direct (Single Step) Analysis

Consider the same two-dimensional aerofoil as above, but let the angle of incidence include the unknown aeroelastic twist θ. The lift acting on the aerofoil at dynamic pressure q and initial angle of incidence θ_0 causes a pitching moment

$$M = q\, ec^2 a_1(\theta_0 + \theta), \tag{8.10}$$

where the unknown twist has been included. The potential/strain energy term is the same as Equation (8.2).

The generalized moment, based on the incremental work done by the pitching moment acting through the incremental angle $\delta\theta$ is

$$Q_\theta = \frac{\partial\,(\delta W)}{\partial\,(\delta\theta)} = \frac{\partial\left[q\, ec^2 a_1(\theta_0 + \theta)\delta\theta\right]}{\partial\,(\delta\theta)} = q\, ec^2 a_1(\theta_0 + \theta). \tag{8.11}$$

Then, application of Lagrange's equations for coordinate θ gives

$$K_\theta \theta = q\, ec^2 a_1(\theta_0 + \theta) \qquad \Rightarrow \qquad \left(K_\theta - q\, ec^2 a_1\right)\theta = q\, ec^2 a_1 \theta_0, \tag{8.12}$$

where it may be seen that the effective structural stiffness is reduced by the aerodynamic term. Solving this equation leads to the twist

$$\theta = \frac{q\, ec^2 a_1}{K_\theta - q\, ec^2 a_1}\theta_0 = \frac{qR}{1 - qR}\theta_0. \tag{8.13}$$

When Equations (8.9) and (8.13) are compared, it may be seen that both approaches give exactly the same value of the elastic twist for a given dynamic pressure q. The elastic twist becomes infinite as q approaches $1/R$, and this defines the so-called divergence speed, as

$$q_{\text{div}} = \frac{1}{R} = \frac{K_\theta}{ec^2 a_1} \tag{8.14}$$

and hence Equation (8.13) becomes

$$\theta = \frac{q/q_{\text{div}}}{1 - q/q_{\text{div}}}\theta_0 \tag{8.15}$$

This analysis demonstrates the physical phenomenon of divergence when the aerodynamic pitching moment overcomes the structural restoring moment. Infinite deflections are not possible, and in practice the structure will fail. Figure 8.2 shows a plot of the ratio of elastic twist to initial angle of incidence against the ratio of dynamic pressure to that at divergence; it can be seen that, for this simple example, the elastic twist equals the initial incidence at $q = q_{\text{div}}/2$ and then increases markedly beyond this point.

In the following sections on static aeroelastic behaviour, the direct (single step) approach will be used.

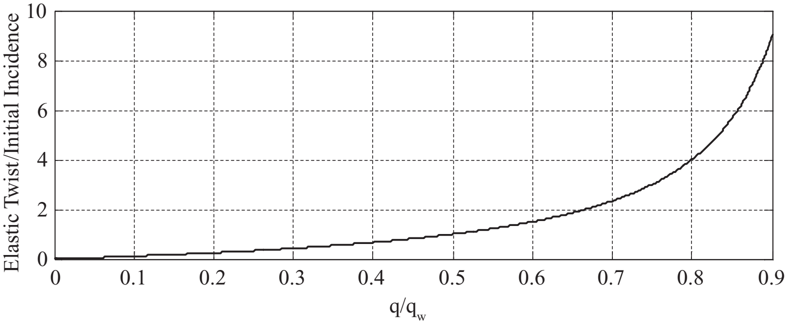

Figure 8.2 Typical twist behaviour for a two-dimensional aerofoil with torsion spring.

8.2 STATIC AEROELASTIC BEHAVIOUR OF A FIXED ROOT FLEXIBLE WING

A more realistic example of static aeroelastic behaviour is now examined for a flexible wing fixed at the root. Consider the wing to be rectangular, with semi-span s, chord c, a symmetric aerofoil section and no initial twist, as shown in Figure 8.3. The flexural axis lies at a distance ec aft of the aerodynamic centre on the quarter chord and the wing torsional rigidity is GJ. The lift curve slope is taken as a_W, with aerodynamic strip theory being used (see Chapter 5). It is also assumed that the wing root incidence θ_0 is fixed; this final assumption does not take into account the trim of the aircraft in steady flight (to be considered later on).

For simplicity, assume that the wing twist behaviour is characterized by the idealized linear relationship

$$\theta = \frac{y}{s}\theta_T, \tag{8.16}$$

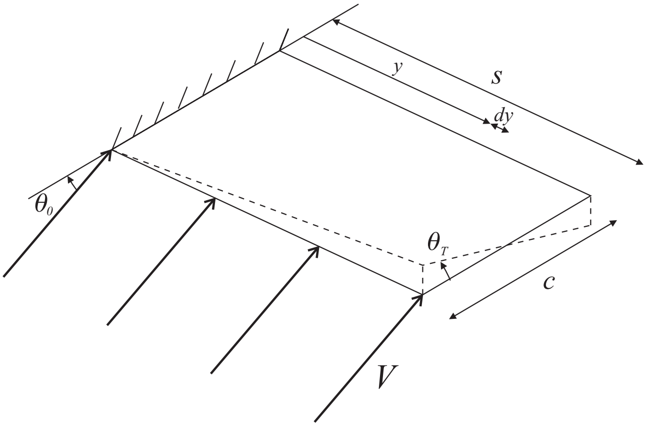

Figure 8.3 Flexible rectangular wing with a fixed root.

where θ_T is the twist at the wing tip (often called a generalized coordinate as it defines the amount of the shape present) and thus the twist increases further away from the wing root. Using such an assumed shape to carry out an approximate analysis is the basis of the Rayleigh–Ritz method introduced in Chapter 3.

8.2.1 Twist and Divergence of the Fixed Root Flexible Wing

The lift is taken as acting at the aerodynamic centre and, because the section is symmetric, there is no pitching moment at zero incidence (see Chapter 5). Using an expression for the lift that takes both the root incidence and aeroelastic twist into account, then the lift on an elemental strip is given by

$$\mathrm{d}L = q\, ca_{\mathrm{W}} \left(\theta_0 + \frac{y}{s}\theta_{\mathrm{T}}\right) \mathrm{d}y, \tag{8.17}$$

and thus the lift increases with distance from the wing root. The total lift on the wing is found by integrating over the semi-span, so that

$$L = \int_0^s q\, ca_{\mathrm{W}} \left(\theta_0 + \frac{y}{s}\theta_{\mathrm{T}}\right) \mathrm{d}s = q\, ca_{\mathrm{W}} \left(s\theta_0 + \frac{s}{2}\theta_{\mathrm{T}}\right). \tag{8.18}$$

As there is no motion of the wing, the kinetic energy $T = 0$. The potential energy occurs from the strain energy due to twist (see Chapter 3), which is given by

$$U = \frac{1}{2}\int_0^s GJ\left(\frac{\mathrm{d}\theta}{\mathrm{d}y}\right)^2 \mathrm{d}y \quad = \quad \frac{1}{2}\int_0^s GJ\left(\frac{\theta_{\mathrm{T}}}{s}\right)^2 \mathrm{d}y \quad = \quad \frac{GJ}{2s}\theta_{\mathrm{T}}^2. \tag{8.19}$$

Now, consider an incremental twist angle being expressed in terms of an incremental generalized coordinate, so that

$$\delta\theta = \frac{y}{s}\delta\theta_{\mathrm{T}}. \tag{8.20}$$

The work done by the aerodynamic forces is determined by considering the pitching moment acting upon each strip doing work through this incremental twist angle. The total incremental work δW is obtained by integrating these work terms across the entire wing semi-span. Thus

$$\begin{aligned} \delta W &= \int_0^s \mathrm{d}L\; ec\; \delta\theta = \int_0^s q\, ca_{\mathrm{W}} \left(\theta_0 + \frac{y}{s}\theta_{\mathrm{T}}\right) \mathrm{d}y\; ec\; \delta\theta \\ &= \int_0^s q\, c^2 a_{\mathrm{W}} \left(\theta_0 + \frac{y}{s}\theta_{\mathrm{T}}\right) \mathrm{d}y\, e\frac{y}{s}\delta\theta_{\mathrm{T}} = q\, ec^2 a_{\mathrm{W}} \left(\frac{s\theta_0}{2} + \frac{s\theta_{\mathrm{T}}}{3}\right)\delta\theta_{\mathrm{T}}, \end{aligned} \tag{8.21}$$

and for the generalized coordinate θ_{T}, Lagrange's equations yield

$$\frac{GJ\theta_{\mathrm{T}}}{s} = q\, ec^2 a_{\mathrm{W}} \left(\frac{s\theta_0}{2} + \frac{s\theta_{\mathrm{T}}}{3}\right) \qquad \Rightarrow \qquad \left(\frac{GJ}{s} - q\, ec^2 a_{\mathrm{W}}\frac{s}{3}\right)\theta_{\mathrm{T}} = q\, ec^2 a_{\mathrm{W}}\frac{s\theta_0}{2}. \tag{8.22}$$

Here again the structural stiffness is seen to be reduced by the aerodynamic term and hence the elastic tip twist is found to be

$$\theta_{\mathrm{T}} = \frac{3q\, ec^2 s^2 a_{\mathrm{W}}}{6GJ - 2q\, ec^2 s^2 a_{\mathrm{W}}}\theta_0. \tag{8.23}$$

The tip twist increases with dynamic pressure and behaves in a similar manner to that shown in Figure 8.2. When the divergence condition is reached the twist tends to infinity; however, in reality, structural failure will occur first. For this fixed root wing, the dynamic pressure at divergence q_{W} is found as

$$q_{\mathrm{W}} = \frac{3GJ}{ec^2s^2a_{\mathrm{W}}}. \tag{8.24}$$

It is possible to make some deductions as to how the dimensions and material of this simplified wing affect the divergence speed, and what design rules could be used to ensure an increase in its value so that it does not occur within the desired flight envelope:

- The smaller the distance between the aerodynamic centre and the flexural axis, and/or the greater the flexural rigidity *GJ*, the greater the divergence speed becomes.
- If the flexural axis lies on the axis of aerodynamic centres there is no twist due to aerodynamic loading and divergence will not occur.
- Should the flexural axis actually lie forward of the aerodynamic centre, the applied aerodynamic moment becomes negative; thus the tip twist is nose downwards and divergence cannot occur.

Unfortunately, these last two design scenarios are not generally possible to implement in practical wing designs, so divergence must always be considered for aeroelastic design, and adequate torsional stiffness is crucial.

8.2.2 Variation of Lift along the Fixed Root Flexible Wing

Having determined the wing twist, the corresponding lift distribution along the fixed root flexible wing may be determined. Combining Equations (8.17) and (8.23), the lift per unit span of the wing is found as

$$\frac{\mathrm{d}L}{\mathrm{d}y} = q\,ca_{\mathrm{W}}\left(\theta_0 + \frac{y}{s}\theta_{\mathrm{T}}\right) = q\,ca_{\mathrm{W}}\left(1 + \frac{3q\,ec^2s^2a_{\mathrm{W}}}{6GJ - 2q\,ec^2s^2a_{\mathrm{W}}}\frac{y}{s}\right)\theta_0, \tag{8.25}$$

and this can be rewritten in terms of the divergence dynamic pressure so that

$$\frac{\mathrm{d}L}{\mathrm{d}y} = q\,ca_{\mathrm{W}}\left(1 + \frac{3\,(q/q_{\mathrm{W}})}{2\,(1-(q/q_{\mathrm{W}}))}\frac{y}{s}\right)\theta_0. \tag{8.26}$$

When the lift per unit span is plotted against the spanwise distance in Figure 8.4, it can be seen that the lift per span increases linearly along the wing span. This is due to the assumed linear twist shape and would differ if a more complicated shape were chosen or if the wing tapered or if modified strip theory were used. As the dynamic pressure increases, the spanwise slope of the lift distribution increases. The lift at the wing root depends solely upon the root incidence.

The total lift is found by integrating Equation (8.26) across the entire wing semi-span, giving

$$L = \int_0^s \frac{\mathrm{d}L}{\mathrm{d}y}\mathrm{d}y = q\,csa_{\mathrm{W}}\left[1 + \frac{3\,(q/q_{\mathrm{W}})}{4\,(1-q/q_{\mathrm{W}})}\right]\theta_0. \tag{8.27}$$

More lift is generated as the air speed (and hence dynamic pressure) increases. As the dynamic pressure q approaches divergence for this fixed root wing model, then the total lift actually becomes infinite.

8.3 EFFECT OF TRIM ON STATIC AEROELASTIC BEHAVIOUR

The above example shows that increasing the air speed leads to a greater wing twist, and thus increased lift. However, in practice, a change in the air speed will require the trim of the aircraft to be adjusted via

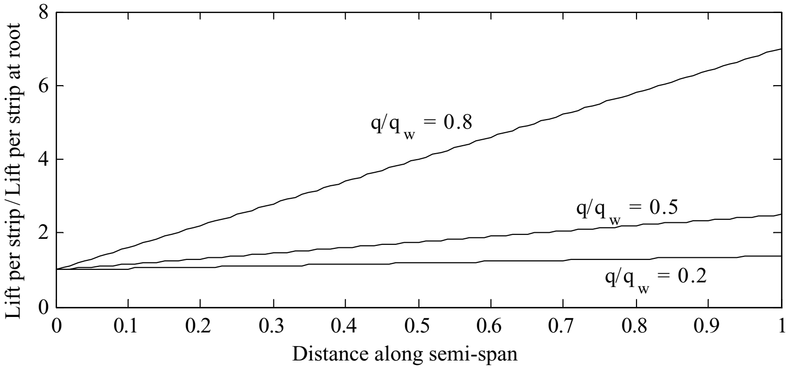

Figure 8.4 Lift per unit span for different dynamic pressures.

the elevator in order to maintain equilibrium of aerodynamic and inertia forces. The following example of a simple flexible aircraft model with a symmetric wing and in-line thrust and drag illustrates how the divergence and load distribution behaviour is changed when the balance of overall forces and moments is preserved; the model has heave and pitch motions, together with the flexible wing effect, represented by adding in a torsional wing branch mode (see Chapter 3).

Later in Chapter 13, where equilibrium manoeuvres are considered, more advanced models, including cambered wing, thrust and drag out-of-line, and downwash effects at the tailplane, will be investigated for accelerated manoeuvres with a steady pitch rate for both rigid and flexible aircraft models.

Note that because the content in the book on static aeroelasticity and flutter has employed the notation in classical texts, there will be some differences in notation in the later parts on manoeuvres where different notation is standard.

8.3.1 Effect of Trim on the Divergence Speed of a Simple Model

Consider the idealized aircraft of weight W in steady level flight as shown in Figure 8.5. The fuselage is rigid, able to undergo heave and pitch motions, and the wings are the same as discussed in the above examples, i.e. wings include flexible motion in torsion and are in effect branch modes for a fixed wing root (as discussed in Chapter 3). Downwash effects of the wing tip vortices at the tailplane are ignored and both the wings and tailplane have symmetric sections, so the tailplane centre of pressure is at the quarter chord and is unaffected by changes in wing root incidence. Also, thrust and drag are assumed to be in line and so do not contribute to the pitching moment terms.

The equations of motion are determined once again using Lagrange's equations. As noted before for the flexible wing, the wing twist θ is taken about the flexural axis, distance ec aft of the wing aerodynamic

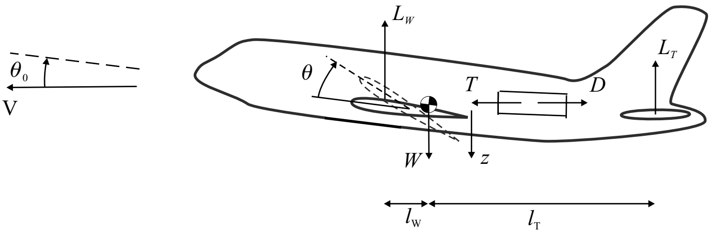

Figure 8.5 Aircraft in steady flight.

centre; the corresponding generalized coordinate is the twist at the wing tip θ_T. However, in this whole aircraft case, the incidence θ_0 and the heave displacement z (positive downwards) at the centre of mass also need to be included as coordinates.

The kinetic energy is zero and the potential/strain energy for both wings is

$$U = 2\frac{1}{2}\int_0^s GJ\left(\frac{\mathrm{d}\theta}{\mathrm{d}y}\right)^2 \mathrm{d}y = GJ\int_0^s \left(\frac{\theta_T}{s}\right)^2 \mathrm{d}y = \frac{GJ}{s}\theta_T^2. \tag{8.28}$$

Consider the work done through incremental displacements for incidence $\delta\theta_0$, wing tip twist $\delta\theta_T$ and heave δz:

$$\begin{aligned}\delta W &= -L_T(\delta z + l_T\delta\theta_0) + W\delta z + 2\int_0^s (q\,ca_W(\theta_0+\theta)\mathrm{d}y)(-\delta z + l_W\delta\theta_0 + ec\delta\theta) \\ &= -L_T(\delta z + l_T\delta\theta_0) + W\,\delta z + 2q\,cs\,a_W\left(\theta_0 + \frac{\theta_T}{2}\right)(-\delta z + l_W\delta\theta_0) + 2q\,ec^2sa_W\left(\frac{\theta_0}{2}+\frac{\theta_T}{3}\right)\delta\theta_T.\end{aligned} \tag{8.29}$$

Application of Lagrange's equations for each of the three coordinates z, θ_0 and θ_T gives the following. Firstly,

$$Q_h = 0 = \frac{\partial(\delta W)}{\partial(\delta z)} = -L_T + W - 2q\,cs\,a_W\left(\theta_0 + \frac{\theta_T}{2}\right), \tag{8.30}$$

which is the equilibrium equation equivalent to resolving forces in the vertical direction and effectively imposes the constraint in steady level flight that the weight of the aircraft is equal to the wing plus tailplane lift. Secondly,

$$Q_{\theta_0} = 0 = \frac{\partial(\delta W)}{\partial(\delta\theta_0)} = -L_T l_T + 2q\,cs\,a_W\left(\theta_0 + \frac{\theta_T}{2}\right)l_W, \tag{8.31}$$

which is the moment equilibrium equation equivalent to the zero pitching moment about the centre of mass. Finally,

$$Q_\theta = \frac{2GJ}{s}\theta_T = 2q\,ec^2sa_W\left(\frac{\theta_0}{2}+\frac{\theta_T}{3}\right), \tag{8.32}$$

which is the elastic mode equilibrium equation. The three unknowns in these equations are θ_0, θ_T and L_T (effectively involving the elevator angle for trim; see Chapter 13); note that z does not appear explicitly because the vertical position of the aircraft does not affect the steady lift. In order to solve these equations, L_T may be eliminated from Equations (8.30) and (8.31), because it is the wing behaviour that is of most interest here, therefore

$$\begin{bmatrix} 2q\,csa_W & q\,cs\,a_W \\ q\,ec^2sa_W & \left(\frac{2}{3}q\,ec^2sa_W - 2\frac{GJ}{s}\right)\end{bmatrix}\begin{Bmatrix}\theta_0 \\ \theta_T\end{Bmatrix} = \begin{Bmatrix}\frac{Wl_T}{l_W+l_T} \\ 0\end{Bmatrix}. \tag{8.33}$$

For the trimmed aircraft, the simultaneous Equations (8.33) are solved to determine the combination of incidence and wing twist that give rise to the equilibrium condition, giving the tip twist as

$$\theta_T = \frac{Wl_T/(l_W+l_T)}{4GJ/(ec\,s) - q\,cs\,a_W/3} = \frac{Wl_T/(l_W+l_T)}{4GJ/[1-q/(4q_W)](ec\,s)} \tag{8.34}$$

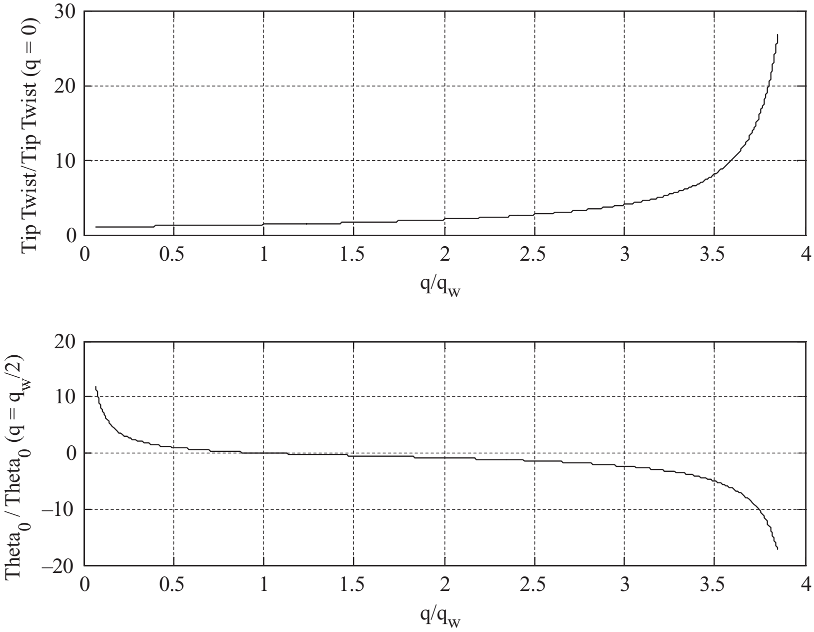

Figure 8.6 Wing tip twist and incidence for an aircraft with a flexible wing in trim.

whereas the root incidence variation is found to be

$$\theta_0 = \frac{\left(6GJ - 2q\,ec^2s^2a_\mathrm{W}\right)Wl_\mathrm{T}/\left(l_\mathrm{T}+l_\mathrm{W}\right)}{q\,cs\,a_\mathrm{W}\left(12GJ - q\,ec^2s^2a_\mathrm{W}\right)} = \frac{Wl_\mathrm{T}/\left(l_\mathrm{T}+l_\mathrm{W}\right)\left(1-q/q_\mathrm{W}\right)}{2q\,cs\,a_\mathrm{W}\left[1-q/(4q_\mathrm{W})\right]} \tag{8.35}$$

Clearly, the tailplane lift required for trim could also be determined from the earlier Equation (8.31). The variation of normalized values of θ_T and θ_0 versus normalized dynamic pressure are shown in Figure 8.6. As before, an increase in the air speed leads to an increase in the wing tip twist; however, it can be seen that the incidence decreases with air speed, and beyond the fixed root wing divergence speed it becomes negative. Beyond this air speed the inboard sections of the wing are at negative angles of incidence.

Considering the denominator of Equations (8.34) shows that the trimmed aircraft divergence speed occurs when

$$q = q_\mathrm{A} = \frac{12GJ}{ec^2s^2a_\mathrm{W}} = 4q_\mathrm{W}, \tag{8.36}$$

where q_A is the trimmed aircraft divergence speed and q_W is the divergence speed for the fixed root flexible wing (this latter value can be obtained from Equations (8.33) by constraining θ_0 and ignoring the first equation). Thus, for this case where trim is maintained at increasing air speed, the dynamic pressure at divergence q_A is four times that of the fixed root flexible wing case (i.e. double the divergence speed). At this air speed both the tip twist and the root incidence tend towards infinity, so again structural failure will occur. In practice, it is unlikely that the divergence speed will be achieved as the aircraft will run out of trim at a lower air speed, i.e. more and more elevator will need to be applied to maintain trim.

Note that including the effects of wing camber, downwash at the tailplane, thrust and drag out-of-line, steady pitch rate, accelerated flight condition, etc., to the model will alter all these results.

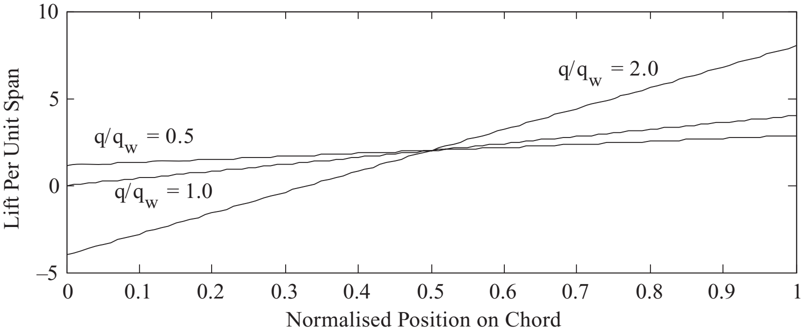

Figure 8.7 Lift distribution for a flexible rectangular wing with aircraft trim.

8.3.2 Effect of Vertical Trim on the Variation of Lift Along the Wing

Substituting the above expressions for θ_0 and θ_T as functions of the dynamic pressure into Equation (8.25) for the lift distribution (lift per unit span) leads to

$$\frac{\mathrm{d}L}{\mathrm{d}y} = \frac{W l_\mathrm{T}/\left(l_\mathrm{T}+l_\mathrm{W}\right)\left[2+q/q_\mathrm{W}\left(3y/s-2\right)\right]}{4s\left[1-q/(4q_\mathrm{W})\right]}. \tag{8.37}$$

For lines of normalized dynamic pressure, as shown in Figure 8.7, the lift increases linearly from the root to the tip. It can be seen that above the fixed root wing divergence speed, negative lift occurs close to the root because of the negative incidence required. The position of the net wing lift force is seen to shift outboard as the air speed increases. Since trim has to be maintained, then the total wing and tailplane lift must remain constant. Because the wing lift is independent of air speed for this simple case (see Section 8.3.3), then the area under each line in this figure remains constant. With the lift shifting outboard, the corresponding wing root bending moments (see Chapters 6 and 18) will increase, and hence these internal loads become greater with increasing air speed due to the aeroelastic effect.

8.3.3 Effect of Trim on Wing and Tail Lift

To maintain trim, the vertical force and moment equilibrium equations must hold at all flight cases. For this special case where the wing has a symmetric section (i.e. no camber), it may be shown that the wing and tailplane lift force remain constant with changes in air speed. However, as will be seen in Chapter 13, the presence of wing camber adds a pitching moment and means that these forces will actually change with air speed, though their sum will still equal the weight.

Assuming that S_T is the tailplane area, a_T is the lift curve slope for the tail, a_E is the lift curve slope for the elevator and η is the elevator angle, the tailplane lift can be expressed in the form

$$L_\mathrm{T} = qS_\mathrm{T}\left(a_\mathrm{T}\theta_0 + a_\mathrm{E}\eta\right), \tag{8.38}$$

so that once the tailplane lift force is determined, then the elevator angle for trim may be found. In this simple example, it may be shown that η must be increased at higher air speeds in order to maintain trim. In practice aircraft will run out of available elevator trim before divergence can occur.

8.4 EFFECT OF WING SWEEP ON STATIC AEROELASTIC BEHAVIOUR

Most aircraft are designed with swept-back wings. The reasons for this are mainly aerodynamic, since for subsonic aircraft sweep-back increases the air speed at which shock waves are formed on the wings, so delaying the associated increase in drag. The sweep also reduces the effective thickness to chord ratio. Supersonic aircraft are designed with the wings swept inside the Mach cone, which also decreases the associated wave drag (Anderson, 2001).

Similar improvements in drag reduction could be obtained through the use of swept-forward wings, which enables other benefits. For swept-forward wings, flow separation occurs initially near the wing root, thus preserving aileron control at the wing tip, whereas for swept-back wings flow separation occurs first towards the wing tips. Very few aircraft (e.g. X-29, Sukhoi-47), however, have been built with swept-forward wings. The main reason for this is the static aeroelastic behaviour of swept wings and in particular the detrimental effect that wing sweep has on the divergence speed.

This section introduces some simple aeroelastic wing models that demonstrate how wing sweep changes the static aerodynamic lift and aeroelastic behaviour. The differences between wings with forwards or backwards sweep are emphasized. Comments on the effect of sweep on the equilibrium manoeuvre and the trimmed condition for a flexible aircraft are included in Chapter 13.

8.4.1 Effect of Wing Sweep on Effective Angle of Incidence

In order to illustrate the effect of wing sweep on a flexible wing, consider the rectangular wing shown in Figure 8.8 subjected to an upwards bending displacement along the mid-chord line (for simplicity); the wing can be unswept, swept-forwards or swept-backwards. Wing bending has a much greater effect on the effective angle of incidence compared to wing twist, but, the actual mode of divergence is still torsion. Of particular importance is the effective angle of incidence of the streamwise strips when the sweep angle is changed (Broadbent, 1954).

The streamwise sections become AC, AD and AB for the no-sweep, sweep-back and sweep-forward cases respectively. When the wing is considered to bend upwards, the following occurs:

(a) For the unswept case (AC), the incidence is unchanged due to bending.
(b) For the sweep-back case (AD), the effective streamwise angle of incidence reduces since point D moves upwards more under bending than point A.
(c) For the sweep-forward case (AB), the effective incidence increases (point A moves upwards more than point B).

Consequently, swept-forward wings have a decreased divergence speed compared to wings with no sweep due to increased effective incidence, whereas swept-back wings have an increased divergence speed.

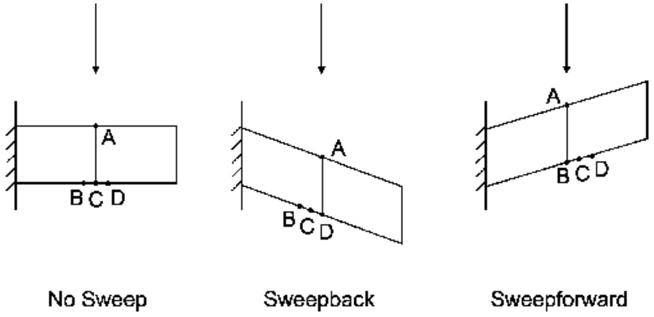

Figure 8.8 Streamwise strips for wings with no sweep, sweep-back and sweep-forward.

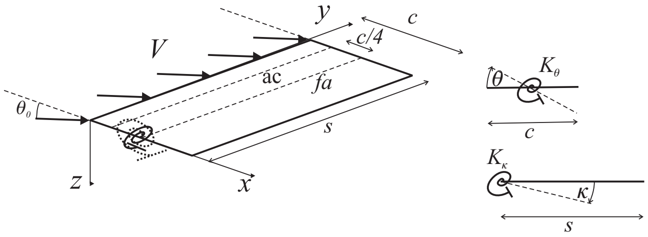

Figure 8.9 Rigid untapered wing attached to the root with pitch and flap springs.

8.4.2 Effective Streamwise Angle of Incidence Due to Flapping/Pitching

Consider now the untapered wing with chord c, semi-span s and sweep angle Λ (taken as positive for sweep-back) in a flow of speed V with an initial root angle of incidence θ_0, as shown in Figures 8.9 and 8.10. Both bending and twisting type deflections need to be included in order to achieve a realistic behaviour; consequently a different mathematical model will be used compared to that in the previous sections. This model will also be used in Chapter 11 on flutter, but without any sweep.

The wing is taken to be rigid, but with two rotational springs at the root, one of stiffness K_κ which controls the flapping motion (i.e. bending about the root) and the other of stiffness K_θ which restrains the pitching motion. The flexural axis is set at the mid-chord (see Chapter 13 for further comments on the effect of sweep on the flexural axis). Flap and pitch motions are assumed to act along and about the flexural axis y' regardless of the sweep angle. Once again strip theory aerodynamics is assumed, with strips aligned in the streamwise direction. Note that, by convention, the span and streamwise chord (and hence wing area) will be kept constant with changes in sweep angle.

Consider the flow over an elemental streamwise strip of width dy at spanwise distance y. The change in the effective angle of incidence depends upon the difference in the deflection of the two ends of the strip (points p and r), and also upon the geometry of points p, q and r. If the wing *pitches* through angle θ about the flexural axis (leading edge upwards), then the increase in angle of incidence of the strip with sweep-back Λ is seen from Figure 8.11 to be

$$\Delta\theta_{\text{pitch}} = \frac{c\theta\cos\Lambda}{c} = \theta\cos\Lambda, \tag{8.39}$$

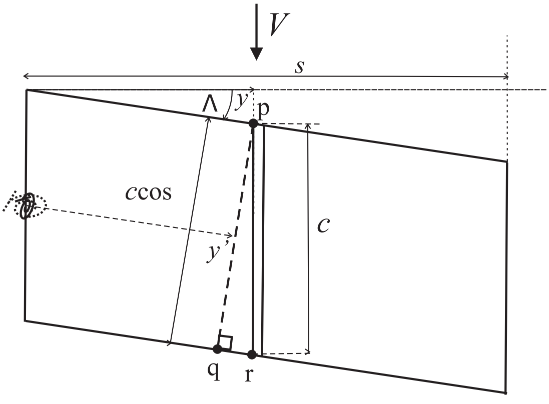

Figure 8.10 Untapered wing with sweep.

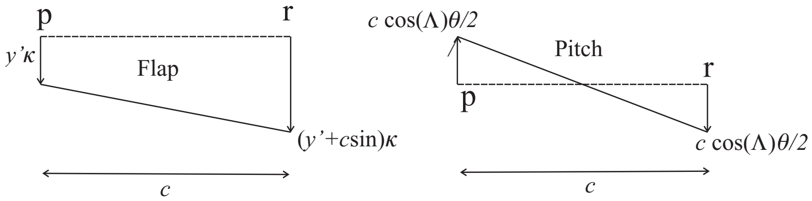

Figure 8.11 Effect of sweep on flap and pitch deflections of a streamwise strip.

since the leading and trailing edges move up and down the same vertical distance about the flexural axis. So for pitch about the flexural axis, sweeping the wing either forwards *or* backwards *decreases* the effective angle of incidence.

Applying the same approach as above, but this time for a *flap* angle *downwards* of κ (to be consistent with later models) implies that points p and q move downwards by $y'\kappa = y\kappa/\cos\Lambda$ whereas point r moves downwards by $(y' + c\sin\Lambda)\kappa$. The resulting angle of incidence increase for flapping downwards can be seen in Figure 8.11 to be

$$\Delta\theta_{\mathrm{Flap}} = \frac{c\kappa\sin\Lambda}{c} = \kappa\sin\Lambda \tag{8.40}$$

Examination of Equation (8.40) shows that sweeping the wing backwards increases the angle of incidence due to the downwards flapping motion, whereas sweeping it forwards reduces the angle of incidence. However, in steady level flight, the wing will flap *upwards* (negative κ), leading to a consequent decrease in the effective angle of incidence due to flapping for the swept-back case and an increase for the swept-forward case.

Consider the more realistic case of a flexible wing undergoing bending and twisting, as opposed to flapping and pitching in the simple model above. The larger bending deflections of a wing dominate the changes in the effective angle of incidence compared to those from wing twist. However, the twisting degree of freedom must also be included in any mathematical model as this is still part of the mechanism that gives rise to divergence.

8.4.3 Effect of Sweep Angle on Divergence Speed

For the same swept untapered wing as above, with an initial root angle of incidence θ_0, the lift acting at the quarter chord of the elemental strip of area $c\,\mathrm{d}y$ when flapping and pitching are considered together is

$$\mathrm{d}L = qa_{\mathrm{W}}c\,\mathrm{d}y\,[(\theta_0+\theta)\cos\Lambda + \kappa\sin\Lambda]\,. \tag{8.41}$$

Thus the work done due to this lift acting through the displacements caused by the incremental angles $\delta\kappa$ and $\delta\theta$, when integrated along the span of the wing, is

$$\begin{aligned}\delta W &= -\int_0^s qa_{\mathrm{W}}c\,\mathrm{d}y\,[(\theta_0+\theta)\cos\Lambda + \kappa\sin\Lambda]\left(\frac{y}{\cos\Lambda} + \frac{c\sin\Lambda}{4}\right)\delta\kappa \quad \text{vertical movement of lift} \\ &\quad + \int_0^s qa_{\mathrm{W}}c\,\mathrm{d}y\,[(\theta_0+\theta)\cos\Lambda + \kappa\sin\Lambda]\,\frac{c\cos\Lambda}{4}\delta\theta \quad \text{moment + ve nose up} \\ &= qa_{\mathrm{W}}c\,[(\theta_0+\theta)\cos\Lambda + \kappa\sin\Lambda]\left[\frac{cs\cos\Lambda}{4}\delta\theta - \left(\frac{s^2}{2\cos\Lambda} + \frac{cs\sin\Lambda}{4}\right)\delta\kappa\right].\end{aligned} \tag{8.42}$$

The potential (or strain) energy is solely due to the two springs, as the wing itself is rigid, so

$$U = \tfrac{1}{2}K_\kappa \kappa^2 + \tfrac{1}{2}K_\theta \theta^2. \tag{8.43}$$

Application of Lagrange's equation for generalized coordinates κ and θ leads to

$$\begin{aligned}
K_\kappa \kappa &= -q a_{\mathrm{W}} \left[(\theta_0 + \theta)\cos\Lambda + \kappa \sin\Lambda\right] \left(\frac{cs^2}{2\cos\Lambda} + \frac{c^2 s \sin\Lambda}{4}\right), \\
K_\theta \theta &= q a_{\mathrm{W}} \frac{c^2 s \cos\Lambda}{4} \left[(\theta_0 + \theta)\cos\Lambda + \kappa \sin\Lambda\right],
\end{aligned} \tag{8.44}$$

which can be rearranged into matrix form as

$$\begin{bmatrix} \left[K_\kappa + q a_{\mathrm{W}} c \left(\dfrac{s^2 \tan\Lambda}{2} + \dfrac{cs \sin^2\Lambda}{4}\right)\right] & q a_{\mathrm{W}} c \left(\dfrac{s^2}{2} + \dfrac{cs \sin\Lambda \cos\Lambda}{4}\right) \\ \dfrac{-q a_{\mathrm{W}} s c^2 \sin\Lambda \cos\Lambda}{4} & \left(K_\theta - \dfrac{q a_{\mathrm{W}} s c^2 \cos^2\Lambda}{4}\right) \end{bmatrix} \begin{Bmatrix} \kappa \\ \theta \end{Bmatrix}$$

$$= \begin{Bmatrix} -q a_{\mathrm{W}} c \left(\dfrac{s^2}{2} + \dfrac{cs \sin\Lambda \cos\Lambda}{4}\right) \\ \dfrac{q a_{\mathrm{W}} s c^2 \cos^2\Lambda}{4} \end{Bmatrix} \theta_0. \tag{8.45}$$

These equations can be solved to give the flap and pitch deflections for a given air speed and root angle of incidence. Note that trim is not taken into account since only the impact of sweep is being considered.

Divergence for the flapping/pitching swept wing occurs when the determinant of the left-hand side square matrix becomes zero; thus

$$\begin{aligned}
&\left[K_\kappa + q a_{\mathrm{W}} c \left(\frac{s^2 \tan\Lambda}{2} + \frac{cs \sin^2\Lambda}{4}\right)\right] \left(K_\theta - \frac{q a_{\mathrm{W}} s c^2 \cos^2\Lambda}{4}\right) \\
&\qquad + (q a_{\mathrm{W}})^2 s c^3 \frac{\sin\Lambda \cos\Lambda}{4} \left(\frac{s^2}{2} + \frac{cs \sin\Lambda \cos\Lambda}{4}\right) = 0
\end{aligned} \tag{8.46}$$

and, since the terms in q^2 cancel out, the dynamic pressure at divergence can be found. Thus the divergence speed may be shown to be

$$V_{\mathrm{div}} = \sqrt{\frac{2K_\theta K_\kappa}{\rho a_{\mathrm{W}} \left[K_\kappa s c^2 \cos^2\Lambda/4 - K_\theta \left(cs^2 \tan\Lambda/2 + c^2 \sin^2\Lambda/4\right)\right]}} \tag{8.47}$$

Figure 8.12 shows how the divergence speed, normalized with respect to the divergence speed for the unswept wing, increases with sweepback ($\Lambda > 0$) and decreases for the sweep-forward case ($\Lambda < 0$). This reduction of the divergence speed becomes the limiting case for sweep-forward designs and consequently very few exist. Experimental aircraft such as the X-29 were only able to have swept-forward wings due to the use of aeroelastic tailoring, where the wing characteristics were altered using composite laminates oriented in such a manner that an upwards bending deflection resulted in a nose down twist.

Note that when there is no sweep ($\Lambda = 0$) then the divergence speed becomes

$$V_{\mathrm{div}} = \sqrt{\frac{8K_\theta}{\rho a_{\mathrm{W}} c^2 s}} \tag{8.48}$$

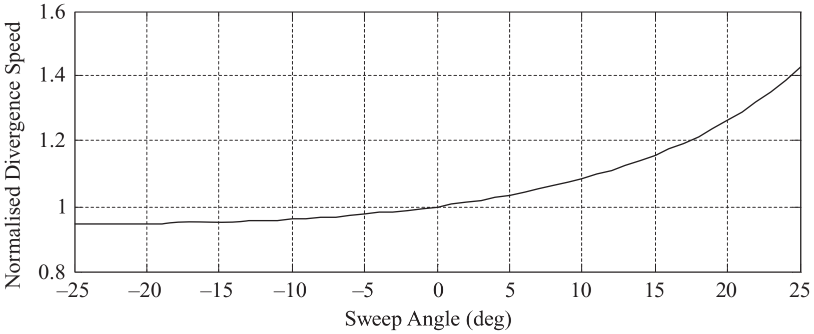

Figure 8.12 Effect of sweep angle on normalized divergence speed.

and this is the divergence speed for the case where only the pitching degree of freedom is included in the rigid wing model with a root rotational spring. This result is to be expected as the flapping degree of freedom has no effect on the steady aerodynamic lift of a streamwise section for the unswept case.

It should be remembered that earlier in this chapter it was shown that by allowing for the trim of the aircraft, the divergence speed changed and a similar effect is found for the swept wing case.

8.4.4 Effect of Sweep Angle on Lift Distribution

The effect of sweep angle on the divergence speed is due to the change in the lift on each streamwise strip, and this will be the same for all strips in this simple case of a rigid wing attached at the root by two springs. By determining the flap and pitch deflections from Equation (8.45) and substituting them into the lift Equation (8.41), the lift on each streamwise strip (i.e. lift per unit span) can be found. Figure 8.13 shows the variation of the lift per unit span with sweep angle (normalized to the zero sweep case); it behaves exactly as expected, with sweep-back reducing the lift for this fixed root incidence case. This analysis for the effect of sweep angle can be extended to take trim effects into account; it may be seen then that the total lift will obviously be independent of sweep but for a swept-back wing the centre of pressure will move inboard, so reducing the wing root bending moment due to lift (see Chapter 13).

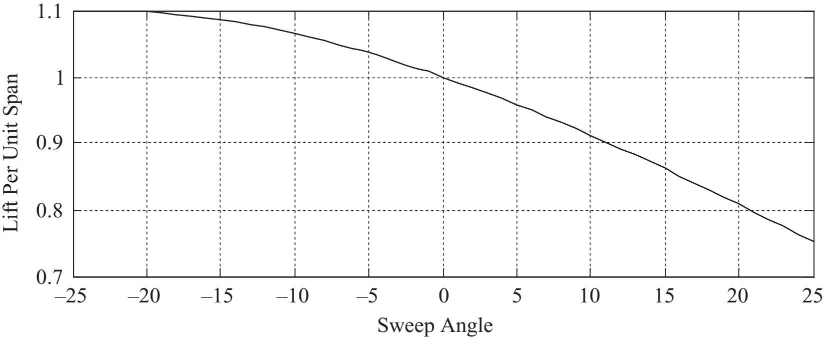

Figure 8.13 Effect of sweep angle on streamwise lift per unit span.

8.4.5 Comments

It should be remembered that there are a number of significant assumptions in the above analysis. Sweepback (or sweep-forward) will increase the aerodynamic interactions between different parts of the wing, which will make the strip theory aerodynamics more inaccurate. It has been assumed that the wing behaves as a beam-like structure, and consequently that the flexural axis remains parallel to the axis of sweep along the mid-chord line. In cases where the wing behaves more like a plate, such as for low aspect ratio tapered swept wings, the structural bending/torsion coupling effects for the swept wing must also be included.

8.5 EXAMPLES

1. Determine the lift distribution and divergence speed of a fixed root rectangular wing of semi-span s, chord c and torsional rigidity *EI* using modified strip theory such that $a_W(y) = a_W(1 - y^2/s^2)$.
2. Determine the lift distribution and divergence speed of a fixed root tapered rectangular wing of semi-span s and chord $c = c_0(1 - y^2/s^2)$ and torsional rigidity $GJ = GJ_0(1 - y^2/s^2)$. Use strip theory.
3. Repeat Examples 1 and 2 but this time for the case where whole aircraft trim is taken into account.
4. Determine the divergence speed and lift distribution for a rectangular fixed root wing of semi-span s, chord c, bending rigidity *EI* and torsional rigidity *GJ* for wing sweep Λ. Use strip theory.
5. Repeat Example 2 with bending rigidity $EI = EI_0(1 - y^2/s^2)$ and wing sweep Λ.

9

Static Aeroelasticity – Effect of Wing Flexibility on Control Effectiveness

It was shown in Chapter 5 how the use of control surfaces changed the effective camber of an aerofoil and that this could be used to change the lift. Thus, control surfaces (e.g. ailerons, rudder) are used to manoeuvre an aircraft in flight and their sizing is an important issue when the aircraft is designed. It is important to know how sensitive an aircraft is to application of the control surfaces and what loads are generated. This is of particular significance for military aircraft where the need to manoeuvre rapidly is essential, but is also of course important in terms of the performance of commercial aircraft.

This chapter will consider the effect that aeroelastic deflections of the flexible wing have on the aerodynamic influence, or *effectiveness*, of the control surfaces in comparison to the rigid wing. It will be shown that as the speed increases the effectiveness reduces until at some critical speed – the *reversal speed* – there is no response to application of the control surface. At speeds greater than the reversal speed, the action of the controls reverses, a phenomenon known as *control reversal*. Although not necessarily disastrous, it is unacceptable that at speeds near to the reversal speed, the aircraft responds either very slowly or not at all to application of the controls, and that the opposite response to that demanded occurs beyond the reversal speed.

There are two basic ways that the aircraft industry considers these static aeroelastic phenomena (although there is motion it is considered to be steady) and these will be illustrated by considering a wing rolling at a constant rate and a wing with a fixed root experiencing a control deflection; in both cases a simple rectangular wing plus aileron is used. In Chapter 13, where equilibrium (or so-called *bookcase*) manoeuvres are considered, the steady application of the elevator to a whole aircraft flexible model is considered; also the steady roll case is revisited and the yaw case examined briefly, both for the whole aircraft. Also, in Chapter 15, the dynamic (or so-called *rational*) manoeuvre using the flight mechanics model allows the flexible aircraft dynamic response to a transient application of a roll or pitch control to be considered, with nonlinear effects able to be included.

Note that static aeroelastic calculations are employed fairly early in the design process to size the control surfaces. However, later on when the flight control system (FCS) has been designed, the flight mechanics model allows rational calculations to be performed in order to see the control effectiveness with nonlinear effects included. The deployment and performance of the controls would then be fine tuned via the FCS to gain the characteristics required; clearly it would then be too late to change the control size.

9.1 ROLLING EFFECTIVENESS OF A FLEXIBLE WING – THE STEADY ROLL CASE

Consider a flexible wing of semi-span s and chord c with a symmetric section (i.e. no camber), a root incidence θ_0 and a rigid full span aileron whose rotation angle is β; this symbol is used as standard in the

---

Introduction to Aircraft Aeroelasticity and Loads J. R. Wright and J. E. Cooper
© 2007 John Wiley & Sons, Ltd

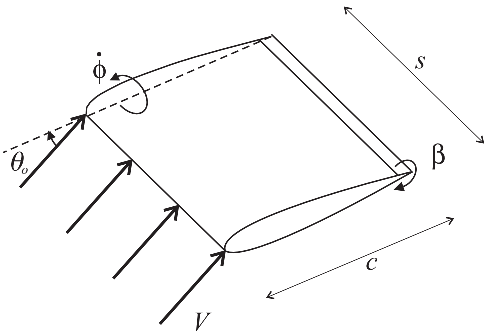

Figure 9.1 Wing with a full span aileron undergoing steady roll.

classical flutter books (e.g. Fung, 1969), but is not to be confused with the usage later in Chapters 13 to 15 for the sideslip angle in the flight mechanics model. The wing undergoes a steady roll rate $\dot{\phi}$ about an axis at the root, as shown in Figure 9.1 (fuselage dimensions are ignored). To avoid problems with signs at this early stage, the port wing with down aileron is considered whereas later in Chapter 15 the normal convention of y positive on the starboard wing will be used.

As in Chapter 8, assume that the wing is flexible in twist, which is taken to vary linearly as

$$\theta = \left(\frac{y}{s}\right)\theta_{\mathrm{T}}. \tag{9.1}$$

The twist is defined as nose up about the flexural axis, taken at distance ec aft of the aerodynamic centre on the quarter chord. Note that no fuselage or tailplane effects are considered. In essence, as in Chapter 8, the aircraft is considered to have a rigid body roll motion, together with a wing torsion branch mode (behaving antisymmetrically on the two sides of the aircraft).

Using the results in Chapter 5, for any section of the wing plus control, the lift and moment (defined positive nose upwards and referred to the flexural axis) coefficients are

$$C_{\mathrm{L}} = a_0 + a_{\mathrm{W}}(\theta_0 + \theta) + a_{\mathrm{C}}\beta \qquad \text{and} \qquad C_{\mathrm{M}} = b_0 + b_{\mathrm{W}}(\theta_0 + \theta) + b_{\mathrm{C}}\beta, \tag{9.2}$$

where $a_0 = b_0 = 0$ for the symmetric aerofoil and $b_{\mathrm{W}} = a_{\mathrm{W}}e$. Figure 9.2 shows the effect of applying a downwards aileron deflection on a flexible (or elastic) wing. Note that the incremental lift due to the control rotation acts towards the aileron hinge line, around the two-third to three-quarter chord. Thus, any applied control rotation provides not only a lift force introducing roll but also a nose down pitching moment, leading to nose down twist for an elastic wing and therefore a reduction in the angle of incidence.

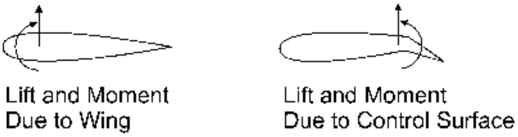

Figure 9.2 Effect on lift distribution of applying a control surface rotation.

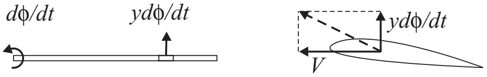

Figure 9.3 Change of incidence due to the downwash from rolling motion.

9.1.1 Determination of Reversal Speed for Steady Roll Case

The lift force and pitching moment acting upon an elemental strip dy for a down aileron application on the port wing are

$$\mathrm{d}L = qc\,\mathrm{d}y\left[a_\mathrm{W}\left(\theta_0 + \frac{y}{s}\theta_\mathrm{T} - \frac{\dot{\phi}y}{V}\right) + a_\mathrm{C}\beta\right] \quad \text{and} \quad \mathrm{d}M = qc^2\mathrm{d}y\left[b_\mathrm{W}\left(\theta_0 + \frac{y}{s}\theta_\mathrm{T} - \frac{\dot{\phi}y}{V}\right) + b_\mathrm{C}\beta\right], \tag{9.3}$$

where q is again the dynamic pressure and $\dot{\phi}y/V$ is the reduction of incidence associated with the downwash due to the rate of roll (port wing moving upwards), as seen in Figure 9.3.

The total work done that is associated with incremental twist $\delta\theta$ and roll $\delta\phi$ angles is

$$\begin{aligned}\delta W &= \int_\mathrm{wing} (\mathrm{d}L\; y\delta\phi + \mathrm{d}M\;\delta\theta)\\ &= 2qc\int_0^s \left[a_\mathrm{W}\left(\frac{y}{s}\theta_\mathrm{T} - \frac{\dot{\phi}y}{V}\right) + a_\mathrm{C}\beta\right]y\delta\phi\,\mathrm{d}y + 2qc^2\int_0^s \left[b_\mathrm{W}\left(\frac{y}{s}\theta_\mathrm{T} - \frac{\dot{\phi}y}{V}\right) + b_\mathrm{C}\beta\right]\delta\theta\,\mathrm{d}y,\end{aligned} \tag{9.4}$$

where a factor of 2 has been applied to include the effect of the starboard wing and the θ_0 terms cancel out on the two sides of the aircraft. Thus the generalized forces in the ϕ and θ_T generalized coordinates are

$$\begin{aligned}Q_\phi &= \frac{\partial(\delta W)}{\partial(\delta\phi)} = 2qc\int_0^s \left[a_\mathrm{W}\left(\frac{y^2}{s}\theta_\mathrm{T} - \frac{\dot{\phi}y^2}{V}\right) + a_\mathrm{C}\beta y\right]\mathrm{d}y\\ &= 2qc\left[a_\mathrm{W}\left(\frac{s^2}{3}\theta_\mathrm{T} - \frac{\dot{\phi}s^3}{3V}\right) + \frac{a_\mathrm{C}\beta s^2}{2}\right]\end{aligned} \tag{9.5}$$

and

$$Q_{\theta_\mathrm{T}} = \frac{\partial(\delta W)}{\partial(\delta\theta_\mathrm{T})} = 2qc^2\int_0^s \left[b_\mathrm{W}\left(\frac{y^2}{s^2}\theta_\mathrm{T} - \frac{\dot{\phi}y^2}{sV}\right) + \frac{b_\mathrm{C}\beta y}{s}\right]\mathrm{d}y = 2qc^2\left[b_\mathrm{W}\left(\frac{s}{3}\theta_\mathrm{T} - \frac{\dot{\phi}s^2}{3V}\right) + \frac{b_\mathrm{C}\beta s}{2}\right]. \tag{9.6}$$

Since the roll motion of the aircraft is steady, the kinetic energy terms associated with roll ϕ and twist θ are constant and do not contribute inertia terms to the roll or twist equations. The potential (or strain) energy for a single wing is the same as in Chapters 3 and 8 so that

$$U = \frac{GJ}{2s}\theta_\mathrm{T}^2. \tag{9.7}$$

Thus, using Lagrange's equations, and evaluating the strain energy for both wings, the relationship between the rate of roll, tip twist and aileron angle is found as

$$\begin{bmatrix} \frac{2q\,cs^3a_W}{3V} & \frac{-2q\,cs^2a_W}{3} \\ \frac{2q\,c^2s^2b_W}{3V} & \left(\frac{2GJ}{s} - \frac{2q\,c^2s\,b_W}{3}\right) \end{bmatrix} \begin{Bmatrix} \dot{\phi} \\ \theta_T \end{Bmatrix} = \begin{Bmatrix} q\,cs^2a_C \\ q\,c^2sb_C \end{Bmatrix} \beta \Rightarrow \begin{bmatrix} 1 & -1 \\ e & (\mu - e) \end{bmatrix} \begin{Bmatrix} \frac{s\dot{\phi}}{V} \\ \theta_T \end{Bmatrix} = \begin{Bmatrix} \frac{3a_C}{2a_W} \\ \frac{3b_C}{2a_W} \end{Bmatrix} \beta, \tag{9.8}$$

where

$$\mu = \frac{3GJ}{q\,c^2s^2a_W}. \tag{9.9}$$

Note that the fixed wing divergence speed may be found again by setting the roll rate to zero.

Solving Equations (9.8) leads to the expressions for the roll rate per control angle, which will provide a measure of the *rolling effectiveness* when compared to the rigid aircraft result, and also for the tip twist per control angle

$$\frac{\dot{\phi}}{\beta} = \frac{3V}{2\mu s a_W}[a_C(\mu - e) + b_C] \qquad \text{and} \qquad \frac{\theta_T}{\beta} = \frac{3(b_C - ea_C)}{2a_W\mu} = \frac{q\,c^2s^2(b_C - ea_C)}{2GJ}. \tag{9.10}$$

It is common practice to define the *control effectiveness in roll* $\Im$ as

$$\Im = \frac{(\dot{\phi}/\beta)_{\text{flexible}}}{(\dot{\phi}/\beta)_{\text{rigid}}}, \tag{9.11}$$

and since for the rigid wing $GJ \to \infty$ and $\mu \to \infty$, then

$$\Im = \frac{(\dot{\phi}/\beta)_{\text{flexible}}}{(\dot{\phi}/\beta)_{\text{rigid}}} = \frac{[3V/(2\mu s a_W)][a_C(\mu - e) + b_C]}{3Va_C/2sa_W} = \frac{a_C(\mu - e) + b_C}{\mu a_C}, \tag{9.12}$$

where it should be noted that $\mu > 0,\ a_C > 0,\ b_C < 0$.

Typical plots of the control effectiveness and tip twist per control angle are shown in Figure 9.4 as a function of velocity normalized to the reversal speed, and demonstrate that the control effectiveness reduces from a value of unity with increasing air speed, reaches zero at the reversal speed and then becomes increasingly negative. Military aircraft are sometimes designed to take advantage of this effect to achieve high manoeuvrability through the use of an active control system that takes into account the opposite effect of the controls beyond reversal. The tip twist also becomes increasingly negative (nose down) and therefore nose down (since b_C is negative) for increases in control angle and dynamic pressure.

At the reversal speed, there is no change of roll rate with respect to control angle, i.e. $\dot{\phi}/\beta = 0$, which occurs when $[a_C(\mu - e) + b_C] = 0$. Thus the dynamic pressure at the reversal speed, q_{rev}, is found as

$$q_{\text{rev}} = \frac{3GJa_C}{c^2s^2a_W(ea_C - b_C)} \tag{9.13}$$

with a corresponding tip twist per aileron angle of

$$\frac{\theta_{T_{\text{rev}}}}{\beta} = -\frac{3a_C}{2a_W} \tag{9.14}$$

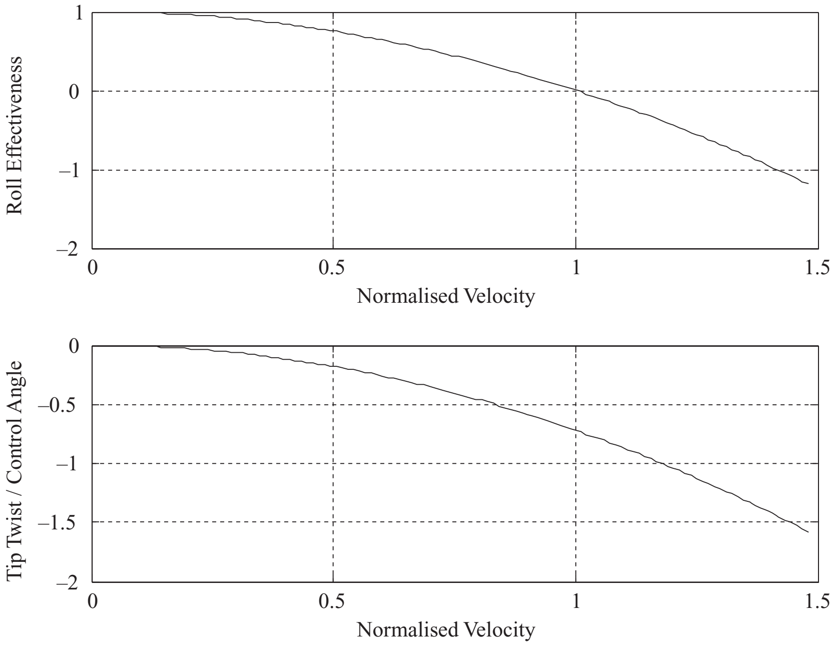

Figure 9.4 Roll effectiveness and tip twist/control angle against velocity normalized to the reversal speed.

At the reversal speed, the pitching moment due to the angle of incidence of the wing is exactly cancelled out by the pitching moment generated by the control angle. Combining Equations (9.12) and (9.13) leads to a different expression for the control effectiveness purely in terms of the dynamic pressure, so that

$$\Im = 1 - \frac{q}{q_{\mathrm{rev}}}. \tag{9.15}$$

Finally, comparing the fixed wing divergence speed to the reversal speed gives

$$\frac{q_{\mathrm{W}}}{q_{\mathrm{rev}}} = \frac{3GJ/(ec^2s^2a_{\mathrm{W}})}{3GJa_{\mathrm{C}}/[c^2s^2a_{\mathrm{W}}(ea_{\mathrm{C}} - b_{\mathrm{C}})]} = \frac{ea_{\mathrm{C}} - b_{\mathrm{C}}}{ea_{\mathrm{C}}} \tag{9.16}$$

and, since b_{C} is negative, the reversal speed is always less here than the fixed wing divergence speed.

9.1.2 Lift Distribution for the Steady Roll Case

Consider the lift acting upon a chordwise elemental strip at distance y from the root. The incremental lift on each chordwise strip dy due to the twist, roll rate and control rotation (i.e. ignoring the steady contribution from the root incidence θ_0) is given by

$$\mathrm{d}L = qc\left[a_{\mathrm{W}}\left(\frac{y}{s}\theta_{\mathrm{T}} - \frac{\dot{\phi}y}{V}\right) + a_{\mathrm{C}}\beta\right]\mathrm{d}y. \tag{9.17}$$

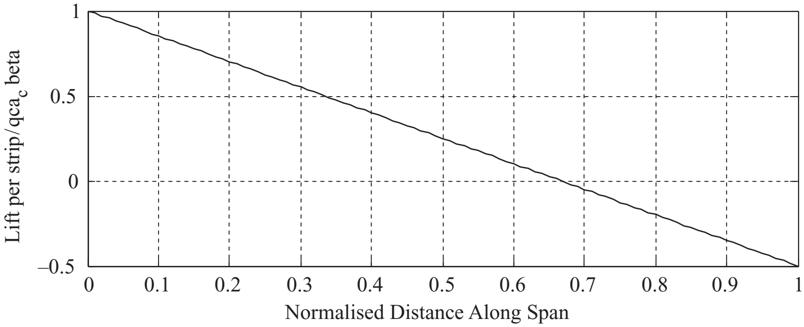

Figure 9.5 Lift per unit span/($qca_C\beta$) along the semi-span.

Substituting the expressions for the roll rate (9.13) and wing twist (9.14) at the reversal condition into this equation leads to the lift per unit span expression at the reversal speed

$$\frac{\mathrm{d}L}{\mathrm{d}y} = q\,ca_C\left(1 - \frac{3y}{2s}\right)\beta. \tag{9.18}$$

Although the lift per unit span increases linearly with dynamic pressure and control angle, Figure 9.5 shows how the lift per unit span reduces with distance from the wing root due to the negative (nose down) twist caused by the control action. In the outboard wing, beyond two-thirds of the semi-span, the lift per unit span is negative and this counteracts the positive lift inboard to give no rolling moment at reversal.

The total lift on one wing at reversal is found by integrating the lift on each strip across the entire wing, such that

$$\text{Total lift} = \int_0^s qca_C\left(1 - \frac{3y}{2s}\right)\beta\,\mathrm{d}y = \frac{qcsa_C}{4}\beta. \tag{9.19}$$

The corresponding rolling moment about the wing root can be found as

$$\int_0^s qca_C\left(1 - \frac{3y}{2s}\right)\beta y\,\mathrm{d}y = qca_C\left(\frac{s^2}{2} - \frac{s^2}{2}\right)\beta = 0, \tag{9.20}$$

which is to be expected as the achieved rate of roll is zero at reversal.

9.2 ROLLING EFFECTIVENESS OF A FLEXIBLE WING – THE FIXED WING ROOT CASE

Consider the same flexible wing model with a full span aileron as used earlier in Section 9.1, but now with the wing root fixed instead of the wing being allowed to undergo a steady roll rate. The effect of applying a control rotation on the lift distribution, and particularly on the wing root bending moment, is of interest.

9.2.1 Determination of Reversal Speed

As the wing is fixed then $\dot{\phi} = \phi = 0$. The lift and pitching moment on the elemental strip dy due to the fixed root incidence θ_0, twist θ and control rotation β are

$$\mathrm{d}L = qc\,\mathrm{d}y\left[a_\mathrm{W}\left(\theta_0 + \frac{y}{s}\theta_\mathrm{T}\right) + a_\mathrm{C}\beta\right] \qquad \text{and} \qquad \mathrm{d}M = qc^2\,\mathrm{d}y\left[b_\mathrm{W}\left(\theta_0 + \frac{y}{s}\theta_\mathrm{T}\right) + b_\mathrm{C}\beta\right]. \tag{9.21}$$

The work done by the lift is zero since the wing is not allowed to roll. However, the work done by the pitching moment acting through an incremental twist $\delta\theta$ for the single wing is found as

$$\delta W = \int_\mathrm{wing} \mathrm{d}M\,\delta\theta = qc^2\int_0^s \left[b_\mathrm{W}\left(\theta_0 + \frac{y}{s}\theta_\mathrm{T}\right) + b_\mathrm{C}\beta\right]\frac{y}{s}\delta\theta_\mathrm{T}\,\mathrm{d}y \tag{9.22}$$

and thus the generalized force in twist is

$$Q_{\theta_\mathrm{T}} = \frac{\partial(\delta W)}{\partial(\delta\theta_\mathrm{T})} = qc^2s\left(\frac{b_\mathrm{W}}{2}\theta_0 + \frac{b_\mathrm{W}}{3}\theta_\mathrm{T} + \frac{b_\mathrm{C}}{2}\beta\right). \tag{9.23}$$

The potential (or strain) energy for a single wing follows as before as in Equation (9.7), and so applying Lagrange's equation gives the expression

$$\frac{GJ}{s}\theta_\mathrm{T} = qc^2s\left(\frac{b_\mathrm{W}}{2}\theta_0 + \frac{b_\mathrm{W}}{3}\theta_\mathrm{T} + \frac{b_\mathrm{C}}{2}\beta\right). \tag{9.24}$$

The wing tip twist is then given by

$$\theta_\mathrm{T} = \frac{qc^2s}{\left(2GJ/s - 2qc^2sb_\mathrm{W}/3\right)}\left(b_\mathrm{W}\theta_0 + b_\mathrm{C}\beta\right) = \frac{qc^2s^2}{2GJ\left(1 - q/q_\mathrm{W}\right)}\left(b_\mathrm{W}\theta_0 + b_\mathrm{C}\beta\right). \tag{9.25}$$

Now consider the effect due to control rotation in isolation from the root incidence effect (examined in Chapter 8). Since b_C is negative, a nose down twist will result from an increased control angle or dynamic pressure. The lift per unit span due to control rotation alone can be determined as

$$\frac{\mathrm{d}L}{\mathrm{d}y} = qc\left[a_\mathrm{W}\frac{y}{s}\theta_\mathrm{T} + a_\mathrm{C}\beta\right], \tag{9.26}$$

and substituting in the relevant part of the expression for the wing tip twist in Equation (9.25) gives

$$\frac{\mathrm{d}L}{\mathrm{d}y} = qc\left[\frac{qc^2s^2a_\mathrm{W}}{2GJ(1 - q/q_\mathrm{W})}\frac{y}{s}b_\mathrm{C} + a_\mathrm{C}\right]\beta. \tag{9.27}$$

The total lift acting on the single wing due to control rotation is

$$L_\mathrm{W} = \int_0^s \frac{\mathrm{d}L}{\mathrm{d}y}\mathrm{d}y = qcs\left[\frac{qc^2s^2a_\mathrm{W}}{4GJ\left(1 - q/q_\mathrm{W}\right)}b_\mathrm{C} + a_\mathrm{C}\right]\beta \tag{9.28}$$

and, in a similar way, the total root bending moment (see internal loads in Chapters 6 and 18) due to application of control rotation is

$$\int_0^s \frac{\mathrm{d}L}{\mathrm{d}y}y\,\mathrm{d}y = qcs^2\left[\frac{qc^2s^2a_\mathrm{W}}{6GJ\left(1 - q/q_\mathrm{W}\right)}b_\mathrm{C} + \frac{a_\mathrm{C}}{2}\right]\beta = qcs^2\left[\frac{qb_\mathrm{C}}{2eq_\mathrm{W}\left(1 - q/q_\mathrm{W}\right)} + \frac{a_\mathrm{C}}{2}\right]\beta \tag{9.29}$$

There is zero total bending moment at the wing root due to control rotation at the reversal speed, so reversal occurs when

$$\frac{qc^2s^2a_\mathrm{W}}{6GJ\,(1-q/q_\mathrm{W})}b_\mathrm{C}+\frac{a_\mathrm{C}}{2}=0. \tag{9.30}$$

Then, following some algebraic manipulation, the dynamic pressure at reversal can be found as

$$q_\mathrm{rev}=\frac{q_\mathrm{W}ea_\mathrm{C}}{ea_\mathrm{C}-b_\mathrm{C}}, \tag{9.31}$$

which is exactly the same as the constant roll rate case in Equation (9.16). The tip twist at reversal is also the same as for the constant roll rate case in Equation (9.14). Note that the root bending moment due to control rotation is equivalent to the total rolling moment, but the former term is more appropriate for a fixed root wing.

9.2.2 Rolling Effectiveness – Fixed Wing Root Case

As for the constant roll rate case, the rolling effectiveness is obtained by comparing the root bending moments for the flexible and rigid wing cases. For a rigid fixed root wing, the lift per unit span due to control rotation is

$$\frac{\mathrm{d}L}{\mathrm{d}y}=qca_\mathrm{C}\beta. \tag{9.32}$$

The total static bending moment due to control rotation for the rigid wing is

$$\int_0^s qca_\mathrm{C}\beta y\,\mathrm{d}y=\frac{qcs^2a_\mathrm{C}}{2}\beta. \tag{9.33}$$

The *static moment effectiveness* is then found by combining Equations (9.29) and (9.33) to give

$$\Im_\text{static moment}=\frac{\text{static bending moment (flexible)}}{\text{static bending moment (rigid)}}=\frac{1-q/q_\mathrm{rev}}{1-q/q_\mathrm{W}} \tag{9.34}$$

Figure 9.6 compares the constant roll rate and static moment effectiveness expressions, Equations (9.15) and (9.34), for the case where the reversal speed is 80% of the divergence speed. It can be seen that

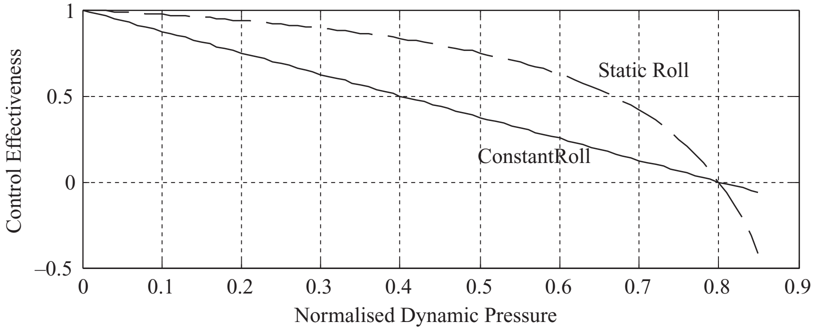

Figure 9.6 Control effectiveness for constant roll rate and static moment cases.

although the estimated reversal speed is the same for both approaches, there is a significant difference between the two curves in the subcritical region.

The actual dynamic roll performance of the aircraft may be examined further when the flight mechanics model is used with the flight control system (FCS) represented and with flexible modes included or with relevant aerodynamic terms corrected for flexible effects (see Chapter 15). The scheduling of different controls (e.g. inboard and outboard ailerons and spoilers) may be adjusted as necessary.

9.3 EFFECT OF SPANWISE POSITION OF THE CONTROL SURFACE

In practice there are usually a number of ailerons along the wings of commercial and military aircraft. They can be used in combination, often to reduce the root bending moment in manoeuvres, and also when a gust load alleviation (or suppression) system is installed.

Consider the same fixed root wing as above, but this time in two different configurations: one with a control surface positioned on the inboard half of the wing and the other with a control surface on the outboard half. Following the same procedure as above, the only difference in the incremental work done occurs in the last term of Equation (9.22), where the control surface term integral has limits $0 \rightarrow s/2$ for the inboard control surface and limits $s/2 \rightarrow s$ for the outboard control surface. The root moments for each configuration are found as

$$M_{\text{inboard}} = qcs^2 \left[\frac{qc^2 s a_{\text{W}}}{24 \left(GJ/s - qc^2 s b_{\text{W}}/3 \right)} b_{\text{C}} + \frac{a_{\text{C}}}{2} \right] \beta. \tag{9.35}$$

and

$$M_{\text{outboard}} = qcs^2 \left[\frac{qc^2 s a_{\text{W}}}{8 \left(GJ/s - qc^2 s b_{\text{W}}/3 \right)} b_{\text{C}} + \frac{a_{\text{C}}}{2} \right] \beta. \tag{9.36}$$

As might be expected, the moment due to the outboard control surface is greater than that for the inboard control surface. Note that if Equations (9.35) and (9.36) are added together, then the same total moment is obtained as that found in Equation (9.29).

Once again, the reversal speed occurs when the moment for each of the two cases is equal to zero, giving

$$q_{\text{rev}_{\text{inboard}}} = \frac{q_{\text{W}} a_{\text{C}} e}{a_{\text{C}} e - b_C/4}, \qquad q_{\text{rev}_{\text{outboard}}} = \frac{q_{\text{W}} a_{\text{C}} e}{a_{\text{C}} e - 3b_{\text{C}}/4}, \tag{9.37}$$

and hence the outboard aileron reaches the reversal speed first (since b_{C} is negative), due to the increased outboard twist. It is common practice in large commercial aircraft to ‘lock’ the outboard ailerons during cruise, as they might otherwise be operating beyond the reversal speed, and to control the aircraft using the inboard ailerons. Alternatively, the controls may be scheduled via the FCS.

9.4 FULL AIRCRAFT MODEL – CONTROL EFFECTIVENESS

In practice, when dealing with the general form of the full aircraft model for static aeroelastic considerations, the generalized (or modal) coordinate equations are used to represent the rigid body and flexible modes (see Chapter 3). In Chapter 23, it is explained that similar approaches to those shown in this chapter may be used in industry to estimate the reversal speed. For the approach considered in Section 9.2, the aircraft is constrained (e.g. fixed wing root) so that no rigid body motion occurs when the control is moved. Then a relevant internal load (such as the wing root bending moment) is examined. However, rather than calculate the internal load directly as in this chapter, a constraint approach may be employed.

For the constant roll rate example given above, consider the generalized coordinate vector

$$\boldsymbol{p} = \begin{Bmatrix} \phi \\ \theta_{\mathrm{T}} \end{Bmatrix} \qquad \begin{matrix} \text{rigid body roll angle (constrained to zero),} \\ \text{wing twist (assume } \infty \text{ fuselage pitch inertia).} \end{matrix} \tag{9.38}$$

Then a constraining moment M needs to be imposed against the roll such that there is no allowed roll angle or roll rate, and Equation (9.8) becomes

$$\begin{bmatrix} 0 & \dfrac{-2qcs^2a_{\mathrm{W}}}{3} \\ 0 & \dfrac{2GJ}{s} - \dfrac{2qc^2sb_{\mathrm{W}}}{3} \end{bmatrix} \begin{Bmatrix} \phi \\ \theta_{\mathrm{T}} \end{Bmatrix} + \begin{Bmatrix} 1 \\ 0 \end{Bmatrix} M = \begin{Bmatrix} qcs^2a_{\mathrm{C}} \\ qc^2sb_{\mathrm{C}} \end{Bmatrix} \beta = \boldsymbol{R}_{\mathrm{con}}, \tag{9.39}$$

where $\boldsymbol{R}_{\mathrm{con}}$ is the vector of control generalized forces. As the rigid body roll angle is constrained to zero, then

$$\mathbf{Z}_{\mathrm{c}}\boldsymbol{p} = \mathbf{0}, \tag{9.40}$$

where $\mathbf{Z}_{\mathrm{c}} = [\,1\ \ 0\,]$ is a constraint matrix. Combining Equations (9.39) and (9.40) leads to

$$\left[\begin{array}{cc|c} 0 & \dfrac{-2qcs^2a_{\mathrm{W}}}{3} & 1 \\ 0 & \dfrac{2GJ}{s} - \dfrac{2qc^2sb_{\mathrm{W}}}{3} & 0 \\ \hline 1 & 0 & 0 \end{array}\right] \left[\begin{array}{c} \phi \\ \theta_{\mathrm{T}} \\ \hline M \end{array}\right] = \left[\begin{array}{c} qcs^2a_{\mathrm{C}} \\ qc^2sb_{\mathrm{C}} \\ \hline 0 \end{array}\right] \beta, \tag{9.41}$$

which leads to the constraining moment

$$M = qcs^2\left[\left(\frac{qc^2sb_{\mathrm{C}}}{3GJ/s - qc^2sb_{\mathrm{W}}}\right) a_{\mathrm{W}} + a_{\mathrm{C}}\right]\beta. \tag{9.42}$$

Once this constraining moment is determined, the ratio of the flexible to rigid moments yields the static effectiveness and the same reversal speed as for the previous approaches.

In general, for an aircraft manoeuvring in roll, pitch or yaw, the constraining equation in matrix form becomes

$$\left(\mathbf{E} + \rho V^2\mathbf{C}\right)\boldsymbol{p} + \mathbf{Z}_{\mathrm{c}}^{\mathrm{T}}\boldsymbol{F} = \boldsymbol{R}_{\mathrm{con}}, \tag{9.43}$$

where $\mathbf{E}$ is the generalized stiffness matrix, $\mathbf{C}$ is the aerodynamic generalized stiffness matrix (see Chapter 10), $\boldsymbol{F}$ are the forces/moments required to constrain the relevant displacements/rotations to zero and $\mathbf{Z}_{\mathrm{c}}$ is the physical constraint matrix setting the relevant displacements/rotations to zero via $\mathbf{Z}_{\mathrm{c}}\boldsymbol{p} = \mathbf{0}$. This leads to

$$\begin{bmatrix} \mathbf{E} + \rho V^2\mathbf{C} & \mathbf{Z}_{\mathrm{c}}^{\mathrm{T}} \\ \mathbf{Z}_{\mathrm{c}} & \mathbf{0} \end{bmatrix} \begin{bmatrix} \boldsymbol{p} \\ \boldsymbol{F} \end{bmatrix} = \begin{bmatrix} \boldsymbol{R}_{\mathrm{con}} \\ \mathbf{0} \end{bmatrix}. \tag{9.44}$$

The upper equation is the overall force/moment balance and the lower equation constrains the defined displacement/rotation to be zero. The effectiveness may be obtained from any of the constraint forces or moments. The same approach may be employed for elevator reversal by constraining the aircraft in the centre fuselage.

9.5 EFFECT OF TRIM ON REVERSAL SPEED

So far it has been assumed that the aircraft can reach and exceed the calculated reversal speed if the wing is sufficiently flexible. However, in practice the trim of the aircraft needs to be maintained by slight adjustments of the controls, i.e. ailerons/rudder for lateral trim and elevator for longitudinal trim. As the reversal condition is approached, the relevant control becomes less effective, not only at controlling the aircraft but also at adjusting trim. Thus the aircraft may 'run out of trim' prior to reversal being reached. Use of multiple control surfaces could mean that one control reaches reversal while the combination of controls retains some effectiveness.

9.6 EXAMPLES

1. Investigate the effect that varying the position of the flexural axis (ec) and the chord/aileron ratio (Ec) have upon the reversal and divergence speeds.
2. For the fixed root case, determine the combinations of e and E that produce the best effectiveness values below the reversal speed.
3. For the fixed root case, explore the effect of the ratio between the dynamic pressures at divergence and reversal on the aileron effectiveness
4. For a wing containing two ailerons that together total the entire semi-span of the wing, determine the size of the two parts such that they have the same reversal speed.
5. For a wing containing two ailerons that together total the entire semi-span of the wing, determine the size of the two parts such that they each give the same root bending moment.

10

Introduction to Unsteady Aerodynamics

So far, when considering static aeroelastic effects in Chapters 8 and 9, the aerodynamic surfaces (such as wings) have been in a steady condition and so the resulting forces and moments have been *steady* (i.e. constant with time). However, for flutter, manoeuvre and gust response analyses the behaviour of aerodynamic surfaces under dynamic motion is required and it is necessary to include the effect of the aerodynamic surface motion upon the resulting forces and moments. These so-called *unsteady* effects are an outcome of the changing circulation and wake acting upon a moving aerofoil, and can have a considerable influence upon the resulting aerodynamic forces and moments. Consequently, a more sophisticated analysis is required than simply considering the angle of incidence. Most aeroelasticity textbooks cover unsteady aerodynamic effects (Scanlan and Rosenbaum, 1960; Fung, 1969; Bisplinghoff *et al.*, 1996; Hodges and Pierce, 2002; Dowell *et al.*, 2004).

In this chapter, the two-dimensional inviscid, incompressible flow over a thin, rigid section aerofoil undergoing small amplitude heave and pitch motions will be considered. Starting with the effect of a sudden step change in incidence on the lift acting on an aerofoil, the lift and moment resulting from a harmonically oscillating aerofoil in a steady flow will be investigated, followed by consideration of how a general motion would be dealt with. Analytical models, using the so-called oscillatory aerodynamic derivatives, will be developed to show how the aerodynamic forces and moments can be expressed via aerodynamic damping and stiffness terms. The results will be used in Chapter 11 on flutter, albeit using a highly simplified version of the derivatives. The related issue of unsteady aerodynamic effects for the aerofoil encountering a sharp-edged or harmonic gust will also be considered, as this will be required for the discrete gust and continuous turbulence response analysis in Chapter 16. Unsteady aerodynamics will not be considered for flight and ground manoeuvres in Chapters 13, 14, 15 and 17.

Simple examples will be used to illustrate the underlying principles rather than addressing the most up-to-date aerodynamic methods. There is a wide range of more advanced methods for computing unsteady aerodynamics for more general three-dimensional geometries and these will be addressed briefly in Chapters 19 and 20.

10.1 QUASI-STEADY AERODYNAMICS

So far in this book, the static aeroelastic cases considered in Chapters 8 and 9 have been for aerofoils fixed relative to the air flow and where the aerodynamic forces and moments are constant with time, i.e. the so-called *steady* aerodynamics case (see Chapter 5).

Where the aerofoil is undergoing a general motion in heave and/or pitch relative to the upstream flow, then the forces and moments vary with time. One simple approach for the calculation of such forces and moments is to assume that at any instant of time the aerofoil behaves with the characteristics of the same aerofoil moving with constant heave and/or pitch velocities equal to the instantaneous values. This is known as the *quasi-steady* assumption and implies that there are no frequency-dependent effects.

Introduction to Aircraft Aeroelasticity and Loads J. R. Wright and J. E. Cooper
© 2007 John Wiley & Sons, Ltd

10.2 UNSTEADY AERODYNAMICS

The *quasi-steady* assumption, while attractive in its simplicity, is not sufficiently accurate for flutter and gust response calculations and a more advanced *unsteady* aerodynamic analysis must be used in order to predict accurately the dependency of aerodynamic forces and moments on the frequency content of dynamic motions.

In order to understand the effect of aerofoil heave and/or pitch motions on the aerodynamic loads and moments generated, the result of instantaneous changes in the angle of incidence and harmonic motion of the aerofoil need to be considered. The key tools to analyse these effects are Wagner's and Theodorsen's functions respectively (Fung, 1969; Bisplinghoff *et al.*, 1996). Wagner's function can be used to consider the case of general motion (in the time domain), whereas the related Theodorsen's function is an important component in predicting the onset of flutter (in the frequency domain) and in the analysis of the response to continuous turbulence.

10.2.1 Instantaneous Change in Angle of Incidence – Wagner's Function

Consider a two-dimensional aerofoil of chord c, initially at some small angle of incidence α and moving at air speed V in still air; assume inviscid and incompressible flow. The aerofoil is then subjected to an instantaneous change in angle of incidence of $\Delta\alpha = \alpha/2$. If a quasi-steady aerodynamic model were used, the lift would increase instantaneously by 50 %, but this does not occur in practice.

Normalizing the lift force so that the initial value is unity in this example, then Figure 10.1 shows how the unsteady lift changes instantaneously to half of the difference between the initial and final steady values, and then increases asymptotically towards the final steady value. Approximately 90 % of the change in lift is achieved after 15 semi-chords have been travelled by the aerofoil; however, there is clearly a considerable delay after the change in incidence before the quasi-steady value is reached. The delay in achieving the new steady lift value occurs due to the time taken for the circulation around the aerofoil to change to that of the new steady flow condition and for changes in the wake to reach a steady state. Since the results are expressed in terms of semi-chords travelled by the aerofoil, a nondimensional

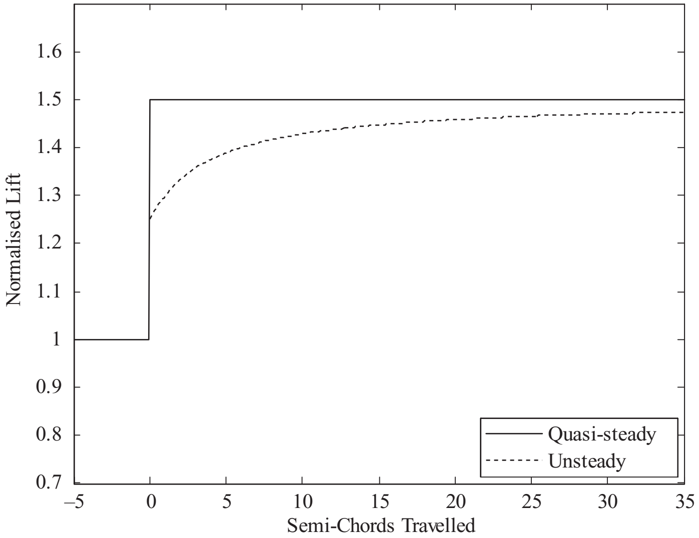

Figure 10.1 Effect on aerofoil lift of a sudden change in the angle of incidence.

measure, this behaviour is independent of chord size or air speed. Note also that the same effect would be found if the air speed were to change suddenly instead.

Wagner's function (Fung, 1969; Bisplinghoff *et al.*, 1996) is used to model how the lift acting at the quarter chord on the aerofoil builds up following the step change of incidence (or air speed) by obtaining the effective downwash at the three-quarter chord point. Downwash is the velocity component normal to the airflow. In terms of nondimensional time $\tau = 2Vt/c = Vt/b$ (i.e. the time taken for the flow to cross a semi-chord b of the aerodynamic surface), the *increase* in lift per unit span following the step change in incidence $\Delta\alpha$ is expressed as

$$\Delta L = \tfrac{1}{2}\rho V^2 c a_1 \Delta\alpha \Phi(\tau) = \tfrac{1}{2}\rho V c a_1 w \Phi(\tau), \tag{10.1}$$

where $w = V\sin\Delta\alpha \approx V\Delta\alpha$ is the change in downwash on the aerofoil (the symbol w is not to be confused with its later usage for the flight mechanics model in Chapters 14 and 15) and $\Phi(\tau)$ is Wagner's function, defined approximately for the incompressible case as (Fung, 1969; Bisplinghoff *et al.*, 1996)

$$\Phi(\tau) = 0, \quad \tau \le 0 \qquad \text{and} \qquad \Phi(\tau) = \frac{\tau+2}{\tau+4}, \quad \tau > 0. \tag{10.2}$$

Wagner's function is often defined using exponential functions as they are easier to manipulate using Laplace transforms when compared to the simple expression in Equation (10.2), but they will not be considered here.

10.2.2 Harmonic Motion – Convolution using Wagner's Function

For a general heave and pitch motion of the aerofoil, Wagner's function may be used to find the lift by obtaining the effective downwash w at the three-quarter chord point and using a convolution integral approach (see Chapter 1). This approach is analogous to determining the response of a system to a general excitation expressed as a superposition of a series of steps, and knowing the step response function. The downwash is then represented by a series of step changes that follow the motion of the aerofoil.

By considering the step change in downwash dw over time $\mathrm{d}\tau_0$, the lift may be written as

$$L(\tau) = \frac{1}{2}\rho V c a_1 \left[w_0 + \int_{\tau_0=0}^{\tau} \Phi(\tau - \tau_0) \frac{\mathrm{d}w}{\mathrm{d}\tau_0} \mathrm{d}\tau_0 \right], \tag{10.3}$$

where $\Phi(\tau - \tau_0)(\mathrm{d}w/\mathrm{d}\tau_0)\mathrm{d}\tau_0$ defines the lift at τ due to the step change in downwash at τ_0. The overall lift time history is obtained by summing (or integrating) the lift obtained from each step.

Figure 10.2 shows the result of the convolution process for the aerofoil oscillating sinusoidally in pitch with an angle of incidence varying as $\alpha = \alpha_0 \sin \omega t$. When the time step is large, the predicted lift time history is somewhat uneven and in error. However, if the time step is reduced then, in the limit, the resulting lift is *sinusoidal* and of the *same frequency* as the oscillation of the aerofoil.

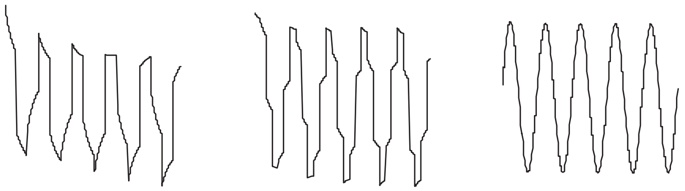

Figure 10.2 Resultant lift for an oscillating aerofoil using the convolution process with decreasing time increments.

10.2.3 Harmonic Motion – Theodorsen's Function

For flutter calculations, the general unsteady aerodynamic behaviour in the time domain is rarely used, since the motion at a single oscillation frequency is of more interest (note, however, that the general motion in the time domain is of interest for the gust response; see Chapter 16). Returning to the example in the previous section, with an aerofoil oscillating in pitch at frequency ω, and applying the convolution approach using Wagner's function to obtain the lift time history, the effect of varying the frequency of the oscillation is now examined. Figure 10.3 shows that, compared to the quasi-steady lift values, there is a *reduction in the magnitude* of the lift and an *introduction of a phase lag* between the aerofoil motion and the unsteady forces (the quasi-steady values are always in-phase by definition). As the frequency increases, the unsteady force amplitude decreases and the phase lag changes.

Further investigation shows that the amplitude attenuation and phase lag are a function of the dimensionless *frequency parameter* ν, defined as

$$\nu = \frac{\omega c}{V}, \tag{10.4}$$

which can be interpreted as the number of oscillations undergone by the aerofoil during the time taken for the airflow to travel across the chord of the aerofoil, multiplied by 2π (the frequency is defined in radians per second). However, often the so-called *reduced frequency k* is used, as in Figure 10.3, and this is defined in terms of the semi-chord $b = c/2$ such that

$$k = \frac{\omega b}{V} = \frac{\omega c}{2V} = \frac{\upsilon}{2}. \tag{10.5}$$

Historically, the fundamental work on unsteady aerodynamics and aeroelasticity in the UK (Frazer and Duncan, 1928; Collar, 1978) used the frequency parameter υ, whereas the equivalent research in the

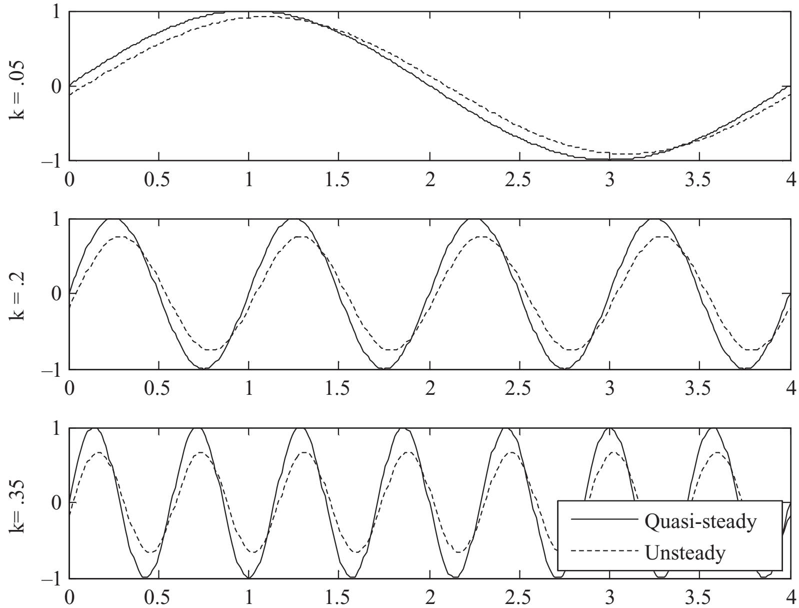

Figure 10.3 Unsteady lift for an oscillating aerofoil at different reduced frequencies.

USA (Theodorsen, 1935) was based upon the reduced frequency, k. For most of this book the reduced frequency k will be employed as this has been used in the classic aeroelasticity textbooks (Fung, 1969; Bisplinghoff *et al.*, 1996). Every time that the reduced frequency is mentioned in a descriptive part of the text, it can simply be replaced with the frequency parameter.

Theodorsen's function is used to model the changes in amplitude and phase of the sinusoidal unsteady aerodynamic forces relative to the quasi-steady forces for different reduced frequencies (or frequency parameter). The function behaves, effectively, as the Fourier transform of Wagner's function, and can be thought of as a filter that modifies the input to a system (i.e. the quasi-steady lift for aerofoil oscillations at some frequency) to give an output (i.e. the unsteady air forces) depending upon the reduced frequency. Theodorsen's function $C(k) = F(k) + iG(k)$, where $C(k)$ is a complex quantity (required since both the amplitude and phase need to change), is expressed (Fung, 1969) as a function of reduced frequency such that

$$C(k) = F(k) + \mathrm{i}G(k) = \frac{H_1^{(2)}(k)}{H_1^{(2)}(k) + \mathrm{i}H_0^{(2)}(k)} = \frac{K_1(\mathrm{i}k)}{K_0(\mathrm{i}k) + K_1(\mathrm{i}k)}, \tag{10.6}$$

where the $K_j(\mathrm{i}k)$ $(j = 0,1,\dots)$ terms are modified Bessel functions of the second kind and $H_n^{(2)}(k)$ are Hankel functions of the second kind. Although an explanation of Bessel and Hankel functions is beyond the scope of this book, these functions are included in many software libraries and are easy to calculate. Approximate expressions for $C(k)$ have been found as (Fung, 1969; Bisplinghoff *et al.*, 1996)

$$\begin{aligned} C(k) &= 1 - \frac{0.165}{1 - \dfrac{0.045}{k}\mathrm{i}} - \frac{0.335}{1 - \dfrac{0.30}{k}\mathrm{i}}, \quad k \le 0.5, \\ &= 1 - \frac{0.165}{1 - \dfrac{0.041}{k}\mathrm{i}} - \frac{0.335}{1 - \dfrac{0.32}{k}\mathrm{i}}, \quad k > 0.5. \end{aligned} \tag{10.7}$$

Figure 10.4 shows the real and imaginary parts, and amplitude and phase, of Theodorsen's function in graphical form. Note that as k increases the magnitude decreases, and the phase lag increases up to a value of around $k = 0.3$ and then reduces again. The complex plane representation is shown in Figure 10.5, with the function following the curve in a clockwise direction for increasing frequency.

For the *quasi-steady aerodynamics* case then $\omega = 0$, thus $k = \nu = 0$ and hence $F = 1$ and $G = 0$, so the unsteady lift may be seen to tend towards the quasi-steady values. In the limit as $k \to \infty$, then $F \to 0.5$ and $G \to 0$, but typically for full size aircraft k has a maximum value of the order of unity.

10.3 AERODYNAMIC LIFT AND MOMENT FOR A HARMONICALLY OSCILLATING AEROFOIL

The solution of the flow around the aerofoil undergoing harmonic oscillations can be divided into two parts:

(a) *Circulatory terms*. Lift and moment terms occurring due to the vorticity in the flow (related to Theodorsen's function).

(b) *Noncirculatory terms*. 'Apparent inertia' forces whose creation is not related to vorticity, i.e. as the aerofoil moves, a cylindrical mass of air accelerates with the aerofoil and introduces a reactive force and moment upon the aerofoil. These terms are of minor importance for bending/torsion type flutter of cantilever wings at low reduced frequencies, but are more important for flutter of control surfaces at higher reduced frequencies.

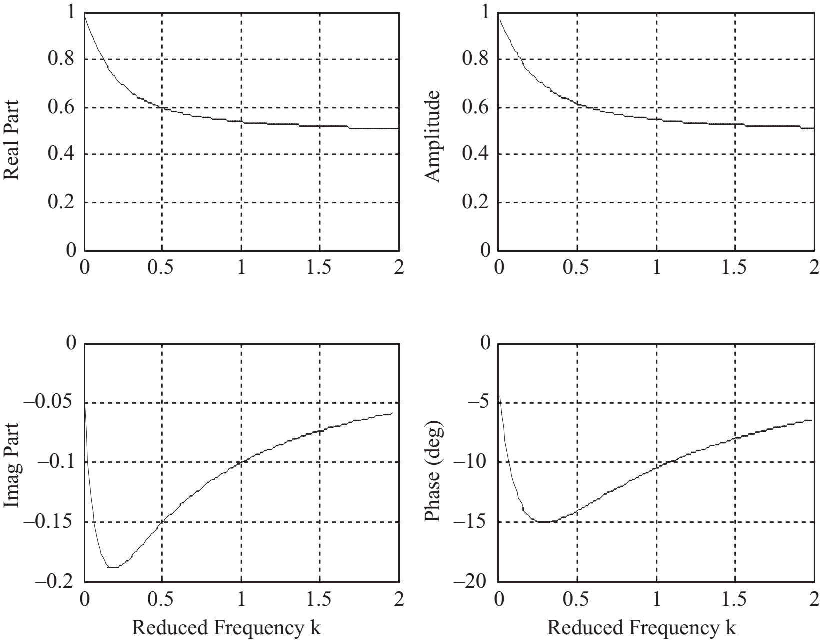

Figure 10.4 Theodorsen's function.

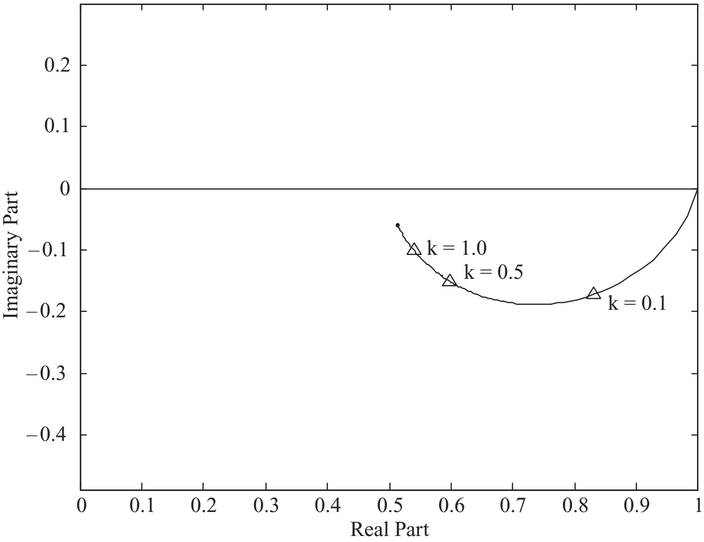

Figure 10.5 Complex plane representation of Theodorsen's function.

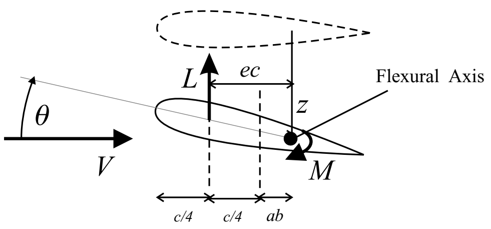

Figure 10.6 Two-dimensional aerofoil undergoing heave and pitch motion.

Consider a symmetric two-dimensional aerofoil ($C_{M_0} = 0$) of chord c, with the flexural axis positioned at distance $ab(= ac/2)$ aft of the mid-chord as shown in Figure 10.6. The aerofoil undergoes oscillatory harmonic motion in heave $z = z_0 e^{\mathrm{i}\omega t}$ (positive downwards) and pitch $\theta = \theta_0 e^{\mathrm{i}\omega t}$ (positive nose up). The classical solution for the lift and moment about the flexural axis, both expressed per unit span, may be written (Theodorsen, 1935; Fung, 1969; Bisplinghoff et al., 1996) as

$$L = \pi\rho b^2\left[\ddot{z} + V\dot{\theta} - ba\ddot{\theta}\right] + 2\pi\rho V b C(k)\Big[\dot{z} + V\theta + b\left(\tfrac{1}{2} - a\right)\dot{\theta}\Big], \tag{10.8}$$

$$\begin{aligned} M = {} & \pi\rho b^2\Big[ba\ddot{z} - Vb\left(\tfrac{1}{2} - a\right)\dot{\theta} - b^2\left(\tfrac{1}{8} + a^2\right)\ddot{\theta}\Big] \\ & + 2\pi\rho V b^2\left(a + \tfrac{1}{2}\right)C(k)\Big[\dot{z} + V\theta + b\left(\tfrac{1}{2} - a\right)\dot{\theta}\Big]. \end{aligned} \tag{10.9}$$

The derivation of these two equations is beyond the scope of this book, but they are included as they help to describe how the aerodynamic lift and moment vary with reduced frequency. The first part of each expression shows the noncirculatory terms and the second part shows the circulatory terms which are dependent upon the value of Theodorsen's function. There are terms dependent upon the displacement, velocity and acceleration of both heave and pitch motions, except for the heave displacement term (the vertical aerofoil position does not affect the lift and moment). Here the two-dimensional lift curve slope has been taken as $a_1 = 2\pi$.

10.4 OSCILLATORY AERODYNAMIC DERIVATIVES

Taking the above expressions for the lift and moment about the flexural axis of the oscillating aerofoil and substituting for the complex form of Theodorsen's function and the heave and pitch motions in complex algebra form (see Chapter 1), then Equations (10.8) and (10.9) become

$$L = \left\{\pi\rho b^2\left[-\omega^2 z_0 + \mathrm{i}\omega V\theta_0 + \omega^2 ba\theta_0\right] + 2\pi\rho V b(F + \mathrm{i}G)\left[\mathrm{i}\omega z_0 + V\theta_0 + \mathrm{i}\omega b\left(\tfrac{1}{2} - a\right)\theta_0\right]\right\}\mathrm{e}^{\mathrm{i}\omega t}, \tag{10.10}$$

$$\begin{aligned} M = {} & \left\{\pi\rho b^2\left(-\omega^2 baz_0 - i\omega Vb\left(\tfrac{1}{2} - a\right)\theta_0 + b^2\omega^2\left(\tfrac{1}{8} + a^2\right)\theta_0\right)\right. \\ & \left. + 2\pi\rho V b^2\left(a + \tfrac{1}{2}\right)(F + iG)\left(i\omega z_0 + V\theta_0 + i\omega b\left(\tfrac{1}{2} - a\right)\theta_0\right)\right\}\mathrm{e}^{i\omega t} \end{aligned} \tag{10.11}$$

These equations can then be written in the oscillatory derivative form

$$\begin{aligned} L &= \rho V^2 b\left[(L_z + \mathrm{i}kL_{\dot{z}})\frac{z_0}{b} + (L_\theta + \mathrm{i}kL_{\dot{\theta}})\theta_0\right]\mathrm{e}^{\mathrm{i}\omega t}, \\ M &= \rho V^2 b^2\left[(M_z + \mathrm{i}kM_{\dot{z}})\frac{z_0}{b} + (M_\theta + \mathrm{i}kM_{\dot{\theta}})\theta_0\right]\mathrm{e}^{\mathrm{i}\omega t}, \end{aligned} \tag{10.12}$$

where L_z, M_z etc., are the nondimensional *oscillatory aerodynamic derivatives* (not to be confused with classical aerodynamic or stability and control derivatives; see Chapters 13 and 14). These derivatives are expressed in terms of the normalised displacement and velocity for heave and pitch, so, for example,

$$L_z = \frac{\partial C_\mathrm{L}}{\partial (z/b)}, \qquad L_{\dot{z}} = \frac{\partial C_\mathrm{L}}{\partial (\dot{z}/V)}, \qquad L_{\dot{\theta}} = \frac{\partial C_\mathrm{L}}{\partial \left(\dot{\theta} c/V\right)}, \qquad \text{etc.} \tag{10.13}$$

Note that there are no acceleration-based terms as they have now been included in the displacement terms via the conversion of the double differentiation to the frequency domain. In terms of Theodorsen's function, comparison of Equations (10.10) and (10.12) leads to the lift derivatives being expressed as

$$\begin{aligned} L_z &= 2\pi\left(-\frac{k^2}{2} - Gk\right), \qquad L_{\dot{z}} = 2\pi F, \\ L_\theta &= 2\pi\left[\frac{k^2 a}{2} + F - Gk\left(\frac{1}{2} - a\right)\right], \qquad L_{\dot{\theta}} = 2\pi\left[\frac{1}{2} + F\left(\frac{1}{2} - a\right) + \frac{G}{k}\right], \end{aligned} \tag{10.14}$$

and, from comparison of Equations (10.11) and (10.12), the relevant moment derivatives are

$$\begin{aligned} M_z &= 2\pi\left[-\frac{k^2 a}{2} - k\left(a + \frac{1}{2}\right)G\right], \qquad M_{\dot{z}} = 2\pi\left(a + \frac{1}{2}\right)F, \\ M_\theta &= 2\pi\left[\frac{k^2}{2}\left(\frac{1}{8} + a^2\right) + F\left(a + \frac{1}{2}\right) - kG\left(a + \frac{1}{2}\right)\left(\frac{1}{2} - a\right)\right], \\ M_{\dot{\theta}} &= 2\pi\left[-\frac{k}{2}\left(\frac{1}{2} - a\right) + kF\left(a + \frac{1}{2}\right)\left(\frac{1}{2} - a\right) + \frac{G}{k}\left(a + \frac{1}{2}\right)\right]. \end{aligned} \tag{10.15}$$

Apart from L_z and $L_{\dot{z}}$, the derivative values depend upon where the flexural axis is located on the chord.

The quasi-steady values of the aerodynamic derivatives ($k \to 0,\ F \to 1,\ G \to 0$) can be found as

$$\begin{aligned} &L_z = 0, \qquad L_{\dot{z}} = 2\pi, \qquad L_\theta = 2\pi, \qquad kL_{\dot{\theta}} = 0, \qquad M_z = 0, \\ &M_{\dot{z}} = 2\pi\left(a + \tfrac{1}{2}\right), \qquad M_\theta = 2\pi\left(a + \tfrac{1}{2}\right), \qquad kM_{\dot{\theta}} = 0. \end{aligned} \tag{10.16}$$

Note the singularity in the expressions for $M_{\dot{\theta}}$ and $L_{\dot{\theta}}$ as $k \to 0$. However, since both $kL_{\dot{\theta}}$ and $kM_{\dot{\theta}}$ tend to zero, then the contribution to the lift and moment from these derivatives is also zero as $k \to 0$. Therefore the concept of quasi-steady derivatives does not apply to the $\dot{\theta}$ derivatives (Hancock *et al.*, 1985). The other derivatives agree with the expressions found earlier for the quasi-steady forces and moments.

10.5 AERODYNAMIC DAMPING AND STIFFNESS

Further insight into the effect of the unsteady aerodynamic forces can be obtained by considering

$$k = \frac{\omega b}{V}, \qquad z = z_0 \mathrm{e}^{\mathrm{i}\omega t}, \qquad \dot{z} = \mathrm{i}\omega z_0 \mathrm{e}^{\mathrm{i}\omega t}, \qquad \theta = \theta_0 \mathrm{e}^{\mathrm{i}\omega t} \qquad \text{and} \qquad \dot{\theta} = \mathrm{i}\omega\theta_0 \mathrm{e}^{\mathrm{i}\omega t}. \tag{10.17}$$

Substituting these expressions into the lift and moment equations (10.12) gives

$$L = \rho V^2\left(L_z z + L_{\dot{z}}\frac{b\dot{z}}{V} + L_\theta b\theta + L_{\dot{\theta}}\frac{b^2\dot{\theta}}{V}\right), \qquad M = \rho V^2\left(M_z bz + M_{\dot{z}}\frac{b^2\dot{z}}{V} + M_\theta b^2\theta + M_{\dot{\theta}}\frac{b^3\dot{\theta}}{V}\right), \tag{10.18}$$

and this can be written in the matrix form

$$\begin{Bmatrix} L \\ M \end{Bmatrix} = \rho V\begin{bmatrix} bL_{\dot{z}} & b^2 L_{\dot{\theta}} \\ b^2 M_{\dot{z}} & b^3 M_{\dot{\theta}} \end{bmatrix}\begin{Bmatrix} \dot{z} \\ \dot{\theta} \end{Bmatrix} + \rho V^2\begin{bmatrix} L_z & bL_\theta \\ bM_z & b^2 M_\theta \end{bmatrix}\begin{Bmatrix} z \\ \theta \end{Bmatrix} = \rho V\mathbf{B}\begin{Bmatrix} \dot{z} \\ \dot{\theta} \end{Bmatrix} + \rho V^2\mathbf{C}\begin{Bmatrix} z \\ \theta \end{Bmatrix}. \tag{10.19}$$

It can be seen that one term is proportional to the heave and pitch velocities, while the other term is proportional to the heave and pitch displacements. Thus, the aerodynamic forces acting on an aerofoil undergoing oscillatory motion can be considered to behave in a similar way to that of damping and stiffness in a structure. Thus **B** and **C** are termed the aerodynamic damping and stiffness matrices respectively. A key difference to structural damping and stiffness matrices is that the aerodynamic matrices are nonsymmetric, and this helps lead to the flutter aeroelastic instability (see Chapter 11); also, the damping and stiffness depend upon the flight condition, including the Mach number.

When applied to aeroelastic systems, as will be shown in the next chapter, the aerodynamic forces are considered together with the structural equations and this leads to equations of motion in the classical form of

$$\mathbf{A}\ddot{\boldsymbol{q}} + (\rho V \mathbf{B} + \mathbf{D})\dot{\boldsymbol{q}} + \left(\rho V^2 \mathbf{C} + \mathbf{E}\right)\boldsymbol{q} = 0, \tag{10.20}$$

where **A**, **B**, **C**, **D**, **E** are the structural inertia, aerodynamic damping, aerodynamic stiffness, structural damping and structural stiffness matrices respectively, and $\boldsymbol{q}$ are the generalized coordinates (typically modal coordinates). It is important to note that the **B**, **C** matrices only apply for the reduced frequency for which they are defined; this can cause some difficulty for flutter calculations and will be discussed later in Chapter 11.

Equation (10.20) is one of the most important equations in this book and describes the fundamental interaction between the flexible structure and the aerodynamic forces. Note that it is usual when considering aeroelastic systems to write the structural inertia, damping and stiffness matrices as **A**, **D**, **E** respectively, rather than the **M**, **C**, **K** notation often used in classical structural dynamics (see Chapter 2).

10.6 UNSTEADY AERODYNAMICS RELATED TO GUSTS

Similar changes in the aerodynamic forces, as shown above for aerofoil heave and pitch motions, occur when the aerofoil encounters a gust field, with the aerodynamic forces also taking time to build up. Here, the gust analysis equivalent of Wagner's and Theodorsen's functions will be briefly considered. The response to 'sharp-edged' and 'sinusoidal' gusts will provide the unsteady aerodynamic tools used for the cases of a rigid or flexible aircraft encountering a discrete gust or continuous turbulence, considered later in Chapter 16.

10.6.1 Lift due to a Sharp-Edged Gust – Küssner's Function

Consider a rigid aerofoil of chord c and unit span moving at air speed V in still air and suddenly encountering a vertical sharp-edged gust of velocity w_g. The increment in lift acting upon the aerofoil is due to the effective change in the angle of incidence caused by the vertical gust velocity, namely

$$\tan \Delta\alpha \approx \Delta\alpha = \frac{w_g}{V}. \tag{10.21}$$

A quasi-steady analysis of this situation assumes that the lift per unit span is developed, as soon as the aircraft enters the gust, according to the expression

$$L = \frac{1}{2}\rho V^2 c a_1 \frac{w_g}{V} = \frac{1}{2}\rho V c a_1 w_g. \tag{10.22}$$

However, in practice, the lift takes time to build up and this effect can be modelled by rewriting the lift as

$$L = \tfrac{1}{2}\rho V a_1 c w_g \Psi(\tau), \tag{10.23}$$

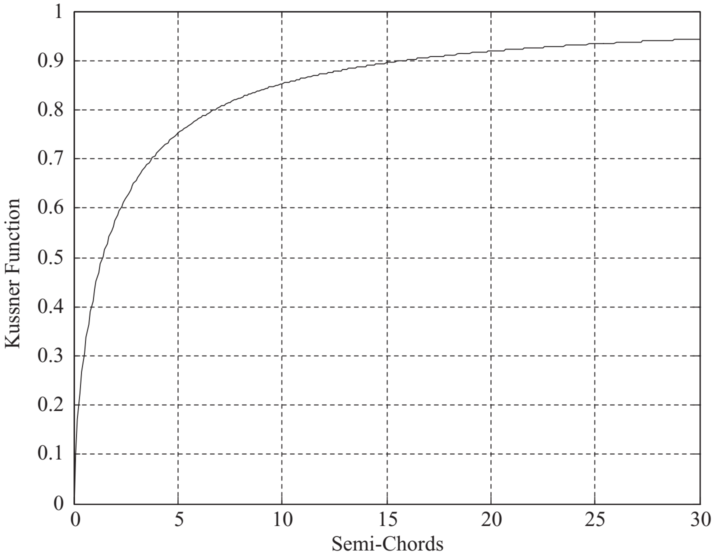

Figure 10.7 Küssner's function.

where $\Psi(\tau)$ is Küssner's function which describes how the aerodynamic forces build up upon entering a gust. The function (Bisplinghoff *et al.*, 1996) is defined approximately in terms of nondimensional time τ (= distance travelled in semi-chords) as

$$\Psi(\tau) = \frac{\tau^2 + \tau}{\tau^2 + 2.82\tau + 0.80}. \tag{10.24}$$

Figure 10.7 shows how this function builds up from zero, when the aerofoil starts to enter the gust, and asymptotically tends towards unity. As with Wagner's function, there is a significant delay before the quasi-steady value is reached. The response to any arbitrary gust field could be determined using a convolution approach (see Chapter 16) similar to that demonstrated earlier with Wagner's function.

10.6.2 Lift due to a Sinusoidal Gust – Sears' Function

Clearly, the response to a general time varying gust velocity field may be obtained using Küssner's function and a convolution approach. However, an alternative way of modelling the response of an aerofoil subjected to continuous turbulence is to perform a frequency domain power spectral density (PSD) based analysis (see Chapters 1, 16 and 18), which is the approach adopted in industry (see Chapter 24). In order to include the unsteady aerodynamic effects in a frequency domain analysis, the effect at each frequency must be evaluated. The resulting force and moment acting on an aerofoil encountering a sinusoidal gust will be attenuated and delayed in-phase with respect to the quasi-steady result, in much the same way as was seen earlier for an oscillating aerofoil in a steady flow field. These effects are dependent on the reduced frequency.

Consider an aerofoil of chord c moving at air speed V within a sinusoidal gust field having a vertical velocity expressed as a function of time as

$$w_{\mathrm{g}} = w_{\mathrm{g}0} \mathrm{e}^{\mathrm{i}\omega t}. \tag{10.25}$$

The lift acting at the quarter chord of the aerofoil can be written as a function of the reduced frequency such that

$$L = \frac{1}{2}\rho V c a_1 w_{g0} e^{i\omega t} \phi(k). \tag{10.26}$$

Here $\phi(k)$ is Sears' function, which is defined as

$$\phi(k) = [J_0(k) - iJ_1(k)]\ C(k) + iJ_1(k), \tag{10.27}$$

where $C(k)$ is Theodorsen's function and $J_j(k)(j = 0,1,\dots)$ are Bessel functions of the first kind. An approximation of the magnitude of the complex Sears function (Fung, 1969) is

$$|\phi(k)|^2 = \frac{d+k}{d + (\pi d + 1)k + 2\pi k^2}, \tag{10.28}$$

where constant $d = 0.1811$ and the phase can be approximated as

$$\begin{aligned} &k \le 0.61, \quad \angle\phi(k) = -48.095k^5 + 87.297k^4 - 61.470k^3 + 21.917k^2 - 3.664k, \\ &k > 0.61, \quad \angle\phi(k) = 0.982k - 0.597. \end{aligned} \tag{10.29}$$

The variation of the real and imaginary parts, and amplitude and phase, of Sears' function for different k values is shown in Figure 10.8, and the complex plane form is shown in Figure 10.9 to have a characteristic spiral shape.

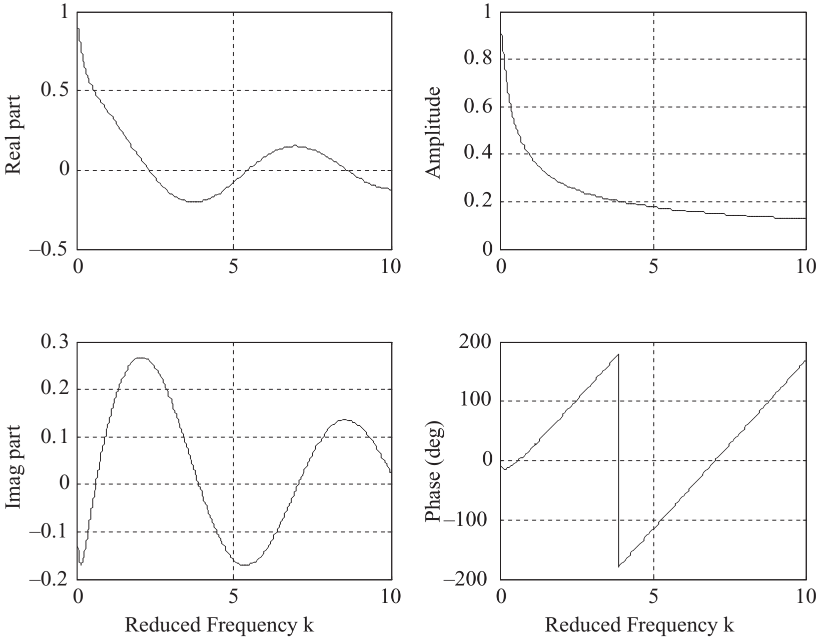

Figure 10.8 Sears' function.

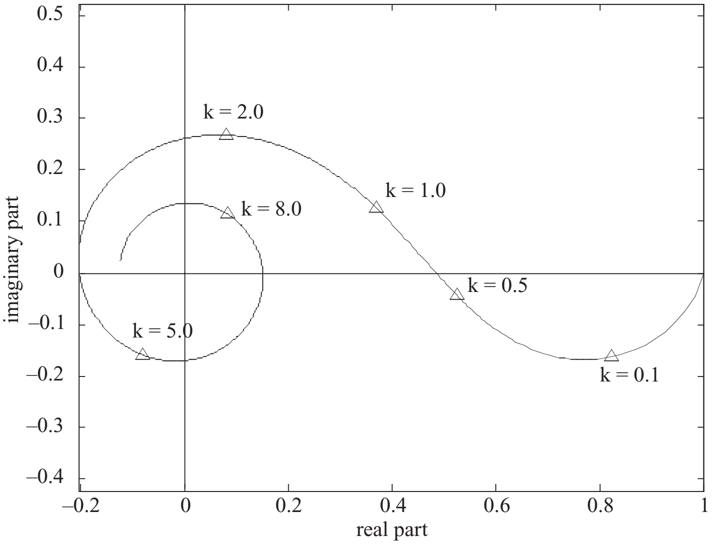

Figure 10.9 Sears' function: complex plane representation.

If the temporal variation of gust velocity is transformed into a spatial variation using $k = \omega b/V$ and $x_g = Vt$, then

$$w_g = w_{g0} \exp\left(\frac{\mathrm{i}kV}{b}t\right) = w_{g0} \exp\left(\frac{ik}{b}x_g\right). \tag{10.30}$$

The wavelength of the sinusoidal gust is then given by $\lambda_g = 2\pi b/k$, which may be compared to the chord length $c = 2b$ for different values of k.

At first sight, it might be thought that the forces developed on an aerofoil that is not moving in heave due to the harmonic gust would be the same as those developed for the aerofoil itself moving with a harmonic heave velocity in a steady air stream. In fact, this is more or less true for gusts where the wavelength is large in comparison with the chord ($\lambda_g \gg c$, i.e. a small reduced frequency) and so the gust velocity is almost constant across the chord, as seen in Figure 10.10. However, where the wavelength is small compared to the chord ($\lambda_g \ll c$, i.e. a high reduced frequency) there will be a significant difference between the two results because the downwash due to the gust velocity will vary significantly across the chord. This argument corresponds to saying that the Theodorsen and Sears functions are very similar for a small reduced frequency, as seen by comparing Figure 10.5 with Figure 10.9.

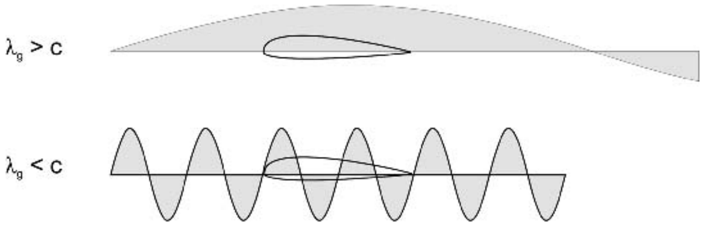

Figure 10.10 Effect of the gust wavelength compared to the chord.

10.7 EXAMPLES

1. Write a MATLAB program to model the change in lift for a step change in incidence for a two-dimensional aerofoil making use of Wagner's function. Apply this approach for a harmonically oscillating aerofoil and explore the effect of different frequency parameters and convolution time steps.
2. Making use of the *besselk* function, write a MATLAB program to determine the Theodorsen function for $0 < k < 10$. Compare these results with the approximation given in Equation (10.7).
3. Write a MATLAB program to determine how the oscillatory aerodynamic derivatives vary with reduced frequency. How great is the difference from the quasi-steady values?
4. Write a MATLAB program to model the change in lift for a two-dimensional aerofoil entering a sharp-edged gust making use of the Küssner function. Extend this to develop a convolution approach for a harmonically oscillating aerofoil and explore the effect of different frequency parameters and convolution time steps.
5. Making use of the *besselj* function, write a MATLAB program to determine Sears' function for $0 < k < 10$. Compare these results with the approximation given in Equations (10.28) and (10.29).
6. Compare the Theodorsen and Sears' functions. For what values of gust wavelengths and reduced frequencies can they be considered to be the same?

11

Dynamic Aeroelasticity – Flutter

Flutter is arguably the most important of all the aeroelastic phenomena (Collar, 1978; Garrick and Reid, 1981) and is the most difficult to predict. It is an unstable self-excited vibration in which the structure extracts energy from the air stream and often results in catastrophic structural failure. Classical binary flutter (Scanlan and Rosenbaum, 1960; Fung, 1969; Hancock *et al.*, 1985; Niblett, 1998; Bisplinghoff *et al.*, 1996; Hodges and Pierce, 2002; Dowell *et al.*, 2004) occurs when the aerodynamic forces associated with motion in two modes of vibration cause the modes to couple in an unfavourable manner, although there have been cases where more than two modes have combined to cause flutter and in industry the mathematical models employ many modes (see Chapters 22 and 23 where a typical industry approach is described).

At some critical speed, known as the flutter speed, the structure sustains oscillations following some initial disturbance. Below this speed the oscillations are damped, whereas above it one of the modes becomes negatively damped and (often violent) unstable oscillations occur, unless some form of nonlinearity (not considered in detail here) bounds the motion. Flutter can take various forms involving different pairs of interacting modes, e.g. wing bending/torsion, wing torsion/control surface, wing/engine, etc.

In this chapter, a simple binary flutter model is developed, making use of strip theory with simplified unsteady aerodynamic terms; the model is then used to illustrate the dynamic characteristics of aeroelastic systems, considering the effect of varying the position of the flexural axis, the mass distribution and the frequency spacing between the two modes. Various methods for determining the critical flutter speeds and associated flutter frequencies are examined, including the realistic case where the aerodynamic terms are reduced frequency-dependent. The final part of the chapter considers the phenomenon of control surface flutter; it also briefly explores flutter in the transonic and supersonic flight regimes, and introduces some effects of nonlinearities. It will be shown that it is important to include unsteady aerodynamic terms and reduced frequency effects in the dynamic models that are used to predict the subcritical aeroelastic behaviour and the onset of flutter. A number of MATLAB codes related to this chapter are included in appendix H in the companion website.

11.1 SIMPLIFIED UNSTEADY AERODYNAMIC MODEL

The full two-dimensional unsteady aerodynamic model was described in Chapter 10 for a harmonically oscillating aerofoil, but here a simplified unsteady aerodynamic model will be introduced. Consider, once again, the two-dimensional aerofoil shown in Figure 11.1 with the flexural axis positioned a distance ec aft of the aerodynamic centre and ab aft of the mid chord, where

$$ec = \frac{c}{4} + ab = \frac{c}{4} + \frac{ac}{2}. \tag{11.1}$$

Introduction to Aircraft Aeroelasticity and Loads J. R. Wright and J. E. Cooper
© 2007 John Wiley & Sons, Ltd

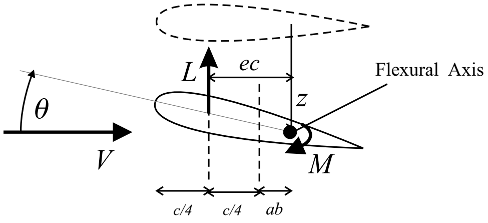

Figure 11.1 Two-dimensional aerofoil.

It was shown in Chapter 10 that the lift and moment per unit span for an aerofoil may be expressed, for a particular reduced frequency, as

$$L = \rho V^2 \left(L_z z + L_{\dot z}\frac{b\dot z}{V} + L_\theta b\theta + L_{\dot\theta}\frac{b^2\dot\theta}{V} \right), \qquad M = \rho V^2 \left(M_z bz + M_{\dot z}\frac{b^2\dot z}{V} + M_\theta b^2\theta + M_{\dot\theta}\frac{b^3\dot\theta}{V} \right). \tag{11.2}$$

In this chapter, V will be taken as the true air speed and ρ is the density at a prescribed altitude.

Taking the *quasi-steady* assumption ($k \to 0$, $F \to 1$, $G \to 0$) for all of the aerodynamic derivatives, then the lift and pitching moment per unit span about the flexural axis become

$$L = \frac{1}{2}\rho V^2 c a_1 \left(\theta + \frac{\dot z}{V}\right), \qquad M = \frac{1}{2}\rho V^2 e c^2 a_1 \left(\theta + \frac{\dot z}{V}\right). \tag{11.3}$$

Compared to the lift force used in the static aeroelastic case, there is now an extra term due to the effective incidence associated with the aerofoil moving downwards with constant heave velocity $\dot z$, causing an effective ‘upwash’. The quasi-steady assumption implies that the aerodynamic loads acting on an aerofoil undergoing variable heave and pitch motions are equal, at any moment in time, to the characteristics of the same aerofoil with constant position and velocity values.

The major drawback in using quasi-steady aerodynamics is that no account is made for the time that it takes for changes in the wake associated with the aerofoil motion to develop (as defined by Wagner’s function) and this can lead to serious aeroelastic modelling errors. Consequently, the $M_{\dot\theta}$ unsteady aerodynamic derivative term in Equation (11.2) will be retained as it has been shown [Hancock et al., 1985] that this has an important effect on the unsteady aerodynamic behaviour. It adds a pitch damping term to the pitching moment Equation (11.3) and the model then becomes

$$L = \frac{1}{2}\rho V^2 c a_1 \left(\theta + \frac{\dot z}{V}\right), \qquad M = \frac{1}{2}\rho V^2 c^2 \left[e a_1 \left(\theta + \frac{\dot z}{V}\right) + M_{\dot\theta}\frac{\dot\theta c}{4V} \right]. \tag{11.4}$$

where $M_{\dot\theta}$ is negative and will initially be assumed to be constant. This ‘simplified unsteady aerodynamic’ model will now be used to develop a binary aeroelastic model. Note that the pitch damping term here differs numerically from that in Hancock *et al.* (1985) by a factor of four, which occurs because the unsteady aerodynamic derivatives are derived in terms of the reduced frequency k rather than the frequency parameter υ.

11.2 BINARY AEROELASTIC MODEL

11.2.1 Aeroelastic Equations of Motion

The simple unswept/untapered (i.e. rectangular) wing model (Hancock *et al.*, 1985) shown in Figure 11.2 is used throughout this chapter to illustrate classical binary flutter. The rectangular wing of span s and chord c is rigid but has two rotational springs at the root to provide flap (κ) and pitch (θ) degrees of

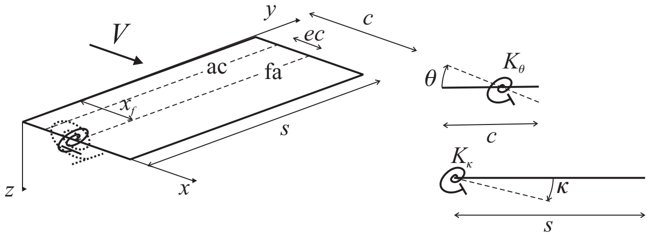

Figure 11.2 Binary aeroelastic model.

freedom. Note that there is no stiffness coupling between the two motions. The springs are attached at a distance *ec* behind the aerodynamic centre (on the quarter chord), defining the position of the flexural axis. The wing is assumed to have a uniform mass distribution and thus the mass axis lies on the mid-chord.

The displacement z (downwards +ve) of a general point on the wing is

$$z(x, y, t) = y\kappa(t) + (x - x_{\mathrm{f}})\theta(t) = \phi_\kappa \kappa + \phi_\theta \theta, \tag{11.5}$$

where κ and θ are generalized coordinates and ϕ_κ and ϕ_θ are simple assumed shapes. They are actually normal mode shapes (i.e. pure flap and pitch) if there is no inertia coupling about the flexural axis.

The equations of motion can be found using Lagrange's equations. The kinetic energy now exists due to the dynamic motion and is

$$T = \int_{\mathrm{wing}} \frac{1}{2} \mathrm{d}m\, \dot{z}^2 = \frac{m}{2} \int_0^s \int_0^c \left(y\dot{\kappa} + (x - x_{\mathrm{f}})\dot{\theta} \right)^2 \mathrm{d}x\, \mathrm{d}y, \tag{11.6}$$

where m is the mass per unit area of the wing. The potential (or strain) energy is due solely to the springs at the root, such that

$$U = \tfrac{1}{2} K_\kappa \kappa^2 + \tfrac{1}{2} K_\theta \theta^2, \tag{11.7}$$

whereas for a general bending and torsional vibration of a flexible wing it would take the form (see Chapter 3)

$$U = \frac{1}{2} \int EI \left(\frac{\mathrm{d}^2 z}{\mathrm{d}y^2} \right)^2 \mathrm{d}y + \frac{1}{2} \int GJ \left(\frac{\mathrm{d}\theta}{\mathrm{d}y} \right)^2 \mathrm{d}y. \tag{11.8}$$

Note that for a dynamic analysis any initial angle of incidence can be ignored as vibrations about the trim condition are considered. Applying Lagrange's equations for both generalized coordinates gives

$$\begin{gathered} \frac{\mathrm{d}T}{\mathrm{d}t}\left(\frac{\partial T}{\partial \dot{\kappa}}\right) = m \int_0^s \int_0^c \left(y^2 \ddot{\kappa} + y\,(x - x_{\mathrm{f}})\,\ddot{\theta} \right) \mathrm{d}x\, \mathrm{d}y = m \left[\frac{s^3 c}{3} \ddot{\kappa} + \frac{s^2}{2} \left(\frac{c^2}{2} - x_{\mathrm{f}} c \right) \ddot{\theta} \right], \\ \frac{\mathrm{d}T}{\mathrm{d}t}\left(\frac{\partial T}{\partial \dot{\theta}}\right) = m \int_0^s \int_0^c \left[y\,(x - x_{\mathrm{f}})\,\ddot{\kappa} + (x - x_{\mathrm{f}})^2\, \ddot{\theta} \right] \mathrm{d}x\, \mathrm{d}y = m \left[\frac{s^2}{2} \left(\frac{c^2}{2} - x_{\mathrm{f}} c \right) \ddot{\kappa} + s \left(\frac{c^3}{3} - c^2 x_{\mathrm{f}} + x_{\mathrm{f}}^2 c \right) \ddot{\theta} \right]. \end{gathered} \tag{11.9}$$

and

$$\frac{\partial U}{\partial \kappa} = K_\kappa \kappa, \qquad \frac{\partial U}{\partial \theta} = K_\theta \theta, \tag{11.10}$$

leading to the equations of motion for the wing, without any aerodynamic forces acting, as

$$\begin{bmatrix} \dfrac{ms^3c}{3} & \dfrac{ms^2}{2}\left(\dfrac{c^2}{2}-cx_\mathrm{f}\right) \\ \dfrac{ms^2}{2}\left(\dfrac{c^2}{2}-cx_\mathrm{f}\right) & ms\left(\dfrac{c^3}{3}-c^2x_\mathrm{f}+cx_\mathrm{f}^2\right) \end{bmatrix} \begin{Bmatrix} \ddot{\kappa} \\ \ddot{\theta} \end{Bmatrix} + \begin{bmatrix} K_\kappa & 0 \\ 0 & K_\theta \end{bmatrix} \begin{Bmatrix} \kappa \\ \theta \end{Bmatrix} = \begin{Bmatrix} 0 \\ 0 \end{Bmatrix}. \tag{11.11}$$

The inertia matrix takes the form

$$\begin{bmatrix} I_\kappa & I_{\kappa\theta} \\ I_{\kappa\theta} & I_\theta \end{bmatrix}$$

which can also be determined from the expressions

$$I_\kappa = \int_0^s y^2\,\mathrm{d}m, \qquad I_\theta = \int_0^c (x-x_\mathrm{f})^2\,\mathrm{d}m \quad \text{and} \quad I_{\kappa\theta} = \int_0^s \int_0^c (x-x_\mathrm{f})\,y\,\mathrm{d}m.$$

These terms are the moments of inertia in the flap and pitch, and the product moment of inertia, respectively.

If there is no inertial coupling ($I_{\kappa\theta} = 0$, i.e. $x_\mathrm{f} = c/2$ for this model) then the flap and pitch natural frequencies are

$$\omega_\kappa = \sqrt{\frac{K_\kappa}{I_\kappa}}, \qquad \omega_\theta = \sqrt{\frac{K_\theta}{I_\theta}}. \tag{11.12}$$

However, the presence of a nonzero value for $I_{\kappa\theta}$ couples the two motions in the mode shapes and the natural frequencies differ.

Generalized forces Q_κ and Q_θ act on the system in the form of unsteady aerodynamic forces; for an oscillatory motion they may be written in terms of the aerodynamic derivatives for a particular reduced frequency $k = \omega c/(2V)$. As shown in Chapter 10, these forces are complex but can be expressed in terms of displacements and velocities, bearing in mind that the result only applies the relevant reduced frequency value. Applying strip theory, together with the simplified unsteady aerodynamics representation, leads to expressions for lift and pitching moment (about the flexural axis) for each elemental strip dy of

$$\mathrm{d}L = \frac{1}{2}\rho V^2 c\,\mathrm{d}y\, a_\mathrm{W}\left(\frac{y\dot{\kappa}}{V}+\theta\right), \qquad \mathrm{d}M = \frac{1}{2}\rho V^2 c^2 \mathrm{d}y\left[ea_\mathrm{W}\left(\frac{y\dot{\kappa}}{V}+\theta\right)+M_{\dot{\theta}}\frac{\dot{\theta}c}{4V}\right], \tag{11.13}$$

where $y\dot{\kappa}$ is the effective heave velocity (+ve downwards) and $M_{\dot{\theta}} < 0$ (Hancock *et al.*, 1985).

The incremental work done over the wing, corresponding to the aerodynamic force/moment doing work through incremental deflections $\delta\kappa$, $\delta\theta$ of the wing is

$$\delta W = \int_\mathrm{wing} [\mathrm{d}L(-y\,\delta\kappa) + \mathrm{d}M\,\delta\theta] \tag{11.14}$$

and so the generalized forces are

$$\begin{aligned} Q_\kappa &= \frac{\partial(\delta W)}{\partial(\delta\kappa)} = -\int_0^s y\,\mathrm{d}L = -\frac{1}{2}\rho V^2 c s^2 a_\mathrm{W}\left(\frac{\dot{\kappa}s}{3V}+\frac{\theta}{2}\right), \\ Q_\theta &= \frac{\partial(\delta W)}{\partial(\delta\theta)} = \int_0^s \mathrm{d}M = \frac{1}{2}\rho V^2 c^2 s\left[ea_\mathrm{W}\left(\frac{\dot{\kappa}s}{2V}+\theta\right)+M_{\dot{\theta}}\frac{\dot{\theta}c}{4V}\right]. \end{aligned} \tag{11.15}$$

Thus, the full aeroelastic equations of motion become

$$\begin{bmatrix} I_\kappa & I_{\kappa\theta} \\ I_{\kappa\theta} & I_\theta \end{bmatrix} \begin{Bmatrix} \ddot{\kappa} \\ \ddot{\theta} \end{Bmatrix} + \rho V \begin{bmatrix} \dfrac{cs^3 a_{\mathrm{W}}}{6} & 0 \\ -\dfrac{ec^2 s^2 a_{\mathrm{W}}}{4} & -\dfrac{c^3 s}{8} M_{\dot{\theta}} \end{bmatrix} \begin{Bmatrix} \dot{\kappa} \\ \dot{\theta} \end{Bmatrix}$$

$$+ \left\{ \rho V^2 \begin{bmatrix} 0 & \dfrac{cs^2 a_{\mathrm{W}}}{4} \\ 0 & -\dfrac{ec^2 s a_{\mathrm{W}}}{2} \end{bmatrix} + \begin{bmatrix} K_\kappa & 0 \\ 0 & K_\theta \end{bmatrix} \right\} \begin{Bmatrix} \kappa \\ \theta \end{Bmatrix} = \begin{Bmatrix} 0 \\ 0 \end{Bmatrix}, \tag{11.16}$$

and it may be seen that the mass and stiffness matrices are symmetric while the aerodynamic matrices are nonsymmetric. Thus the two DoF are coupled and it is this coupling that can give rise to flutter.

11.3 GENERAL FORM OF THE AEROELASTIC EQUATIONS

Equation (11.16) is in the classical second-order form for N DoF discussed earlier in Chapter 10, namely

$$\mathbf{A}\ddot{\boldsymbol{q}} + (\rho V \mathbf{B} + \mathbf{D})\dot{\boldsymbol{q}} + (\rho V^2 \mathbf{C} + \mathbf{E})\boldsymbol{q} = \boldsymbol{0}. \tag{11.17}$$

As is often the case, structural damping has been ignored in the model developed here (i.e. $\mathbf{D} = \boldsymbol{0}$). An alternative representation that is sometimes used is to reform Equation (11.17) in terms of the equivalent air speed V_{EAS} such that

$$\mathbf{A}\ddot{\boldsymbol{q}} + \left(\rho_0 \sqrt{\sigma} V_{\mathrm{EAS}} \mathbf{B} + \mathbf{D}\right)\dot{\boldsymbol{q}} + \left(\rho_0 V_{\mathrm{EAS}}^2 \mathbf{C} + \mathbf{E}\right)\boldsymbol{q} = \boldsymbol{0}, \tag{11.18}$$

where $\sigma = \rho/\rho_0$ is the ratio of air densities at altitude and sea level, defined in Chapter 5.

As these aeroelastic equations have a zero right-hand side (and so are homogeneous), it is not possible to determine the absolute values of the model response. Instead, the stability of the system needs to be explored using an eigenvalue approach.

11.4 EIGENVALUE SOLUTION OF FLUTTER EQUATIONS

The aeroelastic Equation (11.17) can be solved efficiently for an N DoF system using an eigenvalue solution to determine the system frequencies and damping ratios at a particular flight condition (air speed and altitude). Introducing the (trivial) expression

$$\mathbf{I}\dot{\boldsymbol{q}} - \mathbf{I}\dot{\boldsymbol{q}} = \boldsymbol{0}, \tag{11.19}$$

where $\mathbf{I}$ is the $N \times N$ identity matrix, and combining it with Equation (11.17) in partitioned form gives the formulation

$$\begin{bmatrix} \mathbf{I} & \mathbf{0} \\ \mathbf{0} & \mathbf{A} \end{bmatrix} \begin{Bmatrix} \dot{\boldsymbol{q}} \\ \ddot{\boldsymbol{q}} \end{Bmatrix} - \begin{bmatrix} \mathbf{0} & \mathbf{I} \\ -\left(\rho V^2 \mathbf{C} + \mathbf{E}\right) & -(\rho V \mathbf{B} + \mathbf{D}) \end{bmatrix} \begin{Bmatrix} \boldsymbol{q} \\ \dot{\boldsymbol{q}} \end{Bmatrix} = \begin{Bmatrix} \boldsymbol{0} \\ \boldsymbol{0} \end{Bmatrix}. \tag{11.20}$$

This equation may be rewritten as

$$\begin{Bmatrix} \dot{\boldsymbol{q}} \\ \ddot{\boldsymbol{q}} \end{Bmatrix} - \begin{bmatrix} \mathbf{0} & \mathbf{I} \\ -\mathbf{A}^{-1}\left(\rho V^2 \mathbf{C} + \mathbf{E}\right) & -\mathbf{A}^{-1}(\rho V \mathbf{B} + \mathbf{D}) \end{bmatrix} \begin{Bmatrix} \boldsymbol{q} \\ \dot{\boldsymbol{q}} \end{Bmatrix} = \boldsymbol{0} \quad \Rightarrow \quad \dot{\boldsymbol{x}} - \mathbf{Q}\boldsymbol{x} = \boldsymbol{0}. \tag{11.21}$$

Equations (11.21) are now in first-order form but note that the **Q** matrix is $2N \times 2N$, double the size of the matrices in the aeroelastic Equation (11.17). The equation can be solved by assuming $\boldsymbol{x} = \boldsymbol{x_0} e^{\lambda t}$ and thus Equation (11.21) becomes

$$(\mathbf{I}\lambda - \mathbf{Q})\,\boldsymbol{x}_0 = \boldsymbol{0} \qquad \text{or} \qquad (\mathbf{Q} - \mathbf{I}\lambda)\,\boldsymbol{x}_0 = \boldsymbol{0}, \tag{11.22}$$

which is in the classical eigensolution form $(\mathbf{A} - \mathbf{I}\lambda)\,\boldsymbol{x} = \boldsymbol{0}$.

For an oscillatory system, such as the aeroelastic system considered here, the eigenvalues λ of the system matrix **Q** occur in complex conjugate pairs and are in the form (Fraser *et al.*, 1938; Collar and Simpson, 1987)

$$\lambda_j = -\zeta_j \omega_j \pm \mathrm{i}\omega_j \sqrt{1 - \zeta_j^2}, \quad j = 1, 2, \ldots, N, \tag{11.23}$$

where ω_j, $j = 1, 2, \ldots, N$, are the natural frequencies and ζ_j, $j = 1, 2, \ldots, N$, are the damping ratios. The corresponding eigenvectors appear in complex conjugate columns and take the form

$$\boldsymbol{x}_j = \begin{Bmatrix} \boldsymbol{q}_j \\ \lambda \boldsymbol{q}_j \end{Bmatrix}, \quad j = 1, 2, \ldots, N. \tag{11.24}$$

Thus the upper (or lower) halves of the eigenvectors yield the mode shapes in terms of generalized coordinates. Note that due to the influence of the non-symmetric aerodynamic terms these are complex modes (see Chapter 2).

If the real part of the complex eigenvalues is positive then the system becomes unstable. However, if the eigenvalues are real, then the roots are nonoscillatory and do not occur in complex conjugate pairs, although, if the real part becomes positive, the system becomes statically unstable (i.e. divergent; see Chapter 8).

11.5 AEROELASTIC BEHAVIOUR OF THE BINARY MODEL

The dynamic aeroelastic behaviour for the flapping/pitching wing can now be determined at different air speeds and altitudes by forming the eigensolution of matrix **Q** in Equation (11.21) for each flight condition and then calculating the corresponding frequencies and damping ratios. In the following section, the effect of varying different structural and aerodynamic parameters on the frequency and damping trends (so-called $V\omega$ and Vg plots) is investigated.

The baseline system parameters considered are shown in Table 11.1, noting that the mass axis is at the semi-chord ($x_m = 0.5c$) and the flexural axis is at $x_f = 0.48c$ from the leading edge. Note also that the flap and pitch stiffnesses are determined by choosing the desired wind-off (i.e. zero air speed) frequencies for the system without including inertia coupling terms.

Table 11.1 Baseline parameters for the binary flutter model

Semi-span (s)	7.5 m	Flap stiffness (K_κ)	$I_\kappa(5 \times 2\pi)^2$ N m/rad
Chord (c)	2 m	Pitch stiffness (K_θ)	$I_\theta(10 \times 2\pi)^2$ N m/rad
Flexural axis (x_f)	$0.48c$	Lift curve slope (a_W)	2π
Mass axis	$0.5c$	Nondimensional pitch damping derivative ($M_{\dot\theta}$)	-1.2
Mass per unit area	100 kg/m^2	Air density (ρ)	1.225 kg/m^3

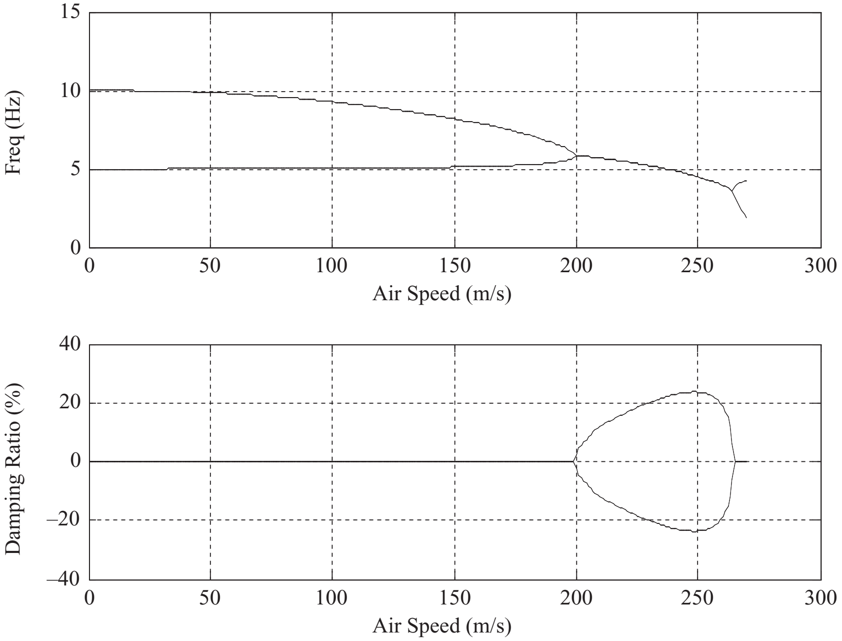

Figure 11.3 Frequency and damping trends for the baseline system with zero aerodynamic and structural damping ($x_f = 0.48c$, $x_m = 0.5c$).

11.5.1 Zero Aerodynamic Damping

If the structural and aerodynamic damping related terms in Equation (11.17) are ignored (i.e. $\mathbf{B} = \mathbf{D} = \mathbf{0}$) then the Vg and $V\omega$ trends in Figure 11.3 for the baseline system show that as the air speed increases, the two frequencies move closer to each other; however, the damping of both modes remains at zero. Once the two frequencies become equal at around 200 m/s, the modes are said to 'coalesce'; one of the damping ratios becomes positive and the other negative. Hence the system becomes unstable, which is the flutter condition. Beyond $V = 264$ m/s, the frequency coalescence stops and both modes become undamped once again.

It is often stated that the frequencies of an aeroelastic system must coalesce for flutter to occur, as in this case of zero aerodynamic damping. However, this is not true for general aeroelastic systems, as will be seen in the later examples when aerodynamic damping is included.

11.5.2 Aerodynamic Damping with Quasi-Steady Aerodynamics

11.5.2.1 Baseline system

When the quasi-steady aerodynamic damping terms due to the flap (and therefore heave) velocity in Equation (11.13) are included in the computations, but the $M_{\dot{\theta}}$ term is still set to zero, then the frequency and damping behaviour become markedly different. The frequencies in Figure 11.4 start to converge gradually with an increase in air speed but do not coalesce at the flutter condition. Both of the damping ratios initially rise with increasing air speed; however, one of them then reduces and becomes zero at the flutter speed of 62.4 m/s. Flutter occurs beyond this speed when this damping ratio becomes negative and the system then becomes unstable.

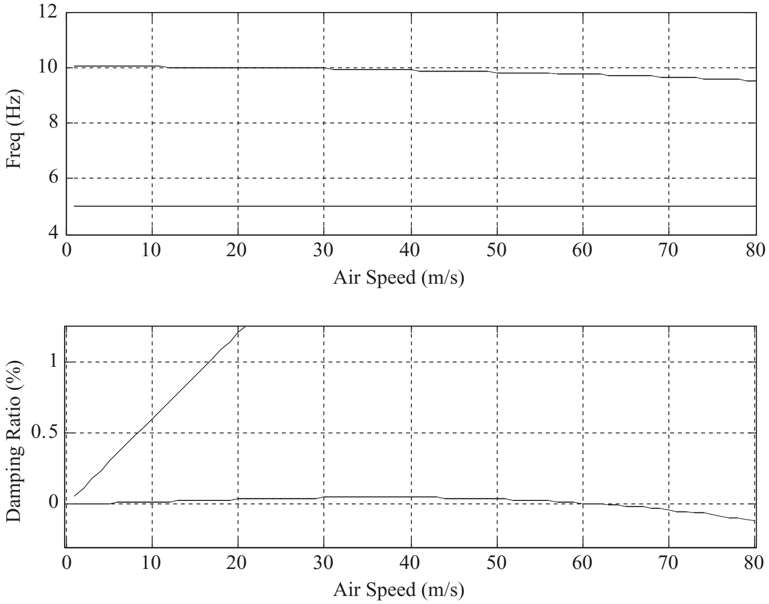

Figure 11.4 Frequency and damping trends for the baseline system with quasi-steady aerodynamic damping included ($M_{\dot{\theta}} = 0, x_f = 0.48c, x_m = 0.5c$).

11.5.2.2 Modified system

Although the $V\omega$ and Vg trends for the baseline system show some typical characteristics of an aeroelastic system, only quasi-steady aerodynamics terms have been included, which can lead to significant modelling errors. For example, consider the same system as in the previous example but now modified to have both the flexural and mass axes on the mid-chord ($x_{\mathrm{f}} = 0.5c$). Figure 11.5 shows that flutter occurs at all speeds above zero air speed (the lowest damping ratio trend is always negative). The unsteady aerodynamic terms must be included for accurate aeroelastic modelling. If only the flutter speed (i.e. searching for zero damping ratios) was sought, then such unrealistic behaviour would not be identified and it is therefore good practice to observe the entire subcritical behaviour.

11.5.3 Aerodynamic Damping with Unsteady Aerodynamics

11.5.3.1 Modified system

The full aeroelastic equations defined in Equation (11.16) are now considered for the modified case considered above in Section 11.5.2, with the flexural axis on the mid-chord ($x_{\mathrm{f}} = 0.5c$). However, now the unsteady aerodynamic term $M_{\dot{\theta}}$ is included (taken here as −1.2, equivalent to the value of −0.3 used in Hancock *et al.* (1985)).

Figure 11.6 shows how the frequency and damping values for this modified system demonstrate classical binary flutter behaviour. As the air speed increases, the frequencies begin to converge. Initially, both of the damping ratios increase, but whereas one of them continues to increase, the second damping starts to decrease and becomes zero at the flutter speed of around 151 m/s. Beyond this air speed the second damping ratio becomes negative and flutter occurs. Note again that the two frequencies do not coalesce, but rather move close enough in frequency for the two modes to couple unfavourably.

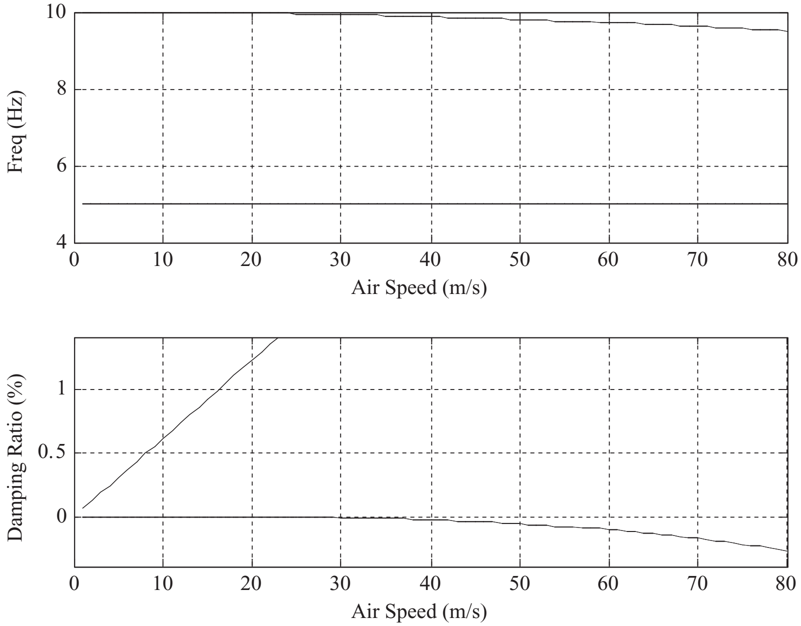

Figure 11.5 Frequency and damping trends for the modified system with quasi-steady aerodynamic damping included ($M_{\dot{\theta}} = 0, x_{\mathrm{f}} = 0.5c, x_{\mathrm{m}} = 0.5c$).

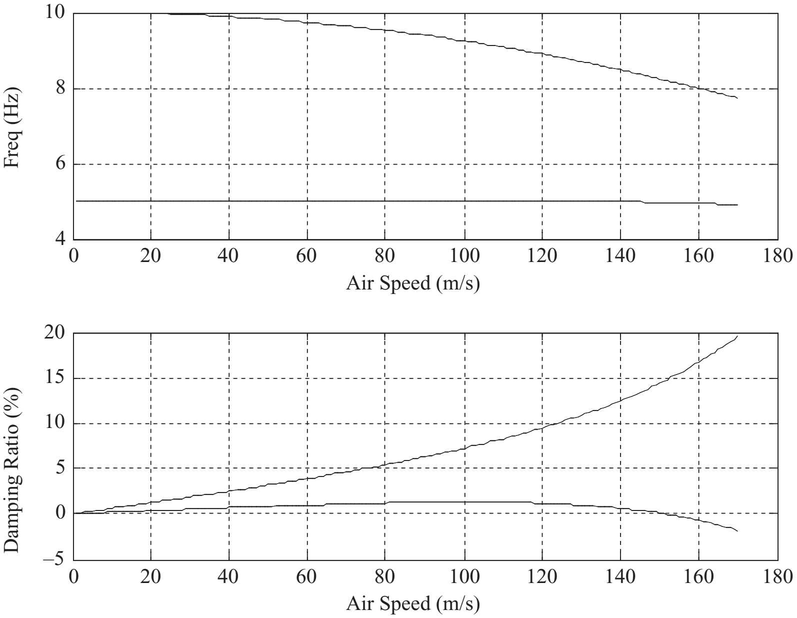

Figure 11.6 Frequency and damping trends for the modified system with the unsteady aerodynamics term included ($M_{\dot{\theta}} = -1.2, x_{\mathrm{f}} = 0.5c, x_{\mathrm{m}} = 0.5c$).

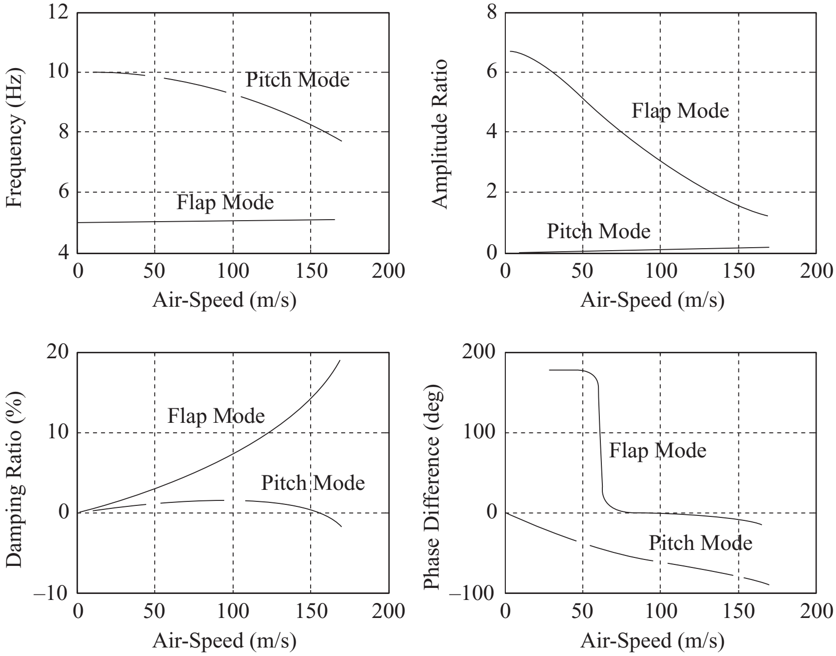

Figure 11.7 Frequency, damping and mode shape trends for the baseline system with $M_{\dot{\theta}} = -1.2$.

Including the unsteady aerodynamic term makes the model more representative of what occurs in practice. This issue is discussed more fully in Hancock et al. (1985).

11.5.3.2 Baseline system

Consider the baseline system ($x_{\mathrm{m}} = 0.48c$) again, but now with the inclusion of the unsteady aerodynamic term $M_{\dot{\theta}}$. The coupling between the modes is illustrated in Figure 11.7. The flutter speed has changed significantly compared to the case without the unsteady aerodynamics term (62.4 m/s) and is now 154 m/s.

The top-right hand plot in Figure 11.7 shows the ratio of the amplitudes of the flap (κ) to the pitch (θ) degrees of freedom. Initially the flap mode contains only a small amount of pitch, and vice versa, but as flutter is approached there is a significant amount of both degrees of freedom in each mode. The bottom right-hand corner plot shows the phase difference between the flap and pitch components in each mode against air speed. As flutter is approached, the phase difference between the two critical components changes to enable the interactions that extract energy from the airflow.

11.5.4 Illustration of Phasing for Flutter

A simplistic illustration as to how the phasing between the pitch and flap motions enables their corresponding lift components to work together to extract energy from the airflow at the flutter condition is shown in Figure 11.8. The quasi-steady aerodynamic components of a two-dimensional aerofoil oscillating in both flap and pitch are considered. In the upper plot, the motions of the flap and pitch components are in phase with each other, and the maximum and minimum values of the resulting lift forces are 90° out-of-phase. However, in the lower plot the flap and pitch motions are 90° out-of-phase, and thus the maximum and minimum lift components are in-phase. This behaviour is illustrated in Figure 11.7.

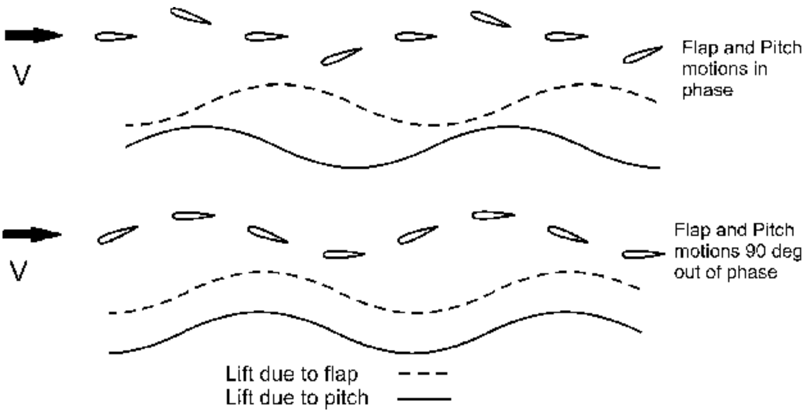
V
Flap and Pitch motions in phase
V
Flap and Pitch motions 90 deg out of phase
Lift due to flap
Lift due to pitch

Figure 11.8 Lift due to flap and pitch components for a two-dimensional aerofoil with different phasing between motions.

Note that, in practice, the presence of unsteady aerodynamic terms means that the phasing of the critical motions at flutter is not 90°.

11.5.5 Soft and Hard Flutter

If the critical damping ratio trend approaches the critical speed with a shallow gradient, this is known as a *soft flutter*. Figure 11.9 shows a case where the system parameters were modified such that the system becomes unstable at 81.4 m/s but becomes stable again beyond 212 m/s. Of course, in practice it would not be possible to fly to this second stable region without flutter occurring first. The presence of structural

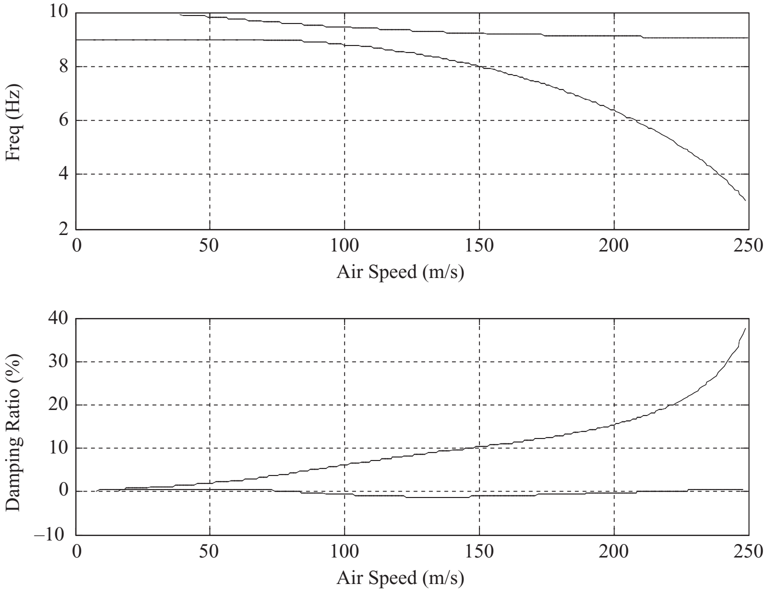

Figure 11.9 Frequency and damping ratio trends for the system with soft flutter.

damping may prevent such a flutter from occurring. If there is a very sudden drop in the damping values with increasing speed towards the flutter condition then this is known as a *hard flutter*. This latter case is of greatest concern during flight flutter testing (see Chapter 26) as a stable system may suddenly become unstable with a relatively small increase in air speed.

11.5.6 Inclusion of Structural Damping

The aeroelastic behaviour will be altered somewhat if structural damping is present. Consider the general aeroelastic model, but now with the addition of a proportional structural damping matrix based upon the structural mass and stiffness matrices (see Chapter 2), namely

$$\mathbf{D} = \alpha \mathbf{A} + \beta \mathbf{E}. \tag{11.25}$$

In order to obtain values of the Rayleigh coefficients α, β for the system, a range of frequencies ω_a and ω_b must be chosen. It can be shown (NAFEMS, 1987) that in order to achieve damping ratios ζ_a, ζ_b at these frequencies, the Rayleigh coefficients must be defined as

$$\begin{aligned} \alpha &= \frac{2\omega_a\omega_b\left(\zeta_a\omega_b - \zeta_b\omega_a\right)}{\omega_a^2\omega_b^2}, \\ \beta &= \frac{2\left(\zeta_a\omega_a - \zeta_b\omega_b\right)}{\omega_b^2 - \omega_a^2}. \end{aligned} \tag{11.26}$$

However, the damping ratios do not remain constant over the specified range of frequencies. If there are only two modes, then the values of ω_a and ω_b may be taken as being equal to the natural frequencies and so dampings for the two modes are defined.

For the baseline system, the two natural frequencies were chosen in this way so as to yield damping ratios of 3 % critical per mode. Figure 11.10 shows the trends of the frequency and damping ratios versus

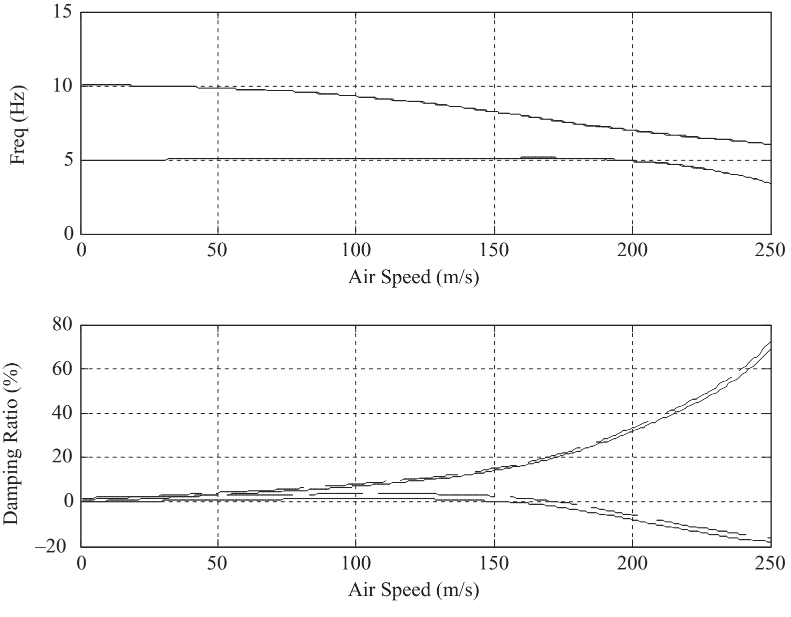

Figure 11.10 Effect of viscous structural damping (— —) on frequency and damping trends.

air speed for the baseline system considered in Figure 11.7 overlaid with the results obtained when damping ratios of 3 % critical are present for each of the modes. Similar trends are obtained as before, with very little change to the frequency behaviour; however, there is a change in the damping trends and the onset of flutter is delayed from 154 to 173 m/s. In general, the presence of structural damping is always beneficial in terms of flutter.

A more usual approach to modelling damping is not to use a Rayleigh model but rather to transform the equations into modal form and then to add a diagonal modal damping matrix where the damping terms are of the form $2\zeta_j\omega_j m_j$, $j = 1, 2, \ldots, N$. The damping ratios ζ_j may be defined based on experience or from a ground vibration test (see Chapter 26). It is explained in Part III how the certification requirements allow some damping to be included, although it is often ignored in aeroelastic models since it can only be determined from measurement; aerodynamic damping tends to dominate anyhow and the flutter predictions will be conservative.

11.5.7 Effect of Changes in Position of the Flexural and Mass Axes

An understanding of how the position of the wing flexural and mass axes affects the aeroelastic behaviour is of great importance in designing wings such that flutter will not occur inside the flight envelope. A slightly modified binary model is now considered compared to the one above, where a strip of mass M per unit length is now attached along the wing leading edge. It can be shown that this now gives the position of the mass axis at a distance

$$x_{\mathrm{cm}} = \frac{mc^2}{2\,(mc + M)} \tag{11.27}$$

from the leading edge. Changes in the mass axis position can then be investigated by varying the value of M, though it is appreciated that the overall mass will alter.

The equations of motion can be found using Lagrange's equations in the same way as before, except now the kinetic energy term contains an extra term such that

$$T = \int_{\text{wing}} \frac{1}{2}\mathrm{d}m\, \dot{w}^2 = \frac{m}{2}\int_0^s \int_0^c \left[y\dot{\kappa} + (x - x_{\mathrm{f}})\dot{\theta}\right]^2 \mathrm{d}x\,\mathrm{d}y + \frac{M}{2}\int_0^s \left(y\dot{\kappa} - x_{\mathrm{f}}\dot{\theta}\right)^2 \mathrm{d}y, \tag{11.28}$$

and this changes the form of the inertia matrix $\mathbf{A}$ to be

$$\mathbf{A} = \begin{bmatrix} \dfrac{ms^3c}{3} + \dfrac{Ms^3}{3} & \dfrac{ms^2}{2}\left(\dfrac{c^2}{2} - cx_{\mathrm{f}}\right) - \dfrac{Ms^2x_{\mathrm{f}}}{2} \\ \dfrac{ms^2}{2}\left(\dfrac{c^2}{2} - cx_{\mathrm{f}}\right) - \dfrac{Ms^2x_{\mathrm{f}}}{2} & ms\left(\dfrac{c^3}{3} - c^2x_{\mathrm{f}} + cx_{\mathrm{f}}^2\right) + Msx_{\mathrm{f}}^2 \end{bmatrix}. \tag{11.29}$$

The spring stiffnesses are determined from the pre-defined natural frequencies in the same way as before, with Equation (11.12) adjusted to include the extra mass in the diagonal terms of the inertia matrix in Equation (11.29).

Figure 11.11 shows how the flutter speed varies due to changes in the position of the flexural and mass axes. By keeping the position of the flexural axis constant, moving the mass axis forward increases the flutter speed. The addition of mass at the wing tip or control surface leading edge is a solution often used by aircraft designers to prevent flutter at too low a speed. When the mass axis is kept constant and the flexural axis is changed, decreasing the distance between the flexural axis and aerodynamic centre increases the flutter speed. Even when the mass and flexural axes are aligned with the aerodynamic centre on the quarter chord, flutter can still occur when unsteady damping terms are included.

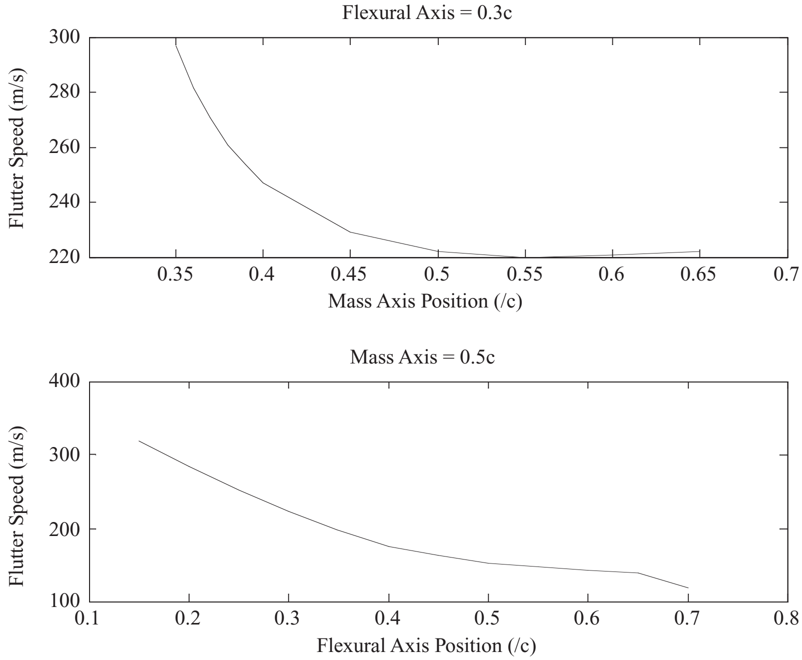

Figure 11.11 Effect of flexural and mass axes position on flutter speed.

11.5.8 Effect of Spacing Between Wind-Off Frequencies

The spacing of the structural (wind-off) natural frequencies has a major influence on the flutter speed as this value influences the interactions that lead to flutter. Figure 11.12 shows the aeroelastic behaviour of the baseline system compared to that when the two structural frequencies are closer together. In general, the closer the wind-off frequencies become, the more rapidly the critical interaction between the modes occurs and the flutter speed reduces. Designers often try to increase the frequency gap between modes (by changing the mass distribution or increasing stiffness) to increase the flutter speed; however, for a complete aircraft, care must be taken to ensure that in solving one problem a different critical flutter mechanism is not created.

11.6 AEROELASTIC BEHAVIOUR OF A FLEXIBLE WING

The same modelling approach as above can be used for the more realistic case of a flexible rectangular wing with a built-in root. Consider the model used in Section 11.2 but ignore the springs and set the flexural and torsional rigidities to be *EI* and *GJ* respectively. Consider the modal behaviour to be represented by bending and torsion assumed modes (see Chapter 3). The deflection of some point (x, y) on the wing can then be written in the same notation as before as

$$z = y^2 q_1 + y(x - x_f) q_2, \tag{11.30}$$

where q_1 and q_2 are generalized coordinates. For each elemental chordwise strip, $q_1 y^2$ is the bending deflection and $q_2 y$ is the angle of twist.

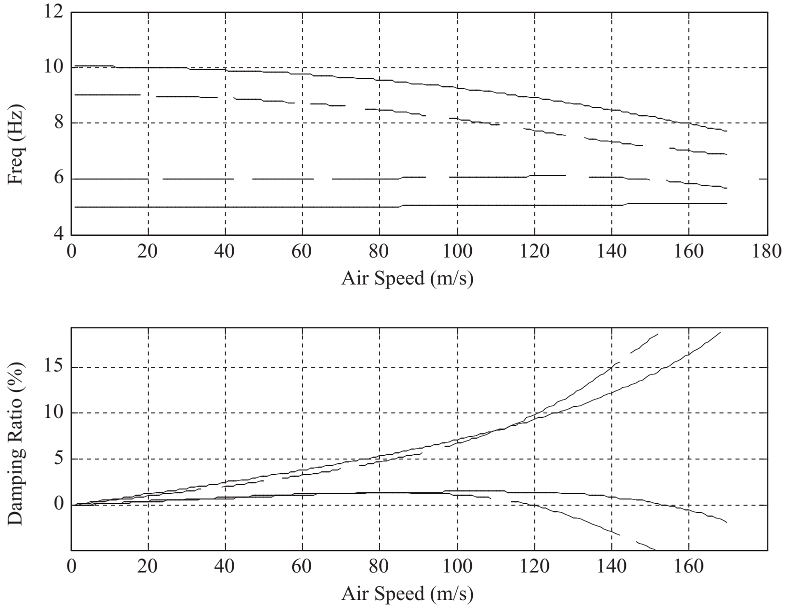

Figure 11.12 Frequency and damping ratio trends for systems with different wind-off frequencies.

Determining the kinetic and potential (or strain) energy and incremental work terms as before may be shown to lead to the equations

$$m\begin{bmatrix} \dfrac{cs^5}{5} & \dfrac{s^4}{4}\left(\dfrac{c^2}{2}-cx_{\mathrm{f}}\right) \\ \dfrac{s^4}{4}\left(\dfrac{c^2}{2}-cx_{\mathrm{f}}\right) & \dfrac{s^3}{3}\left(\dfrac{c^3}{3}-c^2x_{\mathrm{f}}+cx_{\mathrm{f}}^2\right) \end{bmatrix}\begin{Bmatrix} \ddot{q}_1 \\ \ddot{q}_2 \end{Bmatrix} + \rho V\begin{bmatrix} \dfrac{ca_{\mathrm{W}}s^5}{10} & 0 \\ -\dfrac{c^2ea_{\mathrm{W}}s^4}{8} & -\dfrac{c^3s^3M_{\dot{\theta}}}{24} \end{bmatrix}\begin{Bmatrix} \dot{q}_1 \\ \dot{q}_2 \end{Bmatrix}$$

$$+\left(\rho V^2\begin{bmatrix} 0 & \dfrac{cs^4a_{\mathrm{W}}}{8} \\ 0 & -\dfrac{ec^2s^3a_{\mathrm{W}}}{6} \end{bmatrix} + \begin{bmatrix} 4EIs & 0 \\ 0 & GJs \end{bmatrix}\right)\begin{Bmatrix} q_1 \\ q_2 \end{Bmatrix} = \begin{Bmatrix} 0 \\ 0 \end{Bmatrix}. \qquad (11.31)$$

These are in the same classical form as Equation (11.17) except that now the solution is in terms of the generalized coordinates q_1 and q_2 and not physical coordinates. Solutions are found in exactly the same way as for the binary aeroelastic model considered previously and $V\omega$ and Vg trends can be plotted for different flight conditions using the same eigensolution approach. Having determined the complex mode shapes in generalised coordinates from the corresponding eigenvectors, physical coordinate mode shapes can be found from the expression $z = y^2q_1 + y(x - x_{\mathrm{f}})q_2$.

It is possible to improve the model further by introducing more terms into the definition of the deflection shape; e.g. for two bending and two torsion assumed modes, the deflection could be modelled as

$$z = y^2q_1 + y^3q_2 + y(x - x_{\mathrm{f}})q_3 + y^2(x - x_{\mathrm{f}})q_4. \qquad (11.32)$$

The more terms that are included in the model, the more accurate the results (see Chapter 3).

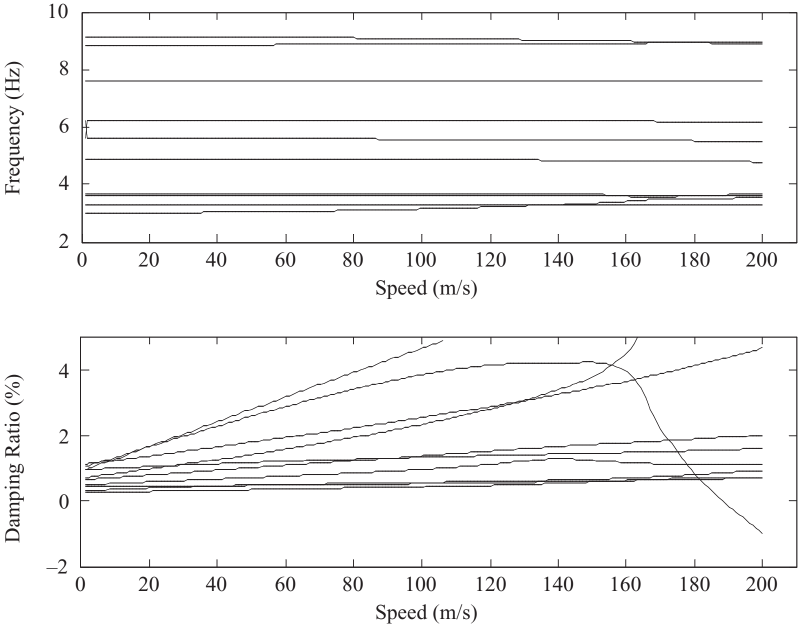

Figure 11.13 Example frequency and damping ratio trends for an aircraft model.

11.7 AEROELASTIC BEHAVIOUR OF A MULTIPLE MODE SYSTEM

If the aerodynamic and structural matrices are known, then the process for plotting the $V\omega$ and Vg plots for a full-scale aircraft model is exactly the same as that described above, making use of the eigensolution approach in Equation (11.22). Figure 11.13 shows a typical set of the first 10 symmetric modes for an aircraft model with unsteady aerodynamics evaluated at a single reduced frequency. The behaviour is much more complicated than for the binary systems considered previously; however, it can be seen that the flutter speed occurs at around 190 m/s, is due to the interaction of the first and third modes, and is a moderately hard flutter. A further multiple mode example is shown in Chapter 20.

11.8 FLUTTER SPEED PREDICTION FOR BINARY SYSTEMS

Instead of plotting the damping trends for different speeds and determining the flutter speed by eye, or by trial and error from the air speed at which zero damping ratio occurs, it is more accurate to calculate the flutter condition directly. This process is straightforward when frequency-independent aerodynamics is considered, but not for frequency-dependent aerodynamics (see later). The approach shown here is based upon the Routh–Hurwitz method described in Chapter 7.

Consider a binary aeroelastic system with frequency-independent aerodynamics, whose equation of motion is

$$\begin{bmatrix} a_{11} & a_{12} \\ a_{21} & a_{22} \end{bmatrix} \begin{Bmatrix} \ddot{q}_1 \\ \ddot{q}_2 \end{Bmatrix} + V \begin{bmatrix} b_{11} & b_{12} \\ b_{21} & b_{22} \end{bmatrix} \begin{Bmatrix} \dot{q}_1 \\ \dot{q}_2 \end{Bmatrix} + \left(V^2 \begin{bmatrix} c_{11} & c_{12} \\ c_{21} & c_{22} \end{bmatrix} + \begin{bmatrix} e_{11} & 0 \\ 0 & e_{22} \end{bmatrix} \right) \begin{Bmatrix} q_1 \\ q_2 \end{Bmatrix} = \begin{Bmatrix} 0 \\ 0 \end{Bmatrix}. \tag{11.33}$$

Assume a solution of the form

$$\begin{Bmatrix} q_1 \\ q_2 \end{Bmatrix} = \begin{Bmatrix} q_1 \\ q_2 \end{Bmatrix}_0 \mathrm{e}^{\lambda t}$$

and also make the substitutions

$$xV^2 = e_{11}, \qquad e_{22} = \mu e_{11} = \mu x V^2, \tag{11.34}$$

where μ is the ratio between the two spring stiffnesses and x is an unknown that has to be found. The nontrivial solution of the equations is defined by

$$\begin{vmatrix} a_{11}\lambda^2 + b_{11}V\lambda + (c_{11} + x)V^2 & a_{12}\lambda^2 + b_{12}V\lambda + c_{12}V^2 \\ a_{21}\lambda^2 + b_{21}V\lambda + c_{21}V^2 & a_{22}\lambda^2 + b_{22}V\lambda + (c_{22} + \mu x)V^2 \end{vmatrix} = 0. \tag{11.35}$$

Solving the determinant gives the quartic equation

$$b_4\lambda^4 + b_3\lambda^3 + b_2\lambda^2 + b_1\lambda + b_0 = 0, \tag{11.36}$$

where $b_0, \ldots, b_4$ are functions of the parameters in Equation (11.35). The roots of the equation are in two complex conjugate pairs, namely

$$\lambda_{1,2} = -\zeta_1\omega_1 \pm \mathrm{i}\omega_1\sqrt{1-\zeta_1^2}, \qquad \lambda_{3,4} = -\zeta_2\omega_2 \pm \mathrm{i}\omega_2\sqrt{1-\zeta_2^2}, \tag{11.37}$$

and at the flutter speed, since one of the damping ratios becomes zero, then one of the root pairs becomes

$$\lambda = \pm\mathrm{i}\omega. \tag{11.38}$$

Substituting Equation (11.38) into the quartic Equation (11.36) gives

$$b_4\omega^4 - \mathrm{i}b_3\omega^3 - b_2\omega^2 + \mathrm{i}b_1\omega + b_0 = 0 \qquad \text{and} \qquad b_4\omega^4 + \mathrm{i}b_3\omega^3 - b_2\omega^2 - \mathrm{i}b_1\omega + b_0 = 0. \tag{11.39}$$

Now, adding and subtracting Equations (11.39) gives

$$b_4\omega^4 - b_2\omega^2 + b_0 = 0 \qquad \text{and} \qquad \mathrm{i}b_3\omega^3 - \mathrm{i}b_1\omega = 0. \tag{11.40}$$

Hence the frequency at the flutter condition is given by

$$\omega = \sqrt{\frac{b_1}{b_3}}. \tag{11.41}$$

Equation (11.41) can be substituted into the quadratic part of Equations (11.40) to give an expression, namely

$$b_4b_1^2 - b_1b_2b_3 + b_0b_3^2 = 0, \tag{11.42}$$

from which the flutter speed may be obtained since the parameters in the equation are functions of V. The same result can be obtained by considering the Routh–Hurwitz stability criteria for the quartic Equation (11.36), leading to the condition for stability

$$b_1b_2b_3 - b_4b_1^2 - b_0b_3^2 > 0. \tag{11.43}$$

Knowing the matrix terms in Equation (11.33) it is possible to determine directly the critical flutter speeds and frequencies of a binary aeroelastic system using the following procedure. On a historical note, this procedure was used by Bairstow and Fage (1916) to investigate the flutter incident of the Handley Page 0-400 bomber (see the book front cover), the first documented flutter analysis.

Expanding the determinant in Equation (11.35) gives the fourth-order characteristic polynomial Equation (11.36) where

$$\begin{aligned} b_4 &= a_{11}a_{22} - a_{21}a_{12}, \\ b_3 &= (a_{11}b_{22} + b_{11}a_{22} - a_{21}b_{12} - a_{12}b_{21})\,V, \\ b_2 &= [(\mu a_{11} + a_{22})\,x + (a_{11}c_{22} + b_{11}b_{22} + c_{11}a_{22} - a_{21}c_{12} - b_{12}b_{21} - c_{21}a_{12})]\,V^2 \\ &= (p_1 x + p_0)\,V^2, \\ b_1 &= [(\mu b_{11} + b_{22})\,x + (b_{11}c_{22} + c_{11}b_{22} - b_{21}c_{12} - c_{21}b_{12})]\,V^3 = (q_1 x + q_0)\,V^3, \\ b_0 &= \left[\mu x^2 + (c_{22} + \mu c_{11})\,x + c_{11}c_{22} - c_{12}c_{21}\right] V^4 = \left(r_2 x^2 + r_1 x + r_0\right) V^4. \end{aligned} \tag{11.44}$$

Substituting Equations (11.44) into expression (11.42) for the critical condition and eliminating a factor of V^6, gives a quadratic equation in terms of the unknown x such that

$$\left(b_4 q_1^2 - b_3 q_1 p_1 + b_3^2 r_2\right) x^2 + \left(2b_4 q_1 q_0 - b_3 q_0 p_1 - b_3 q_1 p_2 + b_3^2 r_1\right) x + \left(b_4 q_0^2 - b_3 q_0 p_2 + b_3^2 r_0\right) = 0 \tag{11.45}$$

The two roots of this equation are then put into Equation (11.34), giving the two critical flutter speeds between which the system is unstable. Obviously the lowest speed is the one that is of interest, since any aircraft will probably have been destroyed long before the second critical condition has been reached. The corresponding flutter frequencies are then found by substituting the estimated flutter speeds and x values into Equation (11.41).

Application of this approach to the baseline model gives critical flutter speeds of 36.6 and 104.5 m/s, with corresponding frequencies of 8.08 and 5.05 Hz respectively, which agree exactly with the predictions obtained from the $V\omega$ and Vg plots.

11.9 FLUTTER CONIC

Further insight into the characteristics of binary flutter systems can be found through the use of the flutter conic (Niblett, 1988). In this case a graphical approach is employed to study the flutter behaviour.

Taking the standard flutter equation without structural damping

$$\mathbf{A}\dot{\boldsymbol{q}} + \rho V\mathbf{B}\dot{\boldsymbol{q}} + (\rho V^2\mathbf{C} + \mathbf{E})\boldsymbol{q} = \boldsymbol{0} \tag{11.46}$$

and assuming a solution of the form $\boldsymbol{q} = \boldsymbol{q}_0 \mathrm{e}^{\mathrm{i}\omega t}$ then the nontrivial solution is defined by

$$\left|-\mathbf{A}\omega^2 + \mathrm{i}\omega\rho V\mathbf{B} + \rho V^2\mathbf{C} + \mathbf{E}\right| = 0. \tag{11.47}$$

In the form of the binary flutter system, Equation (11.33), this becomes

$$\begin{vmatrix} -a_{11}\omega^2 + \mathrm{i}\omega V b_{11} + V^2 c_{11} + e_{11} & -a_{12}\omega^2 + \mathrm{i}\omega V b_{12} + V^2 c_{12} \\ -a_{21}\omega^2 + \mathrm{i}\omega V b_{21} + V^2 c_{21} & -a_{22}\omega^2 + \mathrm{i}\omega V b_{22} + V^2 c_{22} + e_{22} \end{vmatrix} = 0. \tag{11.48}$$

Expanding the determinant of this complex matrix leads to real and imaginary parts that may be separated, since both of these must equal zero at the flutter condition.

The real part of Equation (11.48) gives a quadratic relation between the squares of the frequency and velocity:

$$r_1\omega^4 + r_2V^2\omega^2 + r_3V^4 + r_4\omega^2 + r_5V^2 + r_6 = 0,$$

where

$$\begin{aligned}
r_1 &= a_{11}a_{22} - a_{12}a_{21},\\
r_2 &= a_{12}c_{21} + b_{12}b_{21} + a_{21}c_{12} - a_{11}c_{22} - b_{11}b_{22} - a_{22}c_{12},\\
r_3 &= c_{11}c_{22} - c_{12}c_{21},\\
r_4 &= -e_{11}a_{22} - a_{11}e_{22},\\
r_5 &= e_{11}c_{22} + e_{22}c_{11},\\
r_6 &= e_{11}e_{22},
\end{aligned} \tag{11.49}$$

which is in the mathematical form of a conic when (frequency)^2 is plotted against (velocity)^2. The imaginary part of Equation (11.48) gives a linear relation between ω^2 and V^2 such that

$$s_1\omega^2 + s_2V^2 + s_3 = 0,$$

where

$$\begin{aligned}
s_1 &= a_{12}b_{21} + a_{21}b_{12} - a_{11}b_{22} - a_{22}b_{11},\\
s_2 &= b_{11}c_{22} + c_{11}b_{22} - b_{12}c_{21} - b_{21}c_{12},\\
s_3 &= b_{11}e_{22} + b_{22}e_{11}.
\end{aligned} \tag{11.50}$$

The intersection of the lines formed by these two equations, shown in Figure 11.14 for the baseline system, indicates where the flutter point occurs. The two parts of the conic represent the real part of the equation whereas the straight line represents the imaginary part. The corresponding flutter speed and frequency can be determined from the intersections of the conic and the straight lines and the values agree with those obtained above. If there is no intersection then flutter cannot occur. Note that the flutter

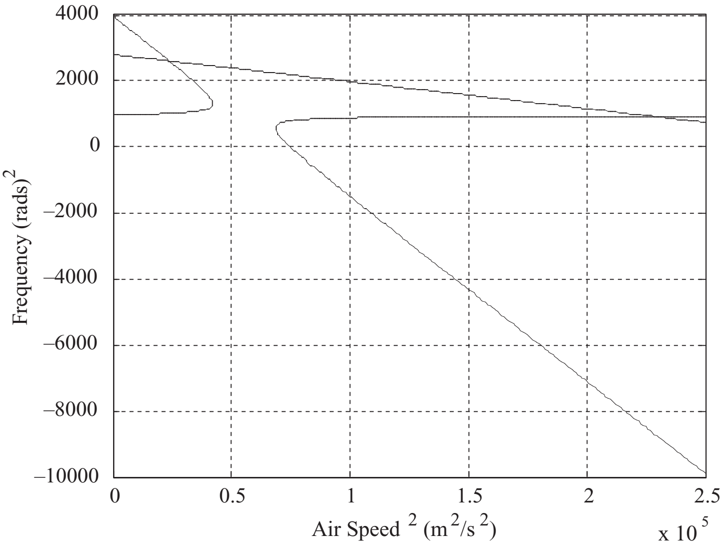

Figure 11.14 Flutter conic plot for the baseline system.

speed can be calculated directly by substituting Equation (11.50) into Equation (11.49). The divergence speed can also be determined from the point where the conic intersects the $\omega = 0$ axis.

The main advantages of using the flutter conic is that it does not matter if the eigenvalues give nonoscillatory solutions and it can be seen immediately whether flutter actually occurs. However, the approach does not lend itself to the analysis of systems greater than second order.

11.10 DIVERGENCE OF AEROELASTIC SYSTEMS

So far, this chapter has only been concerned with determining the flutter speed; flutter normally occurs before divergence but the latter condition does have to be checked. Taking the baseline aeroelastic system of Section 11.5, but this time with the natural frequencies of the pitch and flap modes reversed (somewhat unusual) in order to 'force' divergence to occur at a lower air speed than flutter, Figure 11.15 shows how the frequency, damping and real and imaginary parts of the eigenvalues change with air speed. The pitch mode reduces in frequency and splits into two nonoscillatory solutions at around 136.2 m/s; this is where the imaginary part of the eigenvalue becomes zero. With a further increase in air speed, the system undergoes divergence at 136.7 m/s when the real part of one of the nonoscillatory eigenvalues becomes positive. The $V\omega$ plot indicates a zero frequency at the divergence speed but, as discussed earlier, great care must be taken in interpreting nonoscillatory eigenvalues. The frequency trends do not have any meaning for the nonoscillatory solutions. The divergence speed solution is considered further in Chapter 23.

It is instructive to examine the eigenvalue behaviour on a root locus plot (see Chapter 7), shown in Figure 11.16. The complex conjugate pair of eigenvalues corresponding to the mode that remains oscillatory moves from A to B throughout the speed range. The second mode starts off as a complex conjugate pair at point C; however, at point D the imaginary part becomes zero and the oscillatory motion

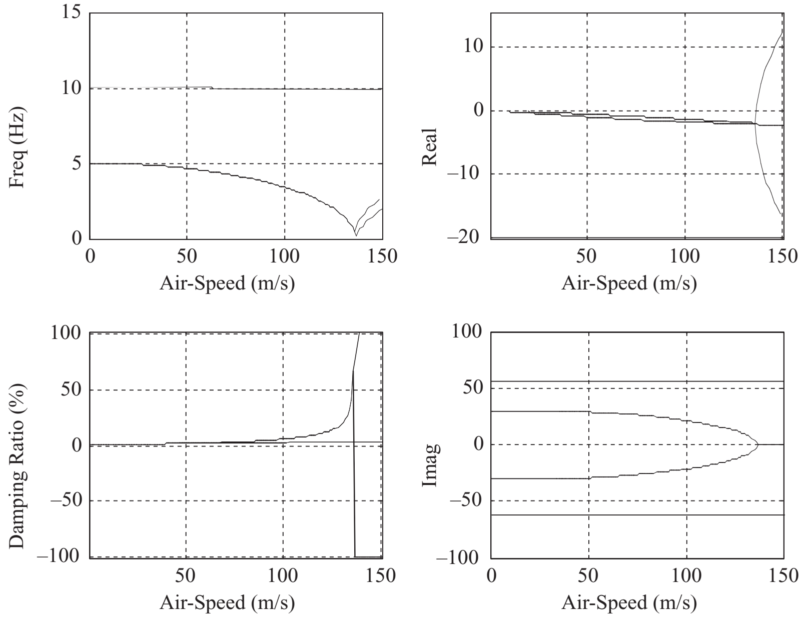

Figure 11.15 Trends of frequency, damping and real/imaginary parts of eigenvalues for the system with reversed order of frequencies ($f_\kappa = 10\,\text{Hz}, f_\theta = 5\,\text{Hz}$).

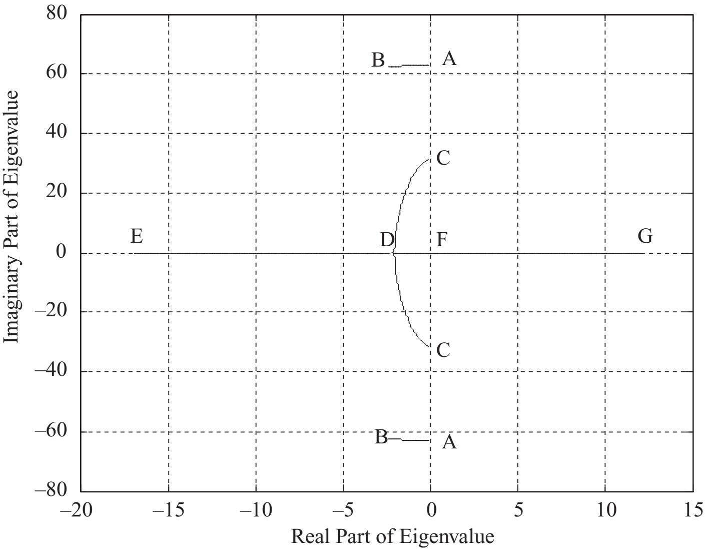

Figure 11.16 Real and imaginary parts of eigenvalues ($f_\kappa = 10\,\text{Hz}, f_\theta = 5\,\text{Hz}$).

ceases. The eigenvalues then split and move along the real axis in both directions towards points E and G. Once the eigenvalue heading for point G crosses the imaginary axis at point F the system becomes statically unstable and divergence occurs.

An exact calculation of the divergence speed for the general aeroelastic system in Equation (11.17) can be found by considering only the displacement related terms, leading to

$$\left(\rho V^2 \mathbf{C} + \mathbf{E}\right) \boldsymbol{q} = \boldsymbol{0}. \tag{11.51}$$

Divergence then occurs at the nontrivial solution defined by

$$\left|\rho V^2 \mathbf{C} + \mathbf{E}\right| = 0, \tag{11.52}$$

or this could be expressed as an eigenvalue problem. When applied to the system considered in this section, a divergence speed of 136.7 m/s is found; this is exactly the same as that obtained from the $V\omega$ plot above and also from the flutter conic method.

In order to determine the static aeroelastic deflections, the initial deformed shape (e.g. wing root incidence) must be included as a right-hand side term (see Chapters 8, 15 and 20). Equation (11.51) then becomes

$$\left(\rho V^2 \mathbf{C} + \mathbf{E}\right) \boldsymbol{q} = -\rho V^2 \mathbf{C} \boldsymbol{q}_0, \tag{11.53}$$

where $\boldsymbol{q}_0$ defines the initial deflection at zero air speed.

11.11 INCLUSION OF UNSTEADY REDUCED FREQUENCY EFFECTS

It has been seen that in order to model aeroelastic systems correctly, the unsteady aerodynamics described in Chapter 10 need to be accounted for. However, so far only the very simplistic approach of including a constant $M_{\dot{\theta}}$ term has been used. In practice, as shown in Chapter 10, the aerodynamic stiffness and damping matrices are reduced frequency-dependent, which leads to the so-called 'frequency matching' problem. If the **B** and **C** matrices in the aeroelastic Equation (11.17) are known, then the eigenproblem posed in Equation (11.21) can be solved. However, the **B** and **C** matrices cannot be formed unless the reduced frequency of interest is known, and this cannot be determined until the eigensolution of the system matrix, **Q**, involving both the **B** and **C** matrices has been solved. There is no direct way of solving this 'chicken and egg' problem and some form of iterative approach, known as 'frequency matching', must be used.

There are a number of ad hoc approaches that have been developed to solve the frequency matching problem. Here, simplified versions of two commonly used approaches, the so-called '*k*' and '*p–k*' methods (Hassig, 1971), will be illustrated on the binary system considered above. Both methods are based upon the assumption that the aerodynamics behaviour is dependent upon a harmonic response. This is fine at the flutter condition but is not true below (and above) this speed; consequently the methods give the same flutter speed and frequency but predict different subcritical behaviour. The methods tend to be fairly robust in their use, although there are concerns about the damping ratio trend predictions for the '*k*' method.

Here, in order to illustrate the two methods, the baseline binary aeroelastic system will be used with a simplified approximation for the frequency dependency of $M_{\dot{\theta}}$ such that

$$M_{\dot{\theta}}(k) = -\frac{5}{2+5k}. \tag{11.54}$$

Clearly, in practice the full unsteady expressions described in Chapter 10 need to be used.

11.11.1 Frequency Matching – '*k*' Method

Consider the classical form of the aeroelastic Equations (11.17), with **B** and **C** now being functions of reduced frequency $k = \omega b/V$, and also include structural (or hysteretic) damping in the form $\mathbf{D} = \mathrm{i}g\mathbf{E}$ (see Chapter 1), where g is the symbol commonly used for the structural damping coefficient in flutter calculations (not to be confused with the symbol for acceleration due to gravity). Assuming a harmonic solution in the form $\boldsymbol{q} = \boldsymbol{q}_0 \mathrm{e}^{\mathrm{i}\omega t}$, and dividing throughout by $-\omega^2$, then Equation (11.17) becomes

$$\left[\mathbf{A} - \mathrm{i}\rho\left(\frac{b}{k}\right)\mathbf{B} - \rho\left(\frac{b}{k}\right)^2\mathbf{C} - \frac{1+\mathrm{i}g}{\omega^2}\mathbf{E}\right]\boldsymbol{q}_0 = \boldsymbol{0}. \tag{11.55}$$

This equation is solely in terms of the reduced frequency k, and is a generalized eigenvalue problem

$$(\mathbf{F} - \lambda\mathbf{E})\boldsymbol{q}_0 = \boldsymbol{0} \quad \text{where} \quad \mathbf{F} = \left[\mathbf{A} - \mathrm{i}\rho\left(\frac{b}{k}\right)\mathbf{B} - \rho\left(\frac{b}{k}\right)^2\mathbf{C}\right] \quad \text{and} \quad \lambda = \frac{1+\mathrm{i}g}{\omega^2}. \tag{11.56}$$

Thus it may be seen that

$$\omega = \frac{1}{\sqrt{\mathrm{Re}(\lambda)}}, \qquad g = 2\zeta = \frac{\mathrm{Im}(\lambda)}{\mathrm{Re}(\lambda)}, \qquad V = \frac{\omega c}{2k}, \tag{11.57}$$

where ζ is the equivalent viscous damping ratio for motion at the natural frequency (see Chapter 1). The '*k*' method is applied in the following manner.

For each reduced frequency of interest:

(a) Calculate the corresponding **B** and **C** matrices.
(b) Solve the complex eigenproblem in Equation (11.56) to yield complex eigenvalues λ.

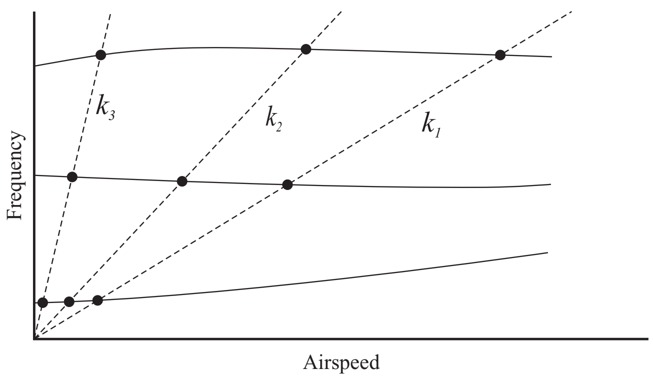

Figure 11.17 The '*k*' method – presentation of frequency points for lines of constant *k*.

(c) Determine the frequencies and damping coefficients (or ratios) from the eigenvalues using Equation (11.57).
(d) Relate these to the air speed via the definition of the reduced frequency *k* in Equation (11.57).

Consider the next reduced frequency and keep repeating the process until all *k* values have been investigated.

Then join up the frequencies and corresponding damping coefficients (or ratios) to form $V\omega$ and Vg plots. Care must be taken in interpreting the results since it is possible for the frequency and damping values to 'fold back', i.e. to have more than one solution for a particular mode at some flight condition.

A sample result is shown in Figure 11.17 where three different reduced frequencies have been considered for a three DOF aeroelastic system. At each reduced frequency *k*, there are three eigenvalues λ that correspond to natural frequencies ω and speeds *V* determined from Equations (11.57). The $V\omega$ and corresponding Vg trends (the latter not shown here) can then be formed, giving an estimate of the aeroelastic behaviour of the system.

The addition of the damping terms in this solution is somewhat artificial; the eigenvalues that are being found actually allow determination of the structural damping required (Garrick and Reid, 1981) to give zero *overall* damping at that flight condition. Consequently, for a stable condition the dampings that are determined are negative, and vice versa for a fluttering system. It is often the convention that flutter plots use these damping coefficients *g* plotted against air speed and so flutter occurs for positive 'required' damping; this is why the classical flutter plot is known as a Vg plot. Care must be taken to confirm what is meant by damping in the interpretation of such plots. In this book true damping values are presented and damping results are a factor of -2 different from the required structural damping approach.

11.11.2 Frequency Matching – '*p–k*' Method

The '*p–k*' method is a widely used frequency matching method and is applied in the following manner.

For each air speed of interest in the flight envelope and for each mode of interest:

(a) Make an initial guess of the frequency for the mode (often the previous air speed or wind-off results are used) and calculate the corresponding reduced frequency for the speed/frequency combination.
(b) Determine the aerodynamic stiffness and damping matrices **B**, **C** using this reduced frequency.
(c) Determine the frequencies for the system at this flight condition using the eigenvalue solution of the real matrix shown in Equation (11.21) for the first-order form,

(d) Take the frequency solution closest to the initial guess and repeat the process.
(e) Continue until the frequency converges (usually after four or five iterations) and note the corresponding damping ratio.

Consider the next mode of interest and repeat until all modes of interest have been investigated. Then consider the next flight speed and repeat until all air speeds of interest have been explored.

A set of frequency, damping and air speed values will then be assembled and plotted, each corresponding to the correct reduced frequency, and the flutter speed may be found where the damping is zero.

11.11.3 Comparison of Results for '*k*' and '*p–k*' Methods

Using the baseline binary aeroelastic system, but with the frequency-dependent $M_{\dot\theta}$ term described above in Equation (11.54), Figure 11.18 shows the frequency and true damping ratio (not 'required' structural damping coefficient) trends for the '*k*' and '*p–k*' methods, where it can be seen that there are some differences in the subcritical behaviour but that, as expected, the same solution is found at the flutter speed.

One major difficulty with these approaches is that, whereas at the flutter condition the critical mode dominates the motion, at subcritical speeds the motion is made up of a number of different modes. The frequency matching process must be undertaken for each mode at a particular flight condition. However, since the aerodynamics is assumed to occur at a single frequency, there will be some error in the estimates. Consequently, the various frequency matching methods give different frequency and damping values at subcritical speeds (or beyond flutter), but give the same estimate at the flutter condition.

More sophisticated frequency matching methods exist (Chen, 2000; Edwards and Weiseman, 2003) but are beyond the scope of this book.

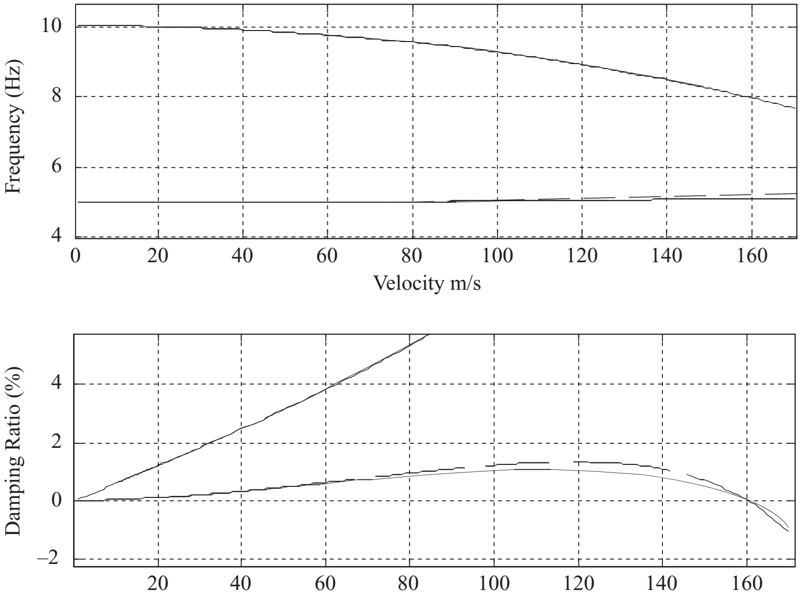

Figure 11.18 Frequency and damping ratio trends from the '*k*' (dashed) and '*p–k*' (solid) methods.

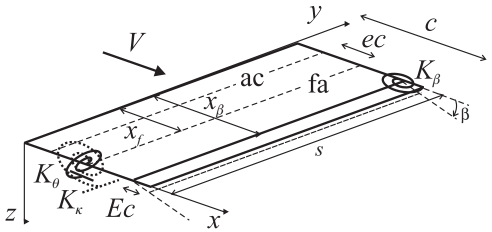

Figure 11.19 Aeroelastic model including a full span control surface.

11.12 CONTROL SURFACE FLUTTER

Historically, flutter involving the control surfaces has occurred more frequently than classical wing bending/torsion flutter. This has often resulted in the loss of control surfaces and/or part of the wing/tail structure but the aircraft has survived. Usually the flutter mechanism still occurs due to the interaction of two modes.

To illustrate some of the characteristics of control surface flutter, consider the three DoF aeroelastic system shown in Figure 11.19. The binary aeroelastic model has now been altered so that a full span control surface is attached to the wing by a torsional spring of stiffness K_β. As before, the nondimensional pitch damping derivative $M_{\dot\theta}$ is included in order to approximate the unsteady aerodynamic behaviour, but now a control aerodynamic damping derivative $M_{\dot\beta}$ is also included (Wright *et al.*, 2003).

The vertical deflection (+ve downwards) is expressed as

$$z = y\kappa + (x - x_\mathrm{f})\theta + \left[x - x_\beta\right]\beta, \tag{11.58}$$

where $[X]$ is the Heaviside function defined by $[X] = 0$ if $X < 0$ and $[X] = X$ if $X \geq 0$. The kinetic energy is given by

$$T = \frac{m}{2}\int_0^s\int_0^{x_\beta}\left\{y\dot\kappa + (x - x_\mathrm{f})\dot\theta\right\}^2 \mathrm{d}x\,\mathrm{d}y + \frac{m}{2}\int_0^s\int_{x_\beta}^{c}\left\{y\dot\kappa + (x - x_\mathrm{f})\dot\theta + \left(x - x_\beta\right)\dot\beta\right\}^2 \mathrm{d}x\,\mathrm{d}y \tag{11.59}$$

and thus the acceleration terms in Lagrange's equations can be found as

$$\begin{Bmatrix} \dfrac{\mathrm{d}}{\mathrm{d}t}\left(\dfrac{\partial T}{\partial\dot\kappa}\right) \\ \dfrac{\mathrm{d}}{\mathrm{d}t}\left(\dfrac{\partial T}{\partial\dot\theta}\right) \\ \dfrac{\mathrm{d}}{\mathrm{d}t}\left(\dfrac{\partial T}{\partial\dot\beta}\right) \end{Bmatrix} = m\begin{bmatrix} \dfrac{cs^3}{3} & \dfrac{s^2}{2}\left(\dfrac{c^2}{2} - cx_\mathrm{f}\right) & \dfrac{s^2}{2}\left(\dfrac{c^2}{2} - cx_\beta + \dfrac{x_\beta^2}{2}\right) \\ & s\left(\dfrac{c^3}{3} - c^2x_\mathrm{f} + cx_\mathrm{f}^2\right) & s\left(\dfrac{c^3}{3} + \dfrac{x_\beta^3}{6} - \dfrac{c^2x_\mathrm{f}}{2} - \dfrac{x_\mathrm{f}x_\beta^2}{2} + cx_\mathrm{f}x_\beta - \dfrac{c^2x_\beta}{2}\right) \\ \text{symmetric} & & s\left(\dfrac{c^3}{3} - \dfrac{x_\beta^3}{3} - c^2x_\beta + cx_\beta^2\right) \end{bmatrix}\begin{Bmatrix} \ddot\kappa \\ \ddot\theta \\ \ddot\beta \end{Bmatrix}, \tag{11.60}$$

which can also be expressed in terms of inertias $I_{\gamma\gamma}$, etc. The potential (or strain) energy is defined as

$$U = \tfrac{1}{2}K_\kappa \kappa^2 + \tfrac{1}{2}K_\theta \theta^2 + \tfrac{1}{2}K_\beta \beta^2 \tag{11.61}$$

and the incremental work done by the aerodynamic force and moments is

$$\delta W = -\int_0^s \mathrm{d}L y \delta\kappa + \int_0^s \mathrm{d}M_{\mathrm{fa}} \delta\theta + \int_0^s \mathrm{d}M_{\mathrm{ha}} \delta\beta \tag{11.62}$$

where M_{fa} and M_{ha} are the aerodynamic moments calculated about the flexural axis and hinge line respectively. The lift and pitching moment about the flexural axis on an elemental strip of the wing are

$$\mathrm{d}L = \frac{1}{2}\rho V^2 \left[a_{\mathrm{W}}\left(\theta + \frac{y\dot{\kappa}}{V}\right) + a_{\mathrm{c}}\beta\right], \qquad \mathrm{d}M_{\mathrm{fa}} = \frac{1}{2}\rho V^2 \left[b_{\mathrm{W}}\left(\theta + \frac{y\dot{\kappa}}{V}\right) + b_{\mathrm{c}}\beta + M_{\dot{\theta}}\frac{\dot{\theta}c}{4V}\right] \tag{11.63}$$

The pitching moment about the hinge line can also be shown to be

$$\mathrm{d}M_{\mathrm{ha}} = \frac{1}{2}\rho V^2 \left[c_{\mathrm{W}}\left(\theta + \frac{y\dot{\kappa}}{V}\right) + c_{\mathrm{c}}\beta + M_{\dot{\beta}}\frac{\dot{\beta}c}{4V}\right], \tag{11.64}$$

where the lift, pitching moment and hinge moment coefficients may be estimated as in Chapter 5 (Fung, 1969):

$$\begin{aligned}
&a_{\mathrm{W}} = 2\pi, \qquad a_{\mathrm{C}} = \frac{a_{\mathrm{W}}}{\pi}\left[\cos^{-1}(1-2E) + 2\sqrt{E(1-E)}\right],\\
&b_{\mathrm{W}} = eca_{\mathrm{W}}, \qquad b_{\mathrm{C}} = -\frac{a_{\mathrm{W}}}{\pi}(1-E)\sqrt{E(1-E)},\\
&c_{\mathrm{W}} = -\frac{T_{12}}{2}, \qquad c_{\mathrm{C}} = -\frac{T_{12}T_{10}}{2\pi},\\
&T_{10} = \sqrt{1-d^2} + \cos^{-1} d, \qquad T_{12} = \sqrt{1-d^2}\,(2+d) + \cos^{-1} d\,(2d+1),\\
&d = \frac{2x_b}{c} - 1, \qquad Ec = c - x_b.
\end{aligned} \tag{11.65}$$

Using Lagrange's energy equations as before yields the aeroelastic equations

$$\begin{bmatrix} I_\kappa & I_{\kappa\theta} & I_{\kappa\beta} \\ I_{\kappa\theta} & I_\theta & I_{\theta\beta} \\ I_{\kappa\beta} & I_{\theta\beta} & I_\beta \end{bmatrix}\begin{Bmatrix} \ddot{\kappa} \\ \ddot{\theta} \\ \ddot{\beta} \end{Bmatrix} + \rho V \begin{bmatrix} \dfrac{cs^3 a_{\mathrm{W}}}{6} & 0 & 0 \\ -\dfrac{cs^2 b_{\mathrm{W}}}{4} & \dfrac{-c^2 M_{\dot{\theta}}}{8} & 0 \\ -\dfrac{cs^2 c_{\mathrm{W}}}{4} & 0 & \dfrac{-c^2 M_{\dot{\beta}}}{8} \end{bmatrix}\begin{Bmatrix} \dot{\kappa} \\ \dot{\theta} \\ \dot{\beta} \end{Bmatrix}$$

$$+ \left(\rho V^2 \begin{bmatrix} 0 & \dfrac{cs^2 a_{\mathrm{W}}}{4} & \dfrac{cs^2 a_{\mathrm{C}}}{4} \\ 0 & -\dfrac{csb_{\mathrm{W}}}{2} & -\dfrac{csb_{\mathrm{C}}}{2} \\ 0 & -\dfrac{csc_{\mathrm{W}}}{2} & -\dfrac{csc_{\mathrm{C}}}{2} \end{bmatrix} + \begin{bmatrix} K_\kappa & 0 & 0 \\ 0 & K_\theta & 0 \\ 0 & 0 & K_\beta \end{bmatrix}\right)\begin{Bmatrix} \kappa \\ \theta \\ \beta \end{Bmatrix} = \begin{Bmatrix} 0 \\ 0 \\ 0 \end{Bmatrix}. \tag{11.66}$$

The flutter behaviour of this system depends upon the interaction of the wing flap, pitch and control rotation motions. In practice, the control stiffness will be low if a mechanical linkage is employed and high if a hydraulic power control unit is used.

The frequency and damping ratio trends in Figure 11.20 show sample characteristics of the three-mode system and it can be seen for the parameters chosen that flutter occurs due to an interaction

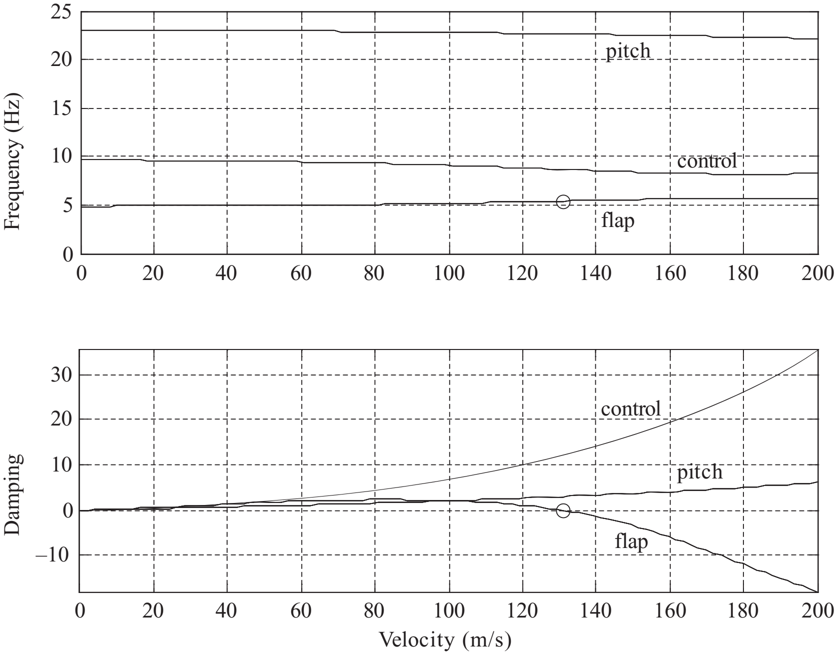

Figure 11.20 Sample wing and control surface frequency and damping ratio trends.

between the flap mode and the control surface rotation. It would also be possible for flutter to occur due to pitch/control rotation coupling, and if a larger value of control stiffness is used, the dominant flutter mechanism would be wing flap/pitch.

The key approach used classically to eliminate control surface flutter is to add extra mass to the control surface in order to change the inertia characteristics (so-called ‘mass balancing’). The use of a ‘horn balance’ to move the control surface centre of mass on to the hinge line is sometimes seen on aircraft control surfaces. In terms of the model above, adding extra mass on the control surface will affect the I_β, $I_{\theta\beta}$ and $I_{\kappa\beta}$ terms. However, whereas adding mass can improve the critical speed of one flutter mechanism, if too great a mass is added it is possible for a different flutter mechanism to occur instead. An alternative way to delay the onset of control surface flutter is to increase the control stiffness.

11.13 WHOLE AIRCRAFT MODEL – INCLUSION OF RIGID BODY MODES

In this chapter, the behaviour of a simple ‘wing-alone’ has been considered, either with a hinged or built-in root; the equations were derived in terms of displacements and/or rotations relative to inertial axes. Historically, flutter calculations were often performed for individual lifting surfaces built in at their root because the natural frequencies were significantly higher than the rigid body frequencies and the aim was for the calculation to be kept at a low model order. However, in recent years it has been normal practice to carry out whole aircraft flutter calculations including both flexible and rigid body modes since computational power is now much greater and rigid body and flexible mode frequencies are often sufficiently close for coupling terms to be relevant and for the flutter behaviour to be influenced somewhat by the rigid body modes. The flutter analysis presented in this chapter can readily be extended to include rigid body modes if desired.

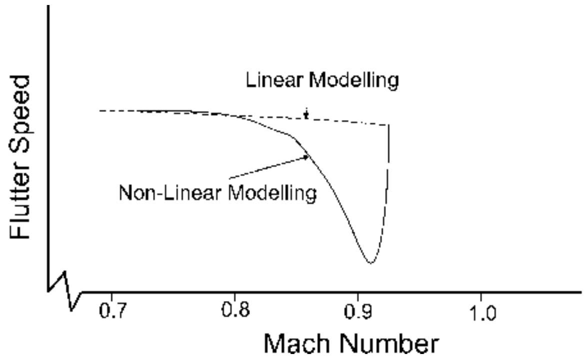

Figure 11.21 Typical flutter speed behaviour in a transonic regime.

In the later chapters on loads, examples of simple models with both rigid body and flexible modes are presented. The inertial axes representation is employed for the equilibrium manoeuvre, gusts and ground loads (see Chapters 13, 16 and 17) whereas the body fixed axes (or so-called flight mechanics) model is used for dynamic manoeuvres (see Chapters 14 and 15). This flight mechanics model with flexible effects included is also used to assess the impact of flexibility upon the aircraft handling, but could also provide another view of any particular flutter mechanism encountered where rigid body effects were important. The inclusion of unsteady aerodynamic effects on the rigid body and flexible modes is considered in Chapter 19.

11.14 FLUTTER IN THE TRANSONIC REGIME

One major limitation with strip theory and panel method aerodynamics (see Chapters 19 and 20) is that they are unable to predict the occurrence of shock waves in the transonic flight regime. A consequence of this is that the prediction of the corresponding flutter boundaries can become inaccurate. Figure 11.21 shows a typical plot of flutter speed versus Mach number, and it can be seen that in the transonic region there is a dramatic reduction in the flutter speed for certain flow conditions. This is known as the 'transonic dip' (or 'flutter bucket') and this cannot be predicted accurately using linear aerodynamic methods; either Euler or Navier–Stokes CFD aerodynamic modelling techniques must be used, coupled with a structural model. It is, however, possible to determine corrections to panel method aerodynamic influence coefficients (AICs) using wind tunnel test or CFD data where transonic effects can be incorporated (see Part III).

11.15 FLUTTER IN THE SUPERSONIC REGIME – WING AND PANEL FLUTTER

Aircraft operating at supersonic speeds have to be cleared for flutter in a similar manner as for those flying at subsonic speeds. For high aspect ratio wings the aerodynamic centre acts at the mid-chord; a similar analysis to that for subsonic flow could be performed. However, aircraft operating at supersonic speeds tend to have delta wings and it is appropriate to use more advanced aerodynamic models such as the Mach "Box" approach.

An aeroelastic phenomenon that occurs solely in supersonic flight is panel flutter. This is characterized by an unstable out-of-plane motion of an aircraft panel, limited in amplitude by nonlinear effects.

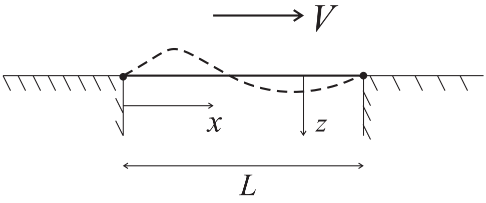

Figure 11.22 Flexible panel subjected to supersonic flow.

Panel flutter can cause unwanted vibrations that can lead to fatigue problems. In supersonic flight, the panels are also subjected to surface heating from the airflow, which tends to cause compressive stresses in the panels.

This section uses a simple two-dimensional model to illustrate the mechanism underlying panel flutter, making use of the piston theory aerodynamics (Dowell *et al.*, 1995) introduced in Chapter 5.

11.15.1 Model of a Panel in Supersonic Flow

Consider the panel of length L, width h, mass per unit length μ and flexural rigidity EI, subjected to a supersonic flow parallel to the surface of speed V, Mach number M and air density ρ. The panel is simply supported at $x = 0, L$ but free along the edges parallel to the x axis, as shown in Figure 11.22.

Assume that the out-of-plane displacement of the panel takes the form (see Chapter 3)

$$z(x,t) = \sin\left(\frac{\pi x}{L}\right) q_1(t) + \sin\left(\frac{2\pi x}{L}\right) q_2(t), \tag{11.67}$$

where each of the sinusoidal shapes satisfies the boundary conditions. From piston theory (Dowell *et al.*, 1995; see Chapter 5), the pressure acting upon an element of the panel for deflection z is given by

$$P = \frac{\rho V^2}{M}\frac{\mathrm{d}z}{\mathrm{d}x} = \frac{\rho V^2}{M}\left[\frac{\pi}{L}\cos\left(\frac{\pi x}{L}\right) q_1 + \frac{2\pi}{L}\cos\left(\frac{2\pi x}{L}\right) q_2\right], \tag{11.68}$$

where M is the Mach number. The panel velocity term, which would add aerodynamic damping, has been neglected.

Once again Lagrange's equations will be used. The kinetic energy for the entire panel is given by the expression

$$T = \frac{1}{2}\int_0^L \mu\left(\sin\left(\frac{\pi x}{L}\right)\dot{q}_1 + \sin\left(\frac{2\pi x}{L}\right)\dot{q}_2\right)^2 \mathrm{d}x. \tag{11.69}$$

The potential (or strain) energy is

$$U = \frac{1}{2}\int_0^L EI\left(\frac{\partial^2 z}{\partial x^2}\right)^2 \mathrm{d}x = \frac{1}{2}\int_0^L EI\left(-\frac{\pi^2}{L^2}\sin\left(\frac{\pi x}{L}\right) q_1 - \frac{4\pi^2}{L^2}\sin\left(\frac{2\pi x}{L}\right) q_2\right)^2 \mathrm{d}x. \tag{11.70}$$

Finally, the incremental work done by the aerodynamic force acting upon the panel (+ve downwards) is given by

$$\delta W = \int_0^L \frac{\rho V^2}{M}\left(\frac{\pi}{L}\cos\left(\frac{\pi x}{L}\right) q_1 + \frac{2\pi}{L}\cos\left(\frac{2\pi x}{L}\right) q_2\right)\left(\sin\left(\frac{\pi x}{L}\right)\delta q_1 + \sin\left(\frac{2\pi x}{L}\right)\delta q_2\right) h\,\mathrm{d}x, \tag{11.71}$$

so the generalized aerodynamic forces are given by

$$\begin{aligned}\frac{\partial(\delta W)}{\partial(\delta q_1)} &= \int_0^L \frac{\rho V^2}{M}\left(\frac{\pi}{L}\cos\left(\frac{\pi x}{L}\right)q_1 + \frac{2\pi}{L}\cos\left(\frac{2\pi x}{L}\right)q_2\right)\sin\left(\frac{\pi x}{L}\right)h\,\mathrm{d}x = -\frac{4\rho V^2 h}{3M}q_2,\\ \frac{\partial(\delta W)}{\partial(\delta q_2)} &= \int_0^L \frac{\rho V^2}{M}\left(\frac{\pi}{L}\cos\left(\frac{\pi x}{L}\right)q_1 + \frac{2\pi}{L}\cos\left(\frac{2\pi x}{L}\right)q_2\right)\sin\left(\frac{2\pi x}{L}\right)h\,\mathrm{d}x = \frac{4\rho V^2 h}{3M}q_1.\end{aligned} \tag{11.72}$$

Applying Lagrange's equations (see Chapter 3 for a similar example) gives

$$\begin{bmatrix} \frac{\mu L}{2} & 0 \\ 0 & \frac{\mu L}{2} \end{bmatrix} \begin{Bmatrix} \ddot{q}_1 \\ \ddot{q}_2 \end{Bmatrix} + \begin{bmatrix} \frac{EI\pi^4}{2L^3} & -\frac{4\rho V^2 h}{3M} \\ \frac{4\rho V^2 h}{3M} & \frac{8EI\pi^4}{L^3} \end{bmatrix} \begin{Bmatrix} q_1 \\ q_2 \end{Bmatrix} = \begin{Bmatrix} 0 \\ 0 \end{Bmatrix}, \tag{11.73}$$

which can be seen to be in the form of a vibrating system with no damping. However, the stiffness matrix is skew-symmetric, with the off-diagonal terms defined by the aerodynamics.

Assuming a solution of the form $\boldsymbol{q} = \boldsymbol{q}_0 \sin\omega t$ leads to a non-trivial solution (see Chapter 2) given by

$$\begin{vmatrix} (-\omega^2 + A) & -B \\ B & (-\omega^2 + 16A) \end{vmatrix} = 0 \quad \text{where} \quad A = \frac{\pi^4 EI}{\mu L^4} \quad \text{and} \quad B = \frac{8\rho V^2 h}{3M\mu L}. \tag{11.74}$$

Solving the resulting quadratic equation in ω^2 then gives an expression for the frequencies at which undamped oscillations can occur in the presence of a supersonic air flow, such that

$$\omega^2 = \frac{17A}{2} \pm \frac{\sqrt{289A^2 - 4(16A^2 + B^2)}}{2}. \tag{11.75}$$

The critical condition is reached when the two frequency solutions are the same (there is no aerodynamic damping); thus the critical frequency and speed condition for the panel are defined as

$$\omega = \sqrt{\frac{17A}{2}} \quad \text{and} \quad 225A^2 - 4B^2 = 0 \quad \Rightarrow \quad V_{\text{crit}} = \sqrt{\frac{45\pi^4 MEI}{16\rho L^3 h}}. \tag{11.76}$$

Finally, the critical mode shape is found from the solution of Equation (11.73) and so

$$\left(-\frac{17A}{2} + A\right)q_1 = Bq_2 \qquad \Rightarrow \qquad \frac{q_2}{q_1} = -1 \tag{11.77}$$

and this ratio may be converted into a physical shape. Figure 11.23 shows the critical flutter mode shape

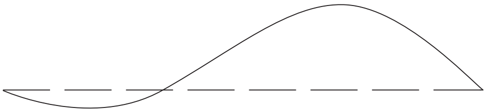

Figure 11.23 Critical mode shape for a panel flutter.

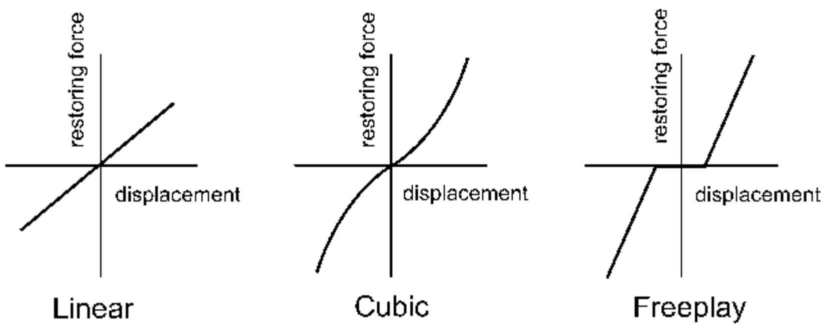

Figure 11.24 Typical structural nonlinearities.

11.16 EFFECT OF NONLINEARITIES – LIMIT CYCLE OSCILLATIONS

All of the aeroelastic modelling that has been considered so far in this book has made the assumption of linearity; the structural deflections are small, the aerodynamic forces are linearly proportional to the response and the control system elements respond linearly with amplitude. In practice, nonlinearities can be present in an aeroelastic system (Dowell *et al.*, 2003) via structural, aerodynamic and control system phenomena. These nonlinearities affect the aeroelastic behaviour and cannot be predicted using linear analysis methods.

Structural nonlinearities occur primarily as nonuniform stiffness effects, including cubic stiffening root attachments of engine pylons, bilinear stiffness of structural joints and freeplay of control surface attachments. Figure 11.24 shows some typical restoring force versus displacement plots for different stiffness nonlinearities. Very flexible aircraft exhibit geometric stiffness nonlinearities due to the large deflections that can occur.

Aerodynamic nonlinearities occur primarily in the transonic flight regime, where shock waves are present upon the wing or control surfaces, and the position of the shock waves changes in response to motion of the wings; the interaction of control surfaces with shock waves is sometimes referred to as 'buzz'. A further aerodynamic nonlinearity is 'stall flutter' when stall occurs at the wing tips and lift is lost on the outer part of the wing.

Control nonlinearities include control surface deflection and rate limits where the control surfaces cannot respond in the manner that is required by control laws. Also, the control surface actuation mechanism tends to be nonlinear as well as the control laws that are used. The use of nonlinear, or multiple, control laws and time delays in their application also leads to nonlinear aeroelastic behaviour.

The main nonlinear aeroelastic response phenomena are limit cycle oscillations (LCOs) which can be considered as bounded flutter and an example of which is shown in Figure 11.25. Sometimes this is referred to as nonlinear flutter. If an aeroelastic system is considered that includes the cubic stiffness shown in Figure 11.24, then at some air speed, depending upon the stiffness at zero deflection, flutter will start to occur and an unstable motion results. However, as the deflections get larger, the stiffness

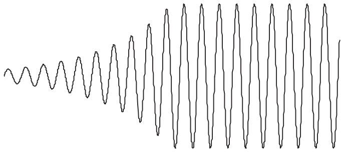

Figure 11.25 Typical limit cycle oscillation.

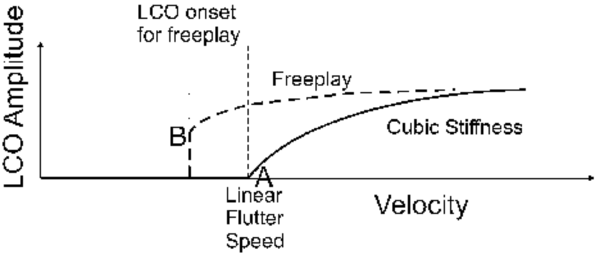

Figure 11.26 Typical limit cycle amplitude versus speed behaviour.

will become greater and the motion will be limited. In some cases the LCOs are made up of multiple sinusoids.

Figure 11.26 shows a typical steady-state LCO amplitude versus speed plot, where it can be seen that below the linear flutter speed the response of the system containing a cubic stiffness following some initial input decays to zero. Beyond the linear flutter speed at point A, an LCO develops and its amplitude grows with speed until finally flutter occurs. Such a response occurs for most of the nonlinearities described above. One exception is the freeplay nonlinearity where, at some critical speed below the linear flutter speed, a limit cycle suddenly occurs with a jump to point B. Much research is currently being undertaken to investigate accurate and efficient ways of predicting LCOs, including nonlinear FE and aerodynamic models.

11.17 EXAMPLES

1. Using the MATLAB code given in Appendix H in the companion website, generate $V\omega$ and Vg plots for the binary flutter system and explore the effect of the following on the aeroelastic behaviour:
   (a) Effect of ratio and spacing between wind-off torsion and bending natural frequencies.
   (b) Effect of position of flexural and mass axes.
   (c) Inclusion of structural damping.
   (d) Altitude and hence plot Mach number vs. speed at flutter.
2. Using the MATLAB code given in Appendix H, examine the effect of the above parameters on the shape of the flutter conic.
3. Develop a MATLAB code to determine the aeroelastic behaviour of the assumed mode representation described in Section 11.6 and explore the effect of including more modes in the mathematical model. Take $EI = 10^6$ N m^2, $GJ = 10^6$ N m^2, $c = 1.5$ m and $s = 7$ m.
4. A wing bending–torsion system (in SI units) is described in terms of coordinates q_1 and q_2 as

$$\begin{bmatrix} 14D^2 + 6VD + \sigma - 6V^2 & -2D^2 + VD + V^2 \\ -2D^2 - 2VD - 5V^2 & D^2 + VD + V^2 \end{bmatrix} \begin{bmatrix} q_1 \\ q_2 \end{bmatrix} = \begin{bmatrix} 0 \\ 0 \end{bmatrix},$$

   where $D = \mathrm{d}/\mathrm{d}t$ and $\sigma = 1 \times 10^5$ N/rad. Determine the critical flutter speeds and corresponding frequencies using the Routh–Hurwitz approach and the flutter conic.

   [73.35 m/s 13.92 Hz, 132.89 m/s 17.74 Hz]
5. A wing bending–torsion system (in SI units) is modelled in terms of coordinates α and θ:

$$\begin{aligned} 12\ddot{\alpha} + 6V\dot{\alpha} + \left(4 \times 10^5 - 9V^2\right)\alpha + 3V\dot{\theta} + 3V^2\theta = 0, \\ -3V^2\alpha + \ddot{\theta} + V\dot{\theta} + V^2\theta = 0. \end{aligned}$$

Determine the critical flutter speeds and corresponding frequencies using the Routh–Hurwitz approach and the flutter conic.

[115.5 m/s 26 Hz, 365 m/s 41 Hz]

6. A binary aeroelastic system (in SI units) takes the form

$$\begin{pmatrix} 130 & 0 \\ 0 & 10 \end{pmatrix}\begin{pmatrix} \ddot{\theta} \\ \ddot{\gamma} \end{pmatrix} + \begin{pmatrix} 6V & 0 \\ -3V & V \end{pmatrix}\begin{pmatrix} \dot{\theta} \\ \dot{\gamma} \end{pmatrix} + \begin{pmatrix} k & 3V^2 \\ 0 & 2k-3V^2 \end{pmatrix}\begin{pmatrix} \theta \\ \gamma \end{pmatrix} = \begin{pmatrix} 0 \\ 0 \end{pmatrix}$$

Find the stiffness value k that gives a critical flutter speed of $V = 250$ m/s and the corresponding flutter frequency. Also find the divergence speed. Confirm these estimates using the flutter conic.

[1.173×10^5 N/m, 11.33 Hz, 279.6 m/s]

7. A binary aeroelastic system (in SI units) takes the form

$$\begin{pmatrix} 120 & 0 \\ 0 & 9 \end{pmatrix}\begin{pmatrix} \ddot{\theta} \\ \ddot{\gamma} \end{pmatrix} + \begin{pmatrix} 6V & 0 \\ -3V & V \end{pmatrix}\begin{pmatrix} \dot{\theta} \\ \dot{\gamma} \end{pmatrix} + \begin{pmatrix} k_1 & 4V^2 \\ 0 & k_2-3V^2 \end{pmatrix}\begin{pmatrix} \theta \\ \gamma \end{pmatrix} = \begin{pmatrix} 0 \\ 0 \end{pmatrix},$$

where $k_1 = 5 \times 10^4$ Nm/rad and $k_2 = 7 \times 10^4$ Nm/rad. Determine the critical flutter speeds and corresponding frequencies using the Routh–Hurwitz and flutter conic approaches. Also, obtain the divergence speed.

[256.8 m/s, 3.29 Hz; 131.9 m/s, 7.30 Hz; 152.8 m/s]

8. The aircraft panel shown in Figure 11.27 (after Dowell *et al.*, 2004) is subjected to a supersonic flow of speed V along its surface. The panel consists of three rigid plates of length L and mass M or $2M$, hinged at each end, and attached to springs of stiffness K and $2K$, as shown in the figure. Making use of piston theory determine the speed at which panel flutter occurs and the shape of the flutter mode in terms of the spring deflections.

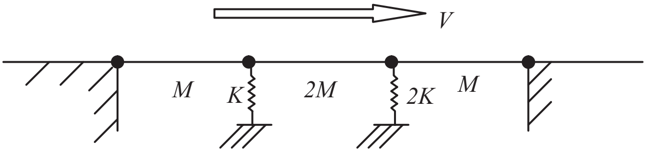

Figure 11.27

12

Aeroservoelasticity

The science of aeroservoelasticity (ASE) extends the aeroelastic interactions between aerodynamic forces and a flexible structure, discussed in Chapters 8, 9 and 11, to include a control system, introduced in Chapter 7. The classic Collar aeroelastic triangle can be extended to form the aeroservoelastic pyramid shown in Figure 12.1, where there are now forces resulting from the control system as well as the aerodynamic, elastic and inertial forces. ASE effects (Zimmermann, 1991; Pratt, 2000; Librescu, 2005) are becoming of increasing importance in modern aircraft design as it is usual nowadays to employ some form of flight control system (FCS) (Pratt, 2000; see also Chapter 14) to improve the handling and stability, flight performance and ride quality throughout the flight envelope, and also to reduce loads and improve service life. For commercial aircraft, the FCS might include a gust and/or manoeuvre load alleviation system in addition to a control system that meets the basic handling requirements. Modern military aircraft are often designed for carefree handling and the ability to fly with reduced, or unstable, open loop static stability so as to improve their manoeuvrability; however, they can only stay airborne through the use of the FCS. All control implementations involve the use of sensors, usually accelerometers and rate gyros placed at the aircraft centre of mass and air data sensors (e.g. angle of incidence, air speed). Some form of control input (defined by a control law; see Chapter 7) is then applied via the control surfaces. It is feasible to develop flutter suppression systems that enable aircraft to fly beyond the flutter speed; however, such an approach has a very high risk and so far has only been demonstrated on wind tunnel models.

ASE effects, sometimes referred to as ‘structural coupling’, can potentially cause a major structural failure due to flutter involving coupling of the aeroelastic and control systems. However, there is also the possibility of causing fatigue damage and reducing control surface actuator performance. Most structural coupling problems occur when the motion sensors detect not only the aircraft rigid body motion but also the motion in the flexible modes, and these vibrations are fed back into the FCS. In this case, the movement of the control surfaces is then likely to excite the flexible modes, so causing the aircraft to vibrate further. Notch filters are often used to remedy this problem by introducing significant attenuation of the response in the region of critical frequencies.

In this chapter, the use of feedback control on a simple binary aeroelastic system with a control surface is considered and the effects of the control law on the stability and response investigated. A simple PI controller (see Chapter 7) is used to demonstrate how the gust response can be reduced and the flutter speed increased. Modelling of ASE systems in the time or frequency domain is also considered, including representation of reduced frequency-dependent aerodynamics and control effects along with the use of state space models. A number of MATLAB codes related to this chapter are included in appendix H in the companion website.

Introduction to Aircraft Aeroelasticity and Loads J. R. Wright and J. E. Cooper
© 2007 John Wiley & Sons, Ltd

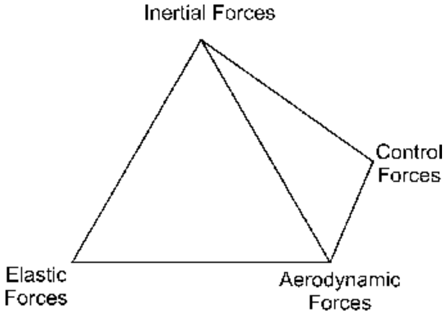

Figure 12.1 Aeroservoelastic pyramid.

12.1 MATHEMATICAL MODELLING OF A SIMPLE AEROELASTIC SYSTEM WITH A CONTROL SURFACE

Consider the binary aeroelastic model examined for its flutter behaviour in Chapter 11; it is composed of a uniform rigid rectangular wing with pitch θ and flap κ degrees of freedom introduced via two springs at the root. As can be seen in Figure 12.2, a full span rigid control surface is now included. It has an infinite stiffness attachment to the wing but can be moved to any angle β that is demanded. The inertial effects of the control surface are ignored. Thus the control surface is not involved in the basic dynamics of the wing but simply acts as an excitation device.

The lift and pitching moment acting upon an elemental strip of wing can be written using the same assumptions and notation as considered before in Chapters 5 and 11, with the $M_{\dot{\theta}}$ term being included to allow for simple unsteady aerodynamic effects on the aerofoil, such that

$$\mathrm{d}L = \frac{1}{2}\rho V^2 c\mathrm{d}y\left[a_{\mathrm{W}}\left(\theta + \frac{y\dot{\kappa}}{V}\right) + a_{\mathrm{C}}\beta\right] \quad \text{and} \quad \mathrm{d}M = \frac{1}{2}\rho V^2 c^2 \mathrm{d}y\left[ea_{\mathrm{W}}\left(\theta + \frac{y\dot{\kappa}}{V}\right) + M_{\dot{\theta}}\frac{\dot{\theta}c}{4V} + b_{\mathrm{C}}\beta\right], \tag{12.1}$$

where there are now lift and moment components due to the application of the control surface through angle β (Fung, 1969), as shown in Chapters 5 and 11.

Evaluation of Lagrange's equations across the entire semi-span of the wing (as in Chapter 11) and adding in the prescribed motion of the control surface gives the expression for the open loop system

$$\begin{bmatrix} I_\kappa & I_{\kappa\theta} \\ I_{\kappa\theta} & I_\theta \end{bmatrix}\begin{Bmatrix} \ddot{\kappa} \\ \ddot{\theta} \end{Bmatrix} + \rho V \begin{bmatrix} \dfrac{cs^3 a_{\mathrm{W}}}{6} & 0 \\ -\dfrac{ec^2 s^2 a_{\mathrm{W}}}{4} & -\dfrac{c^3 s}{8}M_{\dot{\theta}} \end{bmatrix}\begin{Bmatrix} \dot{\kappa} \\ \dot{\theta} \end{Bmatrix} + \left(\rho V^2 \begin{bmatrix} 0 & \dfrac{cs^2 a_{\mathrm{W}}}{4} \\ 0 & -\dfrac{ec^2 s a_{\mathrm{W}}}{2} \end{bmatrix} + \begin{bmatrix} K_\kappa & 0 \\ 0 & K_\theta \end{bmatrix}\right)\begin{Bmatrix} \kappa \\ \theta \end{Bmatrix}$$
$$= \rho V^2 cs \begin{Bmatrix} -\frac{sa_{\mathrm{C}}}{4} \\ \frac{cb_{\mathrm{C}}}{2} \end{Bmatrix}\beta. \tag{12.2}$$

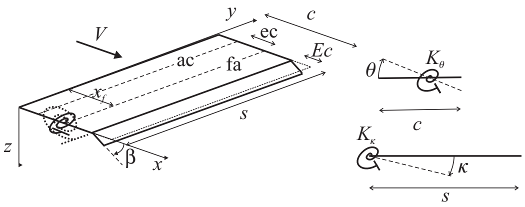

Figure 12.2 Binary flutter system with a control surface.

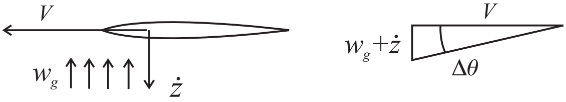

Figure 12.3 Effective angle of incidence due to the vertical gust.

It can be seen that there is now a forcing term on the right-hand side of the equations due to the control surface deflection. Equation (12.2) can be written more compactly in the form

$$\mathbf{A}\ddot{\boldsymbol{q}} + \rho V \mathbf{B}\dot{\boldsymbol{q}} + \left(\rho V^2 \mathbf{C} + \mathbf{E}\right)\boldsymbol{q} = \boldsymbol{g}\beta, \tag{12.3}$$

where for convenience the term ρV^2 is embedded in the excitation vector $\boldsymbol{g}$. Then, using the approach of Chapter 2, a harmonic excitation $\beta = \beta_0 \mathrm{e}^{\mathrm{i}\omega t}$ and response $\boldsymbol{q} = \boldsymbol{q}_0 \mathrm{e}^{\mathrm{i}\omega t}$ lead to the frequency response function between the response degrees of freedom and the control surface rotation. A frequency domain approach may then be used to determine the response of the system due to the input of the control system at any point in the flight envelope. Alternatively, an approach based on time domain numerical integration could be employed for any general excitation input.

For the complete aircraft, the free–free rigid body and flexible modes need to be incorporated, together with the basic FCS. Although some explanation of the FCS model is given in Chapters 14 and 22, and the importance of the FCS emphasized elsewhere, a detailed consideration of the FCS is beyond the scope of this book.

12.2 INCLUSION OF GUST TERMS

The effect of gusts and turbulence will be considered in much greater detail in Chapter 16. However, it is useful here to include the effect of a uniform vertical gust of velocity w_{g} encountered along the whole span of the wing in order to provide a disturbance to the wing (this simplified approach contains a number of assumptions). Figure 12.3 shows that a gust gives rise to an effective instantaneous change of incidence $\Delta\theta$ of

$$\Delta\theta = \frac{w_{\mathrm{g}} + \dot{z}}{V}. \tag{12.4}$$

Thus there is an extra lift term due to the gust velocity, together with that from the vertical velocity term and the incidence due to pitch already considered. The lift and pitching moment of an elemental streamwise strip on the wing now become

$$\begin{aligned} \mathrm{d}L &= \frac{1}{2}\rho V^2 c\,\mathrm{d}y \left[a_{\mathrm{W}} \left(\theta + \frac{w_{\mathrm{g}}}{V} + \frac{y\dot{\kappa}}{V} \right) + a_{\mathrm{C}}\beta \right], \\ \mathrm{d}M &= \frac{1}{2}\rho V^2 c^2 \mathrm{d}y \left[e a_{\mathrm{W}} \left(\theta + \frac{w_{\mathrm{g}}}{V} + \frac{y\dot{\kappa}}{V} \right) + M_{\dot{\theta}} \frac{\dot{\theta} c}{4V} + b_{\mathrm{C}}\beta \right], \end{aligned} \tag{12.5}$$

and hence the open loop equations of motion are found as

$$\begin{bmatrix} I_\kappa & I_{\kappa\theta} \\ I_{\kappa\theta} & I_\theta \end{bmatrix} \begin{Bmatrix} \ddot{\kappa} \\ \ddot{\theta} \end{Bmatrix} + \rho V \begin{bmatrix} \dfrac{cs^3 a_{\mathrm{W}}}{6} & 0 \\ -\dfrac{c^2 s^2 e a_{\mathrm{W}}}{4} & -\dfrac{c^3 s}{8} M_{\dot{\theta}} \end{bmatrix} \begin{Bmatrix} \dot{\kappa} \\ \dot{\theta} \end{Bmatrix} + \left(\rho V^2 \begin{bmatrix} 0 & \dfrac{cs^2 a_{\mathrm{W}}}{4} \\ 0 & -\dfrac{c^2 s e a_{\mathrm{W}}}{2} \end{bmatrix} + \begin{bmatrix} K_\kappa & 0 \\ 0 & K_\theta \end{bmatrix} \right) \begin{Bmatrix} \kappa \\ \theta \end{Bmatrix}$$

$$= \rho V^2 cs \begin{Bmatrix} -\dfrac{s a_{\mathrm{C}}}{4} \\ \dfrac{c b_{\mathrm{C}}}{2} \end{Bmatrix} \beta + \rho V cs \begin{Bmatrix} \dfrac{s}{4} \\ \dfrac{c}{2} \end{Bmatrix} w_{\mathrm{g}} = \begin{Bmatrix} g_1 \\ g_2 \end{Bmatrix} \beta + \begin{Bmatrix} h_1 \\ h_2 \end{Bmatrix} w_{\mathrm{g}}, \tag{12.6}$$

or in a general form,

$$\mathbf{A}\ddot{\boldsymbol{q}} + \rho V \mathbf{B}\dot{\boldsymbol{q}} + \left(\rho V^2 \mathbf{C} + \mathbf{E}\right)\boldsymbol{q} = \boldsymbol{g}\beta + \boldsymbol{h}w_{\mathrm{g}}. \tag{12.7}$$

Again, for convenience, the term ρV is embedded in the gust excitation vector $\boldsymbol{h}$. Now the gust disturbance term is seen to appear on the right-hand side of the equations together with the control surface input. Clearly, the response due to a known gust time history may now be calculated.

12.3 IMPLEMENTATION OF A CONTROL SYSTEM

One of the simplest forms of control system is the PI approach (see Chapter 7), and when implemented here the control surface demand angle is linearly proportional to the velocity and displacement of the system. For simplicity, consider that there is a transducer at the wing leading edge a distance s_0 from the root, and the control surface deflection is taken as being proportional to its displacement and velocity such that

$$\begin{aligned}\beta &= K_{\mathrm{v}}\dot{z}_{\mathrm{wing}} + K_{\mathrm{d}}z_{\mathrm{wing}} = K_{\mathrm{v}}\left(\dot{\kappa}s_0 - \dot{\theta}\frac{c}{2}\right) + K_{\mathrm{d}}\left(\kappa s_0 - \theta\frac{c}{2}\right)\\ &= K_{\mathrm{v}}\begin{Bmatrix} s_0 & -\dfrac{c}{2}\end{Bmatrix}\begin{Bmatrix}\dot{\kappa}\\ \dot{\theta}\end{Bmatrix} + K_{\mathrm{d}}\begin{Bmatrix} s_0 & -\dfrac{c}{2}\end{Bmatrix}\begin{Bmatrix}\kappa\\ \theta\end{Bmatrix},\end{aligned} \tag{12.8}$$

where K_{v} and K_{d} are weightings (commonly called feedback 'gains'; see Chapter 7) applied to the velocity and displacement terms respectively. Thus the aircraft response is fed back via the control surface to modify the aircraft characteristics. This mathematical model of the wing with gust and control input, modified by the feedback law, can be represented by the block diagram shown in Figure 12.4, where the system is generalized to that of an aircraft (not just a wing) (see also Chapters 14 and 22).

12.4 DETERMINATION OF CLOSED LOOP SYSTEM STABILITY

In order to examine the stability of the closed loop system, the feedback law in Equation (12.8) must be combined with the basic wing equations in (12.3). Thus, the closed loop equations of motion (12.3) of the wing plus control surface (but in the absence of a gust disturbance) becomes

$$\begin{aligned}\mathbf{A}\ddot{\boldsymbol{q}} + \rho V \mathbf{B}\dot{\boldsymbol{q}} + \left(\rho V^2 \mathbf{C} + \mathbf{E}\right)\boldsymbol{q} &= \boldsymbol{g}\beta = K_{\mathrm{v}}\begin{Bmatrix} g_1\\ g_2\end{Bmatrix}\begin{Bmatrix} s_0 & -\dfrac{c}{2}\end{Bmatrix}\begin{Bmatrix}\dot{\kappa}\\ \dot{\theta}\end{Bmatrix} + K_{\mathrm{d}}\begin{Bmatrix} g_1\\ g_2\end{Bmatrix}\begin{Bmatrix} s_0 & -\dfrac{c}{2}\end{Bmatrix}\begin{Bmatrix}\kappa\\ \theta\end{Bmatrix}\\ &= K_{\mathrm{v}}\begin{bmatrix} g_1 s_0 & -g_1 c/2\\ g_2 s_0 & -g_2 c/2\end{bmatrix}\begin{Bmatrix}\dot{\kappa}\\ \dot{\theta}\end{Bmatrix} + K_{\mathrm{d}}\begin{bmatrix} g_1 s_0 & -g_1 c/2\\ g_2 s_0 & -g_2 c/2\end{bmatrix}\begin{Bmatrix}\kappa\\ \theta\end{Bmatrix} = \mathbf{F}\dot{\boldsymbol{q}} + \mathbf{G}\boldsymbol{q},\end{aligned} \tag{12.9}$$

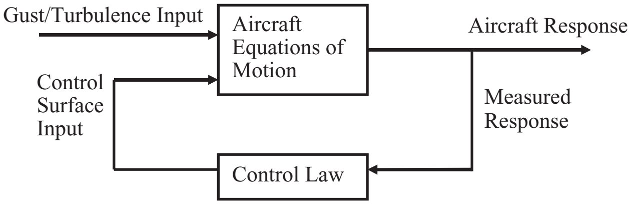

Figure 12.4 Block diagram of an aeroservoelastic system.

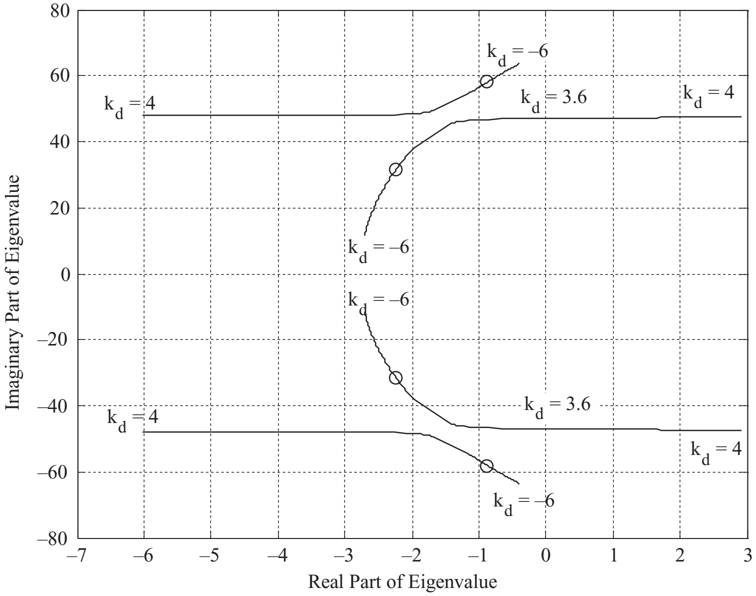

Figure 12.5 System eigenvalues for varying control system gain.

where **F**, **G** are composite feedback matrices with coefficients that are a function of the control gains, density and air speed. This equation can be rearranged as

$$\mathbf{A}\ddot{\boldsymbol{q}} + (\rho V\mathbf{B} - \mathbf{F})\dot{\boldsymbol{q}} + \left(\rho V^2\mathbf{C} + \mathbf{E} - \mathbf{G}\right)\boldsymbol{q} = \mathbf{0} \tag{12.10}$$

and the closed loop system can now be solved to examine its stability. Clearly, the dynamics of the system have now been altered since there are extra stiffness and damping matrices present due to the control system, and this will affect the aeroelastic behaviour including the flutter speed. Equation (12.10) is still in the same general form of the aeroelastic equations and the analysis can be carried out in exactly the same way as in Chapter 11 on flutter, determining the natural frequencies and damping ratios at different flight conditions for different combinations of constant feedback gains $K_{\mathrm{v}},\ K_{\mathrm{d}}$.

The effect of using gain K_{d} alone ($K_{\mathrm{v}} = 0$) for the baseline binary aeroelastic system can be seen in Figures 12.5 and 12.6. In Figure 12.5 the changes in the system eigenvalues are plotted for $-6 < K_{\mathrm{d}} < 4$ at an air speed of 100 m/s. The circles indicate the open loop system characteristics (i.e. $K_{\mathrm{d}} = 0$), and it can be seen that when $\mathrm{K_d}$ reaches 3.6 the system becomes unstable (i.e. a root enters the positive right-hand plane; see Chapter 7). The effect on the flutter speed of changing the gain is shown Figure 12.6, and it can be seen how the flutter speed can be increased or decreased from the open loop value of 154 m/s by changing the gain.

12.5 GUST RESPONSE OF THE CLOSED LOOP SYSTEM

Inclusion of the gust excitation terms on the right-hand side of Equation (12.10) for the closed loop system gives

$$\mathbf{A}\ddot{\boldsymbol{q}} + (\rho V\mathbf{B} - \mathbf{F})\dot{\boldsymbol{q}} + \left(\rho V^2\mathbf{C} + \mathbf{E} - \mathbf{G}\right)\boldsymbol{q} = \boldsymbol{h}w_{\mathrm{g}}, \tag{12.11}$$

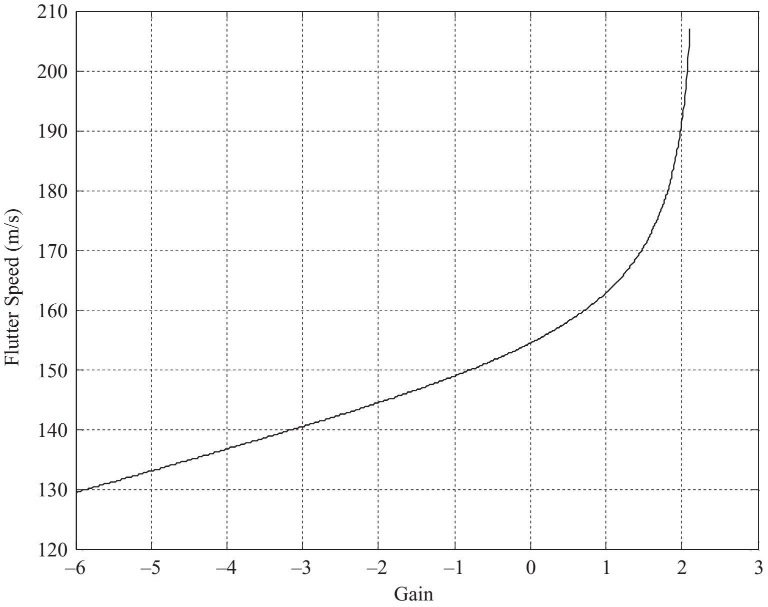

Figure 12.6 Effect of gain K_d on flutter speed.

from which the response of the system to gusts with the inclusion of the feedback control can be calculated. Having determined the responses, the required control angle deflection can be found using Equation (12.8).

Figure 12.7 shows the leading edge tip displacement of the wing for a rapid '1-cosine' gust input to the open loop system and also to the closed loop system employing a different control law ($K_v = -0.01$). The control surface demand angle, determined from Equation (12.8) using the model response, is also shown with the control law applied. It can be seen that the control can be used to reduce the time that it takes for the response to decay. In practice much more sophisticated control laws are used.

One problem with this implementation of control is that the control surface deflection is taken to be linearly related to the wing displacement and velocity. There will be limits to both the control deflection (e.g. $\pm 15^\circ$) and rate (e.g. 60 °/s) that can be realized. Unsteady aerodynamic effects also reduce the control surface effectiveness as the application frequency increases. In practice, more sophisticated models need to be developed to allow for the unsteady aerodynamic behaviour including reduced frequency effects.

12.6 INCLUSION OF CONTROL LAW FREQUENCY DEPENDENCY IN STABILITY CALCULATIONS

In practice, the control gains will also be frequency-dependent due to the presence of so-called 'shaping' (e.g. notch) filters, but these effects can be dealt with through the use of a frequency domain representation in a similar way to that for frequency-dependent aerodynamics (see Chapter 11).

Consider the same ASE system as above, but now with a velocity feedback gain of $K_v T(s)$, where the shaping filter $T(s)$ is frequency dependent. For example, $T(s)$ could have a simple Laplace domain representation of

$$T(s) = \frac{a}{s + a}, \tag{12.12}$$

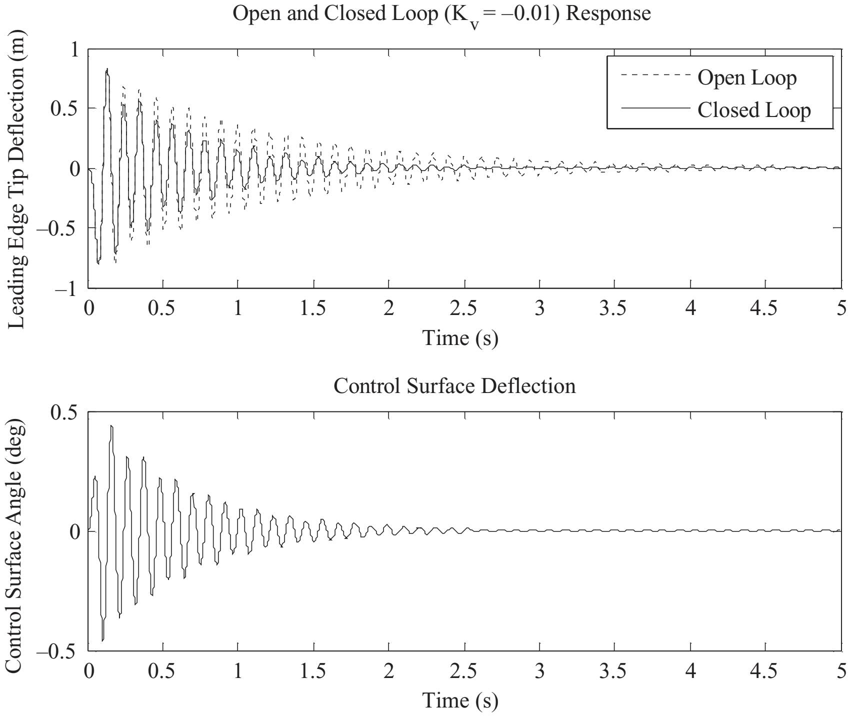

Figure 12.7 Leading edge tip response of wing to gust with/without the control law and control surface demand angle.

where a is a constant and s is the Laplace variable (see Chapter 7); this filter reduces the effective gain and introduces a phase lag as frequency increases. In order to simplify the expressions involved, consider the measurement transducer being moved to the wing elastic axis and only velocity feedback. Then the demanded control angle is given by

$$\beta = K_{\mathrm{v}} T\ \dot{z}_{\mathrm{wing}} = K_{\mathrm{v}} T\ s_0 \dot{\kappa} = K_{\mathrm{v}} T \begin{Bmatrix} s_0 & 0 \end{Bmatrix} \begin{Bmatrix} \dot{\kappa} \\ \dot{\theta} \end{Bmatrix} = K_{\mathrm{v}} T \begin{Bmatrix} s_0 & 0 \end{Bmatrix} \dot{\boldsymbol{q}}, \tag{12.13}$$

where the dependency of T on the Laplace variable s has been omitted from this time domain description for the moment. Then the time domain closed loop equations become

$$\mathbf{A}\ddot{\boldsymbol{q}} + \rho V \mathbf{B} \dot{\boldsymbol{q}} + \left(\rho V^2 \mathbf{C} + \mathbf{E}\right) \boldsymbol{q} = \boldsymbol{g} \beta = K_{\mathrm{v}} T \begin{bmatrix} g_1 s_0 & 0 \\ g_2 s_0 & 0 \end{bmatrix} \begin{Bmatrix} \dot{\kappa} \\ \dot{\theta} \end{Bmatrix} = K_{\mathrm{v}} T \mathbf{F} \dot{\boldsymbol{q}}. \tag{12.14}$$

Transformation to the frequency domain using $\boldsymbol{q} = \boldsymbol{q}_0 \mathrm{e}^{\mathrm{i}\omega t}$ and $s = \mathrm{i}\omega$ gives

$$\left\{-\omega^2 \mathbf{A} + \mathrm{i}\omega \left(\rho V \mathbf{B} - K_{\mathrm{v}} T \mathbf{F}\right) + \left(\rho V^2 \mathbf{C} + \mathbf{E}\right)\right\} \boldsymbol{q}_0 = \mathbf{0}, \tag{12.15}$$

where matrices $\mathbf{B}$, $\mathbf{C}$ are reduced frequency (k) dependent and the filter T is frequency (ω) dependent.

In Chapter 11, the reduced frequency dependency of the $\mathbf{B}$, $\mathbf{C}$ matrices was handled by seeking a matched frequency solution; this approach determined the correct aerodynamic terms at each flight condition and thus the flutter speed was determined. The presence of the shaping filter in this equation may be dealt with in exactly the same way since, for a particular reduced frequency k and air speed V, the frequency $\omega = 2kV/c$ in T will be known and the shaping filter contribution to the equation can be evaluated. More complicated control laws can be utilized using this approach as long as they can be approximated in the form shown above; nonlinear control laws must be approximated by a linear representation.

12.7 RESPONSE DETERMINATION VIA THE FREQUENCY DOMAIN

As the aerodynamic and control terms may be determined for particular reduced frequencies (or frequencies) for a given air speed, it is possible to determine the response to turbulence using a frequency domain representation (see Chapter 16 for a full explanation). Assuming that the ASE system considered above with velocity feedback control including a shaping filter behaves in a linear manner, then encountering a harmonic gust of the form $w_{\mathrm{g}} = w_{\mathrm{g}0}\mathrm{e}^{\mathrm{i}\omega t}$ results in a harmonic response $\boldsymbol{q}_0 = \boldsymbol{q}_0\mathrm{e}^{\mathrm{i}\omega t}$, and Equation (12.11) then becomes

$$\left(-\omega^2\mathbf{A} + \mathrm{i}\omega\left(\rho V\mathbf{B} - K_{\mathrm{v}}T\mathbf{F}\right) + \left(\rho V^2\mathbf{C} + \mathbf{E}\right)\right)\boldsymbol{q}_0 = \boldsymbol{h}w_{\mathrm{g}0}, \tag{12.16}$$

where $\mathbf{B}$, $\mathbf{C}$ and T are evaluated at the appropriate k and ω. Hence, the vector of closed loop transfer functions between the generalized coordinates and the gust excitation (see Chapter 16) is defined by

$$\boldsymbol{q}_0 = \boldsymbol{H}_{\mathrm{qg}}(\boldsymbol{\omega})w_{\mathrm{g}0} \quad \text{where} \quad \boldsymbol{H}_{\mathrm{qg}}(\boldsymbol{\omega}) = \left(-\omega^2\mathbf{A} + \mathrm{i}\omega\left(\rho V\mathbf{B} - K_{\mathrm{v}}T\mathbf{F}\right) + \left(\rho V^2\mathbf{C} + \mathbf{E}\right)\right)^{-1}\boldsymbol{h} \tag{12.17}$$

and that between the deflection at the leading edge (chosen for simplicity) and the gust excitation for the closed loop system is

$$z_{\mathrm{wing}} = \left\{s_0 \ -\frac{c}{2}\right\}\boldsymbol{q}_0 = \left\{s_0 \ -\frac{c}{2}\right\}\boldsymbol{H}_{\mathrm{qg}}(\boldsymbol{\omega})w_{\mathrm{g}0} = H_{z\mathrm{g}}(\boldsymbol{\omega})w_{\mathrm{g}0}. \tag{12.18}$$

The Von Karman frequency representation of turbulence (see Chapter 16) can be used to provide the power spectral density (PSD) input to the system from which the response PSD for the closed loop system can be calculated using Equation (12.17). The control system gains can then be designed such that the resulting deflections and loads are reduced to required levels and required gain and phase margins are achieved.

12.8 STATE SPACE MODELLING

An alternative approach to using second-order models is to employ the first-order state space representation introduced in Chapter 7. The state space formulation is particularly useful for the application of many control design techniques (e.g. optimal control theory).

Equation (12.7) for the open loop system with control and gust input can be reformulated into the first-order state space form, such that

$$\begin{bmatrix}\dot{\boldsymbol{q}}\\ \ddot{\boldsymbol{q}}\end{bmatrix} = \begin{bmatrix}\mathbf{0} & \mathbf{I}\\ -\mathbf{A}^{-1}\left(\rho V^2\mathbf{C} + \mathbf{E}\right) & -\mathbf{A}^{-1}\left(\rho V\mathbf{B}\right)\end{bmatrix}\begin{bmatrix}\dot{\boldsymbol{q}}\\ \boldsymbol{q}\end{bmatrix} + \begin{bmatrix}\mathbf{0}\\ \mathbf{A}^{-1}\boldsymbol{g}\end{bmatrix}\beta + \begin{bmatrix}\mathbf{0}\\ \mathbf{A}^{-1}\boldsymbol{h}\end{bmatrix}w_{\mathrm{g}}, \tag{12.19}$$

or as shown in Chapter 7,

$$\dot{\boldsymbol{x}} = \mathbf{A}_{\mathrm{s}}\boldsymbol{x} + \mathbf{B}_{\mathrm{s}}\boldsymbol{u} + \mathbf{E}_{\mathrm{s}}w_{\mathrm{g}}, \qquad \boldsymbol{y} = \mathbf{C}_{\mathrm{s}}\boldsymbol{x} + \mathbf{D}_{\mathrm{s}}\boldsymbol{u}. \tag{12.20}$$

Here the control input $\boldsymbol{u} = \{\beta\}$ and a gust disturbance term are now present and, when velocity-only measurement on the leading edge is considered, the measured output $\boldsymbol{y}$ is given by

$$\boldsymbol{y} = \left\{\dot{z}_{\mathrm{wing}}\right\} = \left[s_0 \ -\frac{c}{2} \ 0 \ 0\right]\left\{\dot{\kappa} \ \dot{\theta} \ \kappa \ \theta\right\}^{\mathrm{T}} = \mathbf{C}_{\mathrm{s}}\boldsymbol{x}, \tag{12.21}$$

since $\mathbf{D}_s = \mathbf{0}$ is normally assumed. In order to avoid confusion with the notation used earlier in the flutter equation, the subscript 's' has been used here to denote the state space matrices.

To introduce the feedback effect, the control input is written in terms of the measured response $\boldsymbol{y}$ (in this case a velocity), namely

$$\boldsymbol{u} = \{\beta\} = [K_v]\left\{\dot{z}_{\text{wing}}\right\} = \mathbf{K}_s\boldsymbol{y}, \tag{12.22}$$

where $\mathbf{K}_s$ is the state space gain matrix. Then substituting Equation (12.22) into Equation (12.20) and simplifying leads to the revised state equation for the closed loop system

$$\underline{\dot{\mathbf{x}}} = [\mathbf{A}_s + \mathbf{B}_s\mathbf{K}_s\mathbf{C}_s]\,\underline{\mathbf{x}} + \mathbf{E}_s w_g. \tag{12.23}$$

In the same way that a frequency domain representation was used with the second order form of the equations, it is possible to determine the frequencies and damping ratios at a particular flight condition and gain value using the eigensolution of the system matrix $[\mathbf{A}_s + \mathbf{B}_s\mathbf{K}_s\mathbf{C}_s]$ that has been revised to account for control feedback effects. As with the frequency domain approach, the effects of frequency-dependent unsteady aerodynamics and control shaping filters need to be taken into account if accurate models are required. The frequency domain gust response transfer function may also be derived from the state space equations.

These state space equations, and indeed the earlier second-order equations, can be solved in the time domain to give the state response $\boldsymbol{x}$, and hence the measured output $\boldsymbol{y}$, for the closed loop system due to any gust input. In this case, representation of frequency-dependent aerodynamic effects is achieved through the use of so-called rational fraction aerodynamics, which is described in Chapter 20. The effects of structural and control law nonlinearities can be included when a simulation is carried out in the time domain.

12.9 EXAMPLES

Make use of the MATLAB and SIMULINK routines shown in Appendix H in the companion website for the baseline binary aeroelastic system with feedback control input and gust excitation.

1. Determine the response due to '1-cosine' gusts and explore the effect of different gust wavelengths.
2. Determine the response to a 'chirp' (fast sinusoidal sweep) control input of linearly varying frequency and explore the effect of changing the start and end frequencies of the 'chirp'.
3. Explore the effect of varying the gains K_v and K_d on the flutter and divergence speed of the system.
4. Determine the range of gains K_v and K_d that will enable the flutter speed of the baseline system with the control system to be increased by 30 m/s.
5. For '1-cosine' gusts of duration 0.005, 0.01 and 0.05 s, explore the effect of varying the gains K_v and K_d on the closed loop system response.

13

Equilibrium Manoeuvres

Aircraft are controlled by the pilot using the control surfaces (namely aileron/spoiler for roll, rudder for yaw and elevator for pitch) singly or in combination for a range of different manoeuvres. The structure must be designed to withstand these manoeuvres and these load calculations are a critical stage in the aircraft clearance, often involving many thousands of cases. A useful background to meeting most of the loads requirements in the certification specifications (CS-25 and FAR-25) is given in (Howe, 2004, Lomax, 1996).

There is a difference between manoeuvres performed by commercial and military aircraft. Military aircraft (excepting transport and bomber aircraft) are subject to far more severe manoeuvres, involving higher *g* levels, control angles and rates. However, military combat aircraft are generally stiffer than commercial aircraft, with natural frequencies usually greater than 5 Hz, so the manoeuvre loads calculations are sometimes carried out using a rigid aircraft model, often with corrections made to the aerodynamics for flexible effects, though this is changing for more highly flexible combat aircraft and unmanned air vehicles (UAVs). In contrast, although their manoeuvres are less severe, large commercial aircraft are generally significantly more flexible, some (e.g. Airbus A380) with modes of vibration that are even lower than 1 Hz; thus it is becoming more essential to perform loads calculations using a flexible (or elastic) aircraft model that incorporates the rigid aircraft characteristics. This means that the aeroelastic and loads domains are becoming more interdependent, a key reason why this book seeks to balance these two aspects.

There are two types of *flight manoeuvre* that have to be considered in the design of an aircraft, often referred to as:

- equilibrium (or balanced/steady) manoeuvres and
- dynamic manoeuvres.

The calculation methodology is different in each case and these will be addressed in separate chapters.

The term *equilibrium (or balanced) manoeuvre* refers to the case where the aircraft is in a steady manoeuvre. In the symmetric case where *pitching* at a steady pitch rate is usually involved (i.e. zero pitch acceleration), the aircraft will experience accelerations normal to the flight path. Such manoeuvres are intended to represent the aircraft in an emergency pull-up or push-down situation, with the wings idealized as being horizontal; this load case is important for the design of inboard parts of aerodynamic surfaces as well as possibly for engine pylons and fuselage components. A steady banked turn is also an equilibrium manoeuvre. In such accelerated conditions, the aircraft is in effective equilibrium once D'Alembert's principle is used to add inertia forces. The symmetric equilibrium manoeuvre is considered in Howe (2004), Lomax (1996) and Megson (1999) and in ESDU Data Sheets 94009, 97032 and 99033.

Introduction to Aircraft Aeroelasticity and Loads J. R. Wright and J. E. Cooper
© 2007 John Wiley & Sons, Ltd

In this chapter, the process of determining the balanced response (deformation and component loads) in a number of *symmetric* equilibrium (or steady) manoeuvres will be considered, using a progression of fairly basic mathematical models for both rigid and simple flexible aircraft. The flexible aircraft needs to be considered since flexibility can affect the loads distribution; CS-25 states: 'If deflections under load would significantly change the distribution of internal or external loads, this redistribution must be taken into account'. In effect, this is a statement that aeroelastic effects must be accounted for in loads calculations. The ability to correct the rigid aircraft derivatives for flexible effects will also be considered. Note that the axes system used in this chapter will be inertial, i.e. earth fixed, and the unknowns will be displacements, angles and generalized coordinates.

However, there are a number of *asymmetric* manoeuvres involving *rolling* and *yawing* that may also be classed as equilibrium manoeuvres, but these make use of simplified aircraft representations. Some are steady and involve a balance of aerodynamic moments from different sources, while others involve abrupt application of a control and require an inertia couple to balance the aerodynamic control moment at that instant, so leading to a conservative (i.e. over) estimate of loads. In this chapter, these rolling and yawing manoeuvres will be considered briefly, quoting, but not deriving, the models used since these will be considered further in Chapter 14. These balanced manoeuvres for pitching, rolling and yawing are known as *bookcase* manoeuvres, where the load case is often somewhat artificial but will yield load estimates at an early stage in the aircraft life prior to carrying out full dynamic simulations of the aircraft behaviour in time (so-called *rational* cases where a more realistic model and load case are considered; see Chapter 15). Rolling manoeuvres are often important for the outer wing design whereas yawing manoeuvres contribute to rear fuselage and fin design. Note that the treatment of symmetric and asymmetric equilibrium manoeuvres is further considered in Chapter 24. The longitudinal case is the main focus of the book. Some background to static aeroelastic effects for the lateral case may be found in ESDU Data Sheets 01010 and 03011.

In a *dynamic manoeuvre*, the variation with time of the response and loads of the aircraft is determined using a representative dynamic model of the aircraft and performing a *rational* simulation; both symmetric and asymmetric manoeuvres are possible and the types of case will be considered later in Chapter 24. Often, the nonlinear (large angle) flight mechanics model of the aircraft is used, sometimes with flexible modes included especially for highly flexible aircraft; alternatively, a linear (small angle) model may be employed but this is less accurate for manoeuvres with substantial changes of altitude and angle. Therefore, in Chapter 14, the flight mechanics model of the rigid aircraft will be introduced, where axes fixed in the aircraft are used, unknowns are velocities and large angle manoeuvres may be handled. The extension to the flexible aircraft will be considered since flexibility effects are important. In Chapter 15, the application of this flight mechanics model to simple dynamic heave/pitch and roll manoeuvre examples will be considered for both rigid and simple flexible aircraft.

In Chapter 16, the related issues of the response to *gusts* and *continuous turbulence* will be considered, though of course these are not deliberate flight manoeuvres. In Chapter 17, the treatment of *ground manoeuvres* (e.g. taxiing, landing, braking, etc.) will be introduced. In both these cases, inertial axes will be used where unknowns are displacements, rotations and generalized coordinates.

Because a whole range of concepts will be introduced in the next few chapters, the aerodynamics will be kept as simple as possible and strip theory will continue to be used. Later in Chapters 19 and 20, the use of more realistic aerodynamics will be considered. Also, the Rayleigh–Ritz approach for incorporating a flexible free–free mode together with the rigid body motions will be used, thus allowing the whole flexible aircraft to be studied in concept for symmetric flight cases using a total of only three DoF. In Chapter 8, some of the concepts of static aeroelastic deformation for a simple wing model in level flight were introduced.

In this chapter and others on manoeuvres and gusts, the focus will be on determining the aircraft response. In all the cases covered, the aerodynamic and inertia loads distributed over the aircraft give rise to *internal 'MAST' loads* (i.e. moment, axial, shear and torque). The calculation of internal loads will be covered in Chapter 18, since there are many common factors in determination of internal loads for manoeuvre and gust inputs.

13.1 EQUILIBRIUM MANOEUVRE – RIGID AIRCRAFT UNDER NORMAL ACCELERATION

In this section, the aircraft is treated essentially as a ‘particle’ (see Chapter 6) under heave acceleration, i.e. no rotational effects are present. Different manoeuvres are considered and the *load factor* concept is introduced.

13.1.1 Steady Level Flight

Firstly, consider an aircraft of mass m in steady level flight. Because there is no vertical acceleration, there will be no net vertical force and total lift L will balance weight W ($= mg$) so $L = W$. Also, for this simple ‘particle’ representation, thrust T will balance drag D so $T = D$.

13.1.2 Accelerated Flight Manoeuvre – Load Factor

Now consider the aircraft accelerating upwards at a constant acceleration of a (m/s^2), as shown via the free body diagrams (FBDs) (see Chapter 6) in Figure 13.1, but ignoring any velocity component normal to the flight path; a steady turn or a pull out from a dive fall into this category. Velocity components normal to the flight path introduce a change in incidence and become relevant later for dynamic manoeuvres and gust encounters.

Using D’Alembert’s principle (see Chapter 6), the aircraft dynamics may be converted into an equivalent static equilibrium problem by introducing an inertia force equal to ma in the opposite direction to acceleration, as shown in Figure 13.1. Thus, for equilibrium of aerodynamic and inertia forces normal to the flight path

$$L - W - ma = 0 \qquad \text{or} \qquad L = W\left(1 + \frac{a}{g}\right) \qquad \text{or} \qquad L = nW, \tag{13.1}$$

where n is the so-called *load factor*, defined by

$$\text{Load factor } n = \frac{\text{Total Lift}}{\text{Weight}}. \tag{13.2}$$

It is common practice in accelerated flight manoeuvres to use the load factor concept and therefore to balance the lift by the force nW (a combination of weight and inertia force), as shown in Figure 13.1.

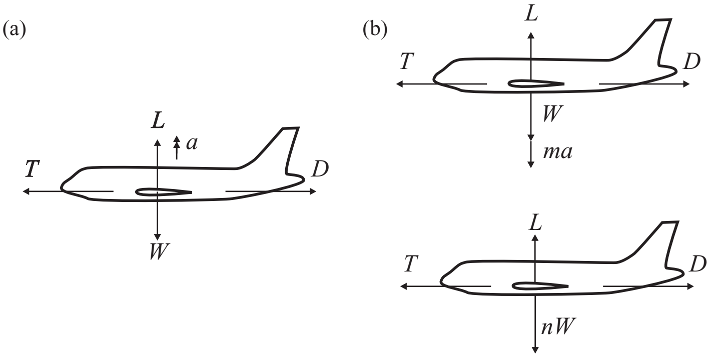

Figure 13.1 Rigid aircraft in accelerated flight: (a) Newton’s law and (b) D’Alembert’s principle.

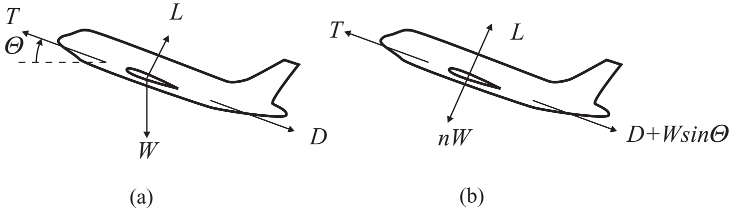

Figure 13.2 Rigid aircraft in steady climb: (a) basic forces and (b) load factor form.

Thus, wherever W appears in equations for steady level flight, it may be replaced by nW for accelerated flight; the usefulness of this concept will be illustrated later in the chapter. Clearly, steady level flight is characterized by a load factor value of $n = 1$. The thrust/drag equation along the flight path remains the same as for steady level flight though changes in lift will affect the drag and therefore the thrust required.

Next, some simple symmetric manoeuvres will be considered to see how load factor relates to flight conditions. The term 'symmetric' is used whenever the response and loads on both sides of the aircraft are the same.

13.1.3 Steady Climb/Descent

Consider an aircraft in a steady climb with its flight path at an angle of inclination Θ to the horizontal, with the FBD shown in Figure 13.2. In this case there will be no velocity of the aircraft normal to the flight path, no pitch rate and no accelerations. For equilibrium *normal* to and *along* the flight path, then

$$L = W \cos \Theta, \qquad T = D + W \sin \Theta \tag{13.3}$$

and so thrust will need to increase for the climb case. The load factor is seen to be given by

$$n = \cos \Theta \quad (n \leq 1) \tag{13.4}$$

13.1.4 Steady Pull-Out and 'Bunt'

Now consider the aircraft in a steady pull-out from a dive. Assume that the aircraft follows a circular path of radius r (not to be confused with yaw velocity in Chapters 14 and 15) in the vertical plane at true air speed (TAS) V (see Chapter 5 for air speed definitions), as shown in Figure 13.3. Again, in this case there will be no velocity of the aircraft normal to the flight path and no acceleration along the flight path. Because the aircraft is following a circular path, it must experience a centripetal acceleration (i.e. towards the centre) of V^2/r.

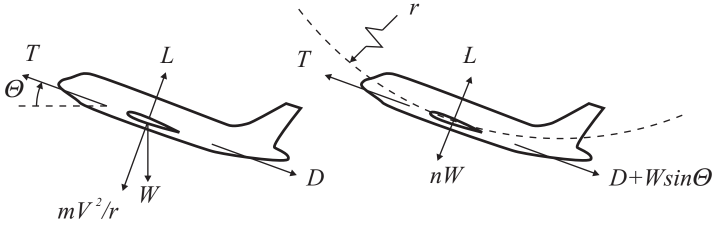

Figure 13.3 Rigid aircraft in steady pull-out – D'Alembert's principle.

It is essential to use TAS (not equivalent air speed, or EAS) when evaluating a centripetal acceleration. Introducing an inertia force and considering equilibrium in a direction *normal* to and *along* the flight path when the aircraft is at an inclination Θ to the horizontal yields

$$L - W\cos\Theta - m\frac{V^2}{r} = 0, \qquad T = D + W\sin\Theta \tag{13.5}$$

and so it may be shown that the load factor is given by

$$n = \cos\Theta + \frac{V^2}{gr}. \tag{13.6}$$

It may be seen from this expression that the load factor increases for higher air speeds and tighter turns (smaller radius). In the pull-out, the aircraft velocity is $V = rq$, where $q = V/r$ is the pitch rate (nose up positive); the symbol q is traditionally used in this way in flight mechanics (see Chapters 14 and 15) and should not be confused with its use elsewhere in this book as a generalized coordinate or dynamic pressure.

When an aircraft 'loops the loop', the load factor varies continuously because of the change in angle to the horizontal; the highest load factor occurs at the bottom of the loop where the inertia force and weight act in the same direction, whereas the lowest load factor occurs at the top of the loop. A manoeuvre where the pitch rate is negative (nose down) is sometimes known as a 'bunt' and can give rise to a zero load factor, or the 'weightless' (zero g) flight condition. Note that in Figure 13.4(a) ($1 > n > 0$) the lift still acts upwards, in Figure 13.4(b) ($n = 0$) the lift and inertia force are both zero (i.e. the weightless condition) and in Figure 13.4(c) ($n = -1$) the lift force actually has a negative value (so is acting downwards while the inertia force acts upwards).

13.1.5 Example of a Pull Out

An aircraft is pulling out of a dive at velocity 200 m/s TAS at 10 000 ft altitude, following a flight path with a radius of 2000 m. Determine the load factor and pitch rate at the bottom of the pull-out. Note that

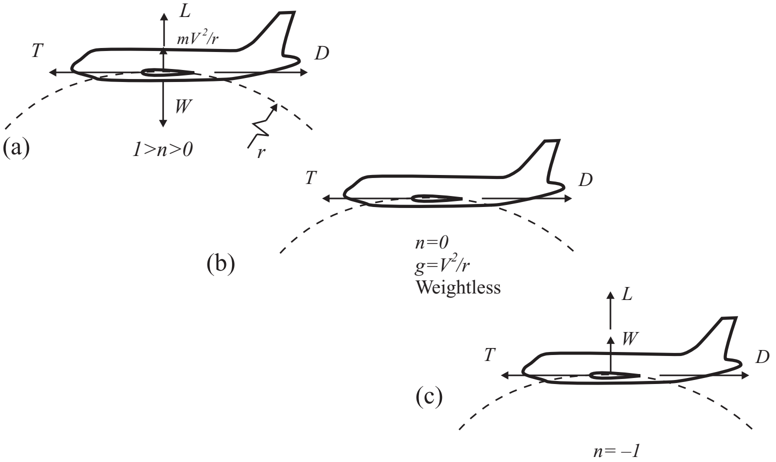

Figure 13.4 Rigid aircraft in steady 'bunt': (a) $1 > n > 0$, (b) $n = 0$ (Weightless) and (c) $n = -1$.

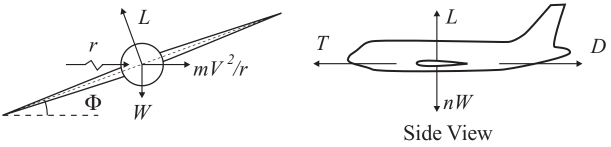

Figure 13.5 Rigid aircraft in steady banked turn – using D'Alembert's principle.

altitude is irrelevant when TAS is used but would be if EAS had been specified because it is the absolute air speed that is important.

$$\text{Load factor } n = \frac{V^2}{gr} = \frac{200^2}{9.81\times 2000} = 2.04$$

$$\text{Pitch rate } q = \frac{V}{r} = \frac{200}{2000} = 0.1\,\text{rad/s} = 5.73\,\text{deg/s}.$$

13.1.6 Steady Turn

A symmetric steady turn manoeuvre is characterized by the aircraft flying at a constant true air speed V around a circular path of radius r in the horizontal plane. The aircraft is oriented at a bank angle Φ as shown in Figure 13.5, such that there is no sideslip (i.e. no net lateral force or acceleration), no roll rate and therefore the lift on each wing is the same; this is known as a banked turn. There is no velocity normal to the flight path.

Recognizing that the aircraft experiences a centripetal acceleration V^2/r, and employing D'Alembert's principle, yields the FBD shown in Figure 13.5. The equilibrium equations in the vertical and horizontal directions are

$$L\cos\Phi = W, \qquad L\sin\Phi - m\frac{V^2}{r} = 0. \tag{13.7}$$

Solving these equations yields the expression for the bank angle and load factor, namely

$$\Phi = \tan^{-1}\left(\frac{V^2}{gr}\right), \qquad n = \frac{1}{\cos\Phi} \quad (n \geq 1). \tag{13.8}$$

The rate of turn is given by $\omega_{\text{Turn}} = V/r$ and so the aircraft experiences steady yaw and pitch rates given by

$$n_{\text{yaw}} = \omega_{\text{Turn}}\cos\Phi = \frac{V}{rn}, \qquad q = \omega_{\text{Turn}}\sin\Phi = \frac{V}{r}\frac{\sqrt{n^2-1}}{n}, \tag{13.9}$$

where n_{yaw} is the yaw rate (n is the standard flight mechanics symbol for yaw rate but the subscript is added here to avoid the confusion with the load factor within the same equation). Thus the pitch rate is related nonlinearly to the load factor and linearly to air speed. Because the lift increases in a steady turn, then so will the drag and therefore the thrust must be increased to maintain the same air speed.

13.1.7 Example: A Turn

An aircraft is in a level steady banked turn at velocity 100 m/s EAS at 10 000 ft (3148 m) altitude ($\sigma = 0.738$), following a flight path with a radius of 1000 m. Determine the bank angle and load factor. Note that altitude is important when EAS is used because load factors depend upon the true air speed

$V_{\mathrm{TAS}} = V_{\mathrm{EAS}}/\sqrt{\sigma} = 116.4\,\mathrm{m/s}$.

$$\text{Bank angle } \Phi = \tan^{-1}\left(\frac{V^2}{gr}\right) = \tan^{-1}\left(\frac{116.4^2}{9.81 \times 1000}\right) = 54.1^\circ,$$

$$\text{Load factor } n = \frac{1}{\cos\Phi} = 1.70.$$

13.2 MANOEUVRE ENVELOPE

Clearly there are an infinite number of combinations of load factor and true air speed that could be considered for loads clearance purposes. However, in order to simplify the position, a *manoeuvre envelope* can be defined to show the boundaries of n and V_{EAS} within which the aircraft must withstand the equilibrium manoeuvre loads for symmetric manoeuvres. In many cases (e.g. pull-out, turn) some steady pitching velocity is involved.

The envelope is defined by the design cruise speed V_{C}, design dive speed V_{D} (to account for a prescribed 'upset' manoeuvre), the positive and negative stall curves (given by the maximum normal force coefficient $\pm C_{\mathrm{N_{Max}}}$), the maximum manoeuvring limit load factor n_1 (typically between 2.5 and 3.8 for a commercial aircraft, depending upon the maximum take-off weight) and the minimum manoeuvring load factor $n_3 = -1$. The positive stall curve defines how the load factor that can be developed is limited by stall, so on the stall boundary

$$L = nW = \frac{1}{2}\rho_0 V_{\mathrm{EAS}}^2 S_{\mathrm{W}} C_{\mathrm{N_{Max}}}, \tag{13.10}$$

where ρ_0 is the sea level air density and S_{W} is the wing planform area. It may be seen that the equivalent air speed (EAS) is used to provide a unified envelope and so avoid needing to construct envelopes for a series of different altitudes. The normal force coefficient $C_{\mathrm{N_{Max}}}$ is normally taken to equal the lift coefficient $C_{\mathrm{L_{Max}}}$. The relationship between n and V_{EAS} along the positive stall curve is then given by

$$n = \frac{\rho_0 S_{\mathrm{W}} C_{\mathrm{L_{Max}}}}{2W} V_{\mathrm{EAS}}^2, \tag{13.11}$$

which is a quadratic expression. Obviously a similar relationship applies for the negative stall curve.

The manoeuvre envelope shown in Figure 13.6 is bounded by the stall curves, the design dive speed and the maximum and minimum load factors, noting that the most severe negative load factor

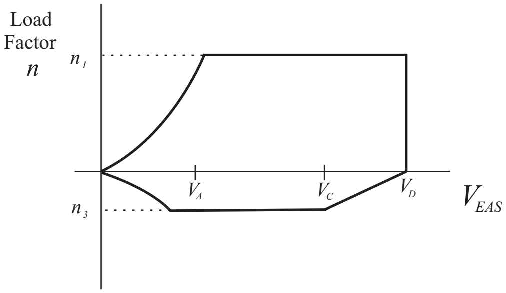

Figure 13.6 Manoeuvre envelope.

is not achievable at V_{D} because it would imply that the aircraft is attempting to go even faster than it was designed for. Boundaries for both flaps up and flaps down cases would be considered. The design manoeuvring speed V_{A} is defined by the intersection of the stall curve and the maximum load factor. Air speeds are specified as a function of altitude.

The aircraft must be designed to withstand loads arising from symmetric (pitching) manoeuvres defined by values of n and V_{EAS}, both on and within the envelope. Usually the corner points are the most critical, but checks along the boundaries would also be needed to ensure that the maximum loads in each part of the aircraft are found (CS-25). Note that the load calculations need to be carried out for the flexible aircraft and with any nonlinearity due to control system constraints and aerodynamics represented.

13.3 EQUILIBRIUM MANOEUVRE – RIGID AIRCRAFT PITCHING

In Section 13.1, the balance of lift, drag, weight, inertia and thrust forces was considered for the aircraft represented as a ‘particle’ in heave, so no pitch effects were included. In this section, the aircraft will be treated as a ‘body’ (see Chapter 6) and pitching effects will be included to show how the tailplane load balances the aircraft in pitch. The elevator angle required to trim the aircraft in the manoeuvre may be determined. At this stage, the aircraft is considered as rigid and the analysis approach applies for both unswept and swept wings.

13.3.1 Inertial Axes System

Before carrying out an analysis on the rigid aircraft undergoing an equilibrium manoeuvre in heave/pitch, it is worth making some comments about the axes system to be employed. For equilibrium manoeuvres, flutter, ground manoeuvres and gust/turbulence encounters, the aircraft behaviour may be referenced to a datum position defined for inertial axes fixed in space because the aircraft excursion from its datum position is considered to be small; the unknowns will be displacements and rotations. In Chapters 14 and 15, on the other hand, axes will be considered to be fixed in the aircraft because for a dynamic manoeuvre the excursion from the initial datum position may be significant and a nonlinear flight mechanics model is used; the unknowns will then be velocities. When aerodynamic derivatives are considered to represent the aerodynamic forces and moments in a compact notation, it is important to recognize which axes system the derivatives are evaluated for.

13.3.2 Determination of External Forces to Balance the Aircraft

In the analysis of the aircraft behaviour in heave and pitch, the tailplane needs to be included and for completeness the thrust and drag lines of action are allowed to be different (though it is assumed for simplicity that they are parallel). The FBD for the aircraft flying horizontally ($\Theta = 0$) but under an accelerated flight condition defined by the vertical load factor n is shown in Figure 13.7 (there is no horizontal load factor as the air speed is assumed to be constant during the manoeuvre); nW is the combined weight/inertia force, T is the thrust, L_{W} is the wing lift, L_{T} is the tailplane lift, D is the drag and $M_{0\mathrm{W}}$ is the wing zero lift pitching moment.

The definitions of pitching moment, lift and drag require expressions involving air speed and density (see Chapter 5); these will be taken as true air speed V and corresponding density ρ (at whatever altitude the aircraft is flying) for most of the remainder of the book, unless indicated otherwise. Thus the wing zero lift pitching moment is given by the expression

$$M_{0\mathrm{W}} = \frac{1}{2}\rho V^2 S_{\mathrm{W}}\bar{c}C_{M_{0\mathrm{W}}} \tag{13.12}$$

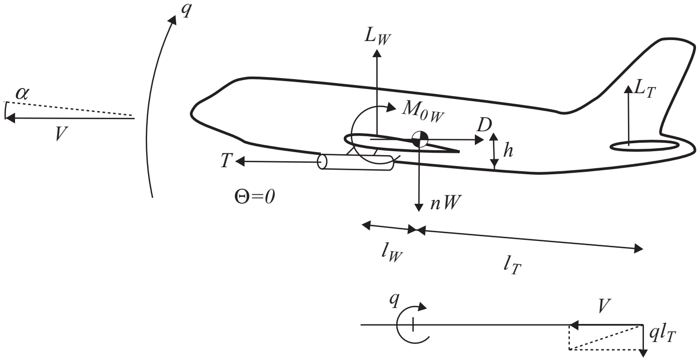

Figure 13.7 Rigid aircraft in an equilibrium manoeuvre, with heave and pitch effects included.

where $\bar{c}$ is the wing mean chord (though in the simple examples considered in this book, wings are usually untapered so the 'bar' will be dropped from now on) and $C_{M_{0W}}$ is the zero lift pitching moment coefficient for the wing (usually negative because of camber). This constant pitching moment coefficient arises when the lift is considered to act at the aerodynamic centre (see Chapter 5). The aircraft dimensions are shown in Figure 13.7. In order to simplify the equations, consider the drag force to act through the aircraft centre of mass.

Taking a view from the side of the aircraft, this FBD is seen to cover all the manoeuvres considered in Section 13.1 for $\Theta = 0$. To cater for inclined flight, the weight component along the flight path also needs to be included. The whole process of introducing inertia forces is defined in the Certification Specifications (CA-25) by the statement 'the linear inertia forces must be considered in equilibrium with the thrust and all aerodynamic loads'.

Now the aircraft shown must be in equilibrium, because of the application of D'Alembert's principle, so there must be no net vertical or horizontal forces and no net pitching moment (about the centre of mass, say). Thus the equations defining equilibrium, assuming that the incidence angle is small ($\cos\alpha = 1$) and that the lift and drag forces act essentially normal to and along the aircraft axis, are

$$nW - L_{\mathrm{W}} - L_{\mathrm{T}} = 0, \qquad T - D = 0, \qquad M_{0\mathrm{W}} + l_{\mathrm{W}} L_{\mathrm{W}} - l_{\mathrm{T}} L_{\mathrm{T}} + hT = 0. \tag{13.13}$$

For a given flight condition, *nW* and $M_{0\mathrm{W}}$ are known and L_{W}, L_{T}, *D* and *T* are unknown. The tailplane is normally designed such that the tailplane lift required for trim is relatively small in cruise and that maximum up and down loads are approximately equal; thus the tailplane usually has a symmetric section, so its zero lift pitching moment $M_{0\mathrm{T}}$ is zero. Thus it may be seen that the overall loads on the aircraft may be determined for a given accelerated flight condition by solving Equations (13.13). There are two different conditions to consider for the solution (see below). A more complete analysis is shown in Lomax (1996) and ESDU Data Sheet 94009.

13.3.3 Thrust and Drag In-Line

When the thrust and drag are *in-line*, then $h = 0$ so the drag is not involved in the moment equation for vertical loads and the lift forces may be solved directly as

$$L_{\mathrm{T}} = \frac{M_{0\mathrm{W}} + nWl_{\mathrm{W}}}{l_{\mathrm{W}} + l_{\mathrm{T}}}, \qquad L_{\mathrm{W}} = nW - L_{\mathrm{T}}. \tag{13.14}$$

These forces express the 'balance' of the aircraft in heave and pitch. It may be seen that the required tailplane lift varies linearly with the load factor. Note that because the zero lift pitching moment for the wing is usually negative, the tailplane lift can sometimes act downwards in steady level flight.

13.3.4 Example: Thrust and Drag In-Line

An aircraft flying at 175 m/s (sea level) has the following characteristics: $m = 20\ 000$ kg, $S_W = 80$ m^2, $c = 3$ m, $l_W = 1$ m, $l_T = 16$ m and $C_{M0W} = -0.06$. Obtain the tailplane lift for load factors of 1 and 3.

$$\begin{aligned} M_0 &= \frac{1}{2}\rho V^2 S_W \bar{c} C_{M0W} = \frac{1}{2} \times 1.225 \times 175^2 \times 80 \times 3 \times -0.06 = -270\,000\,\text{N m},\\ W &= mg = 20000 \times 9.81 = 196\,000\,\text{N}. \end{aligned}$$

Calculating the tailplane lift using Equation (13.14) yields values of -4.3 kN (download) and $+18.7$ kN (upload) respectively for the two load factors. Corresponding wing lift values are 191.7 kN and 569.3 kN.

13.3.5 Thrust and Drag Out-of-Line

When the thrust and drag are *out-of-line* (but parallel), then $h \neq 0$ and the lift forces will depend upon the thrust. However, the thrust is in turn dependent upon the drag and hence upon the wing lift. Thus an iterative approach must be adopted. Initially, the tailplane lift is set to zero so the wing lift is equal to nW, and the wing lift coefficient, drag coefficient, drag and hence thrust are estimated; a first estimate for the tailplane lift force is then obtained using Equations (13.13). The wing lift, drag, thrust and tailplane lift are then re-estimated and this process repeated until the solution converges, usually quite rapidly.

13.3.6 Example: Thrust and Drag Out-of-Line

An aircraft flying at 250 m/s EAS has the following characteristics: $m = 44200$ kg, $S_W = 145$ m^2, $c = 5$ m, $l_W = 0.3$ m, $l_T = 14.9$ m, $C_{M0W} = -0.07$ and drag coefficient $C_D = 0.02 + 0.072 C_{LW}^2$, where C_{LW} is the wing lift coefficient. The drag may be assumed to act through the wing aerodynamic centre and the thrust acts a distance $h = 1.5$ m below the drag. Obtain the tailplane lift for a load factor of 2.5:

$$\begin{aligned} M_{0W} &= \frac{1}{2} \times 1.225 \times 250^2 \times 145 \times 5 \times -0.07 = -1943\,\text{kN m},\\ W &= mg = 44\,200 \times 9.81 = 433.6\,\text{kN}. \end{aligned}$$

Iteration 1 : $L_W = nW = 2.5 \times 433.6\,\text{kN} = 1084\,\text{kN}, \qquad C_{LW} = L_W / \tfrac{1}{2}\rho V^2 S_W = 0.1953,$
$C_D = 0.0227, \qquad T = D = \tfrac{1}{2}\rho V_0^2 S_W C_D = 126.3\,\text{kN},$
$L_T = (M_{0W} + l_W L_W + hT)/l_T = -95.8\,\text{kN}.$

Iteration 2 : $L_W = nW - L_T = 1084 - (-95.8) = 1179.8\,\text{kN}, \qquad C_{LW} = 0.2126,$
$C_D = 0.0233, \quad T = D = 129.1\,\text{kN}, \qquad L_T = -93.6\,\text{kN}.$

The process may then be continued until the required level of accuracy is obtained; e.g. after three iterations the tailplane lift is $L_T = -93.7$ kN.

13.3.7 Determination of Balanced Condition – Thrust/Drag In-Line

In determining the elevator angle for the general manoeuvre with a load factor n, it will be assumed that the aircraft is pitching steadily (nose up) with a rate q; this is true for the pull-up and turn cases but not the descent or climb cases where the pitch rate is zero. The pitch rate effect on wing lift will be ignored as being an unsteady term (see Chapter 10), but the effect on the tailplane lift does need to be included.

The elevator angle required for an equilibrium manoeuvre (or elevator angle to trim) may be found by substituting for the wing and tailplane lift forces in Equations (13.13). The wing lift is given by

$$L_{\mathrm{W}} = -Z_{\mathrm{W}} = \frac{1}{2}\rho V^2 S_{\mathrm{W}} a_{\mathrm{W}}(\alpha - \alpha_0), \tag{13.15}$$

where α is the aircraft incidence (assumed small) and α_0 is the angle of zero lift; the setting angles defining the inclination of the wing and tailplane aerofoil sections to the fuselage are neglected for simplicity. Z_{W} is the downwards force on the wing (in the opposite direction to lift), used because the aircraft z axis points downwards.

To write an expression for tailplane lift in terms of incidence and elevator angle, it should be recognized that there is an effective steady incidence of ql_{T}/V due to the pitch rate effect (i.e. the tail moving forwards at velocity V and downwards with velocity ql_{T}), as shown in Figure 13.7. A further effect that needs to be taken into account for the tailplane is the mean downwash angle ε, i.e. the change in angle of the airflow direction at the tailplane due to the downward flow associated with the wing trailing vortices (see Chapter 5). The tailplane incidence is

$$\alpha_{\mathrm{T}} = \alpha + \frac{ql_{\mathrm{T}}}{V} - \varepsilon, \tag{13.16}$$

and remembering that the tailplane has a symmetric section, the tailplane lift is

$$L_{\mathrm{T}} = -Z_{\mathrm{T}} = \tfrac{1}{2}\rho V^2 S_{\mathrm{T}} \left[a_{\mathrm{T}}\left(\alpha + \tfrac{ql_{\mathrm{T}}}{V} - \varepsilon\right) + a_{\mathrm{E}}\eta\right]. \tag{13.17}$$

Here S_{T} is the tailplane area, a_{T} is the tailplane lift curve slope (defined with respect to incidence), η is the elevator angle and a_{E} is the tailplane lift curve slope (defined with respect to the elevator angle). The mean downwash angle ε may be assumed to be proportional to the effective wing incidence, namely

$$\varepsilon = \frac{\mathrm{d}\varepsilon}{\mathrm{d}\alpha}(\alpha - \alpha_0) = k_{\varepsilon}(\alpha - \alpha_0), \tag{13.18}$$

where $k_{\varepsilon} = \mathrm{d}\varepsilon/\mathrm{d}\alpha$ is typically of the order of 0.35–0.4.

The total aerodynamic lift force required in Equations (13.13) is then given by

$$L_{\mathrm{W}} + L_{\mathrm{T}} = -Z = \frac{1}{2}\rho V^2 \left(S_{\mathrm{W}} a_{\mathrm{W}}(\alpha - \alpha_0) + S_{\mathrm{T}}\left\{a_{\mathrm{T}}\left[(1 - k_{\varepsilon})\alpha + k_{\varepsilon}\alpha_0 + \frac{ql_{\mathrm{T}}}{V}\right] + a_{\mathrm{E}}\eta\right\}\right) \tag{13.19}$$

where it may be seen that the angle of zero lift for the wing influences the tailplane lift via the downwash. It is convenient to write this equation in terms of so-called *aerodynamic derivatives*. For example, the total normal force (in the opposite direction to lift) may be expressed in derivative form as

$$Z = -L = Z_0 + Z_{\alpha}\alpha + Z_q q + Z_{\eta}\eta \tag{13.20}$$

where Z_0 is a constant and, for example, $Z_{\alpha} = \partial Z/\partial\alpha$. For equilibrium manoeuvres, these derivatives are effectively defined with respect to the inertial axes system; other rate dependent derivatives will be introduced in Chapter 16 for gust response analysis. The derivatives obtained with respect to inertial axes are tabulated in Appendix B. Also, note that these derivatives for inertial axes are different to the stability derivatives for wind axes in Chapters 14 and 15 and also to the unsteady aerodynamic derivatives in Chapter 10.

The normal force derivatives in Equation (13.20) are given from inspection of Equations (13.19) and (13.20) as

$$\begin{aligned} Z_0 &= -\tfrac{1}{2}\rho V^2 \left[-S_W a_W + S_T a_T k_\varepsilon\right] \alpha_0, \qquad & Z_q &= -\tfrac{1}{2}\rho V S_T a_T l_T, \\ Z_\alpha &= -\tfrac{1}{2}\rho V^2 \left[S_W a_W + S_T a_T (1 - k_\varepsilon)\right], \qquad & Z_\eta &= -\tfrac{1}{2}\rho V^2 S_T a_E. \end{aligned} \tag{13.21}$$

Negative signs are present because positive incidence, pitch rate and elevator angle cause an upwards force. Similarly, the total aerodynamic pitching moment (nose up positive) about the aircraft centre of mass required in Equations (13.13) is given in aerodynamic moment derivative form as

$$M = M_0 + l_W L_W - l_T L_T = M_0 + M_\alpha \alpha + M_q q + M_\eta \eta, \tag{13.22}$$

where the moment derivative values may be seen by inspection of the lift expressions as

$$\begin{aligned} M_0 &= M_{0W} - \tfrac{1}{2}\rho V^2 \left[S_W a_W l_W + S_T a_T k_\varepsilon l_T\right] \alpha_0, \\ M_\alpha &= \tfrac{1}{2}\rho V^2 \left[S_W a_W l_W - S_T a_T (1 - k_\varepsilon) l_T\right] \\ M_q &= -\tfrac{1}{2}\rho V S_T a_T l_T^2, \\ M_\eta &= -\tfrac{1}{2}\rho V^2 S_T a_E l_T. \end{aligned} \tag{13.23}$$

It should be noted that the constant derivative term M_0 is a combination of the wing zero lift pitching moment M_{0W} and the moment terms caused by the wing and tailplane lift associated with the wing zero lift angle α_0.

When these expressions are substituted into the heave and pitch equations for equilibrium (assuming that thrust and drag are in line and may be omitted from the pitch equation) then it may be shown that

$$-\begin{bmatrix} Z_\eta & Z_\alpha \\ M_\eta & M_\alpha \end{bmatrix} \begin{Bmatrix} \eta \\ \alpha \end{Bmatrix} = \begin{Bmatrix} 1 \\ 0 \end{Bmatrix} nW + \begin{Bmatrix} Z_q \\ M_q \end{Bmatrix} q + \begin{Bmatrix} Z_0 \\ M_0 \end{Bmatrix}. \tag{13.24}$$

The ordering of the unknowns in the left-hand side vector is chosen for convenience to compare with the result for the flexible aircraft determined later in this chapter. The three input terms on the right-hand side are respectively the *inertia input* and *pitch rate input* (both related to the load factor) corresponding to the relevant flight condition and the *aerodynamic input at zero incidence* related to the presence of wing camber and the angle of zero lift. Solving these simultaneous equations for the unknown left hand side vector leads to the elevator angle η required to trim the aircraft in the manoeuvre and the resulting trim incidence α. Hence the external forces for equilibrium may be determined. The analysis may be extended to include the balance of fore-and-aft motion via the thrust and drag. In practice, the aerodynamic forces on the fuselage and nacelles would be included.

If the aircraft is flying near to stall where the lift varies nonlinearly with incidence, then the derivative Z_α will be a nonlinear function and so the solution of Equation (13.24) will be nonlinear (typically found using the Newton–Raphson method). The nonlinear trim condition may then be found. Also, the equations may be modified for large angles of incidence. The same issue applies if a nonlinear flight control system (FCS) is present.

13.3.8 Determination of Balanced Condition – Thrust/Drag Out-of-Line

In the above analysis, the solution was kept relatively simple by assuming that the thrust and drag forces were in line. In the case where the thrust and drag are out of line, it was shown earlier that this led to an iterative solution. The solution may perhaps be seen more clearly by adding the $T - D = 0$ equation to the above analysis and including thrust in the moment equation, with X derivatives used in place of drag (with X defined as positive forward). Thus, Equation (13.24) becomes

$$-\left[\begin{array}{cc|c} Z_\eta & Z_\alpha & Z_\mathrm{T} \\ M_\eta & M_\alpha & M_\mathrm{T} \\ \hline X_\eta & X_\alpha & 1 \end{array}\right]\left\{\begin{array}{c} \eta \\ \alpha \\ \hline T \end{array}\right\} = \left\{\begin{array}{c} 1 \\ 0 \\ \hline 0 \end{array}\right\} nW + \left\{\begin{array}{c} Z_q \\ M_q \\ \hline X_q \end{array}\right\} q + \left\{\begin{array}{c} Z_0 \\ M_0 \\ \hline X_0 \end{array}\right\}, \tag{13.25}$$

where $M_\mathrm{T} = h$ and $Z_\mathrm{T} = 0$ (assuming thrust is perpendicular to lift and parallel to drag). The derivative X_α is a linear function of incidence, and is not constant because the induced drag is proportional to the square of the lift. Thus the solution of Equation (13.25) will be nonlinear, yielding the incidence, elevator angle and thrust required for the balanced state for the appropriate load factor. Such a trimmed or balanced condition (usually at $1g$, $n = 1$) will be the starting point for a dynamic manoeuvre or landing using the flight mechanics model (see Chapters 14, 15 and 17).

13.3.9 Aerodynamic Derivatives

Before moving on, it should be pointed out that in Chapters 14 and 15, other derivatives (actually very similar to the inertially defined derivatives) will be defined with respect to wind (i.e. body fixed) axes for stability and control purposes (Bryan, 1911; Babister, 1980; Cook, 1997; ESDU Data Sheet). In Cook (1997), these *dimensional* derivatives are indicated by using the 'over-o' symbol, e.g. $\overset{\circ}{Z}_q$, and the *nondimensional* derivatives by Z_q; however, since nondimensional derivatives are not used at all in this book, this distinction will not be used and Z_q will indicate a dimensional derivative throughout (see also Chapter 14). The context (i.e. which equations and chapter they are included in) will define which axes the derivatives apply to, i.e. inertial or body fixed.

13.3.10 Static Stability (Stick Fixed)

One important issue related to the equilibrium manoeuvre is the static stability of the aircraft when encountering a disturbance, i.e. the aircraft should return to its balanced state without pilot intervention (stick fixed). The condition for static stability is that $\partial C_\mathrm{M}/\partial\alpha < 0$, where C_M is the overall pitching moment coefficient related to the centre of mass position. This condition may be evaluated and rearranged to give a criterion for the location of the centre of mass for stability, namely

$$l_\mathrm{W} < l_\mathrm{T}\frac{a_\mathrm{T}}{a_\mathrm{W}}\frac{S_\mathrm{T}}{S_\mathrm{W}}(1 - k_\varepsilon). \tag{13.26}$$

Thus the centre of mass must be ahead of the so-called neutral point where the aircraft is neutrally stable (i.e. a change in incidence does not introduce a pitching moment) or else, if it is behind it, the aircraft will be unstable. The static margin is the distance that the centre of mass is ahead of the neutral point.

13.3.11 Example: An Equilibrium Manoeuvre – Rigid Aircraft Pitching

An example using the simple tailplane and wing lift expressions for an equilibrium manoeuvre was given earlier. In this section, the calculation of trim incidence and elevator angle for manoeuvres with different load factors is considered using the simultaneous equations developed for the thrust and drag in-line case. The analysis and example will be repeated later for a simple flexible aircraft.

Consider a rigid aircraft with the following data: $m = 10\,000$ kg, $S_\mathrm{W} = 30$ m^2, $S_\mathrm{T} = 7.5$ m^2, $c = 2.0$ m, $l_\mathrm{W} = 0.6$ m, $l_\mathrm{T} = 7$ m, $a_\mathrm{W} = 4.5$ per rad, $a_\mathrm{T} = 3.2$ per rad, $a_\mathrm{E} = 1.5$ per rad, $k_\varepsilon = 0.35$, $\alpha_0 = -0.03$ rad and $C_{M_{0\mathrm{W}}} = -0.03$. Further parameters will be defined later for the flexible aircraft. It should be noted that the data used corresponds to a static margin of 0.21 m (10 %c) and a flaps-up stall speed of 60 m/s EAS ($C_{\mathrm{L_{Max}}} = 1.5$).

The aim of the example is to determine the trim incidence and elevator angle as (a) a function of load factor between -1.0 and 2.5 at an air speed of 150 m/s EAS and also as (b) a function of air speed in the range 120 to 200 m/s EAS for a load factor of 2.5. A MATLAB program set up to solve the two simultaneous equations is included in appendix I in the companion website. The analysis used in these examples is based upon the solution of Equation (13.24).

Results are shown in Figures 13.8(a) and (b). It may be noted that: (a) the elevator angle to trim is proportional to the trim incidence, (b) the trim incidence increases with the load factor since a larger

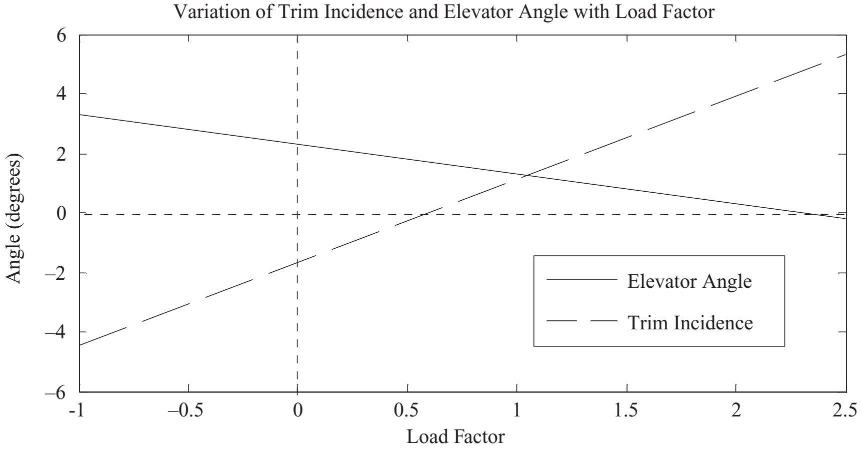

(a) Load factor

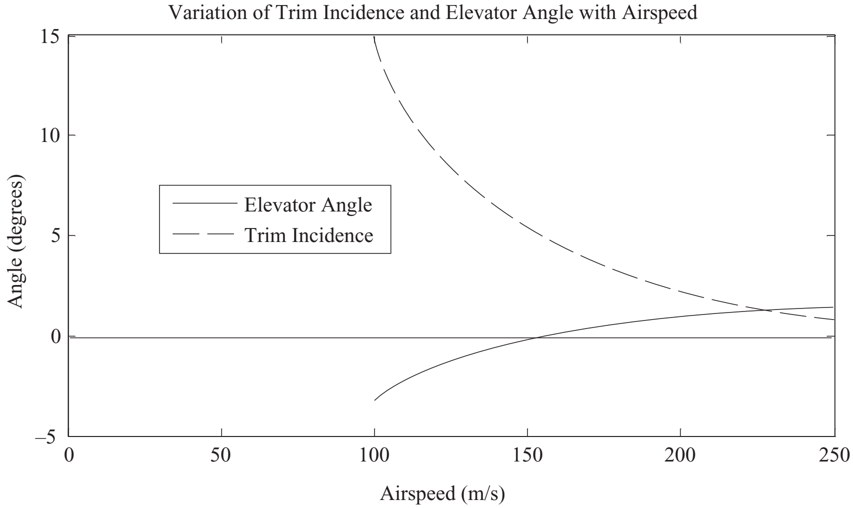

(b) Air speed

Figure 13.8 Results for the example of a rigid aircraft in an equilibrium manoeuvre – trim incidence and elevator angle as a function of (a) load factor (150 m/s EAS) and (b) air speed ($n = 2.5$).

wing lift needs to be developed, (c) the elevator angle to trim may be positive or negative depending upon the air speed and (d) the trim incidence increases at lower air speeds to maintain lift (heading towards stall). The elevator angle acts together with the trim incidence to produce the required tailplane lift force for trim; the trim elevator angle will also depend upon the centre of mass position and whether flaps are deployed (since $C_{M_{0\mathrm{W}}}$ is more negative).

13.4 EQUILIBRIUM MANOEUVRE – FLEXIBLE AIRCRAFT PITCHING

So far, the equilibrium manoeuvres have only been considered for the rigid aircraft, either in heave alone or in combined heave and pitch; also, in the analysis so far, the wing could be unswept/swept and untapered/tapered. In practice, flexible effects can make a significant difference to the balanced/trimmed condition and also to the magnitude and distribution of loads developed on the aircraft in that manoeuvre.

For an unswept wing, if it is assumed that the wing and tailplane aerodynamic centre positions and zero lift pitching moment coefficient are unaffected by flexible effects, then the wing and tailplane lift forces required for balance will not change due to flexible effects; what will change is the trim incidence and elevator angle needed to generate these forces, and also the distribution of the lift loading along the wing. The situation for a swept wing is different and will be discussed later without formal analysis.

In this section, the analysis of a simple aircraft with a flexible fuselage, flexible wing and rigid tailplane will be carried out. To make the treatment more manageable, it is assumed that the wing is unswept and untapered. A single whole aircraft free–free symmetric flexible mode involving fuselage bending and wing bending/twist will be included in the two DoF heave/pitch type analysis covered in the previous section. Solving this three DoF problem, and including the elevator, allows the equilibrium manoeuvre for a simple flexible aircraft to be considered when it experiences a load factor n and a steady pitch rate q (nose up), leading to the flexible aircraft balanced/trimmed state and a revised value for the incidence and elevator angle to trim.

Cases with different mode shapes may be considered after the model has been developed; e.g. wing twist, wing bending or fuselage bending flexible effects may be chosen to be dominant (see Appendix C). It should be noted that the same flexible model will be used in Chapters 15 to 18 and that much of the analysis undertaken in this chapter will be applicable later on.

In the ESDU series, the static aeroelastic behaviour of a flexible aircraft with a swept wing is considered in some detail using assumed modes (ESDU Data Sheet 97032) and normal modes (ESDU Data Sheet 99033).

13.4.1 Definition of the Flexible Aircraft with Unswept Wings

The simplified flexible aircraft consists of uniform, untapered, unswept but flexible wings of chord c and semi-span s, plus a flexible fuselage and rigid tailplane, as shown in Figure 13.9.

The wings are assumed to have a uniform mass distribution with mass μ_{W} and pitch moment of inertia χ_{W} per unit span. The wing mass axis (WM) lies a distance l_{WM} ahead of the aircraft centre of mass (CM) (and is typically around the mid-chord). The mass and pitch moment of inertia of the aircraft fuselage will be represented by discretizing it into three ‘lumps’ of mass m_{F}, m_{C} and m_{T} at the front, centre and rear fuselage; these discrete masses are positioned at the front fuselage (a distance l_{F} forward of the centre of mass), the whole aircraft CM, and at the tailplane aerodynamic centre respectively.

The wing flexural (or elastic) axis WF (typically around a one-third chord) is assumed to lie a distance l_{E} ahead of the wing mass axis (WM) so that wing bending/torsion coupling can occur. The wing aerodynamic centre axis (WA) (typically at the wing quarter chord) is at a distance l_{W} ahead of the centre of mass and a distance l_{A} ahead of the flexural axis. Thus the relationship between the wing chord dimensions is $l_{\mathrm{W}} = l_{\mathrm{A}} + l_{\mathrm{E}} + l_{\mathrm{WM}}$.

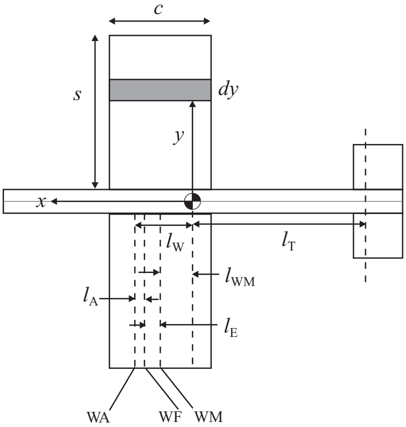

Figure 13.9 Flexible aircraft in an equilibrium manoeuvre – heave and pitch effects included.

If the elastic stiffness distributions along the wing and fuselage were to be specified, then it would be possible to calculate the aircraft modal characteristics using the Rayleigh–Ritz or finite element approaches (see Chapters 3 and 4); different relative stiffnesses between the wing and fuselage would lead to different mode shapes and natural frequencies for the fundamental mode. However, to allow control and modification of the mode shapes and natural frequencies, and to allow an analytical approach to be used, the philosophy here will be to define the type of mode required (e.g. wing bending), to obtain mode shape parameters and modal mass by constraining the flexible mode to be orthogonal to the rigid body heave and pitch modes, and then to examine the effects of natural frequency by simply altering the modal stiffness while retaining the same mode shape.

The analysis in this chapter will be carried out from first principles using Lagrange's equations for the flexible mode equation; so the rigid aircraft derivatives will emerge again. The same concepts are seen in later chapters.

13.4.2 Definition of the Flexible Mode Shape

Selecting a suitable symmetric flexible/elastic mode (subscript e) that allows the illustration of key features in an equilibrium manoeuvre, while keeping the analysis as simple as possible, is not straightforward. In practice, many modes are required to represent the true behaviour of the flexible aircraft, but in the interest of keeping the mathematical model to three DoF, a single flexible mode, having the possibility of including wing twist, wing bending and fuselage bending effects by simply changing a set of mode shape parameters, will be employed. In Chapter 3, the analysis of a free–free flexible aircraft was considered, with rigid body heave and pitch modes combined with a flexible mode; it may be helpful for the reader to refer back to that chapter if not familiar with this kind of analysis.

The symmetric free–free flexible mode shape to be used, illustrated in Figure 13.10 for positive values of all parameters, has the following features:

- The wing twists (nose up) and bends (downwards) according to the assumed shapes, $\gamma_e(y)$ and $\kappa_e(y)$ respectively, both defined relative to the wing flexural axis.
- The fuselage centre section, where the wing is attached and incorporating the aircraft centre of mass location, is treated as rigid and so experiences a slope (nose up) of $\gamma_e(0) = \gamma_{e0}$ and a (downwards) displacement of $\kappa_e(0) = \kappa_{e0}$, both defined at the wing flexural axis location.

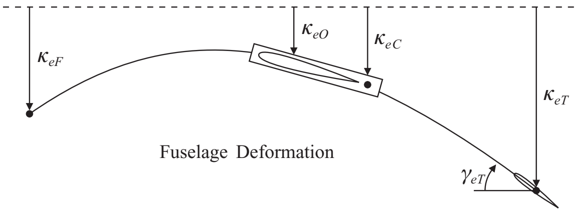

Fuselage Deformation

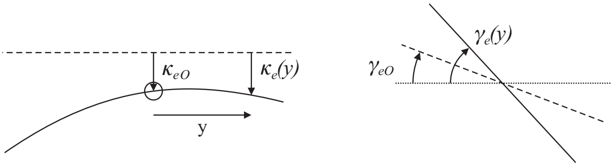

Wing Bending Deformation

Wing Twist Deformation

Figure 13.10 Free–free mode shape for flexible aircraft.

- The fuselage displacements (downwards) at the front fuselage, wing flexural axis, wing mass axis, aircraft centre of mass and tailplane positions are $\kappa_{\mathrm{eF}}, \kappa_{\mathrm{e0}}, \kappa_{\mathrm{eW}}, \kappa_{\mathrm{eC}}, \kappa_{\mathrm{eT}}$ respectively.
- The fuselage bends such that the (nose up) pitch in the mode shape at the rigid tailplane is γ_{eT}.

The generalised coordinate describing the absolute magnitude of the modal deformation is q_{e} (not to be confused with symbol q used elsewhere for pitch rate or dynamic pressure) and so, for example, the absolute displacement at the tailplane in the flexible mode is $\kappa_{\mathrm{eT}}q_{\mathrm{e}}$. The parameters defining the mode shape are considered in more detail in Appendix C, which also defines the modal parameter values to be used later. Flexible modes will be defined that involve wing bending, wing twist or fuselage bending as being dominant.

13.4.3 Expressions for Displacement and Angles Over the Aircraft

Now the flexible mode shape has been defined, expressions for the variation of (downwards) displacement and twist along the wing (and rotation at the tailplane) may be written for the combination of rigid body and flexible motions shown in Figure 13.11. The rigid body motions are defined by a (downward) displacement z_{C} at the centre of mass and angle α (nose up) whereas the flexible mode is defined by the generalized coordinate q_{e}.

The displacements at the *front fuselage* (subscript F), *aircraft centre of mass* (CM) and *tailplane* (T), are

$$z_{\mathrm{F}} = z_{\mathrm{C}} - l_{\mathrm{F}}\alpha + \kappa_{\mathrm{eF}}q_{\mathrm{e}}, \qquad z_{\mathrm{CM}} = z_{\mathrm{C}} + \kappa_{\mathrm{ec}}q_{\mathrm{e}}, \qquad z_{\mathrm{T}} = z_{\mathrm{C}} + l_{\mathrm{T}}\alpha + \kappa_{\mathrm{eT}}q_{\mathrm{e}}, \tag{13.27}$$

where the displacements (downwards positive) are a summation of the heave, pitch and flexible mode effects. The symbol z is commonly used for downwards displacement in aeroelasticity and gusts, and its use here should not be confused with its other use on some occasions as a position coordinate (see also Chapter 3).

Along the axis of *wing aerodynamic centres* (subscript WA), the *wing flexural axis* (WF) and *wing mass axis* (WM) for the starboard wing, the displacement variations are

$$\begin{aligned} z_{\mathrm{WA}}(y) &= z_{\mathrm{C}} - l_{\mathrm{W}}\alpha + [\kappa_{\mathrm{e}}(y) - l_{\mathrm{A}}\gamma_{\mathrm{e}}(y)]\, q_{\mathrm{e}}, \\ z_{\mathrm{WF}}(y) &= z_{\mathrm{C}} - (l_{\mathrm{W}} - l_{\mathrm{A}})\alpha + \kappa_{\mathrm{e}}(y)q_{\mathrm{e}}, \\ z_{\mathrm{WM}}(y) &= z_{\mathrm{C}} - l_{\mathrm{WM}}\alpha + [\kappa_{\mathrm{e}}(y) + l_{\mathrm{E}}\gamma_{\mathrm{e}}(y)]\, q_{\mathrm{e}}, \end{aligned} \tag{13.28}$$

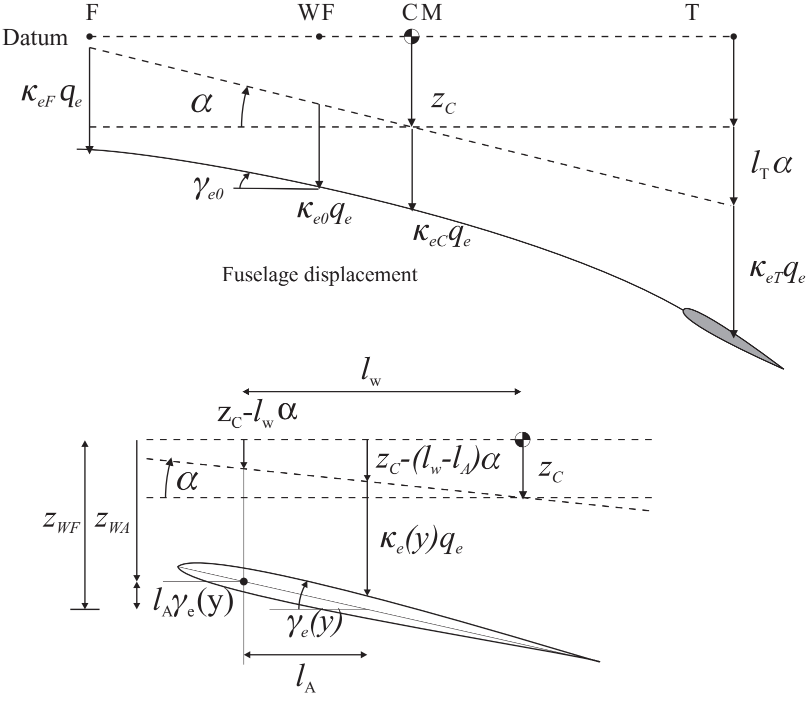
F
WF
CM
T
Datum
$\kappa_{eF} q_e$
α
z_C
$l_T \alpha$
γ_{e0}
$\kappa_{e0} q_e$
$\kappa_{eC} q_e$
$\kappa_{eT} q_e$
l_w
$z_C - l_w \alpha$
$z_C - (l_w - l_A)\alpha$
z_C
α
z_{WF}
z_{WA}
$\kappa_e(y) q_e$
$l_A \gamma_e(y)$
$\gamma_e(y)$
l_A

Fuselage displacement

Wing displacement

Figure 13.11 Aircraft displacements.

where the flexible deformation is a combination of wing bending and twist. The variation of the *effective wing incidence* along the starboard wing, including flexible effects, involves a combination of the trim incidence and the flexible mode twist and is given by

$$\alpha_W(y) = \alpha + \gamma_e(y) q_e. \tag{13.29}$$

These expressions will be required when Lagrange's equations are used to develop the equations of motion.

13.4.4 Aerodynamic Terms

Firstly, the aerodynamic terms due to the wing and tailplane will be determined. The tailplane may be considered as a whole (since it is rigid) whereas evaluating the wing contribution will involve integration using a strip dy because of the flexible twist present (see Chapter 8).

The *wing* incidence α_W on a strip dy at position y is given by Equation (13.29) so the steady lift on the strip is

$$\mathrm{d}L_W = \frac{1}{2}\rho V^2 c\, \mathrm{d}y a_W \left[\alpha - \alpha_0 + \gamma_e(y) q_e\right], \tag{13.30}$$

where a_W is the sectional wing lift curve slope and the additional flexible term may be seen when compared to the earlier analysis. The total wing lift is then given by the integration of this equation over the span, namely

$$L_{\mathrm{W}} = -Z_{\mathrm{W}} = 2\int_{y=0}^{s} \tfrac{1}{2}\rho V^2 c a_{\mathrm{W}}(\alpha - \alpha_0 + \gamma_{\mathrm{e}} q_{\mathrm{e}})\,\mathrm{d}y, \tag{13.31}$$

where it may be noted that the dependency of $\gamma_{\mathrm{e}}, \kappa_{\mathrm{e}}$ on y under the integrals will not always be explicitly stated from now on. It may be seen, as expected, that there is no steady aerodynamic contribution from the wing bending. There is also a zero lift pitching moment for the wing as seen before, namely

$$M_{0\mathrm{W}} = \tfrac{1}{2}\rho V^2 S_{\mathrm{W}} c C_{M_{0\mathrm{W}}}. \tag{13.32}$$

The *tailplane* incidence is given by

$$\alpha_{\mathrm{T}} = \alpha - \varepsilon + \frac{q l_{\mathrm{T}}}{V} + \gamma_{\mathrm{eT}} q_{\mathrm{e}} = \alpha - k_{\varepsilon}(\alpha - \alpha_0) + \frac{q l_{\mathrm{T}}}{V} + \gamma_{\mathrm{eT}} q_{\mathrm{e}}, \tag{13.33}$$

using the expression for mean downwash in Equation (13.18). A term is present to account for the fuselage slope γ_{eT} at the tailplane (nose up positive) in the flexible mode. The effect of the flexible deformation of the wing on downwash is neglected; more advanced aerodynamic methods would account for this effect. The tailplane lift is

$$L_{\mathrm{T}} = -Z_{\mathrm{T}} = \tfrac{1}{2}\rho V^2 S_{\mathrm{T}} \left\{ a_{\mathrm{T}} \left[k_{\varepsilon}\alpha_0 + (1 - k_{\varepsilon})\alpha + \frac{q l_{\mathrm{T}}}{V} + \gamma_{\mathrm{eT}} q_{\mathrm{e}} \right] + a_{\mathrm{E}}\eta \right\}, \tag{13.34}$$

where the effect of the elevator angle η is included to provide trim. Note that the effective incidence due to the nose up pitch rate considered earlier is also included. Again, the symbol q is used for pitch rate and also, with a subscript, for the flexible mode generalized coordinate, hopefully without causing confusion.

13.4.5 Inertia Terms

Because the aircraft is in a steady accelerated manoeuvre with a load factor n, the inertia forces (subscript I) may be considered using D'Alembert's principle. The (downwards) inertia force on the strip of wing will be

$$\mathrm{d}F_{\mathrm{WI}} = n(\mu_{\mathrm{W}}\mathrm{d}y)g \tag{13.35}$$

and the inertia forces for the front fuselage (F), centre fuselage (C) and tailplane (T) are

$$F_{\mathrm{FI}} = n m_{\mathrm{F}} g, \qquad F_{\mathrm{CI}} = n m_{\mathrm{C}} g, \qquad F_{\mathrm{TI}} = n m_{\mathrm{T}} g. \tag{13.36}$$

No inertia moments need to be included in this chapter as the aircraft is not accelerating in pitch. Note that there will be no kinetic energy term T because the manoeuvre is steady.

13.4.6 Stiffness Term

Only the flexible mode will introduce any structural stiffness effects. Rather than evaluate the strain energy using integration over the wing and fuselage using assumed bending and torsional rigidity expressions, it is simpler to write the strain energy as

$$U = \tfrac{1}{2} k_{\mathrm{e}} q_{\mathrm{e}}^2, \tag{13.37}$$

where k_e is the modal stiffness value (see Chapter 3). Adjustment of this stiffness will allow the natural frequency to be controlled readily for a given modal mass.

13.4.7 Incremental Work Done Terms

Incremental displacements at the wing, centre of mass, tailplane and fuselage are required in order to determine the incremental work done and therefore the generalized forces. As an example, the incremental displacement corresponding to the wing aerodynamic centre axis may be written from Equation (13.28) as

$$\delta z_{\mathrm{WA}}(y) = \delta z_{\mathrm{C}} - l_{\mathrm{W}}\delta\alpha + (\kappa_{\mathrm{e}} - l_{\mathrm{A}}\gamma_{\mathrm{e}})\delta q_{\mathrm{e}}. \tag{13.38}$$

The incremental work done for the wing total lift and zero lift pitching moment will then be given by

$$\begin{aligned} \delta W_{\mathrm{WA}} &= -2\int_{y=0}^{s} \mathrm{d}L_{\mathrm{W}}\,\delta z_{\mathrm{WA}} + M_{0\mathrm{W}}\,\delta\alpha, \\ \delta W_{\mathrm{WA}} &= -2\int_{y=0}^{s} \tfrac{1}{2}\rho V^2 c a_{\mathrm{W}}(\alpha - \alpha_0 + \gamma_{\mathrm{e}} q_{\mathrm{e}})\ [\delta z_{\mathrm{C}} - l_{\mathrm{W}}\delta\alpha + (\kappa_{\mathrm{e}} - l_{\mathrm{A}}\gamma_{\mathrm{e}})\delta q_{\mathrm{e}}]\ \mathrm{d}y + M_{0\mathrm{W}}\,\delta\alpha, \end{aligned} \tag{13.39}$$

where the minus sign in the work expression occurs because lift is positive upwards and displacement is positive downwards. The zero lift pitching moment does work through an incremental incidence angle. Similarly, the incremental work done for the tailplane lift is

$$\begin{aligned} \delta W_{\mathrm{TA}} &= -L_{\mathrm{T}}\delta z_{\mathrm{T}} \\ &= -\tfrac{1}{2}\rho V^2 S_{\mathrm{T}} \left\{ a_{\mathrm{T}} \left[k_\varepsilon \alpha_0 + (1 - k_\varepsilon)\alpha + \frac{q l_{\mathrm{T}}}{V} + \gamma_{\mathrm{eT}} q_{\mathrm{e}} \right] + a_{\mathrm{E}}\eta \right\} (\delta z_{\mathrm{C}} + l_{\mathrm{T}}\delta\alpha + \kappa_{\mathrm{eT}}\delta q_{\mathrm{e}}). \end{aligned} \tag{13.40}$$

Finally, the net incremental work done by the wing and fuselage/tailplane inertia forces is

$$\begin{aligned} \delta W_{\mathrm{I}} &= F_{\mathrm{FI}}\delta z_{\mathrm{F}} + F_{\mathrm{CI}}\delta z_{\mathrm{CM}} + 2\int_0^s \mathrm{d}F_{\mathrm{WI}}\delta z_{\mathrm{WM}} + F_{\mathrm{TI}}\delta z_{\mathrm{T}} \\ &= n m_{\mathrm{F}} g\ (\delta z_{\mathrm{C}} - l_{\mathrm{F}}\delta\alpha + \kappa_{\mathrm{eF}}\delta q_{\mathrm{e}}) + n m_{\mathrm{C}} g\ \left(\delta z_{\mathrm{C}} + \kappa_{\mathrm{e_C}}\delta q_{\mathrm{e}}\right) \\ &\quad + 2\int_0^s n\mu_{\mathrm{W}} g\ \{\delta z_{\mathrm{C}} - l_{\mathrm{WM}}\delta\alpha + [\kappa_{\mathrm{e}}(y) + l_{\mathrm{E}}\gamma_{\mathrm{e}}(y)]\,\delta q_{\mathrm{e}}\}\,\mathrm{d}y + n m_{\mathrm{T}} g\ (\delta z_{\mathrm{C}} + l_{\mathrm{T}}\delta\alpha + \kappa_{\mathrm{eT}}\delta q_{\mathrm{e}})\,. \end{aligned} \tag{13.41}$$

In this work expression for inertia forces, the overall term in $\delta\alpha$ will be zero (since masses of fuselage, wing and tailplane have to balance about the overall aircraft centre of mass) and the term in δq_e is also zero, since there must be no net inertia force in a free–free mode. Therefore this work done term can be simplified to

$$\delta W_{\mathrm{I}} = nmg\,\delta z_{\mathrm{C}} = nW\,\delta z_{\mathrm{C}}. \tag{13.42}$$

The right-hand side applied aerodynamic and inertia forces in both the rigid body and flexible modes can now be determined by employing the differentials of these incremental work terms in Lagrange's equations.

13.4.8 Aerodynamic Derivatives – Rigid Body and Flexible

As an example of how the aerodynamic contribution converts to derivative form when applying Lagrange's equation, consider the term in the heave equation for the wing aerodynamics only:

$$\frac{\partial(\delta W_{\mathrm{WA}})}{\partial(\delta z_{\mathrm{C}})} = -2\int_{y=0}^{s} \frac{1}{2}\rho V^2 c a_{\mathrm{W}}(\alpha - \alpha_0 + \gamma_{\mathrm{e}}(y) q_{\mathrm{e}})\,\mathrm{d}y = Z_{\mathrm{W}} = Z_{0_{\mathrm{W}}} + Z_{\alpha_{\mathrm{W}}}\alpha + Z_{\mathrm{e_W}} q_{\mathrm{e}}, \tag{13.43}$$

where each of the derivatives for the wing may be seen by inspection and it may be noted that there is no aerodynamic derivative term associated with the coordinate z_{C}. It may be seen that there is a flexible derivative Z_{eW} denoting the normal force on the wing per unit flexible mode deformation. When tailplane terms are added and the equivalent pitching moment expression is derived, it may be shown that the flexible derivatives (wing + tailplane) that appear in the normal force and pitching moment equations are

$$\begin{aligned} Z_{\mathrm{e}} &= \frac{\partial Z}{\partial q_{\mathrm{e}}} = \tfrac{1}{2}\rho V^2\left(-S_{\mathrm{W}}a_{\mathrm{W}}J_1 - S_{\mathrm{T}}a_{\mathrm{T}}\gamma_{\mathrm{eT}}\right), \\ M_{\mathrm{e}} &= \frac{\partial M}{\partial q_{\mathrm{e}}} = \tfrac{1}{2}\rho V^2\left(S_{\mathrm{W}}a_{\mathrm{W}}l_{\mathrm{W}}J_1 - S_{\mathrm{T}}a_{\mathrm{T}}l_{\mathrm{T}}\gamma_{\mathrm{eT}}\right), \end{aligned} \tag{13.44}$$

where the wing area $S_{\mathrm{W}} = 2cs$ and $J_1 = 1/s\int_{y=0}^{s}\gamma_{\mathrm{e}}\mathrm{d}y$ is a constant that depends upon the wing twist shape. The basic lift and moment derivatives associated with zero lift, incidence, pitch rate and elevator angle are the same as for the rigid aircraft in the previous section.

As an example of finding flexible mode derivatives, consider the flexible mode term for the wing aerodynamics

$$\frac{\partial(\delta W_{\mathrm{WA}})}{\partial(\delta q_{\mathrm{e}})} = -2\int_{y=0}^{s}\tfrac{1}{2}\rho V^2 c a_{\mathrm{W}}(\alpha - \alpha_0 + \gamma_{\mathrm{e}}q_{\mathrm{e}})(\kappa_{\mathrm{e}} - l_{\mathrm{A}}\gamma_{\mathrm{e}})\,\mathrm{d}y = Q_{0_{\mathrm{W}}} + Q_{\alpha_{\mathrm{W}}}\alpha + Q_{\mathrm{e_W}}q_{\mathrm{e}}. \tag{13.45}$$

This term will yield flexible derivatives such as $Q_\alpha = \partial Q/\partial\alpha$ in the generalized equation for the flexible mode. When tailplane terms are added, the derivatives (wing + tailplane) in the flexible mode equation are given by

$$\begin{aligned} Q_0 &= \tfrac{1}{2}\rho V^2\left(S_{\mathrm{W}}a_{\mathrm{W}}J_2 - S_{\mathrm{T}}a_{\mathrm{T}}k_{\varepsilon}\kappa_{\mathrm{eT}}\right)\alpha_0, \\ Q_q &= -\tfrac{1}{2}\rho V S_{\mathrm{T}}a_{\mathrm{T}}l_{\mathrm{T}}\kappa_{\mathrm{eT}}, \\ Q_\alpha &= \tfrac{1}{2}\rho V^2\left(-S_{\mathrm{W}}a_{\mathrm{W}}J_2 - S_{\mathrm{T}}a_{\mathrm{T}}(1-k_{\varepsilon})\kappa_{\mathrm{eT}}\right), \\ Q_{\mathrm{e}} &= \tfrac{1}{2}\rho V^2\left(-S_{\mathrm{W}}a_{\mathrm{W}}J_3 - S_{\mathrm{T}}a_{\mathrm{T}}\gamma_{\mathrm{eT}}\kappa_{\mathrm{eT}}\right), \\ Q_\eta &= -\tfrac{1}{2}\rho V^2 S_{\mathrm{T}}a_{\mathrm{E}}\kappa_{\mathrm{eT}}, \end{aligned} \tag{13.46}$$

where $J_2 = 1/s\int_{y=0}^{s}(\kappa_{\mathrm{e}} - l_{\mathrm{A}}\gamma_{\mathrm{e}})\mathrm{d}y$ and $J_3 = 1/s\int_{y=0}^{s}(\kappa_{\mathrm{e}} - l_{\mathrm{A}}\gamma_{\mathrm{e}})\gamma_{\mathrm{e}}\mathrm{d}y$ are further constants that depend upon the bending and twist shapes. The wing bending deformation dictated by $\kappa_{\mathrm{e}}(y)$ only affects the Q_0, Q_α, Q_{e} derivatives where J_2 and J_3 appear and wing bending should only affect the deformed shape in trim but not the trimmed incidence and elevator angle derivatives. Derivatives are tabulated in Appendix B.

13.4.9 Equations of Motion for Flexible Aircraft Pitching

When Lagrange's equations are used, it may be shown after simplification that the equations may be written in derivative form (defined with respect to inertial axes), namely

$$\left[-\left[\begin{array}{cc|c} 0 & Z_\alpha & Z_{\mathrm{e}} \\ 0 & M_\alpha & M_{\mathrm{e}} \\ \hline 0 & Q_\alpha & Q_{\mathrm{e}} \end{array}\right] + \left[\begin{array}{cc|c} 0 & 0 & 0 \\ 0 & 0 & 0 \\ \hline 0 & 0 & k_{\mathrm{e}} \end{array}\right]\right]\left\{\begin{array}{c} z_{\mathrm{C}} \\ \alpha \\ \hline q_{\mathrm{e}} \end{array}\right\} = \left\{\begin{array}{c} Z_\eta \\ M_\eta \\ \hline Q_\eta \end{array}\right\}\eta + \left\{\begin{array}{c} 1 \\ 0 \\ \hline 0 \end{array}\right\}nW + \left\{\begin{array}{c} Z_q \\ M_q \\ \hline Q_q \end{array}\right\}q + \left\{\begin{array}{c} Z_0 \\ M_0 \\ \hline Q_0 \end{array}\right\}, \tag{13.47}$$

where rigid and flexible terms are partitioned. Additional flexible modes would simply increase the partition dimensions corresponding to the flexible modal coordinates. If Equations (13.47) are examined carefully, it can be seen that the square matrix on the left hand side is singular so these equations cannot apparently be solved in this form. In fact, the rigid body heave displacement z_{C} would not even appear if the equations were written out in longhand form, and so it is therefore not possible to identify its value. This is because any arbitrary value of z_{C} could satisfy the equation, since the model used does not have any means of defining a unique vertical position for the aircraft. However, the three equations may be seen to have three unknowns, namely α, q_{e} and η. Rewriting the equations in terms of these unknowns yields

$$\left[-\left[\begin{array}{cc|c} Z_\eta & Z_\alpha & Z_{\mathrm{e}} \\ M_\eta & M_\alpha & M_{\mathrm{e}} \\ \hline Q_\eta & Q_\alpha & Q_{\mathrm{e}} \end{array}\right] + \left[\begin{array}{cc|c} 0 & 0 & 0 \\ 0 & 0 & 0 \\ \hline 0 & 0 & k_{\mathrm{e}} \end{array}\right]\right] \left\{\begin{array}{c} \eta \\ \alpha \\ \hline q_{\mathrm{e}} \end{array}\right\} = \left\{\begin{array}{c} 1 \\ 0 \\ \hline 0 \end{array}\right\} nW + \left\{\begin{array}{c} Z_q \\ M_q \\ \hline Q_q \end{array}\right\} q + \left\{\begin{array}{c} Z_0 \\ M_0 \\ \hline Q_0 \end{array}\right\}. \tag{13.48}$$

The equations may now be solved for the elevator angle to trim, trim incidence and flexible deformation in the manoeuvre. This form of the equations also applies for models with more flexible modes. The effect of introducing aircraft flexibility may be seen by comparing this equation with that for the rigid aircraft in Equation (13.24); an additional flexible mode equation, coupled aerodynamically to the rigid body motions, is present. The effect of out-of-line thrust and drag may be included as before by adding a drag equation.

13.4.10 General form of Equilibrium Manoeuvre Equations

The equations of motion (13.48) for the trimmed/balanced state may now be written in the more general form (c.f. Chapter 11 for flutter and divergence)

$$\left[\rho V^2 \mathbf{C} + \mathbf{E}\right] \left\{\begin{array}{c} \eta \\ \alpha \\ q_{\mathrm{e}} \end{array}\right\} = \boldsymbol{F}_{\mathrm{I}} nW + \rho V \boldsymbol{F}_{q} q + \rho V^2 \boldsymbol{F}_0 \alpha_0, \tag{13.49}$$

where $\mathbf{C}$ is an aerodynamic stiffness matrix, $\mathbf{E}$ is the structural stiffness matrix and the right-hand side force vectors $\boldsymbol{F}$ correspond to the inertia, pitch rate and zero incidence effects. The dependency upon density and air speed has been highlighted. Clearly, by comparing Equations (13.48) and (13.49), these matrices and vectors may be related to the aerodynamic derivatives.

13.4.11 Values for the Flexible Mode Parameters

In Appendix C, several versions of the whole aircraft symmetric free–free flexible mode are considered, with either fuselage bending, wing bending or wing twist being the dominant feature of the mode shape; the fuselage bending and wing bending/twist contributions are controlled by the bending and torsion rigidities EI_{Fuselage}, EI_{Wing} and GJ_{Wing}, and an individual contribution (e.g. wing bending) becomes 'dominant' when the other two rigidities are allowed to tend to infinity. It is then simple to change an example from one mode type to another. Also, a mode may have all three components if desired, but that case is not considered. Example mode shapes and modal masses are shown in Appendix C for the set of aircraft parameters used in the example to follow.

13.4.12 Lift Distribution and Deformed Shape in the Manoeuvre

Having found the elevator angle, incidence and flexible mode generalized coordinate for the balanced manoeuvre, the lift distribution along the wing and the deformed shape of the aircraft may be determined. The lift per unit span, or lift distribution, may be found by rewriting Equation (13.30) as

$$\frac{\mathrm{d}L_{\mathrm{W}}}{\mathrm{d}y} = \frac{1}{2}\rho V^2 c a_{\mathrm{W}} \left[\alpha - \alpha_0 + \gamma_{\mathrm{e}}(y) q_{\mathrm{e}}\right]. \tag{13.50}$$

Clearly, the lift distribution is only affected by the aircraft flexibility for a mode involving wing torsion; the effect will be to shift the lift outboard (see Chapter 8). The deformation of the wing and fuselage may be found from the mode shape definition shown in Figure 13.10 and the value of the generalized coordinate q_e.

13.4.13 Example: Equilibrium Manoeuvre – Flexible Aircraft Pitching

This example corresponds to the rigid aircraft in Section 13.3.11 but additional parameters are specified to cater for the introduction of flexible effects, namely, fuselage mass terms $m_F = 1500$ kg, $m_C = 4000$ kg, $m_T = 1500$ kg, wing mass/inertia terms $m_W = 2\mu_W s = 3000$ kg, $I_W = 2\chi_W s = 1330$ kg m^2, aircraft pitch moment of inertia $I_y = 144\,000$ kg m^2 and dimensions $s = 7.5$ m, $l_A = 0.25$ m, $l_E = 0.25$ m, $l_{WM} = 0.1$ m and $l_F = 6.8$ m. The modal mass and mode shape parameters for dominant (a) fuselage bending, (b) wing bending and (c) wing twist modes are shown in Appendix C. Then, by varying the value of modal stiffness, the natural frequency of the flexible mode can be altered without changing anything else.

The aim of the example is to determine the effect of the flexible mode natural frequency for the three different mode types on the flexible deformation and on the trim incidence/elevator angle. Only a load factor of 1.0 and air speed of 150 m/s EAS are considered; the results can then be compared to those for the rigid aircraft. A MATLAB program set up to illustrate the process of solving the three simultaneous equations is included in appendix I of the companion website. The analysis used in these examples is based upon the solution of Equation (13.48).

13.4.13.1 Fuselage bending mode

Results for the trim incidence/elevator angle and the fuselage deformation are shown plotted against natural frequency of this fuselage bending mode in Figure 13.12(a) and (b) when the idealized mode involves bending of the fuselage but not wing bending or twist. The wings behave rigidly and heave the same amount as the centre of mass. The trim incidence is unaffected by flexible effects (so rigid and flexible curves overlie each other), but the elevator angle becomes more negative as the aircraft becomes more flexible (i.e. at lower natural frequencies). An attempt will be made to explain what is happening physically.

The fuselage deformation in the balanced state due to flexibility effects may be seen to involve the centre fuselage (and wings) deflecting upwards and the nose/tailplane bending downwards, which corresponds to a negative value of the modal generalized coordinate. This sense of the modal deflection may be understood by considering the modal force generated by the aerodynamic and inertia forces present for the balanced rigid aircraft. It may be shown that the wing lift force and nose/tailplane inertia forces cause a negative modal force that exceeds the positive modal force contribution due to the tailplane lift and centre fuselage/wing inertia forces; the result is the negative modal deformation seen in the results. This deformed shape will not influence the wing lift because there is no wing twist, but it will tend to increase the tailplane lift due to the nose up flexible pitch at the tailplane. Therefore a more negative elevator angle is required to compensate for this effect and so maintain the same tailplane lift force for trim.

For the most flexible 2 Hz natural frequency case (excessively low for this size of aircraft), the fuselage deflections are of the order of 0.05 m and as the effective natural frequency increases, this deformation reduces rapidly. For a higher load factor of 2.5, the behaviour is similar but the flexible deflection increases to around 0.12 m. At higher air speeds, the flexible effect changes because of the revised balance of forces.

13.4.13.2 Wing bending mode

Consider the case where the idealized mode has wing bending but no wing twist or fuselage bending (though there is a small fuselage pitch present). The flexible mode natural frequency only has a very small effect upon the incidence and the elevator angle to trim. However, the variation of wing tip and root

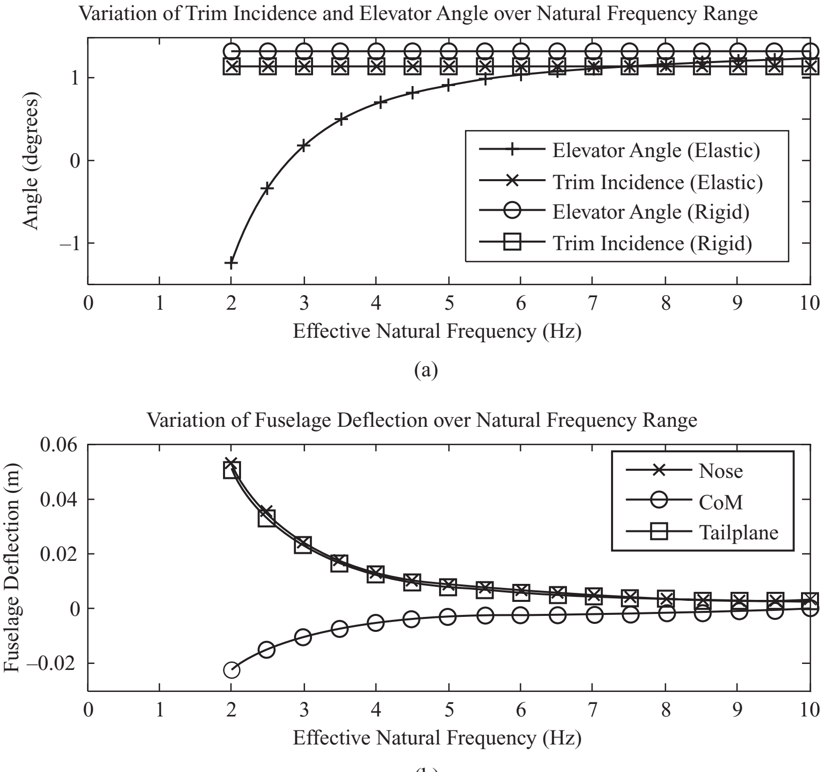
Variation of Trim Incidence and Elevator Angle over Natural Frequency Range

(a)

Variation of Fuselage Deflection over Natural Frequency Range

(b)

Figure 13.12 Results for the example of a flexible aircraft in an equilibrium manoeuvre – fuselage bending mode at 150 m/s EAS and $n = 1$: (a) trim incidence and elevator angle and (b) fuselage deflection.

deflection with natural frequency for 150 m/s air speed and $n = 1$ is seen in Figure 13.13; there is some wing bending deflection due to the wing lift distribution (around 0.25 m upwards at the tip and 0.028 m downwards at the fuselage for the most flexible 2 Hz mode case) and also a very small nose down pitch (around 0.01°). These values reduce quickly with an increase in natural frequency. It is expected that this mode would have no effect on the trimmed state but the small pitch deflection explains the very small flexible effect on trim incidence and elevator angle found (typically there is only about a 1 % change in the angles due to the flexible effect, which is not worth plotting).

13.4.13.3 Wing twist mode

Here the idealized mode has wing twist but no wing or fuselage bending (though there is a small fuselage pitch). The variation of the trim incidence, elevator angle and the wing twist deflection with natural frequency is shown in Figures 13.14(a) and (b); since the deflections at 2 Hz were found to be unrealistic (16° steady twist), the lowest frequency considered was 4 Hz (about 2° twist), but even that frequency is low. Torsional stiffness is a very important parameter in determining the flutter speed and therefore the twist mode occurs at a higher frequency than the bending mode.

For this mode, Figure 13.14(a) shows that both the trim incidence and elevator angle are changed noticeably by flexible effects. The wing twists nose up due to the aerodynamic lift force acting ahead

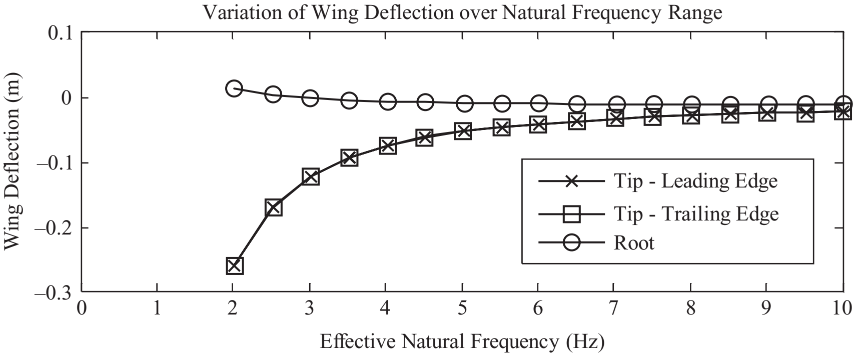

Figure 13.13 Results for the example of a flexible aircraft in an equilibrium manoeuvre – wing bending mode at 150 m/s EAS and $n = 1$: wingtip deflection.

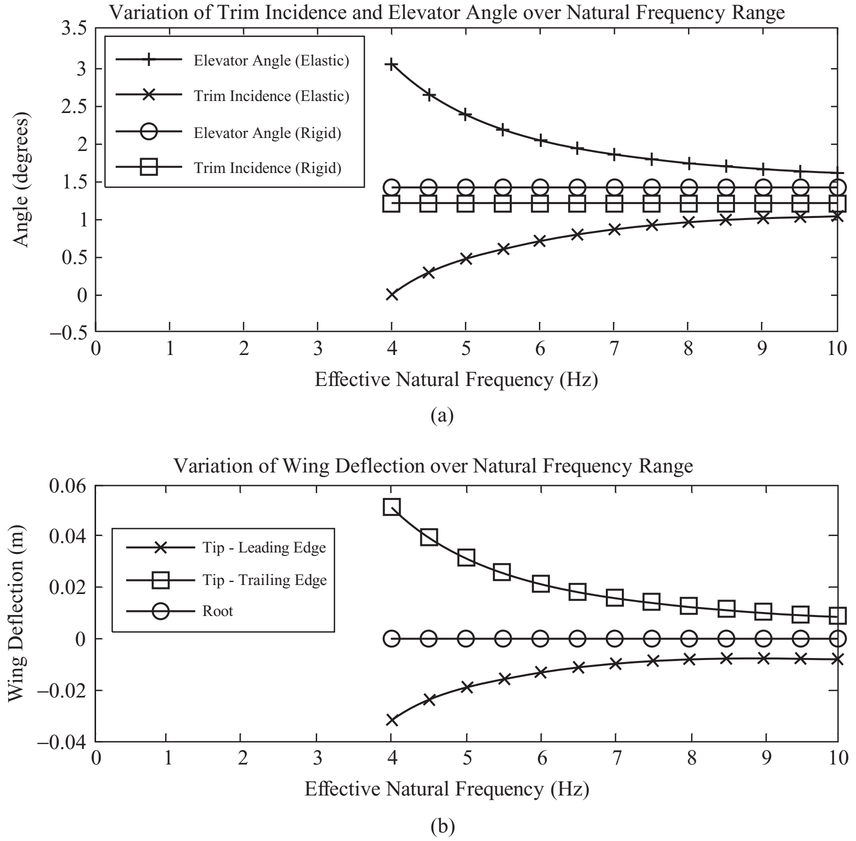

Figure 13.14 Results for the example of a flexible aircraft in an equilibrium manoeuvre – wing twist mode at 150 m/s EAS and $n = 1$: (a) trim incidence and elevator angle and (b) flexible mode deflection.

of the flexural axis and so will tend to increase the wing lift further; in order to maintain the same total wing lift for trim, the trim incidence has to reduce. As a result, the tailplane lift reduces and less of the up elevator is required to maintain the same total lift force. As mentioned earlier, the lift will shift outboard due to the flexible effect and so increase the wing root shear force and bending moment when compared to the rigid aircraft (see also Chapter 18).

13.4.14 Review of Flexible Effects in an Equilibrium Pitching Manoeuvre for an Unswept Wing

The above analysis and examples have demonstrated a number of features for the equilibrium manoeuvre of a simple flexible aircraft, summarized as follows:

- The wing and tailplane lift forces for trim are the same whether the aircraft is rigid or flexible, but the incidence and elevator angle required for trim will change when flexibility is present.
- The flexible aircraft will deform under the aerodynamic and inertia loading for all mode types.
- The presence of a flexible mode involving fuselage bending and/or wing twist can alter the elevator angle to trim and hence affect the control requirements.
- The presence of a flexible mode involving wing bending will not affect the overall trim forces and angles but will cause wing bending deformation.
- The presence of a flexible mode involving wing twist will modify the spanwise aerodynamic loading distribution such that the loading reduces at the root and increases at the tip, so shifting the lift towards the tip and increasing the wing root shear force and bending moment in the manoeuvre.

It should of course be emphasized that, for a real aircraft, symmetric modes will involve both wing and fuselage deformation: while the wing bending mode tends to be the lowest in frequency, for an unswept wing the fuselage bending and wing twist have been seen to be more important with regard to trim. The position is somewhat different for a swept wing, as will be discussed in the next section.

13.4.15 Consideration of Flexible Swept Wing Effects on an Equilibrium Pitching Manoeuvre

In practice, most commercial aircraft of any size have wings that are moderately swept (20–30°) and this alters the effect of aircraft flexibility on the equilibrium manoeuvre. In this section, the likely effect of sweep for a flexible aircraft will be considered, but a full analytical treatment will not be given as it is significantly more difficult than the unswept case.

The manoeuvre calculations for a rigid aircraft with swept wings are carried out in precisely the same way as for unswept wings. However, it should be pointed out that the aircraft aerodynamic centre for swept wings will be somewhat aft of the root quarter chord, depending upon the sweep angle, and this will affect the aircraft centre of mass position needed to achieve trimmed flight. Also, the swept wing mass will have a much greater contribution to the aircraft pitch moment of inertia than for an unswept wing, but this is only relevant when the aircraft experiences pitch acceleration.

There are other key differences between swept and unswept wings when flexible effects are considered:

- The aerodynamic behaviour is significantly more three-dimensional so strip theory is less appropriate.
- The flexural axis is aft of the mid-chord over most of the span (typically around a two-thirds chord for a 30° sweep) but moves further aft as the wing root is approached.
- The simple treatment of a high aspect ratio wing with moderate sweep (20–30°, such as for commercial aircraft) has traditionally considered the wing to be a swept beam with bending rigidity *EI* and torsional rigidity *GJ* aligned with the sweep axis, although of course nowadays the finite element method is normally used to model the entire swept box structure.

- The angle of incidence is not only affected by wing twist but also by bending (see Chapter 8).
- Bending and torsion motions are coupled.

The impact of these features on the equilibrium manoeuvre will be discussed once the effect of flexibility on the incidence has been considered.

13.4.15.1 Effects of a flexible swept wing on incidence

This issue was raised earlier in Chapter 8 when considering the effect of forward or backward sweep on the aircraft divergence speed using the model of a simple rigid wing able to twist and flap elastically. The extension to a fully flexible swept wing involves allowing the wing to twist (nose up positive) and bend (downwards positive) according to the earlier assumed deformation functions γ_e and κ_e respectively. However, in this case the shapes will be defined with respect to the axis of sweep; i.e. the functions would become $\gamma_e(y_s)$ and $\kappa_e(y_s)$ where y_s is the distance from the root along the axis of sweep. Following the approach used earlier, and also given in Niu (1988), the increase of the streamwise angle of incidence associated with any flexible effects is

$$\Delta\alpha_e(y_s) = \gamma_e(y_s)\cos\Lambda + \frac{\partial\kappa_e(y_s)}{\partial y_s}\sin\Lambda, \tag{13.51}$$

where Λ is the angle of sweep. Here the differential is required to find the slope of the wing in the direction of the axis of sweep (i.e. along the beam); the term is related to the earlier flapping angle in Chapter 8. This equation implies that nose up flexible twist increases the effective incidence whereas upwards bending (i.e. a negative slope) will decrease it. Also, if the mode deformations for γ_e and κ_e are defined by simple linear and quadratic functions respectively, the incidence will change linearly along the span due to both types of flexible deformation. For an unswept wing ($\Lambda = 0$), only the twist has an effect on incidence.

13.4.15.2 Effects of a flexible swept wing on equilibrium manoeuvre

In regard to the balanced/trimmed condition for an aircraft with swept wings undergoing an equilibrium manoeuvre, the key difference to the unswept case is that any spanwise change of incidence can alter the fore-and-aft position of the net wing lift force and hence the magnitude of the wing and tailplane lift forces required for balance; this was not the case for the unswept wing. Note that when the aircraft is flying at a positive angle of incidence (in a sufficiently positive load factor manoeuvre), the positive lift distribution will act ahead of the flexural axis and thus have the potential to cause nose up twist and upwards bending of the wing. The different flexible modes will now be considered briefly with regard to their impact on trim in such a manoeuvre.

Fuselage bending mode

The special case of a mode where only the fuselage bends and the wing is rigid in bending and twist is straightforward. The positions and therefore magnitudes of the lift forces for balance will not change and therefore the elevator angle and incidence will alter to maintain the same tailplane lift force once the fuselage has deformed elastically; thus there is little difference to the unswept wing case.

Wing bending mode

In this idealized case, where the wing is rigid in twist and the fuselage rigid in bending, the sweep effect will mean that there will be a greater fuselage pitch in the free–free mode shape and therefore some influence from the tailplane pitch. However, the main effect is that the wing lift distribution will give rise to a bending deflection (upwards for positive lift) and this will reduce the effective incidence according to Equation (13.51) more towards the tip. What this means is that the effective centre of pressure on each wing moves towards the root and therefore forward on the aircraft. Then, in order to maintain balance, the incidence and elevator angle will need to be adjusted but the final balance forces will not be the same as for the rigid aircraft because the flexible effects mean that the wing lift will act further forward and so a somewhat smaller wing lift and larger tailplane lift will be required for balance. The inboard shift in the lift will decrease the wing root bending moment, for example, and so reduce the internal loads. Note that for a forward swept wing, the opposite occurs and the loads increase, as well as causing the reduced divergence speed mentioned earlier.

Wing twist mode

In this idealized case, where the wing twist is assumed to be dominant in the mode, there will be some fuselage pitch as before but no fuselage or wing bending. The wing lift distribution will give rise to a nose up flexible twist and so increase the lift, as well as moving the centre of pressure on each wing outboard towards the tip and therefore aft on the aircraft. In order to maintain trim, the incidence and elevator angle will need to be adjusted but the final balanced state will not be the same as for the rigid aircraft because the flexible effects mean that the wing lift will act further aft and so a larger wing lift and smaller tailplane lift will be required for trim. The outboard shift in the lift will increase the wing root bending moment.

Wing mode with bending and twist

Having investigated the idealized wing twist and bending cases separately, it is important to point out that the nature of the aircraft structure is such that, for a high aspect ratio wing, the wing bending mode will be at a lower frequency than the twist mode (though of course the deformations in any given mode tend to be a combination of both motions). Wing bending will be present in most modes and the reality for a swept wing aircraft is that the first free–free mode will be dominated by wing bending with some twist. Unlike the unswept case, this mode will have the most impact on trim. In Equation (13.51), the bending effect will tend to dominate the twist effect on incidence and so bending would be the most important term; therefore the comments made for wing bending are most relevant.

13.5 FLEXIBLE CORRECTIONS TO RIGID AIRCRAFT PITCHING DERIVATIVES

The analyses in this chapter have shown the combination of rigid body heave/pitch motions with a whole aircraft free–free flexible mode; the extension to more than one flexible mode has been pointed out. In some circumstances, e.g. in dynamic response calculations considered later, it may be useful to solve the rigid aircraft equations with rigid aircraft aerodynamic derivatives modified to account for flexible effects. Calculation of these modified derivatives can be achieved by an approach akin to static Guyan reduction (see Appendix D) and will be illustrated here using the steady model developed.

Consider first the equations for steady motion shown in Equation (13.47) but with a general right-hand side term included to allow for a range of right hand side derivative terms (e.g. zero incidence, control, pitch rate), namely

$$\left[\begin{array}{cc|c} 0 & -Z_\alpha & -Z_\mathrm{e} \\ 0 & -M_\alpha & -M_\mathrm{e} \\ \hline 0 & -Q_\alpha & k_\mathrm{e}-Q_\mathrm{e} \end{array}\right]\left\{\begin{array}{c} z_\mathrm{C} \\ \alpha \\ \hline q_\mathrm{e} \end{array}\right\}=\left\{\begin{array}{c} Z(t) \\ M(t) \\ \hline Q(t) \end{array}\right\}. \tag{13.52}$$

These equations may be rewritten in general matrix form with the rigid and flexible terms partitioned and submatrices indicated by the subscripts ‘r’ (rigid) and ‘e’ (elastic/flexible):

$$\left[\begin{array}{c|c} \mathbf{D}_\mathrm{rr} & \mathbf{D}_\mathrm{re} \\ \hline \mathbf{D}_\mathrm{er} & \mathbf{D}_\mathrm{ee} \end{array}\right]\left\{\begin{array}{c} \boldsymbol{r} \\ \hline \boldsymbol{e} \end{array}\right\}=\left\{\begin{array}{c} \boldsymbol{F}_\mathrm{r} \\ \hline \boldsymbol{F}_\mathrm{e} \end{array}\right\}. \tag{13.53}$$

These partitioned equations may be written separately. A solution for the flexible mode generalized coordinate may be found from the second equation and the result substituted into the first equation to obtain a revised rigid body coordinate equation with flexible effects accounted for:

$$\begin{aligned}&\mathbf{D}_{\mathrm{er}}\boldsymbol{r}+\mathbf{D}_{\mathrm{ee}}\boldsymbol{e}=\boldsymbol{F}_{\mathrm{e}},\\&\boldsymbol{e}=\mathbf{D}_{\mathrm{ee}}^{-1}\left(\boldsymbol{F}_{\mathrm{e}}-\mathbf{D}_{\mathrm{er}}\boldsymbol{r}\right),\\&\mathbf{D}_{\mathrm{rr}}\boldsymbol{e}+\mathbf{D}_{\mathrm{re}}\mathbf{D}_{\mathrm{ee}}^{-1}\left(\boldsymbol{F}_{\mathrm{e}}-\mathbf{D}_{\mathrm{er}}\boldsymbol{r}\right)=\boldsymbol{F}_{\mathrm{r}}.\end{aligned}\qquad(13.54)$$

The modified rigid aircraft matrix equation may then be written as

$$\bar{\mathbf{D}}_{\mathrm{rr}}\boldsymbol{r}=\bar{\boldsymbol{F}}_{\mathrm{r}},\qquad(13.55)$$

where an overbar has been used to indicate modified left- and right-hand side derivative terms given by

$$\begin{aligned}\bar{\mathbf{D}}_{\mathrm{rr}}&=\mathbf{D}_{\mathrm{rr}}-\mathbf{D}_{\mathrm{re}}\mathbf{D}_{\mathrm{ee}}^{-1}\mathbf{D}_{\mathrm{er}},\\\bar{\boldsymbol{F}}_{\mathrm{r}}&=\boldsymbol{F}_{\mathrm{r}}-\mathbf{D}_{\mathrm{re}}\mathbf{D}_{\mathrm{ee}}^{-1}\boldsymbol{F}_{\mathrm{e}}.\end{aligned}\qquad(13.56)$$

Thus the flexible mode equation has been removed (or ‘condensed out’) and the resulting rigid aircraft equation modified to account for flexible deformation. Derivatives modified for flexible effects may now be extracted.

Using the example where only one mode is present, some examples of the modified derivatives are

$$\bar{Z}_\alpha=Z_\alpha+\frac{Z_{\mathrm{e}}Q_\alpha}{k_{\mathrm{e}}-Q_{\mathrm{e}}},\qquad\bar{Z}_\eta=Z_\eta+\frac{Z_{\mathrm{e}}Q_\eta}{k_{\mathrm{e}}-Q_{\mathrm{e}}}\qquad(13.57)$$

In both cases, the flexible mode correction term tends to reduce the value of the rigid aircraft derivative.

Note that many flexible modes may be handled using this process since $\boldsymbol{e}$ is defined as a vector but the resulting expressions will be more complex if written explicitly. This process may be used in practice where only steady aeroelastic effects are considered important, e.g. in some dynamic flight mechanics solutions.

Having determined the flexible corrections to the *magnitude* of certain rigid aircraft derivatives, the effect of flexibility on the *distribution* of rigid aircraft aerodynamic loads may also be determined. From a particular balanced flight case for the flexible aircraft, the incidence, elevator angle and flexible mode generalized coordinate will be known and therefore the corresponding wing (and tailplane) lift distribution in the balanced condition may be determined. The overall ‘shape’ of the lift distribution may then be scaled such that the integrated total lift force over the aircraft per trimmed incidence, for example, matches the corrected derivative $\bar{Z}_\alpha$. Then results determined from the rigid aircraft will have both magnitude and distribution corrected for flexible effects, so allowing loads to be determined as accurately as possibly given the model reduction. This correction will be referred to again in Chapter 22.

13.6 EQUILIBRIUM MANOEUVRES – AIRCRAFT ROLLING AND YAWING

So far in this chapter, the symmetric pitching case has been considered in detail in order to demonstrate an important bookcase manoeuvre and a number of features of symmetric flight, e.g. balance or trim, aerodynamic derivatives, flexible mode effects, sweep effects, flexible corrections, etc. Dynamic pitching manoeuvres using a rational calculation are also required for certification but these will be considered later in Chapters 15 and 24.

However, there are some bookcase requirements for asymmetric manoeuvres that involve rolling or yawing and these will be considered briefly here but without derivation of the mathematical models involved and for the rigid aircraft only. Some approximations are made but it should be remembered that for many manufacturers, these cases are undertaken early in the design process to assist in initial sizing, with more accurate rational calculations performed for certification later in the design cycle. It is important to recognize that the presence of the flight control system (FCS) means that many bookcase loads results are found later to be overestimates.

In order to justify the way in which the load cases are treated, the equations for lateral motion of the aircraft will be written, assuming the aircraft is symmetric and that perturbations about straight and level flight are small. The basic equations of motion in sideslip, roll and yaw for the rigid aircraft use what are known as body fixed axes (Cook, 1999). Using Equations (14.27) and (14.29) of Chapter 14, the equations may be written in the form

$$m\dot{v} + mU_{\mathrm{e}}\dot{\psi} = Y, \qquad I_x\ddot{\phi} - I_{xz}\ddot{\psi} = L, \qquad I_z\ddot{\psi} - I_{xz}\ddot{\phi} = N, \tag{13.58}$$

where Y, L, N are the side force, rolling and yawing moments, ϕ, ψ are the roll and yaw angles, U_{e} is the forward speed, I_x, I_z are the roll and yaw moments of inertia and $I_{xz} = \int xz\,\mathrm{d}m$ is the relevant product moment of inertia. The sideslip angle β is given by the aircraft sideways velocity divided by the total air speed, so $\beta = v/V$ and hence the term $\dot{v} = V\dot{\beta}$ is actually a lateral acceleration term. Note that if the effects of a single elastic mode were included, then four equations of motion would be required; a simple flexible roll case for body fixed axes will be examined in Chapter 15 as a rational calculation.

13.6.1 Equilibrium Manoeuvre – Aircraft Rolling

It will be shown later in Chapter 24 that the basic certification requirements for roll involve a steady roll rate and a maximum roll acceleration case. Loads from both these manoeuvres must be superimposed upon an initial steady load factor.

13.6.1.1 Steady roll rate

Consider firstly the case of *steady roll rate* following a defined aileron deflection, in which case the acceleration terms are zero but various steady terms are nonzero. The applied forces and moments are expanded in derivative form, as used earlier for the pitch model; then, e.g. in the steady roll rate case, the rolling moment can be expanded as

$$L = L_{\xi}\xi + L_{\delta}\delta + L_{\beta}\beta + L_{\dot{\phi}}\dot{\phi}, \tag{13.59}$$

where ξ, δ are the aileron and rudder angles respectively, L_{ξ} is the rolling moment per aileron angle derivative, $L_{\dot{\phi}}$ is the roll damping derivative (from the effective incidence generated by any rolling lifting surfaces), etc. The roll angle is assumed to remain small so that the gravitational term in the y direction may be ignored. The heading is assumed to remain unchanged so the yaw angle is zero. If the derivative expansions are substituted into the equations of motion (13.58), acceleration terms set to zero and the equations rearranged, it may be shown that

$$\begin{bmatrix} Y_{\beta} & Y_{\delta} & Y_{\dot{\phi}} \\ L_{\beta} & L_{\delta} & L_{\dot{\phi}} \\ N_{\beta} & N_{\delta} & N_{\dot{\phi}} \end{bmatrix} \begin{Bmatrix} \beta \\ \delta \\ \dot{\phi} \end{Bmatrix} = - \begin{Bmatrix} Y_{\xi} \\ L_{\xi} \\ N_{\xi} \end{Bmatrix} \xi. \tag{13.60}$$

This equation indicates that a rudder angle and a resulting sideslip angle are required to create a balanced condition of pure steady roll rate. If, for example, the rudder was not deployed, then application of the aileron alone would introduce yaw.

It would be possible to treat this complete solution as a load case with loads developed on all axes. However, for simplicity, cross couplings between roll and yaw may be neglected so only a roll equation is involved (Lomax, 1996) and the aircraft is considered to be balanced in roll, with only the relevant lifting surface bending loads considered. It may be seen from Equation (13.60) that for the rolling manoeuvre, with coupling terms omitted, the equation reduces to

$$L_{\dot{\phi}}\dot{\phi} = -L_{\xi}\xi \tag{13.61}$$

and so the resulting steady roll rate is given by

$$\dot{\phi} = -\frac{L_{\xi}}{L_{\dot{\phi}}}\xi. \tag{13.62}$$

A similar result will be seen later in Chapter 15 when using a rational calculation. The distribution of these aerodynamic loads over the aircraft will be known so the internal loads may be calculated (i.e. bending moments on each lifting surface).

13.6.1.2 Maximum roll acceleration

For the *maximum roll acceleration* case, the bookcase methodology is to react the applied control moment by an inertia couple (and maybe force) at the instant of application so that no velocity or steady response values have yet developed; thus roll and yaw rates will be zero. Also, in this case the acceleration terms will be nonzero, there will be no applied rudder angle and the sideslip angle will be zero. The only relevant derivative terms will be those related to aileron angle so the equations of motion for this condition, starting from a level flight state, may be written as

$$\begin{bmatrix} mV & 0 & 0 \\ 0 & I_x & -I_{xz} \\ 0 & -I_{xz} & I_z \end{bmatrix} \begin{Bmatrix} \dot{\beta} \\ \ddot{\phi} \\ \ddot{\psi} \end{Bmatrix} = \begin{Bmatrix} Y_{\xi} \\ L_{\xi} \\ N_{\xi} \end{Bmatrix} \xi. \tag{13.63}$$

This equation would yield the accelerations at the instant of aileron application, before any response had developed. It may be seen that the yaw and roll accelerations are coupled if the product moment of inertia term is nonzero. Once again (Lomax, 1996), the coupling terms are neglected and so the roll behaviour is given by

$$I_x\ddot{\phi} = L_{\xi}\xi. \tag{13.64}$$

Hence the instantaneous roll acceleration may be determined and the load distribution due to aileron deployment will be balanced by the inertia loading associated with the roll inertia couple $I_x\ddot{\phi}$; the internal loads (i.e. related to bending of the lifting surfaces) may then be found. The way in which this maximum acceleration is determined will lead to an overestimate of loads (conservative) and a rational approach (see Chapters 15 and 24) would produce a more realistic set of loads. In practice, flexible effects will be included, either by adding flexible modes or by determining flexible corrections to the rigid aircraft derivatives; both approaches were considered earlier for the symmetric pitching case.

13.6.2 Equilibrium Manoeuvre – Aircraft Yawing

A somewhat similar approach may be taken for the yawing manoeuvre where (a) a rudder input is suddenly applied, (b) a maximum sideslip overswing is reached, followed by (c) a steady sideslip condition and (d) the rudder is returned to neutral. In effect, steps (a) and (d) involve abrupt rudder application and step (c) requires determination of the steady sideslip condition; the dynamic overswing step (b) (see Chapter 1) may be treated by application of an overswing factor (to allow for the resulting increase in load). Only steps (a) and (b) will be considered in this section, but this manoeuvre will also be considered later in Chapter 24.

13.6.2.1 Abrupt application of rudder

The *abrupt application of rudder* will be balanced by inertia effects and the condition examined prior to any response developing so the yaw and roll angles/rates will be zero. Starting from a steady level flight state ($\beta = \phi = \xi = 0$), the equations may be shown to be the same as in Equation (13.63) but with the rudder replacing the aileron. Therefore

$$\begin{bmatrix} mV & 0 & 0 \\ 0 & I_x & -I_{xz} \\ 0 & -I_{xz} & I_z \end{bmatrix} \begin{Bmatrix} \dot{\beta} \\ \ddot{\phi} \\ \ddot{\psi} \end{Bmatrix} = \begin{Bmatrix} Y_\delta \\ L_\delta \\ N_\delta \end{Bmatrix} \delta. \tag{13.65}$$

If, however, the rudder had been returned abruptly to zero when the aircraft was in a steady sideslip condition (see below), then additional right hand side forcing terms due to the corresponding nonzero steady sideslip, aileron and roll angles would have been included.

The equations could be solved for roll and yaw accelerations and rate of sideslip and loads for all axes considered. Alternatively, for simplicity, the coupling terms could be neglected and the instantaneous yaw acceleration given by

$$I_z \ddot{\psi} = N_\delta \delta. \tag{13.66}$$

Then only the balance of loads in yaw would be considered, rather as for the roll case earlier. In Lomax (1996) reference is made to yawing being a ‘flat’ manoeuvre, presumably indicating that couplings should be neglected wherever possible.

13.6.2.2 Steady sideslip

The *steady sideslip* condition (with zero heading) may be determined by setting all acceleration and velocity terms to zero, but roll angle (assumed small to justify ignoring gravitational forces) and aileron terms must be included in the steady sideslip, Thus the equations are given by

$$\begin{bmatrix} Y_\beta & Y_\xi & Y_\phi \\ L_\beta & L_\xi & 0 \\ N_\beta & N_\xi & 0 \end{bmatrix} \begin{Bmatrix} \beta \\ \xi \\ \phi \end{Bmatrix} = - \begin{Bmatrix} Y_\delta \\ L_\delta \\ N_\delta \end{Bmatrix} \delta \tag{13.67}$$

because $L_\phi = N_\phi = 0$. The solution of these equations (Lomax, 1996) will yield the steady sideslip and the corresponding aileron and roll angles in this balanced case; hence the relevant balanced aerodynamic loads may be determined. If the roll angle had been omitted (not a large value) then the aircraft would have been imbalanced in roll. If, in addition, the aileron angle had been set to zero, then different steady sideslip angles would have been obtained from the side force and yawing moment equations, so one or other would have been imbalanced. Therefore the steady sideslip strictly requires all three equations to be solved and the corresponding aerodynamic loads determined. However, it may be that only the yaw loads would be examined, as these will be dominant for lateral bending of the rear fuselage and tail.

The full yaw manoeuvre case involves four steps, the above two plus the dynamic overswing and return to neutral rudder; this will be discussed further in Chapter 24. A similar bookcase could be carried out for the ‘engine out’ condition, where the yawing moment due to engine out would be balanced by the rudder application (Lomax, 1996).

Note again that flexible effects would need to be included. Also, a rational calculation could be carried out for all the rudder application cases (see Chapter 24).

13.7 REPRESENTATION OF THE FLIGHT CONTROL SYSTEM (FCS)

The flight control system (FCS) has a significant impact upon the dynamic response and loads in a flexible commercial aircraft and will be introduced in Chapter 14. When equilibrium (or steady) manoeuvres are considered, only the steady effect of the FCS is important and so a full FCS model is not required. Instead, the effect of the FCS is represented by including the limits imposed by the FCS on the aircraft behaviour, e.g. in providing a maximum incidence (for high angle of incidence protection) or restricting pitch/roll rate.

13.8 EXAMPLES

1. Draw a basic manoeuvre envelope for the aircraft with the following characteristics: mass 10 000 kg, wing area 30 m^2, maximum lift coefficient 1.6, maximum and minimum load factors 3 and -1, cruise speed 220 m/s EAS and design dive speed 250 m/s EAS. Air density at sea level is 1.225 kg/m^3.
   [Stall speed at $n = 3$ is 100 m/s EAS]

2. For the following manoeuvres of the aircraft above in Example 1, determine the load factors and indicate the manoeuvres on the manoeuvre envelope drawn:
   (a) in a level turn (sea level) at 130 m/s, turning through 180° in 50 s;
   [$n = 1.30,\ \ R = 2069$ m, $\ \phi = 39.8^\circ$]
   (b) in a level turn with bank angle 30° at 210 m/s TAS (at 6000 m where $\sigma = 0.53$);
   [$n = 1.15,\ \ R = 7786\,\text{m}$]
   (c) in a dive at 150 m/s TAS and rate of descent 30 m/s TAS (at 6000 m), pulling out to a rate of climb of 30 m/s TAS in 10 s at constant air speed following a circular path.
   [$n = 0.98 \to 1.58 \to 1.61 \to 1.58 \to 0.98,\ \ R = 3737\,\text{m}$]

3. An aircraft flying at 150 m/s (sea level) has the following characteristics: $m = 100000$ kg, $S_{\text{W}} = 95$ m^2, $c = 3.8$ m, $l_{\text{W}} = 0.4$ m, $l_{\text{T}} = 13$ m, $C_{M_{0\text{W}}} = -0.028$. Obtain the wing and tailplane lift forces for $n = 2.5$. [2390 kN and 63 kN]

4. An aircraft has the following characteristics: $m = 9000$ kg, $S_{\text{W}} = 46$ m^2, $c = 3$ m, $C_{M_{0\text{W}}} = -0.035$ and $l_{\text{W}} + l_{\text{T}} = 8$ m (distance between tailplane and wing aerodynamic centres). If the maximum allowable *download* on the tailplane is 9000 N, what limitations must be imposed upon the centre of mass position to meet this constraint in steady level flight at 180 m/s (sea level)?
   [$l_{\text{W}} > 0.27\,\text{m}$]

5. An aircraft flying at 87.3 m/s EAS is at the point of stalling for a load factor of 2.5. It has the following characteristics: $m = 44200$ kg, $S_{\text{W}} = 145$ m^2, $c = 5$ m, $l_{\text{W}} = 0.3$ m, $l_{\text{T}} = 14.9$ m, $C_{M_{0\text{W}}} = -0.07$, drag coefficient $C_{\text{D}} = 0.02 + 0.072C_{\text{LW}}^2$ where C_{LW} is the wing lift coefficient. The drag may be assumed to act through the wing aerodynamic centre and the thrust acts a distance $h = 1.5$ m below the wing. Estimate the tailplane lift using three iterations. [19.05 kN]

6. Write a MATLAB program to generate the aerodynamic derivatives for a given symmetric flight condition and then to solve the *rigid* aircraft equilibrium manoeuvre for the trim incidence/elevator angle (see Appendix I of companion website). Include the code in a load factor or air speed loop to allow these parameters to be varied. Check the results for the example in this chapter. Then explore the effect of changing air speed, centre of mass position, downwash term and zero lift wing pitching moment coefficient (maintain static stability).

7. Write a MATLAB program to generate the aerodynamic derivatives for a given flight condition and mode type, and then to solve the *flexible* aircraft equilibrium manoeuvre for the trim incidence/elevator

angle (see Appendix I of companion website). Include the code in a load factor or air speed loop to allow these parameters to be varied. Check the results using the example in the chapter. Then explore the effect of changing air speed, centre of mass position, downwash term and zero lift pitching moment coefficient (maintain static stability). Also, generate a new flexible mode for the same aircraft example which is the combination of two of the other modes and investigate the revised behaviour. Finally, develop a data set from another idealized aircraft with a different mass distribution.

14

Flight Mechanics Model for Dynamic Manoeuvres

In Chapter 13, the symmetric equilibrium manoeuvre calculations were considered, where the balanced/trimmed condition was sought and inertial axes fixed in space were used, with displacements and angles as unknowns. In this chapter, some basic concepts related to the large angle nonlinear flight mechanics equations of motion of the aircraft, when undergoing dynamic manoeuvres, will be introduced; this analysis will require a body fixed axes system moving with the aircraft, with velocities as unknowns. This is because, in industry, the flight mechanics equations (sometimes with flexible modes or quasi-flexible effects on aerodynamics included) are often used as the basis for performing flight dynamic manoeuvre calculations to determine loads (Howe, 2004) and to assess stability and handling, so assisting in design of the flight control system (FCS). Linearized versions of these equations are often used to enable basic mathematical treatment of the dynamic stability. In Chapter 15, the equations developed here will be applied to simple heave/pitch and roll manoeuvre conditions for both rigid and flexible aircraft. The nonlinear model with flexible modes is sometimes used for landing calculations (see Chapter 17).

The focus will be on ideas relevant to the response due to manoeuvres, and hence internal loads, for the aircraft and not particularly on performance or stability and control/handling issues. Other texts, e.g. Hancock (1995), Etkin and Reid (1996), Schmidt (1998), Cook (1997), Russell (2003), Stengel (2004) and ESDU Data Sheet 67003, should be consulted for a more thorough treatment of flight mechanics equations, performance, stability and flight dynamics principles. In this book, the flight mechanics concepts are covered, primarily because of their relevance to dynamic manoeuvres (and landing) and the resulting internal loads.

In classical books on flight mechanics, the full nonlinear six DoF equations of motion are usually derived from first principles in three dimensions, linearized in order to study the stability and control behaviour and then terms are gradually eliminated to simplify the picture and allow analytical treatment. The derivation may be performed using approaches in scalars (Cook, 1997; etc.) or vectors (Etkin and Reid, 1996; Russell, 2003; etc.). In order to minimize the mathematics involved and to allow flexible effects to be introduced later in the chapter, the approach taken here will be to carry out the analysis for a symmetric aircraft undergoing two-dimensional longitudinal motion, neglecting fore-and-aft motion to reduce the number of equations further to two, a considerable simplification. An approach based on scalars will be used in order to provide a little more physical appreciation and to avoid an excursion into vectors for only a limited part of the book; however, it must be emphasized that a vector approach is easier and far more elegant for the full three-dimensional case.

In regard to the aerodynamic forces and moments, these are defined in terms of stability and control derivatives derived with respect to body fixed (usually stability or wind) axes; this is in contrast to all other chapters except Chapter 15, where inertial axes are used for static aeroelastic, flutter, manoeuvre and gust cases involving only small excursions (perturbations) from the datum.

Introduction to Aircraft Aeroelasticity and Loads J. R. Wright and J. E. Cooper
© 2007 John Wiley & Sons, Ltd

The aircraft will initially be considered as rigid but the inclusion of flexibility (i.e. elastic deformation) will be introduced later in the chapter. The inclusion of structural deformation means that the instantaneous centre of mass position in the aircraft is not fixed and that the moments of inertia are not constant with time. Performing this analysis will require the introduction of the so-called 'mean axes reference frame' that 'floats' with the aircraft in such a way that its origin always remains at the instantaneous centre of mass. Such a choice of axes allows the inertia coupling terms to be eliminated. The addition of flexible modes into the flight mechanics equation is not straightforward and is a subject of ongoing research; thus as simple an approach as possible will be adopted to highlight some of the key issues. It should be pointed out that the presence of the FCS means that flexible mode dynamics are not always excited during dynamic manoeuvres and therefore introducing quasi-static flexible corrections to the rigid model aerodynamics may often suffice. However, the dynamic landing calculations will certainly require a fully flexible flight mechanics type model.

The chapter concludes with a brief introduction to the aircraft flight control system (FCS), included here because its main function is in connection with the flight mechanics behaviour of the aircraft.

14.1 AIRCRAFT AXES

There are two main types of axes systems in use for aircraft, namely earth and body fixed axes (Cook, 1997).

14.1.1 Earth Fixed Axes

Earth fixed axes ($Ox_E y_E z_E$) are located in the plane of the earth and classically have the x_E axis pointing north and the y_E axis pointing east; the axes assume a 'flat' earth. However, the axes may for convenience be located on the earth surface directly below the aircraft and with the x_E axis pointing along the aircraft direction of flight in the initial trimmed state prior to any manoeuvre. Earth axes may also be located with their origin coinciding with the initial origin of the body fixed axes, but thereafter remaining fixed during any manoeuvre. Provided the effect of the rotation of the earth may be neglected, earth axes may be treated as 'inertial' so that accelerations of the aircraft relative to these axes are absolute. A different approach is required where space travel is being considered since the earth's rotation then becomes significant.

The disadvantage of earth fixed axes, when considering the dynamic response of an aircraft in a manoeuvre where significant motion is experienced, is that the moments of inertia of the aircraft will alter as the aircraft orientation to the earth changes and therefore will become variables. For this reason, body fixed axes are normally used in dynamic manoeuvres whereas inertial axes are satisfactory for static aeroelasticity, equilibrium manoeuvres, ground manoeuvres, gusts and flutter, where only small perturbations are considered.

14.1.2 Body Fixed Axes

Body fixed axes ($Oxyz$) are located in the aircraft, with their origin usually at the centre of mass (CoM), and translate/rotate with it; it is a right-handed system as shown in Figure 14.1. An advantage of using body axes fixed in the aircraft is that the moments of inertia of the aircraft with respect to these axes remain constant during general three-dimensional motion. There are two common types of body axes, as illustrated in Figure 14.2 for two-dimensions.

1. A generalized *body* axis system ($Ox_b y_b z_b$) aligned with the horizontal fuselage datum. For body axes aligned with the principal axes of inertia of the aircraft, by definition the product moments of inertia are zero. However, for nonprincipal or aerodynamic axes these product terms will exist.

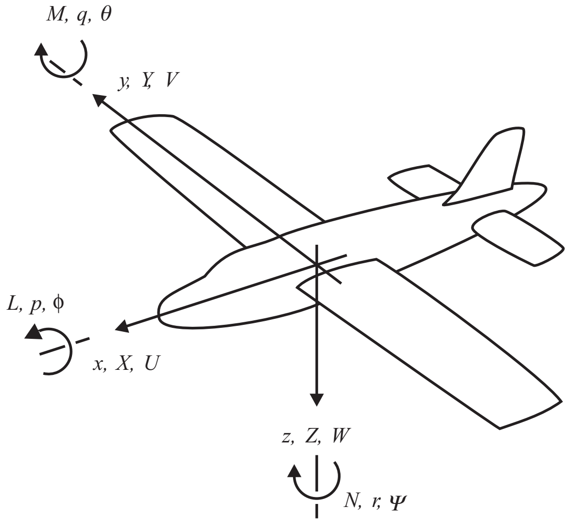

Figure 14.1 Notation for body fixed axes.

2. A special type of body axis (Hancock, 1995; Cook, 1997), where the x axis is aligned with the velocity vector component in the plane of symmetry and *fixed for a particular flight condition*, is known as an *aerodynamic* or *stability* or *wind* axis ($Ox_wy_wz_w$). Such axes have the advantage that the relevant aerodynamic stability derivatives are much easier to derive.

Body and aerodynamic axes differ in orientation by the steady (or equilibrium) body incidence value α_e and are used in different situations, so it is important to apply the necessary transformations to ensure overall consistency of any model used, e.g. derivatives might be calculated for wind axes and then transformed to body axes for response calculation. If calculations are performed using equations for wind axes, then the moments of inertia must be transformed through the steady incidence α_e. The transformations are shown in, for example, Cook (1997).

14.2 MOTION VARIABLES

For body fixed axes, the motion is represented by small or large perturbation variables referred to these moving axes. The aircraft may be considered as being initially in a trimmed (or equilibrium, subscript e) state with total velocity V_0, having components U_e, V_e and W_e along the body axis directions; the trimmed

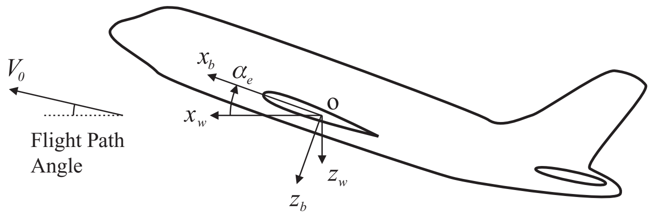

Figure 14.2 Body and wind axes for a two-dimensional symmetric flight.

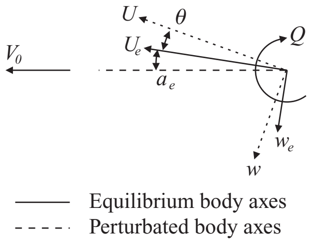

Figure 14.3 Steady and perturbed axes systems in two-dimensional symmetric flight.

pitch attitude (to the horizontal) is θ_e, incidence is α_e and sideslip β_e. There are no rates of rotation in the initial trimmed state.

When the aircraft is disturbed from the trimmed state, there are net forces (X = axial, Y = lateral and Z = normal) and moments (L = rolling, M = pitching and N = yawing) together with centre of mass response velocities (U = axial, V = lateral and W = normal) and rates of rotation (P = roll, Q = pitch and R = yaw), all shown in Figure 14.1. Rotations follow the right-hand rule. The forces and moments acting on the aircraft will be due to aerodynamic, gravitational and propulsion effects. Positive control rotations introduce positive moments.

The change in orientation of the aircraft due to the disturbance, relative to the equilibrium axis set, is defined by the angles ϕ (roll), θ (pitch) and ψ (yaw). The sign convention for these quantities is also shown in Figure 14.1. If the orientation of the aircraft is referred to earth fixed axes, then the absolute angles defining its position are known as Φ (bank), Θ (inclination) and Ψ (azimuth or heading). The steady and perturbed velocities/angles are shown in Figure 14.3 for two-dimensional symmetric flight.

14.3 AXES TRANSFORMATIONS

Once the aircraft has started to undergo a manoeuvre such that it experiences a change of position and orientation with respect to the earth axes, it is important to be able to relate the velocities and rates between the earth and body axes systems (or indeed between any two axes systems). Solution of the equations of motion in the body fixed axes system will yield velocities and rates, relative to the body axes, that must then be transformed to earth axes and finally integrated to obtain changes of position and orientation relative to the earth axes.

The three angles defining the relative angular positions of two sets of axes are known as the Euler angles (e.g. see Cook, 1997), in this case ϕ, θ and ψ. Euler angles may be used to transform between body axes and earth axes or between perturbed axes and equilibrium axes.

14.3.1 Transformation in Two-Dimensions

To demonstrate the basic transformations between body and datum (say, earth) axes using a simple physical approach, consider the behaviour of the aircraft in heave and pitch only. Figure 14.4 shows the velocity diagram with both sets of velocity components. The coincidence of origins does not influence the velocity, rate and angle transformations. By inspection of the figure, it may be seen that the velocities in the datum earth axes directions are given by the summation of the body axes velocities components, namely

$$U_E = U\cos\theta + W\sin\theta, \qquad W_E = -U\sin\theta + W\cos\theta, \tag{14.1}$$

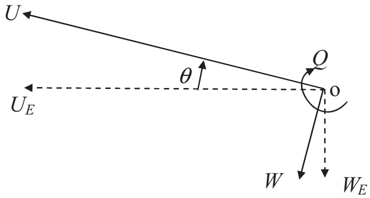

Figure 14.4 Velocity diagram in two-dimensions for body/earth axes transformation.

or in matrix form

$$\begin{Bmatrix} U_{\mathrm{E}} \\ W_{\mathrm{E}} \end{Bmatrix} = \begin{bmatrix} \cos\theta & \sin\theta \\ -\sin\theta & \cos\theta \end{bmatrix} \begin{Bmatrix} U \\ W \end{Bmatrix} = \mathbf{A}_{\mathrm{L}} \begin{Bmatrix} U \\ W \end{Bmatrix}. \tag{14.2}$$

This linear transformation matrix $\mathbf{A}_{\mathrm{L}}$ is in fact the inverse of the matrix of direction cosines in two-dimensions. Also, by inspection it may be seen that the angular velocity Q is identical in both axes systems, so the angular rate transformation is

$$\{\dot{\theta}\} = \{Q\} = \mathbf{A}_{\mathrm{R}}\{Q\}. \tag{14.3}$$

where the rotational transformation matrix for this simple case is $\mathbf{A}_{\mathrm{R}} = [1]$.

Thus a solution of the equations of motion in body axes will yield U, W and Q, with the above transformations allowing the velocities U_{E}, W_{E} and rate of rotation $\dot{\theta}$ relative to earth axes to be calculated.

14.3.2 Transformation in Three-Dimensions

When the equivalent transformation relationships in three-dimensions are sought, the problem is much more difficult as three angles, not one, need to be considered. The transformation between body and earth axes requires two intermediate axes systems through which transformations must be made (Cook, 1997). The order of axis rotations required to generate the transformations is important, namely ψ, then θ and finally ϕ.

It may be shown that the linear and angular transformations are governed by two 3×3 transformation matrices, each involving the Euler angles and leading to complex expressions. Because the focus in this book is on the basic ideas, seen to a large extent in two-dimensions, the expressions will not be quoted in full but are of the form

$$\begin{Bmatrix} U_{\mathrm{E}} \\ V_{\mathrm{E}} \\ W_{\mathrm{E}} \end{Bmatrix} = \mathbf{A}_{\mathrm{L}} \begin{Bmatrix} U \\ V \\ W \end{Bmatrix}, \qquad \begin{Bmatrix} \dot{\phi} \\ \dot{\theta} \\ \dot{\psi} \end{Bmatrix} = \mathbf{A}_{\mathrm{R}} \begin{Bmatrix} P \\ Q \\ R \end{Bmatrix} \tag{14.4}$$

for the velocity components along earth axes and for the Euler rates. Note again that $\mathbf{A}_{\mathrm{L}}$ and $\mathbf{A}_{\mathrm{R}}$ are the linear and rotational transformation matrices. The complete expressions may be found elsewhere (Cook, 1997). It should be noted that for a linearized analysis with small perturbations where the angles may be treated as small, the matrices $\mathbf{A}_{\mathrm{L}}$ and $\mathbf{A}_{\mathrm{R}}$ are considerably simplified (see later).

In this case, the three-dimensional velocity components from the solution of the equations of motion in body fixed axes may be used to determine velocities and rates of rotation of the aircraft in earth axes.

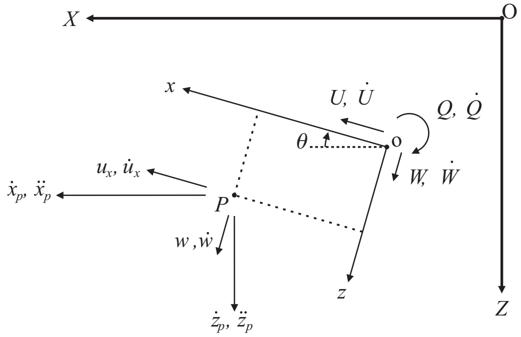

Figure 14.5 Inertial/earth fixed and moving axes frames of reference in two-dimensions.

By integrating these latter velocities and rates, the absolute position and orientation of the aircraft in space may be found.

14.4 VELOCITY AND ACCELERATION COMPONENTS FOR MOVING AXES

To determine the flight mechanics equations of motion based on the axes reference frame moving with the aircraft, the kinematics of the aircraft motion in the moving axes directions are required. The aim is to determine the absolute velocity and acceleration components (i.e. aligned with moving axes directions) of a point in two-dimensions, where flexible behaviour is permissible. Then D'Alembert's principle will be used to determine the equations of motion for a rigid aircraft. Similar principles apply for three-dimensions but with rather more complex expressions.

14.4.1 Position Coordinates in Fixed and Moving Axes Frames

Consider the two-dimensional axes systems shown in Figure 14.5; here OXZ is an inertial frame (such as earth axes) and oxz is a moving frame. It should be noted that the axes arrangement is chosen in order to match the classical flight mechanics sign convention, e.g. z downwards, x forwards, positive pitch nose up, etc. The absolute position of the origin o is given by the coordinates (X_{o}, Z_{o}) and the position of an arbitrary point P is given by coordinates (X_{P}, Z_{P}) with respect to the fixed inertial axes and (x, z) with respect to the moving axes.

By studying the geometry of the system, the position coordinates of P with respect to OXZ (*fixed axes*) *directions* may be written as

$$X_{\mathrm{P}} = X_{\mathrm{o}} + (x\cos\theta + z\sin\theta), \qquad Z_{\mathrm{P}} = Z_{\mathrm{o}} + (-x\sin\theta + z\cos\theta). \tag{14.5}$$

14.4.2 Differentiation with Respect to Time

When considering systems with both fixed and moving axes systems, differentiation with respect to time may apply to inertial axes (sometimes referred to using d/dt) or for moving axes (sometimes referred to using $\partial/\partial t$ or $\delta/\delta t$); in this chapter, the overdot is used to indicate differentiation with respect to time, with the context showing which axes are intended (e.g. $\dot{X} \equiv \mathrm{d}X/\mathrm{d}t$ and $\dot{x} \equiv \partial x/\partial t$).

14.4.3 Velocity Components in Fixed and Moving Axes

Now, differentiating the expressions (14.5) with respect to time yields the absolute velocity components of P, again in the *OXZ* (*inertial axes*) *directions*, so

$$\begin{aligned} \dot{X}_{\mathrm{P}} &= \dot{X}_{\mathrm{o}} + (-x\sin\theta + z\cos\theta)\dot{\theta} + (\dot{x}\cos\theta + \dot{z}\sin\theta), \\ \dot{Z}_{\mathrm{P}} &= \dot{Z}_{\mathrm{o}} + (-x\cos\theta - z\sin\theta)\dot{\theta} + (-\dot{x}\sin\theta + \dot{z}\cos\theta). \end{aligned} \tag{14.6}$$

To understand this differentiation it should be recognized that differentiating a function f of θ with respect to t requires the chain rule; e.g.

$$\frac{\partial f}{\partial t} = \frac{\partial f}{\partial \theta}\frac{\partial \theta}{\partial t}, \qquad \frac{\partial}{\partial t}(\sin\theta) = \frac{\partial}{\partial \theta}(\sin\theta)\frac{\partial \theta}{\partial t} = \cos\theta\,\dot{\theta}. \tag{14.7}$$

Then, to determine the velocity components of point P in the *oxz* directions, the velocity components of the origin o in the *OXZ* (*inertial axes*) *directions*, namely $\dot{X}_{\mathrm{o}}$, $\dot{Z}_{\mathrm{o}}$, need to be expressed in terms of the velocity components in the *oxz* (*moving axes*) *directions*. This is essentially the two-dimensional transformation described in Section 14.3.1 and means that

$$\dot{X}_{\mathrm{o}} = U\cos\theta + W\sin\theta, \qquad \dot{Z}_{\mathrm{o}} = -U\sin\theta + W\cos\theta. \tag{14.8}$$

Considering the geometry of the velocity components shown in Figure 14.5, the absolute velocity components $(v_x,\ v_z)$ of P in the *oxz* (*moving axes*) *directions* will be given by

$$v_x = \dot{X}_{\mathrm{P}}\cos\theta - \dot{Z}_{\mathrm{P}}\sin\theta, \qquad v_z = \dot{X}_{\mathrm{P}}\sin\theta + \dot{Z}_{\mathrm{P}}\cos\theta. \tag{14.9}$$

If the expressions in Equation (14.6) are substituted into Equation (14.9), and the result simplified using Equation (14.8) and the pitch rate relationship $Q = \dot{\theta}$, then it can be shown that the *absolute velocity components of P in the oxz directions* are given by the expressions

$$v_x = U + zQ + \dot{x}, \qquad v_z = W - xQ + \dot{z}. \tag{14.10}$$

The absolute velocity of point P is equal to the absolute velocity of the moving axes origin o, plus a term involving Q to allow for the rotation of the moving axes and a further term to allow for motion of P relative to o (which only applies for a flexible body). The two ‘overdot’ terms are velocities with respect to the moving axes origin.

14.4.4 Acceleration Components in Fixed and Moving Axes

To determine the equivalent relations for the absolute accelerations is more difficult but involves a similar process. Firstly, the expressions in Equation (14.6) are again differentiated with respect to time and then the absolute acceleration components of P in the *OXZ* (*inertial axes*) *directions* are

$$\begin{aligned} \ddot{X}_{\mathrm{P}} &= \ddot{X}_{\mathrm{o}} - \dot{x}s\dot{\theta} - xc\dot{\theta}^2 - xs\ddot{\theta} + \dot{z}c\dot{\theta} - zs\dot{\theta}^2 + zc\ddot{\theta} + \ddot{x}c - \dot{x}s\dot{\theta} + \ddot{z}s + \dot{z}c\dot{\theta}, \\ \ddot{Z}_{\mathrm{P}} &= \ddot{Z}_{\mathrm{o}} - \dot{x}c\dot{\theta} + xs\dot{\theta}^2 - xc\ddot{\theta} - \dot{z}s\dot{\theta} - zc\dot{\theta}^2 - zs\ddot{\theta} - \ddot{x}s - \dot{x}c\dot{\theta} + \ddot{z}c - \dot{z}s\dot{\theta}, \end{aligned} \tag{14.11}$$

where, in order to simplify the expressions, the shorthand notation $s = \sin\theta,\ c = \cos\theta$ has been used.

The acceleration components of the origin o, namely $\ddot{X}_{\mathrm{o}}$, $\ddot{Z}_{\mathrm{o}}$, are now expressed in terms of the velocity and acceleration components in the *oxz* directions by differentiating Equation (14.8), so

$$\ddot{X}_{\mathrm{o}} = -Us\dot{\theta} + \dot{U}c + Wc\dot{\theta} + \dot{W}s, \qquad \ddot{Z}_{\mathrm{o}} = -Uc\dot{\theta} - \dot{U}s - Ws\dot{\theta} + \dot{W}c. \tag{14.12}$$

The absolute acceleration components ($a_x,\ a_z$) of P in the *oxz* (*moving axes*) *directions* are given by a similar expression to that for the velocity in Equation (14.9), namely

$$a_x = \ddot{X}_{\mathrm{P}} \cos\theta - \ddot{Z}_{\mathrm{P}} \sin\theta, \qquad a_z = \ddot{X}_{\mathrm{P}} \sin\theta + \ddot{Z}_{\mathrm{P}} \cos\theta. \tag{14.13}$$

Now, when Equations (14.11) and (14.12) are substituted into Equation (14.13) and the results simplified, it may be shown that the *acceleration components of P in the oxz* (*moving axes*) *directions* are given by

$$a_x = \dot{U} + WQ - xQ^2 + z\dot{Q} + \ddot{x} + 2\dot{z}Q, \qquad a_z = \dot{W} - UQ - zQ^2 - x\dot{Q} + \ddot{z} - 2\dot{x}Q. \tag{14.14}$$

The six terms in each of these expressions have the following meaning (in order from left to right):

(a) acceleration of the origin of the moving axes with respect to inertial axes;
(b) term to account for the effect of rotation of axes on the acceleration of the origin;
(c) centripetal acceleration directed towards the axis of rotation;
(d) changes in the tangential acceleration component due to changes in the rate of rotation;
(e) acceleration of P relative to the moving frame;
(f) Coriolis acceleration term due to the velocity of P relative to the rotating frame.

The last two terms are zero for a *rigid body* but nonzero for a *flexible body*. In order to distinguish between a rigid and a flexible body, the position of the point P relative to the moving axes origin o may be written as the summation of the position coordinates (x_{r}, z_{r}) in the undeformed/rigid aircraft (r) and the displacement components of the elastic deformation (x_{e}, z_{e}) of the structure (e), so

$$x = x_{\mathrm{r}} + x_{\mathrm{e}}, \qquad z = z_{\mathrm{r}} + z_{\mathrm{e}}. \tag{14.15}$$

Because the aircraft is initially assumed to be *rigid*, then from Equation (14.15), $x = x_{\mathrm{r}}$, $z = z_{\mathrm{r}}$ and all the 'overdot' terms in the acceleration component expressions will be zero (i.e. $\dot{x} = \dot{z} = \ddot{x} = \ddot{z} = 0$). Thus, for the rigid aircraft, the acceleration components may be written as

$$a_x = \dot{U} + WQ - x_{\mathrm{r}}Q^2 + z_{\mathrm{r}}\dot{Q}, \qquad a_z = \dot{W} - UQ - z_{\mathrm{r}}Q^2 - x_{\mathrm{r}}\dot{Q}. \tag{14.16}$$

The treatment of the *flexible* aircraft, where the 'overdot' terms are nonzero, will be considered later in this chapter where the flexible deformations are expressed in terms of free–free normal modes.

14.5 FLIGHT MECHANICS EQUATIONS OF MOTION FOR A RIGID AIRCRAFT

Now consider using the above acceleration expressions for the symmetric rigid aircraft in longitudinal motion in two-dimensions (i.e. all yaw and roll terms are zero). The axes systems are inertial (or earth) axes *OXZ* and moving body fixed axes *oxz*, as shown in Figure 14.6. The origin o for the moving axes is taken for convenience to be at the centre of mass, as it allows elimination of several terms in the equations. Some general point P is located at coordinate (x, z) within the aircraft.

14.5.1 Nonlinear Equations for Longitudinal Motion

To determine the equations of motion for the longitudinal behaviour of the symmetric aircraft, consider an elemental mass d*m* at point P and its absolute (inertial) acceleration components in the *oxz* directions.

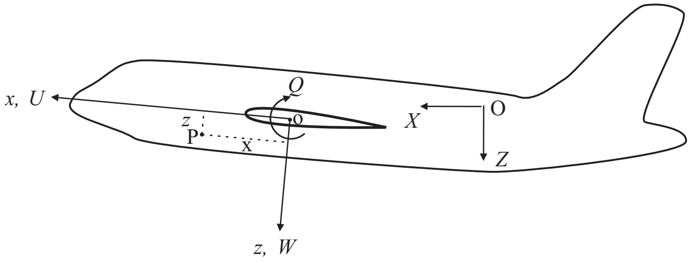

Figure 14.6 Rigid aircraft in longitudinal motion.

The elemental masses are assumed to have no rotational inertia. The D'Alembert inertia force on the mass will have components $-\mathrm{d}m\, a_x$ and $-\mathrm{d}m\, a_z$, aligned with the body axes as shown in Figure 14.7.

If the applied force components in the x and z directions are X and Z, then the body will be in equilibrium, so the applied forces will balance the summation (or integration) of the inertia forces for all the mass elements in the entire body (see Chapter 6) and

$$\int a_x \mathrm{d}m = X, \qquad \int a_z \mathrm{d}m = Z, \tag{14.17}$$

where the summations apply to the entire volume of the aircraft. The moment equation may also be obtained using the inertia forces in Figure 14.7 since for equilibrium the applied moment must balance the total moment of the inertia forces; therefore

$$\int (a_x\, z_\mathrm{r} - a_z\, x_\mathrm{r})\mathrm{d}m = M, \tag{14.18}$$

where the moment arms are the position coordinates of point P in the rigid aircraft.

Now, if the acceleration components from Equations (14.16) are substituted into Equations (14.17) and (14.18), a number of summation terms are present. Note firstly that the summation terms given by $\int x_\mathrm{r}\mathrm{d}m$ and $\int z_\mathrm{r}\mathrm{d}m$ are both zero because the origin of the moving axes system was taken at the rigid aircraft centre of mass and there is no first moment of mass about axes through this point. Also, $m = \int \mathrm{d}m$ is the total aircraft mass and

$$I_y = \int (x_\mathrm{r}^2 + z_\mathrm{r}^2)\mathrm{d}m \tag{14.19}$$

is the moment of inertia of the rigid aircraft about the *oy* axis, i.e. in pitch.

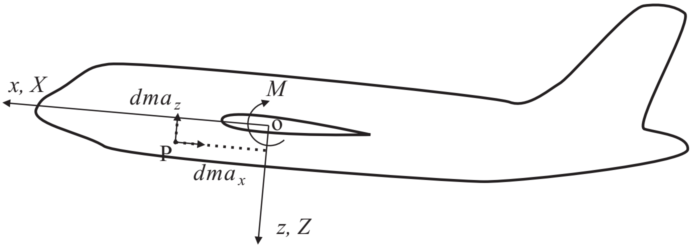

Figure 14.7 Balance of applied and inertia forces for a rigid aircraft.

The nonlinear and coupled equations for longitudinal motion of the symmetric aircraft may then be shown to be

$$m(\dot{U} + QW) = X, \qquad m(\dot{W} - QU) = Z, \qquad I_y\dot{Q} = M. \tag{14.20}$$

14.5.2 Nonlinear Equations for Combined Longitudinal/Lateral Motion

If the acceleration components were obtained in three-dimensions, either using an extension of the two-dimensional approach in Section 14.4 or using vectors, a similar analysis could be performed for the symmetric rigid aircraft undergoing combined longitudinal/lateral motion in three-dimensions. The corresponding nonlinear equations of motion would be given by (Cook, 1997)

$$\begin{aligned}
&m(\dot{U} - RV + QW) = X,\\
&m(\dot{V} - PW + RU) = Y,\\
&m(\dot{W} - QU + PV) = Z,\\
&I_x\dot{P} - (I_y - I_z)QR - I_{xz}(PQ + \dot{R}) = L,\\
&I_y\dot{Q} + (I_x - I_z)PR + I_{xz}(P^2 - R^2) = M,\\
&I_z\dot{R} - (I_x - I_y)PQ + I_{xz}(QR - \dot{P}) = N.
\end{aligned} \tag{14.21}$$

These nonlinear coupled expressions include other moments of inertia and the product moment of the inertia term

$$I_{xz} = \int x_\mathrm{r} z_\mathrm{r} \mathrm{d}m. \tag{14.22}$$

All other product moments of inertia are zero because of the aircraft symmetry and I_{xz} would be zero by definition if the body axes were to be aligned with the principal axes of the aircraft.

These six equations cover general coupled aircraft motion. The equations are nonlinear, thus allowing for large variations in response, such as might occur around the stalled condition and in spinning. The equations require a numerical, not analytical, solution and the forcing terms need to be defined appropriately, i.e. as nonlinear functions of incidence, etc. Also, the full Euler angle transformations need to be employed to convert velocities and rates to earth axes.

14.5.3 Linearized Equations of Motion

Often, the equations of motion are linearized by analytical means for ease of solution, especially for stability and control studies where the behaviour of the aircraft under small perturbations from the trimmed or equilibrium state (denoted by subscript e, not to be confused with its alternative use for elastic deformation) is considered. Initially, for convenience, the datum flight condition is taken as being steady, straight, horizontal flight without sideslip ($V_\mathrm{e} = 0$) and without bank/yaw angles or rates ($\phi = \psi = P_\mathrm{e} = Q_\mathrm{e} = R_\mathrm{e} = 0$).

The total velocity components of the centre of mass in the disturbed flight response are the sum of the equilibrium (trimmed) components and the transient (small) perturbation components (u, v, w), so

$$U = U_\mathrm{e} + u, \qquad V = V_\mathrm{e} + v = v, \qquad W = W_\mathrm{e} + w. \tag{14.23}$$

The equivalent result for the rates of rotation is

$$P = P_\mathrm{e} + p = p, \qquad Q = Q_\mathrm{e} + q = q, \qquad R = R_\mathrm{e} + r = r, \tag{14.24}$$

where the angular disturbance velocities (p, q, r) are also small. All the terms in Equations (14.23) and (14.24) are referred to the moving axes *oxz*.

Substituting the velocity and rate expressions in Equations (14.23) and (14.24) into Equations (14.21), noting that the trimmed velocities are steady and constant, and neglecting small quantities such as products of rates (e.g. pr, p^2, etc.) yields a set of linearized equations. These may be divided into equations for *longitudinal* motion,

$$m(\dot{u} + W_{\mathrm{e}}q) = X, \qquad m(\dot{w} - U_{\mathrm{e}}q) = Z, \qquad I_y\dot{q} = M, \tag{14.25}$$

which are very similar to Equations (14.20), and for *lateral* motion,

$$m(\dot{v} - W_{\mathrm{e}}p + U_{\mathrm{e}}r) = Y, \qquad I_x\dot{p} - I_{xz}\dot{r} = L, \qquad I_z\dot{r} - I_{xz}\dot{p} = N, \tag{14.26}$$

which are considerably simplified. The longitudinal and lateral motions are often treated separately for a symmetric aircraft. Clearly, these equations could also be written in a state space form (see Chapter 7).

Also, because the angles are small, the full nonlinear Euler transformations would not be needed. Using the transformation relationships in Equations (14.4), setting $\cos A = 1$ and $\sin A = A$ with all angles assumed small, and neglecting coupling and second-order terms, yields the following linear and rotational transformations

$$U_{\mathrm{E}} = U_{\mathrm{e}} + W_{\mathrm{e}}\theta, \qquad W_{\mathrm{E}} = -U_{\mathrm{e}}\theta + W_{\mathrm{e}} + w, \qquad \dot{\theta} = q \tag{14.27}$$

for *longitudinal* motion, and

$$\dot{\phi} = p, \qquad \dot{\psi} = r, \qquad V_{\mathrm{E}} = \psi U_{\mathrm{e}} + v - \phi W_{\mathrm{e}} \tag{14.28}$$

for *lateral* motion. These expressions allow transformation of the body axes responses into earth axes.

It should be emphasised that these small disturbance equations can not be applied to conditions where large perturbation flight manoeuvres are expected (e.g. near stall) since the model is only valid in the region of the initial trimmed condition. However, in many cases, the assumption is adequate. In particular, the linearised equations are used to examine stability and control issues.

14.6 REPRESENTATION OF DISTURBING FORCES AND MOMENTS

So far, the applied/disturbing forces and moments have simply been represented by X, Y, Z, L, M, N. These forces, for example, may be written as a summation of the different contributions to them:

$$Z = Z_{\mathrm{a}} + Z_{\mathrm{g}} + Z_{\mathrm{c}} + Z_{\mathrm{p}} + Z_{\mathrm{d}}, \tag{14.29}$$

where the subscripts a, g, c, p and d refer to aerodynamic, gravitational, control, propulsive (power) and disturbance (atmospheric gust) terms respectively (these terms must not be confused with derivatives, where the subscripts correspond to response variables).

For the full nonlinear analysis, some of the aerodynamic forces are nonlinear functions of, for example, incidence and this nonlinearity would need to be represented in the model, obtained from computational fluid dynamics (CFD) and/or wind tunnel tests; this is clearly important for loads purposes but nonlinear aerodynamics are beyond the scope of this book. However, for the linearized analysis often used in stability and control studies, the aerodynamic forces and moments corresponding to small perturbations may be considered. Ignoring the disturbance terms and considering small perturbations, these force and moment components may be written as the summation of *datum* and *perturbation* terms.

In this section, a brief explanation will be given as to how some of these terms are obtained; the focus will be on longitudinal motion only and giving limited examples, as other texts cover this ground extensively (e.g. Cook, 1997).

14.6.1 Aerodynamic Terms (a/c)

The aerodynamic force, for example, may be represented by the summation of datum (equilibrium) and perturbation terms, so

$$Z_{\mathrm{a}} = Z_{\mathrm{a_e}} + \Delta Z_{\mathrm{a}}. \tag{14.30}$$

This perturbation for a typical aerodynamic term is normally written using a first-order Taylor expansion involving all the velocities and rates of change of velocity so, e.g. in two-dimensions again,

$$Z_{\mathrm{a}} = Z_{\mathrm{a_e}} + \Delta Z_{\mathrm{a}} = Z_{a_e} + u\frac{\partial Z_{\mathrm{a}}}{\partial u} + w\frac{\partial Z_{\mathrm{a}}}{\partial w} + q\frac{\partial Z_{\mathrm{a}}}{\partial q} + \dot{u}\frac{\partial Z_{\mathrm{a}}}{\partial \dot{u}} + \dot{w}\frac{\partial Z_{\mathrm{a}}}{\partial \dot{w}} + \dot{q}\frac{\partial Z_{\mathrm{a}}}{\partial \dot{q}}. \tag{14.31}$$

In compact notation, the perturbation term is

$$\Delta Z_{\mathrm{a}} = uZ_u + wZ_w + qZ_q + \dot{u}Z_{\dot{u}} + \dot{w}Z_{\dot{w}} + \dot{q}Z_{\dot{q}}, \tag{14.32}$$

where terms such as Z_w are known as *aerodynamic stability derivatives* (Bryan, 1911; Babister, 1980; Hancock, 1995; Cook, 1997; Russell, 2003; ESDU Data Sheets) and define the perturbation terms about the equilibrium/datum state for this linearized model. Similar terms apply for the control forces, for example $\Delta Z_c = (\partial Z_{\mathrm{c}}/\partial \eta)\eta = Z_\eta \eta$ for the elevator input, where Z_η is the aerodynamic downwards force per elevator angle derivative. Some derivative terms may be negligible.

Note again that the conventional use of the 'over-o' on the dimensional derivative symbol (Cook, 1997) is not used here since nondimensional derivatives are not considered, so there is no need to differentiate between them in this way. Aerodynamic derivatives are often refined or obtained using wind tunnel results.

Under some circumstances, unsteady/oscillatory as opposed to quasi-steady (constant) derivatives may need to be used (see Chapters 10 and 11), but then there is a reduced frequency dependency and so the solution approaches would be different (see also Chapter 16 on gusts). Derivatives are also used elsewhere in the book when inertial axes are employed (see Chapters 13, 16 and 17), but are generally applied to the total forces and moments acting, not perturbation or incremental quantities.

Aerodynamic derivatives are calculated by considering the forces and moments generated in a perturbed flight condition, most conveniently in terms of wind axes, with a transformation to other types of body axes applied afterwards if required. Examples of calculating derivatives are shown in Appendix E, but other references can be consulted for a fuller treatment. It should again be emphasized that the derivatives in this analysis are calculated for wind (body fixed) axes, in comparison to the total derivatives introduced in Chapter 13, where inertial axes are used. Appendix B tabulates the two sets of longitudinal derivatives for the different axes; most are clearly the same while others are different, and some only apply to one case or the other.

14.6.2 Propulsion (or Power) Term (p)

A convenient way of describing the effect of propulsion is to define thrust derivatives e.g.

$$Z_{\mathrm{p}} = Z_{\mathrm{T}}\tau, \tag{14.33}$$

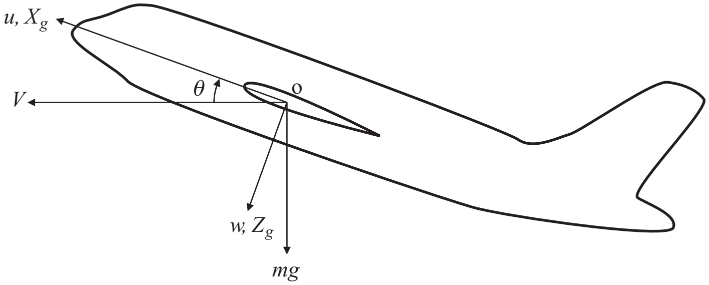

Figure 14.8 Perturbed body axes with gravitational force acting.

where Z_T is the normal force due to thrust and τ is the thrust perturbation, controlled by the throttle setting.

14.6.3 Gravitational Term (g)

The aircraft weight resolved along aircraft body axes introduces steady (datum/equilibrium) force components

$$X_{g_e} = 0, \qquad Z_{g_e} = mg, \tag{14.34}$$

where the datum inclination of the flight path θ_e has been assumed to be zero for simplicity.

During the small perturbation about the equilibrium condition, the attitude perturbation is θ and Figure 14.8 shows the perturbed body axes. It may be seen that the gravitational force components along the body axes directions in the perturbed state are

$$X_g = -mg\sin\theta = -mg\theta, \qquad Z_g = mg\cos\theta = mg, \tag{14.35}$$

with the simplifications allowed because the attitude perturbation θ is small. Therefore the perturbations in gravitational force about the trim condition are

$$\Delta X_g = -mg\theta, \qquad \Delta Z_g = 0. \tag{14.36}$$

The expressions are more complex for nonzero initial attitude and may be seen, for example, in (Cook, 1997).

14.7 EQUATIONS FOR FLEXIBLE AIRCRAFT IN LONGITUDINAL MOTION

So far, the emphasis in this chapter has been upon obtaining the basic flight mechanics equations for a *rigid* aircraft. Such an assumption may often suffice for military aircraft where the natural frequencies for the flexible modes (typically > 5 Hz) are significantly greater than the aircraft rigid body frequencies (e.g. short period and Dutch roll motions). The rigid body dynamic and structural dynamic models may then be considered to be uncoupled and the rigid body model used independently. Loads associated with the aircraft response following a control input may then be sufficiently accurately estimated using a purely *rigid* aircraft model. However, for some large modern commercial aircraft, the natural frequencies (sometimes as low as 1 Hz) are much closer to the rigid aircraft frequencies. Therefore, determining the response to control inputs (and for that matter stability, handling and FCS design) will require an integrated rigid body/flexible aircraft model. Obviously, the same approach could be taken with military aircraft if desired.

The analysis of a flexible aircraft brings a particular challenge in that, as the aircraft vibrates, the position of the instantaneous centre of mass and the moment of inertia values will both change with time. The choice of a suitable origin and orientation for the axes system becomes important in order to keep the equations as simple as possible and in particular to reduce any inertia coupling between the rigid and flexible degrees of freedom. Then couplings only occur due to aerodynamic effects. The development of an integrated flight mechanics model for the deformable aircraft is considered in Milne (1961), Babister (1980), Waszak and Schmidt (1988), Schmidt (1998) and Stengel (2004).

In this section, the basic idea of adding flexible modes into the flight mechanics equations will be introduced for a symmetric aircraft in two-dimensional pitch and heave, using only a single free–free flexible mode in the interests of keeping to a small number of DoF. However, the essential principles that emerge will equally well apply to a full three-dimensional flexible aircraft with multiple flexible modes. Note that care should be taken when comparing different flight mechanics references as there are a number of different notations employed.

14.7.1 Mean Axes Reference Frame

So far, the rigid aircraft in longitudinal motion has a body axis system *oxz* fixed at the centre of mass, which itself is at a fixed point within the structure. The axes system moves with velocities U, W and rotates with a pitch rate of Q. However, when the aircraft is flexible, then in order to minimize any coupling between the rigid body and the flexible mode equations, a 'mean axes reference frame' may be employed (Milne, 1964; Babister, 1980; Waszak and Schmidt, 1988). These axes move or 'float' in phase with the body motion but they are not attached to a fixed point in the aircraft. The mean axes are defined such that the relative linear momentum and angular momentum of the whole aircraft, due to flexible deformation, are zero at every instant of time. Also, the origin of the mean axes system lies at the *instantaneous* centre of mass. In most references, the mean axes conditions and the analysis are expressed in vector form, but here the basic ideas will be expressed in scalars. If a full three-dimensional treatment is sought, then it is recommended that vectors are employed.

For the two-dimensional symmetric flexible aircraft, the position of point P defined by rigid (r) and elastic/flexible deformation (e) components (see Equation (14.15)) is shown in Figure 14.9 while

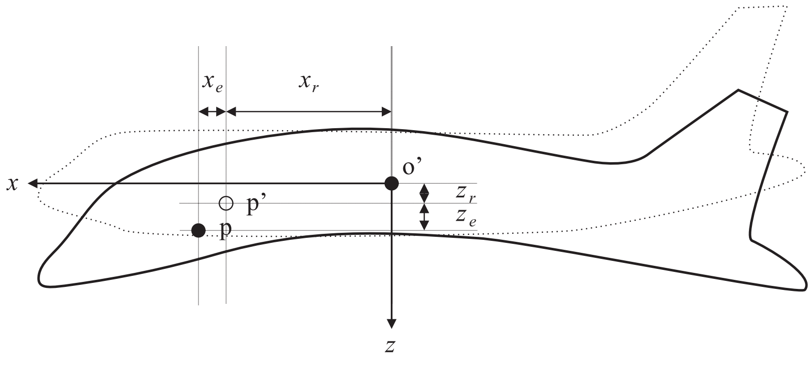

p' ○ Undeformed position with respect to instantaneous CM o'
p ● Deformed

Figure 14.9 Flexible aircraft in longitudinal motion – rigid and flexible displacement components.

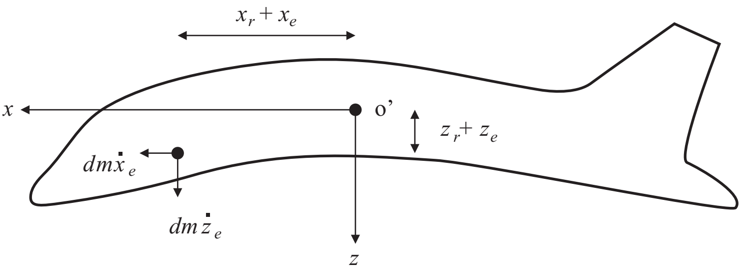

Figure 14.10 Flexible aircraft in longitudinal motion – momentum components.

momentum components for an elemental mass are shown in Figure 14.10. Hence the linear and angular momentum conditions in scalar form are

$$\int \dot{x}_{\mathrm{e}}\,\mathrm{d}m = 0, \qquad \int \dot{z}_{\mathrm{e}}\,\mathrm{d}m = 0, \qquad \int [(z_{\mathrm{r}} + z_{\mathrm{e}})\dot{x}_{\mathrm{e}} - (x_{\mathrm{r}} + x_{\mathrm{e}})\dot{z}_{\mathrm{e}}]\mathrm{d}m = 0. \tag{14.37}$$

If the structural deformation is small, or if the deformation and its rate of change are collinear (i.e. have negligible vector cross-product), the angular condition may be simplified to

$$\int (z_{\mathrm{r}}\dot{x}_{\mathrm{e}} - x_{\mathrm{r}}\dot{z}_{\mathrm{e}})\mathrm{d}m = 0. \tag{14.38}$$

In addition to these conditions, the axes origin is located at the instantaneous centre of mass, defined in two-dimensions by

$$\int (x_{\mathrm{r}} + x_{\mathrm{e}})\mathrm{d}m = 0, \qquad \int (z_{\mathrm{r}} + z_{\mathrm{e}})\mathrm{d}m = 0. \tag{14.39}$$

Now the instantaneous moment of inertia in pitch for the flexible aircraft is given by

$$I_y = \int [(x_{\mathrm{r}} + x_{\mathrm{e}})^2 + (z_{\mathrm{r}} + z_{\mathrm{e}})^2]\mathrm{d}m \tag{14.40}$$

and it may be seen that this value will vary in time as the aircraft deforms. However, in the analysis, the moments of inertia are assumed to be constant with time (i.e. variations due to flexible deformation are small).

The outcome of these assumptions is that any inertia coupling terms between rigid and flexible equations are zero or may be neglected; thus the kinetic energy expression is considerably simplified, having separate rigid and flexible terms. The position and orientation of the axes have been chosen such that the reference frame motions are inertially decoupled from the flexible deformations.

14.7.2 Definition of Flexible Deformation

To simplify the analysis somewhat for the two-dimensional flexible aircraft, the aircraft deformation will be considered as occurring in only the z direction (e.g. bending/torsion). Thus the deformation of the structure in the x direction (x_e) will be zero and so will its derivatives with time. The flexible deformation of the aircraft structure measured with respect to the reference frame will then be expressed as

$$z_e(x, y, t) = \kappa_e(x, y) q_e(t), \tag{14.41}$$

where κ_e is a whole aircraft free–free flexible normal mode shape defining modal displacements in the z direction and $q_e(t)$ is the corresponding generalized coordinate (not to be confused with pitch rate q). The mode is clearly symmetric but could involve wing bending and twisting for an unswept or swept wing.

If the mean axes conditions are applied when a free–free mode is used to define the deformation, then it may be shown (Waszak and Schmidt, 1988) that the modes must be orthogonal to the rigid body translational and rotational modes, namely for two-dimensional motion

$$\int \kappa_e \, dm = 0, \qquad \int \kappa_e x_r \, dm = 0. \tag{14.42}$$

These classical conditions quoted for free–free modes are a consequence of the mean axes assumption. It may also be noted that another way of defining mean axes is that the net inertia force and moment associated with the flexible deformation are zero.

14.7.3 Longitudinal Equations of Motion Including Flexible Effects

The analysis earlier led to the absolute velocity and acceleration components of point P in the oxz axes directions shown in Equations (14.10) and (14.14). Now, when the flexible deformation is present, the x and z values given in Equation (14.15) may be substituted and the resulting acceleration components are

$$\begin{aligned} a_x &= \dot{U} + WQ - (x_r + x_e)Q^2 + (z_r + z_e)\dot{Q} + \ddot{x}_e + 2\dot{z}_e Q, \\ a_z &= \dot{W} - UQ - (z_r + z_e)Q^2 - (x_r + x_e)\dot{Q} + \ddot{z}_e - 2\dot{x}_e Q. \end{aligned} \tag{14.43}$$

Since $x_e = \dot{x}_e = \ddot{x}_e = 0$, if flexible deformation only occurs in the z direction, the equations become

$$\begin{aligned} a_x &= \dot{U} + WQ - (x_r)Q^2 + (z_r + z_e)\dot{Q} + 2\dot{z}_e Q, \\ a_z &= \dot{W} - UQ - (z_r + z_e)Q^2 - (x_r)\dot{Q} + \ddot{z}_e. \end{aligned} \tag{14.44}$$

14.7.4 Equations of Motion Including Flexible Effects – Motion of Axes

The equations of motion for the flexible aircraft consist of equations governing the motion of the undeformed aircraft (i.e. body fixed axes system) and also the flexible mode response. To determine the first set of equations, consider as before the inertia forces associated with an infinitesimal mass dm at point P. The equations of equilibrium are similar to those used earlier in Section 14.5.1 except that the instantaneous position of point P (including flexible deformation) is used in the moment equation, so

$$\begin{aligned} &\int a_x dm = X, \qquad \int a_z dm = Z, \\ &\int [a_x (z_r + z_e) - a_z (x_r + x_e)] dm = M. \end{aligned} \tag{14.45}$$

When the acceleration components are substituted from Equation (14.43) into Equation (14.45) and z_e is replaced by the modal expression in Equation (14.41), the resulting expression initially looks rather complex. However, it may be shown that the equations of motion for the mean axes reference system moving with the body are simply

$$m(\dot{U} + QW) = X, \qquad m(\dot{W} - QU) = Z, \qquad I_y \dot{Q} = M. \tag{14.46}$$

These are of course the rigid body equations found earlier. Note that there are no couplings to the flexible mode generalized coordinate; they have all been eliminated by using mean axes, free–free modes and the simplifying assumptions introduced earlier. Thus the motion of the reference axes system is independent of the structural deformation until couplings are introduced by aerodynamic effects.

Note that the same results would have been obtained if Lagrange's equations had been employed, but it should be noted that the linear and angular velocities of the centre of mass would need to have been defined with respect to an inertial reference frame. Such an approach is taken in (Waszak and Schmidt, 1988).

14.7.5 Equations of Motion Including Flexible Effects – Modal Motion

There are several ways of determining the equation in q_e, the generalized coordinate for the free–free flexible mode, e.g. Lagrange's equations or the principle of virtual displacements (Davies, 1982). However, for simplicity, Lagrange's equations will be employed.

The *kinetic energy* of the two-dimensional flexible aircraft is given by

$$T = \tfrac{1}{2}m(U^2 + W^2) + \tfrac{1}{2}I_y Q^2 + T_s, \tag{14.47}$$

where the inertia coupling terms have been omitted, the moment of inertia is constant and the final term in the expression, T_s, is the kinetic energy associated with the flexible mode deformation in the z direction, namely

$$T_s = \tfrac{1}{2}\int \dot{z}_\mathrm{e}^2 \,\mathrm{d}m = \tfrac{1}{2}\int \kappa_\mathrm{e}^2 \,\mathrm{d}m\, \dot{q}_\mathrm{e}^2 = \tfrac{1}{2}m_\mathrm{e}\, \dot{q}_\mathrm{e}^2, \tag{14.48}$$

where m_e is the modal mass. The *strain energy* term for the flexible aircraft may be expressed in terms of the bending and torsion stiffness distributions over the aircraft, but more conveniently here as

$$U = \tfrac{1}{2}k_\mathrm{e} q_\mathrm{e}^2, \tag{14.49}$$

where k_e is the modal stiffness. Then, applying Lagrange's equation for the flexible mode generalized coordinate and adding in a modal damping term and an external modal generalized force Q_ext yields

$$m_\mathrm{e}\ddot{q}_\mathrm{e} + c_\mathrm{e}\dot{q}_\mathrm{e} + k_\mathrm{e}q_\mathrm{e} = Q_\mathrm{ext}. \tag{14.50}$$

There are no couplings to Equations (14.46) governing the motion of the mean axes set. It may be seen that this is the classical second-order equation for modal space. If more flexible modes were included, then the orthogonality of the flexible modes would need to be exploited and the final result could be expressed in matrix form.

14.7.6 Full Flight Mechanics Equations with Flexible Modes

Now the equations for the underlying flight mechanics behaviour may be combined together with the single flexible mode. Consider the linearized version of Equation (14.46), as quoted in Equation (14.25), and omit the variation in the fore-and-aft direction to keep the overall model to three DoF. Then, adding the modal equation in Equation (14.50), the resulting partitioned equations are

$$\left[\begin{array}{cc|c} m & 0 & 0 \\ 0 & I_y & 0 \\ \hline 0 & 0 & m_\mathrm{e} \end{array}\right] \left\{\begin{array}{c} \dot{w} \\ \dot{q} \\ \hline \ddot{q}_\mathrm{e} \end{array}\right\} + \left[\begin{array}{cc|c} 0 & -mU_\mathrm{e} & 0 \\ 0 & 0 & 0 \\ \hline 0 & 0 & c_\mathrm{e} \end{array}\right] \left\{\begin{array}{c} w \\ q \\ \hline \dot{q}_\mathrm{e} \end{array}\right\} + \left[\begin{array}{cc|c} 0 & 0 & 0 \\ 0 & 0 & 0 \\ \hline 0 & 0 & k_\mathrm{e} \end{array}\right] \left\{\begin{array}{c} \int w \\ \int q \\ \hline q_\mathrm{e} \end{array}\right\} = \left\{\begin{array}{c} Z \\ M \\ \hline Q_\mathrm{ext} \end{array}\right\}. \tag{14.51}$$

These flight mechanics and modal equations are uncoupled dynamically through the use of mean axes though, of course, a given control input could excite a response in both sets of equations. However, once aerodynamic terms are introduced, coupling will occur through the aerodynamic derivatives. Equivalent equations could be written for the nonlinear flight mechanics case and for lateral motion.

14.8 SOLUTION OF FLIGHT MECHANICS EQUATIONS

Finally, once aerodynamic terms are included, the combined flight mechanics equations (linear or nonlinear) could be solved for a variety of control inputs and the responses used to calculate internal loads. Also, the flight control system (FCS) could be added and this will introduce further couplings.

14.8.1 Solving the Longitudinal Nonlinear Equations of Motion

For response determination, the full set of equations is solved in time, so allowing any nonlinear aerodynamic or FCS effects to be included. The resulting accelerations may then be used to obtain inertia force distributions and hence internal loads using the force summation approach described later in Chapter 18.

The equations may be expressed in a block diagram form (cf. analogue computer) and solved using a simulation software package such as SIMULINK. The first part of the simulation solves the differential equations for U, W, Q and q_{e} for the two-dimensional flexible aircraft, whereas the second part converts to velocities in earth axes using the transformation matrices $\mathbf{A}_{\mathrm{L}}$ and $\mathbf{A}_{\mathrm{R}}$ followed by integration to determine the position and orientation of the aircraft. The input forces and moments would be calculated according to the gravitational, aerodynamic, control and propulsive actions. MATLAB and SIMULINK programs to solve the dynamic manoeuvre for a rigid or flexible aircraft in heave and pitch are included in appendix I in the companion website.

14.8.2 Dynamic Stability Modes

A classical analysis using the rigid aircraft linearized flight mechanics equations involves examining the dynamic stability of the aircraft in longitudinal or lateral motion. The equations are written in Laplacian form, relevant transfer functions are generated and the characteristic polynomial (given by the denominator of the transfer function) is solved to yield the roots of the constituent motions (Cook, 1997; also see Chapters 7 and 15). The motion of the aircraft following a disturbance from the trim condition involves a combination of so-called ‘dynamic stability modes’ (Cook, 1997). These modes are different to the rigid body modes (see Chapter 3 and Appendix A) since the dynamic stability modes include the effects of the aerodynamic couplings between the rigid body motions; they are therefore more related to the modes of the aeroelastic system (see Chapter 11) but are based on body fixed axes equations for the rigid aircraft. Some dynamic stability modes are oscillatory whereas others are nonoscillatory, governed respectively by complex and real roots in the characteristic equation. The frequencies of the dynamic stability modes are generally well below any flexible mode frequencies except for very large commercial aircraft.

For *longitudinal* motion, there are two dynamic stability modes, both of which are oscillatory. The very low frequency (and lightly damped) *phugoid* mode involves an oscillation in forward speed, coupled with pitch and height; this mode requires the fore-and-aft motion of the aircraft to be included. The higher frequency (and more heavily damped) *short period* mode is dominated by a pitching oscillation, with the forward speed remaining essentially constant. Each mode will have positive damping for a commercial aircraft but the FCS will be used to create the desired stability and handling characteristics of the aircraft by modifying the dynamic stability modes (see the next section).

For *lateral* motion, the characteristic equation has two real roots and one pair of complex roots, so there are three dynamic stability modes whose stability has to be examined. The *dutch roll* mode involves a damped oscillation in yaw, coupled primarily to roll but also to sideslip. The *spiral* mode is nonoscillatory and is a combination of roll, yaw and sideslip motions. The *roll subsidence* mode (see Chapter 15) is a nonoscillatory rolling motion, largely decoupled from the spiral and Dutch roll modes. It should be noted that the nonoscillatory modes involve an exponentially decaying motion following a disturbance.

When the flexible aircraft is considered, the basic flight mechanics behaviour will alter as the dynamic stability modes will be modified by elastic contributions and the stability may be compromised (see Chapter 15). There will be an overall impact on the FCS design to ensure that the handling qualities of the flexible aircraft remain satisfactory and also the flight simulator model will need to be modified to include elastic effects.

14.9 FLIGHT CONTROL SYSTEM (FCS)

The flight control system (FCS) on modern commercial aircraft is typically driven by software, executed on computers and interfaced with an array of electrical, electronic, mechanical and hydraulic hardware. The FCS is a complex, high integrity system that is essential for safe operation across the full flight envelope and across the full range of expected environmental conditions. There are many features of the FCS that are beyond the scope of this book to cover in any detail; however, the reader is directed to Pratt (2000) for a comprehensive treatment of the FCS, particularly from an industrial viewpoint. The FCS impacts upon manoeuvres, gusts, flutter and static aeroelastic calculations but its primary function relates to aircraft handling and the flight mechanics model – hence the reason for including the FCS in this chapter.

The FCS has a number of functions, namely:

- enabling the aircraft to have the desired stability characteristics and handling qualities;
- avoiding pilot-induced oscillations (PIOs);
- providing the pilot with ‘carefree handling’ such that the aircraft never exceeds aerodynamic, structural or control limits, regardless of pilot input demands;
- reducing manoeuvre loads (e.g. wing root shear force and bending moment) through the use of a manoeuvre load alleviation (MLA) system;
- reducing gust and turbulence response (so improving crew and passenger ride quality) and loads (as for the MLA) through the use of a gust load alleviation (GLA) system.

The FCS involves the use of a range of sensors to measure the aircraft state, namely air data sensors (e.g. altitude, incidence angle, sideslip angle, air speed, Mach number), rate gyros and accelerometers. The FCS also employs a number of actuators, primarily the aerodynamic control surfaces and engine throttle. The aircraft response is fed back, often via multiple feedback loops and control laws, to generate suitable actuation inputs that produce the required behaviour of the aircraft in its closed loop configuration. The aircraft flight condition information, together with mass and centre of mass data, is used to allow the control laws to be ‘scheduled’ in such a way that they are varied as necessary throughout the flight envelope. The replacement of analogue by digital control systems has allowed much more versatile and powerful control systems to be developed.

Historically, mechanical linkages have been used to link the pilot stick/pedals to the control actuators, but many modern aircraft are ‘fly-by-wire’, so electronic signals are used to command the hydraulic or electric actuators, thus avoiding heavy mechanical linkages, although mechanical back-up is still included for critical controls (e.g. elevator and rudder).

One important issue for the control of a flexible aircraft is that the sensors will measure not only the rigid body motions but also deformations of any mode having an influence in the controller bandwidth. These flexible mode contributions will then be processed via the control loops and lead to changes in the actuator demands; the control inputs could then possibly increase the flexible mode responses and lead to an unstable system. Such interaction between the control and structure is known as structural coupling or aeroservoelasticity (Pratt, 2000; also see Chapter 12). To avoid unfavourable effects it is normal to introduce so-called ‘shaping’ or ‘notch’ filters in order to suppress flexible mode contributions. The design of such filtering becomes more difficult as the flexible modes become closer in frequency to the rigid body modes, a growing problem for large commercial aircraft.

The inclusion of feedback control loops in the aircraft dynamic model, consisting of both rigid body and flexible modes, increases the model complexity significantly. Thus the presence of the FCS in manoeuvres and gust encounters will not be considered mathematically in this book, but only some general comments will be made in each case. However, in Chapter 12 it was shown how a simple feedback loop could alter the flutter characteristics of a simple binary wing model; also, the way in which the frequency dependency of shaping filters could be included in the stability calculations was explained. The same principles would apply for the whole free–free flexible aircraft under manoeuvre or gust conditions. The inclusion of the FCS in loads and aeroelastics calculations is also considered briefly in Chapter 22, where a block diagram is included.

15

Dynamic Manoeuvres

In Chapter 13, the balanced aircraft loads, trimmed condition and deformation in a steady symmetric *equilibrium manoeuvre* were considered for both a rigid and a simple flexible aircraft in heave and pitch. Such a manoeuvre is one in which the aircraft undergoes a steady acceleration normal to the flight path and a steady pitch rate (e.g. steady pull-out or banked turn) and where, by the application of D'Alembert's principle, the aircraft may be considered to be in static equilibrium under aerodynamic, thrust and inertia loads. Also, brief consideration was given to lateral equilibrium cases of a steady roll rate and steady sideslip, together with analysis of the abrupt application of the aileron or rudder, where the maximum angular acceleration was determined by balancing the applied aerodynamic moment by an inertia moment. These equilibrium manoeuvres are sometimes known as 'bookcases' (see Chapter 21); they are often somewhat artificial and unrealizable in practice, and may lead to overestimates of the internal loads, but are particularly useful early in the design cycle. However, a more 'rational' (or realistic/accurate; see Chapter 21) approach is often required by the certification specifications and may be used to obtain more realistic loads for some of the bookcases.

A *dynamic manoeuvre* (Lomax, 1996; Howe, 2004) involves applying some form of control input in such a way that a transient (time-varying) response of the aircraft is generated. To obtain accurate responses and loads, a 'rational' calculation will require a more realistic dynamic model and manoeuvre scenario to be used. Certain manoeuvres, e.g. 'unchecked' or 'checked' pitch manoeuvres and also failure cases (see Chapter 24), require a fully rational treatment. The unchecked manoeuvre involves the pilot pulling the stick straight back whereas the checked manoeuvre involves three-quarters of a cycle of harmonic control input; these loading conditions are potential design cases for the rear fuselage and horizontal tailplane. Rolling and yawing manoeuvres may be examined using bookcase (see Chapter 13) or rational calculations, the latter clearly being more accurate. Engine failure cases are best treated rationally. In order to determine the response of the aircraft in a rational manner, the equations of motion must be solved, usually by numerical integration because they may be nonlinear (due to the FCS and/or high incidence aerodynamics). Once the response is known, the variation of internal loads with time may be determined (see later in Chapter 18) via the application of D'Alembert's principle to 'balance' the aircraft at each instant of time. The certification requirements for dynamic manoeuvres may be seen in CS-25 and Lomax (1996) and will be discussed further in Chapter 24.

In Chapter 14, the full flight mechanics model for the rigid aircraft in heave and pitch, employing body fixed axes for large angle nonlinear (and small perturbation linear) manoeuvres, was introduced, where velocities were the basic unknowns. The way in which flexible modes could be included through the use of mean axes was also discussed. Such a flexible flight mechanics model may be used for dynamic flight manoeuvres, though in some cases the effect of the flexible modes is simply included via corrections to the aerodynamics (see Chapter 22), since in many cases the FCS is able to filter out dynamic motion of the flexible modes. The model is also used for assessing the impact of flexibility (i.e. aeroelastic effects) upon the dynamic stability modes (Babister, 1980; Waszak and Schmidt, 1988; Schmidt, 1998; Stengel, 2004), and therefore upon aircraft handling. The model will also yield a further estimate for the control

---

Introduction to Aircraft Aeroelasticity and Loads J. R. Wright and J. E. Cooper
© 2007 John Wiley & Sons, Ltd

effectiveness. Finally, the flight mechanics model is sometimes used for landing simulations with flexible modes included since their dynamic response is important (see Chapter 17).

In this chapter, the flight mechanics model will be applied to the problems of an aircraft undergoing a dynamic manoeuvre in heave/pitch and then, more briefly, in pure roll; these cases allow the concepts to be seen using a small order mathematical model involving both rigid and flexible cases. For simplicity no FCS is included but the way in which a control feedback loop might be represented is considered briefly in Chapter 7. In each case, the response will be calculated, together with the control effectiveness and the dynamic stability modes. Quasi-steady aerodynamics will be employed in determining the aerodynamic derivatives and these will be defined with respect to wind axes (i.e. body fixed) and not inertial axes, as were employed in Chapter 13.

Once again, it should be noted that in this chapter the focus will be on determining the aircraft response. However, a detailed treatment of the impact of aeroelasticity upon the flight mechanics behaviour is beyond the scope of this book. The calculation of loads will be covered in Chapter 18 since there are many common factors in calculating loads for dynamic, ground and equilibrium manoeuvres, as well as for gusts and turbulence.

15.1 DYNAMIC MANOEUVRE – RIGID AIRCRAFT HEAVE/PITCH DUE TO ELEVATOR INPUT

In this section, the dynamic behaviour of a rigid aircraft responding in heave and pitch to an elevator (or pitch control) input will be considered. Such a model allows the rational unchecked and checked pitch manoeuvres to be simulated. The aircraft representation is shown in Figure 15.1, where the notation used is the same as in Chapter 13. For simplicity, the thrust and drag are assumed to be in line, so that they do not contribute to the pitching moment equation. Later in the chapter, the flexible aircraft case will be considered.

15.1.1 Flight Mechanics Equations of Motion – Rigid Aircraft in Pitch

The linearized flight mechanics equations of motion for the longitudinal case (symmetric rigid aircraft) were shown in Chapter 14, for the case of small rates of rotation, to be

$$m(\dot{u} + W_{\mathrm{e}}q) = X, \qquad m(\dot{w} - U_{\mathrm{e}}q) = Z, \qquad I_{\mathrm{y}}\dot{q} = M. \tag{15.1}$$

Now, for the example in this chapter, it is assumed that there are no gravitational terms and no variation in fore-and-aft motion, so u is zero and only two equations are required; this reduced-order model will not therefore represent the long term motion governed by the phugoid (see Chapter 14), but it will approximate

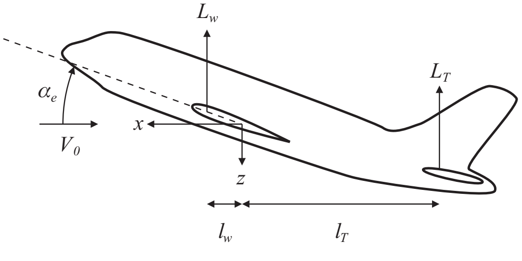

Figure 15.1 Rigid aircraft in dynamic heave/pitch manoeuvre under elevator application.

the short period motion over moderate timescales. Thus the equations governing the heave/pitch motion are

$$m(\dot{w} - U_{\mathrm{e}}q) = Z, \qquad I_{\mathrm{y}}\dot{q} = M. \tag{15.2}$$

The normal force Z and pitching moment M are expressed in terms of aerodynamic stability derivatives as

$$\begin{aligned} Z &= Z_{\dot{\mathrm{w}}}\dot{w} + Z_{\dot{\mathrm{q}}}\dot{q} + Z_{\mathrm{w}}w + Z_{\mathrm{q}}q + Z_{\eta}\eta, \\ M &= M_{\dot{\mathrm{w}}}\dot{w} + M_{\dot{\mathrm{q}}}\dot{q} + M_{\mathrm{w}}w + M_{\mathrm{q}}q + M_{\eta}\eta. \end{aligned} \tag{15.3}$$

Note that these equations may be expressed in body or wind axes (see Chapter 14) and the derivatives must correspond to the axes set chosen i.e. a transformation between axes may be necessary (Cook, 1997).

15.1.2 Aerodynamic Stability Derivatives in Heave/Pitch

The stability derivatives in Equation (15.3) are related to perturbations about axes fixed in the aircraft (usually wind axes) for dynamic manoeuvres, as opposed to the derivatives used in the equilibrium manoeuvres (see Chapter 13) where small angles and displacements about inertial axes (fixed in space) were considered. However, because the perturbations employed in defining stability derivatives are small and not all stability derivatives involve perturbations of the aircraft velocity, many of the values actually turn out to be the same as those obtained for the inertial axes (see the comparison table in Appendix B). It is arguable that using wind axes is preferable to body axes since the derivatives are simpler in form; note that for this simple case of longitudinal motion, the pitch moment of inertia will be the same for both axes sets.

The Z_{w} derivative in Equations (15.3) for the perturbed normal velocity w is derived in Appendix E as an example of how derivatives involving aircraft velocity perturbations may be determined. However, it may be seen in Appendix B that this 'w stability derivative' differs by a factor of V_0 from the 'α inertial derivative' Z_α because of the difference in the equation variable ($\alpha = w/V_0$) and also the drag coefficient C_{D} is present due to the velocity perturbations for the stability derivative. The M_{w} derivative is obtained in a similar way.

The stability derivatives Z_{q}, M_{q}, Z_η, M_η for perturbed q and η turn out to be the same as those derived in Chapter 13 for inertia axes because there are no perturbations of the flight velocities involved. The aerodynamic stability derivatives for heave and pitch acceleration depend upon the downwash lag effect and aerodynamic inertia terms that are often neglected (Cook, 1997); these derivatives will be neglected here, so

$$Z_{\dot{\mathrm{w}}} = Z_{\dot{\mathrm{q}}} = M_{\dot{\mathrm{w}}} = M_{\dot{\mathrm{q}}} = 0. \tag{15.4}$$

Thus, in summary, the nonzero derivatives for wind axes used in Equations (15.3) are given by

$$\begin{aligned} &Z_w = -\tfrac{1}{2}\rho V_0\left(S_{\mathrm{W}}a_{\mathrm{W}} + S_{\mathrm{T}}a_{\mathrm{T}}(1-k_\varepsilon) + S_{\mathrm{W}}C_{\mathrm{D}}\right), \qquad Z_q = -\tfrac{1}{2}\rho V_0 S_{\mathrm{T}}a_{\mathrm{T}}l_{\mathrm{T}} \quad \text{(tailplane effect only)}, \\ &M_w = \tfrac{1}{2}\rho V_0\left[S_{\mathrm{W}}a_{\mathrm{W}}l_{\mathrm{W}} - S_{\mathrm{T}}a_{\mathrm{T}}l_{\mathrm{T}}(1-k_\varepsilon)\right] \text{ or } \tfrac{1}{2}\rho V_0 S_{\mathrm{W}}c\tfrac{\mathrm{d}C_{\mathrm{m}}}{\mathrm{d}\alpha}, \qquad Z_\eta = -\tfrac{1}{2}\rho V_0^2 S_{\mathrm{T}}a_{\mathrm{E}}, \\ &M_q = -\tfrac{1}{2}\rho V_0 S_{\mathrm{T}}a_{\mathrm{T}}l_{\mathrm{T}}^2 \quad \text{(tailplane effect only)}, \qquad M_\eta = -\tfrac{1}{2}\rho V_0^2 S_{\mathrm{T}}a_{\mathrm{E}}l_{\mathrm{T}}, \end{aligned} \tag{15.5}$$

where the notation in (Cook, 1997) has been converted to that used in this book. Note that no zero incidence terms are present in the equations for wind axes fixed in the aircraft.

If the equations were to be expressed in body axes (aligned with principal axes), then these wind axes derivatives would need to be transformed through the trim incidence angle α_{e}, noting that both forces/

moments and linear/angular velocities need to be transformed; the methodology is described in (Cook, 1997).

15.1.3 Solution of the Flight Mechanics Equations – Rigid Aircraft

The flight mechanics equations of motion for the rigid aircraft may then be written in matrix form showing terms due to inertia, use of body fixed axes (see Chapter 14) and aerodynamics as

$$\begin{bmatrix} m & 0 \\ 0 & I_{\mathrm{y}} \end{bmatrix} \begin{Bmatrix} \dot{w} \\ \dot{q} \end{Bmatrix} + \begin{bmatrix} 0 & -mU_{\mathrm{e}} \\ 0 & 0 \end{bmatrix} \begin{Bmatrix} w \\ q \end{Bmatrix} - \begin{bmatrix} Z_{\mathrm{w}} & Z_{\mathrm{q}} \\ M_{\mathrm{w}} & M_{\mathrm{q}} \end{bmatrix} \begin{Bmatrix} w \\ q \end{Bmatrix} = \begin{Bmatrix} Z_\eta \\ M_\eta \end{Bmatrix} \eta \tag{15.6}$$

with the derivatives defined in Equation (15.5). This equation may be solved to determine the response, relative to the wind axes, corresponding to a particular elevator input. The velocity w is difficult to interpret physically so it is arguably easier to consider the variation of incidence using $\alpha = \mathrm{w}/V_0$ for small perturbations. A further useful response parameter is the incremental normal acceleration at an arbitrary position x forward of the centre of mass, namely $a_z = \dot{w} - qU_{\mathrm{e}} - x\dot{q}$ (see Chapter 14).

15.1.4 Pitch Rate Per Elevator Transfer Function

The transfer function relating pitch rate to elevator angle may be written by transforming Equation (15.6) to the Laplace domain (see Chapter 7) such that

$$\begin{bmatrix} sm - Z_{\mathrm{w}} & -mU_{\mathrm{e}} - Z_{\mathrm{q}} \\ -M_{\mathrm{w}} & sI_{\mathrm{y}} - M_{\mathrm{q}} \end{bmatrix} \begin{Bmatrix} w(s) \\ q(s) \end{Bmatrix} = \begin{Bmatrix} Z_\eta \\ M_\eta \end{Bmatrix} \eta(s). \tag{15.7}$$

These matrix equations may be solved for the pitch rate per elevator angle, so that

$$\left(\frac{q}{\eta}(s)\right)_{\mathrm{Rigid}} = \frac{smM_\eta + M_{\mathrm{w}} Z_\eta - M_\eta Z_{\mathrm{w}}}{D(s)}. \tag{15.8}$$

Here the denominator polynomial $D(s)$ is the determinant of the square matrix in Equation (15.7), namely

$$D(s) = s^2\left(I_{\mathrm{y}} m\right) + s\left[-I_{\mathrm{y}} Z_{\mathrm{w}} - mM_{\mathrm{q}}\right] + \left[Z_{\mathrm{w}} M_{\mathrm{q}} - (mU_{\mathrm{e}} + Z_{\mathrm{q}})M_{\mathrm{w}}\right], \tag{15.9}$$

which will define the characteristic (quadratic) equation of the system. The steady state pitch rate per elevator deflection is given by the transfer function at zero frequency, namely

$$\left(\frac{q}{\eta}\right)_{\mathrm{Rigid}} = \frac{M_{\mathrm{w}} Z_\eta - M_\eta Z_{\mathrm{w}}}{Z_{\mathrm{w}} M_{\mathrm{q}} - (mU_{\mathrm{e}} + Z_{\mathrm{q}})M_{\mathrm{w}}}. \tag{15.10}$$

This expression may be compared later to the flexible aircraft result and the elevator effectiveness derived.

When the elevator is deflected (trailing edge upwards, actually negative) for a rigid aircraft then there is a reduced tailplane lift, the aircraft pitches nose up (positive), generates additional incidence and hence sufficient additional wing lift so as to override the tailplane lift reduction and allow the aircraft to heave upwards; this will be seen in the example for a step elevator input in Section 15.1.8.

15.1.5 Short Period Motion

The roots of the quadratic equation (15.9) define the characteristic short period motion of the rigid aircraft. The roots are normally a complex conjugate pair in the form

$$s = -\zeta_{\mathrm{S}}\omega_{\mathrm{S}} \pm \omega_{\mathrm{S}}\sqrt{1 - \zeta_{\mathrm{S}}^2}, \tag{15.11}$$

where ω_S is the undamped frequency of the short period motion (typically 1–10 rad/s) and ζ_S is its damping ratio (stabilizing for a commercial aircraft, typically 20–50 % critical). The mode involves a combination of pitch and heave motion. The short period motion may be significantly affected when the FCS is included in the model.

15.1.6 Phugoid Motion

If the longer term motion were to be studied, then the equation governing u would need to be included, as would the pitch rate/pitch angle equation together with gravitational and thrust terms (Cook, 1997). The characteristic equation would then become a quartic polynomial, giving two sets of complex roots for the phugoid and short period motions. The phugoid mode is a lightly damped, low frequency oscillation in speed u that couples with pitch angle and height but has a relatively constant incidence. The Lanchester approximation to the phugoid mode (Cook, 1997) yields a simple value for the phugoid frequency as $\omega_P = \sqrt{2}\frac{g}{V_0}$ (a very low value, e.g. 0.09 rad/s at 150 m/s TAS).

When the transfer function for the reduced model in Equation (15.8) is used to determine the response to a step elevator input, a steady pitch rate results; however, in practice the long term pitch rate will tend to zero if the full longitudinal equations are used, since the gravitational and drag terms will come into play unless the thrust is adjusted (Cook, 1997). However, an on/off or limited sinusoidal elevator input would lead to a more short term motion and the reduced model is considered to be satisfactory to illustrate such a case.

15.1.7 Conversion to Earth Axes Motion

Once the flight mechanics equations for the pitch rate $q(t)$ and heave $w(t)$ with respect to axes moving with the aircraft have been solved, the motion with respect to earth axes needs to be found. To determine the velocities and position in earth fixed axes, the Euler transformation in Chapter 14 must be employed, namely

$$U_E = U_e + W_e\theta, \qquad W_E = -U_e\theta + W_e + w, \qquad \dot{\theta} = q. \tag{15.12}$$

This equation has been linearized for small perturbations.

Firstly, the pitch rate $\dot{\theta}$ can be determined simply from q and the pitch angle θ may then be found by integrating $\dot{\theta}$ using a suitable initial condition so as to yield the aircraft pitch motion in space. The other two equations may then be employed to find the component velocities in earth axes, followed by integration to find the aircraft position (X_E, Z_E) and hence the flight path during the manoeuvre. Note that prior to the dynamic manoeuvre caused by application of the elevator, the aircraft is assumed to be in straight and level trimmed (or equilibrium, subscript e) flight at velocity U_e $(\theta_e = W_e = 0)$ so the transformation is simplified.

Clearly, the aircraft motion may be seen from the change in earth axes position and/or by considering the perturbations in the flight path angle γ given by $\gamma = \theta - \alpha \cong \theta - w/V_0$ (Cook, 1997). The steady flight path angle γ_e (note different usage of the torsion mode shape symbol) at the commencement of the manoeuvre will be zero since the aircraft is in level flight $(\theta_e = 0)$ and wind axes are used $(\alpha_e = 0)$. Note that for the study of longer term motions, the pitch rate equation needs to be considered together with the three DoF longitudinal equations to allow gravitational and thrust effects to be included (Cook, 1997).

15.1.8 Example: Rigid Aircraft in Heave/Pitch

Consider an aircraft with the following data (essentially the same as that in Chapter 13): $m = 10\,000$ kg, $I_y = 144\,000$ kg m^2, $S_W = 30$ m^2, $S_T = 7.5$ m^2, $c = 2.0$ m, $l_W = 0.3\,c = 0.6$ m, $l_T = 3.5c = 7$ m, $a_W = 4.5$ /rad, $a_T = 3.2$ /rad, $a_E = 1.5$ /rad, $k_\varepsilon = 0.35$, $\alpha_0 = -0.03$ rad, $C_D = 0.1$ and $C_{M_{0W}} = -0.03$. These data are for the rigid aircraft, with further parameters defined later for the flexible aircraft. Note that the data correspond to a static margin of 0.2 m (10 %c). The aim of the example is to determine the short period mode properties and the aircraft response relative to wind and earth axes for the aircraft in straight and level flight at 175 m/s EAS ($U_e = V_0,\ W_e = \theta_e = 0$) when subjected to various elevator (or pitch) control inputs. MATLAB and SIMULINK programmes to solve the dynamic manoeuvre for this rigid aircraft in heave/pitch are included in appendix I in the companion website.

Firstly, it may be shown that the short period mode has a natural frequency of 2.25 rad/s (0.36 Hz) and damping of 56 % at 175 m/s EAS. The frequency varies linearly with velocity but the damping ratio is unaffected. Ideally, the damping would be somewhat lower and this could be achieved by moving the centre of mass further forward. However, it was desired to leave the aircraft centre of mass behind the wing centre of mass in this simple example.

Secondly, when a step elevator input of -1° is applied to the aircraft, then the pitch rate q, incidence α, normal acceleration a_z at the centre of mass, pitch angle θ and flight path angle γ responses are as shown in Figure 15.2. The step elevator input leads to a steady incidence, pitch rate and normal acceleration; the corresponding pitch and flight path angles increase more or less linearly with time, with the flight path angle lagging the pitch angle by about 0.6 s. Examination of the aircraft position in earth axes (X_E, Z_E) shows the aircraft climbing steadily through about 60 m after 4 s. It was pointed out earlier that using the full equations, including forward speed variation and drag effects, etc., would lead to a different long term response due to the phugoid influence.

Thirdly, a single cycle of a sinusoidal elevator input of frequency 0.25 Hz, duration 4 s and amplitude -1° is applied (similar to the checked pitch manoeuvre). The response to this input is shown in Figure 15.3(a). The aircraft pitches nose up, then nose down and settles back at zero pitch rate, normal acceleration and pitch angle; the maximum incremental acceleration is $1.09g$. The flight path angle also returns to zero. This result, together with the aircraft motion in earth axes shown in Figure 15.3(b), indicates that the aircraft has gained about 25 m in height and reached a new level flight condition. Note that different frequencies and numbers of input cycles will yield different responses; e.g. multiple cycles of input will increase the response.

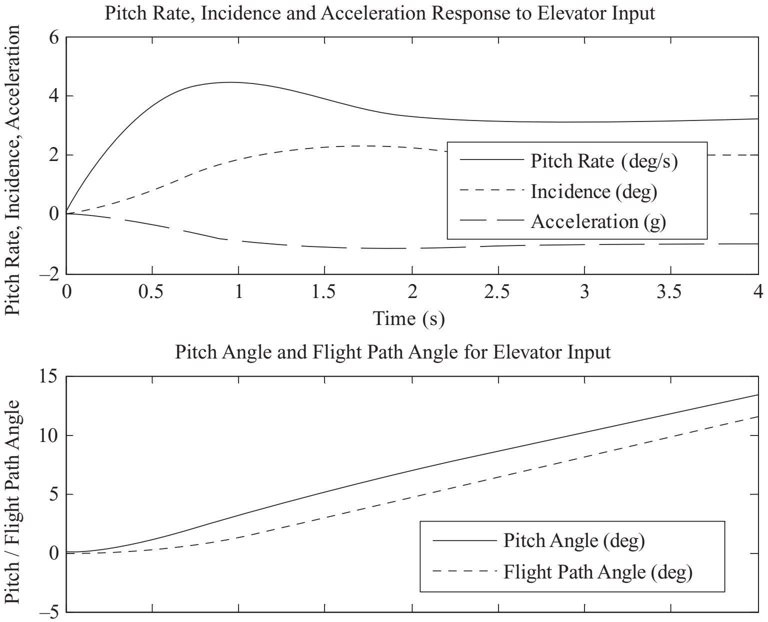

Figure 15.2 Response of a rigid aircraft to a -1° step elevator input at 175 m/s EAS.

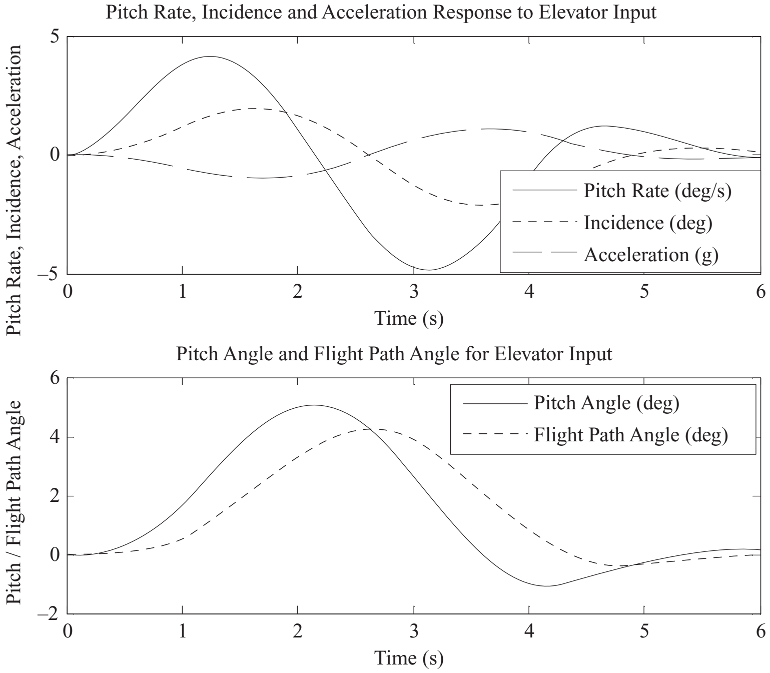

(a) Responses

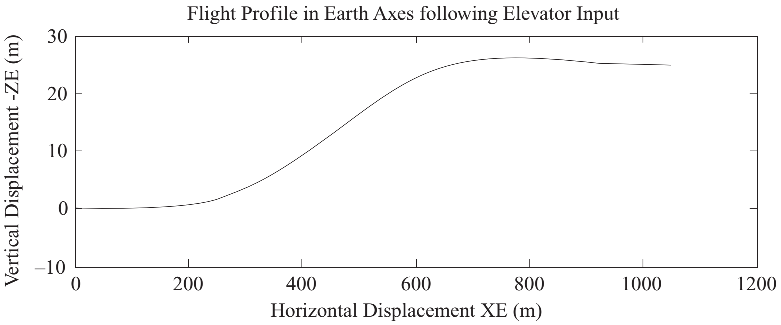

(b) Aircraft Motion in Earth Axes

Figure 15.3 Response of a rigid aircraft to a single cycle of sinusoidal elevator input (0.25 Hz/4 s/-1°): (a) responses and (b) aircraft motion in earth axes.

15.2 DYNAMIC MANOEUVRE – FLEXIBLE AIRCRAFT HEAVE/PITCH DUE TO ELEVATOR INPUT

In Chapter 13, the equilibrium manoeuvre calculation was shown for a simple flexible aircraft in heave and pitch. The motions involved were rigid body heave and pitch, together with a symmetric free–free mode (see Appendix C) with potential wing bending, wing twist or fuselage bending deformations. In this section, the same flexible mode will be added to the flight mechanics equations, in order to investigate the flexible aircraft in a dynamic manoeuvre. Some results from Chapter 13 and this chapter will be used in generating the model.

15.2.1 Flight Mechanics Equations of Motion – Flexible Aircraft in Pitch

In Chapter 14, it was shown how a flexible mode could be introduced into the equation of motions for the flight mechanics model when mean axes were employed, together with certain assumptions (e.g. small deformations). Then the equations for heave and pitch, neglecting fore-and-aft motion as discussed earlier and extended to include the flexible mode, were written with no inertia coupling terms. If the right-hand side aerodynamic forces are written in aerodynamic stability derivative terms and flexible derivatives added, rather as in Chapter 13 but for wind axes, the equations of motion for the flexible aircraft may be simplified to

$$\left[\begin{array}{cc|c} m & 0 & 0 \\ 0 & I_y & 0 \\ \hline 0 & 0 & m_\mathrm{e} \end{array}\right]\left\{\begin{array}{c} \dot{w} \\ \dot{q} \\ \hline \ddot{q}_\mathrm{e} \end{array}\right\} + \left\{\left[\begin{array}{cc|c} 0 & -mU_\mathrm{e} & 0 \\ 0 & 0 & 0 \\ \hline 0 & 0 & c_\mathrm{e} \end{array}\right] - \left[\begin{array}{cc|c} Z_\mathrm{w} & Z_\mathrm{q} & Z_{\dot{\mathrm{e}}} \\ M_\mathrm{w} & M_\mathrm{q} & M_{\dot{\mathrm{e}}} \\ \hline Q_\mathrm{w} & Q_\mathrm{q} & Q_{\dot{\mathrm{e}}} \end{array}\right]\right\}\left\{\begin{array}{c} w \\ q \\ \hline \dot{q}_\mathrm{e} \end{array}\right\}$$

$$\left\{-\left[\begin{array}{cc|c} 0 & 0 & Z_\mathrm{e} \\ 0 & 0 & M_\mathrm{e} \\ \hline 0 & 0 & Q_\mathrm{e} \end{array}\right] + \left[\begin{array}{cc|c} 0 & 0 & 0 \\ 0 & 0 & 0 \\ \hline 0 & 0 & k_\mathrm{e} \end{array}\right]\right\}\left\{\begin{array}{c} \int w \\ \int q \\ \hline q_\mathrm{e} \end{array}\right\} = \left\{\begin{array}{c} Z_\eta \\ M_\eta \\ \hline Q_\eta \end{array}\right\}\eta, \tag{15.13}$$

and this equation may be used to determine the response to any elevator input. Here the matrix partitions separate what are essentially the rigid body and flexible terms; the integral terms are somewhat artificial as they are multiplied by zero, but are included to allow a convenient matrix form of the equations. While the rigid body and flexible equations are actually uncoupled wind-off, the aerodynamic terms introduce couplings between them. If more modes were added, the scalar modal mass, damping and stiffness terms would be replaced by diagonal matrices and additional aerodynamic coupling terms between the modes would be included. It should be noted that the acceleration derivatives have been neglected and that flexible derivatives for both flexible deformation and rate of deformation have been included.

Note that the incremental normal acceleration at position x forward of the centre of mass is $a_\mathrm{z} = \dot{w} - qU_\mathrm{e} - x\dot{q} + \ddot{z}_\mathrm{s}$, where $\ddot{z}_\mathrm{s} = \kappa_{\mathrm{e}x}\ddot{q}_\mathrm{e}$ is the flexible mode contribution to the acceleration and $\kappa_{\mathrm{e}x}$ is the mode shape at position x (see Chapter 14).

15.2.2 Aerodynamic Derivatives for Flexible Aircraft

In considering the derivatives that need to be calculated, there is no need to obtain again the derivatives that appeared in the rigid aircraft equation of motion (15.6) and were tabulated earlier in Equation (15.5), namely Z_w, Z_q, Z_η, M_w, M_q, M_η. Also, the flexible pitch rate and elevator derivatives Q_q, Q_η and the flexible deformation derivatives Z_e, M_e, Q_e corresponding to perturbations in elastic mode deformation may be shown to be the same as those quoted in Chapter 13 for inertial axes, as seen in Appendix B. This means that only the derivative Q_w and the derivatives $Z_{\dot{\mathrm{e}}}$, $M_{\dot{\mathrm{e}}}$, $Q_{\dot{\mathrm{e}}}$ related to perturbations in the rate of elastic deformation need to be obtained here.

To obtain Q_w, a modal force derivative, the incremental work term for the perturbation forces generated by perturbed motion w acting through an incremental flexible deformation may be considered. The perturbation lift forces (upwards) acting on the wing strip and complete tailplane due to perturbation w alone are related to the incidence $\alpha = w/v_0$, so

$$\mathrm{d}L_\mathrm{W} = \tfrac{1}{2}\rho V_0^2 c a_\mathrm{W}\left(\frac{w}{V_0}\right)\mathrm{d}y, \qquad \Delta L_\mathrm{T} = \frac{1}{2}\rho V_0^2 S_\mathrm{T} a_\mathrm{T}\left(\frac{w}{V_0}\right) \tag{15.14}$$

because of the effective incidence produced by the perturbation in heave motion. The corresponding incremental displacements due to incremental flexible mode deformation at the wing and tailplane aerodynamic centres are $[\kappa_\mathrm{e}(y) - l_\mathrm{A}\gamma_\mathrm{e}(y)]\,\delta q_\mathrm{e}$ and $\kappa_{\mathrm{eT}}\delta q_\mathrm{e}$ (both downwards) respectively, where κ_e, γ_e define the symmetric flexible mode shape (see Appendix C). Thus the incremental work done terms may be determined, differentiated with respect to δq_{e}, and the result inspected to yield the derivative for perturbed motion

$$Q_w = \frac{\partial Q}{\partial w} = \tfrac{1}{2}\rho V_0 \left[-S_{\mathrm{W}} a_{\mathrm{W}} J_2 - S_{\mathrm{T}} a_{\mathrm{T}} (1 - k_{\varepsilon}) \kappa_{\mathrm{eT}}\right], \tag{15.15}$$

where $J_2 = (1/s)\int_{y=0}^{s} (\kappa_{\mathrm{e}} - l_{\mathrm{A}}\gamma_{\mathrm{e}})\mathrm{d}y$ and again this derivative is similar to Q_α used for the equilibrium manoeuvres.

Now it is assumed that the flexible rate derivatives $Z_{\dot{\mathrm{e}}}$, $M_{\dot{\mathrm{e}}}$, $Q_{\dot{\mathrm{e}}}$, rather like the pitch rate derivatives, will be dominated by tailplane effects so, for simplicity, terms involving the wing will be neglected. The perturbation tailplane lift force and pitching moment contributions due to perturbed flexible rate effects will be related to the flexible derivatives $Z_{\dot{\mathrm{e}}}$ and $M_{\dot{\mathrm{e}}}$ in the heave and moment equations,

$$\Delta L_{\mathrm{T}} = \tfrac{1}{2}\rho V_0^2 S_{\mathrm{T}} a_{\mathrm{T}} \left(\frac{\kappa_{\mathrm{eT}}\dot{q}_{\mathrm{e}}}{V_0}\right) = -Z_{\dot{\mathrm{e}}}\dot{q}_{\mathrm{e}}, \qquad \Delta M_{\mathrm{T}} = -\tfrac{1}{2}\rho V_0^2 S_{\mathrm{T}} a_{\mathrm{T}} \left(\frac{\kappa_{\mathrm{eT}}\dot{q}_{\mathrm{e}}}{V_0}\right) l_{\mathrm{T}} = M_{\dot{\mathrm{e}}}\dot{q}_{\mathrm{e}}, \tag{15.16}$$

where the vertical velocity at the tailplane due to the flexible rate dictates the effective incidence. The unsteady pitch rate terms associated with the tailplane modal slope γ_{eT} are ignored. Thus, by inspection, the elastic rate derivatives are

$$Z_{\dot{\mathrm{e}}} = -\frac{1}{2}\rho V_0 S_{\mathrm{T}} a_{\mathrm{T}} \kappa_{\mathrm{eT}}, \qquad M_{\dot{\mathrm{e}}} = -\frac{1}{2}\rho V_0 S_{\mathrm{T}} a_{\mathrm{T}} l_{\mathrm{T}} \kappa_{\mathrm{eT}}. \tag{15.17}$$

Finally, the flexible rate derivative in the generalized equation $Q_{\dot{\mathrm{e}}}$ requires the incremental work done due to the tailplane lift force in Equation (15.16) acting through the incremental displacement in the mode at the tailplane, so

$$\delta W_{\dot{\mathrm{e}}} = -\frac{1}{2}\rho V_0^2 S_{\mathrm{T}} a_{\mathrm{T}} \left(\frac{\kappa_{\mathrm{eT}}\dot{q}_{\mathrm{e}}}{V_0}\right)(\kappa_{\mathrm{eT}}\delta q_{\mathrm{e}}). \tag{15.18}$$

Then the relevant generalized force in the modal equation is

$$Q_{\dot{\mathrm{e}}} = -\frac{1}{2}\rho V_0 S_{\mathrm{T}} a_{\mathrm{T}} \kappa_{\mathrm{eT}}^2. \tag{15.19}$$

Thus all the derivatives are available so the flight mechanics equation (15.13) for the flexible aircraft may now be solved and the transformations to earth axes carried out as before.

15.2.3 Pitch Rate Per Elevator Transfer Function

The transfer function relating pitch rate to elevator angle for the flexible aircraft may be written by transforming Equation (15.13) to the Laplace domain

$$\left[\begin{array}{cc|c} sm - Z_{\mathrm{w}} & -mU_{\mathrm{e}} - Z_{\mathrm{q}} & -sZ_{\dot{\mathrm{e}}} - Z_{\mathrm{e}} \\ -M_{\mathrm{w}} & sI_{\mathrm{y}} - M_{\mathrm{q}} & -sM_{\dot{\mathrm{e}}} - M_{\mathrm{e}} \\ \hline -Q_{\mathrm{w}} & -Q_{\mathrm{q}} & s^2 m_{\mathrm{e}} + sc_{\mathrm{e}} + k_{\mathrm{e}} - sQ_{\dot{\mathrm{e}}} - Q_{\mathrm{e}} \end{array}\right] \left\{\begin{array}{c} w(s) \\ q(s) \\ \hline q_{\mathrm{e}}(s) \end{array}\right\} = \left\{\begin{array}{c} Z_\eta \\ M_\eta \\ \hline Q_\eta \end{array}\right\} \eta(s). \tag{15.20}$$

These matrix equations may be solved for pitch rate per elevator angle but the expression will be rather complicated so only its general form will be shown, namely

$$\left(\frac{q}{\eta(s)}\right)_{\text{Elastic}} = \frac{N(s)}{D(s)}. \tag{15.21}$$

Here the denominator polynomial $D(s)$ is the determinant of the square matrix in Equation (15.20) and defines the characteristic quartic equation of the system and its roots (see later), while the numerator polynomial $N(s)$ is a cubic expression.

The steady-state pitch rate per elevator deflection is given by the above transfer function evaluated at zero frequency, namely

$$\left(\frac{q}{\eta}\right)_{\text{Flexible}} = \frac{N(0)}{D(0)}. \tag{15.22}$$

15.2.4 Elevator Effectiveness

The ratio of the flexible to rigid values of the steady-state pitch rate per elevator angle provides a measure of elevator effectiveness, namely

$$\Im_{\text{Elevator}} = \frac{(q/\eta)_{\text{Flexible}}}{(q/\eta)_{\text{Rigid}}}, \tag{15.23}$$

where the constituent terms are given in Equations (15.22) and (15.10). The action of an elevator deflection on the pitch rate for the rigid aircraft was explained in Section 15.1.4. To assist in understanding it, the three different mode cases considered earlier in Chapter 13 will be discussed. Because control effectiveness is under consideration, only the steady case will be looked at and dynamic damping and inertia effects will be ignored.

15.2.4.1 Fuselage bending mode

Consider the aircraft example where the flexible mode involves fuselage bending but the wing is rigid in bending and twist. The downwards tailplane lift due to elevator deflection (trailing edge upwards) will cause bending of the fuselage (in the ‘hogging’ sense) such that the tailplane incidence will increase, so tending to offset the intended elevator action and reducing its effectiveness.

15.2.4.2 Wing bending mode

Consider the aircraft example where the flexible mode involves wing bending only with no fuselage deformation. When the elevator is deflected, the aircraft will pitch nose up, the incidence will increase and additional wing lift will be developed, so causing the wing to bend upwards. In the steady case, this would not be expected to make any difference to the effectiveness. However, as the wing bends upwards, there will be a small downwards fuselage heave component and a small nose down pitch (seen in the mode shape in Appendix C); then the flexible deformation is expected to introduce a small additional down force on the tailplane, therefore actually increasing the effectiveness slightly.

15.2.4.3 Wing torsion mode

Consider the aircraft example where the flexible mode involves wing twist only with no fuselage deformation. When the elevator is deflected, the aircraft will pitch nose up, the incidence will increase and additional wing lift will be developed. However, this lift will cause a nose up twist of the wing and therefore produce further lift. In this case, the effectiveness would increase as velocity increases.

Therefore, as the velocity increases for a given flexible mode frequency, there will be a loss or increase of control effectiveness depending upon the mode shape. This behaviour will be examined later via an example.

15.2.5 Short Period/Flexible Modes

The roots of the quartic characteristic equation define how the short period motion of the aircraft is affected by flexible deformation. The roots are usually two complex conjugate pairs, namely

$$s = -\zeta_S\omega_S \pm \omega_S\sqrt{1-\zeta_S^2} \quad \text{and} \quad s = -\zeta_E\omega_E \pm \omega_E\sqrt{1-\zeta_E^2} \tag{15.24}$$

where ω_S, ω_E are the undamped frequencies and ζ_S, ζ_E are the damping ratios of the constituent motions. The 'S' mode will be a short period type heave/pitch motion modified by the flexible mode while the 'E' mode will be the flexible (or elastic) mode changed by the presence of the rigid body motion. The distinction is rather 'fuzzy' as both roots are likely to end up with short period and flexible mode components; the frequency and mode shape of the flexible mode will dictate how much coupling there will be. Note that it is possible that the aircraft could become unstable in what would in effect be a rigid body/flexible mode coupled flutter. Also, under some circumstances, two real roots could replace the complex roots for the 'S' mode and potentially lead to divergence if one real root were to become positive.

If the phugoid motion were to be included, the additional longitudinal equation would need to be added and a further pair of complex roots obtained. It is likely that aircraft flexibility would modify the phugoid behaviour.

15.2.6 Example: Flexible Aircraft in Heave/Pitch

This example will consider the same data as used for the rigid aircraft example in Section 15.1.8 but additional parameters need to be specified to cater for introduction of idealized flexible effects as used in Chapter 13, namely fuselage mass terms $m_F = 1500$ kg, $m_C = 4000$ kg, $m_T = 1500$ kg, wing mass/inertia terms $m_W = 2\mu_W s = 3000$ kg, $I_W = 2\chi_W s = 1330$ kg m^2, pitch moment of inertia $I_y = 144\,000$ kg m^2, and dimensions $s = 7.5$ m, $l_A = 0.25$ m, $l_E = 0.25$ m, $l_{WM} = 0.1$ m and $l_F = 6.8$ m. The corresponding modal mass and mode shape parameters for (a) fuselage bending, (b) wing bending and (c) wing twist modes being dominant are shown in Appendix C. The effect of air speed and flexible mode natural frequency on the pitch performance (i.e. elevator effectiveness) and stability will be examined using the approaches described earlier. MATLAB and SIMULINK programs to solve the dynamic manoeuvre in heave and pitch are included in appendix I on the companion website.

15.2.6.1 Fuselage bending mode

Consider the fuselage bending case where the wing is rigid. Firstly, several natural frequencies, namely 1.5, 3, 4.5 and 6 Hz, were selected and the elevator effectiveness calculated for a range of velocities; the result is shown in Figure 15.4. As would be expected, the lower the natural frequency, the more flexible the fuselage and the more the effectiveness reduces. The trends in the figure indicate that effectiveness could become small but that elevator reversal will not occur for this aircraft model.

Secondly, the flexible aircraft response to a step elevator input of -1° is calculated at 175 m/s EAS and compared to the rigid aircraft result in Figure 15.2. A low natural frequency of 1.5 Hz with 2 % damping is chosen in order to show a noticeable effect on the response, though fuselage modes are higher in frequency for this size of aircraft. The response is presented in Figure 15.5 and the low frequency decaying oscillation due to the flexible mode is apparent, especially on the pitch rate; the response levels are considerably lower ($\sim$1/4) than for the rigid aircraft due to the loss of effectiveness of around 80 %.

Thirdly, the flexible aircraft stability is examined for the 1.5 Hz fuselage bending mode with 2 % damping. The variation of frequency and damping of the two modes ('S' and 'E') with velocity is shown in Figure 15.6. As the velocity increases so does the 'S' mode natural frequency, much more rapidly than for the rigid aircraft (where the frequency at 250 m/s would be 0.51 Hz), and it becomes closer to the 'E' mode frequency. Eventually at 227 m/s EAS the damping crosses zero and in effect a coupled rigid

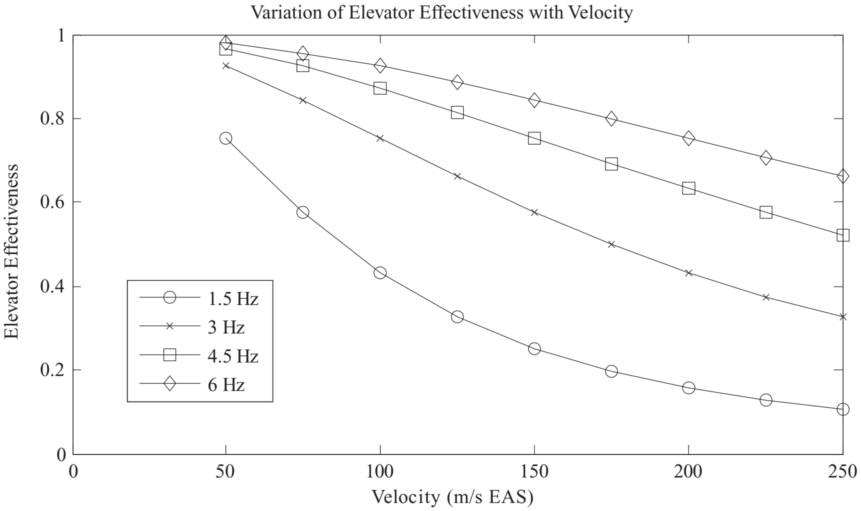

Figure 15.4 Variation of elevator effectiveness with velocity for different fuselage bending natural frequencies.

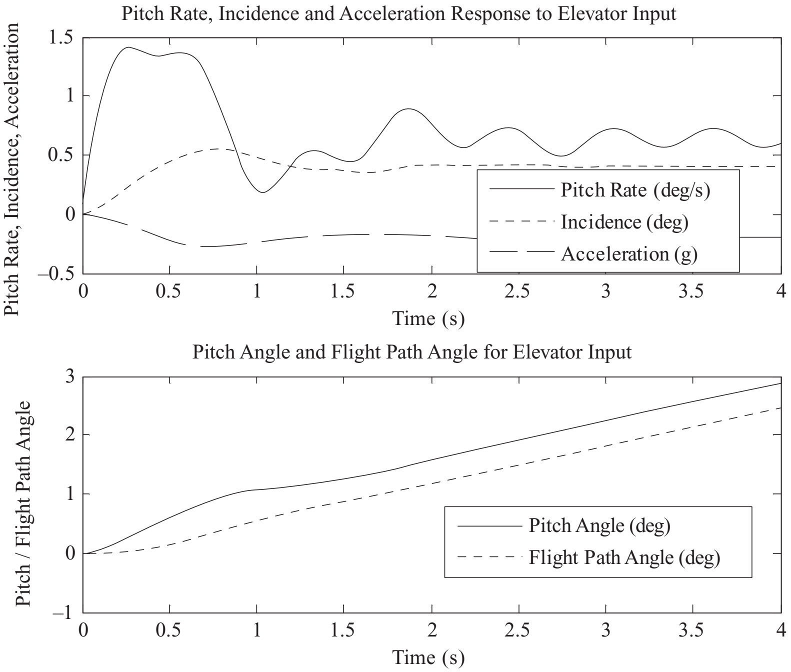

Figure 15.5 Response of a flexible aircraft (1.5 Hz/2 % fuselage bending mode) to a -1° step elevator input at 175 m/s EAS.

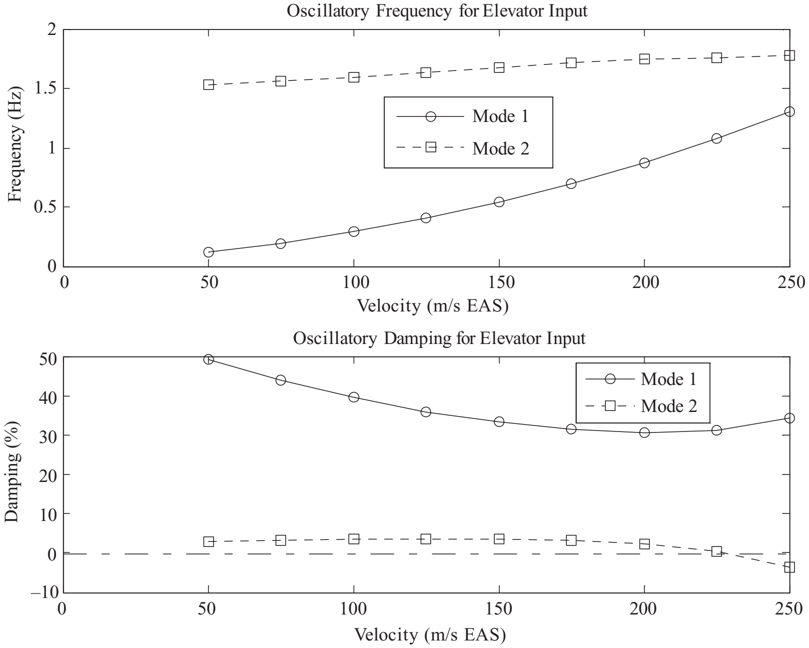

Figure 15.6 Variation of natural frequency and damping with velocity for modes 1 (‘S’) and 2 (‘E’) for the flexible aircraft (fuselage bending mode 1.5 Hz/2 %).

body/flexible mode flutter would occur. For more realistic frequencies of the fuselage bending mode then flutter would not occur at any reasonable velocity.

15.2.6.2 Wing bending mode

Now consider the wing bending mode case where the fuselage is rigid but actually has a small heave and pitch component in the mode shape (see Appendix C). Firstly, several natural frequencies, namely 1.5, 3, 4.5 and 6 Hz, are selected and the effectiveness calculated for a range of velocities; the results show, as anticipated from the discussion in Section 15.2.4, that there is only a very small change in effectiveness due to flexibility, namely an increase of about 3 % for the lowest natural frequency.

Secondly, the flexible aircraft response to a step elevator input of -1° is calculated at 175 m/s EAS to be compared to the rigid aircraft result in Figure 15.2. A low natural frequency of 1.5 Hz with 2 % damping is chosen in order to show whether there is any significant effect on the response; again this value is artificially low. The response to the step input is not presented since there is only a slight difference to the rigid aircraft response (~2 %); the damping for the short period mode has changed from 56 to 59 % with the addition of flexibility.

Thirdly, the flexible aircraft stability is examined for the 1.5 Hz wing bending mode with 2 % damping. The ‘S’ mode frequency increases with velocity (at about the same rate as for the rigid aircraft) but there is very little change in the ‘E’ mode frequency. The damping changes are also small, but at 281 m/s EAS the ‘E’ mode damping crosses zero and a ‘soft’ flutter occurs (see Chapter 11).

15.2.6.3 Wing torsion mode

Now consider the wing torsion case where the fuselage is rigid but the mode shape actually has a small heave and pitch component (see Appendix C). In this case, when the natural frequency was low, the

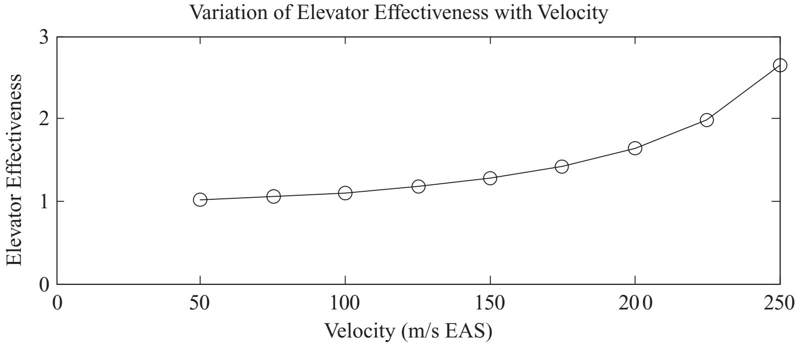

Figure 15.7 Variation of elevator effectiveness with velocity for 9 Hz wing torsion natural frequency.

aircraft quickly became unstable. Therefore a higher value of 9 Hz was selected for examination. In practice, wing torsion modes are at significantly higher frequencies than wing bending modes. Firstly, the effectiveness was calculated for a range of velocities for the 9 Hz mode and the result is shown in Figure 15.7. As anticipated from the discussion in Section 15.2.4, there is a significant increase in elevator effectiveness with velocity.

Secondly, the flexible aircraft response to a step elevator input of -1° is calculated at 175 m/s EAS for a natural frequency of 9 Hz with 2 % damping. The response is similar to the rigid aircraft response but somewhat larger because of the increased effectiveness. However, there is no obvious oscillatory behaviour around 9 Hz.

Finally, the flexible aircraft stability is examined for the 9 Hz wing torsion mode with 2 % damping. The 'E' mode frequency reduces slowly with little damping variation but the 'S' mode damping increases until at 260 m/s the mode is no longer oscillatory but the motion is represented by two negative (i.e. stable) real roots.

15.3 GENERAL FORM OF LONGITUDINAL EQUATIONS

The Equations (15.13) for the linearized flight mechanics representation of longitudinal motion, together with flexible modes, may also be written in the more general form with air speed terms shown explicitly, namely

$$\begin{gathered}\left[\begin{array}{c|c}\mathbf{A}_{\mathrm{r}} & \mathbf{0}\\ \hline \mathbf{0} & \mathbf{A}_{\mathrm{e}}\end{array}\right]\left\{\begin{array}{c}\dot{\boldsymbol{u}}\\ \hline \ddot{\boldsymbol{q}}_{\mathrm{e}}\end{array}\right\}+\left\{\rho V_0\left[\begin{array}{c|c}\mathbf{B}_{\mathrm{rr}} & \mathbf{B}_{\mathrm{re}}\\ \hline \mathbf{B}_{\mathrm{er}} & \mathbf{B}_{\mathrm{ee}}\end{array}\right]+\left[\begin{array}{c|c}\mathbf{D}_{\mathrm{r}} & \mathbf{0}\\ \hline \mathbf{0} & \mathbf{D}_{\mathrm{e}}\end{array}\right]\right\}\left\{\begin{array}{c}\boldsymbol{u}\\ \hline \dot{\boldsymbol{q}}_{\mathrm{e}}\end{array}\right\}\\ +\left\{\rho V_0^2\left[\begin{array}{c|c}\mathbf{0} & \mathbf{C}_{\mathrm{re}}\\ \hline \mathbf{0} & \mathbf{C}_{\mathrm{ee}}\end{array}\right]+\left[\begin{array}{c|c}\mathbf{0} & \mathbf{0}\\ \hline \mathbf{0} & \mathbf{E}_{\mathrm{e}}\end{array}\right]\right\}\left\{\begin{array}{c}\int\boldsymbol{u}\\ \hline \boldsymbol{q}_{\mathrm{e}}\end{array}\right\}=\rho V_0^2\left\{\begin{array}{c}\boldsymbol{F}_{\mathrm{r}}\\ \hline \boldsymbol{F}_{\mathrm{e}}\end{array}\right\}\eta. \qquad (15.25)\end{gathered}$$

Note that the unknown vector for the flexible modes is the vector $\mathbf{q}_{\mathrm{e}}$ of modal/generalized coordinates. However, the unknowns for the rigid aircraft in the flight mechanics equations are based on velocity and rate terms so, for example, in the longitudinal case where the fore-and-aft velocity perturbation is ignored, then $\boldsymbol{u} = \left\{ w \;\; q \right\}^{\mathrm{T}}$. Also, the diagonal inertia matrix $\mathbf{A}_{\mathrm{r}}$ comprises aircraft mass and moments of inertia, $\mathbf{A}_{\mathbf{e}}$ is the diagonal modal mass matrix, $\mathbf{B}$ is the aerodynamic damping matrix, $\mathbf{D}_{\mathrm{r}}$ is a matrix containing the rigid body velocity coupling terms associated with using body fixed axes (e.g. $-mU_{\mathrm{e}}q$), $\mathbf{D}_{\mathrm{e}}$ is the diagonal modal damping matrix, $\mathbf{C}$ is the aerodynamic stiffness matrix, $\mathbf{E}_{\mathrm{e}}$ is the diagonal modal stiffness matrix and the right-hand side input force vectors $\boldsymbol{F}$ correspond to the elevator input terms.

If the longitudinal equations included the fore-and-aft velocity perturbation u then it would appear in the vector of unknown rigid body motions, namely $\boldsymbol{u} = \left\{ u \ w \ q \right\}^{\mathrm{T}}$. The drag terms would then be included in the aerodynamic matrices for the rigid aircraft, there would be additional forcing vectors for gravitational and thrust effects, and the equations relating rates to angles would need to be included to allow the gravitational effects to be calculated. The model would represent the phugoid behaviour as well as short period and flexible effects.

A similar form of equation would apply for the lateral case with aileron, spoiler and rudder inputs. Similar issues of loss of effectiveness and influence of rigid/flexible couplings on the Dutch roll, roll subsidence and spiral modes would be examined. Brief consideration of pure roll will be seen later in this chapter.

Finally, the frequency and damping of the rigid/flexible ‘S’ and ‘E’ type modes would be found from the eigenvalue solution of Equation (15.25) (akin to the flutter solution) and the control effectiveness obtained from the steady-state solution of the rigid and flexible aircraft equations. In practice, the flexible/rigid body couplings are not likely to have as severe an effect as shown in the above examples because the natural frequencies were unrealistically low for an aircraft of the size considered and the models employed were very crude. Also, the flight control system (FCS) would need to be incorporated into the model and would be expected to have a considerable influence on the aircraft dynamics.

15.4 DYNAMIC MANOEUVRE – RIGID AIRCRAFT ROLL DUE TO AILERON INPUT

In this section, the behaviour of an aircraft in pure roll will be considered, both for the rigid and flexible case. When a differential aileron input is applied, the aircraft begins to roll, but due to the presence of the tailplane and fin, it will also experience a response in yaw and sideslip. Thus an analysis of the motion will require three DoF for the rigid aircraft and at least four DoF for a flexible aircraft representation (i.e. with a minimum of one flexible mode). Since one aim of this book is to try wherever possible to keep the number of simultaneous equations to a maximum of three, and to avoid needing to calculate a large number of flexible derivatives, then only a simplified roll case will be considered, namely a rigid aircraft responding in pure roll to an aileron input so that the coupling effects of the tailplane and fin are being neglected. For a rigid aircraft there will only be a single DoF, whereas for an equivalent simple flexible model (see later) two DoF will suffice to show the ideas. In Lomax (1996), for consideration of dynamic rolling manoeuvres, a similar assumption neglects cross-coupling effects. Although the approach here is somewhat crude, it is still essentially ‘rational’ since a simulation will be performed.

The rigid aircraft with a full span aileron is shown in Figure 15.8. Prior to application of the ailerons, the aircraft is assumed to be in straight and level trimmed flight at velocity U_{e} $(W_{\mathrm{e}} = 0)$ so $V_0 = U_{\mathrm{e}}$ (remember that when using the flight mechanics model, the aircraft velocity is V_0 and not V). After applying the ailerons, the aircraft is assumed to roll with an angular velocity p (positive starboard wing down), angular acceleration $\dot{p}$ and instantaneous roll angle ϕ. There are no yaw or sideslip motions for this pure roll case.

15.4.1 Flight Mechanics Equations of Motion–Rigid Aircraft in Roll

The linearized flight mechanics equations of motion for the lateral case (symmetric aircraft) were shown in Chapter 14, for small rates of rotation, to be

$$m(\dot{v} - W_{\mathrm{e}} p + U_{\mathrm{e}} r) = Y, \qquad I_{\mathrm{x}} \dot{p} - I_{\mathrm{xz}} \dot{r} = L, \qquad I_{\mathrm{z}} \dot{r} - I_{\mathrm{xz}} \dot{p} = N. \tag{15.26}$$

These equations may be considered in terms of body or wind axes. If body axes are employed, the aerodynamic derivatives would need transformation from wind axes and this is somewhat complicated

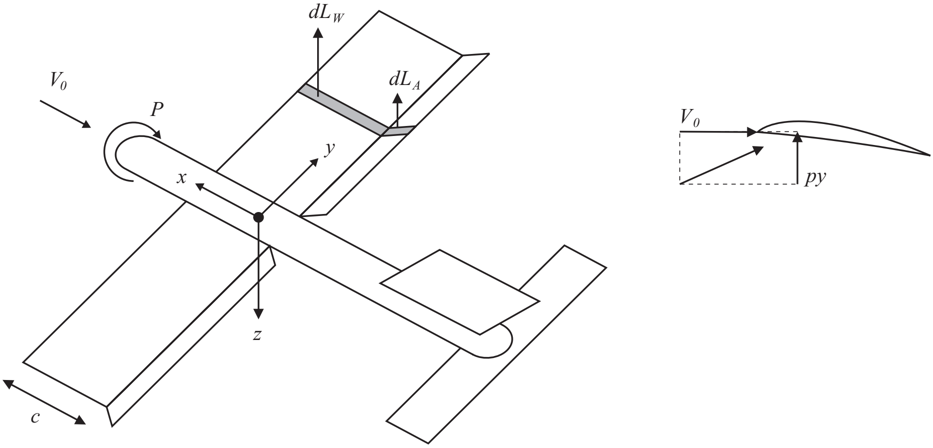

Figure 15.8 Rigid aircraft in roll under aileron application.

for lateral motions (Cook, 1997). On the other hand, if wind axes are employed, the aerodynamic terms are simpler but it is more likely that inertia couplings will occur (i.e. due to a nonzero product moment of inertia). Therefore, for this simple example, wind axes will be chosen and it will be assumed that the product moment of inertia I_{xz} may be set to zero to avoid inertia couplings. Thus the equations of motion may be rewritten as

$$m(\dot{v} + U_{\mathrm{e}}r) = Y, \qquad I_{\mathrm{x}}\dot{p} = L, \qquad I_{\mathrm{z}}\dot{r} = N. \tag{15.27}$$

Clearly the yawing moment N and side force Y must both be zero so as to avoid yaw and sideslip responses and therefore any aerodynamic couplings to roll motion (e.g. derivatives Y_{p}, N_{p}) must also be ignored. Thus the equation governing the simplified aircraft motion is simply the roll equation

$$I_{\mathrm{x}}\dot{p} = L. \tag{15.28}$$

The rolling moment L (the same symbol used as for lift but the difference is made clear by the context of use) may be expressed in terms of aerodynamic stability derivatives (as introduced in Chapter 14), namely

$$L = L_{\mathrm{p}}p + L_{\xi}\xi, \tag{15.29}$$

where L_p and L_ξ are rolling moments due to roll rate p and aileron angle ξ respectively, defined here in wind axes, and other terms involving the null yaw and sideslip motions are omitted. Then the equation of motion is

$$I_{\mathrm{x}}\dot{p} - L_{\mathrm{p}}p = L_{\xi}\xi \tag{15.30}$$

and this equation may be used to determine the response to any aileron input.

15.4.2 Aerodynamic Roll Derivatives

The rolling moment due to the roll rate derivative is based on the change in incidence that occurs when there is a perturbation in wing roll rate. Now, the starboard wing experiences the basic flow field due to the true air speed V_0, but there is also an upwards relative velocity component (py) due to the perturbation in the roll rate. Thus, the perturbation in incidence introduced by the roll rate will given by py/V_0, assuming that $py \ll V_0$. Recognizing that the lift and drag forces in the perturbed condition are inclined to the wind axes, the derivative for an untapered/unswept wing may be shown to be (Appendix E and Cook, 1997)

$$L_{\mathrm{p}} = -\tfrac{1}{2}\rho V_0 \left(\frac{S_{\mathrm{W}} \left(a_{\mathrm{W}} + C_{\mathrm{D}}\right) s^2}{3} \right), \tag{15.31}$$

where fin/tailplane effects are neglected but the roll damping of the wing is the most significant term.

The rolling moment due to the aileron derivative is based on the perturbation of lift when the aileron is perturbed (trailing edge upwards on the starboard wing). A positive aileron angle gives rise to a perturbation force (downwards) on the starboard wing and therefore to a positive roll rate. It may be shown (Appendix E) that the derivative is

$$L_{\xi} = \frac{1}{2}\rho V_0^2 \left(\frac{S_{\mathrm{W}} a_{\mathrm{C}} s}{2} \right). \tag{15.32}$$

where ξ is the aileron angle and a_{C} is the sectional lift coefficient per aileron control angle.

15.4.3 Solution of the Flight Mechanics Equations–Rigid Aircraft

The transient roll rate response of Equation (15.30) to a general aileron input may be solved in the time domain. For a step aileron angle ξ_0, the response may be shown to be

$$p(t) = -\frac{L_{\xi}}{L_{\mathrm{p}}} \left[1 - \exp\left(\frac{L_{\mathrm{p}}}{I_{\mathrm{x}}} t \right) \right] \xi_0. \tag{15.33}$$

The aircraft behaves like a simple lag with a decaying exponent dependent upon the roll damping derivative. The steady-state roll rate following a step aileron input is found by setting the roll acceleration $\dot{p}$ to zero.

15.4.4 Roll Rate Per Aileron Transfer Function

The transfer function between the roll rate and aileron angle may be found by transforming the differential equation of motion (15.30) into Laplace form (see Chapter 7), so

$$\left(\frac{p}{\xi}(s) \right)_{\mathrm{Rigid}} = \frac{L_{\xi}}{I_{\mathrm{x}} s - L_{\mathrm{p}}} \tag{15.34}$$

and this function will show the variation with frequency of the gain and phase lag between the roll rate and an oscillatory aileron input. The denominator, when set to zero, defines the characteristic equation of the system

$$I_{\mathrm{x}} s - L_{\mathrm{p}} = 0. \tag{15.35}$$

The steady-state roll rate per aileron angle is found from the value of the transfer function at zero frequency, so

$$\left(\frac{p}{\xi} \right)_{\mathrm{Rigid}} = -\frac{L_{\xi}}{L_p}. \tag{15.36}$$

This equation will be used later when calculating the aileron effectiveness.

15.4.5 Roll Subsidence

Consider the aircraft to experience a steady roll rate, following an aileron input, when the aileron angle is returned to zero. The roll rate then decays exponentially to zero, an effect known as ‘roll subsidence’ (Cook, 1997; also see Chapter 14). The root of the characteristic equation (15.35) defines the rigid aircraft dynamic stability mode following a disturbance and has a value of L_p/I_x (negative); this root increases linearly with air speed and dictates the rate of decay of the roll mode. The effect of flexibility upon the roll subsidence will be seen later.

15.4.6 Conversion to Motion in Earth Axes

Having solved the flight mechanics equations for the roll rate $p(t)$ relative to wind axes fixed in the aircraft, the motion of the aircraft with respect to earth (inertial) axes needs to be determined. Firstly, the roll rate $\dot{\phi}$ must be determined in earth axes using the Euler transformation outlined in Chapter 14; for this pure roll example, the transformation relationship is a simple one, namely $\dot{\phi} = p$. The roll angle ϕ may then be found by integrating $\dot{\phi}$ using a suitable initial condition so as to yield the aircraft roll motion in earth axes.

15.4.7 Example: Rigid Aircraft in Roll

Consider a rigid aircraft with the following data: $I_x = 56\ 000$ kg m^2, $s = 7.5$ m, $S_W = 30$ m^2, $a_W = 4.5$/rad, $a_C = 1.5$ /rad and $V_0 = 150$ m/s EAS (the drag effect on the roll rate derivative will be neglected). The roll rate (deg/s) and roll angle (deg) responses to a step aileron input of 2 deg are shown

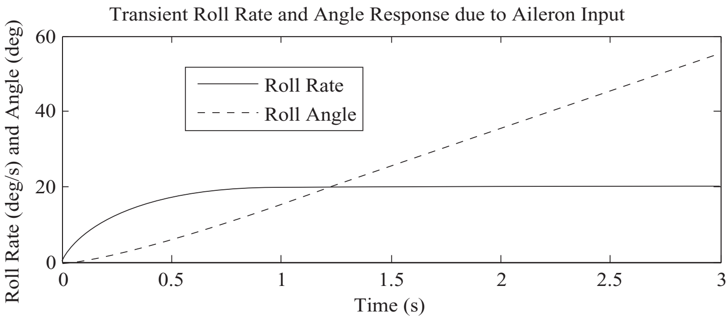

(a) Step Aileron Input

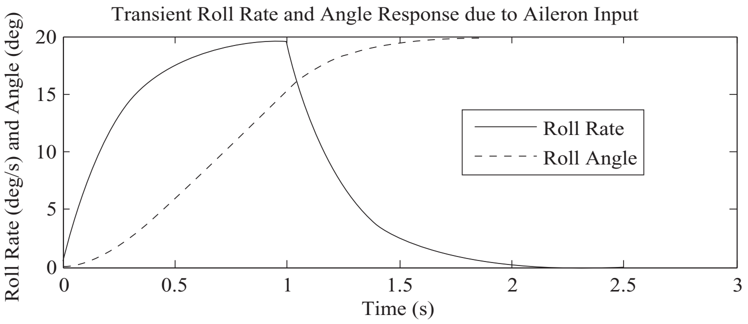

(b) On/Off Aileron Input

Figure 15.9 Roll rate and roll angle variation for (a) step and (b) on/off aileron input – rigid aircraft.

in Figure 15.9(a); as might be expected, the same result was obtained using the above formulae and alternatively a SIMULINK model. A steady-state roll rate of 20 deg/s is achieved after about 2 s and the roll angle is steadily increasing. Figure 15.9(b) shows that a steady 20° bank angle is achieved when an aileron angle of 2° is applied for only 1 s and then returned to the neutral position (on/off aileron input). Albeit only employing a simple model, these calculations are rational.

15.5 DYNAMIC MANOEUVRE – FLEXIBLE AIRCRAFT ROLL DUE TO AILERON INPUT

Having considered the response of an idealized rigid aircraft to an aileron input, the effects of allowing the wing to be flexible may now be examined. In this section, the effect of introducing a flexible antisymmetric wing torsion mode into the pure roll behaviour of the idealised aircraft will be considered. Appendix F considers the whole aircraft antisymmetric free–free bending and torsion modes.

15.5.1 Flexible Wing Torsion Mode

The aircraft model is the same as that in Figure 15.8, with the wing being flexible in twist but rigid in bending. The motion of the flexible rolling aircraft may then be represented using a combination of rigid body roll motion and a flexible antisymmetric free–free mode with a twist variation along the wing (nose up positive on the starboard wing) defined by the mode shape $\gamma_e(y) = y/s$, as illustrated in Figure 15.10. The wing twist due to the flexible deformation at position y is $\gamma_e(y)q_e$. The modal mass is obtained in Appendix F.

15.5.2 Flight Mechanics Equations of Motion – Flexible Aircraft in Roll

In Chapter 14, it was shown that the addition of flexible effects for the longitudinal case, when the equations were linearized, meant the addition of an uncoupled equation for the mode expressed in its flexible (or sometimes referred to as elastic) modal/generalised coordinate q_e. Given that a similar analysis could have been performed for the lateral case, the result will just be assumed here; i.e. using mean axes and certain assumptions (see Chapter 14) eliminates inertia coupling terms between the rigid and flexible equations. Thus the flight mechanics equations of motion for the flexible aircraft in roll are

$$I_x \dot{p} = L, \qquad m_e \ddot{q}_e + c_e \dot{q}_e + k_e q_e = Q_{ext}, \tag{15.37}$$

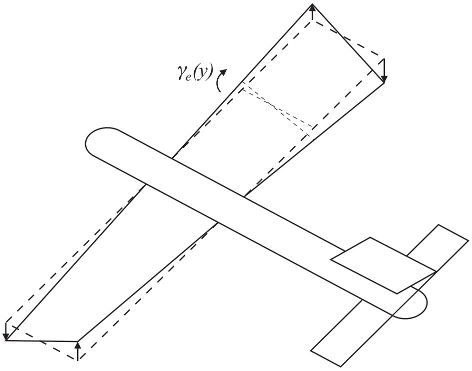

Figure 15.10 Flexible antisymmetric torsion mode for an aircraft in pure roll.

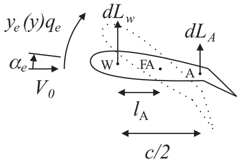

Figure 15.11 Starboard wing section for flexible twist deformation.

where m_e, c_e, k_e, Q_{ext} are the modal mass, damping, stiffness and external force respectively for the antisymmetric torsion mode. The rolling moment and generalized/modal force may be written in derivative form as

$$L = L_p p + L_\xi \xi + L_e q_e, \qquad Q_{ext} = Q_p p + Q_\xi \xi + Q_e q_e, \tag{15.38}$$

where L_p and L_ξ are the same as for the earlier rigid aircraft example. The other derivatives are associated with the flexible deformation of the aircraft; e.g., L_e is the rolling moment due to flexible mode deformation and Q_p is the flexible mode generalized force due to the roll rate.

15.5.3 Aerodynamic Derivatives Associated with the Flexible Mode

Now consider the flexible aircraft experiencing an aileron input ξ (trailing edge upwards/downwards on the starboard/port wings). There will be a perturbed lift contribution due to the upwards velocity of the air stream relative to the wing and also due to the angle of twist; the rate of twist deformation with time may be assumed to cause no net aerodynamic effect if unsteady effects are ignored (i.e. quasi-steady aerodynamics). The wing section geometry was introduced in Chapter 13 and, including a perturbed twist deformation about the flexural axis, is shown again in Figure 15.11. The perturbed lift dL_A due to aileron is shown in its positive sense, though it is negative for aileron up.

Thus the perturbed lift force on the starboard wing strip will be given by

$$dL_{W+A} = dL_W + dL_A = \frac{1}{2}\rho V_0^2 \left\{ a_W \left[\alpha_e + \frac{py}{V_0} + \gamma_e(y) q_e \right] - a_C \xi \right\} c \, dy, \tag{15.39}$$

where the perturbed lift contribution due to flexibility will be used to determine the unknown elastic derivatives. The drag contribution and any effect of perturbed axes (see Appendix E) has been neglected for flexible derivatives. The contribution to rolling moment of the flexible deformation term in this equation will be given by integration, so

$$L_e q_e = -2 \int_0^s \tfrac{1}{2} \rho V_0^2 a_W \gamma_e(y) y c \, dy \, q_e \tag{15.40}$$

and the rolling moment derivative due to flexible deformation can be shown by inspection to be

$$L_e = -\tfrac{1}{2} \rho V_0^2 S_W a_W J_{1R}. \tag{15.41}$$

The negative sign in this derivative occurs because a nose up twist on the starboard wing leads to a negative rolling moment. Here, the constant $J_{1R} = (1/s) \int_{y=0}^{s} y \gamma_e(y) \, dy$ depends upon the mode shape and the subscript R (roll) is used to distinguish these constants from those applying to the heave/pitch example considered earlier.

To determine the derivatives associated with the perturbed flexible mode deformation, the incremental work done by the aerodynamic lift forces moving through the incremental deformation of the mode must be obtained. Now it will be assumed that the lift on the wing (due to the roll rate and twist) acts at the quarter chord (W, for wing aerodynamic centre) and that the additional lift due to the aileron deflection acts at the three-quarter chord (A), as shown in Figure 15.11. Because the flexural axis (FA) lies a distance l_{A} behind the aerodynamic centre, the respective incremental displacements (upwards positive on the starboard wing) are given by

$$\delta z_{\mathrm{W}} = l_{\mathrm{A}} \gamma_{\mathrm{e}}(y) \delta q_{\mathrm{e}}, \qquad \delta z_{\mathrm{A}} = -\left(\tfrac{c}{2} - l_{\mathrm{A}}\right) \gamma_{\mathrm{e}}(y)\, \delta q_{\mathrm{e}} \tag{15.42}$$

and the incremental work done term due to flexible deformation is

$$\delta W_{\mathrm{e}} = 2 \int_0^s \mathrm{d}L_{\mathrm{W}}\ \delta z_{\mathrm{W}} + 2 \int_0^s dL_{\mathrm{A}}\ \delta z_{\mathrm{A}}. \tag{15.43}$$

The generalized/modal force is then given by

$$Q = \frac{\partial(\delta W_{\mathrm{e}})}{\partial(\delta q_{\mathrm{e}})} = Q_{\mathrm{p}} p + Q_{\xi} \xi + Q_{\mathrm{e}} q_{\mathrm{e}} \tag{15.44}$$

and, by inspection, it may be shown that the flexible derivatives are

$$Q_{\mathrm{p}} = \tfrac{1}{2} \rho V_0 S_{\mathrm{W}} a_{\mathrm{W}} l_{\mathrm{A}} J_{1\mathrm{R}}, \quad Q_{\xi} = \frac{1}{2} \rho V_0^2 S_{\mathrm{W}} a_{\mathrm{C}} \left(\frac{c}{2} - l_A\right) J_{2\mathrm{R}}, \quad Q_{\mathrm{e}} = \tfrac{1}{2} \rho V_0^2 S_{\mathrm{W}} a_{\mathrm{W}} l_{\mathrm{A}} J_{3\mathrm{R}}, \tag{15.45}$$

where $J_{2\mathrm{R}} = (1/s) \int_{y=0}^{s} \gamma_{\mathrm{e}}(y)\ \mathrm{d}y$ and $J_{3\mathrm{R}} = (1/s) \int_{y=0}^{s} \gamma_{\mathrm{e}}^2(y)\ \mathrm{d}y$ are constants that again depend upon the mode shape. Again, the signs of these derivatives are consistent with physical understanding.

In Appendix F, the antisymmetric wing torsion mode is considered to have a linear mode shape with unit twist at the tip, so $\gamma_{\mathrm{e}}(y) = y/s$. It is shown there that the modal mass is given by $m_{\mathrm{e}} = I_{\mathrm{W}}/3$, where I_{W} is the total wing moment of inertia in pitch. The J integral terms are given by $J_{1\mathrm{R}} = s/3$, $J_{2\mathrm{R}} = 1/2$, $J_{3\mathrm{R}} = 1/3$.

15.5.4 Solution of the Flight Mechanics Equations – Flexible Aircraft

Now, including these flexible derivative terms in the flight mechanics Equations (15.37) yields the final equations

$$\begin{aligned} I_{\mathrm{x}} \dot{p} &= L_{\mathrm{p}} p + L_{\mathrm{e}} q_{\mathrm{e}} + L_{\xi} \xi, \\ m_{\mathrm{e}} \ddot{q}_{\mathrm{e}} + c_{\mathrm{e}} \dot{q}_{\mathrm{e}} + (k_{\mathrm{e}} - Q_{\mathrm{e}}) q_{\mathrm{e}} &= Q_{\mathrm{p}} p + Q_{\xi} \xi, \end{aligned} \tag{15.46}$$

or in matrix form

$$\begin{bmatrix} I_{\mathrm{x}} & 0 \\ 0 & m_{\mathrm{e}} \end{bmatrix} \begin{Bmatrix} \dot{p} \\ \ddot{q}_{\mathrm{e}} \end{Bmatrix} + \begin{bmatrix} -L_{\mathrm{p}} & 0 \\ -Q_{\mathrm{p}} & c_{\mathrm{e}} \end{bmatrix} \begin{Bmatrix} p \\ \dot{q}_{\mathrm{e}} \end{Bmatrix} + \left\{ \begin{bmatrix} 0 & -L_{\mathrm{e}} \\ 0 & k_{\mathrm{e}} - Q_{\mathrm{e}} \end{bmatrix} \right\} \begin{Bmatrix} \int p \\ q_{\mathrm{e}} \end{Bmatrix} = \begin{Bmatrix} L_{\xi} \\ Q_{\xi} \end{Bmatrix} \xi. \tag{15.47}$$

The flexible aircraft response to any aileron input may be obtained by solving these equations in the time domain, again a rational calculation. The flexible deformation appears as an aerodynamic stiffness term in the roll equation, whereas the roll motion appears as a damping term in the flexible mode equation; these couplings affect the steady-state roll rate. Then, as in Section 15.4.6, the absolute roll angle may be found via the Euler transformation and integration.

15.5.5 Roll Rate Per Aileron Transfer Function

The transfer function relating roll rate to aileron angle may be found from Equation (15.47) in the Laplace domain:

$$\begin{bmatrix} I_x s - L_p & -L_e \\ -Q_p & m_e s^2 + c_e s + (k_e - Q_e) \end{bmatrix} \begin{Bmatrix} p(s) \\ q_e(s) \end{Bmatrix} = \begin{Bmatrix} L_\xi \\ Q_\xi \end{Bmatrix} \xi(s). \tag{15.48}$$

This matrix equation may be solved to give the roll rate per aileron angle

$$\left(\frac{p}{\xi}(s)\right)_{\text{Elastic}} = \frac{s^2 L_\xi m_e + s L_\xi c_e + L_\xi (k_e - Q_e) + L_e Q_\xi}{D(s)}. \tag{15.49}$$

Here the denominator polynomial $D(s)$ is the determinant of the square matrix in Equation (15.48) such that

$$D(s) = s^3 (I_x m_e) + s^2 \left(I_x c_e - L_p m_e\right) + s\left[I_x (k_e - Q_e) - L_p c_e\right] + \left[-L_p (k_e - Q_e) - L_e Q_p\right], \tag{15.50}$$

which, when set to zero, defines the characteristic (cubic) equation. The roots of this polynomial define the characteristic motions of the flexible aircraft in roll, namely a roll subsidence and an oscillatory flexible mode.

The steady state roll rate per aileron deflection is given by the transfer function at zero frequency, namely

$$\left(\frac{p}{\xi}\right)_{\text{Flexible}} = \frac{L_\xi (k_e - Q_e) + L_e Q_\xi}{-L_p (k_e - Q_e) - L_e Q_p}, \tag{15.51}$$

and this may be compared to the rigid aircraft expression in Equation (15.36).

15.5.6 Aileron Effectiveness

The ratio of the flexible to rigid values of the steady-state roll rate per aileron angle provides a measure of aileron effectiveness $\Im_{\text{Aileron}}$ (see Chapter 9), i.e. how the aileron power is influenced by the flexible deformation, so

$$\Im_{\text{Aileron}} = \frac{(p/\xi)_{\text{Flexible}}}{(p/\xi)_{\text{Rigid}}}. \tag{15.52}$$

When the ailerons are deflected (starboard upwards) for a rigid aircraft then lift forces are generated such that the aircraft rolls in a positive sense. However, for flexible wings, the aileron also introduces a pitching moment that will cause wing twist. The resulting lift force due to the twist will act in the opposite sense to that originally intended and so the roll rate achieved will reduce. As the air speed increases for a given flexible mode frequency, there will be a loss of control effectiveness and eventually aileron reversal will occur (see Chapter 9). The reversal condition may be explored either by performing simulations at various air speeds or by checking for a change in sign of the steady roll rate per aileron effectiveness, given by evaluating the effectiveness at various air speeds for a specified natural frequency of the flexible mode.

It is arguable whether the actual reversal speed will ever be reached in practice for a single aileron control since, as that condition is approached, it would be less and less possible to trim the aircraft in roll. However, with multiple ailerons, one control surface (e.g. the outer aileron) could be operating above its reversal speed while another control surface (e.g. the inner aileron) could be below its reversal speed and override the effects of the reversed control. The outer ailerons are often locked at cruise conditions.

It should be noted that the static aeroelastic calculations (see Chapter 9) will be performed early in the design cycle and will allow the control surfaces to be sized. Later in the design, the FCS will have been designed and will influence the control effectiveness, and revised aerodynamic data may also be available. At this stage, the aircraft handling and control will be explored using the flight mechanics model as in this chapter. By this stage in the design, it is too late to modify the control surface sizing so any inadequacies in control effectiveness would be dealt with by control scheduling in the FCS, e.g. suitable mixing of aileron and spoiler contributions.

15.5.7 Stability of the Flexible Rolling Aircraft

The stability of the flexible rolling aircraft may be examined by determining the roots of the characteristic cubic polynomial in Equation (15.50). This equation will have a real root (negative value corresponding to the rigid aircraft roll subsidence) and a pair of complex oscillatory roots due to the addition of the flexible mode. It is possible for the flexible mode to modify the roll subsidence behaviour and for there to be a coupled roll/wing torsion divergent oscillation (or alternatively this could be called a low frequency flexible/rigid body mode flutter). However, it should be pointed out that it is more usual to use the flutter equations (including rigid body modes) to predict any flutter behaviour involving the elastic modes and for the flight mechanics model to be used to assess the impact of flexibility on the dynamic stability modes.

15.5.8 Example: Flexible Aircraft in Roll – Wing Torsion Mode

Consider the same earlier rigid aircraft example, but with different air speeds and with additional parameters specified to cater for the flexible mode case, namely $I_W = 1330$ kg m^2, $c = 2.0$ m, $l_A = 0.25$ m and modal damping $\zeta_e = 4$ %. The effect of air speed and of flexible mode natural frequency on the roll performance (i.e. aileron effectiveness), reversal and stability will be examined using the approaches described above.

Firstly, consider the effect of a change in velocity on the behaviour of the aircraft; increasing the velocity would be expected to make the effects of flexibility more severe. In Figure 15.12, the variation in aileron effectiveness with velocity is shown for torsional natural frequencies of 6, 8 and 10 Hz. It is

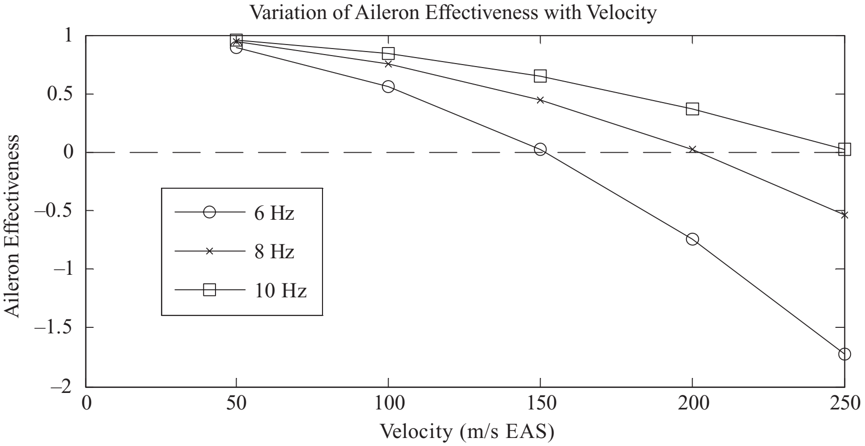

Figure 15.12 Variation of aileron effectiveness with velocity for different wing torsion natural frequencies.

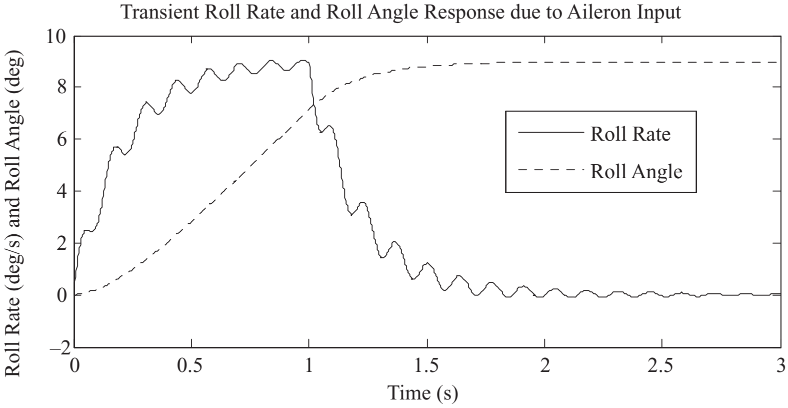

Figure 15.13 Roll rate and roll angle variation for on/off aileron input – flexible aircraft (torsion mode 8 Hz/4 %).

clear that the effectiveness decreases with an increase in air speed and eventually becomes negative; the *reversal* speed for the flexible case is 202 m/s EAS for the 8 Hz mode and reduces for lower natural frequencies. At this point the rolling moment due to deploying the ailerons is exactly balanced by the opposite rolling moment that occurs due to wing twist. As a confirmation of this result, the steady roll rate obtained from rational simulation changed sign at the same speed. This reversal behaviour has been observed here using the dynamic manoeuvre, whereas a similar result could be obtained from a static aeroelastic calculation with the wing root clamped as shown in Chapter 9. The difference with a rational approach such as employed in this chapter is that nonlinear and FCS effects may be examined and the aircraft handling considered.

Secondly, consider the behaviour of the aircraft having an 8 Hz torsional mode, 4 % damping and flying at a velocity of 150 m/s EAS (below reversal speed). Figure 15.13 shows the response when the aileron angle of 2° is applied for 1 s and then returned to zero; the final steady bank angle is about 9° compared to the rigid aircraft value of 20° because the twist of the wing opposes the normal operation of the aileron as mentioned above. There is also a noticeable decaying oscillation of the flexible mode in response to the transient excitation.

Thirdly, the effect of the antisymmetric torsion mode upon the roll subsidence mode with a change in velocity and natural frequency may be seen in Figure 15.14; the magnitude of the root (i.e. decay

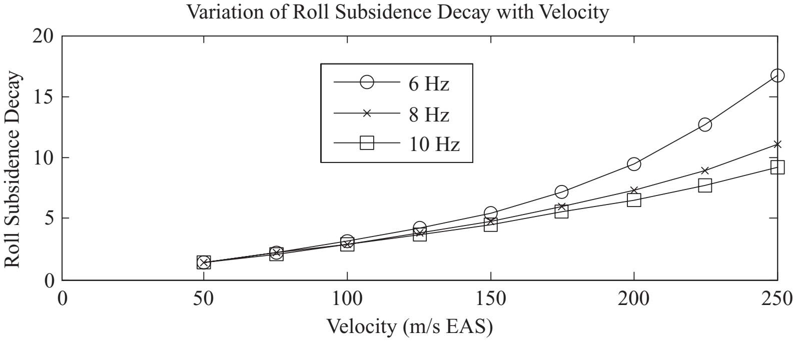

Figure 15.14 Variation of roll subsidence decay with air speed and natural frequency.

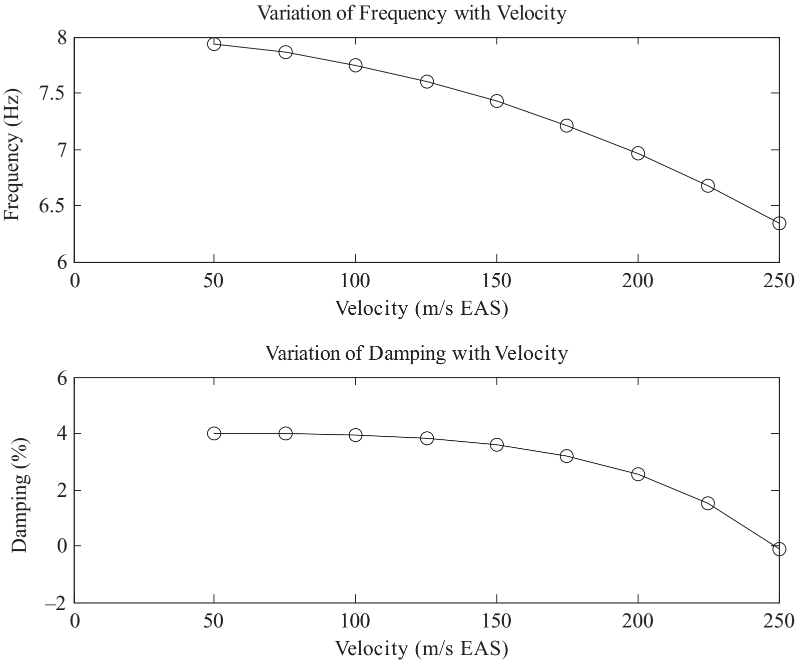

Figure 15.15 Variation of frequency and damping with velocity for a flexible aircraft (torsion mode 8 Hz/4 %).

exponent) is shown. The effect of the torsion mode upon the decay rate increases with air speed and with a reduction in natural frequency.

Finally, consider the variation of the frequency and damping of the oscillatory root with a change in velocity for a torsion mode at 8 Hz with 4 % damping, found by solving the characteristic equation above, and shown in Figure 15.15. It is clear that in addition to the decrease in frequency, the damping decreases until it becomes negative at 240 m/s EAS, which is the speed beyond which divergent oscillations will occur.

In conclusion, it may clearly be seen for this simple example that introducing flexibility to the aircraft wing leads to a loss of control effectiveness (and ultimately reversal) and a potential instability of a rigid body roll mode coupling with a flexible antisymmetric torsion mode. The flexible effects can obviously be important for a manoeuvring aircraft and become more significant as the structure natural frequency reduces. However, the FCS will be designed to suppress such interactions.

Note that the effectiveness, stability and response for a steady roll rate and maximum roll acceleration are considered briefly in Chapters 23 and 24 (CS-25 and Lomax, 1996).

15.5.9 Flexible Wing Bending Mode

Having considered the response of a flexible aircraft to an aileron input for the antisymmetric torsion mode case, the effect of introducing an antisymmetric bending mode for the same basic aircraft will now be considered briefly. The rolling aircraft may now be combined with a free–free flexible antisymmetric wing bending mode; some fuselage roll motion would be present in the mode shape but there would be no fuselage bending. Appendix F shows a typical mode shape and modal mass for this mode.

The incremental aerodynamic force on the wing strip may be written much as in the previous section, only now a term involving the modal velocity will appear in the upwards relative velocity term and there will be no twist term. The equations of motion may then be shown to have no aerodynamic stiffness terms, but additional flexible damping derivatives $L_{\dot{e}}$ and $Q_{\dot{e}}$ will be present. These damping terms will affect the initial but not the steady-state roll rate. The effect on effectiveness and stability may be examined as an exercise.

15.6 FLEXIBLE CORRECTIONS TO FLIGHT MECHANICS EQUATIONS

In Chapter 13, it was shown how the flexible mode equations could be omitted and the effect of flexibility introduced into the rigid body derivatives; this was for the model based on inertial axes. However, a similar approach could be employed for the flight mechanics equations based on body fixed (maybe wind) axes. The rate derivatives would also need correction, using an equivalent to the Guyan reduction.

The dynamic manoeuvres could then be examined using a rigid aircraft flight mechanics model with aerodynamic derivatives corrected for flexible effects. The effect of the flexible mode(s) on the dynamic stability modes (e.g. short period) could then be seen. However, the effect of the rigid body modes on the flexible modes would not be evident; instead, the basic flutter calculations with rigid body modes would be carried out with oscillatory aerodynamics (see Chapter 11). In this present chapter, the flexible mode was included explicitly in order to allow the impact of coupling to the rigid body behaviour to be seen.

Whether employing a flexibility correction, or any other model reduction approach, is a valid simplification depends upon the importance of the dynamic effects of the flexible modes; e.g. flight manoeuvres with a modern FCS might be substantially damped, so flexible modes may not need to be fully modelled, whereas in a landing the flexible mode response would be significant and would need to be included.

15.7 REPRESENTATION OF THE FLIGHT CONTROL SYSTEM (FCS)

For dynamic rational manoeuvres simulated in the time domain, the relevant features of the nonlinear FCS, coupled to the aircraft dynamics, should be represented, including a manoeuvre load alleviation (MLA) system if appropriate (see Chapter 22). Bookcase manoeuvres would only require FCS limits to be imposed. Any transfer function or other studies involving frequency domain analysis would utilize a linearized FCS.

15.8 EXAMPLES

1. Obtain expressions for the short period natural frequency and damping ratio for the *rigid* aircraft in terms of the derivatives. Also, determine an expression for the transfer functions relating incidence ($\alpha = w/V_0$) and normal acceleration to the elevator angle.

2. Write a MATLAB/SIMULINK program (see appendix I in the companion website) to determine (a) the aerodynamic derivatives in wind axes for a given flight condition of the *rigid* aircraft, (b) the static margin, (c) the short period frequency and damping, (d) the response of the aircraft (pitch rate/incidence, etc.) to an elevator input and (e) the aircraft motion in earth axes. Check the results using the example in the chapter. Then explore the effect of changing the centre of mass position, tailplane area, downwash term, etc.

3. For the rigid aircraft used in the text, flying at 175 m/s EAS, determine the pitch rate, normal acceleration and response at the centre of mass relative to earth axes for an oscillatory elevator input of $+ 1^\circ$ at a range of frequencies. What frequency leads to the largest acceleration response in the steady state and how is this related to the undamped or damped short period frequency? Note that this problem may be solved using a simulation or using the transfer function expression evaluated at different frequencies. [Short period mode undamped 0.36 Hz/56 %/damped 0.30 Hz – maximum acceleration 1.06*g* close to damped frequency]

4. Repeat the exercise in Example 2 for the *flexible* aircraft with a fuselage bending mode. Check the results using the example in the chapter. Then explore the effect of changing the centre of mass position; the fuselage mass distribution and hence modal information will need to be altered (see Appendix C). Also, generate a new flexible mode for the same aircraft example, which is the combination of two of the other modes, and investigate the revised behaviour. Finally, develop a data set from another idealized aircraft with a different mass distribution.

5. For the aircraft used in the text, flying at 175 m/s EAS and having a fuselage bending mode with a 2 Hz natural frequency (2 % damping), determine the undamped natural frequency, damping ratio and undamped natural frequency for the 'S' and 'E' modes. Then determine the pitch rate and normal acceleration for an oscillatory input of $+1^\circ$ at these frequencies. What frequency leads to the largest acceleration response in the steady state? Note that this problem may be solved using a simulation or using the transfer function expression evaluated at different frequencies.
   [0.586 Hz, 35.1 %, 2.198 Hz, 3.55 %; 0.50*g* close to 'S' damped frequency and 0.28*g* at 'E' frequency–less than for a rigid aircraft]

6. Determine the cubic characteristic equation for the flexible aircraft and solve it (using MATLAB function *roots*) for Example 5 at a range of velocities and hence determine the coupled rigid/flexible flutter condition.
   [303 m/s]

7. Evaluate the elevator effectiveness for Example 5.
   [0.31]

8. Determine an expression for the initial roll acceleration when a step aileron input is applied to a simple *rigid* aircraft in roll.

9. Consider the rigid aircraft with the following data: $I_x = 40\,000$ kg m^2, $s = 6.25$ m, $S_W = 20$ m^2, $a_W = 4.5$/rad, $a_C = 2$/rad and $V_0 = 150$ m/s EAS. Calculate the maximum roll rate and roll angle responses when the aileron is suddenly deployed at an angle of 2° for 1 s and then returned to zero. This example may be solved using a MATLAB / SIMULINK program (see appendix I) or using the superposition of two steps. Note the effect of varying the input pulse length.
   [29.8 deg/s and 32°]

10. Derive the expressions for the derivatives L_e, Q_p for the *flexible* wing antisymmetric torsion mode.

11. Repeat Example 9 for the flexible aircraft with $I_W = 850$ kg m^2, $c = 1.6$ m, $l_A = 0.2$ m and modal damping $\zeta_e = 4$ % by extending the program in Example 9 to cover flexible effects (see also in appendix I). The natural frequency for the flexible antisymmetric wing torsion mode is 6 Hz. Note the effect of varying the input pulse length.
    [6.2 deg/s and 5.8°]

12. Use the characteristic equation and the roll rate/aileron gain transfer functions to determine the variation of aileron effectiveness with velocity, and reversal and oscillatory divergence speeds for Example 10 with a natural frequency of 8 Hz and damping of 2 %.
    [222 and 248 m/s]

13. For the aircraft in roll with a flexible torsion mode, obtain an expression for the transfer function $q_{\mathrm{e}}(s)/\xi(s)$ and hence for the steady wing twist per aileron deflection. Hence determine the steady wing tip twist for Example 4 with a 2° step aileron input.

14. Derive the equations of motion for the same aircraft in roll but now with an antisymmetric wing bending mode present. Examine the effect of the natural frequency on the aileron effectiveness and step roll response of the aircraft when compared to the behaviour with a torsion mode.

16

Gust and Turbulence Encounters

It is a well known but unfortunate feature of air travel that aircraft regularly encounter atmospheric turbulence (or 'rough air') of varying degrees of severity. Turbulence may be considered as movement of the air through which the aircraft passes. Any component of the velocity of the air (so-called 'gust velocity') that is normal to the flight path, as illustrated in Figure 16.1 for the vertical gust case, will change the effective incidence of the aerodynamic surfaces, so causing sudden changes in the lift forces and hence a dynamic response of the aircraft involving flexible deformation; gust inputs are also considered along the flight path. The response will involve both the rigid body and flexible modes, may give rise to passenger and crew discomfort and will introduce internal loads that need to be considered for aircraft safety. Thus it is important for the safe design of the aircraft to calculate the response and internal loads generated under the conditions defined by the Airworthiness Authorities, and to evaluate the effect on the fatigue life. Gust and turbulence loads are significant throughout the aircraft.

In this chapter, gusts and turbulence will be considered in two idealized forms, namely the tuned discrete gust (1-cosine shaped) and continuous (random) turbulence. The process of determining the response of an aircraft to gusts and continuous turbulence will be shown using a progression of models of differing complexity and using an analysis based in the time or frequency domain as appropriate. The main features of the response analysis are essentially illustrated one at a time, so that the range of issues involved may be seen as clearly as possible. Note that the focus will be on determining the aircraft response with the calculation of loads covered in Chapter 18. The unsteady aerodynamics concepts involved were initially introduced in Chapter 10.

The way in which turbulence has been treated for design has changed significantly over the years, particularly because of the difficulty of defining the external load input and of performing the calculations. A historical perspective is given in Fung (1969), Hoblit (1988), Flomenhoft (1994), Fuller (1995) and Bisplinghof et al. (1996), and, of course, the latest requirements are given in the current certification specifications (CS-25 and FAR-25). Many of the loads calculations required are helpfully explained in Hoblit (1988), Howe (2004) and Lomax (1996). The ESDU series also includes an item on gusts (ESDU Data Sheet 04024). This book will not attempt to catalogue the changes in requirements and philosophy but rather point out the key issues and methods involved by using the earlier rigid and flexible aircraft dynamic models. The approach used in industry and the certification requirements (in particular CS-25) are outlined later in Chapter 24.

It should be noted that the flight mechanics equations of motion will not be used here, since as in the equilibrium manoeuvre, flutter and taxiing calculations, for example, the aircraft encountering a gust is normally in a steady flight condition and the excursions from this datum are relatively small. Thus, an inertial axis system may be employed and rigid body characteristics (e.g. rigid body physical or generalized coordinates) may be combined with flexible modes in the flexible aircraft analysis. The equations of motion are similar to those in Chapter 13 but now with aerodynamic rate derivatives and aircraft acceleration effects present. The similarity of the equations of motion to previous manoeuvre cases means that it is once again convenient to write the equations in terms of aerodynamic derivatives

Introduction to Aircraft Aeroelasticity and Loads J. R. Wright and J. E. Cooper
© 2007 John Wiley & Sons, Ltd

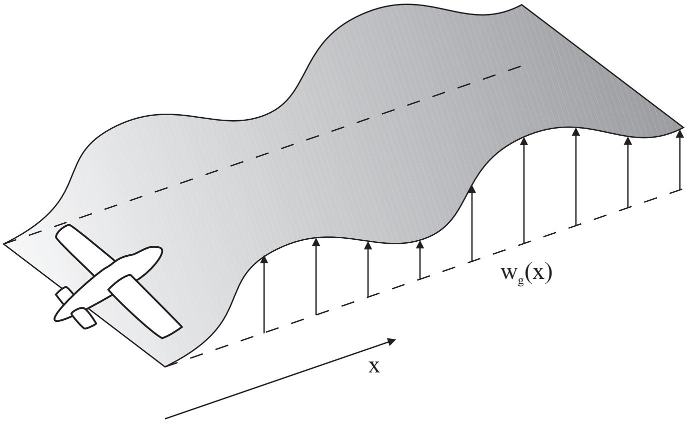

Figure 16.1 Aircraft encountering turbulence.

defined with respect to inertial (and not body fixed) axes where displacements and rotations are the unknowns. Derivatives employed here are tabulated in Appendix B.

16.1 GUSTS AND TURBULENCE

Turbulence, although a complicated phenomenon, is normally considered for design purposes in one of two idealized categories, namely:

(a) *discrete gusts*, where the gust velocity varies in a deterministic manner, often in the form of a '1-cosine' shape (i.e. there is an idealized discrete 'event' that the aircraft encounters), and
(b) *continuous turbulence*, where the gust velocity is assumed to vary in a random manner.

The difference between the two types of turbulence may be seen in Figure 16.2. The discrete gust response is solved in the time domain whereas the continuous turbulence response is usually determined in the frequency domain via a power spectral density method (see Chapter 1). Gusts and turbulence may be vertical, lateral or at any orientation to the flight path, but vertical and lateral cases are normally treated separately. Thus, for a symmetric aircraft, a vertical gust will give rise to heave (or plunge)/pitch motions whereas a lateral gust will cause sideslip/yaw/roll motions; all these motions will be coupled for an asymmetric aircraft. Note that it is normally assumed that there is no variation of the gust velocity across the aircraft span (or with height in the case of lateral gusts). Here only the symmetric vertical gust case

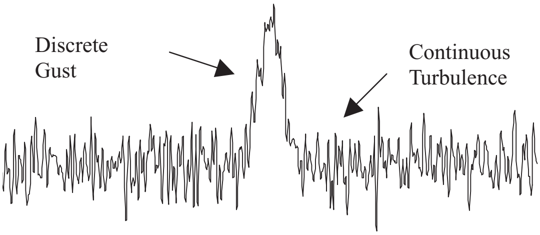

Figure 16.2 Continuous and discrete turbulence.

will be considered. Chapter 24 includes a discussion on lateral and round-the-clock gusts and detail on the magnitude of the gust and turbulence inputs.

16.2 GUST RESPONSE IN THE TIME DOMAIN

Initially, the ‘sharp-edged’ and ‘1-cosine’ discrete gusts will be considered, and the so-called ‘gust penetration effect’ introduced; the sharp-edged gust is included to aid understanding though it is no longer relevant to the gust clearance of large commercial aircraft. The time domain solution for a rigid aircraft entering a sharp-edged gust and responding in heave only will firstly be considered by ignoring separate tailplane aerodynamics and therefore any pitching effects: It will also be assumed that the relevant aerodynamic surface enters the gust instantaneously and develops a lift force proportional to the effective incidence angles produced by the response and gust, i.e. quasi-steady aerodynamics. Then the effect of employing response- and gust-dependent unsteady aerodynamics, the latter allowing for a noninstantaneous lift build-up due to the penetration of the gust by the aerofoil, will be shown using Wagner’s and Küssner’s functions respectively (see Chapter 10).

Later on, the response of a rigid aircraft, with pitching effects included, to a more general gust input (e.g. ‘1-cosine’ gust) will be considered by including the tailplane aerodynamics and the penetration delay between the wing and tailplane. Finally, the gust response of a simple flexible aircraft will be considered. This exercise will allow the general form of the equations of motion to be developed.

16.2.1 Definition of Discrete Gusts

16.2.1.1 ‘Sharp-edged’ gust

The early work on gust response considered the gust input to be in the form of a *sharp-edged or step gust* (Fung, 1969; Fuller, 1995), where the aircraft entered instantaneously into a uniform gust velocity field (see Figure 16.3), defined spatially by

$$w_g(x_g) = \begin{cases} 0, & x_g < 0, \\ w_{g0}, & x_g \geq 0, \end{cases} \tag{16.1}$$

where w_{g0} is the constant gust velocity. Some of the theory for the response to this gust is covered later in this chapter. However, as the prediction methodologies developed, this input was considered to be too unrealistic and others were adopted. (It should be noted that the symbol w_g is a classical notation for gust analysis and should not be confused with the use of w as an aircraft velocity for the flight mechanics model in Chapters 14 and 15, or for downwash in Chapter 19 – all these usages are classical in different areas.)

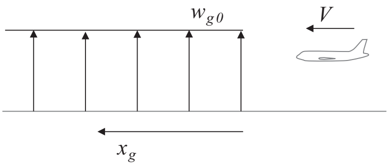

Figure 16.3 ‘Sharp-edged’ gust.

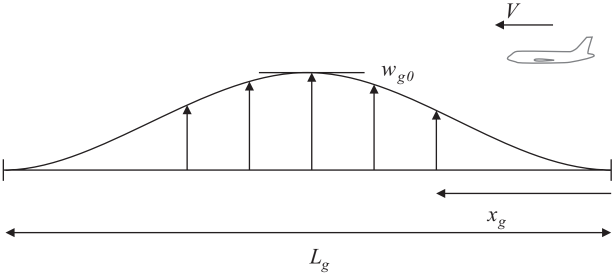

Figure 16.4 Discrete '1-cosine' gust.

16.2.1.2 '1-Cosine' gust

Discrete gusts are currently represented for design purposes by a so-called *'1-cosine' gust*, where the variation in the velocity of the air normal to the path of the aircraft is as shown in Figure 16.4.

The expression governing the *spatial* behaviour of the '1-cosine' gust is

$$w_g(x_g) = \frac{w_{g0}}{2}\left(1 - \cos\frac{2\pi x_g}{L_g}\right), \quad 0 \le x_g \le L_g, \tag{16.2}$$

where x_g is the position of the aircraft in the spatial description of the gust relative to a convenient fixed origin, w_{g0} is the value of the peak, or design, gust velocity and L_g is the gust length (or twice the so-called 'gust gradient' H). The design gust velocity w_{g0} varies with gust length, altitude and speed (CS-25; Hoblit, 1988).

To calculate the aircraft response in the time domain, the gust velocity expression needs to be transformed from a spatial into a temporal function. Consider the aircraft encountering a gust whose vertical velocity varies spatially as shown in Figure 16.5, where the aircraft wing enters the gust at time $t = 0$ and position $x_g = 0$. The tailplane enters the gust shortly after the wing; this is the 'gust penetration effect' (see later). If the aircraft has constant velocity V then the gust velocity w_g experienced by the

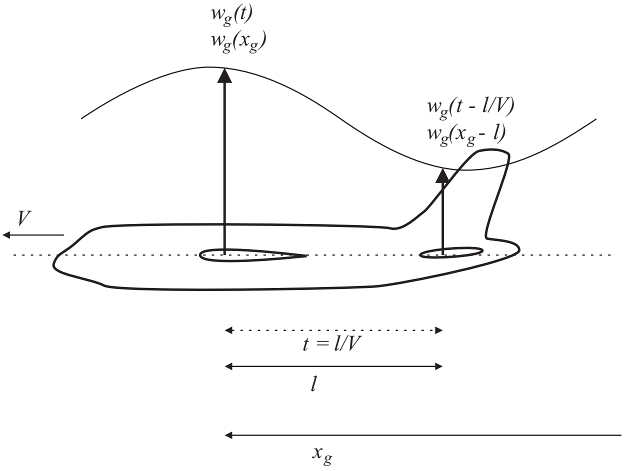

Figure 16.5 Gust penetration effect.

aircraft may be thought of as a function of time since the amount by which the aircraft wing has penetrated the gust will be given by $x_{\mathrm{g}} = Vt$, where in this case V needs to be TAS. For the spatial variation in gust velocity quoted above for the '1-cosine' gust, then the corresponding *temporal* variation of gust velocity, as seen by the aircraft, will be given by

$$w_{\mathrm{g}}(t) = \frac{w_{\mathrm{g0}}}{2}\left(1 - \cos\frac{2\pi V}{L_{\mathrm{g}}}t\right). \tag{16.3}$$

Gust response calculations may be performed in the time domain, using a solution method introduced in Chapter 1, for a series of different gust lengths to seek the so-called 'discrete tuned gust' that causes the maximum value of each internal load (e.g. wing root shear force, torque and bending moment). Nonlinear effects due to the FCS may be included readily. A similar approach will be used for the taxiing case in Chapter 17.

16.2.2 Gust Penetration Effect

It was noted earlier that the wing and tailplane encounter features of the gust at different times, as shown in Figure 16.5, and this delay needs to be represented in the gust response calculations.

If $l = l_{\mathrm{W}} + l_{\mathrm{T}}$ (see Figure 15.1) is the distance between the wing and tailplane aerodynamic centres, then the wing experiences the gust velocity $w_{\mathrm{g}}(t)$ while the tailplane experiences $w_{\mathrm{g}}(t - l/V)$. Clearly, this assumes that the spatial variation of the gust velocity remains the same in the time taken for the aircraft to pass. Downwash effects on the tailplane are ignored at this point. However, even this argument is somewhat simplistic and only applies for lifting surfaces without sweep, since when wing sweep is present then different parts of the wing will encounter a particular feature of the gust at different times. If a strip theory approach is employed, then the wing would be split into strips, each encountering the gust at different times. Alternatively, the penetration effects can be allowed for when using a three-dimensional panel method (see later in Chapters 19 and 20).

16.3 TIME DOMAIN GUST RESPONSE – RIGID AIRCRAFT IN HEAVE

Initially, the time domain solution for a rigid aircraft entering a 'sharp-edged' gust and responding in heave only will be considered in this section by ignoring tailplane effects. Both quasi-steady and unsteady aerodynamic assumptions will be examined and the effect on the heave response discussed. The approach will be extended to a more general gust shape. The arguments presented are partially responsible for the development of the gust alleviation factor, used historically in the load factor approach. Nevertheless, unsteady aerodynamic effects are also crucial when considering current analysis methodologies.

16.3.1 Gust Response of Rigid Aircraft in Heave Using Quasi-Steady Aerodynamics

To simplify the analysis as much as possible, consider the whole aircraft encountering the sharp-edged gust instantaneously (Fung, 1969) and assume that the aircraft will heave (i.e. move up or down) without pitching; thus tailplane and penetration effects are ignored. The term 'plunge' is sometimes used in place of 'heave'. The aircraft is in a trimmed level flight condition before encountering the gust (with lift = weight), so the forces and motions shown below are relative to the initial trimmed state, with the symbol Δ indicating incremental values.

Now, consider the aircraft of mass m as being rigid, moving forwards with velocity V (TAS) and downwards with heave velocity $\dot{z}_{\mathrm{C}}$ at any instant of time (i.e. relative to the initial trimmed state). Because the air is moving upwards with the instantaneous gust velocity w_{g}, it may be seen from the relative velocity

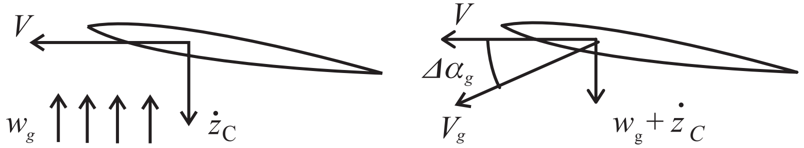

Figure 16.6 Effective incidence due to gust velocity and aircraft response.

between the wing and air in Figure 16.6 that there is an effective instantaneous increase in incidence $\Delta\alpha_g$, given by

$$\Delta\alpha_g \approx \frac{w_g + \dot{z}_C}{V}, \tag{16.4}$$

where small angles are assumed (w_g and $\dot{z}_C \ll V$). Also, the change in the total velocity vector is neglected, so the total velocity in the gust $V_g \approx V$, and if the lift is assumed to be developed instantaneously (essentially the quasi-steady assumption), then the incremental aircraft lift due to the gust velocity is

$$\Delta L = \frac{1}{2}\rho V^2 S_W a \left(\frac{w_g + \dot{z}_C}{V}\right) = \frac{1}{2}\rho V S_W a \left(w_g + \dot{z}_C\right), \tag{16.5}$$

where ρ is the air density, S_W is the wing area and $a = \mathrm{d}C_L/\mathrm{d}\alpha$ is the lift curve slope for the whole aircraft based on using the wing area as the reference. It may thus be seen that the lift developed due to gust velocity is proportional to V (not V^2) and is linearly related to $w_g + \dot{z}_C$. Since pitching effects are neglected, then, using Newton's second law, the heave equation of motion of the aircraft is given by

$$\begin{aligned} m\ddot{z}_C &= -\Delta L = -\tfrac{1}{2}\rho V S_W a \left(w_g + \dot{z}_C\right), \\ m\ddot{z}_C + \tfrac{1}{2}\rho V S_W a \dot{z}_C &= -\tfrac{1}{2}\rho V S_W a w_g \end{aligned} \tag{16.6}$$

or

$$m\ddot{z}_C + \Delta L_z = -\Delta L_g \tag{16.7}$$

where the subscripts z and g indicate that the incremental lift terms are due to the response and gust effects respectively. This form of the equation is included to allow the important distinction between response-dependent and gust-dependent aerodynamic terms to be recognized. The equation could also be written in derivative form, and this will be done later for the rigid (heave/pitch) and flexible aircraft cases.

Dividing Equation (16.7) through by m and defining $\eta_g = \rho V S_W a/(2m)$ (using the subscript g to distinguish from the symbol for elevator angle) leads to the differential equation of motion in the form

$$\ddot{z}_C + \eta_g \dot{z}_C = -\eta_g w_g. \tag{16.8}$$

Given that $w_g(t)$ is a step function of magnitude w_{g0}, the so-called 'sharp-edged' gust, then the displacement and acceleration responses following zero initial conditions $z_C = \dot{z}_C = 0$ at $t = 0$ may be shown to be

$$z_C = \frac{1}{\eta_g} w_{g0}(1 - \mathrm{e}^{-\eta_g t}) - w_{g0} t, \qquad \ddot{z}_C = -\eta_g w_{g0} \mathrm{e}^{-\eta_g t}. \tag{16.9}$$

The heave displacement z_C shows the aircraft climbing steadily after a transient while the acceleration $\ddot{z}_C$ decays from the initial maximum value at $t = 0$. Responses to a step gust will be shown in an example later. The maximum total load factor n (see Chapter 13) occurs at $t = 0$ and is given by

$$n = 1 + \frac{\Delta L}{W} = 1 + \Delta n = 1 - \frac{\ddot{z}_{C\max}}{g} = 1 + \frac{\rho V w_{g0} a}{2W/S_W}, \tag{16.10}$$

where Δn is the increment of load factor and the minus sign appears because both heave displacement and acceleration are defined as positive downwards.

There are significant shortcomings in the above simplified analysis that lead to incorrect estimation of loads, namely:

- The inclusion of the tailplane and penetration effects introduces pitching motion, which modifies the effective incidence of both wing and tailplane at any instant of time.
- The lift force is not developed instantaneously because the surface enters the gust progressively and the changes in incidence do not have an instant effect (i.e. unsteady aerodynamics).
- The flexibility of the aircraft will modify the response.
- The 'sharp-edged' gust is not realistic since in practice the gust velocity takes a finite time to build up.

To account for the instantaneous lift assumption and for replacing the sharp-edged gust by a more 'real' discrete gust, a 'gust alleviation factor' K_g (0.7–0.8) was included in Equation (16.10) to produce more realistic loads.

16.3.2 Gust Envelope

Historically, Equation (16.10) has been written with K_g included and in terms of EAS (equivalent air speed), so

$$n = 1 + \frac{\rho_0 w_{g0EAS}\, a K_g}{2W/S_W} V_{EAS} \tag{16.11}$$

where ρ_0 is the air density at sea level (see Chapter 5). This is known as Pratt's equation and was used to define the load factors for design at different flight conditions. One way of presenting the flight load factors graphically is by generating the 'gust envelope' shown in Figure 16.7. This envelope is constructed by drawing lines of load factor against velocity V_{EAS} for different sharp-edged gust velocities w_{g0EAS}, using Equation (16.11). The points that define the envelope occur at the value of the appropriate gust load factor expression at the specified flight velocity (e.g. V_B = speed for maximum gust intensity, V_C = cruise speed and V_D = design dive speed). The gust velocities at these three flight speeds were defined as 8, 16 and 20 m/s (or 25, 50 and 66 ft/s), with these values reducing at higher altitudes.

Design calculations were then carried out at all the corner (and some intermediate) points on the gust envelope for different flight conditions (i.e. altitudes) and the worst case responses and internal loads obtained, in a somewhat similar way to the manoeuvre envelope in Chapter 13.

Currently, this approach is no longer used for large commercial aircraft (it does not appear in CS-25) and gust loads for aircraft are obtained using more accurate approaches, as will be explained later. In particular, the aircraft model used for gust calculations will include heave and pitch motion together with flexible modes, will approximate the penetration effects, will take account of transient aerodynamic effects and will use both discrete tuned '1-cosine' gust and continuous turbulence representations. Models for lateral gusts are also considered.

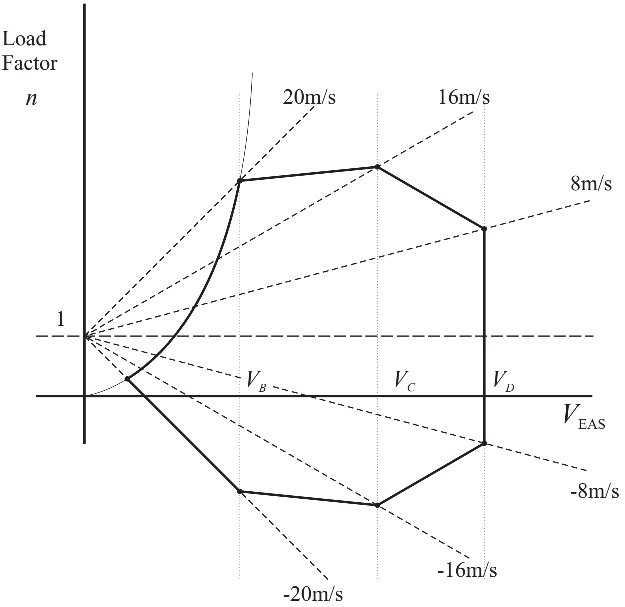

Figure 16.7 Gust envelope.

16.3.3 Unsteady Aerodynamic Effects in the Time Domain

So far, it has been assumed that the aircraft enters the gust instantly and that the aerodynamic forces develop instantaneously following the change in effective incidence caused by the gust and response (i.e. quasi-steady assumption). However, the time taken for the wing section to penetrate the gust and experience the change in effective incidence due to the gust will mean that the *gust-dependent aerodynamic forces* will not be developed instantaneously, but there will be a finite build-up to the steady value. This effect is represented classically by *Küssner's* function $\Psi(\tau)$ (Bisplinghoff *et al.*, 1996), introduced in Chapter 10; it is the ratio between the transient lift and the final steady-state lift on an aerofoil section penetrating a sharp-edged gust. Figure 16.8 shows a typical Küssner's function, where the dimensionless time quantity

$$\tau = \frac{2V}{c}t \tag{16.12}$$

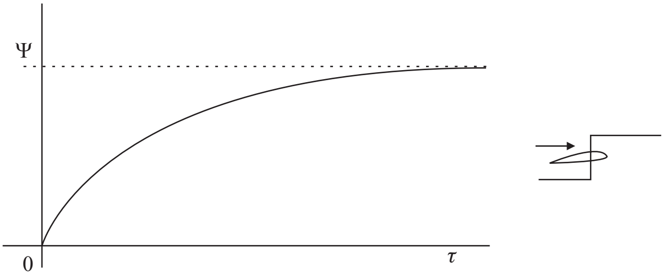

Figure 16.8 Küssner's function (numerical values in Chapter 10).

may be interpreted as the distance travelled by the aerofoil, measured in semi-chords. Thus $\tau = 0$ corresponds to the leading edge entering the gust, whereas at $\tau = 30$ the leading edge has moved 15 chord lengths into the gust and the lift is more or less fully developed.

In addition, the *response-dependent aerodynamic forces* will take time to develop following a change in incidence due to the heave (or plunge) velocity and there will therefore be an attenuation and phase lag between the lift and incidence time histories. This behaviour is accounted for by *Wagner's* function $\Phi(\tau)$ in the time domain (or Theodorsen's function in the frequency domain, see later), also introduced in Chapter 10.

16.3.4 Gust Response of Rigid Aircraft in Heave Using Unsteady Aerodynamics

In this section, the earlier analysis in Section 16.3.1 for the rigid aircraft in heave will be extended to include unsteady aerodynamic effects and a more general input will be allowed for.

16.3.4.1 Küssner's function

From the definition of Küssner's function, the time variation of the increment of *gust-dependent* lift produced on the aircraft entering a sharp-edged gust of velocity w_{g0} is given in terms of dimensional time *t* by

$$\Delta L_{\mathrm{g\,Kussner}}(t) = \frac{1}{2}\rho V^2 S_{\mathrm{W}} a \left(\frac{w_{\mathrm{g}0}}{V}\right) \Psi(t) = \frac{1}{2}\rho V S_{\mathrm{W}} a w_{\mathrm{g}0} \Psi(t). \tag{16.13}$$

This expression is essentially the lift 'step response' following the aerofoil entering a sharp-edged gust, allowing for the finite lift build up. However, Küssner's function was defined in terms of nondimensional time τ so the lift expression should be redefined accordingly.

The variation in lift increment for a *general gust* shape $w_{\mathrm{g}}(t)$ or $w_{\mathrm{g}}(\tau)$ may be determined from the convolution or Duhamel integral written in terms of the step response (introduced in Chapter 1), using $\Psi(0) = 0$ to eliminate the first term in the expression, so that

$$\Delta L_{\mathrm{g\,Kussner}}(\tau) = \frac{1}{2}\rho V S_{\mathrm{W}} a \int_{\tau_0=0}^{\tau} w_{\mathrm{g}}(\tau_0)\Psi'(\tau - \tau_0)\mathrm{d}\tau_0 = \frac{1}{2}\rho V S_{\mathrm{W}} a w_{\mathrm{g\,Kussner}}(\tau), \tag{16.14}$$

where $\Psi' = \mathrm{d}\Psi/\mathrm{d}\tau$ is the equivalent of Küssner's function for an impulsive rather than step gust, $w_{\mathrm{g}}(\tau_0)$ is the gust velocity at τ_0, an integration variable, and $w_{\mathrm{g\,Kussner}}(\tau)$ is the gust velocity after being 'filtered' by Küssner's function through the convolution integral. The above integral could also be written in terms of Küssner's function itself and the rate of change of gust velocity. A shorthand form of either equation may be written as

$$\Delta L_{\mathrm{g\,Kussner}}(\tau) = \frac{1}{2}\rho V S_{\mathrm{W}} a\ w_g {}^* \Psi = \frac{1}{2}\rho V S_{\mathrm{W}} a\ w_{\mathrm{g\,Kussner}}, \tag{16.15}$$

where the symbol $*$ in this context denotes convolution (not complex conjugate) as in Chapter 1. Thus, for any gust velocity profile experienced by the aircraft, the resulting lift force may be obtained as a function of time.

16.3.4.2 Wagner's function

The equivalent expression for the *response-dependent* lift, attenuated via Wagner's function $\Phi(\tau)$, is

$$\Delta L_{\mathrm{z\,Wagner}}(\tau) = \frac{1}{2}\rho V S_{\mathrm{W}} a \frac{2V}{c} \int_{\tau_0=0}^{\tau} \frac{\mathrm{d}z_{\mathrm{C}}}{\mathrm{d}\tau}(\tau_0)\Phi'(\tau - \tau_0)\mathrm{d}\tau_0 \Delta L_z(\tau) = \frac{1}{2}\rho V S_{\mathrm{W}} a \frac{2V}{c} \frac{\mathrm{d}z_C}{\mathrm{d}\tau} * \Phi, \tag{16.16}$$

where the rate of change of z_{C} with the time term has been altered to nondimensional time using

$$\frac{\mathrm{d}z_{\mathrm{C}}}{\mathrm{d}t} = \frac{\mathrm{d}z_{\mathrm{C}}}{\mathrm{d}\tau}\frac{\mathrm{d}\tau}{\mathrm{d}t} = \frac{\mathrm{d}z_{\mathrm{C}}}{\mathrm{d}\tau}\frac{2V}{\mathrm{c}}. \tag{16.17}$$

16.3.4.3 Equation of motion

The equation of motion shown earlier for the rigid aircraft with quasi-steady aerodynamic effects may now be rewritten to account for the finite lift build-up associated with unsteady response and gust-dependent aerodynamics. For convenience, nondimensional time will be retained; thus

$$m\left(\frac{2V}{c}\right)^2\frac{\mathrm{d}^2z_{\mathrm{C}}}{\mathrm{d}\tau^2} + \Delta L_{\mathrm{z\,Wagner}}(\tau) = -\Delta L_{\mathrm{g\,Kussner}}(\tau), \tag{16.18}$$

where both lift functions are the result of convolutions, so

$$m\left(\frac{2V}{c}\right)^2\frac{\mathrm{d}^2z_C}{\mathrm{d}\tau^2} + \frac{1}{2}\rho V S_{\mathrm{W}} a\,\frac{2V}{c}\frac{\mathrm{d}z_C}{\mathrm{d}\tau} * \Phi = -\frac{1}{2}\rho V S_{\mathrm{W}} a\; w_{\mathrm{g}} * \Psi \tag{16.19}$$

Now, defining a mass parameter as

$$\mu_{\mathrm{g}} = \frac{2m}{\rho a S_{\mathrm{W}} c}, \tag{16.20}$$

the differential equation (16.19) may be rewritten as

$$\frac{\mathrm{d}^2z_{\mathrm{C}}}{\mathrm{d}\tau^2} + \frac{1}{2\mu_{\mathrm{g}}}\frac{\mathrm{d}z_{\mathrm{C}}}{\mathrm{d}\tau} * \Phi = -\frac{1}{4\mu_{\mathrm{g}}}\frac{c}{V}\,w_{\mathrm{g}} * \Psi. \tag{16.21}$$

Clearly μ_{g} is a key parameter when the gust response is expressed in terms of the number of chord lengths travelled. The heave response may then be calculated by solving this differential equation; the unsteady aerodynamic effects will reduce the gust response severity when compared to quasi-steady aerodynamics.

16.3.4.4 Gust alleviation factor

This approach was used in Hoblit (1988) to estimate the gust alleviation factor K_{g} mentioned earlier; the response to a '1-cosine' gust of gradient distance of 12.5 chords (or length 25 semi-chords) was used to calculate the load factor (after converting back to dimensional time) and the result was compared to that shown earlier for the sharp-edged gust of the same amplitude but using quasi-steady aerodynamics. Thus

$$\Delta n_{1-\mathrm{cosine}_{\mathrm{US}}} = K_{\mathrm{g}}\Delta n_{\mathrm{Sharp-edged}_{\mathrm{QS}}}, \qquad K_{\mathrm{g}} = \frac{0.88\mu_{\mathrm{g}}}{5.3+\mu_{\mathrm{g}}}. \tag{16.22}$$

The expression for K_{g} in terms of μ_{g} was obtained from a fit to the computational results with different aircraft mass parameters. This gust alleviation factor was in effect an attempt to represent unsteady aerodynamic and real gust effects in terms of the mass parameter before the ability to handle more advanced calculations became available. For the example used later on in this chapter, $K_{\mathrm{g}} = 0.81$.

The analysis shown in this section applies to the rigid aircraft in heave only. When the rigid aircraft in heave and pitch is considered, then a similar approach would be used, except that Wagner's and Küssner's functions would need to be applied to both the wing and tailplane lift forces, recognizing that the wing and tailplane chords, and corresponding nondimensional time definitions, will be different. For a swept wing, each strip contribution could be treated individually. Penetration effects would also need to be included.

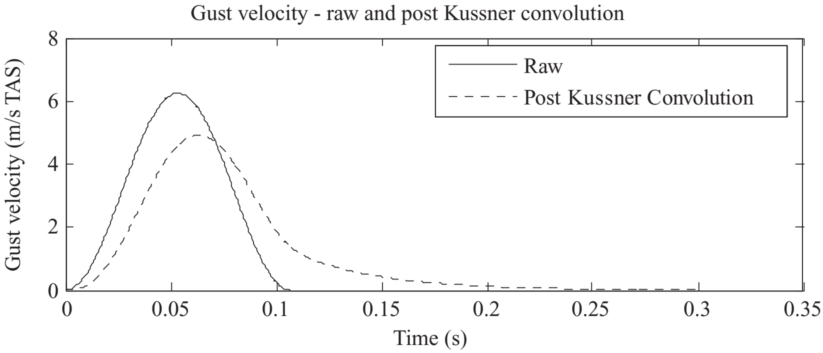

Figure 16.9 Velocity for a ‘1-cosine’ gust – raw and post-Küssner convolution.

16.3.5 Example of Gust Response in the Time Domain Using Unsteady Aerodynamics

It would be possible to calculate a whole series of examples including the Wagner and Küssner effects. However, to save space a simple approach will be used. The aircraft (the parameters are given in Section 16.4.2) is considered as flying at 150 m/s EAS at 14 000 ft but now a short ‘1-cosine’ gust of 20 m wavelength will be used to highlight the gust-dependent effect only. In Figure 16.9, the raw gust velocity w_{g} is compared to the effective gust velocity $w_{\mathrm{g\,Kussner}}$ obtained by filtering the gust through Küssner’s function via the convolution integral. It can be seen that the effect of Küssner’s function is to attenuate the magnitude, widen the pulse and introduce a phase delay; the lift force on the wing due to the gust will be changed accordingly. If Wagner’s function were to be used in the time domain, as described above, then an attenuation and phase lag would be present in each response-dependent lift term.

16.4 TIME DOMAIN GUST RESPONSE – RIGID AIRCRAFT IN HEAVE/PITCH

So far, it has been assumed that the tailplane experienced the same incidence change as the wing and at the same time, so ignoring the penetration delay. The effect of the tailplane and penetration will now be considered.

16.4.1 Equations of Motion – Rigid Aircraft Including Tailplane Effect

Consider the rigid aircraft shown in Figure 16.10 where the heave motion z_{C} (positive downwards) and pitch motion θ (positive nose up) are both referred to the centre of mass. The incremental lift forces

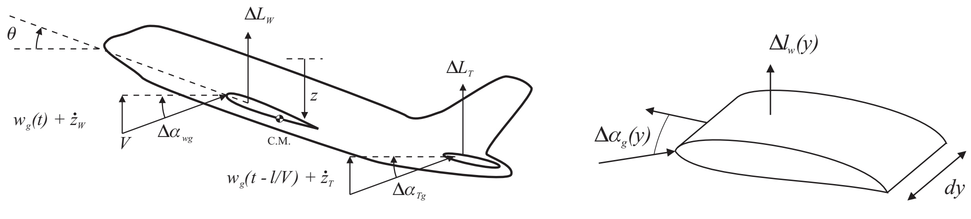

Figure 16.10 Rigid aircraft with heave/pitch motions showing incremental quantities.

ΔL_W, ΔL_T are considered, since the aircraft is assumed to be in a trimmed state prior to entering the gust and the gust loads will then be added to the steady flight loads. The lift forces are shown acting at the aerodynamic centres of the wing and tailplane. For simplicity, the quasi-steady aerodynamic representation will be employed, though unsteady aerodynamic effects are normally included. Downwash effects will initially be excluded here to simplify the expressions, but will be added later when the derivative formulation is used.

It may be seen that the instantaneous pitch angle and heave rate of the aircraft affect the effective incidence of the wing and tailplane. From Figure 16.10, the increments in wing and tailplane incidence are given by

$$\Delta\alpha_{Wg} = \frac{w_g(t) + \dot{z}_W}{V} + \theta, \qquad \Delta\alpha_{Tg} = \frac{w_g(t - l/V) + \dot{z}_T}{V} + \theta, \tag{16.23}$$

where the heave velocities at the aerodynamic centres are now different for the wing and tailplane due to the pitch rate effects, namely

$$\dot{z}_W = \dot{z}_C - l_W\dot{\theta}, \qquad \dot{z}_T = \dot{z}_C + l_T\dot{\theta}. \tag{16.24}$$

The unsteady aerodynamic effect of the rate of change of pitch $\dot{\theta} = q$ (i.e. pitch damping) is neglected here for the gust analysis though it was included for the wing in the earlier treatment of flutter in Chapter 11.

Thus the incremental changes in wing and tail lift (excluding downwash) are given by

$$\Delta L_W = \frac{1}{2}\rho V^2 S_W a_W \left[\frac{w_g(t) + \dot{z}_C - l_W\dot{\theta}}{V} + \theta\right], \quad \Delta L_T = \frac{1}{2}\rho V^2 S_T a_T \left[\frac{w_g(t - l/V) + \dot{z}_C + l_T\dot{\theta}}{V} + \theta\right]. \tag{16.25}$$

It is now possible to write the equations of motion in heave and pitch to allow the response (relative to the initial trimmed state) to be obtained. The net downward force on the aircraft will be equal to the mass × acceleration of the centre of mass and the net nose up pitching moment about the centre of mass is equal to the pitch moment of inertia I_y × pitch acceleration (using the generalized Newton's second law; see Chapter 6), so

$$m\ddot{z}_C = -\Delta L_W - \Delta L_T, \qquad I_y\ddot{\theta} = \Delta L_W l_W - \Delta L_T l_T, \tag{16.26}$$

where positive incremental wing/tailplane lift forces cause nose up/down pitch responses respectively.

The right-hand side of these two equations may be written in derivative form (based on inertial axes, following the approach in Chapter 13). The α and q derivatives here are appropriate for the change of pitch θ and rate of change of pitch $\dot{\theta}$ and are the same as determined in Chapter 13, with pitch rate terms for the wing being neglected. Also, terms associated with the zero lift condition are not required for this incremental case. However, derivatives for the rate of heave $\dot{z}$ appear for the first time in the gust analysis and these are essentially very similar to the w derivatives used for wind axes (see Chapters 14 and 15). Values for these derivatives are given in Appendix B and the downwash terms may now be included.

Thus, building on earlier results, the equations of motion may be written compactly in matrix form as follows:

$$\begin{bmatrix} m & 0 \\ 0 & I_y \end{bmatrix} \begin{Bmatrix} \ddot{z}_C \\ \ddot{\theta} \end{Bmatrix} + \begin{bmatrix} -Z_{\dot{z}} & -Z_q \\ -M_{\dot{z}} & -M_q \end{bmatrix} \begin{Bmatrix} \dot{z}_C \\ \dot{\theta} \end{Bmatrix} + \begin{bmatrix} 0 & -Z_\alpha \\ 0 & -M_\alpha \end{bmatrix} \begin{Bmatrix} z_C \\ \theta \end{Bmatrix}$$
$$= \begin{Bmatrix} Z_{gW} \\ M_{gW} \end{Bmatrix} w_g(t) + \begin{Bmatrix} Z_{gT} \\ M_{gT} \end{Bmatrix} w_g\left[\frac{t-l}{V}\right]. \tag{16.27}$$

It may be seen that gust-related derivatives have now been introduced, which may be shown to be

$$Z_{\mathrm{gW}} = -\frac{1}{2}\rho V S_{\mathrm{W}} a_{\mathrm{W}}, \qquad Z_{\mathrm{gT}} = -\frac{1}{2}\rho V S_{\mathrm{T}} a_{\mathrm{T}}(1-k_{\varepsilon}),$$

$$M_{\mathrm{gW}} = \frac{1}{2}\rho V S_{\mathrm{W}} a_{\mathrm{W}} l_{\mathrm{W}}, \qquad M_{\mathrm{gT}} = -\frac{1}{2}\rho V S_{\mathrm{T}} a_{\mathrm{T}} l_{\mathrm{T}}(1-k_{\varepsilon}). \tag{16.28}$$

It should be noted of course that only the first term on the right-hand side of Equation (16.27) would be included for the initial part of the solution, i.e. before the tailplane enters the gust; this is indicated by the use of square brackets where, if the contents are negative, the term is ignored (i.e. the Heaviside function). The gust tail derivatives are now assumed to be affected by downwash effects and the other derivatives in Appendix B will also be used with downwash effects.

Solution of the equations of motion will yield the heave and pitch responses; the acceleration at the tailplane, for example, will be given by $\ddot{z}_{\mathrm{T}} = \ddot{z}_{\mathrm{C}} + l_{\mathrm{T}}\ddot{\theta}$. The response will be more complicated than for the simple heave model considered earlier. For example, in a sharp-edged gust the aircraft would initially pitch nose up and heave upwards as the wing lift increased over the very short time prior to the tailplane entering the gust, but then the aircraft would pitch nose down due to the tailplane lift, so influencing the wing lift. The aircraft would tend to oscillate in pitch in its short period mode but eventually settle down into a steady condition.

Even though this more advanced model of the aircraft allows for the tailplane effect, the penetration delay and a more complex gust shape, lift forces are still allowed to develop instantaneously and the aircraft is rigid.

16.4.2 Example: Gust Response in the Time Domain for a Rigid Aircraft with Tailplane Effects

Consider an aircraft with the following data: $m = 10\,000$ kg, $S_{\mathrm{W}} = 30$ m^2, $S_{\mathrm{T}} = 7.5$ m^2, $c = 2.0$ m, $l_{\mathrm{W}} = 0.6$ m, $l_{\mathrm{T}} = 7$ m, $a_{\mathrm{W}} = 4.5$/rad, $a_{\mathrm{T}} = 3.2$/rad and $k_{\varepsilon} = 0.35$. These data are for the rigid aircraft, with further parameters being defined later for the flexible aircraft. The aircraft flies at 150 m/s EAS at 14 000 ft ($\sqrt{\sigma} \approx 0.8$), so the velocity is 187.5 m/s TAS. Consider the aircraft entering (a) a '1-cosine' gust of variable length or (b) a sharp-edged gust, both with maximum velocity 5 m/s EAS (or 6.25 m/s TAS). The responses will be evaluated firstly using the heave/pitch model and then using the heave only model discussed earlier (with quasi-steady aerodynamics). MATLAB and SIMULINK programmes to solve the time domain gust response for this rigid aircraft in heave and pitch are presented in appendix I in the companion website.

16.4.2.1 '1-Cosine' gust

Firstly, the centre of mass (CoM) accelerations for '1-cosine' gusts of various lengths are determined. The variation of minimum and maximum values of acceleration for a whole range of gust lengths is shown in Figure 16.11; the maximum acceleration is around +0.51g for a 400 m gust length and the minimum of −0.65g occurs for a 40 m gust length. In Figure 16.12, the variations of pitch rate, pitch angle and nose/CoM/tailplane accelerations with time for the 'tuned' 40 m and 400 m gust lengths are presented (note the different time axes). The aircraft is seen to pitch nose up very slightly, pitch nose down as the tailplane enters the gust and the tailplane lift increases, and then pitch nose up again; the aircraft finishes with zero attitude and pitch rate, having climbed to a slightly higher altitude. The CoM acceleration first peaks at a negative value (i.e. upwards), as the aircraft initially encounters the gust, and then peaks at a positive value (i.e. downwards) as the nose down pitch takes effect; the relative magnitude of the two peaks depends upon the gust length. What is interesting is that there is barely any difference between the accelerations at the CoM and tailplane.

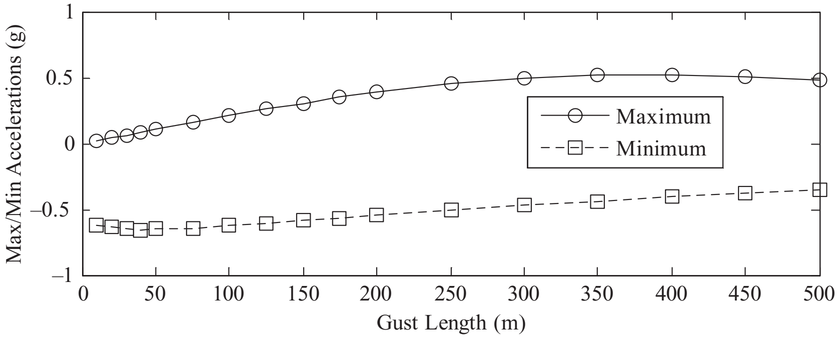

Figure 16.11 Minimum/maximum acceleration response of a rigid aircraft to variable length '1-cosine' gust – heave/pitch model.

Secondly, in Figure 16.13 the results for the heave/pitch model are compared to the heave only model for the 400 m gust length. The heave only model shows the aircraft to have gained more height than the heave/pitch model because the nose down pitch offsets the initial incidence change. The accelerations for the two models are surprisingly similar, although the heave only model underestimates the peaks somewhat because of the absent pitch effect. It should be noted that the 400 m wavelength is longer than would need to be considered under the certification requirements (see Chapter 24).

16.4.2.2 Sharp-edged gust

Some equivalent results for the sharp-edged gust response are presented in Figure 16.14; the overshoot in the acceleration for the heave/pitch model when compared to the heave only model should be particularly noted. The aircraft ends up climbing steadily with no CoM acceleration; the heave only model leads to about twice the rate of climb compared to the heave/pitch model. These results confirm the discussions for the '1-cosine' gust above and show some differences between the two models.

16.5 TIME DOMAIN GUST RESPONSE – FLEXIBLE AIRCRAFT

So far, only the rigid aircraft has been considered, but in practice the flexible deformation of the aircraft will make a difference to the loads developed, especially if any significant frequency content in the gust time history coincides with one or more of the natural frequencies of the aircraft. In this section, in order to keep the mathematics at a manageable level, the flexible aircraft considered earlier in Chapters 13 and 15 will be used, i.e. a single flexible mode with rigid body heave and pitch motions. The equations will refer to inertial axes.

The flexible mode was described in Chapter 13 and Appendix C. However, as a reminder, it permits modes to be considered with fuselage bending, wing bending or wing twist as the dominant components. The mode shape for the general case involves the wing bending and twist shapes defined by the functions $\kappa_e(y)$, $\gamma_e(y)$ respectively and the fuselage deformations defined by $\kappa_{eF}, \kappa_{e0}, \kappa_{eC}, \kappa_{eT}$ at the front fuselage, wing mass axis, aircraft centre of mass/centre fuselage and tailplane respectively. The tailplane modal slope is γ_{eT}.

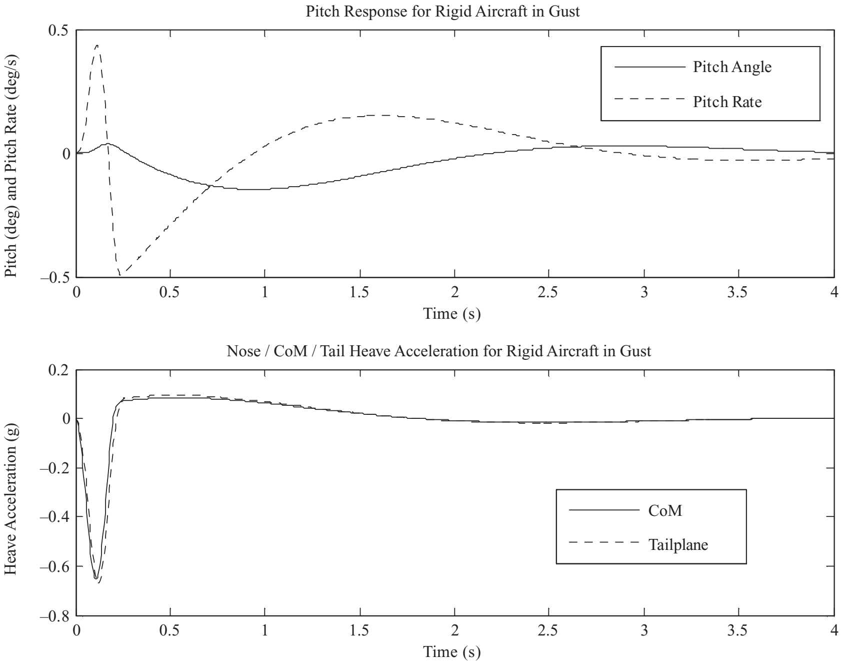

(a) 40 m

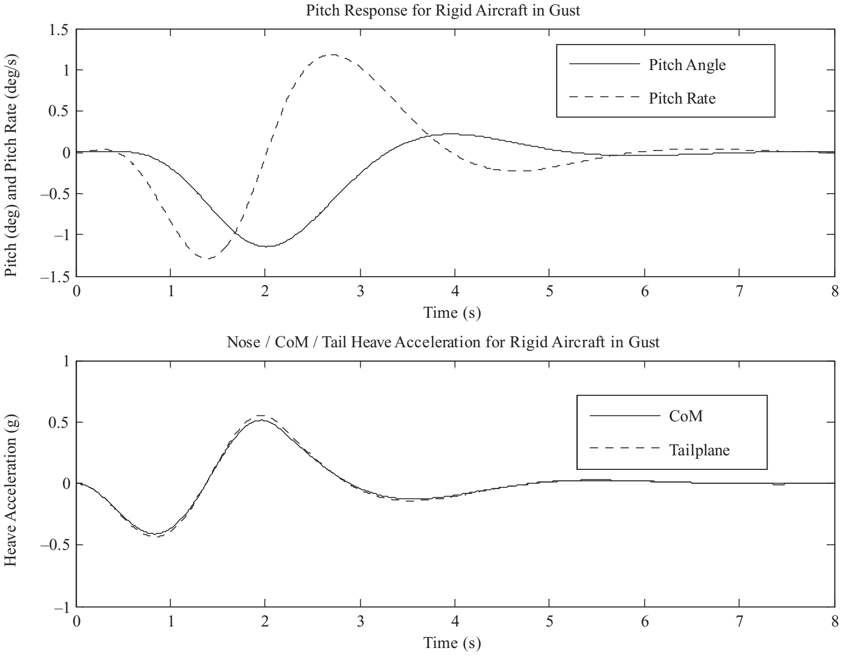

(b) 400 m

Figure 16.12 Response of a rigid aircraft to (a) 40 m and (b) 400 m '1-cosine' gusts – heave/pitch model.

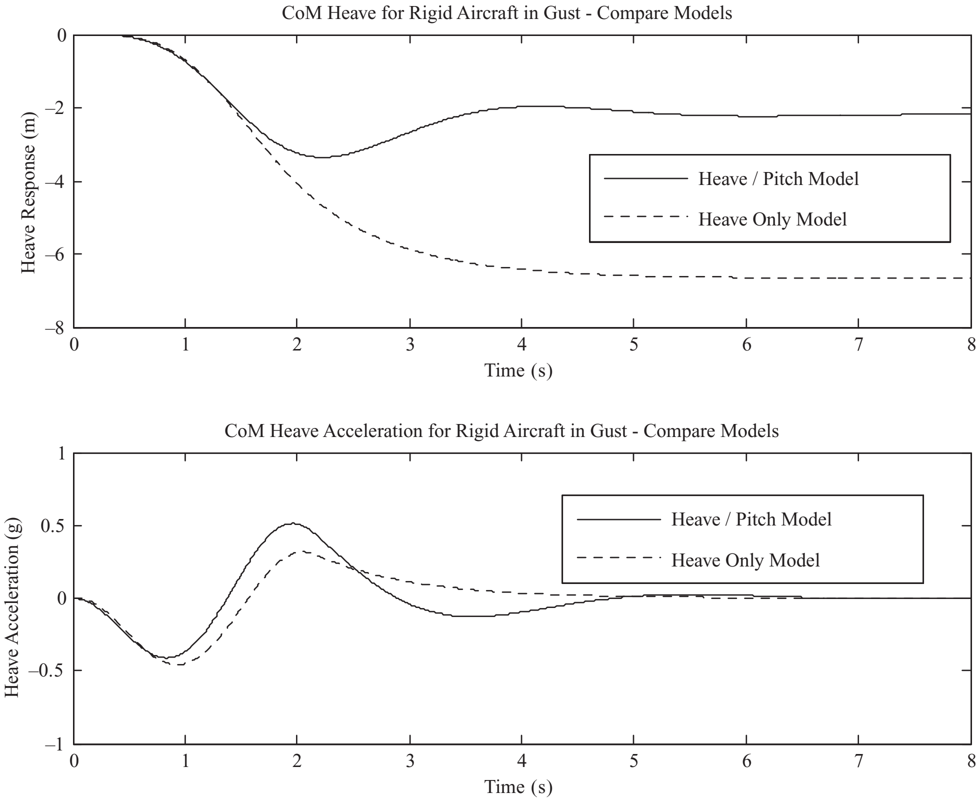

Figure 16.13 Response of a rigid aircraft to the 400 m '1-cosine' gust – comparison of heave only and heave/pitch models.

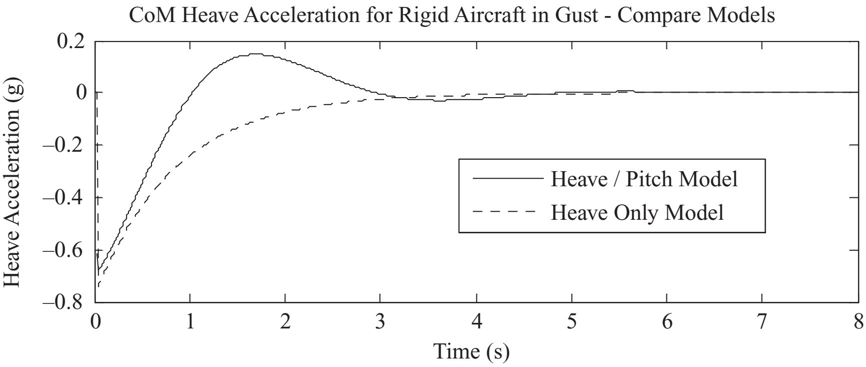

Figure 16.14 Response of a rigid aircraft to the sharp-edged gust – heave only model compared to the heave/pitch model.

16.5.1 Equations of Motion – Flexible Aircraft

In order to save effort and space, the equation of motion for this gust case will simply be written by inspection. Remembering the gust equations for the rigid aircraft and how the flexible mode terms appeared in the equations for the equilibrium and dynamic manoeuvres in Chapters 13 and 15, the equations take the form

$$\left[\begin{array}{cc|c} m & 0 & 0 \\ 0 & I_y & 0 \\ \hline 0 & 0 & m_\mathrm{e} \end{array}\right] \left\{\begin{array}{c} \ddot{z}_\mathrm{C} \\ \ddot{\theta} \\ \hline \ddot{q}_\mathrm{e} \end{array}\right\} + \left\{\left[\begin{array}{cc|c} -Z_{\dot{z}} & -Z_q & -Z_{\dot{\mathrm{e}}} \\ -M_{\dot{z}} & -M_q & -M_{\dot{\mathrm{e}}} \\ \hline -Q_{\dot{z}} & -Q_q & c_\mathrm{e} - Q_{\dot{\mathrm{e}}} \end{array}\right]\right\} \left\{\begin{array}{c} \dot{z}_\mathrm{C} \\ \dot{\theta} \\ \hline \dot{q}_\mathrm{e} \end{array}\right\}$$

$$+ \left\{\left[\begin{array}{cc|c} 0 & -Z_\alpha & -Z_\mathrm{e} \\ 0 & -M_\alpha & -M_\mathrm{e} \\ \hline 0 & -Q_\alpha & k_\mathrm{e} - Q_\mathrm{e} \end{array}\right]\right\} \left\{\begin{array}{c} z_\mathrm{C} \\ \theta \\ \hline q_\mathrm{e} \end{array}\right\} = \left\{\begin{array}{c} Z_\mathrm{gW} \\ M_\mathrm{gW} \\ \hline Q_\mathrm{gW} \end{array}\right\} w_\mathrm{g}(t) + \left\{\begin{array}{c} Z_\mathrm{gT} \\ M_\mathrm{gT} \\ \hline Q_\mathrm{gT} \end{array}\right\} w_\mathrm{g}\left[t - \frac{l}{V}\right]. \qquad (16.29)$$

Flexible derivatives are present as before, and from previous experience the same values are expected as shown in Appendix B for inertial axes.

In this case, there are only two new derivatives that need to be determined, namely those corresponding to the flexible mode generalized force per gust velocity Q_gW, Q_gT. These derivatives require evaluation of the incremental work done for the wing and tailplane lift forces (due to gust velocity) moving through incremental flexible deformations of the mode. The incremental lift force on the wing strip $\mathrm{d}y$ due to wing gust velocity is

$$\Delta l_\mathrm{gW}(y) = \frac{1}{2}\rho V^2 c\,\mathrm{d}y\, a_\mathrm{W} \frac{w_\mathrm{g}(t)}{V} \qquad (16.30)$$

and the effective incremental lift on the tailplane (including downwash effects on the gust velocity at the tailplane) due to tailplane gust velocity is

$$\Delta L_\mathrm{gT} = \frac{1}{2}\rho V^2 S_\mathrm{T} a_\mathrm{T}(1 - k_\varepsilon)\left[\frac{w_\mathrm{g}(t - l/V)}{V}\right]. \qquad (16.31)$$

The corresponding incremental displacements at the wing strip and tailplane aerodynamic centres due to flexible mode deformation will be $(\kappa_\mathrm{e} - l_\mathrm{A}\gamma_\mathrm{e})\delta q_\mathrm{e}$ and $\kappa_\mathrm{eT}\delta q_\mathrm{e}$ (both downwards) respectively. Thus, writing the incremental work done by the lift forces due to the gust moving through the flexible mode displacements, the flexible mode generalized forces due to gust velocity may be obtained and it may be shown that the corresponding flexible mode derivatives are

$$Q_\mathrm{gW} = -\frac{1}{2}\rho V S_\mathrm{W} a_\mathrm{W} J_2, \qquad Q_\mathrm{gT} = -\frac{1}{2}\rho V S_\mathrm{T} a_\mathrm{T} \kappa_\mathrm{eT}(1 - k_\varepsilon), \qquad (16.32)$$

where $J_2 = (1/s)\int_{y=0}^{s} (\kappa_\mathrm{e} - l_\mathrm{A}\gamma_\mathrm{e})\,\mathrm{d}y$ as before. All the derivatives in Equation (16.29) are shown in Appendix B.

The equations of motion in Equation (16.29) will allow the generalized responses to a gust input to be determined and the result may be transformed into the physical response (e.g. acceleration) of the aircraft at any location, depending upon the mode deformation there. Thus, at the tailplane, the downwards acceleration is

$$\ddot{z}_\mathrm{T} = \ddot{z}_\mathrm{C} + l_\mathrm{T}\ddot{\theta} + \kappa_\mathrm{eT}\ddot{q}_\mathrm{e}. \qquad (16.33)$$

The responses may also be used to generate the internal loads as described later in Chapter 18. The equations are in much the same form as those for the heave/pitch rigid aircraft model in Section 16.4 above, but now including aerodynamic terms associated with the flexible mode and also a flexible mode elastic stiffness term. The general form of the time domain equations will be considered later in Section 16.6.

16.5.2 Example: Gust Response in the Time Domain for a Flexible Aircraft

This example uses the same data as in the earlier rigid aircraft example in Section 16.4.2 but additional parameters are specified to cater for idealized flexible effects, namely fuselage mass terms (see Chapter 13 and Appendix C) $m_F = 1500$ kg, $m_C = 4000$ kg, $m_T = 1500$ kg, wing mass/inertia terms $m_W = 2\mu_W s = 3000$ kg, $I_W = 2\chi_W s = 1330$ kg m^2, aircraft pitch moment of inertia $I_y = 144\,000$ kg m^2, and dimensions $s = 7.5$ m, $l_A = 0.25$ m, $l_E = 0.25$ m, $l_{WM} = 0.1$ m and $l_F = 6.8$ m. The modal mass and mode shape parameters for (a) fuselage bending, (b) wing bending and (c) wing twist dominant are shown in Appendix C. Only the vertical '1-cosine' gust will be considered for the flexible aircraft. Again, it should be noted that the natural frequencies are chosen to be artificially low to highlight flexible effects. MATLAB and SIMULINK programs to solve the time domain gust response for this flexible aircraft in heave and pitch are shown in appendix I of the companion website.

Consider firstly the dominant *fuselage bending* mode with a natural frequency of 2 Hz and damping of 4 % for the same flight condition as the rigid aircraft. In Figure 16.15 the pitch rate and CoM accelerations are shown for '1-cosine' gusts of 50, 100, 150 and 200 m lengths. The variation of minimum

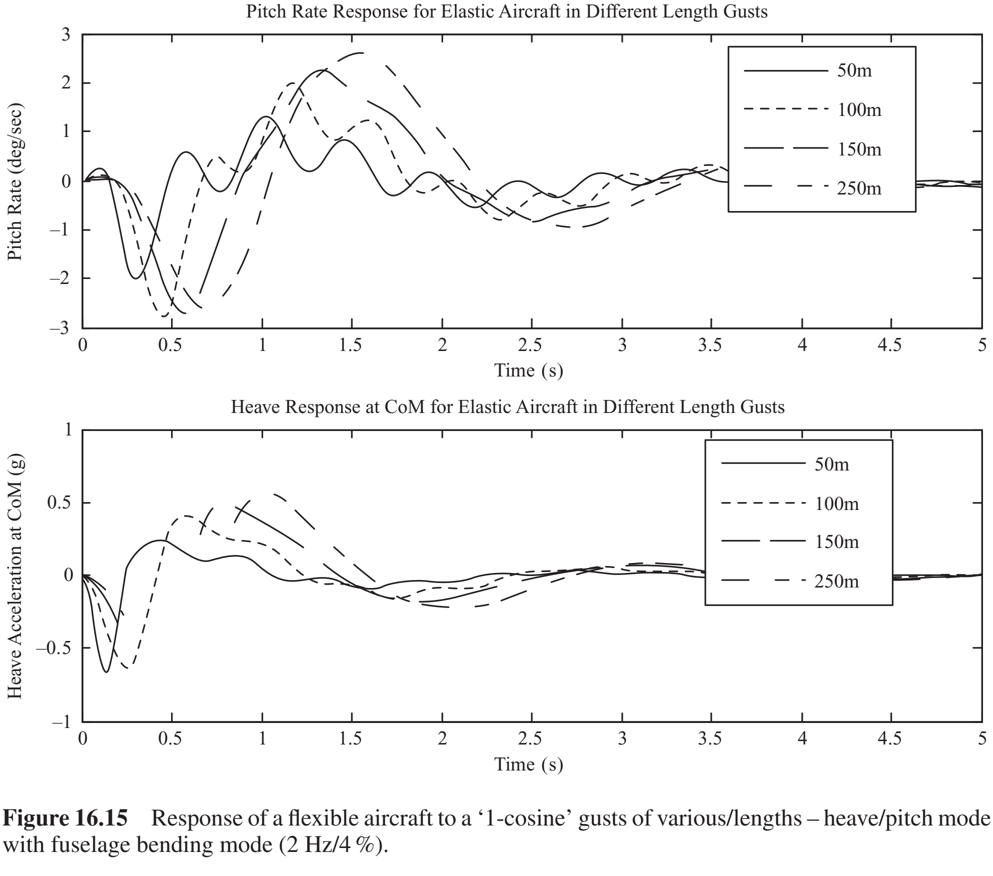

Figure 16.15 Response of a flexible aircraft to a '1-cosine' gusts of various/lengths – heave/pitch mode with fuselage bending mode (2 Hz/4 %).

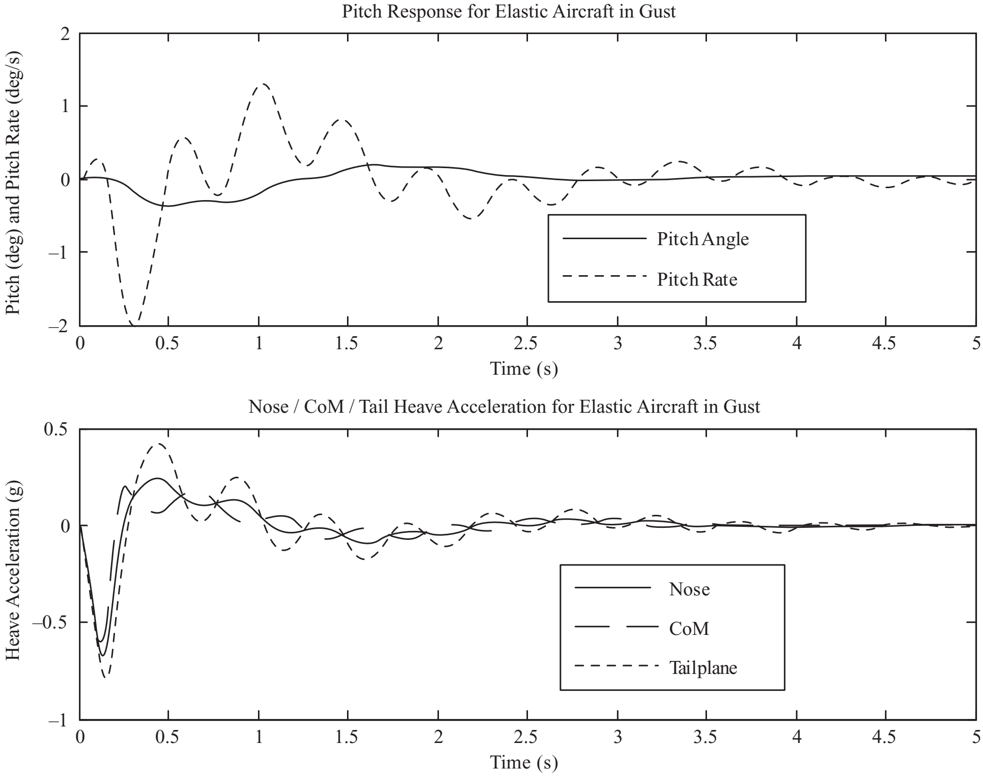

Figure 16.16 Response of a flexible aircraft to a tuned 50 m '1-cosine' gust – heave/pitch model with fuselage bending mode (2 Hz/4 %).

and maximum values of acceleration with gust length was obtained; for the flexible aircraft, the maximum acceleration is around +0.59g for a 225 m gust length, with a minimum of −0.67g for a 50 m gust length. Clearly, the tuned gust length and accelerations have altered when flexible effects are included. The oscillatory modal response is superimposed upon the short period type motion, with the flexible contribution depending on the gust wavelength.

In Figure 16.16, the variations with time of pitch rate, pitch angle and nose/CoM/tailplane accelerations for the 'tuned' 50 m gust length are presented. The presence of the flexible mode may be seen on the pitch rate and particularly on the tailplane and nose accelerations; some of the values are greater than for the rigid aircraft. In any practical case, it is quite possible that a particular internal load may be greater for the flexible case.

Secondly, the dominant *wing bending* case with a flexible mode of frequency 3 Hz and damping 4 % was considered. The acceleration responses to gusts of 20, 40, 60 and 80 m lengths are shown in Figure 16.17. The gust length corresponding to the maximum (negative) acceleration at the CoM ($-0.65g$) was approximately 40 m; the oscillatory response is not very significant on the fuselage, with the behaviour being similar to the rigid aircraft. However, the motion of the wing tip is seen to be dominated by the flexible response, with the maximum wing tip deflection of 108 mm and acceleration of $3.5g$ occurring for a gust in the region of a 40–60 m length.

Finally, the dominant *wing torsion* case with a flexible mode of frequency 9 Hz and damping of 4 % was considered. For a relatively long wavelength gust, there is no real evidence of flexible mode

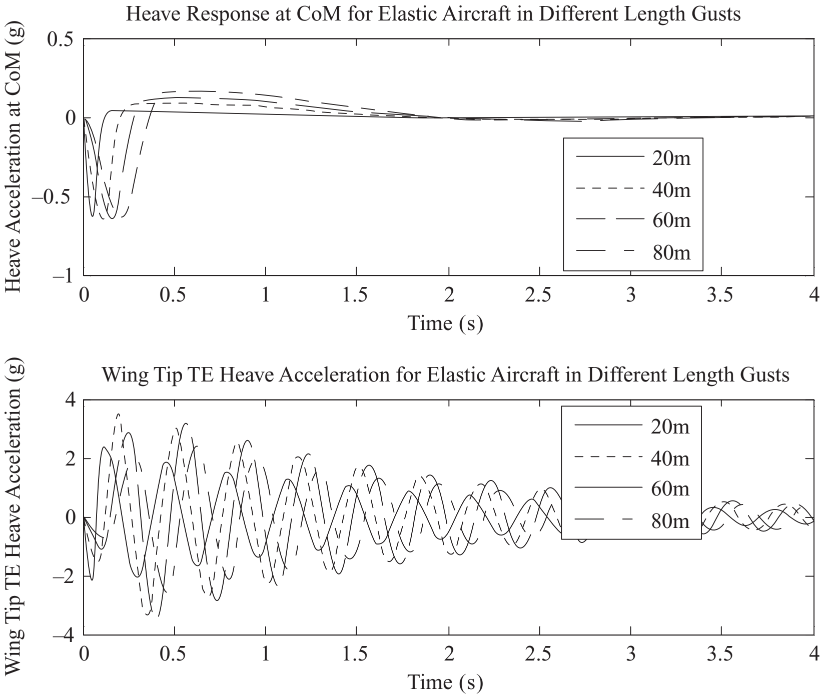

Figure 16.17 Response of a flexible aircraft to a '1-cosine' gust of different lengths – heave/pitch model with wing bending mode (3 Hz/4 %).

oscillations and the behaviour is much the same as for the rigid aircraft. For shorter gusts nearer to the wavelength required to tune the flexible response, there is clear evidence of a flexible mode response. The responses to gust lengths of 10, 20, 35 and 50 m are shown in Figure 16.18. The gust length corresponding to the maximum (negative) acceleration at the CoM ($-0.72g$) was approximately 35 m; the oscillatory response is not very significant on the fuselage, with the behaviour being similar to the rigid aircraft. However, the motion of the wing tip is seen to be dominated by the flexible response, with the maximum wing tip twist of 0.5° and acceleration of $2.88g$ being for a gust in the region of 20 m length. Obviously, the unsteady aerodynamic attenuation effect will be considerable at such a high frequency and will reduce the response levels.

The impact of the flexible mode on gust response clearly depends upon the mode shape, natural frequency and wavelength as well as the response position on the aircraft. Sweep will also affect the gust response, not only because of the coupled wing bending and torsion in the modes but also because of the delayed penetration of the wing tip compared to the root.

16.6 GENERAL FORM OF EQUATIONS IN THE TIME DOMAIN

So far, the examples chosen have deliberately been aimed at introducing different features of gust response calculations in turn. However, in practice all these features will be included together, e.g. realistic gust histories, rigid body plus flexible modes, gust penetration effects, unsteady aerodynamics, etc. In this

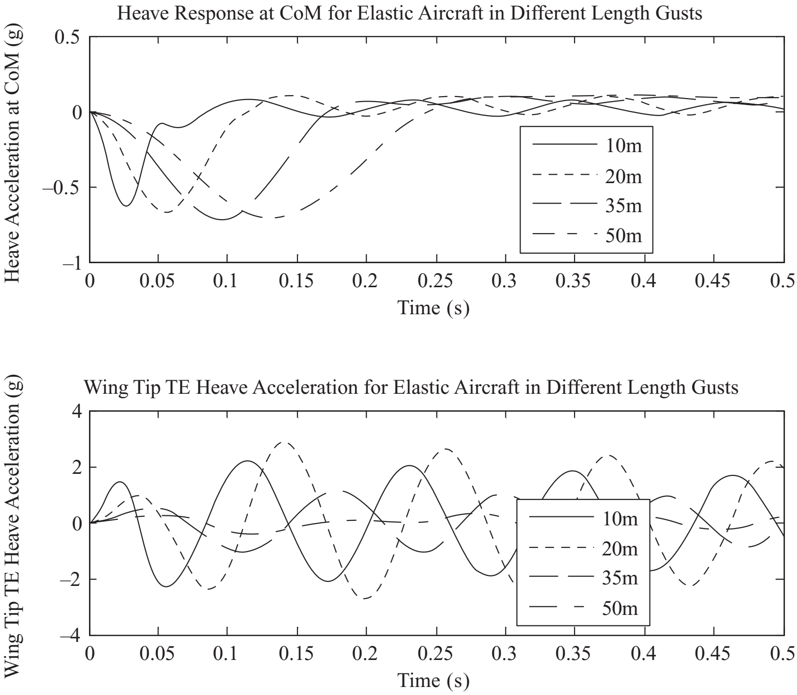

Figure 16.18 Response of a flexible aircraft to '1-cosine' gusts of different lengths – heave/pitch model with wing torsion mode (9 Hz/4 %).

section, a more general expression will be introduced; if the models developed earlier are examined and common features sought, it may be seen that the time domain equations of motion can be written in the general form

$$\mathbf{A}\ddot{\boldsymbol{q}} + \rho V\mathbf{B}\dot{\boldsymbol{q}}^{*}\Phi + \mathbf{E}\mathbf{q} + \rho V^{2}\mathbf{C}\boldsymbol{q}^{*}\Phi = \rho V\boldsymbol{R}_{\mathrm{g}W} w_{\mathrm{g}}(t)^{*}\Psi + \rho V\boldsymbol{R}_{\mathrm{gT}} w_{\mathrm{g}}\left[t - \frac{l}{V}\right]^{*}\Psi, \qquad (16.34)$$

where **q** are generalized coordinates (now both rigid body and flexible modes), **A** is an inertia matrix, **B** and **C** are aerodynamic *response*-dependent matrices, **E** is a structural stiffness matrix (with zero elements corresponding to the rigid body terms) and $\boldsymbol{R}_{\mathrm{gW}}$, $\boldsymbol{R}_{\mathrm{gT}}$ are *gust*-dependent aerodynamic vectors for the wing and tailplane; all these aerodynamic terms are related to the quasi-steady aerodynamic derivatives. The convolutions with Wagner's and Küssner's functions are included to account for unsteady aerodynamic effects. A structural damping matrix **D** may also be introduced if desired.

To examine the response for any general gust time history, for example the '1-cosine' gust, these simultaneous differential equations (16.34) would be solved in the time domain. Nonlinear effects (e.g. FCS) could also be introduced. The equations shown would apply for strip theory type calculations, but if a three-dimensional panel method was used for the unsteady aerodynamics, then both the response and gust dependent aerodynamic terms would be a function of reduced frequency and the results could be expressed in a time domain state space representation using the rational fraction approximation approach (see Chapter 20).

16.7 TURBULENCE RESPONSE IN THE FREQUENCY DOMAIN

So far the response to discrete gusts has been calculated in the *time domain*, normally by numerical integration of the equations of motion. However, the treatment of random continuous turbulence usually requires calculations to be performed in the *frequency domain* using a power spectral density (PSD) approach; this is because the continuous turbulence input is defined via its PSD. The relationship between the PSD of response and excitation for a system was introduced in Chapter 1; the response PSD will yield statistical information about the resulting responses, loads and stresses. In order to determine the PSD of the response to continuous turbulence, the gust response must be considered in the frequency domain and the frequency response functions (FRFs) (see Chapters 1 and 2) of responses to harmonic gusts generated at different frequencies. Therefore the time domain equations need to be transformed into the frequency domain.

Because frequency domain analysis is a linear approach, it is important to recognize that any nonlinearity of the aircraft (e.g. via the FCS) will have to be linearized in some way, leading to an approximation in the predicted response. An alternative approach, that permits nonlinear effects to be included, is to generate a random time signal with the required spectral characteristics to represent the turbulence and then to calculate the response directly in the time domain; this methodology will be considered briefly in Chapter 24.

In the remainder of this chapter, the basic ideas underpinning spectral gust analysis are illustrated for both quasi-steady and unsteady response and gust-dependent aerodynamics. The methodology will initially be based on the heave only model and then extended to the heave/pitch rigid and flexible aircraft cases. This exercise will also allow the equations of motion to be developed in a general form.

16.7.1 Definition of Continuous Turbulence

Continuous turbulence is represented by a random variation in velocity of the air normal to (or sometimes along) the flight path of the aircraft, where the random variable is assumed to have a Gaussian distribution with zero mean and is represented by a gust PSD $\Phi_{gg}(\Omega)$ with units of $(\mathrm{m/s})^2$ / (rad/m); a commonly used spectrum that matches experimentally observed data is that according to Von Karman (Fung, 1969; Hoblit, 1988; CS-25), namely

$$\Phi_{gg}(\Omega) = \sigma_g^2 \frac{L}{\pi} \frac{1 + (8/3)(1.339\Omega L)^2}{[1 + (1.339\Omega L)^2]^{11/6}} \tag{16.35}$$

where $\Omega = \omega / V$ is the scaled frequency (rad/m), σ_g is the root-mean-square turbulence velocity (m/s TAS) and V is the flight speed (m/s TAS). L is the characteristic scale wavelength of the turbulence (typically 762 m, but usually quoted in ft, namely 2500 ft) that dictates the variation of the PSD with frequency. Calculations are usually carried out for a turbulence velocity of 1 m/s root-mean-square and then results factored for the design turbulence velocities specified in CS-25 at the particular flight condition considered. It should be noted that the area under the PSD $\Phi_{gg}(\Omega)$ is equal to the mean square of the turbulence σ_g^2 and so the root-mean-square value σ_g is the square root of the area (see Chapter 1). For turbulence analysis, the PSD is defined as a one-sided spectrum so only a positive frequency axis is relevant.

The variation of the turbulence velocity PSD with scaled frequency for a root-mean-square turbulence velocity of 1 m/s and a scale length of 2500 ft is shown in Figure 16.19. Note that use of the scaled frequency means that the graph is independent of aircraft velocity. The area under this curve is 1 $(\mathrm{m/s})^2$; this is the mean square value of the turbulence velocity, so confirming that the root-mean-square value is 1 m/s.

The PSD may be expressed in terms of frequency (Hz) instead of rad/m by replacing L/π in Equation (16.35) with $2L/V$; the PSD units would then be $(\mathrm{m/s})^2$ / Hz and the frequency axis would be in Hz. The example given later in this chapter will use these dimensional units. Care needs to be taken, when

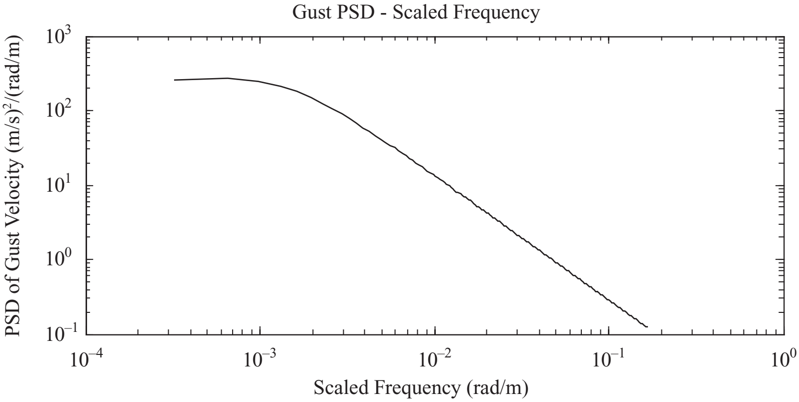

Figure 16.19 Von Karman turbulence PSD in terms of scaled frequency – turbulence velocity of 1 m/s root-mean-square and scale length of 2500 ft.

determining the root-mean-square value from the area under the PSD, that the correct combination of units is used.

16.7.2 Definition of a Harmonic Gust

The frequency domain approach requires a harmonic gust to be defined in order to perform the PSD analysis and process each frequency value separately (the idea was introduced earlier in Chapter 10). Consider a harmonic gust of amplitude w_{g0} and wavelength λ_g, defined spatially by the expression

$$w_g(x_g) = w_{g0} \sin \frac{2\pi x_g}{\lambda_g}, \tag{16.36}$$

as shown in Figure 16.20. Since $x_g = Vt$ then the spatial variation of gust velocity at the wing may be transformed into a temporal variation at frequency $\omega = 2\pi V/\lambda_g$ rad/s, namely

$$w_g(t) = w_{g0} \sin \frac{2\pi V}{\lambda_g} t = w_{g0} \sin \omega t = w_{g0} \exp(i\omega t). \tag{16.37}$$

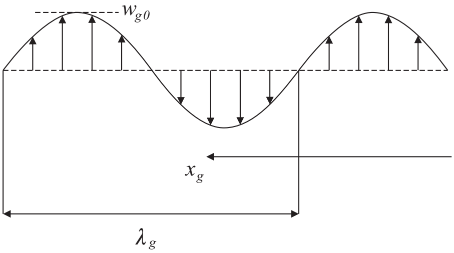

Figure 16.20 Harmonic gust.

Here a complex algebra approach has been used, as introduced in Chapter 1. In order to include the penetration delay for the tailplane, the tailplane gust velocity must also be written in complex algebra form but using a phase lag to account for the delay; therefore at the tailplane

$$w_{\mathrm{g}}\left(t-\frac{l}{V}\right)=w_{\mathrm{g}0}\sin\frac{2\pi V}{\lambda_{\mathrm{g}}}\left(t-\frac{l}{V}\right)=w_{\mathrm{g}0}\sin\left(\omega t-\frac{\omega l}{V}\right)=w_{\mathrm{g}0}\exp\left(\mathrm{i}\omega t-\frac{\omega l}{V}\right). \qquad (16.38)$$

The response at the gust excitation frequency may now be obtained, as illustrated in Chapters 1 and 2.

16.7.3 FRFs for Response per Gust Velocity

To determine the PSD of a response, knowing the PSD of turbulence from Section 16.7.1, the FRF between the response and the gust velocity is needed. For a particular response term (r), the FRF per gust velocity is $H_{\mathrm{rg}}(\omega)$ and this is determined using a complex algebra approach as shown in Chapters 1 and 2. It should be noted that the approach to analysis of a 'response' may also be applied to internal loads.

16.7.4 PSD of Response to Continuous Turbulence

The Von Karman continuous turbulence PSD $\Phi_{\mathrm{gg}}(\omega)$ was defined in Equation (16.35). Thus the PSD $\Phi_{\mathrm{rr}}(\omega)$ of a general response (or internal load/stress) component (r) may be found by the approach introduced in Chapter 1 (and Chapter 2 for multiple degrees of freedom), so

$$\Phi_{\mathrm{rr}}(\omega)=\left|H_{\mathrm{rg}}(\omega)\right|^2\ \Phi_{\mathrm{gg}}(\omega), \qquad (16.39)$$

where this expression only applies for a single response parameter. It is important that care be taken with units; e.g. if the turbulence PSD has units of $(\mathrm{m/s})^2/\mathrm{Hz}$, the acceleration per turbulence velocity FRF has units of $g/(\mathrm{m/s})$ and the acceleration response PSD will have units of $(g)^2/\mathrm{Hz}$. Therefore a simple frequency by frequency multiplication of the modulus squared value of the relevant FRF and the turbulence PSD will yield the response PSD. The root-mean-square value of the response σ_{r} may then be found from the square root of the area under the response PSD curve such that

$$\sigma_{\mathrm{r}}=\sqrt{\int_0^{\omega_{\max}}\Phi_{\mathrm{rr}}(\omega)\,\mathrm{d}\omega}, \qquad (16.40)$$

where $\omega_{\max}$ is the maximum frequency for which the one-sided PSD data are generated. Alternatively, the scaled frequency form of the PSDs may be used. Examples of calculating PSDs and root-mean-square values for responses such as acceleration will be given later in this chapter, but transformation from response to load PSDs is considered in Chapter 18.

16.7.5 Limit Load Definition for Turbulence

In the continuous turbulence design criteria in the certification specifications (CS-25), the following quantity is defined when loads are being considered, namely

$$\bar{A}=\frac{\sigma_{\mathrm{r}}}{\sigma_{\mathrm{g}}}. \qquad (16.41)$$

This is the ratio of the root-mean-square incremental load quantity (e.g. internal load) to the root-mean-square turbulence velocity (in TAS). Any particular limit load (e.g. wing root shear force) may be written in terms of the corresponding steady 1g load (prior to encountering the turbulence) and the turbulence contribution as follows:

$$P_{\text{Limit}} = P_{1g} \pm U_\sigma \bar{A}, \tag{16.42}$$

where U_σ is the limit turbulence intensity (in TAS), a function of air speed and altitude, specified in the certification specifications (see Chapter 24). The calculation of $\bar{A}$ requires load to gust FRFs and these are considered in Chapter 18. Further comments on loads and loads processing are made in Chapter 24.

16.8 FREQUENCY DOMAIN TURBULENCE RESPONSE – RIGID AIRCRAFT IN HEAVE

In this section, the determination of FRFs of response per gust velocity will be considered for the rigid aircraft in heave with quasi-steady and unsteady aerodynamics. The method for determining the FRF of response per gust velocity is illustrated and examples shown.

16.8.1 FRF for Rigid Aircraft Response in Heave per Gust Velocity – Quasi-Steady Aerodynamics

The approach to obtaining an FRF between response and gust velocity will be first illustrated using the simple rigid aircraft in heave with quasi-steady aerodynamics, as considered earlier in Section 16.3.1. The methodology based in the frequency domain is introduced in Chapter 1. Because the quasi-steady assumption requires the lift forces to depend on the instantaneous gust velocity, then the equation of motion for the sharp-edged gust may be revised in terms of a harmonic gust input as

$$m\ddot{z}_{\text{C}} + \Delta L_z(t) = -\Delta L_{\text{g}}(t)$$

or

$$m\ddot{z}_{\text{C}} + \frac{1}{2}\rho V S_{\text{W}} a\, \dot{z}_{\text{C}} = -\frac{1}{2}\rho V S_{\text{W}} a\, w_{\text{g}0} \mathrm{e}^{\mathrm{i}\omega t}, \tag{16.43}$$

where ΔL_z, ΔL_{g} are the response- and gust-dependent lift forces. It is now assumed that the steady-state response to the harmonic gust defined in Equation (16.37) is given by

$$z_{\text{C}}(t) = \tilde{z}_{\text{C}} \mathrm{e}^{\mathrm{i}\omega t}, \tag{16.44}$$

where $\sim$ indicates a complex quantity (i.e. including phase information), as introduced in Chapter 1. Also, the lower case is used for frequency domain amplitude to avoid possible confusion with other symbols (in particular the aerodynamic derivatives). The steady-state response- and gust-dependent lift forces are given by

$$\Delta L_z(t) = \Delta \tilde{L}_z \mathrm{e}^{\mathrm{i}\omega t}, \qquad \Delta L_{\text{g}}(t) = \Delta \tilde{L}_{\text{g}} \mathrm{e}^{\mathrm{i}\omega t}, \tag{16.45}$$

where $\tilde{\Delta} L_z$, $\tilde{\Delta} L_{\text{g}}$ are the complex amplitudes of the relevant lift forces. Then substituting for $z_{\text{C}}(t)$, $\Delta L_z(t)$ and $\Delta L_{\text{g}}(t)$ in Equation (16.43), cancelling out the $\mathrm{e}^{\mathrm{i}\omega t}$ term and simplifying yields the frequency domain expression

$$\left(-\omega^2 m + \mathrm{i}\omega \times \frac{1}{2}\rho V S_{\text{W}} a\right) \tilde{z}_{\text{C}} = -\Delta \tilde{L}_{\text{g}} = -\frac{1}{2}\rho V S_{\text{W}} a w_{\text{g}0}, \tag{16.46}$$

where it may be noted that the quasi-steady gust-dependent lift force amplitude is in-phase with the gust velocity. Hence, rearranging Equation (16.46) yields

$$H_{zg}(\omega) = \frac{\tilde{z}_{\mathrm{C}}}{w_{\mathrm{g0}}} = \frac{-\frac{1}{2}\rho V S_{\mathrm{W}} a}{-\omega^2 m + \mathrm{i}\omega \frac{1}{2}\rho V S_{\mathrm{W}} a}, \tag{16.47}$$

where $H_{zg}(\omega)$ is the frequency response function (FRF) at frequency ω between the (downwards) heave response and the (upwards) gust velocity. This process effectively allows the FRF to be determined over a suitable range of frequencies; only amplitude data are required as use of the modulus squared FRF eliminates phase. The equivalent acceleration FRF result would be obtained by multiplying by $-\omega^2$.

16.8.2 Unsteady Aerodynamic Effects in the Frequency Domain

The analysis in Section 16.8.1 obtained the response of a simple rigid aircraft to a harmonic gust using *quasi-steady* aerodynamic effects. To include *unsteady* aerodynamic effects for the *response dependent* aerodynamics in the frequency domain will involve using Theodorsen's function. However, the *gust-dependent* unsteady aerodynamics will require a frequency domain version of Küssner's function to be used, namely Sears' function (Fung, 1969), somewhat analogous to the relationship between Wagner's and Theodorsen's functions. All these functions were described earlier in Chapter 10.

Consider the aircraft wing 'immersed' in a harmonic gust as shown in Figure 16.20. It may be shown (Fung, 1969) that the attenuation and phase lag associated with a wing moving through a harmonic gust can be allowed for by employing Sears' function $\phi(k)$, a complex function of the reduced frequency $k = \omega c/(2V)$, introduced in Chapter 10. Sears' function is actually very similar to Theodorsen's function at small reduced frequencies. The effect of using unsteady aerodynamics on the *gust-dependent* lift in the frequency domain is to multiply the lift term shown in Equation (16.46) by the complex Sears' function, so

$$\tilde{\Delta} L_{\mathrm{Wg}} = \frac{1}{2}\rho V S_{\mathrm{W}} a w_{\mathrm{g0}}\, \phi(k) = \frac{1}{2}\rho V S_{\mathrm{W}} a w_{\mathrm{g0}}\, \phi\left(\frac{\omega c}{2V}\right). \tag{16.48}$$

This is because convolution in the time domain is equivalent to multiplication in the frequency domain (see Chapter 1). Sears' function attenuates the lift force and introduces a phase lag, both accounting for the gust dependent unsteady aerodynamic effects, which become more significant as the frequency increases. An approximate expression for Sears' function is included in Chapter 10.

In a similar way, Theodorsen's function $C(k)$ may be introduced to account for unsteady aerodynamic effects on the *response dependent* lift in the frequency domain, so

$$\tilde{\Delta} L_z = \frac{1}{2}\rho V S_{\mathrm{W}} a\ \mathrm{i}\omega \tilde{z}_{\mathrm{C}}\ C\left(\frac{\omega c}{2V}\right), \tag{16.49}$$

where again multiplication has replaced convolution.

Theodorsen's and Sears' functions would only be used for large commercial aircraft if strip theory were to be employed (see Chapter 22). More commonly, unsteady aerodynamic computations based on three-dimensional panel methods (e.g. the doublet lattice method; see Chapters 19 and 20) are employed and in effect Theodorsen's and Sears' effects are automatically embedded in the complex aerodynamic influence coefficient (AIC) matrices. These functions are covered in this book to assist in understanding the effect of unsteady aerodynamics, because strip theory type approaches are still used sometimes and also for historical reasons.

16.8.3 FRF for Rigid Aircraft Response in Heave per Gust Velocity – Unsteady Aerodynamics

The FRF between response and gust velocity for a harmonic gust at frequency ω was obtained in Section 16.8.1 using quasi-steady aerodynamics. Because the unsteady gust- and response-dependent aerodynamic effects may be introduced in the frequency domain by a multiplication process, as shown in the previous section, the corresponding FRF may be written by inspection of Equations (16.43), (16.48) and (16.49) as

$$H_{zg}(\omega) = \frac{\tilde{z}_{\mathrm{C}}}{w_{\mathrm{g0}}} = \frac{-\frac{1}{2}\rho V S_{\mathrm{W}} a}{-\omega^2 m + \mathrm{i}\omega \times \frac{1}{2}\rho V S_{\mathrm{W}} a \; C[\omega c/(2V)]}\phi\left(\frac{\omega c}{2V}\right), \tag{16.50}$$

where $C(k)$ and $\phi(k)$ are Theodorsen's and Sears' functions respectively. Thus the aerodynamic attenuation and phase shift are directly applied to the FRF, rather like a filter. The attenuation introduced at each reduced frequency may be seen from the plot of the magnitudes of Theodorsen's and Sears' functions in Chapter 10.

16.8.4 Example: FRF for Rigid Aircraft in Heave for Quasi-Steady and Unsteady Aerodynamics

The FRF between the example aircraft heave response acceleration and gust velocity is plotted in Figure 16.21, both for the quasi-steady case and when attenuated by Sears' function to show unsteady gust-dependent aerodynamic effects. The effect on the higher frequency response (such as for flexible modes) will be important, especially given that the amplitude of the FRF is squared when calculating the response PSD. A similar process using Theodorsen's function allows response dependent unsteady aerodynamics to be seen.

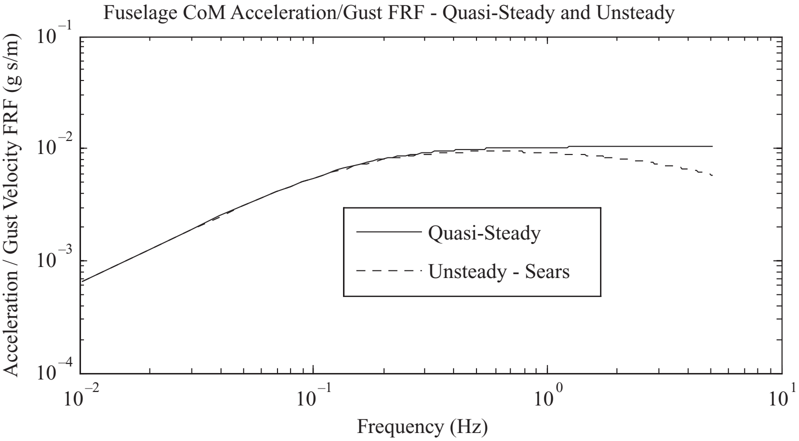

Figure 16.21 FRF for heave acceleration per gust velocity – quasi-steady and unsteady gust dependent aerodynamics.

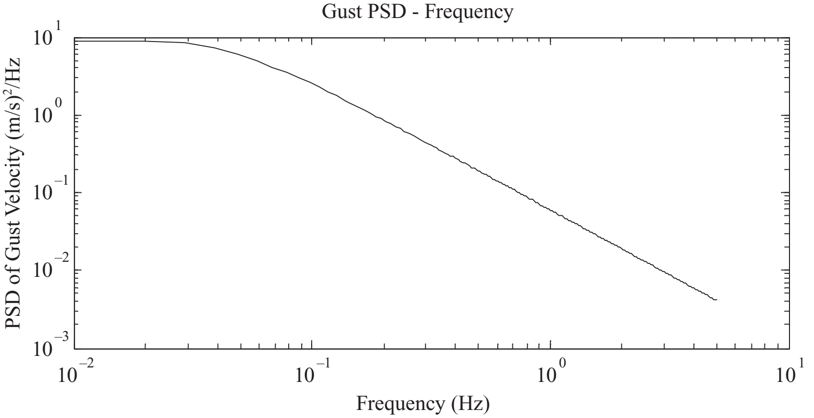

Figure 16.22 Von Karman turbulence PSD in terms of frequency – turbulence velocity of 1 m/s root-mean-square and scale length of 2500 ft.

16.8.5 Example: Turbulence Response in the Frequency Domain for a Rigid Aircraft in Heave

In Section 16.8.1, the determination of FRFs between response and gust velocity was considered. Given the turbulence PSD, the response PSD can be evaluated using the analysis outlined in Section 16.7. In this section, an example showing the FRFs and PSDs for acceleration response quantities will be shown for the rigid aircraft in heave.

For the examples here and in the remainder of this chapter, the Von Karman turbulence PSD is employed with a scale length of 2500 ft and a reference root-mean-square turbulence velocity of 1 m/s; results for design turbulence velocities may be obtained later by simple scaling. The aircraft is flying at 150 m/s EAS at 14 000 ft ($\sqrt{\sigma} \approx 0.8$). The turbulence PSD is shown in Figure 16.22 plotted against frequency in Hz, so the units are in (m/s)^2/Hz. Note that the graphical results would look different if presented in terms of scaled frequency (see Figure 16.19) but the final root-mean-square values of response should of course be the same. The graphs are mostly presented in log–log format, allowing the low frequency behaviour to be seen more clearly.

For the rigid aircraft considered earlier, using the heave only model with quasi-steady aerodynamics, the modulus squared FRF relating CoM acceleration to gust velocity, namely $\left|H_{zg}(\omega)\right|^2$, is shown as a function of frequency (Hz) in Figure 16.23. The acceleration response PSD (g^2/Hz) is then found by multiplying the squared FRF by the gust velocity PSD; the result is also shown in Figure 16.23. The effect of the roll-off in the turbulence velocity PSD may be seen by comparing the two curves. The root-mean-square value of the CoM acceleration is $0.056g$, found from the square root of the area under the acceleration PSD curve. The peak of the acceleration PSD occurs at around 0.1 Hz.

16.9 FREQUENCY DOMAIN TURBULENCE RESPONSE – RIGID AIRCRAFT IN HEAVE/PITCH

So far, the frequency domain analysis has been restricted to the rigid aircraft in heave alone. However, in practice the aircraft will have a tailplane and experience pitch due to the penetration effect, so the desired FRFs would need to be extracted from the heave and pitch equations. Only quasi-steady aerodynamics will be considered here though unsteady effects could be incorporated.

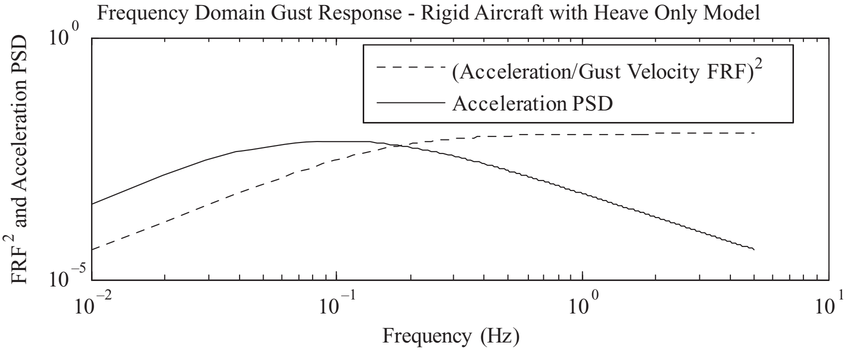

Figure 16.23 Frequency domain gust results for a rigid aircraft heave only model: (CoM acceleration / Gust Velocity FRF)^2 and CoM acceleration PSD.

16.9.1 FRF for Rigid Aircraft Response in Heave/Pitch per Gust Velocity

In order to illustrate the idea, consider the earlier example of the rigid aircraft in heave/pitch in Section 16.4. The key time domain equation is (16.27) and if a harmonic gust input is considered, then the steady-state responses can be written in exponential form as

$$z_{\mathrm{C}} = \tilde{z}_{\mathrm{C}} \mathrm{e}^{\mathrm{i}\omega t}, \qquad \theta = \tilde{\theta} \mathrm{e}^{\mathrm{i}\omega t}. \tag{16.51}$$

If the time domain equation is transformed into the frequency domain by using the complex algebra approach employed in Chapters 1 and 2, then using the expressions for the harmonic gust velocity in Equations (16.37) and (16.38), it may be shown that

$$\begin{aligned} &\left\{ -\omega^2 \begin{bmatrix} m & 0 \\ 0 & I_y \end{bmatrix} + \mathrm{i}\omega \begin{bmatrix} -Z_{\dot{z}} & -Z_q \\ -M_{\dot{z}} & -M_q \end{bmatrix} + \begin{bmatrix} 0 & -Z_\alpha \\ 0 & -M_\alpha \end{bmatrix} \right\} \begin{Bmatrix} \tilde{z}_{\mathrm{C}} \\ \tilde{\theta} \end{Bmatrix} \\ &= \begin{Bmatrix} Z_{\mathrm{gW}} \\ M_{\mathrm{gW}} \end{Bmatrix} w_{\mathrm{g0}} + \begin{Bmatrix} Z_{\mathrm{gT}} \\ M_{\mathrm{gT}} \end{Bmatrix} w_{\mathrm{g0}} \mathrm{e}^{-\frac{\omega l}{V}}, \end{aligned} \tag{16.52}$$

where the delay due to the penetration effect is accounted for using the phase lag term for the tailplane. Then, solving these simultaneous equations for the harmonic response amplitudes in terms of the system dynamics and the turbulence velocity amplitude leads to the expression

$$\begin{aligned} \tilde{\boldsymbol{q}} = \begin{Bmatrix} \tilde{z}_{\mathrm{C}} \\ \tilde{\theta} \end{Bmatrix} = &\left[-\omega^2 \begin{bmatrix} m & 0 \\ 0 & I_y \end{bmatrix} + \mathrm{i}\omega \begin{bmatrix} -Z_{\dot{z}} & -Z_q \\ -M_{\dot{z}} & -M_q \end{bmatrix} + \begin{bmatrix} 0 & -Z_\alpha \\ 0 & -M_\alpha \end{bmatrix} \right]^{-1} \\ &\left\{ \begin{Bmatrix} Z_{\mathrm{gW}} \\ M_{\mathrm{gW}} \end{Bmatrix} + \begin{Bmatrix} Z_{\mathrm{gT}} \\ M_{\mathrm{gT}} \end{Bmatrix} \exp\left(-\frac{\omega l}{V} \right) \right\} w_{\mathrm{g0}} = \boldsymbol{H}_{q\mathrm{g}} w_{\mathrm{g0}}, \end{aligned} \tag{16.53}$$

where $\boldsymbol{H}_{q\mathrm{g}}$ is the vector of FRFs between the two generalized responses and the gust velocity. Then, using Equation (16.33) as an example of obtaining the physical response from the generalized responses above, the relationship between the tailplane harmonic displacement response and the gust velocity may be found and converted to acceleration by multiplying by $-\omega^2$, so

$$\tilde{z}_{\mathrm{T\,Acc}} = -\omega^2 \left\{ 1 \quad l_{\mathrm{T}} \right\} \boldsymbol{H}_{q\mathrm{g}} w_{\mathrm{g0}} = H_{\mathrm{T\,Acc\,g}} w_{\mathrm{g0}}. \tag{16.54}$$

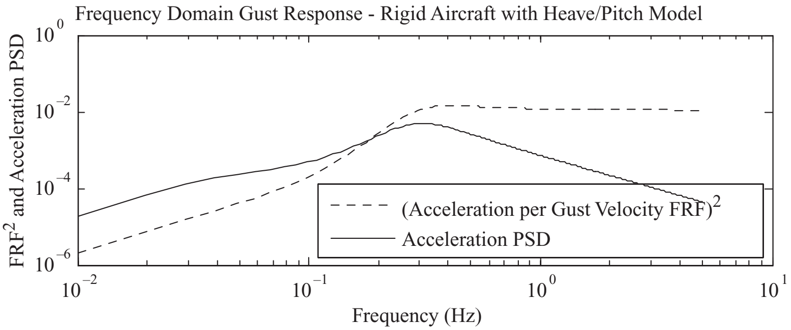

Figure 16.24 Frequency domain gust results for a rigid aircraft heave/pitch model: (CoM acceleration/gust velocity FRF)^2 and CoM Acceleration PSD.

This acceleration FRF $H_{\mathrm{T\,Acc\,g}}$ will show a peak for the short period mode. An example is shown in Section 16.9.2. MATLAB code for this frequency domain calculation is included in appendix I. Unsteady aerodynamics effects could be allowed for simply by multiplying relevant derivatives by Theodorsen's and Sears' functions.

16.9.2 Example: Turbulence Response in the Frequency Domain for a Rigid Aircraft in Heave/Pitch

Here, the rigid aircraft heave/pitch model from the time domain study is used. The FRF modulus squared for CoM acceleration per gust velocity is shown as a function of frequency (Hz) in Figure 16.24. The corresponding acceleration response PSD (g^2/Hz) is also shown in Figure 16.24. The root-mean-square value of the CoM acceleration is $0.051g$, close to that of $0.056g$ for the heave only model. The acceleration PSDs for the CoM and tailplane are similar for the rigid aircraft, with the tailplane root-mean-square value being $0.053g$. The peak of the acceleration PSD corresponds to the short period mode and occurs around 0.3 Hz for this flight condition.

Finally, the heave/pitch and heave only models are compared in terms of acceleration PSDs in Figure 16.25; although the root-mean-square values are fairly similar, the results look rather different for the logarithmic axes. The major difference between the two results occurs below 0.3 Hz. Note that some

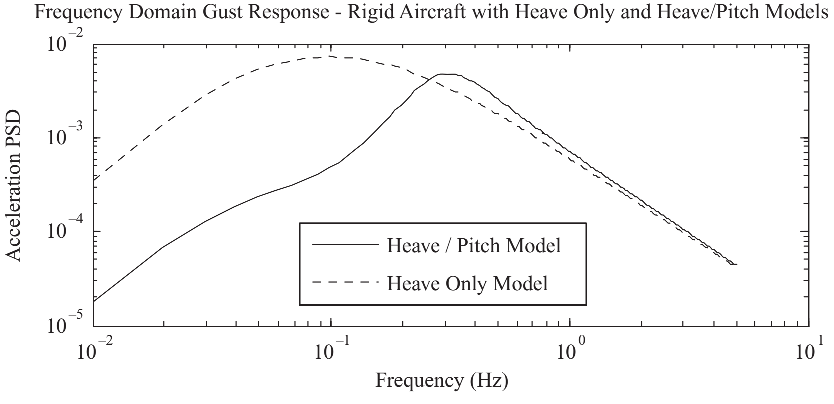

Figure 16.25 Comparison of frequency domain gust results for rigid aircraft heave only and heave/pitch models: CoM acceleration PSD.

sample results are shown in (Hoblit, 1988) for different nondimensional parameters and it is pointed out that the heave only case displays a 'short period' type peak, but of course this is not a mode.

16.10 FREQUENCY DOMAIN TURBULENCE RESPONSE – FLEXIBLE AIRCRAFT

So far, the frequency domain analysis has been restricted to the rigid aircraft in heave/pitch alone. However, in practice the aircraft will be flexible. The flexible aircraft result will simply be quoted, being obtained by inspection of the rigid aircraft results and analysis in earlier chapters.

16.10.1 FRF for Flexible Aircraft Response in Heave/Pitch per Gust Velocity

Consider the earlier example of a flexible aircraft in Section 16.5; the behaviour of the rigid aircraft in heave/pitch may then be seen by inspection. If a harmonic gust input is considered, then the responses can be written as

$$z_{\mathrm{C}} = \tilde{z}_{\mathrm{C}} \mathrm{e}^{\mathrm{i}\omega t}, \qquad \theta = \tilde{\theta} \mathrm{e}^{\mathrm{i}\omega t}, \qquad q_{\mathrm{e}} = \tilde{q}_{\mathrm{e}} \mathrm{e}^{\mathrm{i}\omega t}, \tag{16.55}$$

where $\tilde{q}_{\mathrm{e}}$ is used instead of $\tilde{Q}_{\mathrm{e}}$ to avoid confusion with the flexible derivative Q_{e}. If the time domain equation (16.29) is transformed into the frequency domain by using the complex algebra approach employed in Chapters 1 and 2, then using the expressions for the harmonic gust velocity in Equations (16.37) and (16.38), it may be shown that the final expression equivalent to Equation (16.53) is

$$\tilde{\boldsymbol{q}} = \left\{ \begin{array}{c} \tilde{z}_{\mathrm{C}} \\ \tilde{\theta} \\ \hline \tilde{q}_{\mathrm{e}} \end{array} \right\} = \left[-\omega^2 \left[\begin{array}{cc|c} m & 0 & 0 \\ 0 & I_y & 0 \\ \hline 0 & 0 & m_{\mathrm{e}} \end{array} \right] + \mathrm{i}\omega \left[\begin{array}{cc|c} -Z_{\dot{z}} & -Z_q & -Z_{\dot{\mathrm{e}}} \\ -M_{\dot{z}} & -M_q & -M_{\dot{\mathrm{e}}} \\ \hline -Q_{\dot{z}} & -Q_q & c_{\mathrm{e}} - Q_{\dot{\mathrm{e}}} \end{array} \right] + \left[\begin{array}{cc|c} 0 & -Z_\alpha & -Z_{\mathrm{e}} \\ 0 & -M_\alpha & -M_{\mathrm{e}} \\ \hline 0 & -Q_\alpha & k_{\mathrm{e}} - Q_{\mathrm{e}} \end{array} \right] \right]^{-1}$$

$$\times \left\{ \left\{ \begin{array}{c} Z_{\mathrm{gW}} \\ M_{\mathrm{gW}} \\ \hline Q_{\mathrm{gW}} \end{array} \right\} + \left\{ \begin{array}{c} Z_{\mathrm{gT}} \\ M_{\mathrm{gT}} \\ \hline Q_{\mathrm{gT}} \end{array} \right\} \exp\left(-\frac{\omega l}{\mathrm{V}} \right) \right\} w_{\mathrm{g0}} = \boldsymbol{H}_{q\mathrm{g}} w_{\mathrm{g0}}, \tag{16.56}$$

where $\boldsymbol{H}_{q\mathrm{g}}$ is the vector of FRFs between the three generalized responses and the gust velocity. Then, using Equation (16.33) as an example of obtaining the physical response from the generalized responses above, the relationship between the tailplane harmonic acceleration and the gust velocity will be

$$\tilde{z}_{\mathrm{T\,Acc}} = -\omega^2 \left\{ 1 \quad l_{\mathrm{T}} \quad \kappa_{\mathrm{eT}} \right\} \boldsymbol{H}_{q\mathrm{g}} w_{\mathrm{g0}} = H_{\mathrm{T\,Acc\,g}} w_{\mathrm{g0}}. \tag{16.57}$$

This acceleration FRF $H_{\mathrm{T\,Acc\,g}}$ will now show a resonant peak at the flexible mode natural frequency as well as a peak for the short period mode.

16.10.2 Example: Turbulence Response in the Frequency Domain for a Flexible Aircraft

Consider the flexible aircraft used earlier and include a 2 Hz/4 % *fuselage bending* mode, combined with heave and pitch motions. The MATLAB code for this frequency domain calculation is included in appendix I.

In Figure 16.26, the CoM, tailplane and wing tip trailing edge (TE) acceleration PSDs (g^2/Hz) are shown as a function of frequency (Hz). Peaks are seen corresponding to what are essentially the short period and flexible modes, and the increased flexible mode response at the tailplane is also evident. The corresponding root-mean-square value for the CoM is $0.063g$ (about 20 % larger than the rigid aircraft

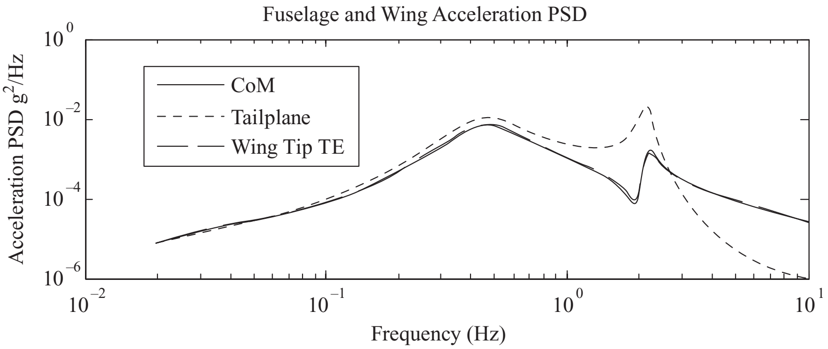

Figure 16.26 Frequency domain gust results for a flexible aircraft with the fuselage bending mode at 2 Hz/4 % showing the CoM, tailplane and wing tip TE acceleration PSDs.

value at the CoM) and for the tailplane is 0.113*g* (80 % larger than at the CoM – a good reason for sitting nearer to the centre of the aircraft for comfort). The wing tip trailing edge results are almost identical to the CoM because for this mode there is no significant wing bending or twist.

Clearly, modes involving any significant wing bending or twist would be apparent on the wing response PSDs. For example, for a *wing bending* mode of 3 Hz frequency and 4 % damping, the response PSDs are shown in Figure 16.27; the wing tip response is much larger than the fuselage response and the root-mean-square values for the fuselage and wing tip were 0.06*g* and 0.31*g* respectively. It should be remembered that the natural frequencies have been set artificially low for the example aircraft in order to exaggerate the effects.

Finally, the results for a *wing torsion* mode of 9 Hz frequency and 4 % damping are shown in Figure 16.28 where the wing tip root-mean-square value is 0.17*g*, noting the different frequency axis used.

It should be noted that the PSD and hence root-mean-square value for load parameters such as the wing root bending moment may also be determined from the responses using the auxiliary equation (see Chapter 18).

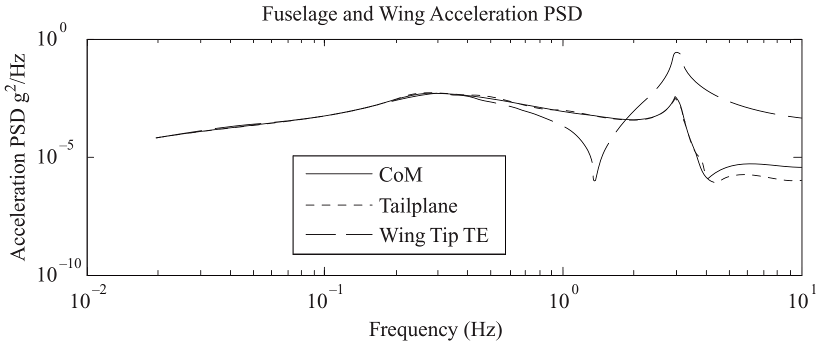

Figure 16.27 Frequency domain gust results for a flexible aircraft with the wing bending mode at 3 Hz/4 % showing the CoM, tailplane and wing tip TE acceleration PSDs.

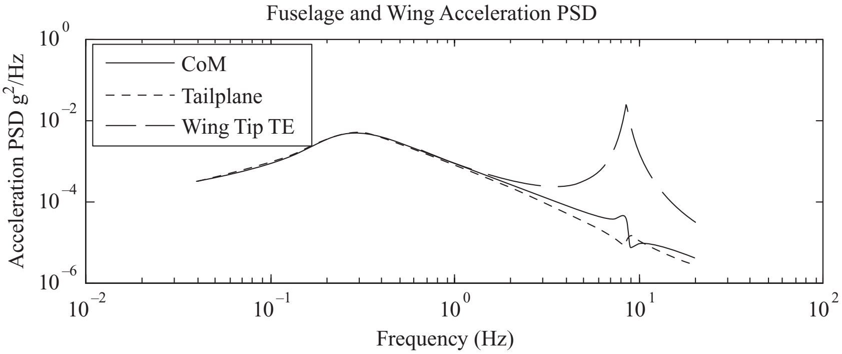

Figure 16.28 Frequency domain gust results for a flexible aircraft with the wing torsion mode at 9 Hz/4 % showing the CoM, tailplane and wing tip TE acceleration PSDs.

16.11 GENERAL FORM OF EQUATIONS IN THE FREQUENCY DOMAIN

In Sections 16.7 to 16.10, the frequency domain approach was illustrated. When the resulting equations are examined their general form may be seen as shown for the time domain in Section 16.6. Thus, when a harmonic gust velocity is introduced, the generalized response vector is assumed to be

$$\boldsymbol{q}(t)=\tilde{\boldsymbol{q}}\mathrm{e}^{\mathrm{i}\omega t}, \tag{16.58}$$

where the frequency domain amplitude is again left as lower case. Then the response may be written, including flexible effects (see Equation (16.56)) and only gust dependent unsteady aerodynamic effects, as

$$\tilde{\boldsymbol{q}} = \left[-\omega^2\mathbf{A} + \mathrm{i}\omega\rho V\mathbf{B} + (\mathbf{E} + \rho V^2\mathbf{C})\right]^{-1}\left\{\rho V\boldsymbol{R}_\mathrm{W} + \rho V\boldsymbol{R}_\mathrm{T}\exp\left(-\frac{\mathrm{i}\omega l}{V}\right)\right\}\phi\left(\frac{\omega c}{2V}\right)w_{\mathrm{g}0} \tag{16.59}$$

or

$$\tilde{\boldsymbol{q}} = \boldsymbol{H}_{q\mathrm{g}}(\omega)\,w_{\mathrm{g}0}, \tag{16.60}$$

where $\boldsymbol{H}_{q\mathrm{g}}$ is the vector of FRFs relating multiple generalized responses to the gust velocity at the relevant flight condition. Note that in Equation (16.59) there is an exponential phase term to account for the tailplane penetration delay. Note also that Theodorsen's function is omitted in this equation for clarity, but it would multiply the left-hand side aerodynamic matrices if used. Employing three-dimensional panel aerodynamics instead of strip theory would mean that the explicit presence of Theodorsen's and Sears' functions would be omitted and the unsteady effects would be catered for via the aerodynamic influence coefficient matrix (see Chapters 19 and 20).

The generalized responses may then be transformed to the desired physical accelerations $\tilde{z}_{\mathrm{Acc}}$ at different positions on the aircraft; e.g.

$$\tilde{\mathbf{z}}_{\mathrm{Acc}} = -\omega^2\mathbf{T}_{\mathrm{zq}}\tilde{\boldsymbol{q}} = -\omega^2\mathbf{T}_{zq}\boldsymbol{H}_{q\mathrm{g}}w_{\mathrm{g}0} = \boldsymbol{H}_{z\,\mathrm{Acc}\,\mathrm{g}}w_{\mathrm{g}0}, \tag{16.61}$$

where the transformation matrix $\mathbf{T}_{zq}$ includes values of the rigid body displacements and flexible modal displacements at the desired spatial positions. This equation may therefore be compared to Equation (16.57) for the tailplane acceleration using $\mathbf{T}_{zq} = \{1 \quad l_\mathrm{T} \quad \kappa_{\mathrm{eT}}\}$. Finally, Equation (16.61) will enable the PSD for each different physical response in the vector to be determined term by term, rather as in Equation (16.39).

Later in Chapter 18, the transformation to load quantities and processing of loads and responses from time and frequency domain analyses will be considered briefly, together with how the structural and aerodynamic model is set up for real aircraft. There is considerable statistical post-processing involved in some aspects of the analysis of continuous turbulence response and Hoblit (1988) covers this thoroughly; mention is made of current certification clearance philosophy for loads due to turbulence in Chapter 24.

16.12 REPRESENTATION OF THE FLIGHT CONTROL SYSTEM (FCS)

The FCS (Pratt, 2000) has an important effect upon the aircraft response and loads caused by a gust or turbulence encounter (see Chapter 14). Of particular interest is the effectiveness of any gust load alleviation (GLA) system upon the resulting response and load levels; such a system uses the normal acceleration to deploy the ailerons and spoilers and so aims to counteract the effects of gusts and turbulence (see Chapter 22). Chapter 12 showed a simple model to demonstrate load alleviation. For the time domain discrete gust simulations, it is possible to incorporate the relevant nonlinear features of the FCS directly into the aircraft dynamic model. However, for turbulence calculations in the frequency domain, a linearized FCS model must be employed. When the effect of nonlinearity on turbulence response is to be considered, then the nonlinear FCS behaviour may be incorporated into a stochastic time domain turbulence representation (see Chapter 24).

16.13 EXAMPLES

Note that some of the examples in Chapters 1 and 2 might be helpful.

1. A rigid aircraft has the following characteristics: $m = 10000$ kg, $S_W = 40$ m^2, $a = 0.09$/deg. The aircraft is flying at 100 m/s at sea level when it meets an upgust of 10 m/s. Find the incremental load factor due to the gust.
   [1.28]

2. Draw a basic gust envelope for the aircraft with the following characteristics: $m = 10200$ kg, $S_W = 50$ m^2, maximum lift coefficient 1.6, $a = 5$/rad, $V_C = 110$ m/s EAS, $V_D = 140$ m/s EAS and $\rho_0 = 1.225$ kg/m^3. Gust velocities are as follows: 20 m/s maximum, 16 m/s at cruise speed and 8 m/s at dive speed. What is the maximum load factor? Ignore the gust alleviation factor.
   [3.69 at cruise speed]

3. An aircraft has the following characteristics: $m = 20000$ kg, $S_W = 80$ m^2, $a_W = 5$/rad, $S_T = 15$ m^2, $a_T = 4$/rad (including downwash). The aircraft is flying at 120 m/s at sea level when it enters a sharp-edged upgust of 10 m/s. Assuming the whole aircraft enters the gust instantly and ignoring unsteady aerodynamic effects, determine the incremental wing and tailplane lift forces and hence the incremental load factor.
   [147 kN, 22 kN and 1.72]

4. Write a MATLAB/SIMULINK program to solve the problem of a rigid aircraft with heave only motion flying through a ‘1-cosine’ gust, check the results given in the chapter for 40 and 400 m gust lengths, and determine the tuned condition that yields the maximum load factor; use quasi-steady aerodynamics.

5. Extend the program in Example 4 to generate the aerodynamic derivatives for a given flight condition and set up the equations of motion and time solution for (a) the heave/pitch model and (b) the flexible model. Repeat the calculations in Example 4. Explore the effect on the solution of changes in aircraft parameters.

6. Perform the convolution of Küssner's function with a '1-cosine' gust of different lengths and plot the degree of unsteady attenuation of the filtered gust magnitude against the gust length.

7. The data in the table below corresponds to the frequency (Hz), gust PSD $(\mathrm{m/s})^2/\mathrm{Hz}$ for a 1 m/s root-mean-square turbulence velocity (Von Karman spectrum) and (CoM acceleration per gust velocity FRF)^2 in $[(\mathrm{m/s}^2)/(\mathrm{m/s})]^2$; a flexible mode is present. Determine the acceleration PSD values, plot the results on linear scales and obtain a rough estimate of the root-mean-square of the acceleration.
[0.6 $\mathrm{m/s}^2$]

Frequency	Gust PSD	FRF^2	Frequency	Gust PSD	FRF^2
1.6	0.027	0.86	0	8.128	0
1.8	0.023	0.64	0.2	0.853	0.05
2.0	0.019	1.07	0.4	0.275	2.05
2.2	0.016	3.56	0.6	0.140	3.00
2.4	0.014	4.01	0.8	0.087	2.01
2.6	0.012	3.46	1.0	0.060	1.59
2.8	0.011	3.07	1.2	0.044	1.33
3.0	0.010	2.82	1.4	0.034	1.10

8. Consider the rigid aircraft heave model used in the examples of this chapter. Obtain the FRF relating heave acceleration per gust velocity and hence the acceleration PSD for turbulence modelled by the Von Karman spectrum with a scale length of 2500 ft and gust velocity of 1 m/s root-mean-square. Obtain the root-mean-square value of the acceleration. Now introduce the Theodorsen and Sears' functions into the FRF and obtain the revised plots and root-mean-square figures.

9. Extend the program in Example 7 for quasi-steady aerodynamics to cater for (a) the heave/pitch model and (b) the flexible mode model. Check the results presented in this chapter. Explore the effect of changing aircraft and modal parameters on the resulting shapes of the acceleration response PSDs.

17

Ground Manoeuvres

The behaviour of an aircraft in contact with the ground is not straightforward, mainly because of the complexity of the landing gears used to absorb energy on landing and to allow ground manoeuvrability. Dynamic loads are developed in the landing gear, and therefore in the airframe, when taxiing, turning, taking off, landing and braking (Lomax, 1996; Howe, 2004); all load cases may be important for dimensioning of some aircraft or gear component.

The certification requirements for ground loads are shown in CS-25 and FAR-25 for large commercial aircraft and some of the calculations are discussed in Lomax (1996) and Howe (2004), though some of the requirements have been revisited since their publication because larger aircraft with more than two main landing gears have been designed. The ground loads certification is considered under the headings of (a) landing and (b) ground handling (taxi, take-off and landing roll, braked roll, turning, towing, tie-down, jacking, etc.). The calculations outlined in CS-25 may be defined as being 'rational' or 'bookcase'. Rational calculations employ a model that seeks to represent more accurately the real physics and dynamics of the system whereas bookcase calculations tend to be more artificial and usually require ground reactions to be balanced by inertia forces (and sometimes moments).

Because of the complexity of the landing gear and some of these ground operations, the treatment in this chapter will be kept fairly simple in order to provide basic understanding of some of the key issues involved. The landing gear will be introduced, followed by relatively simple treatment of the rational taxiing and landing cases, bookcases for braking and turning, simple modelling of braking and wheel spin-up/spring-back, and shimmy. The other load cases and how industry may meet the requirements are discussed in Chapter 25. Note that the calculation of internal loads in the airframe will be considered later in Chapter 18.

17.1 LANDING GEAR

The landing gears for modern aircraft are extremely complex, being required to provide energy absorption on landing and manoeuvrability on the ground (taxiing, turning and braking), as well as needing to be retracted and stowed in flight through one of a variety of kinematic arrangements (Currey, 1988; Niu, 1988; Howe, 2004). It is most common for large commercial aircraft to have a nose/main gear layout; typical main and nose landing gears are shown in Figure 17.1.

Detailed nonlinear mathematical models of the landing gears are required, and loads in each component have to be determined over the whole range of ground manoeuvres. Treatment of landing gear design and construction may be found in Currey (1988) and Niu (1988), though the process of developing a detailed dynamic model for calculation of dynamic responses and loads is not included in these references. In this book, some basic concepts of response calculations will be introduced by treating the gear as a linear or nonlinear 'black box'.

Introduction to Aircraft Aeroelasticity and Loads J. R. Wright and J. E. Cooper

© 2007 John Wiley & Sons, Ltd

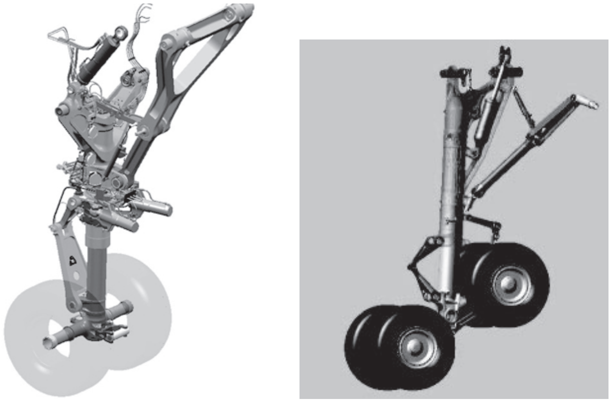

Figure 17.1 Typical nose and main landing gears for a commercial aircraft. (Reproduced by permission of Messier-Dowty Ltd)

17.1.1 Oleopneumatic Shock Absorbers

The main landing gear component relevant to energy absorption and carrying static loads is the shock absorber. Most aircraft use oleopneumatic shock absorbers (gas + oil) as they are the most efficient. The basic idea is shown schematically in Figure 17.2. The idea is that oil is forced through the compression orifices as the shock absorber is compressed (shown by the lower arrow), so dissipating energy and compressing the gas (typically air or nitrogen); then the rebound of the aircraft is controlled by the pressured gas forcing oil back through the recoil orifices (shown by the upper arrow).

The shock absorber provides a 'gas spring' to support the aircraft weight, to prevent 'bottoming' and to provide ride comfort. The *stiffness* characteristics of the gas spring are nonlinear, controlled by the

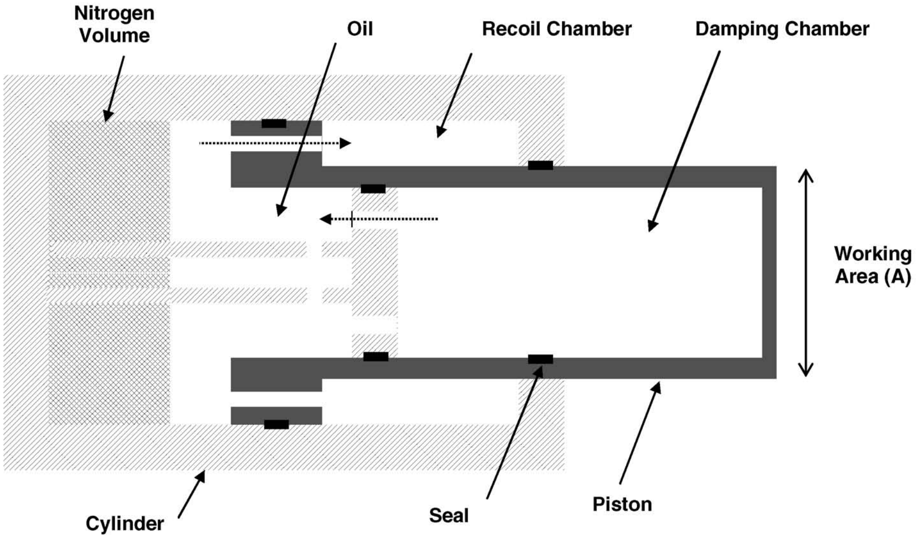

Figure 17.2 Oleopneumatic shock absorber arrangement. (Redrawn with modifications by permission of Messier-Dowty Ltd)

gas law governing the compression of the gas and assuming that the oil is incompressible for a simple model. The ideal gas law (Duncan *et al.*, 1962) is

$$PV^{\gamma} = C, \tag{17.1}$$

where P is the absolute pressure (gauge + atmospheric), V is the volume, C is a constant and γ is the polytropic constant. For *static* loading conditions where there is a steady rate of compression (e.g. taxiing, loading the aircraft), the process may be viewed as isothermal (constant temperature) and $\gamma = 1$ may be used; however, for *dynamic* loading conditions where there is a rapid rate of compression (e.g. landing) the process is assumed to be adiabatic (no heat transfer) and $\gamma = 1.3$–1.4 may be used.

When the gas law is applied to the system to relate the two conditions where the piston is fully extended (subscript ∞) and then partially compressed by an amount z, it may be shown that

$$P(V_{\infty} - Az)^{\gamma} = P_{\infty}V_{\infty}^{\gamma}, \tag{17.2}$$

where A is the piston area. Hence, the absolute pressure/displacement relationship is given by

$$\frac{P}{P_{\infty}} = \left(1 - \frac{z}{z_{\infty}}\right)^{-\gamma}, \tag{17.3}$$

where $z_{\infty} = V_{\infty}/A$ is the fully extended to fully ‘bottomed’ distance (about 10 % greater then the stroke z_{S}).

In order to obtain an estimate of the stroke required for the shock absorber, the energy balance on landing may be considered (Currey, 1988; Howe, 2004). Now, it is normally assumed in the critical part of the landing process for commercial aircraft that lift remains equal to the weight. Then, neglecting the tyre deformation (and therefore the associated energy dissipation), the aircraft kinetic energy must be absorbed by the work done in the shock absorber, so

$$\tfrac{1}{2}mW_{\mathrm{e}}^2 = \eta_{\mathrm{S}}F_{\mathrm{LG_{max}}}z_{\mathrm{S}} = \eta_{\mathrm{S}}n_{\mathrm{LG}}Wz_{\mathrm{S}}, \qquad z_{\mathrm{S}} = \frac{W_{\mathrm{e}}^2}{2\eta_{\mathrm{S}}n_{\mathrm{LG}}g}, \tag{17.4}$$

where m is the aircraft mass (effectively that part supported by each main gear), W_{e} is the vertical landing (or sink/descent) velocity, $F_{\mathrm{LG_{max}}}$ is the maximum landing gear force, η_{S} is the shock absorber efficiency (taking account of losses, typically 0.8) and z_{S} is the stroke. The load factor n_{LG} for a landing gear is defined as the ratio of (static + dynamic reaction load) to (static load); typical values of 2–2.5 for commercial aircraft will occur on landing (Lomax, 1996); note that the definition differs to that for the load factor of a complete aircraft (see Chapter 13). For example, if $W_{\mathrm{e}} = 3$ m/s and $n_{\mathrm{LG}} = 2.5$, then z_{S} 0.23 m.

In order to estimate the values of the other parameters used for the gas spring, the following process may be followed (Currey, 1988), using typical values:

- Determine area A by assuming that the static pressure P_{S} is approximately 100 bar when supporting the aircraft weight.
- Choose P_{C} (C subscript = fully compressed) and P_{∞} to be of order $3P_{\mathrm{S}}$ and $0.25P_{\mathrm{S}}$ respectively.
- Apply the gas law ($\gamma = 1$) to relate fully extended/fully compressed conditions to yield $V_{\infty}/V_C = 12$.
- Recognize that $V_{\infty} = V_{\mathrm{C}} + Az_{\mathrm{S}} = 12Az_{\mathrm{S}}/11$, then $z_{\infty} = 12z_{\mathrm{S}}/11 = 1.091z_{\mathrm{S}}$.

The stiffness curve that may be derived from Equation (17.3) for the static and dynamic cases is shown in Figure 17.3 in terms of the normalized force (strut force per static load) against % compression; note that the atmospheric pressure must be accounted for when the pressure relationship is used in a simulation to generate forces.

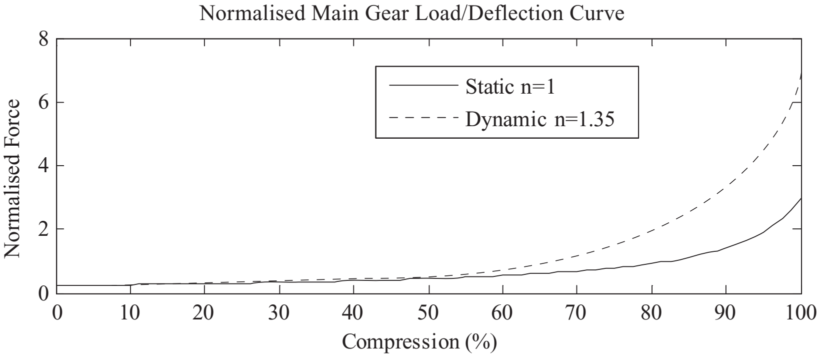

Figure 17.3 Oleopneumatic shock absorber – normalized/compression curve.

The shock absorber also provides friction and a high level of *damping* to help absorb the energy of a landing impact and avoid excessive recoil. The damping is controlled by oil flow through the compression and recoil orifices, and using Bernoulli's theorem and the orifice discharge characteristics (Duncan *et al.*, 1962) it may be seen that the damping is proportional to velocity squared, i.e. nonlinear. The oleo damping force F_D is thus given by

$$F_D = D_C\dot{z}^2, \qquad \dot{z} \geq 0, \qquad F_D = -D_R\dot{z}^2, \quad \dot{z} < 0, \tag{17.5}$$

where D_C, D_R are the compression and recoil damping coefficients and z is the shock absorber compression (or closure); note that D_R is of the order of 15–20 times greater than D_C so as to minimize recoil.

17.1.2 Wheel and Tyre Assembly

A landing gear has two major dynamic elements in series, namely the shock absorber and the wheel/tyre assembly. The dynamic behaviour of this assembly is complex and has an impact upon taxiing, braking, turning, etc. The assembly also influences the landing in that when tyre deformations are included, the required shock absorber stroke reduces somewhat. It is important for the accurate estimation of the landing gear internal loads and the loads at the airframe attachment points that the system is modelled adequately. A very simple representation that includes tyre characteristics is the two DoF model shown in Figure 17.4

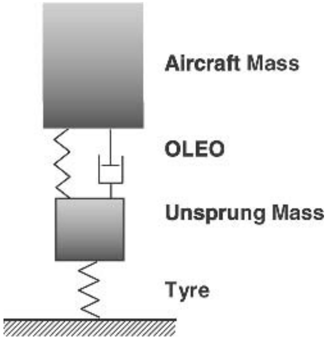

Figure 17.4 Simplified landing gear/tyre model.

where the unsprung mass consists of the sliding tube, axle and wheel/tyre/brake; a linear, undamped tyre model is used for the simple calculations involving vertical motion. In practice, the tyre model is nonlinear, complex (particularly when representing lateral forces) and depends upon material properties, pressure, temperature, tyre wall flexibility, etc.

17.1.3 Determinate and Statically Indeterminate Landing Gear Layouts

When there are only three landing gears on an aircraft, the static loads in each one may be determined by equilibrium considerations alone since the problem is statically determinate. However, for some large commercial aircraft, there are more than three landing gears (e.g. Airbus A340, Boeing 747), and in such cases the problem of finding the static loads is statically indeterminate (or redundant). This means that the elastic deformation of the aircraft and the flexibility of each landing gear (including nonlinear effects) need to be considered when determining the loads carried by the gear units. A nonlinear static balance calculation on the ground will yield these loads. Also, any variation in profile across the runway needs to be considered.

17.2 TAXI, TAKE-OFF AND LANDING ROLL

Taxiing loosely describes the entire phase of ground movement prior to final take off and following landing (Lomax, 1996; Howe, 2004). Clearly the aircraft will need to brake and turn but these are considered as separate operations, with taxiing simply being concerned with straight line motion on the ground. If the runway and taxiways were completely smooth, then taxiing would not be a problem. However, in practice runways and taxiways are ‘rough’ (or nonsmooth) to some extent, i.e. the elevation along the length of the runway does not vary linearly. As a consequence, the aircraft responds dynamically during taxiing, with flexible modes being excited and dynamic loads generated that need consideration for design. Also, the comfort of the crew and passengers is affected. An aircraft that experienced significant dynamic responses during taxiing was the Concorde, since the fuselage was slender and flexible, with the pilot located a long way forward of the nose landing gear when compared to more conventional commercial aircraft; also, the high take-off and landing speeds meant that longer wavelengths of the runway profile became important.

For simplicity in forming the equations in this section, the landing gear will initially be assumed to be a simple linear spring/damper such that a set of linear equations will result. Later, the true nonlinear nature of the gear will be introduced briefly and it will be seen that the aircraft and landing gear equations are arguably better written separately and coupled via the gear forces. The dynamic calculations described for taxiing are rational and broadly similar to the industrial practice used when meeting certification requirements (CS-25; Lomax, 1996).

17.2.1 Runway Profile

To calculate the aircraft dynamic response during taxiing, the runway profile over which the aircraft is operating must be specified. Note that every runway in the world has a different profile. However, it is not possible to consider them all in the design process so only a representative runway is considered, namely San Francisco 28R prior to resurfacing (Lomax, 1996; see also Chapter 25). The profile $h(x_r)$ of a runway is defined relative to a flat datum as shown in Figure 17.5, where the distance along the runway x_r is measured with respect to a convenient origin. The profile is taken as downwards positive, to be consistent with downwards positive displacements on the aircraft. There is no variation of profile across the runway. The analysis has some similarities to that for the simple vertical gust analysis considered in Chapter 16.

Sometimes the response to a particular ‘dip’ or ‘bump’ on an otherwise flat runway may be required, e.g. in meeting the discrete load condition in the certification requirements; the term ‘dip’ will be used

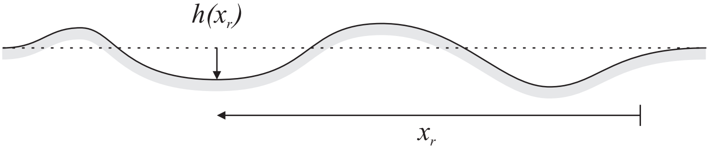

Figure 17.5 Definition of a runway profile.

to describe a negative 'bump'. For example, a '1-cosine' dip of depth Δh_{r} and length L_{r} as shown in Figure 17.6 (not to be confused with the lateral stability derivative given the same symbol) would have a profile

$$h(x_{\mathrm{r}}) = \frac{\Delta h_{\mathrm{r}}}{2}\left(1 - \cos\frac{2\pi x_{\mathrm{r}}}{L_{\mathrm{r}}}\right). \tag{17.6}$$

The aircraft nose and main gears would pass over the 'dip' at different times, so causing both heave and pitch motions of the aircraft (similar to the gust penetration effect in Chapter 16). It is possible that the 'dip' could be 'tuned' to the heave or pitch mode frequency of the aircraft (or indeed to a flexible mode frequency) and so a worst case 'dip' could be envisaged, rather like the tuned '1-cosine' gust case considered in Chapter 16.

When the equations are set up, both $h(t)$ and $\dot{h}(t)$ (i.e. the runway profile and rate of change with time of the profile, as seen by each gear) are required; thus a temporal definition must be obtained from the spatial profile. The value of $h(t)$ is equal to the value of $h(x_{\mathrm{r}})$ at the current location of the aircraft during the taxiing process. The time rate of change of the profile $\dot{h}(t)$ depends upon the local runway slope and the aircraft velocity. Let the aircraft forward velocity be V (TAS) at the instant of time considered. Then, using the chain rule, the rate of change of profile with time is given by

$$\dot{h} = \frac{\mathrm{d}h}{\mathrm{d}t} = \frac{\mathrm{d}h}{\mathrm{d}x_{\mathrm{r}}}\frac{\mathrm{d}x_{\mathrm{r}}}{\mathrm{d}t} = V\frac{\mathrm{d}h}{\mathrm{d}x_{\mathrm{r}}}, \tag{17.7}$$

where the runway slope may be estimated from the profile values near to the point of interest. The treatment in this chapter only covers the effect of the runway profile upon the vertical gear forces; in a more complete model, the effect of a bump or dip upon the wheel drag force would also be included.

17.2.2 Rigid Aircraft Taxiing

Consider a rigid aircraft supported on linear spring/damper gears as shown in Figure 17.7 (see also Chapter 2). The aircraft response is represented by the centre of mass (subscript C) heave z_{C} and pitch θ, relative to any horizontal datum; zero motion corresponds to the aircraft at rest in its static equilibrium position on the datum runway. Thus responses are actually calculated *relative to* this datum state and so are incremental. The aircraft has mass m, pitch moment of inertia about the centre of mass I_y, nose (subscript N) and main (subscript M) gear stiffnesses K_{N}, K_{M} and viscous dampings C_{N}, C_{M}; clearly the main gears on both sides of the aircraft have been combined into one unit.

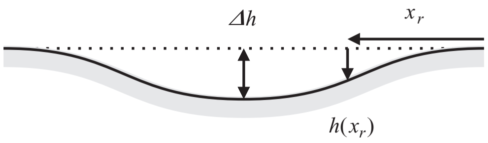

Figure 17.6 '1-Cosine' runway 'dip' profile.

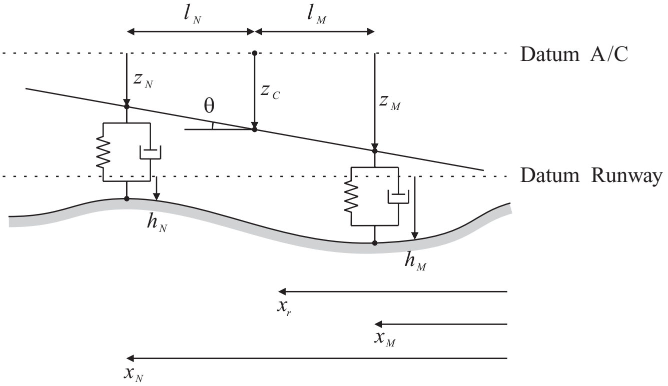

Figure 17.7 Rigid aircraft with a linear landing gear during taxiing.

Consider the aircraft position at any instant, being defined with the centre of mass at distance x_{r} from the runway origin, the nose gear at x_{N} and the main gear at x_{M}. The profile values at the gear positions are then

$$h_{\mathrm{N}} = h(x_{\mathrm{N}}) = h(x_{\mathrm{r}} + l_{\mathrm{N}}), \qquad h_{\mathrm{M}} = h(x_{\mathrm{M}}) = h(x_{\mathrm{r}} - l_{\mathrm{M}}) \tag{17.8}$$

Note that the use of the symbol x here is different to that used for one of the aircraft axes.

The energy dissipation and work done functions depend upon expressions for compression and the rate of compression of the landing gear springs and dampers, and these values will depend on the runway profile and rate of change of the profile. Thus, the compression and rate of compression of the nose and main gears are

$$\begin{aligned} \Delta_{\mathrm{N}} &= z_{\mathrm{N}} - h_{\mathrm{N}} = z_{\mathrm{C}} - l_{\mathrm{N}}\theta - h_{\mathrm{N}}, & \dot{\Delta}_{\mathrm{N}} &= \dot{z}_{\mathrm{C}} - l_{\mathrm{N}}\dot{\theta} - \dot{h}_{\mathrm{N}}, \\ \Delta_{\mathrm{M}} &= z_{\mathrm{M}} - h_{\mathrm{M}} = z_{\mathrm{C}} + l_{\mathrm{M}}\theta - h_{\mathrm{M}}, & \dot{\Delta}_{\mathrm{M}} &= \dot{z}_{\mathrm{C}} + l_{\mathrm{M}}\dot{\theta} - \dot{h}_{\mathrm{M}}. \end{aligned} \tag{17.9}$$

The kinetic energy, strain energy and dissipation function are then given by

$$T = \tfrac{1}{2} m \dot{z}_{\mathrm{C}}^2 + \tfrac{1}{2} I_y \dot{\theta}^2, \qquad U = \tfrac{1}{2} K_{\mathrm{N}} \Delta_{\mathrm{N}}^2 + \tfrac{1}{2} K_{\mathrm{M}} \Delta_{\mathrm{M}}^2, \qquad \Im = \tfrac{1}{2} C_{\mathrm{N}}^2 \dot{\Delta}_{\mathrm{N}} + \tfrac{1}{2} C_{\mathrm{M}} \dot{\Delta}_{\mathrm{M}}^2. \tag{17.10}$$

Then, applying Lagrange's equations with generalized coordinates (z_{C}, θ), it may be shown that the equations of motion for the aircraft taxiing on the nonsmooth runway are

$$\begin{aligned} &\begin{bmatrix} m & 0 \\ 0 & I_y \end{bmatrix} \begin{Bmatrix} \ddot{z}_{\mathrm{C}} \\ \ddot{\theta} \end{Bmatrix} + \begin{bmatrix} C_{\mathrm{N}} + C_{\mathrm{M}} & -l_{\mathrm{N}} C_{\mathrm{N}} + l_{\mathrm{M}} C_{\mathrm{M}} \\ -l_{\mathrm{N}} C_{\mathrm{N}} + l_{\mathrm{M}} C_{\mathrm{M}} & l_{\mathrm{N}}^2 C_{\mathrm{N}} + l_{\mathrm{M}}^2 C_{\mathrm{M}} \end{bmatrix} \begin{Bmatrix} \dot{z}_{\mathrm{C}} \\ \dot{\theta} \end{Bmatrix} \\ &\quad + \begin{bmatrix} K_{\mathrm{N}} + K_{\mathrm{M}} & -l_{\mathrm{N}} K_{\mathrm{N}} + l_{\mathrm{M}} K_{\mathrm{M}} \\ -l_{\mathrm{N}} K_{\mathrm{N}} + l_{\mathrm{M}} K_{\mathrm{M}} & l_{\mathrm{N}}^2 K_{\mathrm{N}} + l_{\mathrm{M}}^2 K_{\mathrm{M}} \end{bmatrix} \begin{Bmatrix} z_{\mathrm{C}} \\ \theta \end{Bmatrix} = \begin{bmatrix} C_{\mathrm{N}} & C_{\mathrm{M}} \\ -l_{\mathrm{N}} C_{\mathrm{N}} & +l_{\mathrm{M}} C_{\mathrm{M}} \end{bmatrix} \begin{Bmatrix} \dot{h}_{\mathrm{N}} \\ \dot{h}_{\mathrm{M}} \end{Bmatrix} \\ &\quad + \begin{bmatrix} K_{\mathrm{N}} & K_{\mathrm{M}} \\ -l_{\mathrm{N}} K_{\mathrm{N}} & l_{\mathrm{M}} K_{\mathrm{M}} \end{bmatrix} \begin{Bmatrix} h_{\mathrm{N}} \\ h_{\mathrm{M}} \end{Bmatrix} \end{aligned} \tag{17.11}$$

It may be seen clearly that the left-hand side of this equation is the same as that in Chapter 2, but now a right-hand side excitation term is present due to the variation in the runway profile. Aerodynamic effects have been ignored in this simple model but steady effects would normally be included to allow the gear compressions to be determined. The taxiing response of the rigid aircraft may be found by solving these differential equations in time, as discussed in Chapters 1 and 2.

17.2.3 Example of Rigid Aircraft Taxiing

A rigid aircraft is considered to pass over a ‘1-cosine’ dip and the resulting heave displacement and acceleration at the nose and main landing gear positions will be examined. The aircraft parameters are $m = 10\,000$ kg, $I_y = 144\,000$ kgm^2, $l_{\mathrm{N}} = 6.8$ m, $l_{\mathrm{M}} = 0.75$ m, $C_{\mathrm{N}} = 3200$ N s/m, $C_{\mathrm{M}} = 19\,200$ N s/m, $K_{\mathrm{N}} = 80\,000$ N/m and $K_{\mathrm{M}} = 240\,000$ N/m. The fuselage mass distribution and component moments of inertia are the same as used for the example in Chapter 13 and Appendix C, but these data only become relevant when the flexible mode is considered later in this chapter. The natural frequencies and damping ratios for the rigid body modes of the aircraft on its linear landing gear are approximately 0.70 Hz/15.1 % and 1.00 Hz/16.1 %. MATLAB and SIMULINK programs for a rigid aircraft taxiing over a ‘1-cosine’ dip are presented in appendix I in the companion website.

Consider a case where the taxiing velocity is 30 m/s and the depth of the dip is 30 mm. The simulation is carried out over 10 s and the nose gear encounters the dip at the start of the simulation. Care needs to be taken when setting up the simulation to ensure that the nose and main gears encounter the dip with the appropriate time delay interval. Clearly, a range of different dip lengths may be examined and the largest acceleration response was found to occur for a dip around 25 m long; the approach is similar to that adopted for the gust in Chapter 16, but the detailed results are not presented here. However, because the flexible aircraft example given later has a maximum acceleration response for a 15 m dip, only this latter case will be considered; this corresponds to an effective 0.5 s duration pulse input. The displacement and acceleration responses are shown in Figure 17.8, with maximum values of approximately 36.4 mm and 0.129g; the motion is predominantly pitching.

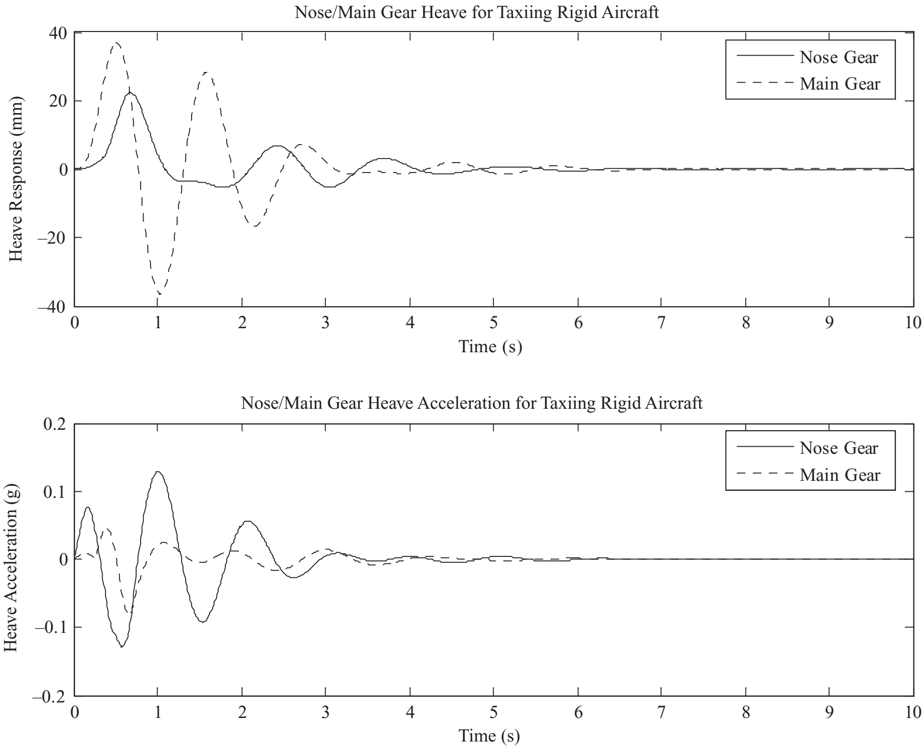

Figure 17.8 Response to taxiing at 30 m/s over a 15 m/30 mm dip for a rigid aircraft.

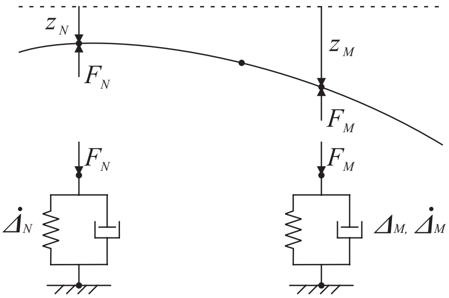

Figure 17.9 Flexible aircraft with linear landing gear during taxiing.

17.2.4 Flexible Aircraft Taxiing

In practice, the taxiing case is always considered with flexible effects included for commercial aircraft. Also, because the landing gear is a complex nonlinear dynamic system in its own right, it is possible that the aircraft and landing gear equations may not be coupled in such a direct way as shown for the rigid aircraft with linear landing gear in Equation (17.11). Instead, the aircraft and landing gear equations can be formed separately, with intercomponent forces (see Chapter 13) and kinematic constraints employed to link the two sets of equations, as shown in Figure 17.9. In this section, the idea will be illustrated together with the inclusion of a flexible mode, rather as was done in Chapters 13 and 16, except that here the aerodynamic forces are ignored.

The sensible option is again to take the deformation of the aircraft at rest on a smooth runway as the datum. The response during taxiing is then *relative to* the initial deformation and will include flexible contributions.

The deformation of the flexible aircraft will be treated via the summation of rigid body and flexible free–free normal modes, such as would emerge from a finite element analysis of a free–free aircraft. Such a model is suitable for taxiing and gust response calculations since the basic dynamics of the airframe (without landing gear) are linear and only relatively small motions away from the datum path occur. The model involves inertial axes with unknown displacements and rotations, so there is therefore no need to consider axes moving with the aircraft, as was the case for dynamic flight manoeuvres in Chapters 14 and 15.

17.2.4.1 Flexible airframe equations

Consider the aircraft shown in Figure 17.9, which is rather similar to the earlier rigid aircraft but now with elastic deformation present and the landing gears and aircraft treated as separate systems. Let the deformation of the aircraft be expressed as the summation of three free–free normal modes for the aircraft without landing gear; the first two modes will be rigid body modes (i.e. heave, pitch) and the other a flexible mode (e.g. fuselage bending). Whole aircraft modes are considered in Chapter 3 and in Appendices A and C. Thus a modal approach including the rigid body behaviour has replaced the previous direct use of heave and pitch coordinates.

The aircraft (downwards) displacement $z(x, y)$ at any position on the airframe and relative to the equilibrium state will then be given by

$$z(x, y) = \kappa_{\mathrm{h}}(x, y)q_{\mathrm{h}} + \kappa_{\mathrm{p}}(x, y)q_{\mathrm{p}} + \kappa_{\mathrm{e}}(x, y)q_{\mathrm{e}}, \tag{17.12}$$

where $q_{\mathrm{h}}, q_{\mathrm{p}}, q_{\mathrm{e}}$ are the modal coordinates used to define the displacements and $\kappa_{\mathrm{h}}, \kappa_{\mathrm{p}}, \kappa_{\mathrm{e}}$ are the heave, pitch and flexible mode shapes. In Appendix A, it is seen that the modal mass values are $m_{\mathrm{h}} = m,\ m_{\mathrm{p}} = I_{\mathrm{y}}$

if the rigid body mode shapes are normalized such that $\kappa_{\mathrm{h}} = 1,\ \kappa_{\mathrm{p}} = -x$. Equation (17.12) then simplifies to

$$z(x, y) = q_{\mathrm{h}} - x q_{\mathrm{p}} + \kappa_{\mathrm{e}}(x, y) q_{\mathrm{e}}. \tag{17.13}$$

The kinetic energy may be expressed in terms of all the modal quantities, whereas the strain energy for the airframe only exists for the flexible mode, so

$$T = \tfrac{1}{2} m_{\mathrm{h}} \dot{q}_{\mathrm{h}}^2 + \tfrac{1}{2} m_{\mathrm{p}} \dot{q}_{\mathrm{p}}^2 + \tfrac{1}{2} m_{\mathrm{e}} \dot{q}_{\mathrm{e}}^2, \qquad U = \tfrac{1}{2} k_{\mathrm{e}} q_{\mathrm{e}}^2, \tag{17.14}$$

where $m_{\mathrm{h}}, m_{\mathrm{p}}, m_{\mathrm{e}}$ are the modal masses and k_{e} is the modal stiffness for the flexible mode. The flexible mode quantities depend upon the mode shape and mode normalization (see Chapter 13 and Appendix C).

The (downwards) displacements of the airframe at the nose and main gear positions are given, using equation (17.13), by

$$\begin{aligned} z_{\mathrm{N}} &= q_{\mathrm{h}} - l_{\mathrm{N}} q_{\mathrm{p}} + \kappa_{\mathrm{e}}(l_{\mathrm{N}}, 0) q_{\mathrm{e}} = q_{\mathrm{h}} - l_{\mathrm{N}} q_{\mathrm{p}} + \kappa_{\mathrm{eN}} q_{\mathrm{e}}, \\ z_{\mathrm{M}} &= q_{\mathrm{h}} + l_{\mathrm{M}} q_{\mathrm{p}} + \kappa_{\mathrm{e}}(-l_{\mathrm{M}}, \pm d_{\mathrm{M}}) q_{\mathrm{e}} = q_{\mathrm{h}} + l_{\mathrm{M}} q_{\mathrm{p}} + \kappa_{\mathrm{eM}} q_{\mathrm{e}}, \end{aligned} \tag{17.15}$$

where $\pm d_{\mathrm{M}}$ are the y positions of the main gear and $\kappa_{\mathrm{eN}}, \kappa_{\mathrm{eM}}$ are the values of the flexible mode shape at the nose and main landing gear positions. Also, the intercomponent forces (compressive positive) between the landing gears and the airframe will be F_{N} and F_{M} (refer to Chapter 13). Then, by determining the incremental work done by these forces moving through incremental nose and main gear displacements, the modal forces due to the presence of the landing gear may be determined, so

$$\delta W = -F_{\mathrm{N}} \delta z_{\mathrm{N}} - F_{\mathrm{M}} \delta z_{\mathrm{M}}$$

or

$$\delta W = -F_{\mathrm{N}} \left(\delta q_{\mathrm{h}} - l_{\mathrm{N}} \delta q_{\mathrm{p}} + \kappa_{\mathrm{eN}} \delta q_{\mathrm{e}} \right) - F_{\mathrm{M}} \left(\delta q_{\mathrm{h}} + l_{\mathrm{M}} \delta q_{\mathrm{p}} + \kappa_{\mathrm{eM}} \delta q_{\mathrm{e}} \right). \tag{17.16}$$

Thus, applying Lagrange's equations, the three DoF equations of motion for the flexible aircraft (see Chapter 3) are found to be

$$\left[\begin{array}{cc|c} m & 0 & 0 \\ 0 & I_y & 0 \\ \hline 0 & 0 & m_{\mathrm{e}} \end{array}\right] \left\{\begin{array}{c} \ddot{q}_{\mathrm{h}} \\ \ddot{q}_{\mathrm{p}} \\ \hline \ddot{q}_{\mathrm{e}} \end{array}\right\} + \left[\begin{array}{cc|c} 0 & 0 & 0 \\ 0 & 0 & 0 \\ \hline 0 & 0 & k_{\mathrm{e}} \end{array}\right] \left\{\begin{array}{c} q_{\mathrm{h}} \\ q_{\mathrm{p}} \\ \hline q_{\mathrm{e}} \end{array}\right\} = -\left\{\begin{array}{c} 1 \\ -l_{\mathrm{N}} \\ \hline \kappa_{\mathrm{eN}} \end{array}\right\} F_{\mathrm{N}} - \left\{\begin{array}{c} 1 \\ l_{\mathrm{M}} \\ \hline \kappa_{\mathrm{eM}} \end{array}\right\} F_{\mathrm{M}}. \tag{17.17}$$

It may be seen that the matrix partitions separate the rigid body and flexible modes. To add more flexible modes would simply mean adding further diagonal modal mass and stiffness terms together with additional mode shape values at the landing gear positions. Damping would also normally be introduced for the flexible mode. Landing gear damping would be involved once the two sets of equations were coupled. These equations are in the general modal form

$$\mathbf{M}_q \ddot{\boldsymbol{q}} + \mathbf{K}_q \boldsymbol{q} = -\boldsymbol{\kappa}_{\mathbf{N}} F_{\mathrm{N}} - \boldsymbol{k}_{\mathbf{M}} F_{\mathrm{M}} \tag{17.18}$$

where, for example, $\boldsymbol{\kappa}_{\mathbf{M}} = \{ 1 \ l_{\mathrm{M}} \ \kappa_{\mathrm{eM}} \}^{\mathrm{T}}$ and by inspection of equation (17.15) it may be seen that $z_{\mathrm{M}} = \kappa_{\mathbf{M}}^{\mathbf{T}} q$. The outcome of this analysis is that Equations (17.17) and (17.18) relate the airframe response to the intercomponent forces applied at the landing gear positions.

17.2.4.2 Landing gear equations – linear

The gear equations relate intercomponent forces to the gear compressions, and thus to the aircraft response and runway profile. The compression and rate of compression vectors for the nose and main gears are

$$\begin{Bmatrix} \Delta_{\mathrm{N}} \\ \Delta_{\mathrm{M}} \end{Bmatrix} = \begin{Bmatrix} z_{\mathrm{N}} \\ z_{\mathrm{M}} \end{Bmatrix} - \begin{Bmatrix} h_{\mathrm{N}} \\ h_{\mathrm{M}} \end{Bmatrix}, \qquad \begin{Bmatrix} \dot{\Delta}_{\mathrm{N}} \\ \dot{\Delta}_{\mathrm{M}} \end{Bmatrix} = \begin{Bmatrix} \dot{z}_{\mathrm{N}} \\ \dot{z}_{\mathrm{M}} \end{Bmatrix} - \begin{Bmatrix} \dot{h}_{\mathrm{N}} \\ \dot{h}_{\mathrm{M}} \end{Bmatrix}. \tag{17.19}$$

The relationship between the gear forces and compressions for a simple *linear* landing gear is

$$\begin{Bmatrix} F_{\mathrm{N}} \\ F_{\mathrm{M}} \end{Bmatrix} = \begin{bmatrix} C_{\mathrm{N}} & 0 \\ 0 & C_{\mathrm{M}} \end{bmatrix} \begin{Bmatrix} \dot{\Delta}_{\mathrm{N}} \\ \dot{\Delta}_{\mathrm{M}} \end{Bmatrix} + \begin{bmatrix} K_{\mathrm{N}} & 0 \\ 0 & K_{\mathrm{M}} \end{bmatrix} \begin{Bmatrix} \Delta_{\mathrm{N}} \\ \Delta_{\mathrm{M}} \end{Bmatrix}. \tag{17.20}$$

The aircraft taxiing response is obtained by simultaneous solution of Equations (17.17) and (17.20), with the kinematic constraints between the airframe and landing gears given by Equations (17.19) and the relationship between the physical and modal coordinates given by Equation (17.15). Solution in the time domain yields the incremental dynamic response of the flexible aircraft as a combination of rigid body and flexible mode motions.

The modal responses and accelerations can then be transformed into physical displacements (and accelerations) anywhere on the airframe, e.g. at the pilot station, the vertical acceleration is given by

$$\ddot{z}_{\mathrm{Pilot}} = \ddot{q}_{\mathrm{h}} - l_{\mathrm{Pilot}} \ddot{q}_{\mathrm{p}} + \kappa_{\mathrm{e\,Pilot}} \ddot{q}_{\mathrm{e}}, \tag{17.21}$$

where $\kappa_{\mathrm{e\,Pilot}}$ is the flexible mode shape value at the pilot position, a distance l_{Pilot} ahead of the centre of mass. A mode will only be excited during taxiing if there is a finite value of the mode shape at one or both of the landing gear positions, i.e. both the gears are not located at node points. Internal airframe loads may also be determined as described later in Chapter 18. Landing gear internal loads may be found knowing the leg forces and compressions, together with the gear dynamic model.

17.2.4.3 Landing gear equations – nonlinear

Since the landing gear is actually *nonlinear*, then the landing gear forces will be a general nonlinear function of the compressions and rates of compression, and it should be noted that the sets of dynamic equations for each gear will be uncoupled, so

$$F_{\mathrm{N}} = f_{\mathrm{NL}}(\Delta_{\mathrm{N}}, \dot{\Delta}_{\mathrm{N}}), \qquad F_{\mathrm{M}} = g_{\mathrm{NL}}(\Delta_{\mathrm{M}}, \dot{\Delta}_{\mathrm{M}}), \tag{17.22}$$

where f_{NL}, g_{NL} are nonlinear functions. The landing gear equations consist of a complete dynamic model, including shock absorber and tyre effects. These nonlinear equations can be solved in conjunction with the airframe equations in place of the linear gear Equation (17.20). (Deriving the full nonlinear landing gear equations is beyond the scope of this book, but some of the nonlinear features of the shock absorber were discussed earlier in Section 17.1.1 and will be considered later for landing.)

17.2.5 Example of Flexible Aircraft Taxiing

A flexible aircraft will now be considered to pass over a '1-cosine' dip and the resulting heave displacement and acceleration at the nose and main gear positions is examined. The aircraft parameters are the same as those used for the rigid aircraft taxiing example, but with a fuselage bending mode added having a natural frequency of 2 Hz and damping of 2 % critical; this artificially low frequency (for this size of aircraft) has been selected to highlight dynamic effects. The fuselage mass idealization and the mode shape are the same as used in Chapter 13 and Appendix C. The mode is the idealized case of fuselage bending with no wing twist or bending. The mode shape values at the nose and main gear locations are $\kappa_{\mathrm{eN}} = -2.382$ and $\kappa_{\mathrm{eM}} = 1$ respectively; these values are obtained by assuming the nose gear to be located at the front fuselage mass position and the main gear on the rigid centre fuselage section (see Appendix C).

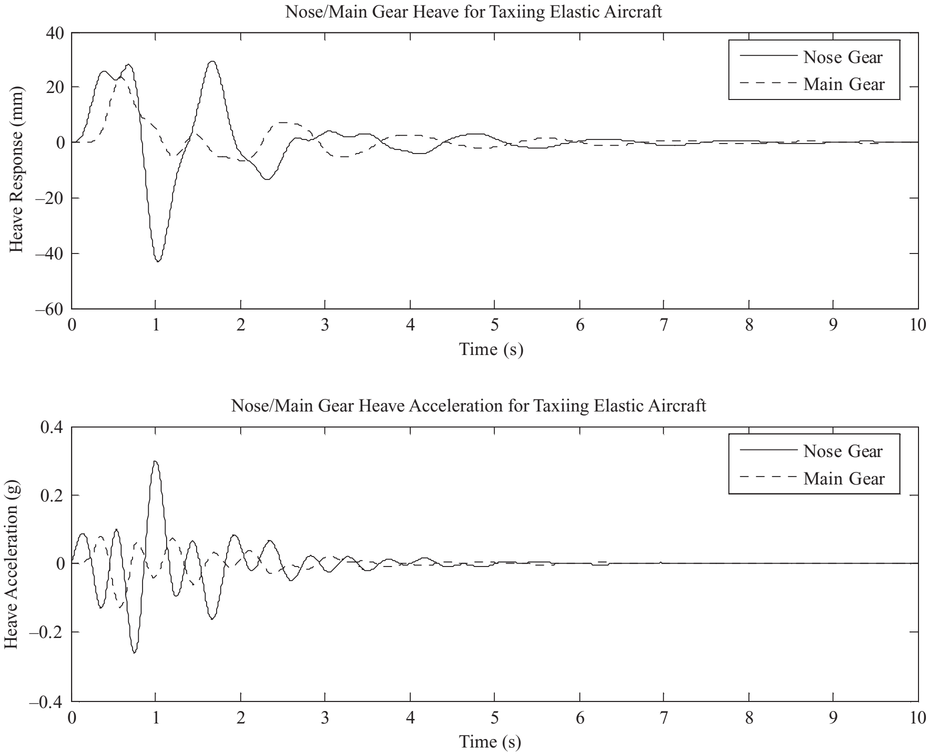

Figure 17.10 Response to taxiing at 30 m/s over a 15 m/30 mm dip for a flexible aircraft.

The modal mass is $m_e = 23\ 340$ kg and the modal stiffness is determined to generate the chosen 2 Hz natural frequency. MATLAB and SIMULINK programs for a flexible aircraft taxiing over a '1-cosine' dip are presented in appendix I of the companion website.

The taxiing velocity is 30 m/s, the depth of the dip is 30 mm and its length is 15 m, as before. The displacement and acceleration responses at the landing gear mounting points are shown in Figure 17.10, with maximum values of approximately 43.2 mm and $0.300g$ respectively; the motion caused by the dip now shows a significant response at the natural frequency of the flexible mode, especially in the acceleration, as would be expected. Clearly, the flexible mode has increased the dynamic response and will change the internal loads.

17.3 LANDING

Landing is a critical load case for the airframe and landing gear (Lomax, 1996; Howe, 2004) since a significant amount of energy has to be dissipated. The main case considered is the aircraft landing on all the main gears simultaneously, with the nose gear still airborne since the aircraft has a positive pitch attitude at the moment of landing prior to final nose down rotation and the nose wheel impacting the ground. The basic landing case (CS-25 and FAR-25) is a descent velocity of 3 m/s (or 10 ft/s) at the design landing weight and with the trimmed attitude/air speed for the $1g$ condition being varied (see also Chapter 25). It will be assumed during the landing of a commercial aircraft that lift remains equal to the weight and that the aircraft is trimmed in attitude on approach by a suitable choice of elevator angle and thrust settings (see Chapter 13). The lift drops off when lift dumpers/spoilers are activated and the

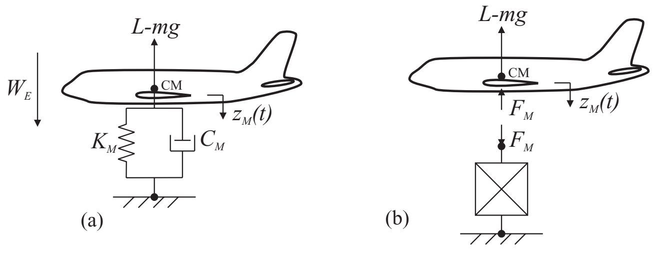

Figure 17.11 Rigid aircraft landing on (a) linear and (b) nonlinear landing gear.

aircraft rotates nose down; this is timed to transfer the weight on to the gear and to avoid the aircraft losing contact with the runway during the landing.

The landing calculations specified in CS-25 are rational, but some bookcases are also included (see Chapter 25). In this section, some simple landing cases will be considered in a rational manner, ranging from a linear spring/damper through a nonlinear shock absorber to a model including the tyre. The effect of the flexible aircraft will be considered briefly. The approach is broadly similar to that employed in industry but no wheel spin-up and consequent spring back effects are included in this model.

17.3.1 Rigid Aircraft Landing – Linear Shock Absorber but No Tyre

Consider the aircraft of mass m (ignoring gear mass) with the main gear shock absorbers represented by a linear model of total damping C_{M} and stiffness K_{M}. Thus a single DoF model is considered, where any fore-and-aft offset of the main gear from the aircraft centre of mass, and consequent pitch motion, has been ignored. The equation for the aircraft as the gear comes into contact with the ground as shown in Figure 17.11 is then

$$m\ddot{z}_{\mathrm{M}} + C_{\mathrm{M}}\dot{z}_{\mathrm{M}} + K_{\mathrm{M}}z_{\mathrm{M}} = L - mg = 0, \tag{17.23}$$

where z_{M} is measured from the aircraft position with the leg uncompressed. The weight mg has been included as a steady force because the final solution (once lift has reduced to zero) must show a steady leg deformation equal to the sag of the aircraft on its landing gear. However, with lift L present for the initial landing impact, sag will not occur since lift offsets the weight; the weight will only transfer on to the gear once the lift is ‘dumped’.

At the moment when the gear comes into contact with the ground, the aircraft is descending at a velocity W_{e} (vertical landing velocity); note that the aircraft is also moving forward (and this will lead to a dynamic ‘spring-back’ of the gear leg that needs to be modelled; see later) but this effect is ignored when using such a simple model to show the energy dissipation in the vertical direction. The initial conditions at the moment of impact are then $z_{\mathrm{M}}(0) = 0,\ \dot{z}_{\mathrm{M}}(0) = W_{\mathrm{e}}$, which will lead to free vibration of the aircraft on its gear. Because the system is a single DoF with an initial velocity W_{e}, the solution of Equation (17.23) for the aircraft response is related to the impulse response function in Chapter 1 and may be written as

$$z_{\mathrm{M}}(t) = \frac{W_{\mathrm{e}}}{\omega_{\mathrm{M}}} \mathrm{e}^{-\zeta_{\mathrm{M}}\omega_{\mathrm{M}}t} \sin(\omega_{\mathrm{M}}\sqrt{1-\zeta_{\mathrm{M}}^2}(\mathrm{t}) \tag{17.24}$$

where $\omega_{\mathrm{M}} = \sqrt{K_{\mathrm{M}}/m}$ is the natural frequency and $\zeta_{\mathrm{M}} = C_{\mathrm{M}}/(2m\omega_{\mathrm{M}})$ is the damping ratio for the aircraft vibrating in heave on its main gears. It may be shown by double differentiation of Equation (17.24) that the presence of damping causes an instant initial deceleration on impact, given by $2\zeta\omega_{\mathrm{M}}W_{\mathrm{e}}$.

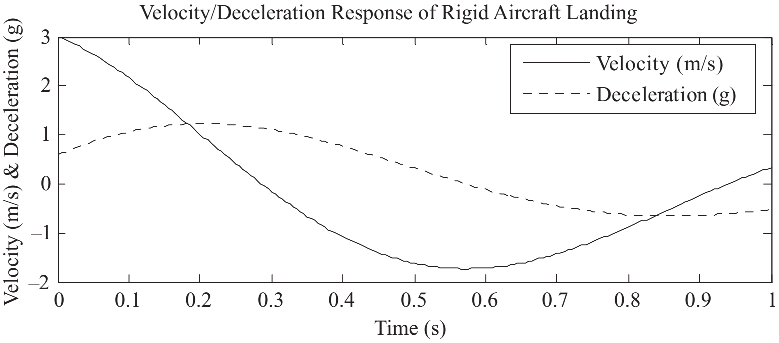

Figure 17.12 Velocity and deceleration responses for landing of a rigid aircraft with a linear shock absorber but no tyre.

An example of a simple landing of a rigid aircraft on a main gear with a linear spring/damper shock absorber but no tyre is now considered. The aircraft parameters are mass $m = 10\,000$ kg, main gear total stiffness $K_{\mathrm{M}} = 240\,000$ N/m and damping $C_{\mathrm{M}} = 19\,200$ N s/m; the natural frequency is 0.78 Hz and the damping ratio 19.6 %. Velocity and deceleration time histories are shown in Figure 17.12, following a 3 m/s initial descent velocity. These results are the same, whether obtained via SIMULINK or analytically from Equation (17.24). The maximum deceleration is $1.23g$. It should be noted that a significant rebound occurs following the initial maximum displacement, which is avoided by suitable design of the nonlinear oleopneumatic shock absorber.

17.3.2 Rigid Aircraft Landing – Nonlinear Shock Absorber but No Tyre

In reality, the main landing gear is highly nonlinear and capable of absorbing the landing impact with minimal rebound. The equations for a rigid aircraft with a nonlinear shock absorber but no tyre can be set up by replacing the linear spring/damper with the nonlinear shock absorber model. Then the aircraft equation will be

$$m\ddot{z}_{\mathrm{M}} + g_{\mathrm{NL}}(\dot{z}_{\mathrm{M}}, z_{\mathrm{M}}) = L - mg = 0, \tag{17.25}$$

where z_{M} is now effectively the main shock absorber compression (equal to the aircraft motion) and g_{NL} is the nonlinear function described earlier in Section 17.1.1, being a combination of the gas spring and orifice damping effects. This equation would then be solved with the same initial conditions as in the previous section and the nonlinear functions added into the simulation via look-up tables (see later).

An example of using a nonlinear shock absorber without a tyre model is now considered. The parameters for a single leg shock absorber are $D_{\mathrm{C}} = 8$ kN s^2/m^2, $D_{\mathrm{R}} = 120$ kN s^2/m^2, $A = 0.005$ m^2, $z_{\mathrm{S}} = 0.4$ m, $V_\infty = 0.0022$ m^3, $z_\infty = 0.44$ m, $P_\infty = 25$ bar (2500 kN/m^2) and $\gamma = 1.35$. The aircraft weight per leg is 50 000 N (i.e. mass of 5000 kg per leg descending) and the descent velocity is 3 m/s. The simulation was carried out using so-called ‘look-up’ tables to cater for the nonlinear damping and stiffness features of the shock absorber, as shown later in Section 17.3.4 and in appendix I of the companion website for the model including the tyre.

The velocity and deceleration shown in Figure 17.13 may be compared to those for the linear gear in Figure 17.12. There is minimal rebound but the deceleration is greater, showing peaks at $1.7g$ and $1.9g$ for the damping and stiffness actions respectively; the initial nonzero deceleration value occurs because the damper acts immediately when subject to the 3 m/s velocity, but in practice the presence of the tyre

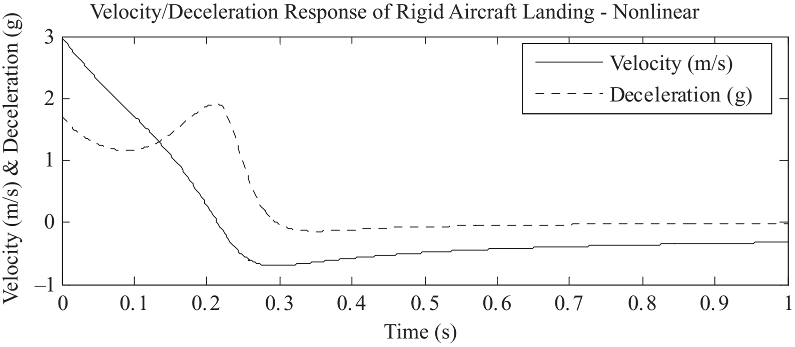

Figure 17.13 Velocity and deceleration responses for landing of a rigid aircraft with a nonlinear shock absorber but no tyre.

dynamics means that the deceleration actually starts from near zero (see the next section). The maximum compression is 85 % of the stroke. The ground load is equal to the aircraft deceleration multiplied by the mass.

17.3.3 Rigid Aircraft Landing – Nonlinear Shock Absorber Plus Tyre

In the previous section example, it was stated that the instantaneous load build-up on the landing gear during landing was unrealistic. This happened because there was no tyre model. A model of the unsprung mass, supported by a linear tyre stiffness k_T, is now included; the small tyre damping forces are neglected in this simple landing model. The equations of motion for the model shown in Figure 17.4 are

$$m\ddot{z}_M + g_{NL}(\dot{z}_{SA}, z_{SA}) = 0, \qquad m_T\ddot{z}_T - g_{NL}(\dot{z}_{SA}, z_{SA}) + k_T z_T = 0, \tag{17.26}$$

where $z_{SA} = z_M - z_T$ is the compression of the shock absorber. Note that the initial velocity for both masses must be equal to the descent velocity W_e. The ground load may be calculated from the relative tyre to ground motion. A MATLAB/SIMULINK model for this system is shown in appendix I, where the use of look-up tables may be seen; a 'look-up' table contains arrays of the force and displacement/velocity, determined using the formulae presented earlier, and SIMULINK interpolates between the values during the solution.

Consider the earlier example in Section 17.3.2 but now include an unsprung mass $m_T = 100$ kg and tyre stiffness $k_T = 1000$ kN/m (equivalent to tyre deformation of approximately 50 mm under the aircraft weight). The displacements and velocities of the aircraft and unsprung mass and the relative shock absorber motions are shown in Figure 17.14 and the ground load normalized to the aircraft weight is shown in Figure 17.15. It may be seen that the total displacement of the aircraft is now a combination of both the shock absorber and tyre deformations; the maximum shock absorber compression is less than that for the model without the tyre. It may also be seen that the tyre will rebound and lose contact with the runway after 0.38 s; the model could be altered to allow for this, but in practice the lift will be dumped so that the aircraft will not usually rebound for a normal landing. Also, the important part of the landing occurs within the first 0.3 s where the loads peak, as seen in Figure 17.15. It may be seen that adding this simple tyre model allows the load to rise from zero, with normalized ground load peaks of 1.39 and 1.6. The inclusion of the tyre avoids the acceleration peak on initial impact. These results are encouragingly similar to those experienced in practice during a drop test. The ground load result shown beyond 0.38 s is meaningless since the tyre load drops to zero when contact is lost.

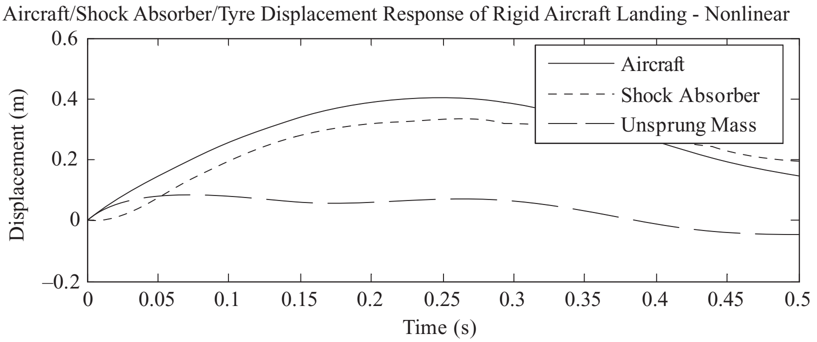

(a) Displacement

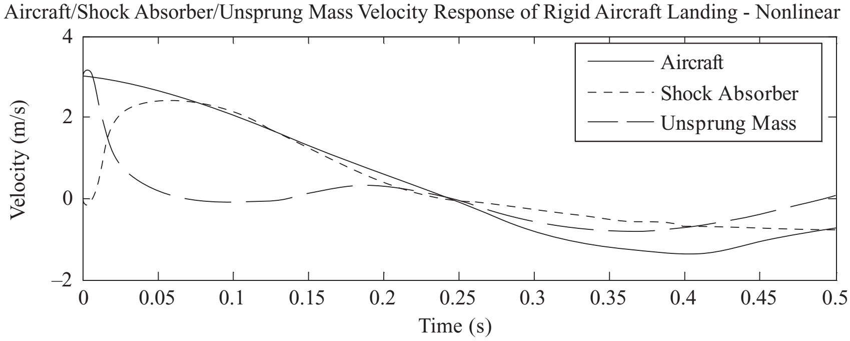

(b) Velocity

Figure 17.14 Response for landing of a rigid aircraft with a nonlinear shock absorber plus tyre: (a) displacement and (b) velocity.

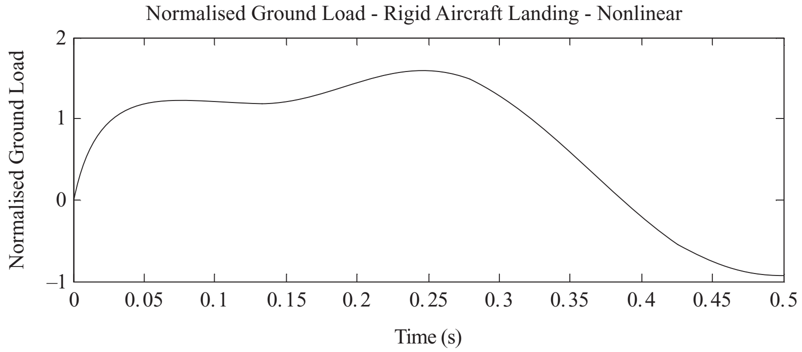

Figure 17.15 Normalized ground load – landing of a rigid aircraft on a nonlinear shock absorber plus tyre.

17.3.4 Flexible Aircraft Landing

When the aircraft is flexible, the situation is more complicated since at the moment of impact the aircraft is in a trimmed state, albeit descending at constant velocity, and elastic deformations of the aircraft will exist because the steady gravitational and aerodynamic forces are differently distributed over the airframe. In Chapter 13, the trim of a flexible aircraft was discussed. It is therefore sensible to consider the response of the aircraft during landing as being *relative to* the deformation of the aircraft on impact with the ground (i.e. incremental quantities). The incremental landing loads would then be added to the steady 1g flight loads present on approach.

The equations for landing of a flexible aircraft on a linear or nonlinear main landing gear may be expressed as a variant of the taxiing Equations (17.18), with only the main gear included in the key phase of the landing:

$$\begin{gathered}\mathbf{M}_q\ddot{\boldsymbol{q}}+\mathbf{K}_q\boldsymbol{q} = -\kappa_{\mathbf{M}}F_{\mathrm{M}},\\ F_{\mathrm{M}} = g_{\mathrm{NL}}(\dot{z}_{\mathrm{M}}, z_{\mathrm{M}}) \qquad z_{\mathrm{M}} = \kappa_{\mathbf{M}}^{\mathbf{T}}\boldsymbol{q},\end{gathered} \tag{17.27}$$

and where vector $\boldsymbol{q}$ now defines the aircraft deformation (heave/pitch/flexible mode) relative to the pre-landing state. The steady aerodynamic and gravitational terms have cancelled out in this incremental calculation. Alternatively, the large angle nonlinear flight mechanics equations for the flexible aircraft developed in Chapter 14 may be employed. Also, high incidence aerodynamic terms may be added as required. Note that the equations will need to be modified to cater for the subsequent nose wheel impact if desired; in practice, the nose gear impact is influenced by pilot control actions, any FCS contribution, aerodynamics, etc.

The initial conditions that need to be set are not immediately obvious. At the moment of impact, the aircraft will not have deformed elastically relative to its pre-landing state so the initial condition is $\boldsymbol{q}(0) = \mathbf{0}$. Also, since only the heave mode has any rate of change at the moment of impact due to the descent velocity, with the pitch and flexible mode generalized coordinates having a zero rate of change, the initial velocity vector may be shown to be $\dot{\boldsymbol{q}}(0) = \{\, W_{\mathrm{e}} \;\; 0 \;\; 0\,\}^{\mathrm{T}}$. Equations (17.27) may then be solved simultaneously in the time domain to determine the aircraft behaviour during the landing. The response and loads will be affected by the flexible mode contribution, being greatest at the aircraft extremities.

17.4 BRAKING

Braking from a high speed landing (or aborted take-off) is a critical design case (Lomax, 1996; Howe, 2004), though braking usually occurs in conjunction with reverse thrust. Part of the forward kinetic energy of the aircraft is converted into heat energy in the main gear braking system. The forces exerted on each wheel due to the application of disc brakes lead to a torque about the axle and hence to a braking force applied at the runway surface, so decelerating the aircraft. The limiting braking that can occur without skidding (or slipping) depends upon the coefficient of friction available between the tyre and the runway, and typically the maximum possible coefficient of friction is 0.8. However, the value depends upon air speed, tyre tread and pressure, runway surface, antiskid system and any torque limitations (ESDU Data Sheets 71025 and 71026); experimental data may be employed in the modelling. Both bookcase and rational calculations will be considered briefly (see also Chapter 25).

17.4.1 Bookcase Braked Roll

Application of the brakes will cause changes in the normal reactions at each gear; e.g. main wheel braking will cause a nose down pitch and hence lead to an increase in the nose gear reaction load. The basic *steady* braked roll case in the certification requirements involves the aircraft with a total braking force F

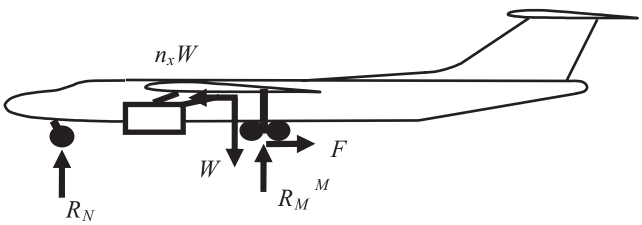

Figure 17.16 Bookcase loads for a steady braked roll.

acting at the main gears, corresponding to a coefficient of friction of 0.8 (so $F = 0.8R_{\mathrm{M}}$), and balanced by a fore-and-aft load factor n_X(i.e. inertia forces $n_X W$); the vertical loads are for a load factor of 1.0 (i.e. static) at the design ramp weight (i.e. the maximum weight for ground handling). Two cases are considered: (a) with the nose gear in contact and (b) with the nose gear not in contact (and pitching effects balanced by a pitch inertia moment). For the first case, the forces are shown in Figure 17.16. Since the steady leg deflections under braking, and hence the forces, will depend upon the nonlinear shock absorber spring curve characteristics, the solution would need to be obtained iteratively. In the second case, no iteration is necessary. In each case, the airframe internal loads may then be determined with the inertia forces distributed over the airframe according to the mass distribution (see Chapters 6 and 18 on loads).

The *dynamic* braked roll bookcase specifies an enhanced nose gear reaction, ‘in the absence of a more rational calculation’; this phrase is often quoted in CS-25 in order to give the manufacturer the opportunity to justify reduced loads by using a more representative calculation or test results.

17.4.2 Rational Braked Roll

If a rational braked roll case is carried out for the steady or dynamic condition, then detailed dynamic models are required to study the loads on the aircraft during braking. The braking force may be applied directly using a suitable coefficient of friction adjusted for the antiskid system in use and justified by test. Alternatively, the braking torque may be considered to be applied with a suitable rise time and tyre-to-runway contact model. The calculation is rather complex.

17.4.3 Effect of Slip Ratio on the Coefficient of Friction

In order to illustrate braking and wheel ‘spin-up’ calculations that are simple but have some degree of rationality, the behaviour at the tyre-to-runway interface needs to be considered. The coefficient of friction between the tyre and the runway behaves in a complex manner and is a nonlinear function of the so-called slip ratio (SR) (ESDU Data Sheets 71025 and 71026) defined by

$$\mathrm{SR} = 1 - \frac{r\dot{\theta}}{V}, \tag{17.28}$$

where r is the effective wheel radius, $\dot{\theta}$ is the angular velocity of the wheel and V (TAS) is the forward speed of the aircraft. The slip ratio is a measure of the relative slip velocity between the tyre and the runway surface. A typical schematic variation of the coefficient of friction μ against slip ratio may be seen in Figure 17.17. When the slip ratio is zero, the wheel is rolling freely so a low rolling coefficient of friction will apply (typically ~0.02), whereas when the slip ratio is unity the wheel is locked and skidding occurs without rolling (coefficient of friction μ_{skid}, typically 0.25 at higher forward speeds and increasing rapidly towards 0.75 as the forward speed reduces). At an intermediate condition,

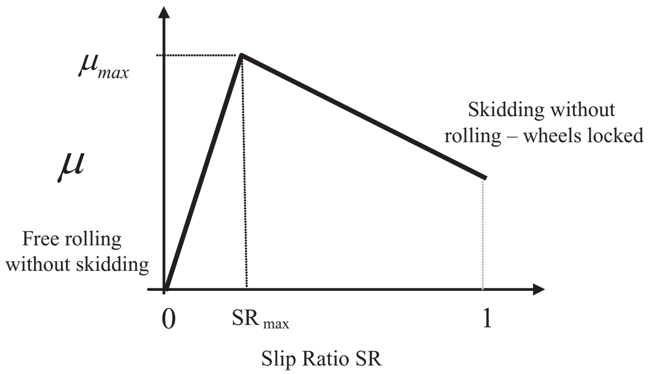

Figure 17.17 Variation of the friction coefficient with slip ratio. (Redrawn from ESDU Data Sheet 71025, Figure 3, with modifications)

typically around a slip ratio of $\mathrm{SR}_{\max} \sim 0.05$–$0.3$, the coefficient of friction reaches a maximum value of $\mu_{\max} \sim 0.8$; at this condition, the tyre is able to grip more effectively than when skidding. These values are quoted for a dry concrete runway and are strongly affected by the condition of the tyre and runway.

This behaviour of the coefficient of friction is relevant for both braking and wheel 'spin-up' on landing (see Section 17.5). For braking, as a braking torque is applied, the operating point on Figure 17.17 moves from left to right whereas in the wheel 'spin-up' case on landing, the operating point moves from right to left.

17.4.4 Simple Braking Model

When a braking torque is applied to a wheel, the tyre mean circumferential speed $r\dot{\theta}$ is less than the forward speed of the aircraft (ESDU Data Sheet 71025) due to tyre deformation and sliding of the tyre tread material relative to the runway within the contact patch. Clearly a complex braking scenario could be envisaged where the coefficient of friction varied significantly with time as the aircraft decelerated. However, a critical braking case at a particular speed is likely to occur when the brakes operate at the condition where the coefficient of friction is a maximum, namely $\mu_{\max} \sim 0.8$, and so the nonlinear variation with slip ratio does not need to be considered. Any braking control system will aim to optimize the braking behaviour.

In order to illustrate braking at a basic level, the case where the braking force is constant will be considered using a simplified model; loads on a single wheel and supporting gear structure for a simplified brake arrangement are shown in Figure 17.18. Simple braking is in essence a quasi-static condition, since the braking force and the airframe deceleration are assumed to be constant at the instant being considered. The diagram shows the braking torque T, the braking force F acting at the runway surface, the normal reaction R at the wheel and intercomponent loads A, B between the wheel and the remainder of the aircraft at the axle bearings; it is assumed for simplicity that the leg carries the relevant proportion of the aircraft weight with no dynamically induced change in reaction. The wheel experiences a forward acceleration $\ddot{x}$ and angular acceleration $\ddot{\theta}$ as shown (for the positive sign convention). The wheel has mass m_{W}, moment of inertia I_{W} and effective tyre radius under braking r (less than the overall wheel radius due to the tyre deformation); the effective mass of the aircraft per supporting wheel is $m_{\mathrm{eff}} = m/N_{\mathrm{W}}$, where N_{W} is the number of wheels active in braking, assuming they all behave in the same way.

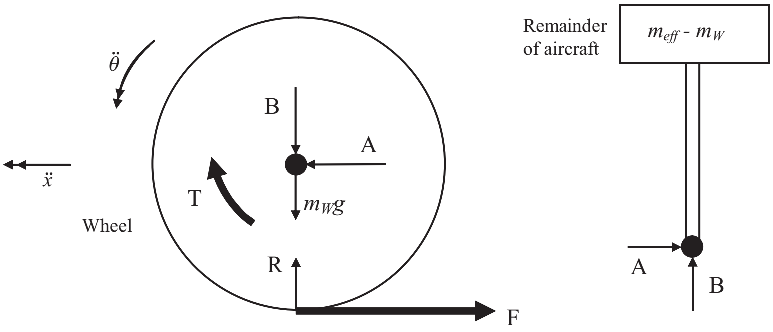

Figure 17.18 Wheel forces during braking.

Now, writing the equations of motion (see Chapter 13) for the wheel and aircraft in this simple case yields

$$\begin{aligned} Fr - T &= I_W\ddot{\theta}, & & -F = m_{\text{eff}}\ddot{x}, \\ A - F &= m_W\ddot{x} & \text{or} \quad & -A = (m_{\text{eff}} - m_W)\ddot{x}, \\ B + m_W g &= R & \text{or} \quad & B = (m_{\text{eff}} - m_W)g. \end{aligned} \tag{17.29}$$

Because it is assumed that $F = \mu_{\max}R$ and R can be determined for a particular deceleration condition (in this case $R = m_{\text{eff}}g$), it may be seen that the aircraft acceleration (negative because it is actually decelerating) and hence the horizontal leg force are given by

$$\ddot{x} = -\frac{F}{m_{\text{eff}}} = -\mu_{\max}g, \qquad A = F\left(1 - \frac{m_W}{m_{\text{eff}}}\right), \tag{17.30}$$

and so $A \approx F$. In the rotation Equation in (17.29), both the torque T and the angular acceleration $\ddot{\theta}$ are unknowns. However, if the moment of inertia of the wheel is neglected ($I_W \ll m_{\text{eff}}r^2$) then the braking torque $T = Fr = \mu_{\max}Rr$, which is achievable provided that the torque is less than or equal to the maximum available torque $T_{\max}$. If, on the other hand, the wheel moment of inertia is included, then whatever torque is applied will give rise to an angular deceleration $\ddot{\theta}$. Also, of course, the brake torque must be reacted on the gear structure.

17.5 'SPIN-UP' AND 'SPRING-BACK' CONDITION

When the aircraft lands then, assuming the wheels are initially stationary, each wheel needs to 'spin-up' (Lomax, 1996; Howe, 2004) from zero rotation speed to an angular speed consistent with rolling at the landing speed of the aircraft (prior to braking); this happens very quickly and is a dynamic condition that will introduce loads into the landing gear. The angular acceleration of the wheel causes the slip ratio to reduce from unity (i.e. skidding without rolling) to zero (i.e. rolling without skidding). Thus the tyre-to-runway contact friction force will be governed by the earlier curve in Figure 17.17 and these nonlinear characteristics will need to be considered (unlike the simplified braking case considered above). As the wheel 'spins up', the force generated at the wheel-to-runway interface will increase to a maximum value (i.e. a better grip is possible) until an optimal slip ratio ($\text{SR}_{\max}$) is reached; beyond this point the contact force will reduce until there is no slip.

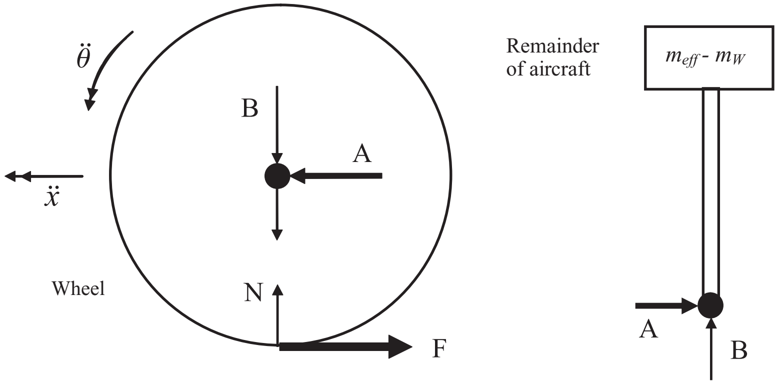

Figure 17.19 Wheel forces during 'spin-up'.

As a simple model, consider the forces acting on the wheel as shown in Figure 17.19; the forces are similar to those for braking but there is no applied torque and the frictional force F is generated by the wheel-to-runway contact on landing. The equations of motion for the wheel in the 'spin-up' case are given by

$$\begin{aligned} Fr &= I_W\ddot{\theta}, \qquad & -F &= m_{\text{eff}}\ddot{x}, \\ A - F &= m_W\ddot{x}, \qquad & B + m_W g &= R. \end{aligned} \tag{17.31}$$

An analysis is required in which the instantaneous frictional contact force F needs to be determined at any stage of the calculation using $F = \mu R$, where the value of μ is dictated by the instantaneous slip ratio according to Figure 17.17. If at any instant $\dot{\theta}$ is known, the slip ratio (SR) may be determined and hence F, $\ddot{\theta}$ and $\ddot{x}$ may be calculated from the dynamics of the wheel (and where necessary the remainder of the aircraft); a revised $\dot{\theta}$ can then be obtained by integration, an updated value of slip ratio determined and so on (in effect a look-up table approach could be employed as in the earlier landing case). The equations governing wheel 'spin-up' are therefore nonlinear.

Two cases need to be considered, depending upon whether the landing gear leg is rigid or flexible:

(a) Consider firstly the landing gear leg structure to be *rigid* and to move forward with the remainder of the aircraft at *constant velocity* (so there is no fore-and-aft acceleration of the wheel and $\ddot{x} = 0$). The equation of motion governing the wheel rotation is

$$Fr = I_W\ddot{\theta} \tag{17.32}$$

and so the frictional force accelerates (or 'spins-up') the wheel in rotation. The frictional force may be determined from the coefficient of friction, defined in Figure 17.17 as a nonlinear function of the slip ratio which may be estimated by integrating $\ddot{\theta}$ to obtain $\dot{\theta}$. Then, knowing the values of F and R, the loads A, B at the axle bearings and hence other loads in the landing gear leg may be obtained from Equation (17.31).

(b) However, in practice the landing gear structure is not rigid but *flexible* and the frictional force due to the wheel 'spin-up' will cause the leg to deform rearwards in bending and then 'spring back' in the forwards direction when the load reduces (Lomax, 1996; Howe, 2004); the gear leg will therefore respond in its bending modes of vibration. Thus, due to this oscillation of the flexible gear, there will be relative motion between the wheel and the aircraft structure, so strictly speaking the velocity of the aircraft will vary during this phase of landing and the wheel will experience fore-and-aft accelerations, giving $\ddot{x} \neq 0$. A suitable dynamic model for the aircraft plus flexible landing gear leg (modelled in fore-and-aft bending using an SDoF or MDoF assumption) would need to be developed so that it may be coupled to the wheel dynamic equations via the intercomponent force A.

At any instant, the frictional force F may then be used to calculate the dynamic response of the aircraft/leg/wheel model; the slip ratio expression would need to be adjusted to use the instantaneous fore-and-aft wheel velocity component $\dot{x}$, which will differ with the speed of the remainder of the aircraft due to leg flexibility. A further complication is that the leg modes will be a function of the vertical closure of the shock absorber at any instant of time and so some form of interpolation between modal properties and leg length will be required.

17.6 TURNING

It is also important for an aircraft to be able to steer in a circular path on the ground without turning over or generating excessive loads (Lomax, 1996; Howe, 2004). A sketch of the basic turning kinematics is shown in Figure 17.20 (Currey, 1988). Usually, the nose wheel is steerable and the main wheels follow, with a small degree of tyre 'scrub' (i.e. rotation about a vertical axis if they are not being steered). Lateral tyre forces are developed to generate the required centripetal acceleration V^2/r in the turn of radius r.

The turning bookcase in CS-25 (see also Chapter 25) is for a $0.5g$ turn where the side forces on each gear are equal to 0.5 times the vertical reaction per gear for the static case; the side forces are balanced by lateral inertia forces and the vertical forces are balanced by the weight. The idea is shown in Figure 17.21 where the subscripts 'o' and 'i' on the main gear reactions refer to the outside and inside of the turn respectively. The equations for the unknown reactions R_{Mi}, R_{Mo}, R_{N}, and hence turning forces, may be derived by equilibrium considerations (zero net vertical force, zero rolling moment and zero pitching moment). Internal loads in the airframe may be found by introducing distributed inertia loads. Obviously, far more rational and therefore complex calculations may be carried out if desired.

17.7 SHIMMY

Shimmy occurs when a wheel (or set of wheels) oscillates at often large amplitudes about its caster axis (i.e. the vertical axis about which the wheel system rotates), with a frequency typically between 10 and

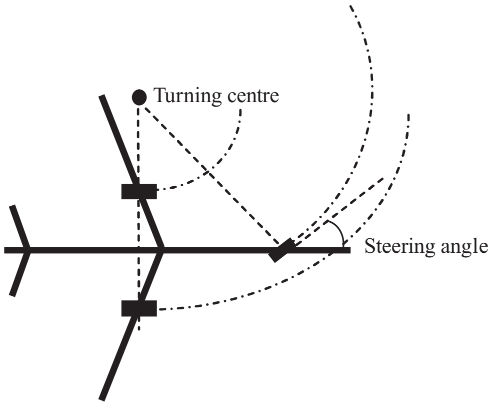

Figure 17.20 Simple turning kinematics.

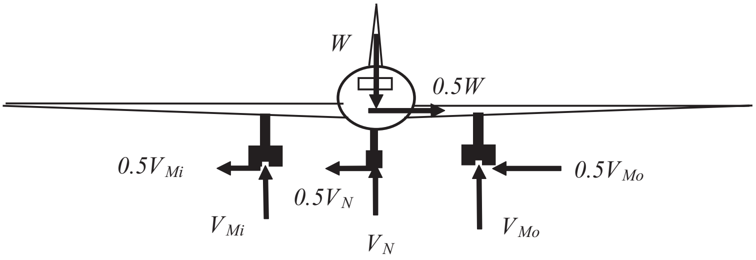

Figure 17.21 Bookcase loads for a 0.5g turn.

30 Hz. It is in essence a self-excited instability, but one that manifests itself as a limit cycle oscillation; i.e. due to nonlinear effects, it reaches a maximum motion. It is most common for nose or main gear cantilevered twin wheel units and does not occur on bogie units. It can occur, for example, when severe vibration occurs on the wheels of a supermarket shopping trolley.

Shimmy can occur due to inadequate torsional stiffness, torsional freeplay, wheel imbalance, etc. It is normally countered by careful design or use of dampers. It is an extremely difficult phenomenon to model as it is nonlinear and requires knowledge of complex tyre response characteristics, etc. The tyre lateral force causes a sideslip angle of the landing gear and in turn the tyre sideslip angle changes, thus modifying the lateral force and potentially leading to an unstable system. A highly simplified two DoF model of the shimmy phenomenon for a trailing wheel nose gear can be developed, following on from Den Hartog (1984). Figure 17.22 shows the wheel and suspension arrangement viewed from above and the position of the landing gear on the front fuselage. The gear-to-aircraft attachment point D moves forward at the speed V (TAS) of the aircraft and is unaffected by feedback from the nose gear dynamic motion (i.e. front fuselage flexibility effects are being ignored). Point B is the bottom of the strut and so it may be seen that the gear strut is flexible, bending through a small displacement y against an effective strut bending stiffness k_y. The tyre is assumed to be rigid. The wheel, whose centre is at point A, lies behind point B by a mechanical trail $a + b$ and yaws through the shimmy angle ψ (assumed small), with the yaw motion restricted by a viscous damper c_ψ. Note that the dynamics would alter if a yaw stiffness k_ψ were present and this could be examined as an exercise. The centre of mass of the combined landing gear is at point C. A follower friction force F acts from the ground on the wheel tread to prevent any sideslip motion of the tyre.

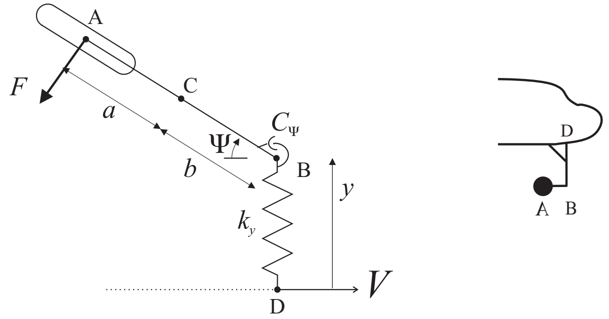

Figure 17.22 Simplified shimmy model.

The kinetic energy term is

$$T = \tfrac{1}{2}m(\dot{y} + b\dot{\psi})^2 + \tfrac{1}{2}I_C\dot{\psi}^2, \tag{17.33}$$

where m is the mass of the combined landing gear and I_C is the moment of inertia of the landing gear about the centre of mass C. The potential energy term for the strut bending and the dissipative term associated with the yaw damper are

$$U = \tfrac{1}{2}k_y y^2, \quad \Im = \tfrac{1}{2}c_\psi \dot{\psi}^2. \tag{17.34}$$

Finally, the incremental work done due to the friction force is

$$\delta W = -F\left[\delta y + (a+b)\delta\psi\right]. \tag{17.35}$$

Applying Lagrange's equations leads to

$$\begin{aligned} m\ddot{y} + mb\ddot{\psi} + k_y y &= -F, \\ mb\ddot{y} + (I_C + mb^2)\ddot{\psi} + c_\psi\dot{\psi} &= -F(a+b). \end{aligned} \tag{17.36}$$

Now the unknown friction force F may be eliminated to combine the two equations into one kinetic equation (with several possible forms); e.g.

$$ma\ddot{y} + (mab - I_C)\ddot{\psi} - c_\psi\dot{\psi} + k_y(a+b)y = 0. \tag{17.37}$$

A further equation may be obtained from the kinematic relationship that there must be no sideslip of the wheel; i.e. the net velocity of the centre of the wheel must act at the angle ψ to the forward direction of the aircraft, so

$$-\frac{\dot{y} + (a+b)\dot{\psi}}{V} = \tan\psi \approx \psi \tag{17.38}$$

and

$$\dot{y} + (a+b)\dot{\psi} + V\psi = 0. \tag{17.39}$$

Combining Equations (17.37) and (17.39) in matrix form leads to the equation

$$\begin{bmatrix} ma & mab - I_C \\ 0 & 0 \end{bmatrix}\begin{Bmatrix} \ddot{y} \\ \ddot{\psi} \end{Bmatrix} + \begin{bmatrix} 0 & -c_\psi \\ 1 & a+b \end{bmatrix}\begin{Bmatrix} \dot{y} \\ \dot{\psi} \end{Bmatrix} + \begin{bmatrix} k_y(a+b) & 0 \\ 0 & V \end{bmatrix}\begin{Bmatrix} y \\ \psi \end{Bmatrix} = \begin{Bmatrix} 0 \\ 0 \end{Bmatrix}, \tag{17.40}$$

giving a nonconservative system. Assuming that the strut displacement and shimmy angle are governed by the exponent exp (λt) as per a flutter solution (see Chapter 11), the roots of the system are given by setting the 2 × 2 determinant to zero, thus yielding a cubic equation in λ:

$$(I_C + ma^2)\lambda^3 + (maV + c_\psi)\lambda^2 + k_y(a+b)^2\lambda + k_y(a+b)V = 0. \tag{17.41}$$

Applying the Routh–Hurwitz criterion (see Chapter 7) yields the following condition for stability:

$$(mab - I_C)V + c_\psi(a+b) > 0. \tag{17.42}$$

Thus the damping, not present in Den Hartog's analysis, is stabilizing and leads to a finite shimmy speed

$$V_{\mathrm{crit}} = \frac{c_\psi (a+b)}{I_{\mathrm{C}} - mab}. \tag{17.43}$$

Above this critical speed, shimmy will occur as an instability involving both y and ψ motions, though of course in practice nonlinear effects will then come into play to limit the response amplitude (i.e. a limit cycle oscillation; see Chapter 11). Clearly, based on this model, shimmy will never occur if $I_{\mathrm{C}} \leq mab$ but this condition is unlikely for practical cases (Den Hartog, 1984). Equation (17.43) also shows that it is important to include damping.

The analysis carried out here is very simplistic. For a real aircraft it should be recognized that the flexibility of the fuselage and landing gear and complex nonlinear flexible tyre dynamics need to be included.

17.8 REPRESENTATION OF THE FLIGHT CONTROL SYSTEM (FCS)

The extent to which the FCS needs to be represented in ground manoeuvres depends upon which, if any, of the FCS functions are relevant to the particular manoeuvre being considered; e.g. if the rotation and de-rotation phases of landing are to be modelled, then the appropriate control laws will be included. The steering and braking control systems should be modelled as required for rational calculations. Bookcase calculations will require any relevant FCS limits to be considered.

17.9 EXAMPLES

Note that some of the examples in Chapters 1 and 2 might be helpful.

1. An aircraft taxiing may be represented as a single degree of freedom system consisting of a mass m supported by a landing gear of linear stiffness k and damping c. The aircraft moves at a velocity V over a harmonically undulating runway surface of wavelength λ and amplitude $\pm h$. Determine the equation of motion for the mass and the amplitude of the steady-state harmonic response as a function of the velocity. Hence find an expression for the most unfavourable value for the velocity of the aircraft.

2. An aircraft of mass 50 000 kg is travelling at a steady speed in high speed taxiing trials. Neglecting aerodynamic forces, the aircraft and its landing gear/tyres can be modelled as a system with a single (vertical) DoF with stiffness of 30 MN/m and damping coefficient of 1.6 MN s/m. The surface of the runway has a sinusoidal profile with amplitude of 10 mm and a wavelength of 15 m. The wheels always remain in contact with the runway. Find the amplitude of vertical displacement of the aircraft and its maximum vertical acceleration when the forward speed of the aircraft is 30 m/s.

   [12 mm, 0.19 g]

3. Write a MATLAB/SIMULINK program to solve the problem of an aircraft taxiing over (a) a harmonically undulating runway and (b) a '1-cosine' dip. The aircraft on its landing gear is modelled as a single DoF system, rather as in Examples 1 and 2 above. Choosing the parameters in Example 2, use part (a) of the program to check the result in Example 2. Then use part (b) to solve for the variation of maximum displacement response of the aircraft as a function of forward speed for a given 'dip' wavelength.

4. Consider the general form of the two DoF heave/pitch taxiing model used in this chapter. The aircraft moves at a velocity V over a harmonically undulating runway surface of wavelength λ and

amplitude $\pm h$. Write the equations governing the steady-state solution in the frequency domain (refer to Chapter 16 for the analogous harmonic gust treatment).

5. Use the taxiing program given in Appendix I for the rigid aircraft in pitch and heave to confirm the results given in this chapter for the worst case velocity for a given 'dip'. Extend the program to cater for the flexible case and again confirm the results given in this chapter.

6. A shock absorber has a piston area of 0.01 m^2, stroke of 0.4 m, pressure when fully extended of 30 bar and fully compressed of 300 bar, polytropic constant 1.35, compression and recoil damping coefficients of 18 and 270 kN s^2/m^2 and effective aircraft weight of 100 000 N per leg (i.e. 10 000 kg mass descending per leg). Generate a MATLAB/SIMULINK model for the landing case, using look-up tables for the stiffness and damping characteristics (see Appendix I). Determine the displacement, velocity and acceleration response following a 3 m/s landing and find the maximum value of acceleration. Examine the effect of changing the values of the two damping coefficients on the relative magnitude of the two acceleration peaks.

   [1.65*g*]

7. Repeat the solution of Example 6 by adding a tyre representation of an unsprung mass of 200 kg and a tyre stiffness of 2000 kN/m.

   [1.41*g* and 1.52*g*]

8. An aircraft of mass 10 000 kg has two main legs with four wheels on each leg. The rolling radius of each wheel is 0.25 m, the wheel mass is 30 kg and the radius of gyration in rolling is 0.2 m. A braking torque of 1250 N m is applied to each wheel. Determine the aircraft deceleration and the horizontal load acting on each leg. What is the ratio of braking force to normal reaction (i.e. effective friction value?

   [3.94 m/s^2, 19 200 N, 0.39]

9. Determine the critical condition for shimmy to occur for the undercarriage system shown in Figure 17.23 (Den Hartog, 1984). Determine the critical shimmy condition for the addition of (a) a translational damper C_y and (b) a rotational stiffness K_θ.

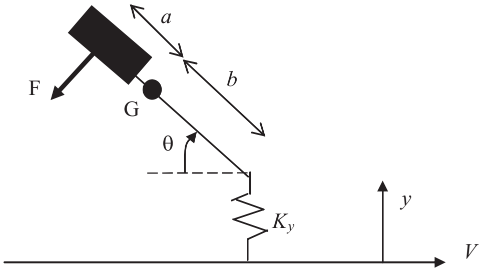

Figure 17.23

18

Aircraft Internal Loads

So far, in Chapters 13 to 17, the different types of manoeuvre and gust inputs have been considered from the point of view of calculating the aircraft response in the rigid body and flexible mode generalized coordinates, and therefore potentially at any physical point on the structure. In this chapter, the way in which these responses are used to obtain the internal loads (i.e. moment, axial, shear and torque, or 'MAST', loads) at reference cross-sections in the airframe will be considered; the method of summation of forces is employed. The focus will be on the internal loads present in the main slender structural components of wing and fuselage.

Some important concepts of loads were introduced in Chapter 6 and it will be assumed that the reader has a grasp of these issues when reading this present chapter. In particular, the use of D'Alembert's principle to allow an accelerating member to be treated as being in effective static equilibrium by adding distributed inertia forces was considered. This approach is powerful in that it allows standard static methods of determining internal loads to be applied to an accelerating slender member subject to a loading which varies with time and is nonuniformly distributed spatially. Indeed, the airworthiness regulations (CA-25 and FAR-25) include direct reference to balancing the applied loads by inertia forces and couples. In Chapter 6, the slender members were considered as firstly continuous, and then represented in a discretized manner. This is because, in practice, the determination of internal loads requires the structure and loading to be idealized into discrete finite width strips and a summation will then replace the integral in the loads analysis. The analysis of the structural behaviour using a discretized representation and the relevant strip theory aerodynamics was introduced in Chapters 4 and 5 respectively. Further consideration of generating a suitable aerodynamic model for a discretized aircraft and coupling it to the structure will be considered in Chapters 19 and 20.

In this chapter, the basic concepts in Chapter 6 are applied to more representative aircraft cases, including where the inertia and aerodynamic loadings are both nonuniformly distributed and time varying, such as would occur for dynamic manoeuvres and gust encounters. Lifting surfaces (e.g. wings) are considered firstly as continuous, in order to be consistent with the Rayleigh–Ritz treatment used extensively earlier in the book, and then as discretized. The effect of discrete external load inputs, such as engine thrust and landing gear reactions, is explained. The loads in the fuselage will only be considered on a discrete basis because the fuselage geometry and mass distribution is not ideal for treating as continuous.

A brief explanation of load sorting, to obtain critical cases for dimensioning, and the importance of loads envelopes is included. Also, the process of using these internal loads to obtain loads and stresses acting on internal structural elements will be mentioned; however, it is a complex procedure and beyond the scope of this book. Some explanation is provided of areas where terminology employed for loads can be confusing. Practical issues are further discussed in Chapters 21 and 25.

Introduction to Aircraft Aeroelasticity and Loads J. R. Wright and J. E. Cooper
© 2007 John Wiley & Sons, Ltd

18.1 LIMIT AND ULTIMATE LOADS

Strength requirements for certification (see Chapter 21) are specified in terms of:

(a) *limit loads*, which are the maximum loads to be expected in service and which the structure needs to support without 'detrimental permanent deformation' and

(b) *ultimate loads* (limit loads multiplied by a factor of safety, normally 1.5 unless otherwise stated), which the structure must be able to support without failure/rupture.

Loads specified in the certification requirements are almost entirely limit loads. Thus the loads calculated for manoeuvres and gust/turbulence encounters are limit loads. The requirements also specify that compliance with the strength and deformation conditions must be demonstrated for each critical loading condition. Further comments on limit and ultimate loads, and on fatigue and damage tolerance, are included in Chapter 21.

18.2 INTERNAL LOADS FOR AN AIRCRAFT

In this section, a brief introduction to the origin of internal loads in a wing and fuselage will be presented. The ESDU series includes an item on internal loads (ESDU Data Sheet 94945).

18.2.1 Internal Loads for a Wing

In general for an aircraft under three-dimensional motion, the external loading is distributed such that the wing is subject to bending moments and shear forces in the vertical and horizontal planes, as well as to torque, which represents the tendency of a component to twist. A typical free body diagram (FBD) for a section of *wing* is shown in Figure 18.1. Vertical bending and shear occur due to a spanwise imbalance between the lift and inertia distribution along the wing whereas horizontal (fore-and-aft) bending and shear occur due to a spanwise imbalance between the drag and fore-and-aft inertia distribution and engine thrust (for wing-mounted engines). Torque occurs because of a chordwise imbalance of wing lift and inertia distribution, as well as of drag, fore-and-aft inertia and thrust. Landing gear loads also influence the internal loads on the inboard wing.

It should be noted that there is more weight, and hence inertia loading, in the fuselage than in the wings whereas the converse is true for the aerodynamic loading. Therefore on the wings the inertia

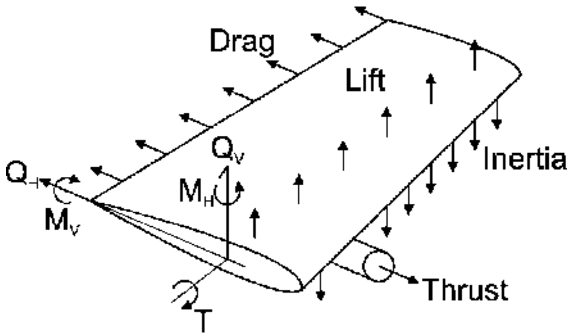

Figure 18.1 External and internal loads on a wing section.

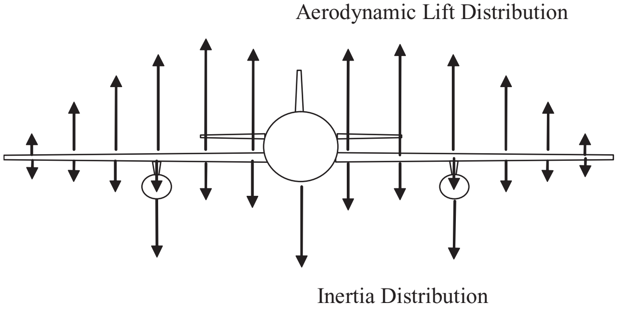

Figure 18.2 Inertia and aerodynamic loading distribution on a wing showing inertia relief.

loads associated with the wing structure (and fuel) and any wing-mounted engines will counteract the aerodynamic loads and so 'relieve' the bending moments and shear forces caused by the aerodynamic loads, as illustrated in Figure 18.2. This is demonstrated in a later example and is one reason why engines are often placed on the wings. In the limit of this argument, it is interesting to note that for a flying wing, if lift and weight (and therefore inertia) could be equally distributed spanwise, then there would be no vertical shear force or bending moment.

18.2.2 Internal Loads for a Fuselage

An FBD for a rear *fuselage* section is shown in Figure 18.3. Vertical bending and shear are experienced due to the imbalance between tailplane/rear fuselage lift and inertia forces, while torsion, lateral bending and shear result from an imbalance of lateral aerodynamic loads and inertia forces acting on the fuselage/tail. Unlike the wing, axial loads will occur due to the imbalance of engine thrust (for rear fuselage mounted engines) and tailplane drag forces (and also cabin pressurization loads). Again, landing gear loads make a significant contribution to the front and centre fuselage when the aircraft is on the ground. The convention adopted for positive internal loads must be chosen carefully and, most importantly, be consistent for loads calculations along any given component for different manoeuvre and gust cases.

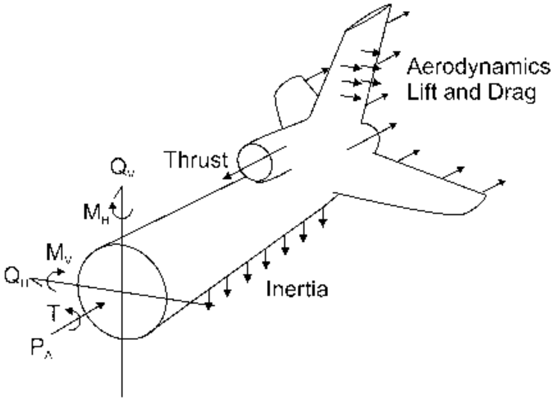

Figure 18.3 External and internal loads on a rear fuselage section.

18.3 GENERAL INTERNAL LOADS EXPRESSIONS – CONTINUOUS WING

In this section, the general case of an aircraft wing experiencing vertical shear/bending/torsion loads under the action of inertia and aerodynamic lift forces during a manoeuvre or gust encounter is considered. The same approach could be used for other lifting surfaces such as the fin and horizontal tailplane. An example will be given of a tapering wing for an aircraft undergoing an equilibrium manoeuvre. In the subsequent sections, application will be made to the aircraft model employed earlier in Chapters 13 to 17.

18.3.1 General Expression for Internal Loads

Consider the wing shown in Figure 18.4 where the aerodynamic lift and inertia forces per unit span are $\lambda_A(\eta, t)$ and $\lambda_I(\eta, t)$ respectively; η defines the spanwise position and the inertia force acts upwards if acceleration $\ddot{z}$ is defined as positive downwards, as has been the case earlier in the book (apart from in Chapter 6 where acceleration was defined positive upwards for convenience – in the direction of the positive applied force). The FBD for the section of wing created by a 'cut' at the spanwise position y is also shown in Figure 18.4, with internal loads introduced to permit equilibrium of the cut section; thus, in essence, the analysis starts at the tip and works towards the root such that the wing root reactions are not required a priori. Taking moments about the cut for equilibrium, the shear force and bending moment expressions are given by integrating over the cut section, so

$$Q(y,t) = \int_{\eta=y}^{s} [\lambda_A(\eta,t) + \lambda_I(\eta,t)]\mathrm{d}\eta, \qquad M(y,t) = \int_{\eta=y}^{s} [\lambda_A(\eta,t) + \lambda_I(\eta,t)](\eta - y)\mathrm{d}\eta. \tag{18.1}$$

The shear force and bending moment may be calculated at any spanwise position as a function of time provided the lift distribution is defined as a function of the wing motion (and, where relevant, gust

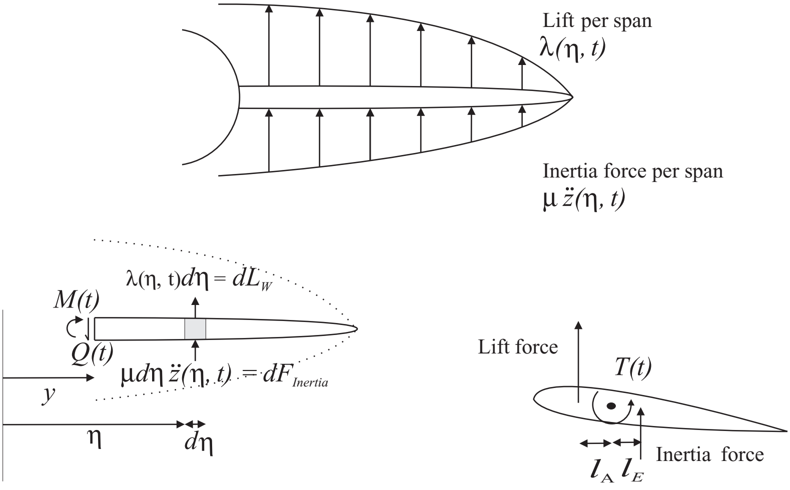

Figure 18.4 Loads on a continuous wing.

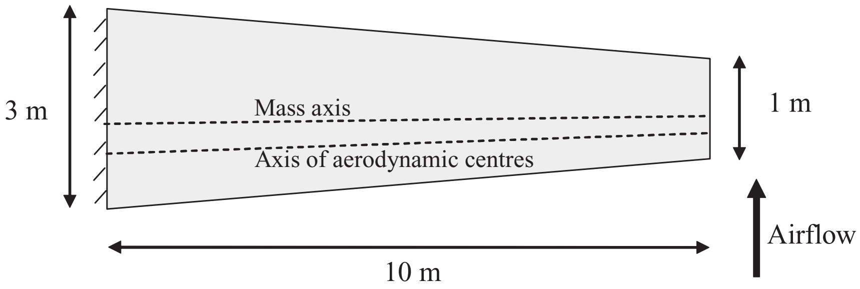

Figure 18.5 Diagram of the tapered wing example.

velocity). Since the lift and inertia forces act at different chordwise positions, as shown in Figure 18.4, then a torque is also present and would need to be calculated using a similar integration approach to that applied above for the shear force and bending moment. For an untapered/unswept wing, then the nose up torque about the flexural axis is

$$T(y,t) = \int_{\eta=y}^{s} [l_A \lambda_A(\eta,t) - l_E \lambda_I(\eta,t)] \mathrm{d}\eta \tag{18.2}$$

where the lift acts a distance l_A forward of the flexural axis and the inertia force a distance l_E behind it. However, the torque expression would differ for a swept or tapered wing.

18.3.2 Example: An Equilibrium Manoeuvre – Continuous Wing

An aircraft whose wing planform is shown in Figure 18.5 has a total mass of 50 000 kg and experiences a steady symmetric pull-up manoeuvre with an incremental acceleration of $2g$, so that the load factor n is 3. Each wing with a full fuel load has a mass of 5000 kg. For ease of analysis the wing is unswept, and it may be assumed that all the aircraft lift is carried by the wings and that the wing mass (including fuel) and wing lift are distributed in proportion to the wing chord; thus any tip effects or flexible mode deformation effects are ignored. At any spanwise location, the lift acts at the quarter chord and the mass axis is assumed to be at 40 % chord. Determine the distributions of the wing shear force, bending moment and torque (about 50 % chord), assuming the sign convention shown in Figure 18.6. Firstly, treat the problem as continuous; the results will be compared later to those obtained from a discretized version. Take $g = 10$ m/s^2 for simplicity.

The total wing lift in the manoeuvre is $L = nW = 3 \times (50\,000 \times 10)/1000 = 1500$ kN, so the lift per wing is 750 kN. Since the area per wing is 20 m^2, the wing loading is $750/20 = 37.5$ kN/m^2. The inertia force per wing (acting downwards and therefore negative) is $nW_{\text{wing}} = 3 \times (5000 \times 10)/1000 =$ 150 kN or 7.5 kN/m^2. The variation of chord with distance η from the root is given by $c(\eta) = 3 - 0.2\eta$. The lift and inertia forces per unit span are then given by $\lambda_A = 37.5c$ and $\lambda_I = -7.5c$ kN/m respectively,

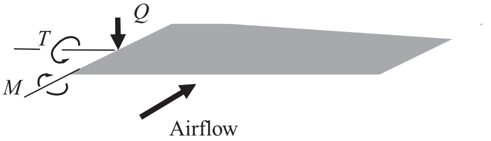

Figure 18.6 Internal load sign convention for the tapered wing example.

so they vary with the chord. Then, considering the forces acting on an element $\mathrm{d}\eta$ and using the approach taken earlier in Section 18.3.1, the shear force, bending moment and torque (at 50 % chord) at position y outboard of the wing root are given by the following expressions:

$$\begin{aligned}
Q(y) &= \int_{\eta=y}^{10} (37.5 - 7.5)c\,\mathrm{d}\eta = \int_{\eta=y}^{10} (37.5 - 7.5)(3 - 0.2\eta)\,\mathrm{d}\eta = 600 - 90y + 3y^2,\\
M(y) &= \int_{\eta=y}^{10} (37.5 - 7.5)\,c(\eta - y)\mathrm{d}\eta = 2500 - 600y + 45y^2 - y^3, \qquad (18.3)\\
T(y) &= \int_{\eta=y}^{10} \left(37.5c\,\frac{c}{4} - 7.5c\frac{c}{10}\right)\mathrm{d}\eta = 373.75 - 77.625y + 5.175y^2 - 0.115y^3.
\end{aligned}$$

The values of these internal loads at the root and 4 m outboard of the root are $Q(0) = 600$ kN, $Q(4) = 288$ kN, $M(0) = 2500$ kN m, $M(4) = 756$ kN m, $T(0) = 373.75$ kN m and $T(4) = 138.69$ kN m. These are ‘exact’ values within the approximations made in the problem and will be seen later to compare closely with the results obtained for the discretised representation when these are plotted along the wing span.

18.4 EFFECT OF WING-MOUNTED ENGINES/LANDING GEAR

If a wing-mounted engine were to be present, a discrete vertical inertia force needs to be introduced and its effect added into the shear force, bending moment and torque expressions inboard of the engine location. Also, the engine thrust would add a further torque component and introduce fore-and-aft shear and bending. Similarly, in a ground manoeuvre, the effect of any landing gear leg reaction force acting on the wing would need to be included in the wing internal load calculations. The effect of such discrete loads for a simple unswept wing would be to introduce a step change in the shear force and torque diagrams and a change of slope in the bending moment diagrams; for a swept wing, there is usually a step change in the bending moment also.

Now, returning to the earlier tapered wing example in Section 18.3.2, consider an engine of mass 2000 kg to be mounted on each wing (instead of on the fuselage) a distance 3 m outboard from the root and with its centre of mass being 1.5 m forward of the wing centre line, as shown in Figure 18.7. Assume that the wing lift in this manoeuvre is unchanged. A thrust of 20 kN acts at a distance 1 m below the wing.

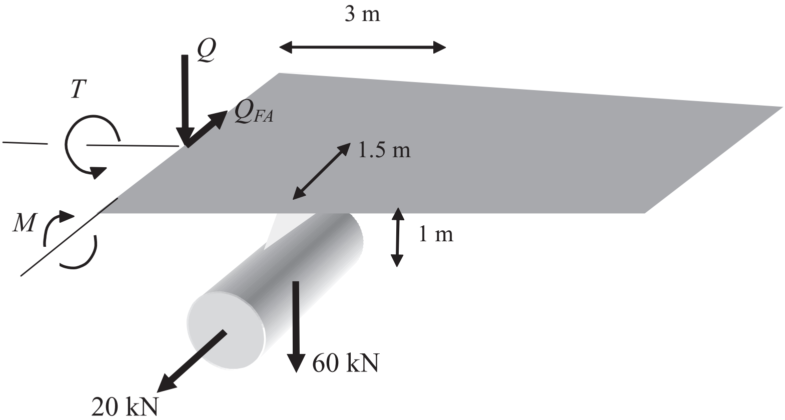

Figure 18.7 Addition of an under-wing engine.

The thrust contributes 20 kN m nose up torque and 20 kN fore-and-aft shear force on the inner wing, as well as a fore-and-aft bending moment (60 kN m at the root). The downwards inertia force associated with the engine is $3 \times (2000 \times 10)/1000 = 60$ kN, so contributing $60 \times 1.5 = 90$ kN m nose down torque about the wing centre line. Thus the net nose down torque due to the thrust and inertia load for the engine is $90 - 20 = 70$ kN m. Therefore the vertical shear force and torque calculated earlier will reduce by 60 kN and 70 kN m respectively, at both positions 4 and 5. The vertical bending moment will reduce by $60 \times 1 = 60$ kN m at position 4 and by $60 \times 3 = 180$ kN m at position 5. The presence of the wing-mounted engine thus alleviates (or relieves) the wing loading in a manoeuvre as mentioned earlier.

18.5 INTERNAL LOADS – CONTINUOUS FLEXIBLE WING

In this section, the general expressions for internal loads will be considered for a flexible aircraft undergoing manoeuvres or encountering gusts. The analysis employs a continuous representation of the wing so as to be compatible with the earlier consideration of manoeuvres and gusts in Chapters 13 to 17 where a single flexible mode was included together with heave and pitch motions; the discretized case will be considered later.

18.5.1 Steady and Incremental Loads

At this point it is worth noting that under some circumstances the dynamic model only yields the incremental response, and hence loads, relative to a steady underlying condition; the steady and incremental loads then need to be added together. This is the case for the gust encounter and also for flight manoeuvres; depending upon the way in which the equations are formed, it may also be the case for some of the ground manoeuvres. Obviously, the equilibrium manoeuvre only generates a steady load.

18.5.2 Internal Loads in An Equilibrium Manoeuvre

The inertia and aerodynamic forces per unit span will be obtained for an equilibrium manoeuvre (see Chapter 13) and then substituted into the general internal load equations derived above. Because it is a steady, and not time-varying, manoeuvre this is a simpler case than the dynamic manoeuvre or gust encounter.

18.5.2.1 Inertia force per unit span

The expression for the inertia force per unit span $\lambda_I(\eta, t)$ depends upon the type of manoeuvre. For an equilibrium pitching manoeuvre at a steady pitch rate, the acceleration is constant with time and the same at every point on the airframe whether it is rigid or flexible; the acceleration is dictated by the load factor n and for a wing with mass per unit span μ the inertia force per unit span is given by

$$\lambda_I(\eta, t) = -\mu n g. \tag{18.4}$$

The minus sign occurs because the inertia force is defined as positive upwards for a positive downwards acceleration whereas the aircraft actually accelerates upwards for a positive load factor (this was the case for the earlier tapered wing example). In the past, a steady pitch acceleration manoeuvre would sometimes be required and in such a case the load factor would vary along the aircraft.

18.5.2.2 Aerodynamic force per unit span

Now consider the aerodynamic lift per span $\lambda_A(\eta, t)$. In this case, for an equilibrium manoeuvre, the lift will be constant with time though it will not normally have a uniform spatial distribution along the wing.

Lift will be a function of the aircraft rigid body and flexible mode responses. Again, referring back to the earlier analyses in Chapter 13, the wing lift per unit span in a symmetric equilibrium manoeuvre for a flexible aircraft is given by

$$\lambda_{\mathrm{A}}(\eta) = \tfrac{1}{2}\rho V^2 c a_{\mathrm{W}}[\alpha - \alpha_0 + \gamma_{\mathrm{e}}(\eta) q_{\mathrm{e}}]. \tag{18.5}$$

Thus the steady lift for this equilibrium manoeuvre is simply a function of incidence, angle for zero lift and wing torsional deformation in the flexible mode, but of course these quantities depend upon the trimmed state and therefore on the rear fuselage deformation and elevator angle. Note here that the symbol η used for the integration variable along the wing should not be confused with that used for the elevator angle.

18.5.2.3 *Internal loads in an equilibrium manoeuvre*

Now that expressions have been obtained for the inertia and aerodynamic forces per span in Equations (18.4) and (18.5), these may be substituted into Equation (18.1) to determine the steady internal loads. For simplicity, consider only the wing root bending moment ($y = 0$). For the flexible aircraft used earlier, the result is given by

$$M(0) = \frac{1}{2}\rho V^2 S_{\mathrm{W}} a_{\mathrm{W}} \frac{s}{4}\left[\alpha - \alpha_0 + \gamma_{\mathrm{e}0}\left(1 + \frac{2B}{3}\right) q_{\mathrm{e}}\right] - \mu n g \frac{s^2}{2}. \tag{18.6}$$

Note that, for any location other than the wing root, each of the four terms in this expression would also be a function of y. It may be seen that the flexible mode deformation will modify the bending moment value due to the spanwise shift in the centre of pressure for a twisted wing. The effect of wing twist for a wing torsion mode will shift the centre of pressure outboard and so increase the wing root bending moment; this phenomenon is illustrated by some wing root bending moment results presented later for the example in Section 18.5.4. The other mode types considered earlier, namely wing bending and fuselage bending, will not affect the distribution of internal loads when compared to the rigid aircraft. The expressions for wing root shear force and torque are similar in appearance to the bending moment. The loads on a swept wing will differ (see Chapter 13).

18.5.3 Internal Loads in a Dynamic Manoeuvre/Gust Encounter

In this section, the inertia and aerodynamic forces per unit span will be determined for a symmetric gust encounter (see Chapter 16) and then substituted into the general expression for the continuous wing. In this case the loadings are time varying. The approach is essentially the same for ground manoeuvres but landing gear leg reaction forces need to be included. The treatment of dynamic flight manoeuvres is similar in principle, but the different axes system needs to be taken into account (see Chapters 14 and 15). Also, control angle terms would be present in the internal load expressions..

For a gust encounter, the incremental internal loads due to the gust need to be added to the internal loads for the initially trimmed steady level flight case ($n = 1$) prior to encountering the gust (see Chapters 16 and 24).

18.5.3.1 *Inertia force per unit span*

For a general gust encounter case, the acceleration will vary over the airframe and with time; also, it will have both rigid body and flexible mode components. Thus the inertia force per span on the wing will be given by

$$\lambda_{\mathrm{I}}(\eta, t) = \mu \ddot{z}_{\mathrm{WM}}(\eta, t), \tag{18.7}$$

where $\ddot{z}_{\mathrm{WM}}$ is the downwards acceleration along the wing mass axis for the spanwise position under consideration (remembering the use of inertial axes). Referring back to Chapters 13 and 16, the displacement at the wing mass axis is dependent upon heave, pitch and flexible mode motions and is given by

$$z_{\mathrm{WM}}(y) = z_{\mathrm{C}} - l_{\mathrm{WM}}\theta + \left[\kappa_{\mathrm{e}}(y) + l_{\mathrm{E}}\gamma_{\mathrm{e}}(y)\right] q_{\mathrm{e}}. \tag{18.8}$$

Therefore the inertia force per unit span is given by

$$\lambda_{\mathrm{I}}(\eta, t) = \mu \ddot{z}_{\mathrm{WM}}(\eta, t) = \mu \left[\ddot{z}_{\mathrm{C}}(t) - l_{\mathrm{WM}}\ddot{\theta}(t) + \left[\kappa_{\mathrm{e}}(y) + l_{\mathrm{E}}\gamma_{\mathrm{e}}(y)\right] \ddot{q}_{\mathrm{e}}(t)\right]. \tag{18.9}$$

The inertia contribution to the internal loads is thus a function of the heave, pitch and flexible mode accelerations. It should be noted that if the aircraft motion involves flexible mode torsional acceleration, then the resulting inertia pitching moments for the wing will affect any torque generated and will have to be included. For a dynamic manoeuvre where a body fixed axes system is employed (see Chapters 14 and 15), the absolute acceleration expression will differ from that above but the principles are the same; the loads in the initial trimmed condition will need to be added to the incremental loads experienced in the dynamic manoeuvre.

18.5.3.2 Aerodynamic force per unit span

When encountering a gust, the wing lift will be a function of incidence and wing twist as before, of the heave, pitch and flexible mode velocities, and also of the gust velocity. Thus, referring back to Chapter 16, and using the same notation, the incremental wing lift per span in a gust encounter, for example, is given by

$$\lambda_{\mathrm{A}}(\eta, t) = \frac{1}{2}\rho V c a_{\mathrm{W}} \left\{w_{\mathrm{g}} + \dot{z}_{\mathrm{C}} - l_{\mathrm{W}}\dot{\theta} + \left[\kappa_{\mathrm{e}}(\eta) - l_{\mathrm{A}}\gamma_{\mathrm{e}}(\eta)\right] \dot{q}_{\mathrm{e}}\right\} + \frac{1}{2}\rho V^2 c a_{\mathrm{W}} \left[\theta + \gamma_{\mathrm{e}}(\eta) q_{\mathrm{e}}\right], \tag{18.10}$$

where both rate- and incidence-dependent terms are present and the dependency of the response quantities on time has been omitted for clarity. The unsteady aerodynamics effects have also been omitted but could employ a convolution process if they were to be included (see Chapters 10 and 16). For a dynamic manoeuvre, the expression would be somewhat similar except for the different axes system (see Chapters 14 and 15). It is important to note that for more advanced panel aerodynamic theories (see Chapters 19 and 20), the lift distribution will be expressed as a function of the motion of the entire wing and not just the motion of the element (or strip) under consideration, and would be a function of reduced frequency.

18.5.3.3 Internal loads in a gust encounter

Now that expressions have been obtained for the inertia and aerodynamic forces per span in Equations (18.9) and (18.10), these may be substituted into Equation (18.1) to determine the shear forces and bending moments. For simplicity, again consider only the wing root bending moment ($y = 0$) and, for the aircraft model used in the earlier chapter on gusts, the result may be shown to be

$$\begin{aligned} M(0, t) = {} & \mu \frac{s^2}{2} \left\{\ddot{z}_{\mathrm{C}} - l_{\mathrm{WM}}\ddot{\theta} + \left[\kappa_{e0}\left(1 + \frac{A}{2}\right) + l_{\mathrm{E}}\gamma_{\mathrm{e0}}\left(1 + \frac{2B}{3}\right)\right] \ddot{q}_{\mathrm{e}}\right\} \\ & + \frac{1}{2}\rho V_0 a_{\mathrm{W}} c \frac{s^2}{2} \left\{\dot{z}_{\mathrm{C}} - l_{\mathrm{W}}\dot{\theta} + \left[\kappa_{\mathrm{e0}}\left(1 + \frac{A}{2}\right) - l_{\mathrm{A}}\gamma_{\mathrm{e0}}\left(1 + \frac{2B}{3}\right)\right] \dot{q}_{\mathrm{e}} + w_{\mathrm{g}}\right\} \\ & + \frac{1}{2}\rho V_0^2 a_{\mathrm{W}} c \frac{s^2}{2} \left[\theta + \gamma_{\mathrm{e0}}\left(1 + \frac{2B}{3}\right) q_{\mathrm{e}}\right], \end{aligned} \tag{18.11}$$

where the bending moment, response variables and the gust velocity are all functions of time. Thus knowing the gust velocity and the generalized coordinate responses, the root bending moment can be calculated. For any other location, each term would also be a function of y. Similar expressions exist for shear force and torque.

18.5.4 Example: Internal Loads during a '1-Cosine' Gust Encounter

To illustrate some results for time-varying internal loads, consider the same time domain gust response example for the simple flexible aircraft used in Chapter 16. The flight case used was for 150 m/s EAS at 14 000 ft with the aircraft encountering 5 m/s EAS '1-cosine' gusts of different lengths. In Chapter 16, only the responses were obtained whereas the sample wing root bending moment, shear force and torque results will be shown here.

18.5.4.1 Steady loads experienced prior to the gust encounter

To determine the overall loads in a gust encounter, both the *steady* and *incremental* components of internal load need to be found. The steady loads are those in the equilibrium flight condition that the aircraft is in prior to encountering the gust whereas the incremental loads are those generated by the gust.

For the *rigid* aircraft in steady level flight, the wing root bending moment, shear force and torque values for this example are 120.3 kN m, 32.1 kN and 15.4 kN m respectively. For the *flexible* aircraft in steady flight, the internal load values depend upon the mode shapes and natural frequencies. For the modes where fuselage bending or wing bending are dominant, the internal loads are unchanged from the rigid aircraft value as there is no change in the local wing incidence due to the flexible modes if the wing is unswept. However, for the mode with wing torsion dominant, the bending moment will increase when compared to the rigid aircraft value since the wing twists and the lift shifts outboard; the bending moment values of 124.7, 130.5 and 145.0 kN m correspond to torsional natural frequencies of 9, 6 and 4 Hz respectively. Shear force and torque are unaffected by the torsion mode.

If the wing is swept, then there is coupling between the bending and torsion modes (see Chapter 13) and so the effect of flexibility on the internal loads will be more complicated, with the effect of bending decreasing the bending moment compared with the rigid aircraft value (i.e. the opposite of the effect of the torsion mode).

18.5.4.2 Incremental loads in the gust encounter

It should be noted that the values presented in the figures below are actually the *incremental* internal loads due to the gust. These loads need to be added to the trim steady level flight loads (i.e. for an $n = 1$ equilibrium manoeuvre) whose generation was described earlier in Section 18.5.2.

Firstly, consider the mode where *fuselage bending* is dominant, with 2 Hz frequency and 4 % damping; note that in this mode shape (see Appendix C) there is a finite heave displacement of the wing and so the mode is excited by a gust input. The variation of the maximum and minimum incremental wing root bending moment with gust wavelength yields a maximum value of 68.4 kN m for around an 80 m wavelength and a minimum value of −62.2 kN m for a 225 m wavelength. A comparison of the bending moment at several different wavelengths is shown in Figure 18.8; both the short period and flexible mode components may be seen in the bending moment time history. Note that the initial internal load peak tends to 'follow' the gust velocity peak. The loads will not necessarily peak at the same wavelength as the response. The equivalent incremental wing root shear force and torque results may also be found from the program in appendix I in the companion website.

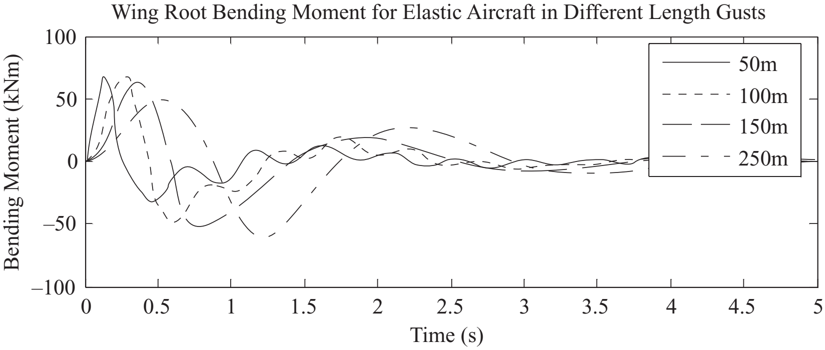

Figure 18.8 Incremental wing root bending moment for a flexible aircraft in a '1-cosine' gust of different lengths – heave/pitch model with a fuselage bending mode (2 Hz/4 %).

The equivalent result for a mode where *wing bending* is dominant, with 3 Hz frequency and 4 % damping, is shown in Figure 18.9; the maximum value of 102.8 kN m occurs for a wavelength of 70 m whereas the minimum value of –98.9 kN m occurs for a 60 m gust. For this mode and low natural frequency, the incremental bending moment is dominated by the oscillatory flexible response.

The results for the mode where *wing torsion* is dominant, with 9 Hz frequency and 4 % damping, show the peak response occurring for small wavelengths where, as seen from the results in Figure 18.10, the incremental bending moment essentially 'follows' the gust velocity. However, it should be noted that these (and the earlier) calculations did not include the unsteady Küssner and Wagner effects (see Chapters 10 and 16) and so in reality these initial peaks would be smaller.

Although the behaviour of the three flexible modes have been shown separately, in practice a number of flexible modes would be involved and the approach involved would be extended by summing the effects of multiple modes, as indicated in Chapter 16.

18.5.5 Form of Internal Loads for a Continuous Wing Representation

Having established typical expressions for inertia and aerodynamic lift forces per unit span for a continuous wing, then by substituting them into the internal load Equations (18.1) the form of the expression for an internal load of the flexible aircraft may be determined. An example was shown earlier for the wing

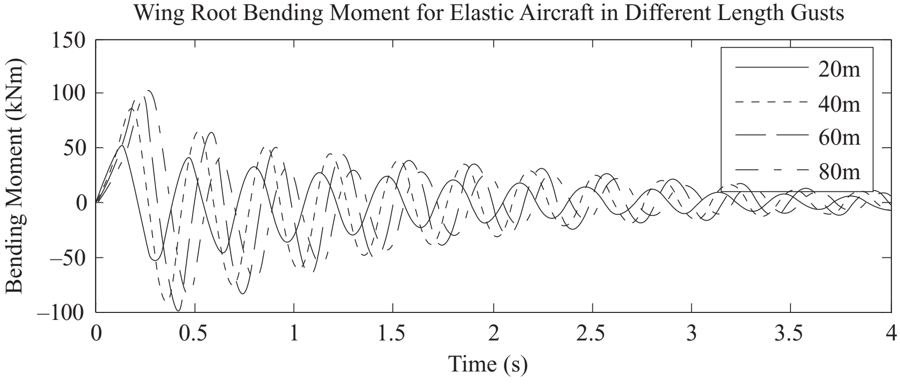

Figure 18.9 Incremental wing root bending moment for a flexible aircraft in a '1-cosine' gust of different lengths – heave/pitch model with a wing bending mode (3 Hz/4 %).

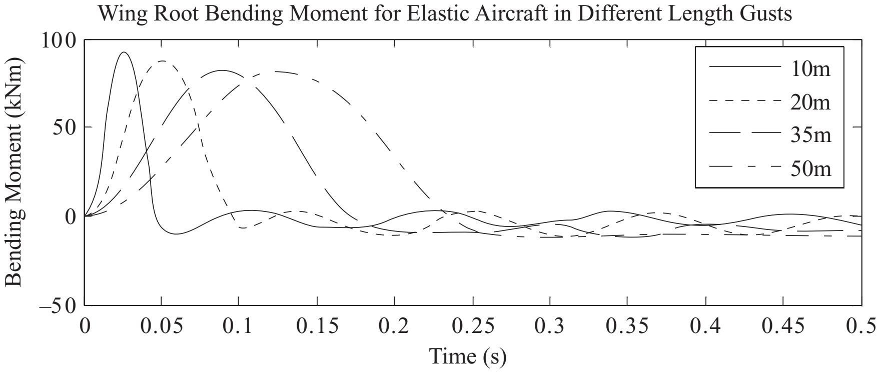

Figure 18.10 Incremental wing root bending moment for a flexible aircraft in a '1-cosine' gust of different lengths – heave/pitch model with a wing torsion mode (4 Hz/4 %).

root bending moment and Equation (18.11) may be written in the more general form for heave, pitch and a single flexible mode:

$$\text{Internal load}\,(y,t) = \{A_1 \quad A_2 \quad A_3\}\ddot{\boldsymbol{q}} + \{B_1 \quad B_2 \quad B_3\}\dot{\boldsymbol{q}} + \{C_1 \quad C_2 \quad C_3\}\boldsymbol{q} + Dw_{\mathrm{g}}, \qquad (18.12)$$

where $\boldsymbol{q} = \{z_{\mathrm{C}} \quad \theta \quad q_{\mathrm{e}}\}^{\mathrm{T}}$ is the response and $A_j,\ B_j,\ C_j \quad (j = 1, 2, 3)$ and D are all functions of y (in general), calculated via the integrals in the internal load equations (18.1). Note that in some circumstances terms related to any control input would be included, e.g. if spoilers were deployed on the wing. Thus, once the responses $\boldsymbol{q}(t),\ \dot{\boldsymbol{q}}(t),\ \ddot{\boldsymbol{q}}(t)$ in a manoeuvre or gust encounter are calculated, the incremental internal loads may be obtained using Equation (18.12) and then added to the steady flight loads to yield the overall loads.

18.6 GENERAL INTERNAL LOADS EXPRESSIONS – DISCRETIZED WING

Since the loads on a real aircraft are not expressed analytically, this section considers the case where both the wing structure and the loading need to be discretized. There are different ways of carrying out the discretization, one possibility being outlined here. In this section, the approach used to obtain internal loads for a discretized structure will be considered (see Chapter 6), together with the general form of the expression. The way in which the aircraft may be represented discretely is discussed further in Chapter 22.

18.6.1 General Expression for Internal Loads – Discretized Wing

Consider the discretized wing with N strips shown in Figure 18.11. In this case, the aerodynamic lift and inertia force on the kth strip of the wing are given by $F_{\mathrm{Aero}\_k}(t)$ and $F_{\mathrm{Inertia}\_k}(t)$. Following a similar argument to that used earlier for the continuous wing, the shear force and bending moment at the inboard end of the jth strip are

$$Q_j(t) = \sum_{k=1}^{j} \left[F_{\mathrm{Aero}\_k}(t) + F_{\mathrm{Inertia}\_k}(t)\right], \qquad j = 1, 2, \ldots, N,$$

and

$$M_j(t) = \sum_{k=1}^{j} \{F_{\mathrm{Aero}\_k}(t) + F_{\mathrm{Inertia}\_k}(t)\}\left(y_k - y_j + \frac{\Delta y}{2}\right). \qquad (18.13)$$

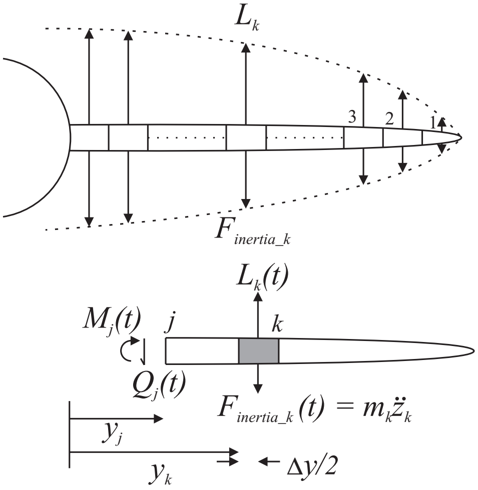
L_k
3
2
1
$F_{inertia\_k}$
$L_k(t)$
$M_j(t)$
j
k
$Q_j(t)$
$F_{inertia\_k}(t) = m_k\ddot{z}_k$
y_j
y_k
$\Delta y/2$

Figure 18.11 Loads on a discretized wing.

Thus the internal loads may be calculated at any spanwise position, defined by the interface between two strips, and as a function of time, provided the lift and inertia distributions are known as a function of the aircraft motion (and, if appropriate, gust velocity). The internal loads do not depend upon the chordwise position of the loadings. A similar expression may be derived for torque, where the chordwise position of the loads is important.

These shear force and bending moment expressions are generally applicable to any unswept wing, although the same principles would apply for a swept wing provided that the strips and internal loads were defined relative to streamwise (i.e. aircraft and not wing) axes. Note that for a swept wing the torque expression would need to allow for the effect of sweep on the moment arm associated with the lift and inertia forces.

18.6.2 Wing Discretization

Consider the wing span to be divided into N strips of equal or unequal width. Assume that the finite element model is either defined as a beam, or condensed to be 'beam-like' (see Chapters 4 and 22), with the beam axis defining a reference axis and load stations being defined on this axis at the inner end of each strip, as seen in Figure 18.12 for example. The aerodynamic force per strip will nominally lie at

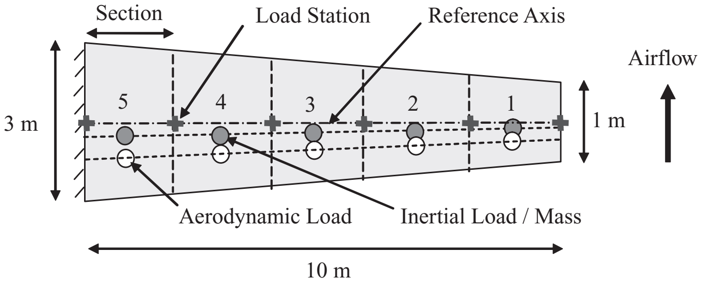
Section
Load Station
Reference Axis
Airflow
3 m
5
4
3
2
1
1 m
Aerodynamic Load
Inertial Load / Mass
10 m

Figure 18.12 Diagram of a discretized tapered wing example.

the aerodynamic centre of the strip, when using the two-dimensional strip theory assumption or when aggregating three-dimensional panel results on to a strip. The mass of each strip is located at the strip centre of mass (i.e. on the mass axis), with any offset of the strip centre of mass from the reference axis being accounted for in the analysis (see Chapter 4).

18.6.3 Example: An Equilibrium Manoeuvre – Discretized Wing

In order to illustrate this discretization further, consider the same wing example as covered in Section 18.3.2 but with the tapered wing shown in Figure 18.5 now divided into five strips of equal width $\Delta y =$ 2 m, as seen in Figure 18.12. The mass axis lies along the 40 % chord and the aerodynamic centre axis lies along the quarter chord. Assume that the reference axis lies along the mid-chord. Having defined the discretization for the earlier example in the previous section, the internal loads at each strip may now be calculated using the direct approach introduced above in Section 18.6.1. The equivalent expression for wing torque (nose up positive) for this particular example, where the mass axis is at 40 % chord, may be shown to be given by

$$T_j(t) = \sum_{k=1}^{j} \left[F_{\text{Aero}\_k}(t)\,\frac{c_k}{4} + F_{\text{Inertia}\_k}(t)\,\frac{c_k}{10} \right], \tag{18.14}$$

where torque is referred to the wing reference axis (i.e. mid-chord). Note that this torque expression only applies to the specific chordwise positions for the lift and inertia forces used in this example (i.e. distances $c_k/4$, $c_k/10$ ahead of the reference axis), but a more general formula could be derived.

The lift and inertia forces per strip of the wing are given in Table 18.1, remembering that the lift and inertia force per unit span (upwards positive) were obtained earlier as $37.5c$ and $-7.5c$ kN/m. The table also shows the internal loads calculated using Equations (18.13) and (18.14). The variation of these three internal loads along the wing is shown in Figure 18.13. At the wing root, the bending moment is 2520 kN m (sag positive) so the wings tend to bend upwards. The wing root torque is 372.6 kN m, with the wing tending to twist nose up. The values in the table agree well with the ‘exact’ values calculated earlier in Section 18.3.2; the shear forces are identical whereas there are relatively small differences ($\sim$1 %) in the bending moments and torques, due to the discretization; using more strips would improve the agreement.

The effect of flexibility would be included by adding the relevant modal terms to the aerodynamic and inertia forces per strip. Also, the dynamic manoeuvre or gust encounter would be treated in a similar way, with the inertia and aerodynamic loads evaluated at the required instant of time.

Table 18.1 Wing properties, external loads and internal loads per strip

Strip j	Mean strip chord (m) c_j	Lift force (kN) F_{Aero_j}	Inertia force (kN) F_{Inertia_j}	Net upwards force (kN) $(F_{\text{Aero}\_j} + F_{\text{Inertia}\_j})$	Shear force (kN) Q_j	Bending moment (kN m) M_j	Torque (kN m) T_j
0	—	—	—	—	0	0	0
1	1.2	90	−18	72	72	72	24.84
2	1.6	120	−24	96	168	312	69
3	2.0	150	−30	120	288	768	138
4	2.4	180	−36	144	432	1488	237.36
5	2.8	210	−42	168	600	2520	372.6

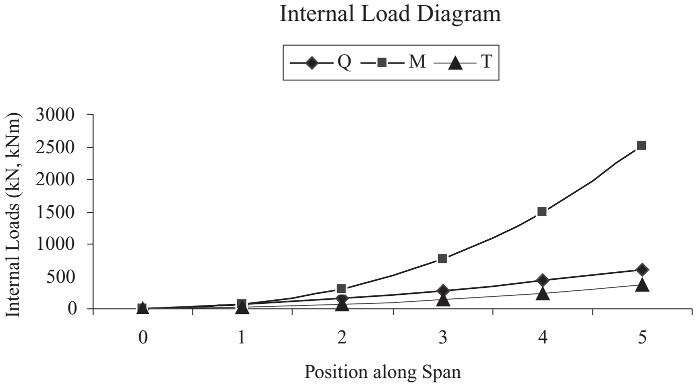

Figure 18.13 Variation of internal loads along a discretized wing for the equilibrium manoeuvre example.

18.6.4 Form of Internal Loads for a Discretized Wing Representation

In Section 18.5.5, the general form for a *continuous* wing internal load at the spanwise position y was illustrated via Equation (18.12). In the general case for any location on the wing, using a *discretized* representation, all the internal loads required at all stations may for convenience be expressed in a matrix form. The idea will be illustrated for the shear forces on a wing structure, but the same approach may be taken for other internal loads and aircraft components. The force summation shown for the wing in Equations (18.13) and (18.14) could be written in the following way for the *inertia* contribution (subscript I), namely

$$\boldsymbol{Q}_{\mathrm{I}} = \begin{Bmatrix} Q_1 \\ Q_2 \\ \vdots \\ Q_N \end{Bmatrix}_{\mathrm{I}} = \begin{bmatrix} 1 & 0 & \cdots & 0 \\ 1 & 1 & \cdots & 0 \\ \vdots & \vdots & \cdots & \vdots \\ 1 & 1 & \cdots & 1 \end{bmatrix} \begin{Bmatrix} F_{\mathrm{I\_1}} \\ F_{\mathrm{I\_2}} \\ \vdots \\ F_{\mathrm{I\_}N} \end{Bmatrix} = \mathbf{T}_{\mathrm{I}} \boldsymbol{F}_{\mathrm{I}}, \tag{18.15}$$

where the transformation (**T**) matrix for the shear force allows the contribution of the inertia forces on each strip to be added into the shear forces at the desired positions. The equivalent **T** matrix for the bending moment would include the moment arm between the load station and the inertia loading point of action; also, the roll inertia moment per strip could be included. If torque loads were being calculated, the pitch inertia moment (and of course any aerodynamic pitching moment) would need to be included. The inertia forces are given by the product of the mass and acceleration for every strip where the mass is lumped, so

$$\boldsymbol{F}_{\mathrm{I}} = \begin{Bmatrix} m_1 \ddot{z}_1 \\ m_2 \ddot{z}_2 \\ \vdots \\ m_N \ddot{z}_N \end{Bmatrix} = \begin{bmatrix} m_1 & 0 & \cdots & 0 \\ 0 & m_2 & \cdots & 0 \\ \vdots & \vdots & \cdots & \vdots \\ 0 & 0 & \cdots & m_N \end{bmatrix} \begin{Bmatrix} \ddot{z}_1 \\ \ddot{z}_2 \\ \vdots \\ \ddot{z}_N \end{Bmatrix} = \mathbf{M}\ddot{\boldsymbol{z}}, \tag{18.16}$$

where the vector $\ddot{\boldsymbol{z}}$ defines the physical acceleration at each mass station. This may in turn be related to the generalized coordinates for the heave, pitch and flexible modes via the modal transformation $\boldsymbol{z} = \boldsymbol{\Phi q}$, where $\boldsymbol{\Phi}$ is the modal matrix, so finally

$$\boldsymbol{Q}_{\mathrm{I}} = \mathbf{T}_{\mathrm{I}}\mathbf{M}\Phi\ddot{\boldsymbol{q}} = \mathbf{A}_{\mathrm{M}}\ddot{\boldsymbol{q}}, \tag{18.17}$$

where $\mathbf{A}_{\mathrm{M}}$ is a modal transformation matrix for the shear force due to inertia effects.

For the *aerodynamic* contribution to the shear force (subscript A), an equivalent expression $\boldsymbol{Q}_{\mathrm{A}} = \mathbf{T}_{\mathrm{A}}\boldsymbol{F}_{\mathrm{A}}$ applies. For the bending moment, a different transformation matrix is used to allow the aerodynamic forces to be defined at different points to the mass (see Chapter 20). These aerodynamic forces may be expressed in terms of the velocities and displacements at the reference positions and the control input η and/or gust velocity w_g (if appropriate), using

$$\boldsymbol{F}_{\mathrm{A}} = \mathbf{B}\dot{\boldsymbol{z}} + \mathbf{C}\boldsymbol{z} + \boldsymbol{R}_{\mathrm{c}}\eta + \boldsymbol{R}_{\mathrm{g}}w_{\mathrm{g}}, \tag{18.18}$$

where $\mathbf{B}, \mathbf{C}$ are the aerodynamic matrices defining the rate and incidence dependent terms and $\boldsymbol{R}_{\mathrm{c}}, \boldsymbol{R}_{\mathrm{g}}$ are the vectors defining the control input and gust velocity terms (with density and air speed terms embedded for all terms). Unsteady aerodynamic effects are neglected. The aerodynamic contribution to the shear force is then

$$\boldsymbol{Q}_{\mathrm{A}} = \mathbf{T}_{\mathrm{A}}\left\{\mathbf{B}\Phi\dot{\boldsymbol{q}} + \mathbf{C}\Phi\boldsymbol{q} + \boldsymbol{R}_{\mathrm{c}}\eta + \boldsymbol{R}_{\mathrm{g}}w_{\mathrm{g}}\right\} = \mathbf{B}_{\mathrm{M}}\dot{\boldsymbol{q}} + \mathbf{C}_{\mathrm{M}}\boldsymbol{q} + \boldsymbol{R}_{\mathrm{Mc}}\eta + \boldsymbol{R}_{\mathrm{Mg}}w_{\mathrm{g}}. \tag{18.19}$$

Therefore the *overall* expression for the wing shear forces is given by a supplementary or *auxiliary equation*

$$\boldsymbol{Q} = \mathbf{A}_{\mathrm{M}}\ddot{\boldsymbol{q}} + \mathbf{B}_{\mathrm{M}}\dot{\boldsymbol{q}} + \mathbf{C}_{\mathrm{M}}\boldsymbol{q} + \boldsymbol{R}_{\mathrm{Mc}}\eta + \boldsymbol{R}_{\mathrm{Mg}}w_{\mathrm{g}}. \tag{18.20}$$

Thus the internal loads may be calculated directly from the generalized responses, control input and gust velocity using an equation that looks somewhat similar to the basic equation of motion of the aircraft. Clearly, the final form is somewhat similar to that found for the continuous wing in Equation (18.12). These matrices are conveniently formed when the initial aeroelastics and loads models are generated. The same form of expression would apply for bending moments and torques except that the content of the transformation matrices would differ. Also, any external forces applied could be included via additional terms. These internal loads may be supplemented by other ‘interesting quantities’ such as accelerations, rates, control forces, strains, etc. (see Chapter 25).

Finally, it should be noted that the approach described above for determination of internal loads is often known as the ‘force summation’ method; it is the most intuitive of methods available. Other approaches sometimes used are the ‘mode displacement’ and ‘mode acceleration’ methods (CA-25).

18.7 INTERNAL LOADS – DISCRETIZED FUSELAGE

The previous sections considered the internal loads present on a continuous or discretized wing in a manoeuvre or gust encounter, but the approach could equally well apply for any other aerodynamic lifting surface such as a tailplane or fin. The case of a fuselage is somewhat different but uses similar principles. In this section, only the discretized fuselage will be considered; the use of an analytical approach would be possible by integrating over the fuselage and adding in the tailplane effects directly, but this is omitted here as it is more ‘messy’ than the wing case and the wing examples are thought to be adequate to illustrate the ideas for continuous analysis.

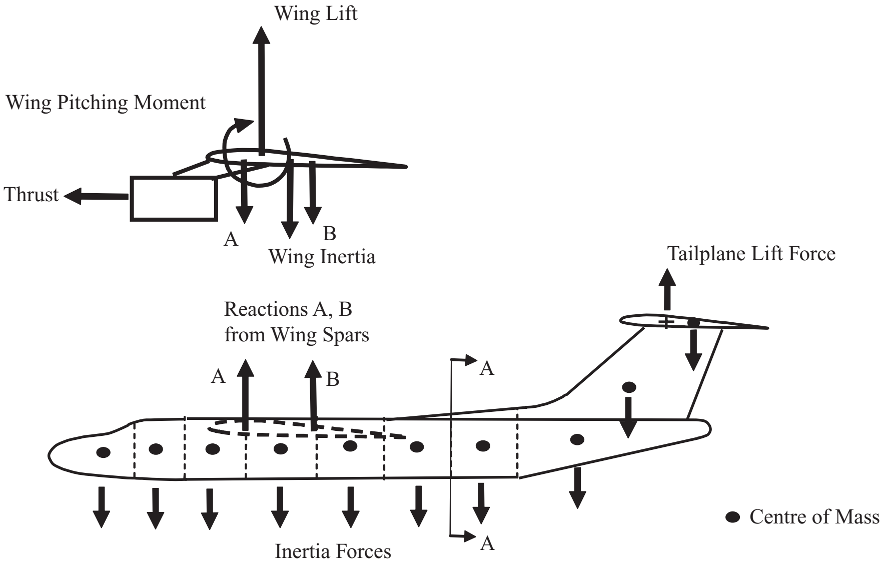

Figure 18.14 Separating wing and fuselage components using intercomponent loads plus forces acting on a discretized fuselage/tail unit.

18.7.1 Separating Wing and Fuselage Components

Note that the wing and fuselage may be considered crudely as separate components by introducing intercomponent forces and moments (see Chapter 6), e.g. at the front and rear spar positions where the wing may be assumed to connect with the fuselage. This is illustrated in Figure 18.14 for the simple case where only vertical loads A, B are present. These intercomponent loads may be obtained from equilibrium of the wing and fuselage components. This approach is reasonable for aircraft where the wing is connected above or below the fuselage using a statically determinate connection arrangement at the main and rear spars (as is the case for some small commercial aircraft). However, it is somewhat idealized for aircraft where the wing/fuselage junction is more integrated and the load path is less distinct; nevertheless, the net effect of the connection may be represented by discrete intercomponent forces as shown here.

A discretization of the fuselage and tail (sometimes called ‘empennage’) is also shown in Figure 18.14. The sections of the fuselage, fin and tailplane have mass components; the interfaces between fuselage sections would usually correspond to frame/bulkhead locations. The fuselage, fin and tailplane are subject to inertia forces for each discrete mass, to a tailplane lift force and to reactions from the wing spars (essentially intercomponent loads). The fuselage/tail unit will be in equilibrium under the forces shown in Figure 18.14. The internal loads may be obtained by considering fuselage sections, such as when analysing the wing, working from the tailplane or nose towards the centre section/wing junction.

18.7.2 Example: Equilibrium Manoeuvre – Discretized Fuselage

In Chapter 13, an equilibrium manoeuvre example for a rigid aircraft was shown, involving the thrust and drag being out-of-line so that an iterative process was required to solve for the balanced condition. The case examined was for a load factor of 2.5 at 250 m/s EAS. The tailplane lift in the equilibrium manoeuvre was $L_T = -93.7$ kN (i.e. acting downwards). In the example here, a sample fuselage internal load calculation is undertaken for this flight condition.

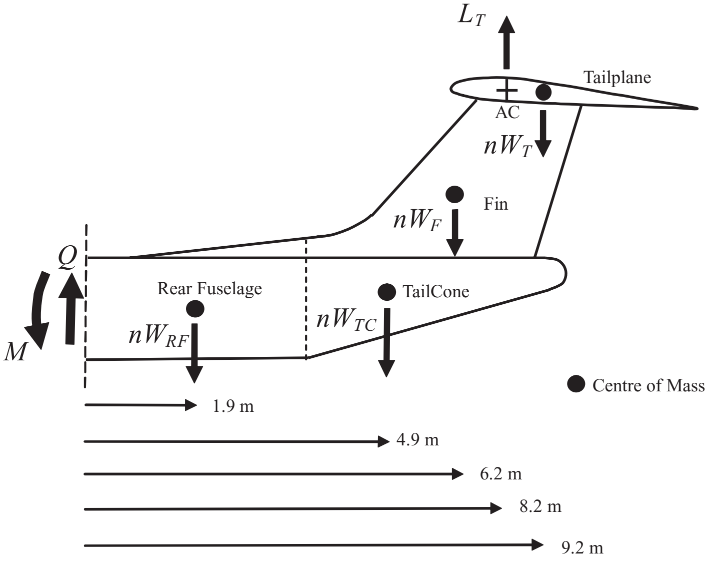

Figure 18.15 Rear fuselage loads in the equilibrium manoeuvre.

To determine internal loads (see Chapter 6), the tailplane/rear fuselage are ‘cut’ away from the remainder of the aircraft at position AA in Figure 18.14 in order to expose the internal loads at this fuselage location, as shown in Figure 18.15. The subsystem under consideration is divided into sections comprising the tailplane, fin, tail cone and rear fuselage; the tailplane lift force and the inertia forces per component are shown on the diagram. The objective is to determine the shear force and bending moment at position AA in the rear fuselage section, as indicated in the figure; this will be an example of the analysis approach that could also be applied at other sections. There is no torque because the manoeuvre, and hence the loading, is symmetric. Axial loads would be present if the effects of aerodynamic drag, engine thrust or cabin pressurization loads were to be included.

The component masses are tailplane m_{T}, fin m_{F}, tail cone m_{TC} and rear fuselage m_{RF}; values are shown in Table 18.2, together with the corresponding inertia forces. Therefore, as an example, for a load factor of 2.5 the inertia force on the fin will be $nW_{\mathrm{F}} = nm_{\mathrm{F}}g = 2.5 \times (900 \times 9.81)/1000 = 22.1$ kN (downwards).

The rear fuselage/fin/tailplane subsystem shown will be in equilibrium under the action of the inertia forces, the tailplane lift force and the internal loads. Considering the equilibrium relationships of zero net vertical force and zero net moment about the cut, and recognizing that the tailplane lift acts downwards, then

$$\begin{aligned} Q &= 24.5 + 22.1 + 9.8 + 78.5 - (-93.7) = 228.6 \text{ kN}, \\ M &= 24.5 \times 9.2 + 22.1 \times 6.2 + 9.8 \times 4.9 + 78.5 \times 1.75 - (-93.7 \times 8.2) = 1316 \text{ kN m}. \end{aligned} \tag{18.21}$$

Table 18.2 Mass and inertia force per component

	Tailplane	Fin	Tail cone	Rear fuselage
Mass (kg)	1000	900	400	3200
Inertia force (kN)	24.5	22.1	9.8	78.5

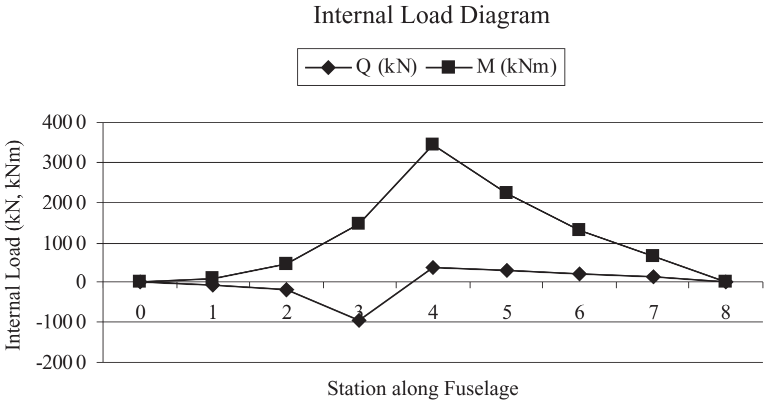

Figure 18.16 Internal load diagram for the fuselage/tail unit example.

Thus, examining the sign convention used in Figure 18.15, the fuselage will bend downwards at the tail (i.e. ‘hog’), with the inertia effects and tailplane lift both acting in the same direction. However, even if the tailplane lift acted upwards, the fuselage would still bend downwards during a positive load factor manoeuvre. When the process is repeated for other positions along the fuselage, the resulting internal load diagram is shown in Figure 18.16. The assumed wing spar/fuselage attachment points are at locations 3 and 4 in this figure. Also, as expected, the internal loads are zero at each end of the aircraft.

18.7.3 Internal Loads for General Manoeuvres and Gusts

The above example was for an equilibrium manoeuvre. However, if the aircraft was subject to a more general acceleration, such as when undergoing a dynamic flight manoeuvre, encountering a gust or landing, the internal loads could be calculated at any instant in time by using the appropriate tailplane (and maybe fuselage) lift as well as the accelerations at each mass section and any landing gear reaction. The general form of the internal load equations would be similar to those for the wing.

18.8 INTERNAL LOADS – CONTINUOUS TURBULENCE ENCOUNTER

So far in this chapter, the generation of internal loads has been sought in the time domain using the output from simulations of steady/dynamic manoeuvres and discrete gust encounters. However, in the analysis of a continuous turbulence response, it is normally required to express the loads behaviour in the frequency domain in terms of spectral incremental loads quantities. In this section, the approach for calculating root-mean-square (RMS) loads from generalized coordinate responses will be outlined. It may be applied to continuous or discretized components but is defined using notation from the latter obtained in Section 18.6.4.

In Chapter 16, the frequency domain power spectral density (PSD) approach was used to obtain the root-mean-square values of response parameters. However, it is now possible, using Equation (18.20), to define transfer functions between each internal load, the vector of generalized coordinates and the gust velocity. Thus, in the frequency domain (referring back to Chapter 16 for the methodology), it may be seen that the vector of shear forces is

$$\tilde{\boldsymbol{Q}} = \left[-\omega^2 \mathbf{A}_{\mathrm{M}} + \mathrm{i}\omega \mathbf{B}_{\mathrm{M}} + \mathbf{C}_{\mathrm{M}}\right] \tilde{\boldsymbol{q}} + \boldsymbol{R}_{\mathrm{M}} w_{\mathrm{g0}} = \mathbf{H}_{Qq} \tilde{\boldsymbol{q}} + \boldsymbol{R}_{\mathrm{M}} w_{\mathrm{g0}}, \tag{18.22}$$

where $\mathbf{H}_{Qq}$ is the frequency response function (FRF) matrix relating the internal load vector (shear force in this case) and the generalized response vector. However, since it was shown in Chapter 16 that these generalized responses could be related to the gust velocity via $\tilde{\boldsymbol{q}} = \boldsymbol{H}_{qg} w_{g0}$, then

$$\tilde{\boldsymbol{Q}} = \mathbf{H}_{Qq} \boldsymbol{H}_{qg} w_{g0} + \boldsymbol{R}_{M} w_{g0} = \left[\mathbf{H}_{Qq} \boldsymbol{H}_{qg} + \boldsymbol{R}_{M}\right] w_{g0} = \boldsymbol{H}_{Qg} w_{g0}. \tag{18.23}$$

Thus an FRF vector $\boldsymbol{H}_{Qg}$ relating the internal loads directly to the gust velocity may be obtained, with the dynamics of the linear aircraft embedded. This allows the continuous turbulence PSD approach to be extended to consideration of internal loads; e.g. the root-mean-square incremental wing root shear force (and therefore relevant stresses) experienced in turbulence may be determined from the relevant internal load PSD.

Once the PSDs for internal loads (and stresses) are found, the statistical implications for fatigue life may be considered; e.g. the limit load may be found from the steady $1g$ load and the limit turbulence intensity multiplied by the ratio of the root-mean-square load to the root-mean-square of gust velocity (see Chapters 16 and 24). Also, positions of the peaks in the PSD dictate the number of cycles of a particular stress level, which can be used with techniques such as rainflow counting and Miner's rule. This area is a complex process and other texts (Hoblit, 1988; Niu, 1988; Megson, 1999) should be consulted for the detail.

18.9 LOADS GENERATION AND SORTING TO YIELD CRITICAL CASES

Calculations need to be carried out for a large range of different loading actions, flight conditions (i.e. air speed, altitude) and centre of mass/mass cases within the design envelope. The aim is to determine the critical cases that will dictate the dimensioning of each part of the aircraft (see also Chapters 21 and 25). Many sets of internal loads values or time histories are generated from different manoeuvre and gust cases, with steady loads added to incremental results as appropriate. The loads are then used to obtain suitable one-dimensional and two-dimensional loads envelopes (explained below) as part of a sorting process employed in order to determine correlated sets of loads that correspond to critical loadings at each location of interest on the aircraft.

The term 'correlated loads' is used to mean a set of loads that is consistent across the aircraft, e.g. extracted at the same instant of time, thus providing balanced loads for subsequent FE analysis. Note that a special approach is required to extract such correlated loads from turbulence response data in the frequency domain. These sorted loads are made available to the stress office. They may also be converted into equivalent loads acting on the reference axes for the FE model of components (see later in this chapter and Chapter 25).

18.9.1 One-Dimensional Load Envelopes

A one-dimensional load envelope shows the maximum and minimum internal loads at each load station along a component such as a wing as part of the loads sorting process, as illustrated in Figure 18.17; the enclosed shaded area contains all the noncritical values. Such a diagram may be drawn for each loading action (equilibrium manoeuvre, dynamic manoeuvre, landing, gust, turbulence, etc.) and the overall worst cases then shown as a composite of all loading actions. It is not possible a priori to determine the relative effects of different load cases since that depends on many factors; however, the different loading actions can often yield quite similar results and are all important somewhere on the aircraft. Such an envelope would be appropriate to use on parts of the aircraft where the design stresses only depend upon one of the 'MAST' quantities, e.g. the effect of the wing bending moment on stresses in parts of the wing cover skins dominated by bending.

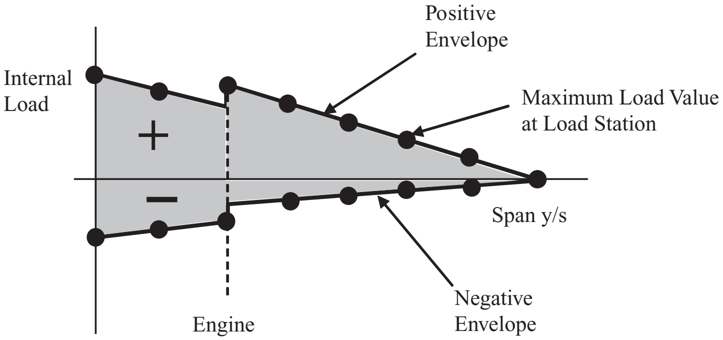

Figure 18.17 One-dimensional load envelope along the wing.

18.9.2 Two-Dimensional Load Envelopes

In the previous section, the one-dimensional load envelope allowed the worst case for a given internal load (e.g. the bending moment) to be seen at a particular load station. More often, the design stresses in structural elements within modern aerospace structures can only be adequately represented by a more complex combination of 'MAST' loads. As an example, for areas where shear stresses dominate, such as spar caps/webs, a step improvement in fidelity can be achieved by considering a two-dimensional envelope of shear and torque since these both contribute to the shear stresses. It is therefore sometimes useful to plot these loads quantities against each other at a particular load station for all the load cases; such a process will help to identify the sets of correlated loads that correspond to the critical design cases for parts of the wing box not dominated by bending.

As an example, consider the approach shown earlier in Section 18.5.4 for obtaining the steady plus incremental loads in response to a '1-cosine' gust. In this section, four different wavelengths of 20, 50, 100 and 200 m will be considered for a 10 m/s EAS '1-cosine' gust at the same flight condition of 150 m/s EAS at 14 000 ft. The incremental wing root shear force and torque for the mode with wing bending dominant are added to the steady internal loads ($n = 1$). When the torque and shear force are plotted against each other, with the locus of the line following time, the result in Figure 18.18 is obtained; the two phases of the load variation involving the response to the initial gust input and the decay of the flexible mode following the input may be seen to give two zones in the plot. The shape of these loci would obviously be different at other load stations, for other loading actions, for other modes and for swept wing aircraft with more than one flexible mode.

In effect, results such as these two-dimensional plots can be generated using a superposition of the many thousands of loads cases investigated (i.e. equilibrium, dynamic, ground and gust) for different flight conditions and mass/centre of mass values to show a complete picture of the torque/shear force load combinations that the aircraft is expected to experience. A 'two-dimensional load envelope' may be defined to embrace this composite plot and so allow the most severe combinations of the shear force and torque to be investigated. It is important that the load sets defined are correlated, i.e. will give rise to a balanced load set. Such composite two-dimensional plots (sometimes called 'potato' plots) are not always simple in shape but depend upon the aircraft modes involved, load station, etc. Clearly the detailed time responses that lie within this load envelope are unimportant and would not need to be plotted. Similar plots could involve the variation of bending moment and torque and also the variation of the wing bending moments for vertical and fore-and-aft bending.

To improve the fidelity of design case sorting/selection further is clearly possible by more directly representing the more complex dependencies of stress within each structural element on the 'MAST' loads. However, this would considerably expand the number of 'design cases' analysed. At this point it

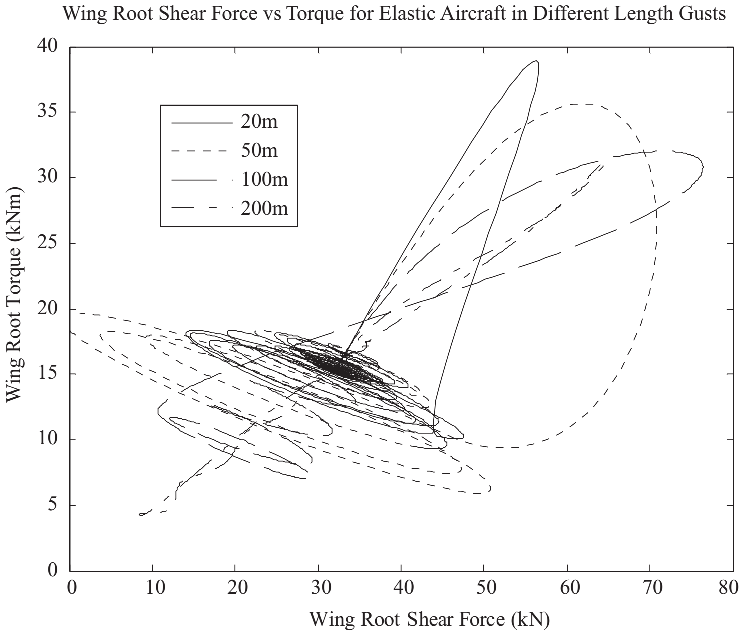

Figure 18.18 Variation of total wing root torque against shear force for a flexible aircraft in a '1-cosine' gust of different lengths – heave/pitch model with a wing bending mode (3 Hz/4 %).

may begin to be worth while reformulating the whole loads solution in terms of structural DoF, again going beyond the scope of this book.

18.10 AIRCRAFT DIMENSIONING CASES

Consider now the importance of different loadings on the aircraft design (Howe, 2004). Shear tends to be of most significance when combined with torque, because these effects generate shear loading in the wing box cover skins and the spar webs (Donaldson, 1993; Megson, 1999; Sun 2006). Shear and torque are also relevant to the inner wing spar and landing gear attachment design, with ground loads such as landing being of the most importance. For the outer wing spar design, the flight loads are usually larger, though dynamic inertia loading on landing can be important in some aircraft. Wing torque is less important than wing bending, with bending loads tending to be most important for the design of spars and of top wing box cover skins (to avoid buckling of the stiffened stringer panels under compression loading in upwards bending); this is the case examined under the ultimate load test (see Chapter 26). Usually the gust/turbulence, dynamic and 2.5*g* equilibrium manoeuvre load envelopes are fairly close in magnitude, depending upon wing loading (lift per area). Downwards bending of the wing is less significant, with bottom cover skins tending to be designed by fatigue/damage tolerance issues (the tension loading present due to upwards bending). The presence of a wing-mounted engine introduces a step change in loads due to thrust and inertia effects (see the earlier example) and possibly also nacelle aerodynamic effects. Also, the envelope of the vertical load factor (i.e. acceleration) is important, with flight and ground loadings causing different levels of acceleration as the different frequency content of the excitation excites different wing modes. High levels of acceleration (typically 20*g* at the wing tip) can introduce large local loads due to system component attachments, fuel inertia loading, etc. Other texts (Niu, 1988; Donaldson, 1993; Megson, 1999) should be sought for further understanding of aircraft loads.

18.11 STRESSES FROM INTERNAL LOADS – COMPLEX LOAD PATHS

In classical stress analysis for simple slender structures where load paths are well defined, the internal loads found from the various manoeuvres and gust encounters could be related directly to stresses (see Chapter 6) so there is no problem of terminology. However, in the analysis of complex built-up structures such as aircraft where load paths are ill-defined, the shear forces, bending moments, etc., would be decomposed into external loads acting, for example, on the reference axis of the component (e.g. the wing) and making up a balanced load case, or, increasingly, decomposed into external 'nodal' loads, so-called because the loads are distributed as realistically as possible directly on to the load-carrying nodes within the structural FE model. Then components would be analysed by the stress office (or equivalent) using the FE method, with the analysis yielding further 'internal' loads or stresses acting on structural elements such as wing spars and ribs. This issue is also addressed briefly in Chapters 21 and 25; the explanation given here is only one of several approaches that can be used for this complex task. There is clearly some room for confusion over terminology since what are referred to as 'internal loads' in this book are sometimes called 'external loads', since they are used to generate equivalent external loads acting on the nodes of the FE model.

18.12 EXAMPLES

Note that it would be helpful to do some of the examples in Chapter 6 first to ensure that the principles for determining internal loads are well understood.

1. An aircraft has the following data: $m = 48\ 000$ kg, $S_W = 160$ m^2, $C_{M_{0W}} = -0.015$, $c = 4$ m, $l_W = 0.4$ m and $l_T = 9$ m. Section AA is 2 m aft of the centre of mass and the section of fuselage/tailplane aft of AA has a mass distribution that can be approximated by lumped masses of 5000, 3000 and 2000 kg at positions that are 2, 4 and 6 m respectively aft of AA. Determine the tailplane lift and the bending moment at AA for a flight case where the air speed is 150 m/s EAS and the load factor $n = 2$.
   [26.0 kN, 485.1 kN m]

2. For the aircraft in Example 1 above, the wing lift acts at quarter chord, the net wing/engine inertia force acts at 40 % chord and the front and rear spars lie at 20 % and 60 % chord. The wing and engine mass is 16 000 kg. Determine the intercomponent forces acting between the wings and centre fuselage at the front and rear spars.
   [Front 558.2 kN and rear −42.6 kN]

3. An aircraft of mass 30 000 kg has the tapered wing planform shown in Figure 18.19. Each wing has a structural mass of 2000 kg and a fuel mass of 2000 kg, with the fuel located only in the inboard half of the wing, as shown in the figure. The wing/fuel mass may be assumed to be uniformly distributed over the relevant wing area whereas the lift may be assumed to be uniformly distributed over the wing and centre fuselage area (i.e. ignore the tailplane effects). The aircraft experiences an $n = 3$ manoeuvre. Determine the shear force and bending moment at the wing root assuming that the structure and loading are continuously distributed. With the wing divided into eight strips, determine and sketch the shear force and bending moment distribution. Would these internal loads increase or reduce if the same manoeuvre were performed with wings (and therefore the aircraft) empty of fuel?
   [Continuous: wing root shear force 264 kN, bending moment 1606 kN m; Discretized: 274 kN, 1608 kN m]

4. For the aircraft in Example 3 above, consider the engines moved from the rear fuselage on to the wing. Each engine mass is 2000 kg and the engine is placed 3.75 m outboard of the fuselage, 2 m

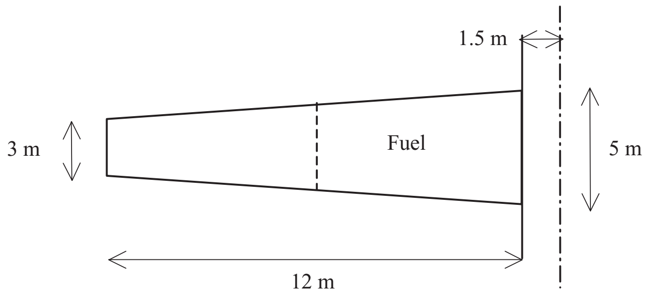

Figure 18.19

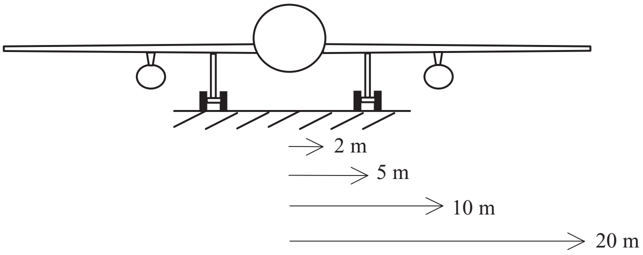

Figure 18.20

forward of the wing centre line and 1 m below it. The engine thrust is 20 kN. Determine and sketch the changes to the internal load diagrams that will result from moving the engines in this way for the full fuel case.
[Wing root shear force 205 kN, bending moment 1387 kN m plus torque 98 kN m]

5. During a heavy landing, at the instant when the vertical force on the landing gear leg reaches a maximum, an aircraft is decelerating in the vertical direction at $2g$ so the load factor is $n = 3$. The spanwise dimensions of the aircraft are shown in Figure 18.20 and both the wing structure mass and lift may be assumed to be uniformly distributed across the span (including the section of wing enclosed by the fuselage). The mass of the complete aircraft is 100 000 kg, the wing mass is 15 000 kg and each engine has a mass of 5000 kg. The attitude and speed of the aircraft are such that the wing lift is equal to 90 % of the aircraft weight. Determine the landing gear reaction force and the bending moment experienced by the wing (a) at the section where the landing gear is attached and (b) at the wing root.
[1030 kN, (a) 506 kN m, (b) 3701 kN m]

6. The aircraft, whose rear fuselage and tail are shown in Figure 18.21, experiences a manoeuvre such that, at some instant of time, the aircraft centre of mass accelerates upwards at 10 m/s^2 (so effectively $n = 2$) and simultaneously the aircraft accelerates nose up in pitch at 1 rad/s^2 about the centre of mass. The aircraft may be assumed to be in a horizontal flight attitude at this instant. The rear fuselage mass of 1200 kg is divided equally at stations A, B and C and the fin and tailplane have masses of 200 and 100 kg respectively. The two engines have a total mass of 1500 kg and develop a net thrust of 30 kN. The net tailplane lift in the manoeuvre is 5 kN and the rear fuselage, fin and tailplane drag forces are 1, 0.5 and 0.5 kN respectively. Determine the inertia loads and draw an FBD. Estimate the bending moment, shear force and axial force defined on the centre line at the fuselage section XX

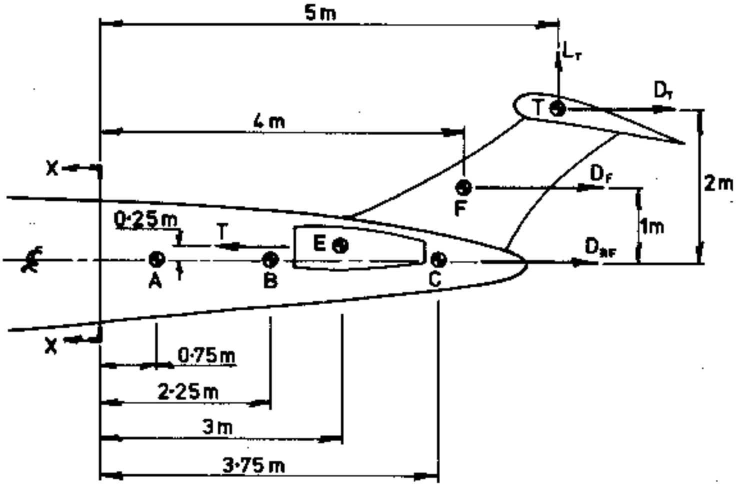

Figure 18.21

which lies 3 m aft of the centre of mass. Note that each section of the structure experiences a different acceleration. Assume for convenience that $g = 10$ m/s^2.
[86.4 kN m, 37.5 kN and 28.0 kN]

7. An aircraft of mass 12 000 kg has the wing planform shown in Figure 18.22, with the mass of each wing (outboard of the fuselage) being 2000 kg and uniformly distributed over the span. The radius of gyration of the aircraft (without wings) in roll is 1 m. The aircraft is flying at 150 m/s EAS when the ailerons are deflected through 5°. The aileron lift curve slope over the local aileron span is $a_C = 1.5/\text{rad}$ and the aileron lift may be assumed to be distributed uniformly over the aileron span. Determine the rolling moment, the aircraft roll moment of inertia, the rolling acceleration and the incremental wing root bending moment in the manoeuvre at the instant of applying the ailerons.
[101 kN m, 115 300 kg m^2, 0.88 rad/s^2, 8.5 kN m]

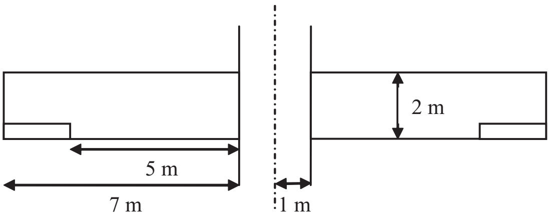

Figure 18.22

8. Obtain the expression for the wing root shear force, equivalent to that for the bending moment presented in Section 18.5.2.3 of this chapter, for the flexible aircraft in an equilibrium manoeuvre.

9. Obtain the expression for the incremental wing root shear force, equivalent to that for the bending moment presented in Section 18.5.3.3 of this chapter, for the flexible aircraft in a gust encounter.

10. Modify the programs developed in the example section of Chapter 13 to include evaluation of the wing root shear force and bending moment in an equilibrium manoeuvre for a rigid and flexible aircraft. Use the programs to determine these internal loads for the aircraft parameters used in that chapter at the corner points of the manoeuvre envelope developed in Example 1 in Chapter 13. Which point on the manoeuvre envelope has the most severe loads?

11. Modify the programs developed in the example section of Chapter 16 to include evaluation of the wing root shear force and bending moment in a ‘1-cosine’ gust for a rigid and flexible aircraft. Use the programmes to determine these internal loads for the aircraft parameters used in that chapter and hence the gust length at which each of these loads has a maximum absolute value.

19

Potential Flow Aerodynamics

The two-dimensional strip theory aerodynamics that has been used so far in this book, for convenience, implies a number of major assumptions about the aerodynamic load distribution (e.g. neglects tip effects) and is only moderately accurate for low speed, high aspect ratio and unswept wings. Of particular importance is the assumption that the aerodynamic forces acting on one chord wise strip have no effect on other chord wise strips. In order to perform a more accurate aeroelastic analysis, aerodynamic theories need to be developed that are able to define more accurate pressure distributions over the entire wing. The so-called three-dimensional *panel* methods were developed to model the interaction between the aerodynamic forces on different parts of the lifting surfaces (wings, fin and horizontal tail surfaces) more accurately. It will be shown in Chapter 20 how it is possible to couple fully the panel method aerodynamics with a finite element (FE) model; consequently, panel methods are the primary aerodynamic tool used by industry for aeroelastic analysis. However, it should be noted that panel methods cannot be used to give accurate lift distributions in the transonic flight regime and corrections based upon wind tunnel tests are often employed. Also only the induced drag is able to be estimated. Consequently, there is an increasing use of higher fidelity computational fluid dynamics (CFD) methods, often solving the full Navier–Stokes equations, coupled with FE models to determine the time response to some initial displacement in the transonic region.

In this chapter, some aspects of inviscid flow analysis will be introduced that enable the velocity at any part of the flow, around a wing for instance, to be defined. Knowing that the flow component normal to the surface of an aerofoil must be zero, the entire flow and resulting pressures can be determined. Following the introduction of the concept of vorticity, the analysis of the flow around two-dimensional thin aerofoils is introduced. Through the use of the Biot–Savart law, the extension to three-dimensional wings is discussed, leading to the panel method analysis of the three-dimensional steady and unsteady cases. The reader is directed to *Low Speed Aerodynamics* by Katz and Plotkin (2001), which provides a complete overview of panel method aerodynamics.

19.1 ELEMENTS OF INVISCID, INCOMPRESSIBLE FLOW ANALYSIS

The classical two-dimensional inviscid flow theory provides a basis for analysing flow motion. Of particular interest are the resulting velocities at a point in the flow which is described by the streamlines (see Chapter 5). The underlying stream function and/or velocity potential of the flow for Cartesian and polar coordinates need to be determined first, and then the velocities at any point can be calculated.

The *stream function* $\Psi(x, y)$ is constant for each streamline and the velocities in the horizontal x, vertical z, radial q_r and tangential q_θ directions are given as

$$u = \frac{\partial \psi}{\partial y}, \qquad w = -\frac{\partial \psi}{\partial x}, \qquad q_r = \frac{1}{r}\ \frac{\partial \psi}{\partial \theta}, \qquad q_\theta = -\frac{\partial \psi}{\partial r}. \tag{19.1}$$

Introduction to Aircraft Aeroelasticity and Loads J. R. Wright and J. E. Cooper
© 2007 John Wiley & Sons, Ltd

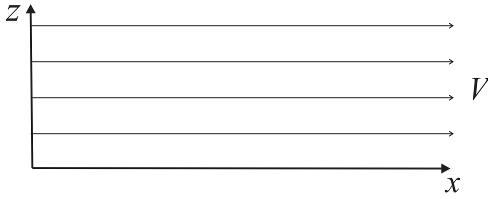

Figure 19.1 Uniform flow streamlines.

The *velocity potential* $\phi\ (x, y)$ is defined as the amount of fluid flowing between two points on a streamline (Houghton and Carpenter, 2001); the equivalent expressions for the velocity components are

$$u = \frac{\partial \phi}{\partial x}, \qquad w = \frac{\partial \phi}{\partial y}, \qquad q_r = \frac{\partial \phi}{\partial r}, \qquad q_\theta = \frac{1}{r}\frac{\partial \phi}{\partial \theta}. \tag{19.2}$$

From inspection of Equations (19.1) and (19.2) it is possible to determine the stream function and velocity potential for a range of different flow cases, as shown in the following examples.

19.1.1 Uniform Flow

For the flow of velocity V parallel to the x axis, as shown in Figure 19.1, using the Cartesian definitions gives

$$u = V, \qquad w = 0 \quad \Rightarrow \quad \psi = Vz \qquad \text{and} \qquad \phi = Vx. \tag{19.3}$$

With the flow along the z axis the expressions change to

$$u = 0, \quad w = V \quad \Rightarrow \quad \psi = -Vx \quad \text{and} \quad \phi = Vz \tag{19.4}$$

and for a flow inclined at $\tan^{-1}\ (V/U)$ then

$$\psi = V\ (z - x) \quad \text{and} \quad \phi = V\ (x + z). \tag{19.5}$$

19.1.2 Point Source and Point Sink

For the source shown in Figure 19.2, where fluid appears at some point in the flow at the flow rate m and moves radially in all directions, then at radius r from the source, using the polar definitions gives

$$\begin{gathered} \phi = \frac{m}{2\pi}\ln(r), \qquad \psi = \frac{m\theta}{2\pi} = \frac{m}{2\pi}\tan^{-1}\left(\frac{z}{x}\right), \\ q_r = \frac{m}{2\pi r}, \qquad q_\theta = 0, \qquad u = \frac{mx}{2\pi r^2}, \qquad w = \frac{my}{2\pi r^2}. \end{gathered} \tag{19.6}$$

The sink is the exact opposite of the source, with flow disappearing into some point at rate m; all of the expressions in Equation (19.6) are preceded by a minus sign. Note that sources and sinks are singular points with an infinite flow velocity where they occur.

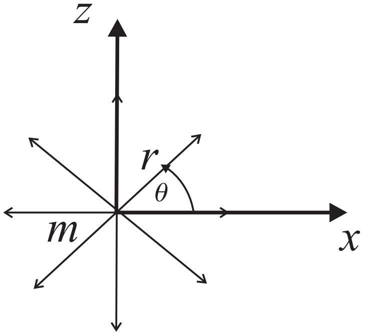

Figure 19.2 Source streamlines.

19.1.3 Source–Sink Pair

Consider the source and sink of equal strength m placed at distances d and $-d$ respectively from the origin on the x axis, as shown in Figure 19.3. The velocity potential and stream function are determined by adding the two component parts together such that

$$\phi = \frac{m}{2\pi}\left[\ln(r_1) - \ln(r_2)\right], \qquad \psi = \frac{m}{2\pi}(\theta_1 - \theta_2),$$
$$u = \frac{m}{2\pi}\frac{x + x_0}{(x+x_0)^2 + z^2} - \frac{m}{2\pi}\frac{x - x_0}{(x-x_0)^2 + z^2}, \qquad w = \frac{m}{2\pi}\frac{z}{(x+x_0)^2 + z^2} - \frac{m}{2\pi}\frac{z}{(x-x_0)^2 + z^2}. \tag{19.7}$$

The streamlines for the combined flows are circles passing through the source and sink as shown in Figure 19.4. When $(\theta_1 - \theta_2) = \pi/2$ the streamline is a semicircle with centre O.

19.1.4 Doublet

If the source and sink in the case above are allowed to approach each other, then $d \to 0$. Now letting $md = \mu/2$, where μ is a constant known as the doublet strength, then the velocity potential and stream function become

$$\phi = \frac{-\mu}{2\pi}\frac{\cos\theta}{r}, \qquad \psi = \frac{\mu}{2\pi}\frac{z}{x^2 + y^2} = \frac{\mu}{2\pi}\frac{\sin\theta}{r}. \tag{19.8}$$

The resulting streamlines are circles that are tangential to each other with centres on the z axis, as shown in Figure 19.5.

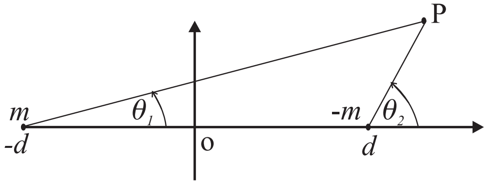

Figure 19.3 Combined source and sink.

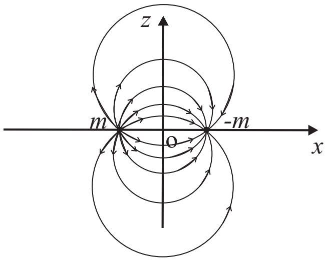

Figure 19.4 Streamlines for a source–sink pair.

19.1.5 Source – Sink Pair in a Uniform Flow (Rankine Oval)

If a uniform flow of V in the x direction is combined with a source–sink pair, as shown in Figure 19.6, then the velocities are found as

$$\phi = Vx + \frac{m}{2\pi}\left[\ln(r_1) - \ln(r_2)\right], \qquad \psi = Vz + \frac{m}{2\pi}(\theta_1 - \theta_2),$$

$$u = V + \frac{m}{2\pi}\frac{x + x_0}{(x + x_0)^2 + z^2} - \frac{m}{2\pi}\frac{x - x_0}{(x - x_0)^2 + z^2}, \qquad w = \frac{m}{2\pi}\frac{y}{(x + x_0)^2 + z^2} - \frac{m}{2\pi}\frac{y}{(x - x_0)^2 + z^2}. \tag{19.9}$$

The so-called stagnation points, where the velocity is zero, are found by determining where both velocities u and w are zero. The streamline passing through the stagnation points is known as the dividing streamline and is defined by $\psi = 0$. The resulting shape is the so-called Rankine oval shown in Figure 19.7 where there are two stagnation points S_1 and S_2 on the x axis. The flow inside the oval is of no interest and consequently the oval can be replaced by a solid body. This is an example of how potential flow analysis can be used to determine the flow around a body.

19.1.6 Doublet in a Uniform Flow

The velocity potential and stream function of a doublet in a uniform flow can be found from superposition of the relevant results above. Taking the doublet strength as $-\mu$, then in polar coordinates

$$\phi = \cos\theta\left(Vr + \frac{\mu}{2\pi r}\right), \qquad \psi = \sin\theta\left(Vr - \frac{\mu}{2\pi r}\right), \tag{19.10}$$

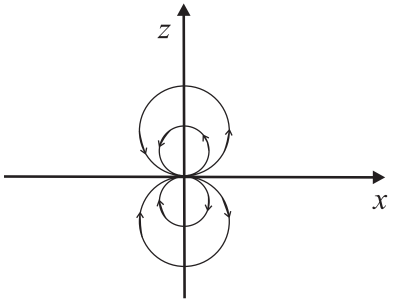

Figure 19.5 Doublet streamlines.

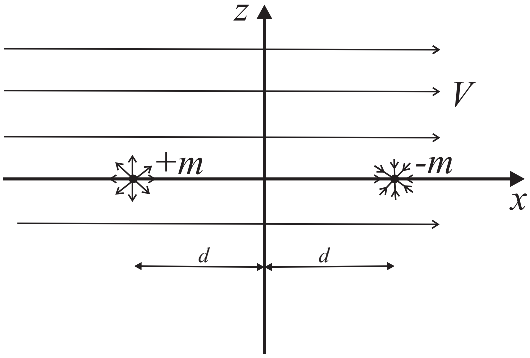

Figure 19.6 Source–sink pair in a uniform flow.

where θ is defined as above and the dividing streamline ($\psi = 0$) is found to be a circle of radius $R = \sqrt{\mu/(2\pi V)}$ with the centre at (0,0), as shown in Figure 19.8. Thus, to achieve a dividing streamline of a given radius R, the required doublet strength is defined as

$$\mu = 2\pi V R^2. \tag{19.11}$$

Once again, the flow inside the dividing streamline may be ignored and may be replaced by a cylindrical body. For the flow around a cylinder of radius R,

$$\begin{aligned} \phi &= V\cos\theta\left(r + \frac{R^2}{r}\right), \qquad \psi = V\ \sin\theta\left(r - \frac{R^2}{r^2}\right), \\ q_r &= V\cos\theta\left(1 - \frac{R^2}{r^2}\right), \qquad q_\theta = -V\ \sin\theta\left(1 + \frac{R^2}{r^2}\right), \end{aligned} \tag{19.12}$$

and on the cylinder surface $q_r = 0$ and $q_\theta = -2V\ \sin\theta$.

The pressure acting around the cylinder can be calculated using Bernoulli's equation (see Chapter 5) so that

$$p_\infty + \frac{\rho V^2}{2} = p + \frac{\rho q_\theta^2}{2}, \qquad \text{giving} \quad p_\infty - p = \frac{\rho V^2}{2}\left(1 - 4\ \sin^2\theta\right) \tag{19.13}$$

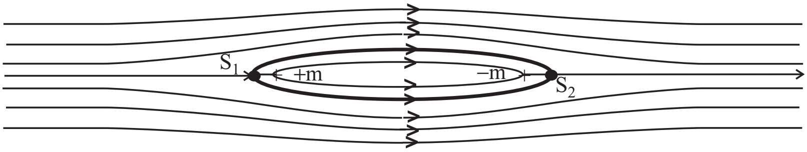

Figure 19.7 Source–sink pair in a uniform flow – streamlines.

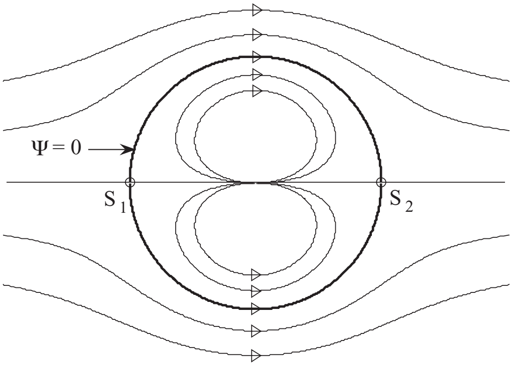

Figure 19.8 Doublet in a uniform flow – streamlines.

on the cylinder surface and a pressure coefficient distribution around the cylinder of

$$C_p = \frac{2(p - p_\infty)}{\rho V^2} = 1 - 4\ \sin^2\theta. \tag{19.14}$$

The lift and drag per unit span on the cylinder can be calculated by integrating the force components in the vertical and horizontal directions due to the pressure acting on elements $R\ \mathrm{d}\theta$ on the cylinder surface. In this case both the lift and drag are zero, due to the symmetry in both the vertical and horizontal planes. In practice the flow around a cylinder will separate from the cylinder, which is not predicted using the above analysis, demonstrating one of the limitations of inviscid theory.

19.2 INCLUSION OF VORTICITY

So far the flow particles have been assumed to maintain their orientation and so are irrotational. A more accurate representation of the fluid motion can be provided by including rotational flow. This can be defined in terms of the vorticity, which is a measure of the angular velocity or spin within the fluid.

19.2.1 Vortices

Consider the 'swirling' flow shown in Figure 19.9 with the vortex positioned at (x_0, z_0). The radial velocity q_r at each point is zero and the tangential velocity q_θ is constant at each radius. Defining the strength, or circulation, of the vortex Γ acting in a clockwise direction as

$$\Gamma = 2\pi r q_\theta, \tag{19.15}$$

the circulation has units of m^2/s in a two-dimensional flow. The consequence of this equation is that the tangential velocity around a vortex reduces in proportion to $1/r$. The velocity potential and stream functions at point P (x, z) for a vortex at point (x_0, z_0) can be shown to be

$$\phi = -\frac{\Gamma}{2\pi}\tan^{-1}\left(\frac{z - z_0}{x - x_0}\right), \qquad \psi = -\frac{\Gamma}{2\pi}\ln\ r, \tag{19.16}$$

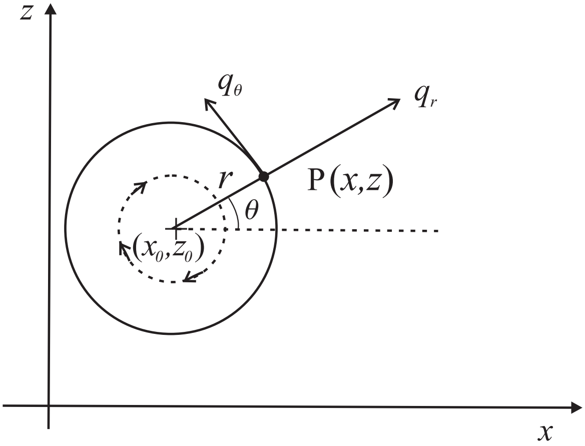

Figure 19.9 Velocities around a vortex.

where r is the distance between the vortex and point P. The velocities at point P can then be found as

$$u = \frac{\Gamma}{2\pi}\frac{(z-z_0)}{(x-x_0)^2+(z-z_0)^2}, \quad w = -\frac{\Gamma}{2\pi}\frac{x-x_0}{(x-x_0)^2+(z-z_0)^2}, \quad q_\theta = -\frac{\Gamma}{2\pi r}, \quad q_r = 0. \tag{19.17}$$

19.2.2 Flow Past a Cylinder with a Vortex at the Centre

Consider the previous case of a doublet of strength $\mu = 2\pi R^2$ in a uniform flow, but this time adding a vortex of strength $-\Gamma$ at the origin. The velocity potential and stream function are found via superposition as

$$\phi = V\ \cos\theta\left(r + \frac{R^2}{r}\right) - \frac{\Gamma}{2\pi}\theta, \qquad \psi = V\ \sin\theta\left(r - \frac{R^2}{r}\right) + \frac{\Gamma}{2\pi}\ln r, \tag{19.18}$$

giving radial and tangential velocities of

$$q_r = V\ \cos\theta\left(1 - \frac{R^2}{r^2}\right), \qquad q_\theta = -V\ \sin\theta\left(1 + \frac{R^2}{r^2}\right) - \frac{\Gamma}{2\pi r}, \tag{19.19}$$

which on the cylinder surface ($r = R$) give

$$q_r = 0, \qquad q_\theta = -2V\ \sin\theta - \frac{\Gamma}{2\pi R}. \tag{19.20}$$

The stagnation points can be found when $q_\theta = 0$ and thus occur where

$$\sin\theta = -\frac{\Gamma}{4\pi R V}. \tag{19.21}$$

Therefore, as long as $\Gamma \leq 4\pi R V$ there is a solution and the stagnation points S_1 and S_2 lie on the dividing streamline which is a circle, as shown in Figure 19.10

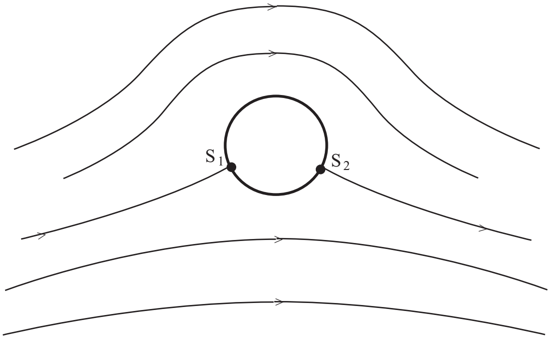

Figure 19.10 Flow around a cylinder with added vortex.

The lift per unit span (positive upwards) is found by integrating around the entire circumference the elemental force acting in the z direction due to the pressure on element $R\ \mathrm{d}\theta$ such that

$$L = \int_0^{2\pi} -pR \sin\theta \ \mathrm{d}\theta. \tag{19.22}$$

Remembering from Bernoulli's equation that

$$p_\infty + \frac{\rho V^2}{2} = p + \frac{\rho q_\theta^2}{2} \quad \to \quad p = p_\infty + \frac{\rho V^2}{2} - \frac{\rho}{2}\left(2V \sin\theta + \frac{\Gamma}{2\pi R}\right)^2, \tag{19.23}$$

the lift per unit span can be shown to be

$$L = \rho V \Gamma. \tag{19.24}$$

This is a very important result which shows that the lift is proportional to the strength of the vortex. Since the flow considered forms a closed loop around the cylinder, Γ is often referred to as the circulation. Note, however, that even with the inclusion of the vortex the drag in this two-dimensional example is still zero; this is because viscosity is neglected.

19.3 NUMERICAL STEADY AERODYNAMIC MODELLING OF THIN TWO-DIMENSIONAL AEROFOILS

It is now possible to start modelling flows around two-dimensional aerofoils. Assuming a two-dimensional incompressible and inviscid steady flow around a thin aerofoil at a small angle of attack, then a number of different flow components can be employed to model the flow; the zero normal flow boundary condition on the solid boundary of the aerofoil is used to determine the strengths of these components. The problem must be modelled in two parts: firstly, a symmetric aerofoil of the same thickness at zero incidence and, secondly, a thin plate of the camber line shape at the prescribed incidence. A further condition that must be met is the so-called Kutta condition, where the flow must leave the sharp trailing edge of the aerofoil smoothly, implying that the velocity there must be finite.

As an example, taking the vortex function described earlier as the fundamental building block, the flow can be modelled as a distribution of vortices along the centre line with differing strengths in a uniform flow. For the aerofoil shown in Figure 19.11, a single vortex is placed at the quarter chord, and it can be shown that the zero normal flow boundary condition needs to be enforced at the three-quarter chord

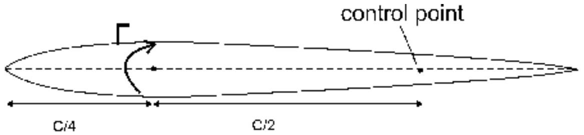

Figure 19.11 Two-dimensional aerofoil modelled as the vortex at the quarter chord and the control point at the three-quarter chord.

control point in order to model the flow correctly. This constraint also ensures that the Kutta condition is met.

If more than a single vortex is used, then the aerofoil is divided into several chordwise elements, each with a vortex and control point. By setting up a series of flow equations from the vortex elements that meet the boundary conditions, the vortex strengths can be determined. Once the vortex distribution has been found, the overall lift and pitching moment can be obtained (the drag is found to be zero for the two-dimensional inviscid case).

As an example (Katz and Plotkin, 2001), consider the two-element cambered aerofoil that is at an angle of incidence of α (radians) to a flow V, as shown in Figure 19.12. A vortex is placed at the quarter chord of each element and the control points are at the three-quarter chord of each element. The camber is represented by angle β at each of the control points. The vortices impose a velocity in the x and z directions at both control points of (u_1, w_1) and (u_2, w_2). Consequently, the flows normal to the surface at both control points are

$$\begin{aligned} n_1 &= (w_1 + V\sin\alpha)\cos\beta_1 + (u_1 + V\cos\alpha)\sin\beta_1, \\ n_2 &= (w_2 + V\sin\alpha)\cos\beta_2 + (u_2 + V\cos\alpha)\sin\beta_2, \end{aligned} \tag{19.25}$$

and as they must both equal zero in order to meet the boundary conditions, then

$$\begin{aligned} w_1\cos\beta_1 + u_1\sin\beta_1 &= -V(\sin\alpha\cos\beta_1 + \cos\alpha\sin\beta_1), \\ w_2\cos\beta_2 + u_2\sin\beta_2 &= -V(\sin\alpha\cos\beta_2 + \cos\alpha\sin\beta_2). \end{aligned} \tag{19.26}$$

The velocities at each control point due to the two vortices can be found using Equation (19.17) for the velocity components, and substitution of these expressions into Equations (19.26) gives

$$\left[\begin{matrix} -\frac{1}{2\pi}\left(\frac{x_{c1}-x_{v1}}{r_{11}^2}\cos\beta_1\right)+\frac{1}{2\pi}\left(\frac{z_{c1}-z_{v1}}{r_{11}^2}\sin\beta_1\right) \\ -\frac{1}{2\pi}\left(\frac{x_{c2}-x_{v1}}{r_{21}^2}\cos\beta_2\right)+\frac{1}{2\pi}\left(\frac{z_{c2}-z_{v1}}{r_{21}^2}\sin\beta_2\right) \end{matrix}\right. \qquad \cdots$$

$$\left.\begin{matrix} -\frac{1}{2\pi}\left(\frac{(x_{c1}-x_{v2})}{r_{12}^2}\cos\beta_1\right)+\frac{1}{2\pi}\left(\frac{(z_{c1}-z_{v2})}{r_{12}^2}\sin\beta_1\right) \\ \frac{1}{2\pi}\left(\frac{x_{c2}-x_{v2}}{r_{22}^2}\cos\beta_2\right)+\frac{1}{2\pi}\left(\frac{z_{c2}-z_{v2}}{r_{22}^2}\sin\beta_1\right) \end{matrix}\right]\begin{bmatrix}\Gamma_1\\ \Gamma_2\end{bmatrix}$$

$$= \begin{bmatrix}\psi_{11} & \psi_{12}\\ \psi_{21} & \psi_{22}\end{bmatrix}\begin{bmatrix}\Gamma_1\\ \Gamma_2\end{bmatrix} = \mathbf{\Psi\Gamma} = -V\begin{bmatrix}\sin\alpha\cos\beta_1+\cos\alpha\sin\beta_1\\ \sin\alpha\cos\beta_2+\cos\alpha\sin\beta_2\end{bmatrix} \tag{19.27}$$

where r_{ij} is the distance between the ith control point and the jth vortex. The ψ_{ij} terms are known as the *influence coefficients* and define the normal flow (or downwash) at the ith control point induced by the jth unit strength vortex. This Equation (19.27) can be solved to find the unknown vortex strength values.

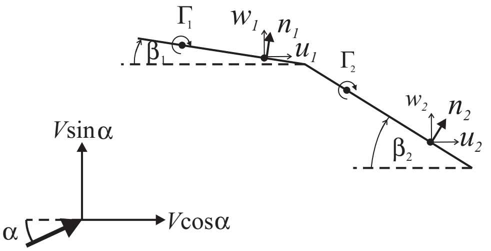

Figure 19.12 Cambered aerofoil with two section vortex elements.

If the simplified case of zero camber and small deflections is considered (i.e. $\beta_1 = \beta_2 = 0$ and $\sin\alpha \to \alpha$), then Equation (19.27) becomes

$$\begin{bmatrix} -\dfrac{2}{c\pi} & \dfrac{2}{c\pi} \\ -\dfrac{2}{3c\pi} & -\dfrac{2}{c\pi} \end{bmatrix} \begin{Bmatrix} \Gamma_1 \\ \Gamma_2 \end{Bmatrix} = -V \begin{Bmatrix} \alpha \\ \alpha \end{Bmatrix} = -V \begin{Bmatrix} 1 \\ 1 \end{Bmatrix} \alpha \quad \Rightarrow \quad \begin{Bmatrix} \Gamma_1 \\ \Gamma_2 \end{Bmatrix} = V\pi c \begin{Bmatrix} \dfrac{3}{4} \\ \dfrac{1}{4} \end{Bmatrix} \alpha. \tag{19.28}$$

The lift on each element L_i is defined as $\rho V \Gamma_i$; thus the total lift is the sum of the lift on the two elements

$$L = \sum_{i=1}^{2} L_i = \rho V \sum_{i=1}^{2} \Gamma_i = \rho V^2 \pi c \alpha, \tag{19.29}$$

whereas the pitching moment about the mid-chord is found as

$$M = \sum_{i=1}^{2} M_i = \rho V^2 \alpha \pi \left(\frac{3c}{4}\frac{3c}{8} - \frac{c}{4}\frac{c}{8} \right) = \frac{\rho V^2 \alpha \pi c^2}{4}. \tag{19.30}$$

Both the lift and pitching moment expressions are exactly the same as those obtained by using strip theory for a unit span aerofoil of chord c and a lift-curve slope of 2π.

It is useful to rewrite the solution for the vortex strength, and hence the lift per unit span acting upon each chordwise element, in terms of a general incidence per element ($\alpha_1 = \alpha + \beta_1,\ \alpha_2 = \alpha + \beta_2$ if camber is present; see Equation (19.27)) as follows:

$$\begin{Bmatrix} L_1 \\ L_2 \end{Bmatrix} = \rho V \begin{Bmatrix} \Gamma_1 \\ \Gamma_2 \end{Bmatrix} = \frac{\rho V^2}{2} \frac{3c\pi}{8} \begin{bmatrix} 2 & 2 \\ -\dfrac{2}{3} & 2 \end{bmatrix} \begin{Bmatrix} \alpha_1 \\ \alpha_2 \end{Bmatrix} = \frac{\rho V^2}{2} \begin{bmatrix} \mathrm{AIC}_{11} & \mathrm{AIC}_{12} \\ \mathrm{AIC}_{21} & \mathrm{AIC}_{22} \end{bmatrix} \begin{Bmatrix} \alpha_1 \\ \alpha_2 \end{Bmatrix}. \tag{19.31}$$

In this important equation, the AIC_{ij} terms are known as the *aerodynamic influence coefficients* (AICs). They relate the lift on each element to the aerodynamics and angle of incidence of each element and also the dynamic pressure. Care must be taken not to confuse the definitions for the *influence coefficients* and the *aerodynamic influence coefficients* as they are quite different, yet closely related, quantities.

The general form of Equation (19.31) is given by

$$\boldsymbol{L} = \rho V \boldsymbol{\Gamma} = -\rho V^2 \boldsymbol{\Psi}^{-1} \boldsymbol{\alpha} = \frac{\rho V^2}{2} \mathbf{AIC} \boldsymbol{\alpha}, \tag{19.32}$$

so the different sets of influence coefficients are related via $\mathbf{AIC} = -2\boldsymbol{\Psi}^{-1}$.

Although only discrete vortices have been used in the above example, it is possible to use any combination of flow components, such as sources, sinks or doublets. Note also that they do not have to be discrete, and can take the form of continuous distributions (e.g. linear or quadratic) along the length of each element.

19.4 STEADY AERODYNAMIC MODELLING OF THREE-DIMENSIONAL WINGS USING A PANEL METHOD

The approach developed above for two-dimensional flows can be extended to the three-dimensional case with the wing being divided up into chordwise and spanwise panels, each with an aerodynamic element. The influence coefficients are calculated for whatever distribution of elements is chosen, and are then used together with the surface boundary conditions at the control points to obtain the element strengths. It is then possible to calculate the lift, pitching moment and, for the three-dimensional case, the induced drag.

19.4.1 Vortex Filaments and the Biot–Savart Law

Assume that it is possible to have a continuous line, or filament, of vortices of constant strength Γ that rotate about that line in three-dimensional space. It can be shown that the vortex filament cannot end in a fluid, but must either form a closed loop or extend to the boundaries of the fluid. A real-life example of this is the trailing tip vortices that form from both wing tips of an aircraft. These vortices extend for many miles behind a commercial aircraft, eventually breaking down due to friction losses, and have a big influence upon the spacing between aircraft allowed by Air Traffic Control.

The Biot–Savart law defines the induced velocity at some point P due to an element of vortex filament. Consider the vortex filament of strength Γ and length $\mathrm{d}s$ passing through point Q in Figure 19.13; the filament is at angle ϕ to PQ. Then the induced velocity $\mathrm{d}w$ at point P in the direction shown is

$$\mathrm{d}w = \frac{\Gamma \sin(\phi)\,\mathrm{d}s}{4\pi r^2}. \tag{19.33}$$

This law can be extended to consider the straight vortex line RS in Figure 19.14 of strength Γ and perpendicular distance h from point P. It can be shown by integrating along the vortex line that the induced velocity at point P is

$$w = \frac{\Gamma}{4\pi h}(\cos\alpha + \cos\beta) \quad \Rightarrow \quad w = \frac{\Gamma}{2\pi h} \quad \text{as} \quad \alpha \to 0,\ \beta \to 0, \tag{19.34}$$

where ($\alpha \to 0$, $\beta \to 0$) is the condition for an infinite vortex line.

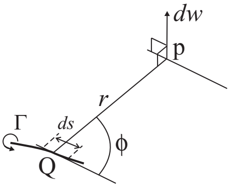

Figure 19.13 Induced velocity at point P due to the vortex filament.

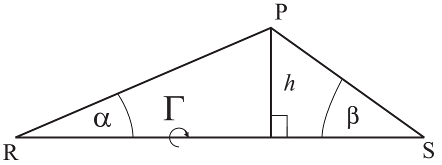

Figure 19.14 Downwash at point P due to the vortex filament RS of strength Γ.

19.4.2 Finite Span Wing – Modelled with a Single Horseshoe Vortex

It is common to model finite wings with vortex elements that tend to infinity and therefore to include the effect of the wake. Consider the wing of span $2s$ and chord c at a small angle of incidence α as shown in Figure 19.15. The wing is modelled as a *horseshoe vortex* that consists of a bound vortex of length $2s$ positioned along the quarter chord and two trailing vortices that tend to infinity. The closing section of the vortex is assumed to have no effect upon the downwash at the wing.

The total downwash w at the control point P, positioned a distance of $0.75c$ from the leading edge at the mid-span, has three contributions, namely those due to the bound vortex and the two trailing vortices. Making use of the Biot–Savart Law gives

$$\begin{aligned} w &= \frac{\Gamma}{4\pi s}\left(\frac{c/2}{\sqrt{s^2+(c/2)^2}}+1\right)+\frac{\Gamma}{4\pi s}\left(\frac{c/2}{\sqrt{s^2+(c/2)^2}}+1\right)+\frac{\Gamma}{4\pi\, c/2}\,\frac{2s}{\sqrt{s^2+(c/2)^2}} \\ &= \frac{\Gamma}{2\pi s}\left(\frac{c}{2\sqrt{s^2+(c/2)^2}}+1\right)+\frac{\Gamma}{\pi c}\frac{s}{\sqrt{s^2+(c/2)^2}} = \Psi\Gamma, \end{aligned} \tag{19.35}$$

where Ψ is the influence coefficient (in this case a scalar value for a single vortex). At the control point, the resulting downwash and the velocity contribution from the airflow (assuming small angles) must equal zero (cf. Equation (19.28)), so giving

$$V\alpha + \Psi\Gamma = 0, \tag{19.36}$$

from which the vortex strength Γ can be found for a given air speed and incidence.

Considering the forces acting upon the wing as shown in Figure 19.16, the lift and drag are found by integrating the force per unit element dy due to the vorticity across the span such that

$$L = \int_{-s}^{s} \rho V \Gamma \, \mathrm{d}y \qquad \text{and} \qquad D = \int_{-s}^{s} \rho V \Gamma \alpha \, \mathrm{d}y, \tag{19.37}$$

where Γ dy is the strength of the vortex element. Note that this is the induced drag and not the total drag, which also has a friction (viscous) drag component that increases with Mach number (see Chapter 5). For a three-dimensional wing, as the span tends to infinity the induced drag tends to zero.

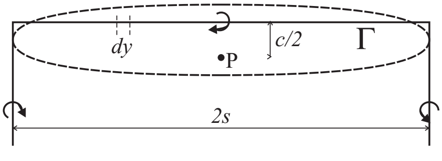

Figure 19.15 Wing modelled as a single horseshoe vortex.

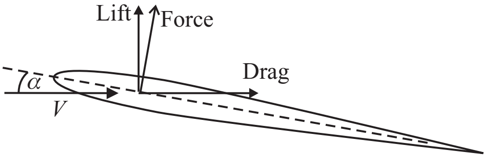

Figure 19.16 Forces acting on the aerofoil.

For this case, a single horseshoe vortex has been used, which implies that there is a constant lift distribution across the entire span. In order to obtain a result in which the lift falls off towards the tip, vorticity needs to be shed all along the wing.

19.4.3 Finite Span Wing – Modelled with a Vortex Lattice

In practice, the variation of lift along the span can be modelled by using a number of horseshoe vortices placed in a 'lattice' arrangement on a series of panels in both the spanwise and chordwise directions; the vortices are placed side by side or behind each other along the quarter chord of each panel. Since the total normal velocity on the control point for each panel, due to all the vortices and the overall flow, must be zero, it is possible to determine the influence coefficients and hence the strength of the vortices for a particular incidence. The following example shows the process when using a lattice of horseshoe vortices.

Consider the wing of span $2s$ and chord c with four equal sized aerodynamic panels each containing a horseshoe vortex, as shown in Figure 19.17. On each panel, the bound vortex runs along the quarter chord and there is a control point at the three-quarter chord on the panel mid-span. Each horseshoe vortex affects all control points, and thus the downwash at each control point has a contribution from each vortex, which can be written using superposition as

$$\boldsymbol{w} = \begin{bmatrix} w_1 \\ w_2 \\ w_3 \\ w_4 \end{bmatrix} = \begin{bmatrix} \psi_{11} & \psi_{12} & \psi_{13} & \psi_{14} \\ \psi_{21} & \psi_{22} & \psi_{23} & \psi_{24} \\ \psi_{31} & \psi_{32} & \psi_{33} & \psi_{34} \\ \psi_{41} & \psi_{42} & \psi_{43} & \psi_{44} \end{bmatrix} \begin{bmatrix} \Gamma_1 \\ \Gamma_2 \\ \Gamma_3 \\ \Gamma_4 \end{bmatrix} = \boldsymbol{\Psi\Gamma}, \tag{19.38}$$

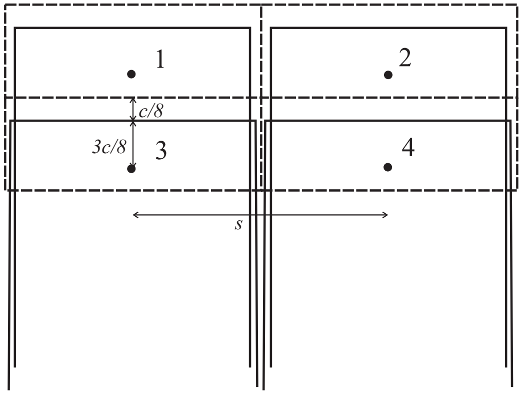

Figure 19.17 Four panel wing with horseshoe vortices.

where the elements of matrix $\boldsymbol{\Psi}$ are the influence coefficients, so ψ_{ij} is the downwash at the ith control point due to the jth horseshoe vortex of unit strength. These influence coefficients can be determined by application of Equation (19.34) for all of the vortices and panels.

As before, the zero normal flow boundary condition at the control points is satisfied via the relation

$$\boldsymbol{\Psi\Gamma} + V\boldsymbol{\alpha} = \mathbf{0}, \tag{19.39}$$

where $\boldsymbol{\alpha}$ is a vector of the angles of incidence of the panels. Equation (12.39) can be solved to find the unknown vortex strengths, but it can also be rearranged to determine the lift on each panel such that

$$\boldsymbol{L} = \rho V \mathbf{S}\boldsymbol{\Gamma} = \frac{\rho V^2}{2}\mathbf{AIC}_{\mathrm{R}}\boldsymbol{\alpha} \tag{19.40}$$

and $\mathbf{AIC}_{\mathrm{R}}$ is the 4×4 matrix of aerodynamic influence coefficients with $\mathbf{AIC}_{\mathrm{R}} = -2\mathbf{S}\boldsymbol{\Psi}^{-1}$ for the 3D case and $\mathrm{S} = \mathrm{diag}\,[\mathrm{s\ s\ s\ s}]$ is the diagonal matrix of the spans of each panel, equal in this example. For this steady case the AIC matrix will be real; however, the subscript R is used since in the unsteady case there will be both real and imaginary terms. The equation is related to the two-dimensional version for an aerofoil section in Equation (19.32).

If the same example were solved using *strip theory*, then two strips of width s and chord c are considered (i.e. one strip for each wing) and the lift curve slope is assumed to be 2π. The lift vector over the two strips is given by

$$\boldsymbol{L} = \frac{\rho V^2}{2}\begin{bmatrix} 2\pi cs & 0 \\ 0 & 2\pi cs \end{bmatrix}\boldsymbol{\alpha} \tag{19.41}$$

and now the AIC matrix is diagonal as the flow over one strip does not affect the other strip.

Panel method aerodynamic methods are formulated for the entire wing span. If only the semi-span is being considered, such as for a fixed root wing, then a further transformation is required (Katz and Plotkin, 2001) to allow for only one half of the aircraft being considered. This ensures that there is a non-zero lift at the wing root.

As in the two-dimensional case, it is also possible to use one of a wide range of different aerodynamic elements that are available, such as sources, sinks and doublets. It is also feasible to use ringed elements (e.g. a vortex ring) rather than the horseshoe modelling approach, and these may contain a distribution of aerodynamic elements across the entire area. In general, the same approach as that above is used to determine the strengths of the aerodynamic components and then to calculate the lift and drag.

19.5 UNSTEADY AERODYNAMIC MODELLING OF WINGS UNDERGOING HARMONIC MOTION

So far in this chapter only steady aerodynamics has been considered. However, for dynamic aeroelastic systems, the motion of the lifting surface needs to be taken into account. It was shown in Chapter 10 how Wagner's and Theodorsen's functions could be used to model the unsteady effects of the motion of a two-dimensional aerofoil for either a general motion (using convolution) or harmonic motion, and also how use of Kussner's and Sears' functions allows representation of gust-dependent unsteady aerodynamics. In this section, the panel method approach is extended in concept to model the aerodynamic forces resulting from unsteady harmonic motion.

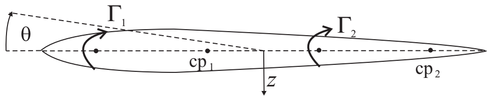

Figure 19.18 Oscillatory motion of a two-dimensional aerofoil.

19.5.1 Harmonic Motion of a Two-Dimensional Aerofoil

Consider the two-dimensional aerofoil that is modelled using two vortices as before, as shown in Figure 19.18, but now the angle of incidence θ and the heave z vary in a harmonic manner. Once a steady state is reached, the resulting lift and pitching moment vary sinusoidally, but with a different amplitude and phase from the quasi-steady predictions (depending upon the reduced frequency); the lift on each element will in general have a different phase. Note also that the wake behind the aerofoil also moves in a sinusoidal manner.

The changing aerodynamic forces due to a predefined structural motion of the aerofoil can be modelled in a 'time-marching' manner by defining a series of vortex rings in the wake (or other aerodynamic elements) and, at each time step, changing the strengths of the vortices on the aerofoil, and also the position of the wake vortices in relation to the motion of the structure. Figure 19.19 shows an example of this sort of process six time instants into the computation (after Katz and Plotkin, 2001). For a given instant in time, the strengths of the aerofoil vortices are determined from the boundary conditions at the control points, then the wake vortices (which cannot change their strength) are moved spatially (which will include roll-up effects) to the next time point and the strength of a new wake vortex close to the wing is determined. The aerofoil itself is then moved in time, and the process repeated.

Whereas such an approach could be applied for any general motion of the aerofoil, it does not lend itself to an efficient aeroelastic analysis and will not be considered further. However, a fully coupled methodology based upon harmonic motion does lead to an effective means of determining the aeroelastic response of an aircraft without calculating the development of the wake and is widely used in industry (Albino and Rodden, 1969; Blair, 1994).

Consider once again the oscillating two vortex aerofoil model shown in Figure 19.18. The panel method approach can be extended to include the unsteady effects by allowing the influence coefficients and aerodynamic influence coefficients to become complex and functions of the reduced frequency. Consequently, as the incidence and heave position of the aerofoil vary harmonically with time, the vortex strengths also vary harmonically with time. The zero normal flow condition at each control point still applies at each instant, but now there is a component due to the structural motion that must be included.

The calculation of the complex aerodynamic influence coefficient matrix for vortex or other aerodynamic elements (e.g. doublets) is beyond the scope of this book. However, the final form of the relationship between the lift on the elements and the motion of the control points is given by the expression

$$\tilde{\boldsymbol{L}}(k) = \frac{\rho V^2}{2}\mathbf{AIC}(k)_{\text{unsteady}}\boldsymbol{h}, \tag{19.42}$$

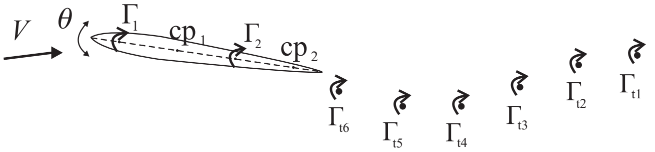

Figure 19.19 Progression of vortices in a time-marching solution for harmonic motion of the aerofoil.

where $\mathbf{AIC}(k)_{\text{Unsteady}}$ is the complex AIC matrix (a function of reduced frequency), $\tilde{\boldsymbol{L}}$ is the vector of lift forces on each panel (with the symbol $\sim$ indicating that it is a complex amplitude; see Chapters 1 and 2) and $\boldsymbol{h}$ is the vector of displacements at the control points (related to the angles of incidence and heave of the panels). Note that there are a number of different ways of writing the AICs and the vector defining the position of the panels; e.g. sometimes the results for panels arranged in a streamwise fashion behind each other are amalgamated into an effective strip. This variation of lift with reduced frequency is analogous to the lift variation with reduced frequency of an oscillating two-dimensional aerofoil described by Theodorsen's function in Chapter 10.

The expression in Equation (19.42) may be rewritten by separating out the real and imaginary parts of the AIC matrix and introducing the reduced frequency such that the complex lift amplitude vector is

$$\tilde{\boldsymbol{L}} = \frac{\rho V^2}{2}\mathbf{AIC}_{\mathrm{R}}\boldsymbol{h} + \mathrm{i}\omega\frac{\rho V}{2}\frac{b}{k}\mathbf{AIC}_{\mathrm{I}}\boldsymbol{h}. \tag{19.43}$$

It may be seen that Equation (19.43) may also be written in a time domain form with structural velocity present:

$$\boldsymbol{L} = \frac{\rho V^2}{2}\mathbf{AIC}_{\mathrm{R}}\boldsymbol{h} + \frac{\rho V}{2}\frac{b}{k}\mathbf{AIC}_{\mathrm{I}}\dot{\boldsymbol{h}}, \tag{19.44}$$

which is similar to the expression involving aerodynamic stiffness and damping for a particular reduced frequency as shown in Chapter 10. The matrices would normally be transformed into modal space for aeroelastic and loads calculations.

19.5.2 Harmonic Motion of a Three-Dimensional Wing

The extension to the three-dimensional case, as shown in Figure 19.20 for an oscillating three-dimensional wing modelled with a single horseshoe vortex, follows the same approach as for the steady case. The vortex filaments on the wing oscillate in strength, whereas the trailing vortices vary in both strength and position.

The most common three-dimensional unsteady panel approach is the doublet lattice (DL) method (Albino and Rodden, 1969; Blair, 1994). In the DL method, the aerodynamic forces resulting from the unsteady motion are modelled using so-called acceleration potential doublets along the quarter chord of each panel. These lead to the calculation of complex AICs that relate the lift acting along the doublet line to the displacement of each panel.

The steady forces corresponding to the underlying steady flow are calculated using the steady vortex lattice method as described above, and Figure 19.21 shows a typical panel set-up with both doublets and vortices. The derivation of the doublet lattice method is well beyond the scope of this book, but the interested reader is directed to Blair (1994) for a comprehensive explanation.

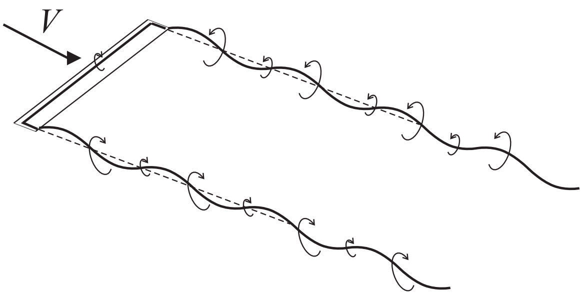

Figure 19.20 Horseshoe vortex on a three-dimensional oscillating wing.

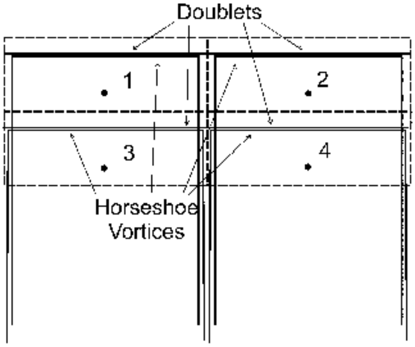

Figure 19.21 Typical doublet and horseshoe vortex set-up for the doublet lattice method.

19.6 AICS IN MODAL SPACE

Up to this point, the use of a panel aerodynamics method has been illustrated using a simple two-dimensional aerofoil and three-dimensional wing model based on physical displacements of the structure. In practice, the aerodynamic forces are calculated for the whole aircraft and it is more efficient and common to consider aeroelastic and loads analysis in terms of the rigid body and flexible modes of the structure.

In this section, the application of AICs to the aeroelastics and loads equations based in modal space is introduced for steady aerodynamics. Comments are also made about the form of the results for the unsteady case. The aerodynamic forces arising from heave, pitch and flexible mode motions for the free–free aircraft are obtained and related to the aerodynamic derivatives employed for manoeuvres and gust encounters earlier in Chapters 13 to 18; the approach is also relevant to static aeroelasticity and flutter for the whole aircraft.

19.6.1 Heave Displacement

Consider firstly the effect of all the panels undergoing heave displacement z (positive downwards), effectively a displacement in the heave rigid body mode. There will be no resulting change of incidence due to this change of position (in the steady case) and therefore no resulting forces on the panels. The net force (downwards) and pitching moment (nose up positive) are therefore zero and so, in essence, are the aerodynamic derivatives, namely $Z_z = M_z = 0$, where, for example, $Z_z = \partial Z/\partial z$ is the downwards force per heave displacement derivative. Likewise, there will be no net force in the elastic mode equations and so the corresponding elastic derivatives for heave displacement are $\boldsymbol{Q}_z = \partial \boldsymbol{Q}/\partial z = \mathbf{0}$.

19.6.2 Pitch Angle

Now consider the effect of the wing, and therefore all the panels, undergoing a pitch θ (nose up), effectively a rigid body pitch mode displacement. The resulting change of incidence vector will be given by

$$\boldsymbol{\alpha} = \left\{ 1\ 1\ \cdots\ 1 \right\}^{\mathrm{T}} \theta = \boldsymbol{e}\theta, \tag{19.45}$$

where $\boldsymbol{e}$ is a unit column vector. Therefore, from Equation (19.40), using the form where AICs are related to the panel incidence, the vector of lift forces on the panels will be given by

$$\boldsymbol{L} = \frac{\rho V^2}{2} \mathbf{AIC}_{\mathrm{R}} \boldsymbol{e}\theta. \tag{19.46}$$

The total heave force (positive downwards) on the wing will be given by the summation of the individual panel forces, so

$$Z = -\sum_{k=1}^{\mathrm{NP}} L_k = -\left\{ 1 \ 1 \ \cdots \ 1 \right\} \boldsymbol{L} = -\boldsymbol{e}^{\mathrm{T}}\boldsymbol{L} = -\frac{\rho V^2}{2}\boldsymbol{e}^{\mathrm{T}}\mathbf{AIC}_{\mathrm{R}}\boldsymbol{e}\theta. \tag{19.47}$$

Thus the *heave force per pitch angle derivative* $Z_\theta = \partial Z/\partial\theta$ will be given in terms of the AIC matrix by

$$Z_\theta = -\frac{\rho V^2}{2}\boldsymbol{e}^{\mathrm{T}}\mathbf{AIC}_{\mathrm{R}}\boldsymbol{e}. \tag{19.48}$$

Following a similar approach, the total pitching moment on the wing due to a nose up pitch angle is given by

$$M = \sum_{k=1}^{\mathrm{NP}} L_k x_k = \left\{ x_1 \ x_2 \ \cdots \ x_{\mathrm{NP}} \right\}^{\mathrm{T}} \boldsymbol{L} = \boldsymbol{x}^{\mathrm{T}}\boldsymbol{L} = \frac{\rho V^2}{2}\boldsymbol{x}^{\mathrm{T}}\mathbf{AIC}_{\mathrm{R}}\boldsymbol{e}\theta, \tag{19.49}$$

where x_k is the distance of the *k*th panel reference grid point forward of the axis, about which the pitching moment is being evaluated. The *pitching moment per pitch angle derivative* is then given by

$$M_\theta = \frac{\rho V^2}{2}\boldsymbol{x}^{\mathrm{T}}\mathbf{AIC}_{\mathrm{R}}\boldsymbol{e}. \tag{19.50}$$

For an elastic aircraft, the lift forces per panel due to the pitch angle introduce a modal force in the elastic mode. If there are M free–free elastic modes of vibration to be considered together with the rigid body heave and pitch modes, then the modal force vector $\boldsymbol{Q}$ due to the pitch angle is given by pre-multiplying the lift force vector by the transpose of the modal matrix defined at the panel grid points (i.e. $\boldsymbol{\Phi}$ is an $\mathrm{NP} \times M$ modal matrix), so

$$\boldsymbol{Q} = -\boldsymbol{\Phi}^{\mathrm{T}}\boldsymbol{L} = -\frac{\rho V^2}{2}\boldsymbol{\Phi}^{\mathrm{T}}\mathbf{AIC}_{\mathrm{R}}\boldsymbol{e}\theta. \tag{19.51}$$

Therefore the modal force per pitch angle derivative vector is given by

$$\boldsymbol{Q}_\theta = -\frac{\rho V^2}{2}\boldsymbol{\Phi}^{\mathrm{T}}\mathbf{AIC}_{\mathrm{R}}\boldsymbol{e}. \tag{19.52}$$

19.6.3 Flexible Mode Motion

The final case to consider is what net lift force, pitching moment and elastic modal force are generated when an elastic mode deformation $\boldsymbol{q}$ occurs. The corresponding derivatives will then be obtained. Firstly, the change in incidence for each panel due to a modal deformation will need to be found using the slope in the mode shape. Consider the *j*th mode and the *l*th panel. The corresponding change in incidence at that panel will be given by the modal slope multiplied by the modal coordinate, so

$$\alpha_{lj} = -\left.\frac{\partial\phi}{\partial x}\right|_{lj} q_j, \tag{19.53}$$

where the negative sign occurs because the mode shape is defined as positive downwards. The vector of all the changes of incidence due to modal displacements in all the modes will then be given by

$$\boldsymbol{\alpha} = -\boldsymbol{\Phi}_x\boldsymbol{q}, \tag{19.54}$$

where $\boldsymbol{\Phi}_x$ is the NP × M matrix of all the modal slopes at the panels. Using Equations (19.40) and (19.54), it can be seen that the vector of lift forces and net heave force due to the modal displacements are given by

$$\boldsymbol{L} = -\frac{\rho V^2}{2}\mathbf{AIC}_{\mathrm{R}}\boldsymbol{\Phi}_x\boldsymbol{q} \Rightarrow Z = -\boldsymbol{e}^{\mathrm{T}}\boldsymbol{L} = \frac{\rho V^2}{2}\boldsymbol{e}^{\mathrm{T}}\mathbf{AIC}_{\mathrm{R}}\boldsymbol{\Phi}_x\boldsymbol{q}. \tag{19.55}$$

Therefore the row vectors of heave force and pitching moment per elastic mode derivatives are given by

$$\boldsymbol{Z}_q = \frac{\rho V^2}{2}\boldsymbol{e}^{\mathrm{T}}\mathbf{AIC}_{\mathrm{R}}\boldsymbol{\Phi}_x \quad \text{and} \quad \boldsymbol{M}_q = -\frac{\rho V^2}{2}\boldsymbol{x}^{\mathrm{T}}\mathbf{AIC}_{\mathrm{R}}\boldsymbol{\Phi}_{\boldsymbol{x}}. \tag{19.56}$$

Finally, using Equation (19.55) and recognizing that the modal force vector is obtained by pre-multiplying the lift forces by the modal matrix, it may be seen that

$$\boldsymbol{Q} = -\boldsymbol{\Phi}^{\mathrm{T}}\boldsymbol{L} = \frac{\rho V^2}{2}\boldsymbol{\Phi}^{\mathrm{T}}\mathbf{AIC}_{\mathrm{R}}\boldsymbol{\Phi}_{\boldsymbol{x}}\boldsymbol{q}. \tag{19.57}$$

Thus the matrix of elastic modal force per modal displacement derivatives is given by

$$\mathbf{Q}_q = \frac{\rho V^2}{2}\boldsymbol{\Phi}^{\mathrm{T}}\mathbf{AIC}_{\mathrm{R}}\boldsymbol{\Phi}_{\boldsymbol{x}}. \tag{19.58}$$

19.6.4 Summary of Steady Aerodynamic Terms

The full set of steady aerodynamics may be expressed as a vector of aerodynamic forces, moments and elastic forces is given in terms of the AICs or the derivatives by

$$\left\{\begin{array}{c} Z \\ M \\ \hline \boldsymbol{Q} \end{array}\right\}_{\text{Steady}} = \frac{\rho V^2}{2}\left[\begin{array}{cc|c} 0 & -\boldsymbol{e}^{\mathrm{T}}\mathbf{AIC}_{\mathrm{R}}\boldsymbol{e} & \boldsymbol{e}^{\mathrm{T}}\mathbf{AIC}_{\mathrm{R}}\boldsymbol{\Phi}_x \\ 0 & \boldsymbol{x}^{\mathrm{T}}\mathbf{AIC}_{\mathrm{R}}\boldsymbol{e} & -\boldsymbol{x}^{\mathrm{T}}\mathbf{AIC}_{\mathrm{R}}\boldsymbol{\Phi}_x \\ \hline \mathbf{0} & \boldsymbol{\Phi}^{\mathrm{T}}\mathbf{AIC}_{\mathrm{R}}\boldsymbol{e} & \boldsymbol{\Phi}^{\mathrm{T}}\mathbf{AIC}_{\mathrm{R}}\boldsymbol{\Phi}_x \end{array}\right]\left\{\begin{array}{c} z \\ \theta \\ \hline \boldsymbol{q} \end{array}\right\} = \left[\begin{array}{cc|c} 0 & Z_\theta & \boldsymbol{Z}_q \\ 0 & M_\theta & \boldsymbol{M}_q \\ \hline \mathbf{0} & \boldsymbol{Q}_\theta & \boldsymbol{Q}_q \end{array}\right]\left\{\begin{array}{c} z \\ \theta \\ \hline \boldsymbol{q} \end{array}\right\}, \tag{19.59}$$

where the $\mathbf{AIC}_{\mathrm{R}}$ terms are at zero reduced frequency for this steady case. The similarity between this derivative matrix and the representation employed in the equilibrium manoeuvre model used earlier in Chapter 13 may be seen clearly, except that only a single mode was employed there and the aerodynamic terms were derived from integrations over strips as opposed to summations over panels. If the wing alone were considered, as in the earlier Chapter 11 on flutter, only the elastic generalized coordinates $\boldsymbol{q}$ would be included.

In practice, the AICs are not usually used to determine the aircraft rigid body aerodynamic derivatives, as these are obtained more accurately from other calculations with wind tunnel test adjustments. However, the AIC results may be used to assist in correcting the rigid aircraft derivatives for elastic effects and adjusting the lift and moment distributions over the span.

19.6.5 Unsteady Aerodynamics

In the analysis shown above, only the steady aerodynamics case was examined, with the AIC matrix being real. Once unsteady aerodynamics are considered, panel methods yield a complex AIC matrix that is reduced frequency dependent. The real part defines the in-phase aerodynamic component and would be in the same form as Equation (19.59), whereas the imaginary part, $\mathbf{AIC}_{\mathrm{I}}$, represents the quadrature component. It should be noted that during dynamic motion, there would be an effective incidence equal to the heave velocity component of any panel divided by the air speed; this means that there would no longer be a slope term $\boldsymbol{\Phi}_x$ in the matrix expressions for the quadrature aerodynamic force but instead the modal matrix $\boldsymbol{\Phi}$ would be used. Also the quadrature forces would be proportional to V not V^2.

The quadrature terms now take the form

$$\left\{\begin{array}{c}\mathbf{Z}\\ \mathbf{M}\\ \hline \boldsymbol{Q}\end{array}\right\}_{\substack{\text{Quad}\\ \text{Aero}}} = \mathrm{i}\omega\frac{\rho V}{2}\frac{b}{k}\left[\begin{array}{cc|c} -\boldsymbol{e}^{\mathrm{T}}\mathbf{AIC}_{\mathrm{I}}\boldsymbol{e} & \boldsymbol{e}^{\mathrm{T}}\mathbf{AIC}_{\mathrm{I}}\boldsymbol{x} & -\boldsymbol{e}^{\mathrm{T}}\mathbf{AIC}_{\mathrm{I}}\boldsymbol{\Phi}\\ \boldsymbol{x}^{\mathrm{T}}\mathbf{AIC}_{\mathrm{I}}\boldsymbol{e} & -\boldsymbol{x}^{\mathrm{T}}\mathbf{AIC}_{\mathrm{I}}\boldsymbol{x} & \boldsymbol{x}^{\mathrm{T}}\mathbf{AIC}_{\mathrm{I}}\boldsymbol{\Phi}\\ \hline -\boldsymbol{\Phi}^{\mathrm{T}}\mathbf{AIC}_{\mathrm{I}}\boldsymbol{e} & \boldsymbol{\Phi}^{\mathrm{T}}\mathbf{AIC}_{\mathrm{I}}\boldsymbol{x} & -\boldsymbol{\Phi}^{\mathrm{T}}\mathbf{AIC}_{\mathrm{I}}\boldsymbol{\Phi}\end{array}\right]\left\{\begin{array}{c}z\\ \theta\\ \hline \boldsymbol{q}\end{array}\right\} = \mathrm{i}\omega\left[\begin{array}{cc|c} Z_{\dot{z}} & Z_{\dot{\theta}} & \mathbf{Z}_{\dot{q}}\\ M_{\dot{z}} & M_{\dot{\theta}} & \mathbf{M}_{\dot{q}}\\ \hline \boldsymbol{Q}_{\dot{z}} & \boldsymbol{Q}_{\dot{\theta}} & \mathbf{Q}_{\dot{q}}\end{array}\right]\left\{\begin{array}{c}z\\ \theta\\ \hline \boldsymbol{q}\end{array}\right\}, \tag{19.60}$$

where $\mathbf{AIC}_{\mathrm{I}}$ is the quadrature/imaginary part of the AIC matrix. Note that there would be rate-dependent derivatives, all of which are nominally nonzero. The total aerodynamic terms for a particular reduced frequency are the sum of the expressions in Equations (19.59) and (19.60).

19.6.6 Gust-Dependent Terms

All the above analysis has been derived for response-dependent aerodynamic terms. However, for flight through gusts and turbulence, the aerodynamic forces due to gust velocity need to be evaluated. The panel methods allow these terms to be obtained, with gust penetration lags present in the frequency domain analysis to allow for the spatial separation of panels on different parts of the wing, and also on the tailplane (Hoblit, 1988).

19.7 EXAMPLES

1. For a two-dimensional aerofoil, develop programs to determine the lift and pitching moment about the mid-chord for distributions of vortices, sources and sinks, and doublets. Investigate the effect of increasing the number of aerodynamic elements included along the chord.
2. Determine the resultant downwash at the three-quarter chord control point of a vortex ring with each side of the ring having the same strength of vortex.
3. Develop programs to determine the steady lift distribution for a three-dimensional wing with either horseshoe vortices or vortex rings. Investigate the effect of increasing the number of aerodynamic panels in both the spanwise and chordwise directions.

20

Coupling of Structural and Aerodynamic Computational Models

The majority of the book so far has shown how aeroelastic and loads models can be developed using continuous approximation models of the structure and aerodynamics. Such an approach is fine for a simplistic aircraft representation; however, real-life structures are non-uniform and consequently are impossible to model accurately using approaches such as the Rayleigh-Ritz method. Instead, industry makes use of discrete approximation methods, such as finite elements (see Chapters 4 and 22), to produce detailed models of the aircraft structure. Similarly, numerical 3D panel methods, such as the vortex or doublet lattice methods (see Chapters 19 and 22), are often used to represent the aerodynamic forces acting on the aircraft. Although more sophisticated computational fluid dynamics (CFD) methods have been developed and used, for example, in performing accurate drag calculations and analysis in the transonic flight regime, the vast majority of the aeroelastic and loads analyses carried out in industry for commercial aircraft are performed using 3D panel methods (sometimes the panel methods are used to correct the rigid aircraft aerodynamics for flexible effects). Such an approach enables the structure and the aerodynamic models to be combined in a very efficient manner so that the static/dynamic aeroelastic and loads behaviour can be determined.

This chapter shows how potential flow aerodynamics can be combined with a structural model to produce static and dynamic aeroelastic (or loads) models. A 2D rigid aerofoil in pitch and heave/pitch is modelled using two vortex elements. Also, a simple 3D built-in wing structure is modelled using only two beam finite elements and four aerodynamic panels in order to illustrate the process of generating a coupled model for both static and dynamic aeroelastic analyses. Finally, the development of a state-space aeroelastic model using a rational fraction approximation to the reduced frequency dependent aerodynamics is described.

20.1 MATHEMATICAL MODELLING – STATIC AEROELASTIC CASE

Before considering simple examples, a general form of the static analysis will be presented for the coupling of 3D panel and finite element representations. The static deflection behaviour of a finite element model relates the displacement vector $\boldsymbol{r}$ to the force vector $\boldsymbol{R}$ via the overall stiffness matrix $\mathbf{K}$ (see Chapter 4), such that

$$\boldsymbol{R} = \mathbf{K}\boldsymbol{r} \tag{20.1}$$

From Chapter 19, in the general case where varying sized panels are used, the aerodynamic panel methods lead to a vector of lift forces, distributed along the quarter chord of each panel, of

$$\boldsymbol{L} = \rho V \mathbf{S}\boldsymbol{\Gamma} \tag{20.2}$$

Introduction to Aircraft Aeroelasticity and Loads J. R. Wright and J. E. Cooper

© 2007 John Wiley & Sons, Ltd

where **S** is the diagonal matrix whose elements are the spans for each panel. The elements of vector $\mathbf{\Gamma}$ are the strengths of the vortices acting on each panel, determined from the zero normal flow boundary condition

$$\mathbf{\Psi\Gamma} = -V\left(\boldsymbol{\theta} + \boldsymbol{\theta}_0\right) \tag{20.3}$$

where Ψ is the matrix of Influence Coefficients, V is the free-stream air speed, $\boldsymbol{\theta}$ is the vector of angles of incidence for each panel due to elastic twist (assuming small angles) and $\boldsymbol{\theta_0}$ is the vector of initial angles of incidence of each panel. The initial angle of incidence allows the wing twist to be determined (see Chapter 8).

The aerodynamic terms depend solely upon the incidence of each panel relative to the free-stream, whereas deflection and initial (wind off) vectors $\boldsymbol{r}$ and $\boldsymbol{r}_0$ for the structure contain translation and rotation terms in all degrees of freedom (DoF). In order to make the two models compatible, equation (20.3) can be rewritten as

$$\mathbf{\Psi\Gamma} = -V\mathbf{T_1}\left(\boldsymbol{r} + \boldsymbol{r_0}\right) \tag{20.4}$$

where the transformation matrix $\mathbf{T_1}$ relates the angles of incidence of each panel to the structural displacements and rotations and so allows a full set of structural DoFs to be included in the equations.

The aerodynamic forces on the panels cause an equivalent set of applied forces and moments to act at the FE model nodes and are a function of the vortex strengths

$$\boldsymbol{R} = \rho V\mathbf{T_2}\mathbf{S}\Gamma \tag{20.5}$$

where $\mathbf{T_2}$ is another transformation matrix that maps forces between the aerodynamic and the structural models. In practice, it is usual for the fluid and structure meshes to be different in terms of density, orientation and node position; consequently the mappings of the panel deflections to the structural displacements and of the fluid forces to the structural grid are not straightforward and must be achieved via some form of interpolation.

Combining equations (20.1), (20.4) and (20.5) gives

$$\mathbf{K}\boldsymbol{r} = \boldsymbol{R} = \rho V\mathbf{T_2}\mathbf{S}\Gamma = -\rho V^2\mathbf{T_2}\mathbf{S}\Psi^{-\mathbf{1}}\mathbf{T}_1\left(\boldsymbol{r}+\boldsymbol{r_0}\right) = \frac{\rho V^2}{2}\mathbf{AIC}\left(\boldsymbol{r}+\boldsymbol{r_0}\right) \tag{20.6}$$

where the aerodynamic influence coefficient matrix **AIC** is defined in Chapter 19 and relates the forces to the deflections such that

$$\mathbf{AIC} = -2\mathbf{T_2}\mathbf{S}\Psi^{-\mathbf{1}}\mathbf{T_1} \tag{20.7}$$

Thus, equation (20.6) becomes

$$\left(\rho V^2\mathbf{T_2}\mathbf{S}\Psi^{-\mathbf{1}}\mathbf{T}_1 + \mathbf{K}\right)\boldsymbol{r} + \rho V^2\mathbf{T_2}\mathbf{S}\Psi^{-\mathbf{1}}\mathbf{T_1}\boldsymbol{r_0} = 0$$

or (20.8)

$$\left(\frac{\rho V^2}{2}\mathbf{AIC} + \mathbf{K}\right)\boldsymbol{r} + \frac{\rho V^2}{2}\mathbf{AIC}\boldsymbol{r_0} = 0$$

which is in the form of the classic static aeroelastic equations

$$\rho V^2\mathbf{C}\left(\boldsymbol{r} + \boldsymbol{r_0}\right) + \mathbf{Er} = \mathbf{0} \tag{20.9}$$

Solution of these equations leads to the aeroelastic deflections **r** from which the vortex strengths can be calculated using equation (20.4). Then the lift and induced drag can be calculated. The divergence

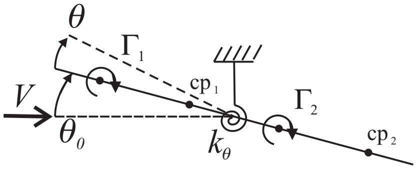

Figure 20.1 Two element wing with torsional spring.

speed can also be determined from equation (20.9), as in Chapter 11, by solving the determinant $\left|\rho V^2\mathbf{C}+\mathbf{E}\right|=0$.

20.2 2D COUPLED STATIC AEROELASTIC MODEL – PITCH

Consider the 2D symmetric aerofoil of chord c, modelled aerodynamically using a 2 element vortex with unknown vortex strengths $\Gamma_{1,2}$ shown in Figure 20.1; the aerofoil rotates on a torsional spring of stiffness k_θ at the mid-chord. The total incidence is the sum of the initial angle θ_0 and the elastic twist θ.

The vortex strengths are calculated from the zero normal flow boundary condition at the control points using the influence coefficient matrix but now the unknown elastic twist θ must be included so (for small angles)

$$\begin{bmatrix} -\dfrac{2}{c\pi} & \dfrac{2}{c\pi} \\ -\dfrac{2}{3c\pi} & -\dfrac{2}{c\pi} \end{bmatrix}\begin{Bmatrix}\Gamma_1\\ \Gamma_2\end{Bmatrix} = -V\begin{Bmatrix}\theta_0+\theta\\ \theta_0+\theta\end{Bmatrix} \quad\Rightarrow\quad \begin{Bmatrix}\Gamma_1\\ \Gamma_2\end{Bmatrix} = \begin{Bmatrix}\dfrac{3}{4}\\ \dfrac{1}{4}\end{Bmatrix}\pi c V\left(\theta_0+\theta\right) \tag{20.10}$$

The aerodynamic moment is balanced by the structural restoring moment so

$$M=\rho V\Gamma_1\frac{3c}{8}-\rho V\Gamma_2\frac{c}{8}=\begin{Bmatrix}\dfrac{3c\rho V}{8} & -\dfrac{c\rho V}{8}\end{Bmatrix}\begin{Bmatrix}\Gamma_1\\ \Gamma_2\end{Bmatrix}=k_\theta\theta \tag{20.11}$$

Combining equations (20.10) and (20.11) leads to

$$\begin{Bmatrix}\dfrac{3c\rho V}{8} & -\dfrac{c\rho V}{8}\end{Bmatrix}\begin{Bmatrix}\dfrac{3}{4}\\ \dfrac{1}{4}\end{Bmatrix}\pi c V\left(\theta_0+\theta\right)=k_\theta\theta \quad\Rightarrow\quad \left(k_\theta-\frac{\rho V^2\pi c^2}{4}\right)\theta=\frac{\rho V^2\pi c^2}{4}\theta_0 \tag{20.12}$$

and thus the elastic angle of twist can be expressed in terms of the initial incidence as

$$\theta=\frac{\rho V^2\pi c^2}{\left(4k_\theta-\rho V^2\pi c^2\right)}\theta_0 \tag{20.13}$$

The vortex strengths may then be determined from equation (20.10), hence the lift and pitching moment. The divergence speed occurs when the twist becomes infinite and so is given by

$$V_{\text{div}}=\frac{2}{c}\sqrt{\frac{k_\theta}{\rho\pi}} \tag{20.14}$$

which is exactly the same result as found using strip theory.

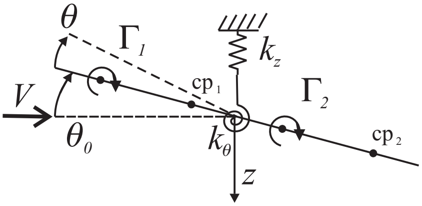

Figure 20.2 Two Element Wing with Heave and Torsional Springs

20.3 2D COUPLED STATIC AEROELASTIC MODEL – HEAVE/PITCH

Consider the same model as above, but a spring of stiffness k_z per unit span in the heave direction (z positive downwards) is also included, as seen in Figure 20.2. The total lift from both vortex elements is

$$L = -(\rho V \Gamma_1 + \rho V \Gamma_2) = -\rho V \{1 \quad 1\} \begin{Bmatrix} \Gamma_1 \\ \Gamma_2 \end{Bmatrix} \tag{20.15}$$

The pitching moment about the mid-chord is given as before in equation (20.11) and the vortex strengths are found from the zero normal flow boundary condition in equation (20.10).

The lift and pitching moment are related to the structural deflections via the stiffness matrix so

$$\begin{Bmatrix} L \\ M \end{Bmatrix} = \begin{bmatrix} k_z & 0 \\ 0 & k_\theta \end{bmatrix} \begin{Bmatrix} z \\ \theta \end{Bmatrix} \tag{20.16}$$

Combining equations (20.10), (20.11) and (20.15) into (20.16) gives the equivalent of equation (20.9), namely

$$\begin{bmatrix} -\rho V & -\rho V \\ \dfrac{3\rho V c}{8} & -\dfrac{\rho V c}{8} \end{bmatrix} \begin{Bmatrix} \Gamma_1 \\ \Gamma_2 \end{Bmatrix} = \begin{bmatrix} -\rho V & -\rho V \\ \dfrac{3\rho V c}{8} & -\dfrac{\rho V c}{8} \end{bmatrix} \begin{Bmatrix} \dfrac{3\pi c V}{4} \\ \dfrac{\pi c V}{4} \end{Bmatrix} (\theta_0 + \theta) = \begin{bmatrix} k_z & 0 \\ 0 & k_\theta \end{bmatrix} \begin{Bmatrix} z \\ \theta \end{Bmatrix} \tag{20.17}$$

which after some rearranging leads to

$$\begin{bmatrix} k_z & \pi \rho c V^2 \\ 0 & \left(k_\theta - \dfrac{\pi \rho c^2 V^2}{4}\right) \end{bmatrix} \begin{Bmatrix} z \\ \theta \end{Bmatrix} = \rho V^2 \begin{Bmatrix} -\pi c \\ \dfrac{\pi c^2}{4} \end{Bmatrix} \theta_0 \tag{20.18}$$

This is in the classical static aeroelastic form of equations. The elastic heave and torsional deflections are then found as

$$\begin{Bmatrix} z \\ \theta \end{Bmatrix} = \begin{Bmatrix} -\dfrac{4k_\theta p}{k_z(4k_\theta - cp)} \\ \dfrac{cp}{(k_\theta - cp)} \end{Bmatrix} \theta_0 \tag{20.19}$$

where $p = \pi \rho c V^2$. The same results for lift and pitching moment are found as for strip theory.

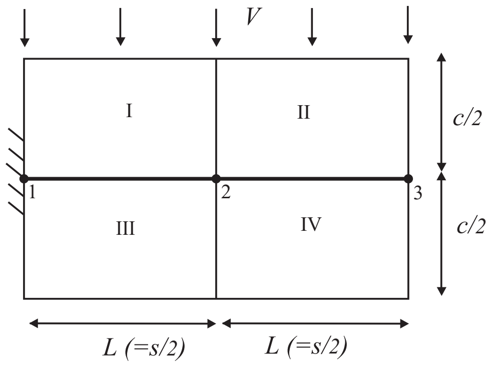

Figure 20.3 Wing represented by Two Beam Elements with Four Aerodynamic Panels.

20.4 3D COUPLED STATIC AEROELASTIC MODEL

In this example, the coupling of panel method aerodynamics with an FE model is considered. The cantilevered wing model in Figure 20.3 has chord c and semi-span $s = 2L$. It consists of two beam elements of length L along the mid-chord to allow for bending and torsion, and four aerodynamic panels whose AICs can be defined from a distribution of vortex elements (see Chapter 19). This model is rather idealised but is employed to illustrate some ideas involved in the solution process. Note that in practice many more finite elements and panels, both chordwise and spanwise, have to be used in order to achieve accurate results.

20.4.1 Structural Model

Consider the general 2-node beam bending/torsional element (see Chapter 4) shown in Figure 20.4. At each node, a vertical deflection z, bending rotation θ and twist ϕ are shown, with corresponding normal force F, moment M and torque T. The element stiffness matrix, for coordinates in the order (z_1, θ_1, ϕ_1, z_2, θ_2, ϕ_2), is

$$\boldsymbol{k} = \begin{bmatrix} 12\frac{EI}{L^3} & 6\frac{EI}{L^2} & 0 & -12\frac{EI}{L^3} & 6\frac{EI}{L^2} & 0 \\ 6\frac{EI}{L^2} & 4\frac{EI}{L} & 0 & -6\frac{EI}{L^2} & 2\frac{EI}{L} & 0 \\ 0 & 0 & \frac{GJ}{L} & 0 & 0 & -\frac{GJ}{L} \\ -12\frac{EI}{L^3} & -6\frac{EI}{L^2} & 0 & 12\frac{EI}{L^3} & -6\frac{EI}{L^2} & 0 \\ 6\frac{EI}{L^2} & 2\frac{EI}{L} & 0 & -6\frac{EI}{L^2} & 4\frac{EI}{L} & 0 \\ 0 & 0 & -\frac{GJ}{L} & 0 & 0 & \frac{GJ}{L} \end{bmatrix} \tag{20.20}$$

Remembering to partition out the terms relating to the nodal degrees of freedom at the wing root (see Chapter 4), the overall system of equations for the two elements may then be shown to be

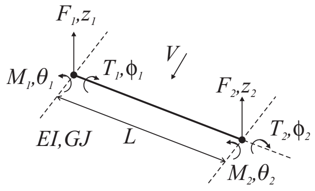

Figure 20.4 2 Node Beam Element.

$$\mathbf{R} = \begin{Bmatrix} F_2 \\ M_2 \\ T_2 \\ F_3 \\ M_3 \\ T_3 \end{Bmatrix} = \begin{bmatrix} 24\dfrac{EI}{L^3} & 0 & 0 & -12\dfrac{EI}{L^3} & 6\dfrac{EI}{L^2} & 0 \\ 0 & 8\dfrac{EI}{L} & 0 & -6\dfrac{EI}{L^2} & 2\dfrac{EI}{L} & 0 \\ 0 & 0 & 2\dfrac{GJ}{L} & 0 & 0 & -\dfrac{GJ}{L} \\ -12\dfrac{EI}{L^3} & -6\dfrac{EI}{L^2} & 0 & 12\dfrac{EI}{L^3} & -6\dfrac{EI}{L^2} & 0 \\ 6\dfrac{EI}{L^2} & 2\dfrac{EI}{L} & 0 & -6\dfrac{EI}{L^2} & 4\dfrac{EI}{L} & 0 \\ 0 & 0 & -\dfrac{GJ}{L} & 0 & 0 & \dfrac{GJ}{L} \end{bmatrix} \begin{Bmatrix} z_2 \\ \theta_2 \\ \phi_2 \\ z_3 \\ \theta_3 \\ \phi_3 \end{Bmatrix} = \mathbf{K}\,\mathbf{r} \tag{20.21}$$

and the notation needs to be converted later from L for the element to s for the wing, using $L = {}^{s}\!/_{2}$.

20.4.2 Aerodynamic Model

The vortex strengths $\Gamma_{\text{I,II,II,IV}}$ may be found from the rearrangement of equation (20.3) for this example, namely

$$\boldsymbol{\Psi} \begin{Bmatrix} \Gamma_{\text{I}} \\ \Gamma_{\text{II}} \\ \Gamma_{\text{III}} \\ \Gamma_{\text{IV}} \end{Bmatrix} = -V \begin{Bmatrix} \alpha_{\text{I}} + \alpha_{0\text{I}} \\ \alpha_{\text{II}} + \alpha_{0\text{II}} \\ \alpha_{\text{III}} + \alpha_{0\text{III}} \\ \alpha_{\text{IV}} + \alpha_{0\text{IV}} \end{Bmatrix} \tag{20.22}$$

where $\boldsymbol{\Psi}$ is the (4×4) influence coefficient matrix determined using the approach described in Chapter 19. The α and α_0 terms are the angles of incidence of each panel due to elastic and initial deflections respectively.

The total angle of incidence depends upon the twist of the beam ϕ which is defined at each node. Therefore, for convenience, take the angle of incidence of each panel to be the average twist between the nodes at each end of the beam that they are attached to. Since there is no chordwise bending of the wing, the angles are equal for the front and rear panels at each spanwise location. Also, the FE model twist is defined as positive nose down so there will be a negative sign present in the relationship between twist and incidence. Thus

$$\alpha_{\text{I}} + \alpha_{0\text{I}} = \alpha_{\text{III}} + \alpha_{0\text{III}} = -\frac{\phi_1 + \phi_{10} + \phi_2 + \phi_{20}}{2} \quad \text{and} \quad \alpha_{\text{II}} + \alpha_{0\text{II}} = \alpha_{\text{IV}} + \alpha_{0\text{IV}} = -\frac{\phi_2 + \phi_{20} + \phi_3 + \phi_{30}}{2} \tag{20.23}$$

Since the wing has a fixed root boundary condition and the FE equations have been partitioned, then the twist at node 1 must be removed from equation (20.23). Obviously the elastic twist at the root is zero, but it will be assumed for simplicity that the initial incidence at the root is also zero. Thus, equation (20.22) becomes

$$\boldsymbol{\Gamma}=\begin{Bmatrix}\Gamma_{\mathrm{I}}\\ \Gamma_{\mathrm{II}}\\ \Gamma_{\mathrm{III}}\\ \Gamma_{\mathrm{IV}}\end{Bmatrix}=-V\boldsymbol{\Psi}^{-1}\begin{bmatrix}0&0&-\dfrac{1}{2}&0&0&0\\ 0&0&-\dfrac{1}{2}&0&0&-\dfrac{1}{2}\\ 0&0&-\dfrac{1}{2}&0&0&0\\ 0&0&-\dfrac{1}{2}&0&0&-\dfrac{1}{2}\end{bmatrix}\left\{\begin{Bmatrix}z_2\\ \theta_2\\ \phi_2\\ z_3\\ \theta_3\\ \phi_3\end{Bmatrix}+\begin{Bmatrix}z_{20}\\ \theta_{20}\\ \phi_{20}\\ z_{30}\\ \theta_{30}\\ \phi_{30}\end{Bmatrix}\right\}=-V\Psi^{-1}\mathbf{T_1}(\boldsymbol{r}+\boldsymbol{r}_0) \tag{20.24}$$

where $\mathbf{T_1}$ is the transformation matrix. Again, in practice, the transformation between the FE displacements and the panel deflections will be much more complicated and is likely to require an interpolation process.

20.4.3 Transformation of Aerodynamic Forces to Structural Model

From equation (20.2), since each panel has the same span $^{s}/_{2}$, the vector of lift forces on each panel is

$$\boldsymbol{L}=\begin{Bmatrix}L_{\mathrm{I}}\\ L_{\mathrm{II}}\\ L_{\mathrm{III}}\\ L_{\mathrm{IV}}\end{Bmatrix}=\rho V\begin{bmatrix}\dfrac{s}{2}&0&0&0\\ 0&\dfrac{s}{2}&0&0\\ 0&0&\dfrac{s}{2}&0\\ 0&0&0&\dfrac{s}{2}\end{bmatrix}\begin{Bmatrix}\Gamma_{\mathrm{I}}\\ \Gamma_{\mathrm{II}}\\ \Gamma_{\mathrm{III}}\\ \Gamma_{\mathrm{IV}}\end{Bmatrix}=\rho V\mathbf{S}\Gamma \tag{20.25}$$

The equivalent forces and moments acting at the element nodes, as shown in Figure 20.5, may be determined based on the idea of kinematically equivalent nodal forces (see Chapter 4). This is a transformation of distributed aerodynamic forces (acting along the ¼ chord of the panels) onto the structural model. It can be shown that the equivalent of equation (20.5) is

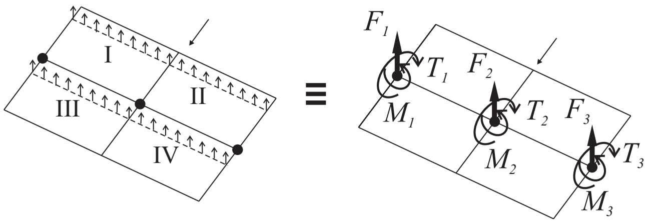

Figure 20.5 Equivalent forces and moments at the beam nodes.

$$\boldsymbol{R} = \begin{Bmatrix} F_2 \\ M_2 \\ T_2 \\ F_3 \\ M_3 \\ T_3 \end{Bmatrix} = \rho V \begin{bmatrix} \frac{1}{2} & \frac{1}{2} & \frac{1}{2} & \frac{1}{2} \\ -\frac{s}{24} & \frac{s}{24} & -\frac{s}{24} & \frac{s}{24} \\ -\frac{3c}{16} & -\frac{3c}{16} & \frac{c}{16} & \frac{c}{16} \\ 0 & \frac{1}{2} & 0 & \frac{1}{2} \\ 0 & -\frac{s}{24} & 0 & -\frac{s}{24} \\ 0 & -\frac{3c}{16} & 0 & \frac{c}{16} \end{bmatrix} \begin{bmatrix} \frac{s}{2} & 0 & 0 & 0 \\ 0 & \frac{s}{2} & 0 & 0 \\ 0 & 0 & \frac{s}{2} & 0 \\ 0 & 0 & 0 & \frac{s}{2} \end{bmatrix} \begin{Bmatrix} \Gamma_{\mathrm{I}} \\ \Gamma_{\mathrm{II}} \\ \Gamma_{\mathrm{III}} \\ \Gamma_{\mathrm{IV}} \end{Bmatrix} = \rho V \mathbf{T_2} \mathbf{S} \Gamma \tag{20.26}$$

where $\mathbf{T_2}$ is the relevant transformation matrix.

20.4.4 Assembly of Aeroelastic Model

All the equations may now be combined to generate a coupled aeroelastic system in the form of equation (20.6)

$$\begin{bmatrix} 192\frac{EI}{s^3} & 0 & 0 & -96\frac{EI}{s^3} & 24\frac{EI}{s^2} & 0 \\ 0 & 16\frac{EI}{s} & 0 & -24\frac{EI}{s^2} & 4\frac{EI}{s} & 0 \\ 0 & 0 & 4\frac{GJ}{s} & 0 & 0 & -2\frac{GJ}{s} \\ -96\frac{EI}{s^3} & -24\frac{EI}{s^2} & 0 & 96\frac{EI}{s^3} & -24\frac{EI}{s^2} & 0 \\ 24\frac{EI}{s^2} & 4\frac{EI}{s} & 0 & -24\frac{EI}{s^2} & 8\frac{EI}{s} & 0 \\ 0 & 0 & -2\frac{GJ}{s} & 0 & 0 & 2\frac{GJ}{s} \end{bmatrix} \begin{Bmatrix} w_2 \\ \theta_2 \\ \phi_2 \\ w_3 \\ \theta_3 \\ \phi_3 \end{Bmatrix} =$$

$$-\rho V^2 \begin{bmatrix} \frac{1}{2} & \frac{1}{2} & \frac{1}{2} & \frac{1}{2} \\ -\frac{s}{24} & \frac{s}{24} & -\frac{s}{24} & \frac{s}{24} \\ -\frac{3c}{16} & -\frac{3c}{16} & \frac{c}{16} & \frac{c}{16} \\ 0 & \frac{1}{2} & 0 & \frac{1}{2} \\ 0 & -\frac{s}{24} & 0 & -\frac{s}{24} \\ 0 & -\frac{3c}{16} & 0 & \frac{c}{16} \end{bmatrix} \mathbf{S}\mathbf{\Psi}^{-1} \begin{bmatrix} 0 & 0 & -\frac{1}{2} & 0 & 0 & 0 \\ 0 & 0 & -\frac{1}{2} & 0 & 0 & -\frac{1}{2} \\ 0 & 0 & -\frac{1}{2} & 0 & 0 & 0 \\ 0 & 0 & -\frac{1}{2} & 0 & 0 & -\frac{1}{2} \end{bmatrix} \left\{ \begin{Bmatrix} w_2 \\ \theta_2 \\ \phi_2 \\ w_3 \\ \theta_3 \\ \phi_3 \end{Bmatrix} + \begin{Bmatrix} w_{20} \\ \theta_{20} \\ \phi_{20} \\ w_{30} \\ \theta_{30} \\ \phi_{30} \end{Bmatrix} \right\} \tag{20.27}$$

The static deflections can be calculated from these equations as a function of the initial deformation. A similar approach is taken when more elements and aerodynamic panels are used and also when the control points of the aerodynamic model and nodes of the structural model do not coincide. However, the interpolation process between the grids for displacements and aerodynamic forces will be far more involved.

20.5 MATHEMATICAL MODELLING – DYNAMIC AEROELASTIC RESPONSE

When the dynamic case is considered, the FE model relates the displacement and acceleration vectors to the force vector $\boldsymbol{R}$ via the mass and stiffness matrices (ignoring structural damping) such that

$$\boldsymbol{R} = \mathbf{M}\ddot{\boldsymbol{r}} + \mathbf{K}\boldsymbol{r} \tag{20.28}$$

For some defined harmonic oscillation at frequency ω (and by implication reduced frequency k), the vectors of forces acting at the quarter chord of each panel is defined in terms of the influence coefficients (usually derived from the doublet lattice method for the dynamic case) such that

$$\boldsymbol{\Psi}\Gamma = -V\mathbf{T}_1\boldsymbol{r} \tag{20.29}$$

where matrix $\boldsymbol{\Psi}$ and the vector of circulation $\boldsymbol{\Gamma}$ are now complex as mentioned in Chapter 19. In this case the flow boundary condition is expressed in terms of the structural displacements and a transformation matrix $\mathbf{T_1}$ as before. The initial deformed shape $\boldsymbol{r}_0$ is not included here since only the flutter solution is sought.

The lift forces on the aerodynamic panels are related to equivalent forces and moments acting at the FE model nodes as before via

$$\boldsymbol{R} = \rho V\mathbf{T}_2\mathbf{S}\boldsymbol{\Gamma} \tag{20.30}$$

Combining equations (20.28) to (20.30) gives

$$\mathbf{M}\ddot{\boldsymbol{r}} + \mathbf{K}\boldsymbol{r} = \boldsymbol{R} = \frac{\rho V^2}{2}\mathbf{AIC}\boldsymbol{r} \tag{20.31}$$

where the AIC matrix is now complex and a function of reduced frequency $k = \omega b/V$. Equation (20.31) can be written in terms of the real and imaginary parts of the AIC matrix (see Chapter 19) as

$$\mathbf{M}\ddot{\boldsymbol{r}} + \mathrm{K}\boldsymbol{r} = \frac{\rho V}{2}\frac{b}{k}\mathbf{AIC_I}\dot{\boldsymbol{r}} + \frac{\rho V^2}{2}\mathbf{AIC_R}\boldsymbol{r} \tag{20.32}$$

This equation can be transformed into modal coordinates $\boldsymbol{q}$ if required (see Chapter 2) via the modal matrix $\boldsymbol{\Phi}$. Then using $\boldsymbol{r} = \boldsymbol{\Phi}\boldsymbol{q}$ and pre-multiplying by $\boldsymbol{\Phi}^{\mathrm{T}}$ yields

$$\mathbf{M_q}\ddot{\boldsymbol{q}} + \mathbf{K_q}\boldsymbol{q} = \frac{\rho V}{2}\frac{b}{k}\boldsymbol{\Phi}^{\mathrm{T}}\mathbf{AIC_I}\boldsymbol{\Phi}\dot{\boldsymbol{q}} + \frac{\rho V^2}{2}\boldsymbol{\Phi}^{\mathrm{T}}\mathbf{AIC_R}\boldsymbol{\Phi}\boldsymbol{q} \tag{20.33}$$

Note that the equations do not apply in this form for quasi-steady motion (zero reduced frequency), so the apparent singularity as $k \to 0$ does not occur. Inspection of equation (20.33) shows that it is in the form of the classic aeroelastic equation with reduced frequency dependent aerodynamic terms

$$\mathbf{A}\ddot{\boldsymbol{q}} + \rho V\mathbf{B}\dot{\boldsymbol{q}} + \left(\rho V^2\mathbf{C} + \mathbf{E}\right)\boldsymbol{q} = \mathbf{0} \tag{20.34}$$

which is sometimes written in the form

$$\boldsymbol{A}\ddot{\boldsymbol{q}} + \boldsymbol{E}\boldsymbol{q} = \frac{\rho V^2}{2}\boldsymbol{Q}\boldsymbol{q} \tag{20.35}$$

where complex matrix **Q** contains the reduced frequency dependent terms, and frequency matching methods discussed in Chapter 11, such as the ‘p-k’ method, must be used.

20.6 2D COUPLED DYNAMIC AEROELASTIC MODEL – BENDING/TORSION

Consider the same aeroelastic 2D aerofoil model as in Section 20.2 but now with numerical values used and taking dynamic effects into account. Then the equations of motion become

$$\begin{bmatrix} M & 0 \\ 0 & I_G \end{bmatrix} \begin{Bmatrix} \ddot{z} \\ \ddot{\theta} \end{Bmatrix} + \begin{bmatrix} k_z & 0 \\ 0 & k_\theta \end{bmatrix} \begin{Bmatrix} z \\ \theta \end{Bmatrix} = \frac{\rho V}{2}\frac{b}{k}\mathrm{AIC}_I \begin{Bmatrix} \dot{z} \\ \dot{\theta} \end{Bmatrix} + \frac{\rho V^2}{2}\mathrm{AIC}_R \begin{Bmatrix} z \\ \theta \end{Bmatrix} \tag{20.36}$$

where M and I_G are the mass and pitch moment of inertia of the aerofoil per unit span. For this example, use numerical values and take the modal mass and stiffness matrices as $\mathbf{M_q} = \mathrm{diag}[1 \quad 1]$, $\mathbf{K_q} = \mathrm{diag}[852 \quad 33070]$. The mode shapes are heave and pitch respectively, with (undamped) natural frequencies of 4.65 and 28.95 Hz.

The 4 AIC values are complex and were calculated in modal format using the doublet lattice method from a well known commercial code. The AICs are dependent upon the reduced frequency and are shown

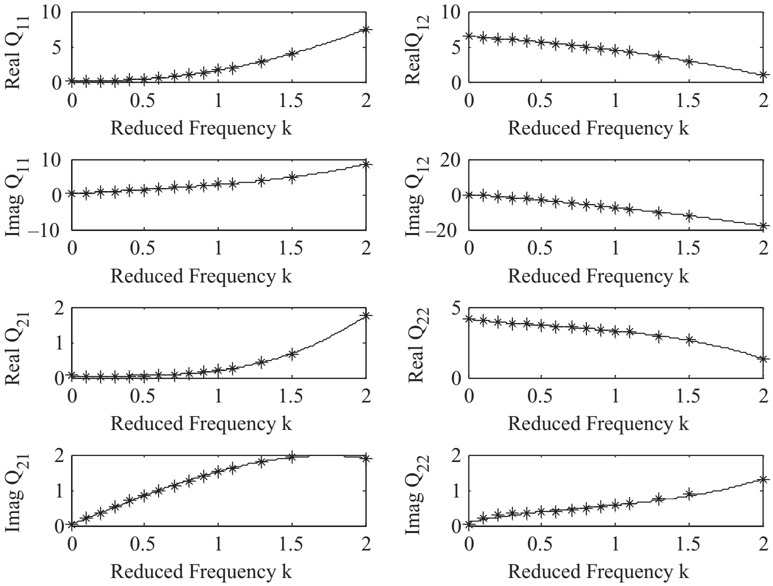

Figure 20.6 Modal AICs for the 2D aerofoil example.

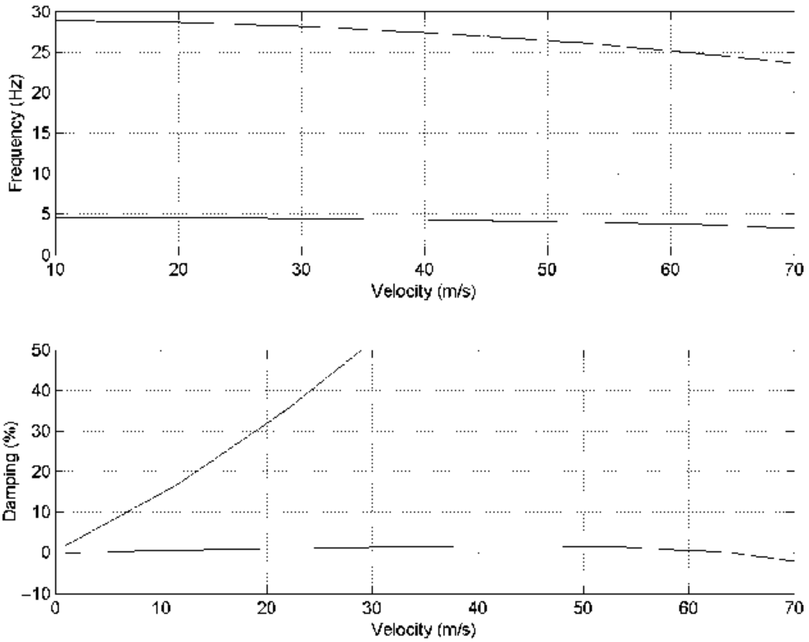

Figure 20.7 Frequency and Damping Ratio Trends for the 2D Aerofoil Example.

in Figure 20.6. The points on each plot indicate the values at which the AICs are explicitly calculated; other intermediate values required when performing a 'p-k' flutter solution may be found by interpolation.

Performing a flutter analysis using the 'p-k' method as described in Chapter 11, then $V\omega$ and Vg trends are shown in Figure 20.7. Flutter occurs at 64.1 m/s, the same answer as given when applying the commercial code. The trends are very sensitive to the values of the AICs and care should be taken when interpolating between the defined reduced frequency values.

20.7 3D FLUTTER ANALYSIS

The same procedure as described above can be performed for a 3D wing or full aircraft. As an example, an analysis was performed on the wing whose FE model is shown in Figure 20.8 and aerodynamic panels shown in Figure 20.9 as part of a study (Taylor et al., 2006) to compare the flutter boundary predictions between potential flow aerodynamics (doublet lattice) and Euler and Navier-Stokes CFD methods.

The resulting frequency and damping ratio trends from a 'p-k' analysis, using AIC matrices for unsteady aerodynamics obtained using the doublet lattice method, are shown in Figure 20.10. This is much more complicated to interpret than the two DoF flutter results as there are many more modes; however, it can be seen that flutter occurs at 332 m/s. Note that the damping results are plotted using the convention that positive damping is unstable (see Chapter 11).

In practice, this analysis would be applied to the whole aircraft model including rigid body modes, as described in Chapter B04, thus enabling the response to flight/ground manoeuvres, gust/turbulence encounters and control inputs as well as static aeroelastic deflections to be obtained.

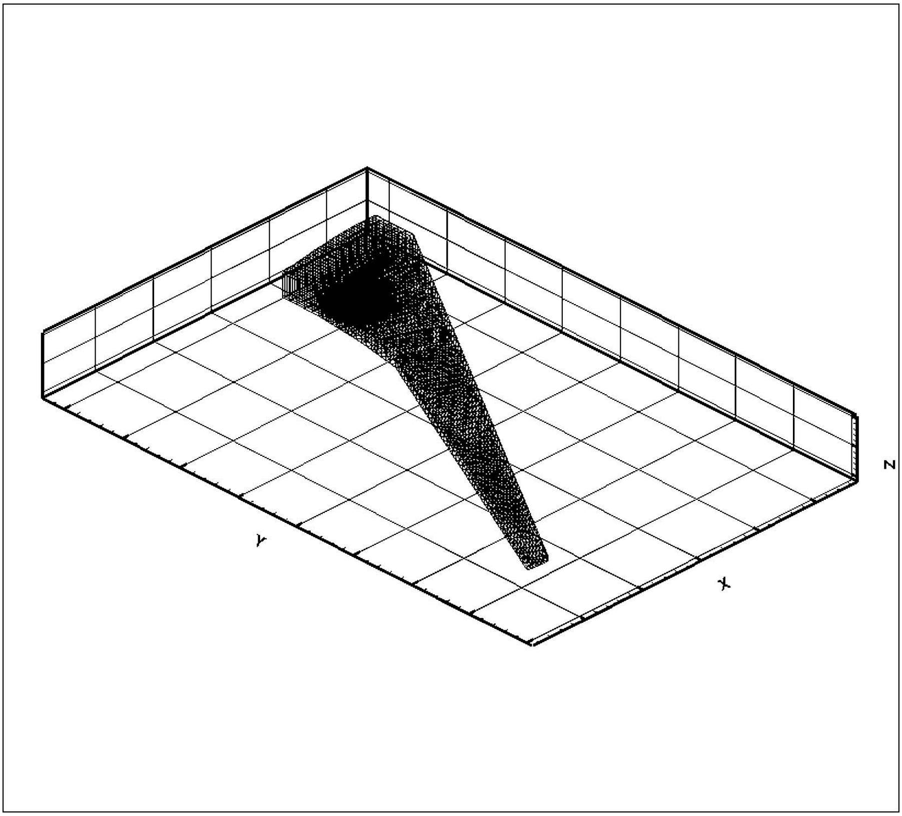

Figure 20.8 FE model of a 3D wing.

20.8 INCLUSION OF FREQUENCY DEPENDENT AERODYNAMICS FOR STATE-SPACE MODELLING – RATIONAL FRACTION APPROXIMATION

It has been shown that the effects of reduced frequency dependent aerodynamics need to be taken into account when performing a *frequency* domain aeroelastic analysis (Chapter 11) or modelling the response to continuous turbulence (Chapter 16); this is possible using the Theodorsen's and Sears' Functions for 2D strip theory or using the relevant AICs from a 3D panel method.

In the same way, if *time* domain models are required for calculations in which non-linear effects are to be examined, then the reduced frequency dependency of the aerodynamics needs to be accounted for; one possibility is to use a convolution employing the Wagner's and Kussner's Functions, but these are based

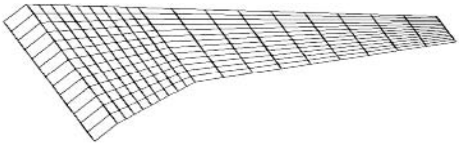

Figure 20.9 Aerodynamic panels for the 3D wing.

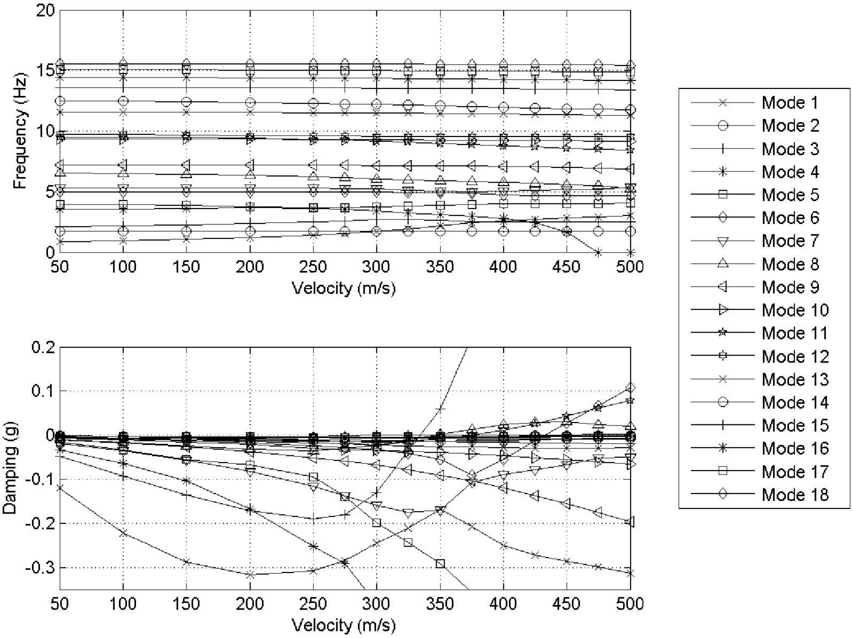

Figure 20.10 Frequency and Damping ratio trends for 3D wing.

on a 2D strip theory approach. If the results from a 3D panel approach are to be used in the time domain, a different method is required. For state-space time domain models (see Chapters 7 and 12), this is achieved through the use of a so-called rational fraction approximation (RFA) for aerodynamics, which approximates the AICs obtained from either doublet lattice modelling or experimental measurements at a range of reduced frequencies for a given flight condition. The approach described here (Eversman and Tewari, 1991) is a variation of the classical approach (Roger, 1977) that doesn't require the computational effort of the well known minimum state method (Karpel, 1982). The way in which the RFA is implemented in the state-space model is described in this section.

Consider the classical aeroelastic model but with the aerodynamic terms placed on the right hand side such that

$$\mathbf{A}\ddot{\boldsymbol{q}} + \mathbf{D}\dot{\boldsymbol{q}} + \mathbf{E}\boldsymbol{q} = -\rho V \mathbf{B}\dot{\boldsymbol{q}} - \rho V^2 \mathbf{C}\boldsymbol{q} = \mathbf{Q}_{\mathbf{Aero}}(t) \tag{20.37}$$

where $\mathbf{Q}_{\mathbf{Aero}}$ is the aerodynamic generalised force vector. Alternatively, in the Laplace domain (Chapter 7)

$$\left(\mathbf{A}s^2 + \mathbf{D}s + \mathbf{E}\right)\boldsymbol{q}(s) = \frac{\rho V^2}{2}\mathbf{Q}(s)\boldsymbol{q}(s) \tag{20.38}$$

where $\mathbf{Q}(s)$ is the rational fraction approximation to the AIC matrix expressed in modal space. The matrix $\mathbf{Q}(s)$ is expanded using a rational fraction approximation in terms of the Laplace variable $s = i\omega$, so that

$$\mathbf{Q}(s) = \mathbf{A_0} + \mathbf{A_1}\frac{sb}{V} + \mathbf{A_2}\left(\frac{sb}{V}\right)^2 + \frac{V}{b}\sum_{n=1}^{N_L}\frac{\mathbf{A_{n+2}}}{\left(s + \dfrac{V}{b}p_n\right)}$$

or

$$\mathbf{Q}(ik) = \mathbf{A_0} + \mathbf{A_1}ik + \mathbf{A_2}\,(ik)^2 + \sum_{n=1}^{N_L} \frac{\mathbf{A_{n+2}}}{(ik + p_n)} \tag{20.39}$$

noting that ${}^{sb}\!/_{V} = ik$. Here p_n are the N_L poles (or lag parameters) used for the approximation of the unsteady aerodynamic matrix **Q**(s) and $\mathbf{A_i},\ i = 0, 1, \ldots N_L + 2$ are unknown matrices to be found.

Now, if $\mathbf{AIC}(k_m),\ m = 1, 2 \ldots N_k$ is a given set of AICs obtained using a panel method or experimental measurements at N_k reduced frequencies, then the square of the error between the RFA (shown here with two aerodynamic lag terms) and $\mathbf{AIC}(k_m)$ for the rs^{th} element is written as

$$\begin{aligned}\varepsilon_{rs} &= \sum_{m=1}^{N_k} \left(\mathbf{Q}_{\text{rs}}\,(ik_m) - \mathbf{AIC}_{rs}\,(ik_m)\right)^2 \\ &= \sum_{m=1}^{N_k} \left(\mathbf{A_0} + \mathbf{A_1}\,(ik_m) + \mathbf{A_2}\,(ik_m)^2 + \frac{\mathbf{A_3}}{(ik_m + p_1)} + \frac{\mathbf{A_4}}{(ik_m + p_2)} - \mathbf{AIC}\,(k_m)\right)_{rs}^2\end{aligned} \tag{20.40}$$

where it should be noted that the subscript ‘rs’ indicates that the rs^{th} element of each matrix is considered so equation (20.40) is actually written in scalar terms. The least squares minimisation between the given data and the rational fraction approximation model for each element is defined as

$$\left(\frac{\partial \varepsilon}{\partial \mathbf{A_n}}\right)_{rs} = 0 \quad \text{for} \quad n = 0, 1, 2, \ldots, N_L + 2. \tag{20.41}$$

which leads to the equations

$$\begin{bmatrix} 1 & ik_1 & -k_1^2 & \dfrac{1}{ik_1 + p_1} & \dfrac{1}{ik_1 + p_2} \\ 1 & ik_2 & -k_2^2 & \dfrac{1}{ik_2 + p_1} & \dfrac{1}{ik_2 + p_2} \\ \vdots & \vdots & \vdots & \vdots & \vdots \\ 1 & ik_{N_k} & -k_{N_k}^2 & \dfrac{1}{ik_{N_k} + p_1} & \dfrac{1}{ik_{N_k} + p_2} \end{bmatrix} \begin{Bmatrix} A_0 \\ A_1 \\ A_2 \\ A_3 \\ A_4 \end{Bmatrix}_{rs} = \begin{Bmatrix} \text{AIC}\,(ik_1) \\ \text{AIC}\,(ik_2) \\ \vdots \\ \vdots \\ \text{AIC}\left(ik_{\text{N}_\kappa}\right) \end{Bmatrix}_{rs} \tag{20.42}$$

and these can be solved using least squares to find the unknown A_{rs} values. Note that the curve fit is performed term by term in the AIC matrix using the same lag values throughout; however a single step matrix approach could be used. The pole values must be positive but their choice is not straightforward and a range of different values should be tried. Better results are obtained if a good distribution of k values is taken over the range of interest but it is usual to have more points at low values of k as these are more important for flutter.

Figure 20.11 shows a typical curve-fit using the above rational fraction approximation approach with 4 aerodynamic lag terms on a sample element (1,2) of the aerodynamic influence coefficient matrix (the “truth”). It can be seen that a reasonable fit can be achieved.

Having estimated the unknown matrix parameters, equation (20.38) can be written in the time domain for two aerodynamic lags and no excitation vector so that

$$\mathbf{A}\ddot{\boldsymbol{q}} + \mathbf{D}\dot{\boldsymbol{q}} + \mathbf{E}\boldsymbol{q} = \hat{\mathbf{A}}_0\boldsymbol{q} + \frac{b}{V}\hat{\mathbf{A}}_{\mathbf{1}}\dot{\boldsymbol{q}} + \left(\frac{b}{V}\right)^2 \hat{\mathbf{A}}_{\mathbf{2}}\ddot{\boldsymbol{q}} + \hat{\mathbf{A}}_{\mathbf{3}}\boldsymbol{q}_{\mathbf{a_1}} + \hat{\mathbf{A}}_{\mathbf{4}}\boldsymbol{q}_{\mathbf{a_2}}$$

where

$$\hat{\mathbf{A}}_{\mathbf{n}} = \frac{\rho V^2}{2}\mathbf{A_n} \tag{20.43}$$

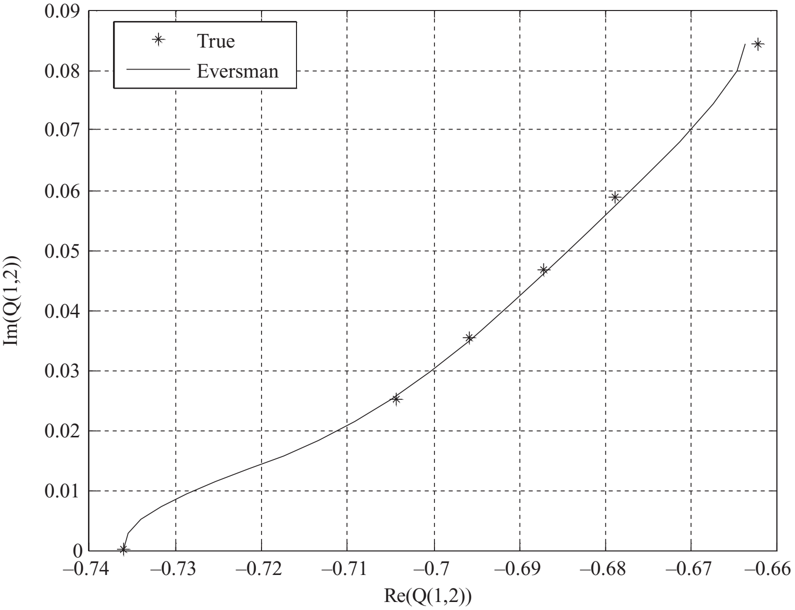

Figure 20.11 Curve fit of AIC data element using rational fraction approximation.

Rewriting this expression yields

$$\left(\mathbf{A}-\left(\frac{b}{V}\right)^2\hat{\mathbf{A}}_2\right)\ddot{\boldsymbol{q}}+\left(\mathbf{D}-\frac{b}{V}\hat{\mathbf{A}}_1\right)\dot{\boldsymbol{q}}+\left(\mathbf{E}-\hat{\mathbf{A}}_0\right)\boldsymbol{q}=\hat{\mathbf{A}}_3\boldsymbol{q}_{\mathbf{a}_1}+\hat{\mathbf{A}}_4\boldsymbol{q}_{\mathbf{a}_2}$$

or (20.44)

$$\tilde{\mathbf{A}}\ddot{\boldsymbol{q}}+\tilde{\mathbf{D}}\dot{\boldsymbol{q}}+\tilde{\mathbf{E}}\boldsymbol{q}=\hat{\mathbf{A}}_3\boldsymbol{q}_{\mathbf{a}_1}+\hat{\mathbf{A}}_4\boldsymbol{q}_{\mathbf{a}_2}$$

where the so-called augmented states, arising from the convolution applied to the inverse Laplace transform of the **Q**(s) matrix, are defined as

$$\boldsymbol{q}_{\mathbf{a}_n}=\int_0^t \boldsymbol{q}e^{-\frac{V}{b}p_n(t-\tau)}d\tau \qquad 1\le n\le N_L \qquad \dot{\boldsymbol{q}}_{\mathbf{a}_n}=\boldsymbol{q}-\frac{V}{b}p_n\boldsymbol{q}_{\mathbf{a}_n} \tag{20.45}$$

but neither term needs to be calculated explicitly. Equation (20.43) can be combined with equation (20.45) to write the system in the classical state-space formulation of

$$\dot{\boldsymbol{x}}=\mathbf{A}_S\boldsymbol{x} \qquad \boldsymbol{x}=\left[\dot{\boldsymbol{q}}^{\mathrm{T}} \quad \boldsymbol{q}^{\mathrm{T}} \quad \boldsymbol{q}_{\mathbf{a}_1}^{\mathrm{T}} \quad \boldsymbol{q}_{\mathbf{a}_2}^{\mathrm{T}}\right]^{\mathrm{T}} \tag{20.46}$$

The system matrix $\mathbf{A}_S$ is

$$\mathbf{A}_S=\begin{bmatrix} -\tilde{\mathbf{A}}^{-1}\tilde{\mathbf{D}} & -\tilde{\mathbf{A}}^{-1}\tilde{\mathbf{E}} & \tilde{\mathbf{A}}^{-1}\hat{\mathbf{A}}_3 & \tilde{\mathbf{A}}^{-1}\hat{\mathbf{A}}_4 \\ \mathbf{I} & \mathbf{0} & \mathbf{0} & \mathbf{0} \\ \mathbf{0} & \mathbf{I} & -\frac{V}{b}p_1\mathbf{I} & \mathbf{0} \\ \mathbf{0} & \mathbf{I} & \mathbf{0} & -\frac{V}{b}p_2\mathbf{I} \end{bmatrix} \tag{20.47}$$

Thus the state space equations of motion can be solved as before (see Chapter 12) but clearly there are additional states present. The model approximates the reduced frequency dependency of the aerodynamics in the time domain by effectively replacing the use of convolution with Wagner's and Kussner's Functions for 2D strip theory.

Part III

Introduction to Industrial Practice

21

Aircraft Design and Certification

The aim of this final part of the book is briefly to outline some of the processes employed in the commercial aerospace industry for aeroelastics and loads analysis. Reference is made to the certification specifications. However, it is recognized that practice across companies and even different aircraft projects will differ so the treatment described is not unique. Where relevant, the processes will be related to the earlier chapters of the book where a simplified approach was taken.

21.1 AEROELASTICS AND LOADS IN THE AIRCRAFT DESIGN PROCESS

Aeroelastic and loads considerations play a part across much of the design and development of an aircraft. The aeroelastic and loads behaviour of the aircraft have an impact upon the concept and detailed structural design, aerodynamic characteristics, weight, jig shape, FCS design, handling qualities, control surface design, propulsion system, performance (effect of flight shape on drag), landing gear design, structural tests, etc.

It can be convenient to think of the design and development cycle as comprising a number of phases:

(a) A *concept phase* in which the intent is to determine the best viable aircraft concept to meet the design aims. Estimates of loads play an important role here in the process of estimating the structural weight of each concept under consideration and so influencing the design trade-offs between alternative options. Aeroelastics is also important in order to eliminate concepts that are likely to be aeroelastically unacceptable or to assist in positioning engines, for example. At this stage of aircraft development the engineering team is relatively small and their need is for rapid turnaround of analyses. Hence the availability of detailed aircraft data is sparse and, instead, there must be a heavy reliance on theoretical analysis calibrated, if at all, mainly by empirical data or data scaled from previous designs in the same family of aircraft. Likewise, the focus of attention will be on those few loading cases that have been identified or are judged to be the most likely design drivers. The analysis methods too are likely to be as simple as they can be, while still capable of delivering worthwhile results, and this will often allow them to be more automated than will be the case later in the design process when practical constraints arising from the detailed design often have to be taken into account. For aircraft that employ an FCS, it is well known that the FCS will have an important effect on loads, but at this early stage of development its concept design will have barely started and there would certainly not be sufficient detail to take rational account of it. Hence it will be necessary to make allowance for the FCS in some other way.

(b) A *pre-design phase* would follow in which the top level architecture of the chosen concept is fleshed out. The start of pre-design usually marks a significant ramp-up of engineering resource on the project (although still an order of magnitude below the expenditure once industrialization gets under

Introduction to Aircraft Aeroelasticity and Loads J. R. Wright and J. E. Cooper
© 2007 John Wiley & Sons, Ltd

way). Reasonable loads estimates are important here in order to determine billet and forging sizes of long-lead items and to contribute to choice of alternative structural architectures (landing gear attachment scheme, position of the primary structural elements within the external contour, two- or three-spar wing design, etc.). In many ways the pre-design phase is one of transition from quick-turnaround methods used for concept selection towards the more rigorous and detailed mainstream methods that are necessary to underpin the loads to be used for detailed design. Pre-design is also just about the last opportunity for aeroelastic drivers to contribute to the fundamental structural concept, so much attention will be paid to ensuring that sufficient analysis is performed to give good confidence that flutter margins will be achievable. Attention will also be paid to ensuring that sufficient control surface static effectiveness is available throughout the design envelope, so as to achieve the required handing qualities and controllability and to provide any load alleviation that may be part of the design concept.

(c) A *detailed design phase* follows, involving a big ramp-up of resourcing costs. This will only follow a formal industrial go-ahead with full financing in place. Once this happens it is a race to complete the detailed design, so a good quality set of loads on which to base the design is needed almost immediately – hence there is a high reliance on the preparatory mathematical modelling undertaken in pre-design. Ideally these loads should not be allowed to increase, although in practice there is often considerable pressure to seek decreases in order to facilitate weight saving. It is evident that as detailed design progresses, the 'best knowledge' of mass properties, aerodynamics, stiffness and systems will change – all potentially influencing calculated loads and aeroelastics characteristics. The focus of attention will therefore naturally turn towards refining mathematical models to track the effects of the evolving design and towards developing solutions to any problems that are identified. Design is naturally an iterative process and the level of detail and confidence in the models employed for analysis will improve cycle by cycle as more information becomes available. The processes by which these design cycles are managed differ from manufacturer to manufacturer and play an important role in the eventual success of the project. (Note that it is quite possible for an iterative process to become divergent).

(d) Finally a *validation and certification phase* follows in which the aircraft (or components) have been built and used in ground and flight testing in order to validate whether the characteristics built into the loads and aeroelastics models are correct. Any adjustments resulting from this and from any late design changes (to the FCS, for example) must be taken into account in producing a set of loads on which the structural certification can be based. There may have to be some late design changes, even at this stage, driven by the evolution of loads or by the need to demonstrate sufficient aeroelastic margins, but the aim is to confine these changes to items that can be changed relatively quickly and without major industrial repercussions, e.g. control law software or fine tuning of control surface mass balance (where used).

There are a number of different customers of loads, each with their own specific requirements. The two that deserve most attention are design and certification.

The customers for *design* (and structural justification) need the loads in order to determine extreme stress levels in their structure or to estimate fatigue damage or damage tolerance. For both purposes they will wish to apply loads cases to their detailed structural models. This usually involves a post-process of decomposition of correlated loads cases supplied from the result of loads calculations into some form of nodal loading that can be applied to specific structural elements. It is therefore important to this analysis that the applied loads are well in balance with constraints. Hence the supplied loads cases must themselves be in balance, for instance as they should be for a specific time instant in a dynamic gust or manoeuvre response. This implies that the loads group must be prepared to deliver as many load cases as are identified as potentially critical on some part of the structure.

For *certification* justification (of the loads themselves) the focus of attention can be more limited, e.g. to the envelope values of the loading quantities of primary interest (such as shear force, bending moment and torque variations along each of the main components).

21.2 AIRCRAFT CERTIFICATION PROCESS

21.2.1 Certification Authorities

Commercial aircraft whose weight is above 5700 kg (12 500 lb) are certified under the ‘large aircraft’ certification requirements, denoted by the number 25 in the regulation description (CS-25 and FAR-25). The certification of aircraft is a complex process and depends upon where in the world the aircraft is manufactured and where it is to be purchased and operated. The US certification is looked after by the FAA (Federal Aviation Administration) and European certification by EASA (European Aviation Safety Agency); until 2003, the European certification of aircraft was overseen by the JAA (Joint Airworthiness Authorities) and prior to that many countries certified aircraft through their own agencies, e.g. CAA (Civil Airworthiness Authority) in the UK.

Any new aircraft model requires type certification by the airworthiness agency corresponding to the area of the world in which the manufacturer is based; this is primary certification. If the aircraft is to be exported to other parts of the world, then secondary certification by the relevant agencies is also required; such an exercise will be eased by any bilateral agreements existing between the agencies.

21.2.2 Certification Requirements

To cover the type certification of large commercial aircraft, the FAA and EASA issue FAR-25 and CS-25 documents respectively. The FAR-25 contains basic FARs (Federal Aviation Regulations, e.g. FAR 25.491 Taxi, Take-off and Landing Roll) and any additional material is contained within ACs (Advisory Circulars, prefixed AC 20 or 25, e.g. AC 25.491). The CS-25 Book 1 contains CS (Certification Specifications) which are standard technical interpretations of the essential airworthiness requirements (e.g. CS 25.491 Taxi, Take-off and Landing Roll); the book is divided into a number of subparts together with appendices. The key subparts for loads and aeroelasticity issues are Subpart B (Flight), C (Structure) and D (Design and Construction). Aeroelastics requirements are fairly well concentrated in CS 25.629, which is within Subpart D. Loads requirements are mainly in Subpart C as the prescription of the loading cases that have to be accounted for in design is a primary prerequisite for assuring structural integrity over the operating environment of the aircraft. Most of the structural airworthiness requirements are related to static (as opposed to fatigue) loads.

CS-25 Book 2 contains what are known as AMCs (Additional Means of Compliance, e.g. AMC 25.491) which are nonexclusive means of demonstrating compliance with airworthiness codes or implementing rules. The AMC (previously termed ACJ when published by JAA) is related to the AC in FAR-25.

Over recent years, there has been considerable effort to rationalize the US and European codes and for most issues they are now the same, though there have been different rates of incorporating changes. An extremely valuable contribution in the field relevant to this book was made by the Loads and Dynamics Harmonisation Working Group (LDHWG), a mix of technical specialists from the US and Europe. The group considered revisions to the codes to assist harmonization and incorporate improvements; a particular area where new work was needed was for large commercial aircraft with more than two main landing gears where the redundant gear layout meant that some of the ground loads requirements were inappropriate and more rational approaches were required. Many of these changes are already in the codes and others are awaiting incorporation.

When revisions are proposed to the requirements, an NPA (Notice of Proposed Amendment) is issued and after consultation it becomes part of the code (e.g. NPA 11/2004 in Europe led to the issue of Appendix K on Interaction of Systems and Structures). For Europe, the current rule-making plans are on the EASA website.

There is a degree of flexibility in meeting the requirements and some room for the manufacturer proposing, and discussing with the certification authorities an alternative approach to a particular issue. The manufacturer can produce a CRI (Certification Review Item) and Special Conditions may be agreed to meet a particular requirement prior to the codes being altered. The need for Special Conditions may be driven by the manufacturer, due to unusual design features in their aircraft, prompting the need for analysis justification beyond the basic requirement, or by the Authority, who often wish to apply a pending NPA as a Special Condition ahead of its adoption into the general requirements.

The certification process depends upon whether an aircraft has ‘new structure’ (e.g. changes in the design philosophy regarding structures and loads have been made or the manufacturer has not built an aircraft of this type before), ‘similar new structure’ (utilizes similar design concepts to an existing tested aircraft) or ‘derivative/similar structure’ (uses structural design concepts almost identical to those on which analytical methods have been validated). Obviously, the more similarity a particular aircraft type has with an existing design or design approach, the simpler the design and certification process. The process of analysis and test depends on what previous test evidence is available. A very useful introduction to the compliance with different loading conditions is given in CS/AMC 25.307 Proof of Structure; e.g. the appropriateness of standard methods and formulae, and the use of the finite element method for complex structures is discussed together with the need for testing.

21.2.3 Design Envelope

It is important for a manufacturer to put the specific loads requirements into the context of the design envelope. CS 25.321(c) requires that enough points on or within the boundary of the design envelope are investigated to ensure that the most extreme loads for each part of the aircraft structure are identified. In this context, the design envelope encompasses the respective ranges of permitted mass/centre of mass envelopes (MTOW, maximum take off weight; MZFW, maximum zero fuel weight; MLW, maximum landing weight; OWE, operating weight empty; etc.), ground design speeds, flight design speed envelopes versus altitude and aircraft (aerodynamic) configuration, flight control law or autopilot mode, etc. Sample envelopes for air speed against altitude and centre of mass/weight against mean aerodynamic chord (MAC) are shown in Figure 21.1 and Figure 21.2. The forward centre of mass limit is often limited by the ability to apply sufficient control and trim, whereas the aft limit depends upon the stability of the aircraft, sensitivity of controls and danger of the aircraft tipping over.

If loads were to be analysed for a large number of different flight and load condition combinations, then this would result in an enormous number of calculations – a prospect that could not be considered in bygone days of limited computing capability. Nevertheless, even with the computational power now

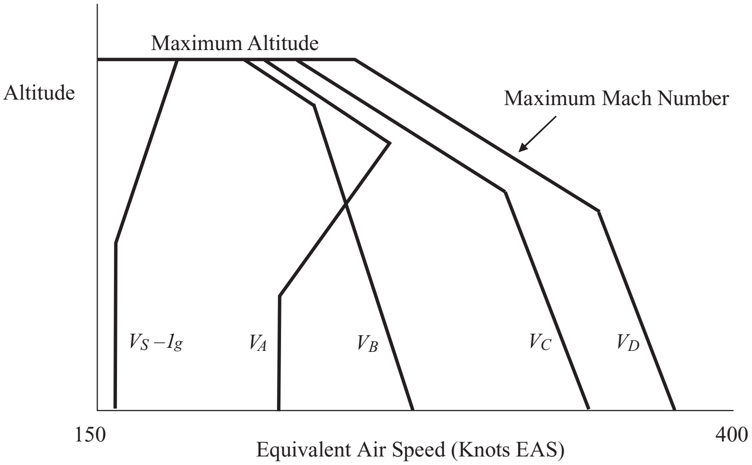

Figure 21.1 Flight envelope – design speed versus altitude. Reproduced by permission of Airbus (redrawn with modifications).

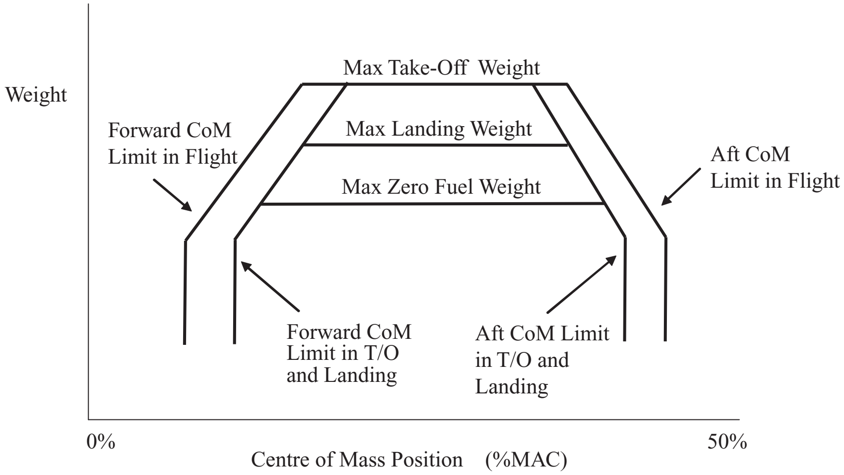
Weight
Max Take-Off Weight
Max Landing Weight
Max Zero Fuel Weight
Forward CoM Limit in Flight
Aft CoM Limit in Flight
Forward CoM Limit in T/O and Landing
Aft CoM Limit in T/O and Landing
0%
50%
Centre of Mass Position (%MAC)

Figure 21.2 Weight versus centre of mass envelope. Reproduced by permission of Airbus (redrawn with modifications).

available, it is still appropriate to take an intelligent approach to case selection, focusing detail where initial calculations or previous studies show the potential for cases to become significant.

21.2.4 Bookcase and Rational Load Cases

The load cases for certification are sometimes classified as either (a) bookcase or (b) rational. The *bookcase* types of load case are often somewhat artificial in that applied loads are assumed and reacted by inertia loads, leading to a static equilibrium problem. They therefore provide simple rules for design but not necessarily a realistic flight case, especially in early stages of the FCS design. The load cases may not be reproduced on the real aircraft; they tend to have been developed when computation methods were in their relative infancy and the loads assumed have been found over the years to lead to aircraft that are judged strong enough. A number of clear examples are shown in the ground loads cases (e.g. turning or braked roll; see Chapters 17 and 25).

On the other hand, *rational* types of load case are those where an attempt is made to model the loads and dynamics of the aircraft as realistically as possible. They have developed as computational methods and the understanding of aircraft behaviour has matured and as nonlinear effects have become more important. In some cases, rational methods have become essential, e.g. where redundant landing gear layouts are introduced by employing more than two main landing gear units. In other cases, use of rational modelling may have allowed reduced loads to be justified (e.g. braking). The rational methods may be classed as 'fully rational' where the full dynamic condition is sought (e.g. landing) or 'quasi-rational' where a trimmed/equilibrium condition is sought from the fully rational (often nonlinear) dynamic model in order to determine a rational balanced condition (e.g. a steady braking case where the static landing gear characteristics are represented).

The bookcase is most useful early on in the design cycle (pre-development and sizing) when the aircraft is at a less mature stage of development and realistic calculations are impractical and probably inaccurate. On the other hand, the rational approach can be used later in the design cycle for loads certification, sensitivity studies, study of failure cases, etc.

Attention to detail is necessary in reading and interpreting the requirements defining load cases for certification. In some cases loads cases are defined in such a way that they can only be applied as a 'bookcase' or as a 'rational' analysis, whereas in other cases the requirement for rational analysis is limited to certain circumstances only. In yet other cases the manufacturer is given the choice of applying a conservative 'bookcase' or alternatively of investing additional time and resources in a more detailed rational analysis in the expectation (not always realized) that it will produce less conservative loads and so allow the aircraft to be more competitive.

21.2.5 Limit and Ultimate Loads

The certification requirements include a number of general requirements that are helpful for the engineer to be aware of. Strength requirements (CS 25.301, 25.303 and 25.305) are specified in terms of:

(a) Limit loads are the maximum loads to be expected in service and which the structure needs to support without 'detrimental permanent deformation'.
(b) Ultimate loads (limit loads multiplied by a factor of safety, normally 1.5 unless otherwise stated) are loads that the structure must be able to support without failure/rupture (for at least 3 seconds).

Limit loads might realistically happen once per lifetime ($\sim 10^5$ hours) for a single aircraft, but once the probabilities of the aircraft actually being at the critical flight state/condition when the event occurs then the probability of experiencing the limit load in practice should be much lower than once per lifetime. The loads specified in CS-25 are almost entirely limit loads. The requirements also specify that compliance with the strength and deformation conditions needs to be demonstrated for each critical loading condition (CS 25.307). How this may be shown by analysis and test is discussed in (CS/AMC 25.307) Proof of Structure.

A recent addition to CS-25 is a requirement on the interaction of systems and structures (CS 25.302/Appendix K) where the structural performance following the possible failure of systems that may influence structural loads must be considered. This requirement is unusual in specifying factors of safety for consideration of loads at the time of occurrence of the failure and factors of safety for consideration of loads for continuation of the flight, which reduce below 1.5 as a function of reducing the probability of occurrence or exposure.

21.2.6 Fatigue and Damage Tolerance

Although often less visible than static design loads, the requirement to provide loads information for fatigue and damage tolerance assessment is nevertheless an important aspect of aircraft design. However, it was decided not to cover this aspect of loads in detail earlier in the book, since it falls into the category of loads post-processing whereas the main focus has been on response and loads determination.

The structural analysis is aimed at an evaluation of an appropriately factored 'life' of a structural element relative to the design life goal of the aircraft or against the maintenance inspection interval schedule. In both cases the key 'loads' input to the structural analysis takes the form of a 'load spectrum' for the anticipated usage (or 'mission') of the aircraft. This is typically generated by the combination for each segment of a 'mission' of a statistical model identifying the frequency of exceeding a global parameter such as gust velocity with sets of loads (sometimes termed 'unit loads' or 'fatigue loads') which provide a relationship between the global parameter and loads in the aircraft structure. Determination of the statistical model is usually based on operational statistics from aircraft in service. The 'mission' definition of an aircraft will be directly linked to the top level aircraft requirements and design characteristics (weights, maximum payload, payload fractions, fuel capacities, speed/altitude profiles, etc.).

The 'fatigue loads' are normally generated using the same mathematical model formulations as used in generating static design loads for stylized conditions. For example, within the airborne part of the mission, they may be provided for the datum 1*g* condition in each segment, plus the incremental loads due to unit root-mean-square (RMS) gust velocity applied in either some form of discrete gust profile or alternatively from a continuous turbulence analysis that will directly facilitate the application of the 'mission analysis' method (see Chapter 24).

In the provision of 'fatigue loads', it is often necessary to identify in some way the frequency of loads occurrences relative to the global parameter on which the statistical model is based. If a deterministic model is used for 'fatigue loads' then this may be needed to account for the contribution to fatigue damage from the second, third and subsequent peak loads in the event time history. If a stochastic model is used (such as continuous turbulence) then the characteristic frequency of the load needs to be identified in order to apply the mission analysis exceedence formula. With this final point in mind, a further useful requirement to be aware of is CS/AMC 25.571 Damage-Tolerance and Fatigue Evaluation of Structures, which includes considerable discussion of how damage and fatigue issues should be handled.

22

Aeroelasticity and Loads Models

In this chapter, the building blocks that make up the aeroelastic and manoeuvre/gust load models will be introduced. Where possible, the models will be related to those used earlier in Part II of the book. Various comments on the requirements for structural and aerodynamic models are made for gusts and flutter in CS/AMC 25.341 and 25.629. Note that what is presented here is one way of developing suitable mathematical models for aeroelastics and loads, but other approaches could be used.

22.1 STRUCTURAL MODEL

22.1.1 Introduction

The basic mathematical model of the aircraft must be able to represent its vibration behaviour over the frequency range of interest, typically 0–40 Hz for large commercial aircraft and 0–60 Hz for small commercial aircraft. Thus the model will need to yield natural frequencies, modal masses and normal mode shapes in these frequency ranges. The model should adequately represent the aircraft complexity, including control surface and engine behaviour, and generate sufficiently accurate mode shapes.

22.1.2 Stiffness Model – ‘Beam-Like’ Representation

The traditional approach to determining a mathematical model for aircraft with fairly slender high aspect ratio wings was to recognize that the structure is ‘beam-like’ and then to represent the major aircraft components (e.g. wing, front fuselage, rear fuselage, tailplane, fin) by beams lying along reference axes positioned at, for example, the locus of shear centres (or flexural axis). The beams are capable of bending, shear, torsional and axial deformations. In such an approach, each beam is divided into several sections or elements. The combination of such ‘beams’ for all parts of the aircraft is called a ‘stick’ or ‘beam’ model and a wing example is shown in Figure 22.1.

The flexural rigidity *EI* and torsional rigidity *GJ* of the beam are traditionally estimated from the member section properties by classical structural analysis methods. The structural stiffness behaviour of each element is represented by a stiffness matrix (effectively the finite element method employing beam elements). This type of model was introduced in Chapter 4.

22.1.3 Stiffness Model – ‘Box-Like’ Representation

The problem with employing beam elements directly for an aircraft structure is that for such a complex structure, the calculated stiffness distribution is rather inaccurate. It may be suitable for an aircraft in early design where the detailed structure has not yet been defined and where scaled stiffness and mass properties from previous aircraft might be employed, but not at the later stages of design and certification

© 2007 John Wiley & Sons, Ltd

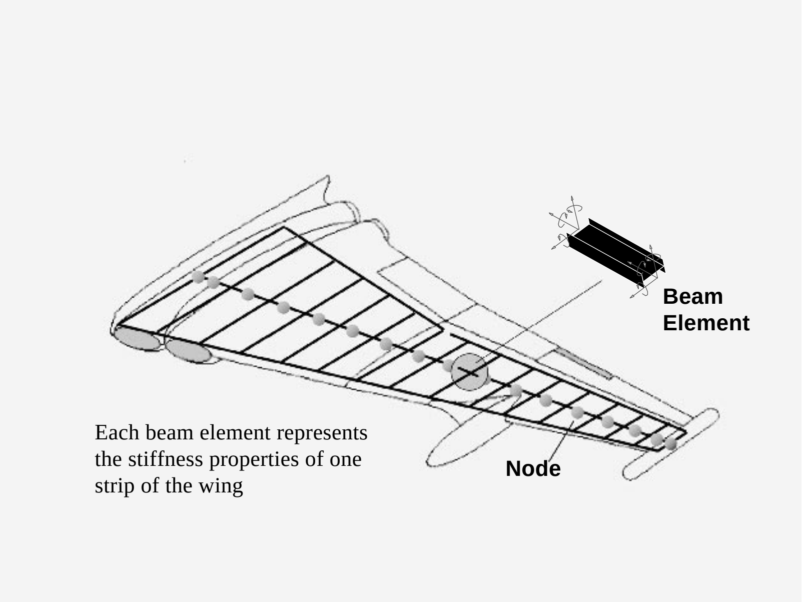

Figure 22.1 Finite element wing model using a 'beam-like' representation. Reproduced by permission of Airbus.

where structural detail is available and important. However, in more recent years, the finite element approach has been used to set up the structural stiffness characteristics for the aircraft by recognizing its detailed 'box-like' construction.

The whole structure, or each separate component, is meshed using a range of finite element types. There are two main ways in which a box-like structure may be modelled, having recognized that such a semi-monocoque structure (Niu, 1988; Megson, 1999) is composed of discrete stiffeners (e.g. spar booms, stringers) and thin-walled panels (e.g. cover skins, webs for spar/rib). The options are for the model to allow for (a) 'overall' bending or for (b) both overall and 'local' bending. Thus, whatever modelling approach is chosen, the model will cater for 'overall' bending which is bending and twisting of the entire structure, such that the cover skins, stiffeners and spar/rib webs essentially carry only in-plane axial and shear loads. The modelling decision is then whether to allow also for 'local' bending of the structure. Local bending implies local bending and twisting of the cover skins, stiffeners and spar/rib webs. This choice depends upon the load paths in the structure. The allowance for local bending is more computationally intensive since more sophisticated elements need to be employed. Thus, if only overall bending is allowed for, the stiffening booms may be modelled using bar (or rod) elements that withstand tension and compression loads; alternatively, if local bending is permitted, beam elements withstanding tension, compression, bending and torsional loads are used. The panels may be represented for overall bending by membrane elements, transferring in-plane axial and shear loads, or alternatively by shell elements where local bending and twisting is also modelled. The compatible element pairs to use are bars/membranes and beams/shells, though use of multipoint constraints (NAFEMS, 1987) allows dissimilar element types to be joined; therefore, for example, a beam/shell model could be attached to a component modelled using bar/membrane elements.

Figure 22.2 shows an example of an FE model for wing and pylons where the representation of the box structure by panel finite elements may be clearly seen. It should be emphasized that the model employed for dynamics purposes may not be as detailed in structural representation as the model used

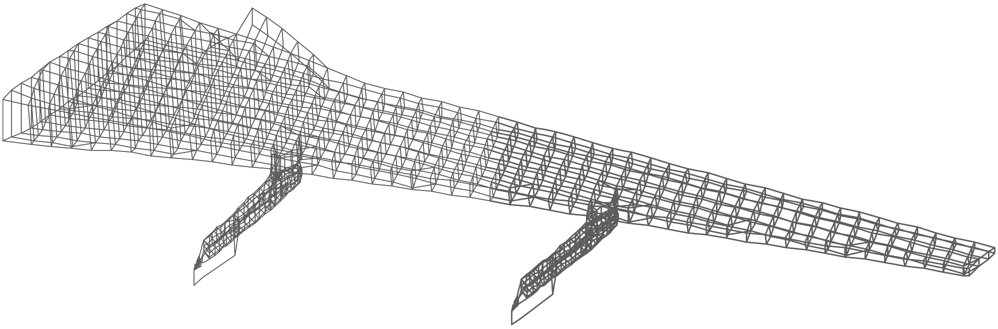

Figure 22.2 Finite element wing model using a 'box-like' representation. Reproduced by permission of Airbus.

for stress analysis. The dynamic idealization for an aircraft structure is relatively crude though the level of sophistication is continually growing.

When modelling a detailed component such as a machined bracket using 'brick' elements, say, the FE model will represent the load paths well and the stresses derived from the stiffness matrix and element deformations will be quite reliable. However, for a complex stiffened aircraft box structure, the level of detail that can be accurately modelled is limited and so the stress output can be rather unreliable. Therefore the FE method often tends to be used to determine load paths via nodal forces that can subsequently act as input loads to a more detailed FE model of a local structure or to a structural element where dedicated design formulae/programs are available; this issue is also referred to in Chapters 4, 18, 21 and 25.

Additional structure to support landing gear, engine/pylon and control surfaces needs to be represented as accurately as possible since local stiffnesses are important for aeroelastics and loads calculations.

22.1.4 Mass Model

A considerable degree of detail is known for the mass distribution on an aircraft structure, but only part of the mass is structural, and therefore associated with the FE structural model, whereas a significant amount of mass is linked with nonstructural elements such as fuel, payload, equipment, etc. Thus, unlike the earlier machined bracket example, where the mass and its distribution would be accurately represented using the brick elements, it is not appropriate to try to link the mass to each finite element in the large box-like aircraft FE model. A different approach is therefore required for an aircraft structure.

What is commonly done for the dynamic modelling of a commercial aircraft with high aspect ratio wings is that the mass is idealized at a limited number of mass reference positions on defined structure (or loads) reference axes. These axes are those at which the internal loads are to be defined and for the beam-like model in Section 22.1.2 will coincide with the beam nodes. However, if the FE model is box-like then it will need to be condensed on to the structural reference axes in order to create an effective beam-like representation (see Section 22.1.5 for the condensed beam model).

Thus, in order to represent the mass distribution, the wing, for example, is divided into a number of sections (or strips), centred on the structural reference points (i.e. nodes) of the beam-like model, as shown in Figure 22.3. For each section, the mass is effectively lumped at the reference positions and attached to the beam axis node by a rigid link element that allows the lumped mass to be represented by section mass, moments of inertia and mass moments. The rigid element will allow for the section centre of mass to be offset from the reference axis and will therefore define the structural mass matrix to accompany the beam-like stiffness matrix; this concept was introduced in Chapter 4.

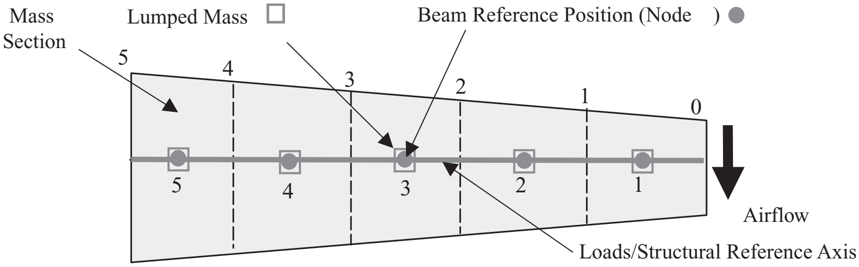
Mass Section
Lumped Mass
Beam Reference Position (Node)
5
4
3
2
1
0
5
4
3
2
1
Airflow
Loads/Structural Reference Axis

Figure 22.3 Arrangement of beam nodes and lumped mass positions.

22.1.5 Stiffness Model – 'Box-Like' Condensed to a 'Beam-Like' Model

It was explained in the last section how lumped masses could be linked rigidly to the nodes of a beam model. However, for the box-like representation of an aircraft, there are a huge number of nodes and so a condensation has to be performed; this process reduces the stiffness model to correspond with a limited number of structural reference (or nodal) points lying on the structural reference axes (or elsewhere as necessary). The condensation is typically carried out using a method such as Guyan reduction (see Appendix D) where the FE stiffness model of original order N is reduced to a significantly smaller set of master degrees of freedom N_m corresponding to the chosen reference axis (and any other chosen points). The master responses, once they have been calculated from the reduced model, may be used to obtain the responses at the slave degrees of freedom $N_\mathrm{s}(= N - N_\mathrm{m})$ that were condensed out. An example of a condensed beam-like model is shown in Figure 22.4 where the lumped masses are shown and where additional condensation points are employed to represent the engine pylon; similar arrangements could be used for the landing gear support points.

The representation of the control surface behaviour depends upon the case being considered. For dynamic loads calculations, the control surface modes may be ignored and control rotation simply treated as imposing forces and moments on the reference axes. However, for aeroelastic calculations such as flutter, the control modes need to be represented and so any reduced model would be extended to include suitable condensation points in the region of the control surface; mass stations would still be linked rigidly to chosen grid points.

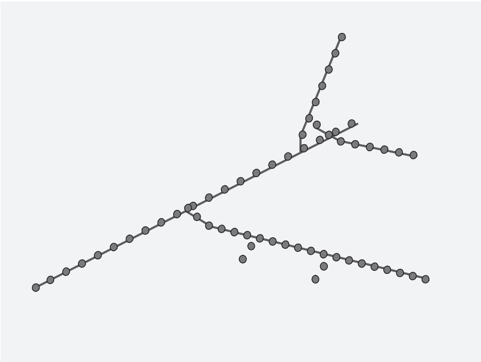

Figure 22.4 Condensed beam-like FE model on structural reference axes. Reproduced by permission of Airbus.

22.1.6 Modal Model

Once the mass representation and the beam-like condensed FE stiffness model are available, the N_m equations of motion governing the modal behaviour of the free–free structure may be determined. The free–free normal modes of vibration may then be calculated (see Chapters 2 and 3), leading to natural frequencies, mode shapes and modal masses for each mode. Both whole aircraft rigid body and flexible modes will be generated.

The diagonal modal mass and modal stiffness matrices may then be obtained using a transformation employing the modal matrix, exactly as originally introduced in Chapter 2. The number of desired flexible modes $N_d(<N_m$ and $<<N)$ to be employed in the aeroelastic or loads analyses must be selected to cover the frequency range of interest with sufficient accuracy; the transformation process effectively discards the excess modes in the uncoupled modal equations. Thus the large set of N finite element degrees of freedom in the box-like representation will have been reduced to a small set of N_d uncoupled single degree of freedom modal equations; typically N_d is of the order of $N^{1/3}$ and maybe only 30–50 modes are retained.

In Figures 22.5 and 22.6, an example of symmetric wing bending and wing torsion mode shapes are shown; the sections on the aircraft (i.e. fuselage, wing, fin, tailplane) are defined by the mass boundaries while the engine is shown as a generic shape scaled for length and diameter. Once mode shapes are known for the condensed (master) degrees of freedom, the values of the even greater number of slave degrees of freedom may be determined and the mode shapes plotted for the entire structural grid if desired.

Note that separate analyses are often performed for symmetric and antisymmetric behaviour of the aircraft and for different fuel and payload states.

22.1.7 Damping Model

It is not possible to model the distributed damping for an aircraft structure in any realistic way. What is normally done is to include an assumed level of modal damping per flexible mode (typically 1 % critical viscous damping or 0.02 structural damping) based on experience, and then to update this level, particularly if lower (e.g. wing bending) or higher values are obtained using results from the ground vibration test (see Chapter 26). If an actuator or flutter damper model is incorporated, then a more

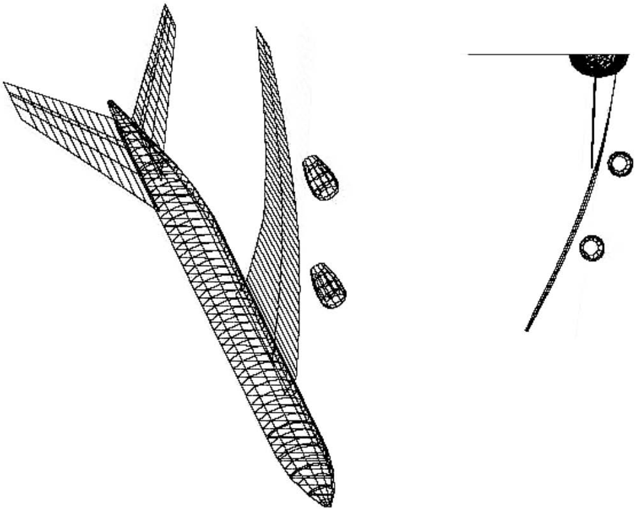

Figure 22.5 Sample symmetric wing bending mode shape. Reproduced by permission of Airbus.

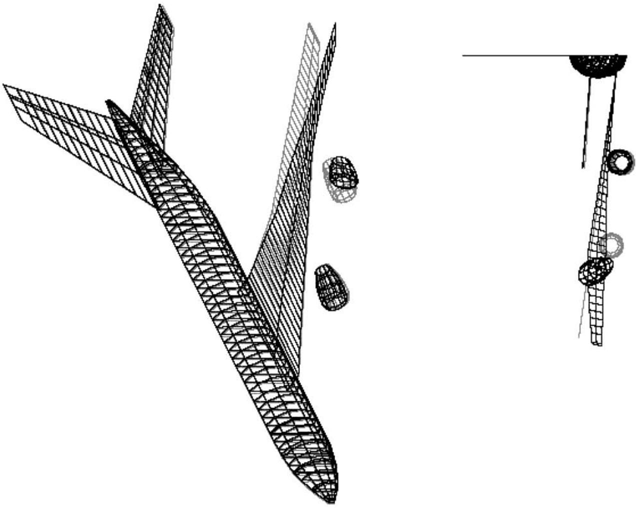

Figure 22.6 Sample symmetric wing torsion/outboard engine lateral mode shape. Reproduced by permission of Airbus.

accurate local damping representation would be available. Sometimes, for flutter calculations, damping is ignored but then a small level of negative damping above V_D would be acceptable as the inherent structural damping would eliminate this flutter in practice.

22.1.8 Rigid Aircraft Model

A model for the rigid aircraft is required for loads and aeroelastics calculations, as well as for flight mechanics studies of course. A linear small angle rigid aircraft model is referenced to inertial axes and is effectively composed of the rigid body heave, pitch and fore-and-aft displacements (for longitudinal motion); this is essentially the same as a modal model represented by rigid body modal coordinates and associated rigid body heave, pitch and fore-and-aft mode shapes (see Appendix A). The alternative rigid aircraft model is the large angle nonlinear flight mechanics model referenced to a body fixed axes system where rigid body velocities are defined relative to these fixed axes, as introduced in Chapter 14. In both cases, flexible modes may be added to the rigid aircraft model by adding the relevant modal equations. In either model, the key mass data required are the mass, centre of mass position and moments, and product moments of inertia for the whole aircraft.

22.2 AERODYNAMIC MODEL

The aerodynamic models used in loads and aeroelastics calculations are vital in allowing the aeroelastic mechanisms to be explored and sufficiently accurate deformations and load distributions to be estimated. Different manufacturers will tend to adopt different practices in detail, though there will be similar core features.

22.2.1 Aerodynamic Model for Flight Mechanics

The aerodynamic models for flight mechanics calculations must include force and moment derivatives for the rigid aircraft at a range of flight conditions (e.g. high incidence). Such information is obtained from a combination of design formulae, data sheets, previous experience on similar configurations, CFD (computational fluid dynamics) models and adjustments from wind tunnel measurements (especially where nonlinear or transonic effects are important); the process will depend upon the complexity of the configuration being considered.

In order to allow for static aeroelastic effects on the derivatives and on the distribution of loads, the results from the three-dimensional panel method analysis at zero reduced frequency (or frequency parameter) may be used to determine suitable corrections such that the rigid aircraft model would be in effect quasi-flexible, i.e. will have both derivatives and distribution corrected for flexibility effects. The rigid aircraft aerodynamics corrected for flexible effects would need to be linked to the panel method grid. Such a model could be employed for dynamic manoeuvres (see Chapter 24) if flexible mode coordinates were not to be included.

22.2.2 Aerodynamic Model for Aeroelastics and Gusts

An unsteady aerodynamic model that represents the forces acting on a flexible structure is required for conditions where aeroelastic effects are present (static aeroelastics, flutter, gusts, etc.). Both response-dependent and gust-dependent aerodynamic models are required (see Chapter 10). The modelling sophistication will depend upon the complexity of the aircraft configuration, the dynamic motions expected, the extent that the flight envelope includes the transonic regime and finally the stage in the design process. Flutter is the phenomenon that requires the most accurate and careful aerodynamic modelling.

Either two-dimensional unsteady strip theory or three-dimensional unsteady panel methods are required by the regulations CS/AMC 25.341 and 25.629. However, the panel methods are much more accurate and therefore more widely used. Basic compressibility effects are included as necessary, but these two approaches do not represent transonic behaviour accurately. Since transonic effects are particularly crucial in flutter prediction, the correction of the calculated two- or three-dimensional aerodynamic results using output from steady CFD and wind tunnel studies, where transonic effects can be included, is important.

The strip theory approach is a relatively crude method though modifications can be introduced to account approximately for tip effects; however, the method is sometimes used, particularly in early design calculations and for less challenging dynamic conditions (e.g. low speed aircraft). The basic idea of strip theory was introduced earlier in the book (see Chapter 5) and has been adopted throughout for simplicity of approach. The unsteady strip theory results will be a function of reduced frequency, and displacements/rotations at the structural and aerodynamic reference axes must be related in order to assemble a coupled aerodynamic/structural model in modal space. When performing gust response calculations in the time domain, the indicial lift effects (via Wagner's and Küssner's functions) should be used for two-dimensional strip analysis, together with penetration lags to account for the position of the strips on swept wings and for tailplane effects. This idea was introduced using the examples in Chapter 16.

For more complex configurations (i.e. most commercial aircraft), aerodynamic forces are usually calculated using a three-dimensional unsteady panel approach, such as the doublet lattice method (DL method), though there is an increased use of CFD methods to cater for transonic effects (see later). The three-dimensional panel method (see Chapter 19) makes allowance for handing the interference between multiple lifting surfaces, all of which are represented by panels (e.g. wing, winglet, tailplane, fin, nacelle and fuselage). A sample DL method panel grid for the whole aircraft is shown in Figure 22.7.

The fact that the structural and aerodynamic data are represented on different grids means that a three-dimensional interpolation/spline approach is required to link the mode shapes with the aerodynamic forces on each panel when assembling a coupled aerodynamic/structural model in modal space (see Chapter 20). The use of a panel method on a simple wing structure was introduced in Chapters 19 and 20. Alternatively, and more simply for convenience, the DL results (in the form of the aerodynamic influence coefficient (AIC) matrix) may be effectively condensed down on to strips on the loads reference axis,

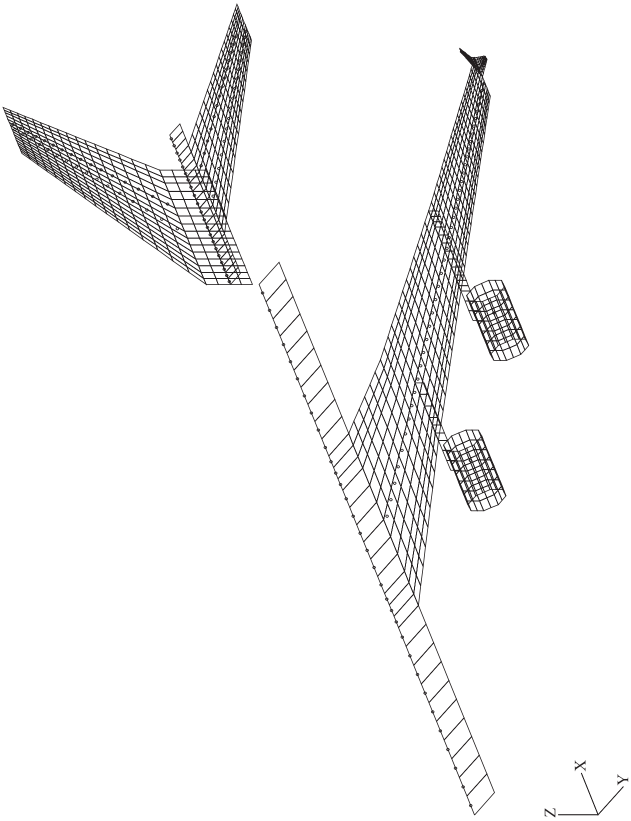

Figure 22.7 Aerodynamic panel grid for the doublet lattice method. Reproduced by permission of Airbus.

thus effectively generating lift and moment coefficients per strip. The approach could be extended when control modes are incorporated.

The aerodynamic model must cater for unsteady effects (i.e. attenuation and phase lag of the aerodynamic forces with respect to the structural motions) so the resulting aerodynamic influence coefficient (AIC) matrix derived from the DL method for oscillatory motion is complex and is a function of the reduced frequency (see Chapter 19); the AIC matrix would therefore be evaluated at a range of reduced frequencies and Mach numbers. Gust dependent effects are based on a harmonic gust input and the AIC matrix from the panel method will allow for gust penetration effects in the frequency domain. When performing gust response calculations in the time domain using a three-dimensional panel method, the frequency domain results for a number of reduced frequencies need to be converted into a time domain representation using the 'rational fraction approximation' discussed in Chapter 20. Unsteady CFD studies can be used additionally to obtain frequency-dependent adjustments to the results.

Aerodynamic matrices for a range of reduced frequencies are required for flutter and gust/turbulence calculations, whereas the zero reduced frequency (quasi-steady) aerodynamics are used for static aeroelastics and manoeuvres.

The aerodynamic model will include terms for both rigid body and flexible modes. This means that at zero reduced frequency, linear rigid aircraft derivatives may be determined (as shown in Chapter 19) and the AIC results may then be corrected using the flight mechanics aerodynamics model. Control surface aerodynamic terms may require greater correction and the sensitivity of results to these values should be studied.

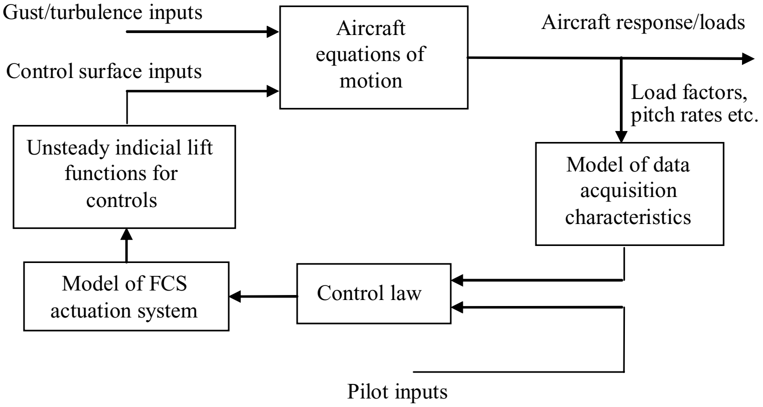
Gust/turbulence inputs
Control surface inputs
Aircraft equations of motion
Aircraft response/loads
Load factors, pitch rates etc.
Unsteady indicial lift functions for controls
Model of data acquisition characteristics
Model of FCS actuation system
Control law
Pilot inputs

Figure 22.8 Representation of aircraft plus the flight control system. Reproduced by permission of Airbus (redrawn with modifications).

Finally, there is a growing interest in performing aeroelastic calculations using coupled CFD/ structure (FE) models. Such a model may be developed for static aeroelastic and flutter calculations (see Chapter 23).

22.3 FLIGHT CONTROL SYSTEM

A nonlinear flight control system (FCS) model will be developed for handling the aircraft (see Chapter 14); it will be coupled with the aircraft dynamic model for a modern commercial aircraft. The FCS commands movements of the aircraft control surfaces depending upon the feedback of information about the aircraft states (e.g. accelerations, rates and air data sensors) and these demands are combined with pilot inputs. The FCS is likely to influence the aircraft loads and aeroelastics behaviour considerably as it will alter the dynamic behaviour of the aircraft (see Chapter 12). A block diagram showing how the FCS integrates with the aircraft model is shown in Figure 22.8. The control law will incorporate multiple control loops as required.

The FCS model nonlinear features may be retained when calculations are performed in the time domain, but it will need to be linearized if a frequency domain solution is to be carried out. Apart from the main function of the FCS of providing ‘envelope protected demand control piloting’, it may also sometimes be used to perform manoeuvre and/or gust load alleviation functions. A gust load alleviation (GLA) system uses measurements of the vertical acceleration of the aircraft to deploy ailerons and spoilers so as to cancel out a proportion of the outer wing gust force generated. A manoeuvre load alleviation (MLA) system uses a similar approach, but is slower acting in order to bring the effective centre of pressure inboard during a manoeuvre. Both have the effect of reducing the wing root bending moment and shear force.

22.4 OTHER MODEL ISSUES

In addition to the stiffness, mass, aerodynamic and control terms, the following models should be available:

(a) a nonlinear large angle landing gear model with oleo, tyre, braking, steering, runway profile, flexible modes, etc. (see Chapters 17 and 25 for more detail);
(b) an engine model with thrust, momentum drag and gyroscopic effects;
(c) a pilot model to allow for the rate of control application.

22.5 LOADS TRANSFORMATIONS

In Chapter 18, it was shown how a transformation could link the response accelerations, velocities and displacements with the control and gust input (if any) to generate the desired internal loads via an auxiliary equation. Part of the required model for loads requires these matrices to be formed for all the quantities that are of interest to the designer.

23

Static Aeroelasticity and Flutter

In this chapter, an outline of typical industrial practice for static aeroelasticity and flutter calculations will be given and related to the earlier chapters in Part II. The certification requirements covering the issues in this chapter are seen primarily in CS/AMC 25.629 under Subpart D, Design and Construction. However, the requirements as written are dominated by considerations of flutter.

23.1 STATIC AEROELASTICITY

There is little specific mention of static aeroelastic phenomena in the certification specifications. The aeroelastic stability requirement (CS 25.629) simply states that 'divergence, control reversal and any undue loss of stability and control as a result of structural deformation' should be evaluated. In CS/AMC 25.629, it is stated that nonoscillatory aeroelastic instabilities (divergence and control reversal) should be analysed to show compliance with CS 25.629 and that loss of control effectiveness should be investigated, but little detail is specified.

However, static aeroelasticity appears indirectly in a number of situations via the effect of structural deformation on the rigid aircraft aerodynamic model and therefore upon gust and manoeuvre loads, etc. It is an important issue that must be considered.

23.1.1 Aircraft Model for Static Aeroelasticity

The aircraft model is traditionally very much the same as that employed for flutter and gust considerations, namely a whole aircraft beam or condensed FE model, but because the calculations for static aeroelastic effects are steady, no dynamic mass and damping matrices are needed. There is no requirement for the control surface modal behaviour to be represented except where it can contribute significantly to the loss of effectiveness through its distortion (including control circuit stiffness). Such a model would be based on rigid body/flexible modal coordinates, with the output converted into physical space where required; however, it is possible to perform calculations directly in physical coordinates by expressing the model differently.

The aerodynamic model could be formulated using two-dimensional strip theory but a three-dimensional panel method such as the vortex lattice method is preferable. Only the zero reduced frequency terms are required for this steady case, with the AIC results scaled to match wind tunnel corrected rigid body aerodynamic data (and steady CFD results if available) to correct for transonic effects. Control surface aerodynamic terms need to be included. The right-hand side load vectors are required for aerodynamic terms of zero incidence and control rotation, together with a $1g$ inertial load. In Chapter 13, the equations for a combined rigid body/flexible aircraft illustrated this model, with such load vectors being included.

© 2007 John Wiley & Sons, Ltd

23.1.2 Control Effectiveness/Reversal

The certification specifications require that the aircraft be adequately controllable over the flight envelope so that there is adequate effectiveness at the boundary of the flight envelope. For control effectiveness/reversal calculations, there are two possible approaches (illustrated in Chapter 9 for a simple wing/control model). In the first method, the structural model is constrained at, say, the wing root (or at a fuselage station aft of the wing) and then an aileron (or elevator) control surface rotation would be applied. For the flexible aircraft, the incremental deformation of the wing (or fuselage) component due to control rotation is obtained from the solution of the equations of motion using the right-hand side control vector; the internal load (such as the wing or fuselage bending moment) at the constraint point would be determined using, for example, the force summation method (described in Chapter 18). The internal load for the rigid aircraft would be derived directly from the distribution of aerodynamic forces due to control rotation. The ratio between the flexible and rigid aircraft load results then indicates the control effectiveness under this manoeuvre initiation (i.e. zero roll or pitch rate).

In the second method, the aircraft model is unconstrained and the aircraft is allowed to roll (or pitch) at a constant rate with linear downwash effects due to roll (or pitch) motion included. Here the ratio of the resulting angular rates for the flexible and rigid aircraft will indicate the control effectiveness. The two approaches will yield the same reversal speed (corresponding to zero effectiveness) but will have different behaviour at lower air speeds. Note that the control effectiveness could be explored further using the dynamic manoeuvre model with FCS (see Chapter 15).

23.1.3 ‘Jig Shape’ – Flexible Deformation and Effect on Loads Distribution

An important issue to address for an aircraft is the relationship between the so-called ‘jig shape’ (i.e. the unstrained aircraft shape when supported in the jigs during manufacture, with no inertial/aerodynamic forces acting) and the symmetric flight shape desired at an optimal (i.e. reference) cruise flight condition; the flight shape has an important influence on the drag acting. The difference between the two shapes is due to elastic deformation under aerodynamic and inertia loads (for a rigid wing there would be no difference).

Assuming the jig shape were to be known and taken as a reference, the trim solution of the static aeroelastic equations to a right-hand side vector (a combination of zero incidence and inertial terms) would yield the flexible deformation and hence the flight shape, as well as the elevator (or stabilizer) angle for trim. The distribution of the aerodynamic forces may then be compared to those for the rigid aircraft and the flexible effects seen. Of course, the jig shape is actually unknown initially though the desired final flight shape and the aerodynamics associated with the design point will be known; an inverse calculation can be performed to determine the jig shape needed to achieve the required flight shape. The distortion between jig and flight shapes is calculated by applying the aerodynamic and inertia loading to the aircraft stiffness representation. Having established the jig shape needed for the optimal flight shape, the calculation of other suboptimal flight points at other flight conditions can be undertaken.

Errors in the predicted jig shape can arise from a number of sources, e.g. errors in the stiffness and mass representation in the structural model and errors in aerodynamic load prediction. Indeed, however refined the aerodynamic theory is, errors in the structural model can spoil the results because of flexibility effects. An inaccurate jig shape will lead to errors in the flight shape; this can mean a greater flight drag than was anticipated when the flight shape was proposed and therefore a suboptimal cruise performance.

The influence of flexible effects in altering the lift distribution was shown in Chapter 8 for a simplified wing. Then the trim calculation for a whole aircraft with rigid body/flexible modes was presented in Chapter 13; this process permitted determination of the trim state, airframe deformation and aerodynamic load distribution.

23.1.4 Correction of Rigid Body Aerodynamics for Flexible Effects

In the previous section, the use of the rigid body/flexible aircraft model to calculate the flexible deformation in steady flight was described and the resulting change of load distribution indicated. In some cases, it could be desirable to use the rigid body equations without the flexible modes (so reducing the model size significantly), so it would then be helpful to correct the rigid aircraft derivatives for flexible effects. By taking the rigid body/flexible equations and removing the flexible degrees of freedom using an approach akin to that of Guyan reduction (see Appendix D), a set of rigid body equations with steady derivatives corrected for flexible effects would be available. This approach was illustrated briefly in Chapter 13.

Having corrected the derivatives themselves, the shape of the rigid aircraft aerodynamic load distribution could be modified to correspond to that found for the flexible aircraft. A quasi-flexible 'rigid' aircraft model would then be available which represented the total forces/moments as well as the distributions, but with flexible effects included. Such a set of corrected derivatives and distributions may also be incorporated in, for example, the flight mechanics model as well as the static aeroelastic model.

23.1.5 Divergence

The divergence condition must be sought using a combined rigid body/flexible model as the phenomenon may occur for either a flexible or rigid body mode (such as the short period mode) or combination of the two. As flight speed increases, a pair of oscillatory roots reduces to zero frequency and becomes two stable real roots on the root locus diagram (see Chapter 7). With a further increase in speed, one root moves towards $-\infty$ and the other root moves towards zero; on the flutter diagram, both roots would have 100 % damping and zero frequency. Divergence occurs when one real root crosses the imaginary axis (i.e. becomes positive); in the flutter 'world' this would correspond to -100 % damping and divergence might be seen on the flutter plot as a curve moving from 100 to -100 % in a single frequency step. Divergence for a simple wing example is considered in Chapters 8 and 11. The concept is mentioned for a whole aircraft with rigid body/flexible modes in Chapter 15.

23.1.6 CFD Calculations

It was pointed out in Chapter 22 that steady CFD calculations allow correction of aerodynamic results for transonic effects. CFD is becoming more widespread in its use. For example, a coupled FE/CFD model could be employed to obtain an improved accuracy in determining the flight shape and drag for suboptimal conditions.

23.2 FLUTTER

The flutter requirements are covered in CS/AMC 25.629 and should be consulted for detailed explanations.

23.2.1 Aircraft Model for Flutter

For linear flutter calculations, a modal model composed of whole aircraft rigid body and free–free flexible modes is normally used, either based on a beam or condensed FE model with a lumped mass distribution, as described in Chapter 22. In particular, the model should represent control surface rotation (including bending and torsional flexible modes) as well as accurate wing/pylon/engine attachment characteristics, since flutter often involves these components. Control surface actuators may be modelled at several levels, e.g. a spring, spring/damper or full linearized hydraulic model. Also, areas where stiffness may be reduced locally should be modelled adequately (e.g. cut-outs/doors) as stiffness is a key parameter in flutter.

An unsteady aerodynamic model is required with terms evaluated at a range of reduced frequencies. Either a modified two-dimensional strip theory or (more usually) a three-dimensional panel method is employed, depending upon the aircraft configuration, though the latter is much more accurate, especially for intersecting lifting surfaces (e.g. wing/winglet), in which case the effect of steady aerodynamic forces and flexible deformations should be included to allow for in-plane coupling effects. Also, the control surface aerodynamic representation is very important for flutter calculations and careful adjustments to hinge moment terms are carried out based on wind tunnel test results. Once again, steady CFD and wind tunnel results are used to adjust the aerodynamic results to make allowance for transonic effects. In addition, unsteady oscillatory CFD calculations enable corrections to be made to the frequency-dependent aerodynamic behaviour.

The influence of damping is represented, in essence, either by a value per mode assumed at 0.02 structural (or 1 % critical viscous) damping or by values obtained from test (see Chapter 26). Thus far, the flutter model is similar to that employed for gusts. The FCS model used for flutter considerations is generally linearized, though the model will still be frequency (and therefore reduced frequency)-dependent; the FCS introduces additional equations into the aeroelastic modal model by involving feedback between structural response and control demand.

23.2.2 Flutter Boundary – Normal and Failure Conditions

The aircraft must be designed to be free from aeroelastic instability for all normal configurations and conditions (i.e. fuel, ice, FCS, thrust settings) within the aeroelastic flight envelope (CS/AMC 25.629); the flight envelope considered for flutter is the normal V_D/M_D versus altitude envelope, but enlarged by 15 % in EAS at both constant Mach number and constant altitude. This enlarged envelope provides a margin of safety for what is an extremely difficult phenomenon to predict accurately. There should be an adequate margin of stability at the V_D/M_D boundary and no rapid reduction in stability near to it. The freedom from flutter must normally be demonstrated by both calculation and flight test (see Chapter 26). There is no quantitative prescription of what defines an acceptable minimum damping in flight for any mode.

Freedom from flutter must also be demonstrated by calculation for a number of failure cases, described fully in CS/AMC 25.629, namely critical fuel loading conditions, failure of any flutter control system, inadvertent ice accumulation, failure of a key structural element supporting a large mass element, various engine failure conditions and potential damage scenarios. Because of the limited probability of occurrence of such failures, the fail-safe clearance envelope within which freedom from flutter must be demonstrated is less extreme than for normal conditions.

Detailed guidance is given in regard to various types of control surface/actuator failure in CS/AMC 26.629. The aircraft must be free from flutter in the presence of freeplay in the control system (represented in a linear model by a stiffness reduction). The FCS and structure should not interact to produce an aeroelastic (or aeroservoelastic) instability. Also, special conditions are specified in CS 25.302, Appendix K, for consideration of flutter in the face of a systems failure likely to impact upon the aircraft dynamic behaviour.

Guidance is given in regard to the incorporation of balance weights and passive flutter dampers. Also, there is sometimes a requirement for investigation of whirl flutter involving gyroscopic effects from engines.

23.2.3 Flutter Calculations

The stability of the aeroelastic equations in modal space is investigated using a suitable approach that allows for the frequency dependency of the aerodynamics (and also the linearized FCS), such as the 'p–k'

method; the flutter condition is 'matched' (see Chapter 11) to the aerodynamic behaviour at each air speed depending upon the solution approach adopted. The calculations are performed for a range of weight, fuel, ice state, centre of mass, engine location, control system characteristics, failure cases, etc. The sensitivity of the flutter results to variation in key parameters, such as the control surface aerodynamics, is examined.

Plots of frequency and damping per mode against air speed or Mach number are examined to study the margins of stability around the edge of the flight envelope as defined above. A sample set of results for a multimode system was shown in Chapters 11 and 20. Such solution issues were considered in Chapter 11 for simplified two or three degree of freedom models; however, to keep the model complexity to a minimum, no rigid body modes were included there. The combination of rigid body and flexible modes was considered in Chapters 13 to 17.

23.2.4 Aeroservoelastic Calculations

In CS/AMC 25.629 it is stated that if control/structure coupling is a potential problem, then aeroelastic stability analyses should include the control system, actuator characteristics, etc. The aeroservoelastic behaviour of the aircraft will need to be investigated using the airframe equations extended to include the linearized flight control system equations; control law stability margins should be determined, together with a study of robustness and potential failure cases. Time domain analyses allow the study of nonlinear FCS behaviour, plus failure case scenarios (CS 25.302, Appendix K), but then a time domain unsteady aerodynamic representation (e.g. the rational fraction aerodynamics approach described in Chapter 20) will be required. Chapter 12 provides a brief introduction to aeroservoelastic analysis.

23.2.5 Nonlinear Aeroelastic Behaviour

There is an increasing interest in predicting the aeroelastic behaviour when nonlinear effects are present; e.g. structural nonlinearities include freeplay in the control surfaces, aerodynamic nonlinearities involve oscillatory motion of the shock waves in transonic flow and control system nonlinearities include rate limits on the motion of the control surfaces. Chapter 11 provides a brief description. The prediction of nonlinear aeroelastic behaviour, particularly in the transonic flight regime, is an area of current research interest using CFD/FE coupled models with time-marching solutions, though more efficient reduced-order modelling methods are also being explored.

24

Flight Manoeuvre and Gust/ Turbulence Loads

In this chapter, the different ways in which flight manoeuvres and gusts are handled in industry when seeking type certification are discussed. The wide range of different cases that have to be considered is examined. From these bookcase and rational design calculations, the internal loads can be determined which then are used to calculate the stresses.

In Chapter 25, the corresponding issue of ground manoeuvre loads will be considered. Also in Chapter 25, the calculation of stresses from internal loads (via loads acting upon components) and loads sorting will be considered briefly. Once again, it should be pointed out that the treatment in this book stops at the generation of shear forces, bending moments, torques, etc., and does not cover calculation of stresses in any detail.

24.1 EVALUATION OF INTERNAL LOADS

In all the following manoeuvre/gust cases, the internal loads and other interesting quantities may be extracted from the response and applied force time histories using the ‘mode displacement’, ‘mode acceleration’ or ‘force summation’ approaches (CS/AMC 25.341). The ‘force summation’ method was illustrated in Chapter 18, showing how suitable transformation matrices allowed summation of inertial and aerodynamic effects via an auxiliary equation when generating internal loads.

It should be noted that in this book, ‘internal’ loads (as far as the whole aircraft is concerned) are taken to be bending moments, shear forces, axial forces and torques (‘MAST’ loads, which are ‘internal’ because the structure has to be ‘cut’ to expose them; see Chapter 6). The loads and aeroelastics department (or equivalent) would generate such internal loads from aerodynamic and inertia forces, calculated using the aircraft dynamic response. The issue of terminology where these internal loads are sometimes later referred to as external loads will be addressed later in Chapter 25.

24.2 EQUILIBRIUM/BALANCED FLIGHT MANOEUVRES

In this book, the distinction has been made between equilibrium and dynamic manoeuvres, but in some cases there is a somewhat ‘fuzzy’ boundary in that some load cases may be solved using an equilibrium balanced analysis or alternatively the same requirements may be met using a rational calculation (see Chapter 21). However, the distinction is considered helpful and will be made as clear as possible, given the differences in practice likely to be found within the industry.

Symmetric equilibrium manoeuvres involve steady motion of the aircraft with a steady pitch rate (zero pitch acceleration). In Chapter 13, it was shown that a pull-out from a dive, a bunt or a steady banked

Introduction to Aircraft Aeroelasticity and Loads J. R. Wright and J. E. Cooper
© 2007 John Wiley & Sons, Ltd

turn all fall into this category. However, in the certification process, such cases are not considered as separate manoeuvres. Instead, the balanced equilibrium flight case involving the application of D'Alembert's principle and the introduction of a load factor n is considered in conjunction with the flight manoeuvre envelope. The equilibrium manoeuvre case is in effect a bookcase, since it does not require a full response simulation; however, it is not completely artificial since such a balanced flight case is realizable in practice unless aerodynamic or FCS limitations prevent large load factors being achieved. It is particularly useful early in the design process when the flight control system (FCS) design is not available or mature.

Asymmetric equilibrium manoeuvres are also possible to analyse. In particular a steady roll rate or a steady sideslip may be viewed as balanced equilibrium steady-state cases where the moment due to control application is balanced by aerodynamic restoring moments. If aerodynamic and inertia couplings between the yaw/sideslip/roll motions are permitted, then the steady roll rate and steady sideslip are realizable conditions (and could be determined by a trim solution of the full equations, applying all control surfaces), but if the approach neglects coupling terms (e.g. pure roll is assumed) the condition is somewhat artificial. In addition, for cases where a control rotation is suddenly applied, the moment due to the control may be balanced by an inertia couple. This is not a steady-state condition but is an artificially generated balanced condition for manoeuvre initiation which leads to conservative angular acceleration and loads estimates. In essence, all these cases are bookcases; however, when using a full dynamic model, some cases are also rational since they can be achieved (see later).

Note that the symmetric equilibrium manoeuvre case was considered extensively in Chapter 13 in order to illustrate the effect of introducing a flexible mode. The asymmetric rolling and yawing cases were also considered briefly in the same chapter for a rigid aircraft with reduced models (Lomax, 1996) to illustrate the concepts of solving for the bookcase manoeuvres.

24.2.1 Aircraft Model for Equilibrium Manoeuvres

The rigid body characteristics for the whole aircraft including the control influences are represented for flight manoeuvres, possibly with symmetric and asymmetric equations considered separately. In CS 25.301, the statement is made that: 'if deflections under load would significantly change the distribution of internal or external loads, this redistribution must be taken into account'. This comment means that the static aeroelastic effects must be accounted for in the model used; i.e. the effect on the aerodynamics of distortion under load must be included. The model is in essence a whole aircraft static aeroelastic model. The model should include thrust and drag representations for the symmetric pitching case and allow for these forces to be out-of-line. Also, nonlinear aerodynamic and FCS effects that would influence the trimmed condition are included, which means that a nonlinear solution of the balanced case may be required. The approach shown in Chapter 13 is similar to that employed in industry for the symmetric manoeuvre. The asymmetric manoeuvre involves a simplified model with certain lateral coupling terms neglected, as illustrated briefly in Chapter 13.

An alternative approach might be to employ a trimmed solution of the large angle nonlinear flight mechanics model introduced in Chapter 14, with all coupling terms present and steady aeroelastic effects included.

24.2.2 Equilibrium Flight Manoeuvres – Pitching

The certification specifications for symmetric balanced pitching manoeuvres (CS 25.321 and 25.331(b)) require that the aircraft limit load strength is met at each combination of air speed and load factor, both on and within the flight manoeuvre envelope (as defined in CS 25.333, based on design speeds defined in CS 25.335 and load factors in CS 25.337), for critical altitudes, weights, centres of mass and thrusts. CS 25.337 allows for the possibility of considering reduced load factors where the physical limitations (such as aircraft stall) would prevent the prescribed load factors being achieved for specific aircraft conditions.

Sufficient points must be investigated to ensure that the maximum load on each part of the aircraft is obtained. The flight manoeuvre envelope was introduced in Chapter 13.

When the manoeuvres involve the aircraft flying in a region where the aerodynamic behaviour is nonlinear, the solution would take this into account. Also, the impact of the FCS on loads must also be accounted for, including potential failure cases. The FCS and aerodynamic limitations (such as stall) may prevent certain balanced manoeuvre conditions on the boundary of the flight envelope from being achieved, and these may be used to limit the load developed within the ‘target conditions’ set by the airworthiness requirements, provided the manufacturer can justify that the constraints applied really exist.

24.2.3 Equilibrium Flight Manoeuvres – Rolling

Here, the rolling manoeuvre conditions described in CS 25.349(a) and Lomax (1996) will be considered using a balanced analysis. The unsymmetrical gust case is covered later. Rolling manoeuvres are assumed to be superimposed upon steady symmetric flight cases defined by a load factor of zero and two-thirds of the maximum load factor for design; the latter case, for example, could correspond to a manoeuvre in which the direction of turn of the aircraft is reversed while remaining at a constant load factor.

Note that cross-coupling effects between roll and yaw degrees of freedom may be neglected for this requirement though they would certainly not be for more fully rational calculations. Torsional flexible deformation should be allowed for. The rolling conditions specified in the certification requirements are therefore nominally of the bookcase type, but the option for a rational calculation is available. The roll manoeuvre contributes to wing and empennage design considerations.

The first condition to be examined is that for a steady roll rate. This is in essence a steady-state solution of the lateral equations with zero roll acceleration and with the rolling moment due to aileron balanced by the aerodynamic moment from the roll damping effect. The other case considered is that of maximum roll acceleration; in the absence of a more rational calculation, the rate of roll would be assumed to be zero, with the aileron rolling moment balanced by a roll inertia couple. This roll initiation condition is conservative. The treatment corresponds to the statement in the requirement that unbalanced aerodynamic moments must be reacted by inertia effects in a rational or conservative manner.

The aileron inputs are defined such that at V_A, the aileron should be deflected suddenly to its maximum value, whereas at V_C and V_D the aileron application should yield respectively a roll rate equal to, or one third of, the roll rate obtained for V_A.

These two cases (i.e. steady roll rate and maximum roll acceleration) may therefore be solved as bookcases via the balanced conditions described above, using, for example, simplified models such as the one in Lomax (1996) where a roll-only equation of motion is shown, with approximate aeroelastic effects included. The basic principles are described in Chapter 13.

Alternatively, the possibility exists to perform a more rational simulation using a mathematical model with five or six rigid degrees of freedom, representing each of the previously mentioned conditions of roll initiation, maximum achieved roll rate and reversal. Indeed, such an approach may be the most practical for an aircraft with an electronic FCS in which the control surface deflections are not directly proportional to the pilot demand through the cockpit control device. A problem to be solved for such a rational simulation is how to represent the degree of piloting control imposed on the nonroll degrees of freedom.

24.2.4 Equilibrium Flight Manoeuvres – Yawing

Here, the yaw manoeuvre conditions described in CS 25.351 and Lomax (1996) will also be considered using a balanced analysis. The manoeuvres involve abrupt application of the rudder followed by a sideslip response and are considered for air speeds between V_{MC} (i.e. the minimum control speed with the critical engine inoperative) and V_D. The aircraft is initially in steady flight with wings level and at zero angle of yaw when the rudder is applied. In essence a ‘flat’ manoeuvre is performed where the wings remain level to maximize sideslip by suitable adjustment of the aileron angle; the roll velocity and acceleration are therefore assumed to be zero. This is a somewhat artificial manoeuvre and is a bookcase condition. In calculating the tail loads, the yawing velocity may be assumed to be zero.

The tail loads are obtained for the following scenario, focusing in turn upon each of the following four aspects that the aircraft is considered to experience: (a) a sudden application of the rudder to its maximum value (or to a value limited by rudder pedal force) and this rudder deflection is maintained, so generating (b) an overswing (or overshoot) sideslip angle, then (c) a steady equilibrium sideslip condition is reached with the maximum rudder deflection maintained and finally (d) the rudder is returned suddenly to neutral (i.e. zero deflection).

Clearly, this sequence could be simulated rationally (see later), but as a bookcase it would actually be solved via four separate calculations. For the sudden rudder applications in (a) and (d) above, the applied yawing moment would be balanced by an inertia couple (rather as for the maximum roll acceleration case above) and this would be conservative. Thus, any unbalanced aerodynamic moments would have been reacted by inertia effects in a rational or conservative manner. The steady sideslip condition (c) would be met via the balance of the aerodynamic yawing moments from control and sideslip angles. Finally, the overswing condition (b) would be obtained by assuming a dynamic overswing factor applied to the steady sideslip result (see Chapter 1).

This case may therefore be solved as four bookcases via the balanced conditions described above, using, for example, simplified models such as the one in Lomax (1996) where two and three degree of freedom equations of motion are shown, with approximate aeroelastic effects included. The basic principles for steps (a) and (c) are described in Chapter 13.

24.2.5 Other Load Cases

A further bookcase to cover unsymmetrical loads on the empennage (CS 25.427) involves applying 100 % of the maximum loading from the symmetric manoeuvre on one side of the tailplane and 80 % on the other side. A similar requirement exists for the gust case (see later).

24.3 DYNAMIC FLIGHT MANOEUVRES

In the above section, the cases of balanced equilibrium manoeuvres involving pitch, roll and yaw were considered as bookcases. In this section, the treatment of the aircraft when undergoing some form of dynamic manoeuvre will be considered. The airworthiness requirements are somewhat inconsistent on whether a steady bookcase and/or a dynamic rational simulation is necessary – both are explicitly required in the pitch axis, but not in the roll and yaw axes. The various dynamic manoeuvres must be considered at a range of altitudes, air speeds, weights, centre of mass positions, thrusts, etc. Sufficient points on and within the boundaries of the design envelope must be investigated to ensure that the maximum load on each part of the aircraft is obtained. Modern commercial aircraft may require many thousands of load cases to be considered, given the combination of multiple loading actions, multiple speed/altitude combinations and multiple mass/centre of mass cases. Efficient loads processing then becomes very important.

As seen later for ground loads, the flight manoeuvre load cases are a mixture of bookcase and rational types, with the former described earlier under equilibrium manoeuvres. The rational manoeuvres will normally be solved in the time domain, giving the potential to undertake the solution with nonlinear aerodynamics and/or with a nonlinear flight control system. Some rational manoeuvres are effectively replacing the bookcases with a more realistic simulation involving the FCS, whereas other rational cases allow investigation of failure cases, FCS design, parametric studies, flight test scenarios and any other manoeuvres of interest to the designers in ensuring a safe aircraft. While very little is said about the rolling and yawing manoeuvres in CS-25, manufacturers have built up experience in design calculations and much is captured in special conditions documentation (see Chapter 21).

It is worth noting that the dynamic manoeuvres described by the airworthiness requirements are not necessarily the most severe manoeuvres that can be envisaged, but they have been shown to be sufficiently severe to ensure that the aircraft is designed to be strong enough to withstand the sort of extreme events that may occur in operational service, however improbable. Manufacturers may well choose to consider manoeuvres more severe than those covered by the requirements in order to provide additional protection; any such manoeuvres should bear in mind the training given to pilots on how the aircraft should be flown. If, during other circumstances, such as the flight test, the aircraft is to be intentionally subject to manoeuvres that may potentially be more severe, then the manufacturer/operator must take additional precautions.

24.3.1 Aircraft Model for Dynamic Manoeuvres

There is a number of ways in which the aircraft may be modelled for calculation of dynamic manoeuvres. The first requirement of the aircraft model is that it should represent the rigid body behaviour of the aircraft following deployment of control surface deflection, adjustments to thrust, engine failure, etc. Also, any nonlinear flight control system must be included since this is likely to influence significantly the response dynamics in the manoeuvre since it effectively filters the control inputs; failure cases will also be examined. Some manufacturers use a linear aircraft model where motion is referred to an inertial axes system (rather as used for the gust encounter in Chapter 16), whereas others may employ the nonlinear large angle flight mechanics model where motion is referred to a body fixed axes system, as introduced in Chapters 14 and 15; the latter model is more accurate for manoeuvres where changes in altitude and incidence may be significant. A pilot model would be included.

The aircraft model should include rigid body aerodynamics, validated by appropriate means, such as the wind tunnel test or increasingly in future by CFD calculation, and with nonlinear effects included if deemed important. If the flexible mode natural frequencies are significantly higher than the rigid aircraft modes (e.g. short period, dutch roll), the rigid aircraft model will often suffice for loads calculations, though correcting the rigid body aerodynamics for static aeroelastic effects is necessary if the influence of such terms is important. Both the coefficients and distributions should be corrected for flexible effects to ensure a sufficiently accurate distribution of loads (particularly spanwise). Thus the aim is for handling qualities/flight mechanics and loads models to be as consistent as possible through the design process.

Where the flexible modes are closer in frequency to the rigid body modes and dynamic flexible response is thought to influence the loads significantly, the flexible modes may be combined with the rigid body modes, leading to additional degrees of freedom, i.e. rigid body motions are combined with modal coordinates as described earlier in Chapter 14. Such a model could be used for the landing calculations where flexible mode effects need to be included (see later) or for flight manoeuvres where flexible dynamic effects are expected. The use of an electronic FCS can mean that the frequency range excited by the control surfaces in flight is reduced and therefore that the flexible mode effects are less important. However, if the flexible modes are part of the model, then both rigid and flexible aerodynamics may be included, most likely for quasi-steady aerodynamics (zero frequency parameter). Creating a coherent set of aerodynamic forces that match the unsteady forces and moments from panel methods with wind tunnel derived terms is not straightforward, especially for the rigid body/flexible aerodynamic coupling terms.

The pitch and roll cases considered in Chapter 15 are rational and indicate the kind of approach used, though without any FCS present. A flexible mode is included together with rigid body motions.

24.3.2 Dynamic Manoeuvres – Pitching

The certification specifications cover abrupt symmetric pitching manoeuvres (CS 25.331(c); Lomax, 1996), which fall into the mandatory dynamic rational category. There are two types of manoeuvre, with the movement of the pitch control often termed ‘unchecked’ and ‘checked’.

The abrupt *unchecked* ‘avoidance’ manoeuvre involves the aircraft in steady level flight at V_A, when the cockpit pitch control (and hence also the elevator in a conventionally controlled aircraft) is suddenly pulled straight back so as to yield an extreme nose up pitching acceleration; typically, the elevator motion may be idealized as a ramp input up to the maximum value feasible. The aim is to provide a design case for the vertical tail load. The manoeuvre need not proceed beyond the point where the positive limit load factor (on the manoeuvre envelope) or where the peak tail load is reached. The aircraft response must be considered so this is nominally a rational case (although peak tail load usually arises from the initial elevator displacement and is reached quite quickly).

The other category is the *checked* manoeuvre with the aircraft in steady level flight between V_A and V_D. In essence, the cockpit pitch control device is moved sinusoidally through three-quarters of a cycle at the natural frequency of the short period motion, though the effect of varying frequency may be explored. The nature of the manoeuvre is such that high pitch accelerations are generated; a pitch motion is initiated and then a recovery begun, in such a way that causes the aircraft to respond significantly in its short period motion. It should be noted that the specifications do not require the pilot to move the elevator back and forth over more than three-quarters of a cycle, nor to consider a short period of greater than 4 s. For aircraft with an electronic FCS the prescribed input will not necessarily translate into a severe elevator command. There may also be some ambiguity about what constitutes the ‘short period motion’ due to the interaction of aircraft and FCS; it may be more appropriate in these circumstances to undertake a frequency search.

For a nose up checked pitching manoeuvre, the amplitude of the cockpit control motion may be scaled down so that the aircraft just reaches the positive limit load factor. Also, for a nose down checked pitch manoeuvre, the input may be scaled down such that the aircraft does not go below a normal acceleration of $0g$ at the centre of mass. If the defined elevator motion for three-quarters of a cycle at the maximum feasible value does not cause the aircraft to reach the positive limit load factor, then the elevator may be allowed to remain at its maximum value after a quarter of a cycle for a period of up to 5 s (i.e. a ‘stretched’ sine), until the limit positive load factor is reached, before completing the remaining half cycle of motion. In these checked manoeuvre cases, conditions are given for when the simulation should stop. It is assumed that the final return to the trimmed condition is carried out smoothly.

In Chapter 15, an example of such a flexible heave/pitch model that could be used for a simple rational calculation was considered.

24.3.3 Dynamic Manoeuvres – Rolling

The rolling manoeuvres described in CS 25.349(a) and Lomax (1996) were considered earlier as equilibrium balanced manoeuvres, with steady roll rate and maximum roll acceleration cases. The rolling conditions specified were therefore nominally of the bookcase type but the option for a rational calculation was said to be available to obtain less conservative results by considering a more representative model and simulation.

One possibility for a simple rational calculation (Lomax, 1996) is to determine, for example, the dynamic response to a ramp up/constant/ramp down aileron deflection profile. The steady roll rate condition would be reached and the resulting roll accelerations would then be lower than for the simple roll initiation bookcase.

Note that, in practice, fully rational manoeuvres would use a model where FCS and roll/yaw/sideslip coupling effects are represented; these more advanced models might be employed in, for example, simulating the steady roll rate and maximum roll acceleration bookcases in a rational manner to gain less conservative results. Other cases may also be examined (see later). In Chapter 15, an example of such a flexible roll model that could be used for a simple rational calculation was considered.

24.3.4 Dynamic Manoeuvres – Yawing

Here, the yaw manoeuvre conditions described in CS 25.351 and Lomax (1996) involve application of the rudder followed by sideslip overswing, steady sideslip and return to neutral. These were treated as four separate bookcase manoeuvres, but the option for a rational calculation is available.

One possibility for a rational calculation (Lomax, 1996) is to determine, using a simplified two or three DoF model (with aeroelastic effects included), the dynamic response to an abrupt rudder input, leading to a dynamic sideslip response including the overswing, followed by the rudder return to neutral. No examples of a dynamic yaw/sideslip model were shown in Part II of this book.

Note that, in practice, fully rational manoeuvres would use a model where FCS and roll/yaw/sideslip coupling effects are represented; these more advanced models might be employed in, for example, simulating the abrupt rudder application bookcases in a rational manner to gain less conservative results. An issue here is to decide how to represent appropriate piloting action to maintain appropriate control in the roll and pitch axes. Other cases may also be examined (see later).

24.3.5 Engine Failure Cases

The unsymmetrical load conditions arising from failure of what is deemed to be the critical engine are considered in CS 25.367. Failures due to fuel flow interruption (a limit case) and mechanical failure of the engine (an ultimate case) must be investigated. Firstly, following an engine failure, there are two relevant steady-state conditions, namely maximum sideslip reached with zero rudder and rudder angle required for zero sideslip. Secondly, a corrective application should be considered, with the rudder applied when maximum yaw velocity is reached (but not earlier than after 2 s). The simulation should include thrust decay and drag build-up effects (more severe for the ultimate failure case) as well as the FCS. Thus, in essence, bookcase or rational calculations may be carried out; in Lomax (1996) simplified linear equations are presented.

24.3.6 Other Load Cases

A fully rational calculation may be carried out to study other proposed failure cases or flight test scenarios, to examine more realistic control actions, to assist in FCS design and to carry out parametric studies (e.g. sensitivity), as well as to perform certification calculations. One issue of growing importance is any failure case involving the FCS and causing control surface runaway or continuous oscillation. Such scenarios would be investigated by rational calculation (CS 25.302, Appendix K), firstly considering loads at the time of occurrence and secondly modified loads that could occur during continuation of the flight.

Other flight cases, such as those specified in CS-25, Subpart B, or flight cases of concern may be investigated by rational calculation as well as by flight test. The model may be validated by comparison with flight test data (including loads; see Chapter 26).

24.4 GUSTS AND TURBULENCE

A considerable effort over many years has been put into deciding how to lay down the certification requirements for loads in gusts and turbulence, with the methodologies becoming more rational and complex (Hoblit, 1988; Lomax, 1996). An extensive experimental program involving measurements on a number of in-service aircraft, namely CAADRP (Civil Aircraft Airworthiness Data Recoding Program), was carried out to help decide upon design gust and turbulence levels using a statistical basis, e.g. the amplitude of the discrete gust is targeted to the 1 in 70 000 flying hours probability level and the variation in amplitude with wavelength adjusted to maintain an equal probability of occurrence. In this section, the main gust and turbulence cases required for certification will be considered (CS/AMC 25.341).

Real gusts and turbulence in the atmosphere tend to occur in patches and to be isotropic in all three dimensions. Airworthiness requirements in general do not require this level of detail in modelling. Rather, for a conventional aircraft at least, the main lifting surfaces respond predominantly to inputs in one or other directions, wings and horizontal tailplane respond to the symmetric vertical component, fins and rear fuselage to the lateral component and high drag devices such as flaps to the fore-and-aft component. Consequently, airworthiness requirements simplify the required analyses to a one-dimensional form only, subject to certain safeguards introduced by 'round-the-clock' gusts, etc. Furthermore, the range of input turbulence manifestations is covered only by the need to consider the two extremes of a single, isolated, 'discrete gust' and of a continuous Gaussian turbulence field. Patches of real turbulence are highly unlikely to be either 'discrete' or 'continuous', but by covering these extremes it is possible to assure robustness of the aircraft structure to gusts and turbulence.

There have been attempts over the years to postulate a gust and turbulence regime that could replace the separate 'discrete' and 'continuous' requirements under one umbrella. One such example, the statistical discrete gust (Jones,1989), allows a range of equiprobable gust patterns, containing the potential to represent complex turbulence shapes for those parts of the aircraft susceptible to more continuous excitation, while allowing for more discrete inputs to those parts of the aircraft more susceptible to these. The so-called matched filter theory (Scott *et al.*, 1993) provides the worst case combination of gust velocities when an aircraft is considered to be linear; however, a search algorithm is required when nonlinearities are present. All such approaches, while being academically attractive, have so far had practical implementation difficulties which have caused them to fail to gain widespread support.

(As an aside it may be of interest to note that limit gust and turbulence have been defined so that they represent the level of severity that a single aircraft might expect to encounter once per lifetime. This implies that the limit load should be encountered less frequently than once per lifetime, allowing for the probability that the aircraft is unlikely to be at its most critical mass/centre of mass/flight condition at the time of the encounter. See also Chapter 21.)

24.4.1 Aircraft Model for Gusts and Turbulence

The aircraft model will include rigid body and flexible modes referenced to the inertial axes system, with the response generally solved in modal coordinates. Structural damping would normally be included (see the model for flutter in Chapter 23). The response dependent and gust-dependent aerodynamics will be unsteady and available at a range of reduced frequencies; typically two-dimensional strip theory (modified) or a three-dimensional panel method such as the DL (doublet lattice) method would be employed (incompressible/compressible, depending upon the complexity of the aerodynamic configuration and flight case). The three-dimensional panel approach (see Chapter 19) will account for the penetration effects of the swept wing and of the tailplane whereas the two-dimensional strip theory would require the penetration effect to be included explicitly. The aerodynamic model was discussed in Chapter 22.

For the response to continuous turbulence, the aerodynamic matrices evaluated at different reduced frequencies would be interpolated to allow frequency domain spectral calculations to be carried out (see Chapter 16). On the other hand, when calculating the response to a discrete gust in the time domain, either two-dimensional indicial lift functions (i.e. Wagner's and Kussner's functions) may be used with two-dimensional strip theory or else the frequency domain aerodynamic forces may be transformed into a time domain representation using a 'rational fraction approximation' (see Chapter 20).

The aircraft model should include models for all relevant modes of any flight control system if any coupling with the structural response is possible. It should also include thrust and gyroscopic effects for the engines.

24.4.2 Discrete Gust Loads

In the certification requirements for discrete gusts, the aircraft is considered to be in level 1*g* flight and subject to symmetric vertical and lateral gusts of the '1-cosine' type introduced earlier in Chapter 16. The incremental loads due to the gust would subsequently be combined with the steady 1*g* flight load solved using a model allowing for static aeroelastic effects (e.g. equilibrium manoeuvre model). Gusts in both positive and negative senses would be considered.

Dynamic response calculations are performed either by direct simulation in the time domain (most suitable if nonlinear effects need to be considered), by convolution or by employing the Fourier transform and impulse response function. These approaches were introduced in Chapters 1 and 2. The approaches are rational and similar in principle to the calculations introduced in Chapter 16. Limit loads must be determined for critical altitudes, weights, centres of mass, air speeds, thrusts, etc. A sufficient number of gust gradient distances H (equal to half the gust wavelength) in the range 9 m (30 ft) to 107 m (350 ft) need to be investigated such that critical responses are found for each load quantity. When a stability augmentation system is employed, any significant system nonlinearity should be taken into account.

The design gust velocity U_{ds} (i.e. the maximum value of the '1-cosine' gust) is expressed in terms of a reference velocity U_{ref}, a flight profile alleviation factor F_{g} and the gradient distance H (in ft) via the formula

$$U_{\mathrm{ds}} = U_{\mathrm{ref}} F_{\mathrm{g}} \left(\frac{H}{350} \right)^{1/6}, \tag{24.1}$$

Thus the longer gusts have a larger gust velocity. For air speeds between V_{B} and V_{C}, the reference gust velocity reduces linearly from 17.07 m/s (or 56 ft/s) EAS at sea level to 13.41 m/s (44 ft/s) EAS at 4572 m (15 000 ft), and again to 6.36 m/s (20.86 ft/s) EAS at 18 288 m (60 000 ft); these values are halved at V_{D}, with values at intermediate air speeds given by linear interpolation. The flight profile alleviation factor F_{g} increases linearly from the sea level value (a function of weight and maximum operating altitude information) to 1.0 at the operating altitude. The intent of this flight profile alleviation factor is to place reduced weighting on those altitudes within the flight envelope where the aircraft is less likely to fly at the design gust speeds.

If a balanced load distribution for the aircraft is required at any instant of time during the response to a discrete gust, then time-correlated results must be used, i.e. all responses and internal loads (shear forces, etc.) are extracted at the same time in the simulation.

Finally, note that a specific requirement is included for wing mounted engines, using a discrete gust at different angles normal to the flight path and also a pair of vertical and lateral gusts in the most severe combination or as a 'round-the-clock' gust.

24.4.3 Continuous Turbulence Loads

The aircraft dynamic response to vertical and lateral continuous turbulence needs to be taken into account for certification. The approach is a rational one and is similar to the methodology introduced in Chapters 16 and 18. A frequency domain power spectral analysis is carried out using the Von Karman turbulence PSD together with a transfer function relating the output response (or load) quantity to the amplitude of a harmonically oscillating gust field. The PSD and root-mean-square value of the response and loads may then be obtained.

The method currently employed in CS-25 for continuous turbulence is the so-called 'design envelope analysis', similar to the way in which discrete gusts are handled; limit loads must be determined for critical altitudes, weights, centres of mass, air speeds, thrusts, etc. An alternative approach, previously popular in the US is 'mission analysis'*;* here, particular mission profiles are set up and analysed in segments using a frequency of exceedance model (Hoblit, 1988). A load spectrum may then be built up by summation of the contributions from all the mission segments and a limit load identified by a nominated frequency of exceedance on that spectrum. The use of one or both of these criteria has been a source of debate between Europe and the US for many years. In fact a 'harmonization agreement' has been reached via the LDHWG (see Chapter 21) to implement what is now the CS-25 text, hence eliminating the mission analysis option. The issue is discussed in detail in Hoblit (1988), but in this book only the design envelope analysis practice will be considered further.

As the name suggests, design envelope analysis is similar to other loads requirements in needing multiple calculations of loads to identify critical mass/centre of mass/flight conditions at which a defined turbulence field is most critical, whereas mission analysis investigates the response to a 'typical' usage of the aircraft. In fact, as mission analysis is both intimately linked to atmospheric turbulence statistics and is capable of representing 'typical' usage of an aircraft, mission analysis remains well suited to producing gust and turbulence load spectra for fatigue and damage tolerance analysis. Its use is expected to continue in this area, at the choice of the manufacturer.

The limit load P_{Limit} for any load of interest (e.g. the wing root bending moment) is determined using the expression

$$P_{\mathrm{Limit}} = P_{1g} \ \pm \ U_{\sigma}\bar{A}, \tag{24.2}$$

where P_{1g} is the corresponding steady $1g$ load for the relevant condition, $\bar{A}$ is the ratio of the root-mean-square incremental load to the root-mean-square (RMS) turbulence velocity and U_{σ} is the limit turbulence intensity; both positive and negative incremental loads need to be considered. Thus the term $U_{\sigma}\bar{A}$ is the incremental load due to turbulence in the limit condition. These issues are discussed in Chapters 16 and 18.

The limit turbulence intensity U_{σ} is a function of air speed and altitude, rather like the reference gust velocity and may be expressed as the product of a reference turbulence intensity $U_{\sigma\mathrm{ref}}$ and the flight profile alleviation factor F_g, namely

$$U_{\sigma} = U_{\sigma\mathrm{ref}}F_{\mathrm{g}}. \tag{24.3}$$

For air speeds between V_{B} and V_{C}, the reference turbulence intensity reduces linearly from 27.43 m/s (or 90 ft/s) EAS at sea level to 24.08 m/s (79 ft/s) EAS at 7315 m (24 000 ft), and then remains constant up to 18 288 m (60 000 ft). These values are halved at V_{D}, with values at intermediate air speeds given by linear interpolation. In essence, the large values of turbulence intensity chosen allow for a probability of exceedance corresponding to the limit condition.

It is worth noting that identifying the 'reference turbulence intensity' for any air speed and altitude does not imply that real continuous turbulence would have an RMS of this magnitude. Rather, U_{σ} can be considered to comprise the product of two scalars, one to represent the RMS of the patch of turbulence most likely to generate a 'limit' gust encounter and another to account for the probability factor to define an appropriate 'extreme event' point on the tail of the assumed Gaussian probability function relative to the RMS (i.e. peak to RMS ratio).

If balanced correlated load distributions are required from a continuous turbulence analysis, then they may be obtained using equiprobable solution results using cross-correlation coefficients (CS-25; Hoblit, 1988). If critical stress values depend upon more than one internal load, then an extension of the correlation coefficient approach is required. The whole statistical processing of results from continuous turbulence is complex and more advanced texts should be consulted if further information is required (Hoblit, 1988).

24.4.4 Handling Aircraft with Nonlinearities

With the advent of widespread use of nonlinear automatic flight control and/or load alleviation systems containing thresholds, authority limits, rate limits, digital logic and nonlinear control surface actuators, there has been a pressing need for manufacturers to be able to address such nonlinearities in the calculation of discrete gust and turbulence loads. In fact, for the calculation of discrete gust loads in the time domain there is no big issue; all that is required is to be able to represent the nonlinear system within the mathematical model used for the simulation.

However, to address continuous turbulence is more difficult and requires an understanding of how the atmosphere model presented in CS 25.341(b) has been simplified. It is particularly important to recognize that it is not the RMS of a load response that is most physically significant for limit loads, rather it is the more extreme peaks or exceedances within the response (after all, if the RMS were the limit load, then the structure would have failed long before an RMS could be established). For a linear Gaussian model (as assumed in the basic airworthiness requirement), this distinction is not important because there will be a constant linear relationship between the RMS and the 'tail' of the Gaussian distribution of the response. However, for a nonlinear aircraft the 'tail' might be stretched or compressed relative to a Gaussian distribution. A large number of different approaches have been studied to the treatment of nonlinearities for determination of continuous turbulence loads, mostly falling into one of two categories:

(a) Linearisation methods, e.g. the 'equivalent gain' method, which, for a limit class of 'symmetric' nonlinearities of the nonlinear gain, seek to identify a linear model with appropriate gain to minimize some error function of the response. This linear model may then be used to produce loads as for a conventional linear formulation.

(b) Timeplane stochastic methods utilize a nonlinear mathematical model of the aircraft to generate a time response to a 'stochastic' gust history, which has been generated to be compatible with the continuous turbulence atmosphere definition. This approach requires a number of issues to be resolved, namely generation of the stochastic gust history itself (Is the turbulence Gaussian?, What is its RMS value?, How much data must be considered for it to be statistically significant?, etc.), the process to identify limit loads in the response (by a level exceedance criterion or by peak counting) and how to generate correlated loads that may be used for structural analysis. CS/AMC 25.341 describes one such solution that has been found acceptable in the past.

24.4.5 Other Gust Cases

The approaches described above are the main gust and turbulence cases that have to be considered and are rational analyses. However, there are a number of other special areas where gusts need to be considered for certification, e.g. loads on high lift devices and other aerodynamic control surfaces, rolling conditions and unsymmetrical loads, fuel and oil loads etc. Some examples will be considered briefly here.

A requirement under the 'Rolling Conditions' heading (CS 25.349) is for the aircraft to be subjected to unsymmetrical vertical gusts, where limit air loads are obtained using the maximum load on the wing from the discrete gust analysis, with 80 and 100 % of this load applied on the two sides of the aircraft respectively. The aircraft is then balanced using inertia forces and so in effect this is a bookcase condition. A very similar bookcase under the 'unsymmetrical loads' heading (CS 25.427) applies to the fin and tailplane. These are of course 'bookcases' designed to give the wing and empennage attachments to the fuselage sufficient robustness to deal with asymmetric loading.

25

Ground Manoeuvre Loads

In this chapter, the treatment of ground loads will be outlined in a somewhat similar manner to that considered for flight manoeuvre and gust loads in Chapter 24. In the certification requirements (CS-25; Lomax, 1996), the load cases are essentially subdivided into the two categories of landing and ground handling, the latter covering taxi, take-off and landing roll, braked roll, turning, jacking, towing, etc. The calculations lead to airframe internal loads, together with landing gear ground, attachment and component loads; the methodologies are similar to those for flight loads except that discrete landing gear loads are also present. As per flight loads, an alternative subdivision would be into 'bookcases' (mainly ground handling) and 'rational' cases requiring flexible or quasi-flexible dynamic modelling (dynamic landing, dynamic taxi, dynamic braked roll, etc.). The calculation of stresses from internal loads (via loads acting upon components) and loads sorting will also be considered.

25.1 AIRCRAFT/LANDING GEAR MODELS FOR GROUND MANOEUVRES

As explained earlier in Chapter 17, the landing gears provide a vital function for landing and ground handling of the aircraft. Landing gears are highly nonlinear for the shock absorber, tyre and gear mechanism. A nonlinear gear model is required for all rationally based requirements, whereas bookcases may (in most cases) use a simpler model as their requirement is usually only to represent a reasonable static closure geometry under the prevailing loading.

Where rational calculations are required, particularly specified in CS-25 for landing and taxi, take-off and landing roll, a nonlinear landing gear model is developed. This model will include the constituent mechanisms of the gear, an oleopneumatic shock absorber with nonlinear stiffness and damping, a dynamic model of the tyre and unsprung mass, and models for braking and steering. A finite element model of the gear should be available to provide modal properties for different shock absorber closures, particularly to cover the spin-up and spring-back behaviour on landing, though a simplified beam model may suffice (see Chapter 17). The ability to interface the model with a runway profile is needed, both for variations in elevation along the runway and also to cater for a convex profile across the runway; the latter is only important for aircraft with more than two main gears, such as the Airbus A340 and Boeing 747. Such landing gear models are developed by both the airframe and gear manufacturers. Nowadays, more use is being made of advanced COTS ('commercial-off-the-shelf') mechanisms software.

The aircraft model depends upon the load case. The landing case employs a flexible aircraft model (often a nonlinear large angle rigid body, i.e. flight mechanics model, based on body fixed axes; see Chapter 14) with quasi-steady aerodynamics for both rigid and flexible deformations (clean wing and high lift) and a fully nonlinear main gear model. The ground handling cases employ a linear airframe model (inertial axes) with rigid body and flexible modes, quasi-steady aerodynamics (rigid body and flexible contributions) and a nonlinear gear model.

Introduction to Aircraft Aeroelasticity and Loads J. R. Wright and J. E. Cooper
© 2007 John Wiley & Sons, Ltd

25.2 LANDING GEAR/AIRFRAME INTERFACE

The gear to airframe attachment arrangement is important in terms of how the loads are transferred. For conventional main gears, the attachment to the airframe via two pintles (providing restraint in $x/y/z$ and y/z respectively) and pinned side brace (providing a tension/compression restraint force) will usually be considered as statically determinate. For nose gears the attachment may be statically indeterminate (or redundant) as the two pintles will provide restraint in $x/y/z$ and x/z, but the drag brace will be attached at two points on either side of the aircraft plane of symmetry; even then, the arrangement will be statically determinate for symmetric loads. Other less conventional gears may have a redundant attachment and so the attachment loads will also depend upon the local airframe flexibility. Any weight benefits gained by structural redundancy will need to be offset against additional analysis costs.

Where rational calculations are carried out, a coupled flexible aircraft/landing gear model will be employed, so the attachment arrangement may be represented whether it is statically determinate or redundant. However, where bookcase calculations are required, any gear model required will depend upon whether the gear/airframe interface is statically determinate or redundant. At best for a statically determinate attachment, no dynamic or flexible model of the gear is required, with specified ground loads simply being transferred to the airframe attachment points via geometric data and simple equilibrium considerations. The shock absorber closure needs to be specified because of its effect on the overall leg length. For a redundant gear/airframe attachment, a gear stiffness model with a simple shock absorber representation coupled to the airframe flexible model is needed in order to allow the attachment loads due to applied ground reactions to be calculated.

25.3 GROUND MANOEUVRES – LANDING

The first category for ground load certification cases is that of landing (CS-25; Lomax, 1996). The fundamental calculation is a fully rational dynamic case (CS 25.473, 25.479 and 25.481) employing a flexible aircraft model (often nonlinear, large angle) and nonlinear landing gear. The aircraft impacts the ground at a prescribed vertical velocity (e.g. 10 ft/s or 3 m/s) for maximum landing weight (MLW), and 6 ft/s at maximum take-off weight (MTOW) with wings level and at a range of air speeds for level and tail down landings. (A trimmed attitude corresponding to the 1*g* condition for a range of air speeds would be a more rational initial condition and then a variety of attitudes could be explored; as it is, a variety of wind speeds would need to be applied in order to match the required initial speed/attitude combinations.)

The dynamic response and loads are calculated using a nonlinear time-stepping solution. Important considerations include the relative contributions of shock absorber stiffness and damping to the vertical load and their correlation with the 'spring back' of the leg due to wheel spin-up drag and the dynamic 'spring-forward' of the leg fore-and-aft bending modes on completion of wheel 'spin-up'. The basic idea, albeit highly simplified in terms of the landing gear model used, was explained in Chapter 17. Note that drop tests (CS/AMC 25.723) on full-scale main landing gears, with and without opposite wheel spin imposed, are carried out to validate the dynamic model.

Apart from the landing calculation providing some design loads for the airframe and gear, the critical vertical leg reaction (i.e. the worst case from all the rational calculations) provides a reference load for bookcases to cover lateral drift and one gear landing (CS 25.483), as well as drag and side load cases (CS 25.485). For aircraft with more than two main gears, and to cater for the case where the gears impact the ground at different times in a nonlevel landing, a rational rolled landing at a reduced descent velocity is carried out.

Additional certification requirements exist to cover emergency landing, and crash simulations are often carried out.

25.4 GROUND MANOEUVRES – GROUND HANDLING

The second and more extensive category for ground load certification is ground handling (CS-25; Lomax, 1996).

25.4.1 Taxi, Take-Off and Roll Case

At present, the only fully rational dynamic ground handling case required for aircraft with two main gears is that for taxi, take-off and roll (CS/AMC 25.491). In this case, which has been treated historically in many different ways, the current recommended process is to carry out dynamic response calculations using a linear flexible airframe model with quasi-steady aerodynamics (rigid body and flexible contributions) and a nonlinear gear model; again the dynamic response and loads will be calculated using a nonlinear time-stepping solution. The basic ‘random’ case employs the San Francisco 28R runway (as surveyed in the 1960s, prior to more recent resurfacing), being seen as a traditionally ‘rough’ runway that was known to lead to high loads and pilot complaints; runs are carried out at a range of steady ground speeds and with zero and maximum thrust (or reverse thrust/braking), depending upon whether take-off or landing is being considered. The basic idea of runway response calculations, albeit significantly simplified, was explained in Chapter 17.

A further rational discrete load case may be carried out by taxiing the aircraft over specified double ‘1-cosine’ bumps, though an alternative bookcase approach is optional. Key considerations here are aircraft ground speed/bump spacing conditions, which give rise to synchronized vertical excitation through the landing gear of the aircraft in heave or pitch or in specific flexible aircraft modes. Note that a bookcase is also specified in order to allow investigation of combined vertical, side and drag loads on the main gear.

25.4.2 Braked Roll, Turning and Other Ground Handling Cases

The remainder of the load cases for ground handling of aircraft with two main gears tend to fall into the bookcase category, though it should be emphasized that the story is far from simple and only an outline will be given here. No aerodynamic model is usually required (or permitted, noting that aerodynamics normally act to relieve the loading on the landing gears) and the specified ground reaction loads (vertical/side/drag) are in most cases reacted by inertia forces (and sometimes moments) distributed over the airframe according to the mass distribution (see Chapter 18). For aircraft with more than two main gears, the approach has had to be altered in many cases, either by adapting the bookcase prescribed ground reaction loads or by carrying out so-called quasi-rational cases where the equilibrium/trim condition is obtained from the model of the quasi-static flexible aircraft (i.e. flexible aircraft and gear stiffness effects represented but no dynamics), with simple nonlinear gear model including leg flexibility.

The braked roll bookcase (CS 25.493) allows calculation of the ground reactions at the gears when a braking force is applied at the braked wheels; both steady and dynamic cases are catered for by specifying different load magnitudes. The steady braking case was shown in Chapter 17. However, a fully rational dynamic or quasi-rational steady approach (based on an aircraft with a shock absorber/tyre model and a brake torque/time input, confirmed using information from brake test data where appropriate) may be employed to justify lower braking loads and to cater for the aircraft with more than two main gears. A reversed braking bookcase (CS 25.507) is also specified.

For turning, a 0.5 *g* bookcase is specified (CS 25.495), with side loads (equal to 0.5 static gear reaction) applied at all wheels and reacted by vertical and side inertia loads distributed over the airframe; this case was shown in Chapter 17. For aircraft with more than two main gears, a rational approach to estimating the distribution of tyre loads in the turn may be required in order to protect against the possibility that any one gear may be subject to a disproportionate loading due to its stiffness characteristics. While it is convenient for the authorities to define and retain the proven conservatism of the turning bookcase, a problem for the manufacturer is that ‘real’ tyres used as part of a rational model may not be able to meet the loads implied by the 0.5 *g* turn.

Additional bookcases cover nose wheel yaw/steering (CS 25.499) by considering the nose gear side load when braking is applied on one side at the main gear and also separately by considering steering torque. Pivoting (where brakes on one side are locked while differential thrust attempts to turn the aircraft, so loading the main gear in torsion) is an additional bookcase related to turning (CS 25.503); this case may need to be revised for redundant gear arrangements. Other bookcases cover towing (CS 25.509) and jacking and tie-down (CS 25.519). Again, in some cases a quasi-rational treatment is required to handle the aircraft with more than two main gears.

As if the picture is not complicated enough, the cases where one or two tyres are deflated (CS 25.511) need to be considered for many of the ground handling cases by applying specified reduction factors. Local redundancy calculations at the wheels may be necessary for the distribution of loads across tyres and bogie units; this is not a straightforward issue. Additional requirements are included to cover the retracting mechanism, wheels, tyres and brakes/braking systems (CS 25.729, 25.731, 25.733, 25.735).

Shimmy studies using a linearised and/or non-linear model may be carried out where appropriate and supplemented by tests.

25.5 LOADS PROCESSING

It should perhaps be emphasized at this stage that the quantities of interest to the designer from loads calculations are more than loads alone but include response accelerations and rates (especially where accelerometer and rate gyros for the FCS are positioned), strains, control forces, values within the FCS loop, aerodynamic pressures, flight mechanics parameters, oleo pressures, etc.

25.5.1 Loads Sorting

The generation of internal loads is a major step in the analysis of the flexible aircraft under static or dynamic loading. As indicated in earlier chapters, a range of calculations will need to be employed so as to cover the many combinations of flight envelope points and mass distributions that could lead to dimensioning loads (i.e. load cases responsible for sizing a particular piece of structure somewhere on the aircraft; see Chapters 18 and 21). Once the appropriate moment, axial force, shear force and torque (‘MAST’) distributions have been determined, often as a function of time, then in essence they need to be processed further (‘sorted’) in order to obtain critical load cases. It is important to use correlated load sets, i.e. loads extracted at the same instant of time to ensure that the loads are balanced in any subsequent analysis; note that correlated loads for turbulence data need special treatment (Hoblit, 1988).

The loads sorting process aims to extract those correlated load sets that identify the most positive, or most negative, internal (‘MAST’) load value somewhere on the aircraft; this process involves huge amounts of data. The idea of using one- and two-dimensional load envelopes to determine critical cases is introduced in Chapter 18. The resulting loads sets are then stored in a database and issued to the stress office for design or certification. These internal loads are then converted to component loads (see the next section) to allow subsequent analyses that provide data to allow individual structural elements to be stressed.

25.5.2 Obtaining Stresses from Internal Loads

The next stage in the loads determination process is now outlined briefly. There are essentially two stages of calculation undertaken for the determination of loads/stresses in an aircraft structure (alluded to in Chapter 6):

(a) In the first stage of calculation, externally applied loads are considered to act on the whole aircraft structure via distributed aerodynamic and inertia effects (including, in the case of ground manoeuvres, discrete landing gear loads acting as reactions). As a result, internal loads (or so-called ‘stress resultants' – moment, axial, shear and torque ('MAST')) are generated at chosen cross-sections of each slender member such as a wing or fuselage. Worst case load conditions are selected by sorting (see above). This stage has been the subject of this chapter so far.

(b) In the second stage of loads calculation, the classical approach (see Chapter 6) is to determine stresses directly from these internal loads using, for example, a formula based methodology, but this assumes that load paths are well defined. However, for more complex semi-monocoque (i.e. stiffened skin) aircraft structures where the load paths are ill defined, this classical approach is inappropriate as there will be no simple formulae linking internal 'MAST' loads to stresses in a structural element such as a wing rib or spar on a swept wing. Instead, the internal 'MAST' loads from the first stage of the analysis will need to be decomposed (or converted) into an equivalent set of 'new' balanced external loads acting, for example, at nodal points on the reference axes of the condensed finite element model (see Chapters 21 and 22). Then, because the FE model will represent the internal load paths, the FE analysis will yield 'new' internal loads (i.e. different to overall 'MAST' loads) and stresses acting on the internal structural elements. Further, more detailed FE models or data sheet/formula approaches on subcomponents may then be employed. Once maximum stress values for different load cases are known, the static strength and fatigue/damage tolerance considerations may be examined for individual structural elements.

Thus, when such subsequent analyses are performed, what have so far been called *internal* loads ('MAST') may sometimes be referred to as *external* loads since they will actually determine the distributed external loads acting at the nodes in the FE model for the component considered. Clearly this can give rise to some confusion of terminology. Since the main focus of the book is on the first stage (namely obtaining moment, axial, shear and torque ('MAST') loads), these have been referred to, in the classical way, as internal loads. The context of a particular external load usage will indicate which type of load is being considered.

Note that the process outlined above, where the internal 'MAST' loads are decomposed on to the reference axis for further analysis, is only one of a number of possible approaches to what is a complex problem. By making use of knowledge of the chordwise mass and aerodynamic pressure distributions (and making assumptions about the fuel mass distribution), the nodal loadings on the FE model may be further refined by being represented along, for example, the front and rear spars. Clearly, the more accurate the analysis, the more precise can be the calculations of stress for design.

26

Testing Relevant to Aeroelasticity and Loads

26.1 INTRODUCTION

The clearance process relating to aeroelastic and loads issues during the design and certification phase of a new aircraft is a combination of numerical modelling backed up by testing. An outline of the main tests used to validate various elements of the aircraft mathematical model for aeroelastic issues is shown in Figure 26.1. Note how there is an opportunity to update the numerical models of each element based upon the test results. A similar series of tests are undertaken to certify aircraft for ground and flight loads. In this chapter, only a very brief outline of the methods will be given.

It must be emphasized is that no one test is capable of providing the information for full validation of the mathematical models used for certification. That must inevitably come by building up a range of test results on different aspects (e.g. structural stiffness, mass, mass distribution, centre of mass, wind tunnel tests, systems tests, etc). The ground tests can be quite accurate and are backed up by checks that show, when assembled together, that the structural dynamic and the flight response properties are both reasonable. However, tests performed in-flight to demonstrate aeroelastic stability and validate flight loads are subject to a number of uncertainties. The test set up for flight flutter testing is much less ideal (e.g. noisy environment, inadequate excitation) than that for ground vibration testing, whereas flight loads have to be determined from strain gauge readings and these calibrations can be problematic.

26.2 WIND TUNNEL TESTS

There are two types of wind tunnel test that are particularly relevant to aeroelasticity and dynamic loads, namely determination of rigid aircraft aerodynamic derivatives and flutter model testing. A wind tunnel model is shown in Figure 26.2.

Aircraft configurations are often complex and accurate prediction of rigid aircraft aerodynamic derivatives is difficult, especially when nonlinearity is important (e.g. near to the stall condition) or the aircraft is in the transonic regime. Therefore model tests for the rigid scale model of a whole aircraft are performed to measure pressure distributions, net forces and moments and so estimate the aerodynamic derivatives at different flight conditions. Values obtained are used to validate and possibly update results calculated using design formulae, data sheets, CFD, etc., and also to scale calculated unsteady aerodynamic results at zero reduced frequency.

A wind tunnel flutter test program (AMC 25.629) may be undertaken using a dynamically scaled model. However, such testing is not sufficiently reliable to use in clearing the aircraft for flutter; instead

Introduction to Aircraft Aeroelasticity and Loads J. R. Wright and J. E. Cooper
© 2007 John Wiley & Sons, Ltd

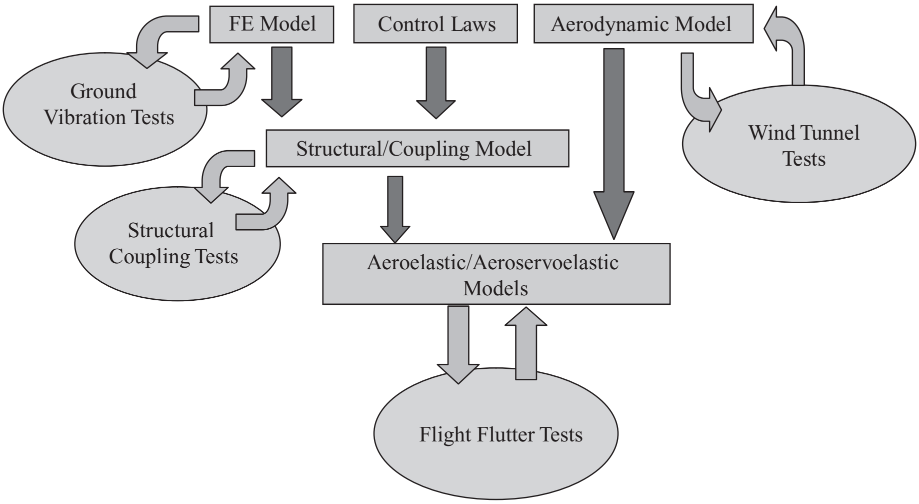
FE Model
Control Laws
Aerodynamic Model
Ground Vibration Tests
Wind Tunnel Tests
Structural/Coupling Model
Structural Coupling Tests
Aeroelastic/Aeroservoelastic Models
Flight Flutter Tests

Figure 26.1 Analysis and test certification process for aeroelasticity.

it helps in the main certification calculations by validating unsteady aerodynamic methodologies, performing parametric studies, studying new configurations, investigating interference and compressibility effects, etc.

26.3 GROUND VIBRATION TEST

The ground vibration test (or GVT, sometimes called a modal test (Ewins, 1995)) is performed on the prototype aircraft to obtain estimates of the whole aircraft normal modes (natural frequencies, damping ratios, mode shapes and modal masses). These modal data may then be used to confirm or adjust the calculated normal modes used in the critical flutter calculations, as well as providing substantiated estimates of damping. Different fuel and hydraulics configurations are studied.

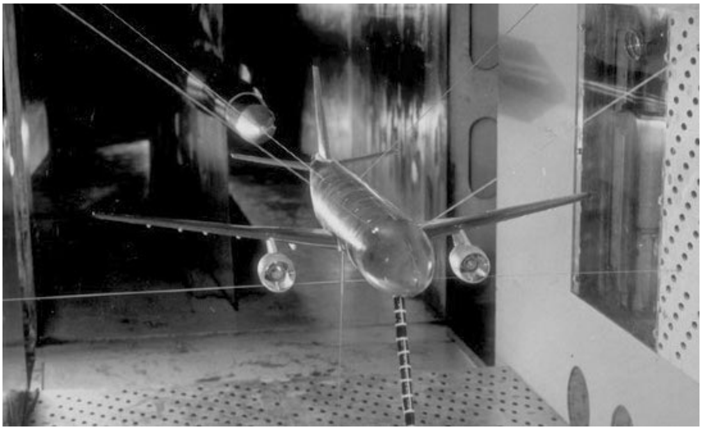

Figure 26.2 Wind tunnel test. Reproduced by permission of ONERA.

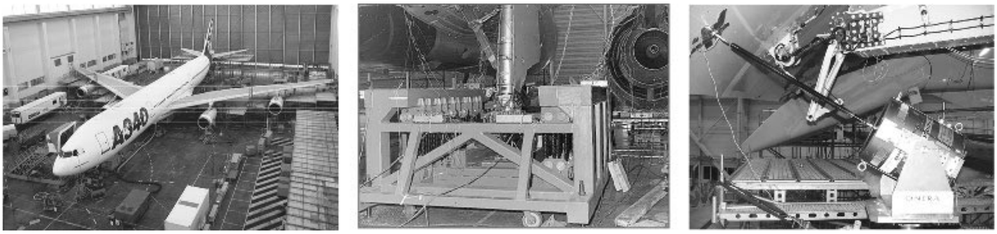

Figure 26.3 Ground vibration test – aircraft under test, main gear bungee support and Flap excitation. Reproduced by permission of Airbus/ONERA/DLR.

The aircraft is usually supported on soft springs (e.g. air bags, elastic bungees or deflated tyres) so that it behaves as near to the free–free condition as possible; the support arrangement may be included in the dynamic model when comparing measurements with calculations. The aircraft is instrumented with, typically, many hundreds of accelerometers to allow adequate mode shape definition, and a number of electrodynamic exciters (typically up to eight) are used to excite vibration of the aircraft at a sufficiently high level. Normally, multiple exciters are applied simultaneously to distribute energy adequately over the structure and to allow modes close in frequency to be identified; exciter positions may need to be varied to excite modes successfully. The excitation signals used to drive the exciters are usually sinusoidal or random, depending upon the test methodology being employed. An example set up for a GVT is shown in Figure 26.3.

There are two main approaches to testing. In one approach, using a phase separation method, a broadband multipoint uncorrelated random excitation or swept sine correlated excitation is applied to the structure using several exciters, a matrix of frequency response functions (FRFs) is estimated and a frequency or time domain identification (i.e. a curve fit) is employed to identify the modal properties.

In an alternative approach, using a phase resonance method, sinusoidal excitation forces are applied at each natural frequency (estimated from an initial broadband test) in turn, and the amplitude and phase of the forces determined from the FRFs or else adjusted iteratively until a normal mode is being excited (indicated by the forces and responses being monophase, with a 90° phase shift between excitation and response such that the structure behaves in essence like a single degree of freedom system). The mode shape is then measured and damping/modal mass estimated usually by varying the excitation frequency around resonance. The latter approach is more suitable for studying important nonlinear effects such as control freeplay, pylon stiffening, etc. However, the identification of multiple-mode nonlinear systems is a challenging area of research.

26.4 STRUCTURAL COUPLING TEST

In AMC 25.629, it is stated that 'the automatic Flight Control System should not interact with the airframe to produce an aeroelastic instability' and that 'when analyses indicate possible adverse coupling, tests should be performed'. These tests include structural coupling tests, which are in effect an extension of the GVT in which additional measurements are performed to include the control system characteristics; e.g. the open loop transfer functions between the response sensors for the control system (e.g. rate gyro/accelerometer) and actuator drive signal (via the flight control computer) would be measured. This would allow the aeroservoelastic model (see Chapter 12) to be checked on the ground at zero air speed where control inertia effects are dominant. Other tests could be carried out to determine the dynamic characteristics of the actuation and systems components.

It is also possible to undertake open and closed loop transfer function measurements in flight to check the flight analytical model; here the aerodynamic effects of the control surface become equally, if not more, important than inertial effects.

26.5 FLIGHT SIMULATOR TEST

A significant amount of testing is undertaken prior to the first flight to assist in FCS design via examination of the aircraft handling qualities; later on, simulators are used for in-service pilot training. The simulator is controlled to match the characteristics of a rigid aircraft dynamic (flight mechanics) model. However, because of the impact of static aeroelastic effects upon the rigid body aerodynamic derivatives, especially for large flexible aircraft, it is important to incorporate static aeroelastic corrections into the aerodynamic model used for the flight simulator. It is not simple to keep the flight mechanics and loads/aeroelastic models in step as the aircraft develops.

It is also worth mentioning the so-called 'Iron Bird' tests, which are a form of simulation not so much directed towards handling qualities as validation of the systems concepts and the real system performance. Typically 'Iron Bird' tests include hardware for hydraulic/electrical systems, the 'real' flight control computers and simulation of the natural aircraft to close the loop. These are of most value in loads and aeroelastics issues by providing system transfer functions and performance constraints for modelling flight control systems.

26.6 STRUCTURAL TESTS

In Chapters 24 and 25, some of the loads requirements in CS-25 were outlined. Most of the structural tests (CS/AMC 25.307) are aimed at demonstrating the limit and ultimate load requirements, and so are strength related; tests are not specifically related to dynamic loads except that certain critical cases may be dynamic in origin and that excessive deformation should not occur. Therefore, only brief mention is made here of structural testing. The amount of testing required will depend upon the classification of the aircraft; e.g. the most extensive test program would be set in place for a new structure, with full scale subcomponent (e.g. spar), component (e.g. wing) and whole aircraft tests carried out to limit and ultimate conditions whereas, for a derivative aircraft, considerably less testing would be required. Also, significant testing at detail, subcomponent, component and whole aircraft level would be carried out in relation to fatigue and damage tolerance conditions, as described in CS/AMC 25.571. Examples of structural strength testing for two different aircraft under near-ultimate wing loading conditions are shown in Figures 26.4(a) and (b), the former showing the loading arrangement and the latter showing the considerable wing deformation that is possible prior to failure.

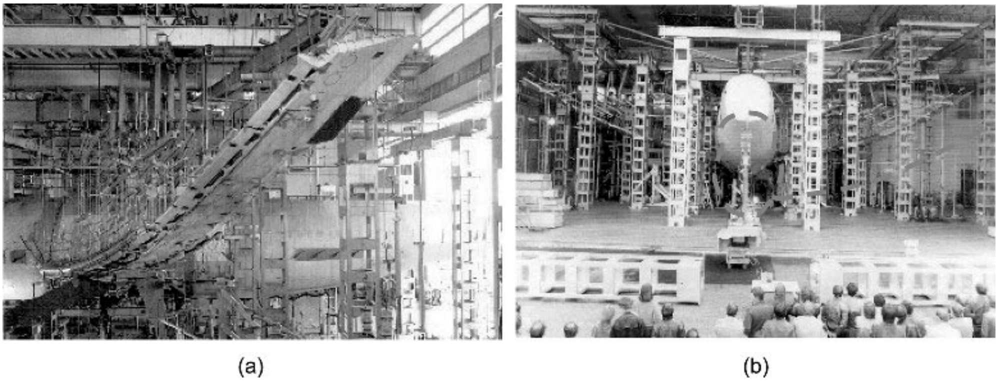

Figure 26.4 Static strength testing of the wings under near-ultimate load conditions; (a) view of the wing loading arrangement and (b) rear view showing wing deformation prior to failure. Reproduced by permission of DGA/CEAT.

26.7 FLIGHT FLUTTER TEST

The uncertainty in the aeroelastic model used for flutter calculations, and especially the unsteady aerodynamics, means that calculated flutter speeds will probably be inaccurate to some extent, especially in the transonic region. It is therefore a requirement of the certification process (AMC 25.629) to validate the flutter behaviour and demonstrate freedom from aeroelastic instability over the flight envelope in a flight flutter test (FFT).

On the basis of calculations, a nominal flight envelope is cleared to permit a first flight to take place. Thereafter, the FFT program precedes every other flight test at each flight envelope point because of the safety critical nature of flutter. The basic FFT philosophy seeks to gradually extend the flight envelope by assessing the flutter stability of the aircraft at progressively increasing speed and Mach number.

It is normal to assess the flutter stability by identifying the frequency and damping of the complex/damped modes (see Chapters 2 and 11) of the aircraft at each test point. The allowable flight envelope is expanded from an initially agreed boundary by examining the results along lines of increasing EAS at constant altitude and lines of constant Mach number, as indicated in Figure 26.5.

The procedure at each test point is: (a) to excite vibration of the aircraft over the frequency range of interest and to measure its response, (b) to curve-fit the excitation and response signals in the time or frequency domain and to identify the model parameters and (c) to determine whether it is safe to proceed to the next test point.

A variety of excitation devices can be used, namely (a) control surface movement via stick/pedal input or explosive charges, (b) control surface movement via a signal from the flight control system, (c) movement of aerodynamic vane fitted to aircraft flying surface or engine/store or (d) inertia exciter mounted in the fuselage. The aircraft response is measured using typically around 20 accelerometers, far fewer than for a GVT.

The most common excitation signals are pulse (via stick/pedal or explosive charge) and chirp (a fast frequency sweep applied as a signal to the control surface, vane or inertia exciter). Where excitation devices are available on both sides of the aircraft, then excitation may be applied in or out of phase in

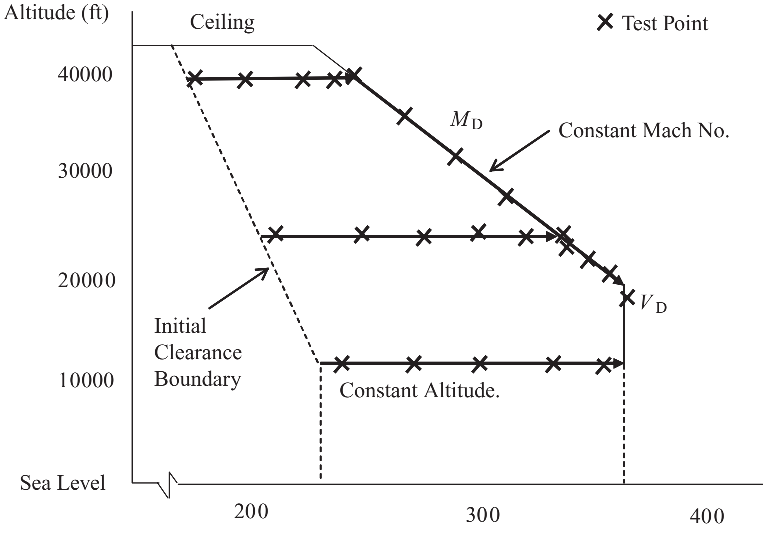

Figure 26.5 Typical flight flutter test clearance envelope.

order to exploit symmetry/antisymmetry and so simplify the analyses. Occasionally a random excitation signal is employed. Sometimes the response of the aircraft to natural turbulence is used (but this is not recommended because the excitation is not 'white' and is not guaranteed to excite adequately all the modes of interest). Where possible, it is preferable that the excitation signal is recorded in order to improve the identification accuracy, but analysis methods are available if this is not the case. Each excitation sequence will probably only last a maximum of 60 s because of the difficulty of holding the aircraft on condition, especially near to the limit of the flight envelope. The test may be repeated and some form of averaging employed to improve the data quality.

Once the test is completed, the results are processed on the ground, either during or after the flight. FRFs are computed or else the raw time data are used directly. Time or frequency domain identification algorithms (i.e. curve-fits) are then employed in order to identify the frequency and damping values for each mode in the data. Again, this process is very similar to modal testing but the levels of noise on the data are far more severe since turbulence (an unmeasured excitation) is exciting the aircraft during the test. The test time is also limited.

The damping values may be compared to results from previous test points and the damping trends for each mode extrapolated to allow progression to the next test point (i.e. by defining a permitted increment in speed or Mach number). Other techniques such as the flutter margin (Zimmermann and Weisenberger, 1964) method can be used to estimate the flutter speed based upon the measured test data. The test process is complete when the extrapolated damping values are still positive at a margin (typically 15 %) above the design dive speed for each Mach number.

These results are compared to the predictions from the model and some basic attempts may be made to reconcile any differences. Any flutter problem (e.g. the flutter speed from test is too low) will require urgent design action (e.g. additional mass balance) and could prove to be extremely costly. Note that in AMC 25.629, the evaluation of phenomena not amenable to analysis (e.g. buffet, buzz, etc.) should be investigated during the flight test program.

26.8 FLIGHT LOADS VALIDATION

In CS 25.301 it is stated that 'methods used to determine load intensities and distribution must be validated by flight load measurement unless the methods used for determining those loading conditions are shown to be reliable'. The definition of such a flight loads test program is considered in AMC 25.301 and depends upon a comparison of design features with previous aircraft (i.e. new features/configurations will require assessment), the manufacturer's experience in load validation and proven accuracy of analysis methods, etc. The aim of the flight loads programme is to demonstrate that the loads calculation and prediction process produces reliable loads for the flight certification cases. In some cases where analytical methods are inadequate, such as for buffet, then flight loads are used for design purposes. The nature of the flight loads programme is explained in AMC 25.301.

A range of flight conditions needs to be investigated, though the flight test need not lead to an exceedance of 80 % of the limit loads. Typically, pitch, yaw, roll and stall entry manoeuvres would be carried out. Clearly, gust loads cannot be validated as the gust conditions may not be arranged, and also failure cases, etc., are not subject to flight test for loads validation purposes.

Flight loads are not measured directly, but rather determined through correlation of predictions with measured strains, accelerations, pressures and flight mechanics parameters. The load intensities and distributions derived from the flight test would be compared to predictions from analysis. Careful correlation is required.

Appendices

A

Aircraft Rigid Body Modes

A.1 RIGID BODY TRANSLATION MODES

The aircraft heave motion may often be represented by a free–free rigid body heave mode (subscript h), instead of using the heave displacement of the centre of mass as a physical coordinate. The mode shape is normalized to have a unit downwards displacement at all points on the aircraft as shown in Figure A.1(a). Thus the mode shape is $\kappa_{\mathrm{h}}(x, y) = 1$ and the corresponding generalized coordinate is q_{h}. The heave mode modal mass $m_{\mathrm{h}} = m$ (i.e. aircraft mass) is found by equating the kinetic energy expressed in terms of the physical and modal masses/coordinates, so

$$T = \frac{1}{2}m_{\mathrm{h}}\dot{q}_{\mathrm{h}}^2 = \frac{1}{2}\int_{A/c}\dot{z}^2\mathrm{d}m = \frac{1}{2}\int_{A/c}[\kappa_{\mathrm{h}}(x, y)\dot{q}_{\mathrm{h}}]^2\mathrm{d}m = \frac{1}{2}m\dot{q}_{\mathrm{h}}^2. \tag{A.1}$$

The other two translational rigid body modes are similar, namely the sideslip and fore-and-aft modes.

A.2 RIGID BODY ROTATION MODES

The pitch, roll and yaw motions may also be represented by rigid body modes of rotation rather than via the pitch, roll and yaw angles. The rigid body pitch mode shape involves a nose up rotation about the aircraft centre of mass, as shown in Figure A.1(b), and if the mode shape is normalized as $\kappa_{\mathrm{p}}(x, y) = -x$

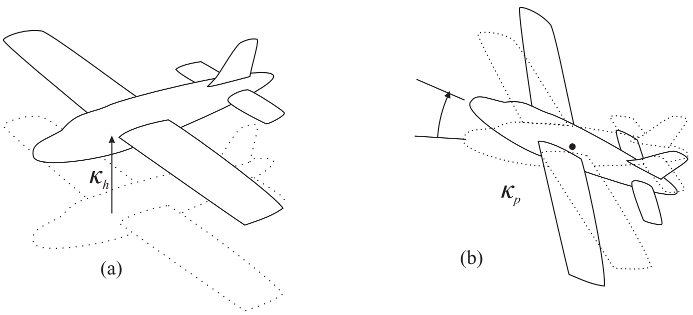

Figure A.1 Rigid body: (a) heave and (b) pitch modes.

Introduction to Aircraft Aeroelasticity and Loads J. R. Wright and J. E. Cooper
© 2007 John Wiley & Sons, Ltd

(i.e. 1 radian rotation) then the pitch generalized coordinate q_p will be equal to the pitch angle. The pitch mode modal mass $m_\mathrm{p} = I_y$ (i.e. the aircraft pitch moment of inertia) may also be found by equating kinetic energies

$$T = \tfrac{1}{2} m_\mathrm{p} \dot{q}_\mathrm{p}^2 = \tfrac{1}{2} \int_{A/c} \dot{z}^2 \mathrm{d}m = \tfrac{1}{2} \int_{A/c} [\kappa_\mathrm{p}(x, y) \dot{q}_\mathrm{p}]^2 \mathrm{d}m = \tfrac{1}{2} I_y \dot{q}_\mathrm{p}^2. \tag{A.2}$$

The other two rotational rigid body modes are similar, namely the roll and yaw modes. Product moments of inertia are considered to be zero for this case where the axes chosen are principal axes.

B

Table of Longitudinal Aerodynamic Derivatives

In the main text, two different axes types have been considered for manoeuvres and gust encounters, namely inertial axes fixed in space and wind/body axes fixed in the aircraft. Inertial axes are appropriate for flutter, equilibrium manoeuvres, most ground manoeuvres and gust/turbulence encounters, where small excursions in angle and displacement about a datum position are considered. The use of derivatives was primarily to yield a convenient and compact representation of the equations. However, wind/body axes are used for dynamic manoeuvres in flight (and possibly landing) and the aerodynamic stability derivatives are obtained by considering small perturbations.

When longitudinal derivatives are obtained for these two different axes types, differences are present in some derivatives, particularly where perturbations in velocity are considered, but they are relatively small. Flexible derivatives are the same for the two cases when using quasi-steady strip theory aerodynamics. Table B.1 presents the derivatives used in the calculation of symmetric manoeuvre loads; the wind axes results were converted into the present notation from Cook (1997).

Table B.1 Derivatives used in the calculation of symmetric manoeuvre loads

	Inertial axes (Chapters 13 and 16)		Wind axes (fixed to aircraft) (Chapters 14 and 15)
Z_0	$-\frac{1}{2}\rho V^2\,[S_W a_W - S_T a_T k_\varepsilon]\,\alpha_0$		
Z_α	$-\frac{1}{2}\rho V^2\,[S_W a_W + S_T a_T(1-k_\varepsilon)]$		
$Z_{\dot{z}}$	$-\frac{1}{2}\rho V\,[S_W a_W + S_T a_T(1-k_\varepsilon)]$	Z_W	$-\frac{1}{2}\rho V_0\,[S_W a_W + S_T a_T(1-k_\varepsilon) + S_W C_D]$
Z_q	$-\frac{1}{2}\rho V S_T a_T l_T$	Z_q	$-\frac{1}{2}\rho V_0 S_T a_T l_T$ (tailplane only)
Z_η	$-\frac{1}{2}\rho V^2 S_T a_E$	Z_η	$-\frac{1}{2}\rho V_0^2 S_T a_E$
Z_e	$\frac{1}{2}\rho V^2\,[-S_W a_W J_1 - S_T a_T \gamma_{eT}]$	Z_e	$\frac{1}{2}\rho V_0^2\,[-S_W a_W J_1 - S_T a_T \gamma_{eT}]$
$Z_{\dot{e}}$	$-\frac{1}{2}\rho V S_T a_T \kappa_{eT}$	$Z_{\dot{e}}$	$-\frac{1}{2}\rho V_0 S_T a_T \kappa_{eT}$
Z_{gW}	$-\frac{1}{2}\rho V S_W a_W$		
Z_{gT}	$-\frac{1}{2}\rho V S_T a_T(1-k_\varepsilon)$		

(*Continued*)

Introduction to Aircraft Aeroelasticity and Loads J. R. Wright and J. E. Cooper
© 2007 John Wiley & Sons, Ltd

Table B.1 Derivatives used in the calculation of symmetric manoeuvre loads (*Continued*)

	Inertial axes (Chapters 13 and 16)		Wind axes (fixed to aircraft) (Chapters 14 and 15)
M_0	$\frac{1}{2}\rho V^2 S_W c C_{M_{oW}}$ $-\frac{1}{2}\rho V^2\left[S_W a_W l_W + S_T a_T k_\varepsilon l_T\right]\alpha_0$		
M_α	$\frac{1}{2}\rho V^2\left[S_W a_W l_W - S_T a_T(1-k_\varepsilon)l_T\right]$		
$M_{\dot{z}}$	$\frac{1}{2}\rho V\left(S_W a_W l_W - S_T a_T(1-k_\varepsilon)l_T\right)$	M_W	$\frac{1}{2}\rho V_0\left(S_W a_W l_W - S_T a_T(1-k_\varepsilon)l_T\right)$
M_q	$-\frac{1}{2}\rho V S_T a_T l_T^2$	M_q	$-\frac{1}{2}\rho V_0 S_T a_T l_T^2$ (tailplane only)
M_η	$-\frac{1}{2}\rho V^2 S_T a_E l_T$	M_η	$-\frac{1}{2}\rho V_0^2 S_T a_E l_T$
M_e	$\frac{1}{2}\rho V^2\left[S_W a_W l_W J_1 - S_T a_T l_T \gamma_{eT}\right]$	M_e	$\frac{1}{2}\rho V_0^2\left[S_W a_W l_W J_1 - S_T a_T l_T \gamma_{eT}\right]$
$M_{\dot{e}}$	$-\frac{1}{2}\rho V S_T a_T l_T \kappa_{eT}$	$M_{\dot{e}}$	$-\frac{1}{2}\rho V_0 S_T a_T l_T \kappa_{eT}$
M_{gW}	$\frac{1}{2}\rho V S_W a_W l_W$		
M_{gT}	$-\frac{1}{2}\rho V S_T a_T l_T(1-k_\varepsilon)$		
Q_0	$\frac{1}{2}\rho V^2\left[S_W a_W J_2 - S_T a_T k_\varepsilon \kappa_{eT}\right]\alpha_0$		
Q_α	$\frac{1}{2}\rho V^2\left[-S_W a_W J_2 - S_T a_T(1-k_\varepsilon)\kappa_{eT}\right]$		
$Q_{\dot{z}}$	$\frac{1}{2}\rho V\left[-S_W a_W J_2 - S_T a_T(1-k_\varepsilon)\kappa_{eT}\right]$	Q_W	$\frac{1}{2}\rho V_0\left[-S_W a_W J_2 - S_T a_T(1-k_\varepsilon)\kappa_{eT}\right]$
Q_q	$-\frac{1}{2}\rho V S_T a_T l_T \kappa_{eT}$	Q_q	$-\frac{1}{2}\rho V_0 S_T a_T l_T \kappa_{eT}$
Q_η	$-\frac{1}{2}\rho V^2 S_T a_E \kappa_{eT}$	Q_η	$-\frac{1}{2}\rho V_0^2 S_T a_E \kappa_{eT}$
Q_{e}	$\frac{1}{2}\rho V^2\left[-S_W a_W J_3 - S_T a_T \gamma_{eT}\kappa_{eT}\right]$	Q_{e}	$\frac{1}{2}\rho V_0^2\left[-S_W a_W J_3 - S_T a_T \gamma_{eT}\kappa_{eT}\right]$
$Q_{\dot{e}}$	$-\frac{1}{2}\rho V S_T a_T \kappa_{eT}^2$	$Q_{\dot{e}}$	$-\frac{1}{2}\rho V_0 S_T a_T \kappa_{eT}^2$
Q_{gW}	$-\frac{1}{2}\rho V S_W a_W J_2$		
Q_{gT}	$-\frac{1}{2}\rho V S_T a_T(1-k_\varepsilon)\kappa_{eT}$		

When inertial axes were used in the main text, the symbol V was used for true air speed, with no air speed perturbations considered. For wind axes, the steady equilibrium value was taken as V_0, with V taken as the perturbed total velocity (in the limit $V \cong V_0$). Note that

$$J_1 = \frac{1}{s}\int_{y=0}^{s}\gamma_{\mathrm{e}}\,\mathrm{d}y, \qquad J_2 = \frac{1}{s}\int_{y=0}^{s}(\kappa_{\mathrm{e}} - l_A\gamma_{\mathrm{e}})\,\mathrm{d}y, \qquad J_3 = \frac{1}{s}\int_{y=0}^{s}(\kappa_{\mathrm{e}} - l_A\gamma_{\mathrm{e}})\gamma_{\mathrm{e}}\,\mathrm{d}y,$$

where $\gamma_{\mathrm{e}} = \gamma_{\mathrm{e}}(y)$, $\kappa_{\mathrm{e}} = \kappa_{\mathrm{e}}(y)$ are functions describing the wing flexible mode shape (see Appendix C).

C

Aircraft Symmetric Flexible Modes

In the treatment of manoeuvres and gust encounters in this book, the whole free–free aircraft is considered, initially as a rigid body and then with a single flexible mode added to illustrate the important effect of flexibility. The aim of the flexible mode representation is to keep the mathematics as basic as possible while illustrating the impact that flexibility might have. In particular, the flexible mode shapes described in this appendix are used in Chapters 13 to 17 for manoeuvres (flight and ground) and gust/turbulence encounters; only one flexible mode is used in each case, but its shape is derived from a 'master' mode template and may be altered. The mode is first introduced in Chapter 13 but some of the content is repeated here for convenience, with modal parameters being derived. In this appendix, the constituent flexible mode shapes and modal parameters will be introduced in order to avoid significant digressions in the main chapters of the book. The idea is to define the flexible mode shapes geometrically, apply conditions of orthogonality to the rigid body modes and so determine the modal masses for the flexible modes; the modal stiffness may then be found simply by choosing the desired natural frequency. Therefore no modal analysis is performed explicitly.

C.1 AIRCRAFT MODEL

The free–free aircraft is shown in Figure C.1. It has unswept and untapered flexible wings with the mass distributed uniformly along the span and with the mass axis aft of the flexural (or elastic) axis. The tailplane is rigid and the engines are mounted on the rear fuselage (but not shown) to leave the wings 'clean'. The fuselage is flexible and for convenience its mass is discretized at three locations: front, centre and rear. The aircraft is somewhat contrived in order to keep it as simple as possible. The essence of the cases considered in this book should not be significantly affected by making the model more realistic, except for the addition of wing sweep, commented on in Chapter 13.

The wings have semi-span s and chord c, with the wing flexural axis a distance l_A aft of the wing aerodynamic centre axis (which is itself at a quarter chord) and a distance l_E ahead of the wing mass axis. The key fuselage dimensions from the aircraft centre of mass to the tail, wing aerodynamic centre, wing mass axis and front fuselage position are l_T, l_W, l_{WM}, l_F respectively. The physical width dimension of the fuselage will be neglected in any spanwise integration over the wings.

The wing mass per unit span is μ_W so the total wing mass is $m_W = 2\mu_W s$. The front, centre and rear fuselage discrete masses, m_F, m_C, m_T, are located at the assumed front fuselage position (e.g. pilot or nose gear), the aircraft centre of mass and the tail respectively; the tail centre of mass is assumed to be coincident with the tailplane aerodynamic centre for convenience. The total mass of the aircraft is $m = m_F + m_W + m_C + m_T$.

By setting the first moment of mass about the centre of mass to zero for the whole aircraft, it may be seen by reference to Figure C.1 that the masses and their positions must be related by the

Introduction to Aircraft Aeroelasticity and Loads J. R. Wright and J. E. Cooper
© 2007 John Wiley & Sons, Ltd

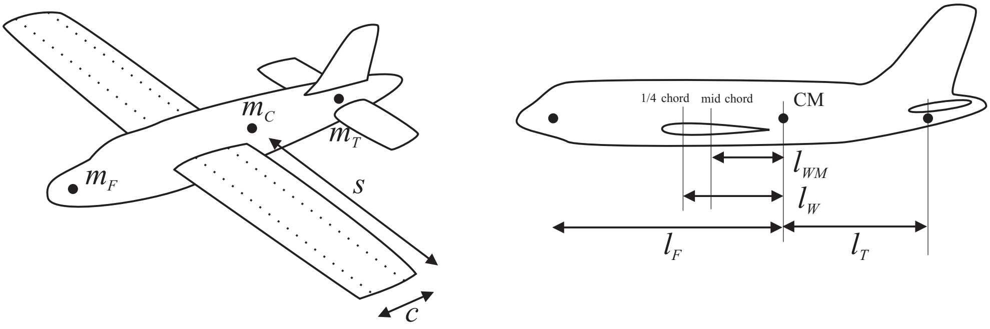

Figure C.1 Free–free flexible aircraft model.

expression

$$m_{\mathrm{F}}l_{\mathrm{F}} + m_{\mathrm{W}}l_{\mathrm{WM}} - m_{\mathrm{T}}l_{\mathrm{T}} = 0. \tag{C.1}$$

The pitch moment of inertia of the wing per unit span is χ_{W} so the total value for the wings about their mass axis is $I_{\mathrm{W}} = 2\chi_{\mathrm{W}}s$. The total pitch moment of inertia of the aircraft about its centre of mass is given by

$$I_y = \left(I_{\mathrm{W}} + m_{\mathrm{W}}l_{\mathrm{WM}}^2\right) + m_{\mathrm{F}}l_{\mathrm{F}}^2 + m_{\mathrm{T}}l_{\mathrm{T}}^2, \tag{C.2}$$

where the wing term employs the parallel axis theorem and the centre fuselage mass term does not appear.

C.2 SYMMETRIC FREE–FREE FLEXIBLE MODE

C.2.1 Description of the Flexible Mode Shape

A free–free flexible (or elastic) mode shape (subscript e), where the wing can deform in bending and twist and the fuselage can deform in bending, is shown in Figure C.2. The flexible mode will be defined by a modal coordinate q_{e}. The wing bending and twist deformations are defined relative to the wing flexural axis by the functions $\kappa_{\mathrm{e}}(y)$ (downwards positive) and $\gamma_{\mathrm{e}}(y)$ (nose up positive) respectively, where the values at the wing root are $\kappa_{\mathrm{e0}} = \kappa_{\mathrm{e}}(0)$ and $\gamma_{\mathrm{e0}} = \gamma_{\mathrm{e}}(0)$.

The fuselage modal deformation (downwards) is defined by displacement values $\kappa_{\mathrm{eF}}, \kappa_{\mathrm{e0}}, \kappa_{\mathrm{eW}}, \kappa_{\mathrm{eC}}, \kappa_{\mathrm{eT}}$ at the front fuselage, wing flexural axis, wing mass axis, aircraft centre of mass (coincident with centre fuselage) and tail positions respectively. The section of fuselage that includes the wing cross-section and the aircraft centre of mass is assumed to behave rigidly and so will heave κ_{e0} and pitch nose up with angle γ_{e0}, relative to the wing flexural axis position. Thus the displacements at the wing and aircraft centres of mass are given by

$$\kappa_{\mathrm{eW}} = \kappa_{\mathrm{e0}} + l_{\mathrm{E}}\gamma_{\mathrm{e0}} \qquad \kappa_{\mathrm{eC}} = \kappa_{\mathrm{e0}} + (l_{\mathrm{WM}} + l_{\mathrm{E}})\gamma_{\mathrm{e0}}. \tag{C.3}$$

The nose up pitch of the tailplane γ_{eT} can be estimated by assuming that the rear and front fuselage deformations in the mode shape vary quadratically; based on this assumption and knowing the displacement and slope of the centre section, it may be shown that the tailplane pitch is given by

$$\gamma_{\mathrm{eT}} = 2\left\{\frac{\kappa_{\mathrm{eT}} - \kappa_{\mathrm{eC}}}{l_{\mathrm{T}}}\right\} - \gamma_{\mathrm{e0}}. \tag{C.4}$$

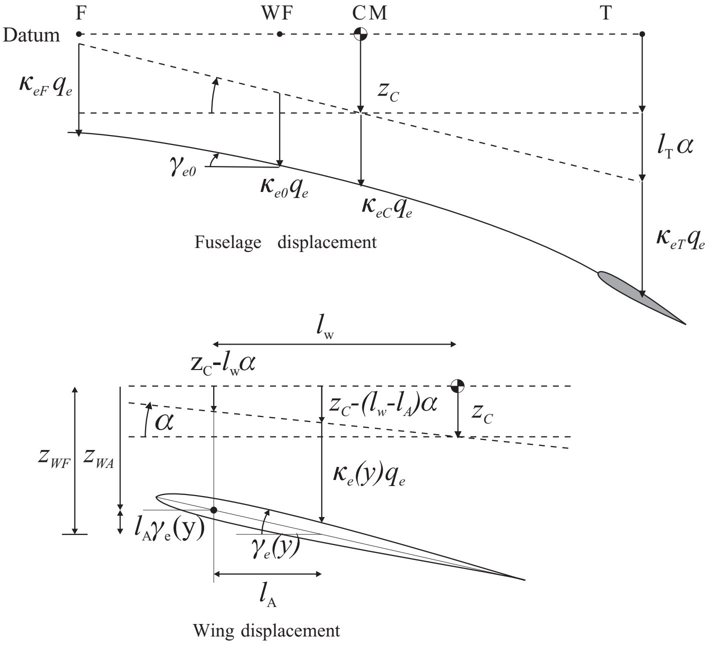

Fuselage displacement

Wing displacement

Figure C.2 Aircraft symmetric free–free flexible mode.

C.2.2 Conditions for Orthogonality with Rigid Body Modes

A free–free symmetric mode is, by definition, orthogonal (see Chapters 2 and 3) to the rigid body heave and pitch modes (described in Appendix A). One way of imposing this orthogonality condition is to ensure that there is no net vertical inertia force or pitching moment in the flexible mode deformation. As an example, the physical inertia force associated with the tail mass modal acceleration is an upwards force of $m_{\mathrm{T}}(\kappa_{\mathrm{eT}}\ddot{q}_{\mathrm{e}})$. When the orthogonality conditions are imposed and the common generalized acceleration terms $\ddot{q}_{\mathrm{e}}$ are cancelled, then it may be shown that the condition for zero net inertia force (upwards positive) is

$$m_{\mathrm{F}}\kappa_{\mathrm{eF}} + 2\int_0^s \mu_{\mathrm{W}}[\kappa_{\mathrm{E}}(y) + l_{\mathrm{E}}\gamma_{\mathrm{E}}(y)]\mathrm{d}y + m_{\mathrm{C}}\kappa_{\mathrm{eC}} + m_{\mathrm{T}}\kappa_{\mathrm{eT}} = 0, \tag{C.5}$$

where the second term is an integral of the wing bending contribution per strip dy. Note that the motion at the wing mass axis is a function of both wing bending and twist. The condition for zero net inertia moment about the aircraft centre of mass (nose down positive) is

$$-m_{\mathrm{F}}\kappa_{\mathrm{eF}}\, l_{\mathrm{F}} - 2\int_0^s \mu_{\mathrm{W}}[\kappa_{\mathrm{E}}(y) + l_{\mathrm{E}}\gamma_{\mathrm{E}}(y)]\mathrm{d}y\, l_{\mathrm{WM}} + 2\int_0^s \chi_{\mathrm{W}}\gamma_{\mathrm{E}}(y)\mathrm{d}y + m_{\mathrm{T}}\kappa_{\mathrm{eT}}\, l_{\mathrm{T}} = 0, \tag{C.6}$$

where the third term is a torsion term which is an integral of the wing twist contribution per strip. The tailplane pitch angle does not appear in this equation because no moment of inertia for the tail was included. These expressions allow the free–free modal parameters to be determined for different types of flexible mode.

C.2.3 Wing Deformation Shapes

In order to be able to apply the above orthogonality expressions, the wing bending and twisting shapes relative to the wing flexural axis need to be defined. To simplify the analysis, basic assumed polynomial expressions will be employed (see Chapter 3). Thus, the wing bending deformation can be written as a quadratic function

$$\kappa_{\mathrm{E}}(y) = \kappa_{\mathrm{e}0}\left[1 + A\left(\frac{y}{s}\right)^2\right], \tag{C.7}$$

where A is an unknown constant defining the amount of bending and the spanwise position of any nodal line running across the wing. The wing twist deformation may be written as a linear function, so

$$\gamma_{\mathrm{E}}(y) = \gamma_{\mathrm{e}0}\left[1 + B\left(\frac{y}{s}\right)\right], \tag{C.8}$$

where B is an unknown constant defining the amount of twist present at the tip relative to the root. The displacement at the wing tip (trailing edge) will be used later to normalize the mode shapes and is given by

$$\kappa_{\mathrm{Tip\_TE}} = \kappa_{\mathrm{e}0}(1 + A) + \gamma_{\mathrm{e}0}(1 + B)l_{\mathrm{TE}}, \tag{C.9}$$

where $l_{\mathrm{TE}} = 3c/4 - l_{\mathrm{A}}$ is the distance from the flexural axis to the wing trailing edge.

When these polynomial functions are substituted into the orthogonality expressions (C.5) and (C.6), assuming that the aircraft deforms in both the wing and fuselage, then the result is

$$\begin{aligned} &m_{\mathrm{F}}\kappa_{\mathrm{eF}} + m_{\mathrm{W}}\left(1 + \frac{A}{3}\right)\kappa_{\mathrm{e}0} + m_{\mathrm{W}}l_{\mathrm{E}}\left(1 + \frac{B}{2}\right)\gamma_{\mathrm{e}0} + m_{\mathrm{C}}\kappa_{\mathrm{eC}} + m_{\mathrm{T}}\kappa_{\mathrm{eT}} = 0, \\ &-m_{\mathrm{F}}\kappa_{\mathrm{eF}}\,l_{\mathrm{F}} - m_{\mathrm{W}}\left(1 + \frac{A}{3}\right)\kappa_{\mathrm{e}0}\,l_{\mathrm{WM}} + \left(I_{\mathrm{W}} - m_{\mathrm{W}}l_{\mathrm{E}}l_{\mathrm{WM}}\right)\left(1 + \frac{B}{2}\right)\gamma_{\mathrm{e}0} + m_{\mathrm{T}}\kappa_{\mathrm{eT}}\,l_{\mathrm{T}} = 0. \end{aligned} \tag{C.10}$$

In order to satisfy these equations, several unknowns need to be chosen and this does not appear to be straightforward or even possible. However, if special cases are selected, then the choice of values is not too difficult. The three cases to be considered are where fuselage bending, wing bending and wing twist each become the dominant component in the mode shape. This approach will allow each effect to be examined separately.

C.2.4 Mode with Fuselage Bending Dominant

Firstly, consider the case where the wing is treated as completely rigid, so $A = B = 0$, but the fuselage is flexible. So that the mode does not involve wing pitch, it will be assumed that $\gamma_{\mathrm{e}0} = 0$ and therefore, from Equation (C.3), $\kappa_{\mathrm{eC}} = \kappa_{\mathrm{e}0}$ and the rigid centre section will simply heave an amount $\kappa_{\mathrm{e}0}$. When these values are substituted into the orthogonality expressions (C.10), and the result simplified, then it may be shown that

$$m_{\mathrm{F}}\kappa_{\mathrm{eF}} + m_{\mathrm{T}}\kappa_{\mathrm{eT}} = -(m_{\mathrm{W}} + m_{\mathrm{C}})\kappa_{\mathrm{e}0} \qquad - m_{\mathrm{F}}l_{\mathrm{F}}\kappa_{\mathrm{eF}} + m_{\mathrm{T}}l_{\mathrm{T}}\kappa_{\mathrm{eT}} = m_{\mathrm{W}}l_{\mathrm{WM}}\kappa_{\mathrm{e}0}. \tag{C.11}$$

Solving these equations leads to the front fuselage and tailplane modal displacements κ_{eF}, κ_{eT} expressed in terms of $\kappa_{\mathrm{e}0}$. The tailplane pitch is then determined using Equation (C.4). The mode shape can be defined using a normalization where, for example, $\kappa_{\mathrm{e}0}$ or the wing tip trailing edge displacement $\kappa_{\mathrm{Tip\_TE}}$ are unity.

C.2.5 Mode with Wing Bending Dominant

Now consider the dominant wing bending case, where the wing is rigid in torsion and $B = 0$. The fuselage is rigid but allowed to pitch by γ_{e0} about the wing flexural axis in order to satisfy orthogonality; however, because the fuselage is rigid, the tailplane pitch γ_{eT} is equal to γ_{e0} and the modal displacements at the front fuselage, centre of mass and tail positions must be a geometric function of the heave and pitch of the fuselage centre section thus

$$\kappa_{\mathrm{eF}} = \kappa_{\mathrm{e0}} - (l_{\mathrm{F}} - l_{\mathrm{WM}} - l_{\mathrm{E}})\gamma_{\mathrm{e0}}, \qquad \kappa_{\mathrm{eC}} = \kappa_{\mathrm{e0}} + (l_{\mathrm{WM}} + l_{\mathrm{E}})\gamma_{\mathrm{e0}}, \qquad \kappa_{\mathrm{eT}} = \kappa_{\mathrm{e0}} + (l_{\mathrm{T}} + l_{\mathrm{WM}} + l_{\mathrm{E}})\gamma_{\mathrm{e0}}. \tag{C.12}$$

If these terms are substituted into the orthogonality equations, the result may be simplified to

$$\left(m + m_{\mathrm{W}}\frac{A}{3}\right)\kappa_{\mathrm{e0}} + m\left(l_{\mathrm{E}} + l_{\mathrm{WM}}\right)\gamma_{\mathrm{e0}} = 0, \qquad -\left(m_{\mathrm{W}}\frac{A}{3}\right) l_{\mathrm{WM}}\kappa_{\mathrm{e0}} + I_y\gamma_{\mathrm{e0}} = 0, \tag{C.13}$$

where the earlier expressions for moment of inertia and first moment of mass have been employed. Both Equations (C.13) yield a value for the ratio $\gamma_{\mathrm{e0}}/\kappa_{\mathrm{e0}}$ as a function of A, and by equating these ratio expressions for a consistent result, it may be shown that A must be given by

$$\frac{m_{\mathrm{W}}}{m}\left[1 + \frac{l_{\mathrm{WM}}(l_{\mathrm{E}} + l_{\mathrm{WM}})}{l_y^2}\right] A = -3, \tag{C.14}$$

where $I_y = ml_y^2$ and l_y is the aircraft pitch radius of gyration. The ratio $\gamma_{\mathrm{e0}}/\kappa_{\mathrm{e0}}$ may then be determined from the value of A. Values of the mode shape for the front, centre and rear fuselage positions can then be determined in terms of κ_{e0} by substituting this ratio into Equations (C.12). The mode shape is then defined as before, based on a normalization where, for example, κ_{e0} or the wing tip displacement $\kappa_{\mathrm{Tip\_TE}}$ are set to unity.

C.2.6 Mode with Wing Twist Dominant

Finally, consider the case where the wing is flexible in twist but rigid in bending and so $A = 0$. Also, the fuselage is rigid in bending but allowed to heave and pitch so the geometric relationships in Equation (3.12) still apply. The tailplane pitch γ_{eT} again equals γ_{e0}. Substituting these terms into the orthogonality Equations (3.10) gives

$$\kappa_{\mathrm{e0}} + \left(l_{\mathrm{E}} + l_{\mathrm{WM}} + \frac{m_{\mathrm{W}}}{m}\frac{B}{2}l_{\mathrm{E}}\right)\gamma_{\mathrm{e0}} = 0, \qquad \left(I_y + \bar{I}_{\mathrm{W}}\frac{B}{2}\right)\gamma_{\mathrm{e0}} = 0, \tag{C.15}$$

where $\bar{I}_{\mathrm{W}} = I_{\mathrm{W}} - m_{\mathrm{W}}l_{\mathrm{E}}l_{\mathrm{WM}}$. Since the fuselage pitch γ_{e0} is nonzero, then $B = -2I_y/\bar{I}_{\mathrm{W}}$ and the ratio $\gamma_{\mathrm{e0}}/\kappa_{\mathrm{e0}}$ may be determined. Values of the mode shape for the front, centre and rear fuselage positions may then be determined in terms of κ_{e0} by substituting this ratio into Equations (C.12) and the mode shape normalized.

C.2.7 Modal Mass Values for the Flexible Aircraft

The modal mass m_{e} for the whole aircraft flexible mode may be defined by writing the kinetic energy associated with motion of the physical masses in the flexible mode deformation and equating it to the value expressed in terms of the modal mass. The general kinetic energy term includes integral expressions for the bending and twisting of the wing, as well as energy terms for each discrete mass, so

$$\begin{aligned}T = \frac{1}{2}m_{\mathrm{e}}\dot{q}_{\mathrm{e}}^{2} = \frac{1}{2}m_{\mathrm{F}}\left(\kappa_{\mathrm{eF}}\dot{q}_{\mathrm{e}}\right)^{2} + \frac{1}{2}2\int_{0}^{s}\mu_{\mathrm{W}}\left\{\left[\kappa_{\mathrm{e}}(y) + l_{\mathrm{E}}\gamma_{\mathrm{e}}(y)\right]\dot{q}_{\mathrm{e}}\right\}^{2}\mathrm{d}y \\ + \frac{1}{2}2\int_{0}^{s}\chi_{\mathrm{W}}\left[\gamma_{\mathrm{e}}(y)\dot{q}_{\mathrm{e}}\right]^{2}\mathrm{d}y + \frac{1}{2}m_{\mathrm{C}}\left[\kappa_{\mathrm{eC}}\dot{q}_{\mathrm{e}}\right]^{2} + \frac{1}{2}m_{\mathrm{T}}\left[\kappa_{\mathrm{eT}}\dot{q}_{\mathrm{e}}\right]^{2}.\end{aligned} \tag{C.16}$$

After carrying out the integrations and cancelling the common factor $\frac{1}{2}\dot{q}_{\mathrm{e}}^{2}$, a general expression for the modal mass may be shown to be

$$\begin{aligned}m_{\mathrm{e}} = m_{\mathrm{F}}\kappa_{\mathrm{eF}}^{2} + m_{\mathrm{W}}\left(1 + \frac{2A}{3} + \frac{A^{2}}{5}\right)\kappa_{\mathrm{e0}}^{2} + \left(I_{\mathrm{W}} + m_{\mathrm{W}}l_{\mathrm{e}}^{2}\right)\left(1 + B + \frac{B^{2}}{3}\right)\gamma_{\mathrm{e0}}^{2} \\ + 2m_{\mathrm{W}}l_{\mathrm{E}}\left[1 + \frac{A}{3} + \frac{B}{2} + \frac{AB}{4}\right]\kappa_{\mathrm{e0}}\gamma_{\mathrm{e0}} + m_{\mathrm{C}}\kappa_{\mathrm{eC}}^{2} + m_{\mathrm{T}}\kappa_{\mathrm{eT}}^{2}.\end{aligned} \tag{C.17}$$

The modal mass may then be estimated for the relevant mode shape, bearing in mind that the numerical value is not unique, but will depend upon the mode shape normalization assumed (see Chapter 2).

Knowing the relevant modal mass m_{e} and assuming a natural frequency ω_{e}(rad/s), the modal stiffness may be determined using $k_{\mathrm{e}} = \omega_{\mathrm{e}}^{2}m_{\mathrm{e}}$, so permitting the flexible mode frequency to be adjusted easily without needing to alter values of bending or torsional stiffness and then having to perform a modal calculation.

C.2.8 Example Data

The following parameter values will be assumed for calculating example values for the mode shape and modal mass in the symmetric manoeuvres and gust encounters: $c = 2.0$ m, $l_{\mathrm{WM}} = 0.1$ m, $l_{\mathrm{E}} = 0.25$ m, $l_{\mathrm{A}} = 0.25$ m, $l_{\mathrm{F}} = 6.8$ m, $l_{\mathrm{T}} = 7$ m, $m = 10\,000$ kg, $m_{\mathrm{F}} = 0.15m$, $m_{\mathrm{W}} = 0.3m$, $m_{\mathrm{C}} = 0.4m$, $m_{\mathrm{T}} = 0.15m$, $I_{\mathrm{y}} = 144\,000$ kg m^{2} and $I_{\mathrm{W}} = 1330$ kg m^{2}. Using different parameters here would lead to different relative fuselage and wing motion in the mode shapes that follow. In each case the modes are arbitrarily normalized with respect to a unit displacement at the wing tip (trailing edge) $\kappa_{\mathrm{Tip\_TE}}$, obtained via Equation (3.9).

C.2.8.1 Fuselage bending dominant

For the chosen parameter values it may be shown that

$$\begin{aligned}&\{\kappa_{\mathrm{eF}}, \kappa_{\mathrm{e0}}, \kappa_{\mathrm{eC}}, \kappa_{\mathrm{eT}}\} = \{-2.382, 1.000, 1.000, -2.285\}, \\ &\{\gamma_{\mathrm{e0}}, \gamma_{\mathrm{eT}}\} = \{0, -0.939\}, \qquad \{\kappa_{\mathrm{Tip\_LE}}, \kappa_{\mathrm{Tip\_TE}}\} = \{1.000, 1.000\}.\end{aligned} \tag{C.18}$$

The resulting mode shape may be seen in Figure C.3 so the fuselage bends in the ‘sagging’ sense but there is no wing twist or bending. The modal mass is $m_{\mathrm{e}} = 23\,340$ kg.

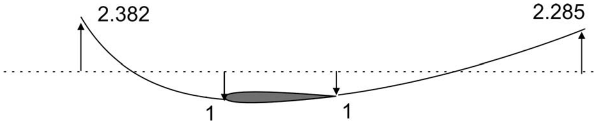

Figure C.3 Aircraft symmetric flexible mode – fuselage bending dominant.

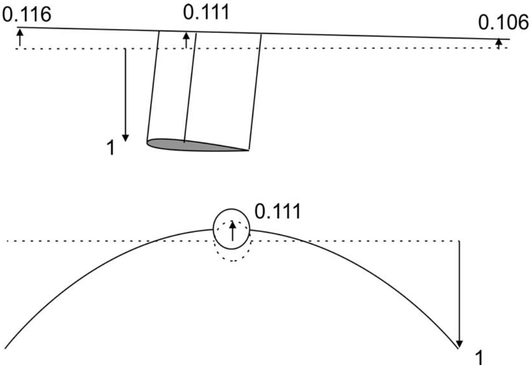

Figure C.4 Aircraft symmetric flexible mode – wing bending dominant.

C.2.8.2 *Wing bending dominant*

For the chosen parameter values then it may be shown that $A = -9.98$. The mode shape values are given by

$$\begin{aligned} &\{\kappa_{\mathrm{eF}}, \kappa_{\mathrm{e0}}, \kappa_{\mathrm{eC}}, \kappa_{\mathrm{eT}}\} = \{-0.116, -0.111, -0.111, -0.106\}, \\ &\{\gamma_{\mathrm{e0}}, \gamma_{\mathrm{eT}}\} = \{0.00077, 0.00077\}, \qquad \{\kappa_{\mathrm{Tip\_LE}}, \kappa_{\mathrm{Tip\_TE}}\} = \{0.999, 1.000\}. \end{aligned} \tag{C.19}$$

The resulting mode shape is shown in Figure C.4 so the wings bend downwards and the fuselage heaves upwards with minimal nose up pitch. The modal mass is $m_{\mathrm{e}} = 616$ kg.

C.2.8.3 *Wing torsion dominant*

For the chosen parameter values then $B = -229$, being a large value since the unswept wing pitch moment of inertia is a relatively small proportion of the value for the whole aircraft. The mode shape values are given by

$$\begin{aligned} &\{\kappa_{\mathrm{eF}}, \kappa_{\mathrm{e0}}, \kappa_{\mathrm{eC}}, \kappa_{\mathrm{eT}}\} = \{0.0222, -0.0004, -0.0017, -0.0262\}, \\ &\{\gamma_{\mathrm{e0}}, \gamma_{\mathrm{eT}}\} = \{-0.0035, -0.0035\}, \qquad \left\{\kappa_{\mathrm{Tip\_LE}}, \kappa_{\mathrm{Tip\_TE}}\right\} = \{-0.600, 1.000\}. \end{aligned} \tag{C.20}$$

The resulting mode shape may be seen in Figure C.5 so the wings twist nose up with a small fuselage nose down pitch and minimal upwards heave at the centre of mass. The modal mass is $m_{\mathrm{e}} = 325$ kg.

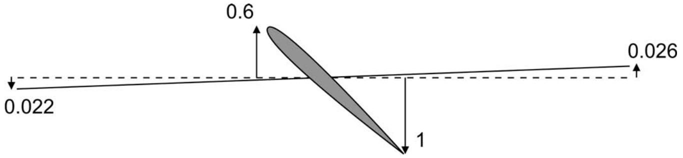

Figure C.5 Aircraft Symmetric flexible mode – wing twist dominant.

C.2.9 'J' Integrals

In the expressions for aerodynamic derivatives associated with the flexible aircraft shown in Chapters 13 to 17 and Appendix B, three integrals involving the wing bending and twisting shapes were quoted. These integrals need to be evaluated and modal quantities substituted when calculating the flexible aircraft aerodynamic derivatives. Using the assumed shapes defined in Equations (C.7) and (C.8) above, then

$$J_1 = \frac{1}{s}\int\limits_{y=0}^{s} \gamma_{\mathrm{e}} \mathrm{d}y = \left(1 + \frac{B}{2}\right)\gamma_{\mathrm{e}0}, \tag{C.21}$$

$$J_2 = \frac{1}{s}\int_{y=0}^{s} (\kappa_{\mathrm{e}} - l_{\mathrm{A}}\gamma_{\mathrm{e}})\mathrm{d}y = \left(1 + \frac{A}{3}\right)\kappa_{\mathrm{e}0} - l_{\mathrm{A}}\left(1 + \frac{B}{2}\right)\gamma_{\mathrm{e}0}, \tag{C.22}$$

$$J_3 = \frac{1}{s}\int_{y=0}^{s} (\kappa_{\mathrm{e}} - l_{\mathrm{A}}\gamma_{\mathrm{e}})\gamma_{\mathrm{e}}\mathrm{d}y = \left(1 + \frac{A}{3} + \frac{B}{2} + \frac{AB}{4}\right)\kappa_{\mathrm{e}0}\gamma_{\mathrm{e}0} - l_{\mathrm{A}}\left(1 + B + \frac{B^2}{3}\right)\gamma_{\mathrm{e}0}^2. \tag{C.23}$$

C.2.10 Other Mode Shapes

If a mode shape had been sought using the above approach with the aim of obtaining combinations of fuselage bending, wing bending and wing twisting motions, it would have been found that insufficient equations were available to obtain a solution. However, a feasible approach is to combine two or more of the above three mode shapes with suitable weightings to create a new mode, recognizing that the summation of two or more shapes that are orthogonal to the rigid body modes will also be orthogonal to them. The modal mass of the combined mode would be obtained by adding the weighted mode shapes within each term in Equation (C.16). It should be noted that the three flexible modes defined above will not be orthogonal to each other, only to the rigid body modes.

D

Model Condensation

The idea of model condensation is that the size of a static or dynamic model in either physical or modal space may be reduced in size and a faster solution obtained with a limited penalty in accuracy. In this appendix, the basic ideas will be illustrated primarily for a physical model (see Chapter 22 for application), but the concept extends to a modal model and this will be commented upon.

D.1 INTRODUCTION

For complex structures such as aircraft, the FE model can be extremely large; a static solution may be readily carried out, but a dynamic solution, such as determining eigenvalues or response, is often preceded by some form of physical 'condensation', or model order reduction.

Firstly, consider the physical equations of motion for an FE model of order *N*:

$$\mathbf{M}\ddot{\boldsymbol{r}} + \mathbf{K}\boldsymbol{r} = \boldsymbol{R}, \tag{D.1}$$

where **M**, **K** are the mass and the stiffness matrices ($N \times N$), $\boldsymbol{r}$ is the displacement vector and $\boldsymbol{R}$ is the vector of applied forces. Now consider dividing the displacements into 'master' (N_{m}) and 'slave' (N_{s}) degrees of freedom $\boldsymbol{r}_{\mathrm{m}}, \boldsymbol{r}_{\mathrm{s}}$, where normally $N_{\mathrm{m}} \ll N$. The master DoFs are those that are to be retained in the analysis, while the slave DoFs are to be removed by physical condensation for the initial analysis, but estimates of the slave DoFs can be recovered later. There are two types of condensation, static and dynamic.

For modal condensation, then clearly in the above equations the matrices are modal mass and stiffness matrices and the vectors are vectors of modal coordinates (see later).

D.2 STATIC CONDENSATION

Consider the static part of Equation (D.1) and write it in partitioned form, separating master and slave DoFs, so

$$\begin{bmatrix} \mathbf{K}_{\mathrm{mm}} & \mathbf{K}_{\mathrm{ms}} \\ \mathbf{K}_{\mathrm{sm}} & \mathbf{K}_{\mathrm{ss}} \end{bmatrix} \begin{Bmatrix} \boldsymbol{r}_{\mathrm{m}} \\ \boldsymbol{r}_{\mathrm{s}} \end{Bmatrix} = \begin{Bmatrix} \boldsymbol{R}_{\mathrm{m}} \\ \boldsymbol{R}_{\mathrm{s}} \end{Bmatrix}. \tag{D.2}$$

Taking the second (or slave) equation, then the slave DoF may be written in terms of the master DoF as follows:

$$\boldsymbol{r}_{\mathrm{s}} = \mathbf{K}_{\mathrm{ss}}^{-1} \left\{ \boldsymbol{R}_{\mathrm{s}} - \mathbf{K}_{\mathrm{sm}} \boldsymbol{r}_{\mathrm{m}} \right\}. \tag{D.3}$$

Introduction to Aircraft Aeroelasticity and Loads J. R. Wright and J. E. Cooper
© 2007 John Wiley & Sons, Ltd

Substituting the slave DoF expression in the first (or master) equation in (D.2) yields an expression for the master DoF alone:

$$\left[\mathbf{K}_{\mathrm{mm}} - \mathbf{K}_{\mathrm{ms}}\mathbf{K}_{\mathrm{ss}}^{-1}\mathbf{K}_{\mathrm{sm}}\right]\boldsymbol{r}_{\mathrm{m}} = \left\{\boldsymbol{R}_{\mathrm{m}} - \mathbf{K}_{\mathrm{ms}}\mathbf{K}_{\mathrm{ss}}^{-1}\boldsymbol{R}_{\mathrm{s}}\right\} \tag{D.4}$$

or

$$\mathbf{K}_{\mathrm{c}}\boldsymbol{r}_{\mathrm{m}} = \boldsymbol{R}_{\mathrm{c}}, \tag{D.5}$$

where the subscript c indicates a 'condensed' matrix or vector. It may be seen that the N equations have been condensed into N_{m} equations and therefore that the master DoF response may be determined from a reduced (or condensed) model. The slave DoF results may then be determined from the transformation in Equation (D.3), noting that no approximations are involved. A static solution of an FE model does not normally require condensation, but the approach may be used in some circumstances for reducing an aeroelastic model.

D.3 DYNAMIC CONDENSATION – GUYAN REDUCTION

Dynamic condensation is normally carried out using Guyan Reduction (Cook *et al.*, 1989). The main assumption in the approach is that for the lower frequency modes, the inertia and damping forces for the slave DoF are less important than the elastic forces associated with the master DoF, i.e. the slave DoF are assumed to behave quasi-statically in response to the master DoFs. The partitioned equations for the damped dynamic case are

$$\begin{bmatrix} \mathbf{M}_{\mathrm{mm}} & \mathbf{M}_{\mathrm{ms}} \\ \mathbf{M}_{\mathrm{sm}} & \mathbf{M}_{\mathrm{ss}} \end{bmatrix} \begin{Bmatrix} \ddot{\boldsymbol{r}}_{\mathrm{m}} \\ \ddot{\boldsymbol{r}}_{\mathrm{s}} \end{Bmatrix} + \begin{bmatrix} \mathbf{D}_{\mathrm{mm}} & \mathbf{D}_{\mathrm{ms}} \\ \mathbf{D}_{\mathrm{sm}} & \mathbf{D}_{\mathrm{ss}} \end{bmatrix} \begin{Bmatrix} \dot{\boldsymbol{r}}_{\mathrm{m}} \\ \dot{\boldsymbol{r}}_{\mathrm{s}} \end{Bmatrix} + \begin{bmatrix} \mathbf{K}_{\mathrm{mm}} & \mathbf{K}_{\mathrm{ms}} \\ \mathbf{K}_{\mathrm{sm}} & \mathbf{K}_{\mathrm{ss}} \end{bmatrix} \begin{Bmatrix} \boldsymbol{r}_{\mathrm{m}} \\ \boldsymbol{r}_{\mathrm{s}} \end{Bmatrix} = \begin{Bmatrix} \boldsymbol{R}_{\mathrm{m}} \\ \boldsymbol{R}_{\mathrm{s}} \end{Bmatrix}. \tag{D.6}$$

In the static condensation, a relationship between the slave and master DoFs was determined from the slave equation; however, in the dynamic case, the external forces are time varying and so cannot be employed in the transformation as they were for the static case. Therefore, in this case, a similar idea is used but the mass, damping and external forcing terms are temporarily neglected in determining the transformation such that there is no net elastic force at the slave DoF and

$$\boldsymbol{r}_{\mathrm{s}} = -\mathbf{K}_{\mathrm{ss}}^{-1}\mathbf{K}_{\mathrm{sm}}\boldsymbol{r}_{\mathrm{m}} = \mathbf{T}_{\mathrm{s}}\boldsymbol{r}_{\mathrm{m}}. \tag{D.7}$$

Then, adding the identity $\boldsymbol{r}_{\mathrm{m}} = \boldsymbol{r}_{\mathrm{m}}$ and combining these two expressions in matrix form yields the transformation

$$\begin{Bmatrix} \boldsymbol{r}_{\mathrm{m}} \\ \boldsymbol{r}_{\mathrm{s}} \end{Bmatrix} = \begin{bmatrix} \mathbf{I} \\ -\mathbf{K}_{\mathrm{ss}}^{-1}\mathbf{K}_{\mathrm{sm}} \end{bmatrix} \boldsymbol{r}_{\mathrm{m}} = \begin{bmatrix} \mathbf{I} \\ \mathbf{T}_{\mathrm{s}} \end{bmatrix} \boldsymbol{r}_{\mathrm{m}} = \mathbf{T}\boldsymbol{r}_{\mathrm{m}}, \tag{D.8}$$

where **I** is the identity matrix and **T** is an $(N \times N_{\mathrm{m}})$ transformation matrix.

This transformation expression may be substituted into Equation (D.6) and the resulting equation pre-multiplied by the transpose of **T**, so leading to the condensed equations of motion

$$\mathbf{M}_{\mathrm{c}}\ddot{\boldsymbol{r}}_{\mathrm{m}} + \mathbf{D}_{\mathrm{c}}\dot{\boldsymbol{r}}_{\mathrm{m}} + \mathbf{K}_{\mathrm{c}}\boldsymbol{r}_{\mathrm{m}} = \boldsymbol{R}_{\mathrm{c}} \tag{D.9}$$

where

$$\mathbf{M}_{\mathrm{c}} = \mathbf{T}^{\mathrm{T}}\mathbf{M}\mathbf{T}, \qquad \mathbf{D}_{\mathrm{c}} = \mathbf{T}^{\mathrm{T}}\mathbf{D}\mathbf{T}, \qquad \mathbf{K}_{\mathrm{c}} = \mathbf{T}^{\mathrm{T}}\mathbf{K}\mathbf{T}, \qquad \boldsymbol{R}_{\mathrm{c}} = \mathbf{T}^{\mathrm{T}}\boldsymbol{R}. \tag{D.10}$$

These are quite complex expressions when written out fully, with the condensed mass matrix involving the stiffness matrix.

The eigenvalue and response calculations may now be carried out for the master DoFs using the relevant parts of Equation (D.9). Estimates of the slave DoF results may then be determined from the master DoF results using Equation (D.7).

Some errors will be present in both the master and slave DoF solutions because of the assumptions made in the transformation. Therefore care must be taken that sufficient master DoFs are included to adequately model the structure over the frequency range of interest and so minimise errors. The analyst has the choice of how many master DoFs to use and where they are located; alternatively, the analysis program can select the master DoFs automatically from the desired frequency range and from the mass and stiffness matrices [Cook *et al*., 1989].

D.4 STATIC CONDENSATION FOR AEROELASTIC MODELS

In Chapter 22, it is explained how a 'beam-like' model may be developed for the aircraft dynamic behaviour. In this case, the static finite element model is 'box-like' (i.e. a reasonably representative structural model) and is condensed statically down to a model where the master structural DoFs lie along suitable reference axes for the wing/fuselage, etc. Thus, in essence the static condensed model becomes a 'beam-like' structure. Because much of the aircraft mass is nonstructural, then masses are effectively lumped at positions offset from, but attached rigidly to, the structural reference axis and near to the master structural DoFs; mass properties are therefore condensed only in the sense that the mass is discretized at suitable structural locations. Thus the condensed dynamic equations of motion are

$$\mathbf{M}_{\mathrm{mm}}\ddot{\boldsymbol{r}}_{\mathrm{m}} + \left[\mathbf{K}_{\mathrm{mm}} - \mathbf{K}_{\mathrm{ms}}\mathbf{K}_{\mathrm{ss}}^{-1}\mathbf{K}_{\mathrm{sm}}\right]\boldsymbol{r}_{\mathrm{m}} = \boldsymbol{R}_{\mathrm{m}}, \tag{D.11}$$

where $\mathbf{M}_{\mathrm{mm}}$ is a mass matrix (not diagonal because of the mass offset; see Chapter 4) representing the effect of the offset masses on the structural DoF. It is clear that any applied forces at the slave positions are neglected. Aerodynamic forces may then be added later based on this reduced model.

D.5 MODAL CONDENSATION

So far in this appendix, the focus has been upon condensation based on physical DoFs. For modal condensation, then clearly in the above equations the matrices and vectors are based in modal space.

The concept of static condensation could be employed to reduce a rigid body/flexible static aeroelastic or equilibrium manoeuvre model expressed in modal coordinates to a rigid body model, so effectively yielding the rigid body aerodynamic derivatives corrected for flexible effects (see Chapter 13). Also, the dynamic condensation approach may be applied to a dynamic aeroelastic model to reduce the model order for dynamic response calculations; in this case the slave DoFs are flexible modes to be condensed out.

D.6 MODAL REDUCTION

When a model has been transformed into modal space by using the modal matrix as a transformation matrix, this process can achieve a considerable reduction in the model order by simple truncation of the model, i.e. discarding some of the modal coordinates. Sufficient modes need to be retained in order to represent the structural behaviour over the frequency range of interest. This truncation is normally carried out prior to calculating the unsteady aerodynamic forces in modal coordinates.

E

Aerodynamic Derivatives in Body Fixed Axes

In Chapter 14, the idea of aerodynamic stability derivatives was introduced for a body fixed (or wind) axes system; these allow the effect on aerodynamic forces and moments, for a small perturbation about the equilibrium condition, to be defined. In this appendix, an example of calculating three such derivatives will be shown. Other references should be consulted for more detail and additional derivative examples (Cook, 1997; ESDU Data Sheets).

E.1 LONGITUDINAL DERIVATIVE Z_W

In this section, the longitudinal derivative Z_w will be obtained for use in Chapter 15, along with many other derivatives that are not derived here.

E.1.1 Perturbed state

The aircraft is in steady level flight at velocity V_0 (equilibrium value) and experiences a small perturbation as shown in Figure E.1; wind axes are used and the lift, drag, pitching moment and thrust are all perturbed quantities. In the *perturbed* condition, the total velocity is V with components U, W along the oxz axes. Then

$$V^2 = U^2 + W^2 \tag{E.1}$$

and

$$U = U_e + u = V\cos\theta, \qquad W = W_e + w = V\sin\theta. \tag{E.2}$$

For wind axes, the pitch attitude perturbation θ is equal to the incidence perturbation α and so for small angles

$$\theta = \alpha = \frac{W}{U}. \tag{E.3}$$

The lift and drag forces produced in the perturbation may be resolved (transformed) into the disturbed aircraft axes, so yielding the perturbed axial/normal forces in the wind axes direction and also the moment, so

$$X = L\sin\theta - D\cos\theta + \tau, \qquad Z = -L\cos\theta - D\sin\theta. \tag{E.4}$$

The moment M requires no transformation. These quantities are then used to find the required derivatives.

Introduction to Aircraft Aeroelasticity and Loads J. R. Wright and J. E. Cooper

© 2007 John Wiley & Sons, Ltd

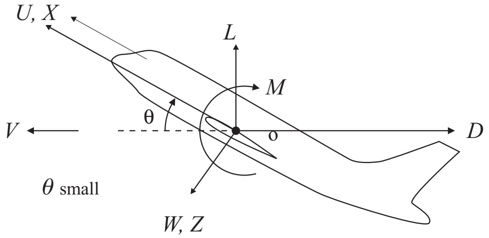

Figure E.1 Perturbed wind axes in heave/pitch.

E.1.2 Derivative for Normal Force due to Normal Velocity Perturbation

Consider, as an example, the normal force derivative due to normal velocity W. Using Equation (E.4) this is

$$Z_{\mathrm{w}} = \frac{\partial Z}{\partial W} = -\frac{\partial}{\partial W}\left[\frac{1}{2}\rho V^2 S_{\mathrm{W}}\left(C_{\mathrm{L}}\cos\theta + C_{\mathrm{D}}\sin\theta\right)\right], \tag{E.5}$$

where C_{L}, C_{D} are the whole aircraft lift and drag coefficients referenced to the wing area. The calculation of this derivative requires certain partial derivatives to be defined, namely from Equations (E.1) to (E.3) then

$$\frac{\partial V}{\partial U} = \frac{U}{V} = \cos\theta \approx 1, \qquad \frac{\partial V}{\partial W} = \frac{W}{V} = \sin\theta \approx 0, \qquad \frac{\partial \alpha}{\partial W} = \frac{\partial \theta}{\partial W} = \frac{1}{U} = \frac{1}{V\cos\theta} \approx \frac{1}{V} \tag{E.6}$$

and also

$$\frac{\partial C_{\mathrm{L}}}{\partial W} = \frac{\partial C_{\mathrm{L}}}{\partial \alpha}\frac{\partial \alpha}{\partial W} = \frac{1}{V}\frac{\partial C_{\mathrm{L}}}{\partial \alpha}, \qquad \frac{\partial(\sin\theta)}{\partial W} = \frac{1}{U} = \frac{1}{V\cos\theta} = \frac{1}{V}. \tag{E.7}$$

Thus, carrying out the differentiation in Equation (E.5), treating angles as small and substituting the above results yields the normal force due to the heave velocity derivative

$$Z_{\mathrm{w}} = -\left[\frac{1}{2}\rho V_0 S_{\mathrm{W}}\left(\frac{\partial C_{\mathrm{L}}}{\partial \alpha} + C_{\mathrm{D}}\right)\right], \tag{E.8}$$

where in the limit the total perturbation velocity tends to the equilibrium value and so $V \cong V_0$ has been used. Note that the value tabulated in Appendix B and used in Chapter 15 is written in terms of separate wing and tailplane lift curve slopes.

Other derivatives may be found in similar ways once changes in lift and moment have been expressed in terms of the velocity perturbations.

E.2 LATERAL DERIVATIVES L_P, L_ξ

Lateral derivatives involve similar principles to longitudinal derivatives but also require integration along the wing and fin using strip theory (Cook, 1997). These derivatives are not accurate and better estimates may be found in data sheets (ESDU). In this section, the lateral derivatives L_{p}, L_ξ will be obtained for use in Chapter 15.

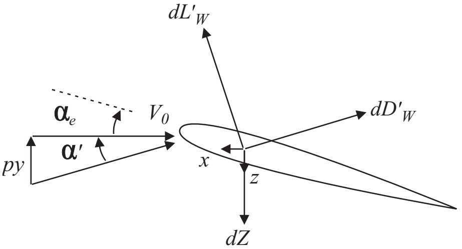

Figure E.2 Wing strip incidence in rolling flight – perturbed state.

E.2.1 Rolling Moment Derivative due to the Roll Rate

This important damping derivative arises largely from the wing, with smaller contributions from the tailplane, fin and fuselage. Consider the aircraft in steady level flight at velocity V_0 and trim incidence α_e. When the aircraft experiences a perturbation in the roll rate p, then there is an effective change of incidence on each wing strip dy, as shown in Figure E.2 for a strip on the starboard wing ($y \geq 0$). The effective increase in incidence for the elemental strip at position y is given by

$$\alpha' = \frac{py}{V_0}, \qquad py << V_0. \tag{E.9}$$

The strip lift and drag in the perturbed state are aligned normal to and along the perturbed velocity vector, so

$$\mathrm{d}L'_\mathrm{W} = \frac{1}{2}\rho V_0^2 c\,\mathrm{d}y a_\mathrm{W}\left(\alpha_\mathrm{e} + \frac{py}{V_0}\right), \qquad \mathrm{d}D'_\mathrm{W} = \frac{1}{2}\rho V_0^2 c\,\mathrm{d}y C_\mathrm{D}. \tag{E.10}$$

Referring to Figure E.2, the normal force in the wind axes direction, corresponding to the perturbed state, will be

$$\mathrm{d}Z = -\mathrm{d}L'_\mathrm{W}\cos\alpha' - \mathrm{d}D'_\mathrm{W}\sin\alpha' \approx -\mathrm{d}L'_\mathrm{W} - \mathrm{d}D'_\mathrm{W}\alpha'. \tag{E.11}$$

The elemental contribution to the rolling moment will be

$$\mathrm{d}L = y\,\mathrm{d}Z = \left(-\mathrm{d}L'_\mathrm{W} - \mathrm{d}D'_\mathrm{W}\alpha'\right)y = -\frac{1}{2}\rho V_0^2\left[a_\mathrm{W}\alpha_\mathrm{e} + (a_\mathrm{W} + C_\mathrm{D})\frac{py}{V_0}\right]cy\,\mathrm{d}y, \tag{E.12}$$

which can be integrated over the wing to determine the rolling moment. When the equivalent expression is obtained for a strip on the port side and the two rolling moment contributions added, the terms involving the trim incidence α_e cancel out as they cause no net roll effect. The total rolling moment may then be written as

$$L = -2\int_0^s \frac{1}{2}\rho V_0^2 c\,(a_\mathrm{W} + C_\mathrm{D})\,\frac{py}{V_0}y\,\mathrm{d}y. \tag{E.13}$$

Evaluating the integral and recognizing that $L = L_p p$ yields the aerodynamic rolling moment due to the roll rate derivative

$$L_p = -\frac{1}{2}\rho V_0 \left[\frac{S_W (a_W + C_D) s^2}{3}\right]. \tag{E.14}$$

The value for L_p agrees with that defined in Cook (1997) for wind axes, when neglecting fin/tailplane effects, but the wing roll damping included here is the most significant term.

E.2.2 Rolling Moment Derivative due to Aileron

In this case, the rolling moment due to deploying the full span aileron through a perturbation in ξ needs to be determined. The lift force perturbation developed on a strip on the starboard wing due to control rotation is

$$\mathrm{d}L_W = -\tfrac{1}{2}\rho V_0^2 c \,\mathrm{d}y\, a_C \xi \tag{E.15}$$

where ξ is the aileron angle (positive trailing edge down) and a_C is the sectional lift coefficient per control angle. The normal force perturbation is then given by $\mathrm{d}Z = -\mathrm{d}L_W$ since the wind axes are not perturbed. The rolling moment from each wing is the same and so, by integration, the total rolling moment is given by

$$L = 2\int_0^s \tfrac{1}{2}\rho V_0^2 c a_C \xi y \,\mathrm{d}y. \tag{E.16}$$

After evaluating the integral, the rolling moment due to aileron derivative is given by

$$L_\xi = \frac{1}{2}\rho V_0^2 \left(\frac{S_W a_C s}{2}\right). \tag{E.17}$$

A more accurate derivative may be found in ESDU.

F

Aircraft Antisymmetric Flexible Modes

In Chapter 15 a simple dynamic roll manoeuvre is introduced for rigid and flexible aircraft and so some definition of simple antisymmetric free–free whole aircraft modes is required.

F.1 AIRCRAFT MODEL

Because of the complexity of the lateral manoeuvres, the effect of the fuselage, fin and tailplane flexibility is ignored in this analysis, so only the wing will behave elastically in twisting or bending. The aircraft once again has unswept and untapered uniform wings which are permitted to bend or twist. Fuselage and empennage roll motion is present for the antisymmetric bending mode.

F.2 ANTISYMMETRIC FREE–FREE FLEXIBLE MODES

F.2.1 Antisymmetric Wing Torsion Mode

In this case, the flexible mode shape involves a (nose up) twist of the starboard wing given by the function $\gamma_e(y)$; the port wing will deform antisymmetrically (nose down), as illustrated in Figure F.1(a). The flexible mode is assumed to involve wing twist with no bending and so essentially the wing mass and elastic (or flexural) axes coincide to avoid bending/torsion coupling. The fuselage would not roll or pitch in the mode shape, since the torsional inertia moments in the two wings are balanced by antisymmetry.

For simplicity, it may be assumed that the wing torsion mode shape is given for $y \geq 0$ (starboard wing) by the linear function (refer to Chapter 3 and Appendix C)

$$\gamma_e(y) = C\frac{y}{s}, \tag{F.1}$$

where C is an unknown normalization constant. The modal mass for the whole aircraft mode may be defined by equating kinetic energies as before in Appendix C, namely

$$T = \tfrac{1}{2}m_e\dot{q}_e^2 = 2\,\tfrac{1}{2}\int_0^s \chi_W[\gamma_e(y)\dot{q}_e]^2\mathrm{d}y, \tag{F.2}$$

where χ_W is the wing torsional moment of inertia in pitch per unit span about the wing mass axis. Thus

$$m_e = 2\int_0^s \chi_W\,[\gamma_e(y)]^2\,\mathrm{d}y = \frac{I_W}{3}C^2 \tag{F.3}$$

Introduction to Aircraft Aeroelasticity and Loads J. R. Wright and J. E. Cooper
© 2007 John Wiley & Sons, Ltd

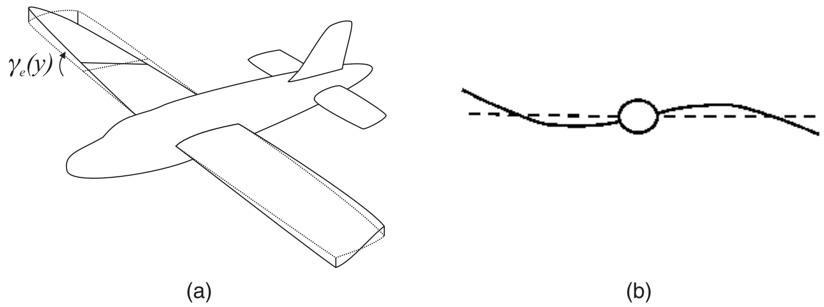

Figure F.1 Aircraft antisymmetric elastic modes: (a) wing torsion and (b) wing bending.

is the modal mass, where I_{W} is the total wing moment of inertia in pitch. Then if the mode shape is normalized to a unit twist at the tip (i.e. $C = 1$), the modal mass is given by $m_{\mathrm{e}} = I_{\mathrm{W}}/3$.

F.2.2 Antisymmetric Wing Bending Mode

Here the wing bends antisymmetrically as shown in Figure F.1(b) and the fuselage rolls such that, to satisfy orthogonality, there is no net inertia rolling moment for the free–free mode. The orthogonality expression is then

$$I_{x\mathrm{F}}\kappa'_{\mathrm{e}0} + 2\int_0^s y\mu_{\mathrm{W}}\kappa_{\mathrm{e}}(y)\,\mathrm{d}y = 0, \tag{F.4}$$

where $I_{x\mathrm{F}}$ is the roll moment of inertia for the fuselage and tailplane, $\kappa_{\mathrm{e}}(y)$ is the wing bending shape and $\kappa'_{\mathrm{e}0} = [\mathrm{d}\kappa_{\mathrm{e}}/\mathrm{d}y]_{y=0}$ is the mode shape slope at the fuselage (i.e. fuselage roll). A suitable assumed shape is

$$\kappa_{\mathrm{e}}(y) = \kappa_{\mathrm{e}0}\left(\frac{y}{s}\right)\left[1 + D\left(\frac{y}{s}\right)\right], \tag{F.5}$$

where D is an unknown constant defining the position of the nodal line along the wing and $\kappa_{\mathrm{e}0}$ is a normalization constant. When this shape is substituted into the orthogonality expression and the equation simplified using the total wing moment of inertia in roll $I_{x\mathrm{W}} = 2\mu_{\mathrm{W}}s^3/3 = m_{\mathrm{W}}s^2/3$ (uniform wings), then

$$D = -\frac{4}{3}\left(1 + \frac{I_{x\mathrm{F}}}{I_{x\mathrm{W}}}\right). \tag{F.6}$$

The mode shape therefore depends on the moment of inertia values assumed in the example. The modal mass may be shown to be given by the expression

$$m_{\mathrm{e}} = m_{\mathrm{W}}\kappa_{\mathrm{e}0}^2\left(\frac{I_{x\mathrm{F}}}{3I_{x\mathrm{W}}} + \frac{1}{3} + \frac{D}{2} + \frac{D^2}{5}\right) \tag{F.7}$$

and clearly a value for $\kappa_{\mathrm{e}0}$ will need to be chosen to define the mode shape (e.g. unity).

References

AGARD *Manual of Aeroelasticity 1956–1970*.

Albino, E. and Rodden, W.P. (1969) A doublet-lattice method for calculating lift distributions on oscillating surfaces in subsonic flows. *AIAA Journal*, **7**(2), 279–85.

Anderson, A. (2001) *Fundamentals of Aerodynamics*, 3rd edn, McGraw-Hill.

Babister, A.W. (1980) *Aircraft Dynamic Stability and Response*, Pergamon Press.

Bairstow, L. and Fage, A. (1916) Oscillations of the tailplane and body of an aircraft in flight. ARC R&M 276, part 2, July.

Benham, P.P., Crawford, R.J. and Armstrong, C.G. (1996) *Mechanics of engineering materials*, 2nd edn, Longman.

Bishop, R.E.D. and Johnson, D.C. (1979) *The Mechanics of Vibration*, Cambridge University Press.

Bisplinghoff, R.L., Ashley, H. and Halfman, R.L. (1996) *Aeroelasticity*, Dover (Addison Wesley, 1955).

Blair, M. (1994) A compilation of the mathematics leading to the doublet lattice method. WL-TR-95-3022.

Broadbent, E.G. (1954) *The Elementary Theory of Aeroelasticity*, Aircraft Engineering.

Bryan, G.H. (1911) *Stability in Aviation*, Macmillan, London.

Chen, P.C. (2000) A damping perturbation method for flutter solution: the g-method. *AIAA Journal*, **38**(9), 1519–24.

Collar, A.R. (1978) The first fifty years of aeroelasticity. *Aerospace*, February, 12–20.

Collar, A.R. and Simpson, A. (1987) *Matrices and Engineering Dynamics*, Ellis Horwood.

Cook, M.V. (1997) *Flight Dynamics Principles*, Arnold.

Cook, R.D., Malkus, D.S. and Plesha, M.E. (1989) *Concepts and Applications of Finite Element Analysis*, John Wiley & Sons, Ltd, Chichester.

CS-25: Certification Specifications for EASA; http://www.easa.eu.int/home/index.html.

Currey, N.S. (1988) *Aircraft Landing Gear Design: Principles and Practices*, AIAA Education Series.

Davies, G.A.O. (1982) *Virtual Work in Structural Analysis*, John Wiley & Sons, Ltd, Chichester.

Den Hartog, J.P. (1984) *Mechanical Vibrations*, Dover.

Donaldson, B.K. (1993) *Analysis of Aircraft Structures: An Introduction*, McGraw-Hill.

Dorf, R.C. and Bishop, R.H. (2004) *Modern Control Systems*, 10th edn, Prentice-Hall.

Dowell, E.H., Clark, R., Cox, D., Curtiss, H.C., Edwards, J.W., Hall, K.C., Peters, D.A., Scanlon, R., Simiu, E., Sisto, F. and Strganac, T.W. (2004) *A Modern Course in Aeroelasticity – Solid Mechanics and Its applications*, 4th revised and enlarged edn, Springer.

Dowell, E.H., Edwards, J.W. and Strganac, T.W. (2003) Nonlinear Aeroelasticity. *Journal of Aircraft*, **40**(5), 857–74.

Duncan, W.J, Thom, A.S. and Young, A.D. (1962) *The Mechanics of Fluids*, Arnold.

Edwards, J.W. and Weiseman, C.D. (2003) Flutter and divergence analysis using the generalized aeroelastic analysis method. In 44th AIAA Conference on *structures, Structural Dynamics and Materials*, 2003, AIAA paper 2003–1489.

Introduction to Aircraft Aeroelasticity and Loads J. R. Wright and J. E. Cooper
© 2007 John Wiley & Sons, Ltd

ESDU Data Sheets.

Etkin, B. and Reid, L.D. (1996) *Dynamics of Flight*, John Wiley & Sons, Ltd, Chichester.

Eversman, W. and Tewari, A. (1991) Consistent rational fraction approximation for unsteady aerodynamics. *Journal of Aircraft*, **28**, September, 545–52.

Ewins, D.J. (1995) *Modal Testing: Theory and Practice*, Research Studies Press.

FAR-25: Certification Specifications for FAA; http://www.faa.gov.

Flomenhoft, H.I. (1994) Brief history of gust models for aircraft design. *Journal of Aircraft*, **31**(5), 1225–7.

Flomenhoft, H.I. (1997) *The Revolution in Structural Dynamics*, Dynaflo Press.

Forsching, H.W. (1974) *Grundlagen der Aeroelastik*, Springer Verlag.

Frazer, R.A. and Duncan, W.J. (1928) The flutter of aeroplane wings. ARC R&M 1155.

Frazer, R.A., Duncan, W.J. and Collar, A.R. (1938) *Elementary Matrices*, Cambridge University Press.

Friedmann, P.P. (1999) Renaissance of aeroelasticity and its future. *Journal of Aircraft*, **36**(1), 105–21.

Fuller, J.R. (1995) Evolution of airplane gust loads design requirements. *Journal of Aircraft*, **32**(2), 235–46.

Fung, Y. (1969) *An Introduction to the Theory of Aeroelasticity*, Dover (original 1955).

Garrick, I.E. and Reid, W.H. (1981) Historical development of aircraft flutter. *Journal of Aircraft*, **18**(11), 897–912.

Golub, G.H. and van Loan, C.F. (1989) *Matrix Computations*, 2nd edn, John Hopkins Press.

Graupe, D. (1972) *Identification of Systems*, Van Nostrand Reinhold.

Hancock, G.J. (1995) *An Introduction to the Flight Dynamics of Rigid Airplanes*, Ellis Horwood,

Hancock, G.J., Simpson, A. and Wright, J.R. (1985) On the teaching of classical flutter. *Aeronautical Journal*, **89** October, 285–305.

Hassig, H.J. (1971) An approximate true damping solution of the flutter equation by determinant iteration. *Journal of Aircraft*, **8**, November, 885–9.

Hoblit, F.M. (1988) *Gust Loads on Aircraft: Concepts and Applications*, AIAA Education Series.

Hodges, D.H. and Pierce, G.A. (2002) *Introduction to Structural Dynamics and Aeroelasticity*, Cambridge University Press.

Houghton, E.L. and Brock, A.E. (1960) *Aerodynamics for Engineering students*, Edward Arnold.

Houghton, E.L. and Carpenter, P.W. (2001) *Aerodynamics for Engineering Students*, 5th edn, Butterworth Heinemann.

Howe, D. (2004) *Aircraft Loading and Structural Layout*, John Wiley & Sons, Ltd, Chichester.

Inman, D.J. (2006) *Vibration with Control*, John Wiley & Sons, Ltd, Chichester.

Jones, J.G. (1989) Statistical discrete gust method for predicting aircraft loads and dynamic response. *Journal of Aircraft*, **26**(4), 382–92.

Karpel, M. (1982) Design for active flutter suppression and gust alleviation using state space aeroelastic modelling. *Journal of Aircraft*, **19**(3), 221–7.

Katz, J. and Plotkin, A. (2001) *Low Speed Aerodynamics*, 2nd edn, Cambridge University Press.

Kuo, B.C. (1995) *Digital Control Systems*, Oxford University Press.

Lanchester, F.W. (1916) Torsional vibration of the tail of an airplane. ARC R&M 276, part 1, July.

Librescu, L. (2005) Advances in the linear/nonlinear control of aeroelastic structural systems. *Acta Mechanica*, **178**, 147–86.

Livne, E. (2003) Future of airplane aeroelasticity. *Journal of Aircraft*, **40**(6), 1066–92.

Lomax, T.L. (1996) *Structural Loads Analysis for Commercial Transport Aircraft: Theory and Practice*. AIAA Education Series.

Megson, T.H.G. (1999) *Aircraft Structures for Engineering Students*, 3rd edn, Arnold.

Meriam, J.L. (1980) *Engineering Mechanics*, Volume 2, *Dynamics*, John Wiley & Sons, Ltd, Chichester.

Milne, R.D. (1964) Dynamics of the deformable aeroplane. R and M 3345.

NAFEMS (1987) *A Finite Element Primer*, DTI.

Newland, D.E. (1987) *An Introduction to Random Vibrations and Spectral Analysis*, Longman.

Newland, D.E. (1989) *Mechanical Vibration Analysis and Computation*, Longman.

Niblett, L.T. (1998) A guide to classical flutter, *Aeronautical Journal*, **92**, 339–54.

Niu, M.C.Y. (1988) *Airframe Structural Design*, Conmilit Press.

Pratt, R.W. (ed.) (2000) *Flight Control Systems: Practical Issues in Design and Implementation*, IEE Control Engineering Series.

Rao, S.S. (1995) *Mechanical Vibrations*, Addison Wesley.

Raven, F.H. (1994) *Automatic Control Engineering*, 5th edn, McGraw-Hill.

Roger, K.L. (1977) Airplane math modelling and active aeroelastic control design. AGARD-CP-228, pp. 4.1–4.11.

Russell, J.B. (2003) *Performance and Stability of Aircraft*, Butterworth-Heinemann.

Scanlan, R.H. and Rosenbaum, R. (1960) *Introduction to the Study of Aircraft Vibration and Flutter*, Macmillan.

Schmidt, L.V. (1998) *Introduction to Aircraft Flight Dynamics*, AIAA Education Series.

Scott, R.C., Pototzky, A.S. and Perry, B. (1993) Computation of maximised gust loads for nonlinear aircraft using matched filter based schemes. *Journal of Aircraft*, **30**(5), 763–68.

Stengel, R.F. (2004) *Flight Dynamics*, Princeton University Press.

Stroud, K.A. and Booth, D.J. (2007) *Engineering Mathematics*, 6th edn, Industrial Press Inc.

Sun, C.T. (2006) *Mechanics of Aircraft Structures*, John Wiley & Sons, Ltd, Chichester.

Taylor, N.V., Vio, G.A., Rampurawala, A.M., Allen, C.B., Badcock, K.J., Cooper, J.E., Gaitonde, A.L., Henshaw, M.J., Jones, D.P. and Woodgate, M.A. (2006) Aeroelastic simulation through linear and non-linear analysis, A summary of flutter prediction in the PUMA DARP. *Aeronautical Journal*, **110**(1107), 333–43.

Theodorsen, T. (1935) General theory of aerodynamic instability and the mechanism of flutter. NACA Report 496.

Thomson, W.T. (1997) *Theory of Vibration with Applications*, 5th edn, Chapman and Hall.

Tse, F.S., Morse, I.E. and Hinkle, R.T. (1978) *Mechanical Vibrations: Theory and Applications*, Allyn and Bacon.

Waszak, M.R. and Schmidt, D.K. (1988) Flight dynamics of aeroelastic vehicles. *Journal of Aircraft*, **25**(6), June.

Wells, D.A. (1967) *Theory and Problems of Lagrangian Dynamics*, Schaum's Outline Series, McGraw-Hill, New York.

Whittle, P. (1996) *Optimal Control, Basics and Beyond*, Wiley.

Wright, J.R., Wong, J., Cooper, J.E. and Dimitriadis (2003) On the use of control surface excitation in flutter testing, *Proc. Instn Mech. Engrs, Part G: J. Aerospace Engineering*, **217**(96), 317–32.

Yates, E.C. (1966) Modified strip analysis method for predicting wing flutter at subsonic to hypersonic speeds. *Journal of Aircraft*, **3**(1), 25–9.

Young, W.C. (1989) Roark's Formulas for Stress and Strain, 6th edn, McGraw-Hill.

Zimmermann, H. (1991) Aeroservoelasticity. *Computer Methods in Applied Mechanics and Engineering*, **90**(13), 719–35.

Zimmermann, N.H. and Weissenberger, J.T. (1964) Prediction of flutter onset speed based on flight testing at subcritical speeds. *Journal of Aircraft*, **1**(4), 190–202.

Index

Aerodynamic derivatives
  body fixed/wind axes, 256, 267, 272, 280, 284, 432, 471, 485
  flexible corrections, 238, 433, 439
  inertial axes, 218, 231, 293, 471
  oscillatory, 159
Aerodynamic Influence Coefficients (AICs), 194, 388–415, 433
  harmonic motion, 394
  modal space, 397
Aerodynamic(s), 69–85, 381–400
  AICs – *see* Aerodynamic Influence Coefficients
  Bernoulli's equation, 73, 385
  Biot-Savart law, 391
  centre of pressure, 74
  centre, 76
  CFD (Computational Fluid Dynamics), 432, 439
  circulation, 386
  damping, 160, 168, 171
  Doublet Lattice method, 396, 409, 432
  doublet, 383
  drag, 74, 81, 213, 218, 267, 485
  dynamic pressure, 72
  gusts, 161, 297, 301, 318
  horseshoe vortex, 392
  Influence coefficients, 389
  Kutta condition, 388
  lift curve slope, 75, 78
  Mach No, 71
  panel method, 81, 405
  point sink/source, 382
  quasi-steady, 153, 168, 173, 256, 295
  Rankine oval, 384
  Rational Fraction Approximation, 412, 434
  stiffness, 160, 171
  stream function, 381
  streamlines, 72
  strip theory, 79, 212, 228, 236, 394, 432
  supersonic flow – Piston theory, 83, 194
  three D oscillating wing, 396
  three D wing modelling, 77, 81, 391
  transonic flows, 84
  two D aerofoil modelling, 388
  two D oscillating aerofoil, 394
  unsteady, 154–165, 167, 187, 300, 313, 318, 325
  velocity potential, 382
  vortex filaments, 391
  Vortex Lattice method, 393
  vorticity, 386
Aeroelastic equations, 171, 402, 408
Aeroservoelasticity (ASE), *see also*, Flutter, 201–209, 441
  closed loop system stability, 204
  control law frequency dependence, 206
  control system implementation, 204
  gust response, 205
  response calculation – frequency domain, 208
  response calculation – time domain, 208
  state space modelling, 208
Aircraft model for certification
  aerodynamic, 432
  beam-like stiffness representation, 53, 65, 427
  box-like stiffness representation, 53, 65, 427
  damping, 431
  dynamic manoeuvre, 446
  equilibrium manoeuvre, 443
  Flight Control System (FCS), 435
  flutter, 439
  ground manoeuvre, 455
  gusts and turbulence encounter, 449
  mass/damping/stiffness/force, 427
  modes, 431
  rigid aircraft, 432
  static aeroelasticity, 437
  stick-like stiffness representation, 46, 49, 53
Atmosphere, 69
Auxiliary equation, *see* Internal load(s)
Axes system
  body fixed/wind, 246
  earth fixed/inertial, 218, 231, 246, 293
  mean, 258
  transformation, 248

Introduction to Aircraft Aeroelasticity and Loads J. R. Wright and J. E. Cooper
© 2007 John Wiley & Sons, Ltd

Balanced manoeuvre, *see* Equilibrium manoeuvre
Bernouilli's equation, *see* Aerodynamics
Bessel Function, 163
Binary aeroelastic model
  control surface term, 202
  flutter, 168, 172
  gust terms, 203
Biot-Savart law, *see* Aerodynamic(s)
Bode plot, 113
Bookcase manoeuvre, 211–244, 423, 443, 455
Braking, 345, 457

Centre of gravity, *see* Centre of mass
Centre of mass, 88, 422
Centripetal acceleration, 212, 252
Certification process
  dynamic aeroelasticity – flutter, 439, 461, 465
  dynamic manoeuvre, 446
  equilibrium manoeuvre, 443
  gust/turbulence encounter, 449
  overall, 421
  static aeroelasticity, 437
Characteristic equation, 111
Checked manoeuvre, 265, 448
Condensation, 66, 429, 433, 481
Continuous system/structure, *see* Vibration
Continuous turbulence, *see* Turbulence
Control effectiveness, *see* Static aeroelasticity
Control reversal, *see* Static aeroelasticity
Control surface, 82, 202
Control systems
  closed loop, 107, 110
  open loop, 107, 110
  PID control, 118
Convolution integral, 12, 34
Coriolis acceleration, 252
Correlated loads, 374, 451, 458
CS-25, *see* Certification process

D'Alembert's principle
  body, 91
  particle, 90
Damping
  coupling, 29
  hysteretic, 9
  proportional/non-proportional, 25
  ratio, 6, 24
  viscous, 4
Design process/envelopes, 419, 422
Dimensioning, 376
Discretised system/structure, *see* Vibration
Divergence, *see* Static aeroelasticity
Doublet Lattice method, *see* Aerodynamic(s)
Duhamel integral, *see* Convolution integral
Dynamic aeroelasticity, *see* Flutter
Dynamic manoeuvre, 211, 245, 265–292, 446
  flexible aircraft in heave/pitch, 271, 448
  flexible aircraft in roll, 283, 448
  rigid aircraft in heave/pitch, 266
  rigid aircraft in roll, 279
Dynamic overswing, 10, 241

Eigenvalue solution
  non-symmetric, 171
  symmetric, 22
Elevator angle to trim, 218, 225
Equilibrium manoeuvre, 211–244, 443
  flexible aircraft in pitch, 225, 444
  rigid aircraft in normal acceleration, 213
  rigid aircraft in pitch, 218
  rigid aircraft in roll and yaw, 239, 445

Failure cases, 440, 449
FAR-25, *see* Certification process
Fatigue/damage tolerance, 424
Finite Element (FE) method, 53
  assembly/solution process, 58, 405
  boundary conditions, 61
  element formulation, 54
  element mass matrix, 57
  element shape function, 55
  element stiffness matrix, 57
  element type
    bar/rod/axial, 64, 448
    bending, 55, 427
    combined bending/torsion, 64, 405
    shell/membrane, 66, 428
    torsion, 63
  kinematically equivalent nodal forces, 58, 407
Flexible aircraft, 225, 273, 289
Flexural axis, 44, 64, 225, 236, 359, 427
Flight Control System (FCS), 263, 435
  Gust Load Alleviation, 263, 435
  Manoeuvre Load Alleviation, 263, 435
Flight flutter test, 465
Flight loads validation, 466
Flight mechanics equations, 245–264, 432
  dynamic stability modes, 262
  flexible aircraft, 246, 257, 432
  rigid aircraft, 252
  solution process, 262
Flight simulator test, 464
Flutter, 167–199, 439
  aerodynamic damping, 173
  aeroservoelastic calculations, 204, 441
  binary, 168, 172
  boundary, 440
  control surface, 191
  eigenvalue solution, *see also* Eigenvalue solution, 171, 182
  flexible wing, 180
  flexural axis position, 167, 179

  flutter conic, 184
  frequency coalesence, 173
  frequency matching – 'k' method, 188
  frequency matching – 'pk' method, 189
  Handley Page 0-400 Bomber, 184
  hard/soft, 177
  mass axis position, 169, 179
  panel, 194
  phasing of motion, 176
  prediction of critical speed, 182, 187
  structural damping, 171, 178
  supersonic flows, 194
  transonic flows, 194
  unsteady aerodynamics, 167–193, 433
  whole aircraft, 193
  wind off frequency spacing, 180
Forced vibration
  harmonic, 7, 31
  random, 16, 34
  transient, 10, 33
Fourier Transform (FT)
  analytical, 14
Fourier Transform (FT)
  discrete, 15
Free vibration, 5, 21
Frequency parameter, *see* Reduced frequency
Frequency Response Function (FRF)
  response per force, 8, 32
  response per gust velocity, 318
Friction coefficient, 345

Generalised coordinate, 38
Generalised equation, 39, 41, 42
Generalised force, 41, 42
Ground manoeuvres, 329–354
Ground vibration test, 28, 33, 179, 431, 462
Gust aerodynamics, *see* Aerodynamic(s)
Gust envelope, 299
Gust Load Alleviation, *see* Flight Control System
Gust loads, *see* Internal loads
Gust response
  flexible aircraft in heave/pitch, 306
  rigid aircraft in heave, 297
  rigid aircraft in heave/pitch, 303
Gust(s), 293–327, 449
  alleviation factor, 299, 302
  (1 – cosine), 296
  design gust velocity, 451
  discrete, 294–313, 451
  flight profile alleviation factor, 451
  gradient distance, 296, 451
  inclusion in binary aeroelastic model, 203
  Loads, *see* internal loads
  penetration effect, 295, 320
  sharp-edged, 295
Guyan reduction, *see* Condensation

Hankel Function, 157
Harmonic gust, 157, 162, 315

Impulse Response Function (IRF), 10
Incremental work, 4, 5, 20, 40, 41, 44
Inertia couple, *see* Loads
Inertia coupling, 44, 64
Inertia force, *see* Loads
Inertia relief, 356
Influence Coefficients, *see also* Aerodynamic(s), 389, 402
Internal load(s), 95, 355–380
  auxiliary equation, 370, 436
  continuous wing, 356, 358
  determination of, 96, 100, 443
  discretised wing, 366
  force summation, 369, 443
  fuselage, 357, 370
  manoeuvre/gust, 361, 362
  MAST loads, 95, 103, 374, 443, 458
  turbulence, 373
  wing-mounted engines/landing gear, 360

Jig shape, 438

Kinetic energy
  bending/torsion, 40, 43
Kussner's Function, *see also* Aerodynamic(s), unsteady, 161, 301, 313, 433

Lagrange's energy equations, 4, 20, 41, 45
Landing
  flexible aircraft, 345, 456
  rigid aircraft, 341
  spin-up and spring-back, 348, 456
Landing gear
  layout, 329, 333, 455
  oleo-pneumatic shock absorber, 330
  wheel/tyre, 332
Laplace Transform, 108
Lift distribution, *see* Static Aeroelasticity
Limit Cycle Oscillations (LCO), 197
Limit load, 316, 356, 424
Load(s)
  external, 93, 356
  Free Body Diagram (FBD), 94, 356, 358
  generation/sorting, 374, 458
  inertia couple, 91, 212, 241
  inertia force, 90, 213, 253, 260
  inter-component, 102, 370
  internal – *see* Internal load(s)
  reactive (reactions), 93, 346, 350
  weight, 93
Load envelopes, 374
Load factor, 213
Lumped parameter system, *see* Vibration

Manoeuvre envelope, 217
Manoeuvre Load Alleviation, *see* Flight Control System
Manoeuvre loads, *see* Internal load(s)
Matrix differentiation, 45
Modal
  mass/damping/stiffness/force, 27
  matrix, 23, 24, 27
  reduction, 30, 484
  space/coordinates, 27
Mode
  branch, 46
  complex, 24, 171
  dimensions, 30
  dynamic stability – *see* Flight mechanics equations
  flapping/pitching, 168
  flexible, 46, 49, 225, 473
  free-free, 31, 46, 49
  fuselage bending dominant, 225, 476
  normal/real, 22, 39, 49
  normalisation, 29
  orthogonality, 27
  rigid body, 31, 46, 49, 193, 469
  shape, 22, 24, 30
  whole aircraft antisymmetric, 283, 489
  whole aircraft symmetric, 225, 473
  wing bending dominant, 225, 476
  wing torsion dominant, 225, 477
Moment of inertia, 89, 25, 259

Natural frequency
  damped, 6
  effective, 24
  undamped, 6, 22
Newton's laws
  body, 88
  particle, 88
  units, 89
Non-linearity, 197, 441, 447, 451
Nyquist plot, 113

Phugoid motion, 262, 269, 275
Power Spectral Density (PSD), 16, 314
Product moment of inertia, 240, 254

Quasi-steady aerodynamics, *see* Aerodynamic(s)

Rational Fraction Approximation, *see* Aerodynamic(s)
Rational manoeuvre, 212, 239, 269–292, 423, 446, 455
Rayleigh damping coefficients, 178
Rayleigh-Ritz method, 38, 127
Reduced frequency, 156, 167, 187, 318, 409, 432,
Reference axes, 427
Reversal, *see* Static aeroelasticity
Rigidity, flexural/torsional, 39, 43
Roll subsidence, 263, 282, 287
Root locus plot, 113
Root-mean-square (RMS), 17, 314, 373
Routh-Hurwitz method, 112, 182

Scaled frequency, 314
Sears' Function, *see also* Aerodynamic(s), unsteady
Shear centre, 44, 427
Shimmy, 350
Short period motion, 262, 268, 275
Slip ratio, 346
Spin-up, *see* Landing
Spring-back, *see* Landing
Stability
  control systems, 111
  gain margin, 114
  phase margin, 114
State Space equations, 116, 208, 412
Static aeroelasticity, 123–151
  control effectiveness
    fixed wing case, 146
    full aircraft model, 149, 274, 286, 438
    steady roll rate case, 141
  deformation
    effect of trim, 129
    fixed wing case, 127
    2D aerofoil, 124
  divergence
    effect of sweep, 134
    effect of trim, 129
    fixed root flexible wing, 127
    full aircraft model, 186, 402, 439
    2D aerofoil, 124
  lift distribution
    effect of sweep, 134
    effect of trim, 129
    fixed wing case, 127, 145
    steady roll rate case, 145
  reversal
    effect of trim, 151
    fixed wing case, 146
    steady roll rate case, 141
Static stability, 223
Step Response Function (SRF), 10
Strain energy
  bending/torsion, 40, 43
Stress, 103, 374, 377, 458
Structural coupling test, 463
Structural test(s), 464
Superposition, 11, 12
Swept wing – flexible effects, 134, 236

Taxiing
  flexible aircraft in heave/pitch, 337, 457
  rigid aircraft in heave/pitch, 334
  runway profile, 333, 457

Theodorsen's Function, *see also* Aerodynamic(s), unsteady, 156, 318
Thrust, 213, 218, 256
Transfer function
  control systems, 108, 110
  flight mechanics, 268, 273, 281, 286
Trimmed manoeuvre, *see* Equilibrium manoeuvre
Turbulence, 314–326, 449
  Design Envelope Analysis, 451
  loads – *see* Internal load(s)
  Mission Analysis, 451
  reference/limit intensity, 452
Turbulence PSD (von Karman), 314
Turbulence response
  flexible aircraft in heave/pitch, 323
  rigid aircraft in heave/pitch, 320
  rigid aircraft in heave, 297
Turbulence response PSD, 316
Turning, 350, 457

Ultimate load, 356, 424, 464
Unchecked manoeuvre, 265, 448
Unsteady aerodynamics, *see* Aerodynamic(s)

Vibration
  continuous systems – Finite Element method, 53–67
  continuous systems – Rayleigh-Ritz method, 38–52
  free-free system, 31, 46, 49
  mutliple DoF systems, 19–36
  single DoF systems, 3–18

Wagner's Function, *see also* Aerodynamic(s), unsteady, 154, 301, 313, 433
Wind tunnel test(s), 432, 461

G

MATLAB/SIMULINK Programs for Vibration

It is beyond the scope of this book to present a detailed treatment of the use of MATLAB and SIMULINK, but instead a few key programs are presented which the reader can use as a template for trying other related calculations. It is assumed that a basic knowledge of the packages will be obtained from other sources.

G.1 FORCED RESPONSE OF AN SDoF SYSTEM

In Chapter 1, the example of an SDoF system excited by a single cycle of a square wave was considered. The response was obtained in three ways, namely using superposition (essentially simple convolution), numerical integration and via the frequency domain (using the Fourier Transform).

G.1.1 Superposition (Essentially Convolution)

The superposition approach treats the double pulse excitation as the combination of three steps. The response to a single step is used as a constituent building block in generating the overall response. Clearly, different inputs such as square waves of different numbers of cycles and periods may be explored by simple modifications of the code.

The program is shown below. The theory in Chapter 1 will be required to follow the program.

```
% Response of SDoF system to single cycle of a square wave
clear all; close all;

% System parameters
f_nat = 2; period = 1 / f_nat; w_nat = 2 * pi * f_nat; zeta = 0.05;
mass = 1000; stiff = w_nat^2 * mass; force = 1000;
w_dpd = w_nat* sqrt(1-zeta^2); psi = atan2(sqrt(1 - zeta^2), zeta);

% Data parameters
T = 8; dt = 0.01; t = [0:dt:T]; [dummy,nt] = size(t);

% Response to step force
for it = 1:nt
   a = exp(-zeta * w_nat * t(it)) / sqrt(1 - zeta^2);
   b = sin(w_dpd * t(it) + psi);
   s(it)= force / stiff * (1 - a * b);
end
```

Introduction to Aircraft Aeroelasticity and Loads J. R. Wright and J. E. Cooper
© 2007 John Wiley & Sons, Ltd

```
% Response to square wave using superposition
% Function p shows 'shape' of excitation force
pulse_width = period / 2; npulse = round(pulse_width / dt);
for it = 1 : npulse
   x(it) = s(it); f(it) = 10;
end
for it = npulse + 1 : 2 * npulse
   x(it) = s(it) - 2 * s(it - npulse);
   f(it) = - 10;
end
for it = 2 * npulse + 1 : nt
   x(it) = s(it) - 2 * s(it - npulse) + s(it - 2 * npulse);
   f(it) = 0;
end

% Plot response in mm
plot(t,x*1000,'k-',t,f,'k:'); axis([0 T -25 25]);
xlabel('Time (s)'); ylabel('Response to Double Pulse (mm)')
```

G.1.2 Numerical Integration

The numerical integration approach uses the SIMULINK package called from MATLAB. The SIMULINK diagram shown in Figure G.1 is built by rewriting the differential equation of motion in terms of the acceleration, so typically

$$\ddot{x} = -\frac{c}{m}\dot{x} - \frac{k}{m}x + \frac{f(t)}{m}. \tag{G.1}$$

The three right-hand side terms are added in the sum block to provide the acceleration, the integrators generate velocity and displacement and the feedback terms provide the inputs to the sum block and so on. The force array corresponding to the required time values is calculated in the MATLAB code from which the SIMULINK function is called. The result of the integration is returned to the workspace for plotting, etc. Clearly, other excitation types may be explored by modifying this code.

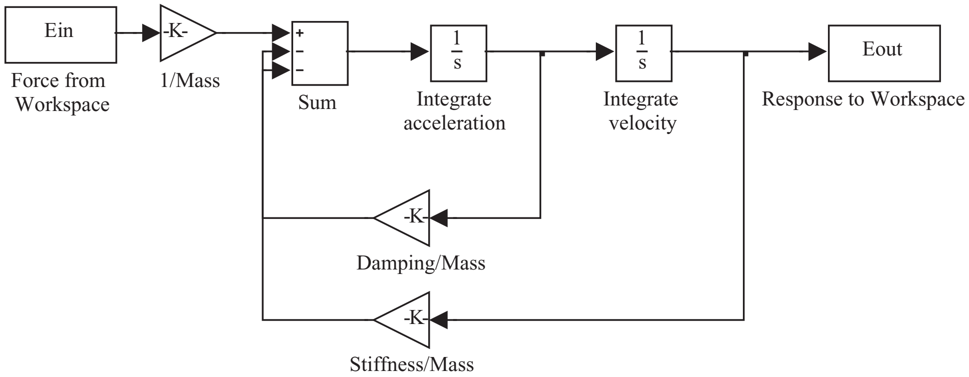
Ein
Force from Workspace
-K-
1/Mass
+
-
-
Sum
1/s
Integrate acceleration
1/s
Integrate velocity
Eout
Response to Workspace
-K-
Damping/Mass
-K-
Stiffness/Mass

Figure G.1 SIMULINK diagram for the SDoF example.

It should be noted that it is possible to solve simultaneous differential equations (linear or nonlinear) using SIMULINK. A further example is shown in Appendix E where manoeuvres and gust encounters are considered.

The program is shown below. The theory in Chapter 1 will be required to follow the program.

```
% Response of SDoF to single cycle of a square wave using SIMULINK
clear all; close all

% System parameters
f_nat = 2; period = 1 / f_nat; w_nat = 2 * pi * f_nat; zeta = 0.05;
mass = 1000; damp = 2 * zeta * mass * w_nat;
stiff = w_nat^2 * mass; force = 1000;

% Simulation parameters
T = 8; dt = 0.01; t = [0:dt:T]; [dummy,nt] = size(t);

% Define excitation f(t)
pulse_width = period / 2; npulse = round(pulse_width / dt);
for it = 1 : npulse
   f(it) = force;
end
for it = npulse + 1 : 2 * npulse
   f(it) = - force;
end
for it = 2 * npulse + 1 : nt
   f(it) = 0;
end

% Run SIMULINK model for SDOF (works with column vectors in
  workspace
% blocks Ein and Eout) using variable step length solver ODE45 with
% outputs at same time intervals dt as for input - note that the
  SIMULINK file
% needs to be in the same directory as the core MATLAB program
Ein = [t',f'];
sim('SDoF_Pulse');

% Access stored data for response x - convert back to row vector for
% consistency with f and t - convert to mm
x = 1000 * Eout';

% Plot response
figure(1); plot(t,x); axis([0 T -25 25]);
xlabel('Time (s)'); ylabel(`Response to Single Cycle of a Square
Wave');
```

G.1.3 Via Frequency Domain

The frequency domain approach uses the Fourier transform. The excitation time sequence is generated, transformed to the frequency domain, multiplied by the frequency response function (FRF) and inverse transformed to yield the response. It will be seen that special care is taken to include the negative frequency values in the FRF in order to match the form of the Fourier transform and so allow inverse transformation to be carried out. Studying this program and its output will help the reader gain some understanding of the use of the Fourier transform in MATLAB. Clearly, other input types and analyses may be tried by suitable modification of the code.

The program is shown below. The theory in Chapter 1 will be required to follow the program.

```
% Response of SDoF to single cycle of a square wave using the
  Fourier Transform and
% transformation into the frequency domain and back again clear all;
close all

% System parameters
f_nat = 2; period = 1 / f_nat; w_nat = 2 * pi * f_nat; zeta = 0.05;
mass = 1000; stiff = w_nat^2 * mass; force = 1000;

% Data parameters in time and frequency domains - note that time
  vector
% stops dt short of T for FT analysis to remain a power of 2 and
  periodic
T = 8; nt = 128; dt = T / nt; t = [0:dt:T - dt];
df = 1 / T; f_nyq = 1 / 2 / dt; frq = [0:df:f_nyq]; [dummy,nf] =
size(frq);

% Define square wave cycle excitation x(t)
pulse_width = period / 2; npulse = round(pulse_width / dt);
for it = 1 : npulse
  f(it) = force;
end
for it = npulse + 1 : 2 * npulse
  f(it) = - force;
end
for it = 2 * npulse + 1 : nt
  f(it) = 0;
end

% Fourier Transform f(t) to frequency domain FF - apply scaling
factor nt
FF = fft(f,nt) / nt;
figure(1)
plot(frq(1:nf),real(FF(1:nf)),'kx',frq(1:nf),imag(FF(1:nf)),'ko');
xlabel('Frequency (Hz)'); ylabel(`Real / Imaginary Parts - FT of
x(t)');
legend('Real Part','Imaginary Part')

% Generate the Frequency Response Function (FRF) for SDoF over 0 -
  f_nyq
for ifq = 1 : nf
  w = 2 * pi * frq(ifq);
  r = w / w_nat;
  H(ifq) = (1 / stiff)/(1 - r^2 + i * 2 * zeta * r);
end
```

```
H(nf) = real(H(nf));

% Generate the FRF 'negative' frequency content (i.e. pack to nt
  complex
% numbers) to be in correct format for inverse FT
for ifq = nf + 1 : nt
   H(ifq) = conj(H(nt - ifq + 2));
end
figure(2)
plot(frq(1:nf),real(H(1:nf)),'kx',frq(1:nf),imag(H(1:nf)),'ko');
xlabel('Frequency (Hz)'); ylabel(`Real / Imaginary Parts - FRF');
legend('Real Part','Imaginary Part')

% Multiply FRF by FT of f(t)(element by element) to get XF - FT of
  x(t)
XF = H. * FF;
figure(3)
plot(frq(1:nf),real(XF(1:nf)),'kx',frq(1:nf),imag(XF(1:nf)),'ko')
xlabel('Frequency (Hz)'); ylabel(`Real /Imaginary Parts - FFT of
y(t)');
legend('Real Part','Imaginary Part');

% Generate response x(t) using the IFT of XF - apply scaling factor
nt
x = ifft(XF) * nt;

% Plot response in mm
figure(4); subplot(211);
plot(t,f,'k');
xlabel('Time (s)'); ylabel(`Excitation (N)');
subplot(212);
plot(t,x*1000,'k'); axis([0 T -25 25]);
xlabel('Time (s)'); ylabel('Response to Single Cycle of a Square
Wave (mm)');
```

G.2 MODAL SOLUTION FOR AN MDoF SYSTEM

In Chapter 2, the modal characteristics of a two DoF aircraft system were considered and the resulting natural frequencies, modal matrix (and hence mode shapes) and modal quantities were presented. In this section, a program is presented for performing these matrix operations and for generating FRF plots. Clearly, other cases such as those explored in Chapters 3 and 4 may be considered by modifying the code.

The program is shown below. The theory in Chapter 2 will be required to follow the program.

```
% Determination of Modal Parameters and FRFs for a 2 DoF system
clear all; close all; nmodes = 2;

% System (2 by 2) mass, stiffness and damping matrices
M = [2 0; 0 1]; K = [3000 -1000; -1000 1000]; C = [6 -2; -2 2];
```

```
% Eigenvalue solution
[vec,val] = eig(M\K);

% Sort eigenvalues / vectors into ascending order of frequency
% and find natural frequencies and mode shapes (psi is modal matrix)
for j = 1:nmodes;
  [max_vec, max_index] = max(abs(vec(:,j))); vec(:,j) = vec(:,j)./
  vec(max_index,j);
  f_nat(j) = sqrt(val(j,j)) / 2 / pi;
end
[f_nat, index] = sort(f_nat);
for j = 1:nmodes;
  psi(:,j) = vec(:,index(j));
end

% Modal matrices
MP = psi' * M * psi; CP = psi' * C * psi; KP = psi' * K * psi;

% Modal masses and dampings
for j = 1:nmodes
  modal_mass(j) = MP(j,j); modal_damping(j) = CP(j,j) / 2 / sqrt
  (MP(j,j) * KP(j,j));
end

% Write out results
f_nat, psi, MP, CP, KP, modal_mass, modal_damping

% Set up parameters for FRF generation and initialise FRF matrix
f_nyq = 10; nt = 1024; nf = nt/2 + 1; frq = linspace(0,f_nyq,nf);
H = zeros(nmodes,nmodes,nf);

% Calculate FRF for each frequency value from DC up to Nyquist
% and set Nyquist frequency value to be real - note that FRF needs to
% be a 3 dimensional array (response r / excitation e / fre-
quency nf)
for ifq = 1:nf
  w = 2 * pi * frq(ifq);
  H(:,:,ifq) = inv(K - (w^2 * M) + (i * w * C));
end
H(:,:,nf) = real(H(:,:,nf));

% Plot first row of FRF matrix - 'squeeze' function needed to bring
  matrix
% from 3 to 2 dimensions in order to plot - use `log' plot to show
FRF more clearly
subplot(211)
semilogy(frq(1:nf), abs(squeeze(H(1,1,1:nf))),'k');
xlabel('Frequency (Hz)'); ylabel(`Direct FRF 11');
subplot(212)
semilogy(frq(1:nf), abs(squeeze(H(1,2,1:nf))),'k');
xlabel('Frequency (Hz)'); ylabel(`Transfer FRF 12');
```

G.3 FINITE ELEMENT SOLUTION

In Chapter 4, the finite element method was introduced and the effect of increasing the number of elements for a uniform cantilever beam was considered. In this section, the generation and assembly of the element stiffness and mass matrices and the generation of natural frequencies is carried out for a range of numbers of elements and also for both consistent and lumped mass representations. Clearly, other cases may be considered by modifying the code.

The program is shown below. The theory in Chapter 4 will be required to follow the program.

```
% FE model of a 'beam' with increasing number of elements
clear all; close all; nelement = 10;

% Loop around increasing numbers of elements
for jelement = 1:nelement
   nw = 4 + (jelement - 1) * 2;

   % Initialise matrices
   kw = zeros(nw); %Overall beam stiffness matrix - unconstrained
   mw = zeros(nw); %Overall beam mass matrix - unconstrained

   % Parameters for beam and element
   s = 10; L = s / jelement; E = 70e9; I = 2e-4; A = 0.04; rho = 2500;
   b = rho * A * L;

   % Element stiffness data and matrix
   k1 = 12 * E * I / L^3; k2 = 6 * E * I / L^2; k3 = 2 * E * I / L;
   k4 = 4 * E * I / L;
   k = [k1 k2 -k1 k2; k2 k4 -k2 k3; -k1 -k2 k1 -k2; k2 k3 -k2 k4];

   % Mass data
   m1 = 156 * b / 420; m2 = 22 * b * L / 420; m3 = 54 * b / 420; m4 =
   13 * b * L / 420;
   m5 = 4 * b * L^2 / 420; m6 = 3 * b * L^2 / 420; m7 = b / 2; m8 =
   b * L^2 / 24;

   % Element consistent mass matrix (comment out lumped mass matrix)
   m = [m1 m2 m3 -m4; m2 m5 m4 -m6; m3 m4 m1 -m2; -m4 -m6 -m2 m5];

   % Element lumped mass matrix (comment out consistent mass matrix)
   % m = diag([m7 m8 m7 m8]);

   % Beam overall stiffness matrix
   kw(1:4,1:4) = k(1:4,1:4);
   if jelement > 1
     for i = 2:jelement
      j = 2 * i - 1; jj = j + 3;
      kw(j:jj, j:jj) = kw(j:jj, j:jj) + k(1:4,1:4);
     end
   end

   % Beam overall mass matrix
   mw(1:4,1:4) = m(1:4,1:4);
   if jelement > 1
     for i = 2:jelement
      j = 2 * i - 1; jj = j + 3;
      mw(j:jj, j:jj) = mw(j:jj, j:jj) + m(1:4,1:4);
     end
   end

   % Select structure stiffness / mass matrices to account for the
   fixed end

   % Origin at tip (comment out origin at root)
   % nwf = nw - 2; kwf = kw(1:nwf,1:nwf); mwf = mw(1:nwf,1:nwf);

   % Origin at root (comment out origin at tip)
   kwf = kw(3:nw,3:nw); mwf = mw(3:nw,3:nw);

   % Solve for eigenvalues
   [r,la] = eig(kwf,mwf); [las,n] = sort(diag(la)); fn = sqrt(las) / 2 /
   pi;

   % disp('Natural frequencies and no of elements');
   % disp(sprintf('%.0f n',jelement)); disp(sprintf('%.3f n',fn));
   [nfn,dummy] = size(fn);
   for jf = 1:nfn
      if jf < 4
       fstore(jf,jelement) = fn(jf);
      end
    end
end
fstore(3,1) = NaN; fstore
element = [1 2 3 4 5 6 7 8 9 10];
hold on; axis([0 10 0 50]);
xlabel('Number of Elements'); ylabel(`Natural Frequencies (Hz)')
plot(element,fstore(1,:),'kx-')
plot(element,fstore(2,:),'kx:')
plot(element,fstore(3,:),'kx-.')
legend('Mode 1','Mode 2','Mode 3')

% Exact natural frequencies (ref Blevins)
lambdaL = [1.8751, 4.69409, 7.85476];
for j = 1:3
  fexact(j) = (lambdaL(j))^2 / 2 /pi * sqrt(E * I / rho / A / s^4);
end
disp('Exact natural frequency'); disp(sprintf('%.3f n',fexact));

% Add exact values to plot
x = [0 10]; y1 = [fexact(1) fexact(1)]; y2 = [fexact(2) fexact(2)];
y3 = [fexact(3) fexact(3)]; line(x,y1); line(x,y2); line(x,y3);

% Note - figure edited to give exact frequency a grey dashed line at
  0.25
% font and the data lines at 1.5 font
```

H

MATLAB/SIMULINK Programs for Flutter

In this appendix, some sample MATLAB programs are given for the calculation of the aeroelastic behaviour of a binary flutter system and also its response to control surface and gust/turbulence inputs.

H.1 DYNAMIC AEROELASTIC CALCULATIONS

In Chapter 11 the characteristics of the flutter phenomenon were described using a binary aeroelastic system. The following code sets up the system equations, including structural damping if required, and then solves the eigenvalue problem for a range of speeds and plots the $V\omega$ and Vg trends.

```
% Flutter Chapter B04 Appendix
% Sets up the aeroelastic matrices for binary aeroelastic model,
% performs eigenvalue solution at desired speeds and determines
the frequencies
% and damping ratios
% plots V_omega and V_g trends
% and plots flutter conic solution

% Initialize variables
clear; clf

% System parameters
s = 7.5;          % semi span
c = 2;            % chord
m = 100;          % unit mass / area of wing
kappa_freq = 5;   % flapping freq in Hz
theta_freq = 10;  % pitch freq in Hz
xcm = 0.5*c;      % position of centre of mass from nose
xf = 0.48*c;      % position of flexural axis from nose
e = xf/c - 0.25;  % eccentricity between flexural axis and aero
                    centre (1/4 chord)

velstart = 1;     % lowest velocity
velend = 180;     % maximum velocity
velinc =0.1;      % velocity increment
```

Introduction to Aircraft Aeroelasticity and Loads J. R. Wright and J. E. Cooper
© 2007 John Wiley & Sons, Ltd

```
a = 2*pi;          % 2D lift curve slope
rho = 1.225;       % air density
Mthetadot = -1.2; % unsteady aero damping term
M = (m*c^2 - 2*m*c*xcm)/(2*xcm);   % leading edge mass term

damping_Y_N = 1;  % =1 if damping included   =0 if not included
if damping_Y_N == 1
    % structural proportional damping inclusion    C = alpha *
      M + beta * K
    % then two freqs and damps must be defined
    % set dampings to zero for no structural damping
    z1 = 0.0;              % critical damping at first frequency
    z2 = 0.0;              % critical damping at second frequency
    w1 = 2*2*pi;           % first frequency
    w2 = 14*2*pi;          % second frequency
    alpha = 2*w1*w2*(-z2*w1 + z1*w2)/ (w1*w1*w2*w2);
    beta = 2*(z2*w2-z1*w1) / (w2*w2 - w1*w1);
end

% Set up system matrices
% Inertia matrix
a11=(m*s^3*c)/3 + M*s^3/3;  % I kappa
a22= m*s*(c^3/3 - c*c*xf + xf*xf*c) + M*(xf^2*s); % I theta
a12 = m*s*s/2*(c*c/2 - c*xf) - M*xf*s^2/2;  %I kappa theta
a21 = a12;
A=[a11,a12;a21,a22];

% Structural stiffness matrix
k1 = (kappa_freq*pi*2)^2*a11;     %  k kappa   heave stiffness
k2 = (theta_freq*pi*2)^2*a22;     %  k theta   pitch stiffness
E = [k1 0; 0 k2];

icount = 0;
for V = velstart:velinc:velend       % loop for different velocities
    icount = icount +1;
    if damping_Y_N == 0;    % damping matrices
        C = [0,0; 0,0];        % =0 if damping not included
    else                    % =1 if damping included
        C = rho*V*[c*s^3*a/6,0;-c^2*s^2*e*a/4,-c^3*s*Mthetadot/8] +
            alpha*A + beta*E;
        % Aero and structural damping
    end
    K = (rho*V^2*[0,c*s^2*a/4; 0,-c^2*s*e*a/2])+[k1,0; 0,k2]; %
        aero / structural stiffness

    Mat = [[0,0; 0,0],eye(2); -A\K,-A\C];   % set up 1st order
                                              eigenvalue solution
                                              matrix
    lambda = eig(Mat);                       % eigenvalue solution

    % Natural frequencies and damping ratios
    for jj = 1:4
        im(jj) = imag(lambda(jj));
        re(jj) = real(lambda(jj));
        freq(jj,icount) = sqrt(re(jj)^2+im(jj)^2);
        damp(jj,icount) = -100*re(jj)/freq(jj,icount);
        freq(jj,icount) = freq(jj,icount)/(2*pi);    % convert
                                                       frequency to
                                                       hertz
    end
    Vel(icount) = V;
end

% Plot frequencies and dampings vs speed
figure(1)
subplot(2,1,1); plot(Vel,freq,'k');
vaxis = axis; xlim = ([0 vaxis(2)]);
xlabel ('Air Speed (m/s) '); ylabel ('Freq (Hz)'); grid

subplot(2,1,2);
plot(Vel,damp,'k')
xlim = ([0 vaxis(2)]); axis([xlim ylim]);
xlabel ('Air Speed (m/s) '); ylabel ('Damping Ratio (%)'); grid
```

H.2 AEROSERVOELASTIC SYSTEM

In Chapter 12 the inclusion of a closed loop control system was introduced via the addition of a control surface to the binary flutter model. The following code enables the response of the binary aeroelastic system subject to control surface excitation and also a vertical gust sequence to be calculated through the use of the SIMULINK function Binary_Sim_Gust_Control shown in Figure H1. The control surface input is defined as a ‘chirp’ with start and end frequencies needing to be specified, and the gust input contains both ‘1-cosine’ and random turbulence inputs. Note that the random signal is generated by specifying an amplitude variation and random phase in the frequency domain via the inverse Fourier transform. All simulations are in the time domain. Note that the feedback loop is not included here but it would be a straightforward addition to the code.

```
% Chapter B05

%%%%%%%%%%%%%%%%%%%%%%%%%%%%%%%%%%%%%%%%%%%%%%%%%%%%%%%%%%%%%%%%%
%    Binary Aeroelastic System plus control plus turbulence    %%
%    Define control_amp, turb_amp, gust_amp_1_minus_cos to     %%
%    determine which inputs are included                       %%
%%%%%%%%%%%%%%%%%%%%%%%%%%%%%%%%%%%%%%%%%%%%%%%%%%%%%%%%%%%%%%%%%

clear all; close all

% System parameters

V = 100;            % Airspeed
s = 7.5;            % semi span
```

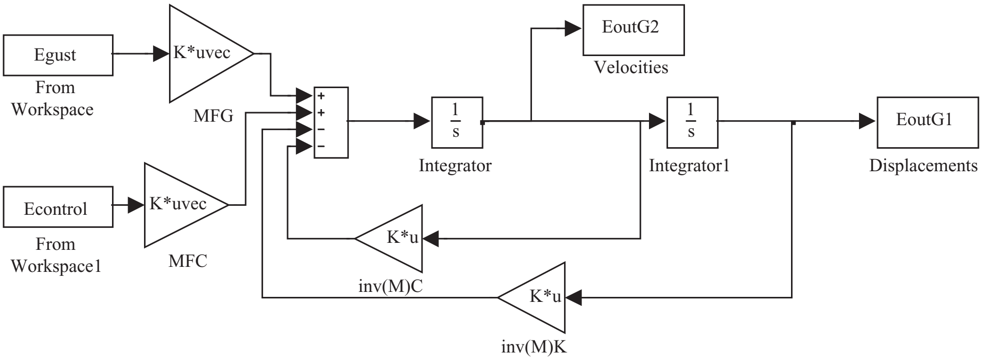
Egust
From Workspace
K*uvec
MFG
Econtrol
From Workspace1
K*uvec
MFC
+
+
−
−
1/s
Integrator
EoutG2
Velocities
1/s
Integrator1
EoutG1
Displacements
K*u
inv(M)C
K*u
inv(M)K

Figure H.1 SIMULINK Implementation for the open loop aeroservoelastic system.

```
c = 2;                % chord
a1 = 2*pi;            % lift curve slope
rho = 1.225;          % air density
m = 100;              % unit mass / area of wing
kappa_freq = 5;       % flapping freq in Hz
theta_freq = 10;      % pitch freq in Hz
xcm = 0.5*c;          % position of centre of mass from nose
xf = 0.48*c;          % position of flexural axis from nose
Mthetadot = -1.2;     % unsteady aero damping term
e = xf/c - 0.25;      % eccentricity between flexural axis and
                        aero centre
damping_Y_N = 1;      % =1 if damping included   =0 if not included

% Set up system matrices
a11 = (m*s^3*c)/3 ;  % I kappa
a22 = m*s*(c^3/3 - c*c*xf + xf*xf*c);   % I theta
a12 = m*s*s/2*(c*c/2 - c*xf);           % I kappa theta
a21 = a12;
k1 = (kappa_freq*pi*2)^2*a11;           % k kappa
k2 = (theta_freq*pi*2)^2*a22;           % k theta
A = [a11,a12; a21,a22];
E = [k1 0; 0 k2];
if damping_Y_N == 0;  %    =0 if damping not included
    C = [0,0; 0,0];
else
    C = rho*V*[c*s^3*a1/6,0; -c^2*s^2*e*a1/4,-c^3*s*Mthetadot/8];
end
K = (rho*V^2*[0,c*s^2*a1/4; 0,-c^2*s*e*a1/2])+[k1,0;0,k2] ;

% Gust vector
F_gust = rho*V*c*s*[s/4 c/2]';

% Control surface vector
EE = 0.1;  % fraction of chord made up by control surface
```

```
ac = a1/pi*(acos(1-2*EE) + 2*sqrt(EE*(1-EE)));
bc = -a1/pi*(1-EE)*sqrt(EE*(1-EE));
F_control = rho*V^2*c*s*[-s*ac/4 c*bc/2]';

% Set up system matrices for SIMULINK

MC = inv(A)*C;
MK = inv(A)*K;
MFG = inv(A)*F_gust;
MFC = inv(A)*F_control;

dt = 0.001;        % sampling time
tmin = 0;          % start time
tmax = 10;         % end time
t = [0:dt:tmax]';  % Column vector of time instances

%%%%%% CONTROL SURFACE INPUT SIGNAL - SWEEP SIGNAL
%%%%%%%%%%%%%%%%%%%%%%%%%%%
control_amp = 5;     % magnitude of control surface sweep input
in degrees
control_amp = control_amp * pi / 180;   % radians
burst = .333;        %  fraction of time length that is chirp
signal  0 - 1
sweep_start = 1;     % chirp start freq in Hertz
sweep_end = 20;      % chirp end freq in Hertz
t_end = tmax * burst;

Scontrol = zeros(size(t));   % control input
xt = sum(t < t_end);
for ii = 1:xt
    Scontrol(ii) = control_amp*sin(2*pi*(sweep_start + (sweep_end -
sweep_start)*ii/(2*xt))*t(ii));
end

%%%%%%%%%%% GUST INPUT TERMS - "1-cosine" and/or turbulence %%%
%%%%%%%%%%%%%%%

Sgust = zeros(size(t));

%%%  1 - Cosine gust
gust_amp_1_minus_cos = 0;       % max velocity of "1 - cosine"
gust   (m/s)
gust_t = 0.05;   %  fraction of total time length that is gust 0 - 1
g_end = tmax * gust_t;
gt = sum(t < g_end);
for ii = 1:gt
    Sgust(ii) = gust_amp_1_minus_cos/2 * (1 - cos(2*pi*t(ii)/g_end));
end

%%% Turbulence input - uniform random amplitude between 0 Hz and
```

```
turb_max_freq Hz %%%
turb_amp = 0;       %   max vertical velocity of turbulence   (m/s)
turb_t = 1;         %   fraction of total time length that is
turbulence    0 - 1
t_end = tmax * turb_t;
turb_t = sum(t < t_end);  % number of turbulence time points required
turb_max_freq = 20;       % max frequency of turbulence(Hz) -
uniform freq magnitude
npts = max(size(t));
if rem(max(npts),2) ~= 0  % code set up for even number
    npts = npts - 1;
end
nd2 = npts / 2;
nd2p1 = npts/2 + 1;
df = 1/(npts*dt);
fpts = fix(turb_max_freq / df) + 1; % number of freq points that form
turbulence input

for ii = 1:fpts  % define real and imag parts of freq domain
                 % magnitude of unity and random phase
    a(ii) = 2 * rand - 1;    % real part  - 1 < a < 1
    b(ii) = sqrt(1 - a(ii)*a(ii)) * (2*round(rand) - 1);
% imag part
end

% Determine complex frequency representation with correct
frequency characteristics
tf =  (a + j*b);
tf(fpts+1 : nd2p1) = 0;
tf(nd2p1+1 : npts) = conj(tf(nd2:-1:2));
Sturb = turb_amp * real(ifft(tf));

for ii = 1:npts
    Sgust(ii) = Sgust(ii) + Sturb(ii); % "1 - cosine" plus
turbulence inputs
end

% Simulate the system using SIMULINK
Egust = [t,Sgust]; % Gust Array composed of time and data columns
Econtrol = [t,Scontrol]; % Control Array composed of time and data
columns

[tout] = sim('Binary_Sim_Gust_Control');

x1 = EoutG1(:,1)*180/pi;   % kappa - flapping motion
x2 = EoutG1(:,2)*180/pi;   % theta - pitching motion
x1dot = EoutG2(:,1)*180/pi;
x2dot = EoutG2(:,2)*180/pi;
figure(1); plot(t,Scontrol,t,Sgust)
```

```
xlabel('Time (s)'); ylabel('Control Surface Angle(deg) and
Gust Velocity(m/s)')
figure(2) ; plot(t,x1,'r',t,x2,'b')
xlabel('Time (s)'); ylabel('Flap and Pitch Angles (deg/s)')
figure(3); plot(t,x1dot,'r',t,x2dot,'b')
xlabel('Time (s)'); ylabel('Flap and Pitch Rates (deg/s)')
```

I

MATLAB/SIMULINK Programs for Flight/Ground Manoeuvres and Gust/Turbulence Encounters

In this appendix, some sample programs for calculation of equilibrium and dynamic manoeuvres, gusts and turbulence, and taxiing and landing are presented.

I.1 RIGID AIRCRAFT DATA

Before proceeding with calculation of results from different manoeuvres and gust/turbulence encounters, the basic aircraft data need to be entered for the rigid or flexible aircraft as appropriate. To save space, the aircraft data will simply be specified for a sample case; clearly, in a normal programme, the reader may choose to enter some parameters via a dialogue and to introduce loops to cover multiple cases (e.g. of air speed). Note that units used throughout for defining data are in N, kg, m, s and rad. Wherever possible, the symbols used in the code below aim to match those used in the main text, with the use of the underscore symbol _ indicating a subscript to follow; therefore, for example, m_W in MATLAB is equivalent to m_W in the text.

```
% Data for Symmetric Aircraft
close all;  clear all

% Mass and Dimensions

m = 10000; W = m * 9.81; m_F = 0.15 * m; m_W = 0.3 * m; m_C = 0.4 *m;
m_T = 0.15 * m; S_W = 30.0; S_T = 7.5; s = 7.5; c = 2.0; s_tp =
3.0; c_tp = 1.25; l_W = 0.3*c; l_T = 3.5 * c; l_A = 0.125 * c; l_E =
0.125 * c; l_WM = l_W - l_A - l_E; l_M = 0.375 * c; l_F = (m_T *
l_T- m_W * l_WM) / m_F; l_WT = l_W + l_T; l_N = l_F; l_M = 0.375 * c;
mu = m_W / 2 / s;

% Moments of Inertia

I_y_fuse = m_F * l_F^2 + m_T * l_T^2; I_y_W = m_W * (c / 3)^2; I_y =
I_y_fuse + I_y_W + m_W * l_WM^2; l_y_W = sqrt(I_y_W / m_W); l_y =
sqrt(I_y / m);
```

Introduction to Aircraft Aeroelasticity and Loads   J. R. Wright and J. E. Cooper
© 2007 John Wiley & Sons, Ltd

```
% Landing gear
C_N = 3200; C_M = 19200; K_N = 80000; K_M = 240000; l_B = l_N + l_M;

% Basic aerodynamics
a_W = 4.5; a_T = 3.2; a_E = 1.5; alpha_0 = - 0.03; C_M0 = - 0.03;
C_D = 0.1; k_epsilon = 0.35;
```

I.2 FLEXIBLE AIRCRAFT DATA

When considering the flexible aircraft, the choice in Appendix F was between three mode types, namely fuselage bending, wing bending or wing twist dominant. This part of the data entry must specify the relevant modal information – mode parameters, mode shape, modal mass, natural frequency, modal stiffness and *J* integrals. The example shown is that for the fuselage bending mode.

```
% Additional Data for Flexible Aircraft (if required) - Example
  of Fuselage Bending dominant
kappa_e0 = 1; gamma_e0 = 0; A = 0; B = 0;

% Normalisation to 1 at wing tip trailing edge
kappa_tip = kappa_e0*(1 + A) + gamma_e0*(1 + B)*(c - c/4 - l_A);
kappa_e0 = kappa_e0/kappa_tip;

% Solution of equations to yield dominant Fuselage Bending mode shape
X = [m_F m_T; -m_F*l_F m_T*l_T]; Y = [- (m_W + m_C)*kappa_e0;
m_W*l_WM*kappa_e0]; Z = X\Y; kappa_eC = 1; kappa_eF = Z(1);
kappa_eT = Z(2); gamma_eT = 2*(kappa_eT - kappa_eC) / l_T - gamma_e0;

% Modal Mass, Natural Frequency and Modal Stiffness for
  Fuselage Bending dominant
m_e = m_F*kappa_eF^2 + m_W*kappa_e0^2 + m_C*kappa_eC^2 + m_T*
kappa_eT^2; f_e = 4.0;  omega_e = 2*pi*f_e;  k_e = omega_e^2*m_e;

% `J' Integrals for aerodynamic derivatives
J1 = gamma_e0*(1 + B / 2);
J2 = kappa_e0*(1 + A / 3) - l_A*gamma_e0*(1 + B / 2);
J3 = gamma_e0*kappa_e0*(1 + A / 3 + B / 2 + A*B / 4) - l_A*
gamma_e0^2*(1 + B + B^2 / 3);
```

This code will need revising for other mode types, using the information given in Appendix F.

I.3 FLIGHT CASE DATA

In this section, the data relevant to the aircraft flight case are generated; once again, a dialogue could be used and loops introduced.

```
% Data for Flight Case-specify EAS (and relative density
  if not at sea level)
V0 = 150;                    % EAS
```

```
rho0 = 1.225;                  % Sea level density
root_sigma  = 0.8;             % Relative density at altitude
V = V0 / root_sigma;           % Convert to TAS for gusts / ground
                                 manoeuvres
```

I.4 AERODYNAMIC DERIVATIVE CALCULATION

The way that manoeuvres and gusts/turbulence have been treated in this book is via the use of rigid and elastic aircraft aerodynamic derivatives, either for inertial or body fixed axes systems; the results seen in Appendix D show that most of the derivatives are the same whereas some are different for each of the two cases. In this section, code is included for calculating the longitudinal derivatives in inertial axes, first for the rigid and then the flexible aircraft, including gust derivatives. The derivatives relative to body fixed axes (in this case wind axes, as used in Chapters 14 and 15) are also included below where they differ to the inertial axes expressions.

```
% Derivatives evaluated using Equivalent Air Speed and sea level
  air density

% Aerodynamic Derivatives (inertial axes)- Heave DoF
Z_0 = -0.5*rho0*V0^2*[- S_W*a_W + S_T*a_T*k_epsilon]*alpha_0;
Z_alpha = -0.5*rho0*V0^2*[S_W*a_W + S_T*a_T*(1 - k_epsilon)];
Z_q = -0.5*rho0*V0*S_T*a_T*l_T;
Z_eta = -0.5*rho0*V0^2*S_T*a_E;
Z_zdot = -0.5*rho0*V0*(S_W*a_W + S_T*a_T*(1 - k_epsilon));
Z_gW = -0.5*rho0*V0*S_W*a_W;
Z_gT = -0.5*rho0*V0*S_T*a_T*(1 - k_epsilon);

% Aerodynamic Derivatives (inertial axes)- Pitch DoF
M_0W = 0.5*rho0*V0^2*S_W*c*C_M0 -0.5*rho0*V0^2*S_W*a_W*l_W*alpha_0;
M_0T = -0.5*rho0*V0^2*S_T*a_T*k_epsilon*l_T*alpha_0;
M_0 = M_0W + M_0T;
M_alpha = 0.5*rho0*V0^2*[S_W*a_W*l_W - S_T*a_T*(1 - k_epsilon)*l_T];
M_q = -0.5*rho0*V0*S_T*a_T*l_T^2;
M_eta = -0.5*rho0*V0^2*S_T*a_E*l_T;
M_zdot = 0.5*rho0*V0*(S_W*a_W*l_W - S_T*a_T*l_T*(1 - k_epsilon));

M_gW = 0.5*rho0*V0*S_W*a_W*l_W;
M_gT = -0.5*rho0*V0*S_T*a_T*l_T*(1 - k_epsilon);

% Additional aerodynamic derivatives for wind axes- Rigid DoF
(if required)
Z_w = -0.5*rho0*V0*(S_W*a_W + S_T*a_T*(1 - k_epsilon)+ S_W*C_D);
M_w = 0.5*rho0*V0*(S_W*a_W*l_W - S_T*a_T*l_T*(1 - k_epsilon));

% Aerodynamic Derivatives-Elastic DoF (if required)
Z_e = 0.5*rho0*V0^2*(-S_W*a_W*J1 - S_T*a_T*gamma_eT);
Z_edot = -0.5*rho0*V0*S_T*a_T*kappa_eT;
M_e = 0.5*rho0*V0^2*(S_W*a_W*l_W*J1 - S_T*a_T*l_T*gamma_eT);
M_edot = -0.5*rho0*V0*S_T*a_T*l_T*kappa_eT;
```

```
Q_0 = 0.5*rho0*V0^2*(S_W*a_W*J2 - S_T*a_T*k_epsilon*kappa_eT)
*alpha_0;
Q_alpha = 0.5*rho0*V0^2*(-S_W*a_W*J2 - S_T*a_T*(1 - k_epsilon)
*kappa_eT);
Q_q = -0.5*rho0*V0*S_T*a_T*l_T*kappa_eT;
Q_eta = -0.5*rho0*V0^2*S_T*a_E*kappa_eT;
Q_e = 0.5*rho0*V0^2*(-S_W*a_W*J3 - S_T*a_T*gamma_eT*kappa_eT);
Q_zdot = 0.5*rho0*V0*(-S_W*a_W*J2 - S_T*a_T*(1 - k_epsilon)
*kappa_eT);
Q_edot = -0.5*rho0*V0*S_T*a_T*kappa_eT^2;
Q_gW = -0.5*rho0*V0*S_W*a_W*J2;
Q_gT = -0.5*rho0*V0*S_T*a_T*kappa_eT;

% Additional aerodynamic derivative for wind axes-Elastic DoF
Q_w = 0.5*rho0*V0*(- S_W*a_W*J2 - S_T*a_T*(1 - k_epsilon)
*kappa_eT);
```

I.5 EQUILIBRIUM MANOEUVRES

In this section, related to Chapter 13, the equations are set up from the aerodynamic derivatives and the solution carried out for the equilibrium manoeuvre of both the rigid and elastic aircraft. In this and later cases, the sections of MATLAB code for aircraft data, flexible aircraft data (if required), flight case and aerodynamic derivatives must be run first.

```
% Load factor and steady pitch rate for equilibrium manoeuvre
  n = 1.0; q_pr = 0;

% Trim response of a rigid aircraft-requires aircraft data,
  flight case and derivative codes
% Setting-up and Solving Equations of Motion for the Rigid Aircraft

ARigid = -[Z_eta Z_alpha; M_eta  M_alpha];
CRigid = [1 ; 0]; DRigid = [Z_q; M_q]; ERigid = [Z_0; M_0];
BRigid = inv(ARigid)*(CRigid*(n*W) + DRigid*q_pr + ERigid);
Bdeg = BRigid*180 / pi;
Trim_Elevator_Rigid = Bdeg(1)
Trim_Incidence_Rigid = Bdeg(2)

% Trim response of an elastic aircraft-requires aircraft
  data, flight case, flexible mode and derivative codes

% Setting-up and Solving Equations of Motion for the Elastic
  Aircraft

AElastic = - [Z_eta  Z_alpha  Z_e;  M_eta  M_alpha  M_e;  Q_eta
Q_alpha  Q_e - k_e];
CElastic = [1 ; 0 ; 0]; DElastic = [Z_q ; M_q ; Q_q];
EElastic = [Z_0 ; M_0 ; Q_0];
BElastic = inv(AElastic)*(CElastic*(n*W) + DElastic*q_pr +
EElastic); Bdeg = BElastic*180 / pi;
Trim_Elevator_Elastic = Bdeg(1)
Trim_Incidence_Elastic = Bdeg(2)

Note that BElastic(3) yields the generalised coordinate for the
fuselage bending mode deformation in the trimmed state and so
the absolute deformation may be obtained by multiplying by the
normalised mode shape.
```

I.6 DYNAMIC MANOEUVRES

In this section, related to Chapters 14 and 15, the equations of motion are defined with respect to the body fixed (in particular wind) axes system and therefore the matrices are structured differently. Only the linearized longitudinal symmetric manoeuvre involving heave and pitch will be considered here, so variations in the fore-and-aft velocity will be ignored. These linearized equations need to be solved against time for a particular control input. In this case, the elevator input will be considered as a step on–step off pulse and will be defined using an input array. Other inputs can be substituted if required.

The first SIMULINK function in Figure I.1 will solve the response w, q to the elevator input in moving axes and integrate $q(=\dot{\theta})$ to determine θ. This output from the moving axes equations will then be used to transform these response velocities into an inertial reference frame fixed with respect to earth, thus yielding the velocities U_E, W_E in earth fixed axes. A further SIMULINK function in Figure I.2 will be used to integrate these velocities in order to determine the position coordinates X_{E}, Z_{E} of the aircraft in earth axes. The reader should refer back to Appendix A for a brief introduction to setting up the SIMULINK block diagram.

It should be possible to analyse both the rigid and elastic aircraft using the same SIMULINK models, but with different equations.

```
% Dynamic response of a symmetric rigid aircraft to an elevator
input-requires aircraft data, flight case and derivative codes

% Simulation data
tmin = 0;  tmax = 5.0; dt = 0.005;
```

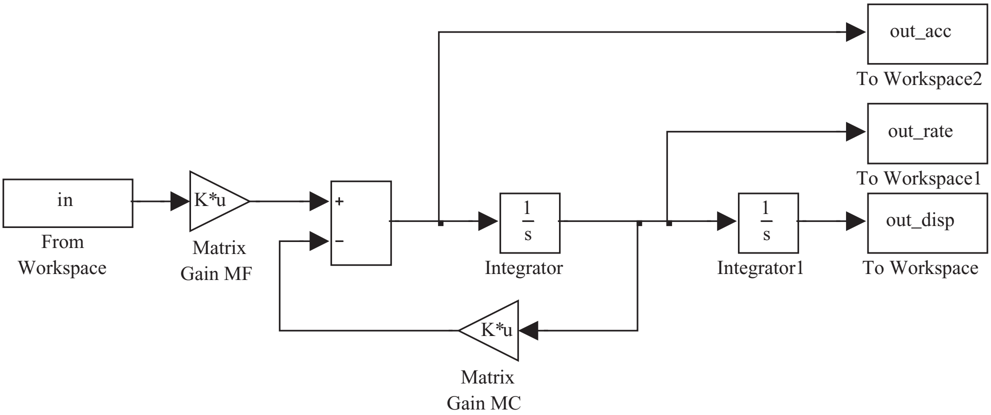

Figure I.1 SIMULINK diagram for a dynamic manoeuvre in body fixed axes.

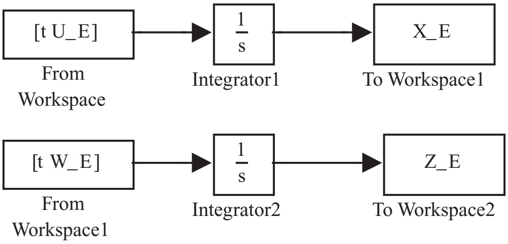

Figure I.2 SIMULINK diagram to integrate velocities in earth axes.

```
% Time increment - will need to be smaller for the elastic
  taircraft (~0.002s)
t = [tmin: dt: tmax]'; [N, dummy] = size(t); eta = zeros(N, 1);

% On / off pulse input to elevator
tpulse = 1.0; npulse = tpulse / dt + 1; eta_in = 2.0;
eta_in = eta_in*pi / 180;
eta(1:npulse) = eta_in*ones(npulse, 1);

% Aircraft initial condition
U_e = V0;  W_e = 0;

% Flight mechanics linearised equations of motion
M = [m 0;0 I_y]; C = [-Z_w -(m*U_e + Z_q); -M_w -M_q];
F = [Z_eta; M_eta];
MC = inv(M)*C; MF = inv(M)*F;

% Simulation of response in body fixed (wind) axes to yield w,q
and then theta
in = [t, eta];
sim('Rigid_Pitch_Dynamic_mdl');

% Output variables
w = out_rate(:,1);          % Downwards velocity
q = out_rate(:,2);          % Pitch rate
wdot = out_acc(:,1);        % Downwards acceleration
theta = out_disp(:,2);      % Integral of q (i.e. theta)
alpha = w / V0;             % Incidence
gamma = theta - alpha;      % Flight path angle - perturbation
az = wdot - q*U_e;          % Normal acceleration at CoM

% Response plots- body fixed axes
figure(1); subplot(311); plot(t, q*180/pi,'k-', t, alpha
*180/pi, 'k:')
title('Pitch Rate and Incidence Response for Elevator Input')
xlabel('Time (s)'); ylabel('Pitch Rate (deg/s), Incidence
(deg)'); legend('Pitch Rate', 'Incidence')
```

```
subplot(312); plot(t, az/9.81, 'k-')
title('Normal Acceleration for Elevator Input'); xlabel
('Time (s)'); ylabel('Normal Acceleration (g)')
subplot(313); plot(t, theta*180/pi, 'k-', t, gamma*180/pi, 'k:')
title('Pitch and Flight Path Angles for Elevator Input')
xlabel('Time (s)');  ylabel('Pitch and Flight Path Angles (deg)');
legend('Pitch Angle', 'Flight Path Angle')

% Transform velocities related to CoM from body fixed to earth
  fixed axes

% Centre of Mass
U_E = U_e + W_e*theta;
W_E = -U_e*theta + W_e + w;

% Tailplane
U_E_tp = U_e + W_e*theta + w.* theta;
W_E_tp = -U_e*theta + W_e + w + l_T*q;

% Response plots - velocities in earth axes
figure(2); plot(t, w, 'k-', t, W_E, 'k:')
title('Vertical Velocity Response (relative to wind / earth axes)
for Elevator Input')
xlabel('Time (s)');  ylabel('Velocity (m/s)')
legend('Vertical velocity relative to wind axes w', 'Vertical
velocity relative to earth axes WE')
figure(3);  plot(t, W_E, t, W_E_tp, 'k-')
title('Vertical Velocity Response (relative to earth axes) for
Elevator Input')
xlabel('Time (s)'); ylabel('Velocity WE (m/s)'); legend
('Centre of mass', 'Tailplane')

% Integrate to yield CoM position coordinates from velocities
in earth axes
sim('EarthAxes_CoM_mdl');

% Response plots - CoM position in earth axes
figure(4);  plot(X_E, -Z_E, 'k-')
title('CoM Flight Profile in Earth Axes following Elevator Input')
xlabel('Horizontal Displacement XE (m)'); ylabel('Vertical
Displacement  ZE (m)')
```

Note that when setting up this and other SIMULINK models involving the transfer of data to and from the workspace, the following settings were used:

(a) From Workspace: set sample time dt, select ‘Interpolation’.
(b) To Workspace: set sample time d*t* and decimation 1; select ‘Array’.

Also, apart from the landing simulation, all initial conditions for the integrators are set to zero.

I.7 GUST RESPONSE IN THE TIME DOMAIN

In this section, related to the treatment of gusts in the time domain in Chapter 16, the equations of motion for the gust response of a rigid aircraft are set up and the response to a ‘1-cosine’ gust is obtained using SIMULINK, set up for the second-order equations of motion referred to inertial axes; the gust time history is defined as an input array.

Note that the distance origin is at the aircraft tail, and at $t = 0$ the aircraft wing is about to enter the gust, as illustrated diagrammatically below (aircraft moving right to left). The simulation ends when the wing reaches the end of the total air space allocated.

```
% Gust response of a rigid aircraft in the time domain-requires
  aircraft data, flight case and derivative codes

% Gust profile                   ***************
% Air space     -----------------------------------------
% Aircraft      W+++++++T                      W+++++++T

% Set-up time array and length of simulation
tmin = 0; tmax = 8.0;
dt = 0.005;           % Time increment - will need to be smaller
                        for the elastic aircraft (~0.002s)
t = [tmin: dt: tmax]'; [Nsim, dummy] = size(t);

% Set-up distance array and size for simulation (important
  to use TAS not EAS)
x_g = V*t;                     % Distance array
dx = V*dt;                     % Distance increment
Nb = round(l_WT / dx+1);       % No of points between wing/tailplane
N = Nsim + Nb - 1;             % No of points for total air space

% Gust velocity profile (1-cosine)
delta_wgt = 5.0;               % Max gust velocity TAS
L_g = 250.0;                   % Gust length
Nd = round(L_g / dx + 1);      % No of points for gust
Nbd = Nb + Nd - 1;             % No of points for a/c and gust
wg = zeros(N, 1);
wg_W = zeros(N, 1);
wg_T = zeros(N, 1);
wg(Nb:Nbd) = (delta_wgt / 2)*
(1 - cos(2*pi*x_g(1:Nd) / L_g));  % Gust velocity array at centre
                                   of mass
wg_W(1:Nsim) = wg(Nb:N);
wg_T(1:Nsim) = wg(1:Nsim);        % Gust velocity array at wing and
                                    tailplane
% Equations of motion for rigid aircraft (elastic is similar
  but with an additional row / column for elastic mode
M = [m 0; 0 I_y]; CC = - [Z_zdot Z_q; M_zdot M_q]; KK = -
[0 Z_alpha; 0 M_alpha];
FW = [Z_gW;  M_gW]; FT = [Z_gT;  M_gT];
```

```
MI = inv(M); MC = MI*CC; MK = MI*KK; MFW = MI*FW; MFT = MI*FT;

% Simulation to find displacements and velocities of response in
  inertial axes
inW = [t, wg_W(1:Nsim)];
inT = [t, wg_T(1:Nsim)];    % Input arrays at wing and tail[lane
sim('Gust_mdl')             % Solve equations via SIMULINK model

% Displacements, velocities and accelerations at CoM, nose and
  tail (all Nsim x 1 arrays)
z_C = out_disp(:,1); zdot_C = out_rate(:,1); zddot_C = out_acc(:,1);
theta = out_disp(:,2); theta_dot = out_rate(:,2); theta_ddot =
out_acc(:,2);
z_F = z_C - l_F*theta; zddot_F = zddot_C - l_F*theta_ddot;
z_T = z_C + l_T*theta; zddot_T = zddot_C + l_T*theta_ddot;

% Plot responses
subplot(211); plot(t, theta*180/pi, 'k-', t, theta_dot *180/pi, 'k:')
title('Pitch Response for Rigid Aircraft in Gust')
xlabel('Time (s)'); ylabel('Pitch (deg) and Pitch Rate (deg/s)');
legend('Pitch Angle', 'Pitch Rate')
subplot(212); plot(t, zddot_C/9.81, 'k-', t, zddot_T/9.81, 'k:')
title('Nose/CoM/Tail Heave Acceleration for Rigid Aircraft in Gust')
xlabel('Time (s)'); ylabel('Heave Acceleration (g)'); legend
('CoM', 'Tailplane')
```

The SIMULINK diagram for the rigid gust case in the time domain is shown in Figure I.3; the same model may be used for the elastic aircraft, with the matrices simply being defined differently in the MATLAB code.

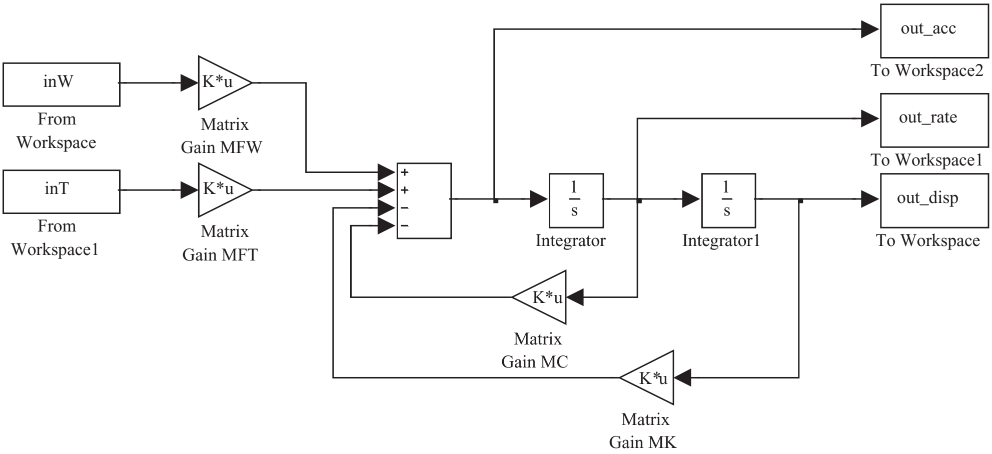
inW
From Workspace
inT
From Workspace1
K*u
Matrix Gain MFW
K*u
Matrix Gain MFT
+
+
−
−
1/s
Integrator
1/s
Integrator1
K*u
Matrix Gain MC
K*u
Matrix Gain MK
out_acc
To Workspace2
out_rate
To Workspace1
out_disp
To Workspace

Figure I.3 SIMULINK diagram for the time domain gust response.

I.8 GUST RESPONSE IN THE FREQUENCY DOMAIN

In this section, related to the treatment of gusts (i.e. continuous turbulence) in the frequency domain in Chapter 16, the equations of motion for the gust response of a rigid aircraft are set up and the power spectral density (PSD) of the response to turbulence is obtained using MATLAB.

```
% Gust response of a rigid aircraft in the frequency domain-
  requires aircraft data, flight case and derivative codes

% RMS gust velocity (TAS) and characteristic scale wavelength
  (2500 ft-converted to m)
sigma_g = 1; L_g = 2500/3.2808;

% Equations of motion for rigid aircraft
M = [m 0; 0 I_y]; CC = [- Z_zdot -Z_q; -M_zdot -M_q];
KK = [0 -Z_alpha; 0 -M_alpha];
FW = [Z_gW; M_gW]; FT = [Z_gT;  M_gT];

% Calculate Gust PSD and FRF for each frequency value from 0 up
  to Nyquist and set Nyquist frequency
% value to be real - note that FRF needs to be 2 dimensional
  (responses and frequency stored)
% The zero frequency value is NaN (Not a Number) because the KK
  Matrix is singular
f_nyq = 5; nt = 1024; nf = nt/2 + 1; frq = linspace(0, f_nyq, nf);
df = frq(2) - frq(1);
H = zeros(2, nf); Hddot = zeros(2, nf); i = sqrt(-1);

for ifq = 1:nf
  w = 2*pi*frq(ifq); omLg = w*L_g/V; OM(ifq) = w/V;
  num = 1 + 8/3*(1.339*omLg)^2; den = (1 + (1.339*omLg)^2)^(11/6);
  psi_gr(ifq) = sigma_g^2
  *L_g/pi*num/den;              % Gust PSD for reduced frequency
  psi_gf(ifq) = sigma_g^2
  *2*L_g/V*num/den;             % Gust PSD for true frequency
  HI = (KK - w^2*M + i*w*CC)^-1; HQG = HI*(FW + FT * exp(- w*l_
  WT/V));
  Hqg(:,ifq) = HQG;  Hqddotg(:,ifq) = - w^2*Hqg(:,ifq);
end
% Plot gust PSD against frequency (not reduced)
  figure(1); loglog(frq(1:nf), psi_gf(1:nf), 'k-');
xlabel('Frequency (Hz)'); ylabel('PSD of Gust Velocity (m/s)^2/Hz');
title('Gust PSD - Frequency')

% Convert to FRF and |FRF|^2 for centre of mass response from
  generalised (heave/pitch) responses
Hz_C = [1 0]*Hqg; Hz_C2 = (abs(Hz_C)).^2; Hzddot_C = [1 0] *
Hqddotg; Hzddot_C2 = (abs(Hzddot_C)).^2;

% Convert to FRF for front fuselage and tailplane response from
  generalised (heave / pitch) responses
```

```
Hz_F = [1 -l_F]*Hqg;  Hz_T = [1 l_T]*Hqg;

% Calculation of centre of mass response PSD from gust PSD and
  response-to-gust |FRF|^2
Pzddot_C2 = psi_gf.*Hzddot_C2;

% Calculate root-mean-square values of acceleration at centre
  of mass (convert from m/s^2 to g)
g2 = 9.81^2;  sumC = 0;
for ifq = 2:nf
  sumC = sumC + Pzddot_C2(ifq) / g2*df;
end
rmsCg = sqrt(sumC)

% Plot centre of mass response PSD against frequency
figure(2); loglog(frq(1:nf), Hzddot_C2(1:nf)/g2,'k:',frq(1:nf),
Pzddot_C2(1:nf)/g2,'k-');
xlabel('Frequency (Hz)'); ylabel('FRF^2 and Acceleration PSD
(g^2 / Hz)');
title('Frequency Domain Gust Response - Rigid Aircraft with
Heave/Pitch Model')
legend('(Acceleration per Gust Velocity FRF)^2', 'Acceleration PSD')
```

I.9 GROUND MANOEUVRES

In this section, the calculation of responses to taxiing and landing as outlined in Chapter 17 is considered.

I.9.1 Taxiing

In this subsection, the equations of motion for the taxiing response of a rigid aircraft are set up and the response to a ‘1-cosine’ dip in the runway is obtained using MATLAB and SIMULINK. Note in this example that the equations are set up in first order state space form and not as second-order equations, as was the case for the gust response; either approach may be employed.

```
% Rigid aircraft taxiing over a 1-cosine dip-requires aircraft data,
  flight case but not derivative codes

% Time and distance data
tmin = 0; tmax = 10.0; dt = 0.01;  % Time increment - will need to
be smaller for the elastic aircraft (~0.002s)
t = [tmin: dt: tmax]'; [Nsim, dummy]=size(t);
x_r = V*t; dx = V*dt; Nb = round(l_B/dx + 1); N = Nsim + Nb - 1;

% Runway profile - define (1-cosine) dip - note similarity
to gust except for the need for hdot terms

%Dip                                ***************
%Runway   ----------------------------------------------------
%Aircraft    N+++++++M                              N+++++++M
```

```
delta_h_r = 0.03; L_r = 60; Ndip = round(L_r / dx + 1); Nbd =
Nb + Ndip - 1;
h = zeros(N, 1); h_N = zeros(N, 1);  h_M = zeros(N, 1);
hdot = zeros(N, 1);  h_Ndot = zeros(N, 1); h_Mdot = zeros(N, 1);
h(Nb:Nbd) = (delta_h_r / 2)*(1 - cos(2*pi*x_r(1:Ndip) / L_r));
hdot(Nb:Nbd) = V*pi*delta_h_r / L_r*sin(2*pi*x_r(1:Ndip) / L_r);

Runway profile defined at nose and main gear positions
h_N(1:Nsim) = h(Nb:N);  h_M(1:Nsim) = h(1:Nsim);
h_Ndot(1:Nsim) = hdot(Nb:N);  h_Mdot(1:Nsim) = hdot(1:Nsim);

% Equations of motion in second order form
M = [m  0; 0  I_y];
CC = [C_N + C_M  -l_N*C_N + l_M*C_M; -l_N*C_N + l_M*C_M l_N^2*
C_N + l_M^2*C_M];
K = [K_N + K_M  -l_N*K_N + l_M*K_M; -l_N*K_N + l_M*K_M l_N^2
*K_N + l_M^2*K_M];
DC = [C_N  C_M;  -l_N*C_N l_M*C_M]; DK = [K_N K_M;  -l_N* K_N
l_M*K_M];
MC = inv(M)*CC; MK = inv(M)*K; MDC = inv(M)*DC; MDK = inv(M)*DK;

% State space equations in first order form
Null22 = zeros(2, 2); I = eye(2); C = eye(4); D = zeros(4, 4);
A = [Null22 I; -MK -MC]; B = [Null22 Null22; MDK MDC];

% State space input vector (Nsim x 4)
u = [h_N(1:Nsim) h_M(1:Nsim) h_Ndot(1:Nsim) h_Mdot(1:Nsim)];

% Simulation in state space to find displacements and velocities
in = [t, u]; sim('SS_taxiing_mdl')

% Displacements at CoM, nose and main gears (all Nsim x 1)
% Dimension of 'out' is Nsim x 4 (zc, theta, zcdot, thetadot)
z_C = out(:,1); z_N = z_C - out(:,2)*l_N; z_M = z_C + out(:,2)*l_M;

% Calculate accelerations from state space equations
% Dimension of 'outdot' is Nsim x 4 (zcdot, thetadot, zcdddot,
thetaddot)
outdot = (A*out' + B*u')'; zddot_C = outdot(:,3); theta_ddot =
outdot(:,4);
zddot_N = zddot_C - theta_ddot*l_N; zddot_M = zddot_C + theta_
ddot*l_M;

% Plot responses at nose and main gear
subplot(211); plot(t, 1000*z_N, 'k-', t, 1000*z_M, 'k:')
title('Nose/Main Gear Heave for Taxiing Rigid Aircraft')
xlabel('Time (s)'); ylabel('Heave Response (mm)'); legend
('Nose Gear', 'Main Gear')

subplot(212); plot(t, zddot_N/9.81, 'k-', t, zddot_M/9.81,'k:')
```

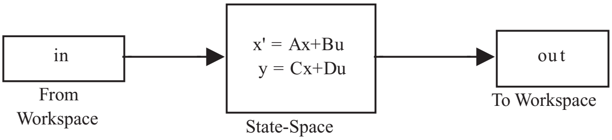
in
From Workspace
x' = Ax+Bu
y = Cx+Du
State-Space
out
To Workspace

Figure I.4 SIMULINK diagram for the time domain taxing response.

```
title('Nose/Main Gear Heave Acceleration for Taxiing Rigid
Aircraft')
xlabel('Time (s)'); ylabel('Heave Acceleration (g)'); legend
('Nose Gear', 'Main Gear')
```

The SIMULINK diagram for the rigid taxiing case is shown in Figure I.4; the same model may be used for the flexible aircraft, with the matrices simply being defined differently in the MATLAB code.

I.9.2 Landing

In this subsection, the MATLAB code and SIMULINK model that were used to generate the results for the nonlinear landing example in Chapter 17 are shown. The example included is a model of the half aircraft mass in heave motion only, the shock absorber and the tyre; look-up tables were used for the nonlinear shock absorber stiffness and damping characteristics. The SIMLINK model is shown in Figure I.5.

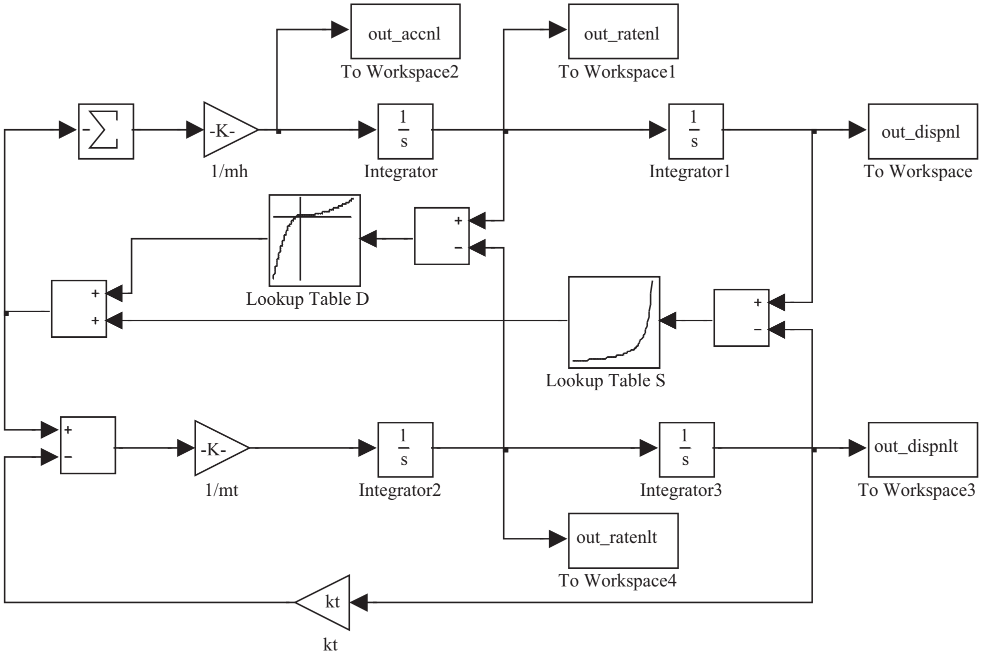
out_accnl
To Workspace2
out_ratenl
To Workspace1
-K-
1/mh
1
s
Integrator
1
s
Integrator1
out_dispnl
To Workspace
Lookup Table D
+
−
+
+
Lookup Table S
+
−
+
−
-K-
1/mt
1
s
Integrator2
1
s
Integrator3
out_dispnlt
To Workspace3
out_ratenlt
To Workspace4
kt
kt

Figure I.5 SIMULINK diagram for the time domain nonlinear landing response.

```
% Rigid aircraft landing - nonlinear gas spring/tyre model -
  requires aircraft data, but not flight case/derivatives
mh = m / 2;                % Factor total mass for half aircraft
Wh = mh*9.81;
Lh = Wh;                   % Lift balances weight
W_e = 3.0;                 % Vertical speed on landing (TAS)

% Single main landing gear parameters leading to non-linear
  behaviour
Pinf = 25e5; PS = 1e7; PC = 3e7; PA = 1e5; zS = 0.4; Area = Wh/PS;
Vratio = PC/Pinf;  Vinf = Vratio*Area*zS / (Vratio - 1);
zinf = Vratio/(Vratio - 1)*zS; ns = 1; nd = 1.35;

% Generate force ~ displacement variation for non-linear shock
  absorber stiffness look-up table
dz = 0.005; z = [0: dz: zS]; [dummy, nz] = size(z);
for j=1:nz
  Pd(j) = Pinf/(1 - z(j) / zinf)^nd;
  Fd(j) = (Pd(j) - PA)*Area;
end

% Generate force ~ velocity variation for nonlinear shock
absorber damping look-up table
Ccomp = 8000; Crecoil = 120000;
zdot = [-1.5: 0.005: 3]; [dummy, nzdot] = size(zdot);
for j=1:nzdot
  if zdot(j) >= 0
Fdamp(j) = Ccomp*zdot(j)^2;
  else
Fdamp(j) = - Crecoil*zdot(j)^2;
  end
end

% Tyre data for half aircraft
mt = 100;  kt = 1000e3; ct = 0;

% Run simulation for aircraft half mass on non-landing gear with
tyre mass/spring representation
tmin = 0; tmax = 0.5; dt = 0.0002; t = [tmin: dt: tmax]';
sim('Rigid_Landing_Gas_Spring_mdl')
% Plot output
figure(1); plot(t, -out_accnl/9.81,'k-'); title('Main Gear
Deceleration for Rigid Aircraft Landing - Non-linear')
xlabel('Time (s)');  ylabel('Main Gear Deceleration (g)')

figure(2);  plot(t, out_dispnl, 'k-', t, (out_dispnl - out_
dispnlt), 'k:', t, out_dispnlt, 'k--')
title('Main Gear/Shock Absorber/Tyre Displacement Response
of Rigid Aircraft Landing - Non-linear')
xlabel('Time (s)'); ylabel('Displacement (m)'); legend('Main
Gear', 'Shock Absorber', 'Unsprung Mass')
```

```
Fgrnd = ct*out_ratenlt +
kt*out_dispnlt;              % Ground reaction force
figure(3);  plot(t, Fgrnd/Wh, 'k-'); title('Normalised Ground
Load - Rigid Aircraft Landing - Non-linear')
xlabel('Time (s)'); ylabel('Normalised Ground Load')
```

Note that the initial condition for the left hand integrator is the landing velocity We.